1
haematologica
Journal of The Ferrata Storti Foundation

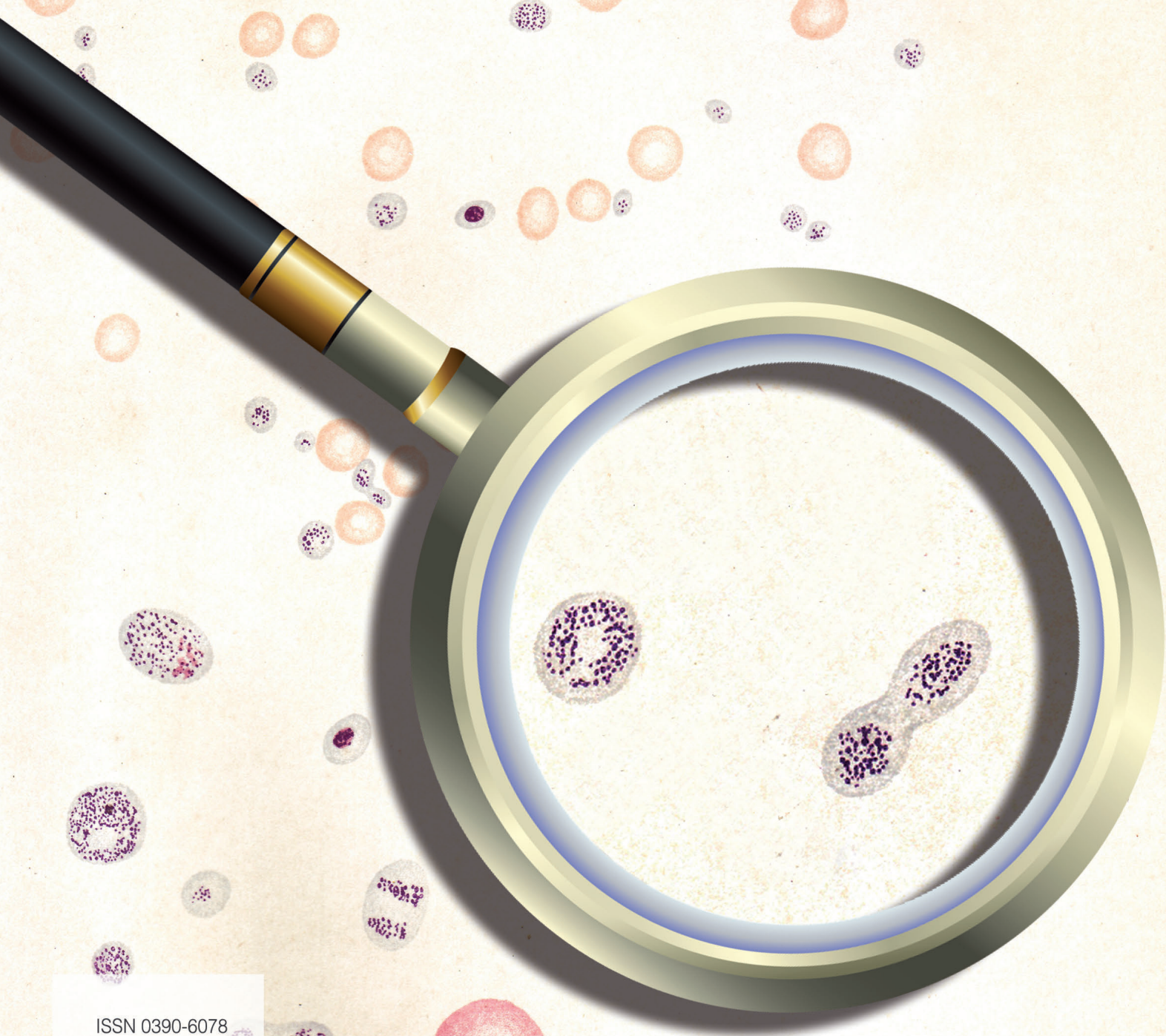

ISSN 0390-6078
Volume 105
MAY
2020 - 05

www.haematologica.org

haematologica
Journal of the Ferrata Storti Foundation

haematologica
Journal of the Ferrata Storti Foundation

Information for readers, authors and subscribers

Haematologica (print edition, pISSN 0390-6078, eISSN 1592-8721) publishes peer-reviewed papers on all areas of experimental and clinical hematology. The journal is owned by a non-profit organization, the Ferrata Storti Foundation, and serves the scientific community following the recommendations of the World Association of Medical Editors (www.wame.org) and the International Committee of Medical Journal Editors (www.icmje.org).

Haematologica publishes editorials, research articles, review articles, guideline articles and letters. Manuscripts should be prepared according to our guidelines (www.haematologica.org/information-for-authors), and the Uniform Requirements for Manuscripts Submitted to Biomedical Journals, prepared by the International Committee of Medical Journal Editors (www.icmje.org).

Manuscripts should be submitted online at http://www.haematologica.org/.

Conflict of interests. According to the International Committee of Medical Journal Editors (http://www.icmje.org/#conflicts), "Public trust in the peer review process and the credibility of published articles depend in part on how well conflict of interest is handled during writing, peer review, and editorial decision making". The ad hoc journal's policy is reported in detail online (www.haematologica.org/content/policies).

Transfer of Copyright and Permission to Reproduce Parts of Published Papers. Authors will grant copyright of their articles to the Ferrata Storti Foundation. No formal permission will be required to reproduce parts (tables or illustrations) of published papers, provided the source is quoted appropriately and reproduction has no commercial intent. Reproductions with commercial intent will require written permission and payment of royalties.

Detailed information about subscriptions is available online at www.haematologica.org. Haematologica is an open access journal. Access to the online journal is free. Use of the Haematologica App (available on the App Store and on Google Play) is free.
For subscriptions to the printed issue of the journal, please contact: Haematologica Office, via Giuseppe Belli 4, 27100 Pavia, Italy (phone +39.0382.27129, fax +39.0382.394705, E-mail: info@haematologica.org).

Rates of the International edition for the year 2019 are as following:

	Institutional	*Personal*
Print edition	*Euro 700*	*Euro 170*

Advertisements. Contact the Advertising Manager, Haematologica Office, via Giuseppe Belli 4, 27100 Pavia, Italy (phone +39.0382.27129, fax +39.0382.394705, e-mail: marketing@haematologica.org).

Direttore responsabile: Prof. Carlo Balduini; Autorizzazione del Tribunale di Pavia n. 63 del 5 marzo 1955.
Printing: Press Up, zona Via Cassia Km 36, 300 Zona Ind.le Settevene - 01036 Nepi (VT)

Associated with USPI, Unione Stampa Periodica Italiana.
Premiato per l'alto valore culturale dal Ministero dei Beni Culturali ed Ambientali

haematologica
Journal of the Ferrata Storti Foundation

Table of Contents

Volume 105, Issue 5: May 2020

About the cover

Editorials

Perspective Article

Review Articles

Articles

Hematopoiesis

Bone Marrow Failure

Iron Metabolism & its Disorders

haematologica
Journal of the Ferrata Storti Foundation

haematologica
Journal of the Ferrata Storti Foundation

Errata Corrige

Letters to the Editor

Letters are available online only at www.haematologica.org/content/105/5.toc

haematologica
Journal of the Ferrata Storti Foundation

Case Reports

Case Reports are available online only at www.haematologica.org/content/105/5.toc

100-year old Haematologica images: the quarrel about the origin of platelets (I)

Carlo L. Balduini

Ferrata-Storti Foundation, Pavia, Italy

E-mail: CARLO L. BALDUINI - carlo.balduini@unipv.it

doi:10.3324/haematol.2020.252908

The textbook of Adolfo Ferrata on Blood Disorders published in 1918, two years before the foundation of Haematologica, devoted six chapters to the origin of platelets.[1] The titles of these chapters are: I. Are platelets precursors of red cells? II. Are platelets living and independent cells? III. Are platelets elements of variable and multiple origin, from erythrocytes, leukocytes and possibly from the vascular endothelium? IV. Are platelets derived from leukocytes? V. Are platelets derived from erythrocytes? VI. Are platelets derived from megakaryocytes? So, at the time of the birth of Haematologica, the origin of platelets was still the subject of vigorous debate.[2]

The image on the cover of this issue has been taken from an article published in Haematologica in 1921 by Aldo Perroncito, who studied under Camillo Golgi when he taught at the University of Pavia.[3] The author was convinced that platelets do not derive from red or white blood cells, and, based on his observation that the number of megakaryocytes does not increase in animals with thrombocytosis induced by bloodletting, he also thought that platelets are not produced by these cells. Although he believed that the origin of the platelets was still to be identified, he gave credit to the hypothesis that these elements are real cells. Moreover, he hypothesized that platelets have the unique ability to duplicate in the peripheral blood. He observed that dog and cat blood with experimentally induced thrombocytosis contained very "large, elongated, biscuit-shaped, and sometimes eight-shaped, platelets" (Figure 1). Moreover, he documented that the number of platelets increased by incubating the blood at 38°C for one or two hours, and concluded that the large and abnormally shaped platelets he identified in peripheral blood are able to divide. Recent studies with refined methodological approaches confirmed his conclusion, a conclusion that he had reached by simple morphological evaluation of blood. Based on current knowledge, the "large, elongated, biscuit-shaped and eight-shaped" elements shown in Figure 1 are proplatelets which have been released, and which have the ability to divide both *in vivo* and *in vitro*, each proplatelet giving the origin to two platelets.

Although Perroncito did not recognize the megakaryocytic origin of platelets, he identified an aspect of platelet biogenesis that has been rediscovered quite recently.[4] Revisiting the Haematologica issues of a century ago shows us that knowledge in the field of hematology was often much more advanced than is commonly thought, this serving to heighten our esteem for the old masters of hematology.

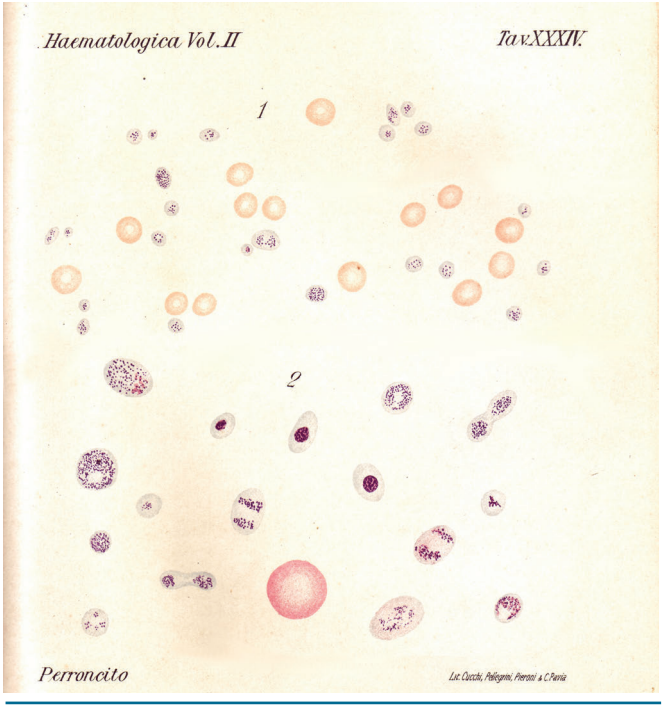

Figure 1. Hand-drawn table that appeared as an illustration in Perroncito's paper "On the derivation of platelets", published in Haematologica in 1921.[3] Based on morphological evaluation of cat and dog blood, the author suggested that the large, elongated, biscuit-shaped platelets shown in the lower part of the figure are able to divide both *in vivo* and *in vitro*. We know today that these elements are proplatelets just released into the blood by megakaryocytes, and that each of them is destined to divide and give the origin to two platelets.

References

1. Ferrata A. [Le emopatie, Trattato per medici e studenti]. Società Editrice Libraria, Milano, 1918.
2. Mazzarello P. One hundred years of Haematologica. Haematologica. 2020;105(1):12-21.
3. Perroncito A. [Sulla derivazione delle piastrine]. Haematologica. 1921;2:510-526.
4. Thon JN, Montalvo A, Patel-Hett S, et al. Cytoskeletal mechanics of proplatelet maturation and platelet release. J Cell Biol. 2010;191(4):861-874.

Immunosuppression and growth factors for severe aplastic anemia: new data for old questions

David J. Young and Cynthia E. Dunbar

Translational Stem Cell Biology Branch, National Heart, Lung, and Blood Institute, NIH, Bethesda, MD, USA

E-mail: DAVID J. YOUNG - david.young2@nih.gov

doi:10.3324/haematol.2020.246512

The arrival of a new patient with severe aplastic anemia (SAA) with severe cytopenias and accompanying risks of bleeding and serious infections strikes fear into the hearts of even experienced hematologists. In most cases, SAA is an acquired disorder driven by a potent autoimmune attack on the most primitive hematopoietic stem and progenitor cell (HSPC) compartment.[1] Treatment requires elimination of the damaging immune response while supporting or replacing the damaged HSPC, either via allogeneic stem cell transplantation (SCT) or intensive immunosuppressive therapy (IST) with horse antithymocyte globulin and cyclosporine.[2,3] Children or younger adults with available donors should undergo upfront allogeneic SCT, since IST does not reverse cytopenias in all patients and requires on average months to result in improvement of cell counts. In addition, IST is associated with both relapse and progression to clonal hematopoietic disorders, including paroxysmal nocturnal hemoglobinuria and myelodysplasia/acute myeloid leukemia in an appreciable fraction of patients followed long-term.[4] In the current issue of *Haematologica*, Tichelli and colleagues present a new analysis of the SAA-granulocyte colony-stimulating factor (G-CSF) trial from the European Group for Blood and Marrow Transplantation (EBMT) Working Party on SAA.[5] In their report, they revisit the use of adjuvant growth factors in SAA treatment and, in doing so, provide the longest follow-up of SAA patients treated with IST to date.

The development and optimization of effective IST for SAA in the late 1980s and early 1990s was punctuated by the identification and clinical availability of hematopoietic cytokines such as G-CSF and erythropoietin. G-CSF was shown to decrease the duration and severity of chemotherapy-induced and inherited neutropenias, rapidly inspiring widespread use in SAA. However, the most primitive HSPC lack the G-CSF receptor, thus at best G-CSF might be expected to accelerate or increase output from a limited number of remaining myeloid progenitor or precursor cells, without improving the underlying profound hematopoietic defects. In addition, early concerns arose that clonal progression could be accelerated or induced by addition of G-CSF to IST, based on retrospective analyses of both children and adults treated with IST.[6-8] A Japanese multicenter, randomized prospective trial that enrolled 101 patients examined the effects of G-CSF added to IST found no increase in progression to myelodysplastic syndromes.[6] At 6 months, the response rate to IST was higher in the G-CSF arm (77% *vs*. 57%), but by the 1 year primary endpoint, response rates were identical and there was no difference in overall survival at 4 years. Interestingly, patients in the G-CSF arm showed fewer relapses (15% *vs*. 42%). In a European trial of 102 SAA patients, higher rates of complete response and 6-month failure-free survival, and faster cell count recovery, were reported, but no significant differences in overall response, 5-year survival or progression to clonal abnormalities could be detected.[9] A number of smaller trials were carried out worldwide with varying designs, assessing the impact of G-CSF, granulocyte-macrophage colony-stimulating factor or erythropoietin, generally showing no consistent benefit or risk in SAA,[10-12] also when pooled via meta-analyses.[13]

The EBMT strove to resolve the confusion by conducting a large, multicenter, randomized trial using optimal IST with and without G-CSF, enrolling 192 patients between 2002 and 2008. The original report published in 2011 showed no impact of G-CSF on primary response or event-free, relapse-free or overall survival rates at 6 years.[14] There was a small but statistically significant reduction in infections and hospitalizations in the G-CSF group. In this initial report, rates of clonal progression were low in both arms, with no apparent impact of G-CSF.

Tichelli and coworkers now provide very illuminating long-term follow-up results from this same EBMT trial.[5] Even the initial report of this trial, as well as registry studies have suggested that all relevant data on the risks and benefits associated with various treatments for SAA are not captured by a sole focus on initial hematologic response and relatively short-term overall survival. Across all ages, regardless of disease severity or treatment, event-free survival continues to decline years after treatment, with continuing increases in the rates of clonal disease and frank second malignancies. Consequently, long-term outcome data provide information on the natural history of treated SAA regardless of the use of growth factors, potentially further informing decisions regarding the initial choice between IST and allogeneic SCT. The authors have been able to provide a median of almost 12 years follow-up in a large well-characterized cohort, an impressive feat in this rare disease. In terms of the original primary endpoints, there was still no impact of G-CSF on response, relapse (in contrast to some previous smaller studies) or overall survival. The primary determinants of outcomes remained age and disease severity at the time of diagnosis, but in patients surviving to 1 year after IST, even these determinants became irrelevant. Regarding clonal disease, the rates at 15 years were congruent with prior estimates, being 8% for cytogenetic abnormalities or myelodysplastic syndrome/acute myeloid leukemia and 10-13% for clinical paroxysmal nocturnal hemoglobinuria. Importantly, G-CSF did not increase the risk of clonal events, and total exposure to G-CSF did not correlate with risk of progression. While Tichelli *et al.* offer additional strong evidence that the addition of G-CSF to IST does not alter overall outcomes

or survival in SAA, they also provide reassurance that G-CSF does not worsen the already significant risk of clonal disease in the post-IST setting. Although their findings definitely do not support the routine use of G-CSF added to IST, they indicate that for high-risk patients with delayed cell count recovery or severe infections, G-CSF may be reasonably added to front-line IST without significant concern for long-term consequences.

However, the most clinically significant findings from this trial have nothing to do with the original questions regarding the risks and benefits of G-CSF in SAA! Regardless of randomization, fully half of all surviving SAA patients experienced significant long-term complications including not only clonal events and relapse, but an array of treatment-related morbidities such as osteonecrosis and kidney disease. Indeed, apart from relapse, non-hematologic complications were more common than clinically relevant clonal progression: 13-16% had chronic kidney disease, with unsurprisingly a higher risk in those requiring prolonged cyclosporine therapy. Furthermore, younger age was not protective against long-term, treatment-related complications. These and prior data indicate that such complications will continue to compound throughout life, underscoring the importance of well-informed initial treatment decisions and further supporting the recommendation for front-line allogeneic SCT in children and younger adults, perhaps employing rapidly available haploidentical family donors given the progressively improving outcomes in the era of post-transplant treatment with cyclophosphamide.[15]

Finally, it is important to mention that in the current era, IST has begun to be augmented not with G-CSF, but instead with the thrombopoietin agonist eltrombopag. Unlike G-CSF, thrombopoietin can act directly on primitive HSPC, which express its receptor, MPL. Initial trials in patients with refractory SAA demonstrated the short-term safety and efficacy of this oral drug as a single agent.[16,17] In a large but single-arm trial at our institution, the addition of eltombopag to IST resulted in improved overall response and complete response in comparison to those in a large historical cohort treated with IST alone.[18] Despite these improved outcome measures, relapse appeared to be just as frequent, and assessment of the impact on clonal progression requires longer follow-up and results from the European ongoing randomized controlled trial of the addition of eltrombopag to IST are awaited. The report from Tichelli and colleagues published in this issue of *Haematologica* educates us regarding the necessity of very long-term and careful analyses of large numbers of patients to inform decisions regarding the best treatment approach for patients with SAA.

References

1. Young NS. Aplastic anemia. N Engl J Med. 2018;379(17):1643-1656.
2. Bacigalupo A. How I treat acquired aplastic anemia. Blood. 2017;129(11):1428-1436.
3. Scheinberg P, Young NS. How I treat acquired aplastic anemia. Blood. 2012;120(6):1185-1196.
4. Socie G, Rosenfeld S, Frickhofen N, Gluckman E, Tichelli A. Late clonal diseases of treated aplastic anemia. Semin Hematol. 2000;37(1):91-101.
5. Tichelli A, Peffault de Latour R, Passweg J, et al. Long-term outcome of a randomized controlled study in patients with newly diagnosed severe aplastic anemia treated with antithymocyte globulin and cyclosporine, with or without granulocyte colony-stimulating factor: a Severe Aplastic Anemia Working Party Trial from the European Group of Blood and Marrow Transplantation. Haematologica. 2020;105(5):1223-1231.
6. Teramura M, Kimura A, Iwase S, et al. Treatment of severe aplastic anemia with antithymocyte globulin and cyclosporin A with or without G-CSF in adults: a multicenter randomized study in Japan. Blood. 2007;110(6):1756-1761.
7. Ohara A, Kojima S, Hamajima N, et al. Myelodysplastic syndrome and acute myelogenous leukemia as a late clonal complication in children with acquired aplastic anemia. Blood. 1997;90(3):1009-1013.
8. Kojima S, Hibi S, Kosaka Y, et al. Immunosuppressive therapy using antithymocyte globulin, cyclosporine, and danazol with or without human granulocyte colony-stimulating factor in children with acquired aplastic anemia. Blood. 2000;96(6):2049-2054.
9. Gluckman E, Rokicka-Milewska R, Hann I, et al. Results and follow-up of a phase III randomized study of recombinant human-granulocyte stimulating factor as support for immunosuppressive therapy in patients with severe aplastic anaemia. Br J Haematol. 2002;119(4):1075-1082.
10. Gordon-Smith EC, Yandle A, Milne A, et al. Randomised placebo controlled study of RH-GM-CSF following ALG in the treatment of aplastic anaemia. Bone Marrow Transplant. 1991;7(Suppl 2):78-80.
11. Shao Z, Chu Y, Zhang Y, Chen G, Zheng Y. Treatment of severe aplastic anemia with an immunosuppressive agent plus recombinant human granulocyte-macrophage colony-stimulating factor and erythropoietin. Am J Hematol. 1998;59(3):185-191.
12. Zheng Y, Liu Y, Chu Y. Immunosuppressive therapy for acquired severe aplastic anemia (SAA): a prospective comparison of four different regimens. Exp Hematol. 2006;34(7):826-831.
13. Gurion R, Gafter-Gvili A, Paul M, et al. Hematopoietic growth factors in aplastic anemia patients treated with immunosuppressive therapy-systematic review and meta-analysis. Haematologica. 2009;94(5):712-719.
14. Tichelli A, Schrezenmeier H, Socie G, et al. A randomized controlled study in patients with newly diagnosed severe aplastic anemia receiving antithymocyte globulin (ATG), cyclosporine, with or without G-CSF: a study of the SAA Working Party of the European Group for Blood and Marrow Transplantation. Blood. 2011;117(17):4434-4441.
15. DeZern AE, Brodsky RA. Haploidentical donor bone marrow transplantation for severe aplastic anemia. Hematol Oncol Clin North Am. 2018;32(4):629-642.
16. Olnes MJ, Scheinberg P, Calvo KR, et al. Eltrombopag and improved hematopoiesis in refractory aplastic anemia. N Engl J Med. 2012;367(1):11-19.
17. Winkler T, Fan X, Cooper J, et al. Treatment optimization and genomic outcomes in refractory severe aplastic anemia treated with eltrombopag. Blood. 2019;133(24):2575-2585.
18. Townsley DM, Scheinberg P, Winkler T, et al. Eltrombopag added to standard immunosuppression for aplastic anemia. N Engl J Med. 2017;376(16):1540-1550.

Recruiting TP53 to target chronic myeloid leukemia stem cells

Steven Grant

Virginia Commonwealth University, Richmond, VA, USA

E-mail: STEVEN GRANT - steven.grant@vcuhealth.org

doi:10.3324/haematol.2019.246306

The problem of eradicating leukemic stem cells (LSC) in chronic myeloid leukemia (CML), as in the case of acute myelogenous leukemia (AML), has long been a therapeutic goal, particularly in relation to agents such as tyrosine kinase inhibitors (TKI), such as imatinib mesylate (IM), that target the oncogenic BCR/ABL kinase. The central conundrum is that CML stem cells appear to be intrinsically resistant to TKI through a variety of mechanisms, including (but not restricted to) increased drug efflux pumps[1] or persistence in a drug-resistant quiescent state. The failure of IM or newer-generation TKI to eradicate CML stem cells presumably underlies the development of drug resistance and/or progression to a more aggressive clinical course e.g. accelerated or blast-phase disease. This inevitable outcome (in transplant-ineligible patients) has prompted the search for new therapeutic strategies capable of eliminating the subset of TKI-resistant stem cells.

In the article by Carter *et al.*, which appears in this edition of Haematologica,[2] the authors expand upon their previous work investigating novel strategies specifically capable of targeting CML LSC. This group had previously shown that the BH3 mimetic Venetoclax (ABT-199), an agent now approved (in combination with hypomethylating agents) in older AML patients, targets LSC, and, when administered in conjunction with IM, effectively eradicated CML stem cells.[3] This group had also shown that disrupting the function of MDM2 (e.g. with nutlin), a protein that binds to and inactivates TP53,[4] also enhanced the activity of IM in a CML blast crisis model. The mechanism(s) by which activating TP53 might sensitize CML stem cells to IM remains to be fully elucidated, but very likely reflects induction of downstream TP53 pro-apoptotic effectors such as NOXA, PUMA, BAX, and BID. For example, NOXA is known to trigger degradation of anti-apoptotic proteins such as MCL-1,[5] which have been shown to serve as a survival factor for leukemia stem cells.[6]

In the present study, the authors examined the effects of a newer MDM2 antagonist (DS-5272) on the sensitivity of CML stem cells to IM using an inducible stem cell promoter-driven CML murine model (Scl-tTa-*BCR/ABL1*). Employing CyTOF-based single-cell proteomics, they found that combined BCR/ABL1 and MDM2 inhibition resulted in the selective upregulation of NOXA and BAX in the CML-LSC population. Importantly, the combination strategy was effective in prolonging survival in this mouse model and in decreasing CML LSC frequency in secondary transplantations. The authors conclude that CML LSC may depend upon TP53 hyperactivation for survival, and that disruption of this process e.g. by MDM2 antagonism may restore TKI sensitivity in these cells. A schematic summary of these concepts is shown in Figure 1. According to this model, CML LSC exhibit relative resistance to TKI, but high activity of TP53, the lethal effects of which are kept in check by MDM2. Disabling of the latter process, e.g. by MDM2 antagonists, results in increased expression of pro-apoptotic TP53-dependent proteins, e.g. NOXA and BAX, which lower the threshold for TKI-mediated cell death (Figure 1A). Activation of TP53 may also lead to downregulation of anti-apoptotic proteins such as MCL-1 indirectly through induction of NOXA. Alternatively, pro-apoptotic proteins such as BCL-2 may be disabled by small molecule BH3-mimetics such as ABT-199, analogously promoting TKI-induced cell death (Figure 1B). The net effect of these events is the selective eradication of CML LSC, an outcome unlikely to be accomplished with TKI alone.

If validated, these findings could have significant implications for the treatment of chronic phase CML by raising the possibility that concomitant administration of MDM2 antagonists with a TKI such as IM might, by targeting quiescent CML stem cells, delay or prevent the emergence of AP or BC. The success of this strategy will be contingent upon the presence of functioning TP53, as the results of earlier studies, as well as this present one, argue strongly that activation of this oncogene is essential for the beneficial actions of MDM2 antagonists. One implication of these findings is that early incorporation of MDM2 inhibitors into TKI-based therapies for CML may be necessary for optimal benefit. For example, in the case of AML, loss of functional TP53 occurs late in the disease and is associated with a particularly poor prognosis.[7] Thus, early eradication of CML stem cells through such a TP53-based strategy may forestall or circumvent the emergence of aggressive clones that have lost functional TP53. Furthermore, while Carter *et al.* have previously described the capacity of the TKI/MDM2 antagonist strategy to target BC cells,[8] the later this approach is applied, the greater the chance of the development of TP53-deficient cells that are resistant to its lethal activity.

One question that arises concerns the mechanism(s) by which addition of an MDM2 antagonist might enhance the activity of TKI against CML stem cells. As noted previously, CML LSC tend to be resistant to TKI because of several factors, including their quiescent state, as well as increased drug efflux in this cell population.[9] To date, there is no evidence that MDM2 inhibitors can directly circumvent these mechanisms and as a consequence, restore TKI sensitivity. Instead, the former agents may primarily operate to modulate the apoptotic threshold e.g. by inducing NOXA, BAX, and potentially other TP53-dependent pro-apoptotic effectors.[10] The ability of the combined TKI/MDM2 antagonist regimen to display superior LSC killing argues that this strategy acts, at least in part, to potentiate the ability of TKI to induce cell death rather than to overcome intrinsic TKI resistance in primitive leukemia progenitors.

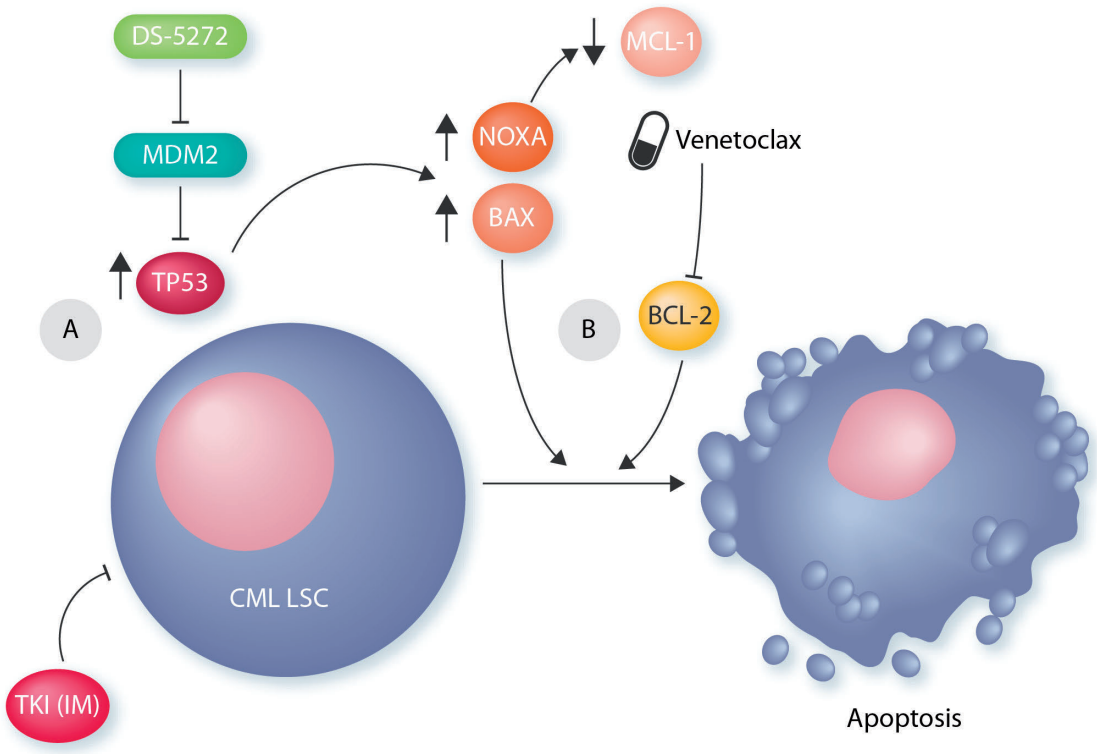

Figure 1. Chronic myeloid leukemia (CML) stem cells are resistant to tyrosine kinase inhibitors (TKI) due to multiple factors, including increased drug efflux. Combined treatment with a TKI and an inhibitor of MDM2 (e.g. OS-5272) leads to hyper-activation of TP53 (A). The latter event results in upregulation of multiple pro-apoptotic effectors including NOXA and PUMA, which trigger LSC apoptosis. This phenomenon may be enhanced by NOXA-mediated degradation of the anti-apoptotic protein MCL-1. Alternatively, disabling of the anti-apoptotic protein BCL-2 (B) e.g. by ABT-199 (Venetoclax) may analogously lower the threshold for TKI-induced cell death in the CML LSC subpopulation. Eradication of such stem cells by simultaneous targeting of oncogenic (BCR/ABL) and orthogonal (TP53) pathways may delay or prevent re-emergence of disease.

While the results of the Carter *et al.* study support the notion that an agent such as OS-5272 may potentiate the activity of a TKI like IM, they also lay a foundation for the development of a wealth of additional strategies capable of targeting CML LSC. For example, apart from the possibility of employing other MDM2 inhibitors, it would be of interest to assess interactions involving other agents that have been used to target BCR/ABL-expressing cells. These would include newer generation TKI such as the multi-kinase inhibitor ponatinib, which is active against BCR-ABL$^+$ cells resistant to IM through the T315 mutation.[11] An alternative candidate for combination with MDM2 inhibitors would be omacetaxine, a protein synthesis inhibitor which down-regulates BCR/ABL among other proteins, and which has shown significant activity against IM-resistant CML.[12] Based upon the present results, there would seem to be a reasonable chance that MDM2 antagonist regimens incorporating these agents would also target LSC. In addition, as noted by the authors, the BCL-2 antagonist ABT-199 is known to target LSC,[13] and has also been shown to increase TKI activity against primitive LSC.[3] If tolerable, adding ABT-199 to the MDM2 antagonist/IM regimen may prove to be particularly effective in eliminating the LSC population. Aside from this approach, recent attention has focused on the development of MCL-1 antagonists as anti-leukemic agents,[14] in part due to evidence that MCL-1 is required by CML LSC for survival.[15] In view of these considerations, the notion of using a clinically relevant MCL-1 antagonist to further enhance the activity of an MDM2 antagonist/TKI regimen against CML LSC appears worthy of investigation.

In summary, the present report argues that, in CML, LSC exhibit a potentially selective activation of TP53 which can be exploited through the use of MDM2 antagonists, and that this phenomenon can act in concert with TKI inhibitors to trigger cell death in this difficult to eradicate leukemic cell subpopulation. Whereas in the past, attention focused on the identification of novel TKI able to overcome mutational forms of resistance, more current approaches are based on the development of strategies designed to disrupt orthogonal, non-oncogenic pathways,[16] including those related to TP53. However, whether such dual-targeting strategies will prove capable of eliminating primitive stem cells has not yet been definitively established. The results presented here strongly support the concept of simultaneous targeting of oncogenic drivers (e.g. BCR/ABL) and orthogonal pathways (e.g. TP53) to eradicate these cells, at least in the case of CML. Given the large array of targeted agents that are now clinically available, including MDM2 inhibitors and modulators of the apoptotic response, LSC-directed therapy in CML and related disorders is currently underway. Determining whether such novel strategies will live up to their pre-clinical promise is only a matter of time.

References

1. Engler JR, Frede A, Saunders VA, Zannettino AC, Hughes TP, White DL. Chronic myeloid leukemia CD34+ cells have reduced uptake of imatinib due to low OCT-1 activity. Leukemia. 2010;24(4):765-770.
2. Carter BZ, Mak PY, Mu H, et al. Combined inhibition of MDM2 and Bcr-Abl tyrosine kinase targets chronic myeloid leukemia stem/progenitor cells in a murine model. Haematologica. 2020;105(5):1274-1284.
3. Carter BZ, Mak PY, Mu H, et al. Combined targeting of BCL-2 and BCR-ABL tyrosine kinase eradicates chronic myeloid leukemia stem cells. Sci Transl Med. 2016;8(355):355ra117.
4. Lau LM, Nugent JK, Zhao X, Irwin MS. HDM2 antagonist Nutlin-3 disrupts p73-HDM2 binding and enhances p73 function. Oncogene. 2008;27(7):997-1003.
5. Willis SN, Chen L, Dewson G, et al. Proapoptotic Bak is sequestered by Mcl-1 and Bcl-xL, but not Bcl-2, until displaced by BH3-only proteins. Genes Dev. 2005;19(11):1294-1305.
6. Yoshimoto G, Miyamoto T, Jabbarzadeh-Tabrizi S, et al. FLT3-ITD up-regulates MCL-1 to promote survival of stem cells in acute myeloid leukemia via FLT3-ITD-specific STAT5 activation. Blood. 2009;114(24):5034-5043.
7. Hunter AM, Sallman DA. Current status and new treatment approaches in TP53 mutated AML. Best Pract Res Clin Haematol. 2019;32(2):134-144.
8. Carter BZ, Mak PY, Mak DH, et al. Synergistic effects of p53 activation via MDM2 inhibition in combination with inhibition of Bcl-2 or Bcr-Abl in CD34+ proliferating and quiescent chronic myeloid leukemia blast crisis cells. Oncotarget. 2015;6(31):30487-30499.
9. Inoue A, Kobayashi CI, Shinohara H, et al. Chronic myeloid leukemia stem cells and molecular target therapies for overcoming resistance and disease persistence. Int J Hematol. 2018;108(4):365-370.
10. Peterson LF, Mitrikeska E, Giannola D, et al. p53 stabilization induces apoptosis in chronic myeloid leukemia blast crisis cells. Leukemia. 2011;25(5):761-769.
11. Pavlovsky C, Chan O, Talati C, Pinilla-Ibarz J. Ponatinib in the treatment of chronic myeloid leukemia and philadelphia chromosome positive acute lymphoblastic leukemia. Future Oncol. 2019;15(3):257-269.
12. Novotny L, Al-Tannak NF, Hunakova L. Protein synthesis inhibitors of natural origin for CML therapy: semisynthetic homoharringtonine (Omacetaxine mepesuccinate). Neoplasma. 2016;63(4):495-503.
13. Mattes K, Gerritsen M, Folkerts H, et al. CD34+ acute myeloid leukemia cells with low levels of reactive oxygen species show increased expression of stemness-genes and can be targeted by the BCL2 inhibitor Venetoclax. Haematologica. 2019 Nov 14. [Epub ahead of print]
14. Wang Q, Hao S. A-1210477, a selective MCL-1 inhibitor, overcomes ABT-737 resistance in AML. Oncol Lett. 2019;18(5):5481-5489.
15. Allan EK, Holyoake TL, Craig AR, Jørgensen HG. Omacetaxine may have a role in chronic myeloid leukaemia eradication through down-regulation of Mcl-1 and induction of apoptosis in stem/progenitor cells. Leukemia. 2011;25(6):985-994.
16. Hanahan D, Weinberg RA. Hallmarks of cancer: the next generation. Cell. 2011;144(5):646-674.

Role of Meningioma 1 for maintaining the transformed state in MLL-rearranged acute myeloid leukemia: potential for therapeutic intervention?

Juerg Schwaller

University Children's Hospital beider Basel (UKBB), Department of Biomedicine (DBM), University of Basel, Switzerland

E-mail: JUERG SCHWALLER - j.schwaller@unibas.ch

doi:10.3324/haematol.2019.246348

Meningioma 1 (MN1) was cloned from a balanced chromosomal translocation in a meningioma as open reading frame encoding for a protein of 1,319 amino acids containing several proline and histidine-rich domains, acting as a transcriptional activator necessary for normal development of the bones of the skull.[1,2] Several studies found mutations or aberrant expression of MN1 in various hematologic malignancies. Characterization of a t(12;22)(p13;q11) chromosomal translocation associated with myeloproliferative disorders revealed a fusion between MN1 and the ETS-family transcription factor ETV6 (a.k.a. TEL).[3] A fusion of MN1 to Friend leukemia virus integration 1 (FLI1) has been shown to be a rare transforming oncogene in acute megakaryoblastic leukemia (AMKL).[4] Aberrant high expression of MN1 was reported in acute myeloid leukemia (AML) with inv(16) leading to the core-binding factor fusion CBFB-MYH11.[5] Clinical studies proposed that high MN1 transcript levels could be used as prognostic marker in cytogenetically-normal (CN) AML.[6] Functional studies in mice demonstrated the oncogenic potential of aberrant MN1 expression. Retroviral MN1 overexpression in murine bone marrow (BM) hematopoietic stem and progenitor cells (HSPC) followed by transplantation rapidly induced a lethal AML in mice.[7] Aberrant MN1 expression due to retroviral insertion was shown to act as collaborative oncogenic event in acute leukemia induction by the MLL-ENL or the MLL-AF9 fusion gene, respectively.[8,9] More recent work suggested that gene expression programs associated with MN1-mediated transformation of hematopoietic cells are controlled by the H3K4 and H3K79 histone methyltransferases MLL1 and DOT1L, respectively.[10] Collectively, these studies indicated that aberrant MN1 expression contributes to malignant transformation of hematopoietic cells towards AML; however, its role in the maintenance of the transformed state remained poorly understood.

In a study published in this issue of Haematologica, Sharma *et al.* functionally addressed the role of MN1 in the maintenance of AML induced by MLL fusion oncogenes.[11] They used Crisper/CAS9 to ablate MN1 in several murine AML lines, including cells transformed by retroviral overexpression of the MLL-AF9 fusion (rMLL-AF9), and in human THP1 and MV4;11 AML cell lines carrying the MLL-AF9 and MLL-AF4 fusions, respectively. They found that inactivation of MN1 impaired the clonogenic activity and proliferation associated with impaired cell cycle progression, and increased differentiation and apoptosis of murine rMLL-AF9 AML cells. Loss of MN1 also

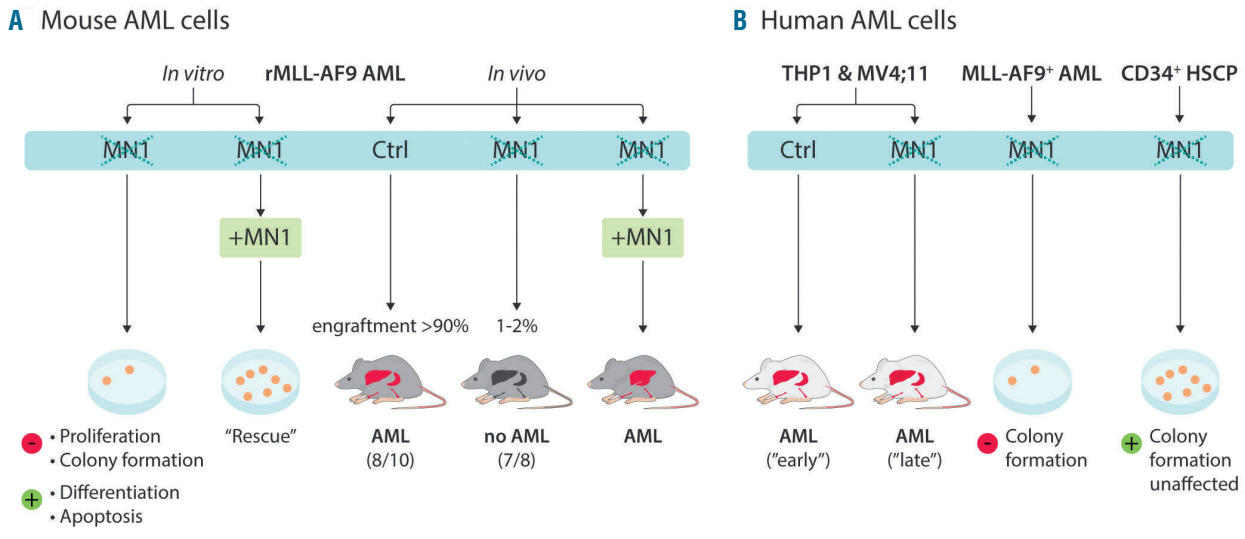

Figure 1. Schematic illustration of the findings by Sharma *et al.* in mouse (A) and human (B) acute myeloid leukemia (AML) cells expressing high levels of Meningioma 1 (MN1) and in CD34+ hematopoietic stem and progenitor cell (HSPC) controls (Ctrl).

reduced *in vivo* leukemia induction after transplanting the cells into syngenic mice. MLL-AF9+ AML cells lacking MN1 were significantly impaired in engrafting upon intravenous injection resulting in AML after long latency or no disease at all (Figure 1A). Notably, MN1 inactivation did not impair homing of transplanted cells to the BM. Most importantly, overexpression of exogenous MN1 'rescued' the anti-leukemic effects of ablation of endogenous MN1 in mouse rMLL-AF9 AML cells resulting in increased proliferation and clonogenic activity *in vitro* and increased engraftment and disease induction *in vivo.* Similar to murine cells, MN1 inactivation also delayed leukemia induction by transplantation of human THP1 or MV4;11 cells into immune deficient NSG mice. As in mouse rMLL-AF9 AML cells, reduced MN1 expression (by siRNA) also impaired clonogenic activity of primary MLL-AF9 human AML cells, whereas colony formation by normal CD34+ hematopoietic stem and progenitor cells (HSPC) was not affected (Figure 1B).

To understand the molecular mechanisms, Sharma *et al.* compared gene expression signatures of MLL-AF9+ leukemic cells before and after MN1 inactivation, and evaluated public chromatin immunoprecipitation sequencing (ChIP-seq) datasets. Enrichment of MN1 together with MLL-AF9, MEIS1 and the DOT1L-mediated H3K79me marks on the distal *Hoxa* gene cluster (Hoxa7-Hoxa10) suggested that MN1 regulates *Hoxa* gene expression. However, MN1 seemed not to co-localize with MLL-AF9, suggesting that MN1 primarily acts as a co-factor of Hoxa9 and Meis1. These observations were supported by reduced expression of the Hoxa9 target *Bcl2* (and other Hoxa9/Hoxa10 targets) upon MN1 inactivation in MLL-AF9+ AML cells. Finally, Sharma *et al.* explored the effects of reduced MN1 levels in primary cells from five AML patients and in CD34+ HSCP from healthy donors. They observed that application of MN1-targeting siRNA, either packed in lipid nanoparticles or transfected, significantly reduced the number and size of colonies formed by primary MLL-AF9+ AML cells but had no effect on colony formation by normal HSPC in methylcellulose. Sharma *et al.* concluded that MN1 is essential to maintain a transformed state of AML cells expressing MLL-AF9.[11]

The experiments by Sharma *et al.* have been performed with well-characterized mouse and human MLL-AF9+ AML cells expressing high levels of MN1 and HOXA9. However, one has to keep in mind that not all AML cells carrying MLL-AF9 or other MLL rearrangements express aberrantly high levels of MN1.[10] Although the effects of increased MN1 expression have been intensively studied, regulation of MN1 expression in hematopoietic cells still remains poorly understood. Previous reports found highest MN1 levels in hematopoietic stem cells (HSC) and early progenitor cells and very similar to HOXA genes, MN1 expression seems down-regulated during myelomonocytic differentiation.[5,12] However, not all AML patients expressing high levels of MN1 also express high levels of the *HOXA* gene cluster. Inv(16)+ AML cells often associated with aberrantly high MN1 levels mostly express very low *HOXA* levels.[13] Although Sharma *et al.* tested the efficacy of anti-MN1-siRNA in the inv(16)+ ME1 cell line, they did not show whether MN1 knockdown impaired colony formation or proliferation of these cells as efficiently as in primary MLL-AF9+ murine AML cells.

Does MN1 expression reflect the cellular origin of transformation? Highest MN1 transcript levels were found in patients with immature CD34+ AML.[14] In addition, transformation by experimental MN1 overexpression was found to depend on activation of MEIS1/AbdB-like HOX proteins present in common myeloid progenitors (CMP) but not in more differentiated granulocyte-macrophage progenitors (GMP).[15] Will the MN1 expression status change upon disease relapse? Experimental data indicated that overexpression of MN1 leads to resistance of AML cells to cytarabine and doxorubicin, suggesting selection for cells expressing highest levels during therapy.[16] However, based on a small number of patients, there seemed to be only a slight trend towards higher *MN1* mRNA expression upon disease relapse.[17] Nevertheless,

highest *MN1* transcript levels were associated with a higher incidence and shorter time to relapse.[14]

How can we then therapeutically target MN1 expression? Although useful to provide proof of concept in experimental studies, clinical siRNA-based knockdown approaches, such as those used by Sharma *et al.*, have so far been hampered by limited delivery into the target cells. However, small molecules have been generated that can interfere with certain transcription factor/co-factor protein-protein interactions or with transcription factor-DNA binding. In addition, transcription activity was successfully targeted by altering levels of ubiquitylation and subsequent proteasome degradation or by interference with regulators of transcription factor expression.[18] To target MN1 as a transcription factor, we would need to know its potential interaction partners on chromatin and/or the critical domains of MN1 that are necessary to maintain the transformed state of AML cells. Targeted genome editing screens could offer a platform to dissect structural needs of MN1 activity in AML cells.[19] Previous work that explored the transforming potential of a large number of MN1 deletion mutants suggested that 221 N-terminal amino acids are critical for induction of AML *in vivo* associated with expression of *HOXA9*, *HOXA10* and *MEIS2*.[20] Similarly, others reported that MN1 lacking amino acids 12-228 was unable to induce leukemia in the BM reconstitution assay, suggesting that overexpression of N-terminal MN1 peptides and small molecules "mimicks" might be able to compete with potentially, yet to be defined, critical protein and/or chromatin interactions.[21] Interestingly, the N-terminal region of MN1 was also shown to interact with the EP300 transcriptional co-activator, raising the question as to whether AML cells expressing high MN1 levels would be particularly sensitive to recently developed small molecule EP300 inhibitors.[22,23]

Collectively, by demonstrating a critical role for MN1 in AML maintenance, the work by Sharma *et al.* suggests that targeting the aberrantly high levels of MN1 expression would have strong anti-leukemic activity. However, the AML patients that would profit from such intervention, and the most efficient clinically applicable strategy, remain to be elucidated.

Acknowledgments

This work was supported by grants from the Swiss Cancer League (KFS-3487-08-2014) and the Swiss National Science Foundation (SNF, 31003_A_173224/1).

References

1. Lekanne Deprez RH, Riegman PH, Groen NA, et al. Cloning and characterization of MN1, a gene from chromosome 22q11, which is disrupted by a balanced translocation in a meningioma. Oncogene. 1995;10(8):1521-1528.
2. Meester-Smoor MA, Vermeij M, van Helmond MJ, et al. Targeted disruption of the Mn1 oncogene results in severe defects in development of membranous bones of the cranial skeleton. Mol Cell Biol. 2005;25(10):4229-4236.
3. Buijs A, Sherr S, van Baal S, et al. Translocation (12;22) (p13;q11) in myeloproliferative disorders results in fusion of the ETS-like TEL gene on 12p13 to the MN1 gene on 22q11. Oncogene. 1995;10(8):1511-1519.
4. Dang J, Nance S, Ma J, et al. AMKL chimeric transcription factors are potent inducers of leukemia. Leukemia. 2017;31(10):2228-2234.
5. Heuser M, Beutel G, Krauter J, et al. High meningioma 1 (MN1) expression as a predictor for poor outcome in acute myeloid leukemia with normal cytogenetics. Blood. 2006;108(12):3898-3905.
6. Carella C, Bonten J, Sirma S, et al. MN1 overexpression is an important step in the development of inv(16) AML. Leukemia. 2007;21(8):1679-1690.
7. Heuser M, Argiropoulos B, Kuchenbauer F, et al. MN1 overexpression induces acute myeloid leukemia in mice and predicts ATRA resistance in patients with AML. Blood. 2007;110(5):1639-1647.
8. Liu T, Jankovic D, Brault L, et al. Functional characterization of high levels of meningioma 1 as collaborating oncogene in acute leukemia. Leukemia. 2010;24(3):601-612.
9. Bergerson RJ, Collier LS, Sarver AL, et al. An insertional mutagenesis screen identifies genes that cooperate with Mll-AF9 in a murine leukemogenesis model. Blood. 2012;119(19):4512-4523.
10. Riedel SS, Haladyna JN, Bezzant M, et al. MLL1 and DOT1L cooperate with meningioma-1 to induce acute myeloid leukemia. J Clin Invest. 2016;126(4):1438-1450.
11. Sharma A, Jyotsana N, Gabdoulline R, et al. Meningioma 1 is indispensable for mixed lineage leukemia-rearranged acute myeloid leukemia. Haematologica. 2020;105(5):1294-1305.
12. Kandilci A, Grosveld GC. Reintroduction of CEBPA in MN1-overexpressing hematopoietic cells prevents their hyperproliferation and restores myeloid differentiation. Blood. 2009;114(8):1596-1606.
13. Ichikawa H, Tanabe K, Mizushima H, et al. Common gene expression signatures in t(8;21)- and inv(16)-acute myeloid leukaemia. Br J Haematol. 2006;135(3):336-347.
14. Jentzsch M, Bill M, Grimm J, et al. Prognostic Impact of Blood MN1 Copy Numbers Before Allogeneic Stem Cell Transplantation in Patients With Acute Myeloid Leukemia. HemaSphere. 2019;3(1):e167.
15. Heuser M, Yun H, Berg T, et al. Cell of origin in AML: susceptibility to MN1-induced transformation is regulated by the MEIS1/AbdB-like HOX protein complex. Cancer Cell. 2011;20(1):39-52.
16. Pardee TS. Overexpression of MN1 confers resistance to chemotherapy, accelerates leukemia onset, and suppresses p53 and Bim induction. PLoS One. 2012;7(8):e43185.
17. Carturan S, Petiti J, Rosso V, et al. Variable but consistent pattern of Meningioma 1 gene (MN1) expression in different genetic subsets of acute myelogenous leukaemia and its potential use as a marker for minimal residual disease detection. Oncotarget. 2016;7(45):74082-74096.
18. Bushweller JH. Targeting transcription factors in cancer - from undruggable to reality. Nat Rev Cancer. 2019;19(11):611-624.
19. Shi J, Wang E, Milazzo JP, Wang Z, Kinney JB, Vakoc CR. Discovery of cancer drug targets by CRISPR-Cas9 screening of protein domains. Nat Biotechnol. 2015;33(6):661-667.
20. Lai CK, Moon Y, Kuchenbauer F, et al. Cell fate decisions in malignant hematopoiesis: leukemia phenotype is determined by distinct functional domains of the MN1 oncogene. PLoS One. 2014;9(11):e112671.
21. Kandilci A, Surtel J, Janke L, Neale G, Terranova S, Grosveld GC. Mapping of MN1 sequences necessary for myeloid transformation. PLoS One. 2013;8(4):e61706.
22. van Wely KH, Molijn AC, Buijs A, et al. The MN1 oncoprotein synergizes with coactivators RAC3 and p300 in RAR-RXR-mediated transcription. Oncogene. 2003;22(5):699-709.
23. Lasko LM, Jakob CG, Edalji RP, et al. Discovery of a selective catalytic p300/CBP inhibitor that targets lineage-specific tumours. Nature. 2017;550(7674):128-132.

A post-stem cell transplant risk score for Philadelphia-negative acute lymphoblastic leukemia

Dietger Niederwieser

University of Leipzig; Lithuanian University of Health Sciences, Kaunas, Lithuania and Aichi Medical University, School of Medicine, Nagakute, Japan

E-mail: DIETGER NIEDERWIESER - dietger@medizin.uni-leipzig.de

doi:10.3324/haematol.2019.246322

Recent decades have seen major advances in understanding the genetic basis of hematologic and non-hematologic malignancies. The discovery of the Philadelphia chromosome (Ph) in chronic myeloid leukemia was a key step forward.[1,2] Since then, many recurrent chromosomal abnormalities, such as t(8,21) and t(15;17), have been found in acute leukemias, paving the way for identification of altered genes.[3] These ongoing discoveries have provided and continue to provide major insights into the mechanisms by which key transcription factors and epigenetic modulators regulate normal hematopoiesis and, if dysregulated, promote leukemic transformation. To date, more than 200 balanced chromosomal rearrangements (translocations, insertions and inversions) defining biologically distinct subsets of acute leukemia have been identified. Chromosome analysis, together with molecular determinations, are now important components of routine clinical practice and essential for appropriate diagnosis. Cytogenetic findings have in addition been repeatedly shown to be among the most important and independent prognostic factors in both acute myeloid leukemia and acute lymphoblastic leukemia (ALL).[4,5] For all these reasons, specific chromosome alterations and their molecular counterparts have been included in the World Health Organization classification of hematologic malignancies and together with morphology, immunophenotype and clinical features are used to define distinct disease entities.[6]

The first comprehensive cytogenetic analysis showing biological and prognostic significance in adult ALL was performed at the Third International Workshop on Chromosomes in Leukemia in 1981.[7] The frequency of abnormal karyotypes was shown to be slightly higher in adult than in pediatric ALL (60-69% *vs.* 58-64%, respectively) with t(9;22)(q34;q11) being the most frequent translocation.[8] Less than 6% of children, but up to 40% of adults ≥40 years of age, with ALL harbor a Ph translocation (Ph^+) with or without additional alterations, which is a poor prognostic feature regardless of age. In contrast, less than 12% of adults, but 25% of children have high hyperdiploidy, a good prognostic feature.[4]

One of the hurdles to developing a more sophisticated cytogenetic profile is the overall incidence and, in particular, the different subsets of Ph^- adult ALL, each of which accounts for less than 10% of the total. Only sparse information is available on Ph^- ALL patients. The most frequent Ph^- chromosomal aberrations include t(4;11)(q21;q23)/*KMT2A-AFFI* (3-7%) involving the *MLL* gene, translocations t(8;14)(q24;q11) (2%) involving *myc*, t(1;19)(q23;p13)/*TCF3-PBX1* (2-3%), t(10;14)(q24;q11) (2%), t(11;19)(q23;13.3) and structural abnormalities such as 9p, 6q, and 12p, 18, 19. Further cytogenetic changes include the multiaberrant karyotype, monosomy 7, monosomy 9, +8, del11 and low hypodiploidy, near triploidy and high hyperdiploidy. ALL study groups, including the Medical Research Council (MRC), Eastern Cooperative Oncology Group (ECOG), Southwest Oncology Group (SWOG), Northern Italy Leukemia Group (NILG), North UK and *Gruppo Italiano Malattie Ematologiche dell'Adulto* (GIMEMA) categorize the cytogenetic alterations at diagnosis into risk groups. Unfortunately, the representation of patients treated with hematopoietic stem cell transplantation (SCT) is limited in these analyses. The largest study with patients undergoing allogeneic SCT was the MRC-ECOG study with 310 patients.[9] Here, four risk categories were identified using the modified MRC-ECOG score (very high, high, intermediate and standard).[10]

In a study reported by Aleksandr Lazaryan *et al.* in this issue of *Haematologica*, the Acute Leukemia Working Committee of the Center for International Blood and Marrow Transplant Research (CIBMTR) investigated the usefulness of the MRC-ECOG score in a large cohort of patients after SCT (n=1731) all of whom were adults with Ph^- ALL.[11] While the standard- risk group had favorable outcomes compared to the intermediate-risk group, the adverse risk group was not clearly inferior using the modified MRC-ECOG score. The analysis of relapse and post-transplant treatment failure revealed that t(8;14), monosomy 7 and complex karyotype were the major important determinants. As a consequence, the authors propose, in addition to the modified MRC-ECOG score at diagnosis, the CIBMTR risk score for transplant, which does not include the t(4;11), t(1;19), t(17;19), t(5;14) and +8, but does include t(8;14), t(11;19), monosomy 7, del(7q), del(11q) and complex karyotype (Figure 1).

Previous studies on ALL patients after SCT have concluded that cytogenetics do not predict overall survival. The difference in respect to the current study might be explained by the high number of patients transplanted in advanced phase disease in addition to the high number of patients with Ph^+ ALL included in one study.[12] Another study found no difference in overall survival between patients with high risk [defined as t(4;11)(q21;q23), t(8;14)(q24;32), low hypodiploidy, complex karyotype] and standard-risk cytogenetics, most probably as a consequence of the low number of patients in the high-risk group.[13] A different study identified t(4;11)/*KMT2A-AFF1* and t(v;14q32)/*IGH* in Ph^- patients, but censored patients at the time of SCT.[14]

A source of uncertainty in the current analysis is the lack of information on cytogenetic results at transplant.[15] Furthermore, molecular information at diagnosis and minimal residual disease might have influenced the results of this retrospective analysis. Despite these flaws, the results

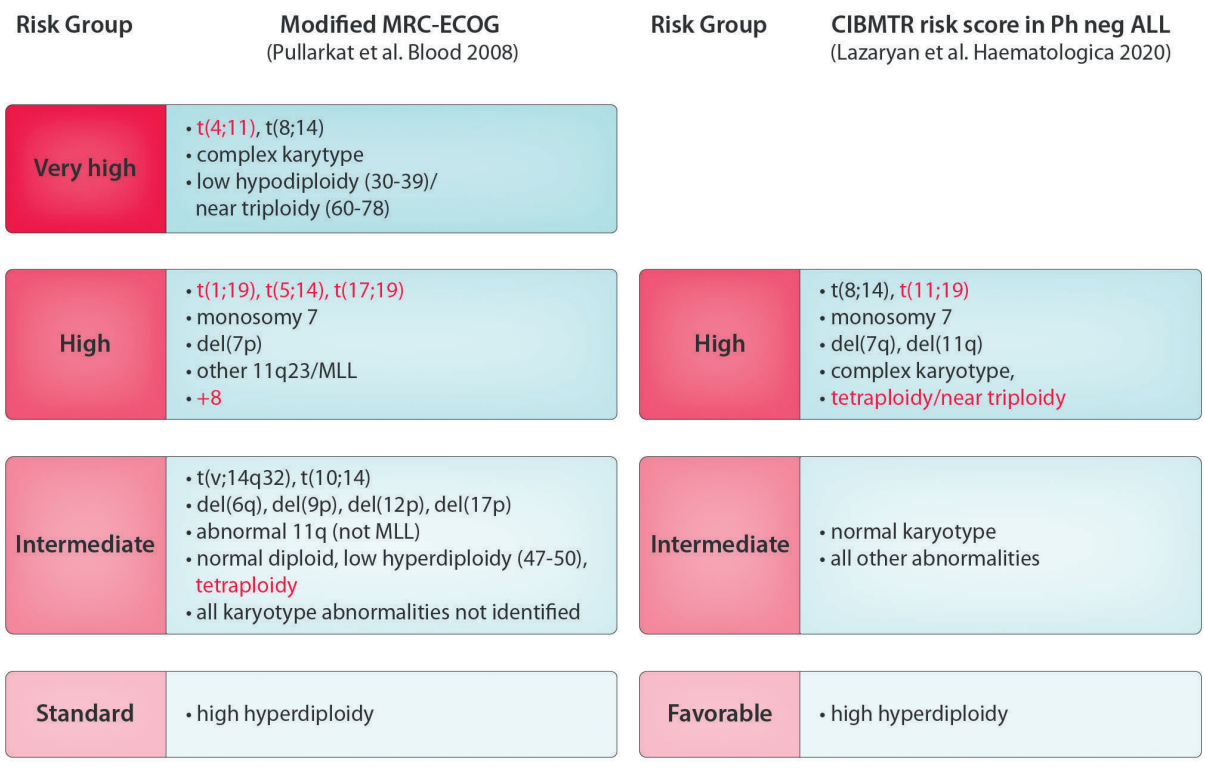

Figure 1. Comparison of two cytogenetic risk classifications for Philadelphia chromosome-negative acute lymphoblastic leukemia. The modified Medical Research Council – Eastern Cooperative Oncology Group (MRC-ECOG) score at diagnosis *versus* the Center for International Blood and Marrow Transplant Research (CIBMTR) risk score for post-transplant Philadelphia chromosome-negative acute lymphoblastic leukemia. Differences between the risk scores are shown in red.

are derived from the largest cohort of Ph- patients treated with SCT to date and show clear distinctions in leukemia-free survival (LFS) using just three risk groups.

Several aspects of the article by Lazaryan *et al.*[11] are of interest. Post-transplant risk scores differ from those for patients treated with conventional therapy. This may be a consequence of graft-*versus*-tumor susceptibility. It is interesting to see that translocations, except for t(8;14) and t(1;19), are noticeably absent from the CIBMTR risk score compared to the modified MRC-ECOG risk score (Figure 1). While t(1;19)(q23;p13), t(4;11)(q21;q23), t(5;14)(q35;q32) and t(17;19)(q22;p13) were identified as risk factors at diagnosis/before SCT, they were not considered to be adverse post-SCT. It is feasible that the abnormal proteins produced by translocations may directly or indirectly affect malignant cell immunogenicity and enhance the graft-*versus*-tumor effect.

The translocations t(8;14) and t(11;19) still remain in the high-risk category. A possible reason might be the association of t(8;14) with the involvement of the *myc* gene on chromosome 8 and of t(11;19) with the *MLL* gene, underlying the prevalence of tumor-specific rather than immunogenic factors.

Multiple mechanisms have been proposed to be responsible for the high relapse rate in diseases with monosomy 7 and complex karyotype, including loss of tumor suppressor genes, haplo-insufficiency or loss of *IKZF1*. These alterations may be less susceptible to graft-*versus*-tumor reactions. The results are similar to those previously seen in acute myeloid leukemia, in which t(11;19),[16-18] monosomy 7, deletion 7q[19,20] and complex karyotype are also risk factors and play an important role in outcome. Similar mechanisms might therefore influence relapse rates after SCT in both acute myeloid leukemia and ALL.

A further consequence of the results of the analysis by Lazaryan *et al.* is the evident need to reduce the relapse rate in high-risk (but also in normal-risk) patients. This may be possible by evaluating minimal residual disease before and after SCT. The important role of minimal residual disease in predicting outcome at an individual level has recently been published.[21] Optimizing SCT outcome by tailoring immunosuppression in the early phase, in response to post-transplant monitoring of disease-specific minimal residual disease or chimerism would be an appropriate approach. The relapse risk in Ph- ALL may be reduced by new drugs, such as blinatumomab, inotuzumab ozogamycin or tisagenlecleucel. In this context, the results presented by Lazaryan *et al.* should provide a stimulus for prospective clinical studies.

Furthermore, those translocations associated with implied susceptibility to graft-*versus*-tumor reactions may provide a lead for the identification of immunogenic tumor-specific antigens, while all translocations are potential targets for small molecules able to neutralize disease-specific products, such as driver kinases or activation pathways. In patients with deletions or monosomy such efforts might be difficult.

Finally, scores might be influenced by the different treat-

ment possibilities available today. Often large datasets are collected over a long time with considerable changes in first-line therapy, such as introduction of pediatric-based regimens, while the number of patients in different categories remains small. Considering the relative homogeneity of transplant procedures in comparison to the different non-transplant protocols, the post-transplant CIBMTR score represents an important prognostic tool.

References

1. Nowell P, Hungerford D. A minute chromosome in human chronic granulocytic leukemia. Science. 1960;132:1497.
2. Rowley JD. A new consistent chromosomal abnormality in chronic myelogenous leukaemia identified by quinacrine fluorescence and Giemsa staining. Nature. 1973;243(5405):290-293.
3. Rowley JD. Identificaton of a translocation with quinacrine fluorescence in a patient with acute leukemia. Ann Genet. 1973. 1973;16(2):109-112.
4. Mrózek K, Heerema NA, Bloomfield CD. Cytogenetics in acute leukemia. Blood Rev. 2004;18(2):115-136.
5. Rowe JM, Buck G, Burnett AK, et al. Induction therapy for adults with acute lymphoblastic leukemia: results of more than 1500 patients from the international ALL trial: MRC UKALL XII/ECOG E2993. Blood. 2005;106(12):3760-3767.
6. Döhner H, Estey E, Grimwade D, et al. Diagnosis and management of AML in adults: 2017 ELN recommendations from an international expert panel. Blood. 2017;129(4):424-447.
7. Mittelman F. The Third International Workshop on Chromosomes in Leukemia. Lund, Sweden, July 21-25, 1980. Introduction. Cancer Genet Cytogenet. 1981(4):96-98.
8. Roberts KG. Genetics and prognosis of ALL in children vs adults. Hematology Am Soc Hematol Educ Program. 2018;2018(1):137-145.
9. Moorman AV, Harrison CJ, Buck GAN, et al. Karyotype is an independent prognostic factor in adult acute lymphoblastic leukemia (ALL): analysis of cytogenetic data from patients treated on the Medical Research Council (MRC) UKALLXII/Eastern Cooperative Oncology Group (ECOG) 2993 trial. Blood. 2007;109(8):3189-3197.
10. Pullarkat V, Slovak ML, Kopecky KJ, Forman SJ, Appelbaum FR. Impact of cytogenetics on the outcome of adult acute lymphoblastic leukemia: results of Southwest Oncology Group 9400 study [eng]. Blood. 2008;111(5):2563-2572.
11. Lazaryan A, Dolan M, Zhang M-J, et al. Impact of cytogenetic abnormalities on outcomes of adult Philadelphia-negative acute lymphoblastic leukemia after allogeneic hematopoietic stem cell transplantation: a study by the Acute Leukemia Working Committee of the Center for International Blood and Marrow Transplant Research [eng]. Haematologica. 2020;105(5):1329-1338.
12. Aldoss I, Tsai N-C, Slovak ML, et al. Cytogenetics does not impact outcomes in adult patients with acute lymphoblastic leukemia undergoing allogeneic hematopoietic cell transplantation. Biol Blood Marrow Transplant. 2016;22(7):1212-1217.
13. Shimizu H, Doki N, Kanamori H, et al. Prognostic impact of cytogenetic abnormalities in adult patients with Philadelphia chromosome-negative ALL who underwent an allogeneic transplant. Bone Marrow Transplant. 2019;54(12):2020-2026.
14. Lafage-Pochitaloff M, Baranger L, Hunault M, et al. Impact of cytogenetic abnormalities in adults with Ph-negative B-cell precursor acute lymphoblastic leukemia. Blood. 2017;130(16):1832-1844.
15. Niederwieser C, Nicolet D, Carroll AJ, et al. Chromosome abnormalities at onset of complete remission are associated with worse outcome in patients with acute myeloid leukemia and an abnormal karyotype at diagnosis: CALGB 8461 (Alliance). Haematologica. 2016;101(12):1516-1523.
16. Döhner H, Weisdorf DJ, Bloomfield CD. Acute myeloid leukemia. N Engl J Med. 2015;373(12):1136-1152.
17. Grimwade D, Hills RK, Moorman AV, et al. Refinement of cytogenetic classification in acute myeloid leukemia: determination of prognostic significance of rare recurring chromosomal abnormalities among 5876 younger adult patients treated in the United Kingdom Medical Research Council trials. Blood. 2010;116(3):354-365.
18. Chen Y, Kantarjian H, Pierce S, et al. Prognostic significance of 11q23 aberrations in adult acute myeloid leukemia and the role of allogeneic stem cell transplantation. Leukemia. 2013;27(4):836-842.
19. Poiré X, Labopin M, Polge E, et al. The impact of concomitant cytogenetic abnormalities on acute myeloid leukemia with monosomy 7 or deletion 7q after HLA-matched allogeneic stem cell transplantation. Am J Hematol. 2020;95(3):282-294.
20. Inaba T, Honda H, Matsui H. The enigma of monosomy 7. Blood. 2018;131(26):2891-2898.
21. Shah MV, Jorgensen JL, Saliba RM, et al. Early post-transplant minimal residual disease assessment improves risk stratification in acute myeloid leukemia 7. Biol. Blood Marrow Transplant. 2018;24(7):1514-1520.

Genetics of "high-risk" chronic lymphocytic leukemia in the times of chemoimmunotherapy

Alexander Ring and Thorsten Zenz

Department of Medical Oncology and Haematology, University Hospital Zurich and University of Zurich, Zurich, Switzerland
E-mail: THORSTEN ZENZ - thorsten.zenz@usz.ch

doi:10.3324/haematol.2020.246504

Chronic lymphocytic leukemia (CLL) is a common leukemic B-cell lymphoma driven by distinct molecular features such as autonomous B-cell receptor signaling and genetic alterations including mutations targeting the DNA damage machinery, RNA processing and splicing, oncogenic signaling pathways (such as Notch) as well as epigenetic and chromatin modification.[1-3] In a simplified model, the "sum" of autonomous B-cell receptor signaling and driver mutations govern CLL progression. In addition, mutations in individual genes, such as *TP53*[4,5] are tightly linked to refractoriness to chemotherapy.[6] This model summarizes current knowledge, but we cannot exclude the possibility that additional (maybe unknown) mechanisms contribute significantly to proliferative drive and may thus predispose (or select for?) driver mutations. The current emergence of additional data and more appropriate statistical tools to query complex molecular data can be expected to provide novel insights into the pathogenesis of CLL.[7]

The study by Jennifer Edelmann and colleagues published in this issue of *Haematologica* is an informative addition to the catalogs of gene mutations in CLL. In this study, Edelmann and colleagues use cohorts of patients treated with chemotherapy/alemtuzumab in multiple trials and high-resolution single nucleotide polymorphism-array profiling and sequencing to characterize copy number variants and a limited mutational landscape of high-risk CLL cases.[8] The analysis summarizes data from 146 patients from CLL trials (CLL8, CLL11, CLL20), in which high risk was defined as either a *TP53* deletion/mutation genotype, "complex" karyotype/ increased genomic complexity or purine-analog refractory cases (progression-free survival <6 months). The authors thus provide a comprehensive description of genomic alterations in high-risk CLL patients that are selected for in the context of chemo(immuno)therapy, by building groups and individually testing for unbalanced incidences of mutations. The results lead to a description of well-known tumor drivers, which appear to contribute to high-risk CLL in addition to *TP53*; *MYC*, [gain (8)(q24)], *CDKN2A/B* [del(9)(p21)] and Notch pathway mutations.

The authors describe mutations in Notch-associated genes and known negative regulators (i.e. *SPEN*, *RBPJ*). They found that the above genes were mutated/deleted in 3.7-8.2% of high-risk CLL patients and showed that mutated cases had higher levels of expression of Notch target genes (e.g. *HES1*, *DTX1* and *MYC*). Furthermore, they revealed that *SNW1* is a potential negative regulator of the Notch signaling pathway. *SNW1* has also been shown to act as a co-activator of Notch-driven transcription.[9]

Notch signaling is an evolutionarily conserved signaling pathway that allows cell-cell interactions regulating a wide range of biological functions.[10] There are four mammalian members of NOTCH transmembrane proteins or receptors (NOTCH1 - 4) which have only partially overlapping functions despite similar structures. These receptors function as ligand-activated transcription factors, interacting with transmembrane ligands (Delta-like1, 3 and 4, and Jagged1 and 2) (Figure 1A, B).

While Notch signaling plays an important physiological role in hematopoiesis and hematopoietic stem cell biology,[11,12] aberrant Notch signaling has been found to be an oncogenic driver in precursor lymphoid and myeloid neoplasms as well as mature B-cell neoplasms with different mechanisms of oncogenic pathway activation including mutations in Notch receptors, mutations in negative regulators (e.g. *FBXW7*) or overexpression of ligands and receptors.[13-15] *NOTCH1* is one of the most frequently mutated genes in CLL,[16] affecting approximately 12% of cases.[17,18] The majority of mutations occur in coding regions leading to stabilization of the Notch intracellular domain (NICD) via loss of the PEST [proline (P), glutamic acid (E), serine (S), and threonine (T)] domain. *NOTCH1* gain-of-function mutations in CLL were first described by Ianni *et al.*[19,20] and were later found in large-scale sequencing studies.[21,22] Additionally, mutations in the non-coding 3' untranslated region have been described.[17,23] These mutational events ultimately lead to the accumulation of NCID and increase Notch signaling activity. Notch activation through mechanisms other than activating mutations also frequently occur in CLL.[18] with roughly 50% of CLL cases exhibiting high levels of NICD without detectable *NOTCH1* mutations.[18,20] Although potential mechanisms of *NOTCH1* mutation-independent pathway activation have been proposed (e.g. *MED12* mutations[24]), the biology remains incompletely understood. Mutations in the negative regulator *FBXW7* have been described in CLL.[25]

NOTCH1 has been found to be an adverse prognostic marker in CLL[26-29] and has been associated with the co-occurrence of other adverse prognostic factors in CLL, such as *IGHV* mutational status[30] and trisomy 12.[31] While *NOTCH1* mutations are more frequently found in CLL with unmutated *IGHV*, the accumulation of NICD without *NOTCH1* mutations seems similarly distributed in CLL with unmutated and mutated *IGHV* genes.[18] Integration of information about the presence or absence of *NOTCH1* mutations into prognostic scoring systems improved survival predictions.[32] *NOTCH1* mutations have not only been linked to progressive disease, but also to the earliest stages of development of CLL.[33]

Current approaches targeting Notch signaling include γ-secretase inhibitors, which block the proteolytic cleavage of NICD. More than 100 γ-secretase inhibitors have been developed,[34] with some demonstrating effects in CLL as single agents or in combination with other drugs.[35,36] Monoclonal antibodies targeting Notch receptors (e.g. OMP-52M51) have been tested in pre-clinical[37] and clinical

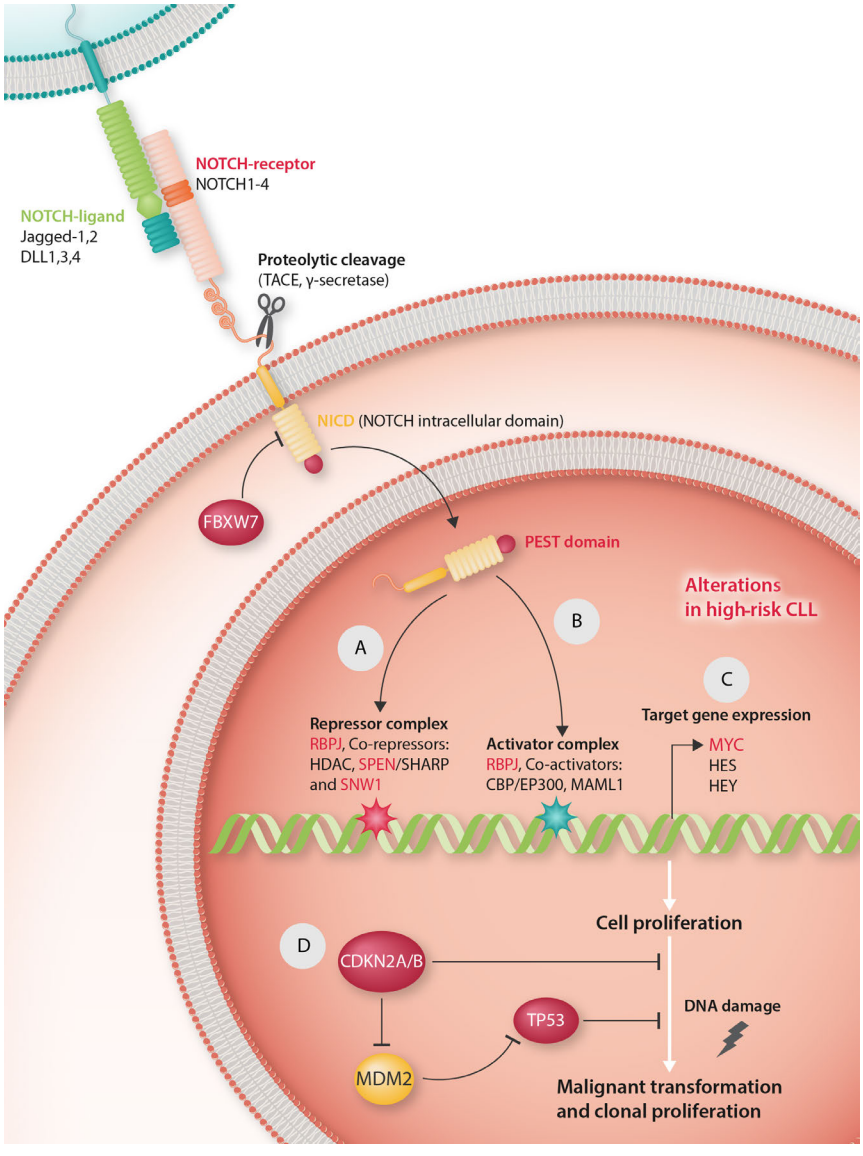

Figure 1. Molecular drivers of high-risk chronic lymphocytic leukemia. (A, B) Notch signaling. In its inactive state the Notch transcriptional complex is bound by co-repressors such as SPEN, histone deacetylases (HDAC) and, potentially, *SNW1* (A). Binding of Notch ligands (Jagged-1,2, DLL1, 3, 4) to Notch receptors leads to proteolytic cleavage of the intracellular domain (NICD) via γ-secretase and translocation of NICD to the nucleus to form a transcriptionally active complex with MAML1 (Mastermind-like protein 1), *RBPJ* (Recombination signal binding protein for immunoglobulin kappa J region) and transcriptional co-activators such as the histone acetyl transferases CBP/EP300, leading to Notch target gene expression (including *MYC*, *HES*, *HEY*) (B). Termination of Notch signaling is achieved mainly via ubiquitination of the PEST degradation domain of NICD by FBXW7 (F-box/WD repeat-containing protein 7). (C) Alterations in MYC activity. *MYC* is a direct target of Notch signaling driving cell proliferation. Gain of the *MYC* locus (8)(q24) enhances activity. (D) DNA damage checkpoint. *TP53* is frequently altered and a hallmark of high-risk chronic lymphocytic leukemia (CLL). Loss of function in *CDKN2A/B* impairs *TP53* tumor suppressor function and cell cycle control. (Gene symbols and gene names in red represent altered/mutated genes in high-risk CLL).

studies (NCT01778439, NCT 01703572). Indirect targeting approaches are also under investigation (e.g. bepridil).[38]

Dysregulation of *MYC* in B-cell tumors has been well established and comprehensively reviewed.[39,40] Edelmann *et al.* have demonstrated that gain of the *MYC* locus [gain (8)(q24)] frequently occurs in high-risk CLL. *MYC* has also been shown to be a direct target of *NOTCH1*[41] (Figure 1C).

Disruption of the DNA damage repair complex and associated cell cycle control or arrest is a hallmark of high-risk CLL. The protein products of both *CDKN2A* and *CDKN2B* (i.e. p16INK4a, p14ARF and p15INK4b, respectively) are central to DNA damage-related cell cycle control by interacting with both p53 and RB1 as well as direct inhibitors of cyclin-dependent kinases (CDK). Both p16INK4a and p15INK4b inhibit CDK4 and CDK6 and lead to the activation of RB1.[42] The alternate reading frame product p14ARF inhibits MDM2, thereby stabilizing p53.[43] (Figure 1D). These mechanisms have important tumor suppressor function guarding against DNA damage with potentially tumorigenic mutations and loss of these tumor suppressors may exert deleterious effects similar to loss of *TP53*. Cases of transformed CLL into aggressive lymphoma (Richter transformation) often exhibit *CDKN2A/B* disruption.[44]

With the advent of chemotherapy-free treatments, it remains to be seen if the results presented will be applicable to current standards of care. For a more comprehensive understanding of CLL, clonal evolution and predictive markers, future studies will leverage comprehensive protein, methylation and RNA expression in addition to DNA-level investigations in a genome-wide manner. As these data emerge and are analyzed with more complex statistical models[7] the mechanisms underlying aggressive disease will become clearer. We hope this will have direct implications for the clinical management of CLL patients. One simple step in this direction is an open approach to data sharing and access, a prerequisite to advance knowledge on rare variants. We are certain that the study groups involved in the analysis by Edelmann *et al.* will also take a lead in this area.

References

1. Baliakas P, Jeromin S, Iskas M, et al. Cytogenetic complexity in chronic lymphocytic leukemia: definitions, associations, and clinical impact. Blood. 2019;133(11):1205-1216.
2. Burger JA, Chiorazzi N. B cell receptor signaling in chronic lymphocytic leukemia. Trends Immunol. 2013;34(12):592-601.
3. Landau DA, Tausch E, Taylor-Weiner AN, et al. Mutations driving CLL and their evolution in progression and relapse. Nature. 2015;526(7574):525-530.
4. Zenz T, Eichhorst B, Busch R, et al. TP53 mutation and survival in chronic lymphocytic leukemia. J Clin Oncol. 2010;28(29):4473-4479.
5. Zenz T, Kröber A, Scherer K, et al. Monoallelic TP53 inactivation is associated with poor prognosis in chronic lymphocytic leukemia: results from a detailed genetic characterization with long-term follow-up. Blood. 2008;112(8):3322-3329.
6. Dietrich S, Oleś M, Lu J, et al. Drug-perturbation-based stratification of blood cancer. J Clin Invest. 2018;128(1):427-445.
7. Argelaguet R, Velten B, Arnol D, et al. Multi–omics factor analysis—a framework for unsupervised integration of multi–omics data sets. Mol Syst Biol. 2018;14(6):e8124.
8. Edelmann J, Holzmann K, Tausch E, et al. Genomic alterations in high-risk chronic lymphocytic leukemia frequently affect cell cycle key regulators and NOTCH1-regulated transcription. Haematologica. 2020;Volume 105(5):1379-1390.
9. Hong M, He J, Li S. SNW1 regulates Notch signaling in neuroblastoma through interacting with RBPJ. Biochem Biophys Res Commun. 2019;509(4):869-876.
10. Fortini ME. Notch sgnaling: the core pathway and its posttranslational regulation. Dev Cell. 2009;16(5):633-647.
11. Pajcini KV, Speck NA, Pear WS. Notch signaling in mammalian hematopoietic stem cells. Leukemia. 2011;25(10):1525-1532.
12. Kojika S, Griffin JD. Notch receptors and hematopoiesis. Exp Hematol. 2001;29(9):1041-1052.
13. Kridel R, Meissner B, Rogic S, et al. Whole transcriptome sequencing reveals recurrent NOTCH1 mutations in mantle cell lymphoma. Blood. 2012;119(9):1963-1971.
14. Lee SY, Kumano K, Nakazaki K, et al. Gain-of-function mutations and copy number increases of Notch2 in diffuse large B-cell lymphoma. Cancer Sci. 2009;100(5):920-926.
15. Karube K, Martínez D, Royo C, et al. Recurrent mutations of NOTCH genes in follicular lymphoma identify a distinctive subset of tumours. J Pathol. 2014;234(3):423-430.
16. Rosati E, Baldoni S, De Falco F, et al. NOTCH1 aberrations in chronic lymphocytic leukemia. Front Oncol. 2018;8:229.
17. Puente XS, Beà S, Valdés-Mas R, et al. Non-coding recurrent mutations in chronic lymphocytic leukaemia. Nature. 2015;526(7574):519-524.
18. Fabbri G, Holmes AB, Viganotti M, et al. Common nonmutational NOTCH1 activation in chronic lymphocytic leukemia. Proc Natl Acad Sci U S A. 2017;114(14):E2011-E2919.
19. Ianni M Di, Baldoni S, Rosati E, et al. A new genetic lesion in B-CLL: A NOTCH1 PEST domain mutation. Br J Haematol. 2009;146(6):689-691.
20. Rosati E, Sabatini R, Rampino G, et al. Constitutively activated Notch signaling is involved in survival and apoptosis resistance of B-CLL cells. Blood. 2009;113(4):856-865.
21. Fabbri G, Rasi S, Rossi D, et al. Analysis of the chronic lymphocytic leukemia coding genome: role of NOTCH1 mutational activation. J Exp Med. 2011;208(7):1389-1401.
22. Puente XS, Pinyol M, Quesada V, et al. Whole-genome sequencing identifies recurrent mutations in chronic lymphocytic leukaemia. Nature. 2011;475(7354):101-105.
23. Bittolo T, Pozzo F, Bomben R, et al. Mutations in the 3′ untranslated region of NOTCH1 are associated with low CD20 expression levels in chronic lymphocytic leukemia. Haematologica. 2017;102(8):e305-e309.
24. Wu B, Słabicki M, Sellner L, et al. MED12 mutations and NOTCH signalling in chronic lymphocytic leukaemia. Br J Haematol. 2017;179(3):421-429.
25. Close V, Close W, Kugler SJ, et al. FBXW7 mutations reduce binding of NOTCH1, leading to cleaved NOTCH1 accumulation and target gene activation in CLL. Blood. 2019;133(8):830-839.
26. Rossi D, Rasi S, Fabbri G, et al. Mutations of NOTCH1 are an independent predictor of survival in chronic lymphocytic leukemia. Blood. 2012;119(2):521-529.
27. Stilgenbauer S, Schnaiter A, Paschka P, et al. Gene mutations and treatment outcome in chronic lymphocytic leukemia: results from the CLL8 trial. Blood. 2014;123(21):3247-3254.
28. Villamor N, Conde L, Martínez-Trillos A, et al. NOTCH1 mutations identify a genetic subgroup of chronic lymphocytic leukemia patients with high risk of transformation and poor outcome. Leukemia. 2013;27(5):1100-1106.
29. Larrayoz M, Rose-Zerilli MJJ, Kadalayil L, et al. Non-coding NOTCH1 mutations in chronic lymphocytic leukemia; their clinical impact in the UK CLL4 trial. Leukemia. 2017;31(2):510-514.
30. López C, Delgado J, Costa D, et al. Clonal evolution in chronic lymphocytic leukemia: Analysis of correlations with IGHV mutational status, NOTCH1 mutations and clinical significance. Genes Chromosom Cancer. 2013;52(10):920-927.
31. Balatti V, Bottoni A, Palamarchuk A, et al. NOTCH1 mutations in CLL associated with trisomy 12. Blood. 2012;119(2):329-331.
32. Döhner H, Stilgenbauer S, Benner A, et al. Genomic aberrations and survival in chronic lymphocytic leukemia. N Engl J Med. 2000;343(26):1910-1916.
33. Damm F, Mylonas E, Cosson A, et al. Acquired initiating mutations in early hematopoietic cells of CLL patients. Cancer Discov. 2014;4(9):1088-1101.
34. Rizzo P, Osipo C, Foreman K, Golde T, Osborne B, Miele L. Rational targeting of Notch signaling in cancer. Oncogene. 2008;27(38):5124-5131.
35. Rosati E, Sabatini R, De Falco F, et al. γ-Secretase inhibitor I induces apoptosis in chronic lymphocytic leukemia cells by proteasome inhibition, endoplasmic reticulum stress increase and notch down-regulation. Int J Cancer. 2013;132(8):1940-1953.
36. López-Guerra M, Xargay-Torrent S, Rosich L, et al. The γ-secretase inhibitor PF-03084014 combined with fludarabine antagonizes migration, invasion and angiogenesis in NOTCH1-mutated CLL cells. Leukemia. 2015;29(1):96-106.
37. Wu Y, Cain-Hom C, Choy L, et al. Therapeutic antibody targeting of individual Notch receptors. Nature. 2010;464(7291):1052-1057.
38. Baldoni S, Del Papa B, Dorillo E, et al. Bepridil exhibits anti-leukemic activity associated with NOTCH1 pathway inhibition in chronic lymphocytic leukemia. Int J Cancer. 2018;143(4):958-970.
39. Nguyen L, Papenhausen P, Shao H. The role of c-MYC in B-cell lymphomas: diagnostic and molecular aspects. Genes (Basel). 2017;8(4).
40. Huh YO, Lin KIC, Vega F, et al. MYC translocation in chronic lymphocytic leukaemia is associated with increased prolymphocytes and a poor prognosis. Br J Haematol. 2008;142(1):36-44.
41. Weng AP, Millholland JM, Yashiro-Ohtani Y, et al. c-Myc is an important direct target of Notch1 in T-cell acute lymphoblastic leukemia/lymphoma. Genes Dev. 2006;20(15):2096-2109.
42. Ruas M, Peters G. The p16(INK4a)/CDKN2A tumor suppressor and its relatives. Biochim Biophys Acta. 1998;1378(2):F115-177.
43. Prives C, Hall PA. The P53 pathway. J Pathol. 1999;187(1):112-126.
44. Fabbri G, Khiabanian H, Holmes AB, et al. Genetic lesions associated with chronic lymphocytic leukemia transformation to Richter syndrome. J Exp Med. 2013;210(11):2273-2288.

Structured assessment of frailty in multiple myeloma as a paradigm of individualized treatment algorithms in cancer patients at advanced age

Monika Engelhardt,[1] Gabriele Ihorst,[2] Jesus Duque-Afonso,[1] Ulrich Wedding,[3] Ernst Spät-Schwalbe,[4] Valentin Goede,[5] Gerald Kolb,[6] Reinhard Stauder[7] and Ralph Wäsch[1]

[1]Department of Medicine I, Hematology, Oncology and Stem Cell Transplantation, Medical Center - University of Freiburg, Faculty of Medicine, University of Freiburg, Freiburg, Germany; [2]Clinical Trials Center Freiburg, Faculty of Medicine, University of Freiburg, Germany; [3]Palliativmedizin Universitätsklinik Jena, Jena, Germany; [4]Vivantes Klinikum Spandau, Innere Medizin, Hämatologie, Onkologie, Palliativmedizin, Berlin, Germany; [5]Geriatrie Köln, St. Marien-Hospital, Köln, Germany; [6]Bonifatius Hospital Lingen, Medizinische Klinik, Fachbereich Geriatrie, Akademisches Lehrkrankenhaus der Westfälischen Wilhelms-Universität Münster, Münster, Germany and [7]Universitätsklinik für Innere Medizin V (Hämatologie und Onkologie), Medizinische Universität Innsbruck, Innsbruck, Austria

Ferrata Storti Foundation

Haematologica 2020
Volume 105(5):1183-1188

Introduction

Life expectancy and incidence of cancer have substantially increased, the latter being closely interlinked to our longevity. Today, 617 million people are ≥65 years; by 2050, this number will have reached 1.6 billion, nearly 20% of the world's population, and the number of "very old" (>80 years) will have more than tripled.[1] This aging of the population involves enormous changes to patient care. For the moment, the most profound changes are to be seen in Japan, Europe and North America. Major risk factors associated with aging include cancer (also multiple cancers in a single patient),[2] and cardiovascular and neurodegenerative diseases, all requiring long-term care. Therefore, especially high-income countries are obliged to meet the challenges.[1]

Multiple myeloma (MM), as one example of cancer, and the 2nd most frequent hematologic malignancy, affects adults of all ages, but is primarily a disease of the elderly. The highest burden of MM-related deaths occurs among persons between 65 and 84 years of age.[3-7] Similarly to the situation in several other types of cancers, management of older MM patients is more demanding due to their often impaired organ function, underlying comorbidities, and co-existing frailty, which may increase therapy-related toxicity, and lead to dose reduction and shorter treatment endurance.[3,4,6-9] The high prevalence of geriatric impairments is increasingly being recognized, but is not always easily detectable without an objective assessment.[3,6,7] Our goal today involves reducing the risk of under-treating fit patients and over-treating those who are frail.[5,10-12] Although eligibility criteria for studies of anti-cancer/-MM agents have traditionally relied on age cut-offs and performance status, geriatric and MM-specific frailty assessments are just beginning to be incorporated into more accurate stratification plans of treatment algorithms.[6,7,11,12] Similarly to MM patients, geriatric assessments (GA) have been defined for patients with chronic lymphocytic leukemia (CLL)[8,13,14] and myelodysplastic syndrome (MDS),[15,16] where determination of frailty *versus* fitness has moved into clinical practice. However, solutions as to how they might be more uniformly used and valued in their daily pratice have not been fully determined.

Recommendations of the geriatric oncology working groups (i.e. German Society of Geriatrics/German Society of Hematoloogy&Oncology) have suggested GA-tools to check comorbidity in patients aged ≥70 years *via* the Charlson Comorbidity Index (CCI), cognition *via* the Mini Mental test (MMST), activity/instrumental activity of daily living (ADL/IADL), mobility *via* the Timed Up and Go test, depression *via* the geriatric depression scale (GDS), and nutrition *via* body mass index (BMI) and Mini Nutritional Status.[6,7,11,12,17] While these GA-tools have been established and validated, their execution is time-consuming, an additional workforce is needed, and the involvement of a geriatric team is advisable.[6,7,9,11,12,17] Whether shorter frailty scores in cancer patients may substitute and/or add to GA-tools is being pursued in single- and multi-center trials (Table 1).

The results were presented in part at the 'American Society of Hematology' (ASH) meetings and the 'German, Austrian and Swiss annual Hematology & Oncology meetings' (DGHO)

Correspondence:

MONIKA ENGELHARDT
monika.engelhardt@uniklinik-freiburg.de

Received: November 14, 2019.
Accepted: January 30, 2020.
Pre-published: April 2, 2020.

doi:10.3324/haematol.2019.242958

Check the online version for the most updated information on this article, online supplements, and information on authorship & disclosures: www.haematologica.org/content/105/5/1183

The aim of this commentary is to define strategies in MM patients, and explore how frailty assessment may be employed in clinical practice and clinical trials.

Instruments to assess vulnerability due to increased treatment options

The epidemiologic and biologic considerations of elderly MM patients, with widely expanding treatment options, have motivated global efforts to validate simple instruments to assess vulnerability of patients, test them in their clinical significance to predict treatment outcome [overall survival (OS) and progression-free survival (PFS)], occurrence of severe adverse events, and to tailor treatment with more or less intensified regimens.[11,12,18]

Under-treatment of fit elderly patients has been demonstrated to occur more frequently than over-treatment.[12] Under-treatment may prevent improvement of organ function, while over-treatment of frail patients can induce unnecessary morbidity and mortality. Both instances reduce patients' health-related quality of life (HRQOL). In a study that assessed HRQOL across >16,000 cancer survivors, those with MM were among those with the lowest HRQOL scores, highlighting the urgent need for this to be improved and for frequent reassessment of HRQOL in cancer patients.[19] The art of managing elderly MM patients involves balancing competing disease-related and patient-specific factors and to make adequate treatment decisions.

Numerous induction (and relapse) MM-treatment options are available today. These include bortezomib-cyclophosphamide-dexamethasone (VCD), bortezomib-lenalidomide-dexamethasone (VRD or VTD), bortezomib-melphalan-prednisone (VMP) or antibody-combinations, autologous stem cell transplantation (ASCT) and 2-drug combinations, such as lenalidomide-dexamethasone (Rd), bortezomib-dexamethasone (Vd), and others.[3,20-22] These largely expanded therapeutic strategies, including immunotherapies,[23] have significantly evolved in recent years, but the beneficial effect is not seen across the age spectrum, with intermediate-fit or frail patients not obtaining the maximal benefit from such new treatment. Part of this failure to achieve benefit relates to the host biology of older patients. Therefore, there is an unmet need to give the right therapy to the patient most suited to benefit from it; the starting point for this approach is an appropriate classification of who is fit and who is frail.

Table 1. Selected clinical trials in multiple myeloma patients with frailty assessments included therein.

#	Institution performing the analysis	Trial title	Phase	Trial#	Retro- *vs.* prospective	N. of patients	Results / Study specifics
1	University of Freiburg (UKF)	Allogeneic (allo)-SCT	IV	NCT00655343	Retrospective	109	R-MCI did improve from 4 before to 3 after allo-SCT. Renal function and age declined over time, but did not neccessarily decrease QoL measures after allo-SCT in long-term survivors.
2	UKF	VBDD	I / II	NCT01394354	Prospective	33	QoL improved in responsive pts: both frailty scores and functional tests were used and showed R-MCI improvement as well as of other frailty scores and functional tests.
3	Ohio State	Frailty + functional assessment in MM	IV Observational	NCT02033928	Prospective	111	Change in Comprehensive Frailty Assessment: before and after transplant (Tx) and non-Tx pts. Study ongoing.
4	City of Hope + University of Rochester	Touchscreen-based geriatric and functional assessment	IV	NCT03068637	Prospective	165	Limited pt time required for survey completion and provider time for results review show mGA can be incorporated into clinical workflow. Real-time mGA results indicating fit/frailty status influenced treatment decisions.
5	Torino, GIMEMA	Rd *vs.* Rd-R in unfit MM pts	II	NCT02215980	Prospective	210	Rd-R improved event-free survial (EFS) end points in unfit MM pts. First results shown at ASH 2018.
6	Indiana University	Maia randomization: standard Dara-Rd *vs.* reduction in frail pts	II, open label	NCT04223661	Prospective	44	Dara-Rd *vs.* reduced dose with frailty index ≥2. Study ongoing.
7	HOVON 143	Efficacy and tolerability of Ixa-Dara-dex in unfit and frail NDMM pts	II	NTR6297	Prospective	n=65 unfit, n=67 frail pts	Dose-adjustment feasible and advisable, but early mortality still occurring. Study ongoing, early ASH results shown 2019: #695.
8	University of Leeds, UK study group	FiTNEss (Frailty-adjusted therapy in Tx Non-Eligible pts with NDMM)	III	NCT03720041	Prospective	740	IRd according to frailty score - randomization into 4 groups. Study ongoing.

pts: patients, #: number, UKF: University of Freiburg Medical Center, allo-SCT: allogeneic stem cell transplantation, R-MCI: Revised Myeloma Comorbidity Index; Tx: transplantation; VBDD: vorinostat-bortezomib-doxorubicin-dexamethason treatment in relapsed/refractory multiple myeloma (RRMM), QoL: Quality of life; ND MM pts: newly diagnosed MM patients; GIMEMA: Italian study group. Rd *vs.* RD-R: Lenalidomide-dexamethason *vs.* continuation of reduced lenalidomide doses without dexamethason in Rd-R, IRd: ixazomib-lenalidomide-dexamethasone; Ixa-Dara-Dex: ixazomib-daratumumab-dexamethasone; Dara-RD: daratumumab-lenalidomide-dexamethasone. For other studies in MM see also Mina *et al.*[51]

Risk parameters in multiple myeloma

That age alone is a much less well-suited discriminator for treatment designation has been shown *via* various risk parameters and comorbidity scores, that are usually described as patient-related factors.[11,12,24-26] These involve simple measures of daily activity, such as constitution *via* Eastern Cooperative Oncology Group (ECOG) or Karnofsky performance status (KPS), organ function, and comorbidities. However, because the KPS/ECOG do not reflect the entire functional status of cancer patients, advances in defining patient fitness more precisely are warranted. In an analysis of 466 consecutive MM patients, the median KPS was determined to be 90%, although a precise reassessment showed this was actually 60%, i.e. 30% lower than that estimated by physicians. This clearly demonstrates that both KPS/ECOG are often over-estimated, and a more precise frailty assessment is valuable.[25] In a subsequent analysis, 13 comorbid conditions were assessed in 801 patients. These were graded and rated according to the Common Terminology Criteria for Adverse Events (CTCAE 4.03), which included: renal-, lung- and KPS-impairment, cardiac, liver or gastrointestinal disease, disability, frailty, infection, thromboembolic events, peripheral neuropathy, pain, and secondary malignancies. In addition, age, cytogenetics *via* fluorescence *in situ* hybridization, renal function and lung disease were determined. The multivariate Cox proportional hazard model based on backward selection revealed five highly significant risks as relevant for OS: renal and lung function, KPS, age, and frailty (Fried definition). Score weights for comorbidities were determined on the basis of regression coefficients of the prognostic factors.[12] Although impairment of organ function such as lung disease had been defined as having nothing to do with MM, in line with other large MM study groups (such as both the German GMMG and DSMM study groups), patients with moderate and severe lung impairment and continued smoking habit were at substantial risk for treatment complications.[11,12] We would, therefore, refrain from ASCT/allogeneic-SCT, triplet and quadruplet therapies in heavy smokers and/or those with impaired lung function.[11,12,24-26] Moreover, disease-related factors add additional complexity in MM, such as cytogenetics, International Staging System (ISS)/revised (R)-ISS stage, bone marrow infiltration, and number of CRAB (C, hypercalcemia; R, renal impairment; A, anemia; B, bone lesions) symptoms. In addition, treatment-related factors, such as how quickly and for how long the disease responds to therapy, are critical.[27-29]

Frailty, organ impairment and myeloma scores

In prior organ function analyses,[11,12,24-26,30] the extent of frailty in MM patients was substantial: 60% for entire (mild to severe) and 40% for severe frailty.[11,12] This led to the development of the revised myeloma comorbidity score (R-MCI). This R-MCI uses weights generated *via* multivariate risk factor assessment with the essential risks being included therein, such as: renal and lung function, KPS, frailty and age, with the option to add cytogenetics.[11,12] Apart from organ impairment, cytogenetic aberrations corroborate with impaired OS in MM patients. The analysis confirmed that cytogenetics provide independent additional information,[31-35] and that patients with unfavorable cytogenetics had higher disease stages, adverse laboratory values, and reduced organ and physical function. Although cytogenetics proved to be a relevant risk factor, the analysis confirmed that others, such as physical and organ conditions, are equally important.[6,7,11,12,18] Moreover, development of the R-MCI showed that the multivariate risks (renal, lung function, KPS, age, frailty) defined patients as fit, intermediate-fit, and frail, which could be improved with inclusion of cytogenetics, (but which could still be used even if this information was unavailable). Weighting of the R-MCI verified that this 9-point score defines three patient groups with clearly different survival,[12] which remained true regardless of treatment or age subgroups.

Comparison of the R-MCI with others and current questions

Comparison of the R-MCI with numerous others [CCI, Kaplan Feinstein (KF), Hematopoietic Cell Transplantation Comorbidity Index (HCT-CI/Sorer),[12] the Satariano Index[24-26] or the International Myeloma Working Group (IMWG frailty score[11]) showed that they all divide patients into risk groups with substantially different OS. However, Brier scores determined the smallest prediction errors with the R-MCI. One reason for the comparability of the R-MCI with others was that most include risks that have some relevance in MM, namely renal and lung function, and physical condition. Compared to the initial non-weighted MCI,[24-26] the R-MCI led to an improvement in group distinction, which highlights the relevance to further improve a risk score, as performed in subsequent analyses.[11,12,24-26,30] Various risk scores that are used in different institutions and within clinical trials in MM patients are summarized in Table 1.[18,36-38]

The question is, therefore, whether one comorbidity score in MM should be put forward or whether more should be developed. Moreover, would harmonization and inclusion of biomarkers improve them?[39] Another question is if MM experts will use these scores and whether treatment decisions are being improved.[40,41] Whether risks determined by a score result in changes in treatment decision has not been fully addressed. Given that MM primarily affects the elderly, whose vulnerabilities may change over time, it is also reasonable to incorporate serial GA throughout treatment in order to potentially modify therapy over time and incorporate this into tumorboards and treatment guidelines. For older, fit patients, intensive treatment with ASCT may be appropriate, while in the very frail, with GA and high R-MCI-scores, end-of-life care discussions can be facilitated.[10,42]

Concrete clinical designations of the use of the R-MCI

1. We have included the R-MCI in the weekly MM tumorboard, where this is being scored before the patient is discussed at an interdisciplinary level. Web applications make it easy to obtain a score end result, as has been achieved for the R-MCI and IMWG-frailty scores.[11,12,18,40] For the R-MCI, each patient's individual risk parameters will generate an R-MCI score.

Training and validation analyses of the R-MCI showed well-discriminated risk profiles in terms of both PFS and OS for fit, intermediate fit, and frail patients.[12] This was true both for more intensively and less intensively treated MM patients.[12] Moreover, if MM patients were risk-assessed *via* the R-MCI rather than the IMWG-frailty score, Kaplan-Meier analysis produced more clearly separated PFS and OS curves with the the R-MCI than with the IMWG-frailty score.[11]

Importantly, if patients are intermediate-fit or frail by R-MCI, precautions for dose reduction of systemic treatment can be made: i.e. if advanced frailty in MM patients is observed, dose reductions can be discussed, including whether the disease aggressiveness needs effective anti-MM treatment to be performed in spite of the patient's frailty. Today, it seems important, given the widely different anti-MM treatment options, that the frailty scoring specifically warns MM experts that complications with intensive treatment may occur. As many precautions as possible can then be taken while treatment is being given, such as inpatient rather than outpatient treatment, observation on the ward until complications no longer occur, prophylactic medications, etc. In line with this, in their joint EMN-paper,[7] the European Myeloma Network (EMN) consensus has stated that in fit MM patients, efficient antimyeloma therapy with the aim of deep remission is key, whereas in unfit or frail patients, the priority is to maintain a good balance between therapy efficacy and safety.

2. Useful dose adaptations have been recommended for individual antimyeloma agents and are published as such in guidelines and chemotherapy manuals.[6,7,43]

3. The R-MCI has also been included in study protocols before therapy initiation and at the end of treatment. This can assess whether a patient's constitution did improve over time, and whether this was associated with myeloma response and better functional comorbidity tests (Table 1).[21,44]

4. The R-MCI has, indeed, allowed a patient's improved constitution to be demonstrated; this has also been assessed in rarer treatment scenarios, such as in younger, high-risk patients undergoing immunotherapy approaches, i.e. allo-SCT. Here, although patients grew older and renal function declined over time, the median R-MCI improved from 4 before allo-SCT to 3 after allo-SCT (Table 1).[23,45]

5. In frail patients, being able to see if there is any deterioration in the R-MCI makes it easier to adapt or interrupt treatment. This underscores its clinical helpfulness. For example, since the QoL in a light chain (AL)-amyloidosis patient did not improve, even though hematologic response was achieved, the use of the R-MCI facilitated supportive treatment rather than continuation of extensive and expensive care.[10,46]

6. Inclusion of the R-MCI in future study protocols at our center, and in discussion with both German MM study groups (DSMM and GMMG) is under way.

Conclusions

Although the IMWG-frailty score is a "reference" comorbidity index,[18] others are more straightforward to use. The inclusion of "Lung function" in the R-MCI had been repeatedly requested by reviewers as a more objective measure than *via* the GOLD criteria, smoking status or dyspnea upon exertion, and is included in the diagnostic workup at our center (i.e. before intensive treatment, such as SCT).[11,12,21,44-47] If unavailable, smoking status, its mandatory cessation before SCT/intensive treatment, no advanced GOLD criteria, and no dyspnea upon exertion have been used as substitutes in prior analyses.[24-26]

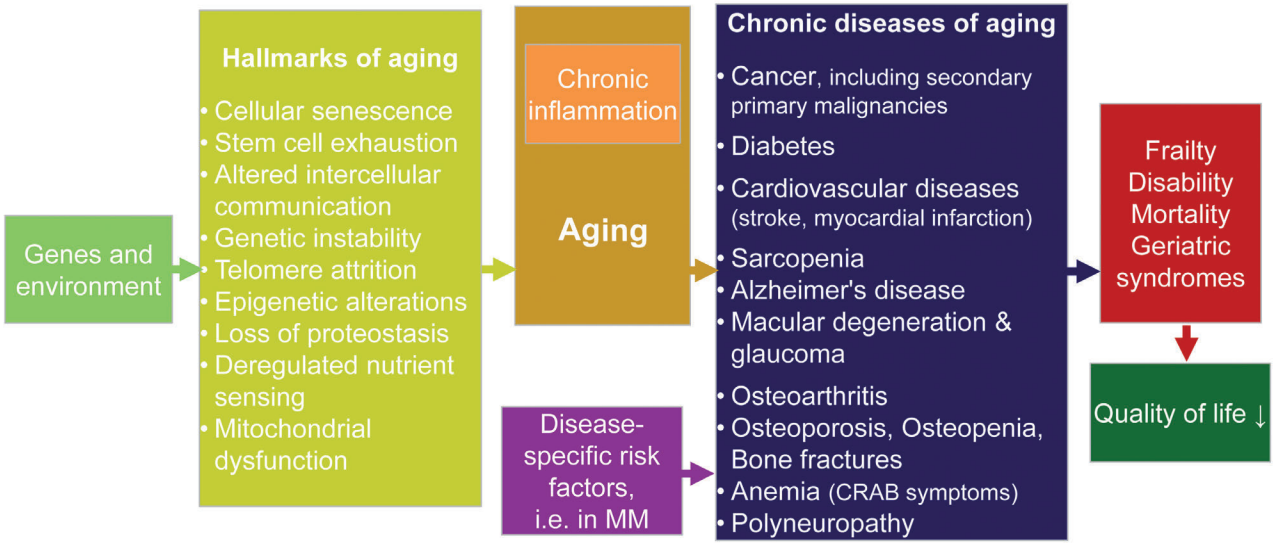

Figure 1. Environmental and genetic factors that influence key cellular processes and pathways defined as hallmarks of aging. Many pathways contribute to the creation of a chronic inflammatory stage and to aging. These in turn increase the risk of chronic disease of aging together with disease-specific risk factors, i.e. in multiple myeloma (MM): polyneuropathy, osteoporosis/osteopenia, bone fractures, anemia. All eventually induce frailty, disability, mortality and geriatric syndromes, and potentially decrease patients' quality of life (adapted and with permission of J. Campisi *et al.*)[50]

We have demonstrated the validity of the R-MCI as a valid prognostic instrument in large MM cohorts treated according to current standards. Based on existing recommendations, the R-MCI can be applied in routine clinical care, multicenter analyses and future clinical trials. It may be used in research to compare risk profiles of MM cohorts, to adjust for imbalanced risks, and to provide a basis to establish new clinical or biologic prognostic factors. Moreover, the R-MCI might be considered to be an integral part in the development of individualized risk-adapted treatment strategies to further improve outcome in MM. This includes correct use of resources, higher inclusion rates of older patients into clinical studies, and avoidance of under-supply for older but fit patients.

In the future, the R-MCI could also help to support treatment decisions, tolerability, and to avoid toxicity. Since any prospective comorbidity, frailty and disability evaluation can be time-consuming, we have implemented the R-MCI within a web-based technology application which allows a quick turnaround of results.[48] Routine measurement of frailty in MM patients is, therefore feasible, and several analyses *via* R-MCI[11,12] (or IMWG frailty scores[18] with various adaptations[6,47]) are available.

All current developments in the field are enthusiastically welcomed, because more effective and individualized treatment offers an opportunity to further improve clinical outcomes, especially among older patients with hematologic malignancies.[21,27,28,49] We have proven tools for a functional, more objective assessment to help guide every-day treatment, and these should be incorporated into tumor boards and may allow better trial comparability, as well as helping to guide trial design. It will be interesting to see whether, in the near future, these risk tools are readily implemented into clinical care and can improve patient management. We are entering an exciting era for research on aging, which holds unprecedented promise for increased patient lifespan, delaying pathologies of aging, allowing patients to grow old, and living a life full of purpose and well-being (Figure 1).[1,50] Future clinical trials that target the aging process and that study biomarkers and intervention programs face considerable challenges, but the potential rewards will far outweigh their risks.[1,50]

Acknowledgments

The authors thank distinguished IMWG, EMN, DSMM and GMMG experts, especially Drs. Thierry Facon (Lille), Hervé Avet-Loiseau (Toulouse), Alessandra Larocca, Sara Bringhen, Francesca Gay (Turin), Gordon Cook (Leeds), Sonja Zweegman (Amsterdam), Heinz Ludwig (Vienna), Hermann Einsele (Würzburg) and Hartmut Goldschmidt (Heidelberg) for their advice and recommendations. We are also grateful of the insightful comments of all myeloma experts and colleagues at the University Clinic Freiburg (UKF), for their inspiring work and thrive for R-MCI topics. The paper is dedicated to Dr. Sandra Maria Woerner, Maximillian Holler, Sophia Scheubeck, Katja Schoeller, Irina Surlan, Mandy Möller, Stefanie Ajayi, Amelie Rösner, Drs. Martina Kleber, Laura Gengenbach, Giulia Graziani, Maximillian Schinke, Heike Reinhardt, Stefan Müller, Matthias Weiß, Johannes Jung, Christine Greil, Michael Rassner, Cornelius Miething, Milena Pantic and Barbara Deschler (UKF, University of Basel and University of Würzburg) for their exceptional support. We are indebted to the interdisciplinary MM tumorboard, the CCFF for incorporation of the R-MCI in its application modus and thank all MM patients who participated in our MM studies. We also thank the 3 insightful, knowledgeable reviewers for their critical comments, which have further improved this article.

Funding

This work was supported by the Deutsche Krebshilfe (grants 1095969 and 111424 [to ME and RWJ]) and Verein Senioren-Krebshilfe (R.S.).

References

1. Dzau VJ, Inouye SK, Rowe JW, Finkelman E, Yamada T. Enabling Healthful Aging for All - The National Academy of Medicine Grand Challenge in Healthy Longevity. N Engl J Med. 2019;381(18):1699-1701.
2. Engelhardt M, Ihorst G, Landgren O, et al. Large registry analysis to accurately define second malignancy rates and risks in a well-characterized cohort of 744 consecutive multiple myeloma patients followed-up for 25 years. Haematologica. 2015;100(10):1340-1349.
3. Engelhardt M, Terpos E, Kleber M, et al. European Myeloma Network recommendations on the evaluation and treatment of newly diagnosed patients with multiple myeloma. Haematologica. 2014;99(2):232-242.
4. Bringhen S, Mateos MV, Zweegman S, et al. Age and organ damage correlate with poor survival in myeloma patients: meta-analysis of 1435 individual patient data from 4 randomized trials. Haematologica. 2013;98(6):980-987.
5. Laubach J. Initial Therapy in Older Patients with Multiple Myeloma. N Engl J Med. 2019;380(22):2172-2173.
6. Zweegman S, Engelhardt M, Larocca A, EHA SWG on 'Aging and Hematology.' Elderly patients with multiple myeloma: towards a frailty approach? Curr Opin Oncol. 2017;29(5):315-321.
7. Larocca A, Dold SM, Zweegman S, et al. Patient-centered practice in elderly myeloma patients: an overview and consensus from the European Myeloma Network (EMN). Leukemia. 2018;32(8):1697-1712.
8. Goede V, Stauder R. Multidisciplinary care in the hematology clinic: Implementation of geriatric oncology. J Geriatr Oncol. 2019;10(3):497-503.
9. Bron D, Ades L, Fulop T, Goede V. Aging and malignant hemopathies. Haematologica. 2015;100(5):571-574.
10. Antoine-Pepeljugoski C, Braunstein MJ. Management of Newly Diagnosed Elderly Multiple Myeloma Patients. Curr Oncol Rep. 2019;21(7):64.
11. Engelhardt M, Dold SM, Ihorst G, et al. Geriatric assessment in multiple myeloma patients: validation of the International Myeloma Working Group (IMWG) score and comparison with other common comorbidity scores. Haematologica. 2016;101(9):1110-1119.
12. Engelhardt M, Domm A-S, Dold SM, et al. A concise revised Myeloma Comorbidity Index as a valid prognostic instrument in a large cohort of 801 multiple myeloma patients. Haematologica. 2017;102(5):910-921.
13. Eichhorst B, Hallek M, Goede V. Management of unfit elderly patients with chronic lymphocytic leukemia. Eur J Intern Med. 2018;58:7-13.
14. Stauder R, Eichhorst B, Hamaker ME, et al. Management of chronic lymphocytic leukemia (CLL) in the elderly: a position paper from an international Society of Geriatric Oncology (SIOG) Task Force. Ann Oncol. 2017;28(2):218-227.
15. Stauder R, Yu G, Koinig KA, et al. Health-related quality of life in lower-risk MDS patients compared with age- and sex-matched reference populations: a European LeukemiaNet study. Leukemia. 2018;32(6):1380-1392.
16. Burgstaller S, Wiesinger P, Stauder R. Myelodysplastic Syndromes in the Elderly: Treatment Options and Personalized Management. Drugs Aging. 2015;32(11):891-905.
17. Friedrich C, Kolb G, Wedding U, Pientka L, Interdisziplinäre Arbeitsgruppe der DGHO/DGG. Comprehensive geriatric assessment in the elderly cancer patient. Onkologie. 2003;26(4):355-360.

18. Palumbo A, Bringhen S, Mateos MV, et al. Geriatric assessment predicts survival and toxicities in elderly myeloma patients: an International Myeloma Working Group report. Blood. 2015;125(13):2068-2074.
19. Kent EE, Ambs A, Mitchell SA, et al. Health-related quality of life in older adult survivors of selected cancers: data from the SEER-MHOS linkage. Cancer. 2015;121(5):758-765.
20. Facon T, Kumar S, Plesner T, et al. Daratumumab plus Lenalidomide and Dexamethasone for Untreated Myeloma. N Engl J Med. 2019;380(22):2104-2115.
21. Gengenbach L, Reinhardt H, Ihorst G, et al. Navigating the changing multiple myeloma treatment landscape: clinical practice patterns of MM patients treated in- and outside German DSMM study group trials<sup/>. Leuk Lymphoma. 2018;59(11):2692-2699.
22. Einsele H, Engelhardt M, Tapprich C, et al. Phase II study of bortezomib, cyclophosphamide and dexamethasone as induction therapy in multiple myeloma: DSMM XI trial. Br J Haematol. 2017;179(4):586-597.
23. Köhler M, Greil C, Hudecek M, et al. Current developments in immunotherapy in the treatment of multiple myeloma. Cancer. 2018;124(10):2075-2085.
24. Kleber M, Ihorst G, Terhorst M, et al. Comorbidity as a prognostic variable in multiple myeloma: comparative evaluation of common comorbidity scores and use of a novel MM-comorbidity score. Blood Cancer J. 2011;1(9):e35.
25. Kleber M, Ihorst G, Gross B, et al. Validation of the Freiburg Comorbidity Index in 466 multiple myeloma patients and combination with the international staging system are highly predictive for outcome. Clin Lymphoma Myeloma Leuk. 2013;13(5):541-551.
26. Kleber M, Ihorst G, Udi J, et al. Prognostic risk factor evaluation in patients with relapsed or refractory multiple myeloma receiving lenalidomide treatment: analysis of renal function by eGFR and of additional comorbidities by comorbidity appraisal. Clin Lymphoma Myeloma Leuk. 2012; 12(1):38-48.
27. Hieke S, Kleber M, König C, Engelhardt M, Schumacher M. Conditional Survival: A Useful Concept to Provide Information on How Prognosis Evolves over Time. Clin. Cancer Res. 2015;21(7):1530-1536.
28. Schumacher M, Hieke S, Ihorst G, Engelhardt M. Dynamic prediction: A challenge for biostatisticians, but greatly needed by patients, physicians and the public. Biom J. 2019 Mar 25. [Epub ahead of print]
29. Caers J, Garderet L, Kortüm KM, et al. European Myeloma Network recommendations on tools for the diagnosis and monitoring of multiple myeloma: what to use and when. Haematologica. 2018;103(11):1772-1784.
30. Kleber M, Ihorst G, Deschler B, et al. Detection of renal impairment as one specific comorbidity factor in multiple myeloma: multicenter study in 198 consecutive patients. Eur J Haematol. 2009;83(6):519-527.
31. Corre J, Munshi N, Avet-Loiseau H. Genetics of multiple myeloma: another heterogeneity level? Blood. 2015;125(12):1870-1876.
32. Moreau P, Cavo M, Sonneveld P, et al. Combination of international scoring system 3, high lactate dehydrogenase, and t(4;14) and/or del(17p) identifies patients with multiple myeloma (MM) treated with front-line autologous stem-cell transplantation at high risk of early MM progression-related death. J Clin Oncol. 2014;32(20): 2173-2180.
33. Neben K, Jauch A, Bertsch U, et al. Combining information regarding chromosomal aberrations t(4;14) and del(17p13) with the International Staging System classification allows stratification of myeloma patients undergoing autologous stem cell transplantation. Haematologica. 2010;95(7):1150-1157.
34. Palumbo A, Avet-Loiseau H, Oliva S, et al. Revised International Staging System for Multiple Myeloma: A Report From International Myeloma Working Group. J Clin Oncol. 2015;33(26):2863-2869.
35. Avet-Loiseau H, Durie BGM, Cavo M, et al. Combining fluorescent in situ hybridization data with ISS staging improves risk assessment in myeloma: an International Myeloma Working Group collaborative project. Leukemia. 2013;27(3):711-717.
36. Binder M, Rajkumar SV, Ketterling RP, et al. Substratification of patients with newly diagnosed standard-risk multiple myeloma. Br J Haematol. 2019;185(2):254-260.
37. Milani P, Vincent Rajkumar S, Merlini G, et al. N-terminal fragment of the type-B natriuretic peptide (NT-proBNP) contributes to a simple new frailty score in patients with newly diagnosed multiple myeloma. Am J Hematol. 2016;91(11):1129-1134.
38. Cook G, Royle K-L, Pawlyn C, et al. A clinical prediction model for outcome and therapy delivery in transplant-ineligible patients with myeloma (UK Myeloma Research Alliance Risk Profile): a development and validation study. Lancet Haematol. 2019;6(3):e154-e166.
39. Pallis AG, Hatse S, Brouwers B, et al. Evaluating the physiological reserves of older patients with cancer: the value of potential biomarkers of aging? J Geriatr Oncol. 2014;5(2):204-218.
40. Engelhardt M, Selder R, Pandurevic M, et al. [Multidisciplinary Tumor Boards: Facts and Satisfaction Analysis of an Indispensable Comprehensive Cancer Center Instrument]. Dtsch Med Wochenschr. 2017;142(9):e51-e60.
41. Soto-Perez-de-Celis E, Li D, Yuan Y, Lau YM, Hurria A. Functional versus chronological age: geriatric assessments to guide decision making in older patients with cancer. Lancet Oncol. 2018;19(6):e305-e316.
42. Abel GA, Klepin HD. Frailty and the management of hematologic malignancies. Blood. 2018;131(5):515-524.
43. Engelhardt M, Mertelsmann R, Duyster J. Das Blaue Buch. Springer; 2020.
44. Waldschmidt JM, Keller A, Ihorst G, et al. Safety and efficacy of vorinostat, bortezomib, doxorubicin and dexamethasone in a phase I/II study for relapsed or refractory multiple myeloma (VERUMM study: vorinostat in elderly, relapsed and unfit multiple myeloma). Haematologica. 2018;103(10):e473-e479.
45. Greil C, Engelhardt M, Ihorst G, et al. Allogeneic transplantation of multiple myeloma patients may allow long-term survival in carefully selected patients with acceptable toxicity and preserved quality of life. Haematologica. 2019;104(2):370-379.
46. Küchlin S, Duffner J, Scheubeck S, et al. Kidney embolization induces prompt organ response in a 86-year-old patient with MGRS-related AL-amyloidosis. Hemodial Int. 2019;23(2):E59-E64.
47. Facon T, Dimopoulos MA, Meuleman N, et al. A simplified frailty scale predicts outcomes in transplant-ineligible patients with newly diagnosed multiple myeloma treated in the FIRST (MM-020) trial. Leukemia. 2020;34(1):224-233.
48. Engelhardt M, Dold SM, Ihorst G, Knaus J, Schumacher M. R-MCI webpage. 2015.
49. Kumar SK, Dispenzieri A, Lacy MQ, et al. Continued improvement in survival in multiple myeloma: changes in early mortality and outcomes in older patients. Leukemia. 2014;28(5):1122-1128.
50. Campisi J, Kapahi P, Lithgow GJ, et al. From discoveries in ageing research to therapeutics for healthy ageing. Nature. 2019;571 (7764):183-192.
51. Mina R, Bringhen S, Wildes TM, Zweegman S, Rosko AE. Approach to the Older Adult With Multiple Myeloma. ASCO Educational Book 2019; vol 39. doi.org/10.1200/EDBK_239067.Am Soc Clin Oncol Educ Book. 2019;39:500-518.

Bone marrow niche dysregulation in myeloproliferative neoplasms

Natalia Curto-Garcia, Claire Harrison and Donal P McLornan

Department of Hematology, Guy's and St Thomas' NHS Foundation Trust, London, UK

Ferrata Storti Foundation

Haematologica 2020
Volume 105(5):1189-1200

ABSTRACT

The bone marrow niche is a complex and dynamic structure composed of a multitude of cell types which functionally create an interactive network facilitating hematopoietic stem cell development and maintenance. Its specific role in the pathogenesis, response to therapy, and transformation of myeloproliferative neoplasms has only recently been explored. Niche functionality is likely affected not only by the genomic background of the myeloproliferative neoplasm-associated mutated hematopoietic stem cells, but also by disease-associated 'chronic inflammation', and subsequent adaptive and innate immune responses. 'Cross-talk' between mutated hematopoietic stem cells and multiple niche components may contribute to propagating disease progression and mediating drug resistance. In this timely article, we will review current knowledge surrounding the deregulated bone marrow niche in myeloproliferative neoplasms and suggest how this may be targeted, either directly or indirectly, potentially influencing therapeutic choices both now and in the future.

Introduction

'Philadelphia chromosome negative' myeloproliferative neoplasms (MPN) are a group of relatively rare hematologic diseases characterized by a clonal proliferation of blood cells, most commonly secondary to acquired hematopoietic stem cell (HSC) mutations that directly or indirectly induce upregulation of the JAK-STAT pathway. The 2016 World Health Organization consensus recognizes the following categories under the MPN classification: chronic myeloid leukemia *BCR-ABL*$^{+}$, chronic neutrophilic leukemia, essential thrombocythemia (ET), polycythemia vera (PV), primary myelofibrosis (PMF) (which includes both the prefibrotic/early stage and overt fibrotic stage), chronic eosinophilic leukemia not otherwise specified, and MPN-unclassifiable.[1] Recent analyses estimate the incidence rates of the classical 'Philadelphia negative'-MPN PV, ET and PMF as 0.7-2.6 cases, 0.34-1.7 cases and 0.1-1.0 cases per 100,000 patients-per-year, respectively.[2] Median age at diagnosis is variable, estimated at between 69-76 years for PMF, 65-74 years for PV, and 64-73 years for ET, although MPN has been described in many younger patients and can manifest at any age.[3] Regarding clinical features, these disorders produce a markedly heterogeneous clinical phenotype. For example, in PMF, patients may range from those lacking any discernible symptomatology to those describing debilitating constitutional symptoms, abdominal discomfort due to splenomegaly, bone pain, and symptomatic anemia, amongst others. The most common complications linked to MPN are thrombotic and hemorrhagic events and an inherent risk of leukemic transformation that is dependent upon the underlying MPN phenotype; this risk is higher for PMF (estimated at a range of 10-20% in the first 10 years from diagnosis) and much lower for both PV (2.3%) and ET (1%).[4] These figures reflect historical data, and it is likely that with the move away from consecutive cytotoxic therapeutic approaches, blastic transformation rates may well be lower.

Following the pivotal reports in 2005 by four different research groups concerning the prevalence of the acquired somatic mutation *JAK2* V617F in MPN, knowledge of the mutational landscape continues to expand.[5-8] The *JAK2* V617F mutation is present in approximately 98% of PV patients, and has an estimated incidence in ET and MF of 50% and 60%, respectively. Mutations in the thrombopoietin receptor (*MPL*) are described in approximately 3% of ET and 5-8% of MF cases, whereas mutations in calreticulin (*CALR*) are evident in 25% of ET and 30% of MF

Correspondence:

CLAIRE HARRISON
claire.harrison@gstt.nhs.uk

Received: November 18, 2019.

Accepted: February 6, 2020.

Pre-published: April 2, 2020.

doi:10.3324/haematol.2019.243121

Check the online version for the most updated information on this article, online supplements, and information on authorship & disclosures: www.haematologica.org/content/105/5/1189

patients.[9-11] Up to 20% with ET and up to 15% of patients with PMF lack detectable mutations in these three genes, as assessed by conventional assays; such patients are termed 'triple negative'.[12-14] Lastly, comprehensive genomic analyses have revealed the presence of additional mutations that can appear before, simultaneously, or following the so-called 'driver mutations' (*JAK2*, *CALR* and *MPL*) in PMF and can affect a wide-array of key genes, such as those involved in epigenetic regulation (*TET2*, *ASXL1*, *EZH2*), splicing (*SRSF2*, *U2AF1*), and cellular signaling (*SH2B3*, *PIAS3*), some of which also affect prognosis.[15]

Multiple factors contribute to the dynamic complexity of the bone marrow niche in MPN, such as the inherent increase in pro-inflammatory cytokines, skewed adaptive and innate immune responses, and 'cross-talk' between the normal and mutated-HSC, endosteal and vascular niches and extracellular matrix. In this review, we will summarize current knowledge concerning bone marrow niche composition in health and how it differs in MPN. Likewise, as we gain further understanding of these dynamics, we will explore what potential there is for therapeutic intervention specifically targeting the niche to provide clinical benefit.

Overview of the bone marrow niche in health

It is evident that much remains to be elucidated concerning the dynamic BM microenvironment, both in normal physiological and disease states. Traditionally, the niche is conceived as being divided into individual compartments with bi-directional 'cross-talk' between the well-defined spatially organized HSC, multiple surrounding permissive cells, and the extracellular matrix (Figure 1). This concept was first delineated by Lord *et al.* and Schofield more than 40 years ago.[16,17] The accumulated evidence demonstrates that multiple additional factors can influence, either directly or indirectly, this niche, such as microenvironmental oxygen tension variations, sympathetic nervous system activity, and endocrine signaling such as the estrogen pathway.[18,19]

Simplistically, the endosteal niche, which is highly vascularized, is considered to be where the 'potent and primitive' HSC reside, rich in long-term (LT)-HSC. The pivotal paper by Nilsson *et al.* demonstrated that, following HSC 'transplantation' in mice, HSC 'homed' to the endosteum, with subsequent maintenance and promotion of HSC development.[20] Later studies by Celso *et al.* and Xie *et al.* showed similar results.[21,22] This niche is formed predominantly by osteoblasts (which mainly line the endosteal bone surface), osteoclasts, and a specific osteoblastic subpopulation known as spindle-shaped N-cadherin$^+$ osteoblasts (SNO cells). Within the niche, both BM mesenchymal stem cells (BMSC) and the N-cadherin$^+$ cell population play an indispensable role in HSC maintenance. Each of these cell populations and their interactions with each other (and with the HSC population) ultimately determines maintenance and proliferation of the hematopoietic stem/progenitor cell pool and downstream lineage differentiation.

Osteoblasts are derived from multipotent BMSC where-

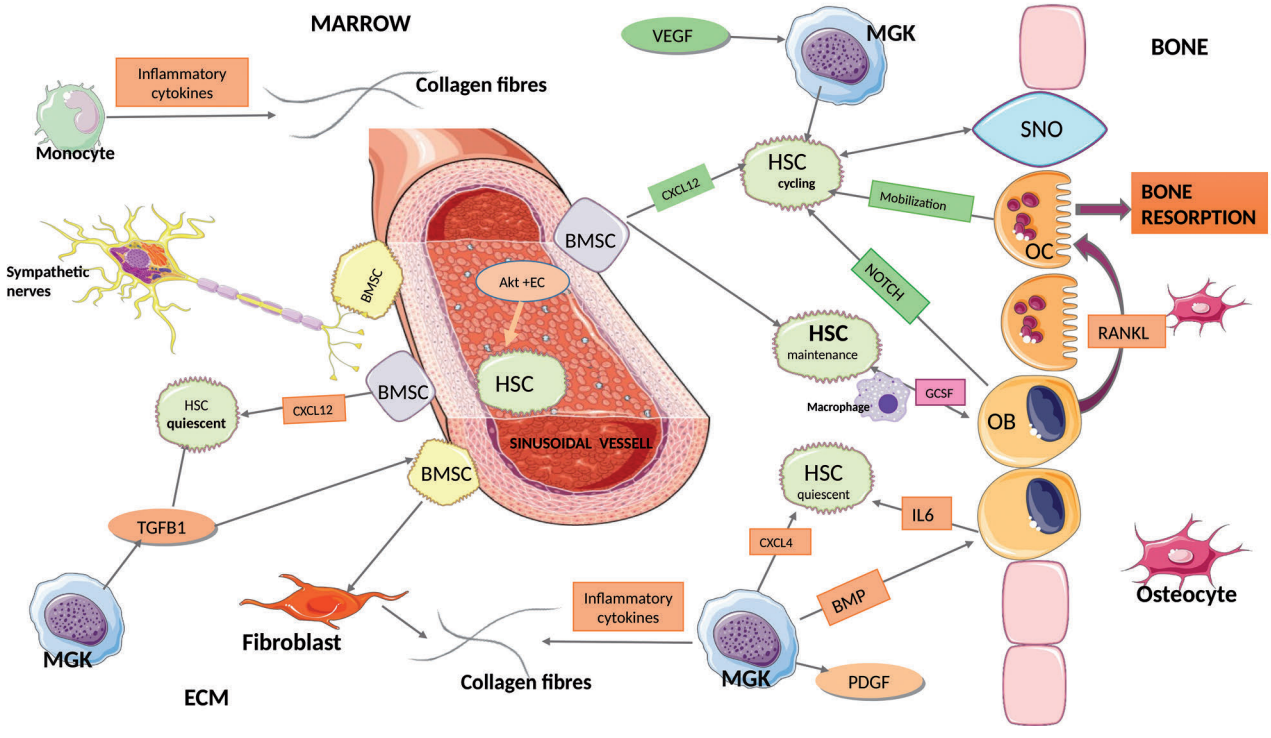

Figure 1. Hematopoietic stem cell (HSC) cycling is regulated by osteoclast (OC), osteoblast (OB) by NOTCH expression and spindle-shaped N-cadherin$^+$ osteoblast (SNO) cells. Different bone marrow mesenchymal cells (BMSC) participate in HSC regulation, such as CXCL12-abundant reticular (CAR) cells that stimulate HSC cycling by producing CXCL12. On the other hand, megakaryocytes (MGK) are activated by vascular endothelial growth factor (VEGF) and participate in the activation of HSC cycling. HSC maintenance is regulated by a reciprocal communication between OB and HSC. CAR cells also participate in this regulation. Finally, HSC quiescent is regulated by both the bone marrow niche (BMN) and the extracellular matrix (ECM), thus, OB and MGK interact in this control. The growth factor TGFb1 and, indirectly, the platelet-derived growth factor (PDGF) (by activating MGK) would participate in the HSC quiescent. Nestin$^+$ BMSC regulate the CXCL12 production and the sympathetic nerves contribute to BMN functionality. EC: endothelial cell.

as osteoclasts originate from CD34+ hematopoietic cells.[23] Early work showed that the two populations were functionally interdependent, e.g. osteoblasts constitutively expressed G-CSF and CD34+ hematopoietic cells enhanced IL-6 production by osteoblasts hence stimulating further investigations into these interactions.[24,25] It is accepted that, in general, osteoblast functionality plays an important role in HSC maintenance, in particular with regard to HSC trafficking. Regulatory roles depend upon osteoblastic differentiation stage, whereby the immature osteoblast progenitor population influences HSC maintenance/proliferation and the mature osteoblasts modulate their differentiation.[26] In murine models, Calvi *et al.* demonstrated that osteoblastic cells influenced HSC functional capacity through NOTCH activation, and it was suggested that HSC are located in close physical proximity to SNO cells, although the role of N-cadherin in these 'cell-cell' interactions remains under debate.[27,28] Multiple soluble factors derived from the osteoblast population play a role in HSC pool fate, including CXCL12, angiopoietin-1 and osteopontin, in addition to multiple other cytokines/chemokines.[29] CXCL12 is a CXC chemokine produced by stromal cells, the major source is from BMSC but also by osteoblasts influenced by circadian oscillations and there is evidence that CXCL12/CXCR4 signaling plays a pivotal role in modulation of HSC trafficking.[30] In addition, the acidic matrix glycoprotein osteopontin is produced by pre-osteoblasts and osteoblasts and negatively regulates both HSC pool 'size' and egress.[27,31] Of note, osteoblasts play an additional role in T lymphopoiesis, whereby DLL4 on the cell surface is pivotal for the production of 'thymic seeding' T progenitors.[32]

As introduced above, osteoclasts derived from monocyte-macrophage lineage cells in the presence of receptor activator of nuclear factor-κB-ligand and macrophage colony-stimulating factor play multiple regulatory roles within the niche in addition to their bone resorption characteristics.[33] Kollet *et al.* demonstrated that, through endosteal component degradation, osteoclasts can promote HSC mobilization.[34] However, the literature also includes contrasting evidence concerning their exact role within the HSC niche, which is most likely context dependent. For example, using the osteopetrotic 'OC/OC'-murine model, absence of functional osteoclasts induced a defective HSC niche with increased mesenchymal precursors, impaired osteoblast development, and resultant aberrant HSC homing.[35] However, Miyamoto *et al.* evaluated hematopoietic activity in three murine models without osteoclasts and showed that HSC mobilization was, in fact, similar, or indeed higher, than that of wild-type animals, suggesting that osteoclasts are not essential for HSC mobilization.[36] Lastly, there is a great deal of cross-talk and interdependency between the osteoblast and osteoclast populations. It has also been shown that osteoclasts can act as antigen presenting cells and activate both CD4+ and CD8+ T cells.[37]

The vascular niche is the other pivotal component of the bone marrow niche and broadly encompasses thin-walled sinusoidal blood vessels, arterioles, transition zone vessels, endothelial cells (that also produce *CXCL12*), stromal elements, fibronectin, and collagen. Functionally, interactions between these perivascular elements determine both HSC dormancy/expansion and migration properties. By way of example, Akt activation in endothelial cells following mTOR recruitment induces upregulation of specific angiocrine factors which promotes expansion of cells with LT-HSC repopulation capacity.[38] Cell-cell contact also appears key. For example, E-selectin expression by endothelial cells in the vascular niche can regulate HSC dormancy and HSC proliferation.[39] Moreover, the vascular niche provides an environment rich in multiple pro-inflammatory chemokines/cytokines, which contribute to niche maintenance. The so-called 'hypoxic-gradient' plays a major role in spatial HSC location within the vascular niche. In this way, quiescent HSC preferentially locate to small arterioles, unsheathed by rare NG2-pericytes, predominantly found in the endosteal bone region. HSC tend to exhibit a strong hypoxic profile, promoting quiescence, irrespective of localization.[40,41] Likewise, in those situations whereby the sinusoids are under stress induced by, for example, myeloablative chemotherapy or irradiation, the endosteal niche becomes an important host of HSC and promotes quiescence.[42]

Bone marrow mesenchymal stem cells encompass a diverse group of cells with multipotent differentiation and self-renewal properties indispensable for HSC maintenance. BMSC can interact in a pleotropic fashion with HSC including direct cell-cell interaction and by the altered production of cytokines and cell markers.[43] CXCL12-abundant reticular cells are a subpopulation of BMSC that produce *CXCL12* and regulate the maintenance and quiescence of the HSC pool. Multiple other cell types, outside the remit of this review, contribute to the regulation of the niche including macrophages which modulate the CXCL12 pathway promoting HSC retention, and monocytic-lineage cells which regulate osteoblasts, facilitate HSC mobilization and also encourage a pro-inflammatory cytokine environment.[31] Concerning the role of the sympathetic nervous system, Mendez-Ferrer *et al*. demonstrated that circulating HSC and their progenitors exhibit marked circadian fluctuations regulated by noradrenaline secretion by the sympathetic nervous system.[30,44] Adrenergic signals *via* the beta-(3)-adrenergic receptor mediate downregulation of CXCL12 and there is a close association between so-called Nestin+ BMSC and adrenergic nerve fibers of the SNS with resultant regulation of HSC functionality and egress. This neuro-hematopoietic axis is exploitable as a therapeutic target, as will be discussed later.

With regard to the extracellular matrix (ECM), this is a non-cellular space that supports the integrity, proliferation and 'elasticity' of the entire bone marrow niche. It acts as a pivotal HSC 'regulator' and ECM-related components critically determine the functionality of HSC lodged within its confines.[45] The 'core matrisome' is a complex structure that consists of up to 300 protein components, enzymes, and growth factors (e.g. *TGFβ1*, *PDGF* and *VEGF*), and overall functionally drives maintenance of the HSC pool.

Bone marrow niche / extracellular matrix disruption in myeloproliferative neoplams

Myeloproliferative neoplasm-associated bone marrow niche homeostasis is disrupted on many levels which collectively can promote the proliferation, survival and migration of mutated MPN HSC. As described by Mead and Mullaly, both 'host' and extrinsic factors can influence MPN HSC behavior, and as the malignant clone expands,

this favors MPN HSC growth over normal HSC expansion.[46] Mullally *et al.* have described that *JAK2*V617F-LT-HSC are capable of initiating and promoting the disease, giving a clonal advantage to dominate the niche against WT cells. In addition, mutated LT-HSC could induce fibrotic changes in the bone marrow niche in WT transplanted mouse models.[47] Furthermore, Lundberg *et al.* proved elevated *JAK2* expression levels impact negatively on the repopulation capacity of LT-HSC and will promote the disease expansion.[48] Finally, acquisition of other mutations, such as *TET2* deletions in *JAK2* V617F-LT-HSC, gives a clonal advantage favoring the disease progression.[49]

Regarding the osteoblast-osteoclast axis, it is clear that aberrant functionality of the endosteal osteoblastic niche plays an important role in MPN maintenance and progression. For example, it has been shown in murine models that osteoblast expansion is functionally altered in MPN and promotes the development of fibrosis.[50] Over time, disease-driven remodeling of the endosteal niche occurs, leading to a self-reinforcing 'leukemia-niche' with impaired normal hematopoiesis. Several mechanisms, as suggested by the authors, are implicated in dysregulated osteoblastic expansion, such as overstimulation of MSC driving production of functionally impaired osteoblasts, resultant direct 'cell-cell contact' with mutated MPN HSC, and up-regulated production of TPO, CCL3, TNF-β and Notch, thus inducing a chronic state of 'inflammation'.[51,52] Expression of *CXCL12*, essential for controlled HSC mobilization, as discussed above, is reduced due to this abnormal osteoblast functionality. Moreover, Spanoudakis *et al.* recently showed that monocytes derived from *JAK2* V617F (heterozygote)-MPN cells had enhanced osteoclast-formation ability compared to wild-type monocytes. An enriched osteoclast environment additionally favors MPN-associated mutated cell population proliferation and survival.[53] Collectively, these findings highlight the importance of the osteoblast-osteoclast axis and its disruption in MPN and how this may be therapeutically exploited.

Clonal-MPN cells additionally have the capacity to disrupt the finely balanced vascular niche. By way of example, *JAK2*-mutated endothelial cells promote the abnormal proliferation and survival of mutated-HSC whilst inhibiting normal HSC functionality. This occurs secondary to alterations within the CXCL12 and stem cell factor pathways. Vascular endothelial growth factor (VEGF), produced by both the endothelial cells and the 'mutated'-HSC, supports neo-angiogenesis and increases both survival and proliferation of these HSC. Therefore, a self-reinforcing vascular niche also develops as a favorable environment for MPN mutated-HSC.[54] Hypoxia-induced signaling also appears to influence HSC behavior by encouraging quiescence and influences long-term repopulating activity.[55] Utilizing transgenic MPN-murine-models, it has been shown that downregulation of HIF-1α induces an enhanced MPN phenotype reflected by increased leukocytosis and significant splenomegaly.[56]

Importantly, BMSC appear pivotal to the development and maintenance of the MPN phenotype. BMSC promote the abnormal expansion of osteoblasts as inflammatory 'myelofibrotic' cells; a conversion mediated by dysregulation of inflammatory signaling pathways with excess production of *TGF-β1*, *Notch*, IL-6, IL-1β and TNF-β and secondary to direct contact between the clonal MPN-HSC and BMSC.[57] Schneider *et al.* has demonstrated that Gli1$^+$-BMSC participate in the activation of myelofibroblasts.[58] Ultimately, the overproduction of inflammatory 'myelofibrotic cells' contributes to progressive BM fibrosis observed in the advanced stages of these diseases.[31] At the same time, excessive osteoblast production perpetuates clonal-MPN cell proliferation.[50] Ramos *et al.* recently demonstrated that BMSC derived from MPN patients (mainly PV and ET) present an altered gene and immunophenotypic expression profile compared to those derived from healthy donors. In PV, BMSC show an overexpression of genes involved in cell differentiation and migration such as *MYADM*, *Angiopoietin-1* expression and decreases in *CXCL12*; that are associated with 'cross-talk' between the mutated-HSC and BMSC.[59] Angiopoietin-1 participates in both angiogenesis and the quiescence of the HSC. Osteoblast production of angiopoietin-1 facilitates interaction with Tie-2, resulting in increased adhesion of HSC to osteoblasts within the niche.[60]

More recently, other studies have explored the neuro-hematopoietic axis, demonstrating that the sympathetic nervous system influences bone marrow niche regulation. Arranz *et al.* elegantly showed that a local neuropathy occurs in MPN-BM, with a reduction in both Nestin$^+$ BMSC and CXCL12 expression and promotion of *JAK2*$^+$ HSC expansion. The relationship, if any, between this local neuropathy and the patient's symptomatology and phenotype is still not clear, although it has been described as a possible therapeutic target, as discussed below.[51,61] Lastly, an increased understanding of the role of estrogen signaling is emerging. In normal HSC, it has been shown that estrogen receptor stimulation *in vivo* led to an increased proliferation of quiescent LT-HSC and tamoxifen induced apoptosis of short-term HSC and multipotent progenitors. In chronic MPN, *JAK2*-mutated murine models, tamoxifen led to preferential restoration of apoptosis in mutated-HSC.[62]

Regarding the ECM, clonal-HSC demonstrate dysregulated 'cross-talk' with augmented levels of cytokines and growth factors within the ECM, enhancing both disease establishment and progression. In MF, there is an intensified deposition of ECM components. Thus, highly fibrogenic *TGFβ1* activates fibrosis deposition by two main routes: (i) skewing BMSC activation towards fibroblastic and osteoblastic genesis; and (ii) an augmented production of collagen. Moreover, *TGFβ1* levels are intimately linked to megakaryocytic activity.[63] Additional growth factors such as PDGF (platelet derived growth factor) and VEGF play a pivotal role in this unbalanced ECM-MPN marrow niche communication. *PDGF* promotes fibrogenesis by activating both megakaryocytes and fibroblasts whereas VEGF contributes towards megakaryocytic maturation and migration.

Other relevant modifiers of the MPN-associated ECM are matrix metalloproteinases (MMP) and Lysyl Oxidase (LOX).[64] In MPN, Wang *et al.* demonstrated downregulation of MMP, supporting the accumulation of ECM substances. Focusing on MF, this study demonstrated decreased MMP3 levels which inversely correlated with increased fibrosis and enhanced expression of tissue inhibitors of the metalloproteinases.[65] Both *MMP2* and *MMP9* are highly expressed in MPN patients and are reduced after treatment with JAK inhibitors.[66] LOX is a potent regulator of fibrogenesis and is involved in collagen cross-linking. Previous studies have demonstrated a link between deregulated megakaryocytic production of PDGF, TGF-β1 and IL-1β and augmented LOX activity,

with resultant collagen accumulation in MF.[64] Tadmor *et al.* demonstrated that, in MF, all LOX members genes are activated compared to the pattern seen in either ET or PV; postulating that this occurred during fibrogenesis. Of interest, *LOXL1* was only expressed in MF, suggesting a relationship with advanced fibrosis.[67]

In summary, it is evident that the bone marrow niche is profoundly dysregulated on multiple, yet interacting levels, in MPN (Table 1). Mutated-MPN-HSC activate a cascade of dysregulated signaling and abnormalities in multiple key players across the niches, compromising functionality of both the osteoblastic and vascular niches and ECM. Consequently, these irregularities promote the abnormal proliferation inherent to these disease states. Although our knowledge of the MPN-associated dysregulated niche has increased in recent years, further studies are required to help understand how this niche can be successfully targeted in therapy.

Direct or indirect targeting of the bone marrow niche in myeloproliferative neoplasms: is there a role?

To date, the only curative treatment for MF remains allogeneic stem cell transplantation, although this is not a feasible option for many due to age, risk profile, co-morbidities, or lack of a suitable donor.[68] Many clinicians have familiarity with the JAK1/JAK2 inhibitor (JAKi) ruxolitinib (Novartis, Switzerland), currently the only licensed agent in MF; which has demonstrated improvement in disease-related symptomatology, induced reductions in spleen size, and prolonged the overall survival (OS) in many MF patients.[69,70] Of note, ruxolitinib has also been used in both PV and ET, particularly in the setting of hydroxycarbamide resistance or intolerance.[71-74] Many other agents have entered the clinical trial arena to address the multiple unmet needs, particularly when individuals are failing or become intolerant of standard therapies, including novel JAKi, BET-inhibitors, BCL-2 inhibitors, HDAC inhibitors, telomerase inhibitors, and MDM2 inhibitors.[75-81] Regarding novel JAKi, pacritinib (which is also a FLT3 inhibitor) has been investigated in MF patients with thrombocytopenia showing improvements in splenic responses within both the PERSIST-I and -II studies.[82,83] The drug was on clinical hold from 2016 due to concerns regarding cardiac toxicity, but following the Food and Drug Administration (FDA) review and removal of the clinical hold, the PAC203 study has now fully recruited and further studies are planned. Momelotinib, a JAK1/2 inhibitor, demonstrated anemia and transfusion responses in both the SIMPLIFY-1 and 2 clinical trials but it failed to meet the pre-defined clinical end points, although some patients demonstrated symptom, spleen and anemia responses.[84,85] This agent will be compared on a randomized basis to danazol in the upcoming MOMEMTUM study. Fedratinib (Inrebic®, Celgene, USA) is a more selective JAKi than ruxolitinib; both JAKARTA-1 and 2 trials showed this agent to have significant efficacy in MF

Table 1. Bone marrow niche in health and myeloproliferative neoplasm.

	Bone marrow niche in health	Bone marrow niche in MPN
Endosteal niche: Osteoblasts, Osteoclasts and spindle-shaped N-cadherin$^+$ osteoblast cells	• Maintenance, proliferation and differentiation of HSC. • **Osteoblasts**: - Interact with CD34$^+$HSC by expressing GSCF and IL6. - Regulate HSC trafficking by expression CXCL12, angiopoietin-1 and osteopontin. • **Osteoclasts**: - Regulatory role. - Bone resorption. - Promote HSC mobilization. • **SNO cells**: - Cell-cell contact with HSC.	Self-reinforcing of clonal cells. - **Osteoblasts**: - Abnormal OB expansion due to overstimulation by BMSC. - Overproduction of inflammatory cytokines. - Promotion of fibrogenesis. - Reduction in CXCL12 expression. - **Osteoclasts**: - Abnormal stimulation by JAK2 positive monocytes. - Favoring survival of clonal HSC. - **SNO**: - No clear role described yet.
Vascular niche: sinusoidal blood vessels, endothelial cells, stromal elements, fibronectin and collagen	• Regulate HSC migration . • Expression of e-selectin by endothelial cells. • Production of inflammatory chemokines and cytokines. • Regulation of hypoxia status . • **BMSC-CAR cells express CXCL12**- maintenance and quiescence HSC. • **Macrophage-** modulate CXCL12 pathway. • **Monocytes**- regulate osteoblasts, promote pro-inflammatory cytokine environment.	• Alteration CXCL12 pathway: upregulated in JAk2$^+$ endothelial cells, downregulated BMSC- promotes expansion mutated HSC. • Clonal endothelial cells support neo-angiogenesis by VEGF production. • Increase survival mutated HSC. • Alteration of HIF-1α and **hypoxia status**. • BMSC promote expansion of osteoblasts by cell contact and excessive TGFβ1, Notch and cytokines. • Overproduction of **inflammatory markers** produce fibrosis.
Sympathetic nervous system	• Noradrenaline secretion regulate HSC circulation and functionality .	• Local **neuropathy** by reduced expression of Nestin$^+$ and CXCL12 promoting HSC expansion.
Extracellular matrix	• Integrity, proliferation and elasticity of BMN. • Presence of growth factors (TGFβ-1, PEGF, VEGF) to maintain HSC.	• Increase **cytokines** and **growth factor** levels (TGFβ-1, PEGF, VEGF) promotes fibrogenesis. • VEGF contributes to MK maturation and migration. • Decrease of MMP and increase of LOX favoring fibrosis.

SNO: spindle-shaped N-cadherin$^+$ osteoblasts; HSC: hematopoietic stem cells; BMSC: bone marrow mesenchymal cells; VEGF: vascular endothelial growth factor; PDG: platelet-derived growth factor; TGFβ1: transforming growth factor beta; HIF-1α: Hypoxia inducible factor 1-alpha; MK: megakaryocytes; MMP: matrix metalloproteinases; LOX: Lysyl Oxidase.

Table 2. Therapies targeting directly or indirectly the bone marrow niche.

Drug	Target	Disease/update results	Reference	
PACRITINIB	JAK2/FLT3 inhibitor	MF with thrombocytopenia Spleen responses 18% volume reduction ≥ 35% – PERSIST I & II trials	82 83	Clinical trials ongoing
MOMELOTINIB	JAK1/2 inhibitor	MF Anemia and transfusion responses in addition to spleen and symptoms: - SIMPLIFY 1 (momelotinib *vs* ruxolitinib): 66.5% transfusion independent at week 24. 26.5% reduction of spleen volume ≥ 35% - SIMPLIFY 2 (momelotinib *vs* BAT): 7% spleen volume ≥ 35%	 84 85	Planned MOMENTUM Study
FEDRATINIB	Selective JAK 2 inhibitor	MF (ruxolitinib resistant or intolerant) Spleen response and symptoms improvement. - JAKARTA-1: reduction spleen volume ≥ 35%, 36% (400mg) and 40% (500-mg compared with placebo. - JAKARTA-2: Second line study 55% of patients achieved spleen volume ≥ 35%. Recent hold due to Wernicke's encephalopathy removed. Approved by FDA in 2019.Fibrosis grade-reduction in 44% (8/18) patients after cycle 6.	 86 87 99	Clinical trials ongoing/ planned
NAVITOCLAX	BCL-2 inhibitor	MF failed ruxolitinib. Clinical trial ongoing in combination with ruxolitinib	No data published available yet	Clinical trial ongoing
PANOBINOSTAT	Histone deacetylase inhibitor	MF -combination with ruxolitinib 36% achieved overall response by IWG-MRT Median spleen reduction was 34% 6.8% decrease in JAK2 allele burden	119	Clinical trial ongoing – expansion phase.
IMETELSTAT	Telomerase inhibitor	MF and ET. - MF clinical trial: Pilot- 33 MF patients- complete and partial response 7(21%) median response 18m. Bone marrow fibrosis reversal in 4 with CR. Molecular response 3 / 4 patients. - Phase-II study: OS 19.9 months in low dose and 29.9 months in higher dose. 93% patients discontinued study (25% due to adverse events). Update data compared with real world showed OS was 30.69 months. Significant myelosuppression and hepatic toxicity in some. ET clinical trial: 16/18 (89%) achieve complete hematological response. And 7/8 molecular response with allele burden reduction between 15-66%. Bone marrow fibrosis reduction of at least 1 grade was described in 4/6 (67%)	 92 93 94 91	Recruitment suspended
IDASANUTLIN	MDM2 inhibitor	PV, ET and MF Alters the MDM2/p53 interaction. PV/ET clinical trial: 58% response on monotherapy and 50% for combined therapy after 6 cycles. Combined with BET inhibitor in MF: Reduction of hematopoietic colony formation CD34+ in MF. Reduction in pro-inflammatory cytokines (decreased the levels of IL-8 in MF MNC by 50% (P=0.0003))	95 96	Clinical trial ongoing
BET inhibitor		Combined with ruxolitinib in MF MF- inhibition of the NF-KB pathway, reduction of inflammatory cytokines. Reduction of bone marrow fibrosis.	120	Clinical trial ongoing

continued on the next page

continued from the previous page

RUXOLITINIB	JAK inhibitor	MF Association between reduction in fibrosis grade and cytokines reduction (AUC=0.85939, *P*=0.0134)	69,97	Single agent studies closed
TAMOXIFEN	Estrogen receptor antagonist	MPN Reduction of JAK2 and CALR allele burden ≥50% at 24 weeks mutation	No data published as yet.	Clinical trial ongoing
PRM-151	Recombinant human pentraxin-2 analogue	MF Fibrosis grade reduced in 25 patients by ≥ 1 initial study. In extension phase, improvements in 71% and 44% of individuals with grade 2&3 fibrosis at baseline. Updated results showed 28% decrease in fibrosis.	100 101 102	Study closed
IPI926	Hedgehog inhibitor	MF No improvements in fibrosis	103,104	Study discontinued
SONIDEGIB (LDE225, NOVARTIS, SWITZERLAND)	SMO receptor antagonist	MF in combination with ruxolitinib Spleen and symptoms responses- 65% of pts achieved a ≥ 50% reduction spleen and 9 pts had resolution of splenomegaly. Reduction of bone marrow fibrosis	105	-
PIRFENIDONE	Antifibrotic agent	MF *In vitro*- reduced both fibroblast activity and ECM components *In vivo*- minimal clinical benefits.	106	-
FRESOLIMUMAB	Monoclonal antibody against TGF-β	MF No relevant changes in fibrosis	107	Clinical trial ongoing
GALUNISERTIB (LY2157299)	TGF-β receptor I kinase	MF Reductions in fibrosis in murine models (*P*=0.02)	108	-
SIMTUZUMAB	Monoclonal antibodies against the Lysyl oxidase like-2	MF- monotherapy and combination with Ruxolitinib Reduced fibrosis score at 24 weeks in 36.7%. Overall limited efficacy	109	-
AZACITIDINE DECITABINE	Hypomethylating agents	MF- high risk and accelerated/blastic phase. Combined with ruxolitinib- 57% fibrosis reduction and spleen responses observed. MF-Blastic phase Increased OS.	110 121	Clinical trial ongoing
MIRABEGRON	Oral β-3 adrenergic agonist	MPN- *JAK2* V617F positive Increase in Nestin$^+$ BMSC (week 24 was 3.52/mm^2 [95%CI: 1.65-5.39]) Mild reduction in fibrosis 1.0 (interquartile range 0–3) to 0.5 (interquartile range 0–2) (*P*=0.01)) Modulation of megakaryocyte clustering	112	
BEVACIZUMAB	Anti-VEGF agent	MPN No significant benefit	113	Study closed
VATALANIB	Anti-VEGF receptors	MF 3% CR and 17% clinical improvement 3/7 patients have bone marrow fibrosis reduction	114	-
BORTEZOMIB	Proteasome inhibitor indirectly inhibits HIF1- α	MF 9/15 patients reduced in the bone marrow vessel density.	118	-

MF: myelofibrosis; CR: complete response; OS: overall survival; PV: polycythemia vera; ET: essential thrombocythaemia; MPN: myeloproliferative neoplasm; CI: confidence interval; MNC: mononuclear cells; BMSC: bone marrow mesenchymal stem cells; VEGF: vascular endothelial growth factor; HIF1-α: hypoxia-inducible factor.

patients, either JAKi naïve or those with resistance or intolerance to ruxolitinib in terms of spleen response and improvement of symptoms.[86,87] The FDA placed the drug on hold due to several cases of Wernicke's encephalopathy, but after further investigations, this clinical hold has now been removed and the agent has recently been approved by the FDA in both the first-line and successive treatment settings in MF.[88]

Multiple alternative pathways are being investigated as potential therapeutic targets for MPN patients; ongoing trials are investigating the use of BET inhibitors, PI3K inhibitors, HDAC inhibitors, BCL-2 inhibitors and MDM2 inhibitors, to name only a few (Table 2). BCL-2 protein inhibitors (BH3-mimetics) have already been investigated in lymphoid and other myeloid disorders.[89] Curiously, these agents trigger remarkable megakaryocytic and

mature platelet apoptosis.[90] A phase II clinical trial of the BCL-2 inhibitor navitoclax in combination with ruxolitinib in MF patients is ongoing and results are awaited with interest. Other emerging agents indirectly targeting the marrow niche are the telomerase inhibitor, imetelstat (GRN163L, Geron, USA), which has been investigated in both ET and MF patients and initial clinical results are encouraging.[91,92] Unfortunately, subsequent studies in MF revealed limited overall spleen responses, significant myelosuppression, and in some patients, hepatic toxicity; therefore, recruitment for the study was suspended (Geron Corporation, June 7 2017, press release). However, the data presented in ASH-2018 showed complete and partial responses in 21% cases, with bone marrow fibrosis reversal in four cases with complete response (CR); OS after 27.4 months of treatment was 19.9 months in the low-dose therapy arm and 29.9 months in the higher-dose therapy arm.[93] Unfortunately, 93% of patients discontinued the study, and of these, 25% were due to adverse events. Recent data presented at the EHA congress 2019 demonstrated that when survival data from the 9.4 mg/kg imetelstat-cohort, from the phase-II trial in ruxolitinib relapsed/refractory higher-risk MF, was compared to 'real world' data for this group of patients treated with best alternative therapy (BAT), there was a potential OS advantage (30.69 months in the imetelstat group, HR 0.35 months, *P*<0019); although this was an unweighted analysis and had inherent comparative limitations.[94] Geron plans to conduct an up-dated phase II trial meeting with the FDA to determine if there is a regulatory path forward for imetelstat in MF in 2020.

MDM2 inhibitors alter the MDM2/p53 interaction, in order to restore p53 functionality/activity. Preliminary data from early phase studies in PV and ET demonstrated favorable clinical responses. Mascarenhas *et al.* recently presented the results of a phase I study in which 13 *JAK2*-mutated PV/ET patients were treated with idasanutlin and combined with pegylated interferon if a partial response was not achieved following cycle 6. Responses were robust: 58% for the monotherapy cohort and 50% for the combination therapy cohort after 6 cycles, with a median treatment duration of 16.8 months.[95] Two multinational clinical trials are currently open investigating the efficacy and safety of the MDM2 inhibitor KRT-232 for ruxolitinib-failure/intolerant MF patients and poorly controlled PV patients. Recently, Lu *et al.* presented early data from a combinatorial study of an MDM2 antagonist and BET inhibitor in MF patients.[96] This combination reduced hematopoietic colony formation by MF-CD34$^+$ cells and targets the microenvironment by reducing the pro-inflammatory cytokine milieu. Results of this particular combinatorial approach are eagerly awaited, as is the combination of a BET inhibitor with JAKi. Lastly, as introduced above, another potential niche pathway target is the estrogen-signaling axis. Inhibition of estrogen-signaling has recently been explored in the TAMARIN trial, investigating clinical benefits and molecular responses induced by the concomitant administration of tamoxifen to patients with MPN established on treatment (excluding interferon).

Historically, the exact relationship between BM fibrosis and clinical outcome/prognosis in MF has been somewhat unclear. An important question is: does improvement in BM fibrosis correlate with improved overall symptom/spleen burden and OS? This has not been comprehensively studied in the clinical trial setting, particularly in the longer term. Kvasnicka *et al.* recently examined the effects of long-term ruxolitinib therapy on BM cytomorphology and fibrosis in 68 patients compared to 192 matching patients with BAT.[97] Compared to baseline reticulin fibrosis grade, ruxolitinib, in contrast to BAT, was associated with augmented odds of fibrosis grade stabilization or improvement and decreased odds of a worsening of reticulin fibrosis. Furthermore, this was often associated with higher degrees of reduction in spleen size. Similar effects have also been noted in a much smaller cohort of patients treated with fedratinib.[98,99] Collectively, these data suggest a possible disease-modifying effect, at least in a subset of those patients undergoing JAKi therapy, which evidently requires a longer duration of drug exposure. Novel therapies such as PRM151, a recombinant human pentraxin-2 analog, have also demonstrated promising findings following reductions in BM fibrosis in some patients with MF. In the first stage of the clinical trial, 27 patients with either primary or secondary MF and ≥ grade 2 reticulin fibrosis were due to receive PRM-151 ± ruxolitinib for 24 weeks; 20 completed therapy.[100] In general, the agent was well tolerated, both alone and with JAKi, with no evidence of myelosuppression. Improvements in symptoms and modest reductions in splenomegaly in some were observed and 11 out of 25 patients evaluated had a reduction in BM fibrosis by ≥ 1 grade. A total of 18 patients were in the open label extension, all of whom received a monthly infusion of PRM-151 at 10 mg/kg, treated for up to 35 cycles (140 weeks).[101] A total of 50% were also receiving ruxolitinib. A similar percentage of patients experiencing reductions in spleen size and improvements in total symptom score (TSS) were seen in both the combination and monotherapy arms. Improvements in reticulin grade was observed in 71% and 44% of those with Grade 2 and 3 marrow fibrosis at baseline, respectively. Recent results presented at the EHA 2019 by Verstovsek *et al.* showed that BM fibrosis decreased at any time point in 28% of patients, and 16-29% patients had a ≥50% reduction in transfusion requirement or hemoglobin improved >10 g/L for 12 consecutive weeks.[102]

Other therapeutic agents have been developed during recent years to specifically target the BM fibrosis and/or relevant pathways in MPN, but with limited success. Inhibitors of hedgehog signaling, important in both primitive and definitive hematopoiesis, cellular proliferation and survival, have been studied both as monotherapies and in combination with ruxolitinib in MF.[103] IPI926, an oral hedgehog-inhibitor, was studied as a monotherapy in MF; however, no significant improvements in fibrosis were reported and the study was discontinued.[104] The SMO-inhibitor sonidegib (LDE225, Novartis, Switzerland) has been investigated in combination with ruxolitinib in a phase-Ib/II study and demonstrated spleen and symptom responses in a minority of patients, and, in some patients, reductions or stability in BM fibrosis.[105] Schneider *et al.* have showed that Gli1$^+$ mesenchymal cells are involved in the fibrosis pathogenesis of MF. The investigators have used GANT61, an inhibitor of Gli1 transcription factor that regulates the hedgehog signaling pathway, in MF murine models and demonstrated reductions in both the fibrosis and the malignant clone. These results suggest a possible new target in reducing marrow fibrosis in MF.[58]

Pirfenidone, an established antifibrotic agent, showed promising results *in vitro* by reducing both fibroblast activ-

ity and ECM components; however, a phase-II study in MF failed to show significant clinical benefits.[106] A study with a monoclonal antibody against TGF-β (fresolimumab) is currently ongoing in MF, although preliminary results have not described any relevant changes in fibrosis.[107] Finally, an inhibitor of the TGF-β receptor-I-kinase, galunisertib (*LY2157299*) has been shown to induce reductions in fibrosis in MPN murine models.[108] Monoclonal antibodies against LOL-2 (simtuzumab) have been tested either as monotherapy or in combination with ruxolitinib in a phase-II study with overall limited efficacy in MF,[109] despite the promising *in vitro* results. Hypomethylating agents such as azacitidine (5-Aza) and decitabine have been investigated in high-risk MF patients and accelerated/blastic phases of the disease. A combined clinical trial with ruxolitinib and 5-Aza is currently ongoing and recent published results have demonstrated marrow fibrosis reductions in 57% of the total cohort (31 cases) at 24 months in addition to acceptable spleen responses.[110] Further research is required to determinate the impact of these hypomethylating agents, with particular attention to the MPN marrow niche.

Therapeutic modulation of the neuro-HSC niche in MPN, introduced above, has recently been explored. Drexler *et al.* report on a phase II trial of an oral β-3 adrenergic agonist (mirabegron) in 39 patients, many of whom had a long duration of disease, with a *JAK2* V617F-mutated MPN who underwent treatment for up to six months. BM core analysis in 20 of the enrolled patients showed increases in Nestin$^+$ BMSC in a proportion of patients (but not in those also receiving hydroxycarbamide); several showed mild reductions in fibrosis and modulation of the characteristic megakaryocyte clustering.[111,112] Although the study end points of a >50% reduction in *JAK2* allelic burden or sustained reductions in splenomegaly were not reached, these intriguing data highlight the potential therapeutic avenues of targeting this neuro-HSC axis in MPN.

With regard to aberrant upregulation of cytokines in MPN, ruxolitinib and other JAKi have been shown to decrease levels of many pro-inflammatory cytokines, including both VEGF and PDGF, as discussed above.[69] The Myeloproliferative Disorders Research Consortium conducted a phase II trial of the anti-VEGF agent (bevacizumab) in 13 patients, 11 of whom were evaluable, to assess if a potential disease modification could be achieved. The dosing strategy was 15 mg/kg intravenously every 21 days; none of the patients demonstrated significant benefits. This lack of response coupled with toxicity led to the premature closure of the study; the authors commented that different dosing strategies may be required.[113] Other drugs have been developed to target VEGF-receptors, like the tyrosine kinase inhibitor vatalanib, but with modest results.[114] Lastly, control or regulation of the marrow hypoxia status could be a potential goal in the management of MPN in view of the key role of oxygen regulation pathways in the pathogenesis and maintenance of these disorders. HIF-1α is essential for HSC maintenance, as discussed. However, in the MPN environment, it participates in both angiogenesis and promotion of suppressor genes, aiding clonal cell adaptation to a hypoxic environment.[115,116] Therefore, targeting HIF1-α has been explored in recent years in both solid and non-solid cancers.[117] Bortezomib, a proteasome inhibitor extensively used in plasma cell dyscrasias, indirectly inhibits HIF-1α in MF patients as demonstrated by Barosi *et al.*[118] Although, to date, few published studies have focused on targeting hypoxia and HIF-pathways in MPN, it remains an attractive area of research.

Conclusions

As our knowledge expands, the complex and dynamic structure of the bone marrow niche in both health and disease is being constantly refined. It is apparent that, in MPN, the mutated-HSC disrupts the harmony of the bone marrow niche, promoting a self-reinforcing environment that facilities their proliferation at the expense of normal hematopoiesis. Furthermore, the MPN-niche can confer therapeutic resistance and potentiate disease progression towards blastic phase disease. Besides the potentially curative procedure of allogeneic stem cell transplantation, attempts to target various components of the MPN-niche have led to variable results and often a lack of sustained clinical benefit. Given the complexity, it is, therefore, increasingly apparent that combinatorial or sequenced therapeutic strategies will be required. As our appraisal of niche dysregulation grows, and we learn more from the current therapeutic trials discussed above, more rational niche-targeted treatment strategies will ultimately be developed.

References

1. Arber DA, Orazi A, Hasserjian R, et al. The 2016 revision to the World Health Organization classification of myeloid neoplasms and acute leukemia. Blood. 2016;127(20):2391-2406.
2. Moulard O, Mehta J, Fryzek J, Olivares R, Iqbal U, Mesa RA. Epidemiology of myelofibrosis, essential thrombocythemia, and polycythemia vera in the European Union. Eur J Haematol. 2014;92(4):289-297.
3. Szuber N, Vallapureddy RR, Penna D, et al. Myeloproliferative neoplasms in the young: Mayo Clinic experience with 361 patients age 40 years or younger. Am J Hematol. 2018;93(12):1474-1484.
4. Yogarajah M, Tefferi A. Leukemic Transformation in Myeloproliferative Neoplasms: A Literature Review on Risk, Characteristics, and Outcome. Mayo Clin Proc. 2017;92(7):1118-1128.
5. James C, Ugo V, Le Couédic JP, et al. A unique clonal JAK2 mutation leading to constitutive signalling causes polycythaemia vera. Nature. 2005;434(7037):1144-1148.
6. Levine RL, Wadleigh M, Cools J, et al. Activating mutation in the tyrosine kinase JAK2 in polycythemia vera, essential thrombocythemia, and myeloid metaplasia with myelofibrosis. Cancer Cell. 2005;7(4):387-397.
7. Kralovics R, Passamonti F, Buser AS, et al. A gain-of-function mutation of JAK2 in myeloproliferative disorders. N Engl J Med. 2005;352(17):1779-1790.
8. Baxter EJ, Scott LM, Campbell PJ, et al. Acquired mutation of the tyrosine kinase JAK2 in human myeloproliferative disorders. Lancet. 2005;365(9464):1054-1061.
9. Vainchenker W, Constantinescu SN, Plo I. Recent advances in understanding myelofibrosis and essential thrombocythemia. F1000Res. 2016;5.
10. Nangalia J, Massie CE, Baxter EJ, et al. Somatic CALR Mutations in Myeloproliferative Neoplasms with Nonmutated JAK2. N Engl J Med. 2013;369(25):2391-2405.
11. Klampfl T, Gisslinger H, Harutyunyan AS, et al. Somatic Mutations of Calreticulin in Myeloproliferative Neoplasms. N Engl J

Med. 2013;369(25):2379-2390.
12. Rumi E, Cazzola M. Diagnosis , riskstratification , and response evaluation in classical myeloproliferative neoplasms. Blood. 2017;129(6):680-693.
13. Shirane S, Araki M, Morishita S, et al. JAK2, CALR, and MPL mutation spectrum in Japanese patients with myeloproliferative neoplasms. Haematologica. 2015;100(2): e46-e48.
14. Ferreira Cristina S, Polo B, Lacerda JF. Somatic Mutations in Philadelphia Chromosome-Negative Myeloproliferative Neoplasms. Semin Hematol. 2018;55(4): 215-222.
15. Nangalia J, Green AR. Myeloproliferative neoplasms: from origins to outcomes. Blood. 2017;130(23):2475-2483.
16. Lord BI, Testa NG, Hendry JH. The relative spatial distributions of CFUs and CFUc in the normal mouse femur. Blood. 1975;46(1): 65-72.
17. Schofield R. The relationship between the spleen colony-forming cell and the haemopoietic stem cell. Blood Cells. 1978;4 (1-2):7-25.
18. Sugiyama T, Nagasawa T. Bone marrow niches for hematopoietic stem cells and immune cells. Inflamm Allergy Drug Targets. 2012;11(3):201-206.
19. Colaianni G, Sun L, Di Benedetto A, et al. Bone marrow oxytocin mediates the anabolic action of estrogen on the skeleton. J Biol Chem. 2012;287(34):29159-29167.
20. Nilsson SK, Johnston HM, Coverdale JA. Spatial localization of transplanted hemopoietic stem cells: inferences for the localization of stem cell niches. Blood. 2001;97(8): 2293-2299.
21. Lo Celso C, Fleming HE, Wu JW, et al. Live-animal tracking of individual haematopoietic stem/progenitor cells in their niche. Nature. 2009;457(7225):92-96.
22. Xie Y, Yin T, Wiegraebe W, et al. Detection of functional haematopoietic stem cell niche using real-time imaging. Nature. 2009;457 (7225):97-101.
23. Taichman RS. Blood and bone: Two tissues whose fates are intertwined to create the hematopoietic stem-cell niche. Blood. 2005;105(7):2631-2639.
24. Taichman RS, Emerson SG. Human osteoblasts support hematopoiesis through the production of granulocyte colony-stimulating factor. J Exp Med. 1994;179(5):1677-1682.
25. Taichman RS, Reilly MJ, Verma RS, et al. Augmented production of interleukin-6 by normal human osteoblasts in response to CD34+ hematopoietic bone marrow cells in vitro. Blood. 1997;89(4):1165-1172.
26. Galán-Díez M, Kousteni S. A bone marrow niche-derived molecular switch between osteogenesis and hematopoiesis. Genes Dev. 2018;32(5-6):324-326.
27. Calvi LM, Adams GB, Weibrecht KW, et al. Osteoblastic cells regulate the haematopoietic stem cell niche. Nature. 2003;425(6960): 841-846.
28. Zhang J, Niu C, Ye L, et al. Identification of the haematopoietic stem cell niche and control of the niche size. Nature. 2003;425 (6960):836-841.
29. Askmyr M, Sims NA, Martin TJ, Purton LE. What is the true nature of the osteoblastic hematopoietic stem cell niche? Trends Endocrinol Metab. 2009;20(6):303-309.
30. Méndez-Ferrer S, Lucas D, Battista M, Frenette PS. Haematopoietic stem cell release is regulated by circadian oscillations. Nature. 2008;452(7186):442-447.
31. Schmitt-Graeff AH, Nitschke R, Zeiser R. The hematopoietic niche in myeloproliferative neoplasms. Mediators Inflamm. 2015;2015:347270.
32. Yu VWC, Saez B, Cook C, et al. Specific bone cells produce DLL4 to generate thymus-seeding progenitors from bone marrow. J Exp Med. 2015;212(5):759-774.
33. Miyamoto T. Role of osteoclasts in regulating hematopoietic stem and progenitor cells. World J Orthop. 2013;4(4):198-206.
34. Kollet O, Dar A, Lapidot T. The Multiple Roles of Osteoclasts in Host Defense: Bone Remodeling and Hematopoietic Stem Cell Mobilization. Annu Rev Immunol. 2007;25:51-69.
35. Mansour A, Abou-Ezzi G, Sitnicka E, W. Jacobsen SE, Wakkach A, Blin-Wakkach C. Osteoclasts promote the formation of hematopoietic stem cell niches in the bone marrow. J Exp Med. 2012;209(3):537-549.
36. Miyamoto T. Regulators of osteoclast differentiation and cell-cell fusion. Keio J Med. 2011;60(4):101-105.
37. Li H, Hong S, Qian J, Zheng Y, Yang J, Yi Q. Cross talk between the bone and immune systems: osteoclasts function as antigen-presenting cells and activate CD4+ and CD8+ T cells. Blood. 2010;116(2):210-217.
38. Kobayashi H, Butler JM, O'Donnell R, et al. Angiocrine factors from Akt-activated endothelial cells balance self-renewal and differentiation of haematopoietic stem cells. Nat Cell Biol. 2010;12(11):1046-1056.
39. Winkler IG, Barbier V, Nowlan B, et al. Vascular niche E-selectin regulates hematopoietic stem cell dormancy, self renewal and chemoresistance. Nat Med. 2012;18(11):1651-1657.
40. Kunisaki Y, Bruns I, Scheiermann C, et al. Arteriolar niches maintain haematopoietic stem cell quiescence. Nature. 2013;502 (7473):637-643.
41. Nombela-Arrieta C, Pivarnik G, Winkel B, et al. Quantitative imaging of haematopoietic stem and progenitor cell localization and hypoxic status in the bone marrow microenvironment. Nat Cell Biol. 2013;15(5):533-543.
42. Boulais P, Frenette P. Making sense of hematopoietic stem cell niches. Blood. 2015;125(17):2621-2630.
43. García-García A, de Castillejo CLF, Méndez-Ferrer S. BMSCs and hematopoiesis. Immunol Lett. 2015;168(2):129-135.
44. Méndez-Ferrer S, Chow A, Merad M, Frenette PS. Circadian rhythms influence hematopoietic stem cells. Curr Opin Hematol. 2009;16(4):235-242.
45. Gattazzo F, Urciuolo A, Bonaldo P. Extracellular matrix: A dynamic microenvironment for stem cell niche. Biochim Biophys Acta. 2014;1840(8):2506-2519.
46. Mead AJ, Mullally A. Myeloproliferative neoplasm stem cells. Blood. 2017;129(12): 1607-1616.
47. Mullally A, Poveromo L, Schneider RK, Al-Shahrour F, Lane SW, Ebert BL. Distinct roles for long-term hematopoietic stem cells and erythroid precursor cells in a murine model of Jak2V617F-mediated polycythemia vera. Blood. 2012;120(1):166-172.
48. Lundberg P, Takizawa H, Kubovcakova L, et al. Myeloproliferative neoplasms can be initiated from a single hematopoietic stem cell expressing JAK2-V617F. J Exp Med. 2014;211(11):2213-2230.
49. Chen E, Schneider RK, Breyfogle LJ, et al. Distinct effects of concomitant Jak2V617F expression and Tet2 loss in mice promote disease progression in myeloproliferative neoplasms. Blood. 2015;125(2):327-335.
50. Schepers K, Pietras EM, Reynaud D, et al. Myeloproliferative neoplasia remodels the endosteal bone marrow niche into a self-reinforcing leukemic niche. Cell Stem Cell. 2013;13(3):285-299.
51. Kollet O, Vagima Y, D'Uva G, et al. Physiologic corticosterone oscillations regulate murine hematopoietic stem/progenitor cell proliferation and CXCL12 expression by bone marrow stromal progenitors. Leukemia. 2013;27(10):2006-2015.
52. Iwasaki H, Suda T. Hematopoietic stem cells and their niche. Cancer Science. 2009;100 (7):1166-1172.
53. Spanoudakis E, Papoutselis M, Bazdiara I, et al. The JAK2V617F point mutation increases the osteoclast forming ability of monocytes in patients with chronic myeloproliferative neoplasms and makes their osteoclasts more susceptible to JAK2 inhibition. Mediterr J Hematol Infect Dis. 2018;10(1):e2018058.
54. Korn C, Méndez-Ferrer S. Myeloid malignancies and the microenvironment. Blood. 2017;129(7):811-822.
55. Mitsumori T, Nozaki Y, Kawashima I, et al. Hypoxia inhibits JAK2V617F activation via suppression of SHP-2 function in myeloproliferative neoplasm cells. Exp Hematol. 2014;42(9):783-792.
56. Velasco-Hernandez T, Tornero D, Cammenga J. Loss of HIF-1α accelerates murine FLT-3 ITD-induced myeloproliferative neoplasia. Leukemia. 2015;29(12):2366-2374.
57. Schepers K, Campbell TB, Passegue E. Normal and Leukemic Stem Cell Niches: Insights and Therapeutic Opportunities. Cell Stem Cell. 2015;16(3):254-267.
58. Schneider RK, Mullally A, Dugourd A, et al. Gli1(+) Mesenchymal Stromal Cells Are a Key Driver of Bone Marrow Fibrosis and an Important Cellular Therapeutic Target. Cell Stem Cell. 2017;20(6):785-800.e8.
59. Ramos TL, Sánchez-Abarca LI, Rosón-Burgo B, et al. Mesenchymal stromal cells (MSC) from JAK2+ myeloproliferative neoplasms differ from normal MSC and contribute to the maintenance of neoplastic hematopoiesis. PLoS One. 2017;12(8): e0182470.
60. Arai F, Hirao A, Ohmura M, et al. Tie2/angiopoietin-1 signaling regulates hematopoietic stem cell quiescence in the bone marrow niche. Cell. 2004;118(2):149-161.
61. Arranz L, Sánchez-Aguilera A, Martín-Pérez D, et al. Neuropathy of haematopoietic stem cell niche is essential for myeloproliferative neoplasms. Nature. 2014;512(7512):78-81
62. Sánchez-Aguilera A, Arranz L, Martín-Pérez D, et al. Estrogen Signaling Selectively Induces Apoptosis of Hematopoietic Progenitors and Myeloid Neoplasms without Harming Steady-State Hematopoiesis. Cell Stem Cell. 2014;15(6):791-804.
63. Vannucchi AM, Bianchi L, Paoletti F, et al. A pathobiologic pathway linking thrombopoietin, GATA-1, and TGF-β1 in the development of myelofibrosis. Blood. 2005;105(9): 3493-3501.
64. Leiva O, Ng SK, Chitalia S, Balduini A, Matsuura S, Ravid K. The role of the extracellular matrix in primary myelofibrosis. Blood Cancer J. 2017;7(2):1-9.
65. Wang JC, Novetsky A, Chen C, Novetsky AD. Plasma matrix metalloproteinase and tissue inhibitor of metalloproteinase in patients with agnogenic myeloid metaplasia

or idiopathic primary myelofibrosis. Br J Haematol. 2002;119(3):709-712.
66. Liu GM, Zhang LJ, Fu JZ, et al. Regulation of Ruxolitinib on matrix metalloproteinase in JAK2V617F positive myeloroliferative neoplasms cells. Zhonghua Xue Ye Xue Za Zhi. 2017;38(2):140-145.
67. Tadmor T, Bejar J, Attias D, et al. The expression of lysyl-oxidase gene family members in myeloproliferative neoplasms. Am J Hematol. 2013;88(5):355-358.
68. McLornan DP, Yakoub-Agha I, Robin M, Chalandon Y, Harrison CN, Kroger N. State-of-the-art review: allogeneic stem cell transplantation for myelofibrosis in 2019. Haematologica. 2019;104(4):659-668.
69. Verstovsek S, Mesa RA, Gotlib J, et al. Long-term treatment with ruxolitinib for patients with myelofibrosis: 5-year update from the randomized, double-blind, placebo-controlled, phase 3 COMFORT-I trial. J Hematol Oncol. 2017;10(1):1-14.
70. Harrison CN, Vannucchi AM, Kiladjian JJ, et al. Long-term efficacy and safety in comfort-II, a phase 3 study comparing ruxolitinib with best available therapy for the treatment of myelofibrosis: 5-year final study results. Blood. 2015;126(23):59.
71. Verstovsek S, Vannucchi AM, Griesshammer M, et al. Ruxolitinib versus best available therapy in patients with polycythemia vera: 80-week follow-up from the RESPONSE trial. Haematologica. 2016;101(7):821-829.
72. Passamonti F, Griesshammer M, Palandri F, et al. Ruxolitinib for the treatment of inadequately controlled polycythaemia vera without splenomegaly (RESPONSE-2): a randomised, open-label, phase 3b study. Lancet Oncol. 2017;18(1):88-99.
73. Harrison CN, Mead AJ, Panchal A, et al. Ruxolitinib vs best available therapy for et intolerant or resistant to hydroxycarbamide. Blood. 2017;130(17):1889-1897.
74. Gunawan A, Harrington P, Garcia-Curto N, McLornan D, Radia D, Harrison C. Ruxolitinib for the Treatment of Essential Thrombocythemia. HemaSphere. 2018;2(4):e56.
75. Harrison CN, McLornan DP. Current treatment algorithm for the management of patients with myelofibrosis, JAK inhibitors, and beyond. Hematology Am Soc Hematol Educ Program. 2017;2017(1):489-497.
76. Bose P, Gotlib J, Harrison CN, Verstovsek S. SOHO State-of-the-Art Update and Next Questions: MPN. Clin Lymphoma, Myeloma Leuk. 2018;18(1):1-12.
77. Tremblay D, Mascarenhas J. Pacritinib to treat myelofibrosis patients with thrombocytopenia. Expert Rev Hematol. 2018;11(9):707-714.
78. Harrington PM, Harrison CN. Beyond JAK-2: potential targets for myeloproliferative neoplasm therapy. Expert Rev Hematol. 2018;11(4):315-324.
79. Kremyanskaya M, Hoffman R, Mascarenhas J, et al. A Phase 2 Study of Cpi-0610, a Bromodomain and Extraterminal (BET) Inhibitor, in Patients with Myelofibrosis (MF). Blood. 2018;132(Suppl 1):5481.
80. Quintás-Cardama A, Kantarjian H, Estrov Z, Borthakur G, Cortes J, Verstovsek S. Therapy with the histone deacetylase inhibitor pracinostat for patients with myelofibrosis. Leuk Res. 2012;36(9):1124-1127.
81. DeAngelo DJ, Tefferi A, Fiskus W, et al. A phase II trial of panobinostat, an orally available deacetylase inhibitor (DACi), in patients with primary myelofibrosis (PMF), post essential thrombocythemia (ET), and post polycythemia vera (PV) myelofibrosis. Blood. 2010;116(21):630.
82. Mesa RA, Vannucchi AM, Mead A, et al. Pacritinib versus best available therapy for the treatment of myelofibrosis irrespective of baseline cytopenias (PERSIST-1): an international, randomised, phase 3 trial. Lancet Haematol. 2017;4(5):e225-e236.
83. Mascarenhas J, Hoffman R, Talpaz M, et al. Pacritinib vs best available therapy, including ruxolitinib, in patients with myelofibrosis: A randomized clinical trial. JAMA Oncol. 2018;4(5):652-659.
84. Mesa RA, Kiladjian JJ, Catalano JV, et al. Simplify-1: A phase III randomized trial of momelotinib versus ruxolitinib in janus kinase inhibitor–naïve patients with myelofibrosis. J Clin Oncol. 2017;35(34):3844-3850.
85. Harrison CN, Vannucchi AM, Platzbecker U, et al. Momelotinib versus best available therapy in patients with myelofibrosis previously treated with ruxolitinib (SIMPLIFY 2): a randomised, open-label, phase 3 trial. Lancet Haematol. 2018;5(2):e73-e81.
86. Pardanani A, Harrison C, Cortes JE, et al. Safety and efficacy of fedratinib in patients with primary or secondary myelofibrosis: A randomized clinical trial. JAMA Oncol. 2015;1(5):643-651.
87. Harrison CN, Schaap N, Vannucchi AM, et al. Janus kinase-2 inhibitor fedratinib in patients with myelofibrosis previously treated with ruxolitinib (JAKARTA-2): a single-arm, open-label, non-randomised, phase 2, multicentre study. Lancet Haematol. 2017;4(7):e317-e324.
88. Harrison CN, Mesa RA, Jamieson C, et al. Case series of potential wernicke's encephalopathy in patients treated with fedratinib. Blood. 2017;130(Suppl 1):4197.
89. Valentin R, Grabow S, Davids MS. The rise of apoptosis: Targeting apoptosis in hematologic malignancies. Blood. 2018;132(12):1248-1264.
90. McArthur K, Chappaz S, Kile BT. Apoptosis in megakaryocytes and platelets: the life and death of a lineage. Blood. 2018;131(6):605-610.
91. Baerlocher GM, Oppliger Leibundgut E, Ottmann OG, et al. Telomerase Inhibitor Imetelstat in Patients with Essential Thrombocythemia. N Engl J Med. 2015;373(10):920-928.
92. Tefferi A, Lasho TL, Begna KH, et al. A Pilot Study of the Telomerase Inhibitor Imetelstat for Myelofibrosis. N Engl J Med. 2015;373(10):908-919.
93. Mascarenhas J, Komrokji RS, Cavo M, et al. Imetelstat Is Effective Treatment for Patients with Intermediate-2 or High-Risk Myelofibrosis Who Have Relapsed on or Are Refractory to Janus Kinase Inhibitor Therapy: Results of a Phase 2 Randomized Study of Two Dose Levels. Blood. 2018;132(Suppl 1):685.
94. Kuykendall A, Wan Y, Mascarenhas J, et al. Favorable overall survival of imetelstat-treated relapsed/refractory myelofibrosis patients compared with closely matched real world data: PS1456. HemaSphere. 2019;3:669-670.
95. Mascarenhas J, Lu M, Kosiorek H, et al. Oral Idasanutlin in Patients with Polycythemia Vera. Blood. 2019;134(6):525-533.
96. Lu M, Xia L, Salama ME, Hoffman R. Combination Treatment with an MDM2 Antagonist and a BET Inhibitor Targets Both Myelofibrosis Hematopoietic Stem/Progenitor Cells and Their Tumor Promoting Microenvironment. Blood. 2017;130(Suppl 1):4225.
97. Kvasnicka HM, Thiele J, Bueso-Ramos CE, et al. Ruxolitinib-Induced Modulation of Bone Marrow Microenvironment in Patients with Myelofibrosis Is Associated with Inflammatory Cytokine Levels. Blood. 2014;124(21):3182.
98. Hasserjian RP, Gotlib J, Cortes JE, et al. Effect Of Treatment With The JAK2-Selective Inhibitor Fedratinib (SAR302503) On Bone Marrow Histology In Patients With Myeloproliferative Neoplasms With Myelofibrosis. Jamieson CHM, ed. Blood. 2013;122(21):2823.
99. Jamieson C, Hasserjian R, Gotlib J, et al. Effect of treatment with a JAK2-selective inhibitor, fedratinib, on bone marrow fibrosis in patients with myelofibrosis. J Transl Med. 2015;13(1):294.
100. Verstovsek S, Mesa RA, Foltz LM, et al. PRM-151 in Myelofibrosis: Durable Efficacy and Safety at 72 Weeks. Blood. 2015;126(23):56.
101. Verstovsek S, Hasserjian RP, Pozdnyakova O, et al. PRM-151 in Myelofibrosis: Efficacy and Safety in an Open Label Extension Study. Blood. 2018;132(Suppl 1):686.
102. Verstovsek S, Talpaz M, Wadleigh M, et al. A randomized, double blind phase 2 study of 3 different doses of prm-151 in patients with myelofibrosis who were previously treated with or ineligible for ruxolitinib: S828. HemaSphere. 2019;3(S1):S829.
103. Tibes R, Mesa RA. Targeting hedgehog signaling in myelofibrosis and other hematologic malignancies. J Hematol Oncol. 2014.
104. Sasaki K, Gotlib JR, Mesa RA, et al. Phase II evaluation of IPI-926, an oral Hedgehog inhibitor, in patients with myelofibrosis. Leuk Lymphoma. 2015;56(7):2092-2097.
105. Gupta V, Koschmieder S, Harrison CN, et al. Phase 1b Dose-Escalation Study of Sonidegib (LDE225) in Combination with Ruxolitinib (INC424) in Patients with Myelofibrosis. Blood. 2014;124(21):712.
106. Mesa RA, Tefferi A, Elliott MA, et al. A phase II trial of pirfenidone (5-methyl-1-phenyl-2-[1H]-pyridone), a novel anti-fibrosing agent, in myelofibrosis with myeloid metaplasia. Br J Haematol. 2001;114(1):111-113.
107. Mascarenhas J, Li T, Sandy L, et al. Anti-transforming growth factor-β therapy in patients with myelofibrosis. Leuk Lymphoma. 2014;55(2):450-452.
108. Yue L, Bartenstein M, Zhao W, et al. Preclinical Efficacy of TGF-Beta Receptor I Kinase Inhibitor, Galunisertib, in Myelofibrosis. Blood. 2015;126(23):603.
109. Verstovsek S, Savona MR, Mesa RA, et al. A phase 2 study of simtuzumab in patients with primary, post-polycythaemia vera or post-essential thrombocythaemia myelofibrosis. Br J Haematol. 2017;176(6):939-949.
110. Masarova L, Verstovsek S, Hidalgo-Lopez JE, et al. A phase 2 study of ruxolitinib in combination with azacitidine in patients with myelofibrosis. Blood. 2018;132(16):1664-1674.
111. Herlihy N, Harrison CN, McLornan DP. Exploitation of the neural-hematopoietic stem cell niche axis to treat myeloproliferative neoplasms. Haematologica. 2019;104(4):639-641.
112. Drexler B, Passweg JR, Tzankov A, et al. The sympathomimetic agonist mirabegron did not lower JAK2-V617F allele burden, but restored nestin-positive cells and reduced reticulin fibrosis in patients with myelopro-

liferative neoplasms: results of phase II study SAKK 33/14. Haematologica. 2019;104(4):710-716.
113. Mesa RA, Silver RT, Verstovsek S, et al. Single agent bevacizumab for myelofibrosis: Results of the myeloproliferative disorders research consortium trial. Haematologica. 2013;98(9):1421-1423.
114. Giles FJ, List AF, Carroll M, et al. PTK787/ZK 222584, a small molecule tyrosine kinase receptor inhibitor of vascular endothelial growth factor (VEGF), has modest activity in myelofibrosis with myeloid metaplasia. Leuk Res. 2007;31(7):891-897.
115. Hermouet S, Bigot-Corbel E, Gardie B. Pathogenesis of Myeloproliferative Neoplasms: Role and Mechanisms of Chronic Inflammation. Mediators Inflamm. 2015;2015:145293.
116. Baumeister J, Chatain N, Hubrich A, et al. Implication of Hypoxia-Inducible Factor-1 (HIF-1) As a New Therapeutic Target in JAK2-V617F Positive Myeloproliferative Neoplasms (MPN). Blood. 2018;132(Suppl 1):4318.
117. Xia Y, Choi H-K, Lee K. Recent advances in hypoxia-inducible factor (HIF)-1 inhibitors. Eur J Med Chem. 2012;49:24-40.
118. Barosi G, Gattoni E, Guglielmelli P, et al. Phase I/II study of single-agent bortezomib for the treatment of patients with myelofibrosis. Clinical and biological effects of proteasome inhibition. Am J Hematol. 2010;85 (8):616-619.
119. Mascarenhas J, Sandy L, Lu M, et al. A phase II study of panobinostat in patients with primary myelofibrosis (PMF) and post-polycythemia vera/essential thrombocythemia myelofibrosis (post-PV/ET MF). Leuk Res. 2017;53:13-19.
120. Kleppe M, Koche R, Zou L, et al. Dual Targeting of Oncogenic Activation and Inflammatory Signaling Increases Therapeutic Efficacy in Myeloproliferative Neoplasms. Cancer Cell. 2018;33(1):29-43.e7.
121. Mascarenhas J, Navada S, Malone A, Rodriguez A, Najfeld V, Hoffman R. Therapeutic options for patients with myelofibrosis in blast phase. Leuk Res. 2010;34(9):1246-1249.

The never ending success story of tranexamic acid in acquired bleeding

Massimo Franchini[1] and Pier Mannuccio Mannucci[2]

[1]Department of Transfusion Medicine and Hematology, Carlo Poma Hospital, Mantova and [2]Fondazione IRCCS Ca' Granda Ospedale Maggiore Policlinico, Angelo Bianchi Bonomi Hemophilia and Thrombosis Center, Milan, Italy

Ferrata Storti Foundation

Haematologica 2020
Volume 105(5):1201-1205

ABSTRACT

Tranexamic acid (TXA) is an anti-fibrinolytic agent that acts by inhibiting plasminogen activation and fibrinolysis. Although its first clinical use dates back more than 50 years, this hemostatic agent is still the object of intense clinical and developmental research. In particular, renewed interest in TXA has arisen following evidence that it has a beneficial effect in reducing blood loss in a variety of medical and surgical conditions at increased risk of bleeding. Given this characteristic, TXA is currently considered a mainstay of Patient Blood Management programs aimed at reducing patients' exposure to allogeneic blood transfusion. Importantly, recent large randomized controlled trials have consistently documented that the use of TXA confers a survival advantage in a number of globally critical clinical conditions associated with acute bleeding, including traumatic injury and post-partum hemorrhage, without increasing the thromboembolic risk.

Introduction

Tranexamic acid (TXA) is a synthetic anti-fibrinolytic amino acid derivative of lysine that acts by competitively blocking the lysine binding sites on plasminogen, thereby inhibiting its interaction with formed plasmin and fibrin.[1,2] Inhibition of plasminogen activation results in the stabilization of the preformed fibrin meshwork produced by the coagulation cascade. Thanks to its ability to inhibit fibrinolysis and clot degradation TXA, which is approved for intravenous, oral and topical applications, has been successfully employed to prevent or decrease blood loss in a variety of clinical conditions characterized by excessive bleeding.[3,4] There is indeed consistent evidence that the early administration of TXA confers a survival benefit in the setting of severe trauma[5,6] and post-partum hemorrhage without an increase in thromboembolic events.[7] In addition, this agent has been successfully used to decrease blood loss in numerous surgical specialties, especially in the frame of cardiac and major orthopedic surgery.[8-11] For this reason, TXA is currently considered a fundamental pillar of the Patient Blood Management (PBM) programs of transfusion medicine, aimed at minimizing blood loss and thus exposure of patients undergoing elective surgery to allogeneic blood.[12-14] In this narrative review we summarize the most recent clinical evidence on the use of TXA for prevention or treatment of bleeding.

Search methods

We analyzed the medical literature for published articles on the use of TXA for bleeding. The MEDLINE electronic database was searched for publications during the last 20 years using English language as a restriction. The Medical Subject Heading and key words used were: "tranexamic acid", "bleeding", "hemorrhage", "treatment", "prevention", "patient blood management", "anti-fibrinolytic", "surgery", "cardiac surgery", "orthopedic surgery", "post-partum hemorrhage", "obstetric", "trauma", "injury" and "traumatic brain injury". We also screened the reference lists of the most relevant review articles for additional studies not captured in our initial literature search. Finally, abstracts from relevant conferences or scientific meetings were hand-searched for additional studies.

Correspondence:

PIER MANNUCCIO MANNUCCI
piermannuccio.mannucci@policlinico.mi.it

Received: March 3, 2020.

Accepted: March 16, 2020.

Pre-published: March 26, 2020.

doi:10.3324/haematol.2020.250720

Check the online version for the most updated information on this article, online supplements, and information on authorship & disclosures: www.haematologica.org/content/105/5/1201

Tranexamic acid for the prevention of bleeding

There is a growing body of evidence documenting the efficacy of TXA in preventing bleeding in a variety of major surgical procedures, especially cardiac surgery, in the frame of PBM programs.[8,13] In a systematic review and meta-analysis, TXA was shown to reduce blood losses in surgical patients by nearly one-third compared to placebo.[15] These results were consistent with those of a Cochrane systematic review, including 129 trials with 10,488 participants, which showed that TXA reduced the probability of receiving a blood transfusion by one third [relative risk (RR) 0.62, 95% confidence interval (95% CI): 0.58-0.65; $P<0.001$).[9] More recently, TXA has been widely used to minimize bleeding and exposure to allogeneic blood transfusion in major orthopedic surgery. Several large randomized controlled trials (RCT) and meta-analyses have consistently confirmed that the intravenous administration of this medication effectively and safely reduces perioperative blood loss and transfusion requirements at the time of major orthopedic operations such as total hip and knee arthroplasty.[10] Some concerns still remained among users over the hypothetical increased risk of thromboembolic complications following the systemic infusion of this anti-fibrinolytic agent, because orthopedic surgery is associated not only with a high risk of bleeding but also of thrombosis. Thus, to refute this unjustified, non-evidence-based perception which represents the main obstacle to a broader use of TXA in this clinical context, we recently conducted a systematic review and meta-analysis of the literature aimed at assessing the safety of intravenous TXA in patients undergoing major orthopedic surgery.[16] After a meta-analytic pooling of 73 RCT involving 4,174 patients and 2,779 controls, there was a similar incidence of venous thromboembolism in patients and controls (2.1% *vs.* 2.0%), which established the safety of this pharmacological treatment in a PBM setting.[16] In addition, a recent systematic review and meta-analysis of five RCT involving 457 patients undergoing total hip arthroplasty concluded that the combined use of intravenous and topical TXA is more effective than intravenous TXA alone in terms of reduction of blood loss, hemoglobin decline and need for transfusion without increasing the rate of thromboembolic complications.[17] The recently published Recommendations for the implementation of PBM programs in orthopedic surgery, edited by the Italian National Blood Center in collaboration with several scientific societies, supported the preoperative and/or postoperative use of TXA in total hip and knee replacement surgery (grade 2A recommendation).[18]

Given the efficacy of TXA in various conditions at potential risk of severe bleeding, several groups also evaluated its use in preventing obstetric hemorrhage.[19,20] Postpartum hemorrhage (PPH) is a leading cause of premature maternal mortality globally, accounting for at least 100,000 deaths each year worldwide.[21] A Cochrane systematic review that evaluated TXA in the prevention of PPH was recently published. In the frame of an analysis of 12 RCT involving 3,285 women, TXA decreased postpartum blood loss, prevented PPH and lowered blood transfusion requirements.[22] We have recently conducted a systematic review and meta-analysis on the use of TXA for PPH prevention in women undergoing Cesarean delivery.[23] After an in-depth analysis of 18 RCT involving 4,557 women, it was found that prophylactic use of TXA significantly reduced the incidence of PPH, total blood loss and transfusion requirements without increasing the risk of thromboembolic complications, thus supporting its beneficial effect in this critical clinical setting. Accordingly, the most recent multidisciplinary consensus statement on prevention and treatment of PPH from the Network for the Advancement of Patient Blood Management, Haemostasis and Thrombosis (NATA) recommends intravenous of TXA for women at increased risk of PPH (grade 1C recommendation).[19]

On the whole, these multiple and consistent findings show that TXA is effective at preventing bleeding complications in a variety of medical and surgical conditions without increasing the risk of thrombosis.

Tranexamic acid in acute bleeding conditions

In addition to the preventive use of TXA, a number of studies have investigated the role of this anti-fibrinolytic agent in patients presenting with acute, critical bleeding.[5,6,24-26] In trauma patients, the largest body of evidence stems from the Clinical Randomisation of an Antifibrinolytic in Significant Haemorrhage (CRASH) trials. In the CRASH-2 trial, 20,211 severely injured adults with confirmed or suspected hemorrhage were randomly assigned within 8 h from the occurrence of trauma to receive TXA (loading bolus dose of 1 g and then an infusion of 1 g over 8 h) or placebo.[27] Despite no difference in bleeding rate and transfusion use, all-cause mortality was lower in the treatment group than in the placebo group (14.5% *vs.* 16%, respectively; RR 0.91; 95% CI: 0.85–0.97, $P=0.0035$). Similarly, the rate of deaths attributed to bleeding was reduced from 5.7% to 4.9% ($P=0.0077$) (Table 1). Yet, from a sub-analysis of CRASH-2, the timing of TXA administration was crucial for patients' outcomes.[28] Early infusion of TXA within 1 h after trauma was associated with the largest survival benefit (absolute reduction = 2.4%, number needed to treat = 41). TXA infused between 1 and 3 h also reduced the risk of death due to bleeding (absolute reduction = 1.3%, number needed to treat = 77), but a later administration (>3 h after trauma) was associated with an increased risk of death from bleeding compared with the risk among patients receiving placebo (RR 1.44, 95% CI: 1.12–1.84; $P=0.004$).[28] There was no evidence that TXA increased the risk of vascular occlusive events and, in a pre-specified analysis of the data collected when TXA was given within 3 h of injury, there was even a reduction in the odds of fatal and non-fatal vascular occlusive events (odds ratio = 0.69, 95% CI: 0.53-0.89; $P=0.005$).[29] Following the publication of this study, the World Health Organization (WHO) included TXA in their list of essential medicines (available at: *http://www.who.int/selection_medicines/committees/expert/18/applications/tranexamic/en*). Since this seminal study, a number of randomized clinical trials, systematic reviews and meta-analyses on the efficacy of anti-fibrinolytic agents have been published. The Cochrane systematic review regarding anti-fibrinolytic drugs for acute traumatic injury found that, after the analysis of four trials involving 20,548 patients, TXA reduced the risk of death by 10% (RR 0.90, 95% CI: 0.85-0.96; $P=0.002$) without increasing the risk of adverse events.[30]

TXA has also been extensively studied in the setting of

Table 1. Main results of randomized clinical trials assessing the use of tranexamic acid for acute bleeding.

Trial	Study design	Patients enrolled	Main results
CRASH-2[27-29]	Trauma patients with or at risk of hemorrhage randomized to receive TXA or placebo	20,211 patients (10,096 in TXA group and 10,115 in placebo group)	Reduction of any cause of death in TXA group *versus* placebo group (RR=0.91, 95% CI: 0.85-0.97, *P*=0.0035); reduction of bleeding-related deaths in TXA group *versus* placebo group (RR=0.85, 95% CI: 0.76-0.96, *P*=0.0077); largest reduction when TXA was administered within 1 h after trauma (RR=0.68, 95% CI: 0.57-0.82, *P*<0.0001)
CRASH-3[33]	Patients with traumatic brain injury (< 3 h) randomized to receive TXA or placebo	12,737 patients (6406 in TXA group and 6331 in placebo group)	Reduction of the risk of head injury-related death in patients with mild-to-moderate head injury receiving TXA (RR 0.78, 95% CI 0.64-0.95); early TXA treatment was more effective than later TXA treatment in patients with mild and moderate head injury (*P*=0.005)
WOMAN[38]	Women with post-partum hemorrhage randomized to receive TXA or placebo	20,060 women (10,051 in TXA group and 10,009 in placebo group)	Reduction of deaths due to bleeding in women given TXA (RR=0.81, 95% CI: 0.65-1.00; *P*=0.045), especially in women given treatment within 3 h of giving birth (RR=0.69, 95% CI: 0.52-0.91; *P*=0.008)

TXA, tranexamic acid; RR, relative risk; CI, confidence interval.

traumatic brain injury, a leading cause of trauma deaths often associated with alterations of hemostasis with the features of hyperfibrinolysis.[24,31] Meta-analysis of two randomized trials examining the effect of TXA on outcomes following traumatic brain injury showed a significant reduction in the progression of intracranial hemorrhage.[32] The results of the CRASH-3 trial were published recently.[33] This trial included 12,737 patients who had isolated acute traumatic brain injury (which occurred within 3 h of random assignment to receive TXA (loading dose 1 g over 10 minutes ,then infusion of 1 g over 8 h) or placebo. TXA failed to reduce the primary endpoint, i.e. the risk of head injury-related death. However, after the exclusion of patients too severe to be saved, namely those with a Glasgow Coma Scale score of 3 or unreactive bilateral pupils at baseline, TXA reduced the risk of head injury-related deaths compared to placebo (12.5% *vs.* 14.0%; RR 0.89, 95% CI: 0.80–1.00). In particular, TXA decreased the risk of injury-related deaths in patients with mild-to-moderate head injury (RR 0.78, 95% CI: 0.64–0.95) but not in those with severe head injury (Table 1). As in CRASH-2, early treatment was more effective than more delayed treatment in patients with mild and moderate head injury (*P*=0.005), with a 10% decrease in treatment effectiveness for every 20 min delay. The risk of vascular occlusive events was similar in the TXA and placebo groups.[33] Notably, the CRASH-3 trial was the first RCT to show that a drug has neuroprotective properties for patients with traumatic brain injury and even reduced mortality. Finally, a very recently published meta-analysis of six RCT on the effect of TXA, compared with placebo, on traumatic brain injury showed that this medication was associated with a reduced mortality (RR 0.91, 95% CI: 0.85-0.97; *P*=0.0004).[34]

Very recent evidence also indicates that TXA usage results in a significant reduction of obstetric bleeding.[35-37] In the landmark randomized, double blind World Maternal Antifibrinolytic (WOMAN) trial, more than 20,000 women with PPH following vaginal or Cesarean delivery were assigned to receive either TXA (1 g TXA intravenously as soon as possible, followed by a further 1 g if bleeding continued after 30 min or restarted within 24 h of the initial dose) or placebo.[38] The trial showed a decreased overall mortality due to bleeding in the TXA group (RR 0.81, 95% CI: 0.65-1.00; *P*=0.045) (Table 1), and no differences in venous or arterial thromboembolic events were observed between women in the two arms. Similarly to the CRASH trials, in the WOMAN trial patients receiving TXA within 3 h from delivery had the most marked mortality reduction (89 deaths in the TXA group *vs*. 127 deaths in the placebo group, RR 0.69, 95% CI: 0.52-0.91; *P*=0.008).[38] Thanks to the results of this global trial, a 2017 World Health Organization recommendation for the treatment of PPH states that TXA should be recognized as a life-saving intervention and thus made readily available for the management of PPH in settings in which emergency obstetric care is provided, regardless of the level of healthcare system resources.[39] In addition, the recent NATA consensus statement recommends the administration of TXA (1 g by intravenous route) as soon as possible within the first 3 h after PPH onset, with this dose repeated after 30 min if bleeding continues (grade 1B recommendation).[19]

All in all, these large trials document with unequivocal evidence the beneficial effect of early administration of TXA in an array of patients with acute critical bleeding, without increasing the risk of adverse events.[40,41]

Conclusions

Although TXA has been known for more than 50 years, its successful use never ceases to amaze us. The incredible current interest in this old drug is demonstrated by the increasing number of PubMed citations (589 in 2019) and by the high number of trials listed at *clinicaltrials.gov* (432 at the time of writing). The current evidence in the literature documents the efficacy and safety of TXA in preventing bleeding in a variety of at-risk conditions and thanks to this effect TXA is nowadays an essential drug in the therapeutic armamentarium of PBM-based protocols developed by the majority of hospitals worldwide with the aim of minimizing patients' exposure to allogeneic blood.[42]

The most recently published data show unequivocally that TXA also plays a prominent role in the management of critical bleeding. Indeed, considering the results of the CRASH-2, CRASH-3 and WOMAN trials (remarkably, CRASH-2 and CRASH-3 trials were truly independent research, not funded by pharmaceutical companies), more than 50,000 bleeding patients have been investigated so far for the hemostatic effect of TXA. Although

with different designs, the results of these trials are very similar and clear: TXA is effective in reducing the risk of death due to bleeding regardless of the cause. Furthermore, all these three trials identified early administration of the drug as a crucial issue for improving patients' outcome.

Additional striking evidence of the beneficial effect of TXA in acute trauma patients comes from the increasing use of this agent in the military setting.[6] Indeed, the positive results of the CRASH-2 trial, conducted in civilian trauma populations, triggered a series of studies evaluating TXA in combat trauma patients.[5] The largest trial was the retrospective observational Military Application of Tranexamic Acid in Trauma Emergency Resuscitation study (MATTERs),[43] which evaluated TXA in subjects with combat-related injury and found that the addition of this anti-fibrinolytic agent to blood component-based resuscitation resulted in a survival improvement, particularly in patients requiring massive transfusion. Thus, on the basis of the findings from the previously mentioned trials, early administration (within 3 h of injury) of TXA is now globally incorporated as an essential therapeutic strategy in the majority of resuscitation protocols, not only in civilian but also in military trauma centers.

Finally, we would like to outline the safety aspects that emerge from an overall analysis of the various RCT. The risk of thromboembolic events – including pulmonary embolism, deep-vein thrombosis, myocardial infarction and stroke – did not differ between the TXA and placebo groups. These data provide definitive strong evidence demonstrating the safety of TXA and render any residual concern unjustified.

References

1. Mannucci PM. Hemostatic drugs. N Engl J Med. 1998;339(4):245-253.
2. Franchini M, Mannucci PM. Adjunct agents for bleeding. Curr Opin Hematol. 2014;21(6):503-508.
3. Schulman S. Pharmacologic tools to reduce bleeding in surgery. Hematology Am Soc Hematol Educ Program. 2012;2012:517-521.
4. Cai J, Ribkoff J, Olson S, et al. The many roles of tranexamic acid: an overview of the clinical indications for TXA in medical and surgical patients. Eur J Haematol. 2020; 104(2):79-87.
5. Ramirez RJ, Spinella PC, Bochicchio GV. Tranexamic acid update in trauma. Crit Care Clin. 2017;33(1):85-99.
6. Lier H, Maegele M, Shander A. Tranexamic acid for acute hemorrhage: a narrative review of landmark studies and a critical reappraisal of its use over the last decade. Anesth Analg. 2019;129(6):1574-1584.
7. Hibbs SP, Roberts I, Shakur-Still H, Hunt BJ. Post-partum haemorrhage and tranexamic acid: a global issue. Br J Haematol. 2018;180(6):799-807.
8. Gerstein NS, Brierley JK, Windsor J, et al. Antifibrinolytic agents in cardiac and non-cardiac surgery: a comprehensive overview and update. J Cardiothorac Vasc Anesth. 2017;31(6):2183-2205.
9. Henry DA, Carless PA, Moxey AJ, et al. Anti-fibrinolytic use for minimising perioperative allogeneic blood transfusion. Cochrane Database Syst Rev. 2011;(3): CD001886.
10. Jiang X, Ma XL, Ma JX. Efficiency and safety of intravenous tranexamic acid in simultaneous bilateral total knee arthroplasty: a systematic review and meta-analysis. Orthop Surg. 2016;8(3):285-293.
11. Lin ZX, Woolf SK. Safety, efficacy, and cost-effectiveness of tranexamic acid in orthopedic surgery. Orthopedics. 2016;39(2):119-130.
12. Franchini M, Muñoz M. Towards the implementation of patient blood management across Europe. Blood Transfus. 2017;15(4):292-293.
13. Franchini M, Liumbruno GM. The key role of tranexamic acid in Patient Blood Management programmes. Blood Transfus. 2018;16(6):471-472.
14. Franchini M, Marano G, Veropalumbo E, et al. Patient Blood Management: a revolutionary approach to transfusion medicine. Blood Transfus. 2019;17(3):191-195.
15. Ker K, Prieto-Merino D, Roberts I. Systematic review, meta-analysis and meta-regression of the effect of tranexamic acid on surgical blood loss. Br J Surg. 2013;100(10):1271-1279.
16. Franchini M, Mengoli C, Marietta M, et al. Safety of intravenous tranexamic acid in patients undergoing major orthopaedic surgery: a meta-analysis of randomised controlled trials. Blood Transfus. 2018;16(1):36-43.
17. Sun Y, Jiang C, Li Q. A systematic review and meta-analysis comparing combined intravenous and topical tranexamic acid with intravenous administration alone in THA. PLoS One. 2017;12(10):e0186174.
18. Vaglio S, Prisco D, Biancofiore G, et al. Recommendations for the implementation of a Patient Blood Management programme. Application to elective major orthopaedic surgery in adults. Blood Transfus. 2016;14(1):23-65.
19. Muñoz M, Stensballe J, Ducloy-Bouthors AS, et al. Patient blood management in obstetrics: prevention and treatment of postpartum haemorrhage – NATA consensus statement. Blood Transfus. 2019;17 (2):112-136.
20. Franchini M, Liumbruno GM. Implementation of a patient blood management programme in obstetrics: let's do it! Blood Transfus. 2019;17(2):87-88.
21. Kassebaum NJ, Bertozzi-Villa A, Coggeshall MS, et al. Global, regional, and national levels and causes of maternal mortality during 1990–2013: a systematic analysis for the Global Burden of Disease Study 2013. Lancet. 2014;384(9947):980-1004.
22. Novikova N, Hofmeyr GJ, Cluver C. Tranexamic acid for preventing postpartum haemorrhage. Cochrane Database Syst Rev. 2015;6(6):CD007872.
23. Franchini M, Mengoli C, Cruciani M, et al. Safety and efficacy of tranexamic acid for prevention of obstetric haemorrhage: an updated systematic review and meta-analysis. Blood Transfus. 2018;16(4):329-337.
24. Gall LS, Davenport RA. Fibrinolysis and antifibrinolytic treatment in the trauma patient. Curr Opin Anesthesiol. 2018;31: 227-233.
25. Godier A, Roquet F, Hamada SR. Tranexamic acid: one more step towards its widespread use. Anaesth Crit Care Pain Med. 2020;39(1):15-17.
26. Roberts I. Tranexamic acid in trauma: how should we use it?. J Thromb Haemost. 2015;13(Suppl. 1):S195-S199.
27. Shakur H, Roberts I, Bautista R, et al. Effects of tranexamic acid on death, vascular occlusive events, and blood transfusion in trauma patients with significant haemorrhage (CRASH-2): a randomised, placebo-controlled trial. Lancet. 2010;376(9734):23-32.
28. Roberts I, Shakur H, Afolabi A, et al. CRASH-2 collaborators. The importance of early treatment with tranexamic acid in bleeding trauma patients: an exploratory analysis of the CRASH-2 randomised controlled trial. Lancet. 2011;377(9771):1096-1101.
29. Roberts I, Perel P, Prieto-Merino D, et al. CRASH-2 Collaborators. Effect of tranexamic acid on mortality in patients with traumatic bleeding: prespecified analysis of data from randomised controlled trial. BMJ. 2012;345:e5839.
30. Ker K, Roberts I, Shakur H, Coats TJ. Antifibrinolytic drugs for acute traumatic injury. Cochrane Database Syst Rev. 2015;5:CD004896.
31. Maegele M, Schochl H, Menovsky T, et al. Coagulopathy and haemorrhagic progression in traumatic brain injury: advances in mechanisms, diagnosis, and management. Lancet Neurol. 2017;16(8):630-647.
32. Zehtabchi S, Abdel Baki SG, Falzon L, Nishijima DK. Tranexamic acid for traumatic brain injury: a systematic review and meta-analysis. Am J Emerg Med. 2014;32(12):1503-1509.
33. CRASH-3 trial, collaborators. Effects of tranexamic acid on death, disability, vascular occlusive events and other morbidities in patients with acute traumatic brain injury (CRASH-3): a randomised, placebo-

controlled, trial. Lancet. 2019;394(102210): 1713-1723.
34. Chen H, Chen M. The efficacy of tranexamic acid for brain injury: a meta-analysis of randomized controlled trials. Am J Emerg Med. 2020 Oct 14. [Epub ahead of print]
35. Ducloy-Bouthors AS, Jude B, et al. EXADELI Study Group. High-dose tranexamic acid reduces blood loss in postpartum haemorrhage. Crit Care. 2011;15(2):R117.
36. Gayet-Ageron A, Prieto-Merino D, Ker K, Shakur H, Ageron FX, Roberts I. Antifibrinolytic Trials Collaboration. Effect of treatment delay on the effectiveness and safety of antifibrinolytics in acute severe haemorrhage: a meta-analysis of individual patient-level data from 40 138 bleeding patients. Lancet. 2018;391(10116):125-132
37. Alam A, Choi S. Prophylactic use of tranexamic acid for postpartum bleeding outcomes: a systematic review and meta-analysis of randomized controlled trials. Transfus Med Rev. 2015;29(4):231-241.
38. WOMAN Trial Collaborators. Effect of early tranexamic acid administration on mortality, hysterectomy, and other morbidities in women with post-partum haemorrhage (WOMAN): an international, randomised, double-blind, placebo-controlled trial. Lancet. 2017;389(10084):2105-2116.
39. World Health Organization. WHO Recommendation on Tranexamic Acid for the Treatment of Postpartum Haemorrhage. Geneva: World Health Organization; 2017.
40. Godier A, Roberts I, Hunt BJ. Tranexamic acid: less bleeding and less thrombosis? Crit Care. 2012;16(3):135.
41. Spahn DR, Bouillon B, Cerny V, et al. The European guideline on management of major bleeding and coagulopathy following trauma: fifth edition. Crit Care. 2019;23 (1):98.
42. Desai N, Schofield N, Richards T. Perioperative Patient Blood Management to improve outcomes. Anesth Analg. 2018;127(5):1211-1220.
43. Morrison JJ, Dubose JJ, Rasmussen TE, Midwinter MJ. Military application of tranexamic acid in trauma emergency resuscitation (MATTERs) Study. Arch Surg. 2012;147(2):113-119.

Ferrata Storti Foundation

Haematologica 2020
Volume 105(5):1206-1215

Early growth response 1 regulates hematopoietic support and proliferation in human primary bone marrow stromal cells

Hongzhe Li,[1,2] Hooi-Ching Lim,[1,2] Dimitra Zacharaki,[1,2] Xiaojie Xian,[2,3] Keane J.G. Kenswil,[4] Sandro Bräunig,[1,2] Marc H.G.P. Raaijmakers,[4] Niels-Bjarne Woods,[2,3] Jenny Hansson,[1,2] and Stefan Scheding[1,2,5]

[1]Division of Molecular Hematology, Department of Laboratory Medicine, Lund University, Lund, Sweden; [2]Lund Stem Cell Center, Department of Laboratory Medicine, Lund University, Lund, Sweden; [3]Division of Molecular Medicine and Gene Therapy, Department of Laboratory Medicine, Lund University, Lund, Sweden; [4]Department of Hematology, Erasmus MC Cancer Institute, Rotterdam, the Netherlands and [5]Department of Hematology, Skåne University Hospital Lund, Skåne, Sweden

ABSTRACT

Human bone marrow stromal cells (BMSC) are key elements of the hematopoietic environment and they play a central role in bone and bone marrow physiology. However, how key stromal cell functions are regulated is largely unknown. We analyzed the role of the immediate early response transcription factor EGR1 as key stromal cell regulator and found that EGR1 was highly expressed in prospectively-isolated primary BMSC, down-regulated upon culture, and low in non-colony-forming $CD45^{neg}$ stromal cells. Furthermore, EGR1 expression was lower in proliferative regenerating adult and fetal primary cells compared to adult steady-state BMSC. Overexpression of EGR1 in stromal cells induced potent hematopoietic stroma support as indicated by an increased production of transplantable $CD34^{+}CD90^{+}$ hematopoietic stem cells in expansion co-cultures. The improvement in bone marrow stroma support function was mediated by increased expression of hematopoietic supporting genes, such as *VCAM1* and *CCL28*. Furthermore, EGR1 overexpression markedly decreased stromal cell proliferation whereas EGR1 knockdown caused the opposite effects. These findings thus show that EGR1 is a key stromal transcription factor with a dual role in regulating proliferation and hematopoietic stroma support function that is controlling a genetic program to co-ordinate the specific functions of BMSC in their different biological contexts.

Correspondence:

STEFAN SCHEDING
stefan.scheding@med.lu.se

Received: January 14, 2019.

Accepted: July 19, 2019.

Pre-published: August 1, 2019.

doi:10.3324/haematol.2019.216648

Check the online version for the most updated information on this article, online supplements, and information on authorship & disclosures: www.haematologica.org/content/105/5/1206

Introduction

Hematopoietic stem cell (HSC) niches are specialized local tissue microenvironments that maintain and regulate HSC. Aside from being skeletal stem cells with multilineage differentiation capacity, bone marrow mesenchymal stromal cells (BMSC) are essential constituents of the HSC niche. Despite this key role in hematopoiesis, and despite recent progress in the identification of primary BMSC,[1,2] little is known about how proliferation, differentiation and hematopoietic support functions of these important niche cells are regulated.

We therefore approached the identification of potential BMSC regulators by investigating specific gene expression of highly-purified primary BMSC that were prospectively isolated from human bone marrow samples using recently-identified surface marker combinations.[1] Previously reported array-based comparative gene expression analysis showed high *expression of early growth response 1 (EGR1)* in primary BMSC compared to non-colony-forming cells (for details see *Online Supplementary Table S1* in *Li et al.*[1]). Interestingly, EGR1 is an important regulator of different cellular processes[3-5] and has been identified as a cell-intrinsic regulator of HSC proliferation and mobilization.[6] Furthermore, data from knockout mice indicated a role of EGR1 on bone formation *in vivo*.[7] These findings suggested that

EGR1 might also have a role in human primary non-hematopoietic bone marrow stromal cells.

We therefore investigated the role of EGR1 in human BMSC and found that EGR1 was highly expressed in steady-state primary BMSC compared to regenerating adult and fetal BMSC. Overexpression of EGR1 increased BMSC hematopoietic stroma support function and inhibited cell proliferation, whereas decreased EGR1 expression caused the opposite effects. Our data thus indicate a key dual role of EGR1 in BMSC regulation, which has important implications for stroma repair and replacement approaches, and possibly also for the understanding of important developmental aspects of hematopoietic stroma formation.

Methods

Human bone marrow and cord blood cells

Human bone marrow (BM) cells were collected at the Hematology Department, University of Lund, Sweden, from consenting healthy donors by aspiration from the iliac crest. Cord blood (CB) samples were obtained from consenting donors at the maternity wards at Lund, Helsingborg and Malmö Hospitals, Sweden. BM aspirates from patients with acute myeloid leukemia (AML), BM controls, and fetal long bones were obtained with informed consent at the Erasmus Medical Center, the Netherlands, as described previously.[8] The processing of BM mononuclear cells (BM-MNC), isolation and characterization of primary bone marrow stroma cells (BMSC), and generation of cultured stroma cells including EGR1 over-expressing and knockout cells from sorted $CD45^-CD271^+CD140a^-$ BMSC, is provided in the *Online Supplementary Appendix*: *experimental procedures*. The use of human samples was approved by the corresponding Institutional Review Board of the University of Lund and the Erasmus Medical Center, respectively, in accordance with the Declaration of Helsinki.

Co-culture of cord blood $CD34^+$ cells with stromal cells

FACS-sorted GFP^+ stromal cells (EGR1 knockdown, EGR1 over-expressing cells, and corresponding controls) were plated as adherent feeder cells into 96-well plates at 10,000 cells per well and cultured in MSC medium for three days. Medium was then removed and 5,000 CB $CD34^+$ cells were added in serum-free expansion medium (SFEM, STEMCELL Technologies) supplemented with or without stem cell factor, thrombopoietin, and FLT-3 ligand (all at 25 ng/mL, STF25) (*Online Supplementary Appendix*). Expanded CB cells were harvested, counted and analyzed after four days of co-culture.

Conditioned MSC medium was prepared by replacing the MSC expansion medium with serum-free expansion medium (SFEM) and collecting the conditioned media after four days.

Transwell cultures were performed using the HTS Transwell-96 System (Corning, New York, NY, USA); 10,000 BMSC in standard MSC culture medium were plated in the transwell reservoir. After three days of culture, the MSC culture medium was removed and replaced with SFEM (STF25), and 5,000 CB $CD34^+$ cells in SFEM (STF25) were loaded into the insert (membrane pore size: 0.4 μm). After four days of co-culture, cells were harvested, counted and analyzed.

To evaluate the role of VCAM1 and CCL28 on CD34 expansion, stromal cells were pretreated with 100 ng/mL VCAM1 or CCL28 blocking antibody and control IgG, respectively, at 37°C for two hours followed by co-culture with $CD34^+$ cells in either standard SFEM (STF25) or cytokine-free conditions at 37°C for four days.

Other methods

The details of the other methods used in this study, i.e. generation of cultured MSC, EGR1 knockdown and EGR1 over-expressing stroma cells, FACS sorting and analysis, CFU-F assays, *in vitro* differentiation assays, real-time polymerase chain reaction (PCR), *in vivo* HSC repopulation assay, CCL28 ELISA, Illumina array, RNA-seq and proteome analysis, as well as information on the deposition of gene expression and proteomics data, are all provided in the *Online Supplementary Appendix*: *experimental procedures*.

Results

EGR1 is highly expressed in primary bone marrow stromal cells

Our previous gene expression profiling data demonstrated that expression levels of *EGR1* in primary CFU-F (colony-forming unit, fibroblast)-enriched $lin^-CD45^-CD271^+$ BMSC were substantially higher compared to non-colony-forming cells ($lin^-CD45^-CD271^-$).[1] We therefore proceeded to investigate EGR1 expression and function in highly purified $lin^-CD45^-CD271^-CD140a(PDGFR\alpha)^-$ BMSC, which we have recently demonstrated as a (close to) pure population of putative BM stromal stem cells with high CFU-F frequency, typical *in vitro* and *in vivo* differentiation capacities, and potent hematopoietic stroma function.[1] Expression of EGR1 was 128.9±28.4-fold higher in $lin^-CD45^-CD271^+CD140a^-$ BMSC compared to non-colony-forming cells ($lin^-CD45^-CD271^-CD140a^-$), and 2.8±0.6-fold higher compared to $lin^-CD45^-CD271^+CD140a^+$ stromal cells, which have only limited CFU-F activity (Figure 1A).[1] In addition, EGR1 expression was significantly higher in steady-state adult BMSC ($CD31^-CD271^+$) in comparison to fetal BMSC, BMSC in regenerating marrow, and BM endothelial cells ($CD31^+CD9^+$) (Figure 1B). None of the other EGR transcription factor family members were expressed at comparable levels in BMSC or endothelial cells (*Online Supplementary Figure S1A and B*).

Upregulation of EGR1 increases BMSC cell hematopoietic stroma-support

Motivated by the selective high expression of EGR1 in hematopoiesis-supporting BMSC, we went on to investigate the functions of EGR1 employing gain-of-function and loss-of-function approaches.

Effective reduction of EGR1 expression in BMSC was induced by two (shEGR1-1 and shEGR1-4) of four tested EGR1-specific shRNA (*Online Supplementary Figure S2A*). EGR1 overexpression in BMSC by more than two-fold was realized using the lentiviral vector encoding full length human EGR1 (*Online Supplementary Figure S2B*).

BMSC cell hematopoietic stroma supporting function was evaluated by co-culturing CB $CD34^+$ cells with EGR1 knockdown stromal cells, EGR1 over-expressing stromal cells and corresponding controls, respectively, as adherent feeder cells. Total numbers of hematopoietic cells increased when $CD34^+$ cells were expanded on stroma feeder layers compared to cultures without stroma support, but no differences were observed between the different stromal cell groups (Figure 2A and B). However, EGR1 knockdown feeder cells failed to effectively support the $CD34^+$ phenotype while the EGR1 over-expressing stromal cells efficiently maintained this population

(Figure 2C). Furthermore, although not significant, both percentages and absolute numbers of transplantable CD34$^+$CD90$^+$ cells were reduced when CD34$^+$ cells were co-cultured on EGR1 knockdown stromal cells (1.76±0.76 fold for shEGR1 *vs.* 2.64±1.47 fold for scramble control compared with no stroma control), whereas the production of CD34$^+$CD90$^+$ cells was significantly increased with EGR1 over-expressing stroma feeder cells (6.97±4.53-fold) compared to controls (3.11±2.65-fold) (Figure 2D). Accordingly, transplantation into NSG mice demonstrated that CB CD34$^+$ cells expanded on EGR1 over-expressing stroma exhibited higher long-term in vivo reconstitution levels with stable lymphoid and myeloid lineage engraftment compared with controls and EGR1 knockdown feeder cells (Figure 2E-G). These data therefore clearly indicated that EGR1 expression regulates the hematopoietic stroma support function of BM stromal cells.

EGR1-induced enhanced hematopoietic support is mediated through soluble factors and cell-cell interaction

Cord blood CD34$^+$ expansion experiments using transwell cultures showed that numbers and percentages of *ex vivo* expanded CD34$^+$ cells and CD34$^+$CD90$^+$ as well as total nucleated cells were reduced in all transwell co-cultures compared to stroma-contact conditions (Figure 3A-C and *Online Supplementary Figure S3*). Reductions were even more drastic in cultures stimulated with conditioned media from EGR1 knockdown and over-expressing cell cultures, respectively, instead of feeder cells. Numbers of total CD34$^+$ and CD34$^+$CD90$^+$ cells generated were highest in the EGR1 overexpression groups, both in standard and transwell co-cultures, but also in non-stroma cultures stimulated by conditioned medium collected from EGR1 over-expressing stromal cells. These data thus indicated that EGR1 effects were both cell-cell contact and soluble factor-mediated, and confirmed the role of EGR1 in hematopoietic support regulation.

Stromal EGR1 induces expression of hematopoietic supporting genes that contribute to preserve primitive phenotype of CD34$^+$ cells

To further explore the mechanism of EGR1-mediated hematopoiesis support, an array-based gene expression analysis was performed comparing EGR1 cells and control cells. In total, 189 genes were significantly up-regulated in EGR1 over-expressing cells, including genes involved in signal transduction, as well as adhesion molecule and cytokine genes (*Online Supplementary Table S1 and Online Supplementary Figure S4A*). Six of the up-regulated genes (*CCL28, VCAM1, TIMP3, TNC, ENPP2* and *MFAP4*) (Figure 4A) have been reported to be genes supporting hematopoiesis,[9-14] and we chose to further investigate CCL28 and VCAM1 as representatives for soluble factors and surface expressed, cell-cell contact mediating molecules, respectively.

First, CCL28 levels secreted by stromal cells in culture were assessed. CCL28 levels were higher in cultures with EGR1 over-expressing cells compared to controls (Figure 4B). Exogenous CCL28 enhanced the expansion of functional progenitor cells in co-cultures with EGR1 knockdown stroma feeder cells (Figure 4D-F and *Online Supplementary Figure S4B-D*). Furthermore, *ex vivo* expansion of CD34$^+$ and CD34$^+$CD90$^+$ cells in co-culture with EGR1 over-expressing stroma was dramatically inhibited by CCL28 blocking antibody in both standard medium and cytokine-free conditions (Figure 4G-I and *Online Supplementary Figure S4E-G*).

VCAM1 was slightly up-regulated in EGR1 over-expressing cells (Figure 4C). Functionally, the production of CD34$^+$ and CD34$^+$CD90$^+$ cells in EGR1 over-expressing BMSC co-cultures was dramatically reduced when VCAM1 was blocked by a neutralizing antibody. Expansion rates were further reduced when CCL28 and VCAM1 blocking antibodies were used concurrently (Figure 4G-I and *Online Supplementary Figure S4E-G*).

Taken together, these data indicated that EGR1 overexpression enhanced BMSC stroma supporting capacity and,

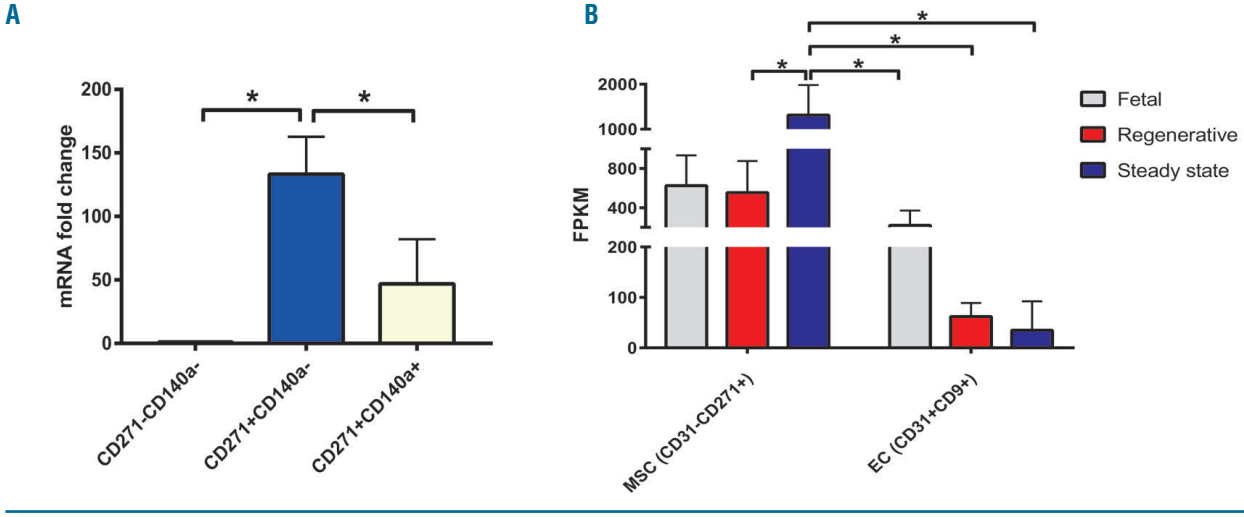

Figure 1. EGR1 is highly expressed by primary bone marrow mesenchymal stromal cells (BMSC). (A) Quantitative real-time polymerase chain reaction (rtPCR) of EGR1 expression in sorted lin$^-$CD45$^-$CD271$^+$CD140a$^-$ BMSC compared to CD271$^+$CD140a$^+$ and lin$^-$CD45$^-$CD271$^-$CD140a$^-$ cells. Results are shown as fold mRNA change after standardizing with GAPDH levels. (B) Transcript analysis by massive parallel RNA sequencing of EGR1-4 expression in BMSC (CD31$^-$CD271$^+$) isolated from human fetal, regenerative and steady-state BMSC compared to CD31$^+$CD9$^+$ endothelial cells (EC). FPKM: fragments per kilobase million. Data are shown as mean±standard deviation, n=3-10. *P<0.05.

consequently, improved *ex vivo* expansion of hematopoietic cells by up-regulating a panel of hematopoiesis-supporting genes, including cytokines and cell surface expressed molecules such as CCL28 and VCAM1.

EGR1 knockdown induces bone marrow stromal cell proliferation mediated by elevated reactive oxygen species

EGR1 functions either as a cell cycle promoter or a cell proliferation inhibitor depending on the cell type and the environment. We therefore investigated how EGR1 expression impacted BMSC proliferation. Our data showed that EGR1 knockdown BMSC exhibited higher percentages of dividing cells, shorter population doubling times, and enhanced colony-forming capacities (Figure 5A-C and *Online Supplementary Figure S5A*). On the other hand, CFU-F activity was virtually absent in EGR1 overexpressing cells and population doubling times were sub-

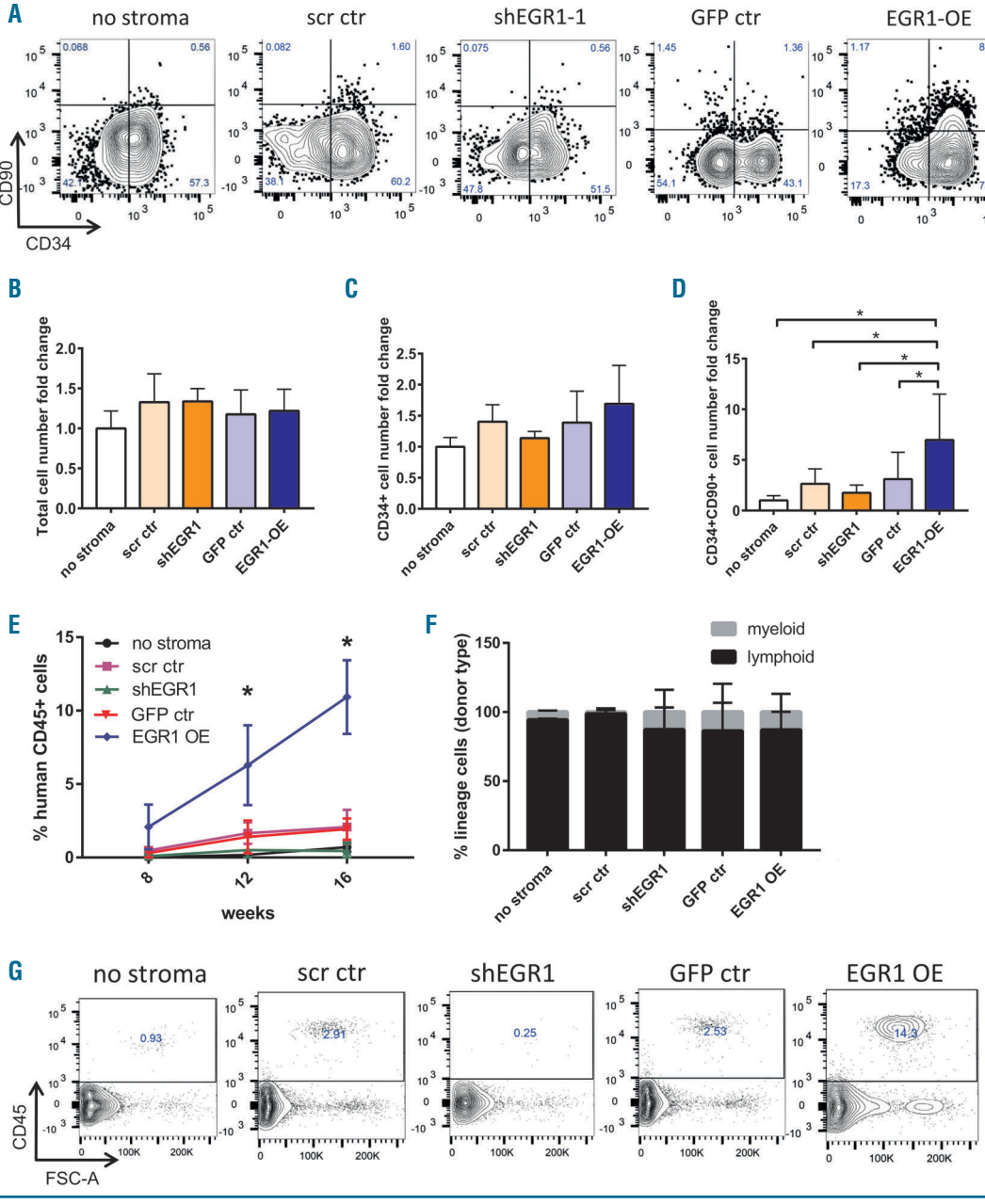

Figure 2. Increased EGR1 expression in mesenchymal stromal cells (MSC) promotes the *ex vivo* expansion of transplantable cord blood CD34⁺ cells. Five thousand cord blood CD34⁺ cells were co-cultured for four days on a feeder layer of 10,000 BMSC transfected with scramble control, shEGR1, green fluorescent protein control (GFP ctr) and EGR1 overexpression plasmids, respectively, in SFEM supplemented with 25 ng/mL of SCF, TPO and Flt3L (STF25). (A) Representative FACS profiles of co-culture generated cells are shown. The type of feeder cells is indicated on top of the respective FACS plot. (B-D) Fold change of total number of hematopoietic cells (B), CD34⁺ cells (C), and CD34⁺CD90⁺ cells (D) produced after four days in culture. Results are shown as fold change relative to the cell number of standard CD34⁺ culture (STF25) without stroma support. N=9-12. *P<0.05. (E-G) Analysis of human hematopoietic cell engraftment following intravenous transplantation of the culture equivalent (4 days culture in SFEM, STF25) of 50,000 input CD34⁺ cells into NSG mice. Human engraftment was assessed 8, 12 and 16 weeks after transplantation by flow cytometry using human-specific antibodies against CD45, CD15/CD33/CD66b and CD19. *P<0.05 between EGR1 OE and each of the other groups. (E) Percentage of human CD45⁺ cells in the peripheral blood of NSG mice at different time points after intravenous transplantation. Data represent the mean±standard deviation (SD) of a total of 4-5 mice per time point except no stroma control, which shows the data for two mice. (F) Lineage distribution of human cells (mean±SD, n= 2-5) and (G) representative FACS plots 16 weeks after transplantation.

stantially increased accordingly (Figure 5B and C).

Proteomic analysis was performed to investigate the mechanisms behind the EGR1 knockdown-induced increased proliferation. Of a total of 4,520 identified proteins, 190 were differentially expressed between EGR1 knockdown stromal cells and scramble and non-transfected controls (*Online Supplementary Tables S4* and *S5* and *Online Supplementary Figure S4E-G*). A group of ten proteins (HSD17B11, UQCRC1, CYP1B1, NDUFA8, TXNDC17, CYCS, FADS3, PDIA5, PCYOX1, QSOX1) related to oxidative-reduction processes was expressed lower in EGR1 knockdown cells (Figure 6A and B) as were GLS1, GPX1 and GSTP1, which are also associated with intracellular reactive oxygen species (ROS) accumulation.[15-17] Accordingly, ROS levels in EGR1 knockdown cells were increased compared to controls (Figure 6C and D).

Inhibiting ROS using an antioxidant cocktail (L-ascorbic acid and citric acid), N-acetylcysteine (NAC), or apocynin considerably reduced ROS production in EGR1 knockdown cells (Figure 6E). ROS reduction caused a decrease in the fraction of dividing EGR1 knockdown cells (Figure 6F) and in the numbers of CFU-F with complete abrogation of colony formation when using the antioxidant cocktail (Figure 6G). In contrast, neither myeloperoxidase (MPO) inhibitor 4-ABAH nor the small molecule inhibitor LY2228820 (Figure 6E-G) affected ROS levels, percentages of proliferating cells or CFU-F numbers.

Consistent with the increased proliferation in EGR1-knockdown BMSC, gene expression profiling identified a group of down-regulated genes involved in cell death and apoptosis (*BFAR, EIF4G2, TSPO, RABEP1, MCL1, TNFRSF12A, TBRG4, MYC, DDIT4*) in EGR1 knockdown cells (*Online Supplementary Table S2* and *Online Supplementary Figure S5B and C*). Furthermore, positive regulators of cell proliferation and negative regulators of apoptosis were down-regulated in EGR1 over-expressing cells (*Online Supplementary Table S3* and *Online Supplementary Figure S5D*), which is consistent with the

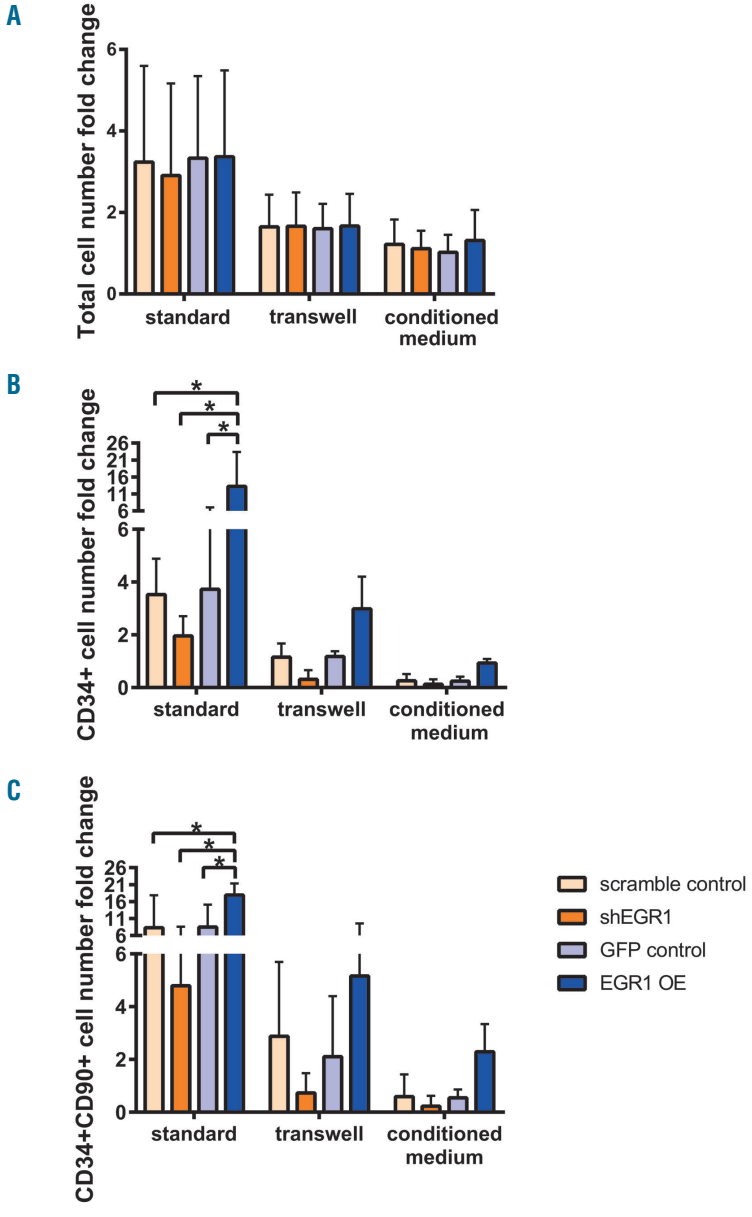

Figure 3. EGR1-induced *ex vivo* expansion of CB CD34⁺ cells is mediated by both soluble and membrane-bound factors. Five thousand cord blood (CB) CD34⁺ cells were co-cultured for four days with 10,000 feeder bone marrow mesenchymal stromal cells (BMSC) transfected with scramble control, shEGR1, green fluorescent protein control (GFP ctr) and EGR1 overexpression plasmids, respectively, in serum-free expansion medium supplemented with 25 ng/mL of SCF, TPO and Flt3L. Co-cultures were performed in either standard culture plates (standard) or transwell culture plates with the stromal cells in the bottom well and CD34⁺ cells in the insert (transwell). For conditioned medium cultures, 10,000 BM-derived stromal cells transfected with scramble control, shEGR1, GFP control and EGR1 overexpression plasmids, respectively, were cultured with 200 μL serum-free expansion medium supplemented with 25 ng/mL of SCF, TPO and Flt3L for four days. Conditioned media were collected and used to stimulate cultures with CB CD34⁺ cells (without feeder cells). Fold change of total cell number (A), cell number of CD34⁺ cells (B) and CD34⁺CD90⁺ cells (C) produced after four days in culture are shown as mean±standard deviation. Three independent experiments were performed with cells from different donors. Representative results are shown for one of the experiments. *P<0.05.

reduced proliferation of EGR1 over-expressing cells.

These data therefore indicate that increased proliferation of EGR1 knockdown cells is, at least partly, mediated by increased ROS levels and downregulation of cell death genes, whereas downregulation of cell proliferation and apoptosis inhibiting genes was observed upon EGR1 overexpression. Thus, whereas increased EGR1 expression improved the stroma supporting function of BMSC, cell proliferation was substantially inhibited, indicating a dual role of EGR1 in the regulation of BMSC growth and function. On the other hand, other BMSC functions, such as multi-differentiation capacity (adipogenic, osteogenic and chondrogenic) and surface marker expression profile of BMSC were not affected by changes in EGR1 expression (*Online Supplementary Figure S6A and B*).

Discussion

Bone marrow is the major site of residence of both HSC and BMSC. The most crucial functions of BMSC are to maintain the turnover of the BM stroma and skeletal tissues and to provide critical hematopoietic support. However, the mechanisms that regulate these different

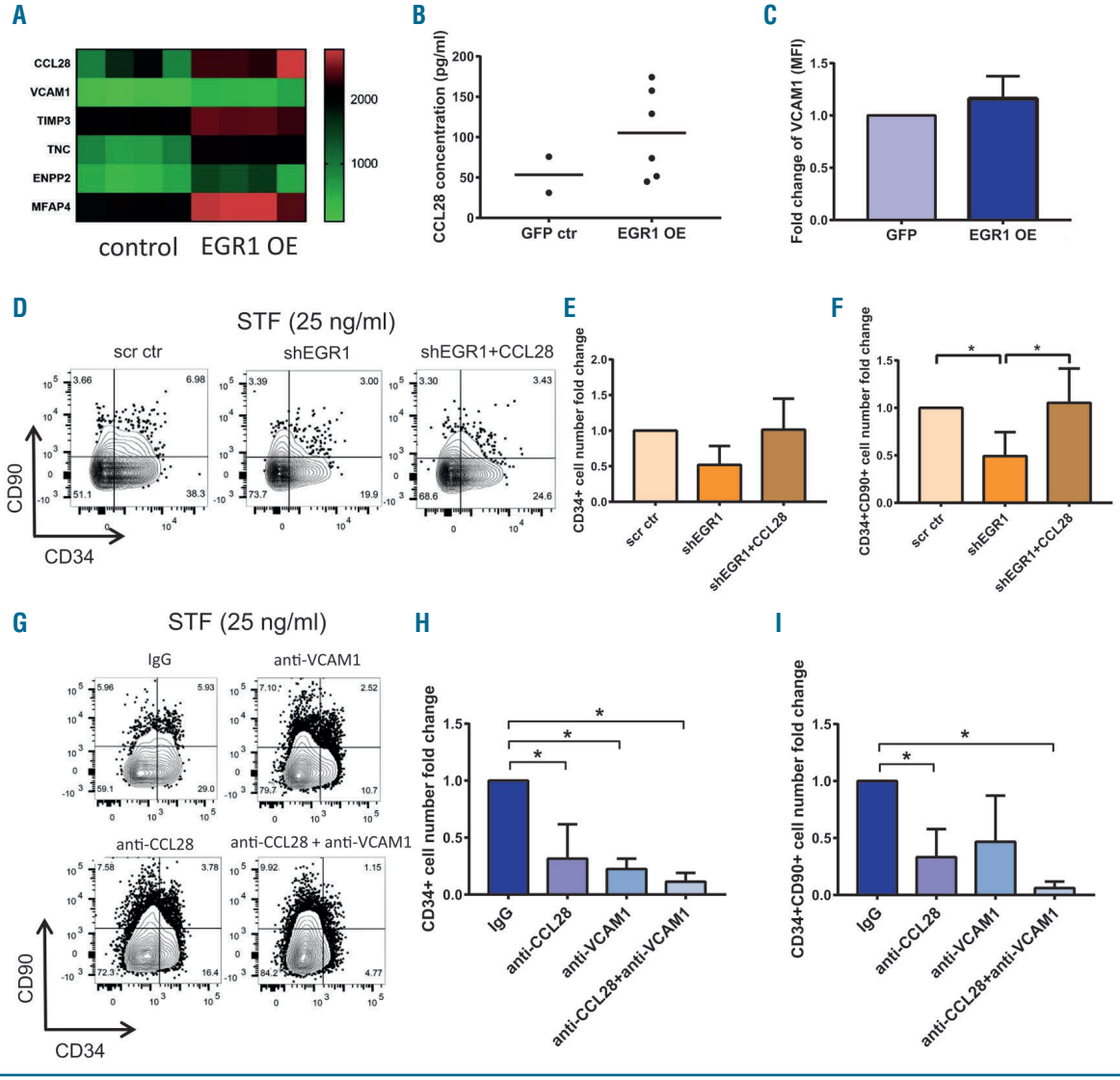

Figure 4. Hematopoiesis-supporting genes are up-regulated in EGR1 over-expressing mesenchymal stromal cells (MSC). (A) Heatmap of significantly up-regulated hematopoietic supporting genes in EGR1 overexpression cells *versus* controls (n=4). (B) Secreted CCL28 concentrations in cell culture supernatants of EGR1 over-expressing bone marrow stromal cells (BMSC) (EGR1 OE) and green fluorescent protein control (GFP ctr) (n=2-6). (C) Fold change of surface expression of VCAM1 (CD106) in EGR1 over-expressing cells compared with GFP control cells. VCAM1 expression is shown as fold change of the geometric mean fluorescence intensity (MFI) after standardizing with GFP control cells (n=3-4). (D-F) 5,000 cord blood CD34$^+$ cells were co-cultured for four days with 10,000 BM-derived feeder stromal cells transfected with scramble control and shEGR1 plasmids, respectively, in cytokine-free or standard STF25 culture conditions supplemented with or without 100 ng/mL CCL28. Standard culture (STF25): SFEM supplemented with 25 ng/mL of SCF, TPO and Flt3L (n=3). (D) Representative FACS profiles of co-culture generated cells in standard culture. The type of feeder cells is indicated on top of the FACS plots. Fold change of total numbers of CD34$^+$ cells and CD34$^+$CD90$^+$ cells produced in standard STF25 cultures (E and F). (G-I) 5,000 cord blood CD34$^+$ cells were co-cultured for four days with 10,000 EGR1 overexpression cells as feeder cells in standard culture media supplemented with neutralizing antibody against CCL28, VCAM1 and IgG control (all at 100 ng/mL) for four days. (G) Representative FACS profiles of co-culture generated cells. Total number of CD34$^+$ cells (H) and CD34+CD90+ cells (I) produced in the co-cultures without/with neutralizing antibodies as indicated by the x-axis labels (n=3). *P<0.05

functions are not well known. Murine studies using inducible gene deletion strategies in BMSC indicated a tight control of key BMSC functions to maintain homeostasis of the hematopoietic and the skeletal system.[18, 19] Here we report for the first time that EGR1 is a key regulator in human BMSC.

EGR1 is a member of the immediate early response transcription factor family with a role in regulating development, growth control and stress response in many tissues. Based on our *EGR1* expression data in primary BMSC,[1] and information on the role of EGR1 in stromal cell growth factor production regulation and hematopoietic stem cell regulation,[6,20] we hypothesized that EGR1 could also be an important regulator of BM stromal stem cells.

In accordance with our previous data[1] we found that EGR1 expression was substantially higher in highly CFU-F-enriched primary lin$^-$CD45$^-$CD271$^+$CD140a$^-$ BMSC (Figure 1A). In addition, EGR1 was significantly higher expressed in steady-state adult BMSC in comparison to fetal BMSC and BMSC in regenerating marrow (Figure 1B), which have higher proliferation rates as indicated by high cell cycle activator expression levels in fetal BMSC (*data not shown*) and previously reported proliferation data.[21,22] Moreover, EGR1 was the only member of the EGR family (EGR1-4) that was highly expressed in BMSC (*Online Supplementary Figure S1A and B*), in contrast to other cell types that also co-express other EGR family members.[23,24]

These data implied that EGR1 expression levels might be connected to the regulation of key BMSC functions, i.e. hematopoietic support in steady-state and stroma proliferation in situations with regenerative demands. In fact, EGR1 overexpression increased BMSC hematopoietic stroma-supporting function and facilitated the effective generation of transplantable hematopoietic stem cells, while EGR1 knockdown abrogated the stroma contribution in HSC expansion co-cultures (Figure 2). Furthermore, a clear reduction in *ex vivo* expanded HSC was recorded in transwell cultures and when using conditioned medium (Figure 3). Our data thus indicated that EGR1 regulated BMSC stroma support functions mediated by both cell-cell contact and soluble factors, both of which are required to realize effective *ex vivo* HSC expansion.[25-28] Accordingly, gene array expression profiling identified hematopoiesis-supporting genes as EGR1 downstream targets, which corresponded to both secreted and surface-expressed molecules (Figure 4A). Of these, we investigated the functional role of CCL28 and VCAM1 as examples for a potent niche-secreted soluble growth factor[11] and an adhesion molecule, respectively. Here, CCL28 supplementation and blocking experiments (Figure 4D-I) clearly indicated a contributing role of CCL28 in EGR1-mediated *ex vivo* expansion of CB CD34$^+$ cells on EGR1 over-expressing stromal cells. Similarly, the role of VCAM1 was demonstrated by blocking VCAM1 with neutralizing antibodies (Figure 4G-I).

Successful *ex vivo* expansion of HSC represents a promising approach to provide sufficient numbers of transplantable stem cells and to facilitate the development of cell and gene therapies. A number of approaches to expand HSC have been pursued, including enhancing positive signals and inhibiting negative signals for HSC self-renewal.[29,30] Our results indicate that modification of feeder cell regulation by EGR overexpression represents a novel approach to generate an optimized microenvironment that supports HSC self-renewal and growth with the potential to improve current HSC expansion culture conditions. Furthermore, one can envision strategies to increase EGR1 expression *in vivo* to improve hematopoietic stromal support function, for example, in transplantation patients with poor graft function, and possibly even in patients with insufficient hematopoiesis, such as low-risk myelodysplastic syndrome.

The effect of EGR1 on cell proliferation depends on the biological context.[31,32] Our data clearly demonstrated that high expression of EGR1 inhibited proliferation and colony-formation of human BMSC, whereas reduced EGR1 levels caused the opposite effects (Figure 5). Thus, EGR1 expression modulation might not only be used to modify BMSC stroma support function, but could also be utilized to increase BMSC proliferation *in vitro* to optimize BMSC expansion strategies, and possibly also *in vivo* to induce stroma and bone tissue growth.

Proteomic analysis of EGR1 knockdown cells identified a group of down-regulated proteins related to oxidative-reduction processes. Accordingly, increased ROS levels were observed in EGR1 knockdown cells (Figure 6C),

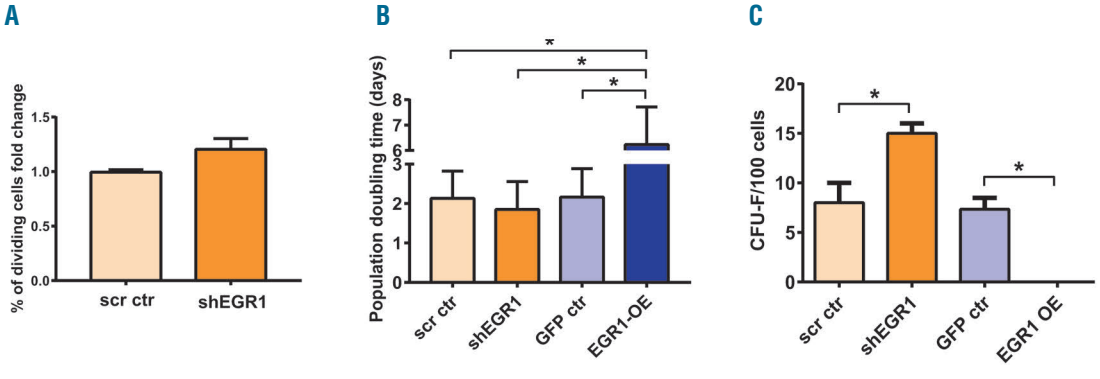

Figure 5. Proliferation of EGR1 knockdown bone marrow mesenchymal stromal cells (BMSC) is increased. (A) Percentage of dividing cells in EGR1 knockdown BMSC in comparison with scramble control. Data are shown as mean±standard deviation (SD) (n=5) for passage 2-5 cells. (B) Population doubling times of passage 2-5 BMSC transfected with scramble control, shEGR1, green fluorescent protein control (GFP ctr) and EGR1 overexpression plasmids, respectively. Data are shown as mean±SD (n=3). (C) Frequencies of colony-forming units-fibroblasts (CFU-F) in BM-derived MSC (passage 2-5) transfected with scramble control, shEGR1, GFP ctr and EGR1 overexpression plasmids, respectively. Data are presented as mean±SD (n=3). *P<0.05.

which have been reported to promote cell proliferation, differentiation and survival.[33-35] Furthermore, experiments using different ROS inhibitors showed that ROS production in BMSC was mostly affected by oxidative pathway changes, and to a lesser extent by p38 pathway alterations or 4-ABAH induced inhibition of myeloperoxidase (MPO).

In addition to the role of EGR1 in regulating key BMSC functions *in vitro* as demonstrated here, we observed that EGR1 expression levels were significantly different in different (patho)physiological situations. These expression data were generated with prospectively isolated BMSC and can therefore be considered to accurately reflect the *in vivo* situation. We found that EGR1 was significantly

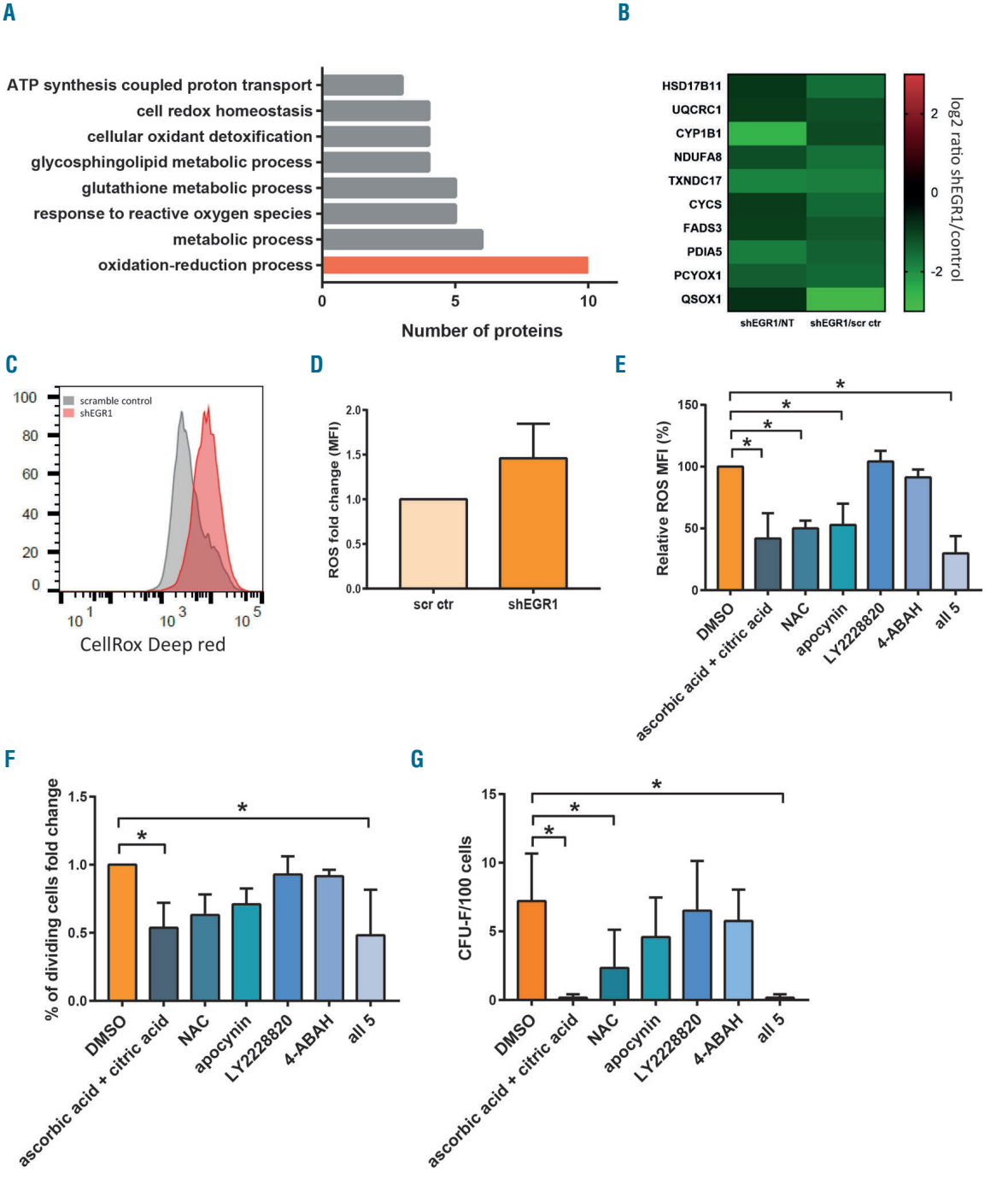

Figure 6. Increased proliferation in EGR1 knockdown bone marrow mesenchymal stromal cells (BMSC) is mediated by reactive oxygen species (ROS). (A) Biological process annotations for down-regulated proteins in EGR1 knockdown cells were identified using the DAVID Bioinformatics Resources 6.8. (B) Heatmap of down-regulated proteins related to oxidative-reduction processes in EGR1 knockdown cells *versus* controls. NT: non-transfected cells; scr ctr: scramble control. (C) Representative FACS histogram of ROS levels in EGR1 knockdown cells compared with scramble control. (D) Fold change of ROS in EGR1 knockdown cells in comparison with scramble control. Data are shown as mean fluorescence intensity (MFI) fold change±standard deviation (SD) (n=3). ROS MFI levels relative to dimethyl sulfoxide (DMSO) controls (E), percentage of dividing cells expressed as fold change compared to DMSO controls (F), and colony-forming units-fibroblast (CFU-F) frequencies (G) in EGR1 knockdown cells after ROS inhibitor treatment. Data are shown as mean±SD (n=3). NAC: N-acetylcysteine. **P*<0.05.

higher expressed in adult steady-state BMSC compared with fetal BMSC and BMSC in regenerating marrow (Figure 1B), both of the latter showing higher proliferation compared to steady-state BMSC. Thus, these data point to a possible key role *in vivo* of EGR1, regulating the response to the different requirements in development and under pathological conditions. In the fetal period, there is demand for a high proliferation of BMSC with potent osteogenic and stroma differentiation potential. Likewise, primarily cellular regeneration is required after stromal damage, for example, following myelotoxic chemo- or radiotherapy. In addition, murine data demonstrated that BMSC expanded considerably following irradiation and BM transplantation.[22] In contrast, hematopoietic support is most important in steady-state adult BM, whereas there is only a limited need for BMSC proliferation. However, whether or not a demand-controlled EGR1 regulation of proliferation and stroma function is operative *in vivo* has not yet been investigated, but is certainly an interesting and highly relevant topic for future research.

Taken together, we demonstrate that EGR1 is a key dual regulator of human BMSC which controls a genetic program co-ordinating specific functions of BMSC in their different biological contexts. High EGR1 expression induced potent hematopoietic stroma support by expression of high levels of hematopoiesis-supporting genes and suppressed BMSC proliferation, whereas EGR1 downregulation promoted BMSC proliferation at the expense of hematopoietic support function. These data thus considerably expand our current understanding of the regulation of BMSC under distinct physiological and developmental conditions. Furthermore, they have clear implications for the development of stroma replacement and repair strategies, for example, for optimizing BMSC expansion protocols *in vitro* and to improve stroma function in transplantation patients with poor graft function, as well as stroma-mediated HSC expansion approaches.

Funding

This work was supported by funds from the HematoLinné and StemTherapy Program, the Swedish Cancer Foundation, the Swedish Childhood Cancer Foundation, Gunnel Björk's Testament, Gunda Nilsson's Testament, the Åke och Inger Bergkvists stiftelse, ALF (Government Public Health Grant), and the Skåne County Council Research Foundation.

Acknowledgments

The authors would like to thank Helene Larsson and Anna Jonasson for their help to collect bone marrow samples and the Lund Stem Cell Center FACS facility personnel for technical assistance. Furthermore, support from the Swedish National Infrastructure for Biological Mass Spectrometry (BioMS) is gratefully acknowledged. We would also like to thank Professors Axel Schambach, Manuel Grez, and Thomas Moritz for providing the A2UCOE-EFS promoter used to generate the lentivector driving expression of EGR1, and Jonas Larsson for crtically reading the manuscript.

References

1. Li H, Ghazanfari R, Zacharaki D, et al. Low/negative expression of PDGFR-alpha identifies the candidate primary mesenchymal stromal cells in adult human bone marrow. Stem Cell Reports. 2014;3(6):965-974.
2. Tormin A, Li O, Brune JC, et al. CD146 expression on primary nonhematopoietic bone marrow stem cells is correlated with in situ localization. Blood. 2011; 117(19):5067-5077.
3. Christy BA, Lau LF, Nathans D. A gene activated in mouse 3T3 cells by serum growth factors encodes a protein with "zinc finger" sequences. Proc Natl Acad Sci U S A. 1988; 85(21):7857-7861.
4. Milbrandt J. A nerve growth factor-induced gene encodes a possible transcriptional regulatory factor. Science. 1987;238(4828):797-799.
5. Lemaire P, Revelant O, Bravo R, Charnay P. Two mouse genes encoding potential transcription factors with identical DNA-binding domains are activated by growth factors in cultured cells. Proc Natl Acad Sci U S A. 1988;85(13):4691-4695.
6. Min IM, Pietramaggiori G, Kim FS, Passegue E, Stevenson KE, Wagers AJ. The transcription factor EGR1 controls both the proliferation and localization of hematopoietic stem cells. Cell Stem Cell. 2008;2(4):380-391.
7. Reumann MK, Strachna O, Lukashova L, et al. Early growth response gene 1 regulates bone properties in mice. Calcif Tissue Int. 2011;89(1):1-9.
8. Kenswil KJG, Jaramillo AC, Ping Z, et al. Characterization of Endothelial Cells Associated with Hematopoietic Niche Formation in Humans Identifies IL-33 As an Anabolic Factor. Cell Rep. 2018;22(3):666-678.
9. Zhang CC, Kaba M, Ge G, et al. Angiopoietin-like proteins stimulate ex vivo expansion of hematopoietic stem cells. Nat Med. 2006;12(2):240-245.
10. Nakajima H, Ito M, Smookler DS, et al. TIMP-3 recruits quiescent hematopoietic stem cells into active cell cycle and expands multipotent progenitor pool. Blood. 2010;116(22):4474-4482.
11. Karlsson C, Baudet A, Miharada N, et al. Identification of the chemokine CCL28 as a growth and survival factor for human hematopoietic stem and progenitor cells. Blood. 2013;121(19):3838-3842.
12. Nakamura-Ishizu A, Okuno Y, Omatsu Y, et al. Extracellular matrix protein tenascin-C is required in the bone marrow microenvironment primed for hematopoietic regeneration. Blood. 2012;119(23):5429-5437.
13. Li H, Yue R, Wei B, Gao G, Du J, Pei G. Lysophosphatidic acid acts as a nutrient-derived developmental cue to regulate early hematopoiesis. EMBO J. 2014;33(12):1383-1396.
14. Mazo IB, Massberg S, von Andrian UH. Hematopoietic stem and progenitor cell trafficking. Trends Immunol. 2011; 32(10):493-503.
15. Kanwal R, Pandey M, Bhaskaran N, et al. Protection against oxidative DNA damage and stress in human prostate by glutathione S-transferase P1. Mol Carcinog. 2014;53(1):8-18.
16. Okazaki A, Gameiro PA, Christodoulou D, et al. Glutaminase and poly(ADP-ribose) polymerase inhibitors suppress pyrimidine synthesis and VHL-deficient renal cancers. J Clin Invest. 2017;127(5):1631-1645.
17. Dokic I, Hartmann C, Herold-Mende C, Regnier-Vigouroux A. Glutathione peroxidase 1 activity dictates the sensitivity of glioblastoma cells to oxidative stress. Glia. 2012;60(11):1785-1800.
18. Omatsu Y, Seike M, Sugiyama T, Kume T, Nagasawa T. Foxc1 is a critical regulator of haematopoietic stem/progenitor cell niche formation. Nature. 2014;508(7497):536-540.
19. Seike M, Omatsu Y, Watanabe H, Kondoh G, Nagasawa T. Stem cell niche-specific Ebf3 maintains the bone marrow cavity. Genes Dev. 2018;32(5-6):359-372.
20. Kerpedjieva SS, Kim DS, Barbeau DJ, Tamama K. EGFR ligands drive multipotential stromal cells to produce multiple growth factors and cytokines via early growth response-1. Stem Cells Dev. 2012; 21(13):2541-2551.
21. Guillot PV, Gotherstrom C, Chan J, Kurata H, Fisk NM. Human first-trimester fetal MSC express pluripotency markers and grow faster and have longer telomeres than adult MSC. Stem Cells. 2007;25(3):646-654.
22. Abbuehl JP, Tatarova Z, Held W, Huelsken J. Long-term engraftment of primary bone marrow stromal cells repairs niche damage and improves hematopoietic stem cell transplantation. Cell Stem Cell. 2017; 21(2):241-255.e6.
23. Shao H, Kono DH, Chen LY, Rubin EM, Kaye J. Induction of the early growth

response (Egr) family of transcription factors during thymic selection. J Exp Med. 1997;185(4):731-744.
24. Poirier R, Cheval H, Mailhes C, et al. Distinct functions of egr gene family members in cognitive processes. Front Neurosci. 2008;2(1):47-55.
25. Harvey K, Dzierzak E. Cell-cell contact and anatomical compatibility in stromal cell-mediated HSC support during development. Stem Cells. 2004;22(3):253-258.
26. Kawada H, Ando K, Tsuji T, et al. Rapid ex vivo expansion of human umbilical cord hematopoietic progenitors using a novel culture system. Exp Hematol. 1999;27(5):904-915.
27. Thiemann FT, Moore KA, Smogorzewska EM, Lemischka IR, Crooks GM. The murine stromal cell line AFT024 acts specifically on human CD34+CD38- progenitors to maintain primitive function and immunophenotype in vitro. Exp Hematol. 1998;26(7):612-619.
28. Breems DA, Blokland EA, Ploemacher RE. Stroma-conditioned media improve expansion of human primitive hematopoietic stem cells and progenitor cells. Leukemia. 1997;11(1):142-150.
29. Guo B, Huang X, Lee MR, Lee SA, Broxmeyer HE. Antagonism of PPAR-gamma signaling expands human hematopoietic stem and progenitor cells by enhancing glycolysis. Nat Med. 2018;24(3):360-367.
30. Talkhoncheh MS, Subramaniam A, Magnusson M, Kumar P, Larsson J, Baudet A. Transient inhibition of NF-kappaB signaling enhances ex vivo propagation of human hematopoietic stem cells. Haematologica. 2018;103(9):1444-1450.
31. Thiel G, Cibelli G. Regulation of life and death by the zinc finger transcription factor Egr-1. J Cell Physiol. 2002;193(3):287-292.
32. Adamson ED, Mercola D. Egr1 transcription factor: multiple roles in prostate tumor cell growth and survival. Tumour Biol. 2002;23(2):93-102.
33. Kobayashi CI, Suda T. Regulation of reactive oxygen species in stem cells and cancer stem cells. J Cell Physiol. 2012;227(2):421-430.
34. D'Autreaux B, Toledano MB. ROS as signalling molecules: mechanisms that generate specificity in ROS homeostasis. Nat Rev Mol Cell Biol. 2007;8(10):813-824.
35. Atashi F, Modarressi A, Pepper MS. The role of reactive oxygen species in mesenchymal stem cell adipogenic and osteogenic differentiation: a review. Stem Cells Dev. 2015;24(10):1150-1163.

Ferrata Storti Foundation

Haematologica 2020
Volume 105(5):1216-1222

Prion protein deficiency impairs hematopoietic stem cell determination and sensitizes myeloid progenitors to irradiation

Capucine Siberchicot,[1,2,3,4] Nathalie Gault,[1,3,4,5,6] Nathalie Déchamps,[1,3,4,6] Vilma Barroca,[1,3,4,5,6] Adriano Aguzzi,[7] Paul-Henri Roméo,[1,3,4,5,6] J. Pablo Radicella,[1,2,3,4] Anne Bravard,[1,2,3,4,5,6] Jacqueline Bernardino-Sgherri[1,2,3,4,5,6]

[1]French Alternative Energies and Atomic Energy Commission (CEA)/Direction of Fundamental Research (DRF)/Institute of Biology François Jacob (IBFJ)/Institute of Cellular and Molecular Radiobiology (iRCM), 92265 Fontenay-aux-Roses Cedex, France; [2]Laboratory of Research in Genetic Instability (LRIG), 92265 Fontenay-aux-Roses Cedex, France; [3]Université Paris-Diderot, Sorbonne Paris Cité, Paris, France; [4]Université Paris-Sud, Paris, France; [5]Laboratory of Repair and Transcription in Hematopoietic Stem Cells (LRTS), 92265 Fontenay-aux-Roses Cedex, France; [6]Inserm U967, 92265 Fontenay-aux-Roses Cedex, France and [7]Institute of Neuropathology, University of Zurich, Zurich, Switzerland

ABSTRACT

Highly conserved among species and expressed in various types of cells, numerous roles have been attributed to the cellular prion protein (PrPC). In hematopoiesis, PrPC regulates hematopoietic stem cell self-renewal but the mechanisms involved in this regulation are unknown. Here we show that PrPC regulates hematopoietic stem cell number during aging and their determination towards myeloid progenitors. Furthermore, PrPC protects myeloid progenitors against the cytotoxic effects of total body irradiation. This radioprotective effect was associated with increased cellular prion mRNA level and with stimulation of the DNA repair activity of the Apurinic/pyrimidinic endonuclease 1, a key enzyme of the base excision repair pathway. Altogether, these results show a previously unappreciated role of PrPC in adult hematopoiesis, and indicate that PrPC-mediated stimulation of BER activity might protect hematopoietic progenitors from the cytotoxic effects of total body irradiation.

Correspondence:

JACQUELINE BERNARDINO-SGHERRI
jacqueline.bernardino@cea.fr

ANNE BRAVARD
anne.bravard@cea.fr

Received: September 3, 2018.

Accepted: July 15, 2019.

Pre-published: August 14, 2019.

doi:10.3324/haematol.2018.205716

Check the online version for the most updated information on this article, online supplements, and information on authorship & disclosures: www.haematologica.org/content/105/5/1216

Introduction

Radiotherapy is commonly used alone or in combination with genotoxic drugs for treatment of numerous solid tumors. Despite progress in its targeting, radiotherapy can be deleterious to two tissues, the gastrointestinal tract and the bone marrow (BM), and can lead to secondary effects commonly defined as Acute Radiation Syndrome.[1] Irradiation of the BM damages hematopoietic stem and progenitor cells (HSPC) and perturbs the hematopoietic microenvironment,[2,3] resulting in radiation-induced acute myelosuppression[4,5] and increased susceptibility to infections.[6,7]

Numerous types of DNA lesions are induced by cell exposure to ionizing radiation. They include base modifications, apurinic/apyrimidic sites (AP sites), and single- (SSB) and double (DSB)-strand breaks. DSB are the main lesions affecting cell survival. They can arise not only directly by deposition of energy on the DNA, but also as a consequence of the formation of AP sites or SSB.[8,9] Indeed, base excision repair (BER) activities, and in particular the processing of abasic sites, have been shown to contribute to radiation-induced DNA damage.[10,11]

Apurinic/apyrimidic endonuclease-1 (Ape1) is the unique enzyme that converts AP sites into SSB intermediates during BER. Ape1 3'-phosphodieterase and -phosphate activities (for a review, see Laev *et al.*[12]) also contribute to the processing of radiation-induced DNA strand break extremities[13] during the single strand break repair pathway (SSBR). Accordingly, protection of neuronal cells from radiation-induced damage requires Ape1.[14,15]

The cellular prion protein (PrPC) is a highly conserved glycoprotein that, when structurally modified, plays a critical role in the pathogenesis of neurodegenerative

disorders called prion diseases.[16] The normal prion protein was shown to protect cells from oxidative stress.[17-20] It also gives protection from DNA damage by promoting Ape1 DNA repair activity and cell survival through an interaction with Ape1.[21] During hematopoiesis, PrPC is highly expressed in HSC and hematopoietic progenitors[22-24] and PrPC deficiency is associated with decreased HSC self-renewal.[25] As oxidative stress and DNA damage help determine HSC cell fate,[26] PrPC might participate in the maintenance of the hematopoietic system and its response to cytotoxic stresses. To address these points, we used *Prnp* knockout mice to study the consequences of PrPC deficiency on hematopoiesis of young and old adult mice, and on the response of hematopoietic stem cells (HSC) and hematopoietic progenitors to gamma-irradiation.

Methods

Mice

Mice experiments were carried out in compliance with the European Community Council Directive (EC/2010/63) and were approved by our institutional ethics committee (CetEA-CEA-DRF–n. 17-096). The B6.129S7-Prnptm1Cwe/Orl mice were from the European Mutant Mouse Archive and bred in our animal facility. We also used *Prnp* ZH3/ZH3 mice provided by A. Aguzzi (Zurich, Switzerland) and C57BL/6 mice were purchased from Charles River.

Cell sorting and flow cytometry analysis of bone marrow cells

Murine BM cells were flushed out of femurs, tibiae, hip bone and humeruses using a syringe filled with DPBS and filtered through a 70 µm-cell strainer. After red blood cell lysis using NH_4Cl solution (STEMCELL Technologies), mononuclear cells were phenotyped using different antibody cocktails from Biolegend, e-Bioscience or Beckton Dickinson. Flow cytometry analysis was performed with a BD FACS LSRII™ flow cytometer (BD Biosciences) and cell sorting with a FACS Influx cell sorter (Becton Dickinson). Data were analyzed with FlowJo software. Antibodies and gating strategies for hematopoietic subset analysis and sorting are described in the *Online Supplementary Methods*. For RT-PCR and Ape1 endonuclease activity experiments, aliquots of 50,000 myeloid progenitor cells were sorted in PBS whereas aliquots of 10,000 HSC and multi-potent progenitors (MPP) were sorted in PBS/1%BSA.

Ape1 endonuclease activity

Cell extracts were obtained by sonication of pelleted BM sorted cells in 20mM Tris-HCl, pH 7.5, 250mM NaCl, 1mM EDTA, 20mM sucrose, and protease inhibitor cocktail 0.1% (Sigma-Aldrich P2714). For progenitor analysis, 50,000 cells were suspended in 125 µL extraction buffer. For HSC or MEP analysis, 10,000 sorted cells were suspended in 30µL extraction buffer. After sonication, the homogenate was centrifuged at 20,000 x g for 30 minutes (min) at 4°C and aliquots of the supernatant were stored at -80°C. Ape1 endonuclease activity was measured using a 5'-end labeled 34-mer oligonucleotide containing a single tetrahydrofuranyl artificial AP site at position 16 hybridized to its complementary oligonucleotide containing a cytosine opposite the lesion (Eurogentec). To measure Ape1 activity in BM progenitors, 1-4 µL of cell extract were incubated for 30 min at 30°C in 10 µL of reaction buffer containing 25mM Tris-HCl pH 7.5, 5mM $MgCl_2$, 5% glycerol, 52mM NaCl, BSA 1 µg/µL and 150 fmoles of the hybridized oligonucleotide. To determine Ape1 activity in BM HSC and MPP, 1-4 µL of cell extract were incubated for 10 min at 30°C in 10 µL reaction buffer containing 25mM Tris-HCl pH 7.5, 5mM MgCl2, 5% glycerol, 52mM NaCl, and 150 fmoles of the hybridized oligonucleotide. The reaction was stopped by adding 4µL of denaturating buffer (80% formamide, 0.1% bromophenol blue, 10mM EDTA) followed by heating for 5 min at 95°C. The products of the reaction were resolved by denaturating 7M urea-20% polyacrylamide gel electrophoresis. Gels were scanned using a Typhoon 5 (GE Healthcare Life Sciences) and band intensifies were quantified with ImageQuant TL 8.1 (GE Healthcare Life Sciences).

Statistical analyses

Quantitative data are presented as the mean±standard error of mean (SEM). Statistical significance was assayed using the non-parametric Mann Whitney U-test (GraphPad Prism software).

Additional information concerning the materials and methods used are to be found in the *Online Supplementary Methods.*

Results

Cellular prion protein is differentially expressed in hematopoietic stem cells and myeloid progenitors and is involved in hematopoietic stem cell expansion during aging

To address the potential functions of PrPC in hematopoietic stem and progenitor cells (HSPC), we first characterized the expression pattern of *Prnp* in different purified hematopoietic subpopulations, i.e. common myeloid progenitors (CMP), granulocyte-monocyte progenitors (GMP), megakaryocyte-erythrocyte progenitors (MEP), MPP, and hematopoietic stem cells (HSC). The highest level of *Prnp* mRNA was found in MEP while they were 2.7-fold and 4.3-fold lower in CMP and GMP, respectively (Figure 1A). These differences in mRNA expression were also found at the protein level (Figure 1B and *Online Supplementary Figure S1A*). The *Prnp* mRNA level in purified HSC was 2.5-fold higher than in MPP (Figure 1C).

To determine if PrPC has a role in hematopoiesis, we first compared BM from 3-month old $Prnp^{+/+}$ (WT) and $Prnp^{-/-}$ (KO) mice. WT and KO mice showed similar peripheral blood counts (*data not shown*) and BM cellularity (*Online Supplementary Figure S1B*). However, the frequency of CMP, GMP and MEP was significantly reduced in KO mice compared to WT mice (Figure 1D), whereas CLP, MPP, ST-HSC and LT-HSC frequencies were similar (Figure 1E). The differences between KO and WT myeloid progenitor frequencies were not associated with increased apoptosis (*Online Supplementary Figure S1C)* or cell cycle alteration (*Online Supplementary Figure S1D*) but with a higher percentage of quiescent MPP and ST-HSC (Figure 1F). These results suggest a defect of determination of HSPC (MPP and ST-HSC) towards the myeloid lineage in $Prnp^{-/-}$ mice. Finally, clonogenic assay using purified CMP and GMP showed a significantly decreased plating efficiency of $Prnp^{-/-}$ CMP and GMP (Figure 1G). Taken together, these results show intrinsic myeloid differentiation deficiencies in $Prnp^{-/-}$ HSC and progenitors and suggest that the reduction of cycling MPP and ST-HSC contributes to the lower myeloid progenitor content in the BM from KO compared to WT mice.

Aging of HSC is associated with an increased percent-

age of HSC in BM, decreased HSC self-renewal, and accumulation of DNA damage.[27] As PrPC has been implicated in HSC self-renewal[25] and in DNA repair,[21] we investigated the effect of PrPC loss in HSC numbers and DNA repair capacity during aging in *Prnp*$^{+/+}$ and *Prnp*$^{-/-}$ mice. *Prnp* mRNA level in HSC was 2.7-fold higher in 11-month old compared to 3-month old mice (Figure 1H) but did not change in MPP (Figure 1H). BM from 11-month old WT and KO mice displayed similar cellularity (*Online Supplementary Figure S1E*). As in 3-month old mice, a lower frequency of myeloid progenitors but not MPP (Figure 1I) was found in 11-month old KO mice (*Online*

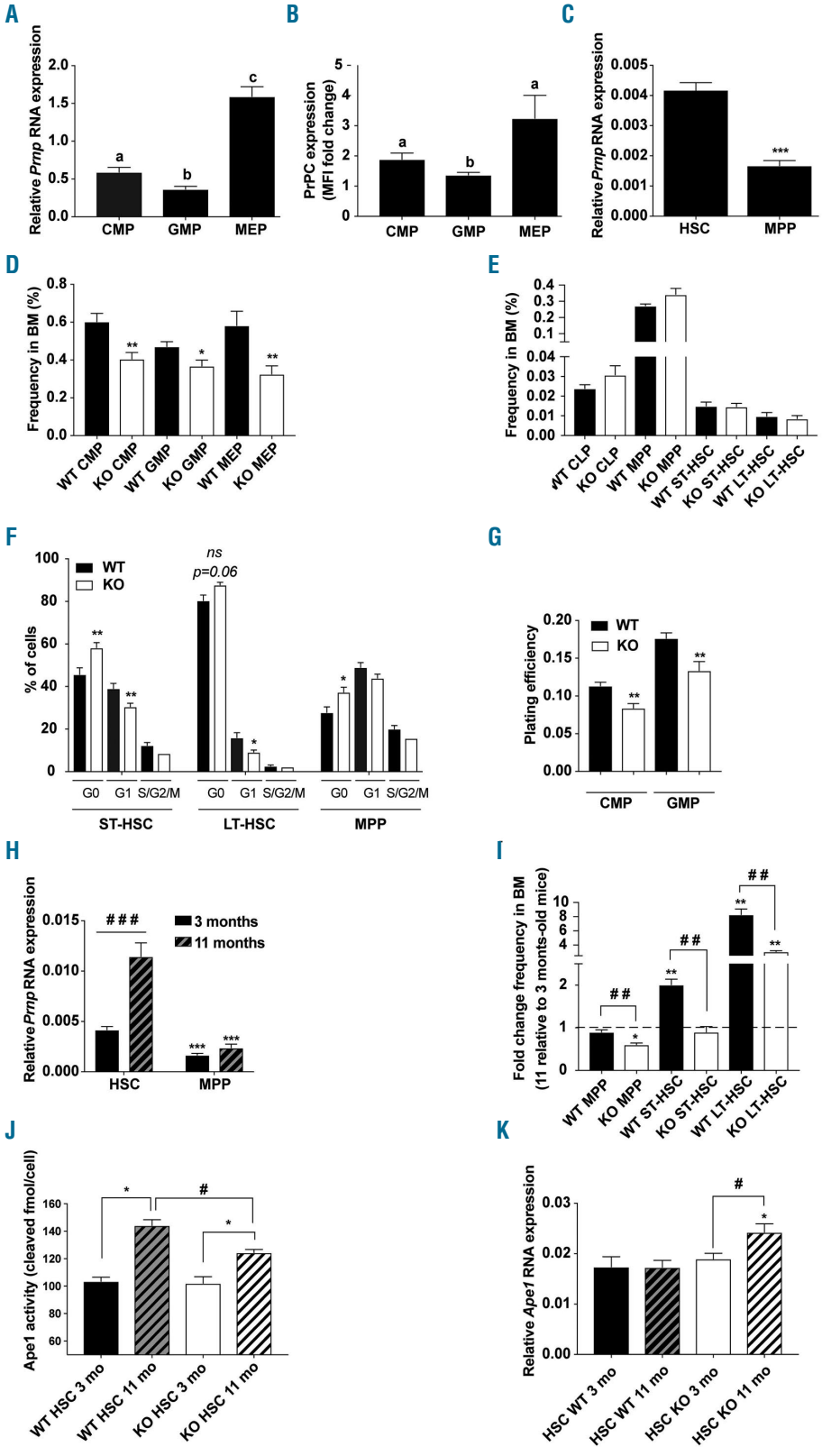

Figure 1. PrPC contributes to mouse hematopoietic homeostasis. (A) quantative real-time polymerase chain reaction (qRT-PCR) analysis of *Prnp* expression, normalized to *Rplp0* in the indicated bone marrow (BM) subpopulations: CMP: common myeloid progenitor; GMP: granulocyte-macrophage progenitor; MEP: megakaryocyte-erythrocyte progenitor purified by flow cytometry from BM of 3-month old mice (n=7-9). Data are presented as mean±standard error of mean (SEM). Means with different letters are significantly different (P<0.05). (B) Flow cytometry analysis of the PrPC protein expression in the indicated BM supopulations. Graph depicts ratio of median fluorescence intensity (MFI) in wild-type (WT) and knock-out (KO) control cells (n=5-6). Data are presented as mean±SEM. Means with different letters are significantly different (P<0.05) (CMP *vs.* MEP, P=0.06). (C) qRT-PCR analysis of *Prnp* expression, normalized to *Actb* in hematopoietic stem cell (HSC) (LSK CD135$^-$) and in multipotent progenitor (MPP) (LSK CD135$^+$) purified by flow cytometry from BM of 3-month old mice (n=9); Data are presented as mean±SEM. ***P<0.001. (D) Frequencies of myeloid progenitors in WT (black bars) and KO (white bars) BM from 3-month old mice (n=6-10). Data are presented as mean±SEM. *P<0.05; **P<0.01. (E) Frequencies of lymphoid progenitors (CLP), MPP, ST- and LT-HSC in the BM from WT (black bars) and KO (white bars) mice (n=6). Data are presented as mean±SEM. (F) Distribution of WT (black bars) and KO (white bars) HSC and MPP in each phase of the cell cycle. Data are presented as mean±SEM. *P<0.05; **P<0.01. ns: not significant. (G) *In vitro* plating efficiency of CMP and GMP purified by flow cytometry from BM of WT (black bars) and KO (white bars) mice (n=6-9). Data are presented as mean±SEM. **P<0.01. (H) qRT-PCR analysis of *Prnp* expression, normalized to Actb in WT and KO HSC and MPP purified by flow cytometry from BM of 3-month and 11-month old mice (n=6-9). Data are presented as the mean±SEM. ***P<0.001 or ###P<0.001. (I) Frequencies of MPP, ST- and LT-HSC in BM from 3-month and 11-month old WT (black bars) and KO (white bars) mice. Data are presented as the mean±SEM fold change of the frequencies in 11-month relative to 3-month old mice (n=6-10). **P<0.01 or ##P<0.01. (J) Ape1 endonuclease activity in 3-month (opened) and 11-month (hatched) old WT (dark) and KO (light) HSC. Data are presented as the mean±SEM. (n=4-5). *P<0.05 or #P<0.05. (K) qRT-PCR analysis of *Ape1* expression, normalized to *Actb* in WT (dark) and KO (light) HSC purified by flow cytometry from BM of 3-month (opened bars) and 11-month (hatched bars) old mice. Data are presented as mean±SEM. (n=7-9). *P<0.05 or #P<0.05.

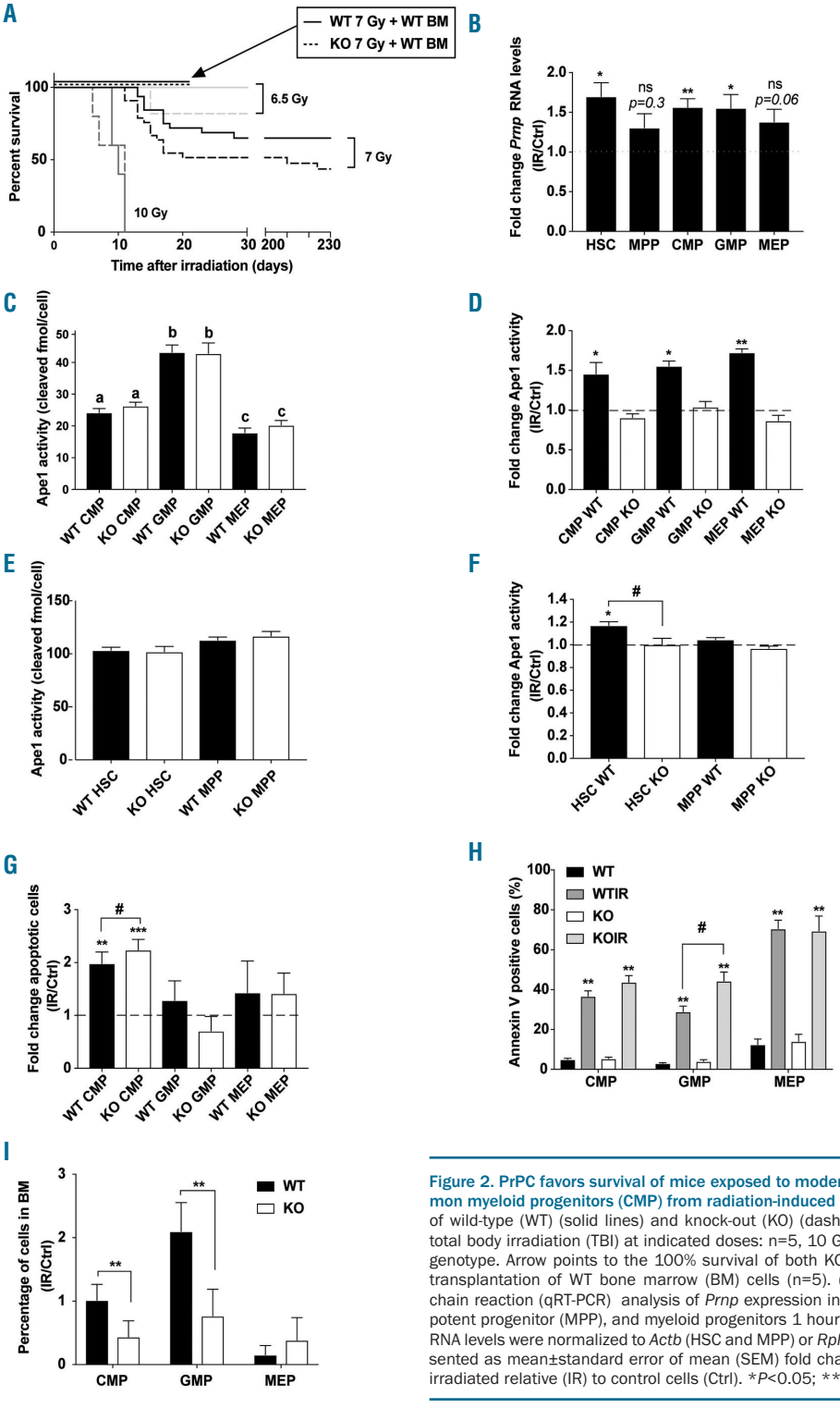

Figure 2. PrPC favors survival of mice exposed to moderate doses of γ-rays and protects common myeloid progenitors (CMP) from radiation-induced death. (A) Kaplan-Meier survival plots of wild-type (WT) (solid lines) and knock-out (KO) (dashed lines) mouse overall survival after total body irradiation (TBI) at indicated doses: n=5, 10 Gy; n=13, 6.5 Gy; n=28, 7 Gy; for each genotype. Arrow points to the 100% survival of both KO and WT irradiated mice (7 Gy) after transplantation of WT bone marrow (BM) cells (n=5). (B) Quantitative real-time polymerase chain reaction (qRT-PCR) analysis of *Prnp* expression in hematopoietic stem cell (HSC), multipotent progenitor (MPP), and myeloid progenitors 1 hour (h) after irradiation (7 Gy) (n=6). *Prnp* RNA levels were normalized to *Actb* (HSC and MPP) or *Rplp0* (myeloid progenitors). Data are presented as mean±standard error of mean (SEM) fold change of normalized *Prnp* RNA levels in irradiated relative (IR) to control cells (Ctrl). **P*<0.05; ***P*<0.01.

(C) Ape1 endonuclease activity in myeloid progenitor subpopulations from WT (black bars) and KO (white bars) mice (n=5-8). Data are presented as mean±SEM. Means with different letters are significantly different (*P*<0.05). (D) Ape1 endonuclease activity in myeloid progenitors from WT (black bars) and KO (white bars) mice (n=5-8) 1 h after irradiation (7 Gy). Data are presented as mean±SEM fold change of Ape1 endonuclease in irradiated relative to non-irradiated control cells. **P*<0.05; ***P*<0.01. (E) Ape1 endonuclease activity in HSC and MPP from WT (black bars) and KO (white bars) mice (n=5-8). Data are presented as mean±SEM. (F) Ape1 endonuclease activity in HSC and MPP from WT (black bars) and KO (white bars) mice (n=4-5) 1 h after irradiation (7 Gy). Data are presented as mean±SEM fold change of Ape1 endonuclease in irradiated relative to non-irradiated control cells. **P*<0.05 or #*P*<0.05. (G) Percentage of apoptotic myeloid progenitors (AnnexineV-positive cells) in BM from WT (black bars) and KO (white bars) mice (n=6-8) 1 h after irradiation (7 Gy). Data are presented as mean±SEM fold change of percentage of apoptotic cells in irradiated relative to non-irradiated control myeloid progenitors. ***P*<0.01; ***P<0.001; #*P*<0.05. (H) Percentage of apoptotic myeloid progenitors (AnnexineV-positive cells) in BM from WT (dark gray bars, WTIR) and KO (light gray bars, KOIR) mice (n=6-8) 1 h after irradiation (7 Gy). Data are presented as mean±SEM. Non-irradiated control WT (black bars) and KO (white bars) myeloid progenitors are shown. ***P*<0.01; #*P*<0.05. (I) Percentage of myeloid progenitors in BM from WT (black bars) and KO (white bars) mice (n=6-7) 18 h after irradiation (7 Gy). Data are presented as mean±SEM of the percentage of cells remaining in BM 18 h after irradiation compared to non-irradiated control. ***P*<0.01.

Supplementary Figure S1F). In contrast, compared to their 3-month old counterparts, ST- and LT-HSC frequencies respectively increased 2- and 8.3-fold in 11-month old WT mice but did not change (ST-HSC) or was only 3-fold increased (LT-HSC) in 11-month old KO mice (Figure 1I). DNA repair was slightly dependent on PrPC in aged HSC. A 1.4-fold increased activity of Ape1 in WT HSC was found between three months and 11 months without any change in *Ape1* mRNA level. In KO HSC, Ape1 activity also increased between three months and 11 months, but to a lesser extent (1.2-fold) than in WT HSC. Interestingly, this increased activity was associated with an increased *Ape1* mRNA level (Figure 1J and K).

Altogether, these results show that PrPC deficiency is associated with decreased HSC determination towards the myeloid lineage, and decreased number of HSC and decreased Ape1 activity in old mice.

Prnp expression is up-regulated in myeloid progenitors and hematopoietic stem cell subpopulations after *in vivo* radiation exposure

Hematopoietic stem cell aging is associated with increased oxidative stress[28] and PrPC has been shown to protect cells from oxidative stress.[17-20] To characterize the role of PrPC during the oxidative stress of hematopoiesis, we performed total body irradiation (TBI) on WT and KO mice. Survival curves of WT and KO mice exposed to increasing gamma-radiation doses showed that a higher percentage of irradiated KO mice died earlier than irradiated WT mice even if statistical significance between both genotypes was not reached (P=0.0792 at 7 Gy) (Figure 2A). When KO mice were grafted with BM from non-irradiated WT mice 24 hours (h) after a 7 Gy irradiation, they did not die, indicating that the higher sensitivity of KO mice to TBI was not due to the BM microenvironment of KO mice and that they died from hematopoietic syndrome.

One hour after a 7 Gy TBI, a 1.5-fold increase in *Prnp* mRNA level was found in HSC, CMP and GMP but not in MPP and MEP (Figure 2B). These data are consistent with the observed *Prnp* upregulation in neuronal tissues after exposure to genotoxic stress,[21] and suggest a potential role of PrPC in response to radiation in GMP, CMP, and HSC.

Cellular prion protein-dependent increase in the DNA repair activity of Ape1 is associated with radioprotection of CMP and GMP

Cellular prion protein prevents cell death in response to alkylating agent or H_2O_2 exposure by directly stimulating the DNA repair activity of Ape1.[21] Without irradiation, Ape1 activity was similar in WT and KO progenitors (Figure 2C). One hour after a 7 Gy TBI, Ape1 activity increased in all WT irradiated myeloid progenitors analyzed (from 1.5- to 1.7-fold) but not in their KO counter parts (Figure 2D). In HSC and MPP, Ape1 activity was similar in WT and KO mice (Figure 2E) but increased only in WT HSC after a 7 Gy TBI (Figure 2F). Whatever the subpopulation analyzed, the radiation-induced Ape1 activity was not associated with an increase in *Ape1* mRNA level (*Online Supplementary Figure S2A and B*). These data show that, after irradiation, Ape1 activity in all myeloid progenitor subpopulations and in HSC is stimulated in a PrPC-dependent manner.

As the radiation-induced death of myeloid progenitors is dependent on apoptosis,[5] we quantified apoptosis in WT and KO myeloid progenitors 1 and 12 h after TBI at 7 Gy. One hour after irradiation, apoptotic (Annexin V-positive cells) and dead cell (Annexin V-negative and Hoechst-positive cells) fractions increased only in CMP and were higher in KO compared to WT CMP (Figure 2G and *Online Supplementary Figure S2C*). Twelve hours after irradiation, both apoptotic (Figure 2H) and dead (*Online Supplementary Figure S2D*) cell fractions increased in all myeloid progenitor subpopulations in both WT and KO mice. However, higher rates of apoptosis and cellular death were observed in irradiated KO compared to WT GMP. In accordance with this, significantly lower frequencies of CMP and GMP were found in KO *versus* WT irradiated mice 18 h after irradiation (Figure 2I). Myeloid progenitors from *Prnp* ZH3/ZH3 mice exhibited the same radiation sensitivity than those from *Prnp*$^{-/-}$ mice, shown by a similar reduced number compared to mice in non-irradiated conditions (*Online Supplementary Figure S2E*). Altogether, these results suggest that PrPC-dependent stimulation of the DNA repair activity of Ape1 is required for the radioprotection of myeloid progenitors.

Discussion

Despite numerous studies, the physiological role of PrPC remains elusive. Recently, we showed that PrPC can stimulate an important DNA repair pathway, the BER, in neuronal tissues through interaction with and stimulation of its key enzyme, APE1.[21] Here we show that the same mechanism can be proposed for the radioprotection of myeloid progenitors, HSC determination, and the expansion of the HSC compartment during aging.

Previous studies[22-24,29] indicated a decreased *Prnp* expression during differentiation of hematopoietic cells. Here, we performed an extended study of *Prnp* expression in different hematopoietic subpopulations and showed a 3-fold higher *Prnp* expression level in MEP compared to their progenitors CMP, suggesting that the correlation between *Prnp* downregulation and cellular differentiation[24] may not be a general feature in hematopoiesis. Furthermore, and contrary to a previous study,[25] we found that KO mice have less myeloid progenitors. This discrepancy could be explained by the fact that, in the previous study, younger mice were analyzed (7-10-week old mice compared to the 3-month and 11-month old mice used in the present study) and by the number of backcrosses (4 *vs.* >10) that might influence the phenotype of *Prnp* knockout mice.[30] Finally, we found a higher frequency of KO ST-HSC and KO MPP in the G0 phase. These populations being the direct precursors of myeloid progenitors, the increased quiescence of these cells might account for the decreased myeloid progenitor subpopulations.[31] Strikingly, both KO CMP and GMP exhibited a lower plating efficiency despite no significant change in their cell cycle *in vivo*. Whether the microenvironment of these cells could compensate *in vivo* for an intrinsic growth deficiency observed *in vitro* remains to be clarified.

Prnp expression in the HSC compartment increased 8-fold with age. This higher expression was associated with the known elevated frequency of both ST- and LT-HSC.[27,32] PrPC deficiency was associated with no increase in ST-HSC and with a diminished increase in LT-HSC with age, suggesting that PrPC plays a role in the age-dependent increase in HSC. Although an aging-associated increase in HSC numbers has been known for a long time and is

known to be cell-intrinsic,[33,34] the underlying mechanisms are not fully understood. The results presented here indicate a significant involvement of PrPC in the age-dependent increase in HSC frequency. This increase may be accounted for by a PrPC-dependent upregulation of Ape1 repair activity. Independently of its DNA repair activity,[35,36] Ape1 has a redox activity shown to be necessary for normal embryonic hematopoiesis,[37] stem cell pool maintenance,[38,39] and hematopoietic progenitor colony formation.[40] Thus, the PrPC-dependent stimulation of the Ape1 DNA repair activity might contribute to hematopoietic homeostasis.

We found a modest but recurrent radiation sensitization of *Prnp* KO mice that contrasts with a previous study showing that the absence of PrPC protected rather than sensitized mice to an 8 Gy TBI.[41] However, this work was performed on a mixed 129/C57BL6 background, whereas we used a pure C57BL6 background. Furthermore, that study used a dose of X rays that was lethal for WT animals, while we used different doses of non-lethal γ-rays. BM myeloid cells are particularly sensitive to chemical and radiation cytotoxicity.[4,42,43] Accordingly, we found a dramatic decrease in BM myeloid progenitors within the first 24 h after radiation exposure that was exacerbated in *Prnp* KO irradiated mice. The reduced frequency of KO irradiated myeloid progenitors was associated with higher CMP and GMP apoptosis, within the first 12 h after irradiation, as well as with an absence of stimulation of Ape1 activity in these subpopulations 1 h after irradiation. In contrast, in WT irradiated myeloid progenitors and HSC, upregulation of *Prnp* gene expression was associated with an increase in Ape1 activity in these subpopulations. PrPC has been shown to protect HSC from myelotoxic injury by 5-FU, commonly used in chemotherapy,[25] and we now extend its myeloprotective role to radiotherapy.

Finally, a similar basal reduced number of myeloid progenitors and a similar radiation sensitivity of myeloid progenitors were found in the co-isogenic *Prnp*$^{ZH3/ZH3}$ mouse line[44] and the *Prnp*$^{-/-}$ mouse line. These results rule out the involvement of any *Prnp* flanking gene polymorphism previously described by Nuvolone *et al.*[45]

Altogether, these results suggest that PrPC is involved in the homeostasis of steady-state hematopoiesis and that PrPC-dependent activation of base excision repair contributes to the radioprotection of the myeloid progenitors of the mouse bone marrow.

Acknowledgments

The authors thank Véronique Neuville and staff of the IRCM animal facility for animal care and breeding, and Petra Schwarz for managing Prnp ZH3/ZH3 mice supply. Flow cytometry and cell sorting were performed at the IRCM Flow Cytometry Shared Resource, established by equipment grants from DIM-Stem-Pôle, INSERM, Foundation ARC, and CEA.

Funding

This work was supported by the French National Electricity Company (EDF), the Transverse Division N°4 (Segment n°4 Radiobiologie – headed by Christophe Carles) and the Radiobiology Program of the French Alternative Energies and Atomic Energy Commission (CEA).

References

1. Dörr H, Meineke V. Acute radiation syndrome caused by accidental radiation exposure - therapeutic principles. BMC Med. 2011;9(1):126.
2. Simonnet AJ, Nehmë J, Vaigot P, Barroca V, Leboulch P, Tronik-Le Roux D. Phenotypic and functional changes induced in hematopoietic stem/progenitor cells after gamma-ray radiation exposure. Stem Cells. 2009;27(6):1400-1409.
3. Shao L, Luo Y, Zhou D. Hematopoietic Stem Cell Injury Induced by Ionizing Radiation. Antioxid Redox Signal. 2014;20(9):1447-1462.
4. Down JD, Boudewijn A, van Os R, Thames HD, Ploemacher RE. Variations in radiation sensitivity and repair among different hematopoietic stem cell subsets following fractionated irradiation. Blood. 1995; 86(1):122-127.
5. Mohrin M, Bourke E, Alexander D, et al. Hematopoietic stem cell quiescence promotes error-prone DNA repair and mutagenesis. Cell Stem Cell. 2010;7(2):174-185.
6. Kim JH, Thimmulappa RK, Kumar V, et al. NRF2-mediated Notch pathway activation enhances hematopoietic reconstitution following myelosuppressive radiation. J Clin Invest. 2014;124(2):730-741.
7. Zachman DK, Leon RP, Das P, et al. Endothelial cells mitigate DNA damage and promote the regeneration of hematopoietic stem cells after radiation injury. Stem Cell Res. 2013;11(3):1013-1021.
8. Ensminger M, Iloff L, Ebel C, Nikolova T, Kaina B, Löbrich M. DNA breaks and chromosomal aberrations arise when replication meets base excision repair. J Cell Biol. 2014;206(1):29-43.
9. Bauer NC, Corbett AH, Doetsch PW. The current state of eukaryotic DNA base damage and repair. Nucleic Acids Res. 2015; 43(21):10083-10101.
10. Fung H, Demple B. Distinct roles of Ape1 protein in the repair of DNA damage induced by ionizing radiation or bleomycin. J Biol Chem. 2011;286(7):4968-4977.
11. Wang H, Wang X, Chen G, et al. Distinct roles of Ape1 protein, an enzyme involved in DNA repair, in high or low linear energy transfer ionizing radiation-induced cell killing. J Biol Chem. 2014;289(44):30635-30644.
12. Laev SS, Salakhutdinov NF, Lavrik OI. Inhibitors of nuclease and redox activity of apurinic/apyrimidinic endonuclease 1/redox effector factor 1 (APE1/Ref-1). Bioorganic Med Chem. 2017;25(9):2531-2544.
13. Parsons JL, Dianova II, Dianov GL. APE1 is the major 3 -phosphoglycolate activity in human cell extracts. Nucleic Acids Res. 2004;32(12):3531-3536.
14. Vasko MR, Guo C, Thompson EL, Kelley MR. The repair function of the multifunctional DNA repair/redox protein APE1 is neuroprotective after ionizing radiation. DNA Repair (Amst). 2011;10(9):942-952.
15. Ströbel T, Madlener S, Tuna S, et al. Ape1 guides DNA repair pathway choice that is associated with drug tolerance in glioblastoma. Sci Rep. 2017;7(1):1-13.
16. Prusiner SB. Novel proteinaceous infectious particles cause scrapie. Science. 1982; 216(4542):136-144.
17. Milhavet O, Lehmann S. Oxidative stress and the prion protein in transmissible spongiform encephalopathies. Brain Res Brain Res Rev. 2002;38(3):328-339.
18. Rachidi W, Vilette D, Guiraud P, et al. Expression of prion protein increases cellular copper binding and antioxidant enzyme activities but not copper delivery. J Biol Chem. 2003;278(11):9064-9072.
19. McLennan NF, Brennan PM, McNeill A, et al. Prion protein accumulation and neuroprotection in hypoxic brain damage. Am J Pathol. 2004;165(1):227-235.
20. Krebs B, Wiebelitz A, Balitzki-Korte B, et al. Cellular prion protein modulates the intracellular calcium response to hydrogen peroxide. J Neurochem. 2007;100(2):358-367.
21. Bravard A, Auvré F, Fantini D, et al. The prion protein is critical for DNA repair and cell survival after genotoxic stress. Nucleic Acids Res. 2015;43(2):904-916.
22. Kent DG, Copley MR, Benz C, et al. Prospective isolation and molecular characterization of hematopoietic stem cells with durable self-renewal potential. Blood. 2009;113(25):6342-6350.
23. Liu T, Li R, Wong B-S, et al. Normal Cellular Prior Protein Is Preferentially Expressed on Subpopulations of Murine Hemopoietic Cells. J Immunol. 2001;166 (6):3733-3742.

24. Panigaj M, Glier H, Wildova M, Holada K. Expression of prion protein in mouse erythroid progenitors and differentiating murine erythroleukemia cells. PLoS One. 2011;6(9):e24599.
25. Zhang CC, Steele AD, Lindquist S, Lodish HF. Prion protein is expressed on long-term repopulating hematopoietic stem cells and is important for their self-renewal. Proc Natl Acad Sci U S A. 2006;103(7):2184-2189.
26. Weiss CN, Ito K. DNA damage: A sensible mediator of the differentiation decision in hematopoietic stem cells and in leukemia. Int J Mol Sci. 2015;16(3):6183-6201.
27. Rossi DJ, Seita J, Czechowicz A, Bhattacharya D, Bryder D, Weissman IL. Hematopoietic stem cell quiescence attenuates DNA damage response and permits DNA damage accumulation during aging. Cell Cycle. 2007;6(19):2371-2376.
28. Chen F, Liu Y, Wong NK, Xiao J, So KF. Oxidative Stress in Stem Cell Aging. Cell Transplant. 2017;26(9):1483-1495.
29. Dodelet VC, Cashman NR. Prion protein expression in human leukocyte differentiation. Blood. 1998;95(5):1556-1561.
30. Schmitz M, Greis C, Ottis P, et al. Loss of Prion Protein Leads to Age-Dependent Behavioral Abnormalities and Changes in Cytoskeletal Protein Expression. Mol Neurobiol. 2014;50(3):923-936.
31. Susek KH, Korpos E, Huppert J, et al. Bone marrow laminins influence hematopoietic stem and progenitor cell cycling and homing to the bone marrow. Matrix Biol. 2018;6747-62.
32. Kowalczyk MS, Tirosh I, Heckl D, et al. Single-cell RNA-seq reveals changes in cell cycle and differentiation programs upon aging of hematopoietic stem cells. Genome Res. 2015;25(12):1860-1872.
33. Rossi DJ, Bryder D, Zahn JM, et al. Cell intrinsic alterations underlie hematopoietic stem cell aging. Proc Natl Acad Sci U S A. 2005;102(26):9194-9199.
34. Geiger H, De Haan G, Carolina Florian M. The ageing haematopoietic stem cell compartment. Nat Rev Immunol. 2013;13(5):376-389.
35. Tell G, Quadrifoglio F, Tiribelli C, Kelley MR. The Many Functions of APE1/Ref-1: Not Only a DNA Repair Enzyme. Antioxid Redox Signal. 2008;11(3):601-620.
36. Xie J, Zhang L, Li M, et al. Functional analysis of the involvement of apurinic/apyrimidinic endonuclease 1 in the resistance to melphalan in multiple myeloma. BMC Cancer. 2014;14:11.
37. Zou GM, Luo MH, Reed A, Kelley MR, Yoder MC. Ape1 regulates hematopoietic differentiation of embryonic stem cells through its redox functional domain. Blood. 2007;109(5):1917-1922.
38. Wang K, Zhang T, Dong Q, Nice EC, Huang C, Wei Y. Redox homeostasis: The linchpin in stem cell self-renewal and differentiation. Cell Death Dis. 2013;4:e537.
39. Domenis R, Bergamin N, Gianfranceschi G, et al. The redox function of APE1 is involved in the differentiation process of stem cells toward a neuronal cell fate. PLoS One. 2014;9(2):e89232.
40. Rohrabaugh SL, Hangoc G, Kelley MR, Broxmeyer HE. Mad2 haploinsufficiency protects hematopoietic progenitor cells subjected to cell-cycle stress in vivo and to inhibition of redox function of Ape1/Ref-1 in vitro. Exp Hematol. 2011;39(4):415-423.
41. Strup-Perrot C, Vozenin MC, Monceau V, et al. PrP c deficiency and dasatinib protect mouse intestines against radiation injury by inhibiting of c-Src. Radiother Oncol. 2016;120(1):175-183.
42. Pilzecker B, Buoninfante OA, van den Berk P, et al. DNA damage tolerance in hematopoietic stem and progenitor cells in mice. Proc Natl Acad Sci U S A. 2017;114(33):E6875-E6883.
43. Roth RB, Samson LD. 3-Methyladenine DNA glycosylase-deficient Aag null mice display unexpected bone marrow alkylation resistance. Cancer Res. 2002;62(3):656-660.
44. Nuvolone M, Hermann M, Sorce S, et al. Strictly co-isogenic C57BL/6J- Prnp –/– mice: A rigorous resource for prion science. J Exp Med. 2016;213(3):313-327.
45. Nuvolone M, Kana V, Hutter G, et al. SIRP polymorphisms, but not the prion protein, control phagocytosis of apoptotic cells. J Exp Med. 2013;210(12):2539-2552.

ARTICLE

Long-term outcome of a randomized controlled study in patients with newly diagnosed severe aplastic anemia treated with antithymocyte globulin and cyclosporine, with or without granulocyte colony-stimulating factor: a Severe Aplastic Anemia Working Party Trial from the European Group of Blood and Marrow Transplantation

André Tichelli,[1] Régis Peffault de Latour,[2] Jakob Passweg,[1] Cora Knol-Bout,[3] Gérard Socié,[4] Judith Marsh,[5] Hubert Schrezenmeier,[6] Britta Höchsmann,[6] Andrea Bacigalupo,[7] Sujith Samarasinghe,[8] Alicia Rovó,[9] Austin Kulasekararaj,[10] Alexander Röth,[11] Dirk-Jan Eikema,[3] Paul Bosman,[3] Peter Bader,[12] Antonio Risitano[13] and Carlo Dufour[14] on behalf of the SAA Working Party of the EBMT

[1]Division of Hematology, University Hospital Basel, Basel, Switzerland; [2]Université de Paris, and Hematology-Transplantation, Saint Louis Hospital (AP-HP), Paris, France; [3]EBMT Registry Office, Leiden, the Netherlands; [4]Université de Paris, INSERM U976 and Hematology-Transplantation, Saint Louis Hospital (AP-HP), Paris, France; [5]Department of Haematological Medicine, King's College Hospital/King's College London, London, UK; [6]Institute of Tranfusion Medicine, University of Ulm and Institute of Clinical Transfusion Medicine and Immunogenetics Ulm, German Red Cross Blood Transfusion Service Baden-Württemberg-Hessen and University Hospital Ulm, Ulm, Germany; [7]Instituto di Ematologia, Fondazione Policlinico Universitario Gemelli IRCSS, Università Cattolica del Sacro Cuore, Roma, Italy; [8]Sujith Samarasinghe, Great Ormond Street Hospital, London, UK; [9]Department of Hematology and Central Hematology Laboratory, Bern University Hospital, University of Bern, Bern, Switzerland; [10]Department of Haematological Medicine, King's College Hospital, NIHR/Wellcome King's Clinical Research Facility, London, UK; [11]Department of Hematology, West German Cancer Center, University Hospital Essen, University of Duisburg-Essen, Essen, Germany; [12]University Children's Hospital Frankfurt, Frankfurt, Germany; [13]Hematology Department of Clinical Medicine and Surgery, Federico II University of Naples, Naples, Italy and [14]Hemato-Onco-SCT Pole, Hematology Unit. G. Gaslini Children's Research Hospital, Genova, Italy.

Ferrata Storti Foundation

Haematologica 2020
Volume 105(5):1223-1231

Correspondence:

ANDRÉ TICHELLI
tichelli@datacomm.ch

Received: March 20, 2019.

Accepted: September 30, 2019.

Pre-published: October 3, 2019.

doi:10.3324/haematol.2019.222562

Check the online version for the most updated information on this article, online supplements, and information on authorship & disclosures: www.haematologica.org/content/105/5/1223

ABSTRACT

This follow-up study of a randomized, prospective trial included 192 patients with newly diagnosed severe aplastic anemia receiving antithymoglobulin and cyclosporine, with or without granulocyte colony-stimulating factor (G-CSF). We aimed to evaluate the long-term effect of G-CSF on overall survival, event-free survival, probability of secondary myelodysplastic syndrome (MDS) or acute myeloid leukemia (AML), clinical paroxysmal nocturnal hemoglobinuria, relapse, avascular osteonecrosis and chronic kidney disease. The median follow-up was 11.7 years (95% CI, 10.9-12.5). The overall survival rate at 15 years was 57±12% in the group given G-CSF and 63±12% in the group not given G-CSF (P=0.92); the corresponding event-free survival rates were 24±10% and 23±10%, respectively (P=0.36). In total, 9 patients developed MDS or AML, 10 only a clonal cytogenetic abnormality, 7 a solid cancer, 18 clinical paroxysmal nocturnal hemoglobinuria, 8 osteonecrosis, and 12 chronic kidney disease, without any difference between patients treated with or without G-CSF. The cumulative incidence of MDS, AML or isolated cytogenetic abnormality at 15 years was 8.5±3% for the G-CSF group and 8.2±3% for the non-G-CSF group (P=0.90). The cumulative incidence of any late event including myelodysplastic syndrome or acute myeloid leukemia, isolated cytogenetic abnormalities, solid cancer, clinical paroxysmal nocturnal hemoglobinuria, aseptic osteonecrosis, chronic kidney disease and relapse was 50±12% for the G-CSF group and 49±12% for the non-G-CSF group (P=0.65). Our results demonstrate that it is unlikely

that G-CSF has an impact on the outcome of severe aplastic anemia; nevertheless, very late events are common and eventually affect the prognosis of these patients, irrespectively of their age at the time of immunosuppressive therapy (NCT01163942).

Introduction

Acquired aplastic anemia is a rare disease defined by peripheral pancytopenia associated with hypocellularity of the bone marrow. The aim of treatment of aplastic anemia is to improve peripheral blood counts and obtain transfusion independency. First-line treatment for younger patients (≤40 year old) with a matched sibling donor is allogeneic stem cell transplantation (SCT). The standard of care for adult patients not eligible for SCT is immunosuppressive therapy (IST), including a combination of horse antithymocyte globulin (ATG) and cyclosporine (CSA).[1] In contrast to patients undergoing SCT, those treated with IST are not cured from their disease and are at risk of late complications such as relapse and development of late clonal diseases, including paroxysmal nocturnal hemoglobinuria (PNH), myelodysplastic syndrome (MDS) or acute myeloid leukemia (AML).[2] Furthermore, the delayed recovery of peripheral blood counts exposes patients to infectious and hemorrhagic complications.[3]

Immunosuppression remains a suboptimal treatment, since about 30% of the patients fail to respond and even in responding patients, blood counts often remain subnormal, possibly requiring maintenance IST with CSA. Efforts have been made for 40 years to improve the standard horse ATG plus CSA treatment.[1] Other immunosuppressive combinations as well as the use of high-dose cyclophosphamide have been evaluated, without showing the expected breakthrough.[4-7] Great hopes have been placed in the development of hematopoietic growth factors. The role of granulocyte colony-stimulating factor (G-CSF) added to standard IST with ATG and CSA, tested in six small prospective randomized trials, was inconclusive.[8-13] Therefore, in 2001 a prospective randomized study was initiated to evaluate the short- and long-term effects of G-CSF added to standard IST. Patients with newly diagnosed severe aplastic anemia (SAA) were randomized to treatment with ATG and CSA, with or without G-CSF (NCT01163942). The study demonstrated that G-CSF added to ATG and CSA decreases the rate of early infectious episodes and days of hospitalization in patients with very SAA patients, but has no significant impact on overall survival (OS), event-free survival (EFS), relapse, or death rates.[14] The role of G-CSF in triggering late clonal evolution to a hematologic malignancy has been debated for years.[15-18] and we lacked follow-up in our previous study for a meaningful assessment of this risk.[14]

Early death occurs secondary to infection, bleeding, or complications of severe anemia. Limited data are available on late malignant and non-malignant complications after IST. Today, 16 years after initiation, this randomized controlled study is a unique opportunity to assess the long-term outcome of SAA patients treated with IST. We thus aimed to evaluate the durability of response to treatment, survival outcomes, and the risk of long-term complications of patients treated with ATG and CSA, with or without G-CSF.

Methods

Design

The design and methodology of the randomized study have been described previously.[14] It was an open-label, multicenter randomized study conducted by the Severe Aplastic Anemia Working Party of the European Group for Blood and Marrow Transplantation (EBMT). Disease severity was assessed with the use of standard criteria and categorized into SAA and very SAA. Patients of any age were included, but patients with congenital SAA, such as Fanconi anemia, as well as patients with hypoplastic MDS were excluded. A total of 192 patients with newly diagnosed SAA, not eligible for SCT, were randomly assigned in a multicenter trial to receive horse ATG and CSA with (49.5%) or without G-CSF (50.5%). Patients randomized to receive G-CSF were given a dose of 150 μg/m^2/day from day 8 through day 240 except for subjects who achieved complete remission before. Methylprednisolone (or prednisone) 1 mg/kg/day was administered on days 1-14. After 14 days, corticosteroids were tapered off over the subsequent 14 days. In the case of serum sickness, a longer tapering schedule, as clinically indicated, was allowed. Complete response was defined as transfusion independency with a hemoglobin level ≥110 g/L, a neutrophil count ≥1.5 x10^9/L and a platelet count ≥150 x10^9/L. Partial response was defined as no longer meeting the criterial of SAA and no transfusion dependence for platelets and/or red blood cells. Continuous transfusion dependency was classified as no response. Relapse was defined as a decrease in blood counts to values either requiring transfusions or needing re-treatment of the aplastic anemia with immunosuppression or SCT. For late complications, the participating centers were asked to report the date of first appearance of a clonal evolution to a hematologic malignancy (MDS or AML, whichever appeared first; or an isolated cytogenetic abnormality), solid cancer, clinical PNH, osteonecrosis and chronic kidney disease. The diagnosis of clinical PNH was retained in patients with a measurable PNH clone who developed either thromboembolic complications or active intravascular hemolysis. Chronic kidney disease was defined as persistence of abnormal creatinine or glomerulation filtration rates more than 1 year after randomization. The present analysis included all 192 randomized patients (Table 1). The study was approved by the ethics committee of each center including patients in the study. All patients gave informed written consent to inclusion in the study.

Outcome measures

Given that at the time of first publication 44 of the original 192 patients had died, the follow-up was done for the remaining 148 patients. Endpoints of the present study were OS, EFS, causes of death, and probability of clonal evolution to a hematologic malignancy (including secondary MDS/AML and an isolated cytogenetic abnormality), solid cancer, clinical PNH, relapse, avascular osteonecrosis and chronic kidney disease by 15 years, comparing for each endpoint patients treated with or without G-CSF. Causes of deaths were classified as related to aplastic anemia (infection, bleeding, undefined), to secondary neoplasm (MDS, AML, solid cancer), transplantation related in patients who received SCT for treatment failure, unrelated to aplastic anemia, or of unknown cause. We analyzed the risk of osteonecrosis because of the use of steroids,[19-21] and of chronic

kidney disease because of the treatment with ATG and CSA.[22,23] Furthermore, for patients with aseptic osteonecrosis we compared those who needed more than one course of ATG and were therefore more exposed to steroids, to those treated with a single course of ATG; for patients with chronic kidney disease we compared patients who were either dependent on CSA or needed a subsequent course of CSA to those who received a single course of ATG without being dependent on CSA. Time to an event started from the day of randomization, except for survival of patients treated with SCT. For OS, patients were censored either at the time of last follow-up or at the time of transplantation, used as salvage therapy. For EFS analysis, events were defined as relapse, non-response at day 120, subsequent SCT, the occurrence of MDS/AML, solid cancer, clinical PNH or death.

Statistical analysis

Group differences were analyzed with the use of the Mann-Whitney U test for continuous variables and the χ^2 test for categorical variables. Survival probabilities were calculated with the use of the Kaplan-Meier estimator. Time at risk started from the date of randomization and ended on the date of death for OS, and on the date of an event for EFS, or the date of last known assessment, whichever came first. For the cumulative incidence of a late complication, death from other cause was considered as a competing risk. The log-rank test with a two-sided significance level was used for comparison in the Kaplan-Meier estimates. The time to an event was computed from the date of randomization to the date of death or the date of last contact. Univariate competing risk analyses were performed using the Gray test. Multivariate analysis was performed to calculate hazard ratios and their 95% confidence intervals, adjusted for all covariates, using a Cox proportional hazards regression model. Factors considered were age at randomization, severity of aplastic anemia and the use of G-CSF. All *P*-values are two-sided with a type I error rate fixed at 0.05. Statistical analyses were performed with SPSS Statistic 25 software (IBM Corp., Chicago, IL, USA); cumulative incidence curves were constructed with NCSS 2004 (Statistics and Systems, Kaysville, UT, USA).

Table 1. Characteristics of the study patients, overall and according to randomization to treatment with or without granulocyte colony-stimulating factor.

Variable	All 192	No G-CSF 95	With G-CSF 97	*P*
Median age (range), years	46 (2-81)	41 (9-80)	50 (2-78)	0.322
Age group				
- <20 years	31 (16%)	15 (16%)	16 (16%)	
- 20-39 years	51 (26%)	27 (28%)	24 (25%)	0.362
- 40-59 years	51 (26%)	29 (31%)	22 (23%)	
- ≥60 years	59 (31%)	24 (25%)	35 (36%)	
Gender				
- Male	94 (49%)	46 (48%)	48 (49%)	0.883
- Female	98 (51%)	49 (52%)	49 (51%)	
Severity				
- Very SAA	70 (37%)	39 (41%)	31 (32%)	0.191
- SAA	122 (63%)	56 (59%)	66 (68%)	
Median number of days with G-CSF	na	na	160 (1-544)	-
Patients with ≥240 days of G-CSF	na	na	21/97 (22%)	
Type of response at last follow-up				
- Complete remission	71	35	36	
o After IST	54	26	28	
o After BMT	17	9	8	
- Partial response	29	13	16	0.815
- No response	5	3	2	
- Secondary MDS/AML	8	4	4	
- Solid cancer	1	0	1	
- Missing data	13	9	4	
Number of deaths	65 (34%)	31 (33%)	34 (35%)	0.723
Post-randomization complications				
- Relapse	48 (26%)	21 (24%)	27 (28%)	
- Clonal myeloid malignancy				
o MDS/AML	9 (5%)	5 (5%)	4 (4%)	
o Cytogenetic abnormality only	10 (5%)	4 (4%)	6 (6%)	0.824
- Solid cancer	7 (4%)	3 (3%)	4 (4%)	
- PNH	18/113 (16%)	9/52 (17%)	9/61 (15%)	
- Aseptic osteonecrosis	8 /113 (7%)	3 /54 (6%)	5/59 (8%)	
- Chronic kidney disease	12/101 (12%)	5 /53 (9%)	7 /48 (15%)	
Subsequent allogeneic SCT	28 (15%)	16 (17%)	12 (12%)	0.380
Median (95% CI) follow-up time in years since randomization*	11.7 (10.9-12.5).	11.2 (9.6-12.7)	11.9 (11.0-12.9)	0.892

G-CSF: granulocyte colony-stimulating factor; SAA: severe aplastic anemia; na: not applicable; IST: immunosuppressive therapy; BMT: bone marrow transplantation; MDS: myelodysplastic syndrome; AML: acute myeloid leukemia; PNH: paroxysmal nocturnal hemoglobinuria; SCT: stem cell transplantation. *P* values: Mann-Whitney U test for continuous variables and the χ^2 test for categorical variables. *Using the reverse Kaplan-Meier method.

Results

Overall survival and event-free survival

OS and EFS rates at 15 years for all patients were 60±9% and 24±7%, respectively. The OS rate was 57±12% for the G-CSF group and 63±12% for the non-G-CSF group (P=0.92) (Figure 1A). The EFS rate was 24±10% for the G-CSF group and 23±10% for the non-G-CSF group (P=0.36) (Figure 1B). At last follow-up, among 127 alive patients, 71 were in complete remission (54 after IST, 17 after subsequent transplantation), 29 in partial response and five had not responded. Data on remission status of SAA were missing for 13 patients, and not applicable in nine cases (8 with secondary MDS/AML and 1 with solid cancer). There was no difference with respect to remission state at last follow-up between the patients in the G-CSF and non-G-CSF groups (P=0.81). In the 65 patients who died, cause of death was infection (n=26), bleeding (n=3), SAA not further specified (n=3), MDS/AML (n=4), solid cancer (n=4), transplant-related mortality (n=8), cardiovascular/aging (n=9), or unspecified (n=8). There was no difference in the causes of death between patients treated with or without G-CSF.

The most important risk factors for OS of patients treated with horse ATG and CSA with or without G-CSF were age and severity of the disease at randomization: the OS rate at 15 years was 89±12% for patients aged <20 years, 81±13% for patients 20-39 years old, 55±15% for patients 40-59 years old, and 32±16% for patients ≥60 years old (P<0.001) (Figure 2A). The OS rate for patients with SAA was 64±11% and that for patients with very SAA was 52±13% (P=0.021). However, for patients surviving 1 year or longer after first IST, there was no longer any difference in survival according to disease severity: the OS rate is 71±11% for patients with SAA and 74±16% for patients with very SAA (P=0.636) (*Online*

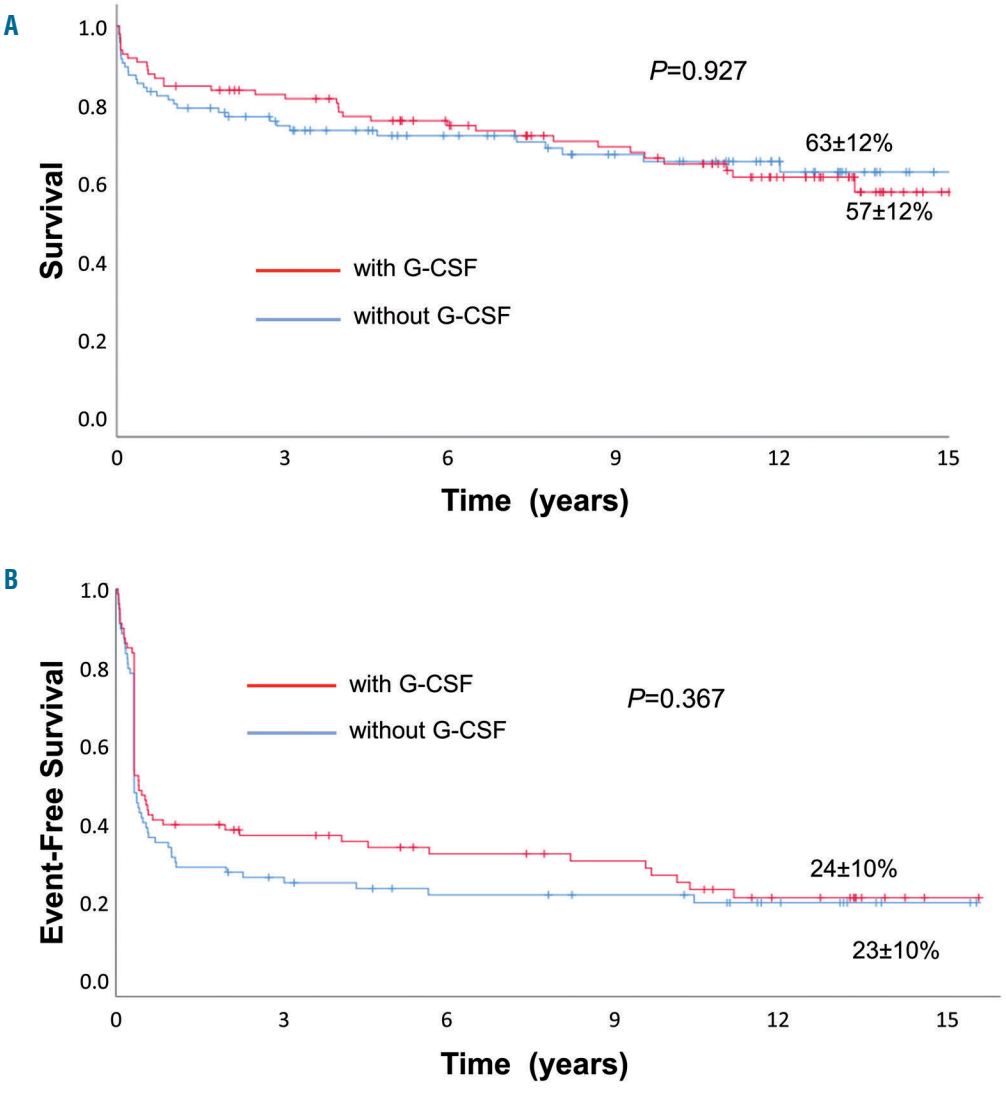

Figure 1. Outcomes of patients with severe aplastic anemia treated with horse antithymocyte globulin and cyclosporine with or without granulocyte colony-stimulating factor. (A, B) Overall survival (A) and event-free survival (B) of patients with severe aplastic anemia treated with horse antithymocyte globulin and cyclosporine with or without granulocyte colony-stimulating factor. Events included relapse, non-response at day 120, subsequent stem cell transplantation, myelodysplastic syndrome/acute myeloid leukemia, solid cancer, paroxysmal nocturnal hemoglobinuria or death. G-CSF: granulocyte colony-stimulating factor.

Supplementary Figure S1A, B). In multivariate analysis including age, severity and randomization for G-CSF as variables, treatment with G-CSF was not associated with better survival [G-CSF; relative risk (RR) 0.91, 95% confidence interval (95% CI): 0.55-1.49; *P*=0.70]; the relative risk was increased for very SAA (RR 1.95, 95% CI 1.19-3.21, *P*=0.008) and older age (reference age <20 years; 20-39 years, RR 1.77, 95% CI: 0.48-6.67, *P*=0.40; age 40-59 years, RR 4.96, 95% CI: 1.48-16.65, *P*=0.009; age ≥60 years, RR 9.08, 95% CI 2.78-29.73, *P*<0001). EFS at 15 years according to age group was as follows: 27%±17% for patients aged <20 years, 28±16% for patients 20-39 years old, 30±14% for patients 40-59 years old, and 12±12% for patients 60 years or older (*P*=0.023) (Figure 2B). In multivariate analysis, age group was no longer significantly different for EFS (Table 2), although a notable, non-significant trend remained for patients 60 years or older.

Relapse, non-response to immunosuppression and need for subsequent stem cell transplantation

We evaluated relapse, non-response to immunosuppression and the need for either subsequent SCT or subsequent courses of IST. There was no difference between patients treated with or without G-CSF with respect to relapse and the need for second-line treatment: the cumulative incidence of relapse for patients responding at day 120 was 30±10% for the G-CSF group, and 25±10% for the non-G-CSF group (*P*=0.54) (Figure 3A). Forty patients needed a second-line therapy for relapse (n=17), refracto-

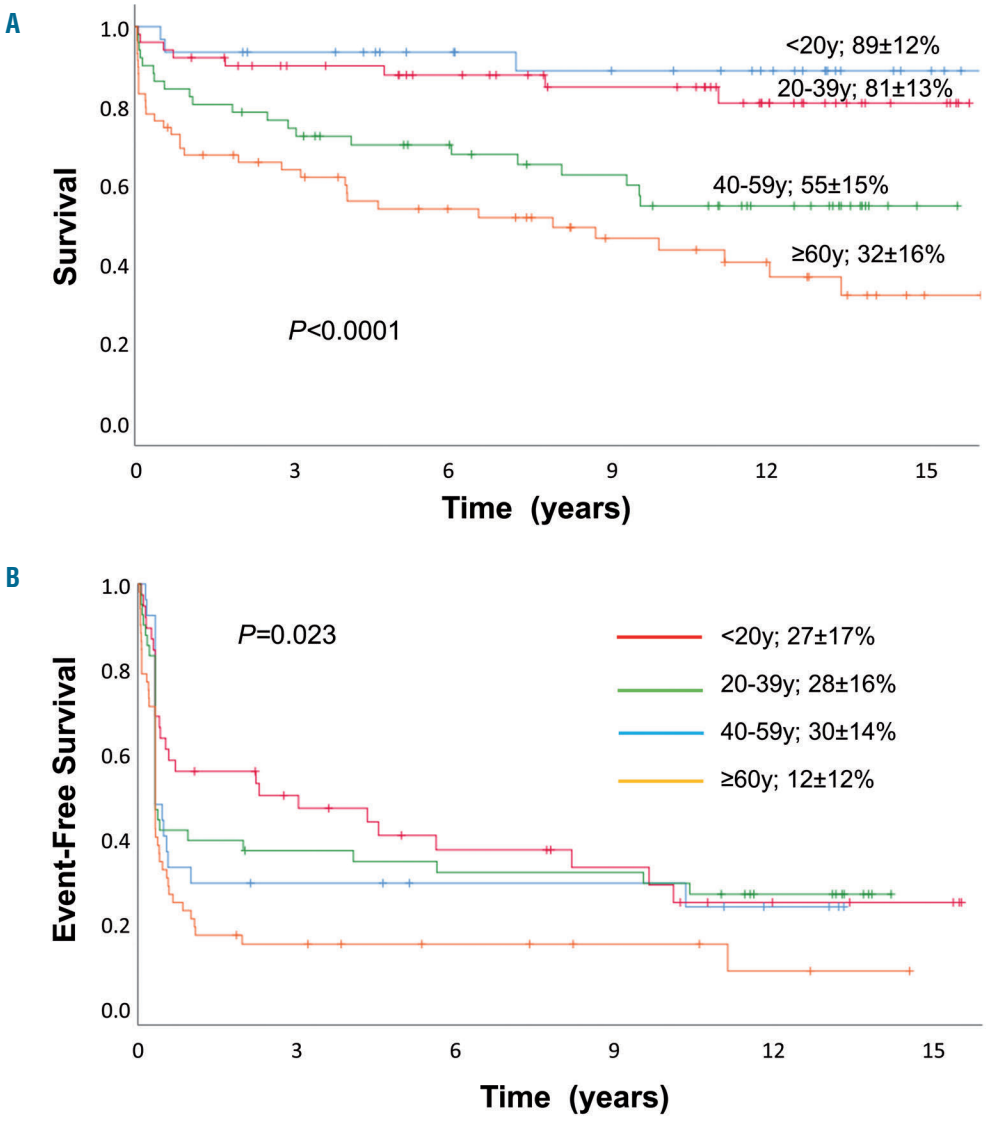

Figure 2. Overall survival and event-free survival according to age groups. (A, B) Overall survival (A) and event-free survival (B) of patients with severe aplastic anemia treated with horse antithymocyte globulin and cyclosporine with or without granulocyte colony-stimulating factor according to age groups at time of randomization: patients <20 years, patients 20-39 years, patients 40-59 years, patients 60 years or older. Events included relapse, non-response at day 120, subsequent stem cell transplantation, myelodysplastic syndrome/acute myeloid leukemia, solid cancer, paroxysmal nocturnal hemoglobinuria or death. G-CSF: granulocyte colony-stimulating factor.

ry disease (n=8), or incomplete response (cyclosporine dependency, n=7; decreasing values but still in partial remission, n=8), 24 in the G-CSF group, and 16 in the non-G-CSF group (*P*=0.35). Sixteen patients needed a third-line therapy for relapse (n=5), refractory disease (n=7), or incomplete response (decreasing values but still in partial remission, n=4), 12 in the G-CSF group, and four in the non-G-CSF group (*P*=0.60). Twenty-eight patients needed allogeneic SCT as second-line or subsequent treatment, 12 in the G-CSF group, and 16 in the non-G-CSF group, because of non-response/relapse (n=23), or MDS/AML (n=5). The cumulative probability of being treated with SCT at 15 years was 14±8% for patients who had been given G-CSF, and 22%±10% for those who had not (*P*=0.38) (Figure 3B). The 10-year survival after transplantation was 63±18%.

Long-term follow-up

Next, we evaluated the probability of malignant and non-malignant late complications. During the follow-up, 52 of the 192 patients developed a late complication. Some of them developed more than one late event: 44 patients developed one, five developed two, and three developed three or more late complications. Nine patients developed clinical or morphological signs of MDS/AML, ten developed isolated cytogenetic abnormalities (2 cases with del(7q), 1 in the G-CSF group and 1 in the non-G-CSF group, and 1 case with each of the following abnormalities: del(13q), del(9), loss of chromosome X in a female patient, loss of chromosome Y in a male patient, anomaly of chromosome 11 and translocation t(6;10); 2 cases with undefined abnormality), seven developed a solid cancer (colon, pancreas, glioblastoma, gastric, adenocarcinoma and squamous cell carcinoma of unknown origin, unspecified, 1 of each), and 19 developed clinical PNH. At 15 years, the cumulative incidence of MDS/AML or isolated cytogenetic abnormalities was 8.5±3% in the G-CSF group, and 8.2±3% in the non-G-CSF group (*P*=0.90) (Figure 3C); the cumulative incidence of clinical PNH was 10.1±5% in the G-CSF group, and 13.3±7% in the non-G-CSF group (*P*=0.499). With regards to non-clonal late complications, there were eight cases of avascular osteonecrosis, and 12 of chronic kidney disease. The cumulative incidence of chronic kidney failure at 15 years was 13%±11% in the G-CSF group, and 16±11% in the non-G-CSF group (*P*=0.51). Likewise, there was not a difference for aseptic osteonecrosis, although there were not enough events to provide an estimate. Patients needing longer CSA treatment had a higher risk of chronic kidney disease (6/22; 27%) compared to patients who received a single course of CSA (6/79; 7.6%; *P*=0.021). In contrast, patients needing more steroids (1/13; 7.7%) did not have a higher risk of osteonecrosis than patients needing steroids only for one ATG course (7/100;6.2%; *P*=0.453). The cumulative incidence of all late events at 15 years (i.e., including MDS/AML, isolated cytogenetic abnormalities, solid cancer, clinical PNH, osteonecrosis, kidney disease, relapse) was 50±12% in the G-CSF group, and 49±12% in the non-G-CSF group (*P*=0.65) (Figure 3D).

We also evaluated a possible effect of duration of treatment with G-CSF on long-term events. Patients randomized to receive G-CSF, were given the growth factor for a

Table 2. Multivariate analysis for overall survival and event free-survival.

	Hazard ratio	95% Confidence interval		*P*
		Lower	Higher	
Overall survival				
G-CSF randomization				
- No G-CSF (ref)	1	-	-	
- With G-CSF	0.91	0.55	1.49	0.703
Age group at randomization				
- <20 years (ref)	1	-	-	-
- 20-39 years	1.77	0.47	6.67	0.400
- 40-59 years	4.96	1.49	16.65	0.009
- ≥60 years	9.08	9.09	29.73	<0.001
Severity of aplastic anemia				
- SAA (ref)	1	-	-	0.008
- Very SAA	1.95	1.19	3.21	
Event free survival				
G-CSF randomization				
- No G-CSF (ref)	1	-	-	0.250
- With G-CSF	0.81	0.56	1.16	
Age groups at randomization				
- < 20 years (ref)	1	-	-	-
- 20-39 years	0.83	0.46	1.49	0.525
- 40-59 years	0.93	0.53	1.64	0.805
- ≥60 years	1.61	0.96	2.73	0.080
Severity of aplastic anemia				
- SAA (ref)	1	-	-	0.215
- Very SAA	1.27	0.87	1.83	

G-CSF: granulocyte colony-stimulating factor; SAA: severe aplastic anemia.

median of 160 days (range, 1-544 days). Of these patients, 21 received G-CSF for ≥240 days. Patients who received G-CSF for ≥240 days were not more likely to develop MDS/AML, isolated cytogenetic abnormalities, second solid cancers, clinical PNH, aseptic osteonecrosis or chronic kidney disease.

Discussion

G-CSF had been shown to reduce infections and days of hospitalization in the first 3 months of its administration in patients with SAA.[14] The expectation from adding G-CSF to standard IST was to improve the long-term outcome and sustainability of remission, as has been envisaged recently with the use of eltrombopag.[24] We show here that the addition of G-CSF to horse ATG and CSA has no impact on the long-term outcome of patients with acquired SAA: OS, EFS, non-response, relapse and need for a subsequent SCT were similar in the groups that did or did not receive G-CSF. G-CSF treatment during IST is an option of effective supportive care, possibly to combat or prevent infectious complications, even if it does not have any beneficial effect as an adjunct to standard IST in the long-term.[25] Clonal malignant evolution was always a concern with the use of G-CSF in SAA patients receiving

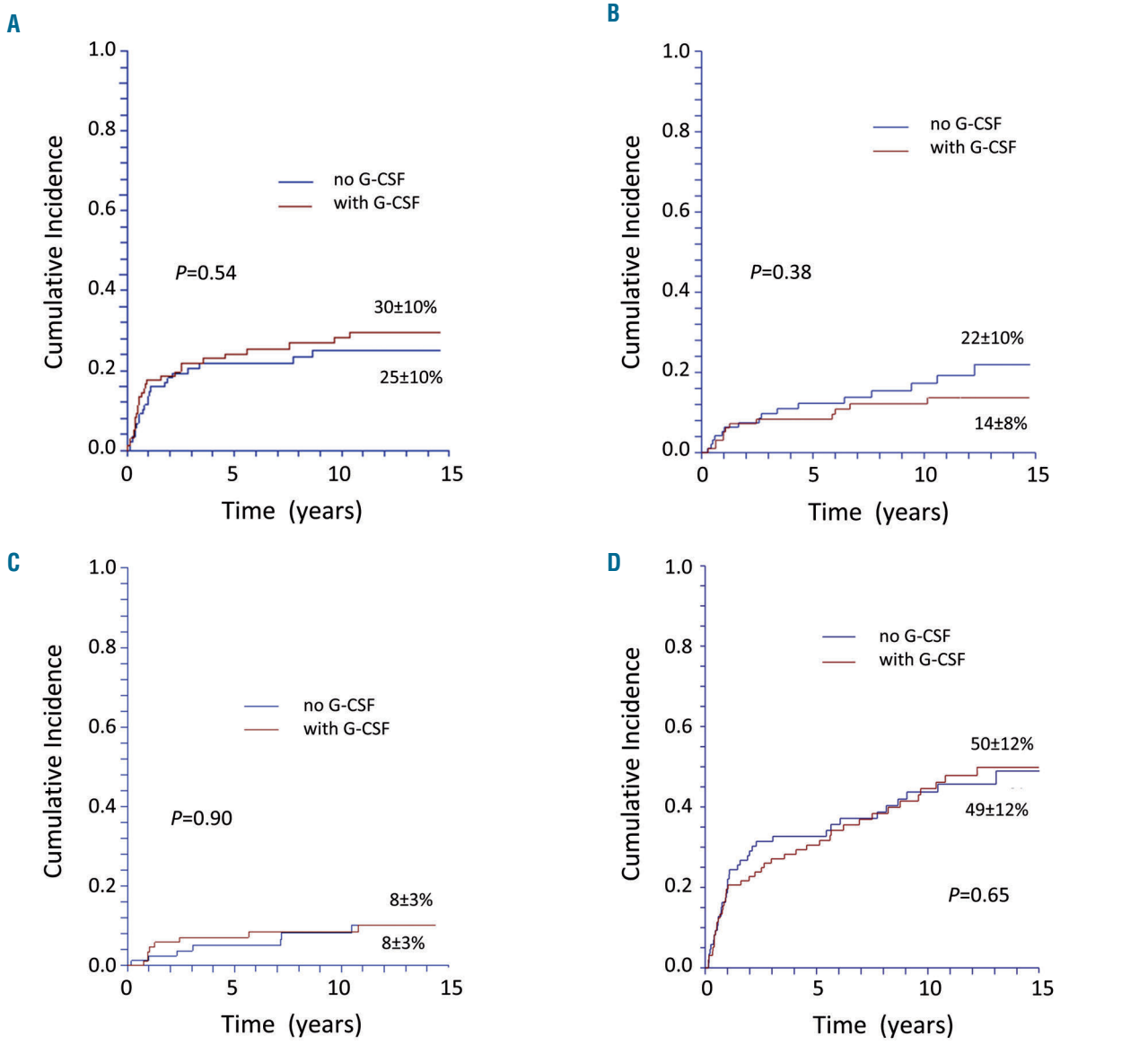

Figure 3. Cumulative incidence of late complications of patients with severe aplastic anemia treated with horse antithymocyte globulin and cyclosporine with or without granulocyte colony-stimulating factor. (A) Cumulative incidence of relapse of patients with severe aplastic anemia (SAA) treated with horse antithymocyte globulin (ATG) and cyclosporine (CSA) with or without granulocyte colony-stimulating factor (G-CSF). (B) Cumulative probability of being transplanted (death without transplant is the competing event) of patients with SAA treated in first-line with horse ATG and CSA with or without G-CSF. (C) Cumulative incidence of clonal evolution to a hematologic malignancy (myelodysplastic syndrome/acute myeloid leukemia or isolated cytogenetic abnormality) of patients with SAA treated with horse ATG and CSA with or without G-CSF. (D) Cumulative incidence of any late event (relapse, myelodysplastic syndrome/acute myeloid leukemia, isolated cytogenetic abnormality, solid cancer, clinical paroxysmal nocturnal hemoglobinuria, aseptic osteonecrosis, chronic kidney disease) of patients with SAA treated with horse ATG and CSA with or without G-CSF.

IST. We could not demonstrate a higher risk for the development of MDS/AML or cytogenetic abnormalities in patients randomized to receive G-CSF. Patients were analyzed for the risk of clonal evolution to a hematologic malignancy according to their initial randomization group (i.e. with or without G-CFS). However, data on patients in the non-G-CSF group who eventually received G-CSF (dose and duration) later in the course of their disease are not available. Thus, it is fair to state that G-CSF given as part of the initial treatment within this randomized clinical trial does not seem to increase the risk of clonal evolution to MDS/AML. Patients with SAA had a baseline risk of developing clonal evolution to a hematologic malignancy; this risk was not increased for patients treated with G-CSF, when compared to those in the non-G-CSF arm.

The strength of our trial is the prospective, randomized design with a follow-up time (median 11.7 years) that is longer than the interval, 10 years after IST,[15] within which secondary MDS/AML usually occur. Previous studies were less powerful to investigate this issue for various reasons. They were either retrospective,[15,18,26] not randomized, randomized without a non-G-CSF arm[16,17] or had a lower number of patients and shorter follow-up.[10,12] However, it is not obvious why few among these studies showed a relationship between the use of G-CSF and a clonal evolution to MDS/AML. Factors explaining the difference from our results could be patient selection (more patients with pre-existing clonal karyotype at diagnosis of SAA).[18] ethnic reasons, differences in dose and duration of G-CSF,[16] or the retrospective nature of the analysis.[15] The present study goes a step further in the long-term observation than most of the previous studies on SAA patients treated with ATG and CSA. We, too, could not demonstrate a higher risk of clinical PNH (the archetype of a benign clonal evolution), second solid cancer or non-malignant late events such as chronic kidney disease and aseptic osteonecrosis in the G-CSF group. Second solid cancers in SAA patients treated with immunosuppression have been shown to be more frequent than expected in a general population[27] and to affect OS strongly.[15] However, we found that G-CSF has no impact on the development of second solid cancers.

This study highlights two significant messages. First, G-CSF is unlikely to be linked with an increased risk of clonal transformation into a hematologic malignancy; however, available clinical data do not support the routine unse of G-CSF along with IST. G-CSF can be considered as an effective supportive care to combat or prevent infectious complications.[25] Second, irrespectively of G-CSF, SAA patients receiving IST are particularly vulnerable to a number of late malignant and non-malignant complications, either because of an intrinsic pre-cancerous nature of the disease or alternatively because of long-term stressed hematopoiesis and prolonged immunosuppression. Severity of the disease and age of the patient at first IST are the most important risk factors for survival. Interestingly, severity seems to have an impact only during the early phase after treatment, due to the higher risk of death from infections. In patients surviving 1 year or longer severity no longer has any impact on survival. It is somewhat disappointing that in this carefully followed cohort, irrespective of the age, less than 25% of patients are alive and event-free 15 years after initial treatment, and about 20% of them required an allogeneic SCT. Among the late events, relapses remain the most common, since, quite surprisingly, they continue to occur for at least 10 years after the initial treatment. Despite an excellent OS, young adults, have a similar risk of malignant and non-malignant complications after IST as older patients. The only difference is that the mortality rate in younger patients (aged <40 years) is lower, likely due to other salvage treatment options (mostly SCT) which are associated with different mortality based on age.[28]

Our study has a number of limitations. Firstly, despite it being the largest randomized study on the use of G-CSF in patients treated with horse ATG and CSA, because of the slow accrual for this rare disease and the withdrawal of horse ATG in Europe, the EBMT was forced to close the study early.[14] However, it is unlikely that a larger number of patients would have changed the findings. Secondly, we do not have the cumulative dose of G-CSF, particularly for non-responding and relapsed patients who have been retreated with immunosuppression. The study design is based on the principle of an intention-to-treat analysis in order to provide unbiased assessments of treatment efficacy.[29] Thirdly, not all late events have the same impact on the outcome of the patients. The occurrence of secondary malignancy, MDS, AML or solid cancer, strongly affect-OS.[2] Relapse of aplastic anemia does not have the same poor prognosis as relapse of a malignant disease. Although relapse is common, the majority of relapsed patients respond to the reintroduction of IST and relapse does not influence survival.[30] Finally, another limitation of our work is the non-exhaustiveness of the cytogenetic analysis in the context of clonal evolution, mainly related to failure to obtain results and also because the long-term evaluation had not been part of the original protocol.

Taken together, our data suggest that G-CSF added to standard IST has no impact on long-term outcome of patients with acquired aplastic anemia and is not directly related with late effects. However, regardless of the use of G-CSF, SAA patients treated with immunosuppression are particularly vulnerable to a number of late malignant and non-malignant complications. In particular, SAA patients treated with IST continue to relapse even at 10 years after initial treatment; therefore, alternative non-transplant treatment strategies are more than welcome. The addition of eltrombopag on top of standard IST resulted in an increased response rate in a phase II study[31,32] and is presently being evaluated in a randomized trial (EudraCT number 2014-000363-40). Furthermore, given the dramatic improvement of outcome after SCT, the possibility of early front-line SCT with an alternative donor might be considered for selected young patients who lack a matched sibling donor.[33] Clinical trials in this setting remain the only opportunity to investigate the best strategies to improve the rate of cure in SAA, possibly minimizing the risk of early and late events that affect survival.

Acknowledgments

The authors thank all the patients and the centers whose participation made this study possible. The list of participating centers is shown in the appendix of the Online Supplementary Material.

References

1. Scheinberg P, Young NS. How I treat acquired aplastic anemia. Blood. 2012;120(6):1185-1196.
2. Socie G, Rosenfeld S, Frickhofen N, Gluckman E, Tichelli A. Late clonal diseases of treated aplastic anemia. Semin Hematol. 2000;37(1):91-101.
3. Bacigalupo A. Antithymocyte globulin and cyclosporin: standard of care also for older patients with aplastic anemia. Haematologica. 2019;104(2):215-216.
4. Tisdale JF, Dunn DE, Geller N, et al. High-dose cyclophosphamide in severe aplastic anaemia: a randomised trial. Lancet. 2000;356(9241):1554-1559.
5. Scheinberg P, Wu CO, Nunez O, Young NS. Predicting response to immunosuppressive therapy and survival in severe aplastic anaemia. Br J Haematol. 2009;144(2):206-216.
6. Scheinberg P, Wu CO, Nunez O, et al. Treatment of severe aplastic anemia with a combination of horse antithymocyte globulin and cyclosporine, with or without sirolimus: a prospective randomized study. Haematologica. 2009;94(3):348-354.
7. Cle DV, Atta EH, Dias DSP, et al. Rabbit antithymocyte globulin dose does not affect response or survival as first-line therapy for acquired aplastic anemia: a multicenter retrospective study. Ann Hematol. 2018;97(11):2039-2046.
8. Gluckman E, Rokicka-Milewska R, Hann I, et al. Results and follow-up of a phase III randomized study of recombinant human-granulocyte stimulating factor as support for immunosuppressive therapy in patients with severe aplastic anaemia. Br J Haematol. 2002;119(4):1075-1082.
9. Gordon-Smith EC, Yandle A, Milne A, et al. Randomised placebo controlled study of RH-GM-CSF following ALG in the treatment of aplastic anaemia. Bone Marrow Transplant. 1991;7 Suppl 2:78-80.
10. Kojima S, Hibi S, Kosaka Y, et al. Immunosuppressive therapy using antithymocyte globulin, cyclosporine, and danazol with or without human granulocyte colony-stimulating factor in children with acquired aplastic anemia. Blood. 2000;96(6):2049-2054.
11. Shao Z, Chu Y, Zhang Y, Chen G, Zheng Y. Treatment of severe aplastic anemia with an immunosuppressive agent plus recombinant human granulocyte-macrophage colony-stimulating factor and erythropoietin. Am J Hematol. 1998;59(3):185-191.
12. Teramura M, Kimura A, Iwase S, et al. Treatment of severe aplastic anemia with antithymocyte globulin and cyclosporin A with or without G-CSF in adults: a multicenter randomized study in Japan. Blood. 2007;110(6):1756-1761.
13. Zheng Y, Liu Y, Chu Y. Immunosuppressive therapy for acquired severe aplastic anemia (SAA): a prospective comparison of four different regimens. Exp Hematol. 2006;34(7):826-831.
14. Tichelli A, Schrezenmeier H, Socie G, et al. A randomized controlled study in patients with newly diagnosed severe aplastic anemia receiving antithymocyte globulin (ATG), cyclosporine, with or without G-CSF: a study of the SAA Working Party of the European Group for Blood and Marrow Transplantation. Blood. 2011;117(17):4434-4441.
15. Socie G, Mary JY, Schrezenmeier H, et al. Granulocyte-stimulating factor and severe aplastic anemia: a survey by the European Group for Blood and Marrow Transplantation (EBMT). Blood. 2007;109 (7):2794-2796.
16. Kojima S, Ohara A, Tsuchida M, et al. Risk factors for evolution of acquired aplastic anemia into myelodysplastic syndrome and acute myeloid leukemia after immunosuppressive therapy in children. Blood. 2002;100(3):786-790.
17. Locasciulli A, Bruno B, Rambaldi A, et al. Treatment of severe aplastic anemia with antilymphocyte globulin, cyclosporine and two different granulocyte colony-stimulating factor regimens: a GITMO prospective randomized study. Haematologica. 2004;89(9):1054-1061.
18. Ohara A, Kojima S, Hamajima N, et al. Myelodysplastic syndrome and acute myelogenous leukemia as a late clonal complication in children with acquired aplastic anemia. Blood. 1997;90(3):1009-1013.
19. Marsh JC, Zomas A, Hows JM, Chapple M, Gordon-Smith EC. Avascular necrosis after treatment of aplastic anaemia with antilymphocyte globulin and high-dose methylprednisolone. Br J Haematol. 1993;84(4):731-735.
20. Park J, Jun J, Kim Y, Lee J, Kim C, Hahn S. Osteonecrosis of the hip in patients with aplastic anemia. J Korean Med Sci. 2002;17(6):806-810.
21. Socie G, Cahn JY, Carmelo J, et al. Avascular necrosis of bone after allogeneic bone marrow transplantation: analysis of risk factors for 4388 patients by the Societe Francaise de Greffe de Moelle (SFGM). Br J Haematol. 1997;97(4):865-870.
22. Barakat RK, Schmolck JP, Finkel KW, Foringer JR. Prolonged renal failure secondary to antithymocyte globulin treatment in severe aplastic anemia. Ann Pharmacother. 2007;41(5):895-898.
23. Gupta N, Mahapatra M, Rathi S, et al. Acute renal failure following antithymocyte globulin therapy for aplastic anaemia-report of two cases and review of literature. Ann Hematol. 2011;90(2):239-241.
24. Olnes MJ, Scheinberg P, Calvo KR, et al. Eltrombopag and improved hematopoiesis in refractory aplastic anemia. N Engl J Med. 2012;367(1):11-19.
25. Dufour C, Svahn J, Bacigalupo A, Severe Aplastic Anemia-Working Party of the EBMT. Front-line immunosuppressive treatment of acquired aplastic anemia. Bone Marrow Transplant. 2013;48(2):174-177.
26. Imashuku S, Hibi S, Nakajima F, et al. A review of 125 cases to determine the risk of myelodysplasia and leukemia in pediatric neutropenic patients after treatment with recombinant human granulocyte colony-stimulating factor. Blood. 1994;84(7):2380-2381.
27. Socie G, Henry-Amar M, Bacigalupo A, et al. Malignant tumors occurring after treatment of aplastic anemia. European Bone Marrow Transplantation-Severe Aplastic Anaemia Working Party. N Engl J Med. 1993;329(16):1152-1157.
28. Giammarco S, Peffault de Latour R, Sica S, et al. Transplant outcome for patients with acquired aplastic anemia over the age of 40: has the outcome improved? Blood. 2018;131(17):1989-1992.
29. Montori VM, Guyatt GH. Intention-to-treat principle. CMAJ. 2001;165(10):1339-1341.
30. Rosenfeld S, Follmann D, Nunez O, Young NS. Antithymocyte globulin and cyclosporine for severe aplastic anemia: association between hematologic response and long-term outcome. JAMA. 2003;289(9):1130-1135.
31. Townsley DM, Scheinberg P, Winkler T, et al. Eltrombopag added to standard immunosuppression for aplastic anemia. N Engl J Med. 2017;376(16):1540-1550.
32. Scheinberg P. Activity of eltrombopag in severe aplastic anemia. Blood Adv. 2018;2(21):3054-3062.
33. Dufour C, Veys P, Carraro E, et al. Similar outcome of upfront-unrelated and matched sibling stem cell transplantation in idiopathic paediatric aplastic anaemia. A study on behalf of the UK Paediatric BMT Working Party, Paediatric Diseases Working Party and Severe Aplastic Anaemia Working Party of EBMT. Br J Haematol. 2015;171(4):585-594.

Ferrata Storti Foundation

Haematologica 2020
Volume 105(5):1232-1239

Iron absorption from supplements is greater with alternate day than with consecutive day dosing in iron-deficient anemic women

Nicole U. Stoffel,[1] Christophe Zeder,[1] Gary M. Brittenham,[2] Diego Moretti[1*] and Michael B. Zimmermann[1*]

[1]ETH Zurich, Department of Health Science and Technology, Institute of Food, Nutrition and Health, Laboratory of Human Nutrition, Zürich, Switzerland and [2]Columbia University, Department of Pediatrics, College of Physicians and Surgeons, New York, NY, USA

These authors are co-senior authors

ABSTRACT

In iron-depleted women without anemia, oral iron supplements induce an increase in serum hepcidin (SHep) that persists for 24 hours, decreasing iron absorption from supplements given later on the same or next day. Consequently, iron absorption from supplements is highest if iron is given on alternate days. Whether this dosing schedule is also beneficial in women with iron-deficiency anemia (IDA) given high-dose iron supplements is uncertain. The primary objective of this study was to assess whether, in women with IDA, alternate-day administration of 100 and 200 mg iron increases iron absorption compared to consecutive-day iron administration. Secondary objectives were to correlate iron absorption with SHep and iron status parameters. We performed a cross-over iron absorption study in women with IDA (n=19; median hemoglobin 11.5 mg/dL; mean serum ferritin 10 μg/L) who received either 100 or 200 mg iron as ferrous sulfate given at 8 AM on days 2, 3 and 5 labeled with stable iron isotopes 57Fe, 58Fe and 54Fe; after a 16-day incorporation period, the other labeled dose was given at 8 AM on days 23, 24 and 26 (days 2, 3 and 5 of the second period). Iron absorption on days 2 and 3 (consecutive) and day 5 (alternate) was assessed by measuring erythrocyte isotope incorporation. For both doses, SHep was higher on day 3 than on day 2 (P<0.001) or day 5 (P<0.01) with no significant difference between days 2 and 5. Similarly, for both doses, fractional iron absorption (FIA) on days 2 and 5 was 40-50% higher than on day 3 (P<0.001), while absorption on day 2 did not differ significantly from day 5. There was no significant difference in the incidence of gastrointestinal side effects comparing the two iron doses (P=0.105). Alternate day dosing of oral iron supplements in anemic women may be preferable because it sharply increases FIA. If needed, to provide the same total amount of iron with alternate day dosing, twice the daily target dose should be given on alternate days, as total iron absorption from a single dose of 200 mg given on alternate days was approximately twice that from 100 mg given on consecutive days (P<0.001). In IDA, even if hepatic hepcidin expression is strongly suppressed by iron deficiency and erythropoietic drive, the intake of oral iron supplements leads to an acute hepcidin increase for 24 hours. The study was funded by ETH Zürich, Switzerland. This study has been registered at *www.clinicaltrials.gov as #NCT03623997*.

Introduction

Anemia affects ~33% of the world population and accounts for 8.8% of global disability.[1] Iron deficiency (ID) is considered the most prevalent cause of anemia globally.[1] In the United States, nearly 10% of 12 to 49-year-old females have ID.[1,2]

Correspondence:

NICOLE STOFFEL
nicole.stoffel@hest.ethz.ch

Received: March 1, 2019.

Accepted: August 12, 2019.

Pre-published: August 14, 2019.

doi:10.3324/haematol.2019.220830

Check the online version for the most updated information on this article, online supplements, and information on authorship & disclosures: www.haematologica.org/content/105/5/1232

Oral iron supplementation with ferrous sulfate ($FeSO_4$) is recommended to treat ID and iron deficiency anemia (IDA).[3] Because iron absorption from oral supplements tends to be low, current recommendations call for daily provision of high doses of $FeSO_4$, in the range of 60-200 mg, preferably split into 2 or 3 daily doses.[4-7] With larger iron doses,[8] the proportion of the dose absorbed, termed the fractional iron absorption (FIA), decreases, and large amounts of unabsorbed iron can cause gut inflammation[9,10] and increase free radical production and peroxidation in the gut mucosa.[11,12] This may result in gastrointestinal side effects, which are common[9] and typically dose dependent.[13] Furthermore, an increase in colonic iron can reduce abundances of beneficial commensal gut bacteria and increase abundances of potential enteropathogens.[14,15]

Hepcidin, the central systemic controller of iron homeostasis in mammals is a 25-amino acid peptide mainly produced by the liver, and is regulated by iron, hypoxia, inflammation and erythropoiesis.[16] Hepcidin binds to ferroportin, mainly expressed on enterocytes, hepatocytes and macrophages, leading to internalization and degradation of ferroportin. Thus, high serum hepcidin (SHep) reduces dietary iron absorption and recycling of iron from senescent erythrocytes. Large oral doses of iron acutely increase SHep in a dose-dependent fashion, with the increase in SHep persisting for ~24 hours (h).[8,17] The increase after iron administration is distinct[18] from the natural circadian increase in SHep over the day.[19] We previously showed that twice daily administration of 60 mg oral iron sharply augments the circadian SHep increase and results in higher SHep on the next day compared to once daily dosing with 120 mg iron.[17]

In iron-depleted young women given doses ≥60 mg of oral iron in the morning, SHep increases and is followed by a decrease in iron absorption on the following day.[8] Consequently, alternate day dosing results in a higher FIA compared to daily dosing.[8] In a study comparing iron absorption from 60 mg doses during 28 days of alternate day *versus* 14 days of consecutive day supplementation, FIA was significantly higher (+33%) with alternate day dosing.[17] In addition, due to the acute SHep increase after an oral iron dose, splitting a dose into two daily divided doses did not increase iron absorption.[17] However, these studies were conducted in iron-depleted women without anemia. Whether oral iron supplements, given at higher doses in women with IDA also induce an acute SHep increase and inhibit absorption of daily doses of iron is uncertain.[20]

Besides the iron-induced increase in SHep, a putative 'mucosal block' may decrease iron absorption from daily iron doses. According to the 'mucosal block' theory, enterocytes exposed to a large dose of iron will not absorb subsequent iron doses until they are replaced by new enterocytes after five to six days; therefore, provision of iron doses at weekly intervals might increase absorption.[21] If the increase in SHep subsides after 48 h, any residual inhibition on absorption would be consistent with this view of the 'mucosal block'. The World Health Organisation recommends weekly intermittent iron doses in women who experience significant side effects taking oral iron doses.[22] Therefore, the aim of our study was to measure the magnitude and duration of the acute SHep increase after high-dose oral iron supplementation and the effect on iron absorption in women with IDA. Our hypotheses regarding women with IDA were: a) single oral iron doses of 100 and 200 mg acutely increase SHep and this increase persists for 24 h, but not 48 h; b) FIA from both doses would be lower on the following day, but not differ from baseline 48 h post administration (alternate day dosing), suggesting there is no 'mucosal block'; and c) FIA would be lower from the 200 mg dose than the 100 mg dose.

Methods

Subjects

We recruited healthy women participating in the blood donation drive at the University of Zürich, and we conducted this study at the Human Nutrition Laboratory of the ETH Zürich, Switzerland. Detailed inclusion criteria are described in the *Online Supplementary Materials* and *Methods*. In this cross-over study, we compared iron absorption from consecutive and alternate day dosing in women with IDA, using 100 and 200 mg doses of iron as ferrous sulfate ($FeSO_4$). This study was approved by the Cantonal Ethics Committee in Zürich, Switzerland. All participants gave informed written consent.

Participants went through two study cycles of 6 days each, with 16 days in between (Figure 1). To all subjects, we administered oral doses of $FeSO_4$ in the morning on two consecutive days (days 2 and 3) and a third dose 48 h later (day 5), each dose was labeled with ^{57}Fe, 58Fe or ^{54}Fe. Subjects were randomly assigned to first receive either three doses of 100 mg or three doses of 200 mg. They were given the iron dose under standardized conditions. Detailed supplement administration is described in the *Online Supplementary Material* and *Methods*. On day 1, before iron supplementation, baseline venipuncture blood samples were taken at 8:00 AM and at 4:00 PM. Iron was administered at 8:00 AM on days 2, 3 and 5. Blood samples were taken at 8:00 AM (before dosing) and at 4:00 PM on days 2, 3 and 5. Additional blood samples were taken on day 4 and day 6 at 8:00 AM. Using a questionnaire, subjects were asked whether they had gastrointestinal side effects during the visits. We assessed iron absorption by measuring isotopic enrichment in red blood cells 16 days after administration of the third dose in both supplementation periods.[23-25] Hemoglobin (Hb), SHep, iron- and inflammatory biomarkers were measured as described in the *Online Supplementary Materials* and *Methods*.

Based on previous studies in our laboratory at the ETH Zürich using iron supplements in women we expected a standard deviation (SD) of the difference between pairs of 0.18 in log FIA. The study was powered to detect a relevant difference of 30% in FIA on a linear scale (such as 15% and 20%), which on a log scale, corresponds to 0.125 units of log FIA. This yielded a minimal sample size of 18 subjects, assuming a power of 0.8 and an alpha of 0.05. We recruited an additional subject to account for possible attrition, and enrolled 19 women in the study.

Statistical analysis

We performed the statistical analyses using SPSS (IBM SPSS statistics, Version22), as described in detail in the *Online Supplementary Materials* and *Methods*. We used linear mixed effect model analysis with Bonferroni corrected multiple comparisons to assess the effect of consecutive versus alternate day dosing with 100 and 200 mg on different variables. Dose and time (reflecting the supplement

administration day) were defined as fixed effects, participants as random effects (intercept) using a variance component structure matrix. Spearman correlation was applied. Incidences of side effects were compared using χ^2 test. *P*-values<0.05 were considered statistically significant.

Results

We began recruiting on October 10, 2017, and during October and November 2017, we enrolled 19 women in the study. Three women were included in the study based on their Hb concentration before blood donation; 16 women were included in the study based on their Hb concentration after blood donation. We completed the study on January 8, 2018. Three women left the study after completing the first supplementation period: two after the 100 mg dosing (one because of gastrointestinal side effects, one because of travels away from the study site) and one after the 200 mg dosing (because of travels away from the study site). The data from these three women from the first supplementation period were included in the final analysis.

Baseline characteristics

Table 1 shows the subject characteristics at baseline (day 1) and at day 22, by randomization group. At baseline, four subjects were borderline anemic with a baseline Hb between 12.0-12.5 g/dL (two in each group) and three subjects, who received 100 mg iron first, had a mild upper respiratory tract infection and had an elevated baseline c-reactive protein (CRP); all of these subjects were included in the analysis. There were no significant within-group or

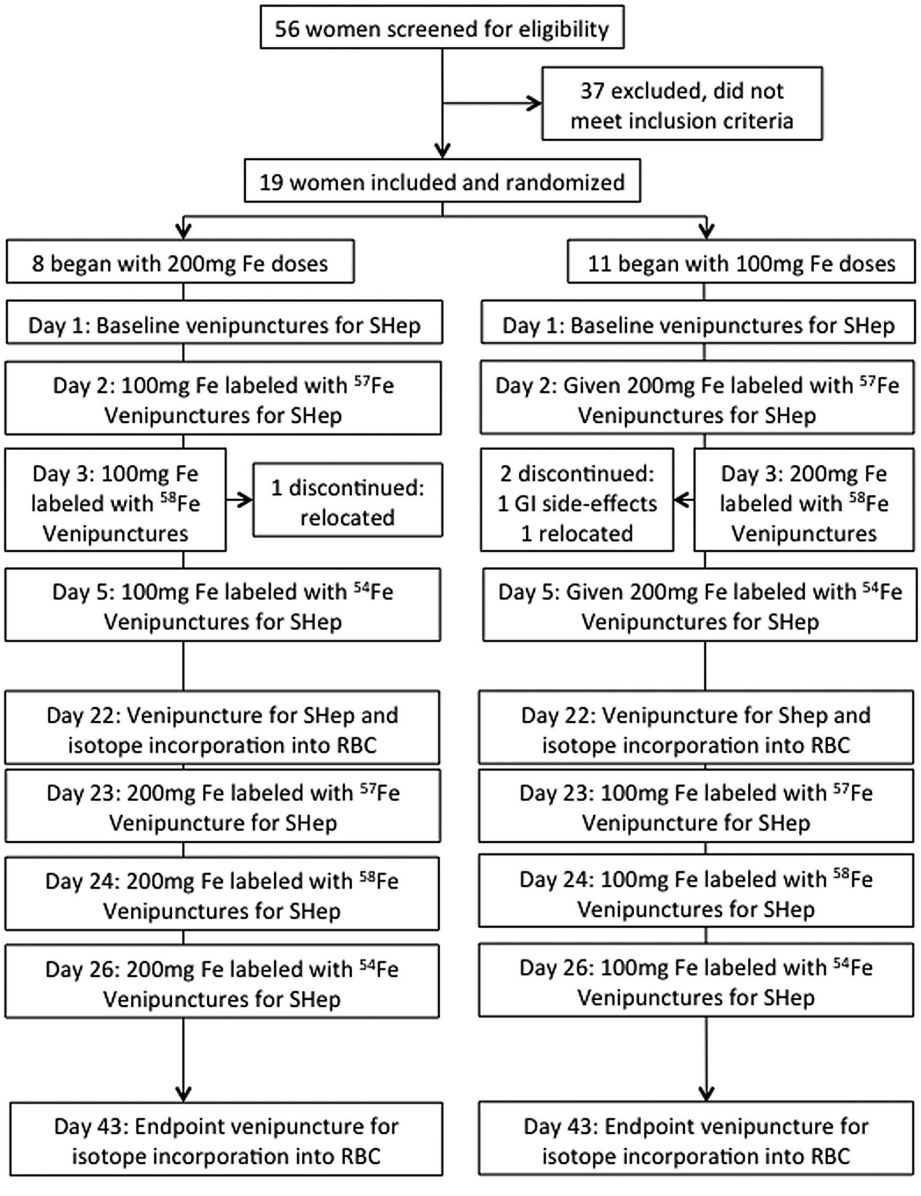

Figure 1. Study design. SHep: serum hepcidin; RBC: red blood cells.

between-group differences in age, body mass index (BMI) or iron and inflammatory parameters at days 1 and 22 (Table 1).

Hepcidin profiles and iron absorption during daily and intermittent oral iron dosing

As shown in Figure 2, median (IQR) SHep (nM) at 8 AM before administration of the 100 mg dose on days 2, 3 and 5 was 0.24 (0.19-0.38), 0.60 (0.44 - 1.09) and 0.46 (0.20-0.62), and at 8 AM before administration of the 200 mg dose on days 2, 3 and 5 was 0.26 (0.13-0.37), 0.74 (0.38-1.62) and 0.42 (0.29-0.74). SHep was significantly affected by time (P<0.001) but not by dose (P=0.733), and there was no significant time-dose interaction (P=0.815). For both doses, SHep was significantly higher on day 3 compared to day 2 (P<0.001) or day 5 (P<0.01). There was no significant difference in SHep between days 2 and 5 (P=0.115). Individual SHep data for each participant on days 2, 3 and 5 for both doses are shown in the *Online Supplementary Figure S1*.

Summing the 3 doses from each supplementation period, there was a significant dose effect (100 *vs.* 200 mg iron) on both FIA and total iron absorption (TIA) (P<0.001 for both), but no significant time-dose interaction on FIA or TIA (P=0.737; P=0.763). For both doses, there was a significant time effect on FIA (Figure 3A-B) and TIA (P<0.001 for both). Geometric mean (-SD, +SD) FIA (%) from the 100 mg dose on days 2, 3 and 5 was 23.5 (17.2, 32.2), 17.0 (12.3, 23.6) and 25.0 (16.8, 37.2), respectively, and from the 200 mg dose on days 2, 3 and 5 was 17.3 (12.1, 24.8), 11.9 (8.5, 16.6) and 16.8 (10.8, 25.9), respectively. FIA and TIA on day 2 and day 5 was significantly higher than on day 3 (P<0.001), but did not differ significantly comparing days 2 and 5, independent of the dose (Figure 3). Individual FIA data for each participant on days 2, 3 and 5 for both doses are shown in the *Online Supplementary Figure S2*. FIA from daily dosing (day 3) with 100 mg was not significantly different from alternate dosing (day 5) with 200 mg (P=0.792), but TIA was greater from the 200 mg dose on the alternate day (P<0.001). There was no significant correlation between baseline Hb and the difference in FIA between alternate (day 5) and consecutive (day 3) dosing (r_S = -0.292; P=0.240).

The effects of high oral iron doses on iron- and inflammatory status

Iron and inflammatory status indicators are shown in Table 2. There was a significant dose (100 *vs.* 200 mg iron) and time effect on serum ferritin (SF) (P<0.01, P<0.001). For both doses, SF on days 3 and 5 was significantly higher than on day 2 (P<0.001) and SF was also significantly higher on day 3 than on day 5 (P<0.05). There were significant time effects on serum iron (SFe), total iron binding capacity (TIBC) and transferrin saturation (TSAT) (P<0.05 for all). SFe and TSAT on days 3 and 5 were significantly higher than on day 2 (P<0.05 for all), but did not differ signifi cantly comparing days 3 and 5, independent of the dose. TIBC on days 3 and 5 was significantly lower than on day 2 (P<0.05, P<0.01), but did not differ significantly comparing days 3 and 5, for both doses. The iron doses had no significant effect on erythropoietin (EPO), and there was no significant difference

Table 1. Characteristics of the women (n=19) at day 1 (baseline, before beginning the first set of iron doses) and at day 22 (before beginning the second set of iron doses), by group.

	Group first receiving 100 mg iron doses	Group first receiving 200 mg iron doses
	Day 1	
Age, y[1]	21 (19-24)	22 (20-26)
Body mass index, kg/m^2	22.7±2.3	21.6±2.2
Hemoglobin, g/dL	11.3±1.1	11.6±0.6
Serum ferritin, μg/L	9.6±4.3	12.0±4.7
Serum sTfR, mg/L	5.2 (4.5-6.7)	5.2 (4.5-6.3)
Serum hepcidin, nM	0.32 (0.16-0.44)	0.19 (0.14-0.44)
Serum C-reactive protein, mg/L	0.50 (0.34-8.35)	0.37 (0.13-4.0)
Serum alpha glycoprotein, g/L	0.47 (0.38-0.59)	0.49 (0.32-0.62)
	Day 22	
Hemoglobin, g/dL	12.1±0.7	12.0±1.2
Serum ferritin, μg/L	9.4±3.4	8.1±3.9
Serum sTfR, mg/L	5.9 (5.4-8.8)	6.7 (4.5-8.4)
Serum hepcidin, nM	0.10 (0.06-0.27)	0.16 (0.02-0.22)
Serum C-reactive protein, mg/L	0.25 (0.16-2.14)	1.23 (0.30-2.75)
Serum alpha glycoprotein, g/L	0.54 (0.36-1.21)	0.47 (0.40-0.79)

[1]All such data as medians (IQR). [2]All such data as means ± standard deviation (SD). sTFR=soluble transferrin receptor. There were no significant differences between groups at day 1 and day 22, as well as no significant differences within groups comparing days 1 and 22. For between group comparisons, independent sample t-test was used for normally distributed data and Mann-Whitney U test was used for not normally distributed data. For within group comparisons, dependent sample t-test was used for normally distributed data and Wilcoxon matched-pair signed-rank test was used for not normally distributed data.

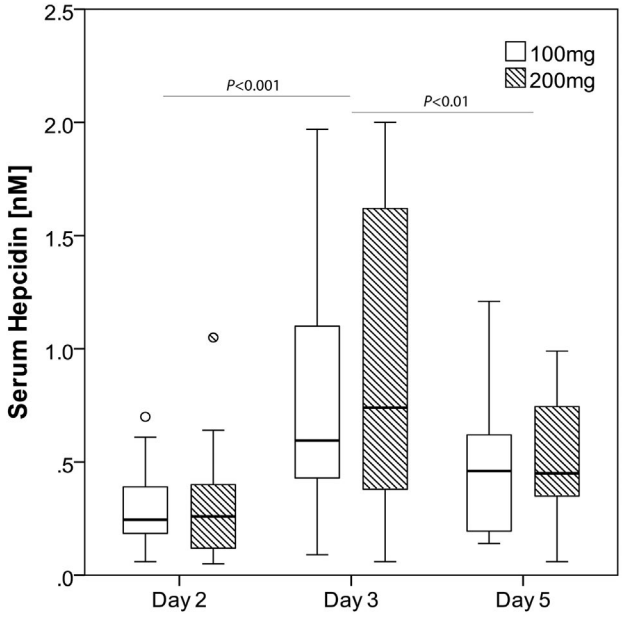

Figure 2. Serum hepcidin in iron-deficient anemic women. In women with iron deficiency anemia (IDA) who received 100 mg and 200 mg oral iron supplements on consecutive (day 3) and alternate days (day 5), serum hepcidin increases at 24 hours (h) and returns to baseline by 48 h .

Table 2. Iron and inflammatory indices in iron-deficient anemic women (n=19) receiving 100 or 200 mg of oral iron as $FeSO_4$ on days 2, 3 and 5.

	100 mg iron supplement			200 mg iron supplement			*P*	
	Day 2	Day 3	Day 5	Day 2	Day 3	Day 5	Dose	Time (day)
Serum ferritin, μg/L[1]	9.62 (5.75, 16.09)	18.19 (10.93, 30.26)	14.35 (7.73, 26.67)	10.02 (6.59, 15.26)	21.99 (13.79, 35.05)	18.46 (10.37, 32.84)	<0.01	<0.001
Serum sTfR, mg/L[2]	6.10 (5.24-7.16)	5.67 (4.88-6.29)	5.82 (4.69-6.91)	6.35 (4.92-7.49)	5.16 (4.71-6.66)	5.58 (4.51-6.25)	0.413	<0.001
Serum iron, μM	6.87 (3.90, 12.10)	11.26 (6.56, 19.33)	9.74 (5.97, 15.88)	7.69 (4.45, 13.29)	12.09 (5.65, 25.85)	12.44 (8.08, 19.14)	0.061	<0.001
TIBC, μM	86.68 (74.64, 100.66)	81.49 (73.91, 89.84)	82.00 (72.45, 92.81)	91.71 (80.96, 103.90)	84.38 (73.66, 96.66)	83.12 (72.93, 94.74)	0.268	<0.01
TSAT, %	7.92 (4.49, 13.99)	13.82 (8.18, 23.37)	11.87 (7.00, 20.13)	8.61 (4.87, 15.21)	15.68 (7.96, 30.90)	15.06 (9.41, 24.10)	0.106	<0.001
Serum EPO, mIU/mL	15.35 (8.60, 27.38)	15.09 (8.09, 28.13)	17.02 (9.95, 29.12)	15.12 (7.87, 29.04)	18.21 (9.67, 34.29)	16.43 (8.74, 30.86)	0.727	0.590
CRP, mg/L	0.53 (0.24-2.83)	0.52 (0.21-3.21)	0.38 (0.25-1.20)	0.89 (0.43-2.12)	0.78 (0.31, 2.84)	0.46 (0.23, 1.97)	0.556	0.072
AGP, g/L	0.54 (0.32, 0.91)	0.56 (0.35, 0.91)	0.46 (0.29, 0.72)	0.57 (0.36, 0.90)	0.46 (0.23, 0.93)	0.31 (0.16, 0.62)	0.101	<0.01

[1]All such data as geometric means (-SD,+SD). [2]All such data as medians (IQR). Analyzed by Linear Mixed Model Analysis with Bonferroni corrected multiple comparisons. There were no significant dose by time interactions. sTFR: soluble transferrin receptor; TIBC: total iron binding capacity; TSAT: transferrin saturation; EPO: erythropoietin; CRP: C-reactive protein; AGP: alpha-1-acid glycoprotein.

in EPO between the two doses on any of the study days (Table 2).

The increases in SHep and TSAT in the afternoon after oral iron administration (Figure 4A-B) reflected the dose. Linear mixed model analysis showed significant time and daytime effects (P<0.001 for both), but no dose effect (P=0.168) on SHep. There was a significant time by daytime interaction (P<0.001), but there were no dose by time, dose by daytime or dose by time by daytime interactions (P=0.981, P=0.390, P=0.940). Linear mixed model analysis showed significant dose, time and daytime effects (P<0.001 for all), on TSAT. There were significant dose by daytime and time by daytime interactions (P<0.01, P<0.001), but there were no dose by time or dose by time by daytime interactions (P=0.265, P=0.185).

Gastrointestinal side effects

All reported adverse events were grade I-II. The most common adverse event was nausea/epigastric pain for both doses: five cases in five women during 100 mg dosing and 12 cases in eight women during 200 mg dosing. There were three cases of vomiting ~5h after the iron intake: one after the first 100 mg dose and two after the first 200 mg iron dose. The total incidence of the gastrointestinal side effects that were assessed (epigastric pain/nausea/diarrhea/vomiting) was 40% lower with 100 mg dosing than with 200 mg dosing, however this difference was not statistically significant (P=0.105).

Discussion

Our main findings in women with IDA are: a) single oral iron doses of 100 and 200 mg acutely increased SHep and these increases persisted for 24 h; b) FIA from both iron doses was lower with consecutive *versus* alternate day dosing; and c) TIA was higher from the 200 mg dose than the 100 mg dose while FIA was lower; d) with both doses, we did not detect a decrease in iron absorption after 48 h from the last dose, evidence against the postulate of a mucosal block lasting up to five or six days.

In this study, for both iron doses, SHep was significantly higher with consecutive day doses (on day 3 compared to day 2, P<0.01) and significantly lower with alternate day doses (on day 5 compared to day 3, P<0.05), with no significant difference in SHep between days 2 and 5. These data support our previous oral iron supplementation studies in iron-deficient, mostly non-anemic, subjects.[8,17] In those studies, we assessed the magnitude and duration of the SHep increase after an oral iron dose and found that oral iron doses ≥60 mg significantly increased SHep at 24 h, which returned to baseline by 48 h.[8] In a second study, we provided 14 oral iron doses of 60 mg to iron-depleted women either on 14 consecutive days or on alternate days over 28 days and showed that during the first 14 days of supplementation in both groups, SHep was higher in the consecutive day group than in the alternate day group, likely driven by the higher iron supplement frequency in the consecutive day group.[17] Therefore, taken together, the available data suggest that in iron-deficient women with or without anemia, high oral iron doses acutely increase SHep and that this increase persists for 24 h but returns to baseline by 48 h.

In this study, alternate day dosing resulted in a significantly higher FIA (by 40-50%) compared to daily dosing for both 100 and 200 mg doses (P<0.001). FIA was significantly lower on day 3 compared to day 2 (P<0.001) and significantly greater on day 5 compared to day 3 (P<0.001) with no significant difference in FIA between days 2 and 5. Again, these results are consistent with those previously shown in iron-depleted, non-anemic women, where FIA was lower from an oral iron dose ≥60 mg given the next day (at 24 h after a first dose) (8). Over 14 oral iron doses given either on 14 (consecutive) or 28

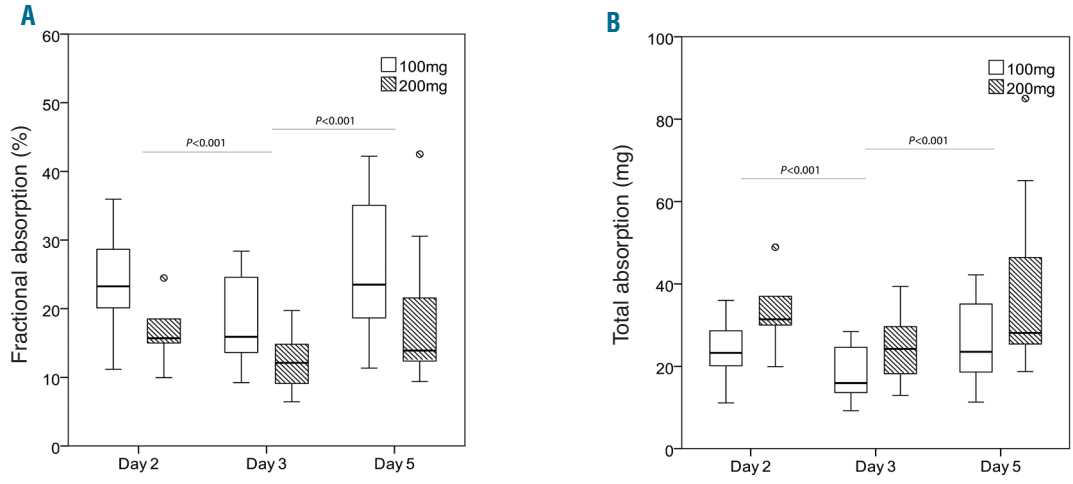

Figure 3. Iron absorption in iron-deficient anemic women. (A) Fractional iron absorption from 100 and 200 mg oral iron doses was higher during alternate day dosing (day 5) compared to consecutive day dosing (day 3); (B) Total iron absorption from 100 and 200 mg oral iron doses was higher during alternate day dosing (day 5) compared to consecutive day dosing (day 3).

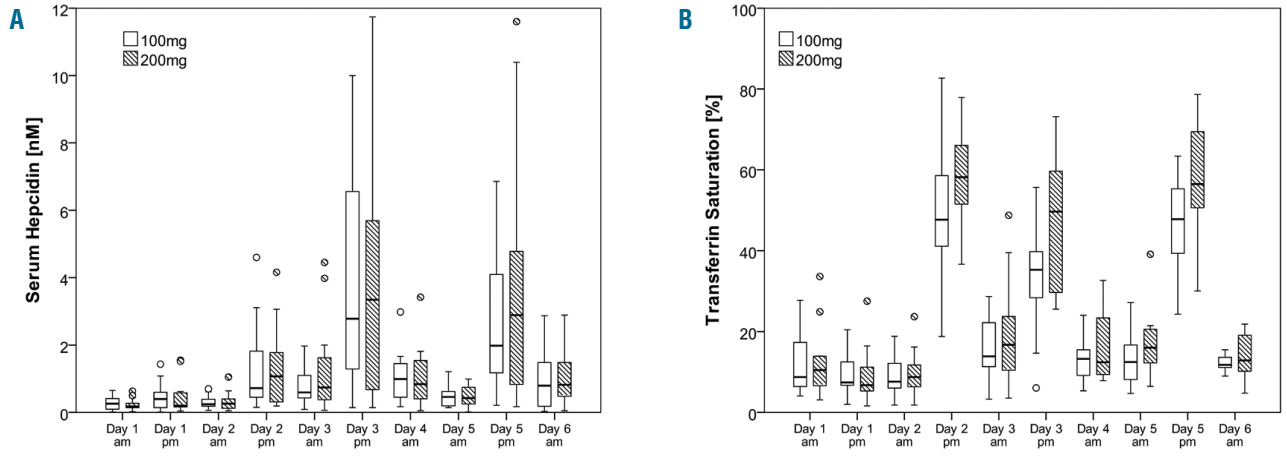

Figure 4. Serum hepcidin and transferrin saturation profiles in iron-deficient anemic women. (A) Serum hepcidin (Shep) profile during alternate day dosing (day 5) and consecutive day dosing (day 3) with 100 and 200 mg oral iron; (B) Transferrin saturation profile (TSAT) during alternate day dosing (day 5) and consecutive day dosing (day 3) with 100 and 200 mg oral iron.

(alternate) days, alternate day dosing resulted in a 34% higher FIA compared to consecutive day dosing.[17] In the current study, there was no residual absorption inhibition at 48 h post-administration; this is evidence against the postulate of a mucosal block lasting up to 5 or 6 days.[26] This finding suggests that increasing the dosing interval beyond 48 h would not result in a further increase in iron absorption. Taken together, the available data suggest that in iron-deficient women with or without anemia, alternate day dosing with oral iron doses in the range of 60 to 200 mg results in a sharply higher FIA compared to daily dosing.

In this study, FIA from 200 mg was significantly lower compared to FIA from 100 mg iron (P<0.001). Thus, even in iron-deficient anemic women, who are maximizing enterocyte iron uptake from the gut lumen by upregulation of divalent metal transporter 1 (DMT1) expression,[27] and who are maximizing enterocyte iron transfer to the circulation *via* low baseline SHep and high ferroportin expression, low oral iron doses are more efficiently absorbed than higher doses. Previous studies have generally demonstrated that FIA of oral iron decreases with increasing dose, but many of these studies were done in non-anemic subjects.[8] In this study, there was no significant difference in FIA comparing daily dosing (day 3) with 100 mg *versus* alternate day dosing with 200 mg (day 5). Consequently, TIA from a single dose of 200 mg given on alternate days was approximately twice that from 100 mg given on consecutive days (P<0.001). This suggests that TIA would be similar from alternate day dosing of 200 mg compared to daily dosing of 100 mg.

In women with IDA, the SHep increase of ~0.4 nM after doses of 100 and 200 mg was much smaller than the SHep increase of ~2 nM (about 1.85 nM after correction for method comparison)[28] after doses of 120 mg in non-anemic iron depleted women.[8] A potential explanation

for the lower increase in SHep in response to oral iron in anemic women compared to iron deficient non-anemic women is that hepatic hepcidin expression is more strongly suppressed by ID and erythropoetic drive; the latter mechanism may be particularly important in our subjects who had recently donated blood.[16]

The strengths of this study are that we used a cross-over design providing two high oral iron doses (100 and 200 mg) to women with IDA together with a standardized diet, and precisely quantified iron absorption using multiple iron stable isotopic labels on multiple days, with each subject acting as her own control. SHep and iron status parameter profiles were accurately and repeatedly quantified using an immunoassay with high sensitivity over two to six days; tolerability and gastrointestinal side effects were assessed by a standardized interview. Furthermore, study participants were otherwise healthy and free of comorbidities. Limitations of the study are that our subjects were only mildly, or for some, borderline, anemic, with Hb values ranging from 8.6 to 12.5 g/dL. Confirmation of these findings in women with more severe anemia (with Hb <8 g/dL) would require further study. At inclusion, most of the participants had just donated blood, which contributed to their anemia. The recent loss of 500 mL blood during donation could have influenced the response to the supplemental iron doses: for example, acute blood loss can stimulate renal EPO production which can suppress hepatic hepcidin synthesis.[29,30] However, despite prevailing high EPO concentrations (Table 2), we saw clear increases in SHep in response to the iron doses. Whether the response of SHep would differ in subjects with chronic anemia cannot be concluded from our data. However, chronic anemia would also increase the chance for gastrointestinal or other inflammatory conditions affecting iron absorption, and we can exclude that these had an effect in the current study. Finally, based on our study design, it is unclear if the effect of iron supplement dosing on consecutive days (day 2, 3) prior to the alternate day dosing (day 3, 5) effected our comparisons. To address this, an alternate design could have been to test consecutive day dosing and then have a washout period and then test the alternate day dosing. However, a disadvantage of this approach would be an increase in the number of test meals and subject burden, as well as potential changes in subjects' inflammatory and/or iron status during the washout period that would increase variability.

In conclusion, as in our previous studies using a daily dose of 60 mg in iron-depleted non-anemic women, our data show that with higher doses of 100 to 200 mg iron in women with IDA, alternate day dosing results in higher FIA and a trend for lower incidence of gastrointestinal side effects compared to consecutive day dosing. These potential benefits need to be confirmed in long-term intervention studies in anemic women with clinical endpoints, such as change in Hb, iron status and side effects, as primary outcomes. If confirmed, this dosing regimen may allow the use of lower iron doses, which may reduce side effects and improve compliance.

Acknowledgments

The authors thank the participating women, the nursing staff, Bérénice Hansen, Dr. Reinhard Henschler and Dr. Beat Frey for their support of the study.

References

1. Kassebaum NJ, Jasrasaria R, Naghavi M, et al. A systematic analysis of global anemia burden from 1990 to 2010. Blood. 2014; 123(5):615-624.
2. Cogswell ME, Looker AC, Pfeiffer CM, et al. Assessment of iron deficiency in US preschool children and nonpregnant females of childbearing age: National Health and Nutrition Examination Survey 2003-2006. Am J Clin Nutr. 2009;89(5):1334-1342.
3. Cook JD. Diagnosis and management of iron-deficiency anaemia. Best Pract Res Clin Haematol. 2005;18(2):319-332.
4. Camaschella C. Iron deficiency: new insights into diagnosis and treatment. Hematology Am Soc Hematol Educ Program. 2015;2015:8-13.
5. CDC. Recommendations to Prevent and Control Iron Deficiency in the United States. Atlanta: Centers for Disease Control and Prevention (CDC). 1998 [cited 2018 21.09]; Available from: https://www.cdc.gov/mmwr/preview/mmwrhtml/00051880.htm
6. Stoltzfus RJ, Dreyfuss ML. Guidelines for the use of iron supplements to prevent and treat iron deficiency anemia: International Nutritional Anemia Consultative Group (INACG), 1998. Available from: motherchildnutrition.org/nutrition-protection-promotion/pdf/mcn-guidelines-for-iron-supplementation.pdf
7. Pavord S, Myers B, Robinson S, et al. UK guidelines on the management of iron deficiency in pregnancy. Br J Haematol. 2012; 156(5):588-600.
8. Moretti D, Goede JS, Zeder C, et al. Oral iron supplements increase hepcidin and decrease iron absorption from daily or twice-daily doses in iron-depleted young women. Blood. 2015;22;126(17):1981-1989.
9. Tolkien Z, Stecher L, Mander AP, Pereira DI, Powell JJ. Ferrous sulfate supplementation causes significant gastrointestinal side-effects in adults: a systematic review and meta-analysis. PloS One. 2015;10(2): e0117383.
10. Kortman GA, Raffatellu M, Swinkels DW, Tjalsma H. Nutritional iron turned inside out: intestinal stress from a gut microbial perspective. FEMS Microbiol Rev 2014; 38(6):1202-1234
11. Lund EK, Fairweather-Tait SJ, Wharf SG, Johnson IT. Chronic exposure to high levels of dietary iron fortification increases lipid peroxidation in the mucosa of the rat large intestine. J Nutr. 2001;131(11):2928-2931.
12. Lund EK, Wharf SG, Fairweather-Tait SJ, Johnson IT. Oral ferrous sulfate supplements increase the free radical-generating capacity of feces from healthy volunteers. Am J Clin Nutr. 1999;69(2):250-255.
13. Rimon E, Kagansky N, Kagansky M, et al. Are we giving too much iron? Low-dose iron therapy is effective in octogenarians. Am J Med. 2005;118(10):1142-1147.
14. Jaeggi T, Kortman GA, Moretti D, et al. Iron fortification adversely affects the gut microbiome, increases pathogen abundance and induces intestinal inflammation in Kenyan infants. Gut. 2015;64(5):731-742.
15. Paganini D, Uyoga MA, Kortman GAM, et al. Prebiotic galacto-oligosaccharides mitigate the adverse effects of iron fortification on the gut microbiome: a randomised controlled study in Kenyan infants. Gut. 2017;66(11):1956-1967.
16. Sangkhae V, Nemeth E. Regulation of the iron homeostatic hormone hepcidin. Adv Nutr. 2017;8(1):126-136.
17. Stoffel NU, Cercamondi CI, Brittenham G, et al. Iron absorption from oral iron supplements given on consecutive versus alternate days and as single morning doses versus twice-daily split dosing in iron-depleted women: two open-label, randomised controlled trials. Lancet Haematol. 2017;4(11): e524-e533.
18. Schaap CC, Hendriks JC, Kortman GA, et al. Diurnal rhythm rather than dietary iron mediates daily hepcidin variations. Clin Chem. 2013;59(3):527-535.
19. Troutt JS, Rudling M, Persson L, et al. Circulating human hepcidin-25 concentrations display a diurnal rhythm, increase with prolonged fasting, and are reduced by growth hormone administration. Clin Chem. 2012;58(8):1225-1232.
20. Camaschella C. New insights into iron deficiency and iron deficiency anemia. Blood Rev. 2017;31(4):225-233.
21. Pena-Rosas JP, De-Regil LM, Gomez

Malave H, Flores-Urrutia MC, Dowswell T. Intermittent oral iron supplementation during pregnancy. Cochrane DB Syst Rev. 2015 19(10):CD009997.
22. Pena-Rosas JP, Nesheim MC, Garcia-Casal MN, et al. Intermittent iron supplementation regimens are able to maintain safe maternal hemoglobin concentrations during pregnancy in Venezuela. J Nutr. 2004; 134(5):1099-1104.
23. Hotz K, Krayenbuehl PA, Walczyk T. Mobilization of storage iron is reflected in the iron isotopic composition of blood in humans. J Biol Inorg Chem. 2012;17(2):301-309.
24. Brown E, Bradley B, Wennesland R, Hodges JL, Hopper J, Yamauchi H. Red Cell, Plasma, and Blood Volume in Healthy Women Measured by Radichromium Cell-Labeling and Hematocrit. J Clin Invest. 1962;41:2182-2190.
25. Hosain F, Marsaglia G, Noyes W, Finch CA. The nature of internal iron exchange in man. Trans Assoc Am Physicians. 1962; 75:59-63.
26. Hallberg L. Combating iron deficiency: daily administration of iron is far superior to weekly administration. Am J Clin Nutr. 1998;68(2):213-217.
27. Zoller H, Koch RO, Theurl I, et al. Expression of the duodenal iron transporters divalent-metal transporter 1 and ferroportin 1 in iron deficiency and iron overload. Gastroenterology. 2001;120(6): 1412-1419.
28. Stoffel NU, Zeder C, Fort E, Swinkels DW, Zimmermann MB, Moretti D. Prediction of human iron bioavailability using rapid c-ELISAs for human plasma hepcidin. Clin Chem Lab Med. 2017;26;55(8):1186-1192.
29. Maeda H, Hitomi Y, Hirata R, et al. The effect of phlebotomy on serum erythropoietin levels in normal healthy subjects. Int J Hematol. 1992;55(2):111-115.
30. Schotten N, Laarakkers CM, Roelofs RW, Origa R, van Kraaij MG, Swinkels DW. EPO and hepcidin plasma concentrations in blood donors and beta-thalassemia intermedia are not related to commercially tested plasma ERFE concentrations. Am J Hematol. 2017;92(3):E29-E31.

Ferrata Storti Foundation

Haematologica 2020
Volume 105(5):1240-1247

Extensive multilineage analysis in patients with mixed chimerism after allogeneic transplantation for sickle cell disease: insight into hematopoiesis and engraftment thresholds for gene therapy

Alessandra Magnani,[1,2] Corinne Pondarré,[3,4] Naïm Bouazza,[5] Jeremy Magalon,[6] Annarita Miccio,[7,8] Emmanuelle Six,[8,9] Cecile Roudaut,[1] Cécile Arnaud,[3] Annie Kamdem,[3] Fabien Touzot,[10] Aurélie Gabrion,[1] Elisa Magrin,[1,2] Chloé Couzin,[1] Mathieu Fusaro,[11] Isabelle André,[8,9] Jean-Paul Vernant,[12] Eliane Gluckman,[13] Françoise Bernaudin,[3] Dominique Bories[14*] and Marina Cavazzana[1,2,8,9*]

[1]Department of Biotherapy, Necker-Enfants Malades University Hospital, Assistance Publique-Hôpitaux de Paris, Paris, France; [2]Biotherapy Clinical Investigation Center, Groupe Hospitalier Universitaire Ouest, Assistance Publique-Hôpitaux de Paris, INSERM CIC 1416, Paris, France; [3]Centre de référence de drépanocytose, CHIC Centre Hospitalier Intercommunal de Créteil, Créteil, France; [4]Inserm U955, Paris XII University, Créteil, France; [5]Université Paris Descartes, EA7323, Sorbonne Paris Cité, CIC-1419 Inserm, Cochin-Necker, Paris, France; [6]Cell Therapy Unit, Hôpital de la Conception, AP-HM, INSERM CIC BT 1409, Marseille, France; [7]Laboratory of Chromatin and gene regulation during development, Imagine Institute, Paris, France; [8]Paris Descartes–Sorbonne Paris Cité University, Imagine Institute, Paris; [9]Human Lymphohematopoiesis Laboratory, Inserm UMR 1163, Imagine Institute, University Paris Descartes Sorbonne Paris Cité, Paris, France; [10]Department of Immunology-Allergy-Rheumatology, CHU Sainte-Justine, University of Montreal, Montreal, Quebec, Canada; [11]Study Center for Primary Immunodeficiencies, Assistance Publique-Hôpitaux de Paris (AP-HP), Necker-Enfants Malades University Hospital, Paris, France; [12]Hematology Department, Pitié-Salpêtrière Hospital, Paris, France; [13]Monacord Hôpital Saint Louis Paris, Centre Scientifique de Monaco, Monaco and Eurocord, Hôpital Saint Louis, Université Paris Diderot, Paris, France and [14]Hématologie Moléculaire, Hôpital Henri Mondor, Université Paris Est, Créteil, France

*These authors are co-senior authors

Correspondence:

ALESSANDRA MAGNANI
alessandra.magnani@aphp.fr

Received: May 24, 2019.

Accepted: September 18, 2019.

Pre-published: September 19, 2019.

doi:10.3324/haematol.2019.227561

Check the online version for the most updated information on this article, online supplements, and information on authorship & disclosures: www.haematologica.org/content/105/5/1240

ABSTRACT

Although studies of mixed chimerism following hematopoietic stem cell transplantation in patients with sickle cell disease (SCD) may provide insights into the engraftment needed to correct the disease and into immunological reconstitution, an extensive multilineage analysis is lacking. We analyzed chimerism simultaneously in peripheral erythroid and granulomonocytic precursors/progenitors, highly purified B and T lymphocytes, monocytes, granulocytes and red blood cells (RBC). Thirty-four patients with mixed chimerism and ≥12 months of follow-up were included. A selective advantage of donor RBC and their progenitors/precursors led to full chimerism in mature RBC (despite partial engraftment of other lineages), and resulted in the clinical control of the disease. Six patients with donor chimerism <50% had hemolysis (reticulocytosis) and higher HbS than their donor. Four of them had donor chimerism <30%, including a patient with AA donor (hemoglobin >10 g/dL) and three with AS donors (hemoglobin <10 g/dL). However, only one vaso-occlusive crisis occurred with 68.7% HbS. Except in the patients with the lowest chimerism, the donor engraftment was lower for T cells than for the other lineages. In a context of mixed chimerism after hematopoietic stem cell transplantation for SCD, myeloid (rather than T cell) engraftment was the key efficacy criterion. Results show that myeloid chimerism as low as 30% was sufficient to prevent a vaso-occlusive crisis in transplants from an AA donor but not constantly from an AS donor. However, the correction of hemolysis requires higher donor chimerism levels (*i.e.* ≥50%) in both AA and AS recipients. In the future, this group of patients may need a different therapeutic approach.

Introduction

Sickle cell disease (SCD) is a severe, monogenic disease associated with high mortality and morbidity rates.[1] Together with β-thalassemia, SCD constitutes the world's most prevalent inherited disorder.[2,3] Allogeneic human leukocyte antigen (HLA)-matched hematopoietic stem cell transplantation (HSCT) is the only curative treatment. Non-transplanted patients with SCD have a significantly shortened life expectancy, and experience disease-related complications throughout their lives.[4–6] With the aim of improving care for patients with SCD, non-myeloablative, reduced-intensity conditioning regimens and haploidentical transplants are now being investigated.[7–13] Furthermore, recent advances in gene therapy offer new perspectives for the treatment of this serious disease.[14,15] However, the curative level of engraftment by genetically modified cells has yet to be determined.

Following HSCT, SCD patients may develop mixed chimerism (MC), *i.e.* the co-existence of host- and donor-derived cells, which can nevertheless result in the clinical control of the disease.[16–21] MC is favored by the increasing use of non-myeloablative reduced-intensity conditioning regimens[9–11] and high doses of antithymocyte globulin.[22] The minimum level of donor chimerism required to reverse the clinical symptoms of SCD is still subject to debate.[21,23] Some literature data show that a donor white blood cell (WBC) percentage as low as 11% is enough to provide clinically adequate disease control[20] probably because the healthy cells have a survival advantage over SCD erythroid cells.[24] This advantage is also observed in beta-thalassemia.[25,26] However, donor chimerism at different stages of hematopoietic differentiation/development has yet to be analyzed in detail in a large cohort of SCD patients. Furthermore, donor chimerism (typically quantified as the proportion of donor-derived total circulating WBC) might be a poor indicator of the clinical outcome in patients with MC.

We therefore decided to perform an extensive analysis of donor chimerism in different cell lineage populations among a cohort of SCD patients having a mixed chimerism defined in the present study as host cells >0.05% after a full myeloablative conditioning regimen and then genoidentical HSCT. Our objective was to study the hematopoietic reconstitution after HSCT in SCD patients and determine the engraftment threshold for stable disease control. To this end, we performed a multilineage analysis of donor chimerism concomitantly in highly purified peripheral blood myeloid and lymphoid lineages, in erythroid and granulomonocytic progenitors/precursors, and mature RBC in a large cohort of SCD patients with MC at last follow up.

Our present results may have implications not only for allogeneic HSCT but also for gene therapy trials based on the autologous transplantation of genetically modified $CD34^+$ cells.

Methods

Between May 1990 and December 2013, 119 patients with SCD (registered at the Paris region's Pediatric Reference Center for SCD (Créteil, France)) underwent HLA-matched allogeneic HSCT at various transplantation centers. These patients are part of the French cohort previously published.[4,22] Patients with symptomatic SCD (genotype: S/S or S/ 0) and an HLA-identical sibling donor (hemoglobin [Hb] genotype: AA, AS, A/ 0 or A/D-Punjab) underwent HSCT. The myeloablative conditioning regimen consisted of busulfan, cyclophosphamide (total dose: 200 mg/kg), and rabbit anti-thymocyte globulin (total dose: 20 mg/kg). The total dose of intravenous busulfan was adjusted to the recipient's body weight: 12.8 mg/kg for >34 kg, 15.2 mg/kg for 23-34 kg, 17.6 mg/kg for 16-23 kg, and 19.2 mg/kg for 9-16 kg.

The main inclusion criteria for the present study were the development of MC for total WBC, at least 12 months of follow-up, and regular monitoring at the Reference Center. Post-HSCT blood samples were collected as part of routine care at last follow up. The patients' medical records were analyzed retrospectively.

Sorting of hematopoietic subpopulations

Cells were stained with specific, directly labeled monoclonal antibodies, according to the manufacturer's instructions. Chimerism was analyzed only when the population purity was ≥90%.

Clonogenic assay and DNA extraction

Erythroid burst-forming-units (BFU-E) and granulocyte-macrophage colony-forming-units (CFU-GM) progenitors/precursors were grown in semisolid methylcellulose medium with or without supplemented erythropoietin.

Hemoglobin fraction analysis

Values for Hb fractions HbS, HbF, and HbA were determined by cation-exchange high-performance liquid chromatography (HPLC).

Chimerism analysis in mature lymphoid and myeloid populations and in progenitors/precursors

Chimerism was determined in sorted, mature myeloid and lymphoid populations and concomitantly in BFU-E and CFU-GM. Analysis was performed in the Molecular Hematology Laboratory at Henri Mondor Hospital (Creteil, France). Chimerism was first analyzed using quantitative real-time PCR assays for indel genomic polymorphisms (KimerDx kit, GenDX, Netherlands), using a method adapted from a previous publication[27] and by PCR-STR when the level was above 10%. Mixed chimerism was defined as a recipient cell percentage above 0.05%. Patients were divided into three groups according to the level of donor chimerism. The 70% and 95% cutoffs were chosen on the basis of published data[22] and according to the limit usually employed in clinics, respectively. The donor chimerism in peripheral mature RBC was obtained by calculating the post-HSCT proportion of donor HbA.

Statistical analyses

Statistical analysis was performed with *ad hoc* routines implemented in R software (*http://www.R-project.org*). The data are presented as proportions for categorical data and as median, interquartile range and range for quantitative data. Quantitative variables were compared with the non-parametric Wilcoxon tests and proportions with the Fisher's exact tests or the chi-squared tests, as appropriate. Correlations between continuous variables were calculated using the non-parametric Spearman's rank correlation test. Wilcoxon signed-rank test for paired data was used to compare donor chimerism levels in RBC relative to BFU-E, CFU-GM and $CD15^+$ cells. A *P*-value of 0.05 was considered statistically significant for all analyses. Two-sided tests were used in all analyses. Please see the *Online Supplementary Materials and Methods* for a more detailed description of the methods used.

Results

The study population and clinical outcomes

A total of 34 patients with MC and more than 12 months of follow-up at the Pediatric Reference Center were included in the study and then divided into three groups, according to the level of total WBC donor chimerism at last follow-up: <70% (group 1, n=10), 70-95% (group 2, n=14), and 95-99.95% (group 3, n=10). Six of the patients in group 1 had a donor chimerism level below 50% (Table 1 and *Online Supplementary Table S1*).

In the study population as a whole, the median (range) age at transplant was 7.2 years (3.4-14.2); the median age did not differ significantly when comparing the three groups (8.1, 7 and 7.1 years in groups 1, 2 and 3, respectively; *P*=0.8). The median duration of post-HSCT follow-up was 54.5 months (12-155); no significant differences were observed when comparing the three groups (58.5, 56 and 42 months in groups 1, 2 and 3, respectively; *P*=0.67). The donor genotypes were as follows: n=13 for AA, n=19 for AS, n=1 for A/β0, and n=1 for A/D-Punjab donor. The proportion of AS donors was similar in the three groups (50% in groups 1 and 2, and 70% in group 3). Examples of MC following HSCT with an AA or AS donor are shown

Table 1. Characteristics of the study population, and donor chimerism in cell subsets and progenitors/precursors.

Variable	Level	Total (n=34)	Group 1 (n=10)	Group 2 (n=14)	Group 3 (n=10)	*P*
Age at HSCT (years)	median [iqr] (range)	7.2 [5.8, 9.1] (3.4, 14.2)	8.1 [6.0, 10.5] (3.4, 12.5)	7.0 [6.0, 8.6] (4.1, 12.5)	7.1 [5.0, 9.1] (4.1, 14.2)	0.80
Follow-up after HSCT (months)	median [iqr] (range)	54.5 [37.2, 81.8] (12.0, 155.0)	58.5 [37.0, 122.5] (21.0, 155.0)	56.0 [46.8, 76.2] (12.0, 91.0)	42.0 [36.2, 92.5] (12.0, 127.0)	0.67
Donor Hb genotype	AA, A/β^0 or A/D-Punjab	15 (44.1%)	5 (50.0%)	7 (50.0%)	3 (30.0%)	
	AS	19 (55.9%)	5 (50.0%)	7 (50.0%)	7 (70.0%)	0.69
Donor HbS (%)	median [iqr] (range)	32.0 [0.0, 37.5] (0.0, 44.6)	16.6 [0.0, 38.5] (0.0, 44.6)	15.8 [0.0, 35.7] (0.0, 39.8)	33.6 [7.9, 37.7] (0.0, 38.7)	0.62
Donor HbA (%)	median [iqr] (range)	53.0 [51.7, 54.7] (46.9, 57.4)	54.0 [52.8, 55.4] (51.7, 57.4)	52.7 [49.2, 53.8] (47.9, 54.8)	53.3 [52.2, 55.2] (46.9, 57.3)	0.46
Hb level at last follow-up (g/dL)	median [iqr] (range)	12.9 [11.5, 13.4] (8.4, 14.4)	10.8 [9.9, 13.1] (8.4, 14.2)	13.1 [12.8, 13.3] (9.6, 14.4)	12.9 [11.9, 13.5] (10.9, 13.7)	0.19
Reticulocytes at last follow-up (G/L)	median [iqr] (range)	36.0 [30.0, 57.3] (16.5, 407.0)	135.0 [38.6, 209.5] (31.2, 407.0)	36.4 [27.8, 55.8] (16.5, 161.0)	30.0 [24.8, 34.5] (20.6, 55.0)	0.0037
HbA (%)	median [iqr] (range)	53.8 [49.2, 82.3] (24.0, 87.5)	66.2 [45.1, 79.8] (24.0, 84.5)	53.8 [49.0, 85.9] (44.0, 87.5)	53.0 [50.1, 73.1] (48.8, 84.0)	0.71
HbS (%)	median [iqr] (range)	33.0 [0.0, 38.1] (0.0, 68.1)	20.6 [4.6, 45.1] (0.0, 68.1)	16.4 [0.0, 37.2] (0.0, 41.2)	33.7 [8.1, 39.1] (0.0, 40.3)	0.46
HbF (%)	median [iqr] (range)	1.0 [0.0, 1.9] (0.0, 6.5)	1.2 [0.2, 1.8] (0.0, 4.4)	1.0 [1.0, 2.6] (0.0, 6.5)	1.1 [0.0, 1.7] (0.0, 5.5)	0.87
Chimerism analysis						
Whole blood (%)	median [iqr] (range)	89.3 [60.0, 95.7] (16.0, 99.8)	37.0 [19.5, 56.0] (16.0, 66.0)	89.3 [85.3, 91.9] (72.0, 93.4)	97.2 [96.3, 98.8] (95.7, 99.8)	< 0,0001
CD3$^+$ (%)	median [iqr] (range)	73.5 [58.8, 91.8] (12.0, 99.9)	41.8 [31.8, 45.5] (12.0, 70.0)	73.5 [70.5, 77.2] (63.0, 88.5)	93.8 [92.6, 97.4] (89.0, 99.9)	< 0,0001
CD19$^+$ (%)	median [iqr] (range)	94.0 [56.0, 97.8] (11.0, 99.9)	36.5 [15.5, 49.8] (11.0, 90.0)	95.2 [88.2, 97.8] (73.0, 98.7)	98.6 [96.9, 99.4] (93.5, 99.9)	< 0,0001
CD14$^+$ (%)	median [iqr] (range)	96.5 [52.5, 99.6] (9.4, 100.0)	33.5 [18.5, 56.8] (9.4, 98.5)	96.4 [94.6, 98.5] (72.0, 99.9)	99.7 [99.5, 99.9] (98.2, 100.0)	0.00013
CD15$^+$ (%)	median [iqr] (range)	95.0 [64.0, 99.5] (5.4, 100.0)	24.5 [14.5, 51.2] (5.4, 95.0)	96.2 [92.5, 97.8] (63.0, 99.9)	99.8 [99.7, 100.0] (95.1, 100.0)	0.00022
BFU-E (%)	median [iqr] (range)	97.7 [65.5, 99.9] (0.0, 100.0)	39.0 [31.0, 61.0] (0.0, 76.0)	98.1 [94.5, 99.1] (52.0, 99.9)	99.9 [99.9, 99.9] (97.2, 100.0)	< 0,0001
CFU-GM (%)	median [iqr] (range)	98.0 [64.0, 99.4] (8.0, 99.9)	38.5 [14.5, 46.5] (8.0, 60.0)	98.2 [89.8, 99.2] (76.0, 99.9)	99.4 [99.1, 99.8] (80.0, 99.9)	< 0,0001
RBC (%)	median [iqr] (range)	87.5 [82.7, 97.2] (46.4, 104.1)	81.6 [79.7, 84.5] (46.4, 98.7)	89.7 [86.1, 97.0] (47.9, 101.5)	94.1 [84.9, 99.2] (79.0, 104.1)	0.039

HSCT : hematopoietic stem cell transplantation ; Hb: hemoglobin; BFU-E: erythroid burst forming units; CFU-GM: granulocyte-macrophage colony-forming-units; RBC: red blood cells.

in the *Online Supplementary Figure S1*.

Hemoglobin levels (overall median [range] concentration: 12.9 g/dL [8.4-14.4]) were generally stable and clinically satisfactory. Median Hb level was lower in group 1 (10.8 g/dL) than in group 2 (13.1 g/dL) or group 3 (12.9 g/dL), although the difference was not statistically significant (P=0.18). There was no difference in the mean Hb level between the set of patients with an AS donor (median [range] 12.8 g/dL [8.4-14.3]) and the set with a non-AS donor (median [range] 13.1 g/dL [9.6-14.4]) (P=0.61). A reticulocyte count at last follow-up greater than $100x10^9$/L was observed in patients with WBC donor chimerism <50%. However, this was associated with Hb levels <10 g/dL solely in patients with AS donor (see below).

The HbS fractions in patients after HSCT were similar to those of the donors, with the exception of the six patients with donor chimerism <50% (*see below*). With the exception of patient #2 (who experienced a single vaso-occlusive crisis (VOC) with confirmed liver involvement; *see below*), no VOC were observed after transplantation.

Donor chimerism in mature myeloid and lymphoid cells, and in granulomonocytic progenitors

The chimerism profiles of mature lymphoid/myeloid lineages and of progenitors/precursors often differed from those recorded for total WBC (Table 1 and *Online Supplementary Table S1*). The levels of donor chimerism were correlated for CD15$^+$ *versus* CD14$^+$ cells (rho=0.93, P=0.002), CD15$^+$ *versus* CD19$^+$ cells (rho=0.66, P=0.076), and CD14$^+$ *versus* CD19$^+$ cells (rho=0.69, P=0.028) but not for CD15$^+$ *versus* CD3$^+$ cells (rho=-0.14, P=0.752), CD14$^+$ *versus* CD3$^+$ cells (rho=-0.18, P=0.632) or CD19$^+$ *versus* CD3$^+$ cells (rho=0.44, P=0.199) (Figure 1). The donor chimerism in CFU-GM correlated with that in CD15$^+$ cells (rho=0.8, P<0.001) (*Online Supplementary Figure S2*). We limited our correlation analyses to group 1, in order to avoid bias due to the higher overall levels of donor chimerism in groups 2 and 3. Our analysis of chimerism in mature blood lineages showed that T-cell chimerism was independent of the other lineages.

The selective advantage of donor erythroid cells

In order to investigate the donor chimerism in peripheral RBC in patients with MC, we compared HbS fractions in patients after HSCT and in their donors. Overall, there was an excellent correlation between the HbS fraction in patients after HSCT and the fraction in the donors (rho=0.94, P<0.001) (Figure 2). The intra-class correlation coefficient (95% confidence interval [CI]) between these two variables was estimated to be 0.95 (0.81 – 0.99). In all the patients other than the six with MC <50% (*see below*), HbS levels were similar to those observed in the donors.

In order to investigate this putative selective advantage over the course of erythroid development, we compared donor chimerism among mature RBC, BFU-E, CFU-GM and CD15$^+$ cells (Figure 3). The CD15$^+$ cell population was chosen as a benchmark for bone marrow engraftment because it lacks a selective advantage, is short-lived, and is thus unlikely to accumulate over time. As expected, there were no differences in myeloid lineage donor chimerism between CD15$^+$ cells and CFU-GM (P=0.313). Inversely we observed a progressive enrichment in cells of donor origin during the development of the erythroid lineage in the periphery, with higher levels of donor chimerism in peripheral RBC *versus* CFU-GM and in BFU-E *versus* CFU-GM (P=0.016 and P=0.03, respectively). A median (IQR) 2.0-fold (1.4-2.5) increase between donor chimerism in peripheral RBC *versus* BFU-E was observed, whereas, a 1.5-fold (1.2-2.2) increase was observed between BFU-E and CFU-GM.

Taken as a whole, these results evidenced a lineage-specific, selective advantage in donor erythroid cells. Full donor chimerism was achieved in peripheral RBC, independently of the level in other lineages. Interestingly, this

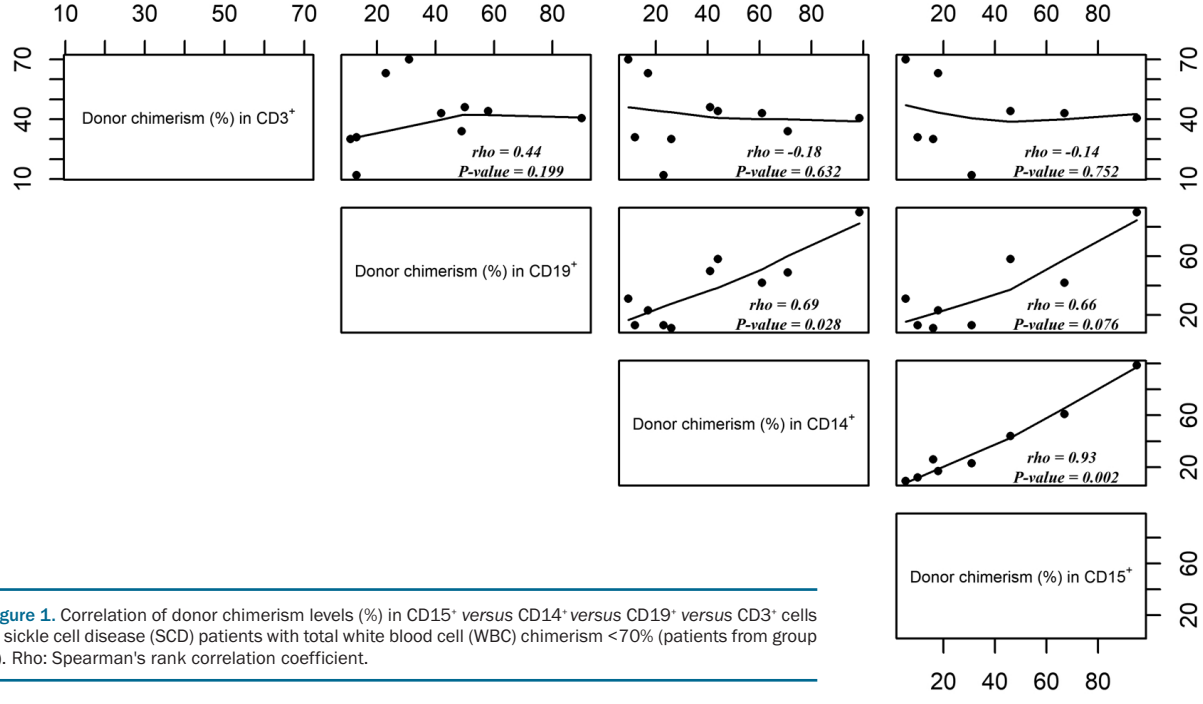

Figure 1. Correlation of donor chimerism levels (%) in CD15$^+$ *versus* CD14$^+$ *versus* CD19$^+$ *versus* CD3$^+$ cells in sickle cell disease (SCD) patients with total white blood cell (WBC) chimerism <70% (patients from group 1). Rho: Spearman's rank correlation coefficient.

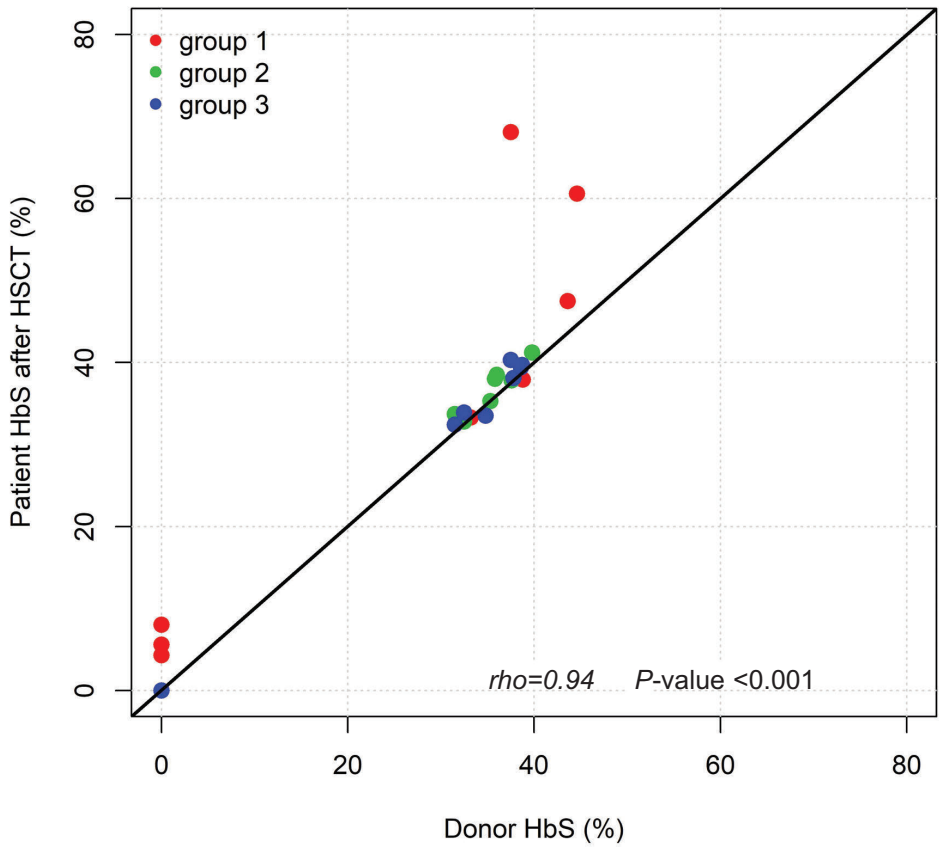

Figure 2. Correlation between HbS in patients after hematopoietic stem cell transplantation (HSCT) and in donors, regardless of the donor's genotype, divided into group 1 (mixed chimerism [MC] <70%, red dots), group 2 (MC 70-95%, green dots) and group 3 (MC 95-99.5%, blue dots). The line corresponds to y=x. Rho: Spearman's rank correlation coefficient.

selective advantage was observed not only in the peripheral compartment but also in erythroid progenitors/precursors.

Patients with WBC donor chimerism ≤50%

Six patients in group 1 (three with AA donors and three with AS donors) presented with a total WBC donor chimerism level ≤50% (median [range]: 20% [16-44%]) (Table 1, *Online Supplementary Table S1*). A unique chimerism profile was observed, with higher levels of donor chimerism in the $CD3^+$ cells than in the other lineages unlike most of the included patients (*Online Supplementary Figure S3-4*).

This subgroup of patients was characterized by younger age at transplant (median [range]: 7.15 years [3.4-10.8]), a longer post-HSCT follow-up period (median [range]: 68.5 months [33-153]), and lower Hb levels (median [range]: 10.1 g/dL [8.4-11.8]), when compared with the other patients in group 1. As mentioned above, HbS levels in these patients were higher than the corresponding donors (Figure 2, *Online Supplementary Table S1*). For these six patients, the reticulocyte count at last follow-up was greater than $100x10^9$/L; however, this was associated with a Hb level <10 g/dL only in three with very low myeloid chimerism (≤21%) and transplanted with AS donors (patients #2, #8 and #9, *Online Supplementary Table S1*). In these three cases, reticulocyte count was higher than $150x10^9$/L and associated with an HbS >47.5%. The three patients transplanted with an AS donor (patients #2, #8 and #9) presented a particularly low level of donor myeloid chimerism (5.4%, 10% and 16%, respectively–the lowest levels in the whole cohort) and highest HbS levels (68.1%, 60.6% and 47.5%, respectively) (*Online Supplementary Table S1*). The three patients received donor lymphocyte infusions (DLI); this treatment did not modify the donor chimerism and was not associated with graft-*versus*-host disease (GvHD) occurrence. Two of the patients (#2 and #9) required sporadic RBC transfusions between 24 and 43 months after HSCT. Neither of them has required RBC transfusions since then. The three patients developed hemolytic anemia (patients #2, #8 and #9), but only one had a suspected VOC with liver involvement (patient #2; hepatic sequestration was confirmed by a histological assessment). Before HSCT, patient #8 had presented with severe, SCD-related cerebral vasculopathy (bilateral stenosis of the cervical carotid arteries, and aneurism of the internal carotid arteries); this condition was stable after HSCT. Patients #8 and #9 are dizygotic twins who received grafts from different sibling AS donors (HbS fractions in the donors: 44.6% and 43.6%, respectively) at 5 years of age in 2003 and at 4 years of age in 2002, respectively. The level of donor chimerism fell rapidly in both twins, and then stabilized at a value below 20% in the second year post-HSCT. The HbS fraction progressively rose to a value of 60.6% and 47.5% in patients #8 and #9, respectively.

Interestingly, one patient (#6, with an AA donor) displayed a WBC donor chimerism level as low as 19% and myeloid chimerism of 31% but had a total Hb level of 11.8 g/dL and an HbS percentage of 5.6%.

Our results showed that HbS levels were closely correlated with chimerism in the myeloid compartment. The analyses of a subgroup of patients with low donor chimerism suggested that a myeloid chimerism of 30% is sufficient for preventing VOC in transplants from AA donors but not constantly from AS donors; in contrast, the

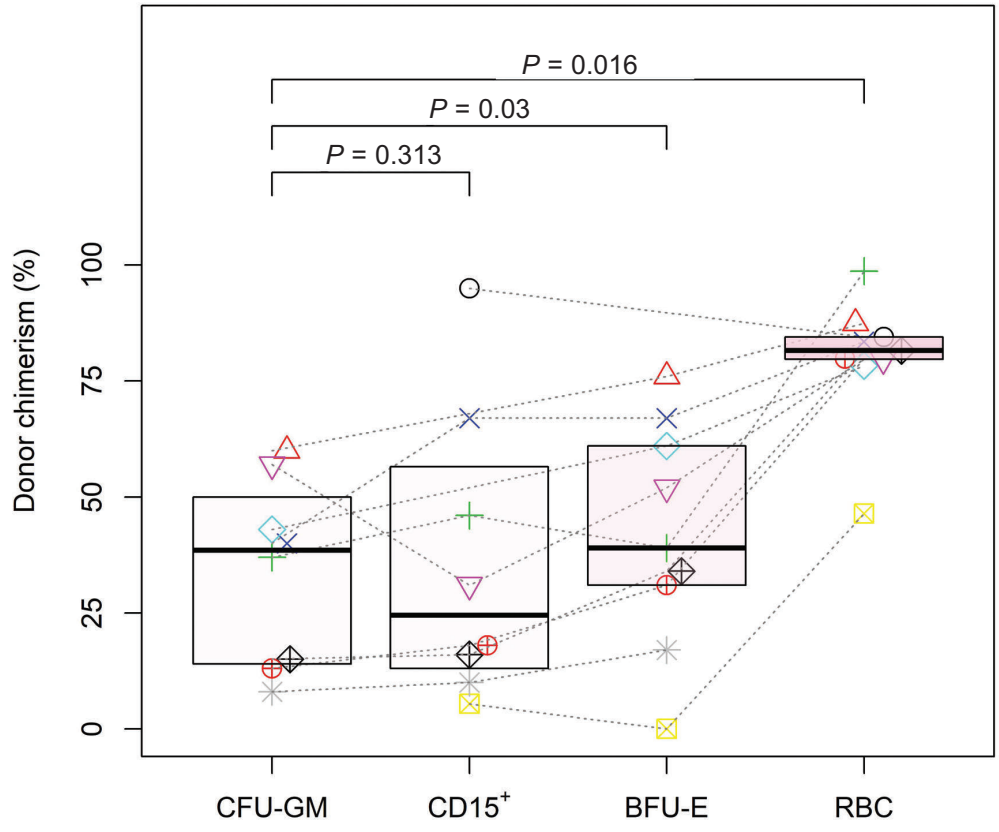

Figure 3. Donor chimerism (%) in peripheral red blood cells (RBC), erythroid burst forming units (BFU-E), CD15+ cells and granulocyte-macrophage colony-forming-units (CFU-GM) progenitors/precursors in patients with donor chimerism <70% (group 1), independently of the donor's genotype. Each patient is represented by a different symbol.

full correction of hemolytic anemia requires a higher level of myeloid donor chimerism (*i.e.* >50%) - particularly in patients with an AS donor.

Discussion

After HSCT, the majority of our patients with SCD will develop mixed chimerism (as defined in the *Methods* section). This condition is associated with a sufficient level of disease control, and represents an ideal setting for investigating (i) the reconstitution of the hematopoietic lineages following HSCT, and (ii) the minimum level of correction required to prevent the recurrence of clinical signs of SCD.

Chimerism analysis of total WBC is frequently used to evaluate donor cell engraftment following HSCT. However, in the context of MC, this tool does not provide an exhaustive analysis of donor engraftment. The present study is the first to have featured detailed, simultaneous analyses of chimerism in several different mature myeloid and lymphoid subpopulations, erythroid and myeloid progenitors/precursors, and peripheral RBC in a large cohort of patients having undergone myeloablative conditioning.

When simultaneously analyzing the donor/recipient origin of different hematologic lineages, we observed a linear correlation between $CD15^+/CD14^+$, $CD15^+/CD19^+$ and $CD14^+/CD19^+$ cells; this was also observed in our gene therapy trials (*unpublished data*). Chimerism of $CD3^+$ cells was not correlated with other cell populations. With the exception of the subgroup of patients with the lowest levels of recipient chimerism (including the three symptomatic patients), patients had a lower percentage of donor cells in the $CD3^+$ population than in the other lineages. Hence, T-cell reconstitution appears to be independent of the other lineages. An alternative explanation to this observation is that a minimum level of T-cell chimerism may be necessary for any myeloid chimerism, and/or that particular T-cell subsets may be critical for myeloid engraftment. Data available at the moment cannot formally confirm this hypothesis, however to our knowledge no myeloid chimerism was observed with no T-cell engraftment. It is possible that especially for low levels of donor chimerism a T-cell population could be necessary to allow the engraftment of myeloid cells in the bone marrow.

This finding shows that whole blood chimerism analysis is not appropriate for evaluating engraftment - especially in patients with MC, and provides an insight into the hematopoietic reconstitution after HSCT in these patients.

One of the present study's main objectives was to evaluate the minimum level of donor engraftment needed to prevent the recurrence of clinical signs of SCD. Most SCD-related morbidity is caused by altered RBC; hence, we focused on changes in donor chimerism during erythroid development. Nearly all the patients displayed full donor chimerism in peripheral RBC, despite variable degrees of MC in other cell populations; this suggests that donor RBC have a lineage-specific selective advantage in

the recipient. In order to investigate this putative selective advantage over the course of erythroid development, we compared donor chimerism among compartments at different stages of development. Our results show that not only the peripheral donor RBC have a selective advantage related to the shortened lifetime of SCD RBC but also the earlier erythroid progenitor/precursors. Despite the results of studies suggesting that the selective advantage is restricted to RBC in the periphery,[23,28] our hypothesis has already been proposed in small series of patients.[17,20] Indeed, the selective advantage of donor erythroid progenitor/precursors could be due to the ineffective erythropoiesis in SCD, as shown by the loss of SCD erythroblasts reported in patients with MC.[24] Interestingly, in a SCD patient with MC, the expression of the apoptotic regulator Fas was significantly higher in recipient than in donor erythroblasts and RBC,[29] suggesting that SCD "ineffective" erythroid cells undergo apoptosis, while donor cells have a survival advantage.

We further focused on a group of patients with low levels of donor chimerism (<70% for total WBC), and in particular on a subgroup of six patients who presented a donor chimerism level ≤50%. Indeed, as reported in the overall French cohort,[22] donor chimerism values as low as 16%, 18% and 21% for total WBC were recorded; these patients were the only ones to display high (>45%) HbS levels, hemolytic anemia and (in one case) a hepatic VOC. All three patients had an AS donor. These patients also presented the lowest level of donor chimerism in $CD15^+$ cells (5.4%, 10% and 16%), which was more closely correlated than WBC chimerism with the HbS level.

In contrast, patients with total WBC chimerism ≤50% and AA donors had low HbS levels and no anemia, although high reticulocyte counts were recorded. In the study population as a whole, there were no significant differences between patients with an AA donor and those with an AS donor. However, when the level of donor chimerism was low, having an AA donor was an advantage.

Three patients with the lowest levels of donor myeloid chimerism received donor lymphocyte infusions during follow up in order to stabilize donor cells engraftment. Of note no modification in donor chimerism was observed after infusion. The use of donor lymphocyte infusion in this context is debated as the risks might exceed the benefits.

Although our results came from a small number of patients, they show that individuals with a myeloid donor chimerism level above 30% have stable, sufficient levels of total Hb and no longer display the clinical signs of SCD - regardless of the donor's Hb genotype. In contrast, the full correction of hemolytic anemia requires higher myeloid donor chimerism levels (*i.e.* >50%) - particularly for patients with an AS donor. A myeloid donor chimerism level as low as 30% was sufficient to prevent VOC in patients with AA donors but not constantly in those with AS donors. For patients with very low degree of myeloid donor engraftment, an AS graft is associated with a higher risk of SCD symptoms.

By defining the level of correction needed to obtain clinical remission in SCD, the present study provides important information for patients undergoing autologous transplantation of genetically modified hematopoietic stem cells (HSC). It is important to note that today's lentiviral-based gene addition strategies and genome-editing approaches aimed at reactivating the expression of the anti-sickling fetal γ-globin at best generate a heterozygous phenotype *in vitro*; therapeutic hemoglobin accounts for at most 60% of the total Hb types, *e.g.* in RBC derived from HSC harboring multiple copies of the vector.[30] Under these optimal conditions (i.e. generation of AS-like HSC), our analyses of SCD patients with MC suggested that an HSC genetic modification rate below 30% would not be sufficient to ameliorate the SCD clinical phenotype, whereas a myeloid donor chimerism level ≥30% would probably lead to clinical improvements. Furthermore, our present results suggest that in order to fully control hemolysis, this threshold should be raised to >50%. Under suboptimal conditions (*i.e.* therapeutic Hb <60%), we predict that a donor chimerism level largely exceeding 30% would be required to correct the SCD clinical phenotype.

Consistently, the initial clinical data from gene therapy trials highlighted the absence of clinical benefit in patients with SCD harboring 10-30% of transduced HSC and low therapeutic Hb levels (*i.e.* 0.1-1.2 g/dL, which probably accounts for <10% of the total Hb types [31]. In contrast, clinical remission was observed in a SS patient with a mean vector copy number per cell of ~2, >60% of genetically modified HSC, and therapeutic Hb levels accounting for ~50% of the total Hb.[14]

In conclusion, these findings show that the degree of myeloid donor engraftment (rather than T cells) is a better predictor of the disease control in these patients - as shown by the inverse correlation between HbS levels and the chimerism in the myeloid lineage. According to these observations the whole blood chimerism could be appropriate for evaluating engraftment when donor chimerism is higher than 50%, but it looks unsatisfactory for patients developing lower donor chimerism; in this case a lineage-specific chimerism analysis should be preferred.

Our results provide a new insight into the selective advantage of donor erythroid cells in SCD patients. In particular, we show that not only donor peripheral RBC but also progenitors/precursors have a selective advantage over the recipient cells. Lastly, our study provides important clues for future gene therapy trials, and suggests that higher levels of gene correction will be needed to obtain full disease control.

Acknowledgments

The authors would like to thank patients and their families.

Funding

This work was funded by grants from "Cordons de Vie" charity and Agence Nationale de la Recherche (ANR-10-IAHU-01 "Investissements d'Avenir" program). This project has received funding from the European Union's Horizon 2020 research and innovation program under grant agreement No 693762 - Gene For Cure.

References

1. Kato GJ, Piel FB, Reid CD, et al. Sickle cell disease. Nat Rev Dis Prim. 2018;4:18010.
2. Williams TN, Weatherall DJ. World distribution, population genetics, and health burden of the hemoglobinopathies. Cold Spring Harb Perspect Med. 2012; 2(9):a011692.
3. Piel FB, Patil AP, Howes RE, et al. Global epidemiology of sickle haemoglobin in neonates: a contemporary geostatistical model-based map and population estimates. Lancet. 2013;381(9861):142-151.
4. Bernaudin F, Socie G, Kuentz M, et al. Long-term results of related myeloablative stem-cell transplantation to cure sickle cell disease. Blood. 2007;110(7):2749-2756.
5. Bhatia M, Walters MC. Hematopoietic cell transplantation for thalassemia and sickle cell disease: past, present and future. Bone Marrow Transplant. 2008;4(2):109-117.
6. Gluckman E, Cappelli B, Bernaudin F, et al. Sickle cell disease: an international survey of results of HLA-identical sibling hematopoietic stem cell transplantation. Blood. 2017;129(11):1548-1556.
7. Bernaudin F, Kuentz M. Haplo-BMT: cure or back to sickle cell? Blood. 2012;120(22): 4276-4277.
8. Gaziev J, Isgrò A, Sodani P, et al. Haploidentical HSCT for hemoglobinopathies: improved outcomes with TCR +/CD19+-depleted grafts. Blood Adv. 2018;2(3):263-270.
9. Krishnamurti L, Neuberg DS, Sullivan KM, et al. Bone marrow transplantation for adolescents and young adults with sickle cell disease: Results of a prospective multicenter pilot study. Am J Hematol. 2019; 94(4):446-454.
10. Hsieh MM, Fitzhugh CD, Weitzel RP, et al. Nonmyeloablative HLA-matched sibling allogeneic hematopoietic stem cell transplantation for severe sickle cell phenotype. JAMA 2014;312(1):48-56.
11. King AA, Kamani N, Bunin N, et al. Successful matched sibling donor marrow transplantation following reduced intensity conditioning in children with hemoglobinopathies. Am J Hematol. 2015; 90(12): 1093-1098.
12. Bhatia M, Jin Z, Baker C, et al. Reduced toxicity, myeloablative conditioning with BU, fludarabine, alemtuzumab and SCT from sibling donors in children with sickle cell disease. Bone Marrow Transplant. 2014;49(7): 913-920.
13. Bolaños-Meade J, Fuchs EJ, Luznik L, et al. HLA-haploidentical bone marrow transplantation with posttransplant cyclophosphamide expands the donor pool for patients with sickle cell disease. Blood. 2012;120(22):4285-4291.
14. Ribeil J-A, Hacein-Bey-Abina S, Payen E, et al. Gene therapy in a patient with sickle cell disease. N Engl J Med. 2017;376(9):848 855.
15. Cavazzana M, Antoniani C, Miccio A. Gene therapy for β-hemoglobinopathies. Mol Ther. 2017;25(5):1142-1154.
16. Andreani M, Testi M, Lucarelli G. Mixed chimerism in haemoglobinopathies: from risk of graft rejection to immune tolerance. Tissue Antigens. 2014;83(3):137-146.
17. Wu CJ, Gladwin M, Tisdale J, et al. Mixed haematopoietic chimerism for sickle cell disease prevents intravascular haemolysis. Br J Haematol. 2007;139(3):504-507.
18. Andreani M, Testi M, Battarra M, et al. Split chimerism between nucleated and red blood cells after bone marrow transplantation for haemoglobinopathies. Chimerism. 2011;2 (1):21-22.
19. Andreani M, Testi M, Gaziev J, et al. Quantitatively different red cell/nucleated cell chimerism in patients with long-term, persistent hematopoietic mixed chimerism after bone marrow transplantation for thalassemia major or sickle cell disease. Haematologica. 2011;96(1):128-133.
20. Walters MC, Patience M, Leisenring W, et al. Stable mixed hematopoietic chimerism after bone marrow transplantation for sickle cell anemia. Biol Blood Marrow Transplant. 2001;7(12):665-673.
21. Abraham A, Hsieh M, Eapen M, et al. Relationship between mixed donor-recipient chimerism and disease recurrence after hematopoietic cell transplantation for sickle cell disease. Biol Blood Marrow Transplant. 2017;23(12):2178-2183.
22. Bernaudin F, Dalle JH, Bories D, et al. Long-term event-free survival, chimerism and fertility outcomes in 234 patients with sickle-cell anemia younger than 30 years after myeloablative conditioning and matched-sibling transplantation in France. Haematologica. 2019 May 16. [Epub ahead of print]
23. Fitzhugh CD, Cordes S, Taylor T, et al. At least 20% donor myeloid chimerism is necessary to reverse the sickle phenotype after allogeneic HSCT. Blood. 2017;130(17):1946-1948.
24. Wu CJ, Krishnamurti L, Kutok JL, et al. Evidence for ineffective erythropoiesis in severe sickle cell disease. Blood. 2005;106(10):3639-3645.
25. Miccio A, Cesari R, Lotti F, et al. In vivo selection of genetically modified erythroblastic progenitors leads to long-term correction of beta-thalassemia. Proc Natl Acad Sci U S A. 2008;105(30):10547-10552.
26. Andreani M, Manna M, Lucarelli G, et al. Persistence of mixed chimerism in patients transplanted for the treatment of thalassemia. Blood. 1996;87(8):3494-3499.
27. Alizadeh M, Bernard M, Danic B, et al. Quantitative assessment of hematopoietic chimerism after bone marrow transplantation by real-time quantitative polymerase chain reaction. Blood. 2002;99(12):4618-4625.
28. Altrock PM, Brendel C, Renella R, et al. Mathematical modeling of erythrocyte chimerism informs genetic intervention strategies for sickle cell disease. Am J Hematol. 2016;91(9):931-937.
29. Marziali M, Isgrò A, Sodani P, et al. Peripheral red blood cell split chimerism as a consequence of intramedullary selective apoptosis of recipient red blood cells in a case of sickle cell disease. Mediterr J Hematol Infect Dis. 2014;6(1):e2014066.
30. Weber L, Poletti V, Magrin E, et al. An optimized lentiviral vector efficiently corrects the human sickle cell disease phenotype. Mol Ther Methods Clin Dev. 2018;10:268-280.
31. Kanter J, Tisdale J, Kwiatkowski J et al. Outcomes for initial patient cohorts with up to 33 months of follow-up in the Hgb-206 phase 1 trial. Blood. 2018;132(Suppl 1):1080.

Ferrata Storti Foundation

Haematologica 2020
Volume 105(5):1248-1261

Appropriation of GPIbα from platelet-derived extracellular vesicles supports monocyte recruitment in systemic inflammation

Myriam Chimen,[1,2] Aigli Evryviadou,[1] Clare L. Box,[1] Matthew J. Harrison,[1] Jon Hazeldine,[2] Lea H. Dib,[1] Sahithi J. Kuravi,[1] Holly Payne,[1] Joshua M.J. Price,[2] Dean Kavanagh,[1] Asif J. Iqbal,[1] Sian Lax,[1] Neena Kalia,[1] Alex Brill,[1,3,4] Steve G. Thomas,[1,3] Antonio Belli,[2] Nicholas Crombie,[2] Rachel A. Adams,[5] Shelley-Ann Evans,[5] Hans Deckmyn,[6] Janet M. Lord,[2] Paul Harrison,[2] Steve P. Watson,[1,3] Gerard B. Nash[1] and G. Ed Rainger[1]

[1]Institute of Cardiovascular Sciences, College of Medicine and Dentistry, University of Birmingham, Birmingham, UK; [2]NIHR Surgical Reconstruction and Microbiology Research Centre, Institute of Inflammation and Ageing, Birmingham University Medical School, Birmingham, UK;[3]Centre of Membrane Proteins and Receptors, University of Birmingham and Nottingham, The Midlands, UK; [4]Sechenov First Moscow State Medical University (Sechenov University), Moscow, Russia; [5]Cardiff School of Health Sciences, Cardiff Metropolitan University, Cardiff, UK and [6]Laboratory for Thrombosis Research, KU Leuven Campus Kulak Kortrijk, Kortrijk, Belgium

ABSTRACT

Interactions between platelets, leukocytes and the vessel wall provide alternative pathological routes of thrombo-inflammatory leukocyte recruitment. We found that when platelets were activated by a range of agonists in whole blood, they shed platelet-derived extracellular vesicles which rapidly and preferentially bound to blood monocytes compared to other leukocytes. Platelet-derived extracellular vesicle binding to monocytes was initiated by P-selectin-dependent adhesion and was stabilised by binding of phosphatidylserine. These interactions resulted in the progressive transfer of the platelet adhesion receptor GPIbα to monocytes. GPIbα$^+$-monocytes tethered and rolled on immobilised von Willebrand Factor or were recruited and activated on endothelial cells treated with TGF-β1 to induce the expression of von Willebrand Factor. In both models monocyte adhesion was ablated by a function-blocking antibody against GPIbα. Monocytes could also bind platelet-derived extracellular vesicle in mouse blood *in vitro* and *in vivo*. Intratracheal instillations of diesel nanoparticles, to model chronic pulmonary inflammation, induced accumulation of GPIbα on circulating monocytes. In intravital experiments, GPIbα$^+$-monocytes adhered to the microcirculation of the TGF-β1-stimulated cremaster muscle, while in the *ApoE*$^{-/-}$ model of atherosclerosis, GPIbα$^+$-monocytes adhered to the carotid arteries. In trauma patients, monocytes bore platelet markers within 1 hour of injury, the levels of which correlated with severity of trauma and resulted in monocyte clearance from the circulation. Thus, we have defined a novel thrombo-inflammatory pathway in which platelet-derived extracellular vesicles transfer a platelet adhesion receptor to monocytes, allowing their recruitment in large and small blood vessels, and which is likely to be pathogenic.

Introduction

The recruitment of leukocytes during inflammation occurs in the haemodynamically permissive environment of the post capillary venules. In this environment, vascular endothelial cells responding to pro-inflammatory mediators such as cytokines express adhesion receptors and activating stimuli such as chemokines, which ensure efficient and localised trafficking of leukocytes into the affected tissues.[1-4] It has become clear more recently that in pathological situations, platelets can also play a

Correspondence:

MYRIAM CHIMEN
chimenm@bham.ac.uk

Received: December 21, 2018.

Accepted: August 23, 2019.

Pre-published: August 29, 2019.

doi:10.3324/haematol.2018.215145

Check the online version for the most updated information on this article, online supplements, and information on authorship & disclosures: www.haematologica.org/content/105/5/1248

role in leukocyte recruitment in other vascular beds.[5] Thus, the integrated function of the thrombotic and inflammatory systems results in recruitment of leukocytes to arterioles in models of ischaemic injury of the liver and other tissues.[6-10] Moreover, there is substantial evidence supporting a role for platelets in the preferential recruitment of monocytes to the artery wall during atherogenesis. For example, inhibition of platelet adhesion to the artery wall, or induction of thrombocytopenia, significantly reduces monocyte trafficking and the burden of atherosclerotic disease in genetically susceptible strains of mice.[11-14] In addition, instillation of activated platelets exacerbates the formation of atherosclerotic plaques in such models.[11-14] There is also direct evidence that platelet P-selectin plays a role in plaque formation in the *ApoE*$^{-/-}$ mouse.[11-14] Other studies demonstrate that platelet derived chemokines such as CCL5 (RANTES) and CX3CL1 (fractalkine), once deposited on vascular endothelial cells, can selectively recruit monocytes in these models.[11-15]

The examples described above require platelet activation at the vessel wall to facilitate leukocyte recruitment and trafficking. However, interactions between platelets and leukocytes also occur in circulating blood under pathological conditions. Indeed, formation of platelet-leukocyte aggregates has been described in diseases as diverse as bacterial infection, rheumatoid arthritis, diabetes and inflammatory bowel disease.[16-22] In cardiovascular disease (CVD) the number of platelet-leukocyte aggregates increases significantly, and one can measure an increased incidence of such heterotypic aggregates in individuals with independent risk factors for CVD, such as hypertension.[23-25] Indeed, it has been proposed that an increase in the incidence of platelet-leukocyte aggregates may in itself, be an independent risk factor for CVD.[26] The formation of platelet leukocyte aggregates may also play an important role in acute and severe inflammatory responses. Thus, in patients with acute trauma or trauma associated sepsis, an enhanced capacity for platelet activation and platelet interaction with monocytes and neutrophils has been reported in response to exogenous activation of their blood with the ionophore, ionomycin.[27,28]

Extracellular vesicles which can be detected in the blood, urine and other bodily fluids are heterogeneous particles 40-1,500 nm in diameter that are derived from the plasma membrane (microvesicles) or by exocytosis of multi-vesicular bodies (exosomes).[29] They are released from cells of the vasculature, including platelets, endothelial cells (EC) and leukocytes, and specific populations can be identified using appropriate methodology (*e.g.* flow cytometry), as they express surface markers derived from their cell of origin. There is now mounting evidence that platelet-derived extracellular vesicles (PEV) (otherwise and often referred to as microparticles or microvesicles) are heterogeneous in nature. For example, *in vitro*, PEV have been generated in response to shear stress, thrombin, calcium ionophore, adenosine diphosphate (ADP), collagen and collagen related peptide.[30-33] Interestingly, these studies show that PEV derive by using different platelet agonists and differ in abundance, as well as the cargo that they convey. Indeed, there is now good evidence that platelets can shed large vesicles which contain organelles such as mitochondria.[34] Until recent technological advancements it had been impossible to analyse the concentration and composition of vesicles using a single platform. Flow cytometry does not detect vesicles <200-300 nm and does not accurately measure larger vesicles due to the disparity in the refractive index of biological vesicles and the latex beads used as size standards on this platform.[35] However, electron microscopy studies show that the majority of PEV are small. Thus, although Ponomereva *et al.* described calcium ionophore derived PEV as large as 1,500 nm, particles were predominantly in the range of 50-130 nm.[36] Similarly, Aatonen *et al.* described the main population of PEV as being 100-250 nm, with in excess of 90% of all vesicles being smaller than 500 nm irrespective of the platelet agonist used for PEV biogenesis.[35] Mitochondria containing vesicles, referred to above, were in the range of 500-1,500 nm. Importantly, the study of the functions of distinct subsets of PEV is not a well-developed field, however, bearing in mind the diversity of the PEV generated upon platelet activation, vesicles with discrete functional roles cannot be ruled out. The diversity of platelet microparticles has recently been reviewed.[37]

There is mounting evidence that PEV play a pathophysiological role in inflammation.[38] An increased concentration of circulating PEV is associated with a number of diseases. In diabetic retinopathy, the number of PEV was associated with the severity of disease,[39] while the levels of PEV circulating in patients with type-1 diabetes correlated with the degree of pro-atherogenic dyslipidaemia.[40] There was a correlation with vascular dysfunction (assessed by measuring arterial elasticity and flow-dependent vasodilatation of the brachial artery) in patients with type-2 diabetes.[41] Interestingly, the number of PEV was higher in patients with acute coronary syndromes than those with stable angina,[42] implying an association with the onset of athero-thrombotic disease. The roles of PEV in inflammation and pathogenesis of inflammatory disease are not well understood. However, they possess adhesion receptors such as glycoprotein (GP)Ibα, αIIbβ3-integrin and P-selectin, meaning that they could interact with the vessel wall and circulating leukocytes to promote recruitment of the later. Importantly, as these receptors ordinarily regulate the process of haemostasis, PEV might provide an avenue of leukocyte recruitment to the disease environment which falls outside of regulatory pathways which ordinarily limit the duration and magnitude of the inflammatory response.

Here, using assays of heterotypic aggregate formation we have characterised the adhesive interactions between leukocytes and PEV in whole blood and identified a novel route by which the platelet adhesion receptor, GPIbα, promotes monocyte recruitment in both *in vitro* and *in vivo* models of vascular inflammation.

Methods

Full Methods can be found in the *Online Supplementary Materials and Methods.*

Blood donors

Blood was obtained from healthy donors with informed consent and with local ethical approval (ERN_07-058). Blood from the Golden Hour cohort (drawn within 1 hour of suffering traumatic injury) was obtained under the National Research Ethics Committee (reference 13/WA/0399). Specimen collection and informed consent procedures were approved and permission granted by the Biomedical Science Ethic Committee.

Animal experiments

All experiments were performed in accordance with the Home Office Guidelines. In each experiment C57BL/6 *IL4R/GPIbα*–Tg or *ApoE*$^{-/-}$ or wild-type (WT) animals with the same background were allocated at random to experimental groups. Mice from the same litter were randomly distributed amongst experimental groups.

Results

Platelet activation in whole blood leads to formation of PEV and their adhesion to monocytes

We investigated the effect of platelet activation on platelet-leukocyte interactions in whole blood. When thrombin receptor activating peptide (TRAP), an agonist of the platelet protease activated receptor-1 (PAR-1), was added to sheared whole blood, a time dependent increase in the percentage of monocytes bearing the platelet receptor GPIbα (CD42b) as well as CD41 (GPIIb) and in the intensity of GPIbα and CD41 staining, was observed (Figure 1A-C; *Online Supplementary Figure S1A-C* and *S2*). In unstimulated blood, few monocytes (~5%) possessed measurable levels of GPIbα, showing that shear did not activate platelets. During analysis monocytes were subdivided into two subsets using standard markers as previously described.[43] Classical monocytes (CD14^{+}CD16^{-}) represent 90% of cells in the circulation and non-classical/intermediate monocytes (CD14$^{+/dim}$CD16^{+}) 10% (*Online Supplementary Figure S1A*). In our studies, we have compared classical to non-classical/intermediate monocytes grouped together. This is because the low numbers of isolated intermediate and non-classical monocytes do not allow appropriate functional testing of these subsets individually in our assays. The interaction between platelets and monocytes was similar when classical and non-classical/intermediate monocytes were assayed, showing similar patterns of GPIbα and CD41 accumulation over time (Figure 1B-C; *Online Supplementary Figure S1A-C* and *S2*). Interestingly, only a modest accumulation of GPIbα was evident on neutrophils stimulated with TRAP and even less when whole blood was stimulated with CRP-XL (Figure 1D and *Online Supplementary Figure S1D-E*). We observed no accumulation of GPIbα on lymphocytes (Figure 1D and *Online Supplementary Figure S1D*).

The median fluorescent intensity (MFI) of GPIbα on monocytes after 30 minutes (min) of TRAP stimulation was well below the intensity on individual platelets (Figure 2A). Moreover, the time course of the acquisition of GPIbα by monocytes demonstrated a progressive accumulation that ruled out the binding of whole platelets (Figure 2B). This pattern of accumulation is consistent with the adhesion of PEV, which was confirmed using confocal microscopy (Figure 2C and *Online Supplementary Figure S3*). For comparison, we show a monocyte bearing whole platelets generated under different experimental conditions *i.e.* in the absence of shear (Figure 2D).

Here, we have reported the formation of PEV in response to thromboxane A2, ADP and cross linked collagen related peptide (CRP-XL). Activation of platelets in whole blood using CRP-XL, ADP, the thromboxane mimetic U46619, or the C-type lectin-like receptor (CLEC-2) agonist, rhodocytin, resulted in the same pattern of accumulation of GPIbα on monocytes, showing that different routes of platelet activation resulted in PEV production and adhesion to monocytes (*Online Supplementary Figure S4A-D*).

PEV binding to monocytes is rapid

Accumulation of PEV on monocytes after stimulation of whole blood was progressive over a prolonged period of time (*i.e.* 30 min) (Figure 1B-C and *Online Supplementary Figure S4*). An important question is whether this pattern of accumulation is dependent upon the dynamics of PEV-monocyte interaction and adhesion, or whether the genesis of PEV from activated platelets is the rate-limiting step. Here we used the addition of isolated and pre-labelled PEV (1x10^{9}/mL) generated by stimulating platelets (3x108) with CRP-XL (1 µg/mL), to unstimulated whole blood to investigate this. After CRP-XL activation of isolated platelets, GPIbα stained PEV were readily discernible by flow cytometry in platelet supernatants (Figure 3A and *Online Supplementary Figure S5A-E*). A similar pattern was observed for CD41 on PEV (*Online Supplementary Figure S5C* and *S6*). Interestingly, ~25% of the large vesicles detected by flow cytometry contained mitochondrial fragments, as previously described[34] (*Online Supplementary Figure S7A*). Analysis using nanoparticle tracking showed that 3x10^{8} platelets could yield 1.2±0.3x10^{9} PEV compared to an average 1.3x10^{8}±2.8x10^{7} vesicles in untreated conditions (Figure 3B and *Online Supplementary Figure S5D-E*) with a mean diameter of 274±188 nm. To date it has not been possible to simultaneously count vesicles, size them and analyse protein cargo using a single platform. The Exo View-R100 is a new platform which allows such analysis providing previously unattainable information in a single protocol.[44] Using this assay we observed that PEV from CRP-XL stimulated platelets captured by a CD9 antibody had a mean size of 54 nm while those captured by a CD41a antibody had a mean size of 82.3 nm (*Online Supplementary Figure S7B*). Upon analysis using the Exo View system, we observed the majority of PEV were captured by CD41a and CD9 (which are abundant on platelets), but not CD63 or CD81 (which are expressed on exosomes) (*Online Supplementary Figure S7C*). This was also confirmed by secondary labelling of captured PEV using fluorescent antibodies against CD9, CD63 and CD81 (*Online Supplementary Figure S7D*). Labelled PEV were added to whole blood at a concentration of 1x10^{9}/mL and their interactions with leukocytes assayed by flow cytometry. Many monocytes acquired GPIbα within 5 min, but neutrophils or lymphocytes did not (Figure 3C-D). The proportion of monocytes acquiring GPIbα slowly increased thereafter, while intensity of GPIbα staining increased steadily (Figure 3C-D). Interestingly, we found that most of the GPIbα signal detected by flow cytometry was intracellular (~80%) on both monocyte subsets (*Online Supplementary Figure S8A-B*) and in agreement with the confocal imaging data described in Figure 2C. We also analysed the adhesion of PEV labelled with the lipophilic dye PKH67 to exclude antibody-mediated interaction of PEV with monocytes. PKH67 labelled all of the PEV in the activated-platelet supernatant (Figure 3E). The dynamics of PEV binding to monocytes, neutrophils or lymphocytes (Figure 3F) was similar to that for the antibody-labelled PEV (Figure 3C).

The mechanistic basis for the preferential accumulation of GPIbα on monocytes was investigated using adhesion-blocking reagents. Inclusion of a function-neutralising

anti-P-selectin antibody inhibited GPIbα accumulation on both monocytes and neutrophils, strongly implicating this platelet receptor in heterotypic adhesion with the two cells (Figure 4A and *Online Supplementary Figure S9A-B*). We measured the density of the P-selectin counter receptor P-selectin Glycoprotein Ligand 1 (PSGL-1) on blood leukocytes because the efficiency of GPIbα accumulation might reflect the surface density of this molecule. Figure 4B shows that there is substantially more PSGL-1 on monocytes than neutrophils, which could account for the differential levels of GPIbα accumulating on these cells. However, T cells, which did not accumulate GPIbα, also possessed abundant PSGL-1. Thus additional and cell specific adhesive interactions may be required to stabilise P-selectin mediated adhesion under shear. Using a panel of function-neutralising antibodies against known platelet and leukocyte adhesion molecules, we could find no contribution to heterotypic aggregate formation from CD31, ICAM-2 or β2-integrins (Figure 4C-E). However, an anti-phosphatidylserine (PS) antibody significantly reduced GPIbα accumulation on both neutrophils and monocytes (Figure 4C-E). The function of PS as a stabilising interactant is concordant with its documented patterns of interaction with monocytes and neutrophils, while its potential lack of interaction with T cells would account for the lack of GPIbα accumulation on these cells.

An important question was whether monocyte activa-

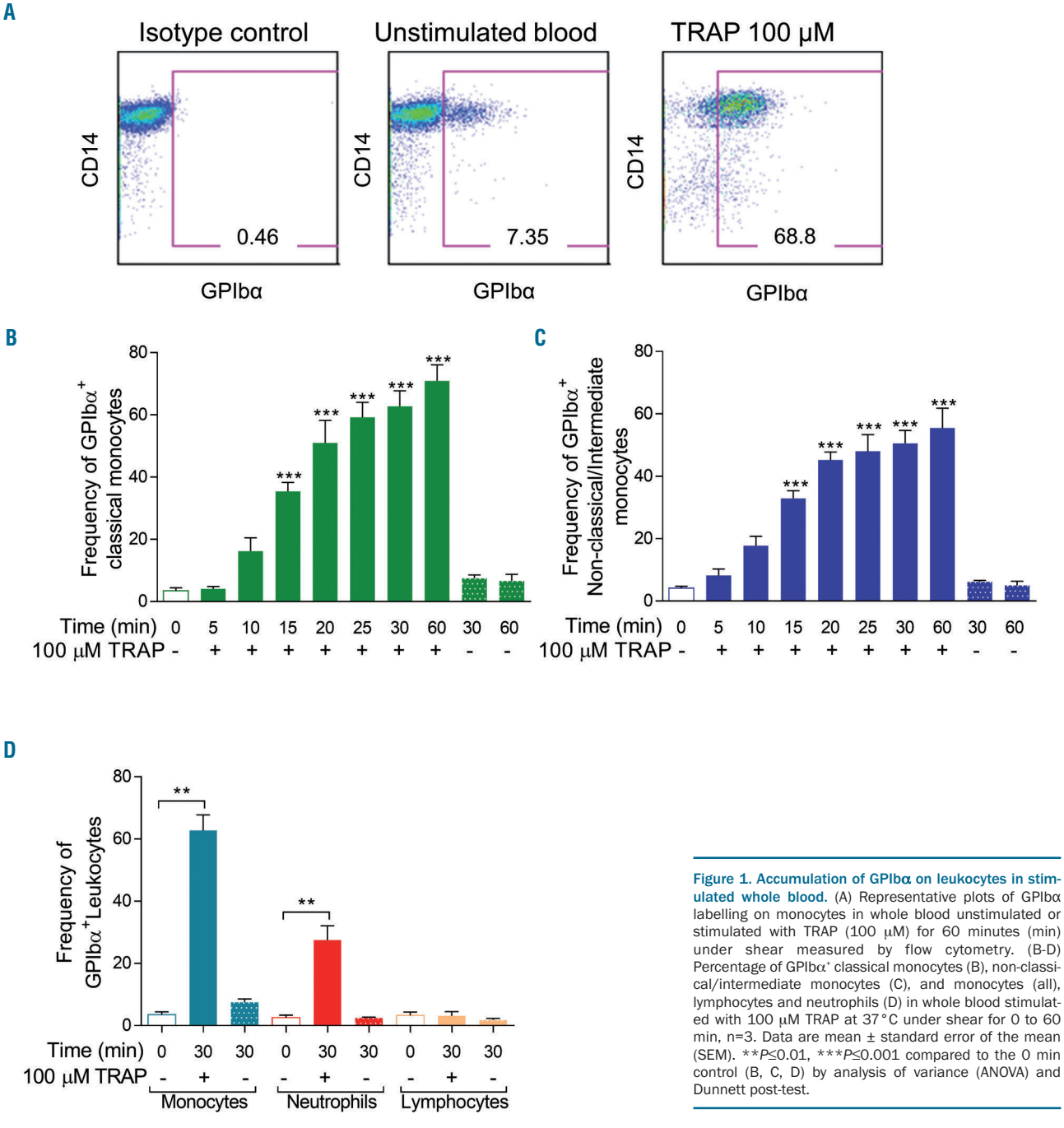

Figure 1. Accumulation of GPIbα on leukocytes in stimulated whole blood. (A) Representative plots of GPIbα labelling on monocytes in whole blood unstimulated or stimulated with TRAP (100 µM) for 60 minutes (min) under shear measured by flow cytometry. (B-D) Percentage of GPIbα+ classical monocytes (B), non-classical/intermediate monocytes (C), and monocytes (all), lymphocytes and neutrophils (D) in whole blood stimulated with 100 µM TRAP at 37°C under shear for 0 to 60 min, n=3. Data are mean ± standard error of the mean (SEM). ***P*≤0.01, ****P*≤0.001 compared to the 0 min control (B, C, D) by analysis of variance (ANOVA) and Dunnett post-test.

tion contributed to GPIbα accumulation. For these studies, we used CRP-XL to stimulate whole blood, as this agonist does not directly activate monocytes and would thus allow analysis of whether secondary activation of monocytes downstream of platelet activation was prerequisite for PEV adhesion. We assessed the expression of the activation marker αMβ2-integrin (CD11b/CD18) on monocytes 30 min after the addition of CRP-XL to whole blood. There was some increase in both integrin subunits CD11b and CD18 (*Online Supplementary Figure S9C-D*), however, this was inconsistent and monocyte subset specific. When a function neutralising antibody against CD18 was included in the assay it had no effect on GPIbα accumulation (Figure 4C-E), indicating that monocyte activation was not required for PEV adhesion.

Adopted GPIbα is a functional adhesion molecule supporting monocyte rolling on von Willebrand Factor

As GPIbα is known to mediate binding of platelets from flowing blood to von Willebrand Factor (VWF), we tested whether VWF could also recruit PEV-treated monocytes (Figure 5A-E). Monocytes lacking GPIbα showed low levels of adhesion when perfused across immobilised human VWF (Figure 5B, E). However, acquisition of PEV-derived-GPIbα supported capture and rolling (66.8±4.1% of adherent cells rolling) of monocytes on VWF (Figure 5C, E). Importantly, the adhesion of PEV-treated monocytes was inhibited by a function-neutralising antibody against GPIbα (Figure 5D, E).

Monocytes bearing GPIbα bind to EC in a model of vascular inflammation

Transforming growth factor beta-1 (TGF-β1) promotes the expression of a matrix of VWF on the surface of EC which recruits platelets from flowing blood, which in turn function as adhesive bridges for the preferential recruitment of monocytes to EC *in vitro* and *in vivo*.[15] Here we used this model to determine whether PEV-derived GPIbα could support monocyte adhesion directly to stimulated endothelium. A low level of monocyte adhesion to TGF-β1-stimulated EC was observed without PEV (Figure 6A, D). However, PEV-treated monocytes adhered in significantly higher numbers, an adhesive interaction blocked by a GPIbα blocking antibody (Figure 6B-D). As previously observed, recruited monocytes did not roll on the EC. Thus 6.1±0.9% of adherent cells were observed rolling, with the remaining 93.9% becoming activated and stably adherent. Interestingly, the acquisition of PEV increased the efficiency with which monocytes transmigrated across the EC monolayer (Figure 6E). We could attribute this increase in PEV-treated monocytes recruitment to PEV rather than soluble factors such as chemokines, as supernatants generated from PEV filtered using a 10 KDa size filter (to remove

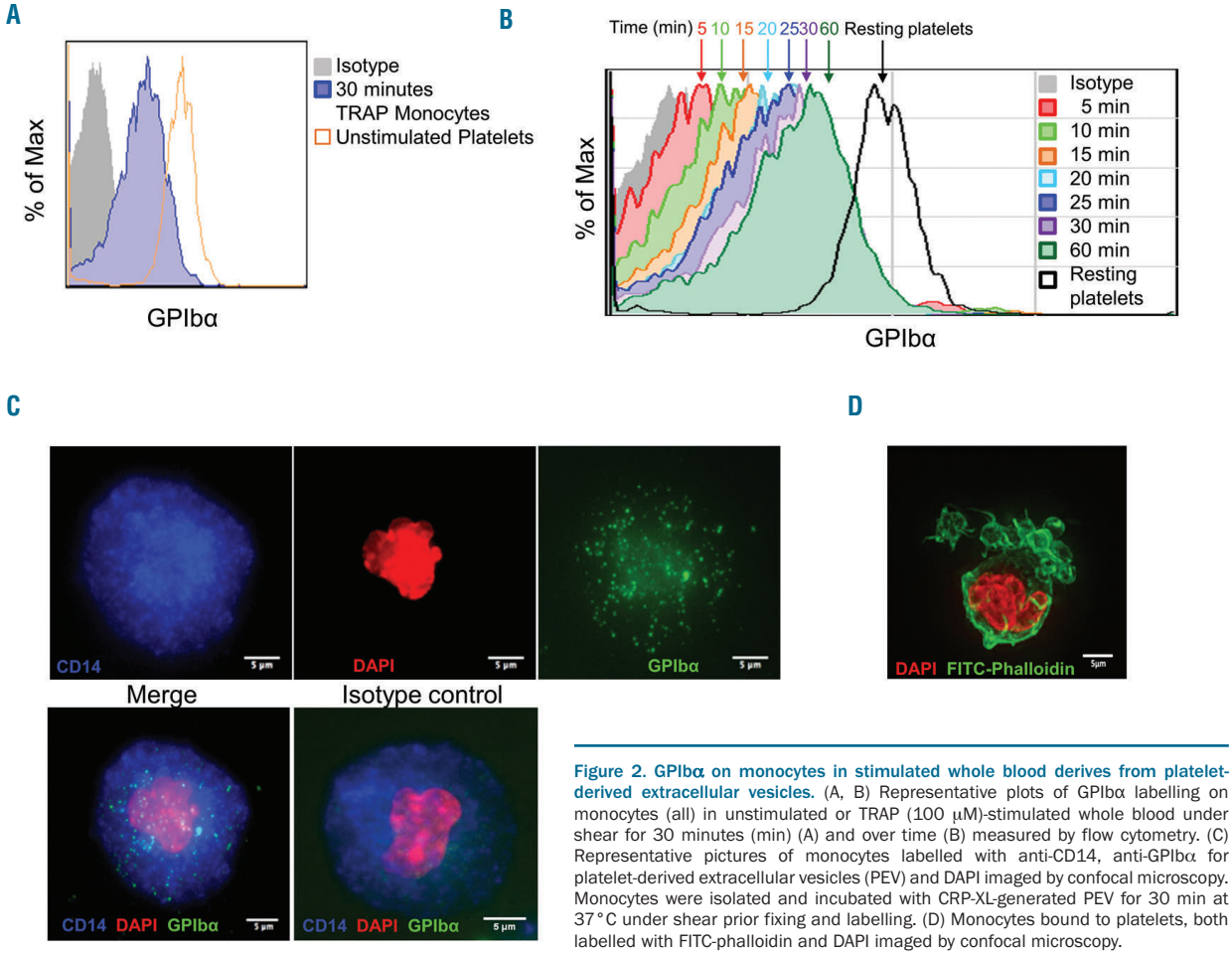

Figure 2. GPIbα on monocytes in stimulated whole blood derives from platelet-derived extracellular vesicles. (A, B) Representative plots of GPIbα labelling on monocytes (all) in unstimulated or TRAP (100 μM)-stimulated whole blood under shear for 30 minutes (min) (A) and over time (B) measured by flow cytometry. (C) Representative pictures of monocytes labelled with anti-CD14, anti-GPIbα for platelet-derived extracellular vesicles (PEV) and DAPI imaged by confocal microscopy. Monocytes were isolated and incubated with CRP-XL-generated PEV for 30 min at 37°C under shear prior fixing and labelling. (D) Monocytes bound to platelets, both labelled with FITC-phalloidin and DAPI imaged by confocal microscopy.

vesicles) did not induce monocyte adhesion and transmigration (Figure 6D, E).

PEV-treated murine monocytes bearing GPIbα can be generated and recruited in mice

Prior to moving to *in vivo* assays of monocyte recruitment, we determined whether murine PEV derived-GPIbα could accumulate on murine monocytes. Using the *ex vivo* whole blood assay under shear, we observed a high proportion of murine monocytes rapidly accumulated GPIbα and CD41 after addition of ADP to the blood (Figure 7A and *Online Supplementary Figure S10A-C*). To examine monocytes/PEV aggregate formation *in vivo* we induced pulmonary inflammation by instillation of air pollution particles into the lungs. A significant increase in the number of monocytes bearing GPIbα and CD41 (αIIb-integrin) was observed in animals exposed to air pollution particles, but not vehicle control (PBS) (Figure 7B-C). Importantly, and in concordance with human studies, GPIbα and CD41 intensities of expression was below the level on individual platelets (*Online Supplementary Figure S10D*), demonstrating that monocytes bind PEV in this model.

Using an intravital preparation of the TGF-β1-stimulated, mouse cremaster muscle to observe monocyte interactions with the microvasculature in real time, we tracked

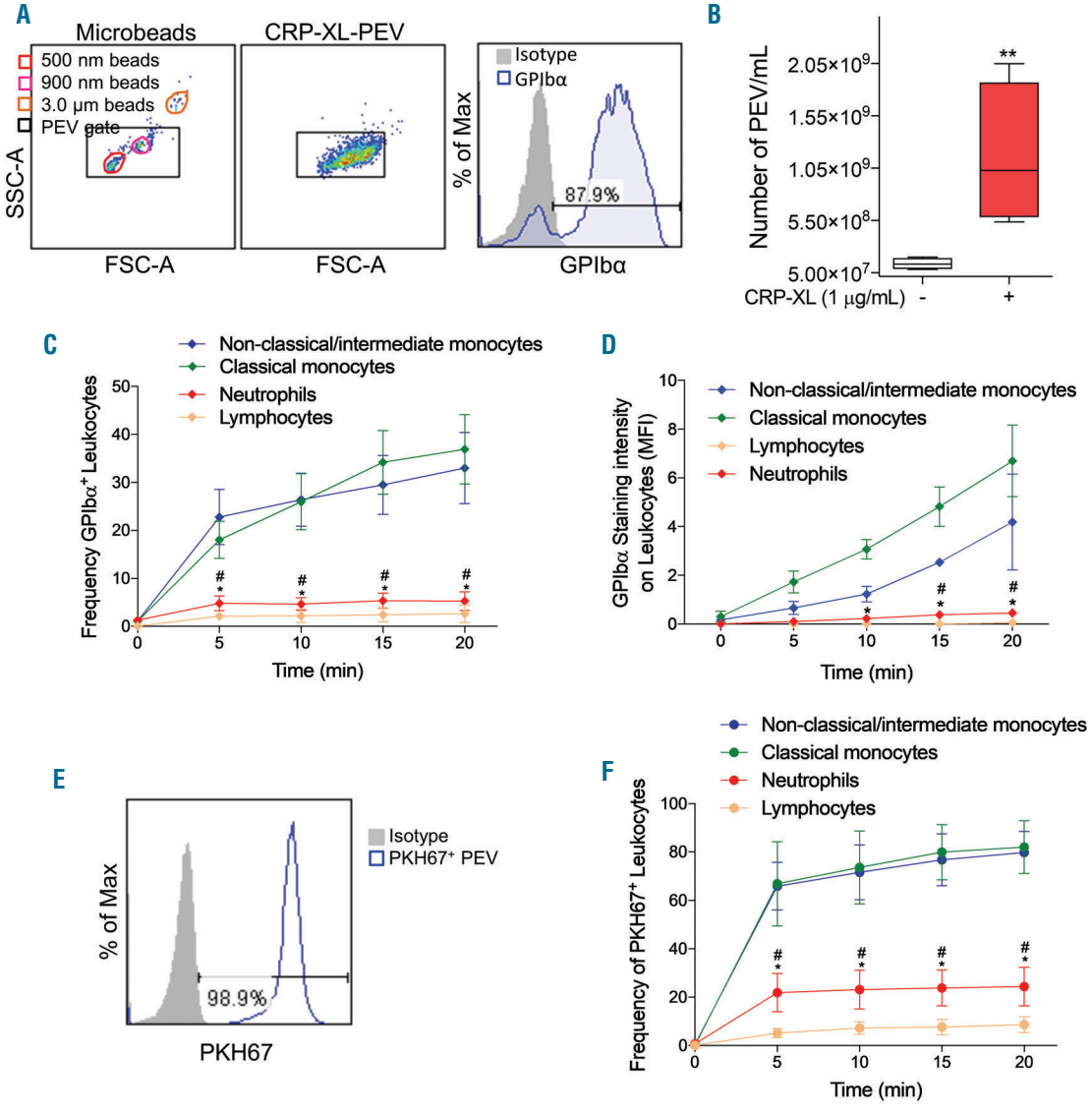

Figure 3. Rapid and specific binding of platelet-derived extracellular vesicles to monocytes. (A) Platelet-derived extracellular vesicles (PEV) gate was determined using microbeads to select events under 900 nm in size (left dot plots). Representative plot of GPIbα intensity on PEV generated by stimulation of platelets with 1 µg/mL CRP-XL for 30 minutes (min) analysed by flow cytometry (right histogram). (B) Concentration of PEV generated by stimulation of platelets with 1 µg/mL CRP-XL for 30 min, n=4. (C, D) Percentage (C) and median fluorescent intensity (MFI) (D) of GPIbα⁺ leukocytes in unstimulated whole blood supplemented with CRP_XL (1 µg/mL)-generated-PEV at 37°C under shear determined by flow cytometry, n=4. (E) Representative plot of PEV generated by stimulation of platelets with 1 µg/mL CRP-XL for 30 min labelled with PKH67. (F) Percentage of PKH67+ leukocytes in unstimulated whole blood supplemented with CRP_XL (1 µg/mL) generated PEV at 37°C under shear determined by flow cytometry, n=4. Data are mean ± standard error of the mean (SEM). $^{**}P \leq 0.01$ by (B) unpaired t-test. * or $^{\#}P \leq 0.01$ (C, D, F) by repeated measures two-way ANOVA followed by Bonferroni post-test for neutrophils and lymphocytes compared to * classical monocytes and # to non-classical/Intermediate monocytes.

human mouse PEV-treated monocytes (*Online Supplementary Figure S10E-F*). We used the hIL4R/GPIbα–Tg mouse which expressed human IL-4 receptor under the GPIbα promoter. This allows the animals to be rendered thrombocytopenic by injection of an antibody against hIL4R. Adoptively transferred WT platelets or PEV are however retained within the circulation. Using mice depleted of endogenous platelets using an anti-hIL4R antibody, we observed higher numbers of adoptively transferred WT PEV-treated monocytes rolling on the microvasculature compared to untreated monocytes; the number was significantly reduced by a GPIbα blocking antibody (Figure 7D-G). Detailed analysis revealed two populations of rolling cells: those exhibiting stable rolling (interactions >300 ms) with a velocity of 241±82 μm/s (Figure 7D, F); those exhibiting transient rolling (interactions <300 ms) with a velocity of 478±65 μm/s (Figure 7D, G). We also infused human monocytes into *ApoE*$^{-/-}$ mice that had been on a western diet for six weeks and observed the carotid artery by intravital microscopy. Murine PEV-treated monocytes adhered to the artery wall with significantly greater efficiency than untreated monocytes (Figure 7H). In this environment a mixture of adhesive behaviors was observed with stationary adhesion, stable rolling and transient rolling adhesion evident (Figure 7H).

Monocytes with platelet markers appear within 1 hour of severe trauma and are rapidly cleared from the circulation

We investigated whether rapid production and binding of extracellular vesicles to monocytes could be detected following an acute event such as traumatic injury. In the Golden Hour study blood samples in the pre-hospital setting (mean time to blood sampling =43 min) were acquired from traumatically-injured patients (injury sever-

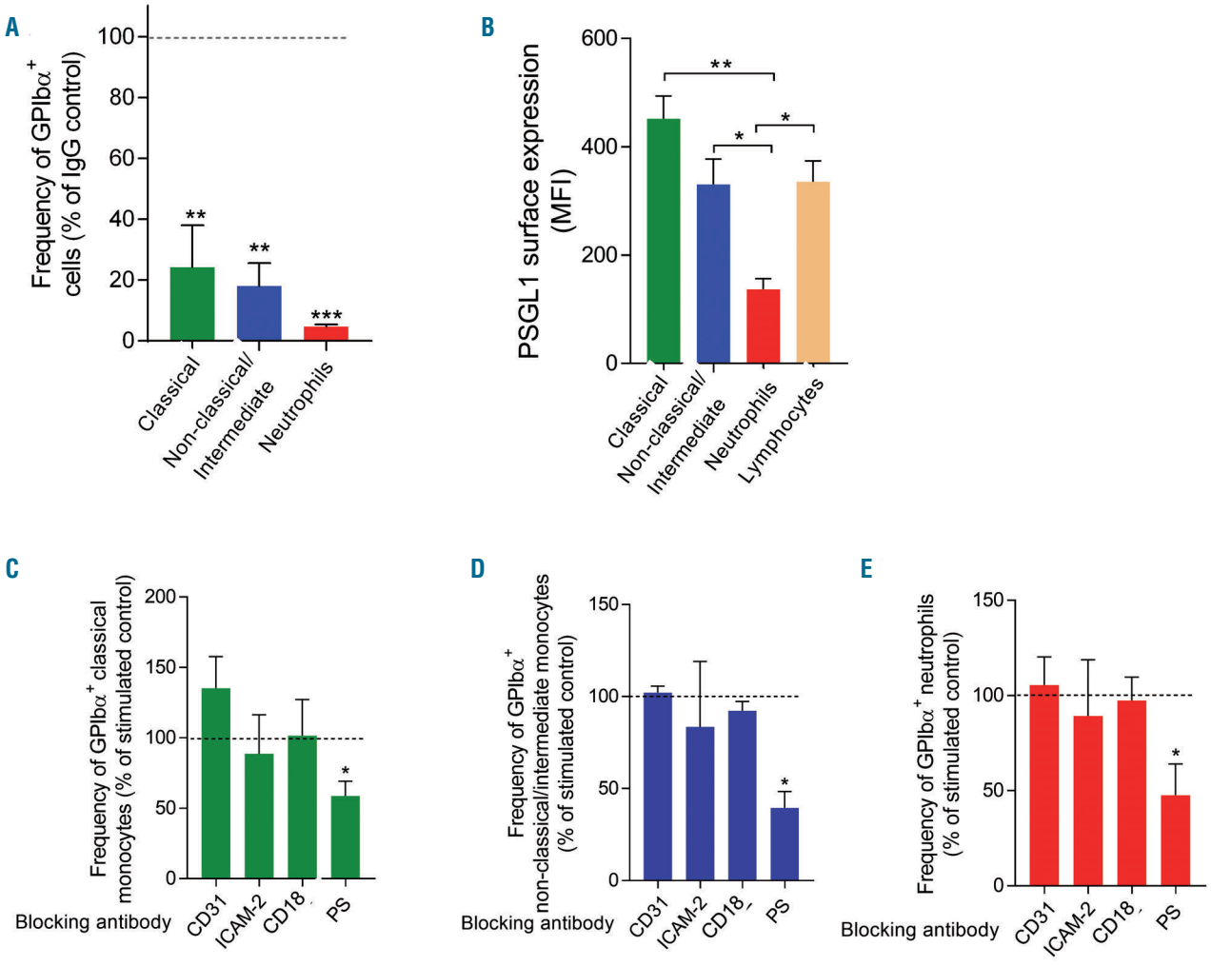

Figure 4. Blocking of GPIbα$^+$ platelet-derived extracellular vesicles to leukocytes. (A) Binding of platelet-derived extracellular vesicles (PEV) on classical monocytes, non-classical/intermediate monocytes and neutrophils with blockade of P-selectin in TRAP (100 μM)-stimulated whole blood for 30 minutes (min) under shear, n=3. (B) Surface expression (MFI: median fluorescence intensity) of PSGL1 (P-selectin ligand) on monocyte subsets, neutrophils and lymphocytes determined by flow cytometry, n=3. (C-E) Binding of PEV on classical monocytes (C), non-classical/intermediate monocytes (D) and neutrophils (E) with blockade of CD31, ICAM-2, CD18 (β2) and Phosphatidylserine (PS) in TRAP (100 μM)-stimulated whole blood for 30 min under shear, n=3-5. Data are mean ± standard error of the mean (SEM). *P≤0.05, **P≤0.01 compared the normalised IgG control (A) by analysis of variance (ANOVA) and Dunnett post-test or Bonferroni post-test (B) and one sample t-test to 100% of TRAP control (C-E).

ity score [ISS] >8). Analysis by flow cytometry showed acquisition of CD41 by circulating leukocytes with preferential binding to monocytes (Figure 8A-B and *Online Supplementary Figure S11A-B*). The CD41 measured on monocytes was likely derived from PEV, as the intensity of fluorescent staining at 4 hours post trauma (2,226±474) was substantially below that of a single platelet (13,702±964) (*Online Supplementary Figure S11B*). Both the number of CD41$^+$ monocytes and the intensity of staining for CD41 on them (MFI), correlated significantly with the severity of trauma (Figure 8C-D). Lastly, there was a marked loss of CD41$^+$ monocytes from the blood within 4 to 12 hours, which was sustained for up to 72 hours (Figure 8E) and a decrease in circulating platelet counts which reflects platelet activation and PEV generation (*Online Supplementary Figure S11C*).

Discussion

We have defined a new thrombo-inflammatory route of monocyte recruitment *via* an adhesion molecule transferred from platelets. Recruitment is reliant upon platelet-derived GPIbα, which allows monocyte capture by VWF exposed on the vessel wall. Previous studies have indicated that platelet-derived chemokines can then induce arrest and migration.[45] *Online Supplementary Figure S12* summarises the steps we propose in this thrombo-inflammatory cascade. Importantly, the cascade may diverge from the normal pathways of leukocyte trafficking in a manner that could contribute to disease, as plasma borne PEV preferentially deliver functional GPIbα to the monocyte surface. Transfer of GPIbα can support adhesion of monocytes *in vitro* and *in vivo*, in human and murine models of

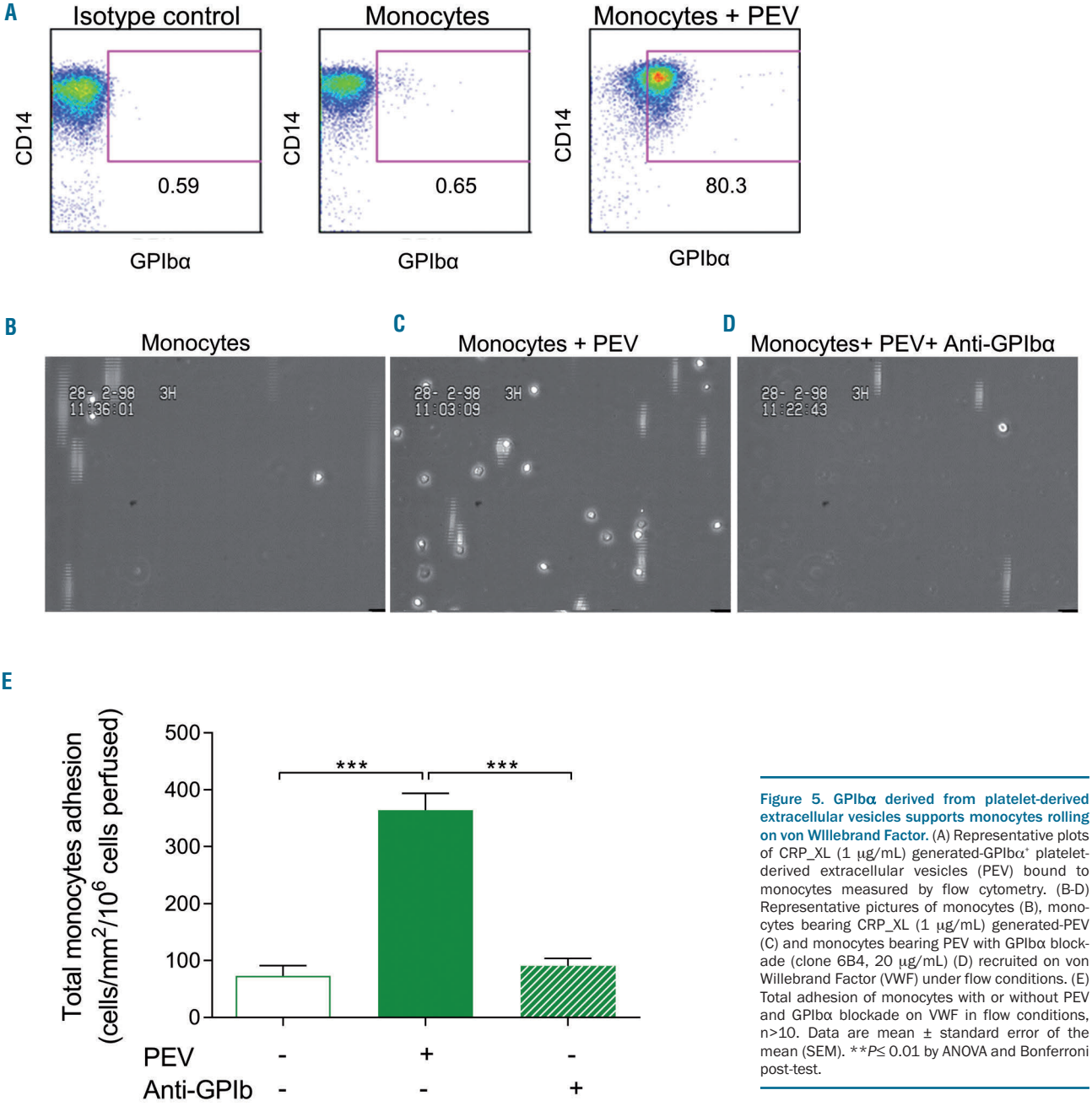

Figure 5. GPIbα derived from platelet-derived extracellular vesicles supports monocytes rolling on von Willebrand Factor. (A) Representative plots of CRP_XL (1 μg/mL) generated-GPIbα$^+$ platelet-derived extracellular vesicles (PEV) bound to monocytes measured by flow cytometry. (B-D) Representative pictures of monocytes (B), monocytes bearing CRP_XL (1 μg/mL) generated-PEV (C) and monocytes bearing PEV with GPIbα blockade (clone 6B4, 20 μg/mL) (D) recruited on von Willebrand Factor (VWF) under flow conditions. (E) Total adhesion of monocytes with or without PEV and GPIbα blockade on VWF in flow conditions, n>10. Data are mean ± standard error of the mean (SEM). $^{**}P \leq 0.01$ by ANOVA and Bonferroni post-test.

vascular inflammation. This process means that circulating monocytes may be recruited to the vessel wall through a pathway outside of the tightly regulated physiological inflammatory system. We believe that such monocyte recruitment may be particularly relevant in the dysregulated inflammatory responses seen in chronic inflammatory disease, which leads to tissue damage and loss of function (such as atherosclerosis and rheumatoid arthritis). In addition, it may be important in inflammation associated with severe trauma, where the drivers of inflammation are substantial and acute tissue damage, and extensive activation of the coagulation and haemostatic pathway. However, we believe that during acute responses initiated by inflammatory cytokines in a coordinated and controlled manner, and where timely and comprehensive resolution is the norm, platelet-mediated pathways of leukocyte trafficking are likely to be of lesser importance.

Other studies show that whole platelets can bind leukocytes, a process dependent upon platelet and/or leukocyte activation and linked to pathological conditions.[46] Moreover, if PEV are mixed with isolated monocytes they are able to activate the leukocytes so that they show enhanced levels of recruitment to EC *in vitro*, although direct binding between PEV and leukocytes was not demonstrated in that study.[47] Here, we show that monocytes preferentially accumulate PEV rather than whole platelets through an adhesive pathway reliant upon P-selectin. In the context of leukocyte recruitment to vascular EC, P-selectin supports a distinct form of rolling adhesion which is based on the transient nature of the bonds formed with PSGL-1 under conditions of shear.[48] Here we propose that the P-selectin-PSGL-1 mediated interactions between PEV and leukocytes are also transient under the shear conditions of our assay and in flowing blood *in vivo*. However, on monocytes and neutrophils, PS in the PEV membrane acts to stabilise heterotypic adhesion upon interaction with membrane receptors on the leukocytes. In the case of T lymphocytes, which also possess abundant PSGL-1, the transient interactions formed with P-selectin under shear are not stabilised by PS, which has not been reported to bind T cells to our knowledge.

In fact, much of the data on heterotypic aggregate formation in human blood does not discriminate between platelets and PEV binding to leukocytes, and it is unclear which is being assessed. Studies that do report platelet

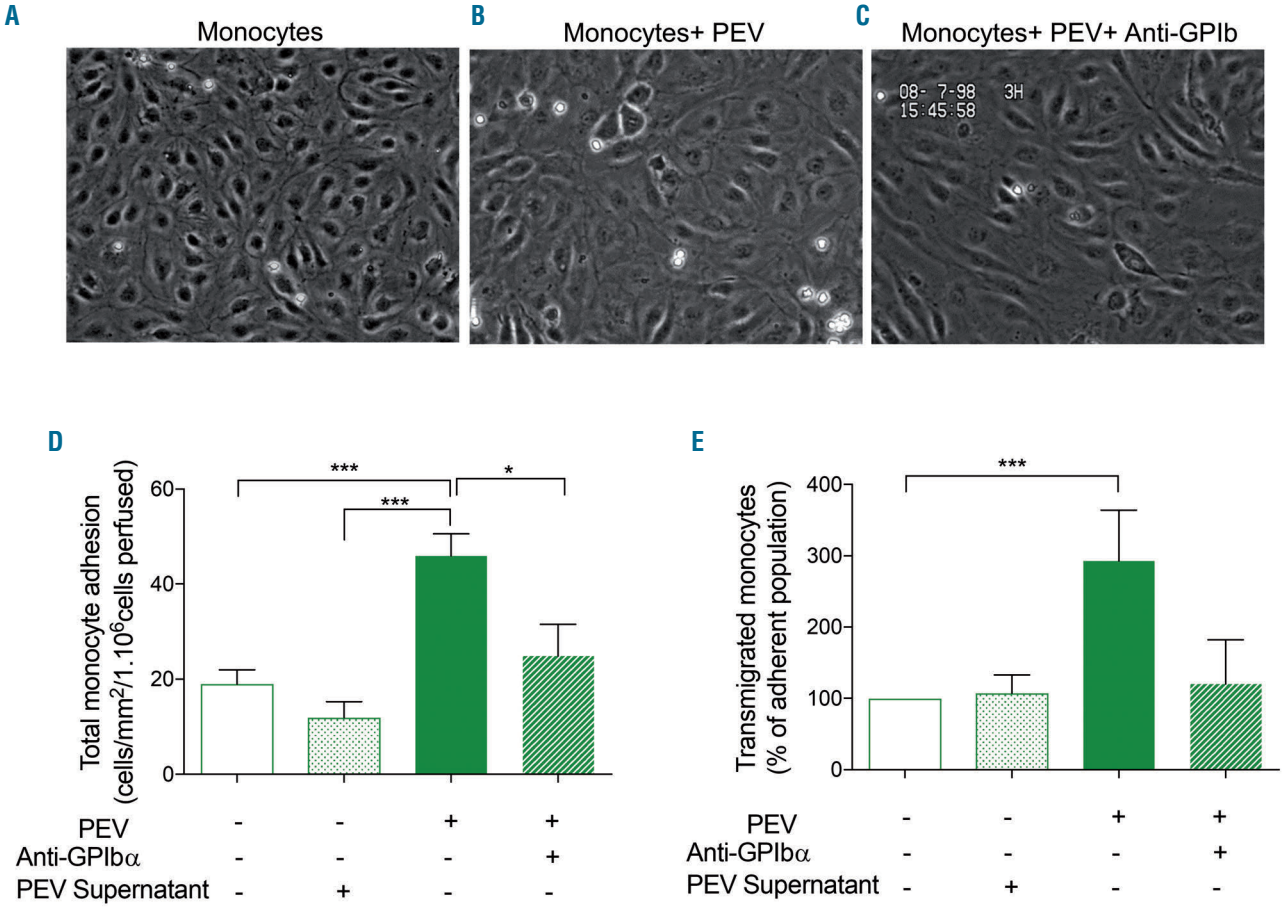

Figure 6. GPIbα derived from platelet-derived extracellular vesicles supports monocytes recruitment on TGF-β1 stimulated endothelial cells. (A-C) Representative pictures of monocytes (A), monocytes bearing CRP_XL (1 μg/mL) generated-PEV (B) and monocytes bearing PEV with GPIbα blockade (clone 6B4, 20 μg/mL) (C), adhered on TGF-β1 (10 ng/mL) stimulated EC in flow conditions. (D, E) Total adhesion (D) and transmigration (E) of monocytes with or without PEV, GPIbα blockade and filtered PEV through a 10 KDa filters to remove PEV and leave potential soluble factors on TGF-β1 stimulated EC in flow conditions, n=3-5. Data are mean ± standard error of the mean (SEM). *$P \leq 0.05$, **$P \leq 0.01$ by ANOVA and Bonferroni post-test.

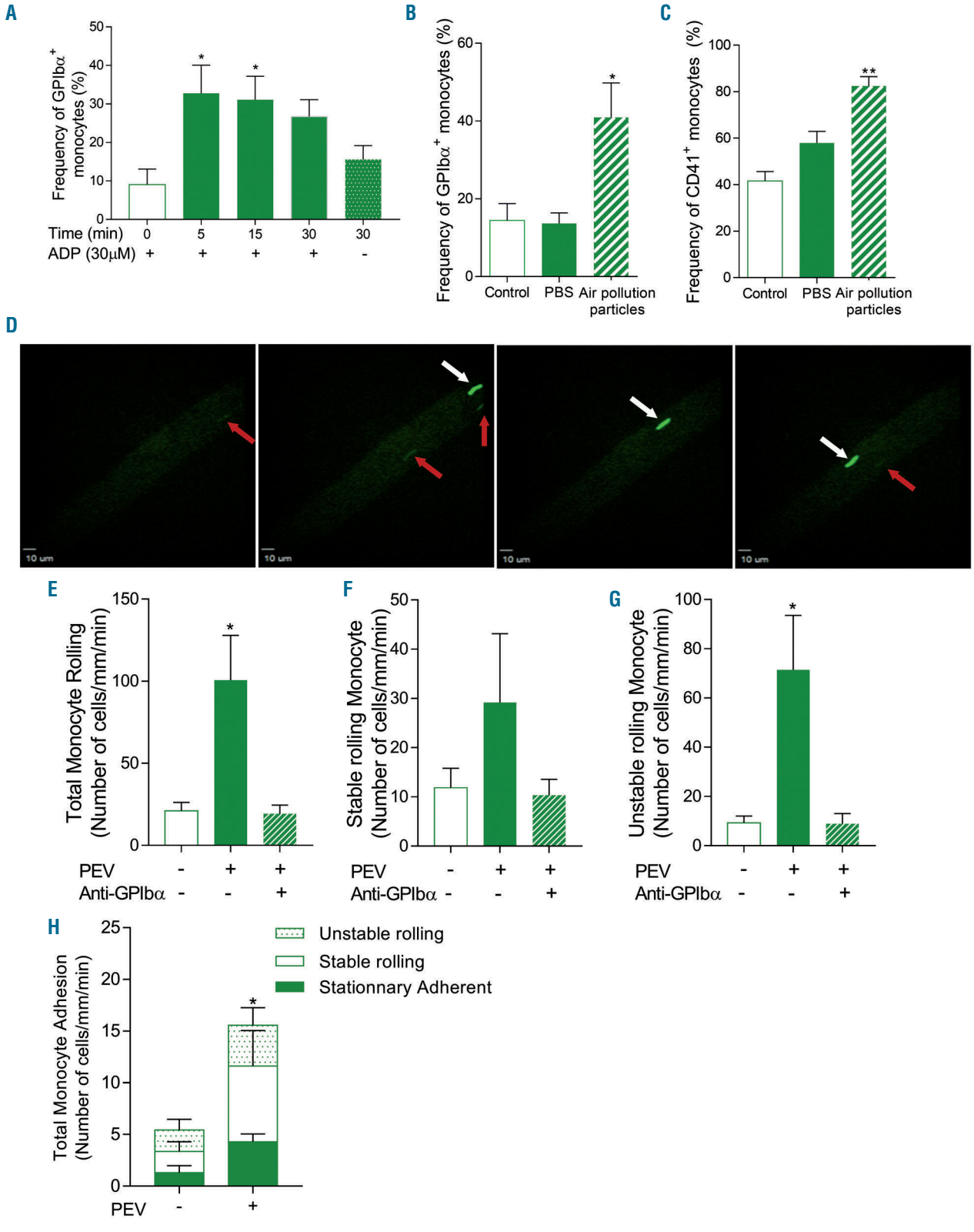

Figure 7. GPIbα from platelet-derived extracellular vesicles mediates recruitment of monocytes *in vivo*. (A) Percentage of GPIbα$^+$ monocytes in whole murine blood stimulated with 30 μM ADP at 37°C under shear determined by flow cytometry, n=4. (B) Percentage of GPIbα$^+$ and (C) CD41$^+$ monocytes in murine blood 48 hours after intratracheal instillation of air pollution particles (400 μg) measured by flow cytometry, n=5-6. (D) Representative images of the recruitment of human monocytes bearing GPIbα from mouse platelet-derived extracellular vesicles (PEV) to the TGF-β1 (80 μg/kg)-stimulated vasculature in the cremaster muscle using intravital microscopy. Red arrows point to unstable rolling monocytes, white arrows to stable rolling monocytes. Total rolling (E) stable rolling (F) and unstable rolling (G) of human monocytes bearing GPIbα from mouse PEV with or without with GPIbα blockade (clone Xia.B2, 50 μg/mL) adoptively transferred in the platelet depleted IL4R/GPIbα−Tg mice measured by intravital microscopy of the TGFβ1-stimulated cremaster muscle, n=3. (H) Total adhesion and behaviors of human monocytes bearing mouse PEV adoptively transferred in western diet fed *ApoE*$^{-/-}$ mice measured by intravital microscopy of the right carotid artery, n=3. Data are mean ± standard error of the mean (SEM). *P≤0.05, **P≤0.01 compared to the 0 minute (min) control (A) or control (B, C) by analysis of variance (ANOVA) and Dunnett post-test and by unpaired *t*-test, by two-way ANOVA (H).

binding are routinely performed *ex vivo* under the non-physiological condition of stasis *in vitro*, where the number of platelet-leukocyte aggregates formed is a direct function of the time of incubation.[49] Thus, patient blood may have a greater propensity to form aggregates with platelets under static conditions *ex vivo*, but this probably does not reflect the situation *in vivo*. Such aggregation may be a surrogate endpoint for the degree of platelet and/or leukocyte activation present in patient blood. In support of this, the patterns of PEV associated with circulating monocytes that we report here are in strong accord with a recent report from Fendl *et al*. who analysed the effects of pre-analytical blood handling (which included the imposition of shear) on the association of extracellular vesicles with leukocytes.[50]

Interestingly, upon addition of purified PEV to whole blood, we observed rapid accumulation of GPIbα on monocytes, implying assimilation of PEV was extremely efficient. However, when a platelet activating agonist was added to whole blood the process was continuous and prolonged, leading to an incremental increase in GPIbα expression. The latter profile of accumulation of GPIbα likely reflects the dynamics of PEV formation and release by platelets in whole blood, implying that the rate-limiting step in this thrombo-inflammatory pathway is not PEV-monocyte interaction, but rather the process of PEV release after platelet activation. In addition, accumulation of PEV was more prevalent in monocytes compared to neutrophils and lymphocytes. In a previous study, we observed different patterns of recruitment, migration and reverse migration *in vitro* between classical and non-classical/intermediate monocytes.[43] We characterised a novel process of crosstalk mediated by cytokines between the two subsets that allowed a balanced regulation of endothelial cell activation. Other studies have shown that changes in proportional representation of monocyte subsets in the circulation are associated with vascular diseases.[51,52] However, in this study we observed no preferential binding of PEV between classical and non-classical/intermediate monocytes, which was consistent with similar levels of PSGL1 expression exhibited by all subsets.

GPIbα is an adhesion receptor mediating a specialised form of platelet recruitment during haemostasis. Bonds forming between GPIbα and VWF exhibit high on rates, meaning that adhesion can occur between rapidly flowing

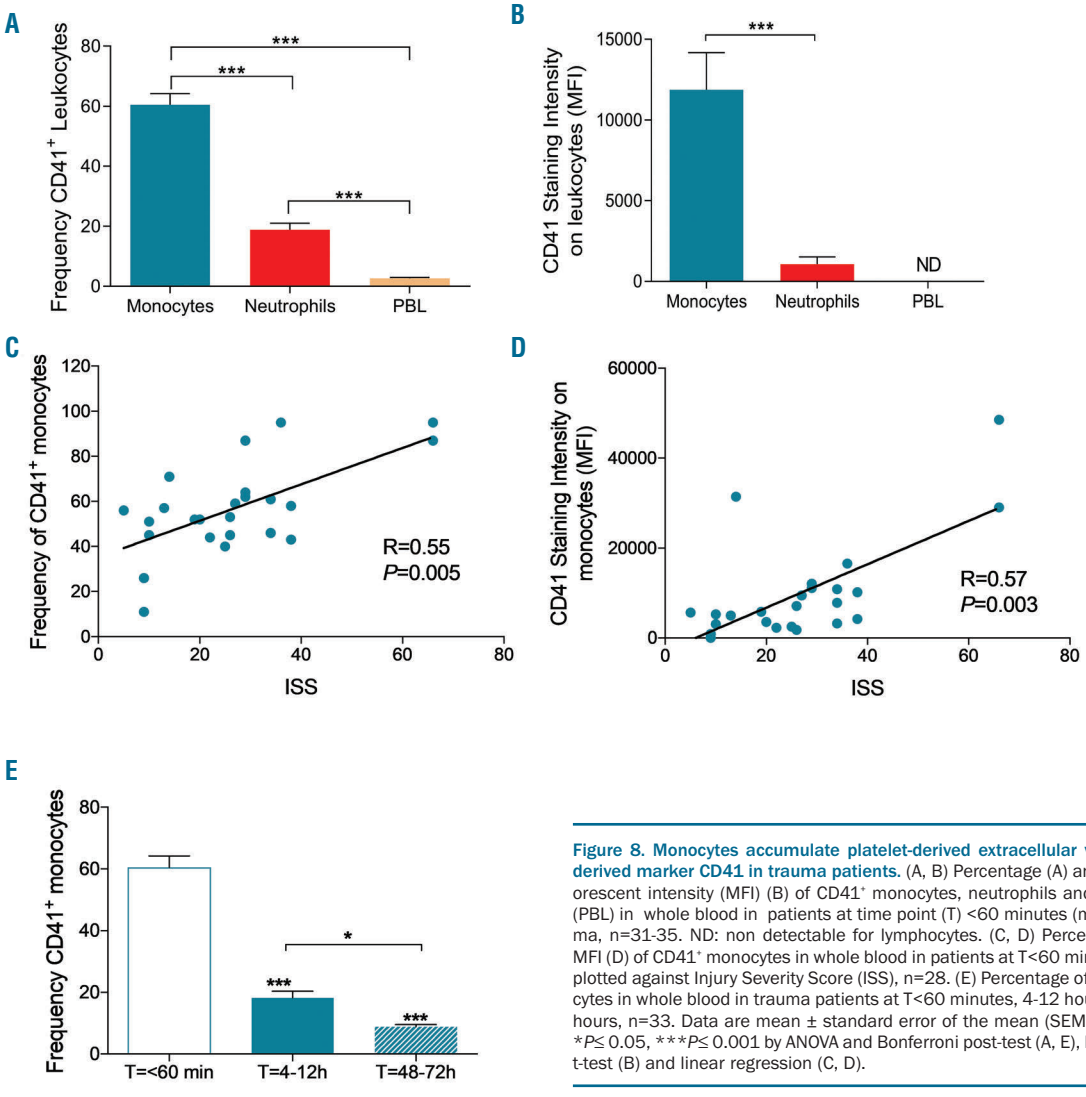

Figure 8. Monocytes accumulate platelet-derived extracellular vesicles (PEV) derived marker CD41 in trauma patients. (A, B) Percentage (A) and median fluorescent intensity (MFI) (B) of CD41+ monocytes, neutrophils and lymphocytes (PBL) in whole blood in patients at time point (T) <60 minutes (min) after trauma, n=31-35. ND: non detectable for lymphocytes. (C, D) Percentage (C) and MFI (D) of CD41+ monocytes in whole blood in patients at T<60 min after trauma plotted against Injury Severity Score (ISS), n=28. (E) Percentage of CD41+ monocytes in whole blood in trauma patients at T<60 minutes, 4-12 hours and 48-72 hours, n=33. Data are mean ± standard error of the mean (SEM) (A, B and E). *$P \leq 0.05$, ***$P \leq 0.001$ by ANOVA and Bonferroni post-test (A, E), Mann Whitney t-test (B) and linear regression (C, D).

platelets and the substrate.[15,53] However, these bonds also exhibit high off rates. Thus, under conditions of shear stress (*i.e.* blood flow) the rapid formation and dissolution of bonds supports rolling adhesion.[15,53] We observed that monocytes bearing GPIbα also rolled on purified VWF. However, on EC bearing VWF, monocytes were rapidly activated, which is consistent with our previous observations on the activity of EC derived stimuli such as C-C chemokine ligand 2 (CCL2).[15]

Trogocytosis is the phenomenon by which lymphocytes extract surface molecules from antigen presenting cells through transfer of plasma membrane at the immunological synapse.[54] This process has been observed for T, B and NK cells and neutrophils[54,55] and is a fast and efficient means of transferring molecules involved in the regulation of immune functions.[54] We cannot completely exclude that monocytes in whole blood do not bind whole platelets and acquire GPIbα and CD41 via a trogocytosis like process, although a synapse like structure has not been reported in this context to our knowledge. However, both trogocytosis and PEV accumulation by monocytes require activation dependent cytoskeletal rearrangement to achieve the transfer of membrane cargo that alters the function of the recipient cells. Thus, the processes may not be unrelated in their mechanisms of initiation and progression. However, trogocytosis does appear to be specific to the immunological synapse or related structures.[54,56] Here however, we have shown that purified labelled PEV bind to isolated monocytes or monocytes in whole blood with the same dynamics as agonist stimulated systems. This clearly demonstrates that a trogocytosis like process is not required for accumulation of PEV once they have been generated by platelet activation (Figure 3). Our colleagues have also shown that PEV levels increase dramatically after trauma and thus are likely to be the source of GPIbα found on leukocytes in trauma patients.[57]

Using intravital microscopy we observed GPIbα-dependent recruitment of PEV-treated monocytes to the vasculature. Interestingly, the short-lived adhesive interactions, here termed 'transient rolling' which did not result in prolonged monocyte localisation and activation at the vessel wall, have previously been shown to have physiological roles. Thus, under steady-state conditions (non-inflamed), circulating platelets expressing GPIbα are able to interact transiently with sinusoidal Kupffer cells in the liver *via* surface-expressed VWF, interactions which are important for host defence, as they facilitate uptake and disposal of bacteria by liver resident macrophages (Kupffer cells).[58] In the context of CVD, we showed that induction of pulmonary inflammation with pollution nanoparticles, a known risk factor for thrombo-inflammatory disease associated with atherosclerosis,[59] induced the formation of circulating monocyte-PEV aggregates. Moreover, such aggregates showed a significantly enhanced capacity to bind to the artery wall in the *ApoE*$^{-/-}$ mouse after induction of disease by feeding a high fat western diet. Thus, we propose that the transfer of platelet cargo to monocytes by PEV can contribute to the progression of plaque formation by promoting the recruitment of inflammatory monocytes. It would be interesting to investigate the functional and phenotypical changes induced by binding and internalisation of PEV by monocytes. In this study we did not observe major changes in integrin expression as a marker of activation. However, we do not exclude changes in monocyte activation and/or function relevant to vascular disease over longer periods of interaction.

The paradigm discussed above may provide a novel thrombo-inflammatory mechanism for the continuous low levels of monocyte delivery in chronic inflammatory conditions such as atherosclerosis. However, our Golden Hour data suggest that acquisition of this pathway of monocyte recruitment could also lead to the clearance of monocytes from the blood during acute and severe trauma. Indeed, in this injured patient cohort, PEV counts increase in the circulation[57] and monocytes rapidly acquired CD41-derived from PEV (1 hour after trauma) which we believe led to their clearance from the circulation, as frequency of CD41^{+} monocyte numbers are lower 4 hours after trauma. This may be due to clearance by the reticulo-EC system, or alternatively by the expedited recruitment to damaged and inflamed tissues, or indeed a combination of both. Whatever the pathway of their removal from the circulation, we speculate that the rapid clearance of immune cells from the circulation may exacerbate cell turnover and result in immune suppression and the increased risk of septic complications. In addition, monocytes bearing pro-coagulant PEV could also contribute to the initiation and propagation of disseminated intravascular coagulation (DIC) which is a potential and serious complication of traumatic injury.[27]

In conclusion, we believe that this new paradigm for leukocyte recruitment is an important step in understanding the contribution of platelets to thrombo-inflammatory pathology. By acquiring GPIbα in the circulation, monocytes may be provided with a means of interacting with the vessel wall, which is ordinarily restricted to platelets during haemostasis. In chronic diseases such as atherosclerosis, this process may occur with a low frequency over protracted periods of time. Nevertheless, the dynamic nature of PEV-monocyte interaction demonstrated in this study implies that such routes of thrombo-inflammation may be major contributors to pathology.

Funding

This work was supported by a British Heart Foundation (BHF) programme grant (RG/12/7/29693 to GER), a BHF Chair (CH/03/003 to SPW), a Royal Society Dorothy Hodgkin research fellowship (DH160044 to MC) and a BHF studentship (FS/14/42/30956, GER). This work was also supported by grants from the NIHR Surgical Reconstruction Microbiology Research Centre (SRMRC) (JL, JH) and the Scar Free foundation (JL, PH). The NIHR-SRMRC is a partnership between University Hospitals Birmingham NHS Foundation Trust, the University of Birmingham and the Royal Centre for Defence Medicine. The views expressed are those of the author(s) and not necessarily those of the NHS, the NIHR or the Department of Health. AB is supported by British Heart Foundation Senior Basic Science Research Fellowship (FS/19/30/34173). This work was also supported by a BHF Accelerator Award (AA/18/2/34218).

References

1. Kansas GS. Selectins and their ligands: current concepts and controversies. Blood. 1996;88(9):3259-3287.
2. Ley K, Laudanna C, Cybulsky MI, Nourshargh S. Getting to the site of inflammation: the leukocyte adhesion cascade updated. Nat Rev Immunol. 2007;7(9):678-689.
3. Liu Y, Shaw SK, Ma S, Yang L, Luscinskas FW, Parkos CA. Regulation of leukocyte transmigration: cell surface interactions and signaling events. J Immunol. 2004;172(1):7-13.
4. Springer TA. Traffic signals on endothelium for lymphocyte recirculation and leukocyte emigration. Annu Rev Physiol. 1995;57:827-872.
5. McEver RP. Adhesive interactions of leukocytes, platelets, and the vessel wall during hemostasis and inflammation. Thromb Haemost. 2001;86(3):746-756.
6. Cooper D, Russell J, Chitman KD, Williams MC, Wolf RE, Granger DN. Leukocyte dependence of platelet adhesion in postcapillary venules. Am J Physiol Heart Circ Physiol. 2004;286(5):H1895-900.
7. Kuroda T, Shiohara E. Leukocyte and platelet depletion protects the liver from damage induced by cholestasis and ischemia-reperfusion in the dog. Scand J Gastroenterol. 1996;31(2):182-190.
8. Lefer AM, Campbell B, Scalia R, Lefer DJ. Synergism between platelets and neutrophils in provoking cardiac dysfunction after ischemia and reperfusion: role of selectins. Circulation. 1998;29;98(13):1322-1328.
9. Nishijima K, Kiryu J, Tsujikawa A, et al. In vivo evaluation of platelet--endothelial interactions after transient retinal ischemia. Invest Ophthalmol Vis Sci. 2001;42(9):2102-2109.
10. Salter JW, Krieglstein CF, Issekutz AC, Granger DN. Platelets modulate ischemia/reperfusion-induced leukocyte recruitment in the mesenteric circulation. Am J Physiol Gastrointest Liver Physiol. 2001;281(6):G1432-1439.
11. Burger PC, Wagner DD. Platelet P-selectin facilitates atherosclerotic lesion development. Blood. 2003;101(7):2661-2666.
12. Huo Y, Schober A, Forlow SB, et al. Circulating activated platelets exacerbate atherosclerosis in mice deficient in apolipoprotein E. Nat Med. 2003;9(1):61-67.
13. Massberg S, Brand K, Gruner S, et al. A critical role of platelet adhesion in the initiation of atherosclerotic lesion formation. J Exp Med. 2002;196(7):887-896.
14. Sachais BS, Turrentine T, Dawicki McKenna JM, Rux AH, Rader D, Kowalska MA. Elimination of platelet factor 4 (PF4) from platelets reduces atherosclerosis in C57Bl/6 and apoE-/- mice. Thromb Haemost. 2007;98(5):1108-1113.
15. Kuckleburg CJ, Yates CM, Kalia N, et al. Endothelial cell-borne platelet bridges selectively recruit monocytes in human and mouse models of vascular inflammation. Cardiovasc Res. 2011;91(1):134-141.
16. Elalamy I, Chakroun T, Gerotziafas GT, et al. Circulating platelet-leukocyte aggregates: a marker of microvascular injury in diabetic patients. Thromb Res. 2008;121(6):843-848.
17. Goncalves R, Zhang X, Cohen H, Debrabant A, Mosser DM. Platelet activation attracts a subpopulation of effector monocytes to sites of Leishmania major infection. J Exp Med. 2011;208(6):1253-1265.
18. Harding SA, Sommerfield AJ, Sarma J, et al. Increased CD40 ligand and platelet-monocyte aggregates in patients with type 1 diabetes mellitus. Atherosclerosis. 2004;176(2):321-325.
19. Joseph JE, Harrison P, Mackie IJ, Isenberg DA, Machin SJ. Increased circulating platelet-leucocyte complexes and platelet activation in patients with antiphospholipid syndrome, systemic lupus erythematosus and rheumatoid arthritis. Br J Haematol. 2001;115(2):451-459.
20. McCabe DJ, Harrison P, Mackie IJ, et al. Platelet degranulation and monocyte-platelet complex formation are increased in the acute and convalescent phases after ischaemic stroke or transient ischaemic attack. Br J Haematol. 2004;125(6):777-787.
21. Parimon T, Li Z, Bolz DD, et al. Staphylococcus aureus alpha-hemolysin promotes platelet-neutrophil aggregate formation. J Infect Dis. 2013;208(5):761-770.
22. Tekelioglu Y, Uzun H. Circulating platelet-leukocyte aggregates in patients with inflammatory bowel disease. J Chin Med Assoc. 2013;76(4):182-185.
23. Gkaliagkousi E, Corrigall V, Becker S, et al. Decreased platelet nitric oxide contributes to increased circulating monocyte-platelet aggregates in hypertension. Eur Heart J. 2009;30(24):3048-3054.
24. Nomura S, Kanazawa S, Fukuhara S. Effects of efonidipine on platelet and monocyte activation markers in hypertensive patients with and without type 2 diabetes mellitus. J Hum Hypertens. 2002;16(8):539-547.
25. Wrigley BJ, Shantsila E, Tapp LD, Lip GY. Increased formation of monocyte-platelet aggregates in ischemic heart failure. Circ Heart Fail. 2013;6(1):127-135.
26. Lippi G, Montagnana M, Salvagno GL, et al. Risk stratification of patients with acute myocardial infarction by quantification of circulating monocyte-platelet aggregates. Int J Cardiol. 2007;115(1):101-102.
27. Gando S, Otomo Y. Local hemostasis, immunothrombosis, and systemic disseminated intravascular coagulation in trauma and traumatic shock. Crit Care. 2015;19:72.
28. Ogura H, Kawasaki T, Tanaka H, et al. Activated platelets enhance microparticle formation and platelet-leukocyte interaction in severe trauma and sepsis. J Trauma. 2001;50(5):801-809.
29. Raposo G, Stoorvogel W. Extracellular vesicles: exosomes, microvesicles, and friends. J Cell Biol. 2013;200(4):373-383.
30. Cloutier N, Tan S, Boudreau LH, et al. The exposure of autoantigens by microparticles underlies the formation of potent inflammatory components: the microparticle-associated immune complexes. EMBO Mol Med. 2013;5(2):235-249.
31. Holme PA, Rosger M, Solum NO, Brosstad F, Larsen AM, Hovig T. Glycoprotein IIb-IIIa on platelet-derived microparticles, and microparticle structures studied by electron microscopy, confocal laser microscopy and crossed radio-immunoelectrophoresis. Platelets. 1996;7(4):207-214.
32. Nomura S, Tandon NN, Nakamura T, Cone J, Fukuhara S, Kambayashi J. High-shear-stress-induced activation of platelets and microparticles enhances expression of cell adhesion molecules in THP-1 and endothelial cells. Atherosclerosis. 2001;158(2):277-287.
33. Shai E, Rosa I, Parguina AF, Motahedeh S, Varon D, Garcia A. Comparative analysis of platelet-derived microparticles reveals differences in their amount and proteome depending on the platelet stimulus. J Proteomics. 2012;76 Spec No.:287-296.
34. Boudreau LH, Duchez AC, Cloutier N, et al. Platelets release mitochondria serving as substrate for bactericidal group IIA-secreted phospholipase A2 to promote inflammation. Blood. 2014;124(14):2173-2183.
35. Aatonen MT, Ohman T, Nyman AT, Laitinen S, Gronhilm M, Siljander PRM. Isolation and characterisation of platelet-derived extracellular vesicles. J Extracell Vesicles. 2014;3.
36. Ponomareva AA, Nevzorova TA, Mordakhanova ER, Andrianova IA, Litvinov RI. Structural characterisation of platelets and platelets microvesicles. Cell Tissue Biol. 2016; 10(3):217-226.
37. Boilard E, Duchez AC, Brisson A. The diversity of platelet microparticles. Curr Opin Hematol. 2015;22(5):437-444.
38. Varon D, Hayon Y, Dashevsky O, Shai E. Involvement of platelet derived microparticles in tumor metastasis and tissue regeneration. Thromb Res. 2012;130 Suppl 1:S98-99.
39. Ogata N, Imaizumi M, Nomura S, et al. Increased levels of platelet-derived microparticles in patients with diabetic retinopathy. Diabetes Res Clin Pract. 2005;68(3):193-201.
40. Nomura S, Suzuki M, Katsura K, et al. Platelet-derived microparticles may influence the development of atherosclerosis in diabetes mellitus. Atherosclerosis. 1995;116 (2):235-240.
41. Feng B, Chen Y, Luo Y, Chen M, Li X, Ni Y. Circulating level of microparticles and their correlation with arterial elasticity and endothelium-dependent dilation in patients with type 2 diabetes mellitus. Atherosclerosis. 2010;208(1):264-269.
42. Biasucci LM, Porto I, Di Vito L, et al. Differences in microparticle release in patients with acute coronary syndrome and stable angina. Circ J. 2012;76(9):2174-2182.
43. Chimen M, Yates CM, McGettrick HM, et al. Monocyte Subsets Coregulate Inflammatory Responses by Integrated Signaling through TNF and IL-6 at the Endothelial Cell Interface. J Immunol. 2017;198(7):2834-2843.
44. Daaboul GG, Gagni P, Benussi L, et al. Digital Detection of Exosomes by Interferometric Imaging. Sci Rep. 2016; 6:37246.
45. Mause SF, von Hundelshausen P, Zernecke A, Koenen RR, Weber C. Platelet microparticles: a transcellular delivery system for RANTES promoting monocyte recruitment on endothelium. Arterioscler Thromb Vasc Biol. 2005;25(7):1512-1518.
46. van Gils JM, Zwaginga JJ, Hordijk PL. Molecular and functional interactions among monocytes, platelets, and endothelial cells and their relevance for cardiovascular diseases. J Leukoc Biol. 2009;85(2):195-204.
47. Barry OP, Pratico D, Lawson JA, FitzGerald GA. Transcellular activation of platelets and endothelial cells by bioactive lipids in platelet microparticles. J Clin Invest. 1997;99(9):2118-2127.
48. Ley K. The role of selectins in inflammation and disease. Trends Mol Med. 2003;9(6):263-268.
49. Harding SA, Din JN, Sarma J, et al. Flow cytometric analysis of circulating platelet-monocyte aggregates in whole blood: methodological considerations. Thromb Haemost. 2007;98(2):451-456.
50. Fendl B, Weiss R, Fischer MB, Spittler A,

Weber V. Characterization of extracellular vesicles in whole blood: Influence of pre-analytical parameters and visualization of vesicle-cell interactions using imaging flow cytometry. Biochem Biophys Res Commun. 2016;478(1):168-173.
51. Shantsila E, Wrigley B, Tapp L, et al. Immunophenotypic characterization of human monocyte subsets: possible implications for cardiovascular disease pathophysiology. J Thromb Haemost. 2011;9(5):1056-1066.
52. Yang J, Zhang L, Yu C, Yang XF, Wang H. Monocyte and macrophage differentiation: circulation inflammatory monocyte as biomarker for inflammatory diseases. Biomark Res. 2014;7;2(1):1.
53. Andre P, Denis CV, Ware J, et al. Platelets adhere to and translocate on von Willebrand factor presented by endothelium in stimulated veins. Blood. 2000;96(10):3322-3328.
54. Ahmed KA, Munegowda MA, Xie Y, Xiang J. Intercellular trogocytosis plays an important role in modulation of immune responses. Cell Mol Immunol. 2008;5(4):261-269.
55. Valgardsdottir R, Cattaneo I, Klein C, Introna M, Figliuzzi M, Golay J. Human neutrophils mediate trogocytosis rather than phagocytosis of CLL B cells opsonized with anti-CD20 antibodies. Blood. 2017;129(19):2636-2644.
56. Dopfer EP, Minguet S, Schamel WW. A new vampire saga: the molecular mechanism of T cell trogocytosis. Immunity. 2011;35(2):151-153.
57. Kuravi SJ, Yates CM, Foster M, et al. Changes in the pattern of plasma extracellular vesicles after severe trauma. PLoS One. 2017;12(8):e0183640.
58. Wong CH, Jenne CN, Petri B, Chrobok NL, Kubes P. Nucleation of platelets with blood-borne pathogens on Kupffer cells precedes other innate immunity and contributes to bacterial clearance. Nat Immunol. 2013;14(8):785-792.
59. Brook RD, Rajagopalan S. Particulate matter air pollution and atherosclerosis. Curr Atheroscler Rep. 2010;12(5):291-300.

Ferrata Storti Foundation

Haematologica 2020
Volume 105(5):1262-1273

Oncogenic fusion protein BCR-FGFR1 requires the breakpoint cluster region-mediated oligomerization and chaperonin Hsp90 for activation

Malalage N. Peiris,[1] April N. Meyer,[1] Katelyn N. Nelson,[1] Ezra W. Bisom-Rapp,[1] and Daniel J. Donoghue[1,2]

[1]Department of Chemistry and Biochemistry, University of California San Diego and
[2]Moores Cancer Center, University of California San Diego, La Jolla, CA, USA

ABSTRACT

Mutation and translocation of fibroblast growth factor receptors often lead to aberrant signaling and cancer. This work focuses on the t(8;22)(p11;q11) chromosomal translocation which creates the breakpoint cluster region (BCR) fibroblast growth factor receptor1 (FGFR1) (BCR-FGFR1) fusion protein. This fusion occurs in stem cell leukemia/lymphoma, which can progress to atypical chronic myeloid leukemia, acute myeloid leukemia, or B-cell lymphoma. This work focuses on the biochemical characterization of BCR-FGFR1 and identification of novel therapeutic targets. The tyrosine kinase activity of FGFR1 is required for biological activity as shown using transformation assays, interleukin-3 independent cell proliferation, and liquid chromatography/mass spectroscopy analyses. Furthermore, BCR contributes a coiled-coil oligomerization domain, also essential for oncogenic transformation by BCR-FGFR1. The importance of salt bridge formation within the coiled-coil domain is demonstrated, as disruption of three salt bridges abrogates cellular transforming ability. Lastly, BCR-FGFR1 acts as a client of the chaperonin heat shock protein 90 (Hsp90), suggesting that BCR-FGFR1 relies on Hsp90 complex to evade proteasomal degradation. Transformed cells expressing BCR-FGFR1 are sensitive to the Hsp90 inhibitor Ganetespib, and also respond to combined treatment with Ganetespib plus the FGFR inhibitor BGJ398. Collectively, these data suggest novel therapeutic approaches for future stem cell leukemia/lymphoma treatment: inhibition of BCR oligomerization by disruption of required salt bridges; and inhibition of the chaperonin Hsp90 complex.

Correspondence:

DANIEL J. DONOGHUE
ddonoghue@ucsd.edu

Received: March 1, 2019.

Accepted: August 14, 2019.

Pre-published: August 22, 2019.

doi:10.3324/haematol.2019.220871

Check the online version for the most updated information on this article, online supplements, and information on authorship & disclosures: www.haematologica.org/content/105/5/1262

Introduction

Fibroblast growth factor receptors (FGFR) are part of the receptor tyrosine kinase (RTK) family and are responsible for cell growth and proliferation. The FGFR family is composed of four homologous receptors; all contain three extracellular immunoglobulin-like domains, a transmembrane domain, and a split kinase domain. When these receptors are bound to fibroblast growth factor (FGF) and heparin sulfate proteoglycans, they are able to dimerize, which leads to auto-phosphorylation of the kinase domain and activation of downstream cell signaling pathways including signal transducer and activator of transcription (STAT), mitogen activated protein kinase (MAPK), protein kinase B (AKT), and phospholipase C gamma (PLCγ). FGFR signaling results in cellular migration, cell proliferation, angiogenesis, and wound healing.[1]

FGFRs are often aberrantly activated in cancer by overexpression, mutation, or translocation. Specifically, FGFR1 is involved in stem cell leukemia/lymphoma (SCLL), also known as 8p11 myeloproliferative syndrome (EMS).[2] SCLL is characterized by a chromosomal translocation that produces a dimerizing protein partner fused to the kinase domain of FGFR1.[3] Although SCLL is rare, it can aggressively progress to atypical chronic myeloid leukemia (CML), acute myeloid leukemia (AML), or B-cell lymphoma. Despite extensive chemotherapy, the only known cur-

ative option for SCLL patients is hematopoietic stem cell transplantation. Although both Ponatinib and Pemigatinib (INCB054828) have been used to treat patients with mixed results, few other alternative treatment plans exist for patients who are either awaiting or are unable to receive transplantation.[4,5] This work focuses on the t(8;22)(p11;q11) chromosomal translocation resulting in the BCR-FGFR1 fusion protein with exon 4 of the breakpoint cluster region (BCR) fused to exon 9 of FGFR1. Although BCR was first identified fused to Abelson murine leukemia viral oncogene homolog-1 (ABL), also known as the Philadelphia chromosome, BCR has since then been identified fused to ret proto-oncogene (RET), Janus kinase 2 (JAK2), and platelet derived growth factor receptor alpha (PDGFRA).[6-9] Although a common fusion partner, the endogenous function of the *BCR* gene remains obscure. The fusion protein BCR-FGFR1 retains the coiled-coil dimerization/oligomerization domain, putative serine/threonine kinase domain, and partial RhoGEF domain from BCR.[10]

The BCR-FGFR1 fusion is not well characterized, and this work seeks to elucidate the underlying mechanisms behind BCR-FGFR1 mediated SCLL. Although tyrosine kinase inhibitor therapies (TKI) are traditionally used to treat certain hematological cancers, the use of TKI often results in drug resistance in patients. Thus, it is crucial to determine additional therapeutic strategies in treating hematopoietic cancers. Here we suggest disruption of the BCR coiled-coil dimerization domain and Hsp90 inhibition as novel therapeutic targets for BCR-FGFR1 driven SCLL. Data presented here may also allow for additional approaches in treating BCR-ABL mediated CML, due to the similarity between BCR-ABL and BCR-FGFR1 fusion proteins.

Methods

DNA Constructs

The *BCR* gene (pSG65-Bcr) was purchased from Addgene (Watertown, MA, USA) and was subcloned into pcDNA3. *FGFR1* and *FGFR1-K656E* were previously described.[11] To construct *BCR-FGFR1*, a BamHI site was introduced by PCR-based site-directed mutagenesis after amino acid L584 in *BCR* and before amino acid V429 in *FGFR1*. This unique internal BamHI site was used together with an upstream site of EcoRI to subclone the 5' region of *BCR* into the *FGFR1* pCDNA3 plasmid, creating a fusion breakpoint of BCR exon 4 fused to *FGFR1* exon 9. The BamHI site adds 6 bases which code for a GS linker between the 5' BCR and the 3' *FGFR1*. *FGFR1-K514A*[12] and all other mutations described were introduced by PCR-based site-directed mutagenesis. *FGFR1* or *BCR-FGFR1* clones were subcloned into the pLXSN expression plasmid for use in NIH3T3 or 32D cells. Details of plasmid DNA used are in the *Online Supplementary Material and Methods*.

Cell transfection, immunoprecipitation, immunoblot analysis

HEK293T cells were transfected with 3 μg of the pcDNA3 plasmid constructs using calcium phosphate transfection as described.[13] Immunoblotting was performed as described.[14] NIH3T3 focus assays were performed as described.[15] Number of foci were, normalized by transfection efficiency, and quantitated relative to a positive control +/-standard error of the mean (SEM).

The Hsp90 inhibitor, Ganetespib was added to HEK293T transfected cells at a concentration of 200 nM for 4 hours (h) during cell starvation at 10% CO2, 37°C. Transfected NIH3T3 cells were maintained with 0, 10, 20, 23, 25, or 30 nM Ganetespib for 14 days, and fixed and scored as described. For combination drug treatment, 15 nM Ganetespib was used with the FGFR inhibitor BGJ398 at 0, 2.5, or 10 nM. All cell assays were performed a minimum of three times. More detailed information is provided in the *Online Supplementary Materials and Methods*.

Interleukin-3 (IL-3) independent growth in 32D cells

A total of $1x10^6$ 32D cells were electroporated (1,500V, 10 ms, 3 pulses) by Neon Transfection system using 30 μg of *FGFR1* or *BCR-FGFR1* derivatives in pLXSN in triplicate. 48 h after transfection, cells were selected with 1.5 mg/mL Geneticin (G418) for 10 days to generate stable cell lines before starting IL-3 independent growth assays. Triplicate flasks were seeded with the cell lines at $4x10^4$ cell/mL in the presence or absence of mouse IL-3. In addition, 1 nmol/L of FGF and 30 ug/mL of heparin was added to a set of flasks in the absence of IL-3. On days 1, 3, 5, 7, and 9 samples were counted and measured for MTT metabolic activity as described.[16] For Ganetespib treatment, cells were seeded with 0, 2.5, or 5.0 nM Ganetespib –/+ IL-3. MTT metabolic activity was measured on days 3, 5, and 7. A concentration of 10 nM or higher of Ganetespib was found to be toxic to 32D cells in the presence of IL-3.

Mass spectrometry sample preparation

Liquid chromatography/mass spectroscopy (LC-MS/MS) for phosphopeptide analysis was as described previously.[16] Complete information is available in the *Online Supplementary Material and Methods.*

Results

Signaling cascade activation by BCR-FGFR1

The role of BCR in this fusion protein has remained unclear, as BCR-FGFR1 retains the coiled-coil oligomerization domain, putative serine/threonine kinase domain, and partial RhoGEF domain from BCR. In order to elucidate if BCR-FGFR1 relies on the tyrosine kinase activity of FGFR1, a K514A kinase dead mutation,[12] or a K656E kinase activating mutation,[11,15] were introduced in the FGFR1 tyrosine kinase domain in both FGFR1 and BCR-FGFR1 backgrounds (Figure 1A). These studies were performed in HEK293T cells, as they have previously been used in FGFR signal transduction and protein phosphorylation studies.[16] HEK293T cells expressing either full-length FGFR1 or BCR-FGFR1 variants were analyzed for MAPK, STAT3 and STAT5 activation, and FGFR1 receptor phosphorylation. Expression of FGFR1 shows slight activation of the MAPK pathway, while expression of the activated FGFR1-K656E shows elevated phosphorylation levels of MAPK (Figure 1B, panel 7). Expression of BCR-FGFR1 or BCR-FGFR1-K656E also resulted in MAPK phosphorylation. Additionally, STAT3 and STAT5 phosphorylation were strongly elevated by BCR-FGFR1 and BCR-FGFR1-K656E, in comparison to FGFR1 or FGFR1-K656E, indicating that BCR-FGFR1 induces both MAPK and STAT pathway activation (Figure 1B, panel 3 and 5).

To examine the phosphorylation of each fusion construct compared with FGFR1, FGFR1-K656E and FGFR1-K514A were expressed in HEK293T cells, collected and immunoprecipitated with a C-terminal FGFR1 antibody, and probed for tyrosine phosphorylation. An increase in tyrosine phosphorylation was observed in both BCR-

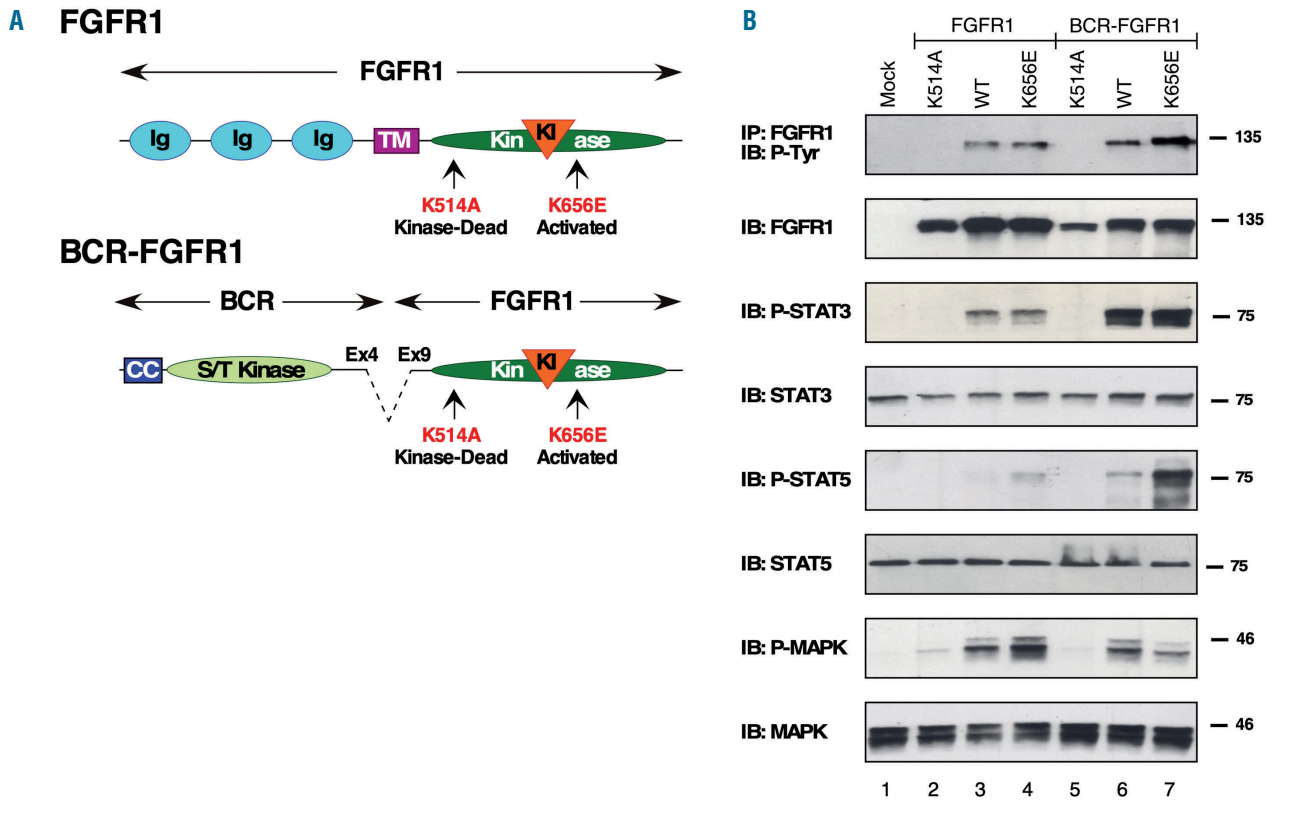

Figure 1. Cell signaling activated by BCR-FGFR1. (A) Schematic of FGFR1 and BCR-FGFR1 with K514A kinase dead, and K656E kinase activating mutations shown. FGFR1 contains an extracellular ligand binding domain with immunoglobulin-like domains (Ig), a transmembrane domain (TM), a split tyrosine kinase domain, and kinase insert domain (KI). BCR-FGFR1 contains breakpoint cluster region (BCR) exon 4 at the N-terminus fused to the kinase domain of fibroblast growth factor receptor 1 (FGFR1) at exon 9. BCR contributes a coiled-coil (CC) and a putative serine/threonine (S/T) kinase domain to the BCR-FGFR1 fusion. (B) Lysates of HEK293T cells expressing either FGFR1 or BCR-FGFR1 derivatives were immunoprecipitated with anti-FGFR1 antibody and immunobotted with phosphotyrosine antibody (panel 1). These lysates were immunoblotted with anti-FGFR1 antibody to detect expression of transfected clones (panel 2). Lysates were examined for activation of the STAT3, STAT5 and MAPK pathways using phospho-specific antibodies; phospho-STAT3 (Y705) (panel 3), phospho-STAT5 (Y694) (panel 5) and phospho-MAPK (T202/Y204) (panel 7). Membranes were stripped and reprobed for total STAT3, STAT5 and MAPK shown in panels 4, 6 and 8, respectively.

FGFR1, and BCR-FGFR1-K656E expressing cells, when compared to FGFR1, indicating that the contribution of *BCR* as a partner gene to this fusion increases the constitutive phosphorylation of FGFR1 (Figure 1B, top panel). Interestingly, although the putative serine/threonine kinase domain in BCR is present in the BCR-FGFR1 fusion protein, HEK293T cells expressing BCR-FGFR1-K514A, which contains BCR fused to a kinase-dead FGFR1, does not activate MAPK or STAT pathways (Figure 1B). In addition, no tyrosine phosphorylation of FGFR1 was detected for cells expressing BCR-FGFR1-K514A, suggesting that BCR-FGFR1 relies on the constitutive kinase activity of FGFR1 for activation of downstream cell signaling.

Cell transforming ability of BCR-FGFR1 by focus assay

In order to investigate the transforming ability of BCR-FGFR1 and subsequent mutants, these constructs were assayed in a NIH3T3 cell transforming assay. NIH3T3 cell transformation assays were one of the original assays used to discover and characterize novel oncogenes such as activated *RAS, MUC4, AKT* and various other oncogenes.[16,17] NIH3T3 cells expressing BCR-FGFR1, BCR-FGFR1-K656E, and FGFR1-K656E exhibited high levels of focus formation (Figure 2B, D and G). *FGFR3-TACC3*, a known fusion oncogene,[15,16] was used as a positive control. Interestingly, BCR-FGFR1 and BCR-FGFR1-K656E exhibited nearly three-fold higher focus formation in comparison to FGFR3-TACC3. NIH3T3 cells expressing either FGFR1, FGFR1-K514A, or BCR-FGFR1-K514A did not form any visible foci (Figure 2C, E-F), indicating that the kinase activity of FGFR1 is critical to the transforming ability of this fusion.

BCR-FGFR1 promotes IL-3 independent cell growth

The BCR-FGFR1 fusion protein has been solely discovered in hematopoietic cancers to date. Previous studies have utilized either Ba/F3 or 32D hematopoietic cell lines to demonstrate oncogenic and proliferative potential in these IL-3 dependent cell lines.[16,18] 32D cells were used to investigate the proliferative potential of cells expressing FGFR and BCR-FGFR1 derivatives in the presence and absence of IL-3, and in the absence or presence of aFGF (Figure 3).

FGFR1, FGFR1-K656E, BCR-FGFR1, and *BCR-FGFR1-K656E* were electroporated into 32D cells. Only 32D cells which expressed either BCR-FGFR1 or BCR-FGFR1-K656E were able to proliferate in the absence of IL-3, as seen through MTT metabolic assays and cell counts (Figure 3A and D). The addition of aFGF in the absence of IL-3 resulted in a slight increase in cell growth for FGFR1 and FGFR1-K656E, but no change for BCR-FGFR or BCR-FGFR1-K656E (Figure 3B and E), as expected since the

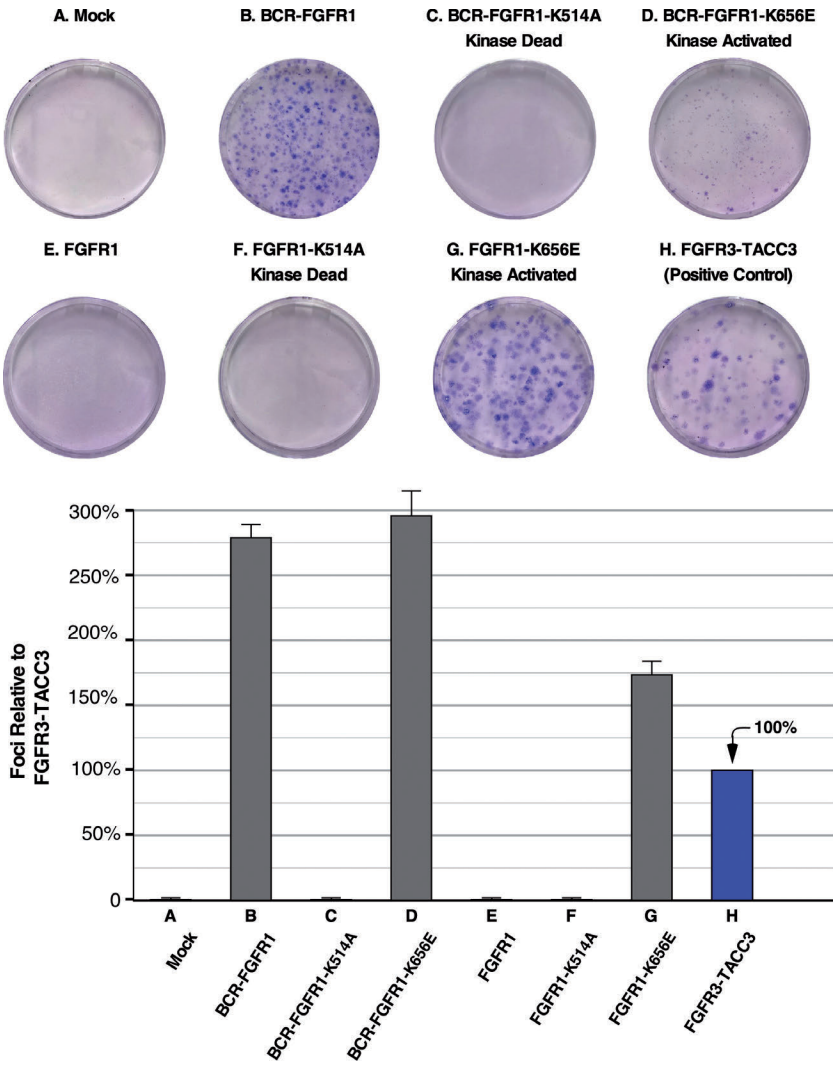

Figure 2. Cell transformation of NIH3T3 cells by BCR-FGFR1. Representative plates from a focus assay are shown, with transfected constructs indicated. The graph shows the number of foci scored, normalized for transfection efficiency and calculated as a percentage of transformation relative to FGFR3-TACC3 –/+ standard error of the mean (SEM). Assays were performed a minimum of three times *per* each DNA construct.

extracellular ligand binding domain of FGFR1 is removed in the fusion proteins. All transfected constructs displayed cell viability in the presence of IL-3 (Figure 3C and F). Thus, these data demonstrate that the BCR-FGFR1 fusion protein requires the N-terminal contribution of BCR for IL-3-independent proliferation as assayed in 32D cells.

LC-MS/MS analysis identifies novel phosphorylation sites

The strong tyrosine phosphorylation signal seen in BCR-FGFR1 and BCR-FGFR1-K656E lysates though immunoblotting (Figure 1) led to the inquiry of whether there were any novel phosphorylation sites within these fusion proteins. To investigate this question, HEK293T cell lysate expressing either FGFR1 or BCR-FGFR1 derivatives were immunoprecipitated and analyzed by LC-MS/MS as described.[16]

Both BCR-FGFR1 and BCR-FGFR1-K656E exhibit high phosphorylation levels on key tyrosine residues in the FGFR1 kinase domain, whereas BCR-FGFR1-K514A exhibited only slight phosphorylation (Figure 4). The lack of phosphorylation on the activation loop tyrosine residues in BCR-FGFR1-K514A indicates that FGFR1 kinase activity is critical for activation of the BCR-FGFR1 fusion.

Additional serine, threonine, and tyrosine phosphorylation sites were also detected in BCR-FGFR1 or BCR-FGFR1-K656E (Figure 4B-C) which have not been previously reported. To determine the role of these novel phosphoacceptor sites within the BCR domain of BCR-FGFR1 fusion proteins, phosphorylated serine or threonine residues were mutated to alanine, and phosphorylated tyrosine residues in *BCR* were mutated to phenylalanine. Each construct was assayed for focus formation. In addition to these mutations, a BCR(Y177F)-FGFR1 mutant was also assayed as it mutates the Grb2 binding site, previously shown to reduce activation of the BCR-FGFR1 fusion protein.[19,20]

The Y177F Grb2 mutation in BCR-FGFR1 shows a 50% decrease in transforming ability when compared to NIH3T3 cells expressing BCR-FGFR1. However, all additional mutations in BCR phosphoacceptor sites displayed little to no difference in transforming ability (Table 1). The mutant BCR(T359A/S367A/S369A/S377A)-FGFR1, which mutates phosphorylated residues within the ABL SH2 binding domain present in BCR, was also transforming. Taken together, LC-MS/MS data and cell transformation assays suggest that tyrosine phosphorylation on activation loop residues within the FGFR1 kinase domain is critical for BCR-FGFR1 activation. BCR-FGFR1 relies on an active

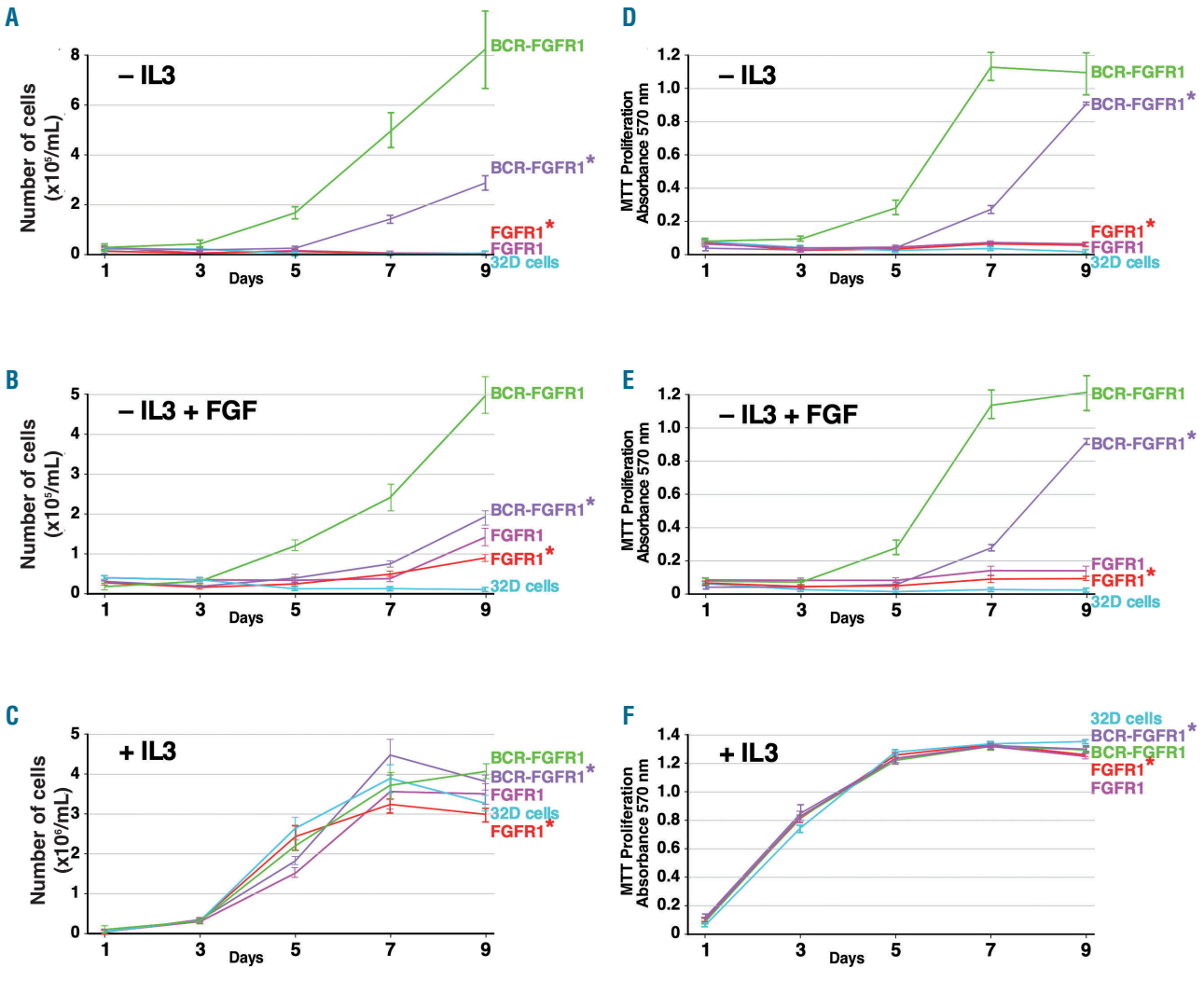

Figure 3. BCR-FGFR1 supports interleukin-3-independent proliferation. 32D control cells and cell lines selectively expressing FGFR1, FGFR1-K656E (FGFR1*), BCR-FGFR1 and BCR-FGFR1-K656E (BCR-FGFR1*) were cultured in the absence of interleukin-3 (IL-3) (A and D), in the presence of aFGF/Heparin (B and E) and in the presence of IL-3 (C and F). Total number of cells were counted on days 1, 3, 5, 7 and 9 to examine IL-3 independent growth (A, B, and C). Cell viability was determined by MTT metabolic assay (D, E, and F). All control cells and cell lines were assayed in triplicate. Standard deviation is shown.

FGFR1 kinase domain for transformation, while phosphorylation on residues within the BCR domain does not appear to be critical.

Salt bridge disruption in BCR dimerization domain abrogates cell transforming ability

The coiled-coil oligomerization domain of BCR is an attractive therapeutic target, as it is essential for cell transformation as demonstrated with assays done in BCR-ABL.[21] Previous work has shown the necessity of salt bridge formation for the activation of oncogenic fusion protein ETV6-NTRK3, which is found in AML.[22] Here we investigated the importance of salt bridge formation in the BCR coiled-coil domain as a potential requirement for the oligomerization and oncogenic activation of BCR-FGFR1.

The coiled-coil oligomerization region of BCR spans amino acid residues 3-75 and has been proposed to contain two interhelical salt bridges stabilizing the two coils in an antiparallel coiled-coil[23] (Figure 5). The first salt bridge (Salt Bridge #1) was proposed to form between residues Glu34 and Arg55, whereas the second salt bridge (Salt Bridge #2), between Glu46 and Arg53 is visible in the crystal structure of the BCR oligomerization domain (Figure 5B).[23-25] Each salt bridge residue was individually mutated to a residue of the opposite charge to abolish the electrostatic interaction. When residues Glu34 or Arg55 in BCR Salt Bridge #1 were mutated to the opposing charge, E34R or R55E respectively, little to no effect was observed in cell transformation (Figure 5C, mutants 2 and 8). Likewise, when residues Glu46 or Arg53 in BCR Salt Bridge #2 were mutated to the opposing charge, E46R or R53E respectively, no effect in cell transformation was observed (Figure 5C, mutants 3-4).

We also became aware of the possible importance of a putative intrahelical salt bridge (Salt Bridge #3) involving E52 and R55[23] (Figure 5A-B). Since R55 is also involved in Salt Bridge #1, this means that mutation of R55E to probe the importance of Salt Bridge #1 inadvertently disrupts the intrahelical Salt Bridge #3. This extra layer of complexity was analyzed as shown in Table 2. The upper portion of

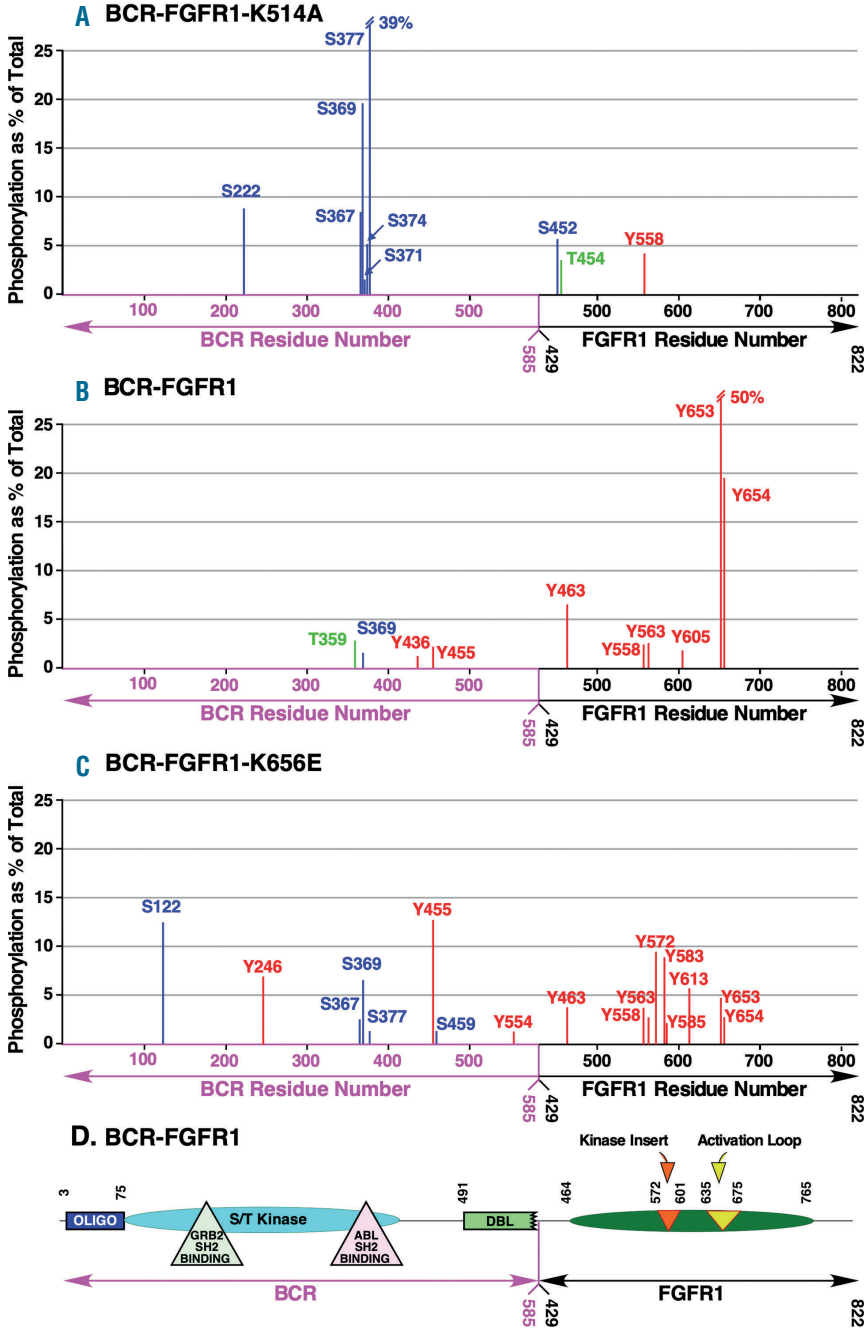

Figure 4. Phosphorylated residues in BCR-FGFR1 derivatives identified by mass spectrometry analysis. FGFR1 and BCR-FGFR1 derivatives were transfected into HEK293T cells and examined for phosphorylation by mass spectrometry as described in the Methods. The phosphorylation sites are indicated that were greater than 1% of the total phosphorylation detected in the sample. P-Tyr is shown in red; P-Thr is shown in green; P-Ser is shown in blue. Duplicate, independent samples were averaged; (A) BCR-FGFR1-K514A, (B) BCR-FGFR1, (C) BCR-FGFR1-K656E. There was no significant difference in the phosphorylation sites detected in the FGFR1 kinase domains in BCR-FGFR1 fusions compared to the FGFR1 derivatives (data not shown). (D) A schematic presentation of the BCR-FGFR1 fusion protein with key amino acid positions and domains labeled. The oligomerization domain (OLIGO), the Grb2 and the Abl SH2 binding domains are shown. Also shown is the partial DBL-homologous (DBL) domain, which is a structural RhoGEF domain of guanine nucleotide exchange factors for Rho/Rac/Cdc42-like GTPases.

the table lists all possible mutations in Salt Bridges #1 and #2 (mutants 2-5) which do not disrupt Salt Bridge #3. The lower portion of the table lists all possible mutations in Salt Bridges #1 and #2 which also perturb Salt Bridge #3 (mutants 7-12).

When only Salt Bridge #3 was disrupted in the E52R mutation (Figure 5C, mutant 6), little effect was observed. When various combinations of mutations were examined, affecting Salt Bridge #3 together with either Salt Bridge #1 or Salt Bridge #2, the effects on biological activity were variable (Figure 5C, mutants 7-10). However, cell-transforming ability by BCR-FGFR1 was significantly reduced or completely abrogated when all three salt bridges were disrupted simultaneously: the mutant E34R/E46R/E52R exhibited <1% transformation activity, and the mutant R53E/R55E exhibited only 14% (Figure 5C, mutants 11-12). These data suggest that these three salt bridges in the BCR coiled-coil domain together provide a critical and partially redundant role in the oligomerization and activation of BCR-FGFR1. Figure 5D presents focus assay plates for BCR-FGFR1 (Figure 5D, mutant 1), and for selected mutants that disrupt either 2 or 3 salt bridge simultaneously (Figure 5D, mutants 5, 7, 9-12).

BCR-FGFR1 is an HSP90 addicted oncoprotein

Hsp90 is a highly conserved, ubiquitously expressed molecular chaperone that controls the stability of certain proteins.[26] Prior work has shown that Hsp90 is overexpressed in certain cancers, and the Hsp90 complex provides stability for various oncogenic proteins, which are necessary for cancer cell survival.[27] Many of these oncogenes, such as mutated P53 or BCR-ABL take advantage of

the Hsp90 chaperone system to avoid ubiquitination and proteasomal degradation.[28] Here, we aim to uncover if BCR-FGFR1 is a client of Hsp90 and possibly relies on the Hsp90 complex for stability and cellular survival.

HEK293T cell lysate expressing either FGFR1 or BCR-FGFR1 derivatives were immunoprecipitated with FGFR1 antisera and immunoblotted for Hsp90. An interaction was observed between Hsp90 and BCR-FGFR1 derivatives (Figure 6A). To further analyze if BCR-FGFR1 is dependent on Hsp90 for cellular stability and activity, assays with potent Hsp90 inhibitor, Ganetespib, were performed. HEK293T cells expressing either FGFR1 or BCR-FGFR1 derivatives were treated with 200 nM Ganetespib for 4 h, then analyzed for overall FGFR1 expression and activation of downstream cell signaling pathways (Figure 6B). A significant reduction in BCR-FGFR1 expression is observed following Ganetespib

Table 1. Biological activity of mutations in phosphoacceptor sites.

Construct	Foci relative to BCR-FGFR1 (%)	SEM (%)
Mock	0	0
BCR-FGFR1	100	11
BCR(Y177F)-FGFR1	55	16
BCR(Y436F)-FGFR1	120	2
BCR(Y455F)-FGFR1	108	9
BCR(S122A)-FGFR1	97	1
BCR(Y246F)-FGFR1	105	7
BCR(S459A)-FGFR1	129	1
BCR(Y554F)-FGFR1	126	11
BCR(T359A/S367A/S369A/S377A)-FGFR1	129	3

BCR: breakpoint cluster region; FGFR1: fibroblast growth factor receptor 1; SEM: standard error of the mean.

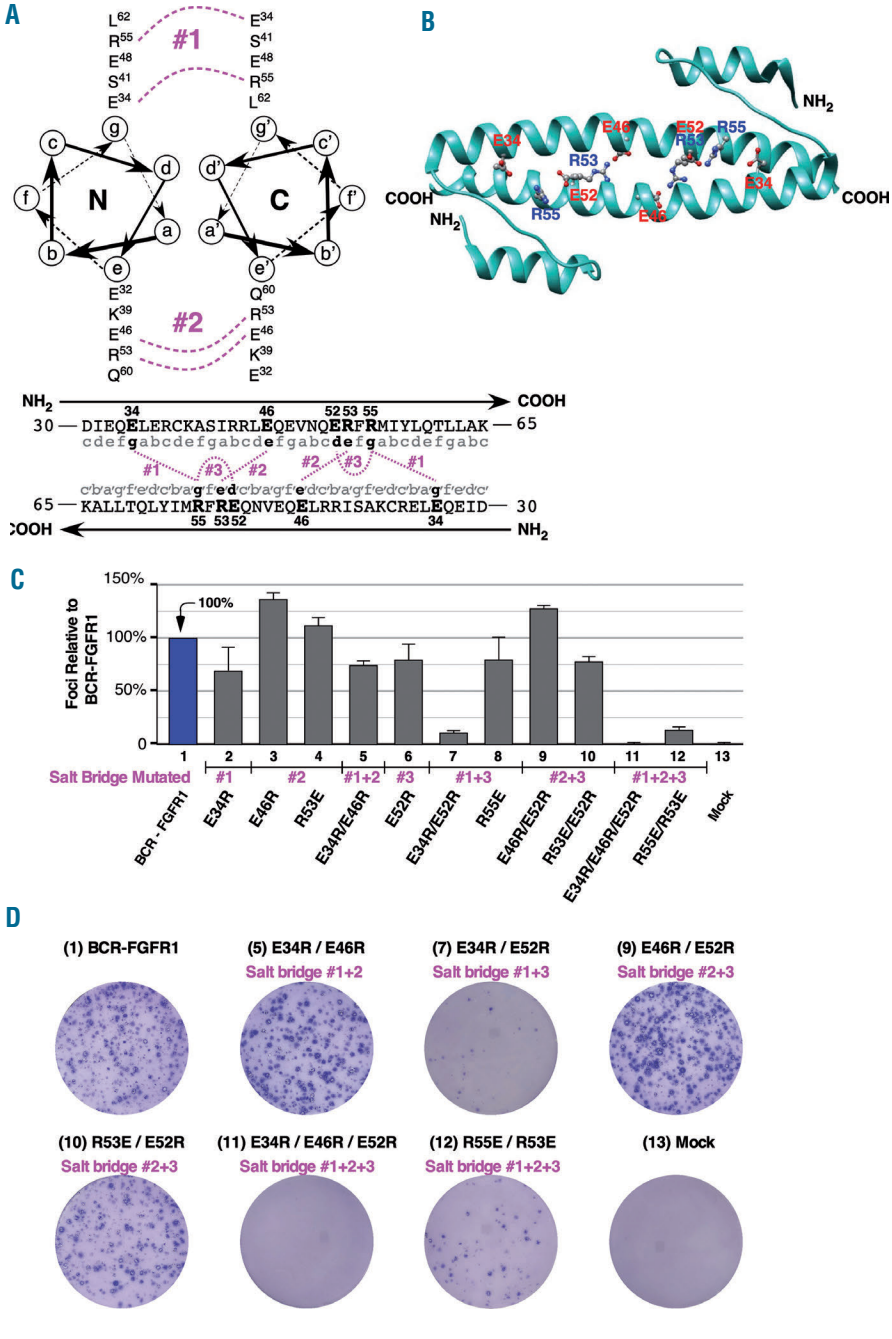

Figure 5. Three salt bridges are required for BCR-FGFR1 activity. Focus assay results with salt bridge mutations made in BCR coiled-coil domain. (A) The anti-parallel heptad repeats of the coiled-coil domain of BCR showing the residues in the "e" and "g" positions.[23] The two *interhelical* salt bridges are indicated between residues E34 and R55 (#1) in the "g" positions, and between E46 and R53 (#2) in the "e" positions. Below, residues 30 through 65 of the anti-parallel region are shown with the salt bridges indicated. Also shown in the linear sequence is the location of the *intrahelical* salt bridge involving E52-R55 in the "d" and "g" positions. (B) The crystal structure of the breakpoint cluster region (BCR) coiled-coil oligomerization domain is shown (PDB code 1K1F), as viewed using Chimera software.[24,25] Positive residues R53 and R55 are in blue while negative residues E34, E46, and E52 are in red. (C) Results from NIH3T3 transformation assay expressing BCR-FGFR1 fusions with salt bridge mutations. Foci were scored, normalized for transfection efficiency and quantitated relative to BCR-FGFR1 –/+ standard error of the mean (SEM). Each DNA construct was assayed at least three times. (D) Representative plates from a focus assay are shown. In the interest of space, plates are shown only for selected mutants that disrupt either two or three salt bridges simultaneously, as indicated.

treatment (Figure 6B, top panel). Furthermore, treatment with this Hsp90 inhibitor shows a decrease in phosphorylated STAT3, and complete ablation of phosphorylated Tyr on BCR-FGFR1, when compared to control cells treated (Figure 6B, panel 4 and 6). Interestingly, MAPK retains phosphorylation, despite the loss of phosphorylated BCR-FGFR1 (Figure 6B, panel 2). Although unexpected, this result could be due to the Grb2 binding site present in BCR, which activates downstream Ras and MAPK pathways independently of FGFR1 activation.[19] The dra-

Table 2. Mutations affecting interhelical Salt Bridges #1 and/or #2, and intrahelical Salt Bridge #3. Mutated residues shown in bold font; missing salt bridge indicated by ⊗ . Wt: wild-type.

Mutant Name	Mutated Salt Bridges	Salt Bridge #1 Residues	Salt Bridge #2 Residues	Salt Bridge #3 Residues	Activity
(1) BCR-FGFR1 WT	None	E34 • R55	E46 • R53	E52 • R55	Active
(2) E34R	#1	**E34R** ⊗ R55	E46 • R53	E52 • R55	Active
(3) E46R	#2	E34 • R55	**E46R** ⊗ R53	E52 • R55	Active
(4) R53E	#2	E34 • R55	E46 ⊗ **R53E**	E52 • R55	Active
(5) E34R/E46R	#1 + 2	**E34R** ⊗ R55	**E46R** ⊗ R53	E52 • R55	Active
(6) E52R	#3	E34 • R55	E46 • R53	**E52R** ⊗ R55	Active
(7) E34R/E52R	#3 + 1	**E34R** ⊗ R55	E46 • R53	**E52R** ⊗ R55	Reduced
(8) R55E	#3 + 1	E34 ⊗ R55E	E46 • R53	E52 ⊗ **R55E**	Active
(9) E46R/E52R	#3 + 2	E34 • R55	**E46R** ⊗ R53	**E52R** ⊗ R55	Active
(10) R53E/E52R	#3 + 2	E34 • R55	E46 ⊗ **R53E**	**E52R** ⊗ R55	Active
(11) E34R/E46R/E52R	#3 + 1 +2	**E34R** ⊗ R55	**E46** ⊗ R53	**E52R** ⊗ R55	Inactive
(12) R55E/R53E	#3 + 1 +2	E34 ⊗ **R55E**	E46 ⊗ **R53E**	E52 ⊗ **R55E**	Reduced

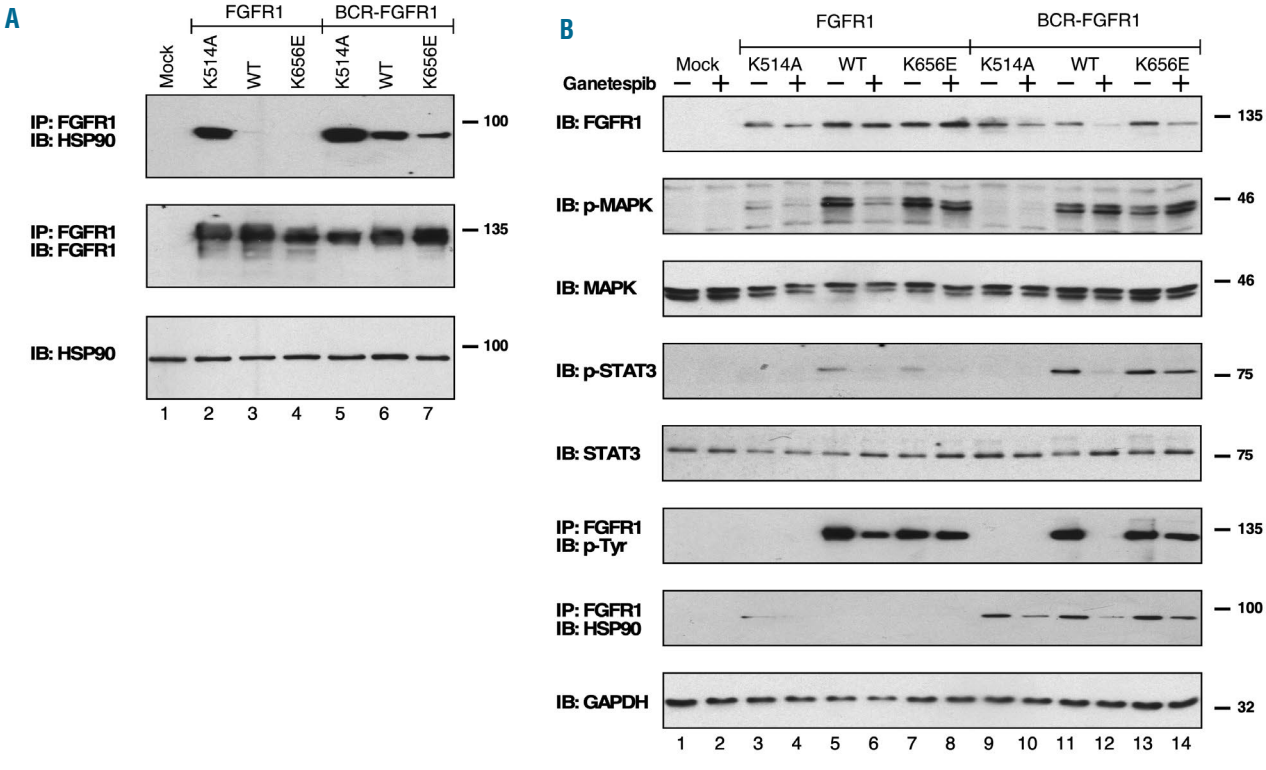

Figure 6. BCR-FGFR1 activity relies upon Hsp90. (A) Lysates from HEK293T cells expressing FGFR1 and BCR-FGFR1 derivatives were immunoprecipitated with FGFR1 and immunoblotted with anti-Hsp90 antibody (top panel). The membrane was reprobed for total FGFR1 (panel 2). The bottom panel shows the Hsp90 expression in lysate samples. (B) HEK293T cells expressing FGFR1 and BCR-FGFR1 derivatives were treated with –/+ 200 nM Ganetespib for 4 hours (h) prior to lysing. Lysates were examined for expression of the clones with anti-FGFR1 (panel 1), examined for activation of MAPK and STAT3 pathways using phospho-specific antibodies; phospho-MAPK (T202/Y204) (panel 2) and phospho-STAT3 (Y705) (panel 4). Membranes were stripped and reprobed for total MAPK and STAT3 shown in panel 3 and 5, respectively. Tyrosine phosphorylation of FGFR1 and BCR-FGFR1 derivatives was examined by immunoprecipitating FGFR1 followed by immunoblotting with anti-phosphotyrosine antibody (panel 6). The Hsp90 interaction was examined by immunoblotting with anti-Hsp90 antibody on FGFR1 immunoprecipitations (panel 7). The bottom control panel shows expression of GAPDH.

matic decrease in BCR-FGFR1 expression with the addition of Ganetespib suggests that BCR-FGFR1 may be a client protein of Hsp90 and potentially uses the Hsp90 complex for protein stability within the cell.

To investigate if BCR-FGFR1 relies on Hsp90 for cell transformation, NIH3T3 cells expressing FGFR1 or BCR-FGFR1 derivatives were treated with increasing concentrations of Ganetespib. Ganetespib concentrations were titrated to allow for a dose that effectively treated BCR-FGFR1 expressing cells without harming non-expressing NIH3T3 cells. A reduction of cell transformation and focus formation is observed with increasing concentrations of

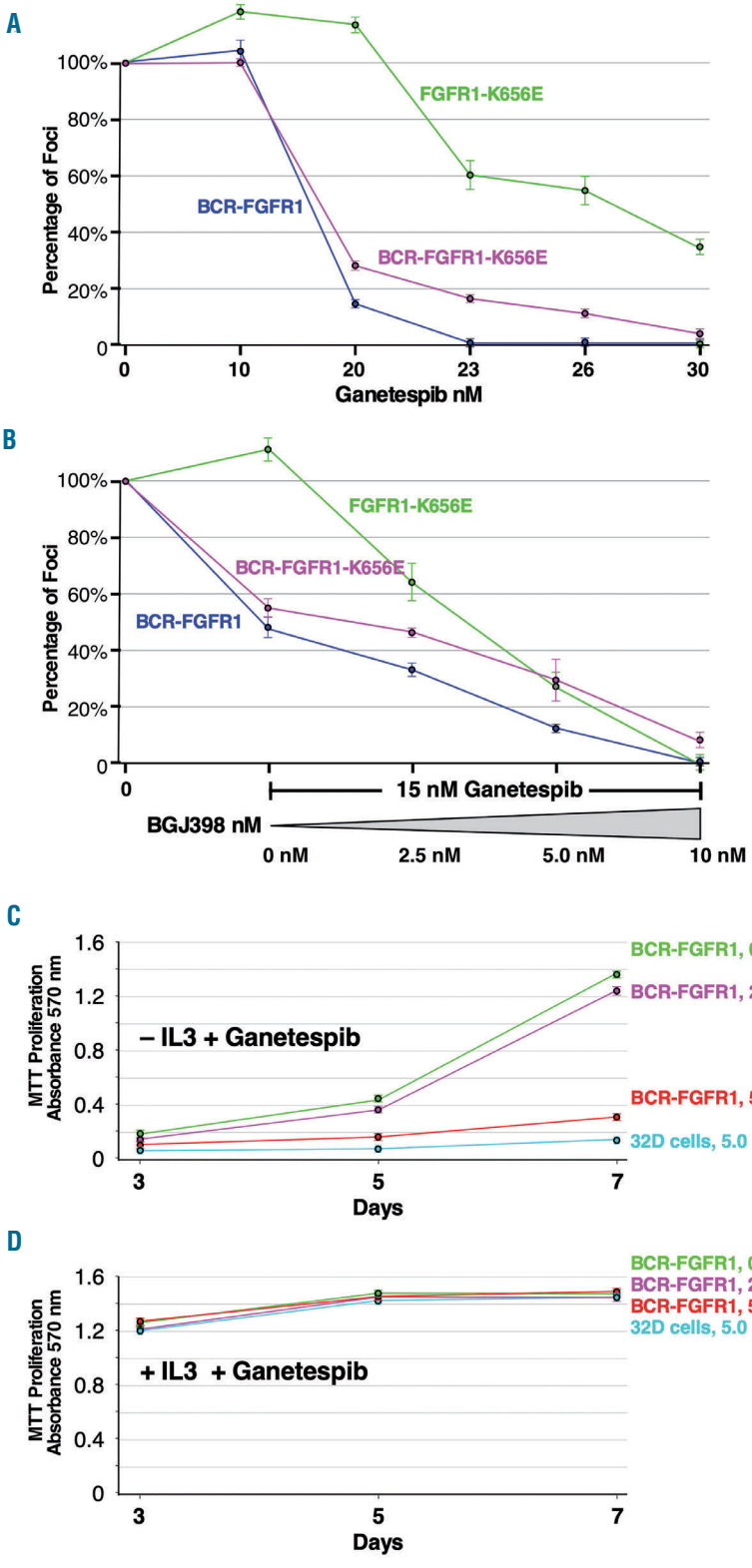

Figure 7. Effects of Ganetespib on BCR-FGFR1 activity in cellular assays. (A) NIH3T3 transformation assay. Cells expressing FGFR1-K656E, BCR-FGFR1 and BCR-FGFR1-K656E were treated with increasing concentrations of the Hsp90 inhibitor, Ganetespib (10, 20, 23, 26 and 30 nM). After 14 days (d), foci were scored and each sample was normalized by transfection efficiency set to 100% as the starting value under conditions of no Gantespib. Mock transfected cells and cells expressing FGFR1 were also included in this assay; no foci were observed. (B) Effects of Ganetespib (15 nM) together with increasing concentrations of FGFR-specific TKI BGJ398 in NIH3T3 transformation assays. Quantitation as in (A) above. Mock transfected cells and cells expressing FGFR1 were also included in this assay; again, no foci were observed (C and D). Ganetespib inhibits 32D cell proliferation stimulated by BCR-FGFR1. 32D control cells and cells selectively expressing BCR-FGFR1 were cultured in panel C in the absence of IL-3 and, in panel D, in the presence of IL-3, together with Ganetespib at 0, 2.5, and 5.0 nM. Cells expressing FGFR1 were also included in this assay and showed no cell proliferation in the absence of IL-3, as shown earlier (Figure 3A and D). Cell viability was determined by MTT metabolic assay. All control cells and cell lines were assayed in triplicate. Standard error is shown.

Ganetespib (Figure 7A). The BCR-FGFR1 derivatives were more sensitive to the Ganetespib than FGFR1-K656E, possibly due to the lack of HSP90 association with FGFR1-K656E (Figure 6).

Furthermore, in order to determine if the effects of Ganetespib were synergistic with FGFR inhibition, a combinatorial experiment was performed on NIH3T3 cells expressing either BCR-FGFR1 or FGFR1 derivatives, which were simultaneously treated with Ganetespib and a TKI. These cells were treated with a constant 15 nM Ganetespib and were dosed with increasing concentrations of BGJ398, a potent FGFR inhibitor (Figure 7B). A potentially synergistic effect is observed between Ganetespib and BGJ398, as foci production among cells expressing either BCR-FGFR1 or FGFR1 derivatives dramatically decreases. These data suggest that the use of Hsp90 inhibition combined with TKI treatment may be beneficial for BCR-FGFR1 expressing cells.

The effect of Ganetespib was also examined using 32D IL-3-dependent cells. The IL-3-independent proliferation of the BCR-FGFR1 expressing 32D cells was reduced by treatment with Ganetespib as measured by MTT assay (Figure 7C). The Ganetespib did not affect the normal dependence of the cells on IL-3, as shown in Figure 7D. Therefore, these data suggest that BCR-FGFR1 is dependent on the molecular chaperone Hsp90 for cellular transformation.

Discussion

Considerable advances have been made in our understanding of the molecular basis of hematological cancers. Since the identification of BCR-ABL almost 60 years ago,[29] over 500 oncogenic translocations have been identified in hematopoietic cancers alone, which emphasizes the importance of identifying and characterizing these oncogenic drivers.[30] With the emergence of personalized medicine, the characterization of activators of SCLL, such as BCR-FGFR1, is critical in determining additional therapeutic targets. Although the use of TKI to treat SCLL is becoming more commonplace, TKI treatment often results in drug resistance in patients, highlighting the need for additional therapies for SCLL.[31]

Biological and biochemical characterization of BCR-FGFR1

Through the data presented, we were able to extensively characterize the fusion protein BCR-FGFR1. We demonstrate that the N-terminal fusion of BCR results in constitutive activation of FGFR1. Through our cell signaling studies, we demonstrate that BCR-FGFR1 activates ERK/MAPK and JAK/STAT pathways, and possesses transforming activity in NIH3T3 cells (Figure 1-2). However, BCR-FGFR1-K514A was unable to activate either pathway, or transform NIH3T3 cells, indicating that BCR-FGFR1 relies on the kinase activity of FGFR1 for activation. Furthermore, 32D cells expressing BCR-FGFR1 or BCR-FGFR1-K656E were able to proliferate in the absence of IL-3, indicating the oncogenic potential of this fusion protein (Figure 3).

LC-MS/MS data additionally demonstrate that BCR-FGFR1 relies on the kinase activity of FGFR1 for oncogenic activity. Phosphorylation on key tyrosine residues in the FGFR1 kinase domain, including Y653 and Y654 in the activation loop, is observed in BCR-FGFR1 and BCR-FGFR1-K656E, which is absent in kinase-dead BCR-FGFR1-K514A (Figure 4). Although novel phosphorylation sites were detected on BCR, these phosphoacceptor sites do not appear to be critical for the cell transformation or oncogenic ability of BCR-FGFR1 (Table 1).

Novel therapeutic targets for SCLL induced by BCR-FGFR1

Currently, hematopoietic stem cell transplantation is the primary curative option for patients who have SCLL. Here, we have described two novel potential therapeutic approaches: disruption of ionic bonding that stabilizes BCR oligomerization, and inhibition of the chaperonin Hsp90 complex.

The coiled-coil oligomerization domain of BCR has previously been demonstrated to be essential for the transforming ability of BCR-ABL.[21] However, the requirement of electrostatic interactions within the coiled-coil domain for oligomerization has not been investigated. Here, we have described a novel inhibition of BCR-FGFR1 mediated cell transformation through abolishing three salt bridge interactions in the coiled-coil domain of BCR. This ablation of cell transformation is seen through focus forming assays, as the disruption of these salt bridges in the *BCR-FGFR1* mutant E34R/E46R/E52R (mutant 11) almost completely abolishes focus formation (Figure 5). Furthermore, the intrahelical Salt Bridge #3, formed by residue Glu52 with Arg55 in BCR, plays a crucial role in providing stability for the coiled-coil domain in BCR. The apparent ability of Arg55 to form complex salt bridges with Glu34 and Glu52 highlights the potential importance of cooperativity exhibited by complex salt bridges and their contribution to protein stability.[32] Taken together, these data suggest that these three salt bridges provide a critical role in the activation of BCR-FGFR1. The potential loss of oligomerization and near absence in focus formation suggests that the coiled-coil domain of BCR is an attractive therapeutic target for SCLL.

Additionally, we have shown that BCR-FGFR1 is a client of the Hsp90 chaperone complex, and potentially uses this complex to avoid proteasomal degradation in the cell. Previous work has shown that the FGFR1OP2-FGFR1 fusion is also a client of the Hsp90 complex, and that targeting the Hsp90 complex resulted in reduced activity of this fusion protein.[33] The interaction and dependence of BCR-FGFR1 on the Hsp90 complex is established through cell transformation assays, and analysis of downstream cell signaling (Figure 6-7). A decrease in overall expression of BCR-FGFR1 is detected with the addition of Ganetespib, a potent Hsp90 inhibitor. Furthermore, BCR-FGFR1 expressing cells treated with Ganetespib displayed a reduction in STAT and MAPK activation, and no FGFR1 phosphorylation. Additionally, the transformation ability of cells expressing BCR-FGFR1 decreases when treated with increasing concentrations of Ganetespib (Figure 7A), indicating that this fusion protein relies on the Hsp90 complex for cellular stability, and is sensitive to Hsp90 inhibition. We also examined the combined effects of Ganetespib with the FGFR inhibitor BGJ398 in NIH3T3 cell transformation assays (Figure 7B), and in 32D cell proliferation assays in the absence and presence of IL-3 (Figure 7C-D). Taken together, these data show that BCR-FGFR1 may rely on the Hsp90 molecular chaperone complex to avoid proteasomal degradation.[34]

Through this work, we have described potential approaches to inhibit BCR-FGFR1 induced SCLL. Although TKI therapies have been used to traditionally treat certain hematopoietic cancers, their use has often resulted in drug resistance. Recently it has been discovered that FGFR1 fusion kinases are associated with the upregulation of MYC, which drives SCLL.[35] Targeting the MYC complex in addition to chemotherapy, and the approaches described here may also be therapeutically beneficial for patients with SCLL.

Relevance for *BCR-ABL* driven cancers

Since the initial characterization of *BCR-ABL*, the emergence of cancer genome sequencing has played a vital role in the detection of other translocation-induced malignances. *BCR-ABL* is detected in 95% of CML cases, and variants of this gene exist with alternative breakpoints. The most commonly found transcript is the *BCR-ABL* p210 variant which contains a breakpoint of BCR exon 13 fused to exon 1 of ABL.[10] In comparison to *BCR-FGFR1, BCR-ABL* retains more of the BCR gene in this fusion. However, both fusions retain the oligomerization domain, putative serine threonine/kinase domain and GEF domain. Due to the similarity between these fusions, we propose that the work described here will be relevant to *BCR-ABL* fusions as well. In particular, the inhibition of the BCR coiled-coil domain through salt bridge disruption may be an additional therapeutic target for BCR-ABL. Furthermore, retention of the GEF domain in *BCR-FGFR1* has been shown to result in reduced leukemogenesis.[36]

Although TKI are usually the first line of treatment for CML, many patients will require concurrent forms of therapy to ensure complete remission.[37] Hsp90 inhibition has become an attractive therapeutic target in treating *BCR-ABL* induced CML. More recently, aminoxyrone was shown to be effective in inhibiting imatinib resistant CML.[37] While Ganetespib binds to the N-terminal ATP binding site in Hsp90, Aminoxyrone binds to the C-terminal tail of Hsp90, preventing its dimerization. The combination of Hsp90 inhibition with traditional chemotherapy and TKI treatment may be beneficial in patients with CML or SCLL. These recent findings again highlight the importance of the characterization of oncogenic translocations as well as the development of additional therapeutic targets to treat therapy-refractory leukemia.

Acknowledgements

We thank all current lab members particularly Juyeon Ko, Fangda Li, and Clark Wang for advice and encouragement, Leo Gallo and Dan Crocker for additional support, and Alexandre R. Campos from Sanford Burnham Prebys (SBP) Medical Discovery Institute for analysis of samples by mass spectrometry. MNP gratefully acknowledges support from a UC San Diego San Diego Fellowship, and DJD gratefully acknowledges generous philanthropic support from the UC San Diego Foundation. Support to the SBP Proteomics Facility from grant P30 CA030199 from the National Institutes of Health is also gratefully acknowledged.

Dedication

MNP dedicates this work in memory of her parents Swarnakanthie Peiris (1947-2005) and Donald Peiris (1949-2018), as this work would not have been possible without their inspiration, love and support.

References

1. Gallo LH, Nelson KN, Meyer AN, Donoghue DJ. Functions of Fibroblast Growth Factor Receptors in cancer defined by novel translocations and mutations. Cytokine Growth Factor Rev. 2015;26(4):425-449.
2. Macdonald D, Reiter A, Cross NC. The 8p11 myeloproliferative syndrome: a distinct clinical entity caused by constitutive activation of FGFR1. Acta Haematol. 2002;107(2):101-107.
3. Nelson KN, Peiris MN, Meyer AN, et al. Receptor tyrosine kinases: translocation partners in hematopoietic disorders. Trends Mol Med. 2017;23(1):59-79.
4. Khodadoust MS, Luo B, Medeiros BC, et al. Clinical activity of ponatinib in a patient with FGFR1-rearranged mixed-phenotype acute leukemia. Leukemia. 2016;30(4):947-950.
5. Verstovsek S, Rambaldi A, Asatiani E, et al. Phase 2, open-label, multicenter study to evaluate the efficacy and safety of INCB054828 in patients with myeloid/lymphoid neoplasms with fibroblast growth factor receptor 1 (FGFR1) rearrangement. Cancer Res. 2017;77(13 Suppl):Abstract nr CT057.
6. Cuesta-Dominguez A, Ortega M, Ormazabal C, et al. Transforming and tumorigenic activity of JAK2 by fusion to BCR: molecular mechanisms of action of a novel BCR-JAK2 tyrosine-kinase. PLoS One. 2012;7(2):e32451.
7. Ballerini P, Struski S, Cresson C, et al. RET fusion genes are associated with chronic myelomonocytic leukemia and enhance monocytic differentiation. Leukemia. 2012;26(11):2384-2389.
8. Baxter EJ, Hochhaus A, Bolufer P, et al. The t(4;22)(q12;q11) in atypical chronic myeloid leukaemia fuses BCR to PDGFRA. Hum Mol Genet. 2002;11(12):1391-1397.
9. Peiris MN, Li F, Donoghue DJ. BCR: a promiscuous fusion partner in hematopoietic disorders. Oncotarget. 2019;10(28):2738-2754.
10. Laurent E, Talpaz M, Kantarjian H, Kurzrock R. The BCR gene and philadelphia chromosome-positive leukemogenesis. Cancer Res. 2001;61(6):2343-2355.
11. Hart KC, Robertson SC, Kanemitsu MY, et al. Transformation and Stat activation by derivatives of FGFR1, FGFR3, and FGFR4. Oncogene. 2000;19(29):3309-3320.
12. Hu Y, Fang X, Dunham SM, et al. 90-kDa ribosomal S6 kinase is a direct target for the nuclear fibroblast growth factor receptor 1 (FGFR1): role in FGFR1 signaling. J Biol Chem. 2004;279(28):29325-29335.
13. Gallo LH, Meyer AN, Motamedchaboki K, et al. Novel Lys63-linked ubiquitination of IKKbeta induces STAT3 signaling. Cell Cycle. 2014;13(24):3964-3976.
14. Meyer AN, McAndrew CW, Donoghue DJ. Nordihydroguaiaretic acid inhibits an activated fibroblast growth factor receptor 3 mutant and blocks downstream signaling in multiple myeloma cells. Cancer Res. 2008;68(18):7362-7370.
15. Nelson KN, Meyer AN, Wang CG, Donoghue DJ. Oncogenic driver FGFR3-TACC3 is dependent on membrane trafficking and ERK signaling. Oncotarget. 2018;9(76):34306-34319.
16. Nelson KN, Meyer AN, Siari A, et al. Oncogenic gene fusion FGFR3-TACC3 is regulated by tyrosine phosphorylation. Mol Cancer Res. 2016;14(5):458-469.
17. Mulcahy LS, Smith MR, Stacey DW. Requirement for ras proto-oncogene function during serum-stimulated growth of NIH 3T3 cells. Nature. 1985;313(5999):241-243.
18. Daley GQ, Baltimore D. Transformation of an interleukin 3-dependent hematopoietic cell line by the chronic myelogenous leukemia-specific P210bcr/abl protein. Proc Natl Acad Sci U S A. 1988;85(23):9312-9316.
19. Ma G, Lu D, Wu Y, et al. Bcr phosphorylated on tyrosine 177 binds Grb2. Oncogene. 1997;14(19):2367-2372.
20. Roumiantsev S, Krause DS, Neumann CA, et al. Distinct stem cell myeloproliferative/T lymphoma syndromes induced by ZNF198-FGFR1 and BCR-FGFR1 fusion genes from 8p11 translocations. Cancer Cell. 2004;5(3):287-298.
21. McWhirter JR, Galasso DL, Wang JY. A coiled-coil oligomerization domain of Bcr is essential for the transforming function of Bcr-Abl oncoproteins. Mol Cell Biol. 1993;13(12):7587-7595.
22. Cetinbas N, Huang-Hobbs H, Tognon C, et al. Mutation of the salt bridge-forming residues in the ETV6-SAM domain interface

blocks ETV6-NTRK3-induced cellular transformation. J Biol Chem. 2013;288(39):27940-27950.
23. Taylor CM, Keating AE. Orientation and oligomerization specificity of the Bcr coiled-coil oligomerization domain. Biochemistry. 2005;44(49):16246-16256.
24. Zhao X, Ghaffari S, Lodish H, et al. Structure of the Bcr-Abl oncoprotein oligomerization domain. Nat Struct Biol. 2002;9(2):117-120.
25. Pettersen EF, Goddard TD, Huang CC, et al. UCSF Chimera--a visualization system for exploratory research and analysis. J Comput Chem. 2004;25(13):1605-1612.
26. Taipale M, Jarosz DF, Lindquist S. HSP90 at the hub of protein homeostasis: emerging mechanistic insights. Nat Rev Mol Cell Biol. 2010;11(7):515-528.
27. Whitesell L, Lindquist SL. HSP90 and the chaperoning of cancer. Nat Rev Cancer. 2005;5(10):761-772.
28. Neckers L. Hsp90 inhibitors as novel cancer chemotherapeutic agents. Trends Mol Med. 2002;8(4 Suppl):S55-61.
29. Nowell PC, Hungerford DA. Chromosome studies on normal and leukemic human leukocytes. J Natl Cancer Inst. 1960;25:85-109.
30. Nambiar M, Kari V, Raghavan SC. Chromosomal translocations in cancer. Biochim Biophys Acta. 2008;1786(2):139-152.
31. Musumeci F, Greco C, Grossi G, et al. Recent studies on ponatinib in cancers other than chronic myeloid leukemia. Cancers (Basel). 2018;10(11).
32. Gvritishvili AG, Gribenko AV, Makhatadze GI. Cooperativity of complex salt bridges. Protein Sci. 2008;17(7):1285-1290.
33. Jin Y, Zhen Y, Haugsten EM, Wiedlocha A. The driver of malignancy in KG-1a leukemic cells, FGFR1OP2-FGFR1, encodes an HSP90 addicted oncoprotein. Cell Signal. 2011; 23(11):1758-1766.
34. Gallo LH, Ko J, Donoghue DJ. The importance of regulatory ubiquitination in cancer and metastasis. Cell Cycle. 2017;16(7):634-648.
35. Hu T, Wu Q, Chong Y, et al. FGFR1 fusion kinase regulation of MYC expression drives development of stem cell leukemia/lymphoma syndrome. Leukemia. 2018;32(11): 2363-2373.
36. Hu T, Chong Y, Lu S, et al. Loss of the BCR-FGFR1 GEF Domain Suppresses RHOA Activation and Enhances B-Lymphomagenesis in Mice. Cancer Res. 2019;79(1):114-124.
37. Bhatia S, Diedrich D, Frieg B, et al. Targeting HSP90 dimerization via the C terminus is effective in imatinib-resistant CML and lacks the heat shock response. Blood. 2018; 132(3):307-320.

Ferrata Storti Foundation

Combined inhibition of MDM2 and BCR-ABL1 tyrosine kinase targets chronic myeloid leukemia stem/progenitor cells in a murine model

Bing Z. Carter,[1] Po Yee Mak,[1] Hong Mu,[1] Xiangmeng Wang,[1] Wenjing Tao,[1] Duncan H. Mak,[1] Elisha J. Dettman,[2] Michael Cardone,[2] Oleg Zernovak,[3] Takahiko Seki,[3] and Michael Andreeff[1]

[1]Section of Molecular Hematology and Therapy, Department of Leukemia, The University of Texas MD Anderson Cancer Center, Houston, TX, USA; [2]Eutropics, Cambridge, MA, USA and [3]Daiichi Sankyo Co. Ltd., Oncology Laboratories, R&D Division, 2-58, Hiromachi 1-Chrome, Shinagawa-ku, Tokyo, Japan

Haematologica 2020
Volume 105(5):1274-1284

Correspondence:

BING Z. CARTER
bicarter@mdanderson.org

MICHAEL ANDREEFF
mandreef@mdanderson.org

Received: February 11, 2019.

Accepted: July 26, 2019.

Pre-published: August 1, 2019.

doi:10.3324/haematol.2019.219261

Check the online version for the most updated information on this article, online supplements, and information on authorship & disclosures: www.haematologica.org/content/105/5/1274

ABSTRACT

Although highly effective, BCR-ABL1 tyrosine kinase inhibitors do not target chronic myeloid leukemia (CML) stem cells. Most patients relapse upon tyrosine kinase inhibitor therapy cessation. We reported previously that combined BCR-ABL1 and BCL-2 inhibition synergistically targets CML stem/progenitor cells. p53 induces apoptosis mainly by modulating BCL-2 family proteins. Although infrequently mutated in CML, p53 is antagonized by MDM2, which is regulated by BCR-ABL1 signaling. We hypothesized that MDM2 inhibition could sensitize CML cells to tyrosine kinase inhibitors. Using an inducible transgenic Scl-tTa-*BCR-ABL1* murine CML model, we found, by RT-PCR and CyTOF proteomics increased p53 signaling in CML bone marrow (BM) cells compared with controls in $CD45^+$ and linage-$SCA\text{-}1^+C\text{-}KIT^+$ populations. CML BM cells were more sensitive to exogenous BH3 peptides than controls. Combined inhibition of BCR-ABL1 with imatinib and MDM2 with DS-5272 increased NOXA level, markedly reduced leukemic linage-$SCA\text{-}1^+C\text{-}KIT^+$ cells and hematopoiesis, decreased leukemia burden, significantly prolonged the survival of mice engrafted with BM cells from Scl-tTa-*BCR-ABL1* mice, and significantly decreased CML stem cell frequency in secondary transplantations. Our results suggest that CML stem/progenitor cells have increased p53 signaling and a propensity for apoptosis. Combined MDM2 and BCR-ABL1 inhibition targets CML stem/progenitor cells and has the potential to improve cure rates for CML.

Introduction

Chronic myeloid leukemia (CML) originates from the t(9;22) chromosomal translocation that results in the BCR-ABL1 fusion gene and constitutive activation of the BCR-ABL1 tyrosine kinase in hematopoietic stem cells.[1-3] CML stem cells are quiescent,[4] yet can self-renew, proliferate, differentiate, and promote expansion of the myeloid lineage. The development of imatinib and other tyrosine kinase inhibitors (TKI) has made CML, once a deadly disease, highly manageable with a 10-year overall survival rate of over 90%.

Although extremely effective in eliminating proliferating CML cells, TKI are inactive against quiescent CML stem cells, despite inhibition of BCR-ABL1 activity,[5-7] and several clinical trials have demonstrated that approximately 50% of patients eventually relapse after ceasing TKI therapy.[8-11] Long-term treatment with TKI is expensive, and may lead to the development of inhibitor resistance, or intolerance to therapy. Furthermore, the persistence of CML stem cells contributes to the generation of new clones with additional acquired mutations, which can lead to progression to acute disease over time. Thus, eradicating CML stem cells is the ultimate goal in curing CML.

Numerous combinatorial strategies have been proposed pre-clinically and shown to be effective in eradicating CML stem cells.[12-16] Among them, concomitant targeting of

anti-apoptotic BCL-2 proteins enhances TKI activity in CML,[17-19] and we demonstrated that BCL-2 is a key survival factor of CML stem cells, and targeting BCL-2 with ABT-199, combined with a TKI, enhanced eradication of CML stem cells.[20]

Among its numerous tumor suppressor functions, p53 activates the expression of the pro-apoptotic BCL-2 proteins BAX, PUMA, NOXA, and BID triggering apoptosis.[21-23] Altered p53 and MYC transcriptional network in CML stem cells was recently reported, and targeting both p53 and MYC selectively eliminated CML stem cells.[24] Activation of p53 by inhibition of SIRT1 or MDM2, in combination with TKI has been explored in CML.[25,26] We reported that TKI in combination with the MDM2 inhibitor nutlin3a enhanced apoptosis induction in proliferating and quiescent blast crisis CML progenitor cells *in vitro*.[27]

The expression of p53 can be induced when cells are stressed, including those associated with oncogenic stimulation. Like other oncogenes, the hyper-proliferative signal from *BCR-ABL1* can activate p53 and induce cell cycle block and senescence to counterbalance oncogenic stimulation signals. This may also contribute to CML stem cell maintenance. However, the role of p53 signaling proteins in BCR-ABL1 oncogene-driven CML/CML stem cells and the response of CML stem cells to the combined MDM2 and BCR-ABL1 inhibition have not been fully investigated.

Using an inducible, stem cell promoter (Scl)-driven transgenic CML murine model (Scl-tTa-*BCR-ABL1* mice),[15,20,28,29] we here determine the expression of p53 and its signaling proteins in bone marrow (BM) cells and lineage-SCA-1$^+$C-KIT$^+$ (LSK) cells from CML and control mice, and in BM cells in CML mice treated with the MDM2 inhibitor DS-5272, the TKI imatinib, or both, using novel CyTOF mass cytometry, which measures single-cell protein expression in phenotypically-defined cell populations. We also investigated the anti-leukemia activity of combined MDM2 and BCR-ABL1 inhibition in this model.

Methods

Mouse model and cells

Mouse experiments were performed in accordance with MD Anderson Cancer Center Animal Care and Use Committee approved protocols. Scl-tTa-BCR-ABL1 FVB/N mice[28,29] were provided by Dr. R. Bhatia (University of Alabama at Birmingham, AL, USA). BM cells were collected from mice 3-4 weeks after tetracycline cessation (Tet-off) or from controls (Tet-on).

Human cells

Cells from newly diagnosed chronic phase CML (CML-CP) patients (*Online Supplementary Table S1*) and normal controls were obtained as described in the *Online Supplementary Methods*.

Real-time polymerase chain reaction

Real-time polymerase chain reaction (RT-PCR) was carried out as previously described[20] using freshly isolated mouse or human BM cells. Primers are shown in *Online Supplementary Table S2*. The abundance of each transcript relative to that of *Abl1* or *ABL1* was calculated using the $2^{-\Delta Ct}$ method, expressed as copies of each mRNA/1000 copies of *Abl1* or *ABL1*.

Western blot

Western blot was performed as described previously.[20] Antibodies against human p53 and BAX were purchased from Santa Cruz (Dallas, TX, USA).

Mass cytometry

Mouse BM cells were stained with metal-tagged antibodies for cell surface markers and intracellular proteins (*Online Supplementary Table S3*) and subjected to mass cytometry (CyTOF) analysis as previously described[16,20,30] and as briefly described in the *Online Supplementary Methods*.

Mitochondrial priming

BH3 priming assay as previously described[31] is described briefly in the *Online Supplementary Methods*.

In vivo experiments

GFP$^+$ CML cells from donor mice as previously described[15,20] were injected ($0.6x10^6$ cells/mouse) into FVB/N recipient mice (The Jackson Laboratory) irradiated at 900 cGy. After CML developed, assessed by flow cytometry measurement of GR-1 (LY6G)$^+$ cells, mice were treated daily (oral gavage) with imatinib (100 mg/kg; vehicle: acidified water, pH 5.0) for four weeks, DS-5272 (50 mg/kg; vehicle: 0.5% w/v methylcellulose 400) for two weeks (initiated two weeks after imatinib group), imatinib for two weeks and then plus DS-5272 for two additional weeks, or vehicle control (1:1 volume of each vehicle). Two sets of experiments were performed.

Experiment I: at the end of treatments, BM and spleen cells (n=3-5/group) were collected and stained with a lineage cocktail and antibodies against SCA-1 (eBioscience, ThermoFisher Scientific), C-KIT (CD117), CD34, FcγRII/III, GR-1 (LY6G), and MAC-1 (CD11b) (all from BioLegend, San Diego, CA, USA) to measure leukemia LSK, myeloid progenitors, and myeloid cells as previously described.[20] Peripheral blood (PB) leukemia burden was measured by total and GFP$^+$ white blood cell (WBC) count (CD45$^+$) and total and GFP$^+$ neutrophils (Ly6G$^+$) using flow cytometry. Mouse survival was recorded.

Experiment II: BM cells were collected at the end of treatments for secondary transplantation as described previously.[20] At 16 weeks, PB engraftment was determined, and the frequency of leukemia long-term hematopoietic stem cells (LT-HSC) was calculated. Green fluorescent protein (GFP) positivity and BCR-ABL1 RNA levels in BM cells from mice that received $0.25x10^6$ cells/mouse were determined.

Statistical analysis

Results are expressed as mean±standard error of the mean. $P<0.05$ was considered statistically significant (two-sided Student *t*-test). Correlation coefficient was determined by Pearson correlation analysis. Mouse survival was estimated by the Kaplan-Meier method and data were analyzed using the log-rank test. LT-HSC frequency was calculated using the Extreme Limiting Dilution Analysis software program (*http://bioinf.wehi.edu. au/software/elda/*).[32]

Results

BCR-ABL1 oncogene increases the expression of p53 and p53 targets

To determine p53 expression and p53 signaling in hematopoietic cells of CML mice and compare with those of controls, we collected BM cells from Tet-off CML and Tet-on control Scl-tTa-*BCR-ABL1* FVB/N mice, and determined the RNA levels of p53 and its target genes by RT-PCR. We found that BCR-ABL1 induction significantly increased *Trp53 (p53)* RNA and that of its target genes including *Bax, Pmaip1 (Noxa), Mdm2*, and *Cdkn1a* (*p21*) (Figure 1A) ($P<0.001$ for all genes analyzed), supporting oncogenic induction of p53.

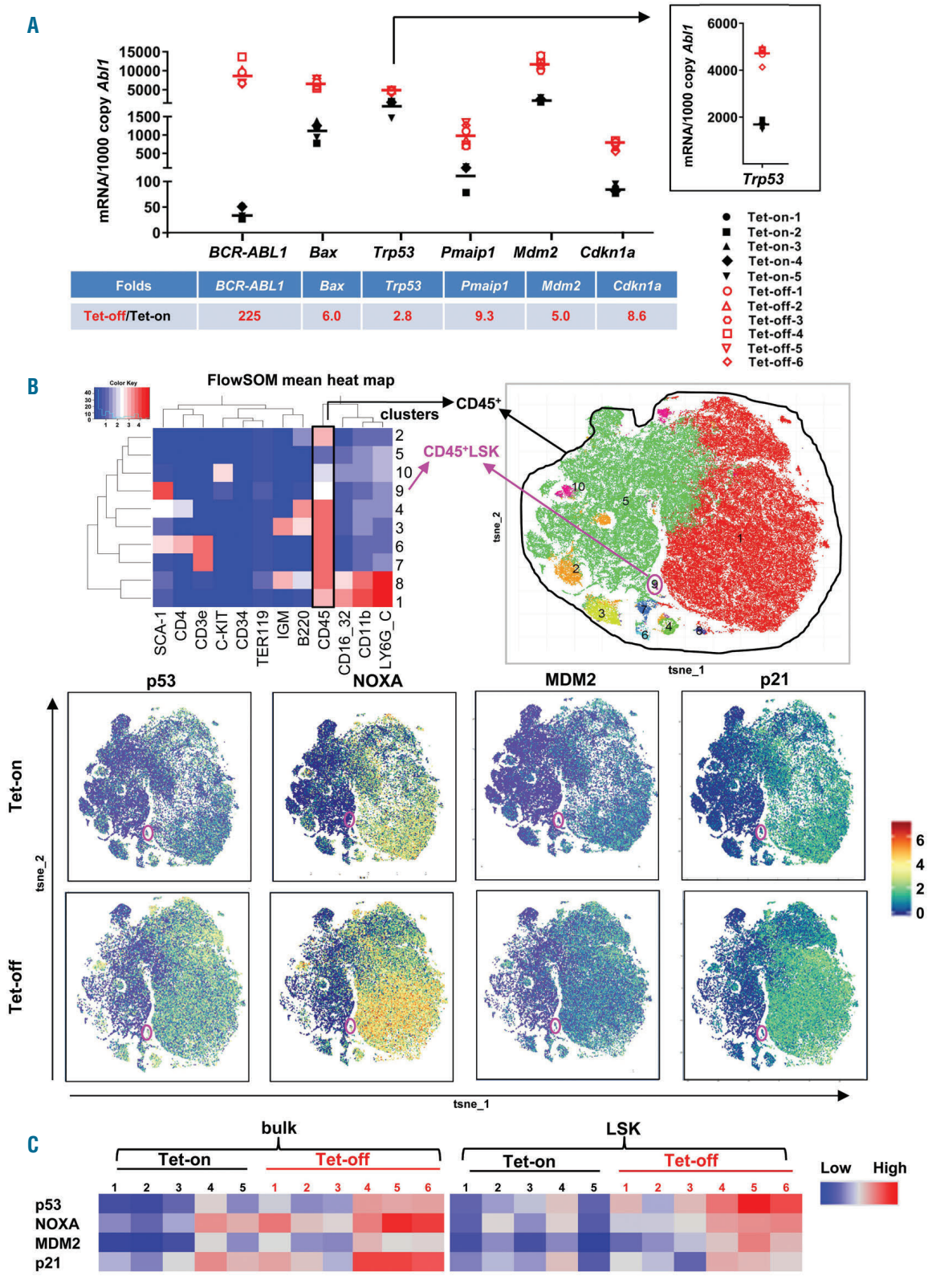

Figure 1. Expression of p53 and target genes in Tet-off chronic myeloid leukemia (CML) and Tet-on control mice. (A) RNA levels of *Trp53* (also shown in the insert) and its target genes in Tet-off CML and Tet-on control mouse bone marrow (BM) cells, determined by Taq-Man real-time polymerase chain reaction (RT-PCR). (B) Heat map and cell subset clusters by RPhenoGraph based on mouse cell surface markers (upper) and protein expression of p53 and p53 targets in BM cells of Tet-off and Tet-on mice, shown by RPhenoGraph (constructed from all the samples in each group) (lower panel) determined by CyTOF mass cytometry analysis. (C) Heat map showing protein expression of p53 and target genes in individual Tet-off CML and Tet-on control mouse BM CD45$^+$ (bulk) and lineage-SCA-1$^+$C-KIT$^+$ (LSK) cells as determined by CyTOF mass cytometry, quantified by FlowJo software, and expressed in ArcSinh. BM cells were collected from mice 3-4 weeks after tetracycline cessation (Tet-off) (n=6) or from age-matched controls (Tet-on) (n=5).

We next stained BM cells from Tet-off and Tet-on SCL-tTa-BCR-ABL1 FVB/N mice with a panel of metal-tagged antibodies for cell surface and intracellular proteins (*Online Supplementary Table S3*) and performed CyTOF mass cytometry analysis. Following Cytofkit unsupervised subset detection based on RPhenoGraph clustering algorithms, expression of various proteins was determined in bulk CD45$^+$ and LSK (cluster 9, pink circle) cells (see Figure 1B). We found increased levels of p53 and its targets, including NOXA, MDM2, and p21 in CD45$^+$ and LSK cells from Tet-off BM cells compared with their Tet-on counterparts, as displayed by RPhenoGraph (Figure 1B) as well as in a heat map showing the expression of each protein in each individual mouse (Figure 1C). We previously reported that BAX, another target of p53, was also higher in BM CD45$^+$ and LSK cells from Tet-off CML mice compared to that in control mice.[20]

To demonstrate that increased expression of p53 and its target proteins also occurs in newly-diagnosed CML-CP patients, we first performed RT-PCR using RNA isolated from fresh BM samples of patients (n=5) (*Online Supplementary Table S1*) and normal controls (n=6). Although there were high individual variations, overall BM cells from CML patients expressed higher levels of RNA representing p53 signaling proteins compared with those from normal controls, with statistically significantly higher *BAX* (P=0.009) and markedly higher *PMAIP1 (NOXA)* (P=0.06) (Figure 2A).

We next isolated CD34$^+$ cells from fresh BM or PB samples of newly-diagnosed CML patients (n=7) (*Online Supplementary Table S1*) and fresh BM samples from normal controls (n=5) and obtained sufficient material for determining p53 and BAX protein levels by western blot analysis. We found that CD34$^+$ cells from CML-CP patient

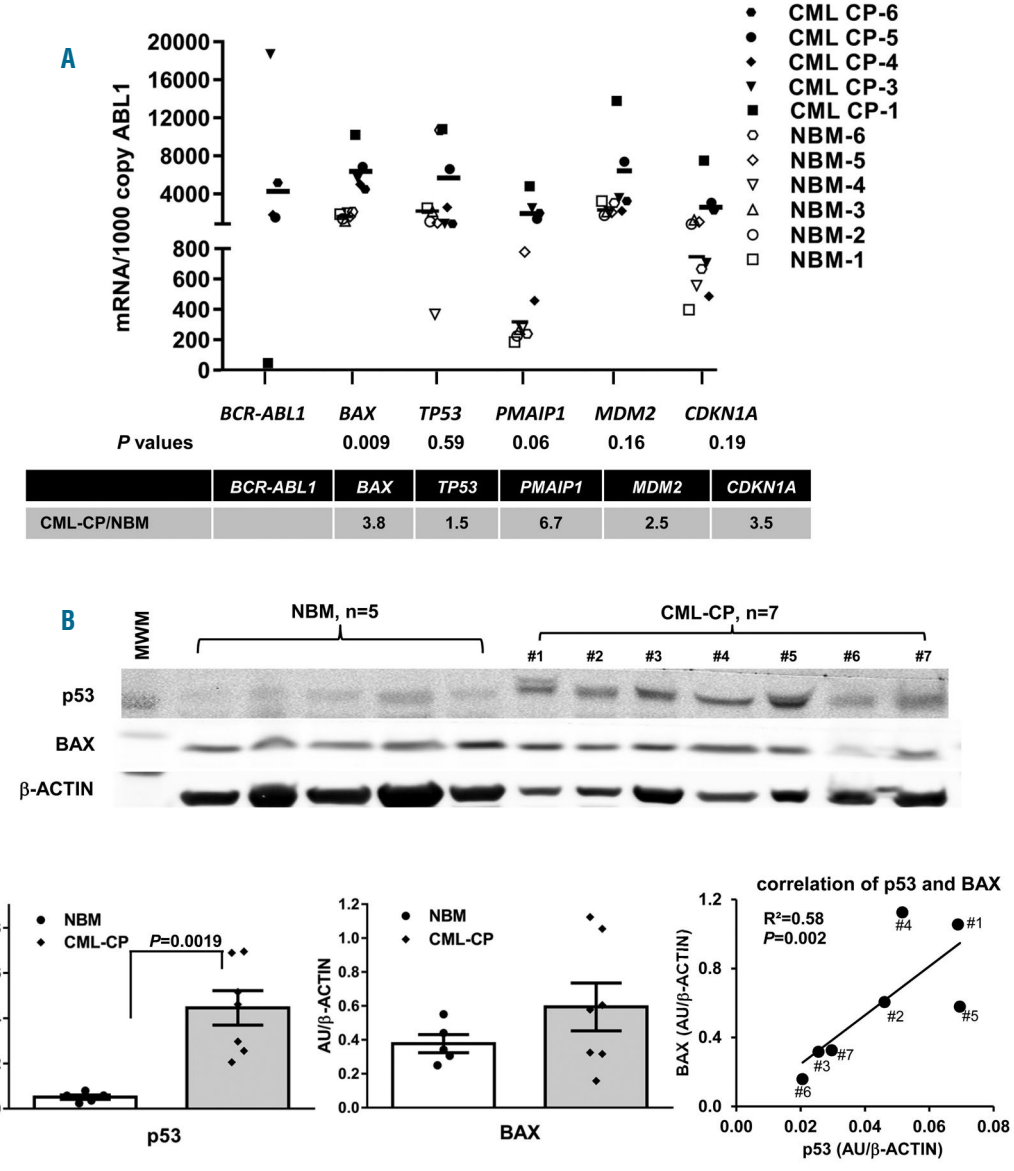

Figure 2. Expression of p53 and target genes in samples from patients with chronic phase chronic myeloid leukemia (CML)-CP and normal bone marrow (BM) controls (NBM). RNA and protein lysates were prepared from freshly collected samples and CML samples were obtained from untreated newly diagnosed CML-CP patients. (A) RNA levels of *TP53* and its target genes in CML patient samples (n=5) and NBM controls (n=6), determined by Taq-Man real-time polymerase chain reaction. (B) p53 and BAX protein levels in CD34$^+$ cells of NBM (n=5) or of untreated newly diagnosed CML-CP patients (n=7) were determined by western blot analysis and the correlation of the two proteins in patient samples was shown. MWM: molecular weight markers. Error bars indicate standard error of the mean.

samples expressed statistically significantly higher p53 (P=0.019) and, although non-significant, higher BAX protein levels, and that p53 and BAX levels in the CML-CP samples were highly correlated (R^2=0.58, P=0.002) (Figure 2B). Note among the seven CML-CP samples tested, sample #6, that had the lowest levels of p53 and BAX, was a PB sample. All of the other samples were derived from BM. All the normal controls were derived from BM.

Bone marrow lineage-SCA-1$^+$C-KIT$^+$ cells from chronic myeloid leukemia mice are sensitive to BH3 peptide-induced apoptosis

Induction of apoptosis is one of the major functions of p53, which occurs primarily through transcriptional activation of pro-apoptotic BCL-2 family proteins such as BAX and NOXA. Our previous study of the overexpression of BCL-2 proteins[20] and the present assessment of

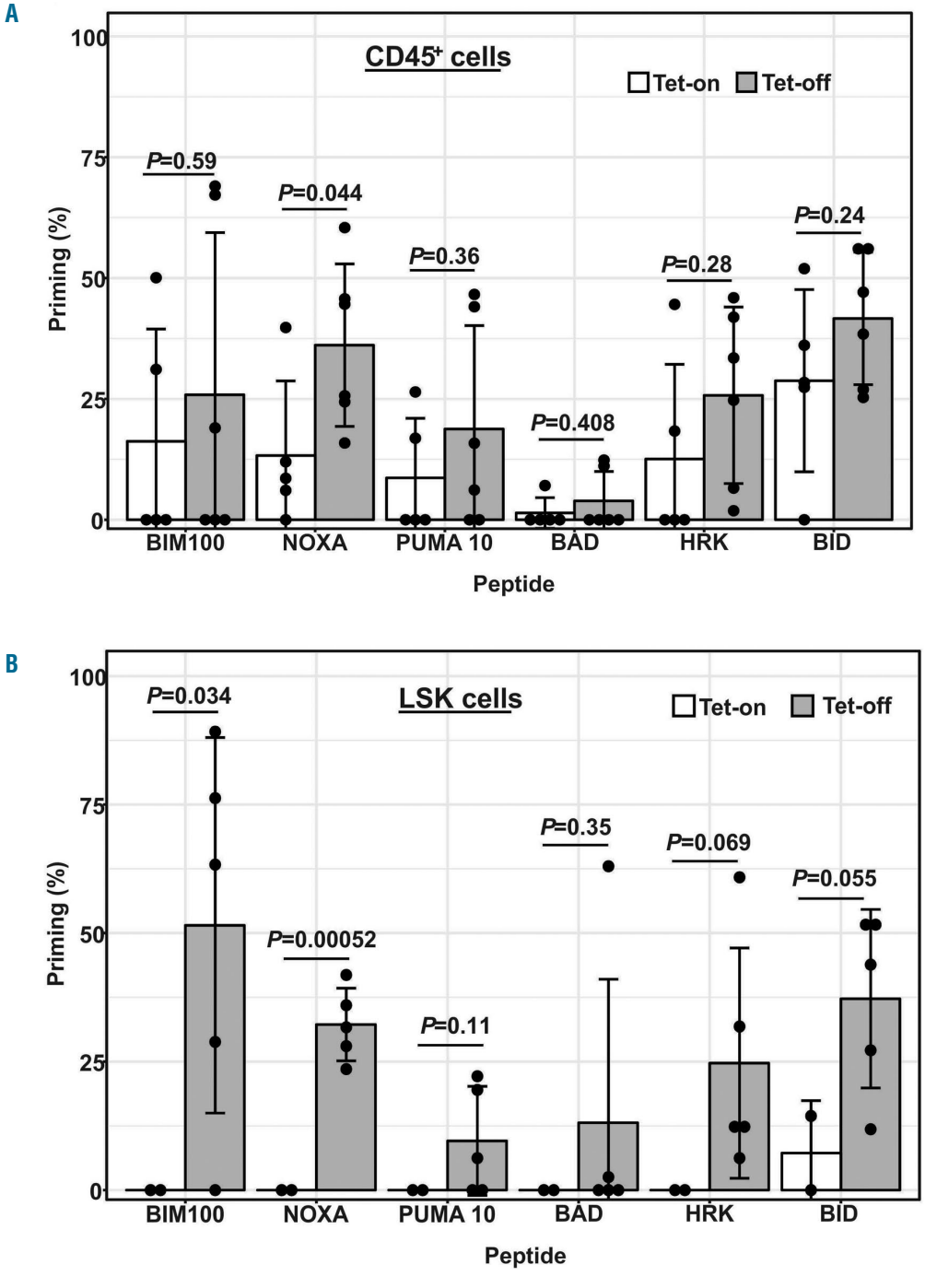

Figure 3. Priming analysis of bone marrow (BM) cells from Tet-off chronic myeloid leukemia (CML) and Tet-on control mice to BH3 peptides. BM cells were treated with various BH3 peptides (PUMA, 10 μM; all others, 100 μM) for 2 hours and 15 minutes. CD45$^+$ or lineage-SCA-1$^+$C-KIT$^+$ (LSK) cells were analyzed using flow cytometry after the cells were stained with JC-1 and priming was calculated for each peptide. Error bars indicate standard error of the mean. BM cells were collected from mice 3-4 weeks after tetracycline cessation (Tet-off) (n=6) or from age-matched controls (Tet-on) (n=5). (A) Results of CD45$^+$ cells (n=6 for Tet-off and n=5 for Tet-on). (B) Results of LSK cells (n=5 for Tet-off and n=2 for Tet-on).

increased p53 signaling in the BM of CML mice suggested that CML cells are protected from cell death, but possibly could still have a propensity for p53-mediated apoptosis. Consequently, they could be more sensitive to BH3 peptides than normal controls. To test this, we treated BM cells from Tet-off CML (n=6) and Tet-on control (n=5) mice with various BH3 peptides in order to assess the pool of sequestered pro-apoptotic, BH3-only proteins (priming) in CD45$^+$ and CD45$^+$LSK cells. Owing to the limited number of cells available in the LSK population, priming results were calculated for only those samples in which sufficient LSK cells (>10 cells) were measured (n=5 for Tet-off and n=2 for Tet-on).

Although the variations were large, (likely due, in part,

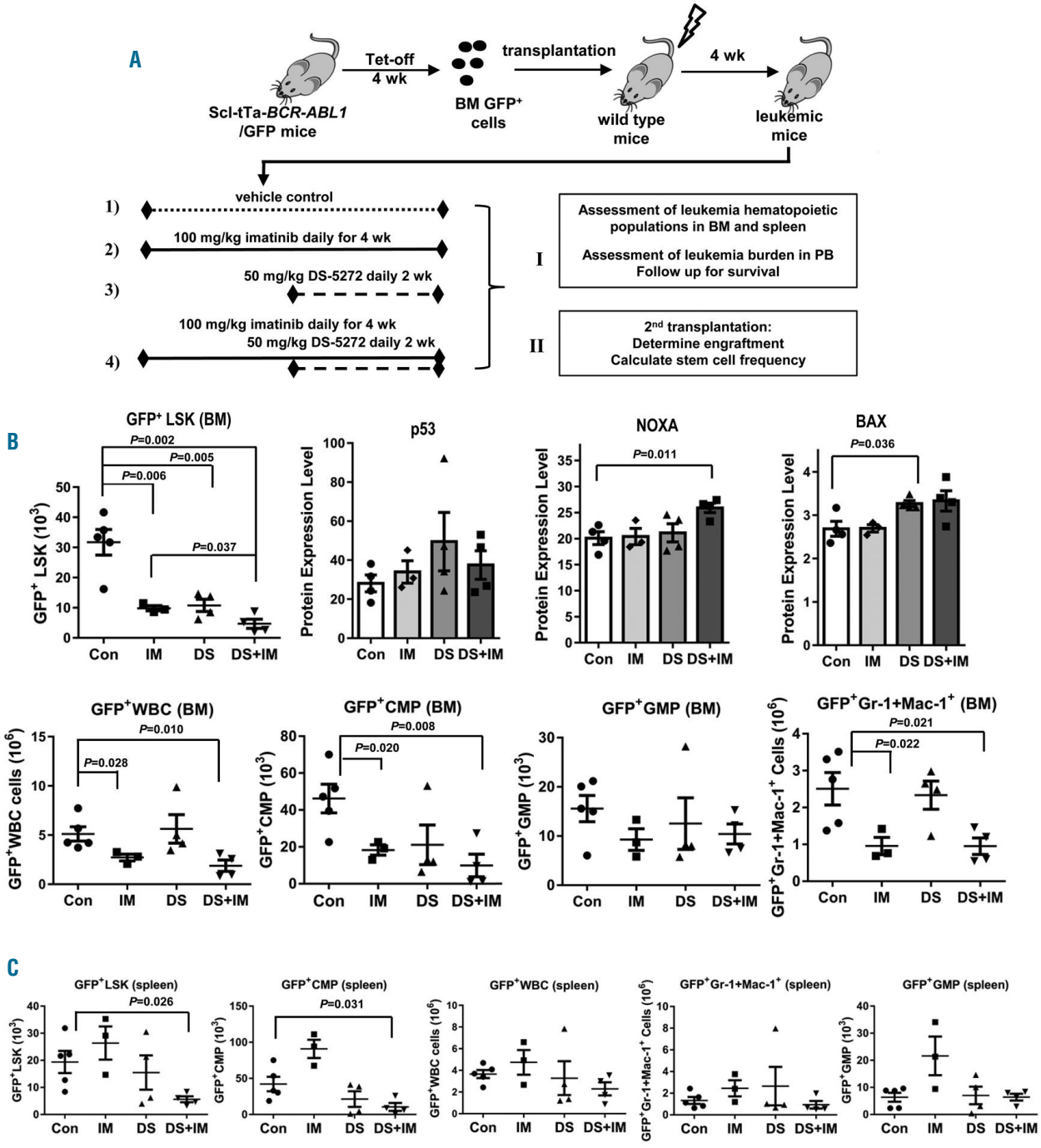

Figure 4. Effects of combined activation of p53 by MDM2 inhibition and inhibition of BCR-ABL1 by imatinib *in vivo*. (A) Experimental scheme. (B) The combination of the MDM2 inhibitor DS-5272 (DS) and imatinib (IM) significantly decreases chronic myeloid leukemia (CML) lineage-SCA-1$^+$C-KIT$^+$ (LSK) frequency, increases p53 signaling in CML LSK cells, and reduces leukemia cells in various cell subsets in mouse bone marrow (BM). (C) The combination of DS and IM significantly decreases CML LSK frequency and reduces leukemia cells in various cell subsets in the mouse spleen. The analysis was carried out in cells collected at the end of the treatments. Con: control. (B and C) N=3, 4, and 4 for IM, DS, and IM+DS treatment groups; respectively. In the control group, n=5 for measuring CML cell numbers in various populations, and n=4 for determining protein levels by CyTOF mass cytometry.

to limited cell numbers in some samples), CML mouse BM CD45$^+$ cells tended to be more sensitive to the BH3 peptides tested, but were statistically significantly more sensitive than cells from control mice to the NOXA peptide (P=0.044) (Figure 3A). CML mouse BM LSK cells overall were statistically significantly more sensitive to BH3 peptides, especially to BIM (P=0.034) and NOXA (P=0.00052), than were controls (Figure 3B). These results indicated that CML cells, and stem/progenitor cells, were more sensitive to BH3 peptide-induced apoptosis than controls.

Combined activation of p53 and inhibition of BCR-ABL1 demonstrates strong anti-leukemia activity and inhibits leukemic lineage-SCA-1$^+$C-KIT$^+$cells in chronic myeloid leukemia mice

Bone marrow cells from Tet-off Scl-tTa-*BCR-ABL1*/GFP mice were injected into irradiated recipient FVB/N mice. After confirming the development of neutrophilic leukocytosis in PB (4 weeks after cell injection), mice were untreated, or treated with imatinib, DS-5272, or the combination, following the scheme shown in Figure 4A. At the

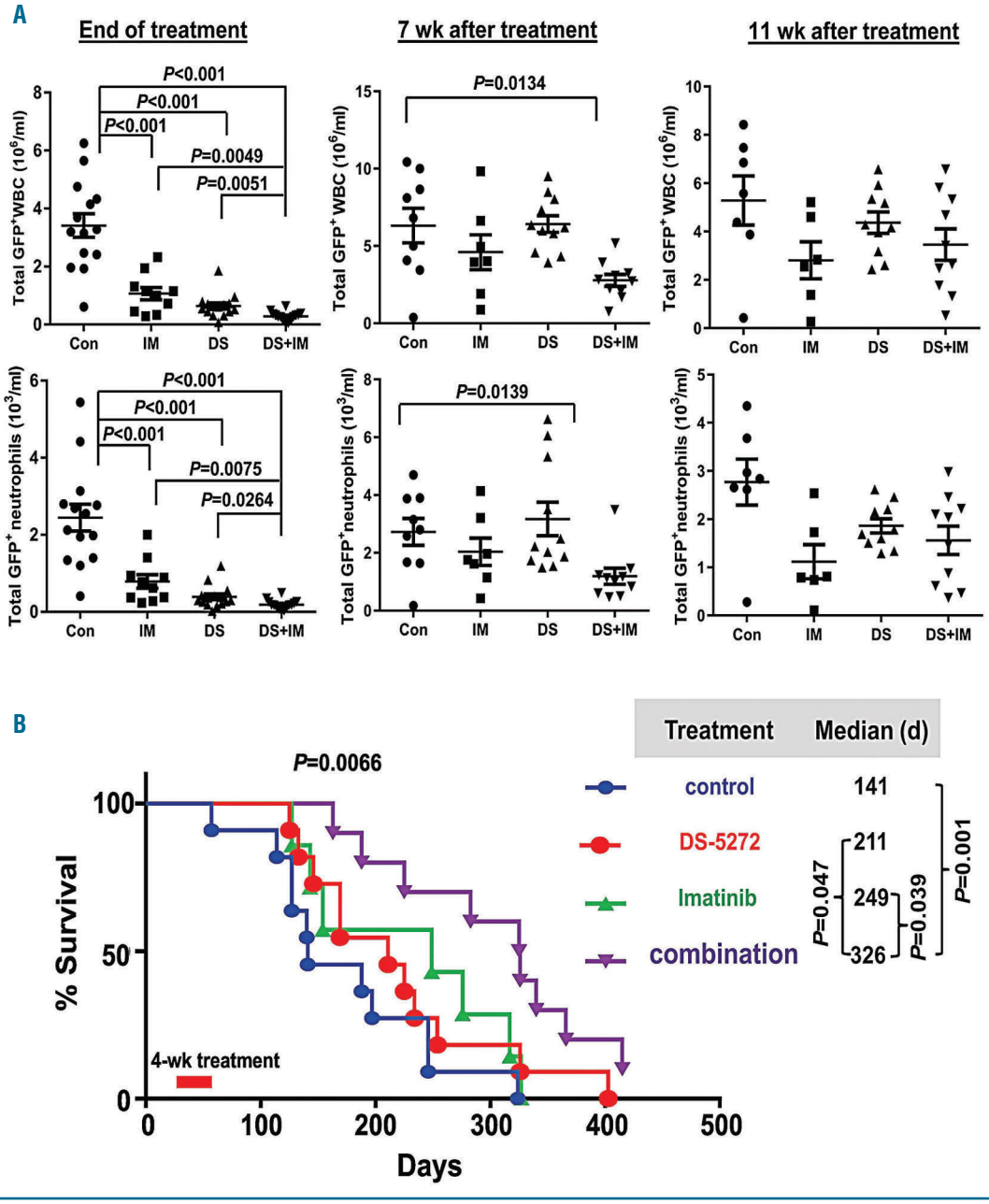

Figure 5. Anti-leukemia activity of combined activation of p53 by MDM2 inhibition and inhibition of BCR-ABL1 by imatinib in a mouse model of chronic myeloid leukemia (CML). (A) Leukemia burden in each treatment group at the end of treatments and 7 and 11 weeks (wk) after treatments was assessed using flow cytometry measuring total GFP$^+$ white blood cell (WBC) count and neutrophils in mouse peripheral blood (PB). Con: control; IM: imatinib; DS: DS-5272. (B) Kaplan-Meier curves for overall survival. Each dot/mark represents the result from an individual mouse; d: days.

end of the 4-week treatments, BM and spleen cells were collected (n=3-5 from each group) and leukemia hematopoiesis was analyzed. Flow cytometry analysis showed that the number of GFP$^+$LSK cells was significantly reduced in the BM in all treatment groups compared to controls (Figure 4B). The combination was the most effective (P=0.002 *vs.* control; GFP$^+$LSK cell numbers in combination was 14.9% of that in control group) and was statistically significantly better than imatinib alone (P=0.037) (Figure 4B). The combination also statistically significantly decreased the number of GFP$^-$LSK cells (P=0.026 *vs.* control), but to a much lesser degree, and GFP$^-$LSK cells in the combination treated group was 38.5% of that in the control, suggesting that a therapeutic window exists for the respective treatments (*Online Supplementary Figure S1A*).

We determined the levels of p53 and its target proteins in the LSK cell population by CyTOF mass cytometry and observed some increases in these proteins, particularly significant increases of NOXA in the combination group and BAX in the DS-5272-treated group (Figure 4B). BAX level was also increased in the combination group, but did not reach statistical significance (Figure 4B). Imatinib and the combination also statistically significantly decreased the number of GFP$^+$ WBC, common myeloid progenitor (CMP) cells, and mature myeloid cells, and granulocyte-monocyte progenitor (GMP) cells were not significantly

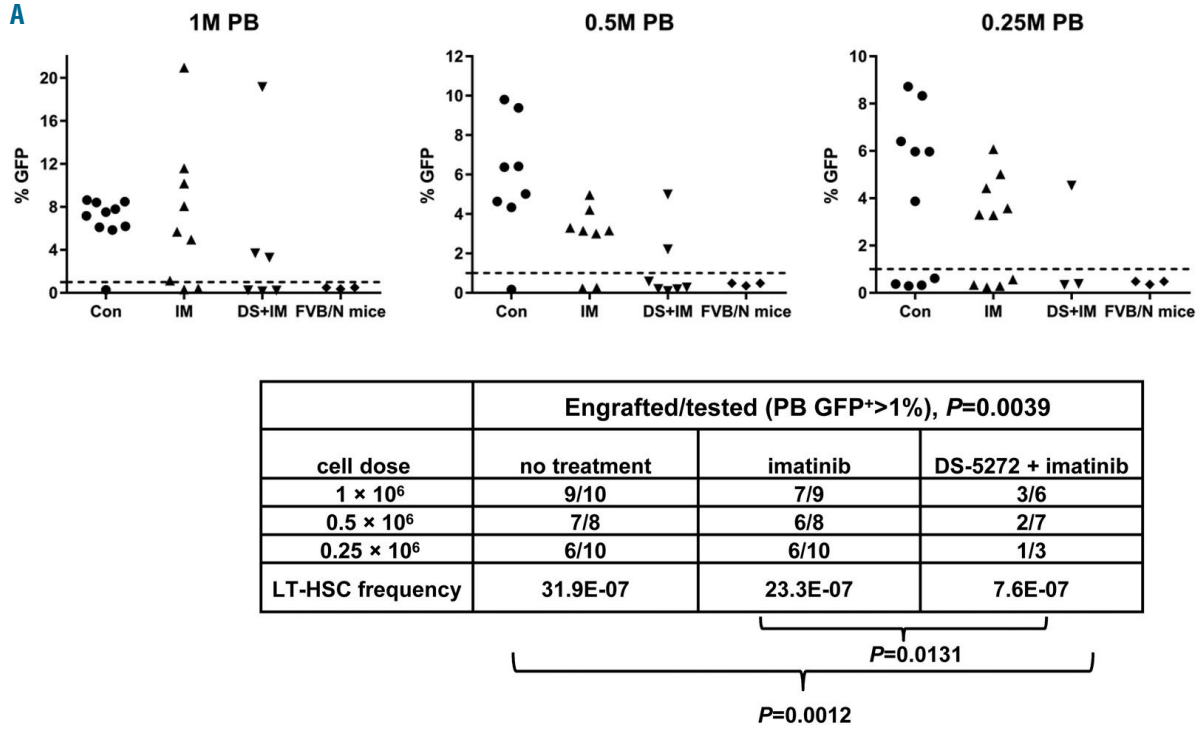

	Engrafted/tested (PB GFP$^+$>1%), P=0.0039		
cell dose	no treatment	imatinib	DS-5272 + imatinib
1 × 10^6	9/10	7/9	3/6
0.5 × 10^6	7/8	6/8	2/7
0.25 × 10^6	6/10	6/10	1/3
LT-HSC frequency	31.9E-07	23.3E-07	7.6E-07

P=0.0131

P=0.0012

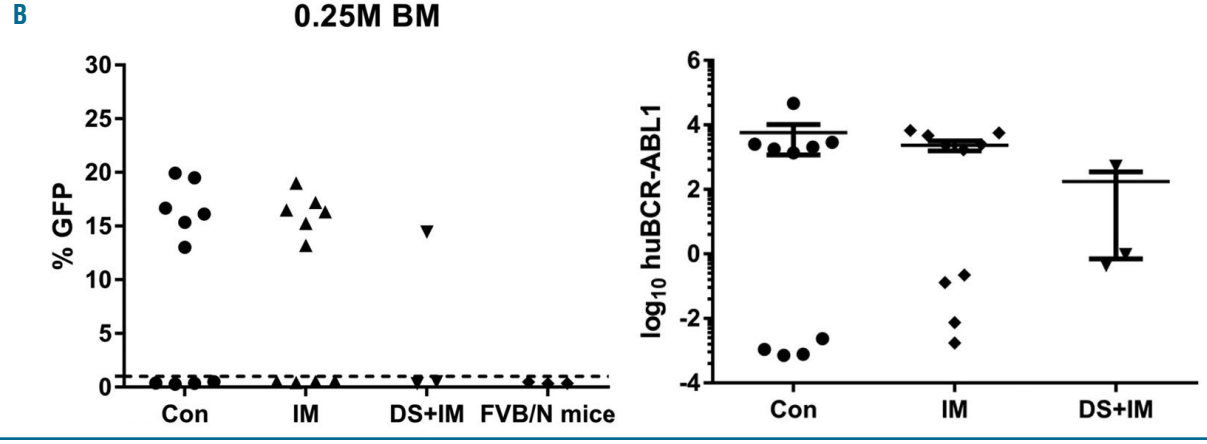

Figure 6. Effects of combined inhibition of MDM2 and BCR-ABL1 on chronic myeloid leukemia (CML) stem cells *in vivo* after secondary transplantation. (A) Green fluorescent protein (GFP) positivity (top panels) and numbers of engrafted *versus* total transplanted mice and leukemia long-term hematopoietic stem cell (LT-HSC) frequency (lower panel) are shown at 16 weeks after secondary transplantation in peripheral blood (PB) of mice injected with various cell dilutions for each treatment group. (B) GFP positivity at 16 weeks after secondary transplantation in bone marrow (BM) of mice injected with 0.25x10^6 cells/mouse in each treatment group, as well as BM *BCR-ABL1* RNA levels in these mice. Each dot/mark represents the result from an individual mouse. M: one million cells.

affected by the treatments (Figure 4B) at this time point.

Although we did not observe decreased spleen leukemic hematopoiesis by imatinib (but rather some increase) or DS-5272, the combination statistically significantly reduced leukemia GFP$^+$LSK (Figure 4C), while neither single agent alone, nor their combination, statistically significantly altered the number of GFP$^-$LSK in mouse spleen (*Online Supplementary Figure S1B*). In addition, the combination also statistically significantly decreased GFP$^+$CMP cells in spleen and tended to reduce leukemia WBC and mature myeloid cells (Figure 4C). Again, the treatments did not affect GMP cells in the spleen.

Mice that received DS-5272 were treated for only two weeks during the second half of the treatment (Figure 4A). Although DS-5272 by itself did not statistically significantly decrease CML cells in several cell populations, it greatly enhanced the activity of imatinib, especially in suppressing GFP$^+$LSK cells, both in BM and spleen.

To further assess the anti-leukemia activity of each agent and the combination, we determined circulating leukemia at the end of and at 7 and 11 weeks after treatments by flow cytometry measurement of GFP$^+$ total WBC and GFP$^+$ neutrophils. As shown in Figure 5A, at the end of the treatments, all treated groups had statistically significantly fewer GFP$^+$WBC and neutrophils compared with the control group (P<0.001), and the combination was statistically significantly more effective than imatinib (P<0.01 for both WBC and neutrophils) or DS-5272 alone (P<0.01 for WBC and P=0.0264 for neutrophils; left panel). At 7 weeks after treatments, only the combination group demonstrated statistically significant decreases in GFP$^+$WBC (P=0.0134) and GFP$^+$ neutrophils (P=0.0139) compared with the control group (middle panel). At 11 weeks after treatments, although all treatment groups still showed lower leukemia burden compared with controls, no statistical significance was reached (right panel). However, only 50% (7 of 14) of mice in the control group, compared to 60% (6 of 10) in the imatinib-treated group, 67% (10 of 15) in the DS-5272-treated group, and 71% (10 of 14) in the combination treatment group, remained alive at the end of treatment.

Treatments greatly improved overall survival in CML-bearing mice (P=0.0066) (Figure 5B). Although not statistically significant, the median overall survival for the DS-5272 or imatinib group was 211 and 249 days, respectively; both were markedly longer than that of the untreated control group (141 days). The mice treated with the combination had a median overall survival of 326 days, which was statistically significantly longer than that of the control (P=0.001), the imatinib-treated (P=0.039), and the DS-5272-treated (P=0.047) groups. The mice seemed to tolerate the treatments well. No obvious weight loss was observed in the treated mice (*Online Supplementary Figure S2*).

These data indicated that, like imatinib, inhibition of MDM2 by DS-5272 also had anti-leukemia activity in CML, and the combination had significantly more than each agent alone. The mice treated with the combination had deeper and longer lasting responses, suggesting that combined inhibition of MDM2 and BCR-ABL1 may target CML stem cells.

Combined inhibition of MDM2 and BCR-ABL1 targets chronic myeloid leukemia stem cells in BCR-ABL1 transgenic mice

To determine whether combined inhibition of MDM2 and BCR-ABL1 targeted CML stem cells, we carried out another set of experiments (see Figure 4A). At the end of treatments, BM cells were obtained from each group for the secondary transplantation. Unfortunately, we did not obtain sufficient cells from the DS-5272 treatment group and the secondary transplantation was conducted using only cells from the untreated control and imatinib or imatinib/DS-5272 treated mice. The number of mice with evidence of engraftment in PB at 16 weeks was determined by flow cytometry. Engraftment was defined as GFP levels >1% (above the background levels in the PB of FVB/N mice without cell injection).

Figure 6A shows the percentage of GFP$^+$ cells in PB samples of mice injected with various amounts of cells from mice treated with different agents. Based on the engrafted and total mice transplanted in each group, we calculated the leukemia LT-HSC frequency. The CML LT-HSC frequency was statistically significantly different among the groups (P=0.0039) (Figure 6A), and statistically significantly decreased by the combination treatment compared with imatinib alone (P=0.0131) or the untreated control (P=0.0012). No statistically significant difference was observed between imatinib-treated and untreated groups (P=0.38), as expected. For every LT-HSC detected in the combination-treated group, three times as many cells were detected in the imatinib group, and four times as many cells were detected in the control group.

We also collected BM cells from mice that received $0.25x10^6$ cells/mouse and determined GFP positivity by flow cytometry and BCR-ABL1 RNA levels by RT-PCR. As shown in Figure 6B, engraftment rates in BM were similar to those in PB samples (Figure 6A). The number of mice showing markedly lower BM BCR-ABL1 RNA levels (3 logs lower than that in controls) was consistent with the number of mice with GFP <1% in both BM and PB samples (Figure 6B).

Discussion

Effectively treating patients with blast crisis CML, and eradicating CML stem cells to achieve cures and prevent disease progression to blast crisis, are two major challenges facing CML therapy. We previously reported that combination of TKI with a MDM2 inhibitor enhanced apoptosis induction in not only proliferating but also quiescent blast crisis CML progenitor cells *in vitro*.[27] In the current study, we investigated if this combination strategy has the potential to target CML stem cells and improve cure rates in CML-CP.

Using an inducible transgenic Scl-tTa-BCR-ABL1 mouse model, we demonstrated that CML and CML stem/progenitor cells have increased p53 signaling and are more sensitive to BH3 peptide-induced apoptosis. This increase was further validated in samples obtained from patients with newly-diagnosed CML compared with normal BM controls, indicating oncogenic induction of p53. This observation supports the idea that CML cells have a propensity to death induction, and activation of p53 by MDM2 inhibition sensitizes CML to TKI. Indeed, we demonstrated that combined inhibition of MDM2 and BCR-ABL1 activated p53 signaling, targeted CML stem/progenitor cells, prolonged mouse survival, and decreased CML LT-HSC.

In contrast to the report by Abraham *et al.*,[24] we found

increased levels of p53 and several of its targets in CML BM cells compared to those from normal controls, in both mouse models and human samples. These findings are consistent with a previous report that the BCR-ABL1 fusion protein in CML cells promotes p53 accumulation, but antagonizes its activity by modulating the p53-MDM2 regulatory loop.[33] A recent study also showed that CD34$^+$ progenitor cells from CML-CP patients expressed statistically significantly higher phosphorylated p53 (Ser15) compared to CD34$^+$ cells from health donors.[34]

We found that pro-apoptotic BAX and NOXA were increased in CML cells compared with normal controls. BCR-ABL1 is known to up-regulate anti-apoptotic proteins such as MCL-1 and BCL-XL to support CML cell survival. We previously reported higher anti-apoptotic BCL-2 levels in CML cells and LSK cells in the same mouse model.[20] These anti-apoptotic BCL-2 proteins likely antagonize the pro-apoptotic BCL-2 proteins tilting the balance towards cell survival, which makes CML cells more dependent on anti-apoptotic BCL-2 proteins. This notion is consistent with our results showing that BM CD45$^+$ cells and LSK cells from the CML mice were more sensitive to BH3 peptide-induced apoptosis than those cells from the control mice. Furthermore, it was previously reported that, although imatinib does not directly affect p53 levels, it abrogated nutlin-3-induced p21,[35] which is known to block the cell cycle and suppress apoptosis.[36]

We were able to detect increased p53, NOXA, and BAX in CML LSK cells from mouse BM treated with DS-5272, or the combination, 24 hours after treatments. The short in vivo half-life of DS-5272 may contribute to the diminished induction of p53 and its target proteins. It is important to point out that although TKI are inactive against CML stem cells, they do inhibit BCR-ABL1 activity in these cells.[6] The balance of pro- and anti-apoptotic proteins decides cell death or survival. Activation of p53-induced apoptotic signaling by MDM2 inhibition together with inhibition of BCR-ABL1-regulated survival pathway by TKI likely push CML cells/stem cells towards death. This is supported by our previous study in blast crisis CML demonstrating that nutlin3a induced p53 and pro-apoptotic proteins PUMA and BAX, while nilotinib suppressed BCR-ABL1 signaling and decreased anti-apoptotic proteins BCL-XL and MCL-1, and that their combination synergistically induced cell death even in blast crisis CML cells resistance to TKI.[27] Wendel *et al*. reported that loss of p53 hampers the anti-leukemia response to BCR-ABL inhibition in a BCR-ABL1 transgenic mouse model,[37] suggesting that activation of p53 signaling may enhance TKI activities in CML.

You *et al*. recently demonstrated that JNJ-26854165, another MDM2 inhibitor, is active in CML cells through promoting BCR-ABL proteosomal degradation, independent of p53.[38] This is not surprising since several reports have shown p53-independent anticancer activity of JNJ-26854165.[39-41] DS-5272, derived from a candidate MDM2 inhibitor by chemical modifications to improve its potency and physicochemical property, is a highly selective and potent MDM2 inhibitor.[42] Although we cannot state that DS-5272 works entirely in a p53-dependent manner, especially since MDM2 has functions other than antagonizing p53, its use alone or in combination with a TKI increased p53, NOXA, and BAX, suggesting that it functions, at least in part, through increasing the p53 signaling.

Tyrosine kinase inhibitors have been proven to be highly effective in controlling CML, but in most cases they do not cure the disease. Although imatinib significantly deceased CML LSK cells in BM at the end of the treatment in the transgenic mouse model, the combination was more effective. Imatinib had no effect on spleen leukemia LSK. The different effects of imatinib on BM and spleen CML LSK is not clear and it may involve microenvironmental factors. However, the combination also significantly decreased spleen CML LSK cells. Importantly, imatinib by itself did not significantly reduce leukemia LT-HSC frequency in second transplantation, but rather did so only when combined with DS-5272. Similarly, nilotinib itself also did not decrease leukemia LT-HSC frequency in a second transplantation, as shown in our previous study.[20]

The mechanism of BCR-ABL1-driven p53 activation is not fully understood. However, BCR-ABL1-mediated hyper-proliferative signals likely contribute to the activation. The combination of MDM2 inhibition and TKI profoundly prolonged overall survival in our mouse model. In addition to modulating apoptosis regulators, other pathways may also be involved. For example, it was reported that TKI nilotinib inhibits MDM2 and induces a p53-independent apoptosis by down-regulating XIAP.[43] Kojima *et al*.[44] showed that inhibition of MDM2 with nutlin decreased CXCL12 in stromal cells, a critical component of the BM microenvironment that supports leukemia-BM microenvironment interactions and confers drug resistance. Furthermore, whether mouse immunity is regulated by the combination treatment is unknown, which warrants future investigation.

Data from this study, together with our previous report in blast crisis CML,[27] demonstrate that combined inhibition of MDM2 and BCR-ABL1 tyrosine kinase can target CML cells and CML stem/progenitor cells, and it has the potential to overcome TKI resistance and significantly improve outcomes in CML. Furthermore, we have demonstrated that BCL-2 is a key survival factor of CML stem cells, and targeting BCL-2, combined with a TKI, had the potential to eradicate CML stem cells.[20] Adding a MDM2 inhibitor, which activates p53 and induces pro-apoptotic BCL-2 proteins to the combination, will likely further improve the therapeutic potential for patients with CML, which certainly warrants future clinical investigations.

Funding

The authors would like to thank the research funding from Daiichi Sankyo (to BZC) and by National Institutes of Health grants P01CA49639 and P30CA016672 and the Paul and Mary Haas Chair in Genetics (to MA) and by NCI-SBIR grant 2R44CA203610-02A1 (to Eutropics) for supporting this study.

Acknowledgments

Erica Goodoff from Scientific Publication at MD Anderson Cancer Center and Numsen Hail, Jr. for editing and assisting with the manuscript preparation.

References

1. Heisterkamp N, Stephenson JR, Groffen J, et al. Localization of the c-ab1 oncogene adjacent to a translocation break point in chronic myelocytic leukaemia. Nature. 1983;306(5940):239-242.
2. Nowell PC, Hungerford DA. Chromosome studies in human leukemia. II. Chronic granulocytic leukemia. J Natl Cancer Inst. 1961;27:1013-1035.
3. Rowley JD. Letter: A new consistent chromosomal abnormality in chronic myelogenous leukaemia identified by quinacrine fluorescence and Giemsa staining. Nature. 1973;243(5405):290-293.
4. Holyoake T, Jiang X, Eaves C, Eaves A. Isolation of a highly quiescent subpopulation of primitive leukemic cells in chronic myeloid leukemia. Blood. 1999;94(6):2056-2064.
5. Copland M, Hamilton A, Elrick LJ, et al. Dasatinib (BMS-354825) targets an earlier progenitor population than imatinib in primary CML but does not eliminate the quiescent fraction. Blood. 2006;107(11):4532-4539.
6. Corbin AS, Agarwal A, Loriaux M, Cortes J, Deininger MW, Druker BJ. Human chronic myeloid leukemia stem cells are insensitive to imatinib despite inhibition of BCR-ABL activity. J Clin Invest. 2011;121(1):396-409.
7. Graham SM, Jorgensen HG, Allan E, et al. Primitive, quiescent, Philadelphia-positive stem cells from patients with chronic myeloid leukemia are insensitive to STI571 in vitro. Blood. 2002;99(1):319-325.
8. Mahon FX, Rea D, Guilhot J, et al. Discontinuation of imatinib in patients with chronic myeloid leukaemia who have maintained complete molecular remission for at least 2 years: the prospective, multicentre Stop Imatinib (STIM) trial. Lancet Oncol. 2010;11(11):1029-1035.
9. Rea D, Nicolini FE, Tulliez M, et al. Discontinuation of dasatinib or nilotinib in chronic myeloid leukemia: interim analysis of the STOP 2G-TKI study. Blood. 2017;129(7):846-854.
10. Ross DM, Branford S, Seymour JF, et al. Safety and efficacy of imatinib cessation for CML patients with stable undetectable minimal residual disease: results from the TWISTER study. Blood. 2013;122(4):515-522.
11. Saussele S, Richter J, Hochhaus A, Mahon FX. The concept of treatment-free remission in chronic myeloid leukemia. Leukemia. 2016;30(8):1638-1647.
12. Carter BZ, Andreeff M. Eradication of CML stem cells. Oncoscience. 2016;3(11-12):313-315.
13. Hamad A, Sahli Z, El Sabban M, Mouteirik M, Nasr R. Emerging therapeutic strategies for targeting chronic myeloid leukemia stem cells. Stem Cells Int. 2013;2013:724360.
14. Holyoake TL, Vetrie D. The chronic myeloid leukemia stem cell: stemming the tide of persistence. Blood. 2017;129(12):1595-1606.
15. Zhang B, Strauss AC, Chu S, et al. Effective targeting of quiescent chronic myelogenous leukemia stem cells by histone deacetylase inhibitors in combination with imatinib mesylate. Cancer Cell. 2010;17(5):427-442.
16. Zhou H, Mak PY, Mu H, et al. Combined inhibition of beta-catenin and Bcr-Abl synergistically targets tyrosine kinase inhibitor-resistant blast crisis chronic myeloid leukemia blasts and progenitors in vitro and in vivo. Leukemia. 2017;31 (10):2065-2074.
17. Goff DJ, Court Recart A, Sadarangani A, et al. A Pan-BCL2 inhibitor renders bone-marrow-resident human leukemia stem cells sensitive to tyrosine kinase inhibition. Cell Stem Cell. 2013;12(3):316-328.
18. Kuroda J, Kimura S, Strasser A, et al. Apoptosis-based dual molecular targeting by INNO-406, a second-generation Bcr-Abl inhibitor, and ABT-737, an inhibitor of anti-apoptotic Bcl-2 proteins, against Bcr-Abl-positive leukemia. Cell Death Differ. 2007;14(9):1667-1677.
19. Mak DH, Wang RY, Schober WD, et al. Activation of apoptosis signaling eliminates CD34+ progenitor cells in blast crisis CML independent of response to tyrosine kinase inhibitors. Leukemia. 2012;26(4):788-794.
20. Carter BZ, Mak PY, Mu H, et al. Combined targeting of BCL-2 and BCR-ABL tyrosine kinase eradicates chronic myeloid leukemia stem cells. Sci Transl Med. 2016;8(355):355ra117.
21. Miyashita T, Reed JC. Tumor suppressor p53 is a direct transcriptional activator of the human bax gene. Cell. 1995;80(2):293-299.
22. Sax JK, Fei P, Murphy ME, Bernhard E, Korsmeyer SJ, El-Deiry WS. BID regulation by p53 contributes to chemosensitivity. Nat Cell Biol. 2002;4(11):842-849.
23. Yu J, Wang Z, Kinzler KW, Vogelstein B, Zhang L. PUMA mediates the apoptotic response to p53 in colorectal cancer cells. Proc Natl Acad Sci U S A. 2003;100(4):1931-1936.
24. Abraham SA, Hopcroft LE, Carrick E, et al. Dual targeting of p53 and c-MYC selectively eliminates leukaemic stem cells. Nature. 2016;534(7607):341-346.
25. Li L, Wang L, Li L, et al. Activation of p53 by SIRT1 inhibition enhances elimination of CML leukemia stem cells in combination with imatinib. Cancer Cell. 2012;21(2):266-281.
26. Peterson LF, Mitrikeska E, Giannola D, et al. p53 stabilization induces apoptosis in chronic myeloid leukemia blast crisis cells. Leukemia. 2011;25(5):761-769.
27. Carter BZ, Mak PY, Mak DH, et al. Synergistic effects of p53 activation via MDM2 inhibition in combination with inhibition of Bcl-2 or Bcr-Abl in CD34+ proliferating and quiescent chronic myeloid leukemia blast crisis cells. Oncotarget. 2015;6(31):30487-30499.
28. Huettner CS, Koschmieder S, Iwasaki H, et al. Inducible expression of BCR/ABL using human CD34 regulatory elements results in a megakaryocytic myeloproliferative syndrome. Blood. 2003;102(9):3363-3370.
29. Koschmieder S, Gottgens B, Zhang P, et al. Inducible chronic phase of myeloid leukemia with expansion of hematopoietic stem cells in a transgenic model of BCR-ABL leukemogenesis. Blood. 2005;105(1):324-334.
30. Han L, Qiu P, Zeng Z, et al. Single-cell mass cytometry reveals intracellular survival/proliferative signaling in FLT3-ITD-mutated AML stem/progenitor cells. Cytometry A. 2015;87(4):346-356.
31. Ishizawa J, Kojima K, McQueen T, et al. Mitochondrial Profiling of Acute Myeloid Leukemia in the Assessment of Response to Apoptosis Modulating Drugs. PLoS One. 2015;10(9):e0138377.
32. Hu Z, Pan XF, Wu FQ, et al. Synergy between proteasome inhibitors and imatinib mesylate in chronic myeloid leukemia. PLoS One. 2009;4(7):e6257.
33. Levav-Cohen Y, Goldberg Z, Zuckerman V, Grossman T, Haupt S, Haupt Y. C-Abl as a modulator of p53. Biochem Biophys Res Commun. 2005;331(3):737-749.
34. Ricciardi MR, Salvestrini V, Licchetta R, et al. Differential proteomic profile of leukemic CD34+ progenitor cells from chronic myeloid leukemia patients. Oncotarget. 2018;9(31):21758-21769.
35. Kurosu T, Wu N, Oshikawa G, Kagechika H, Miura O. Enhancement of imatinib-induced apoptosis of BCR/ABL-expressing cells by nutlin-3 through synergistic activation of the mitochondrial apoptotic pathway. Apoptosis. 2010;15(5):608-620.
36. Carter BZ, Mak DH, Schober WD, et al. Simultaneous activation of p53 and inhibition of XIAP enhance the activation of apoptosis signaling pathways in AML. Blood. 2010;115(2):306-314.
37. Wendel HG, de Stanchina E, Cepero E, et al. Loss of p53 impedes the antileukemic response to BCR-ABL inhibition. Proc Natl Acad Sci U S A. 2006;103(19):7444-7449.
38. You L, Liu H, Huang J, et al. The novel anticancer agent JNJ-26854165 is active in chronic myeloid leukemic cells with unmutated BCR/ABL and T315I mutant BCR/ABL through promoting proteosomal degradation of BCR/ABL proteins. Oncotarget. 2017;8(5):7777-7790.
39. Jones RJ, Gu D, Bjorklund CC, et al. The novel anticancer agent JNJ-26854165 induces cell death through inhibition of cholesterol transport and degradation of ABCA1. J Pharmacol Exp Ther. 2013;346(3):381-392.
40. Kojima K, Burks JK, Arts J, Andreeff M. The novel tryptamine derivative JNJ-26854165 induces wild-type p53- and E2F1-mediated apoptosis in acute myeloid and lymphoid leukemias. Mol Cancer Ther. 2010;9(9):2545-2557.
41. Lehman JA, Hauck PM, Gendron JM, et al. Serdemetan antagonizes the Mdm2-HIF1alpha axis leading to decreased levels of glycolytic enzymes. PLoS One. 2013;8(9):e74741.
42. Miyazaki M, Uoto K, Sugimoto Y, et al. Discovery of DS-5272 as a promising candidate: A potent and orally active p53-MDM2 interaction inhibitor. Bioorg Med Chem. 2015;23(10):2360-2367.
43. Zhang H, Gu L, Liu T, Chiang KY, Zhou M. Inhibition of MDM2 by nilotinib contributes to cytotoxicity in both Philadelphia-positive and negative acute lymphoblastic leukemia. PLoS One. 2014;9(6):e100960.
44. Kojima K, McQueen T, Chen Y, et al. p53 activation of mesenchymal stromal cells partially abrogates microenvironment-mediated resistance to FLT3 inhibition in AML through HIF-1alpha-mediated down-regulation of CXCL12. Blood. 2011;118(16):4431-4439.

ARTICLE

Phosphorylation of BECLIN-1 by BCR-ABL suppresses autophagy in chronic myeloid leukemia

Chuanjiang Yu,[1] Sivahari P. Gorantla,[1] Alina Müller-Rudorf,[1,2] Tony A. Müller,[1] Stefanie Kreutmair,[1] Corinna Albers,[3] Lena Jakob,[1] Lena J. Lippert,[1] Zhenyu Yue,[4] Monika Engelhardt,[1] Marie Follo,[1] Robert Zeiser,[1,2] Tobias B. Huber,[5,6,7] Justus Duyster[1,2] and Anna L. Illert[1,2]

[1]Department of Internal Medicine I, Medical Center, Faculty of Medicine, University of Freiburg, Freiburg, Germany; [2]German Cancer Consortium (DKTK) and German Cancer Research Center (DKFZ), Heidelberg, Germany; [3]Department of Medicine, Klinikum rechts der Isar, Technical University München, München, Germany; [4]Department of Neurology and Neuroscience, Friedman Brain Institute, Mount Sinai School of Medicine, New York, NY, USA; [5]Department of Medicine, University Medical Center Hamburg-Eppendorf, Hamburg, Germany; [6]Department of Medicine, Medical Center, Faculty of Medicine, University of Freiburg, Freiburg, Germany and [7]BIOSS Center for Biological Signalling Studies and Center for Systems Biology (ZBSA), Albert-Ludwigs-University, Freiburg, Germany

Ferrata Storti Foundation

Haematologica 2020
Volume 105(5):1285-1293

ABSTRACT

Autophagy is a genetically regulated process of adaptation to metabolic stress and was recently shown to be involved in the treatment response of chronic myeloid leukemia (CML). However, *in vivo* data are limited and the molecular mechanism of autophagy regulators in the process of leukemogenesis is not completely understood. Here we show that *Beclin-1* knockdown, but not *Atg5* deletion in a murine CML model leads to a reduced leukemic burden and results in a significantly prolonged median survival of targeted mice. Further analyses of murine cell lines and primary patient material indicate that active BCR-ABL directly interacts with BECLIN-1 and phosphorylates its tyrosine residues 233 and 352, resulting in autophagy suppression. By using phosphorylation-deficient and phosphorylation-mimic mutants, we identify BCR-ABL induced BECLIN-1 phosphorylation as a crucial mechanism for BECLIN-1 complex formation: interaction analyses exhibit diminished binding of the positive autophagy regulators UVRAG, VPS15, ATG14 and VPS34 and enhanced binding of the negative regulator Rubicon to BCR-ABL-phosphorylated BECLIN-1. Taken together, our findings show interaction of BCR-ABL and BECLIN-1 thereby highlighting the importance of BECLIN-1-mediated autophagy in BCR-ABL$^+$ cells.

Introduction

The BCR-ABL fusion kinase has been identified in more than 95% of chronic myeloid leukemia (CML) and 20% of acute lymphoblastic leukemia (ALL) cases.[1,2] Oncogenic BCR-ABL activates several aberrant kinase-dependent pathways including anti-apoptosis, proliferation and differentiation,[3,4] leading to the development of several successful tyrosine kinase inhibitors (TKI) in BCR-ABL$^+$ leukemia treatment.[5,6] However, there are still unsolved issues in TKI-based therapies for patients with CML: Suppression of the disease relies in most patients on continuous and lifelong TKI therapy[7,8] and disease relapse occurs due to emerged TKI resistance.[9-11] Thus, identification of additional important mediators could significantly improve CML therapy.

Autophagy is an evolutionarily conserved mechanism for the degradation of cytoplasmic components including organelles and proteins and plays an important role in cellular homeostasis. Because of its potential role in metabolism and cell survival, altered autophagy processes are critical for cancer cell fate. Several reports indicate

Correspondence:

ANNA LENA ILLERT
lena.illert@uniklinik-freiburg.de

Received: January 18, 2019.

Accepted: August 7, 2019.

Pre-published: August 8, 2019.

doi:10.3324/haematol.2018.212027

Check the online version for the most updated information on this article, online supplements, and information on authorship & disclosures: www.haematologica.org/content/105/5/1285

that autophagy may be a promising target pathway in BCR-ABL+ leukemia treatment.[12-18] However, the distinct role of autophagy in the process of leukemogenesis is not completely understood and crucial autophagy mediators have not been evaluated in *in vivo* leukemogenesis mouse models.

BECLIN-1, a master regulator of autophagy, is essential for the formation of the autophagosome and autolysosome as a part of the Rubicon, VPS15, VPS34, ATG14, UVRAG and BECLIN-1 complex.[19-23] An *in vitro* study has discovered that a treatment strategy combining TKI and inhibitors of BECLIN-1-mediated autophagy may be beneficial for BCR-ABL+ CML therapy,[16] but *in vivo* data are missing and the molecular mechanisms underlying this effect remain unclear.

Methods

GST-pulldown assay, immunoprecipitation and Western blotting

All *Beclin-1* fragments were cloned into PGEX-4T2 vector, which were confirmed by Sanger sequencing. Those constructs were transformed into Bl21 competent cells, and a single clone was picked for culture in LB medium at 37°C with vigorous shaking. IPTG was added when the OD600 of the bacterial suspension reached 0.6. After an additional 2 hours (h) of incubation, bacterial cells were harvested, lysed using lysozyme and sonification and incubated for 3 h with glutathione-agarose beads in NETN buffer (0.5% NP40, 20 mM Tris/HCl, 100 mM NaCl, 1 mM EDTA, 1 mM PMSF, 1 mM Benzamidin, protease inhibitor cocktail [Roche]) at 4°C. The beads were then incubated with K562 cell lysates over night at 4°C. Immunoprecipitation and Western blotting were performed as described previously.[24-26] Briefly, immunoprecipitation was performed by adding IP lysis buffer (40 mM HEPES, 120 mM NaCl, 1 mM EDTA, 10 mM pyrophosphate, 50 mM NaF, 0.3% CHAPS, 1 mM sodium orthovanadate, 1 mM glycerolphosphate, protease inhibitor cocktail) to the cells for 1 h on ice. Pre-clearing of the lysates was performed using protein A or G agarose beads, followed by incubation with anti flag beads (Sigma) or antibody plus protein A or G beads (GE healthcare) overnight at 4°C. Protein extraction for Western blotting was performed using protein lysis buffer (10 mM Tris/HCl, 130 mM NaCl, 5 mM EDTA, 0.5% Triton X-100, 20 mM Na_2HPO_4/NaH_2PO_4, 10 mM sodium pyrophosphate, 1 mM sodium orthovanadate, 20 mM NaF, 1 mM glycerole 2-phosphate, protease inhibitor cocktail).

In vitro kinase assay

In vitro kinase assay was performed as described previously.[27] Briefly, recombinant active ABL (ProQinase GmbH) was incubated with 10 μCi [γ-^{33}P]ATP (PerkinElmer) and 1 μg recombinant GST-BECLIN-1 fragment in 50 μL kinase buffer (70 mM HEPES, 25 mM β-glycerophosphate, 3 mM $MgCl_2$, 3 mM $MnCl_2$, 1.2 mM DTT, 50 μg/mL PEG20.000, and 1% DMSO). Reactions were incubated at 30°C for 40 min. Proteins were separated by 10% SDS-PAGE, and phosphorylation was visualized by autoradiography.

Flow cytometry

Flow cytometric staining was performed as previously described.[28-30]

Mice

Mice were caged in special caging system with autoclaved food and acidified water at the University of Freiburg in accordance with national and institutional guidelines for animal care. All animal studies have been approved by the Ethics committees of the University Medical Center Freiburg and the district government in Freiburg (approval no. 35-9185.81/G-13/05).

Statistics

Statistical comparisons were performed using GraphPad Prism 6 software. Detailed statistical tests and significance cutoffs are indicated in each figure legend. All data represent the mean ± standard error of the mean (SEM).

Study approval

The studies using human samples were conducted according to the Declaration of Helsinki principles. All biological samples were obtained following written informed consent from the patient and upon approval by the Ethics Committee of the University Medical Center Freiburg.

Additional methodology is provided in the *Online Supplementary Materials and Methods.*

Results

Knockdown of *Beclin-1* delays BCR-ABL-mediated leukemogenesis *in vivo*

To further investigate the impact of autophagy in CML we examined the role of BECLIN-1, a master autophagy mediator, in BCR-ABL induced transformation and colony forming assays. *Beclin-1* was downregulated using a targeted genetic approach with an individualized micro RNA-based knockdown of *Beclin-1* in BCR-ABL-overexpressing Ba/F3 cells and bone marrow derived cells (BMDC). Specific knockdown of *Beclin-1* with two individually designed siRNA resulted in significantly lower proliferation of BCR-ABL transduced Ba/F3 cells compared to cells infected with a control miR sequence (Figure 1A-B). As the secondly designed *Beclin-1* miR resulted in the most efficient *Beclin-1* knockdown, we performed all further experiments solely with *Beclin-1* miR2. We could detect higher apoptosis levels, but no decrease in cell cycle rate in *Beclin-1* miR cells (Figure 1C, *Online Supplementary Figure S1A*).

Furthermore, we could show significantly lower colony formation in BCR-ABL-expressing primary BMDC with *Beclin-1* downregulating miR in comparison to control BMDC (Figure 1D-E).

Next, we examined the effects of *Beclin-1* knockdown in a CML mouse model *in vivo*. BMDC from 5-FU pretreated animals were infected with a vector expressing BCR-ABL and the specific *Beclin-1* (pMmiRBec–BCR-ABL) or control miR sequence (pMmiRCtrl–BCR-ABL) on one construct and under the LTR promoter. Survival of mice transplanted with BCR-ABL-expressing *Beclin-1* knockdown BMDC was sustained and significantly prolonged compared to the control group (median survival 28 *vs.* 50 days, $P<0.0001$) (Figure 1F). Furthermore, the white blood cell count (WBC) and the leukemic burden of mice transplanted with *Beclin-1* knockdown BCR-ABL BMDC was significantly lower (87.3 *vs.* 14.8 x 10^3/μL on day 17, $P<0.0001$) compared to the control group (Figure 1G).

Immunoblotting of splenocyte extracts of transplanted mice confirmed efficient downregulation of *Beclin-1* one month after transplantation (Figure 1H). Upon disease induction, fluorescence-activated cell sorting (FACS) analyses of transplanted animals showed no differences in the immune phenotype of the BCR-ABL induced disease by *Beclin-1* downregulation (*Online Supplementary Figure S1B-D*). To test whether the impact of *Beclin-1* knockdown on CML cells is due to a general effect of autophagy inhibition or more due to a specific role of BECLIN-1 in BCR-ABL induced diseases, we also deleted another main autophagy regulator, ATG5 in a CML mouse model: *Atg5*

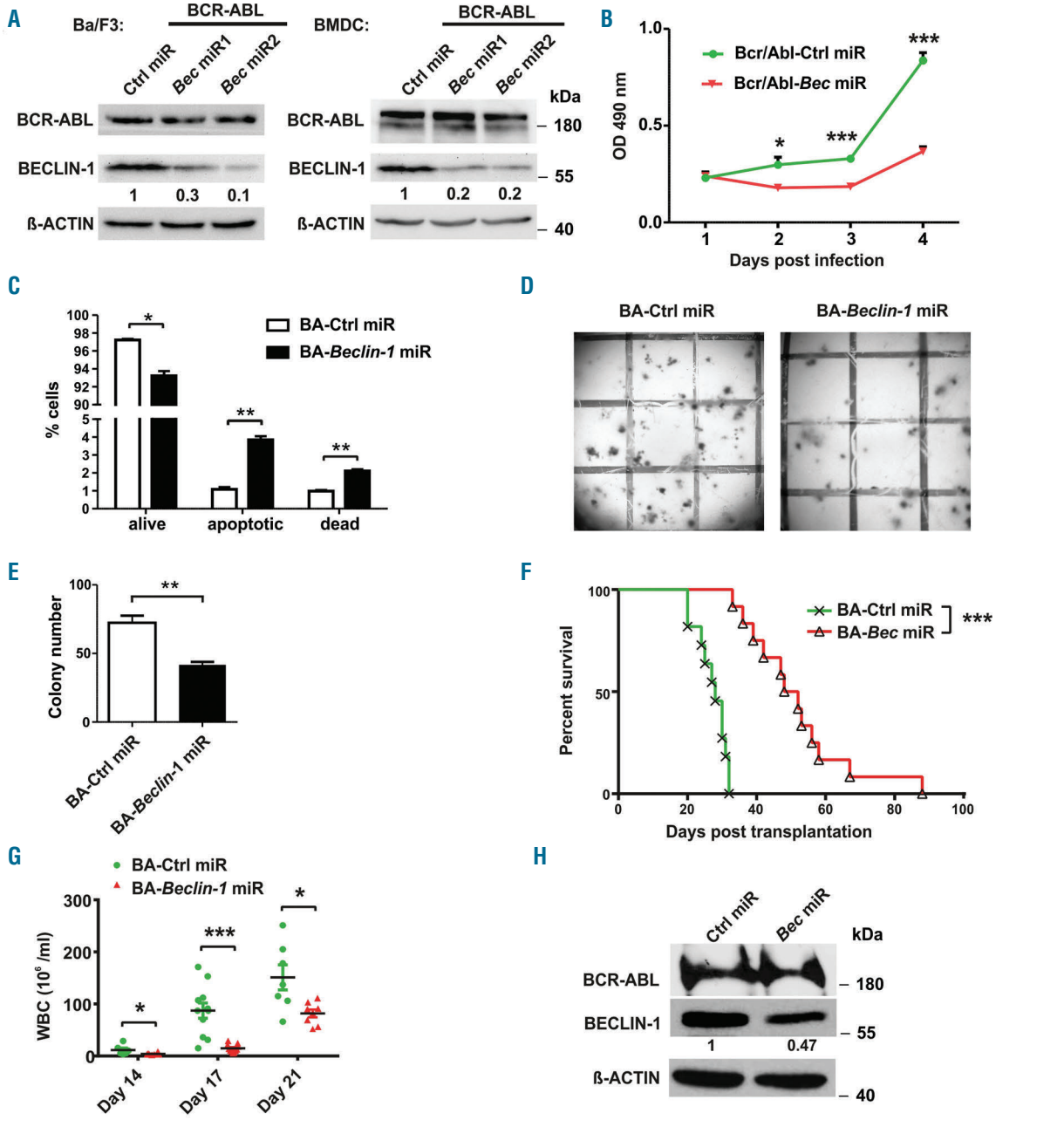

Figure 1. BECLIN-1 downregulation delays BCR-ABL-mediated proliferation *in vitro* and *in vivo*. (A) Immunoblot analyses were used to confirm downregulation of BECLIN-1 using two different *Beclin-1* directed miR in Ba/F3 cells and BMDC. (B) Cell proliferation measurement was performed by MTT assay in Ba/F3 cells infected with indicated construct towards IL-3 withdrawal, indicating that BCR-ABL-mediated cell proliferation is impaired by *Beclin-1* knockdown. ***P<0.001, *P<0.05, Student's *t*-test. (C) Statistical analysis of flow cytometric staining showing Annexin-V$^-$/ propidium iodide (PI)- ("alive"), Annexin-V$^+$/ PI$^-$("apoptotic") and Annexin-V$^+$/ PI$^+$ ("dead") Ba/F3 cells with indicated construct. **P<0.01, *P<0.05, Student's *t* test. (D) Methylcellulose (MC) colony formation assay of primary 5-FU enriched bone marrow cells showed impaired colony formation upon BCR-ABL expression in *Beclin-1* knockdown cells compared to control miR expressing cells. 1,000 EGFP$^+$ BMDC infected with the indicated construct were plated into methylcellulose in the absence of growth factors and colonies were quantified 10 days later. One representative well is shown. Three independent experiments were performed in doublets. Grid size is 5 x 5 mm. (E) Quantitation of the MC shown in (D) (72 *vs.* 55.7 colony-forming unit [CFU], *P<0.05, and 72 *vs.* 41.7 CFU, **P<0.01, respectively, student's *t*-test). (F) Kaplan-Meier curve demonstrates a significantly prolonged survival of mice transplanted with *Beclin-1* knockdown BCR-ABL+ BMDC compared to control mice (Median survival 28 *vs.* 50 days, ***P<0.001 in two independent transplantations, Log-rank test (n=11, control miR; n=13, *Beclin-1* miR)). (G) WBC from peripheral blood (PB) showed a significant reduction of leukemic progression in mice transplanted with *Beclin-1* knockdown cells (11.6 *vs.* 4 million/mL, day 14, *P<0.05; 87.3 *vs.* 14.8 million/mL, day 17, ***P<0.001; 151.1 *vs.* 81.9 million/mL, day 21, *P<0.05). (H) Efficient and durable knockdown of Beclin-1 was proven by immunoblot analyses of spleen cells of transplanted mice (day 27).

conditional knockout BMDC[31] were infected with a BCR-ABL-Cre fusion vector and transplanted into wild-type (wt) recipient mice. Interestingly, deletion of *Atg5* was not able to induce a delay in leukemia induction or progression of BCR-ABL transplanted mice (*Online Supplementary Figure S1E*). Furthermore, *Atg5* deletion had no influence on the WBC of the transplanted animals (*Online Supplementary Figure S1F*), despite efficient deletion of the floxed *Atg5* alleles upon Cre expression in BCR-ABL positive BMDC (*Online Supplementary Figure S1G*).

In order to exclude toxic effects of *Beclin-1* knockdown on normal hematopoiesis, we transplanted solely *Beclin-1* miR infected BMDC into mice, which exhibited no differences in survival, WBC or lineage phenotype compared to the control group (*Online Supplementary Figure S2A-G*).

Our results from the *in vivo* CML mouse model show a significant and specific impact of *Beclin-1* knockdown on CML disease induction.

Active BCR-ABL suppresses autophagy through the BECLIN-1 complex

It has been shown previously that BCR-ABL kinase inhibitors induce autophagy. Accordingly, inhibition of BCR-ABL kinase activity by nilotinib led to an induction of autophagy measured by increased LC3-II expression and punctual LC3 accumulation (*Online Supplementary Figure S3A-C*). To differentiate, whether the autophagy induction by nilotinib is caused by specific BCR-ABL inhibition or due to an unspecific nilotinib effect, we treated nilotinib-resistant Ba/F3-BCR-ABL-T315I cells with nilotinib and could show that this treatment failed to induce autophagy, suggesting that active BCR-ABL indeed sup-

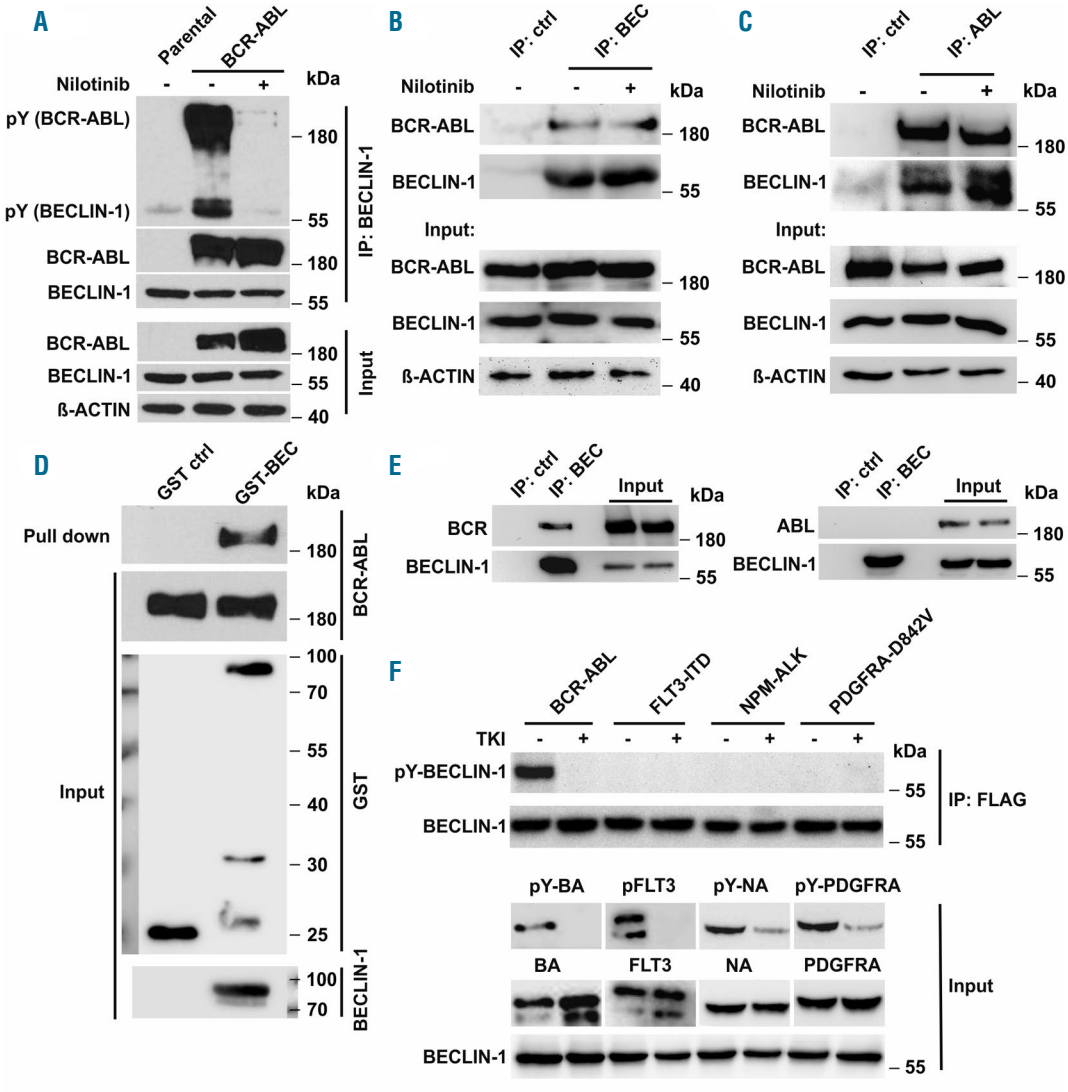

Figure 2. BCR-ABL interacts with and phosphorylates BECLIN-1. (A) Co-immunoprecipitation analyses in BCR-ABL-tranfected HEK293T cells demonstrate, that BCR-ABL strongly phosphorylates and binds BECLIN-1. A phosphotyrosine antibody was used for phospho-BECLIN-1 and phospho-BCR-ABL detection. (B) Immunoprecipitation of BCR-ABL with BECLIN-1 and (C) BECLIN-1 with ABL in K562 cells confirms the interaction reciprocally and at endogenous level. (D) GST-pull-down of BCR-ABL with recombinant GST-Beclin-1 in K562 cells corroborated the interaction between BCR-ABL and BECLIN-1. (E) BECLIN-1 immunoprecipitation in *Beclin-1* transfected HEK293T cells demonstrates that BECLIN-1 is interacting with BCR but not with ABL. (F) BECLIN-1 is exclusively phosphorylated by BCR-ABL among several oncogenic tyrosine kinases in HEK293T cells. For TKI treatment, specific inhibitors (nilotinib for BCR-ABL, sorafenib for FLT3-ITD and PDGFRA-D842V, and TAE684 for NPM-ALK) were added into medium four hours before cell harvest.

presses autophagy. Moreover, addition of interleukin-3 (IL-3), which rescues cells from nilotinib-induced cell death but does not rescue BCR-ABL inhibition, could not block autophagy (*Online Supplementary Figure S3D-F*).

Based on our mouse model data, we hypothesized that BECLIN-1 may be an essential player in autophagy suppression by BCR-ABL. BECLIN-1 has a crucial role in autophagosome formation as being part of the UVRAG-VPS15-ATG14-VPS34-RUBICON-BECLIN-1 complex. Interestingly, we could show that the formation of the UVRAG-VPS15-ATG14-VPS34-RUBICON-BECLIN-1 complex was altered in a BCR-ABL positive human cell line (K562) after nilotinib treatment (*Online Supplementary Figure S3G*): recruitment of positive regulators of autophagosome formation (VPS15, VPS34, UVRAG and ATG14) to BECLIN-1 was increased upon BCR-ABL inhibition, whereas the recruitment of the negative regulator RUBICON to BECLIN-1 was impaired after nilotinib treatment. These results indicate that BCR-ABL kinase activity modulates the BECLIN-1 complex composition and thereby leads to autophagy suppression.

BCR-ABL interacts with BECLIN-1

Next, we aimed to investigate how BCR-ABL kinase activity modulates BECLIN-1 complex composition. We found that BCR-ABL strongly binds to BECLIN-1, independent of ABL kinase activity.

Furthermore, BECLIN-1 was tyrosine phosphorylated in a complex with kinase active BCR-ABL indicating that BCR-ABL may directly phosphorylate BECLIN-1 (Figure 2A). Immunoprecipitation of endogenous BCR-ABL in K562 cells confirmed the BCR-ABL/BECLIN-1 interaction (Figure 2B-C) and GST-pulldown-assays using purified BECLIN-1 suggest that BCR-ABL and BECLIN-1 may bind directly to each other (Figure 2D).

We could also detect BCR-ABL/BECLIN-1 co-localization using immunofluorescence staining (*Online Supplementary Figure S4A*). To investigate which region of BCR-ABL binds to BECLIN-1, we performed binding assays by overexpressing either *BCR* or *ABL* together with *Beclin-1* in 293T cells. Immunoprecipitations revealed that BCR interacts with BECLIN-1 but not ABL (Figure 2E).

BCR-ABL directly phosphorylates BECLIN-1 at specific tyrosine residues Y233 and Y352

We next investigated, whether BECLIN-1 is exclusively phosphorylated by BCR-ABL. Interestingly, all other tested oncogenic kinases (FLT3-ITD, NPM-ALK and PDGFRA-D842V) failed to induce BECLIN-1 phosphorylation, implying that BECLIN-1 is a specific substrate of BCR-ABL and not a general target of oncogenic tyrosine kinase signaling (Figure 2F). Moreover, we were able to confirm BECLIN-1 tyrosine phosphorylation in all tested samples of primary CML patient material, whereas BECLIN-1 phosphorylation was absent in healthy control samples (*Online Supplementary Figure S4B*).

To test whether BECLIN-1 is a direct target of BCR-ABL we performed an *in vitro* kinase assay, and identified specific phosphorylation in two distinct regions of BECLIN-1: One spanning amino acid (aa) region 141 - 277 and another aa region 338 - 450 (Figure 3A). Furthermore, we generated a series of tyrosine residue mutants to determine specific BECLIN-1 tyrosine residues phosphorylated by BCR-ABL. Strong phosphorylation by BCR-ABL could be detected on BECLIN-1 tyrosine residues Y233 and Y352, whereas Y162 and Y338 show minor phosphorylation (Figure 3B). Western blot analyses of single and double phosphorylation-deficient mutants of those distinct BECLIN-1 tyrosine residues validated our results (Figure 3C) and demonstrated that BCR-ABL phosphorylates BECLIN-1 specifically at tyrosine residues Y233 and Y352. Interestingly, tyrosine Y352 (AA352-355 YCSG) is part of a STAT5 Src Homology 2 (SH2) domain binding motif (Y[VLTFIC]xx).[37]

Phospho-mimic mutant *Beclin-1* Y233E/Y352E suppresses autophagy through BECLIN-1 complex alterations whereas the phospho-deficient *Beclin-1* Y233F/Y352F mutant induces autophagy

To evaluate whether phosphorylation of BECLIN-1 regulates autophagy, we generated a BECLIN-1 phosphorylation-mimic (Y233E/Y352E) and a phosphorylation-deficient mutant (Y233F/Y352F). In an LC3 puncta assay in K562 cells, we found that the phosphorylation-mimic BECLIN-1 mutant suppresses autophagy, whereas the phosphorylation-deficient BECLIN-1 mutant induces increased autophagy (Figure 4A-B). By immunoblotting, we could confirm that the phosphorylation-mimic mutant Y233E/Y352E decreases autophagy, whereas expression of the phosphorylation-deficient mutant Y233F/Y352F induces autophagy (Figure 4C). Our findings therefore suggest that phosphorylation of BECLIN-1 by BCR-ABL suppresses autophagy induction.

Next we sought to know, whether the impaired autophagy induction of the phospho-mimic mutant Y233E/Y352E may be due to an altered recruitment of complex components to BECLIN-1. It has been shown recently, that lack of BECLIN-1 leads to downregulation of the BECLIN-1 complex binding partners.[38] Indeed, *Beclin-1* deficient, BCR-ABL expressing MEF showed downregulation of BECLIN-1 binding partners, which could be rescued by re-expression of either wt *Beclin-1* or both phospho-mutants ((BEC FF and EE). Furthermore, expression of the *Beclin-1* Y233E/Y352E mutant leads to decreased UVRAG and ATG14 levels, whereas Rubicon levels were increased compared to phosphorylation-deficient BECLIN-1 cells (Figure 4D).

From our results we hypothesized that the phosphorylation status of BECLIN-1 is important for the stabilization and recruitment of the different binding partners to the BECLIN-1 complex. Interestingly, co-immunoprecipitation of BECLIN-1 complex components revealed that autophagy activating proteins like VPS15, VPS34 and ATG14 were recruited less to the phospho-mimic BECLIN-1 (BEC EE) complex compared to the phospho-deficient BECLIN-1 (BEC FF) complex (Figure 4E, *Online Supplementary Figure S4C*). These results indicate that the altered autophagy by the two mutants is due to altered binding capacities of positive regulators to the BECLIN-1 core complex and thereby alters BECLIN-1 complex activity.

Next we asked, whether expression of the phospho-mimic *Beclin-1* mutant could overcome the TKI-induced BCR-ABL inhibition-mediated autophagy induction and indeed, expression of *Beclin-1 EE* Y233E/Y352E impaired nilotinib-induced autophagy measured by LC3-II expression (Figure 4F) and LC3 puncta accumulation (Figure 4G-H). BCR-ABL inhibition by nilotinib was not able to enhance the autophagy-stimulatory effect of the phosphorylation-deficient BECLIN-1 Y233F/Y352F mutant com-

pared to wt BECLIN-1, pointing to a BECLIN-1-specific autophagy regulation by BCR-ABL (Figure 4F-H).

In further BECLIN-1 complex analyses, we could demonstrate that the resistance of the phospho-mimic *Beclin-1* mutant to nilotinib-induced autophagy is caused by an altered composition of the BECLIN-1 core complex with an impaired recruitment of the activation components ATG14, UVRAG, VPS15 and a gain of the negative regulator RUBICON to the BECLIN-1 core complex (*Online Supplementary Figure S5A*). BECLIN-1 phosphorylation with subsequent resistance to TKI-induced autophagy may thereby provide a novel explanation of how leukemic cells can escape autophagy-induced cell death and develop TKI resistance.

Recently, it has been shown that BECLIN-1 S90 phosphorylation is involved in starvation-mediated autophagy.[39] To test whether BECLIN-1 phosphorylation at Y233/Y352 can influence starvation-mediated or rapamycin-mediated autophagy, we starved K562 cells or treated them with rapamycin and found that cellular autophagy is induced in *Beclin-1* wt cells (*Online Supplementary Figure S5B-D*) and no differences could be demonstrated in K562 cells expressing either BECLIN-1 Y233E/Y352E or BECLIN-1 Y233F/Y352F (*Online Supplementary Figure S5E-H*). These results indicate that tyrosine phosphorylation of BECLIN-1 at Y233 and Y352 is not involved in starvation- or rapamycin-mediated autophagy but rather seems to be specific for tyrosine kinase-mediated autophagy processes.

Discussion

Recently, several studies have suggested that autophagy, a mechanism maintaining cellular homeostasis, plays an essential role in CML. However, the precise machinery of autophagy in CML development is not completely understood and crucial autophagocytotic mediators have not been investigated *in vivo* for their role in leukemogenesis in relevant CML mouse models.

Here, we define a molecular mechanism of autophagy suppression by BCR-ABL-specific BECLIN-1 phosphorylation. Silencing of *Beclin-1* by siRNA technology led to a significantly prolonged survival of BCR-ABL transplanted mice, whereas no profound differences could be found for *Atg5* deletion. Binding of BECLIN-1 to BCR-ABL led to phosphorylation at tyrosine residues Y233 and Y352, alteration of the BECLIN-1 interactome, and suppression of autophagy function.

Several active oncogenic kinases were demonstrated to serve as negative regulators of autophagy processes, whereas inhibition of oncogenic tyrosine kinases can reverse this effect. Until now, some links of BCR-ABL to autophagy processes have been described: BCR-ABL activates the PI3K/AKT signaling pathway, which is considered as a pathway inhibiting autophagy. Furthermore, TKI treatment itself triggers autophagy in BCR-ABL$^+$ cells and TKI-induced cell death can potentially be increased by targeting autophagy proteins in addition. Recently, it was demonstrated that Ponatinib-resistant CML cells can

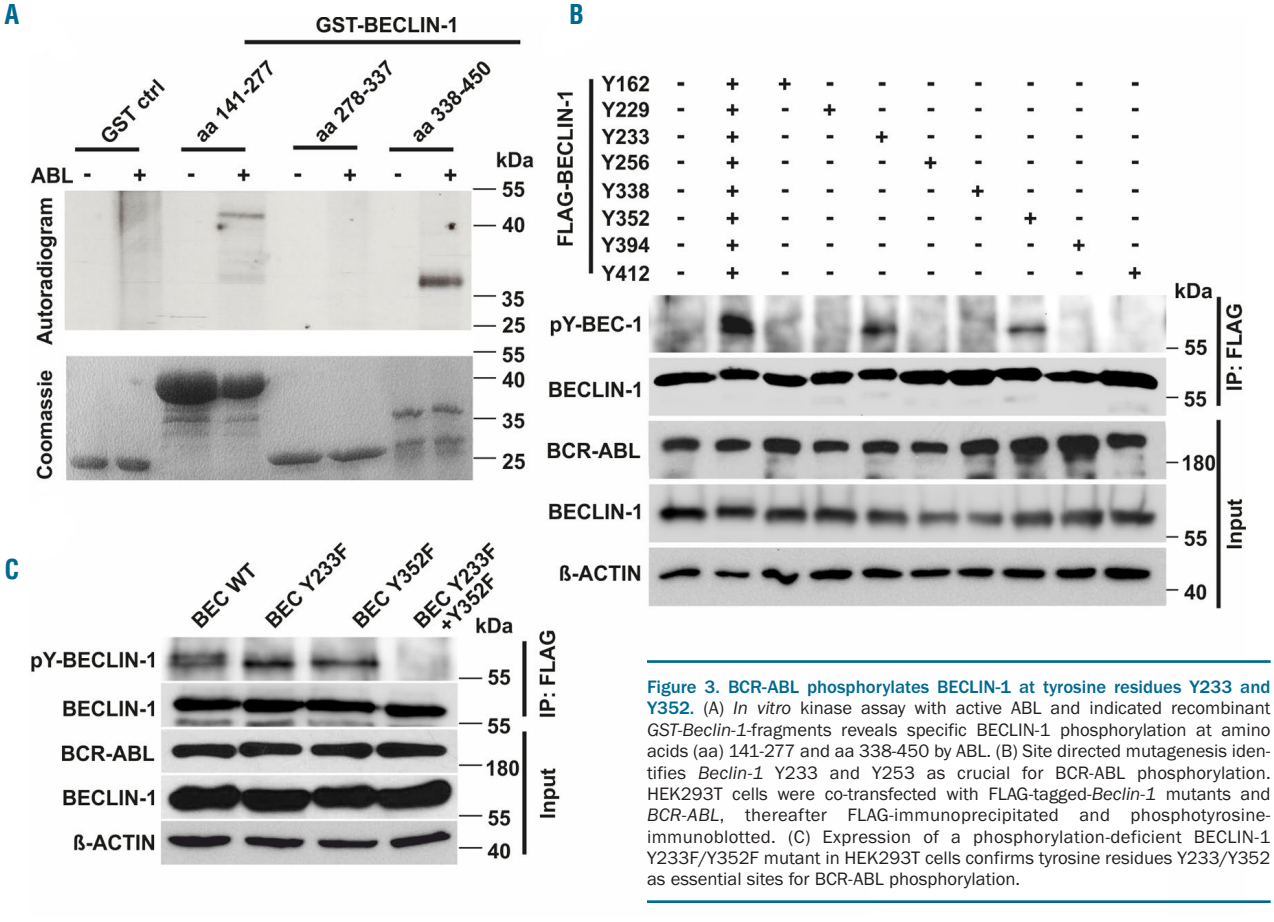

Figure 3. BCR-ABL phosphorylates BECLIN-1 at tyrosine residues Y233 and Y352. (A) *In vitro* kinase assay with active ABL and indicated recombinant *GST-Beclin-1*-fragments reveals specific BECLIN-1 phosphorylation at amino acids (aa) 141-277 and aa 338-450 by ABL. (B) Site directed mutagenesis identifies *Beclin-1* Y233 and Y253 as crucial for BCR-ABL phosphorylation. HEK293T cells were co-transfected with FLAG-tagged-*Beclin-1* mutants and *BCR-ABL*, thereafter FLAG-immunoprecipitated and phosphotyrosine-immunoblotted. (C) Expression of a phosphorylation-deficient BECLIN-1 Y233F/Y352F mutant in HEK293T cells confirms tyrosine residues Y233/Y352 as essential sites for BCR-ABL phosphorylation.

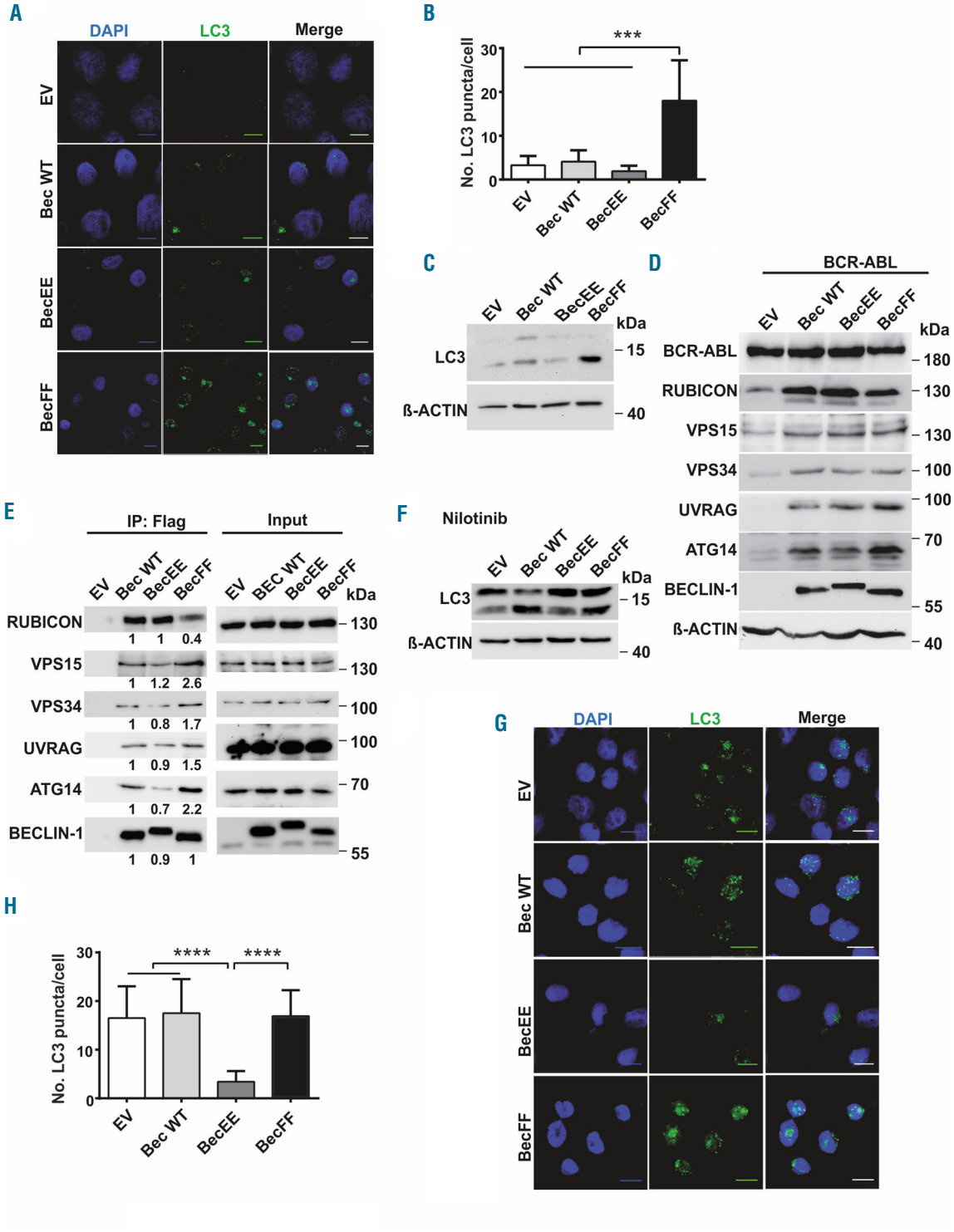

Figure 4. BCR-ABL mediated BECLIN-1 phosphorylation leads to suppression of autophagy and altered BECLIN-1 complex formation. (A) Confocal microscopy of K562 cells reveals significant induction of autophagy in BECLIN-1 Y233F/Y352F-expressing cells indicated by increased number of LC3 puncta. (B) Statistical analysis of LC3 puncta count in *Beclin-1*-mutant-transduced K562 cells (3.3, 4.1, 1.9, and 18 units respectively; ****P<0.0001 Student's t-test; Scale bar 10 μm). (C) Upregulation of LC3-II in K562 cells transduced with the phosphorylation-deficient *Beclin-1* Y233F/Y352F mutant. (D) Immunoblot analyses were used for the detection of ATG14, UVRAG, VPS34 and RUBICON expression levels in *Beclin-1* knockout MEF transduced with BCR-ABL and the indicated *Beclin-1* construct. (E) Immunoprecipitation of FLAG-tagged phosphorylation-deficient BECLIN-1 Y233F/Y352F mutant (BecFF) in K562 cells indicates altered autophagy complex formation compared to the phosphorylation-mimic BECLIN-1 mutant (BecEE). (F) *Beclin-1* tyrosine phosphorylation-mimic mutation blocks nilotinib-induced autophagy seen by reduced LC3-II levels compared to empty vector, *Beclin-1* wt, and *Beclin-1* FF. LC3 levels were evaluated by immunoblotting in the indicated *Beclin-1* mutant-transduced K562 cells. (G) LC3 puncta formation was measured using confocal microscopy in K562 cells transduced with mCherry-EGFP-LC3 and the indicated *Beclin-1* construct upon nilotinib treatment. Cells were stained with anti-LC3 antibody and nuclei were counterstained with DAPI. Scale bar, 10 μm. (H) Quantitation of LC3 puncta (16.5, 17.5, 3.4, and 16.9 dots/cell, respectively; P<0.0001 for comparison of *Beclin-1* EE to empty vector [EV], *Beclin-1* wt and *Beclin-1* FF). K562 cells transduced with mCherry-EGFP-LC3 and the indicated *Beclin-1* constructs were used for LC3 puncta measurement via Olympus ScanR screening station. Bars represent the mean±SD. ****P<0.0001 by Student's t-test. EV: empty vector; wt: wild-type *FLAG-Beclin-1*; EE: *FLAG-Beclin-1* Y233E/Y352E; FF: *FLAG-Beclin-1* Y233F/Y352F.

acquire BCL-ABL-independent resistance through autophagy inhibition by activation of mTOR.[46] Therefore, we hypothesize that BECLIN-1 may play similar roles in the resistance-acquired signaling cascade. BECLIN-1 is a central autophagy mediating protein in mammalian cells, and EGFR and AKT kinase have been shown to phosphorylate BECLIN-1 leading to inactivation of the protein and suppression of autophagy. Interestingly, active EGFR has been shown to phosphorylate the same tyrosine residues Y233/Y352 as BCR-ABL, further highlighting the importance of these tyrosine residues for autophagy suppression.[42] In line with these previous findings, we have demonstrated in the present study that BCR-ABL phosphorylates BECLIN-1 and thereby suppresses autophagy. Interestingly, this effect is mediated by the alteration of BECLIN-1 affinity to BECLIN-1 binding partners (ATG14, VPS34 and VPS15), known as the BECLIN-1 core complex. Our results therefore provide a novel explanation for the suppression of autophagy in CML and expand our knowledge regarding BECLIN-1-associated pathogenic mechanisms in BCR-ABL$^+$ leukemia.

A role for BECLIN-1 has been proposed in various malignancies, such as breast or lung carcinomas. However, the precise role of BECLIN-1 in tumorigenesis remains unclear: On one hand, *Beclin-1* is considered as a tumor suppressor and its overexpression is favorable for treatment of various solid tumors.[51-54] Furthermore, low expression of *Beclin-1* is a marker of poor prognosis and enhanced aggressiveness in breast cancer[55] and loss of one *Beclin-1* allele leads to enhanced tumor development in mice. On the other hand, our present study demonstrates that knockdown of *Beclin-1* prolongs the survival of BCR-ABL$^+$ leukemic mice, which is consistent with a previous *in vitro* study in CML cell lines.[16] Gene array analysis of CML patient samples revealed upregulated *Beclin-1* levels in CML patients compared to healthy controls (fold change: 1.22; *q*-value: <0.1%).[56] Importantly, we could show that CML patients exhibit a significant increase of phosphorylated BECLIN-1 levels. Targeting BECLIN-1 in specific approaches might thereby represent an elegant and alternative treatment option for TKI-resistant or intolerant CML patients by rendering CML cells sensitive to targeted therapies.

Recently, a study uncovered a kinase-independent role of EGFR in autophagy, showing that inactive oncogenic EGFR reversely triggers autophagy.[57] These findings support the hypothesis that cells can develop TKI-resistance through autophagy induction, which might be caused or even triggered through the inactive oncogenic kinase itself. This sheds some light on the role of autophagy on cellular survival rather than cell death and gives a rationale to explore the combinatory effect of kinase inhibitors with autophagy inhibitors. A number of drugs (Chloroquine, Bafilomycin A1, MAPK inhibitors and PI3K inhibitors) were described to have inhibitory effects on autophagy, however, most of them are poorly selective, limiting their therapeutic application. Therefore, the development of highly specific and selective autophagy inhibitors remains a mandatory necessity for the successful evaluation of the therapeutic combination therapy with TKI in CML. Moreover, accurate target identification among major autophagy players is fundamental for successful therapeutic application: BECLIN-1 seems an attractive target, as its role in kinase-driven cancer is not only shown for solid cancers but also for hematopoietic malignancies in our study. For ATG5, we were not able to prove essential function in CML development in mice, whereas Liu *et al*. were able to demonstrate a crucial role of the protein in MLL-AF9 mediated AML induction in mice.[61] ATG3 expression was shown to be indispensable for effective CML progression.[14] These results indicate that autophagy induction is highly specific and stringently regulated, not only depending on the particular malignancy, but also on the involvement of the master regulators.

Taken together, in this study we uncover a crucial role of BECLIN-1 in BCR-ABL mediated transformation *in vivo* and were able to identify a molecular mechanism by which BCR-ABL kinase activity regulates autophagy. We show that BCR-ABL binds and phosphorylates BECLIN-1 on tyrosine residues 233 and 352, thereby leading to alterations of the UVRAG-VPS15-ATG14-VPS34-RUBICON-BECLIN-1 complex. Moreover, the BCR-ABL/ BECLIN-1 interaction suppresses autophagy and thereby bypasses the negative effect of autophagy on cancer cell survival and proliferation. Importantly, these data may be of clinical relevance, as CML patients exhibit upregulated BECLIN-1 phosphorylation levels. Our findings provide a novel link between BCR-ABL and BECLIN-1 and shed some light on how specific oncogenes influence autophagy.

Funding

The authors would like to thank their funding agencies. This work was supported by research grants from the Deutsche José Carreras Leukämie-Stiftung (DJCLS R14/22 to JD and ALI and DJCLS 02 FN/2017 to TAM). ALI was supported by a research grant from the University Medical Center Freiburg and from the government Baden-Württemberg (BSL). JD and TAM were supported by a DFG grant (FOR 2033). TBH was supported by the DFG (CRC1140, CRC 992, HU 1016/8-1), by the BMBF (01GM1518C), by the Else-Kröner Fresenius Stiftung (NAKSYS), by the European Research Council-ERC grant 616891 and by the H2020-IMI2 consortium BEAt-DKD.

References

1. Marcucci G, Perrotti D, Caligiuri MA. Understanding the molecular basis of imatinib mesylate therapy in chronic myelogenous leukemia and the related mechanisms of resistance. Commentary re: A. N. Mohamed et al., The effect of imatinib mesylate on patients with Philadelphia chromosome-positive chronic myeloid leukemia with secondary chromosomal aberrations. Clin. Cancer Res., 9: 1333-1337, 2003. Clin Cancer Res. 2003; 9(4):1248-1252.
2. Talpaz M, Shah NP, Kantarjian H, et al. Dasatinib in imatinib-resistant Philadelphia chromosome-positive leukemias. N Engl J Med. 2006;354(24):2531-2541.
3. Melo JV, Barnes DJ. Chronic myeloid leukaemia as a model of disease evolution in human cancer. Nat Rev Cancer. 2007; 7(6):441-453.
4. Ren R. Mechanisms of BCR-ABL in the pathogenesis of chronic myelogenous leukaemia. Nat Rev Cancer. 2005;5(3):172-183.
5. Weisberg E, Manley PW, Cowan-Jacob SW, Hochhaus A, Griffin JD. Second generation inhibitors of BCR-ABL for the treatment of imatinib-resistant chronic myeloid leukaemia. Nat Rev Cancer. 2007;7(5):345-356.
6. An X, Tiwari AK, Sun Y, Ding PR, Ashby CR Jr., Chen ZS. BCR-ABL tyrosine kinase inhibitors in the treatment of Philadelphia chromosome positive chronic myeloid leukemia: a review. Leuk Res. 2010; 34(10):1255-1268.
7. Bhatia R, Holtz M, Niu N, et al. Persistence of malignant hematopoietic progenitors in

chronic myelogenous leukemia patients in complete cytogenetic remission following imatinib mesylate treatment. Blood. 2003; 101(12):4701-4707.
8. Mahon FX, Rea D, Guilhot J, et al. Discontinuation of imatinib in patients with chronic myeloid leukaemia who have maintained complete molecular remission for at least 2 years: the prospective, multicentre Stop Imatinib (STIM) trial. Lancet Oncol. 2010;11(11):1029-1035.
9. de Lavallade H, Apperley JF, Khorashad JS, et al. Imatinib for newly diagnosed patients with chronic myeloid leukemia: incidence of sustained responses in an intention-to-treat analysis. J Clin Oncol. 2008; 26(20):3358-3363.
10. Holyoake TL, Helgason GV. Do we need more drugs for chronic myeloid leukemia? Immunol Rev. 2015;263(1):106-123.
11. Druker BJ, Guilhot F, O'Brien SG, et al. Five-year follow-up of patients receiving imatinib for chronic myeloid leukemia. N Engl J Med. 2006;355(23):2408-2417.
12. Helgason GV, Karvela M, Holyoake TL. Kill one bird with two stones: potential efficacy of BCR-ABL and autophagy inhibition in CML. Blood. 2011;118(8):2035-2043.
13. Sheng Z, Ma L, Sun JE, Zhu LJ, Green MR. BCR-ABL suppresses autophagy through ATF5-mediated regulation of mTOR transcription. Blood. 2011;118(10):2840-2848.
14. Altman BJ, Jacobs SR, Mason EF, et al. Autophagy is essential to suppress cell stress and to allow BCR-Abl-mediated leukemogenesis. Oncogene. 2011; 30(16):1855-1867.
15. Bellodi C, Lidonnici MR, Hamilton A, et al. Targeting autophagy potentiates tyrosine kinase inhibitor-induced cell death in Philadelphia chromosome-positive cells, including primary CML stem cells. J Clin Invest. 2009;119(5):1109-1123.
16. Yu Y, Yang L, Zhao M, et al. Targeting microRNA-30a-mediated autophagy enhances imatinib activity against human chronic myeloid leukemia cells. Leukemia. 2012;26(8):1752-1760.
17. Mitchell R, Hopcroft LEM, Baquero P, et al. Targeting BCR-ABL-independent TKI resistance in chronic myeloid leukemia by mTOR and autophagy inhibition. J Natl Cancer Inst. 2018;110(5):467-478.
18. Karvela M, Baquero P, Kuntz EM, et al. ATG7 regulates energy metabolism, differentiation and survival of Philadelphia-chromosome-positive cells. Autophagy. 2016; 12(6):936-948.
19. He C, Levine B. The Beclin 1 interactome. Curr Opin Cell Biol. 2010;22(2):140-149.
20. Sun Q, Fan W, Zhong Q. Regulation of Beclin 1 in autophagy. Autophagy. 2009; 5(5):713-716.
21. Zhong Y, Wang QJ, Li X, et al. Distinct regulation of autophagic activity by Atg14L and Rubicon associated with Beclin 1-phosphatidylinositol-3-kinase complex. Nat Cell Biol. 2009;11(4):468-476.
22. Zhong Y, Wang QJ, Yue Z. Atg14L and Rubicon: yin and yang of Beclin 1-mediated autophagy control. Autophagy. 2009; 5(6):890-891.
23. Matsunaga K, Saitoh T, Tabata K, et al. Two Beclin 1-binding proteins, Atg14L and Rubicon, reciprocally regulate autophagy at different stages. Nat Cell Biol. 2009; 11(4):385-396.
24. Grundler R, Thiede C, Miething C, Steudel C, Peschel C, Duyster J. Sensitivity toward tyrosine kinase inhibitors varies between different activating mutations of the FLT3 receptor. Blood. 2003;102(2):646-651.
25. Illert AL, Kawaguchi H, Antinozzi C, et al. Targeted inactivation of nuclear interaction partner of ALK disrupts meiotic prophase. Development. 2012;139(14):2523-2534.
26. Illert AL, Zech M, Moll C, et al. Extracellular signal-regulated kinase 2 (ERK2) mediates phosphorylation and inactivation of nuclear interaction partner of anaplastic lymphoma kinase (NIPA) at G2/M. J Biol Chem. 2012;287(45):37997-38005.
27. Grundler R, Brault L, Gasser C, et al. Dissection of PIM serine/threonine kinases in FLT3-ITD-induced leukemogenesis reveals PIM1 as regulator of CXCL12-CXCR4-mediated homing and migration. J Exp Med. 2009;206(9):1957-1970.
28. Muller TA, Grundler R, Istvanffy R, et al. Lineage-specific STAT5 target gene activation in hematopoietic progenitor cells predicts the FLT3(+)-mediated leukemic phenotype. Leukemia. 2016;30(8):1725-1733.
29. Illert AL, Albers C, Kreutmair S, et al. Grb10 is involved in BCR-ABL-positive leukemia in mice. Leukemia. 2015; 29(4):858-868.
30. Albers C, Illert AL, Miething C, et al. An RNAi-based system for loss-of-function analysis identifies Raf1 as a crucial mediator of BCR-ABL-driven leukemogenesis. Blood. 2011;118(8):2200-2210.
31. Liu S, Hartleben B, Kretz O, et al. Autophagy plays a critical role in kidney tubule maintenance, aging and ischemia-reperfusion injury. Autophagy. 2012; 8(5):826-837.
32. Mizushima N, Yoshimori T, Levine B. Methods in mammalian autophagy research. Cell. 2010;140(3):313-326.
33. Ultimo S, Simioni C, Martelli AM, et al. PI3K isoform inhibition associated with anti Bcr-Abl drugs shows in vitro increased anti-leukemic activity in Philadelphia chromosome-positive B-acute lymphoblastic leukemia cell lines. Oncotarget. 2017;8(14):23213-23227.
34. Morita M, Nishinaka Y, Kato I, et al. Dasatinib induces autophagy in mice with Bcr-Abl-positive leukemia. Int J Hematol. 2017;105(3):335-340.
35. Kang R, Zeh HJ, Lotze MT, Tang D. The Beclin 1 network regulates autophagy and apoptosis. Cell Death Differ. 2011; 18(4):571-580.
36. McKnight NC, Zhenyu Y. Beclin 1, an essential component and master regulator of PI3K-III in health and disease. Curr Pathobiol Rep. 2013;1(4):231-238.
37. Uyar B, Weatheritt RJ, Dinkel H, Davey NE, Gibson TJ. Proteome-wide analysis of human disease mutations in short linear motifs: neglected players in cancer? Mol Biosyst. 2014;10(10):2626-2642.
38. McKnight NC, Zhong Y, Wold MS, et al. Beclin 1 is required for neuron viability and regulates endosome pathways via the UVRAG-VPS34 complex. PLoS Genet. 2014;10(10):e1004626.
39. Wei Y, An Z, Zou Z, et al. The stress-responsive kinases MAPKAPK2/MAPKAPK3 activate starvation-induced autophagy through Beclin 1 phosphorylation. Elife. 2015;4.
40. Goussetis DJ, Gounaris E, Wu EJ, et al. Autophagic degradation of the BCR-ABL oncoprotein and generation of antileukemic responses by arsenic trioxide. Blood. 2012;120(17):3555-3562.
41. Liu X, Rothe K, Yen R, et al. A novel AHI-1-BCR-ABL-DNM2 complex regulates leukemic properties of primitive CML cells through enhanced cellular endocytosis and ROS-mediated autophagy. Leukemia. 2017; 31(11):2376-2387.
42. Wei Y, Zou Z, Becker N, et al. EGFR-mediated Beclin 1 phosphorylation in autophagy suppression, tumor progression, and tumor chemoresistance. Cell. 2013;154(6):1269-1284.
43. Wang RC, Wei Y, An Z, et al. Akt-mediated regulation of autophagy and tumorigenesis through Beclin 1 phosphorylation. Science. 2012;338(6109):956-959.
44. Kharas MG, Janes MR, Scarfone VM, et al. Ablation of PI3K blocks BCR-ABL leukemogenesis in mice, and a dual PI3K/mTOR inhibitor prevents expansion of human BCR-ABL+ leukemia cells. J Clin Invest. 2008;118(9):3038-3050.
45. Klejman A, Rushen L, Morrione A, Slupianek A, Skorski T. Phosphatidylinositol-3 kinase inhibitors enhance the anti-leukemia effect of STI571. Oncogene. 2002;21(38):5868-5876.
46. Mitchell R, Hopcroft LEM, Baquero P, et al. Targeting BCR-ABL-Independent TKI Resistance in Chronic Myeloid Leukemia by mTOR and Autophagy Inhibition. J Natl Cancer Inst. 2018;110(5):467-478.
47. Yue Z, Jin S, Yang C, Levine AJ, Heintz N. Beclin 1, an autophagy gene essential for early embryonic development, is a haploinsufficient tumor suppressor. Proc Natl Acad Sci U S A. 2003;100(25):15077-15082.
48. Liang XH, Jackson S, Seaman M, et al. Induction of autophagy and inhibition of tumorigenesis by beclin 1. Nature. 1999; 402(6762):672-676.
49. Dang CV. Links between metabolism and cancer. Genes Dev. 2012;26(9):877-890.
50. Liu J, Xia H, Kim M, et al. Beclin1 controls the levels of p53 by regulating the deubiquitination activity of USP10 and USP13. Cell. 2011;147(1):223-234.
51. Qu X, Yu J, Bhagat G, et al. Promotion of tumorigenesis by heterozygous disruption of the beclin 1 autophagy gene. J Clin Invest. 2003;112(12):1809-1820.
52. Ahn CH, Jeong EG, Lee JW, et al. Expression of beclin-1, an autophagy-related protein, in gastric and colorectal cancers. APMIS. 2007;115(12):1344-1349.
53. Shen Y, Li DD, Wang LL, Deng R, Zhu XF. Decreased expression of autophagy-related proteins in malignant epithelial ovarian cancer. Autophagy. 2008;4(8):1067-1068.
54. Won KY, Kim GY, Kim YW, Song JY, Lim SJ. Clinicopathologic correlation of beclin-1 and bcl-2 expression in human breast cancer. Hum Pathol. 2010;41(1):107-112.
55. Tang H, Sebti S, Titone R, et al. Decreased BECN1 mRNA expression in human breast cancer is associated with estrogen receptor-negative subtypes and poor prognosis. EBioMedicine. 2015;2(3):255-263.
56. Diaz-Blanco E, Bruns I, Neumann F, et al. Molecular signature of CD34(+) hematopoietic stem and progenitor cells of patients with CML in chronic phase. Leukemia. 2007;21(3):494-504.
57. Tan X, Thapa N, Sun Y, Anderson RA. A kinase-independent role for EGF receptor in autophagy initiation. Cell. 2015;160(1-2):145-160.
58. Dalby KN, Tekedereli I, Lopez-Berestein G, Ozpolat B. Targeting the prodeath and prosurvival functions of autophagy as novel therapeutic strategies in cancer. Autophagy. 2010;6(3):322-329.
59. Wang C, Hu Q, Shen HM. Pharmacological inhibitors of autophagy as novel cancer therapeutic agents. Pharmacol Res. 2016; 105:164-175.
60. Pasquier B. Autophagy inhibitors. Cell Mol Life Sci. 2016;73(5):985-1001.
61. Liu Q, Chen L, Atkinson JM, Claxton DF, Wang HG. Atg5-dependent autophagy contributes to the development of acute myeloid leukemia in an MLL-AF9-driven mouse model. Cell Death Dis. 2016; 7(9):e2361.

Ferrata Storti Foundation

Meningioma 1 is indispensable for mixed lineage leukemia-rearranged acute myeloid leukemia

Amit Sharma,[1] Nidhi Jyotsana,[1] Razif Gabdoulline,[1] Dirk Heckl,[2] Florian Kuchenbauer,[3] Robert K. Slany,[4] Arnold Ganser[1] and Michael Heuser[1]

[1]Department of Hematology, Hemostasis, Oncology and Stem Cell Transplantation, Hannover Medical School, Hannover, Germany; [2]Department of Pediatric Hematology and Oncology, Hannover Medical School, Hannover, Germany; [3]British Columbia Cancer Agency, Vancouver, British Columbia, Canada and [4]Department of Genetics, Friedrich-Alexander-University Erlangen-Nürnberg, Erlangen, Germany

Haematologica 2020
Volume 105(5):1294-1305

ABSTRACT

Mixed lineage leukemia (*MLL/KMT2A*) rearrangements (MLL-r) are one of the most frequent chromosomal aberrations in acute myeloid leukemia. We evaluated the function of Meningioma 1 (MN1), a co-factor of HOXA9 and MEIS1, in human and murine MLL-rearranged leukemia by CRISPR-Cas9 mediated deletion of MN1. MN1 was required for *in vivo* leukemogenicity of MLL positive murine and human leukemia cells. Loss of MN1 inhibited cell cycle and proliferation, promoted apoptosis and induced differentiation of MLL-rearranged cells. Expression analysis and chromatin immunoprecipitation with sequencing from previously reported data sets demonstrated that MN1 primarily maintains active transcription of HOXA9 and HOXA10, which are critical downstream genes of MLL, and their target genes like BCL2, MCL1 and Survivin. Treatment of MLL-rearranged primary leukemia cells with anti-MN1 siRNA significantly reduced their clonogenic potential in contrast to normal $CD34^+$ hematopoietic progenitor cells, suggesting a therapeutic window for MN1 targeting. In summary, our findings demonstrate that MN1 plays an essential role in MLL fusion leukemias and serve as a therapeutic target in MLL-rearranged acute myeloid leukemia.

Correspondence:

MICHAEL HEUSER
heuser.michael@mh-hannover.de

Received: November 6, 2018.

Accepted: August 8, 2019.

Pre-published: August 14, 2019.

doi:10.3324/haematol.2018.211201

Check the online version for the most updated information on this article, online supplements, and information on authorship & disclosures: www.haematologica.org/content/105/5/1294

Introduction

Acute myeloid leukemia (AML) is associated with a plethora of genetic alterations such as chromosomal rearrangements and mutations,[1] with some of them being generic for different types of leukemias and cancers.[1] MLL1 (Mixed lineage leukemia 1/KMT2A) rearrangements are one such example that are found in myeloid as well as lymphoid leukemias.[2] Approximately 135 different MLL rearrangements have been identified so far, but only nine specific gene fusions (including AF4, AF9, ENL, and AF6) account for more than 90% of all oncogenic recombinations.[3,4] A unifying hallmark of all MLL-rearranged (MLL-r) leukemias is the deregulation of clustered HOXA/MEIS1 genes.[2] Transcriptional activation of MLL target genes (HOXA9/MEIS1) is associated with an increase in histone H3 lysine79 dimethylation (H3K79me2) across the respective gene locus, which is specifically mediated by histone methyltransferase DOT1.[2,5] Recently, several studies in patients and murine models have highlighted the importance of co-operating genetic alterations in MLL-r leukemia progression. In 40-50% of MLL-r AML cases, RAS and FLT3 mutations have been shown to accelerate leukemogenesis, and Mn1, Bcl11a and Fosb have been identified as co-operating oncogenes in a murine leukemia virus insertional mutagenesis model.[4,6]

MN1 (Meningioma-1) is frequently over-expressed in AML patients and is associated with a poor prognosis.[7-13] However, in patients with inv(16), highest *MN1* expression has been reported with favorable prognosis to current therapeutics.[11] MN1 functions as a transcriptional regulator that co-operates with the nuclear receptors for retinoic acid (RAR) and vitamin D, by acting as co-activator or co-repressor, depending on the interacting partners.[14-16] In addition, *MN1* is frequently over-expressed and occasionally fused to *TEL* as part of the rare MN1-TEL translocation.[17] Mn1 is known

to be co-operating partner of several oncogenic fusion genes (NUP98–HOXD13,[18] CALM–AF10,[19] MLL–AF9[6] and MLL–ENL)[20] and mutated RUNX1,[21] and as a common target of insertional mutagenesis in a hematopoietic stem cell (HSC) gene therapy trial,[22] thereby promoting leukemogenesis.

Interestingly, MN1-induced AML is also dependent on Hoxa cluster genes and Meis1.[23] Multipotent progenitor cells (MPP) and common myeloid progenitors (CMP) have been identified as the cell of origin in MN1-induced AML, while granulocyte-macrophage progenitors (GMP) cannot be transformed.[23] We found that the differential expression of *Hoxa9, Hoxa10* and *Meis1* in MPP/CMP compared to GMP cells was responsible for the ability of MN1 to transform the more immature, but not the more mature, progenitor cells.[23] One important difference between MN1 and MLL-r leukemia is that MN1 cannot activate *Hox* gene expression by itself, while MLL-AF9 can.[23,24] Therefore, MN1 is unable to transform GMP cells, while MLL-AF9 can transform myeloid progenitor cells down to the differentiation state of a GMP. Both MLL-AF9- and MN1-induced leukemias depend on the H3K79 methyltransferase DOT1L.[14,25,26] In addition, deletion of Mll and Dot1l in MN1-expressing cells abrogated the cell of origin-derived gene expression program, including the expression of Hoxa cluster genes, and impaired the leukemogenic activity of MN1 *in vivo*.[14] However, it is not known whether MLL-AF9 transformed cells also depend on MN1.

High *MN1* expression confers resistance to all-trans retinoic acid (ATRA)-induced differentiation and chemotherapy-induced cytotoxicity.[7,27] Recent studies have shown that pyrimethamine [a dihydrofolate reductase (DHFR) inhibitor] and DOT1L inhibitors possess anti-leukemic effects in MN1^{hi} AML cells.[14,27] However, the mechanism of MN1-induced AML and drug resistance is still not completely understood due to its little structural/functional similarity to any other protein.[14] Mn1 null mice have severe defects in bones of the cranial skeleton, yet the effects of its deletion in hematopoiesis/leukemia are not known.[28] Here, we show that CRISPR–Cas9-mediated deletion of MN1 in MLL-r leukemias, and consequently treatment of MLL-r leukemias with an anti-MN1 siRNA, led to strong anti-leukemic effects, including increased terminal myeloid differentiation and suppression of leukemic growth *in vitro* and *in vivo*.

Methods

Viral vectors, vector production, and CRISPR

Briefly, helper-free recombinant retrovirus harvested from supernatants of the transfected ecotropic Phoenix packaging cell line was used to transduce 5-fluoro-uracil treated mouse bone marrow cells to generate an immortalized MLL-AF9 cell line, as described before.[15,29] CRISPR lentiviral vector L40C-CRISPR.EFS.dTomato (Addgene # 89392) was kindly provided by Dr. Dirk Heckl, Hannover Medical School, Hannover, Germany.[30] CRISPR-Cas9 target sites in the Mn1/MN1 gene were selected using the CCTop selection tool.[31] Single guide RNA (sgRNA) were cloned in the CRISPR-Cas9 vector. The list of sgRNA is summarized in *Online Supplementary Table S1*.

Cell lines and primary cells

Bone marrow from healthy donors was obtained from the transplantation unit of Hannover Medical School. Mononuclear cells from peripheral blood or bone marrow were isolated by density gradient centrifugation. CD34$^+$ cells were isolated using the CD34 microbead kit (Miltenyi Biotech, Bergisch Gladbach, Germany), as per manufacturer's protocol. AML patient samples were taken from the AML-myelodysplastic syndromes (AML-MDS) repository of Hannover Medical School. Written informed consent was obtained for the use of patient samples in accordance with the Declaration of Helsinki, and the study was approved by the institutional review board of Hannover Medical School (ethical vote 1187-2011).

Mouse transplantation and homing assay

NOD-SCID and NOD/SCID/IL2rgnull (NSG) mice were bred and maintained in pathogen-free conditions in the animal laboratory of Hannover Medical School, Hannover, Germany. All animal experiments were approved by the Lower Saxony state office for consumer protection, Oldenburg, Germany.

siRNA and lipid nanoparticles

All siRNAs (MN1 and control/AHA1) were purchased from Axolabs GmbH (Kulmbach, Germany). siRNAs were packaged in lipid nanoparticles (LNP), as described previously.[32]

Gene expression and chromatin immunoprecipitation sequencing analysis

We performed gene expression profiling of *in vitro* cultured MLL-AF9/Mn1wt *versus* MLL-AF9/Mn1null cells in triplicate. RNA was extracted using the standard trizol method and was further used for gene expression profiling. Gene expression profiling using extracted RNA from MLL-AF9/MNn1wt and MLL-AF9/MNn1null cells was performed on Affymetrix GeneChip Mouse 430 2.0 arrays (43,000 probes). The whole dataset can be found at GEO (GSE130631) for public access.

Chromatin immunoprecipitation sequencing (Chip-Seq) DNA binding data were taken for H3K79me2 from GSE55038,[33] MLL-AF9 from GSE29130,[25] Hoxa9 from GSE33518,[34] and MN1 and MEIS1 from our previous publication.[23]

Statistical analysis

Pairwise comparisons were performed by Student t-test for continuous variables. Two-sided significance was set at $P<0.05$. Comparison of survival curves were performed using the log rank test. Statistical analyses were performed with Microsoft Excel (Microsoft, Munich, Germany) and GraphPad Prism 5 (GraphPad Software, La Jolla, CA, USA).

More detailed information on the materials and methods used can be found in the *Online Supplementary Appendix*.

Results

MLL-AF9 cell proliferation depends on Meningioma 1

To study the effects of MN1 gene inactivation in leukemia cells, we generated CRISPR-Cas9 engineered MN1null murine and human leukemia cells and characterized these cells *in vitro* and *in vivo* (Figure 1A). MN1 was deleted in murine cells transformed by MLL-AF9, HOXA9, HOXA9MEIS1, E2A-HLF and 10 human leukemia cell lines: THP-1, MV-4-11, NB4, OCI-AML2, OCI-AML3, U937, K562, Kasumi-1, HL-60 and HEL. Ninety-six to 288 transduced cells per cell line were single cell sorted and the outgrowing clones were evaluated for MN1 deletion by qualitative RT-PCR (qRT-PCR), western blot and sequencing (*Online Supplementary Tables S2* and *S3* and *Online Supplementary Figure S1A-F*). While up to

30% of the single sorted cells grew out as clones, only 0-8.9% of the single sorted clones were MN1-deleted, and only one MN1-deleted clone was obtained from four different murine cell lines with HOX-dependent oncogene expression (*Online Supplementary Table S2*), suggesting that MN1 loss impairs clonogenicity of MLL-r and HOXA9-transformed cells. Subsequently, in parallel to MLL-AF9 mouse cells, we also studied THP-1 and MV-4-11 (positive for MLL-AF9 and MLL-AF4, respectively) and the non-MLL-r human cell line U937. Loss of MN1 more potently reduced proliferation in MLL-r cells as compared to non-MLL-r leukemia cells (Figure 1B-D and *Online Supplementary Figure S2A*). The inhibitory effect of MN1 loss in U937 cells may be due to high HOXA9 and MEIS1 expression (*Online Supplementary Figure S2B* and *C*). The cell lines K562, Kasumi-1 and HL-60 had the lowest HOXA9 and MEIS1 expression levels, but had the highest rate of MN1-deleted clones (*Online Supplementary Table S2*), indicating a dependence on MN1 in MLL-r and HOXA9/MEIS1 expressing cells.

MN1 deletion drastically impaired the colony-forming potential up to 22-fold and reduced the size of the colonies in MLL-AF9 transformed murine cells (Figure 1E and 1F). Due to potential unpredictable off-target effects, we tested one additional sgRNA (sgRNA-4; positioned at a different location), which had a similar effect as the initial sgRNA (*Online Supplementary Figure S3A* and *B*). Thus, *in vitro* proliferation and colony-forming potential of MLL-rearranged cells require MN1 expression both in murine and human leukemia cells.

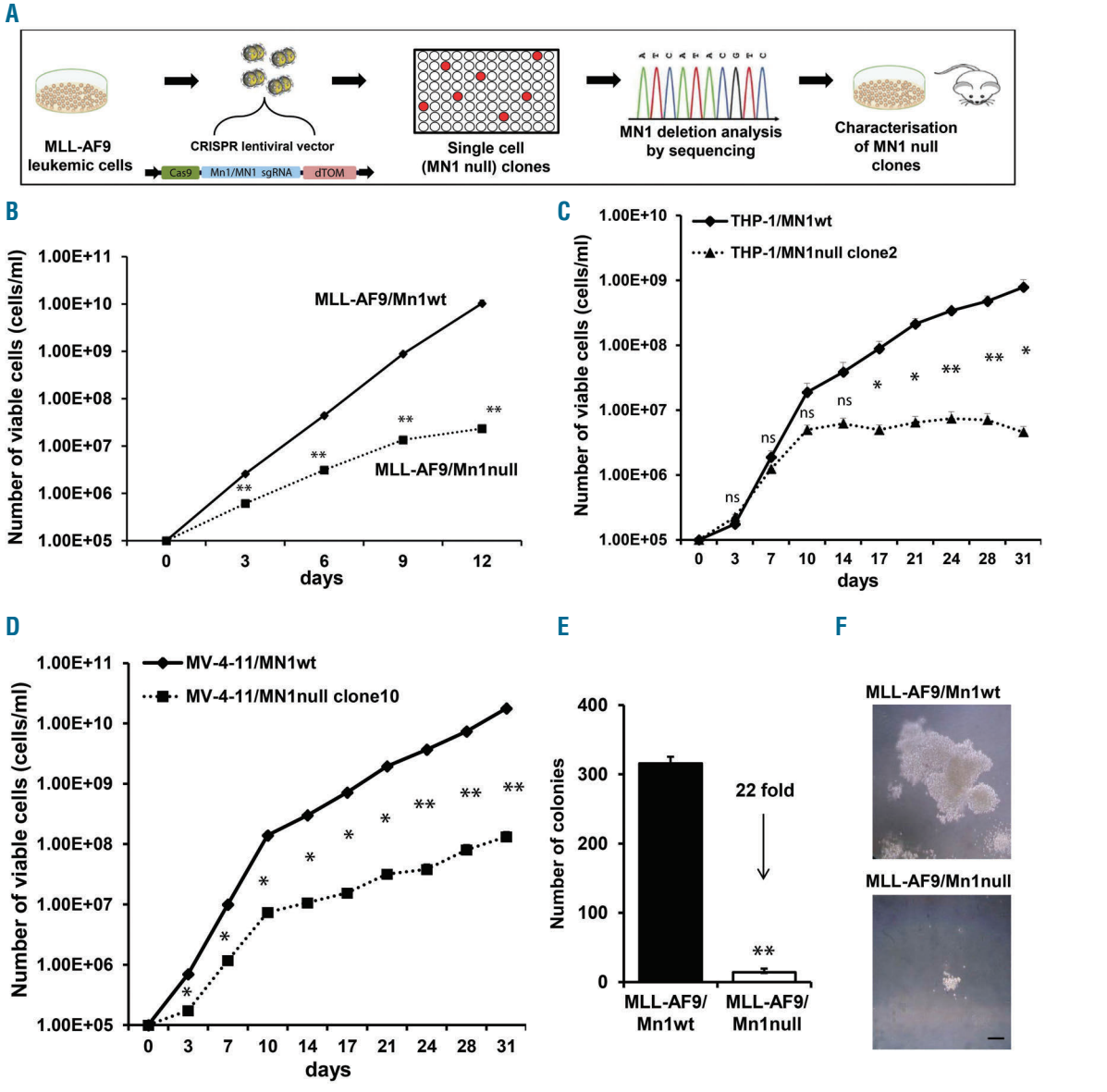

Figure 1. MLL-AF9 cell proliferation depends on Meningioma 1 (MN1). (A) Schematic outline of the strategy for deletion of MN1/Mn1 in murine and human cell lines. (B) Cumulative cell counts of MLL-AF9/Mn1wt and MLL-AF9/Mn1null cells [mean±standard error of mean (SEM), n=3]. (C) Cumulative cell counts of THP-1 MN1wt and MN1null cells (mean±SEM, n=3). (D) Cumulative cell counts of MV-4-11 MN1wt and MN1null cells (mean±SEM, n=3). (E) Colony-forming cell (CFC) counts of MLL-AF9/Mn1wt and MLL-AF9/Mn1null cells (mean±SEM, n=3). (F) Morphology of representative CFC colonies of MLL-AF9/Mn1wt and MLL-AF9/Mn1null cells. Black scale bar represents 0.25 mm. *P<0.05; **P<0.01; ns: not significant.

Meningioma 1 regulates cell cycle, apoptosis and differentiation in MLL-AF9 cells

Next, we explored the impact of *MN1* deletion on cell cycle, apoptosis and differentiation in MLL positive leukemic cell lines. Loss of MN1 inhibited cell cycle progression resulting in more cells in G0/G1 phase and fewer cells in S phase of the cell cycle compared to MN1wt cells (Figure 2A and *Online Supplementary Figure S4A*). In addition, cell cycle progression was negatively associated with MN1 null cells by gene set enrichment analysis (GSEA) of gene expression profiling data (*Online Supplementary Tables S4* and *S5* and *Online Supplementary Figures S4B* and *S5A-D*). The proportion of Annexin V positive cells was significantly increased and the gene sets for apoptosis and the p53 pathway were highly enriched in MLL-AF9/Mn1null cells (Figure 2B, *Online Supplementary Table S4* and *Online*

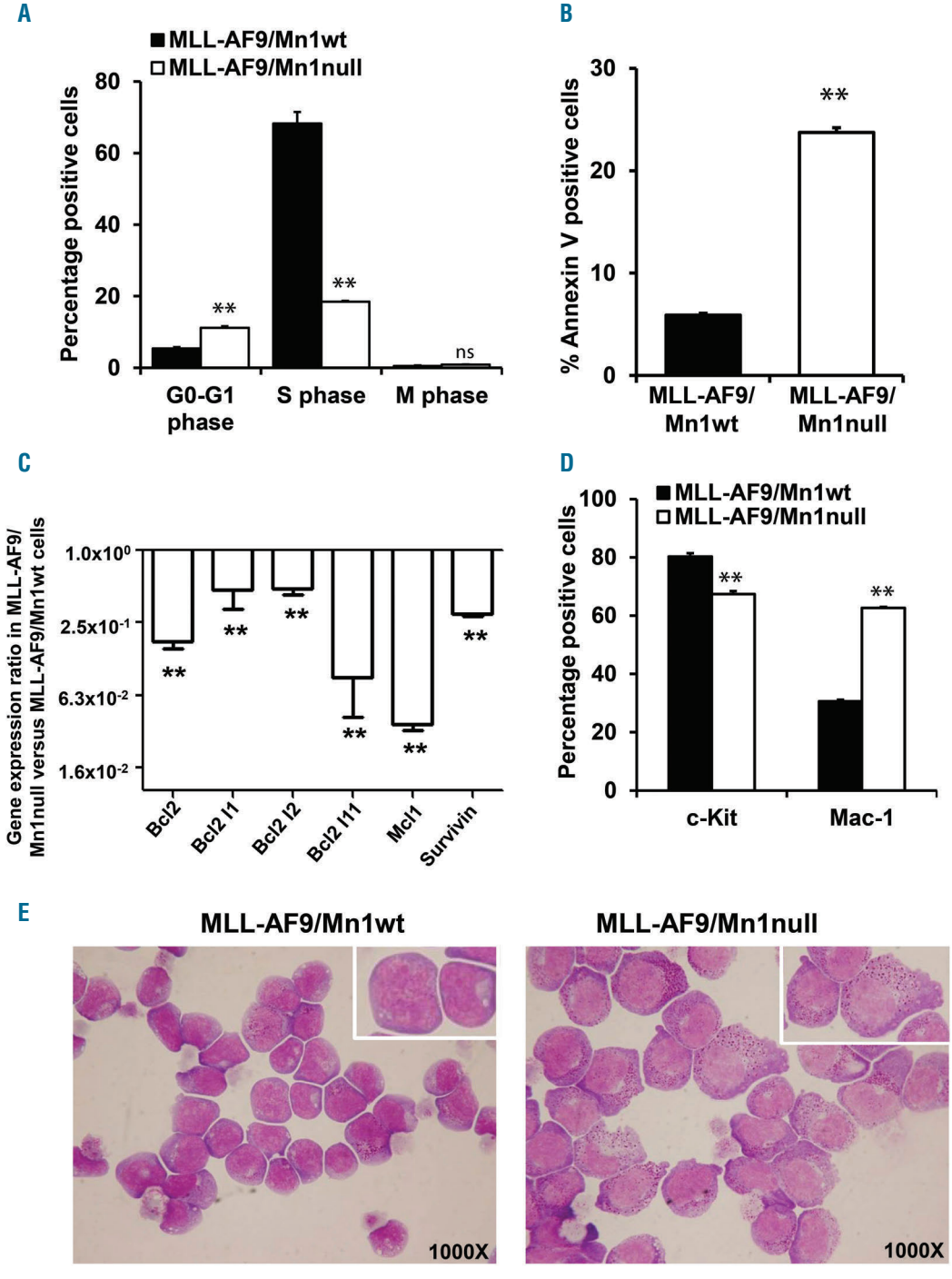

Figure 2. Meningioma 1 (MN1) regulates cell cycle, apoptosis and differentiation in MLL-AF9 cells. (A) Cell cycle analysis of MLL-AF9/Mn1wt and MLL-AF9/Mn1null cells [mean±standard error of mean (SEM), n=3]. (B) Proportion of apoptotic cells in MLL-AF9/Mn1wt and MLL-AF9/Mn1null cells (mean±SEM, n=3). (C) Relative gene expression of differentially expressed genes normalized to Abl1 in MLL-AF9/Mn1wt and MLL-AF9/Mn1null cells (mean±SEM, n=3). (D) Immunophenotype of *in vitro* cultured MLL-AF9/Mn1wt and MLL-AF9/Mn1null cells (mean±SEM, n=3). (E) Morphology of in vitro cultured MLL-AF9/Mn1wt and MLL-AF9/Mn1null cells (original magnification 1,000-fold). *P<0.05; **P<0.01; ns: not significant.

Supplementary Figure S4E and *F*). In support of the GSEA analysis, a strong downregulation of the anti-apoptotic Bcl2 gene family, Mcl1 and Survivin was shown by qRT-PCR (Figure 2C). MLL-AF9/Mn1null cells showed low levels of the hematopoietic stem/progenitor cell marker c-Kit/CD117 but high expression of the mature myeloid cell marker Mac1/CD11b and Gr-1/Ly-6G in Mn1 null cells compared to MLL-AF9/Mn1wt cells (Figure 2D and *Online Supplementary Figure S6A*). This observation was also supported by morphological analysis, as Mn1 null cells had a lower nuclear-cytoplasmic ratio and were more granulated (Figure 2E), and gene sets were enriched for myeloid and lymphoid cell differentiation (*Online Supplementary Tables S4* and *S5,* and *Online Supplementary Figures S4B* and *S6B* and *C*). MLL-AF9 oncogene expression was found to be unaltered or increased upon loss of Mn1 in MLL-AF9/Mn1null cells when compared with MLL-AF9/Mn1wt cells, excluding the possibility that downregulation of the oncogene is responsible for the anti-leukemic effects of MN1 loss (*Online Supplementary Figure S7A-C*). Hence, MN1 deletion suppresses cell cycle, promotes apoptosis, and induces differentiation in MLL positive leukemia cells.

MLL-AF9-induced leukemogenesis requires Meningioma 1

To further investigate the role of Mn1 deletion in MLL-AF9 leukemogenesis *in vivo*, we transplanted MLL-AF9/Mn1wt and MLL-AF9/Mn1null cells in syngeneic mice and monitored onset of leukemia and survival. Mice transplanted with MLL-AF9/Mn1null cells had <1% engraftment in all ten mice, whereas mice transplanted with MLL-AF9/Mn1wt cells showed >90% engraftment at week 4 (Figure 3A). At eight weeks, engraftment in MLL-AF9/Mn1null was below 2% (except for one mouse with 88% MLL-AF9 expressing cells, which consequently died), while 8 of 10 MLL-AF9/Mn1wt mice died from leukemia and the two surviving mice showed >90% engraftment (Figure 3A). Correspondingly, white blood cell (WBC) counts were significantly lower in MLL-AF9/Mn1null than in MLL-AF9/Mn1wt mice (Figure 3B). Loss of Mn1 significantly prolonged survival as compared to Mn1wt mice (Figure 3C). At death, mice transplanted with MLL-AF9/Mn1 null cells had significantly lower spleen weight (Figure 3D). Since loss of Mn1 in MLL-AF9 cells did not show a potent engraftment ability, and to exclude the possibility of homing defects, we transplanted equal numbers of MLL-AF9 (Mn1wt/null) cells intravenously in sub-lethally irradiated mice. Mice were sacrificed after 8 and 24 hours and MLL-AF9/Mn1null cells showed better homing in bone marrow than mice transplanted with MLL-AF9/Mn1wt cells, suggesting that differences in homing could not account for the differences in survival (Figure 3E). In addition, to rule out the presence of any immunological effects against MLL-AF9/Mn1null cells, we transplanted MLL-AF9 (Mn1wt or null) cells in NSG mice (lacking cellular and humoral immunity) and monitored leukemia onset and survival. Similar to syngeneic mouse transplantation studies, MLL-AF9/Mn1null mice did not develop leukemia, while their MLLAF9/Mn1wt counterpart quickly died from leukemia (*Online Supplementary Figures S8A* and *B* and *S9A-H* for blood counts). Thus, MLL-AF9 positive murine leukemia requires *MN1* expression to induce leukemia *in vivo*.

MLL-AF9 and MLL-AF4 rearranged human leukemias also depend on Meningioma 1

Besides syngeneic MLL-AF9 transplantation studies, we also assessed the role of MN1 deletion in MLL-AF4 (MV-4-11) and MLL-AF9 (THP-1) leukemias *in vivo*. Equal numbers of THP-1 and MV-4-11 (MN1wt or MN1null) cells were transplanted intravenously in NSG mice, and the onset of leukemia and survival were assessed. MN1null cells showed lower engraftment of transplanted cells in peripheral blood at four weeks and improved blood counts compared to their wild-type counterparts (Figure 4A and B and *Online Supplementary Figures S10* and *S11*). MN1 deletion significantly prolonged survival of mice transplanted with THP-1/MN1null and MV-4-11/MN1null clones (Figure 4C and D). At death, engraftment in bone marrow and spleen weight were also found lower in mice transplanted with MN1 deletion clones of THP-1 and MV-4-11 (Figure 4E and F and *Online Supplementary Figure S12A* and *B*). In addition, we also evaluated the tumor-forming ability of THP-1/MN1null and MV-4-11/MN1null clones by subcutaneous transplantation in NOD-SCID mice. Tumor volumes were monitored every five days starting 15 days after transplantation. Deletion of MN1 led to significantly reduced tumor volumes for 2 of 3 MN1null clones as compared to wild-type MN1 human leukemic cell lines (*Online Supplementary Figure S13A* and *B*). Our *in vivo* transplantation studies suggest that loss of MN1 critically affects leukemia proliferation in human MLL-rearranged AML.

Meningioma 1 overexpression restores leukemogenicity in MLL-AF9/Mn1null cells

In an attempt to rescue the deleterious effects caused by Mn1 deletion, we over-expressed control (MIY) vector or MN1 in MLL-AF9/Mn1 null cells and characterized its properties *in vitro* and *in vivo*. MLL-AF9/Mn1null cells transduced with MN1 overcame the reduced proliferative capacity of MLL-AF9/Mn1null cells similarly to MLL-AF9/Mn1wt cells (Figure 5A). Similarly, MLL-AF9/Mn1null cells with MN1 expression restored the reduced colony-forming potential of MLL-AF9/Mn1null cells akin to MLL-AF9/Mn1wt cells (Figure 5B and C). We also studied the leukemogenic potential of MLL-AF9/Mn1null cells rescued by MN1 expression in comparison with MLL-AF9 (Mn1wt or null) cells transduced with vector control. As previously mentioned in our manuscript, MLL-AF9/Mn1null cells do not possess the ability to engraft in mice. However, MLL-AF9/Mn1null cells with ectopic MN1 expression engrafted in mice and induced a leukemic phenotype with short survival similar to MLL-AF9/Mn1wt mice (Figure 5D and E and *Online Supplementary Figure S14*). Hence, deleterious effects caused by loss of MN1 expression can be rescued by restoring the expression of MN1.

Meningioma 1 maintains expression of the distal HOXA cluster and MEIS1

MLL-AF9-mediated leukemogenesis is primarily mediated by upregulation of the Hox/Meis1 gene cluster and their target genes.[33,35] DOT1L methylates histone H3 on lysine 79 (H3K79me2), which has been associated with MLL-AF9 binding and expression of Hoxa cluster genes and Meis1 in normal hematopoietic progenitors and MLL-r leukemias.[25] Gene expression analysis by qRT-PCR in MLL-AF9/Mn1null and Mn1wt cells showed that *Hoxa3*

through *Hoxa7* were not significantly dysregulated, while *Hoxa9, Hoxa10* and *Meis1* were strongly down-regulated in MLL-AF9/Mn1null cells (Figure 6A). We also performed global gene expression analysis in MLL-AF9/Mn1wt versus MLL-AF9/Mn1null cells with significant differentially expressed genes (*Online Supplementary Table S6* and *Online Supplementary Figure S15A*).

To evaluate a direct transcriptional effect of MLL-AF9 and MN1 on the distal Hoxa cluster genes, we analyzed the binding of MN1, MLL-AF9, Hoxa9, MEIS1 and dimethyl marks of H3K79 (representing DOT1L binding) at the Hoxa cluster locus from available chromatin immunoprecipitation-sequencing (ChIP-Seq) data sets. MN1 chromatin marks were enriched at distal Hoxa cluster genes (*Hoxa7* to *Hoxa10*) similar to MLL-AF9, MEIS1 and H3K79me2 marks (Figure 6B), suggesting that MN1 is a direct regulator of *Hoxa* cluster gene expression. However, genome-wide co-localization of MLL-AF9 and MN1 chromatin did not show any overlap of a significant number of chromatin marks, in contrast to the high overlap of MN1 with *Hoxa9* and MEIS1 (Figure 6C-E), suggesting that MN1 is essential for MLL-AF9 primarily due to its role as a co-factor of *Hoxa9* and *Meis1*.

To substantiate this observation, we evaluated the expression of Bcl2 in MLL-AF9/Mn1 wild-type and null cells, as Bcl2 is a known target of *Hoxa9* but not of MLL-

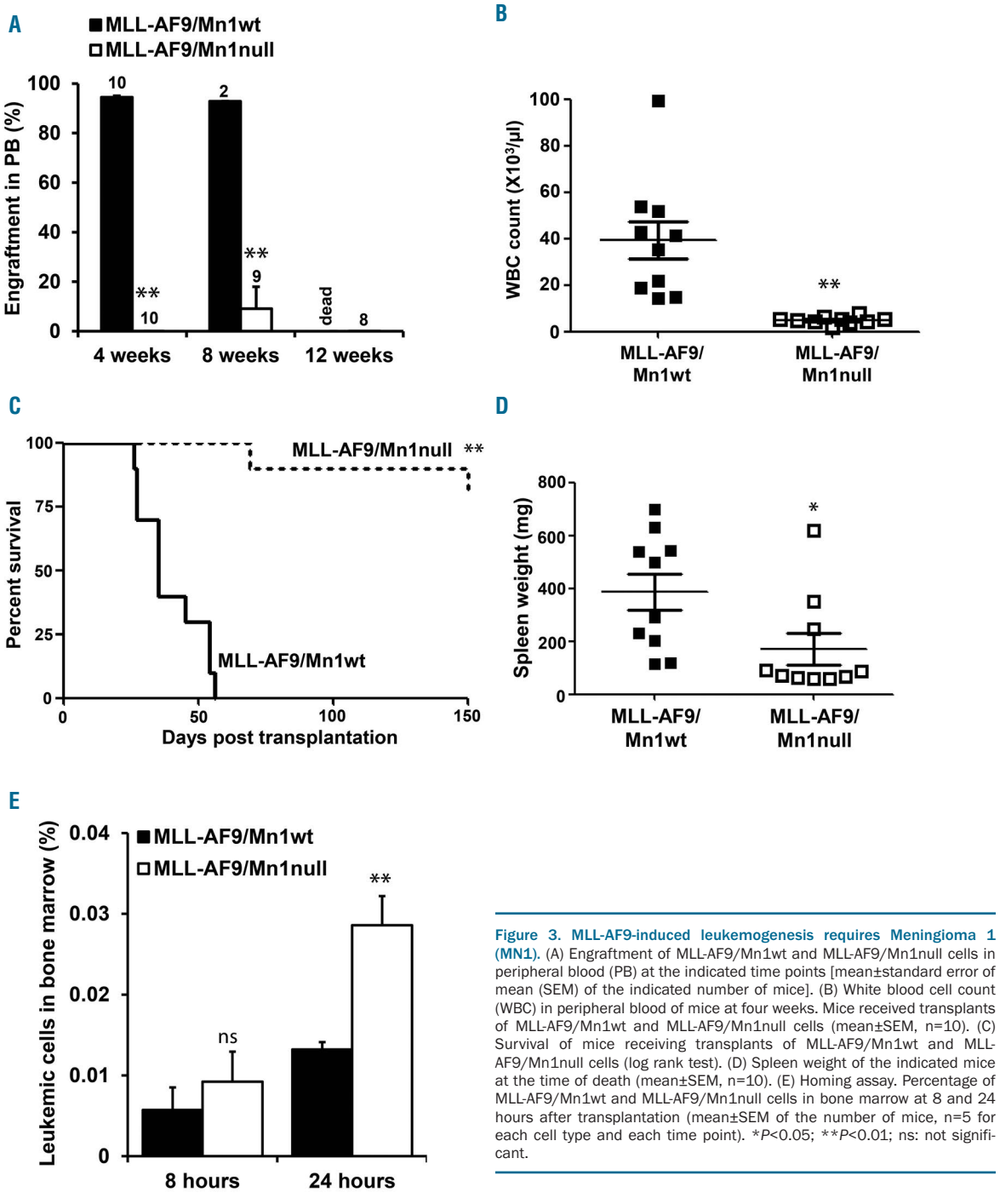

Figure 3. MLL-AF9-induced leukemogenesis requires Meningioma 1 (MN1). (A) Engraftment of MLL-AF9/Mn1wt and MLL-AF9/Mn1null cells in peripheral blood (PB) at the indicated time points [mean±standard error of mean (SEM) of the indicated number of mice]. (B) White blood cell count (WBC) in peripheral blood of mice at four weeks. Mice received transplants of MLL-AF9/Mn1wt and MLL-AF9/Mn1null cells (mean±SEM, n=10). (C) Survival of mice receiving transplants of MLL-AF9/Mn1wt and MLL-AF9/Mn1null cells (log rank test). (D) Spleen weight of the indicated mice at the time of death (mean±SEM, n=10). (E) Homing assay. Percentage of MLL-AF9/Mn1wt and MLL-AF9/Mn1null cells in bone marrow at 8 and 24 hours after transplantation (mean±SEM of the number of mice, n=5 for each cell type and each time point). *P<0.05; **P<0.01; ns: not significant.

AF9 (Figure 6F).[36] In agreement with this, Bcl2 and related genes were strongly down-regulated upon deletion of Mn1 in MLL-AF9 cells (Figure 2C), confirming the critical role of MN1 in *Hoxa9/Meis1* regulated gene expression. We also identified putative *Hoxa9/Hoxa10* targets differentially expressed and regulated in our gene expression data and GSEA analysis in MLL-AF9 (Mn1wt *vs.* Mn1null) cells (*Online Supplementary Table S7* and *Online Supplementary Figure S15B* and *C*). Significantly, more *Hoxa9/Hoxa10* target genes were down-regulated in MLL-AF9/Mn1null (P=0.027, from hypergeometric distribution). Thus, our data suggest that MN1 is required in MLL-r leukemia to

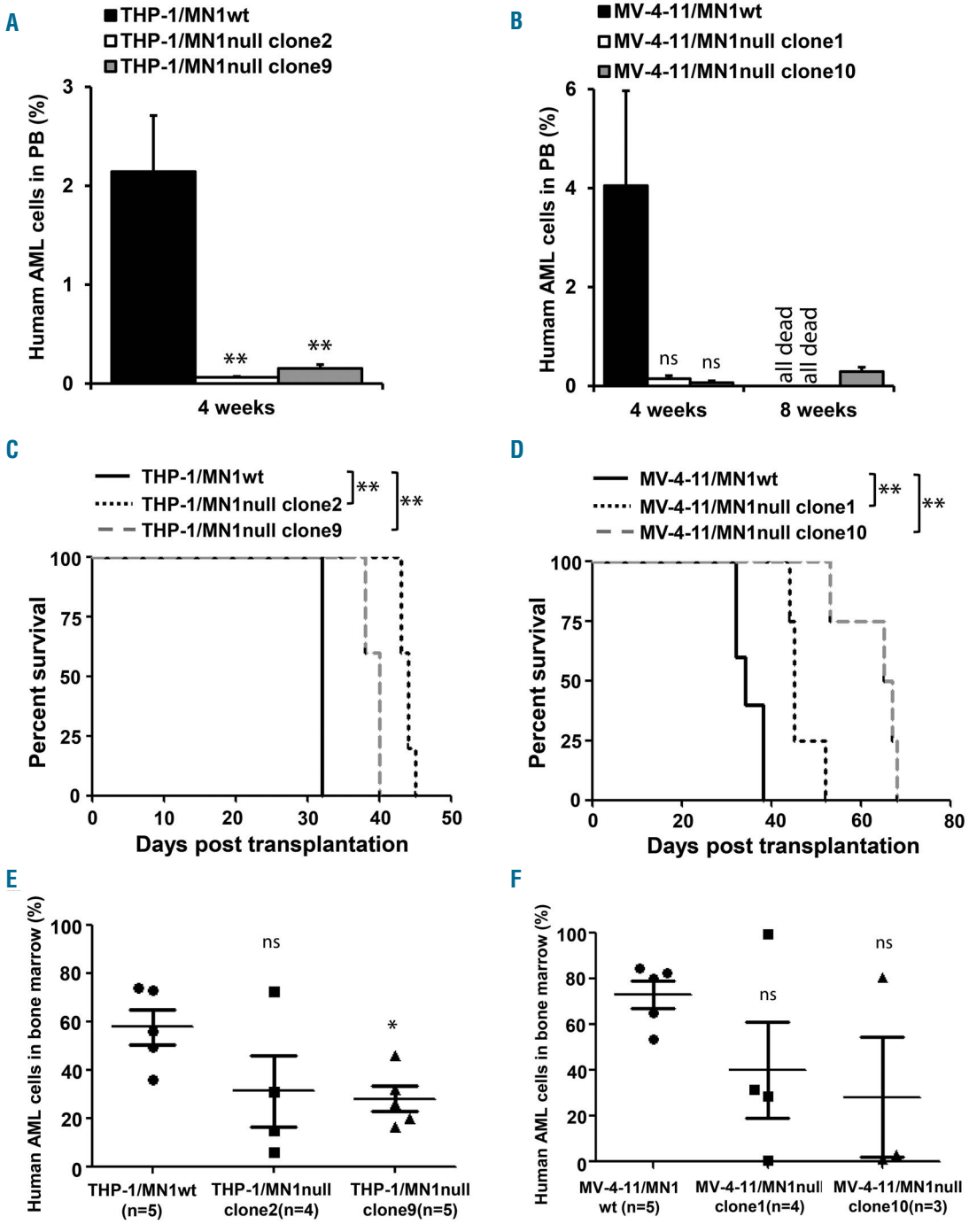

Figure 4. MLL-AF9 and MLL-AF4 rearranged human leukemias also depend on Meningioma 1 (MN1). (A) Engraftment of THP-1/MN1wt and THP-1/MN1null cells in peripheral blood (PB) at four weeks [mean±standard error of mean (SEM), n=5 for THP-1/MN1wt, THP-1/MN1null clone2 and 9]. (B) Engraftment of MV-4-11/MN1wt and MV-4-11/MN1null cells in peripheral blood (PB) at 4 and 8 weeks (mean±SEM; n=5 for MV-4-11/MN1wt, n=4 for MV-4-11/MN1null clone1 and 10). (C) Survival of mice receiving transplants of THP-1/MN1wt and THP-1/MN1null cells (log rank test); (n=5 for THP-1/MN1wt, THP-1/MN1null clone2 and 9). (D) Survival of mice receiving transplants of MV-4-11/MN1wt and MV-4-11/MN1null cells (log rank test); (n=5 for MV-4-11/MN1wt, n=4 for MV-4-11/MN1null clone1 and 10). (E) Percentage of THP-1 (MN1wt or MN1null clone) cells in bone marrow at death (mean±SEM; n=5 for THP-1/MN1wt and THP-1/MN1null clone9, n=4 for THP-1/MN1null clone2). (F) Percentage of MV-4-11 (MN1wt or MN1null clone) cells in bone marrow at death (mean±SEM; n=5 for MV-4-11/MN1wt, n=4 for MV-4-11/MN1null clone1 and n=3 for MV-4-11/MN1null clone10). AML: acute myeloid leukemia; **P<0.01; ns: not significant.

maintain expression of the distal Hoxa cluster and Meis1 and as a co-factor of the *Hoxa9/Meis1* transcriptional complex and their target genes, which also includes MLL.

Meningioma 1 as therapeutic target in MLL-AF9 acute myeloid leukemia

To evaluate MN1 as a therapeutic target in MLL positive AML, we tested the effect of MN1 siRNA in primary human AML cells. As a proof of principle, we first tested *MN1* knockdown using LNP packaged with anti-*MN1* siRNA in the ME-1 cell line, which expresses MN1 at high levels. *MN1* expression was reduced up to 4-fold in anti-MN1 siRNA treated cells as compared to control siRNA treated cells (*Online Supplementary Figure S16A*). Furthermore, we evaluated the effect of MN1 knockdown in CD34$^+$ hematopoietic progenitor cells from four

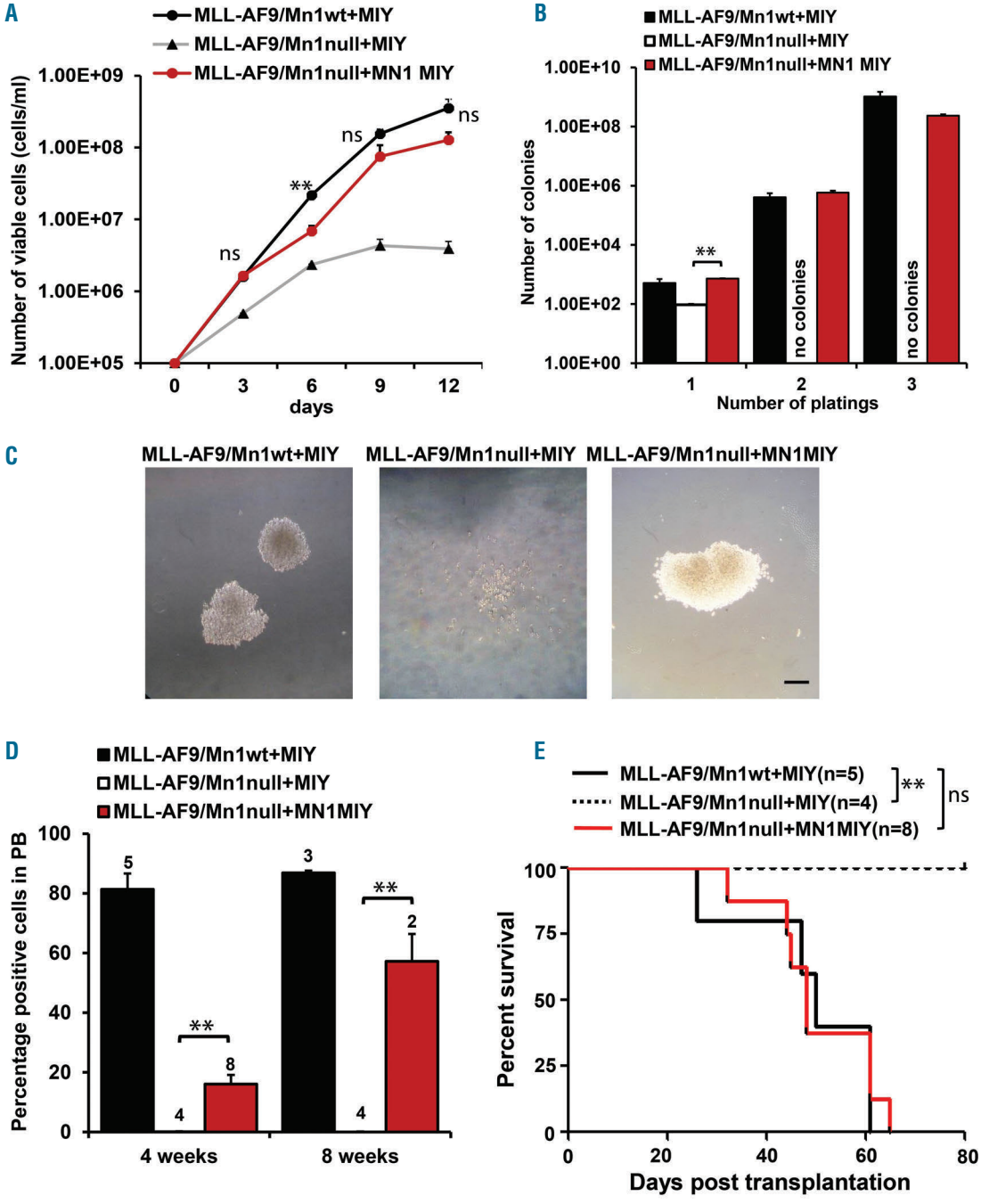

Figure 5. Meningioma 1 (MN1) overexpression restores leukemogenicity in MLL-AF9/Mn1null cells. (A) Cumulative cell counts of MLL-AF9/Mn1wt and MLL-AF9/Mn1null cells transduced with control or MN1MIY plasmid [mean±standard error of mean (SEM), n=3]. (B) Colony-forming cell (CFC) counts of MLL-AF9/Mn1wt and MLL-AF9/Mn1null cells transduced with control or MN1MIY plasmid (mean±SEM, n=3). (C) Morphology of representative CFC colonies of MLL-AF9/Mn1wt and MLL-AF9/Mn1null cells transduced with control or MN1MIY plasmid. Black scale bar represents 0.25 mm. (D) Engraftment of MLL-AF9/Mn1wt and MLL-AF9/Mn1null cells transduced with control or MN1MIY plasmid in peripheral blood (PB) at 4 and 8 weeks after transplantation (mean±SEM of the indicated number of mice). (E) Survival of mice receiving transplants of MLL-AF9/Mn1wt and MLL-AF9/Mn1null cells transduced with control or MN1MIY plasmid (log-rank test). ***P*<0.01; ns: not significant.

healthy stem cell donors and five MLL-AF9 positive AML patients in colony forming cell (CFC) assays. Colony numbers and size were significantly reduced in MLL-AF9 positive AML cells treated with anti-MN1 siRNA compared to CD34+ cells from healthy donors when normalized to control siRNA treated cells (Figure 7A and B). Cell numbers from CFC assays were also found significantly reduced in MLL-AF9 positive AML cells treated with anti-MN1 siRNA (Figure 7C). In order to exclude toxic effects of the LNP/siRNA formulation, we tested an additional anti-MN1 siRNA (MN1 siRNA-3) and found similar specific inhibitory effects with anti-MN1 siRNA-3 against MLL-AF9 positive primary human AML cells (*Online Supplementary Figure S16B* and *C*). Thus, *MN1* expression is critical for proliferation of MLL-transformed leukemic cells while it has no effect on CD34+ cells from healthy donors, suggesting MN1 as a therapeutic target in MLL-transformed AML.

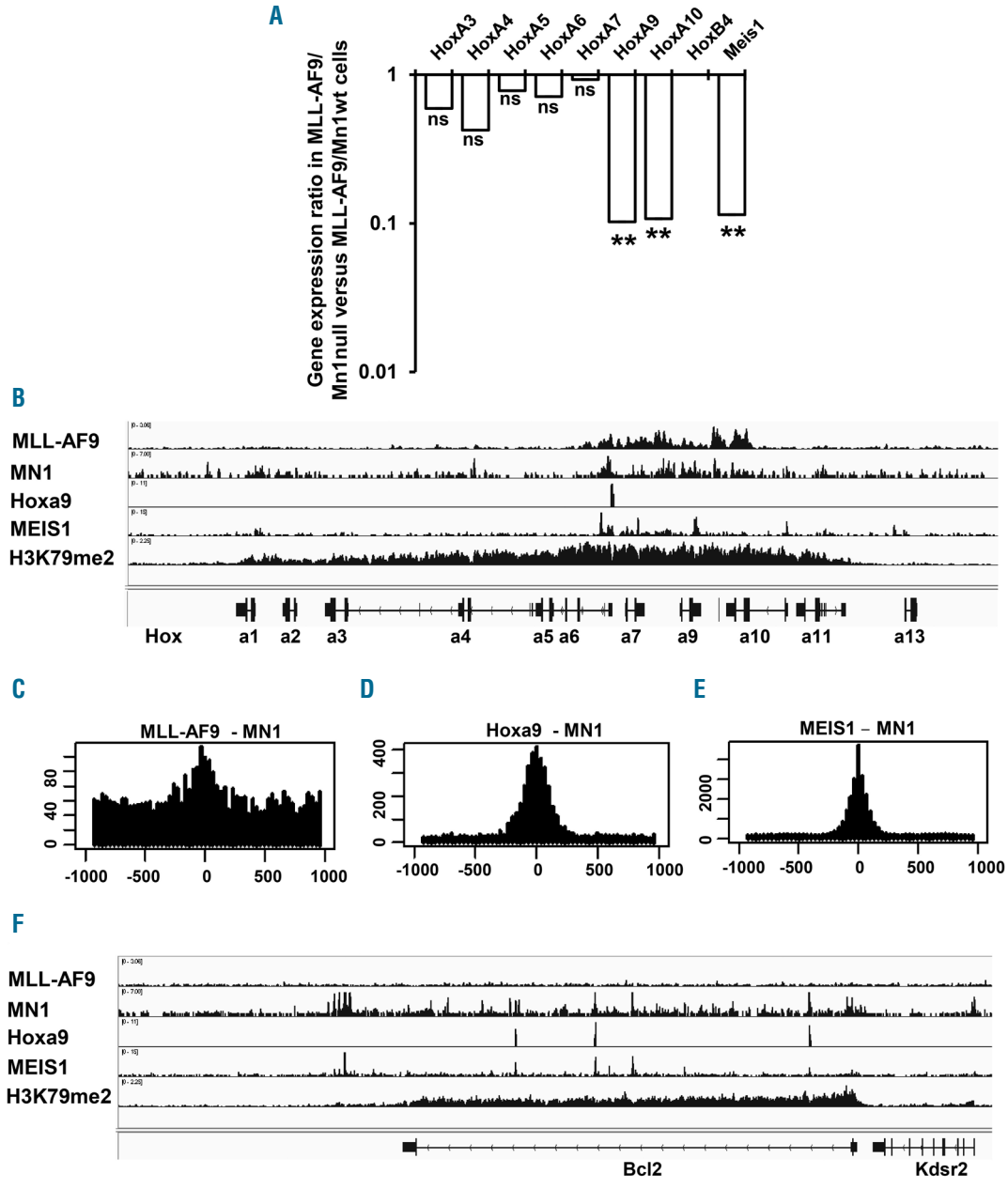

Figure 6. Mn1 maintains distal Hoxa cluster and Meis1 expression. (A) Relative gene expression of differentially expressed genes normalized to Abl1 in MLL-AF9/Mn1wt andMLL-AF9/Mn1null murine cells [mean±standard error of mean (SEM), n=3]. (B) Chromatin immunoprecipitation-sequencing (ChIP-Seq) for MLL-AF9, MN1, Hoxa9, MEIS1 and H3K79me2 in different leukemic cell lines (details in Methods). Screen shot of the Hoxa cluster with binding peaks of the above mentioned proteins. (C) Histogram showing the distance between peak maxima of MLL-AF9 peaks to their closest MN1 peak, indicating that MN1-binding sites are less frequently enriched at MLL-AF9-binding sites. (D) Histogram showing the distance between peak maxima of Hoxa9 peaks to their closest MN1 peak, indicating that MN1-binding sites are highly enriched at Hoxa9-binding sites. (E) Histogram showing the distance between peak maxima of MEIS1 peaks to their closest MN1 peak, indicating that MN1-binding sites are highly enriched at MEIS1-binding sites. (F) ChIP-Seq for MLL-AF9, MN1, Hoxa9, MEIS1 and H3K79me2 in different leukemic cell lines (details in Methods). A screen shot of the Bcl2 gene with binding peaks of the aforementioned proteins. **P*<0.05; ***P*<0.01; ns: not significant.

Discussion

Acute myeloid leukemia pathogenesis requires a multitude of genetic and epigenetic alterations for its initiation and progression.[1] One such genetic alteration is high expression of MN1, which is widely reported as an independent poor prognostic marker in AML patients, and its induced overexpression in mouse cells induces aggressive AML.[7-9,12,13,23] In the knockout studies of MN1, mice died young from cleft palate and severe defects in development

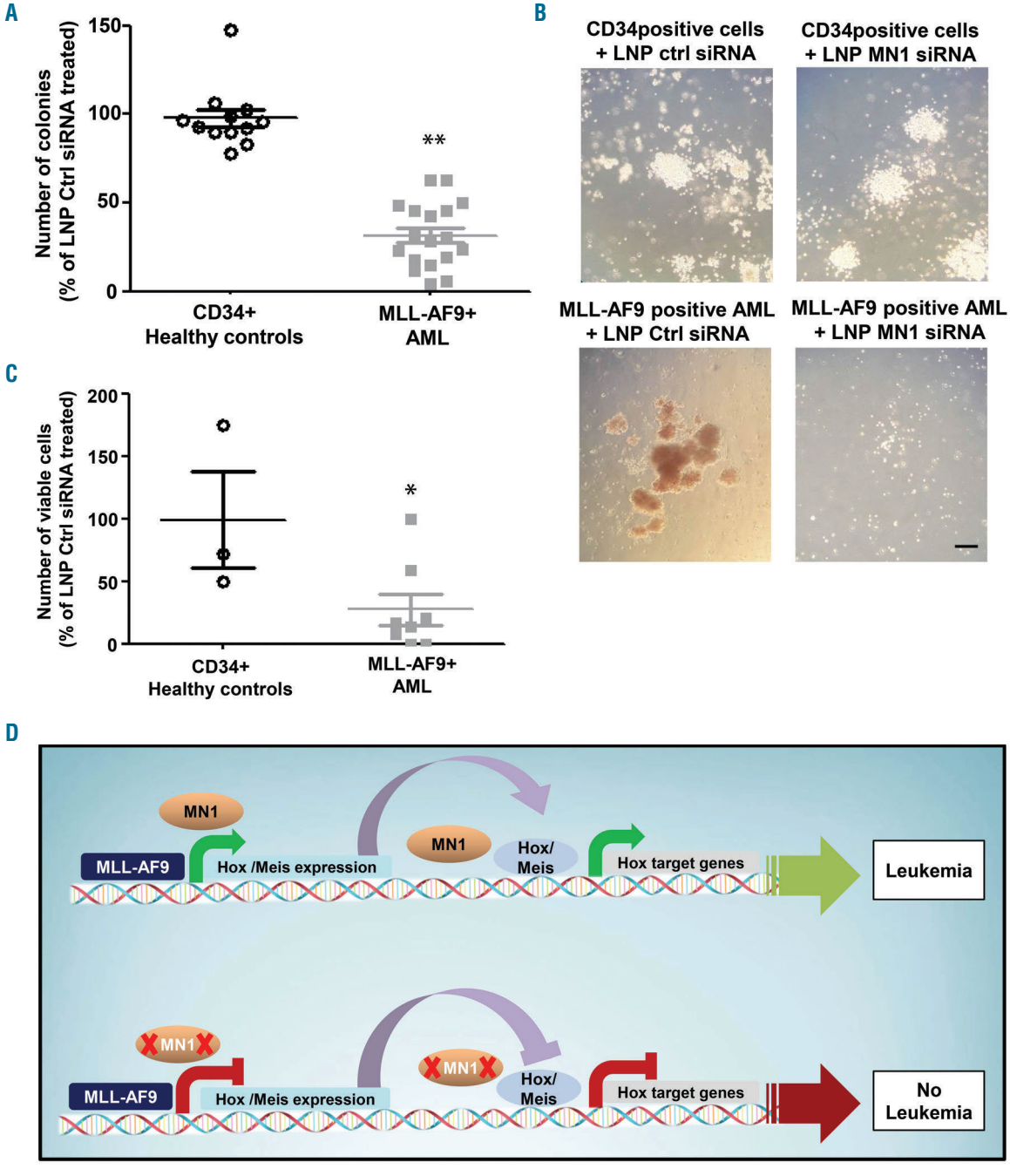

Figure 7. Meningioma 1 (MN1) as therapeutic target in MLL-AF9 acute myeloid leukemia (AML). (A) Colony-forming cell (CFC) counts of CD34$^+$ healthy controls (Ctrl) and MLL-AF9 positive AML patient cells treated with anti-MN1 siRNA/LNP formulation normalized to control siRNA/lipid nanoparticle (LNP) formulation [mean±standard error of mean (SEM), cells from n=4 CD34$^+$ healthy donors with 3 repeats, and cells from n=4 MLL-AF9 positive AML patients with 4 repeats and 2 repeats from 1 patient]. (B) Morphology of representative CFC colonies of CD34$^+$ healthy controls and MLL-AF9 positive AML patient cells treated with control or anti-MN1 siRNA/LNP formulation. Black scale bar represents 0.25 mm. (C) Number of viable cells from colonies of CD34$^+$ healthy controls and MLL-AF9 positive AML patient cells treated with anti-MN1 siRNA/LNP formulation normalized to control siRNA/LNP treated cells (mean±SEM, cells from n=1 CD34$^+$ healthy donor in triplicate, and cells from n=4 MLL-AF9 positive AML patients in duplicate from each patient). *P<0.05; **P<0.01; ns: not significant. (D) Model of MN1-dependency in MLL-rearranged AML. MLL-AF9 and MN1 induces expression of HOXA cluster genes and MEIS1. MN1 is a critical co-factor of the HOXA9/MEIS1 transcriptional complex. Loss of MN1 affects HOXA expression and renders the HOXA9/MEIS1 complex inactive, and loss of this critical downstream complex of MLL-AF9 blocks its transforming ability.

of various bones in the skull. In addition, MN1 KO mice apparently did not develop hematopoietic defects during the first few weeks of life until they died, suggesting that MN1 inhibition or deletion has a therapeutic window when targeted in leukemic cells.[28] It has been previously reported that transient *MN1* knockdown *via* siRNA in human leukemia cell lines reduces their proliferation;[20] however, perpetual loss of *MN1* expression has not been comprehensively studied in murine or human leukemias. Our study shows that CRISPR-Cas-mediated loss of MN1 substantially impairs leukemogenesis in MLL-r leukemias. MN1 loss prevents *in vitro* proliferation and colony-forming potential of MLL-AF9 and MLL-AF4-dependent cells. Correspondingly, we demonstrate that MN1 inactivation inhibits cell cycle, promotes apoptosis and induces differentiation in MLL-r leukemic cells. In addition, loss of MN1 significantly impairs MLL-AF9-mediated murine leukemogenesis and reduces leukemic and tumor growth of human MLL-rearranged leukemias *in vivo*. Our results are supported by a previous study, which found that Mn1 cooperated with Mll-AF9 in leukemogenesis in an *in vivo* transplantation assay.[6] The homing potential of MLL-AF9/Mn1null cells is not affected by Mn1 deletion. We also show that re-expression of MN1 in MLL-AF9/Mn1null cells restores the leukemic potential of MLL-AF9.

Both MN1 and MLL-AF9-induced leukemias rely on expression of the *Hoxa9/Meis1* complex.[2,25,33,35,37,38] On a genome-wide level chromatin binding of MN1 largely over-lapped with HOXA9 and MEIS1 binding, suggesting that the previously described function of MN1 as a co-factor of HOXA9/MEIS1 is its major contribution to the leukemogenic activity of MLL-AF9, as illustrated in our study (Figure 7D). This is supported by our gene expression data showing that HOXA9 target genes are primarily down-regulated upon MN1 deletion. Previous studies have found that both MLL-AF9 and MN1-induced leukemias are dependent on *Dot1l*.[14,25,26] MLL fusions misdirect DOT1L to the promoters of Hoxa cluster genes and Meis1 leading to H3K79 methylation and constitutive activation of these genes.[2,25,33] It is important to note that MN1 transformed HSC have high expression of HOXA9 irrespective of DOT1L expression.[14] In support of this observation, we show that loss of MN1 can overcome the effect of MLL-AF9 and DOT1L-directed dysregulation of HOXA cluster genes and MEIS1.

The leukemogenicity of MLL-positive leukemias is dependent on genes such as the Mll wild-type allele, AF9, Dot1l, JMJD1C, PU.1, CBX8, Hoxa7, Hoxa9 and S6K1, which mediate the leukemogenic activity of MLL-AF9 predominantly by Dot1l gene activation.[26,33,37-41] Our data provide additional insights into MLL-rearranged leukemia through the addition of MN1 as a crucial co-factor regulating the HOXA cluster, MEIS1 and their target genes. As U937 cells were moderately affected by MN1 deletion, we speculate that cells with high HOXA9/MEIS1 expression may also depend on MN1 like MLL-r cells. Therefore, we predict that MN1 is not only required for MLL-transformed leukemias, but for approximately 50% of AML cases, which show dysregulated expression of the clustered homeobox genes.

High MN1 expression has been reported as a poor prognostic marker in AML patients, and its overexpression induces ATRA resistance and AML in mouse cells.[7-9,12,13,23] Also, it is most highly expressed in CMP, and scantily expressed in HSC and more differentiated cells.[23] Interestingly, induced MN1 expression cannot transform stem cells, as previously described,[23] and we hereby report that proliferation of $CD34^+$ cells remain unaffected by depletion of MN1 expression. Hence, the expression characteristics of MN1 seem to be favorable for therapeutic targeting. A potential therapeutic index is indicated by lack of an inhibitory effect in normal stem/progenitor cells and a specific inhibitory effect in AML cells. Therefore, targeting MN1 by LNP/siRNA formulations holds a strong potential therapeutic avenue, as suggested by our previous proof-of-principle study in a PDX model of acute lymphoblastic leukemia *in vivo*.[32]

In summary, we identify MN1 as an essential protein in MLL fusion gene leukemia *in vivo* and highlight its importance as a co-factor of the HOXA9/MEIS1 complex. An LNP/siRNA formulation against MN1 effectively inhibits the colony-forming potential of MLL-r primary AML cells, suggesting that MN1 is a valid and druggable target in AML.

Acknowledgments

We thank Silke Glowotz, Annett Reinsch, Basem Othman, Kerstin Goerlich, Martin Wichmann, Nadine Kattre and Renate Schottmann for technical help. We also thank Dr. Matthias Ballmaier and the staff of the Cell Sorting Core Facility of Hannover Medical School for their excellent service (supported in part by the Braukmann-Wittenberg-Herz-Stiftung).

Funding

This study was supported by the Rudolf- Bartling Stiftung, an ERC grant under the European Union's Horizon 2020 research and innovation program (n. 638035), Deutsche Krebshilfe (70112697) and DFG grants HE 5240/5-1, HE 5240/5-2, HE 5240/6-1 and HE 5240/6-2.

References

1. Papaemmanuil E, Gerstung M, Bullinger L, et al. Genomic Classification and Prognosis in Acute Myeloid Leukemia. N Engl J Med. 2016;374(23):2209-2221.
2. Slany RK. The molecular mechanics of mixed lineage leukemia. Oncogene. 2016;35(40):5215-5223.
3. Meyer C, Burmeister T, Groger D, et al. The MLL recombinome of acute leukemias in 2017. Leukemia. 2018;32(2):273-284.
4. Milne TA. Mouse models of MLL leukemia: recapitulating the human disease. Blood. 2017;129(16):2217-2223.
5. Mueller D, Garcia-Cuellar MP, Bach C, Buhl S, Maethner E, Slany RK. Misguided transcriptional elongation causes mixed lineage leukemia. PLoS Biol. 2009;7(11):e1000249.
6. Bergerson RJ, Collier LS, Sarver AL, et al. An insertional mutagenesis screen identifies genes that cooperate with Mll-AF9 in a murine leukemogenesis model. Blood. 2012;119(19):4512-4523.
7. Heuser M, Argiropoulos B, Kuchenbauer F, et al. MN1 overexpression induces acute myeloid leukemia in mice and predicts ATRA resistance in patients with AML. Blood. 2007;110(5):1639-1647.
8. Heuser M, Beutel G, Krauter J, et al. High meningioma 1 (MN1) expression as a predictor for poor outcome in acute myeloid

leukemia with normal cytogenetics. Blood. 2006;108(12):3898-3905.
9. Langer C, Marcucci G, Holland KB, et al. Prognostic importance of MN1 transcript levels, and biologic insights from MN1-associated gene and microRNA expression signatures in cytogenetically normal acute myeloid leukemia: a cancer and leukemia group B study. J Clin Oncol. 2009; 27(19):3198-3204.
10. Schwind S, Marcucci G, Kohlschmidt J, et al. Low expression of MN1 associates with better treatment response in older patients with de novo cytogenetically normal acute myeloid leukemia. Blood. 2011;118(15): 4188-4198.
11. Haferlach C, Kern W, Schindela S, et al. Gene expression of BAALC, CDKN1B, ERG, and MN1 adds independent prognostic information to cytogenetics and molecular mutations in adult acute myeloid leukemia. Genes Chromosomes Cancer. 2012;51(3):257-265.
12. Carella C, Bonten J, Sirma S, et al. MN1 overexpression is an important step in the development of inv(16) AML. Leukemia. 2007;21(8):1679-1690.
13. Metzeler KH, Dufour A, Benthaus T, et al. ERG expression is an independent prognostic factor and allows refined risk stratification in cytogenetically normal acute myeloid leukemia: a comprehensive analysis of ERG, MN1, and BAALC transcript levels using oligonucleotide microarrays. J Clin Oncol. 2009;27(30):5031-5038.
14. Riedel SS, Haladyna JN, Bezzant M, et al. MLL1 and DOT1L cooperate with meningioma-1 to induce acute myeloid leukemia. J Clin Invest. 2016;126(4):1438-1450.
15. Sharma A, Yun H, Jyotsana N, et al. Constitutive IRF8 expression inhibits AML by activation of repressed immune response signaling. Leukemia. 2015;29(1):157-168.
16. van Wely KH, Molijn AC, Buijs A, et al. The MN1 oncoprotein synergizes with coactivators RAC3 and p300 in RAR-RXR-mediated transcription. Oncogene. 2003;22(5):699-709.
17. van Wely KH, Meester-Smoor MA, Janssen MJ, Aarnoudse AJ, Grosveld GC, Zwarthoff EC. The MN1-TEL myeloid leukemia-associated fusion protein has a dominant-negative effect on RAR-RXR-mediated transcription. Oncogene. 2007;26(39):5733-5740.
18. Slape C, Hartung H, Lin YW, Bies J, Wolff L, Aplan PD. Retroviral insertional mutagenesis identifies genes that collaborate with NUP98-HOXD13 during leukemic transformation. Cancer Res. 2007;67(11):5148-5155.
19. Caudell D, Harper DP, Novak RL, et al. Retroviral insertional mutagenesis identifies Zeb2 activation as a novel leukemogenic collaborating event in CALM-AF10 transgenic mice. Blood. 2010;115(6): 1194-1203.
20. Liu T, Jankovic D, Brault L, et al. Functional characterization of high levels of meningioma 1 as collaborating oncogene in acute leukemia. Leukemia. 2010;24(3):601-612.
21. Watanabe-Okochi N, Kitaura J, Ono R, et al. AML1 mutations induced MDS and MDS/AML in a mouse BMT model. Blood. 2008;111(8):4297-4308.
22. Braun CJ, Boztug K, Paruzynski A, et al. Gene therapy for Wiskott-Aldrich syndrome--long-term efficacy and genotoxicity. Sci Transl Med. 2014;6(227):227ra33.
23. Heuser M, Yun H, Berg T, et al. Cell of origin in AML: susceptibility to MN1-induced transformation is regulated by the MEIS1/AbdB-like HOX protein complex. Cancer Cell. 2011;20(1):39-52.
24. Krivtsov AV, Twomey D, Feng Z, et al. Transformation from committed progenitor to leukaemia stem cell initiated by MLL-AF9. Nature. 2006;442(7104):818-822.
25. Bernt KM, Zhu N, Sinha AU, et al. MLL-rearranged leukemia is dependent on aberrant H3K79 methylation by DOT1L. Cancer Cell. 2011;20(1):66-78.
26. Nguyen AT, Taranova O, He J, Zhang Y. DOT1L, the H3K79 methyltransferase, is required for MLL-AF9-mediated leukemogenesis. Blood. 2011;117(25):6912-6922.
27. Sharma A, Jyotsana N, Lai CK, et al. Pyrimethamine as a Potent and Selective Inhibitor of Acute Myeloid Leukemia Identified by High-throughput Drug Screening. Curr Cancer Drug Targets. 2016; 16(9):818-828.
28. Meester-Smoor MA, Vermeij M, van Helmond MJ, et al. Targeted disruption of the Mn1 oncogene results in severe defects in development of membranous bones of the cranial skeleton. Mol Cell Biol. 2005;25(10):4229-4236.
29. Heuser M, Sly LM, Argiropoulos B, et al. Modeling the functional heterogeneity of leukemia stem cells: role of STAT5 in leukemia stem cell self-renewal. Blood. 2009;114(19):3983-3993.
30. Reimer J, Knoss S, Labuhn M, et al. CRISPR-Cas9-induced t(11;19)/MLL-ENL translocations initiate leukemia in human hematopoietic progenitor cells in vivo. Haematologica. 2017;102(9):1558-1566.
31. Stemmer M, Thumberger T, Del Sol Keyer M, Wittbrodt J, Mateo JL. CCTop: An Intuitive, Flexible and Reliable CRISPR/Cas9 Target Prediction Tool. PLoS One. 2015;10(4):e0124633.
32. Jyotsana N, Sharma A, Chaturvedi A, et al. RNA interference efficiently targets human leukemia driven by a fusion oncogene in vivo. Leukemia. 2018;32(1):224-226.
33. Deshpande AJ, Deshpande A, Sinha AU, et al. AF10 regulates progressive H3K79 methylation and HOX gene expression in diverse AML subtypes. Cancer Cell. 2014;26(6):896-908.
34. Huang Y, Sitwala K, Bronstein J, et al. Identification and characterization of Hoxa9 binding sites in hematopoietic cells. Blood. 2012;119(2):388-398.
35. Argiropoulos B, Humphries RK. Hox genes in hematopoiesis and leukemogenesis. Oncogene. 2007;26(47):6766-6776.
36. Brumatti G, Salmanidis M, Kok CH, et al. HoxA9 regulated Bcl-2 expression mediates survival of myeloid progenitors and the severity of HoxA9-dependent leukemia. Oncotarget. 2013;4(11):1933-1947.
37. Zhou J, Wu J, Li B, et al. PU.1 is essential for MLL leukemia partially via crosstalk with the MEIS/HOX pathway. Leukemia. 2014;28(7):1436-1448.
38. Ayton PM, Cleary ML. Transformation of myeloid progenitors by MLL oncoproteins is dependent on Hoxa7 and Hoxa9. Genes Dev. 2003;17(18):2298-2307.
39. Tan J, Jones M, Koseki H, et al. CBX8, a polycomb group protein, is essential for MLL-AF9-induced leukemogenesis. Cancer Cell. 2011;20(5):563-575.
40. Zhu N, Chen M, Eng R, et al. MLL-AF9- and HOXA9-mediated acute myeloid leukemia stem cell self-renewal requires JMJD1C. J Clin Invest. 2016;126(3):997-1011.
41. Ghosh J, Kobayashi M, Ramdas B, et al. S6K1 regulates hematopoietic stem cell self-renewal and leukemia maintenance. J Clin Invest. 2016;126(7):2621-2625.

Ferrata Storti Foundation

Haematologica 2020
Volume 105(5):1306-1316

TARP is an immunotherapeutic target in acute myeloid leukemia expressed in the leukemic stem cell compartment

Barbara Depreter,[1,2] Karin E. Weening,[2,3] Karl Vandepoele,[2,4] Magnus Essand,[5] Barbara De Moerloose,[1,2,6] Maria Themeli,[7] Jacqueline Cloos,[7] Diana Hanekamp,[7] Ine Moors,[8] Inge D'hont,[6] Barbara Denys,[2,4] Anne Uyttebroeck,[9] An Van Damme,[10] Laurence Dedeken,[11] Sylvia Snauwaert,[12] Glenn Goetgeluk,[3] Stijn De Munter,[2,3] Tessa Kerre,[2,8] Bart Vandekerckhove,[2,3] Tim Lammens[1,2*] and Jan Philippé[2,3,4*]

[1]Department of Internal Medicine and Pediatrics, Ghent University, Ghent, Belgium; [2]Cancer Research Institute Ghent, Ghent University, Ghent, Belgium; [3]Department of Diagnostic Sciences, Ghent University, Ghent, Belgium; [4]Department of Laboratory Medicine, Ghent University Hospital, Ghent, Belgium; [5]Science for Life Laboratory, Department of Immunology, Genetics and Pathology, Uppsala University, Uppsala, Sweden; [6]Department of Pediatric Hematology-Oncology and Stem Cell Transplantation, Ghent University Hospital, Ghent, Belgium; [7]Department of Hematology, VU University Medical Center, Amsterdam, the Netherlands; [8]Department of Hematology, Ghent University Hospital, Ghent, Belgium; [9]Department of Pediatrics, University Hospital Gasthuisberg, Louvain, Belgium; [10]Department of Pediatric Hematology Oncology, University Hospital Saint-Luc, Brussels, Belgium; [11]Department of Pediatric Hematology Oncology, Queen Fabiola Children's University Hospital, Brussels, Belgium and [12]Department of Hematology, AZ Sint-Jan Hospital Bruges, Bruges, Belgium

**JP and TL contributed equally to this work as co-senior authors.*

ABSTRACT

Immunotherapeutic strategies targeting the rare leukemic stem cell compartment might provide salvage to the high relapse rates currently observed in acute myeloid leukemia (AML). We applied gene expression profiling for comparison of leukemic blasts and leukemic stem cells with their normal counterparts. Here, we show that the T-cell receptor γ chain alternate reading frame protein (TARP) is over-expressed in *de novo* pediatric (n=13) and adult (n=17) AML sorted leukemic stem cells and blasts compared to hematopoietic stem cells and normal myeloblasts (15 healthy controls). Moreover, TARP expression was significantly associated with a fms-like tyrosine kinase receptor-3 internal tandem duplication in pediatric AML. TARP overexpression was confirmed in AML cell lines (n=9), and was found to be absent in B-cell acute lymphocytic leukemia (n=5) and chronic myeloid leukemia (n=1). Sequencing revealed that both a classical TARP transcript, as described in breast and prostate adenocarcinoma, and an AML-specific alternative TARP transcript, were present. Protein expression levels mostly matched transcript levels. TARP was shown to reside in the cytoplasmic compartment and showed sporadic endoplasmic reticulum co-localization. TARP-T-cell receptor engineered cytotoxic T-cells *in vitro* killed AML cell lines and patient leukemic cells co-expressing TARP and HLA-A*0201. In conclusion, TARP qualifies as a relevant target for immunotherapeutic T-cell therapy in AML.

Correspondence:

TIM LAMMENS
tim.lammens@ugent.be

Received: March 21, 2019.

Accepted: July 12, 2019.

Pre-published: August 1, 2019.

doi:10.3324/haematol.2019.222612

Check the online version for the most updated information on this article, online supplements, and information on authorship & disclosures: www.haematologica.org/content/105/5/1306

Introduction

Acute myeloid leukemia (AML) is a heterogeneous hematologic malignancy, accounting for 80% of adult[1-4] and 20% of pediatric[5-7] leukemia. Despite initial clinical remission rates of 60-90%,[2,5,6] patients exhibit a high relapse risk and therapy-related mortality, resulting in a 5-year overall survival of 30% in adult AML[1,3] and 65-70% in pediatric AML (pedAML).[5,8] Especially the prognosis of patients with fms-like tyrosine kinase receptor-3 internal tandem duplications (*FLT3*-ITD) remains extremely poor.[2,8,9] The high relapse rate is thought to arise from a chemotherapy-resistant cell fraction with unlimited self-renewal capacities,

denominated as leukemic stem cells (LSC).[4,10-14] In CD34$^+$ AML, stem cell characteristics were shown to be present in all four CD34/CD38 phenotypic compartments, though the CD34$^+$CD38$^-$ fraction was the most LSC-enriched.[15] Moreover, a high LSC load at diagnosis was shown to be a significant adverse prognostic factor.[16-19] Unfortunately, current chemotherapeutic regimens were shown to perform inadequate towards LSC eradication[14] and they induce important toxicity.[5,6,20] Also hematopoietic stem cell transplantation, performed in high-risk (HR) patients or as salvage therapy, carries a high mortality and morbidity risk,[2,5] highlighting the need for alternative treatments. Thus, identifying LSC aberrations is crucial to tackle the high relapse rate and to develop therapeutic targeting strategies for LSC elimination, while ensuring salvage of normal hematopoietic stem cells (HSC).

Targeted therapy has led to remarkable progress in the survival rates of multiple cancers. The introduction of tyrosine kinase inhibitors in the treatment of chronic myeloid leukemia (CML) accomplished a major breakthrough, and CD19-directed chimeric antigen receptor (CAR) therapy has led to an enormous improvement in survival in relapsed/refractory pediatric ALL.[21,22] These successes paved the way for the exploration of the clinical applicability of targeting antibodies and CAR- or T-cell receptor (TCR)-transgenic cytotoxic T cells (CTL) in AML.[2,23-28] Although an increasing number of LSC-specific membrane markers have been identified over recent years,[18,23,29,30] only a few reports address the molecular abnormalities of LSC compared to HSC,[15,31-37] especially in pedAML.

Here, we identified the T-cell receptor (TCR)γ chain alternate reading frame protein (TARP) as an AML-specific target, expressed in the LSC and blasts of pediatric and adult AML, while absent in their normal counterparts. *TARP* transcript expression was associated with *FLT3*-ITD in pedAML. In addition, we provide *in vitro* evidence that TARP may serve as a novel immunotherapeutic target in AML for TARP-TCR engineered CTL.

Methods

Patients

We retrospectively selected diagnostic material from 13 pedAML and 17 adult AML patients based on the sample availability, LSC load, CD34 positivity, *FLT3* mutational status, and HLA-status (Table 1 and *Online Supplementary Table S1*). At diagnosis, mononuclear cells (MNC) were isolated from bone marrow (BM) or peripheral blood (PB) by Ficoll density gradient (Axis-shield) and cryopreserved in 90% fetal calf serum (FCS) and 10% dimethylsulfoxide (DMSO). Samples were thawed, followed by 30 minutes (min) incubation at room temperature (RT) in 20 mL RPMI with 20% FCS, 200 µL DNase I (1 mg/mL, grade II bovine pancreas), and 200 µL MgCl2 (1 M) (Sigma-Aldrich). After incubation, cells were spinoculated (10 min, 400 rpm) and washed once more with RPMI/20% FCS.

In addition, we prospectively collected material from 15 healthy subjects. Normal bone marrow (NBM, n=6) was collected from posterior iliac crest of pediatric patients (4-18 years) undergoing scoliosis surgery. Umbilical cord blood (CB, n=7) was obtained after normal vaginal deliveries at full term. Mobilized peripheral blood stem cells (mPBSC, n=2) were collected by apheresis of adult donors pre-allotransplant. All patients or their guardians gave their informed consent and approval was obtained by the ethical committee, in accordance with the Declaration of Helsinki. Buffy coats from donors were obtained from the Red Cross (Mechelen, Belgium) and used for CTL isolation and the preparation of feeder cell medium.

Flow cytometry analysis and cell sorting

Cell pellets were surface stained (*Online Supplementary Table S2*), followed by 20 min incubation at 4°C and washing with PBS$^+$2% BSA. For cell-sorting, labeled cells were resuspended in medium and sorted on a FACSAria III with red, blue, and violet lasers (BD Biosciences). For flow cytometry (FCM) analysis, cells were resuspended in PBS+2% BSA and analyzed on a LSR II or a FACSCanto II, equipped with four or three solid-state lasers, respectively (both BD Biosciences). All scatters were devoid of doublets based on FSC-H/FSC-A, and propidium iodide (PI) was used to exclude dead cells. Sorting strategies are described in *Online Supplementary Data 2.2.* Regarding FCM-based cytotoxicity and cytokine assays (*Online Supplementary Data 2.9*), living cells were selected using a LIVE/DEAD staining (1:10000 dilution, ThermoFisher Scientific) instead of PI. Target cells were stained with a Violet CellTrace™ (VT) Cell Proliferation Kit (5 mM, 1:10000 dilution, ThermoFisher Scientific) prior to incubation with TCR-engineered CTL. After incubation and before surface staining, Flow-Count™ Fluorospheres (1:20 diluted, Beckman Coulter) were added to each well to enable target quantification (measurement of minimum 1000 Fluorospheres/well).

Transcript expression

Details on micro-array profiling, RNA isolation, cDNA synthesis, quantitative polymerase chain reaction (qPCR) conditions and primers can be found in *Online Supplementary Data 2.3, 2.4, 2.5* and *Online Supplementary Table S3*. qPCR data analysis was performed according to state-of-the-art methods.[38,39] Relative quantity (RQ) values were normalized against housekeeping genes *GAPD, HPRT1* and *TBP*. For *TARP* expression, normalized relative quantities were calibrated (calibrated normalized relative quantity, CNRQ) *versus* a single calibrator to allow interrun comparison. For the investigation of the subcellular localization of TARP, delta (d) Ct between cytoplasmic and nuclear compartments were calculated and compared to *MALAT1* and *TBP* expression. Functional TCRG gene rearrangements were excluded if sufficient material remained using DNA TCRG GeneScan analysis40 and/or TRGV(J)C qPCR (*Online Supplementary Table S4*).

Protein detection

Details on western blotting and confocal microscopy are provided in *Online Supplementary Data 2.6*.

Viral transduction of acute myeloid leukemia cell lines and generation of T-cell receptor-transgenic cytotoxic T cells

All transfer and helper plasmids used, and procedures for transformation, plasmid isolation, transfection and transduction are described in *Online Supplementary Data 2.7 and 2.8*.

Six AML cell lines (HL-60, Kg-1a, MOLM-13, HL-60-Luc, MOLM-13-Luc and MV4;11-Luc) were transduced with HLA-A*0201 MHC-I encoding retrovirus, hereafter defined as A2+. Transgenic TARP overexpression (OE) cell lines were generated for OCI-AML3 and THP-1, next to mock controls. TARP was knocked down in four TARP-high AML cell lines (HL-60, Kg-1a, MV4;11 and THP-1) using three different shRNA, next to mock controls.

TARP-TCR engineered CTL were generated by transduction with lentiviral (LV) or retroviral (RV) particles encoding a TCRA8-T2A-TCRB12 sequence directed against the HLA-A*0201-restrict-

Table 1. Characteristics of *de novo* acute myeloid leukemia (AML) patients used for sorting CD34$^+$CD38$^+$ and CD34$^+$CD38$^-$ cell fractions and qualitative polymerase chain reaction evaluation.

	Pediatric AML (n=13) Median (Range)		Adult AML (n=17) Median (Range)	
Age, years	10 (2-16)		48 (20 - 76)	
WBC count, x 10^9/L	66 (2.7-336)		15 (6-274)†	
Morphological blast count				
BM, %	81 (34-96)		77 (28-90)†	
PB, %	67 (1-95)		73 (7-93)‖	
	N	%	N	%
Gender				
F	7	53.8%	9	52.9%
M	6	46.2%	8	47.1%
Sample				
BM	8	61.5%	11	64.7%
PB	5	38.5%	6	35.3%
CD34 positivity	13	100.0%	15	88.2%
Fusion transcript	6	46.2%	3*	18.8%
CBF leukemia	4	30.8%	2	11.8%
WT1 overexpression	10	76.9%	10‡	71.4%
Mutation status				
NPM1	0	0.0%	5‡	35.7%
FLT3-ITD	8	61.5%	9†	60.0%
Risk classification				
SR	7	53.8%	Favorable	423.5%
HR	5	38.5%	Intermediate-I/II	741.2%
Unknown	1	7.7%	Adverse	317.6%
			Unknown	317.6%

Pediatric acute myeloid leukemia (pedAML) patients were diagnosed in Belgium and treated according to the DB AML-01 (n=9, 69%) or NOPHO-DBH AML 2012 (n=4, 31%) protocol. Pediatric patients were risk stratified as previously published[8] and categorized according to the French-American-British (FAB) classification into M0 (n=1), M1 (n=1), M2 (n=4), M3 (n=1), M4 (n=3), M5 (n=2), and M7 (n=1). Adult AML samples were from patients treated at the Ghent University Hospital, Ghent, Belgium (n=12, 71%) or VUmc, Amsterdam, the Netherlands (n=5, 29%). Belgian patients were treated according to local and international guidelines, whereas Dutch patients were included in the HOVON 102 (n=3) or HOVON 132 (n=2) study. Adults were risk stratified according to the European LeukemiaNet 2010 guidelines[1] and categorized according to the FAB classification into M1 (n=6), M2 (n=6), and M3 (n=2). *WT1* overexpression was interpreted according to in-house or published cut-offs. Core binding factor (CBF)-positive leukemias comprised AML with t(8;21)(q22;q22) (pedAML=3) and inv(16)(p13q22) (pedAML=1, adult AML=2). Other fusion transcripts detected were *DEK-NUP214* (pedAML=1) and *PML-RARA* (pedAML=1, adult AML=1). *One, †two, ‡three or ‖five missing data. BM: bone marrow; F: female; M: male; *NPM1*: nucleophosmin; PB: peripheral blood; WBC: white blood cell; WT1: Wilms' tumor 1.

ed synthetic TARP peptide TARP(P5L).[4-13] Regarding RV transduced TARP-TCR CTL, mock CTL were used to correct for non-TARP mediated lysis, and CMV-TCR transduced CTL to evaluate aspecific killing.

Results

Discovery of T-cell receptor γ chain alternate reading frame protein transcript expression in acute myeloid leukemia

In order to identify LSC-specific antigens, we re-analyzed the gene set enrichment (GSE) 17054 micro-array dataset from Majeti *et al.*,[31] which included gene expression profiles of CD34$^+$CD38$^-$ sorted fractions of four healthy adults (HSC) and nine adult AML patients (LSC). *TARP* ranked first amongst the top differentially expressed genes, with all four probes in the top 20 (range log2-FC 5.13-6.92), showing a significantly higher expression in LSC compared to HSC (P<0.01) (*Online Supplementary Figure S1*). TARP had previously been identified as a truncated TCR transcript expressed in androgen-sensitive prostate and breast adenocarcinoma (*Online Supplementary Figure S2*).[41,42] We further explored *TARP* expression in pedAML by micro-array profiling CD34$^+$CD38$^+$ (n=4, leukemic blast) and CD34$^+$CD38$^-$ (n=3, LSC) sorted cell populations from four pedAML patients (2 *FLT3*-ITD and 2 *FLT3* WT) (*Online Supplementary Table S1*). In addition, sorted CD34$^+$CD38$^+$ (n=3) and CD34$^+$CD38- (n=2) cells from CB were profiled to examine the expression in their normal counterparts (*Online Supplementary Figure S3*). TARP appeared to be more highly expressed in leukemic blasts and LSC from *FLT3*-ITD patients compared to *FLT3* WT patients and CB (Figure 1A). This finding suggested that TARP might represent a LSC-associated target within HR pedAML patients harboring *FLT3*-ITD.

To validate these data in a larger patient group, we sorted CD34$^+$CD38$^+$ and CD34$^+$CD38$^-$ cell populations from nine additional pedAML (resulting in a total of 13 pedAML patients), 17 adult AML (Table 1) and 15 control samples (n=7 CB, n=6 NBM, n=2 mPBSC). qPCR analysis using TARP short primers (*Online Supplementary Table S3 and Online Supplementary Figure S2*) showed that *TARP* transcripts were consistently low in HSC and myeloblasts

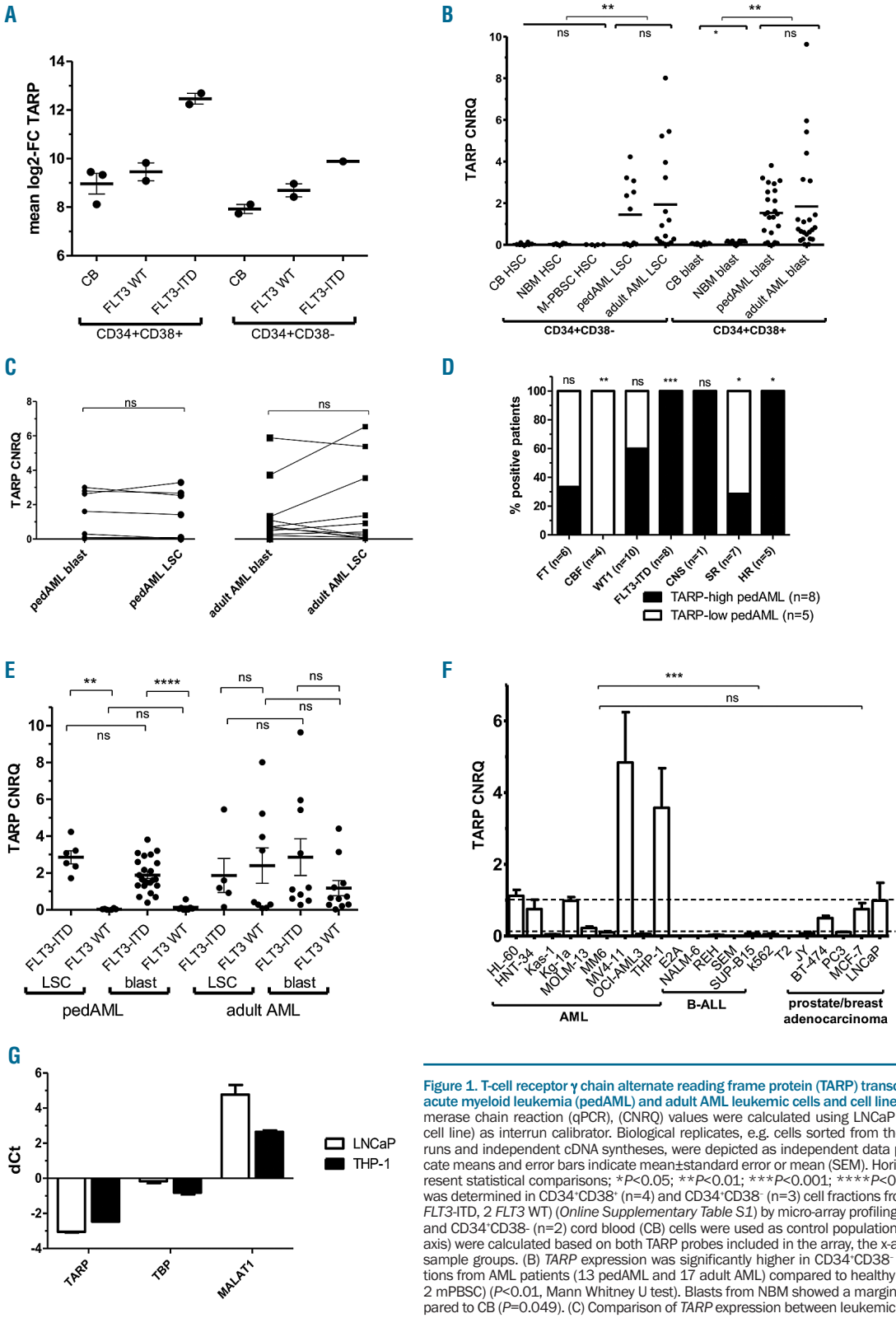

Figure 1. T-cell receptor γ chain alternate reading frame protein (TARP) transcript expression in pediatric acute myeloid leukemia (pedAML) and adult AML leukemic cells and cell lines. For TARP qualitative polymerase chain reaction (qPCR), (CNRQ) values were calculated using LNCaP (prostate adenocarcinoma cell line) as interrun calibrator. Biological replicates, e.g. cells sorted from the same patient in different runs and independent cDNA syntheses, were depicted as independent data points. Horizontal bars indicate means and error bars indicate mean±standard error or mean (SEM). Horizontal square brackets represent statistical comparisons; *P<0.05; **P<0.01; ***P<0.001; ****P<0.0001. (A) TARP expression was determined in CD34$^+$CD38$^+$ (n=4) and CD34$^+$CD38$^-$ (n=3) cell fractions from four pedAML patients (2 *FLT3*-ITD, 2 *FLT3* WT) (*Online Supplementary Table S1*) by micro-array profiling. Sorted CD34$^+$CD38$^+$ (n=3) and CD34$^+$CD38- (n=2) cord blood (CB) cells were used as control populations. Mean log2-FC values (y-axis) were calculated based on both TARP probes included in the array, the x-axis represents the different sample groups. (B) *TARP* expression was significantly higher in CD34$^+$CD38$^-$ and CD34$^+$CD38$^+$ cell fractions from AML patients (13 pedAML and 17 adult AML) compared to healthy controls (7 CB, 6 NBM and 2 mPBSC) (P<0.01, Mann Whitney U test). Blasts from NBM showed a marginally higher expression compared to CB (P=0.049). (C) Comparison of *TARP* expression between leukemic stem cells (LSC) and blasts within pedAML (circles, n=10) and adult AML (squares, n=12) on a per patient basis showed no significant differences (P>0.05, paired sample t-test). (D) Bars display the percentage of patients (%), harboring the characteristic shown in the x-axis (dichotomous variables, for details see Table 1), for TARP-high (black, n=8) and TARP-low (white, n=5) pedAML patients. The total number of patients positive for each characteristic is shown between parentheses. Patients without central nervous system (CNS) involvement all showed negative lumbar punctures. Data on CNS involvement and risk profile is lacking for one patient. The number of patients harboring *FLT3*-ITD (P<0.001) and HR profiles (P<0.05) were significantly higher in the TARP-high group, whereas TARP-low pedAML patients included significantly more CBF-leukemia (P<0.01) and SR profiles (P<0.05) (χ^2 test). (E) Differential *TARP* expression between LSC and blasts sorted from pediatric and adult AML patients with *FLT3*-ITD *versus FLT3* WT. A significant higher *TARP* expression in LSC (P<0.01) and blasts (P<0.0001) was only detected for *FLT3*-ITD positive pedAML patients (Mann Whitney U test). (F) *TARP* expression in nine AML cell lines, five B-ALL cell lines, the CML cell line K562, the Epstein-Barr virus (EBV)-immortalized B-cell line JY and T2 cell line, next to two breast (BT-474, MCF-7) and two prostate (LNCaP, PC3) adenocarcinoma cell lines. Dashed lines indicate the expression observed in PC3 and LNCaP, serving as low and high reference, respectively, in agreement with previous literature.[43] (G) Delta (d) Ct values were calculated for TARP, *MALAT1* and *TBP* between cytoplasmic and nuclear compartments of THP-1 and LNCaP, in order to examine the subcellular location of *TARP*. THP-1 showed a cytoplasmic residence for TARP, in agreement with LNCaP. FC: fold change; FT: fusion transcript; Kas-1: Kasumi-1; MM-6: MONO-MAC6; mPBSC: mobilized peripheral blood stem cells; NBM: normal bone marrow.

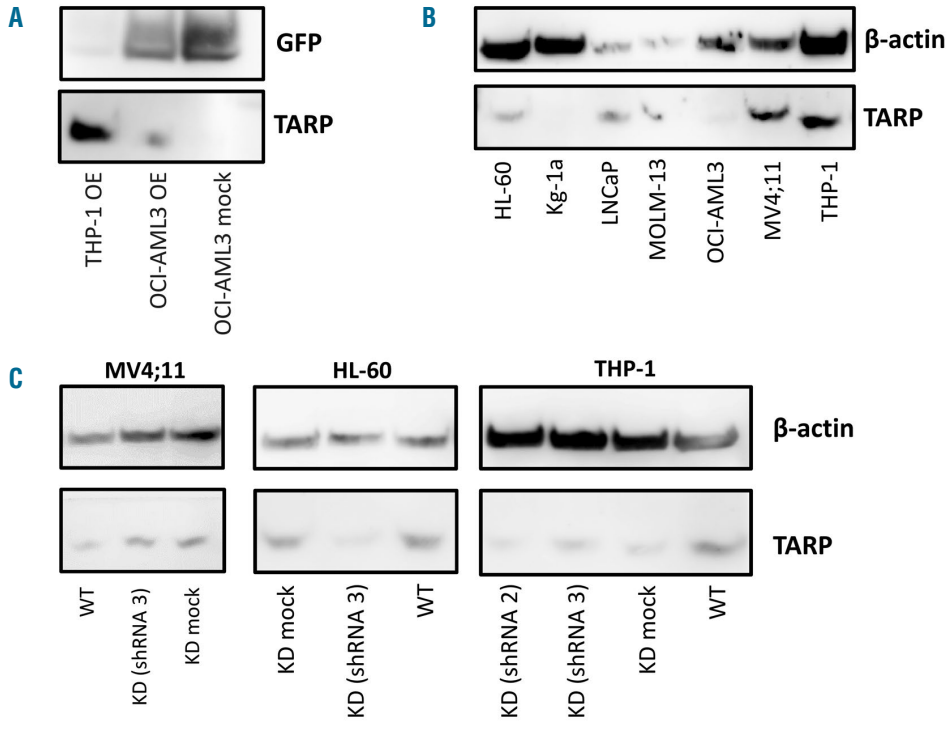

Figure 2. T-cell receptor γ chain alternate reading frame protein (TARP) expression in cell lines evaluated by western blotting. Whole-blot images with ladders used for size estimation are shown in *Online Supplementary Figure* S7. (A) TARP transgenic (OE) cell lines generated for OCI-AML3 and THP-1 showed a 27 kDa protein for GFP and a 15-25 kDa protein for TARP. In agreement with low TARP transcript levels, the OCI-AML3 mock cell line only showed a 27 kDa GFP protein. TARP expression in THP-1 OE was higher than OCI-AML3 OE, most likely resulting from both transgenic and cognate TARP protein expression, since THP-1 was categorized by qualitative polymerase chain reaction (qPCR) as a TARP-high acute myeloid leukemia (AML) cell line. (B) Immunoblotting of TARP and β-actin in AML cell lines (HL-60, Kg-1a, MOLM-13, OCI-AML3, MV4;11 and THP-1) next to LNCaP. Protein expression mostly matched transcript levels, except for Kg-1a, although confocal microscopy did allow TARP protein staining in Kg-1a. β-actin expression appeared to be lower for LNCaP and MOLM-13, although equal amounts of protein were loaded. (C) Immunoblotting of TARP and β-actin in selected shRNA-mediated knockdown (KD) AML cell lines for MV4;11, HL-60 and THP-1, next to their respective mock and wild-type (WT) cell line. For HL-60, a stable knockdown was introduced by shRNA 3 (19.4% compared to mock). KD: knockdown; OE: overexpression.

sorted from CB, NBM and mPBSC (Figure 1B), although blasts from NBM showed a marginally higher expression compared to CB (mean CNRQ 0.12 *vs.* 0.045, P=0.049). In sharp contrast, LSC and blasts from pediatric and adult AML showed significantly (P<0.01) higher expressions compared to their normal counterparts. Paired comparison between LSC and blasts on a per patient basis showed no significant differences (Figure 1C).

A cut-off for elevated TARP expression was determined based on the highest expression in control fractions plus two times the standard deviation. Classification of patients into TARP-high (8 pedAML, 13 adult AML) and TARP-low (5 pedAML, 4 adult AML) revealed that *FLT3*-ITD (P<0.001), CNS involvement and HR profile (P<0.05) were exclusively present in TARP-high pedAML patients (Figure 1D). TARP expression was shown to be significantly higher in sorted LSC (P<0.01) and blasts (P<0.0001) from *FLT3*-ITD compared to *FLT3* WT pedAML (Figure 2E). In adult AML, high TARP expression was not restricted to *FLT3*-ITD. On the other hand, all pediatric (Figure 1D) and adult (*Online Supplementary Figure S4A*) core-binding factor (CBF) leukemia were classified as TARP-low patients (P<0.01). TARP-low pedAML patients were included in the standard risk (SR) groups (P<0.05). No significant differences in age, white blood cell (WBC) count, or blast percentages were observed between TARP-high and -low pediatric or adult AML patients (*Online Supplementary Figure S4B and C*). We thus conclude that TARP is highly and specifically expressed in AML leukemic cells from both adults and children, showing a significant association with *FLT3*-ITD in pedAML.

Next, we evaluated TARP transcript levels in cell lines of various origin. Expression in breast and prostate adenocarcinoma (PC3, BT-474, LNCaP and MCF-7) was in agreement with previous findings[42] (Figure 1F). No expression was detected in five B-ALL cell lines, CML cell line K562, EBV-immortalized B-cell line JY and T2 cell line. Expression in AML cell lines, on the other hand, was significantly increased (P<0.001, one-way ANOVA). The highest expression was observed in HL-60, HNT-34, Kg-1a, MV4;11 and THP-1 (median CNRQ 1.12, range 0.75-4.84), whereas low transcript levels were observed in Kas-1, MOLM-13, MONO-MAC6 and OCI-AML3 (median CNRQ 0.080, range 0.049-0.22). Furthermore, fractionation revealed a mainly cytoplasmic localization of TARP mRNA in THP-1 (Figure 1G), as previously shown in LNCaP43.

To evaluate whether the TARP transcript detected in AML is identical to previous reports, we sequenced the TRGC region of different TARP amplicons obtained by qPCR for AML cell lines and pedAML leukemic cells. Using TARP long primers, we observed a single band for

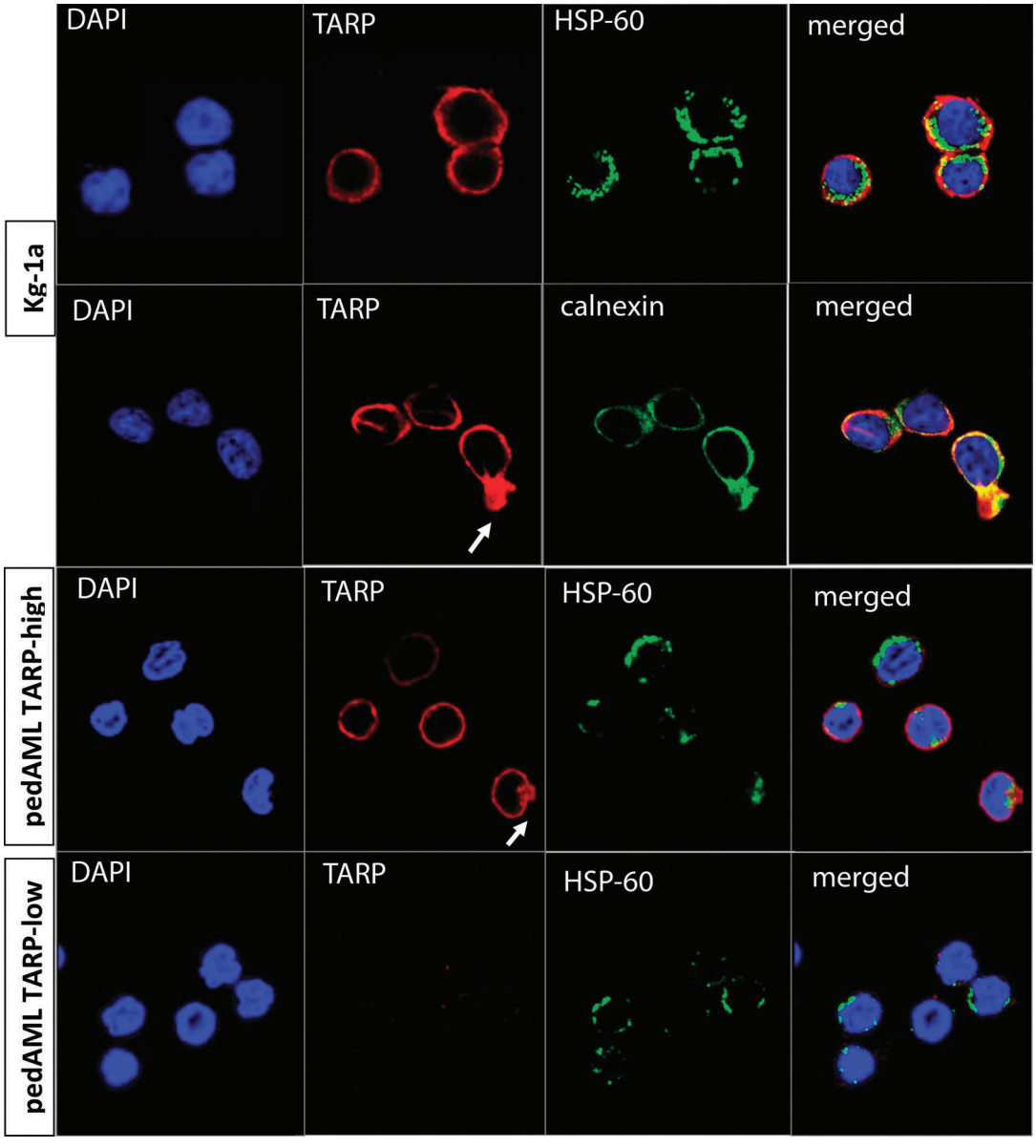

Figure 3. T-cell receptor γ chain alternate reading frame protein (TARP) protein detection in Kg-1a and patient leukemic cells by confocal microscopy. Merged patterns visualize TARP (red) and HSP-60 (top lane) or calnexin (bottom lane) (both in green) co-localization (yellow fusion signals) together with DAPI nuclear counterstaining (blue). Leukemic cells were sorted from two pediatric acute myeloid leukemia (pedAML) patients, classified as TARP-high and TARP-low by qualitative polymerase chain reaction. Calnexin staining was not performed on primary cells due to lack of material. Within Kg-1a and the sorted TARP-high leukemic cells, TARP expression was enriched at the cells' protrusions, indicated by arrows.

Kg-1a, which was similar to the LNCaP and TRGC1 reference sequence (*Online Supplementary Figure S5A*). Unexpectedly, three fragments were observed in the sorted blasts and LSC from TARP-high pedAML patients and the MV4;[11] cell line. Cloning and sequencing of each fragment (*Online Supplementary Figure S5B*) revealed that the largest fragments were artificial heteroduplexes,[44] whereas the smallest fragments were identical to the fragments from Kg-1a and LNCaP. Medium-sized fragments were consistently 48 bp longer, and showed the same size as the HSB-2 amplicon, a T-cell acute lymphoblastic leukemia (T-ALL) cell line with functional TRGC2 rearrangements.[45] As TRGC2 contains a duplicated second exon (48 bp) compared to TRGC145 (*Online Supplementary Figure S2*), we hypothesized that there might be an alternative TARP transcript in AML. Indeed, most AML cell lines, but none of the prostate and breast adenocarcinoma cell lines, showed TRGC1 as well as TRGC2 amplicons (*Online Supplementary Figure S5C and E*). Single bands for exon 3 and exon 1 amplicons in all cell lines provided evidence that the occurrence of the second transcript is related to the TRGC2 duplicated second exon. Altogether, TARP was highly expressed in approximately half of the AML cell lines evaluated, and both TRGC1- and TRGC2-related transcripts co-existed in AML.

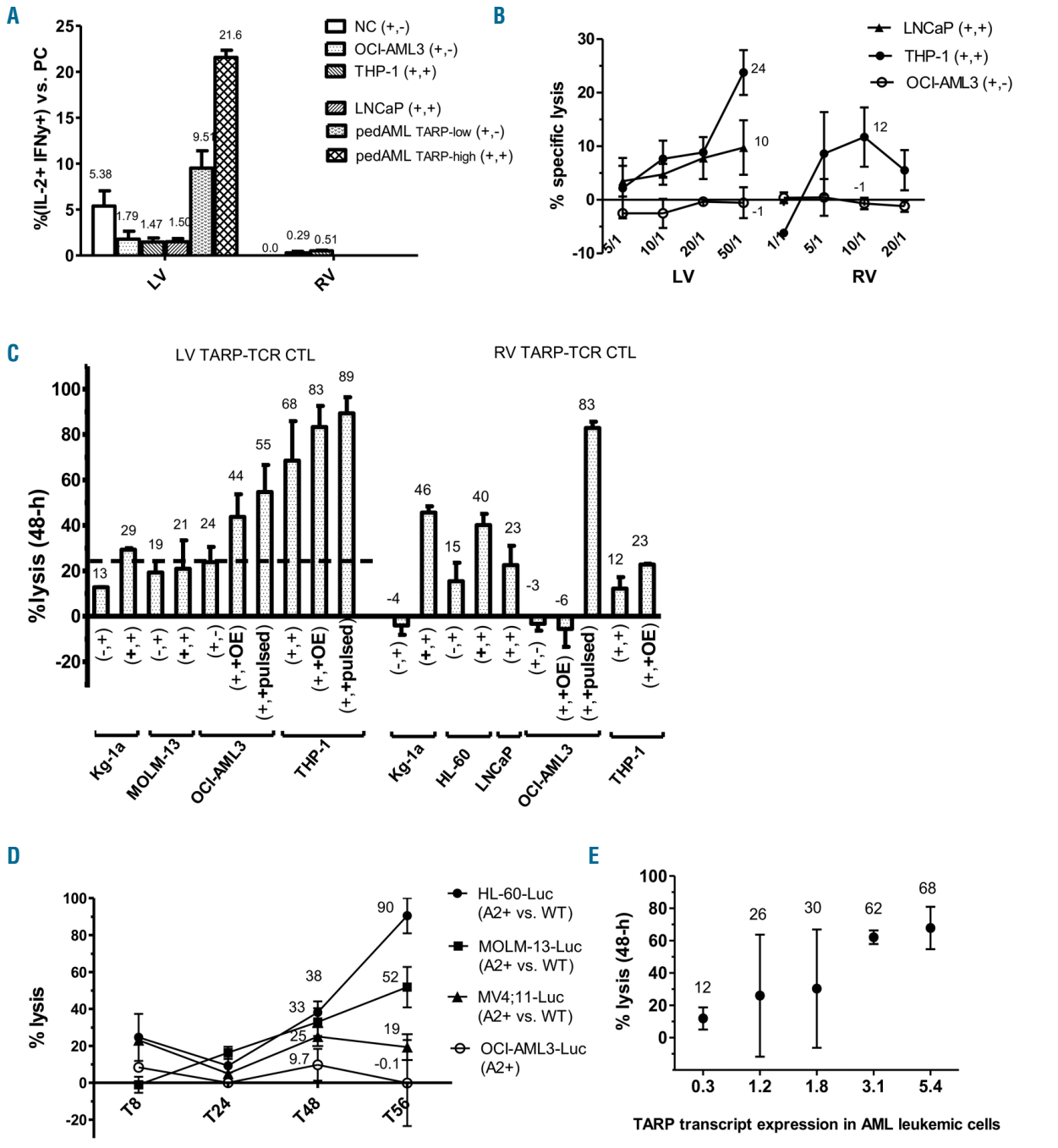

Figure 4. Functional evaluation of T-cell receptor (TCR)-transgenic cytotoxic T cells (CTL) towards cognate and modified cell lines and patient leukemic cells. (A) Cytokine response (IFN-γ/IL-2 expression within the $CD3^+/CD8^+$ compartment) by co-incubation (1 hour, h) with OCI-AML3 and THP-1 was evaluated by both lentiviral (LV) and retroviral (RV) TCR-T-cell receptor γ chain alternate reading frame protein (TARP) CTL. LNCaP and patient leukemic cells (single experiment) were only evaluated by LV transduced TARP-TCR CTL. For each target, positive (+) or negative (-) HLA-A*0201 and TARP expression, in this respective order, is indicated between brackets. HLA-A*0201 and TARP co-expressing cell lines (LNCaP and THP-1) were unable to trigger higher cytokine release than OCI-AML3 with low TARP expression. Leukemic cells from a TARP-high pediatric acute myeloid leukemia (pedAML) patient triggered a 2-fold higher cytokine release compared to a TARP-low pedAML patient. (B) Lytic response of LV and RV TARP-TCR CTL *versus* HLA-A*0201-positive TARP-high (black symbols) and TARP-low (white symbols) targets, measured by a chromium[51] release assay after 4 h. Highest lysis of TARP-high cell lines was observed at E/T ratio 50/1 for LV and 10/1 for RV TARP-TCR CTL (percentages indicated between brackets), whereas OCI-AML3 (HLA-A*0201$^+$, TARP$^-$) remained unaffected. (C) Lytic response of LV and RV TARP-TCR CTL *versus* towards wild-type (WT), transgenic and pulsed AML cell lines, measured by a 48-h FCM-based cytotoxicity assay. The dashed line indicates the highest level of non-TARP mediated background killing observed for LV TARP-TCR CTL, as no mock CTL could be constructed. Positive (+) or negative (-) expression for HLA-A*0201 and TARP is shown, in this respective order, between brackets. Bold symbols indicate the expression differing from wild-type, either by retroviral transduction or pulsing. HLA-A*0201 transgenic AML cell lines were more efficiently lysed compared to their HLA-A*0201-negative counterparts (Kg-1a, MOLM-13, HL-60). Higher lysis was observed for transgenic TARP OE or peptide-pulsed cell lines compared to the WT cell line (OCI-AML3, THP-1), except for killing of TARP OE OCI-AML3 cell line by RV TARP-TCR CTL. (D) Lysis by LV TARP-TCR CTL, measured at different time points (8h, 24h, 48h and 56h, as indicated on x-axis), based on the luminescence release by transgenic HLA-A*0201-expressing TARP-high AML cell lines with respect to the HLA-A*0201 WT cell line (HL-60-Luc, MOLM-13-Luc and MV4;11-Luc: black symbols). In addition, lysis of the TARP-low, cognate HLA-A*0201-positive OCI-AML3 cell line was evaluated (white symbols). Mean lysis (%) observed after 48 h is indicated next to whiskers, representing the mean±standard error of mean. (E) 48-h FCM-based cytotoxicity assay evaluating lysis of primary leukemic cells (adult AML=5, all FLT3-ITD mutated) by LV TARP-TCR transduced CTL (biological duplicates). TARP transcript expression (CNRQ) is shown in the x-axis for each target. IFN-γ: interferon gamma; IL-2: interleukin-2; INF: influenza.

T-cell receptor γ chain alternate reading frame protein is expressed in acute myeloid leukemia cell lines and patient leukemic cells

We generated TARP transgenic cell lines in order to optimize western blot experiments and evaluate TARP protein expression in AML. THP-1 and OCI-AML3 OE cell lines showed a significant higher *TARP* transcript expression ($P<0.01$) compared to mock controls (*Online Supplementary Figure S6A*). Western blotting confirmed presence of TARP and GFP proteins in both OE cell lines, with a size of around 20 kDa and 27 kDa, respectively (Figure 2A and *Online Supplementary Figure S7*). Concordantly, the OCI-AML3 mock cell line, negative for TARP, only showed a 27 kDa GFP protein. WT AML cell lines HL-60, MV4;11, THP-1 and MOLM-13, as well as LNCaP, also showed a 20 kDa TARP protein, with expression corresponding to the transcript levels (Figure 2B and *Online Supplementary Figure S7*). TARP knockdown (KD) cell lines were generated for HL-60, Kg-1a, MV4;11 and THP-1 using TARP-targeting shRNA, next to mock controls. Transcript levels were efficiently down-regulated (*Online Supplementary Figure S8*), and KD cell lines for HL-60, MV4;11 and THP-1 showing the highest transcript downregulation were selected for western blotting (Figure 2C and *Online Supplementary Figure S7*). Protein levels were efficiently down-regulated in HL-60 transduced with shRNA 3 (19.4% compared to mock). This downregulation was less clear in MV4;11 and THP-1: 116% (shRNA 3) and 108% (shRNA 3) *versus* 63% (shRNA 2), respectively.

To confirm western blot data and determine the subcellular location of TARP, confocal microscopy was performed using TARP antibodies combined with mitochondrial (HSP-60) and endoplasmic reticulum (ER, calnexin) staining. The over-expressing OCI-AML3 and THP-1 cell lines (*Online Supplementary Figure S6B and C*) and TARP-high WT AML cell lines showed a perinuclear membranous-type TARP staining pattern (Kg-1a (Figure 3), HL-60, MV4;11 and THP-1 (*Online Supplementary Figure S9*). This finding was in contrast to the barrel-shaped TARP pattern with mitochondrial co-localization reported in LNCaP.[43] Co-localization with calnexin, presenting as a speckled pattern throughout the ER, was more abundant in some cell lines, e.g. Kg-1a, showing TARP enrichment at the cells' protrusions. TARP-low cell lines concordantly showed weak or negative TARP protein staining (*Online Supplementary Figure S8*). Importantly, the leukemic cells sorted from a TARP-high and TARP-low pedAML patient also illustrated differential TARP protein expression in agreement with the transcript levels, again showing limited mitochondrial overlap (Figure 3).

T-cell receptor γ chain alternate reading frame protein transgenic cytotoxic T cells display specific anti-leukemic activity

To explore if TARP might represent an immunotherapeutic target in AML, we evaluated the cytokine and cytotoxicity response of TARP-TCR transgenic CTL, encoding a previously developed TCRA8-T2A-TCRB12 sequence targeting the HLA-A2 enhanced affinity TARP(P5L)$_{4\text{-}13}$ epitope.[46,47] As concomitant HLA-A*0201 and TARP expression is required to trigger TCR-mediated killing, HLA-A*0201 transgenic cell lines were generated for 3 WT cell lines (HL-60, Kg-1a and MOLM-13) and 3 Luc-positive cell lines (HL-60-Luc, MOLM-13-Luc, MV4;11-Luc).

First, target specificity of the TARP-TCR was examined in a non-competitive environment using T2 cells (endogenous HLA-A*0201+) pulsed with exogenous peptides (*Online Supplementary Table S3*). As expected, we found stronger cytokine responses (*Online Supplementary Figure S10A*) and higher killing rates (*Online Supplementary Figure S10B and C*) towards the TARP(P5L)$_{4\text{-}13}$ than to the cognate TARP$_{4\text{-}13}$ peptide for both RV and LV transduced CTL, with LV TARP-TCR CTL generally reacting stronger. T2 cells pulsed with non-TARP-related peptides (INF, CMV) were not affected, although CMV-pulsed T2 cells were efficiently recognized by CMV-TCR CTL, indicating a high specificity of the TARP-TCR.

Second, we explored the immunogenicity of cell lines with endogenous HLA-A*0201 presentation. Exposure to LNCaP and THP-1 appeared to be insufficient to trigger cytokine release for both LV and RV transduced TARP-TCR CTL (Figure 4A). Using a chromium^{51} release assay, we observed a lytic response by LV transduced TARP-TCR CTL starting from effector to target ratio (E/T) 10/1, with a maximal average response at 50/1 (LNCaP 10%, THP-1 24%), whereas RV transduced TARP-TCR CTL performed best at 10/1 (THP-1 12%) (Figure 4B). The TARP-low AML cell line OCI-AML3 remained unaffected under all conditions. Altogether, as the TARP-TCR targets the enhanced HLA-A2 TARP(P5L)$_{4\text{-}13}$ binding peptide, we observed weaker responses against endogenous TARP-expressing cell lines compared to pulsed T2 cells.

Third, lysis of TARP-high HLA-A*0201-negative cell lines was evaluated *versus* their HLA-A*0201 transgenic counterparts in a 48-h FCM-cytotoxicity assay. In addition, killing of TARP transgenic or TARP-pulsed HLA-A*0201-positive cell lines was compared to the respective TARP-low WT cell line (Figure 4C). A non-TARP mediated lysis by LV TARP-TCR CTL of maximal 20% was observed (indicated by dashed line). Stable transduction of HLA-A*0201 increased killing for Kg-1a compared to the WT cell line (29% *vs.* 13%), whereas killing of MOLM-13, with lower TARP expression levels, remained unaffected when HLA-A*0201 was introduced. Transgenic TARP OE and TARP(P5L)$_{4\text{-}13}$ pulsed OCI-AML3 cells were prone to a higher lysis than the WT cell line (44% and 55%, respectively, *vs.* 24%). Killing of TARP OE/pulsed THP-1 cells was only marginally up-regulated, most likely due to an already high endogenous expression. These data were confirmed using RV TARP-TCR CTL, and corrected for non-TARP mediated lysis using mock CTL. HLA-A*0201 expression again increased killing of Kg-1a (46% *vs.* -4%) and HL-60 (40% *vs.* 15%) compared to the WT cell line. Up-regulated killing of transgenic TARP OE THP-1 cells was again limited. For OCI-AML3, lysis was up-regulated after pulsing, but remained low for the TARP OE transgenic cell line. Killing by LV TARP-TCR CTL was additionally evaluated in a bioluminescence imaging (BLI)-based assay using Luc-positive AML cell lines with high TARP expression (HL-60 and MV4;11) and low TARP expression (MOLM-13 and OCI-AML3) (Figure 4D). A higher lysis was observed for HL-60-Luc and MV4;11-Luc when expressing HLA-A*0201 at 48 h and 56 h, indicating that also in long-term cytotoxicity experiments HLA-A*0201 restricted TARP-specific killing could be detected.

Finally, we explored the feasibility of therapeutic targeting of primary leukemic cells by LV TARP-TCR CTL. Co-incubation with blasts sorted from a TARP-high pedAML patient resulted into a 2-fold higher IFN-γ and IL-2 production compared to a TARP-low pedAML patient (22%

vs. 10%) (Figure 4A). Moreover, TARP-TCR CTL were also capable of killing leukemic cells from *de novo* adult AML patients (n=5) (Figure 4E). Lysis ranged between 12% and 68%, and borderline correlated to *TARP* transcript levels (Spearman's coefficient 0.82, P=0.089).

Discussion

We demonstrated increased *TARP* expression in AML LSC ($CD34^+CD38^-$) and blasts ($CD34^+CD38^+$) from primary patients compared to their normal counterparts as well as AML cell lines. We also showed that TARP protein is expressed in primary AML leukemic cells and are adequately presented on HLA molecules, which makes the cells targetable for immunotherapy.

TARP expression has only been investigated in prostate tissue and androgen-sensitive prostate adenocarcinoma and breast adenocarcinoma,[42,43,48] next to a single report on salivary adenoid cystic carcinoma.[49] We found that *TARP* expression was significantly (P<0.001) higher in *FLT3*-ITD compared to *FLT3* WT pedAML patients at diagnosis, whereas no significant difference was observed in adult AML. Importantly, enormous differences in the genomic landscape in adult compared to pedAML were shown,[50,51] potentially explaining some of the differential associations observed in our cohorts. The association between *TARP* expression and a poor prognosis is in agreement with a recent report, investigating the association between transcript expression and clinical outcome in pedAML, ranking *TARP* within the top genes significantly associated with a detrimental outcome.[52] To shed light on the link between *FLT3*-ITD and *TARP*, mRNA sequencing of the transgenic OE and KD cell lines compared to their WT cell line is ongoing. As it was recently shown that the *FLT3*-ITD regions encode immunogenic, HLA-presented neo-epitopes,[53] the benefit of CTL therapy targeting both leukemogenic molecules in pedAML could be of great interest. On the other hand, CBF leukemias, representing a favorable cytogenetic subgroup,[2,8] were only present (P<0.01) in the TARP-low group for both pediatric and adult patients. AML cell lines derived from pediatric cases (MV4;11, THP-1) and LSC-enriched cell lines (Kg-1a, HNT-34), showed the highest TARP levels, confirming a relation between TARP, the LSC compartment and pedAML, although also HL-60 (adult, $CD34^-$) showed high expression. Whether TARP remains differentially expressed within LSC outside the predominant $CD34^+CD38^-$ compartment, as it does within $CD34^-$ AML,[15,54] needs to be explored further. In addition, we showed that transcripts differ from those in solid tumors and are derived from both the TRGC1 and TRGC2 coding regions. Sequencing analysis indicated the presence of a second, AML-exclusive, TARP transcript encoding TRGC2 instead of TRGC1.

TARP protein expression was in agreement with transcript levels, showing a 15-25 kDa fragment in AML cell lines. In breast and prostate adenocarcinoma, TARP had previously been defined as a 7 kDa protein,[42,48] although also a 9 kDa fragment was reported in MCF-7.[42,48] Fritzsche *et al*. detected protein sizes in prostate carcinoma of 20-25 kDa,[55] comparable to our findings, whereas Yue *et al*. reported a 15 kDa protein.[49] Besides its size, the subcellular localization of TARP in AML needs to be refined. qPCR analysis revealed cytoplasmic localization, and confocal microscopy showed sporadic ER overlap, in contrast to previously reported mitochondrial co-localization.[43] We observed an enrichment of TARP at the cells' protrusions in Kg-1a and sorted leukemic cells. Protrusions are kinetic cytoskeletal abnormalities formed during chemokine-induced cell migration, e.g. homing of $CD34^+$ HSC towards the bone marrow niche.[56] The presence of molecular abnormalities in $CD34^+$ progenitor cells was shown to increase protrusion formation.[57] Indeed, LSC were reported to compete with HSC for endosteal niche engraftment, where they are protected from chemotherapy-induced apoptosis.[12,58] Whether TARP interferes in homing and chemoprotection of leukemic AML cells in the BM microenvironment needs to be elucidated. Although protein expression was readily up-regulated in TARP transgenic cell lines, shRNA-mediated knockdown appeared to be less efficient. Possible explanations are the presence of escape mechanisms and alternative translation pathways during silencing or a very high stability of the TARP protein, persisting in the cell for a long period of time.

To explore TARP as an immunotherapeutic target in AML, we evaluated the cytokine release and cytotoxic killing capacities of TARP-TCR transgenic CTL *in vitro*. TARP and HLA-A*0201 co-expressing cell lines were efficiently lysed, and although evaluated on a limited number of patients (n=5), TARP-TCR CTL were able to kill primary leukemic cells with a borderline correlation to the *TARP* transcript expression. Interestingly, weaker responses were observed for the cognate $TARP_{4\text{-}13}$ peptide, since the TCR is directed against the HLA-A*0201 enhanced affinity $TARP(P5L)_{4\text{-}13}$ peptide. Moreover, pulsed T2 cells appeared to be more susceptible than AML cells. This finding is in agreement with previous data,[47,59] and several reasons may account for this phenomenon. First, peptide processing, transport and/or MHC-I presentation may be disturbed in leukemic cells.[60] Second, high and stable HLA-A*0201 expression is vital for triggering lytic responses, and transgenic expression might diminish during culture. Therefore, we cannot exclude the possibility that HLA-A*0201-mediated TARP presentation within the transgenic OCI-AML3 cell line had diminished during long-term culture. Third, competition between transgenic and endogenous MHC-I molecules might block HLA-A*0201-guided peptide presentation. Indeed, the TARP-TCR was shown to suffer from low MHC-I avidity compared to foreign epitope-directed TCR.[61] Cloning the $TARP_{4\text{-}13}$-TCR sequence into a retroviral construct enabled higher transduction efficiencies and the generation of mock CTL to correct non-TARP mediated lysis, which are lacking in previous reports.[37,49] As promoters driving TCR expression differed between constructs, and functional activity is known to correlate with TCR cell-surface expression,[62] it was no surprised that different killing rates between LV and RV transduced CTL were osberved. In addition, intrinsic reactivity, HLA status and endogenous TCR repertoire of each donor as such might have an impact.[62] In addition, comparing reactivity by effectors from an allogeneic *versus* autologous setting will be implemented in future experiments.

In conclusion, we showed that *TARP* is highly expressed in AML leukemic cells, including the $CD34^+CD38^-$ LSC compartment, while absent in normal counterparts. Moreover, *TARP* expression was associated with *FLT3*-ITD in pedAML. We provide *in vitro* evidence that

TARP-directed CTL effectively kill TARP and HLA-A*0201 co-expressing cell lines and primary leukemic cells, and thus hold great promise for immunotherapeutic T-cell therapy.

Acknowledgments

Our gratitude goes to Dr. F. Plasschaert, the staff of the Department of adult Hematology and Pediatric Hematology and Oncology of the Ghent University Hospital (Ghent, Belgium), and C. Matthys of the Cord Blood Bank, for providing samples. The authors thank all patients and their parents for their participation in the study, as well as the data managers involved in the clinical trials. We are indebted to S. Vermaut for cell sorting and all technicians of the Childhood Cancer Foundation and Laboratory of the Ghent University Hospital (Ghent, Belgium). We thank our collaborators from the LL Biology Working Group for their relevant contributions, in particular Prof. Dr. GJ Kaspers for taking interest in our research.

Funding

This research was supported by the Belgian Foundation against Cancer (grant 2014–265), FOD-KankerPlan (Actie29, grant to JL) and vzw Kinderkankerfonds (grant to TL). The Research Foundation - Flanders (Fonds voor Wetenschappelijk Onderzoek Vlaanderen, FWO) supported TK (grant 1831312N) and BD (grants 1113117 and V433317N). This work is submitted in partial fulfilment of the requirement for the PhD of candidate BD at Ghent University.

References

1. Dohner H, Estey EH, Amadori S, et al. Diagnosis and management of acute myeloid leukemia in adults: recommendations from an international expert panel, on behalf of the European LeukemiaNet. Blood. 2010;115(3):453-474.
2. Dohner H, Estey E, Grimwade D, et al. Diagnosis and management of AML in adults: 2017 ELN recommendations from an international expert panel. Blood. 2017;129(4):424-447.
3. De Kouchkovsky I, Abdul-Hay M. Acute myeloid leukemia: a comprehensive review and 2016 update. Blood Cancer J. 2016; 6(7):e441.
4. Bonnet D, Dick JE. Human acute myeloid leukemia is organized as a hierarchy that originates from a primitive hematopoietic cell. Nat Med. 1997;3(7):730-737.
5. Rasche M, Zimmermann M, Borschel L, et al. Successes and challenges in the treatment of pediatric acute myeloid leukemia: a retrospective analysis of the AML-BFM trials from 1987 to 2012. Leukemia. 2018; 32(10):2167-2177.
6. Creutzig U, van den Heuvel-Eibrink MM, Gibson B, et al. Diagnosis and management of acute myeloid leukemia in children and adolescents: recommendations from an international expert panel. Blood. 2012;120(16):3187-3205.
7. von Neuhoff C, Reinhardt D, Sander A, et al. Prognostic impact of specific chromosomal aberrations in a large group of pediatric patients with acute myeloid leukemia treated uniformly according to trial AML-BFM 98. J Clin Oncol. 2010;28(16):2682-2689.
8. De Moerloose B, Reedijk A, de Bock GH, et al. Response-guided chemotherapy for pediatric acute myeloid leukemia without hematopoietic stem cell transplantation in first complete remission: Results from protocol DB AML-01. Pediatr Blood Cancer. 2019;66(5):e27605.
9. Meshinchi S, Woods WG, Stirewalt DL, et al. Prevalence and prognostic significance of Flt3 internal tandem duplication in pediatric acute myeloid leukemia. Blood. 2001; 97(1):89-94.
10. Hope KJ, Jin L, Dick JE. Acute myeloid leukemia originates from a hierarchy of leukemic stem cell classes that differ in self-renewal capacity. Nat Immunol. 2004; 5(7):738-743.
11. Shlush LI, Mitchell A, Heisler L, et al. Tracing the origins of relapse in acute myeloid leukaemia to stem cells. Nature. 2017;547(7661):104-108.
12. Ishikawa F, Yoshida S, Saito Y, et al. Chemotherapy-resistant human AML stem cells home to and engraft within the bone-marrow endosteal region. Nat Biotechnol. 2007;25(11):1315-1321.
13. Thomas D, Majeti R. Biology and relevance of human acute myeloid leukemia stem cells. Blood. 2017;129(12):1577-1585.
14. Griessinger E, Anjos-Afonso F, Pizzitola I, et al. A niche-like culture system allowing the maintenance of primary human acute myeloid leukemia-initiating cells: a new tool to decipher their chemoresistance and self-renewal mechanisms. Stem Cells Transl Med. 2014;3(4):520-529.
15. Ng SW, Mitchell A, Kennedy JA, et al. A 17-gene stemness score for rapid determination of risk in acute leukaemia. Nature. 2016;540(7633):433-437.
16. Terwijn M, Zeijlemaker W, Kelder A, et al. Leukemic Stem Cell Frequency: A Strong Biomarker for Clinical Outcome in Acute Myeloid Leukemia. PLoS One. 2014; 22:9(9):e10758.
17. van Rhenen A, Feller N, Kelder A, et al. High stem cell frequency in acute myeloid leukemia at diagnosis predicts high minimal residual disease and poor survival. Clin Cancer Res. 2005;11(18):6520-6527.
18. Hanekamp D, Denys B, Kaspers GJL, et al. Leukaemic stem cell load at diagnosis predicts the development of relapse in young acute myeloid leukaemia patients. Br J Haematol. 2018;183(3):512-516.
19. Witte KE, Ahlers J, Schafer I, et al. High Proportion of Leukemic Stem Cells at Diagnosis Is Correlated with Unfavorable Prognosis in Childhood Acute Myeloid Leukemia. Pediatr Hemat Oncol. 2011;28(2):91-99.
20. Annesley CE, Brown P. The Biology and Targeting of FLT3 in Pediatric Leukemia. Front Oncol. 2014;4:263.
21. Hunger SP, Lu X, Devidas M, et al. Improved survival for children and adolescents with acute lymphoblastic leukemia between 1990 and 2005: a report from the children's oncology group. J Clin Oncol. 2012;30(14):1663-1669.
22. Maude SL, Laetsch TW, Buechner J, et al. Tisagenlecleucel in Children and Young Adults with B-Cell Lymphoblastic Leukemia. N Engl J Med. 2018;378(5):439-448.
23. Hanekamp D, Cloos J, Schuurhuis GJ. Leukemic stem cells: identification and clinical application. Int J Hematol. 2017;105(5):549-557.
24. Felipe Rico J, Hassane DC, Guzman ML. Acute myelogenous leukemia stem cells: from Bench to Bedside. Cancer Lett. 2013;338(1):4-9.
25. Perna F, Berman SH, Soni RK, et al. Integrating Proteomics and Transcriptomics for Systematic Combinatorial Chimeric Antigen Receptor Therapy of AML. Cancer Cell. 2017;32(4):506-519.
26. Pollyea DA, Gutman JA, Gore L, et al. Targeting acute myeloid leukemia stem cells: a review and principles for the development of clinical trials. Haematologica. 2014;99(8):1277-1284.
27. Jen EY, Ko CW, Lee JE, et al. FDA Approval: Gemtuzumab Ozogamicin for the Treatment of Adults with Newly Diagnosed CD33-Positive Acute Myeloid Leukemia. Clin Cancer Res. 2018;24(14):3242-3246.
28. Parigger J, Zwaan CM, Reinhardt D, et al. Dose-related efficacy and toxicity of gemtuzumab ozogamicin in pediatric acute myeloid leukemia. Expert Rev Anticancer Ther. 2016;16(2):137-146.
29. van Rhenen A, Moshaver B, Kelder A, et al. Aberrant marker expression patterns on the CD34+CD38- stem cell compartment in acute myeloid leukemia allows to distinguish the malignant from the normal stem cell compartment both at diagnosis and in remission. Leukemia. 2007;21(8):1700-1707.
30. Bonardi F, Fusetti F, Deelen P, et al. A proteomics and transcriptomics approach to identify leukemic stem cell (LSC) markers. Mol Cell Proteomics. 2013;12(3):626-637.
31. Majetl R, Becker MW, Tian Q, et al. Dysregulated gene expression networks in human acute myelogenous leukemia stem cells. Proc Natl Acad Sci U S A. 2009;106(9):3396-3401.
32. Eppert K, Takenaka K, Lechman ER, et al. Stem cell gene expression programs influence clinical outcome in human leukemia. Nat Med. 2011;17(9):1086-1093.
33. Forsberg EC, Passegue E, Prohaska SS, et al. Molecular signatures of quiescent, mobilized and leukemia-initiating hematopoietic stem cells. PloS One. 2010;5(1):e8785.
34. Gal H, Amariglio N, Trakhtenbrot L, et al. Gene expression profiles of AML derived stem cells; similarity to hematopoietic stem cells. Leukemia. 2006;20(12):2147-2154.

35. Gentles AJ, Plevritis SK, Majeti R, et al. Association of a leukemic stem cell gene expression signature with clinical outcomes in acute myeloid leukemia. JAMA. 2010;304(24):2706-2715.
36. Saito Y, Kitamura H, Hijikata A, et al. Identification of therapeutic targets for quiescent, chemotherapy-resistant human leukemia stem cells. Sci Transl Med. 2010;2(17):17ra9.
37. de Leeuw DC, Denkers F, Olthof MC, et al. Attenuation of microRNA-126 expression that drives CD34+38- stem/progenitor cells in acute myeloid leukemia leads to tumor eradication. Cancer Res. 2014;74(7):2094-2105.
38. Hellemans J, Mortier G, De Paepe A, et al. qBase relative quantification framework and software for management and automated analysis of real-time quantitative PCR data. Genome Biol. 2007;8(2):R19.
39. Vandesompele J, De Preter K, Pattyn F, et al. Accurate normalization of real-time quantitative RT-PCR data by geometric averaging of multiple internal control genes. Genome Biol. 2002;3(7):Research0034.
40. van Dongen JJ, Langerak AW, Bruggemann M, et al. Design and standardization of PCR primers and protocols for detection of clonal immunoglobulin and T-cell receptor gene recombinations in suspect lymphoproliferations: report of the BIOMED-2 Concerted Action BMH4-CT98-3936. Leukemia. 2003;17(12):2257-2317.
41. Essand M, Vasmatzis G, Brinkmann U, et al. High expression of a specific T-cell receptor gamma transcript in epithelial cells of the prostate. Proc Natl Acad Sci U S A. 1999;96(16):9287-9292.
42. Wolfgang CD, Essand M, Vincent JJ, Lee B, Pastan I. TARP: A nuclear protein expressed in prostate and breast cancer cells derived from an alternate reading frame of the T cell receptor gamma chain locus. Proc Natl Acad Sci U S A. 2000;97(17):9437-9442.
43. Maeda H, Nagata S, Wolfgang CD, et al. The T cell receptor gamma chain alternate reading frame protein (TARP), a prostate-specific protein localized in mitochondria. J Biol Chem. 2004;279(23):24561-24568.
44. Qi C, Jia X, Lu L, et al. HEK293T Cells Are Heterozygous for CCR5 Delta 32 Mutation. PloS One. 2016;11(4):e0152975.
45. Lefranc MP, Forster A, Rabbitts TH. Genetic polymorphism and exon changes of the constant regions of the human T-cell rearranging gene gamma. Proc Natl Acad Sci U S A. 1986;83(24):9596-9600.
46. Carlsson B, Totterman TH, Essand M. Generation of cytotoxic T lymphocytes specific for the prostate and breast tissue antigen TARP. Prostate. 2004;61(2):161-170.
47. Hillerdal V, Nilsson B, Carlsson B, et al. T cells engineered with a T cell receptor against the prostate antigen TARP specifically kill HLA-A2+ prostate and breast cancer cells. Proc Natl Acad Sci U S A. 2012; 109(39):15877-15881.
48. Wolfgang CD, Essand M, Lee B, et al. T-cell receptor gamma chain alternate reading frame protein (TARP) expression in prostate cancer cells leads to an increased growth rate and induction of caveolins and amphiregulin. Cancer Res. 2001; 61(22):8122-8126.
49. Yue H, Cai Y, Song Y, et al. Elevated TARP promotes proliferation and metastasis of salivary adenoid cystic carcinoma. Oral Surg Oral Med Oral Pathol Oral Radiol. 2017;123(4):468-476.
50. Farrar JE, Schuback HL, Ries RE, et al. Genomic profiling of pediatric acute myeloid leukemia reveals a changing mutational landscape from disease diagnosis to relapse. Cancer Res. 2016;76(8):2197-2205.
51. Bolouri H, Farrar JE, Triche T, et al. The molecular landscape of pediatric acute myeloid leukemia reveals recurrent structural alterations and age-specific mutational interactions. Nat Med. 2017;24(1):103-112.
52. Lamba JK, Cao X, Raimondi SC, et al. Integrated epigenetic and genetic analysis identifies markers of prognostic significance in pediatric acute myeloid leukemia. Oncotarget. 2018;9(42):26711-26723.
53. Graf C, Heidel F, Tenzer S, et al. A neoepitope generated by an FLT3 internal tandem duplication (FLT3-ITD) is recognized by leukemia-reactive autologous CD8+ T cells. Blood. 2007;109(7):2985-2988.
54. Quek L, Otto GW, Garnett C, et al. Genetically distinct leukemic stem cells in human CD34- acute myeloid leukemia are arrested at a hemopoietic precursor-like stage. J Exp Med. 2016;213(8):1513-1535.
55. Fritzsche FR, Stephan C, Gerhardt J, et al. Diagnostic and prognostic value of T-cell receptor gamma alternative reading frame protein (TARP) expression in prostate cancer. Histol Histopathol. 2010;25(6):733-739.
56. van Buul JD, Voermans C, van Gelderen J, et al. Leukocyte-endothelium interaction promotes SDF-1-dependent polarization of CXCR4. J Biol Chem. 2003;278(32):30302-30310.
57. Salgia R, Li JL, Ewaniuk DS, et al. BCR/ABL induces multiple abnormalities of cytoskeletal function. J Clin Invest. 1997; 100(1):46-57.
58. Boyd AL, Campbell CJV, Hopkins CI, et al. Niche displacement of human leukemic stem cells uniquely allows their competitive replacement with healthy HSPCs. J Exp Med. 2014;211(10):1925-1935.
59. Oh S, Terabe M, Pendleton CD, et al. Human CTLs to wild-type and enhanced epitopes of a novel prostate and breast tumor-associated protein, TARP, lyse human breast cancer cells. Cancer Res. 2004;64(7):2610-2618.
60. Coulie PG, Van den Eynde BJ, van der Bruggen P, et al. Tumour antigens recognized by T lymphocytes: at the core of cancer immunotherapy. Nat Rev Cancer. 2014; 14(2):135-146.
61. Hillerdal V, Boura VF, Bjorkelund H, et al. Avidity characterization of genetically engineered T-cells with novel and established approaches. BMC Immunol. 2016;17(1):23.
62. Heemskerk MH, Hagedoorn RS, van der Hoorn MA, et al. Efficiency of T-cell receptor expression in dual-specific T cells is controlled by the intrinsic qualities of the TCR chains within the TCR-CD3 complex. Blood. 2007;109(1):235-243.

ARTICLE

Dissecting molecular mechanisms of resistance to NOTCH1-targeted therapy in T-cell acute lymphoblastic leukemia xenografts

Valentina Agnusdei,[1] Sonia Minuzzo,[2] Marica Pinazza,[1] Alessandra Gasparini,[1] Laura Pezzè,[3] Adriana Agnese Amaro,[4] Lorenza Pasqualini,[1§] Paola Del Bianco,[1] Martina Tognon,[1] Chiara Frasson,[5] Pietro Palumbo,[6] Yari Ciribilli,[3] Ulrich Pfeffer,[4] Massimo Carella,[6] Alberto Amadori[1,2] and Stefano Indraccolo[1]

[1]Istituto Oncologico Veneto IOV - IRCCS, Padova; [2]Department of Surgery, Oncology and Gastroenterology, University of Padova, Padova; [3]Laboratory of Molecular Cancer Genetics, Department of Cellular, Computational and Integrative Biology (CIBIO), University of Trento; [4]Tumor Epigenetics, IRCCS Ospedale Policlinico San Martino, Genova; [5]Istituto di Ricerca Pediatrica, Fondazione Città della Speranza, Padova and [6]Medical Genetics Unit, Fondazione IRCCS Casa Sollievo della Sofferenza, San Giovanni Rotondo, Italy

[§]Current address: Diagnostics and genomics group, Agilent Technologies Inc. Santa Clara, CA, USA

Ferrata Storti Foundation

Haematologica 2020
Volume 105(5)1317-1328

ABSTRACT

Despite substantial progress in treatment of T-cell acute lymphoblastic leukemia (T-ALL), mortality remains relatively high, mainly due to primary or acquired resistance to chemotherapy. Further improvements in survival demand better understanding of T-ALL biology and development of new therapeutic strategies. The Notch pathway has been involved in the pathogenesis of this disease and various therapeutic strategies are currently under development, including selective targeting of NOTCH receptors by inhibitory antibodies. We previously demonstrated that the NOTCH1-specific neutralizing antibody OMP52M51 prolongs survival in TALL patient-derived xenografts bearing *NOTCH1/FBW7* mutations. However, acquired resistance to OMP52M51 eventually developed and we used patient-derived xenografts models to investigate this phenomenon. Multi-level molecular characterization of T-ALL cells resistant to NOTCH1 blockade and serial transplantation experiments uncovered heterogeneous types of resistance, not previously reported with other Notch inhibitors. In one model, resistance appeared after 156 days of treatment, it was stable and associated with loss of Notch inhibition, reduced mutational load and acquired *NOTCH1* mutations potentially affecting the stability of the heterodimerization domain. Conversely, in another model resistance developed after only 43 days of treatment despite persistent down-regulation of Notch signaling and it was accompanied by modulation of lipid metabolism and reduced surface expression of NOTCH1. Our findings shed light on heterogeneous mechanisms adopted by the tumor to evade NOTCH1 blockade and support clinical implementation of antibody-based target therapy for Notch-addicted tumors.

Introduction

T-cell acute lymphoblastic leukemia (T-ALL) is an aggressive hematological disease that results from clonal expansion of transformed lymphoid progenitors at different developmental stages.[1] Cure rates for pediatric ALL are currently approximately 90%, but prognosis for children who experienced relapse remains poor, and it has only marginally improved over the past two decades. Therefore, more efforts are required for patients with chemotherapy-resistant leukemia to identify effective treatment strategies.[2,3]

The Notch pathway plays a crucial role in T-cell lineage specification and thymic development and its deregulated activation has been linked to T-ALL development and maintenance.[1,4] Notably, about 50-60% of T-ALL samples show

Correspondence:

STEFANO INDRACCOLO
stefano.indraccolo@unipd.it

Received: February 8, 2019.

Accepted: August 26, 2019.

Pre-published: August 29, 2019.

doi:10.3324/haematol.2019.217687

Check the online version for the most updated information on this article, online supplements, and information on authorship & disclosures: www.haematologica.org/content/105/5/1317

activating mutations in the *NOTCH1* gene[5,6] and 15% of T-ALL cases present mutations or deletions in its ubiquitin ligase *FBW7*.[7] The role of Notch in solid and hematological malignancies suggests targeting of this pathway for therapeutic purposes in Notch-driven malignancies. Consolidated therapeutic approaches include the use of gamma secretase inhibitors (GSI) that block Notch processing, alternative molecules that affect Notch signaling and antibodies or decoy peptides to target specific Notch receptors or their ligands, hypothetically overcoming adverse effects due to the pan-Notch signaling inhibition associated with GSI.[8]

We have recently shown the therapeutic efficacy of the NOTCH1-specific monoclonal antibody OMP52M51 (Brontictuzumab) in pediatric T-ALL xenografts bearing *NOTCH1/FBW7* mutations, including samples derived from relapsed and difficult-to-treat patients.[9] OMP52M51 has been in clinical trial in patients with relapsed or refractory lymphoid malignancies (*trial ID: NCT01703572*) and with relapsed or refractory advanced solid tumors (*trial ID: NCT01778439*), although it has not been considered for further clinical development. Preliminary experiments in our lab showed that T-ALL PDX acquire resistance to OMP52M51 and this event may likely occur also in patients enrolled in clinical trials with this Notch inhibitor. Moreover, state-of-the-art knowledge about the molecular mechanisms of resistance to Notch blockade stems from various experimental models which utilized almost exclusively GSI to block Notch signaling.[10] We were therefore interested in exploiting PDX models to investigate possible novel mechanisms of resistance to antibody-mediated NOTCH1 blockade with the long-term aim to support clinical development of antibodies targeting Notch in cancer.

Methods

Establishment of T-ALL xenografts and development of resistant PDX *in vivo*

Xenografts (PDTALL) establishment and their genetic characterization are reported elsewhere.[9] To develop resistance to Notch blockade, PDTALL cells were intravenously (i.v.) injected in NOD/SCID mice ($5x10^6$ cells/mouse; 5-6 mice/group) and animals were intraperitoneally (i.p.) treated with the humanized anti-human NOTCH1 mAb OMP52M51 (Oncomed Pharmaceuticals Inc., Redwood, CA, USA) or control antibody (Rituximab, Roche, Basel, Switzerland) until disease progression. Both antibodies were administrated weekly at 20 mg/Kg, starting two days after i.v. injection of T-ALL cells. In the acute treatment experiment, mice were treated with OMP52M51 four days prior to sacrifice. Procedures involving animals conformed current laws and policies (EEC Council Directive 86/609, OJ L 358, 12/12 1987) and were authorized by the Italian Ministry of Health (894/2016-PR). T-ALL growth was monitored by periodic blood drawings and flow cytometric analysis of CD5 and CD7 (the antibodies used were both from Coulter, Fullerton, CA, USA). Leukemic cells were recovered from the spleen and used for the following analyses.

Reverse transcription-PCR (RT-PCR) and quantitative PCR (qPCR)

Total RNA was isolated using TRIzol Reagent (Life Technologies, Paisley, UK) according to the manufacturer's instructions. cDNA was synthesized from 1-1.5 μg of total RNA using the High Capacity RNA-to-cDNA kit (Life Technologies). For analysis of the Notch pathway activation, a panel of 21 NOTCH-target genes were evaluated in duplicates by Custom TaqManArray Cards as described before[9] using the TaqMan Universal PCR Master Mix (Life Technologies) and ABI Prism 7900 Sequence Detection System. Relative quantification was done using the ΔΔCt method, normalizing to β2-microglobulin mRNA. Primers used for validation of microarray results are reported in the *Online Supplementary Material and Methods*.

Western blot analysis

Western blot methods used in this study have been previously published.[11] Immunoprobing was performed using antibodies reported in the *Online Supplementary Material and Methods* section. Antigens were identified by luminescent visualization using the Western Lightning Plus ECL (Perkin Elmer) or ECL Select (Amersham, GE Healthcare, Chicago, IL, USA) and signal intensity was measured using a Biorad XRS chemiluminescence detection system. In a set of experiments we used subcellular fractionation, which was performed as previously described in Pinazza *et al.*[12]

Preparation of cRNA, GeneChip microarray analysis and data normalization

Samples were prepared with GeneChip® WT PLUS Reagent Kit (Affymetrix, Santa Clara, CA, USA). Total RNA and cRNA quality were evaluated with the Agilent RNA 6000 Nano Kit and Agilent 2100 Bioanalyzer (Agilent Technologies, Santa Clara, CA, USA) before microarray hybridization. cDNA was quantified by Implen NanoPhotometer (Implen, München, Germany). Labeled sense-strand cDNA was used for screening of GeneChip® Human Transcriptome Array 2.0 (Affymetrix). Each sample consisted of a single mouse (n=4-5 samples/group). Hybridization and scanning were conducted on the Affymetrix platform. Further experimental details can be found in the *Online Supplementary Material and Methods.*

Metabolomic analysis

Experimental details can be found in the *Online Supplementary Material and Methods.*

NGS analysis and Sanger sequencing

Experimental details can be found in the *Online Supplementary Material and Methods.*

Results

Resistance to OMP52M51 occurs with heterogeneous kinetics and Notch signaling activity in T-ALL PDX

We previously demonstrated that treatment with OMP52M51 delays engraftment of T-ALL cells bearing *NOTCH1/FBW7* mutations. Responder PDX disclosed increased T-ALL cell apoptosis, reduction of proliferation and marked inhibition of the Notch transcriptional signature.[9] To investigate whether and when resistance to NOTCH1 blockade occurs in a regimen of continuous administration of OMP52M51 mAb, we treated n=3 xenografts bearing activating *NOTCH1* mutations[9] and initially responsive to OMP52M51 (PDTALL8, PDTALL11, PDTALL19) until the appearance of leukemia. For each PDX, leukemia bearing mice (n=5-6 per group) were treated with OMP52M51 or control antibody once a week. Development of leukemia was evaluated by regular blood drawings and flow cytometric analysis of human CD5 and CD7 T-ALL markers and mice were sacrificed

when they presented ~20-25% circulating blasts (Figure 1A). Percentages of T-ALL cells in the spleen were evaluated at sacrifice, confirming an almost complete infiltration (>87%) of this hematopoietic organ by leukemic cells both in control and OMP52M51-resistant mice (*Online Supplementary Figure S1A*). In PDTALL19 model, leukemia engraftment and development of resistance to OMP52M51 were followed by optical imaging (*Online Supplementary Figure S1B*). Resistance to OMP52M51 treatment arose in all mice but with different kinetics in the three PDX analyzed, ranging from 43 days of PDTALL19 to 80 days of PDTALL11 and 156 days of

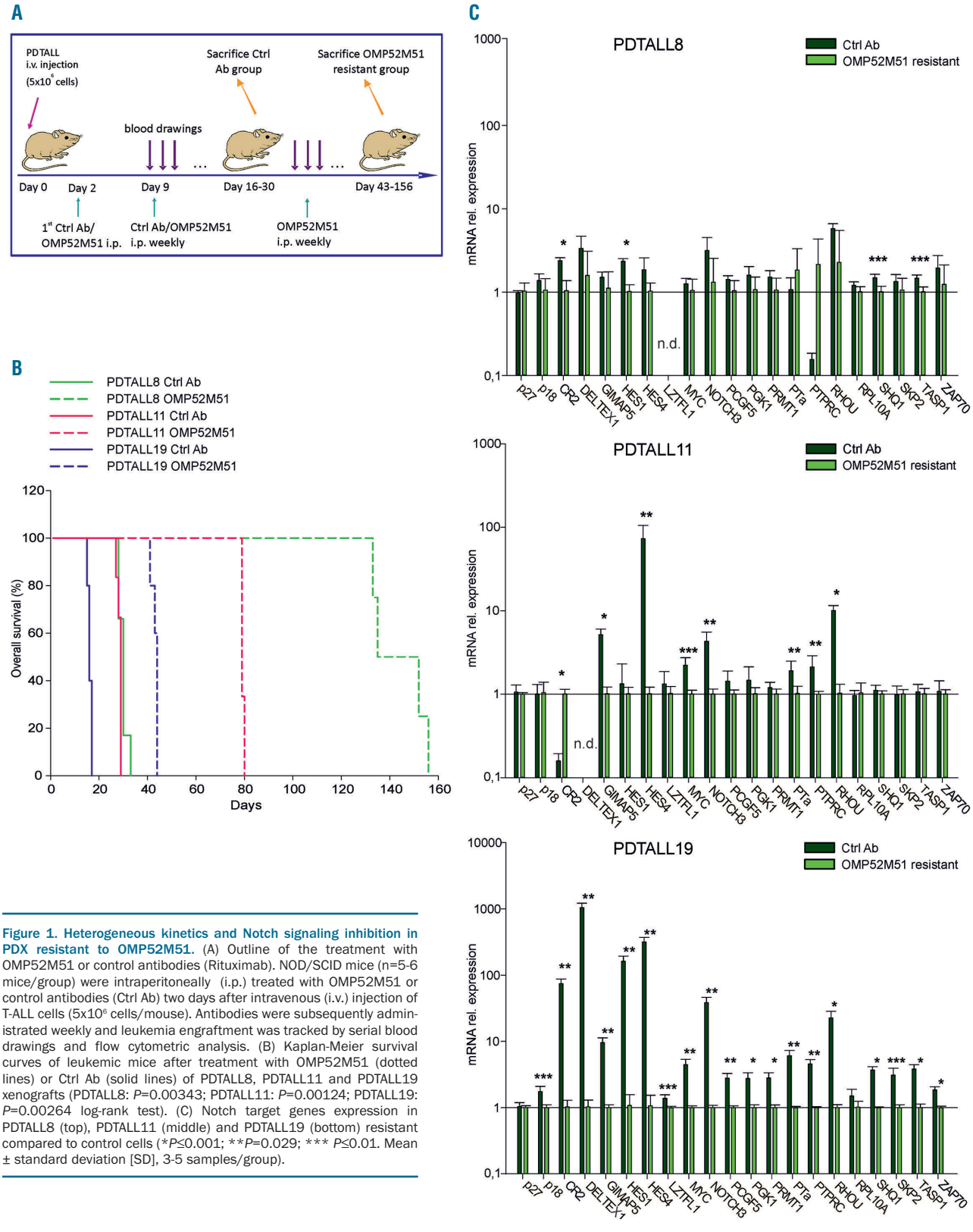

Figure 1. Heterogeneous kinetics and Notch signaling inhibition in PDX resistant to OMP52M51. (A) Outline of the treatment with OMP52M51 or control antibodies (Rituximab). NOD/SCID mice (n=5-6 mice/group) were intraperitoneally (i.p.) treated with OMP52M51 or control antibodies (Ctrl Ab) two days after intravenous (i.v.) injection of T-ALL cells (5x10^6 cells/mouse). Antibodies were subsequently administrated weekly and leukemia engraftment was tracked by serial blood drawings and flow cytometric analysis. (B) Kaplan-Meier survival curves of leukemic mice after treatment with OMP52M51 (dotted lines) or Ctrl Ab (solid lines) of PDTALL8, PDTALL11 and PDTALL19 xenografts (PDTALL8: *P*=0.00343; PDTALL11: *P*=0.00124; PDTALL19: *P*=0.00264 log-rank test). (C) Notch target genes expression in PDTALL8 (top), PDTALL11 (middle) and PDTALL19 (bottom) resistant compared to control cells (*$P \leq 0.001$; **$P=0.029$; *** $P \leq 0.01$. Mean ± standard deviation [SD], 3-5 samples/group).

PDTALL8 (Figure 1B). Notably, the dynamic tracking of the percentage of T-ALL cells in blood uncovered substantially different profiles in these models. In fact, we observed a steep increase in the case of PDTALL8 model, compared with the mild increase observed in the PDTALL19 model (*Online Supplementary Figure S2*), suggesting different mechanisms of adaptation to OMP52M51.

Following treatment of T-ALL PDX with OMP52M51, we previously observed a strong reduction of Notch target gene expression in good responders and we considered this phenomenon as indirect evidence of reduced Notch signaling.[9] Therefore, we wondered if this inhibition was still present in mice which developed resistance to OMP52M51 therapy. To investigate this hypothesis, we analyzed expression levels of 21 Notch target genes by qPCR. In the PDTALL8 model, expression levels of Notch target genes were very similar in OMP52M51-resistant and control cells (Figure 1C, top). On the contrary, in PDTALL11 xenograft several genes were significantly downregulated in cells recovered from OMP52M51-resistant compared to control mice (Figure 1C, middle). In the PDTALL19 model, inhibition of Notch signaling was maintained in resistant cells (Figure 1C, bottom) and it was comparable to that previously measured following acute treatment with OMP52M51.[9]

Serial transplantation experiments disclosed two types of resistance to OMP52M51

To elucidate whether resistance to OMP52M51 was a stable trait, we performed serial transplantation experiments. T-ALL cells from the spleen of donor mice resistant to OMP52M51 were i.v. injected into naïve recipient mice, which were then weekly treated with OMP52M51 or control antibody according to the standard protocol until the appearance of the signs of disease (Figure 2A). We found that resistance was a stable trait in the PDTALL8 model, the PDX in which resistance developed 156 days after OMP52M51 treatment (late onset). In fact, in the serial transplantation experiment, both OMP52M51-treated and control mice developed leukemia 39 days after T-ALL cell injection (Figure 2B). In contrast, resistance to OMP52M51 was lost upon serial transplantation in PDTALL19 model, the PDX with early onset of resistance. PDTALL19 cells recovered from the spleen of OMP52M51-resistant mice and injected into näïve mice were initially sensitive to OMP52M51 treatment, as no evidence of T-ALL cells was found in the blood of these mice at day 18, when control mice were sacrificed. When administration of OMP52M51 was repeated, however, mice became gradually resistant to therapy and they were eventually sacrificed 41 days after T-ALL cell injection, a time point very similar to that observed in the initial experiment (Figure 2B). It is important to note, however, that following repeated (n=5) cycles of treatment of PDTALL19 cells with OMP52M51, resistance became stable, replacing the initial unstable form of resistance seen in this model (*Online Supplementary Figure S3*), with possibly different underlying mechanisms. In the PDTALL11 model, the onset of resistance was intermediate between the other two models previously described (Figure 2B). Finally, Notch pathway activation was investigated in secondary treated and non-treated resistant cells. Results disclosed marked differences in the expression of several Notch target genes in the case of PDTALL11 and PDTALL19 and only marginal differences in the case of PDTALL8 (Figure 2C), in line with results of the first round of treatment.

Resistance to OMP52M51 is not associated with PTEN or *FBW7* alterations

It is well known that the PTEN/PI3K/AKT pathway is frequently altered in T-ALL and that PTEN loss is involved in resistance induced by GSI[13] and other therapies.[14] Therefore, we analyzed the expression of PTEN in the three PDX models. PTEN was expressed in all models and resistance was not associated with loss of PTEN, since the protein was detectable at comparable levels in treated and control cells (*Online Supplementary Figure S4*). In line with this finding, comparable levels of AKT activation (determined as $pAKT^{Ser473}$ and $pAKT^{Thr308}$)[15] were found in OMP52M51 compared with control cells (*Online Supplementary Figure S4*). Furthermore, we sequenced the *FBW7* gene, since mutations in this gene have also been correlated with GSI resistance.[7] Sequencing of *FBW7* in PDTALL8, PDTALL11 and PDTALL19 models revealed that neither parental nor resistant cells were harboring a mutated version of FBW7 (*Online Supplementary Table S2*). We conclude that resistance to OMP52M51 did not involve mechanisms reported in previous studies with GSI.

Resistance to OMP52M51 is associated with a distinct transcriptional signature in PDTALL19 model

We exploited transcriptome analysis to investigate the mechanisms of resistance to OMP52M51 in the PDTALL8 and PDTALL19 models, which presented completely different phenotypes of resistance. In the PDTALL8 model – the PDX characterized by late onset and stable resistance to OMP52M51 – only a few ProbeSet ID without an associated gene annotation were modulated, so we concluded that the gene expression profiles of resistant cells were superimposable to control ones (*Online Supplementary Figure S5*). In contrast, in the PDTALL19 model – the PDX characterized by early onset and transient resistance to OMP52M51 – we identified 327 up- and 257 down-regulated genes in the comparison between OMP52M51-resistant and control cells (Figure 3A, *Online Supplementary Table S3-4*). Gene set enrichment analysis (GSEA) identified 20 pathways significantly down-regulated in OMP52M51-resistant T-ALL samples (*Online Supplementary Figure S6*). Among them, we found the Notch pathway (Figure 3B), confirming the inhibition measured by TaqMan arrays, oxidative phosphorylation, unfolded protein response, pathways related to proliferative processes - such as the G2/M checkpoint and mitotic spindle – and MYC targets, a well-known mediator of Notch activity. Interestingly, GSEA disclosed also metabolic pathways significantly down-regulated in resistant compare to control cells, including cholesterol homeostasis, adipogenesis and fatty acid metabolism (Figure 3B). Selective transcriptome findings were validated by quantitative RT-PCR (*Online Supplementary Figure S7*). In order to unravel if these modulations were due to inhibition of Notch signaling or were hallmarks of resistance to OMP52M51, we performed gene expression profile analysis in mice engrafted with PDTALL19 cells and acutely treated with OMP52M51. The majority of pathways identified by GSEA were present also in these samples (*Online*

Supplementary Figure S8-9), but with a higher level of down-regulation compared to OMP52M51 resistant cells (*Online Supplementary Figure S10*), suggesting that the inhibitory effect of the antibody on signaling is partially lost when resistance develops.

Resistance to OMP52M51 is associated with rewiring of lipid metabolism in PDTALL19 cells

These results prompted investigation of the effects of Notch blockade on lipid metabolism. To this end, we performed tandem mass spectrometry (MS/MS) for different

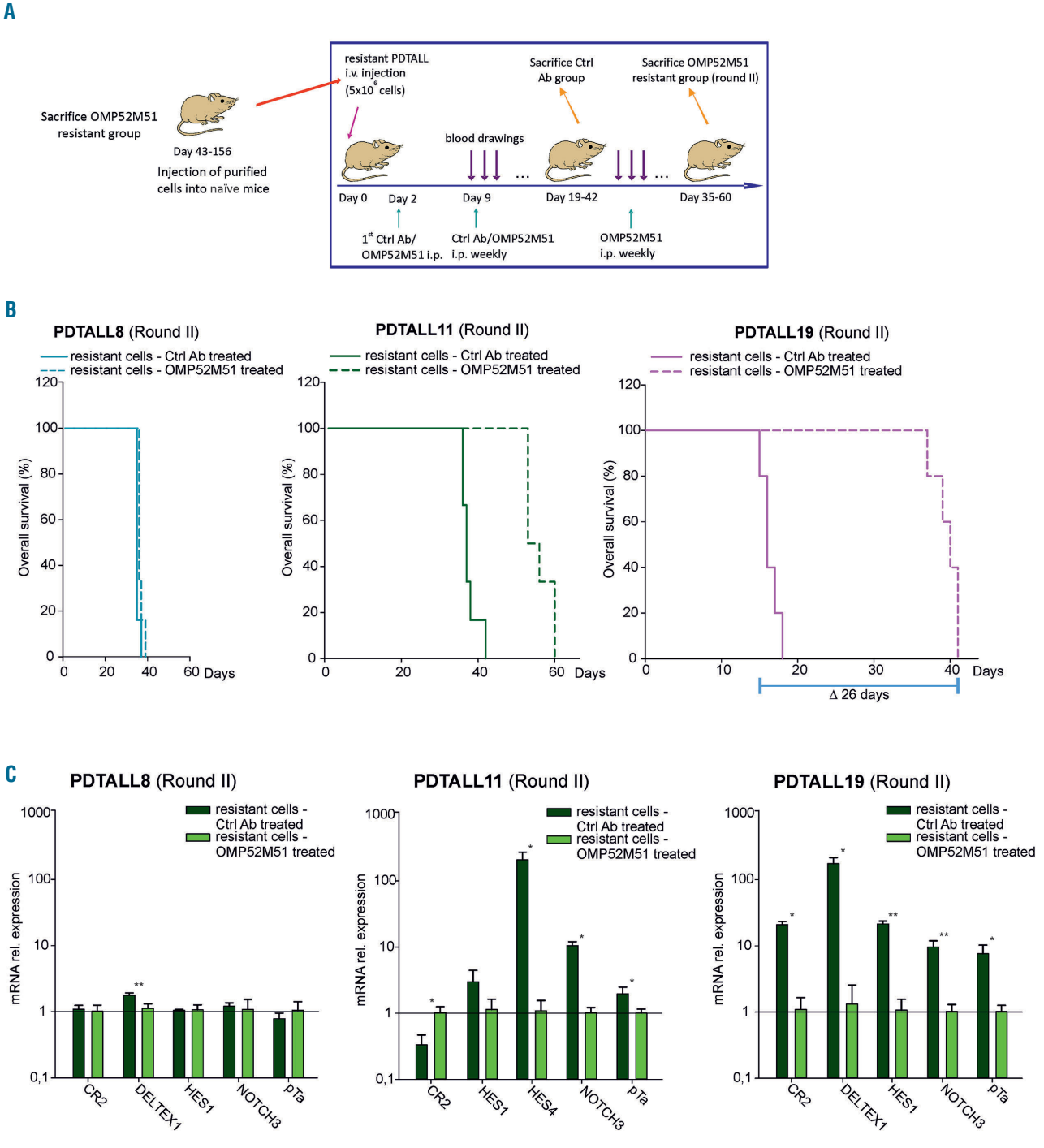

Figure 2. Serial transplantation experiments disclose different phenotypic traits of resistance. (A) Outline of the experiment. Resistant cells were recovered from the spleen of OMP52M51-treated mice and injected into naïve mice (5-6 mice/group). Recipient mice were then treated weekly with OMP52M51 or control monoclonal antibodies (Ctrl mAb) according to the standard protocol. (B) Kaplan-Meier survival curves of PDTALL8, PDTALL1 and PDTALL19 mice after a second course of treatment with OMP52M51. In these experiments, mice transplanted with PDTALL8, PDTALL11 or PDTALL19 resistant cells from the first round of treatment (PDTALL8: P=0.0441; PDTALL11: P<0,001; PDTALL19: P=0.00181 log-rank test). (C) Expression levels of selected Notch target genes in T-ALL cells obtained from the spleen of mice after the second course of OMP52M51 treatment (*P<0,05; **P<0,001. Mean ± standard deviation [SD], 3-6 samples/group).

classes of metabolites. This analysis revealed that numerous constituents of cell membranes were less abundant in OMP52M51-resistant versus control PDTALL19 samples, including members of glycerophospholipids, sphingomyelins and ceramides families, as well as oxysterols and one cholesterol ester. Only few metabolites in these classes were enriched in OMP52M51-resistant cells (Figure 4A). Quantification of the cellular contents of lipid droplets by flow cytometry confirmed a significant reduction of lipid storage in OMP52M51-resistant cells compared to controls (*Online Supplementary Figure S11*). Moreover, MS/MS analysis discovered an imbalance

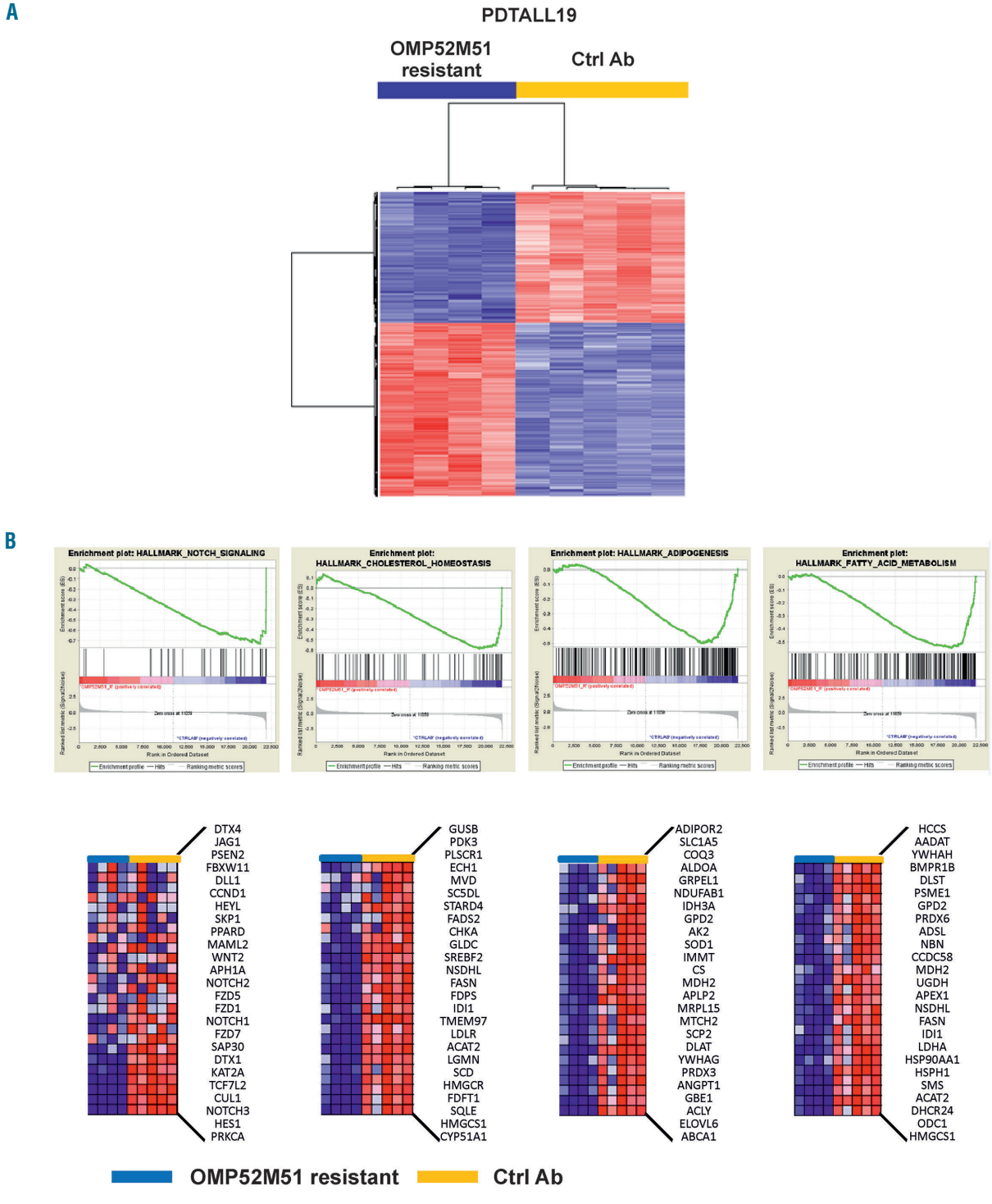

Figure 3. Transcriptome analysis of OMP52M51-resistant PDTALL19 cells. (A) Heatmap of genes modulated comparing OMP52M51 resistant and control cells (4-5 samples/group). Red and blue colors indicate higher and lower expression levels, respectively. The columns represent individual samples (B) top: Gene set enrichment analysis (GSEA) plots of four enrichment sets down-regulated in resistant cells. Bottom: Heatmaps and lists of the top 25 differentially expressed genes of the corresponding plots reported above.

between saturated and (poly-) unsaturated lipids and identified a trend towards reduction of the unsaturation degree in OMP52M51-resistant samples (Figure 4B). Notably, acute treatment of PDTALL19 mice with OMP52M51 did not cause significant alterations in lipids (*Online Supplementary Figure S12*), indicating that dis-regulated lipid metabolism is a feature of resistance.

Since NOTCH1 is a membrane-bound protein, we hypothesized that a different composition of lipid constituents could affect the fluidity of the membrane and the surface levels of the receptor. To this end, we analyzed NOTCH1 protein levels by Western blot (WB) analysis both in whole cell lysates (Figure 5A) and in plasma membrane fractions (Figure 5B). OMP52M51-resis-

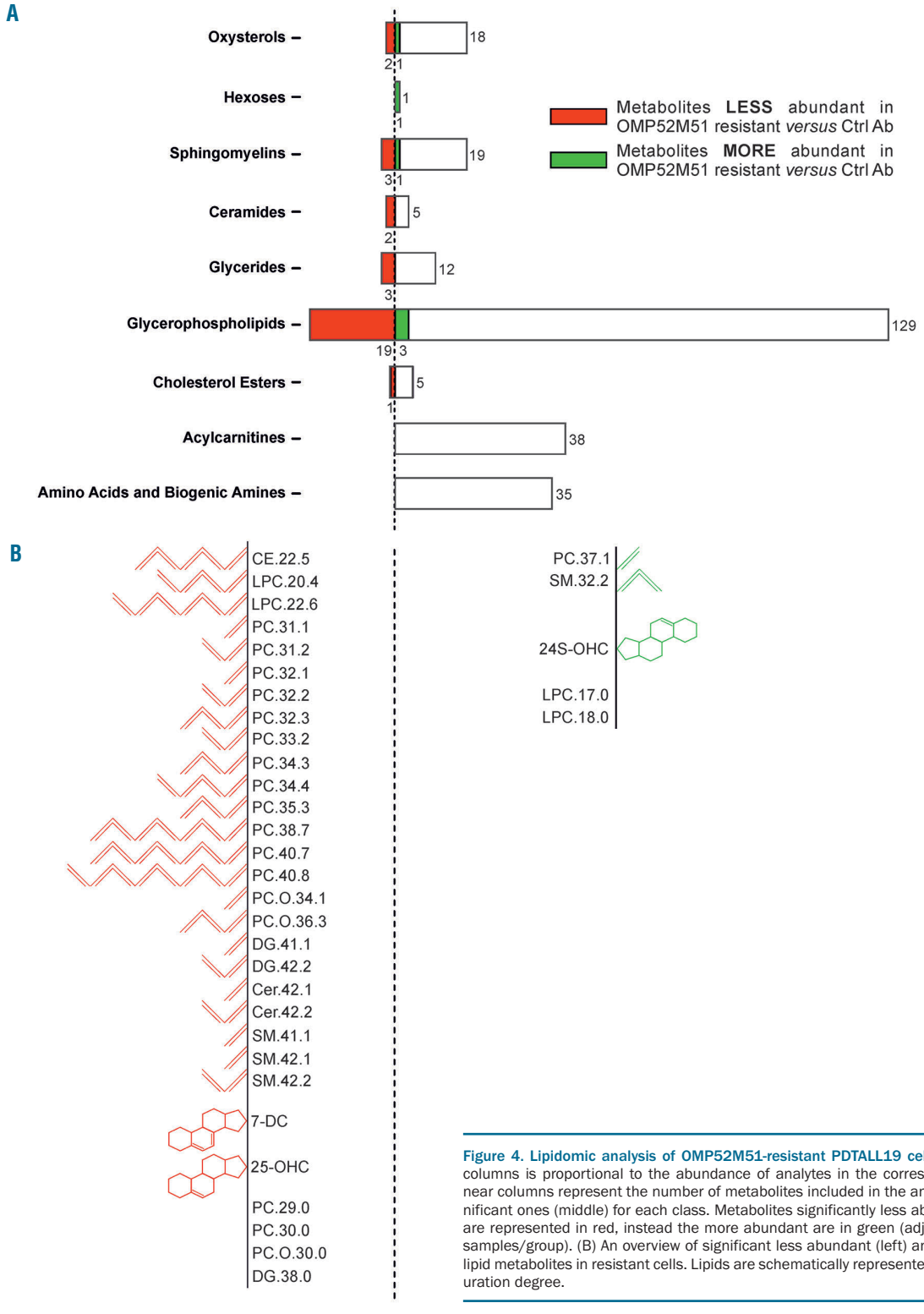

Figure 4. Lipidomic analysis of OMP52M51-resistant PDTALL19 cells. (A) The length of the columns is proportional to the abundance of analytes in the corresponding class. Numbers near columns represent the number of metabolites included in the analysis (right) and the significant ones (middle) for each class. Metabolites significantly less abundant in resistant cells are represented in red, instead the more abundant are in green (adjusted *P*-value<0.05, five samples/group). (B) An overview of significant less abundant (left) and more abundant (right) lipid metabolites in resistant cells. Lipids are schematically represented depending on their saturation degree.

tant samples revealed a clear reduction in trans-membrane (TM) and intracellular domain (ICD) forms, a result that was expected since binding of the antibody should prevent activation of the pathway. These results were confirmed by WB analysis of whole cell lysates using the NOTCH1 ICD-specific Val1744 monoclonal antibody (mAb) (Figure 5A). Interestingly, we also observed a decrease in the full-length NOTCH1 form, which was not anticipated and suggested lower levels of NOTCH1 on the cell surface (Figure 5A-B). This modulation in NOTCH1 protein levels was not observed in OMP52M51-resistant PDTALL8 and PDTALL11 cells,

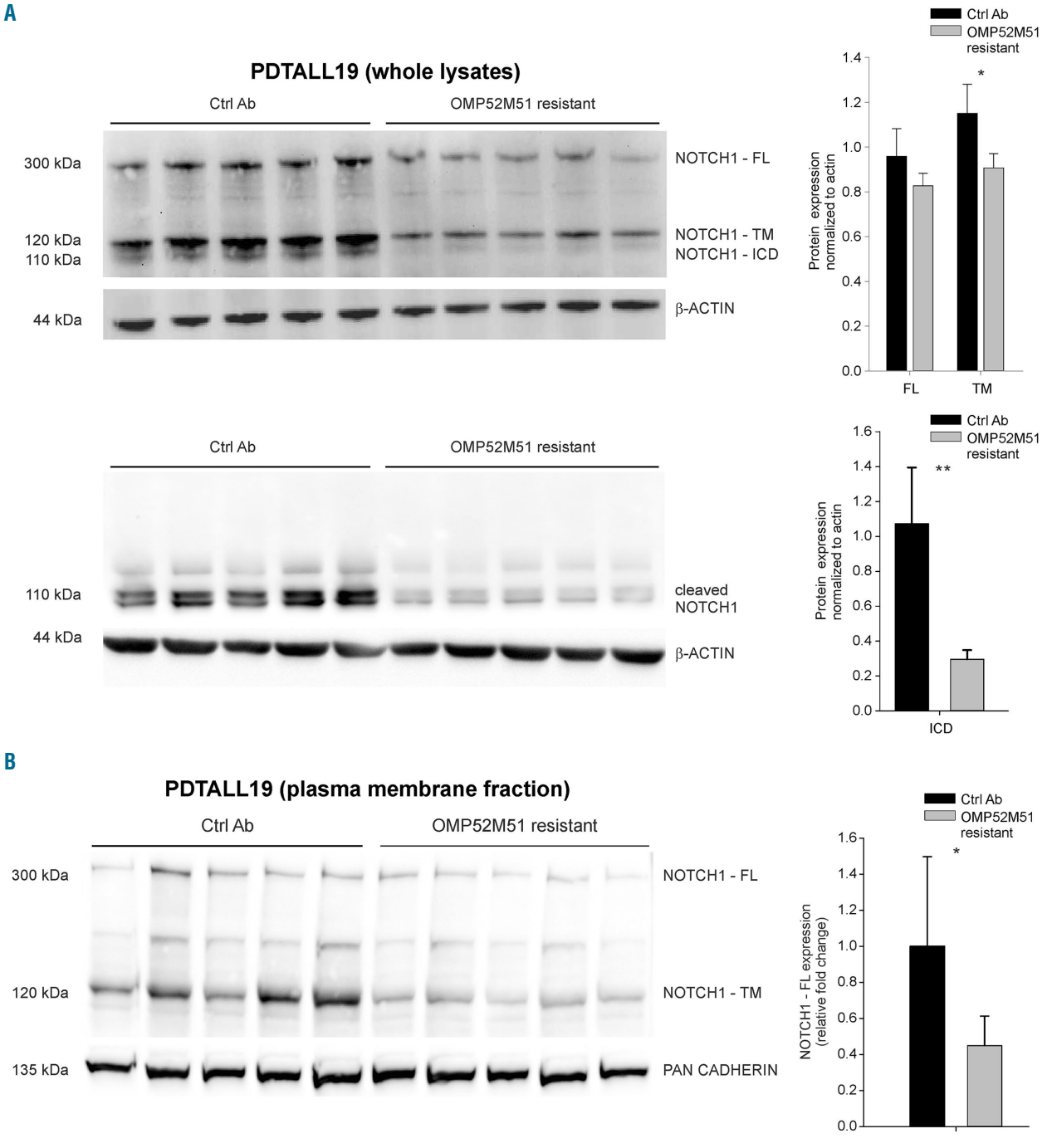

Figure 5. OMP52M51-resistant PDTALL19 cells show reduction of surface NOTCH1 protein. (A) Left: NOTCH1 full-length (FL), transmembrane (TM) and intra-cellular domain (ICD) expression levels were measured by Western blot analysis on whole cell lysates. Cleaved NOTCH1 levels (mid panel) were determined by probing the filters with the Val1744 antibody. Right: quantification of NOTCH1 FL, TM and ICD levels normalized to β-actin expression (mean ± standard deviation [SD]) of control and resistant cells (five samples/group. **P*=0.005; ***P*<0.001). (B) Left: Analysis of NOTCH1 expression on plasma membrane lysates obtained by subcellular fractionation. Right: Quantification of NOTCH1-FL expression in control antibodies (Ctrl Ab) and resistant cells, normalized to the corresponding housekeeping protein pan-cadherin and normalized to controls (mean ± SD, 10 samples/group.**P*=0.001).

consistent with marginal variations in genes involved in lipid metabolism in these models (*Online Supplementary Figure S13*). However, acute treatment of PDTALL19 mice with OMP52M51 was also associated with reduced NOTCH1 FL and ICD levels (*Online Supplementary Figure S12*), indicating that these changes were related to NOTCH1 blockade rather than to resistance. Finally, given the marked changes in lipid metabolism seen in the PDTALL19 model, we investigated other possible phenotypic changes associated with resistance. By flow cytometry analysis, we found that OMP52M51-resistant cells exhibited a smaller size compared with control cells and there were also significant changes in surface expression of the T-cell markers CD3 and CD7 and the pan-leucocyte marker CD11a (*Online Supplementary Figure S14*).

Assessment of the genetic background of OMP52M51 resistance in the PDTALL8 model

In the case of PDTALL8 model, transcriptional data suggested that mechanisms underlying the stable resistance to OMP52M51 treatment could involve an "on target" mutation of the Notch pathway selected during treatment and serial transplantation experiments, leading to the loss of sensitivity to OMP52M51.

To investigate this hypothesis, we performed single nucleotide polymorphism (SNP) arrays and whole exome sequencing (WES) of paired control-resistant mice (see *Online Supplementary Table S5* for WES metrics details), allowing the identification of variants that could be not detected by Sanger sequencing due to a relatively low variant frequency. Cytoscan arrays failed to identify copy number variations associated with resistance to OMP52M51 in PDTALL8 cells (*Online Supplementary Figure S15*). However, bioinformatics analysis of WES revealed that control mice displayed a higher tumor mutational load than OMP52M51-resistant samples, both considering the total number of variants (34,641 variants in controls compared to 12,206 in OMP52M51-resistant samples) and shared confident non-synonymous calls (440 *vs.* 54; Figure 6A-B and *Online Supplementary Table S6*). This difference could be explained by the "tumor clonal selection" model. Speculatively, the OMP52M51 antibody could act as a selective agent, favouring outgrowth of a subpopulation of cells from the initial tumour. Interestingly, WES analysis highlighted the presence of two NOTCH1 activating variants mapping to the heterodimerization domain (HD),[16] *i.e.* p.Q1584H and p.L1585P, present only in the OMP52M51-resistant mice (Figure 6C). We validated these mutations by Sanger sequencing and extended analysis to additional samples from the same experiment (four to five mice/group; *Online Supplementary Figure S16*). Sanger sequencing confirmed that both mutations were present in OMP52M51 resistant mice and were lacking in controls (Figure 6D).

To investigate whether these mutations occurred at low level in parental cells, we performed targeted sequencing analysis. All treated xenograft (three replicates/group) presented p.L1585P and p.Q1584H variants in cis (*Online Supplementary Figure S17*). On the other hand, at a depth of 300X the p.L1585P and p.Q1584H variants were not identified in control samples and therefore, if present prior to treatment, must have been present at a frequency of less than 5%, which was the estimated sensitivity of the next-generation sequencing (NGS) assay.

Finally, according to the literature, these mutations destabilize the structure of the HD domain[17] and therefore could affect binding of OMP52M51. This was indeed shown by flow cytometry experiments showing that the binding of OMP52M51 is lower in PDTALL8 resistant compared with control cells (Figure 6E).

Discussion

In the last 10 years, personalized treatment of cancer has improved substantially thanks to the identification of specific genetic alterations and consequent development of target therapies against oncogenic drivers. In this landscape, the resistance of cancer cells to pharmacological treatment remains the major challenge to face in order to increase the efficacy of new drugs.[18] Although we are aware of some intrinsic limitations of xenografts, such as the lack of the immune system, the systemic T-ALL models used in this study are suitable to study effects of drugs directly targeting tumors cells, and we used them to investigate the molecular mechanisms of resistance to Notch targeted therapy. Our results demonstrate that the resistance appeared following long-term administration of OMP52M51 antibody in each of the three PDX models tested, though with different timing. In fact, PDTALL8, the PDX with a late onset of resistance and loss of Notch signaling inhibition, was characterized by a stable resistance. On the contrary, in the PDTALL19 model, resistance appeared earlier, Notch signaling was inhibited and, importantly, it was an unstable trait. Analysis of the slope of the percentage of T-ALL cells in blood of these mice during serial drawings suggested that adaptation to OMP52M51 in this model consisted mainly of a delayed but constant growth of the PDX without the development of true resistance during the first round of treatment. However, upon repeated rounds of treatment with OMP52M51 stable resistance eventually occurred, suggesting a two-stage form of resistance in this model. PDTALL11 disclosed an intermediate behavior both regarding the time of development of resistance, the stability of resistance and Notch signaling inhibition, likely due to a mixture of different mechanisms. Speculatively, an additional round of treatment might lead to the selection of a completely resistant clone also in the PDTALL11 model, although this was not investigated here.

Intriguingly, previous studies elegantly addressed the issue of clonality of T-ALL xenografts and correlated the genetic complexity of T-ALL cells with the speed of leukemia development in xenograft models.[19,20] Specifically, in the case of delayed T-ALL growth, leukemia cells were in part genetically diverse, the resulting xenograft leukemia arising from different but branched subclones present in the original sample. Although not investigated in our study, it could be speculated that the clonal architecture of the PDX might have an influence on the time of development and the type of resistance to anti-NOTCH1 therapy.

In the PDX tested, the resistance was never associated with the loss of PTEN, AKT activation or mutations in *FBW7* gene, which represent some of the previously described mechanisms of resistance to Notch inhibition by GSI.[7,13] The strikingly different phenotypes of the PDTALL8 and PDTALL19 models underscored two novel mechanisms of resistance. In the case of PDTALL19, we

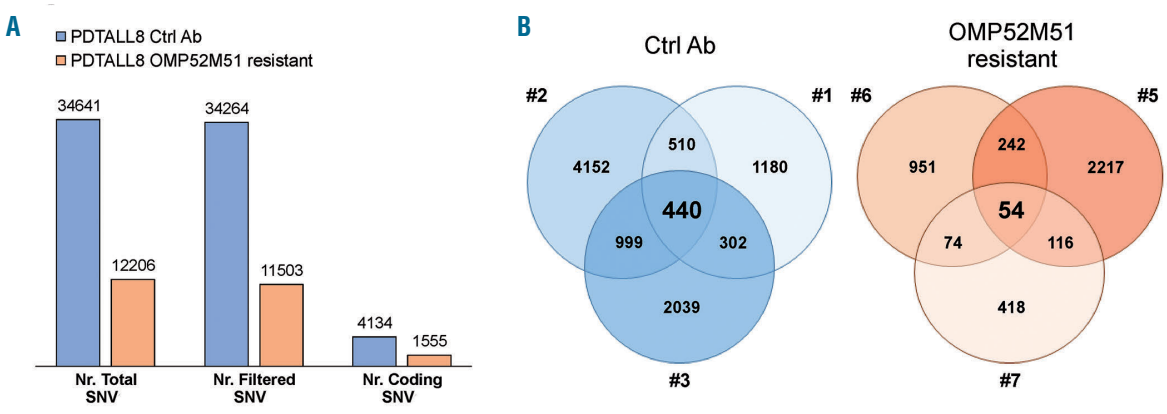

C

Sample	c.Annot	p.Annot	VAF	AD	DP
PDTALL8 OMP52M51 resistant #5	c.[4752G>C;4754T>C]	p.[Q1584H; L1585P]	31.5	40	127
			31.2	41	128
PDTALL8 OMP52M51 resistant #6	c.[4752G>C;4754T>C]	p.[Q1584H; L1585P]	26.4	43	163
			25.3	39	158
PDTALL8 OMP52M51 resistant #7	c.[4752G>C;4754T>C]	p.[Q1584H; L1585P]	30.8	32	104
			29.4	32	109

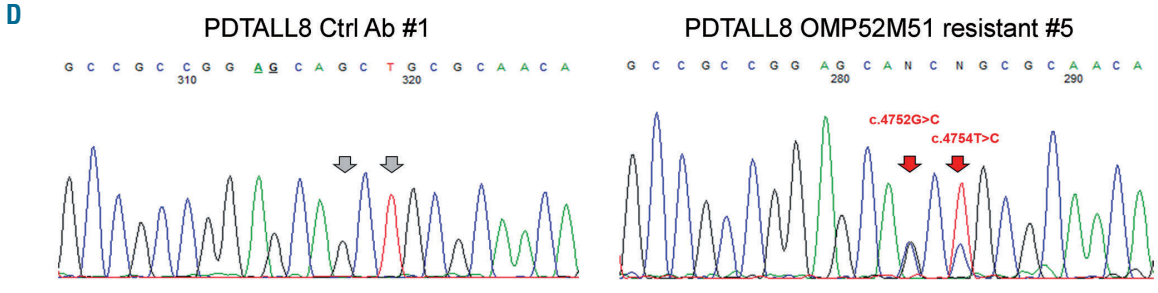

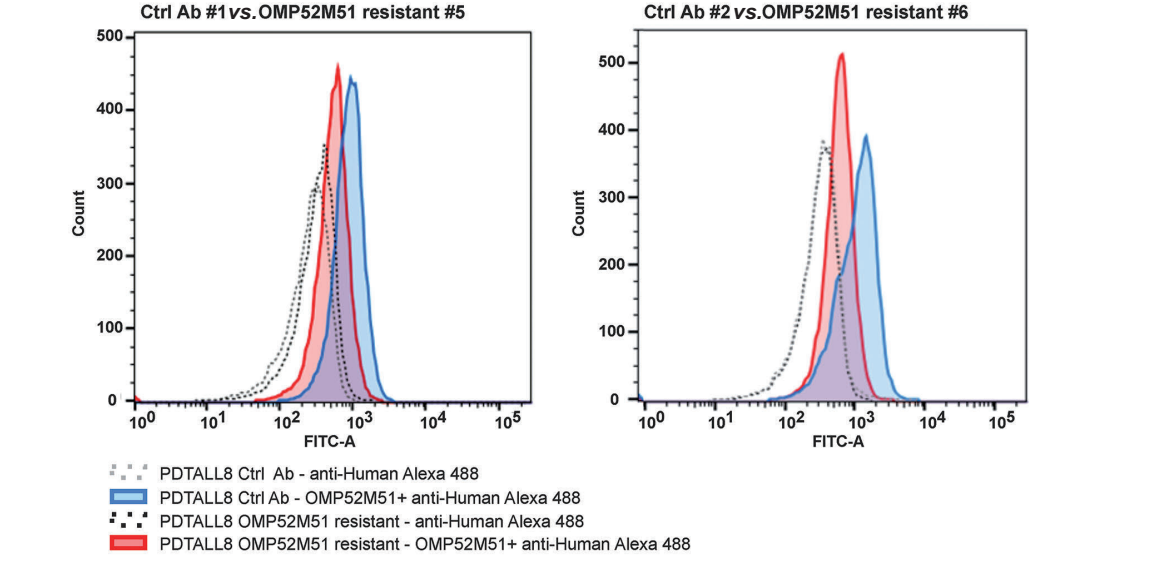

Figure 6. Molecular profiling of PDTALL8 control and OMP52M51 resistant T-cell acute lymphoblastic leukemia cells. (A) Comparison between the average mutational burden in PDTALL8 untreated and resistant cells based on whole exome sequencing (WES) results. Total: total number of single-nucleotide variant (SNV); filtered: variants with a variant allele fraction (VAF) >10% and coverage depth (DP) >30 excluding common polymorphisms; coding: filtered coding variants excluding synonymous genetic alterations. (B) Venn diagrams of coding variants for each mouse. 440 SNV and 54 SNV are shared respectively between control (#1-3) and resistant mice (#5-7) inside each group. (C) *NOTCH1* variants found only in OMP52M51 resistant samples. cDNA coordinates, amino acidic changes, VAF, alternative allele depth (AD) and DP are reported. (D) Direct sequencing of exon 26 in a representative control (Ctrl Ab #1) and resistant (OMP52M51 resistant #5) pair. Resistance-related mutations are indicated with the red arrows. (E) Flow cytometric analysis of surface expression of NOTCH1 in T-cell acute lymphoblastic leukemia (T-ALL) cells from the spleen of PDTALL8 mice treated with either OMP52M51 or control antibody. Two representative samples per group are shown.

found that tumor adaptation to anti-NOTCH1 therapy was accompanied by a distinct transcriptomic and metabolic signature. Alterations converged on lipid metabolism, hinting at significant alterations in constituents of cell membranes such as phosphatidylcholines, lysophosphatidylcholines, sphingomyelins and ceramides. Moreover, there was a trend towards the reduction of the unsaturation degree of lipids in OMP52M51-resistant samples, hypothetically suggesting a modulation of membrane fluidity, since saturated fatty acids are more densily packed.[21] Some years ago, a well-designed study correlated a different composition of phospholipids with an increase in endocytosis and therefore a reduction in EGFR and Notch signaling, due to the fact that these receptors were less abundant on the cell membrane.[22] Albeit performed in Drosophila, we speculated that the different composition and/or unsaturation degree of membrane components could affect the amount of NOTCH1 receptor on cell surface and, therefore, the amount of target available for binding the therapeutic antibody. For a linear pathway such as Notch, the exposure of the receptor on cell surface is fundamental and, therefore, the number of NOTCH1 receptors are strictly regulated.[23-25] However, we found reduced NOTCH1 levels also after short-term treatment with OMP52M51, a condition where lipid alterations were not detected, indicating that the alterations in lipid metabolism are in fact a feature associated with the resistance in the PDTALL19 model, but this does not likely cause reduced NOTCH1 FL levels in these cells. In any case, recent findings gave prominence to new functions of membrane components, beyond the structural one. Phosphatidylcholines, lysophosphatidylcholines, sphingomyelins and ceramides could, in fact, be involved in cell signaling and behave as messengers frequently altered in pathologic conditions such as cancer.[26-29] Therefore, it could be possible that the variations in membrane components observed in PDTALL19 model could influence the microenvironment and/or T-ALL cell behaviour. Along this line, our finding that T-ALL cells resistant to OMP52M51 had reduced size and showed lower surface levels of CD3, CD4 and CD11a compared with control cells supports this hypothesis.

In a recent paper, Herranz and colleagues identified glucose metabolism and glutaminolysis as key determinants in cell resistance to Notch blockade with GSI.[30] In our model, we also found an increase in the amount of hexoses in resistant cells, but the innovative finding was represented by the association between the resistance to OMP52M51 antibody and the modulations of the sterol biosynthetic pathway. Moreover, in our model we did not observe the activation of autophagy (*data not shown*), which other groups previously detected in cells after Notch inhibition by GSI.[30] Regarding the PDTALL19 model, finally, the comparison between resistant cells and acute treatment with OMP52M51 disclosed that the antibody inhibited the same GSEA pathways but with a different strength.

Another possible hypothesis behind the reduction of surface NOTCH1 receptor regards DELTEX1. Many studies performed in *Drosophila* have shown that the activation, degradation and recycling of Notch receptors could depend on their ubiquitination pattern.[31,32] DELTEX1 is an ubiquitin-ligase that could act as a positive or a negative regulator of Notch signaling depending on the cellular context and could influence endocytic trafficking of the receptor.[33-35] Notably, in our models *DELTEX1* was one of the most down-regulated genes in PDTALL19 cells, whereas it was not detectable in PDTALL11 cells and was not modulated in PDTALL8 cells (Figure 1C), PDX in which we did not observe any reduction of surface NOTCH1 protein.

In the PDTALL8 model, given the stability of the resistance and the loss of Notch signaling inhibition, the most likely explanation for the observed resistance was the selection of a mutated clone no longer responsive to therapy. To address this possibility, NGS analysis performed in control and resistant cells disclosed a selection of clones of the initial tumour, since treated samples presented a lower mutational burden compared to control. Moreover, NGS analysis revealed the presence of two activating mutations in *NOTCH1* gene - p.Q1584H and p.L1585P - in the OMP52M51 resistant mice. These variants, reported as T-ALL associated in CIViC database (36), were in cis and cause the introduction of a positive charge (p.Q1584H) and a break (p.L1585P) to the α2-helix in the HD domain,[16] adding steric bulk in the HD core. These modifications potentially affect the stability of HD domain and could influence binding of the OMP52M51 antibody, causing the loss of responsiveness to the therapy. Notably, we confirmed the p.Q1584H and the p.L1585P mutations by targeted sequencing but could not find them in the parental cells prior to treatment. However, as all of the independently derived resistant PDTALL8 tumor samples disclosed the same p.Q1584H and p.L1585P variants, it is extremely likely that these variants must have been present in a minor sub-clone prior to selective pressure with OMP52M51.

Finally, the possible role of the microenvironment must be taken into consideration, since different tumours could differ, not only in intrinsic lesions but also in their dependence on the niche – therefore, different T-ALL cases might respond distinctly to the same treatment. A better characterization of both cell-autonomous lesions and cues from the microenvironment, which was apart from the purpose of this paper, would extend the complete understanding of how the malignancy progresses and resistance develops.[1]

In conclusion, our study highlights heterogeneity in the phenotypic and molecular features of resistance to OMP52M51. Notably, traits associated with resistance differ from those previously described following treatment with GSI, suggesting that leukemia cells can adopt several strategies to evade Notch inhibition according to the therapeutic drug used.

Ackowledgments

We thank Dr. Erich Piovan (University of Padova, Padova, Italy) for providing the PTEN antibody and Dr. Tim Hoey (Oncomed Pharmaceuticals Inc., Redwood, CA, USA) for providing the OMP52M51 antibody.

Funding

This work was supported by AIRC (Grant n. IG18803 to SI).

References

1. Oliveira ML, Akkapeddi P, Alcobia I, et al. From the outside, from within: Biological and therapeutic relevance of signal transduction in T-cell acute lymphoblastic leukemia. Cell Signal. 2017;38:10-25.
2. Pierro J, Hogan LE, Bhatla T, Carroll WL. New targeted therapies for relapsed pediatric acute lymphoblastic leukemia. Expert Rev Anticancer Ther. 2017;17(8):725-736.
3. Pui CH, Yang JJ, Hunger SP, et al. Childhood Acute Lymphoblastic Leukemia: Progress Through Collaboration. J Clin Oncol. 2015;33(27):2938-2948.
4. Aifantis I, Raetz E, Buonamici S. Molecular pathogenesis of T-cell leukaemia and lymphoma. Nat Rev Immunol. 2008;8(5):380-390.
5. Weng AP, Ferrando AA, Lee W, et al. Activating mutations of NOTCH1 in human T cell acute lymphoblastic leukemia. Science. 2004;306(5694):269-271.
6. Sulis ML, Williams O, Palomero T, et al. NOTCH1 extracellular juxtamembrane expansion mutations in T-ALL. Blood. 2008; 112(3):733-740.
7. O'Neil J, Grim J, Strack P, et al. FBW7 mutations in leukemic cells mediate NOTCH pathway activation and resistance to gamma-secretase inhibitors. J Exp Med. 2007;204(8):1813-1824.
8. Platonova N, Lesma E, Basile A, et al. Targeting Notch as a therapeutic approach for human malignancies. Curr Pharm Des. 2017;23(1):108-134.
9. Agnusdei V, Minuzzo S, Frasson C, et al. Therapeutic antibody targeting of Notch1 in T-acute lymphoblastic leukemia xenografts. Leukemia. 2014;28(2):278-288.
10. Hales EC, Taub JW, Matherly LH. New insights into Notch1 regulation of the PI3K-AKT-mTOR1 signaling axis: targeted therapy of gamma-secretase inhibitor resistant T-cell acute lymphoblastic leukemia. Cell Signal. 2014;26(1):149-161.
11. Pinazza M, Borga C, Agnusdei V, et al. An immediate transcriptional signature associated with response to the histone deacetylase inhibitor Givinostat in T acute lymphoblastic leukemia xenografts. Cell Death Dis. 2016;6:e2047.
12. Pinazza M, Ghisi M, Minuzzo S, et al. Histone deacetylase 6 controls Notch3 trafficking and degradation in T-cell acute lymphoblastic leukemia cells. Oncogene. 2018;37(28):3839-3851.
13. Palomero T, Sulis ML, Cortina M, et al. Mutational loss of PTEN induces resistance to NOTCH1 inhibition in T-cell leukemia. Nat Med. 2007;13(10):1203-1210.
14. Brown KK, Toker A. The phosphoinositide 3-kinase pathway and therapy resistance in cancer. F1000Prime Rep. 2015;7:13.
15. Zeng Z, Shi YX, Tsao T, et al. Targeting of mTORC1/2 by the mTOR kinase inhibitor PP242 induces apoptosis in AML cells under conditions mimicking the bone marrow microenvironment. Blood. 2012; 120(13):2679-2689.
16. Gordon WR, Roy M, Vardar-Ulu D, et al. Structure of the Notch1-negative regulatory region: implications for normal activation and pathogenic signaling in T-ALL. Blood. 2009;113(18):4381-4390.
17. Breit S, Stanulla M, Flohr T, et al. Activating NOTCH1 mutations predict favorable early treatment response and long-term outcome in childhood precursor T-cell lymphoblastic leukemia. Blood. 2006;108(4):1151-1157.
18. Pazarentzos E, Bivona TG. Adaptive stress signaling in targeted cancer therapy resistance. Oncogene. 2015;34(45):5599-5606.
19. Clappier E, Gerby B, Sigaux F, et al. Clonal selection in xenografted human T cell acute lymphoblastic leukemia recapitulates gain of malignancy at relapse. J Exp Med. 2011;208(4):653-661.
20. Poglio S, Lewandowski D, Calvo J, et al. Speed of leukemia development and genetic diversity in xenograft models of T cell acute lymphoblastic leukemia. Oncotarget. 2016;7(27):41599-41611.
21. Rysman E, Brusselmans K, Scheys K, et al. De novo lipogenesis protects cancer cells from free radicals and chemotherapeutics by promoting membrane lipid saturation. Cancer Res. 2010;70(20):8117-8126.
22. Weber U, Eroglu C, Mlodzik M. Phospholipid membrane composition affects EGF receptor and Notch signaling through effects on endocytosis during Drosophila development. Dev Cell. 2003; 5(4):559-570.
23. Fortini ME. Notch signaling: the core pathway and its posttranslational regulation. Dev Cell. 2009;16(5):633-647.
24. Yamamoto S, Charng WL, Bellen HJ. Endocytosis and intracellular trafficking of Notch and its ligands. Curr Top Dev Biol. 2010;92:165-200.
25. Fortini ME, Bilder D. Endocytic regulation of Notch signaling. Curr Opin Genet Dev. 2009;19(4):323-328.
26. Drzazga A, Sowińska A, Koziołkiewicz M. Lysophosphatidylcholine and lysophosphatidylinosiol--novel promissing signaling molecules and their possible therapeutic activity. Acta Pol Pharm. 2014;71(6):887-899.
27. Furse S, de Kroon AI. Phosphatidylcholine's functions beyond that of a membrane brick. Mol Membr Biol. 2015;32(4):117-119.
28. Ridgway ND. The role of phosphatidylcholine and choline metabolites to cell proliferation and survival. Crit Rev Biochem Mol Biol. 2013;48(1):20-38.
29. Ryland LK, Fox TE, Liu X, Loughran TP, Kester M. Dysregulation of sphingolipid metabolism in cancer. Cancer Biol Ther. 2011;11(2):138-149.
30. Herranz D, Ambesi-Impiombato A, Sudderth J, et al. Metabolic reprogramming induces resistance to anti-NOTCH1 therapies in T cell acute lymphoblastic leukemia. Nat Med. 2015;21(10):1182-1189.
31. Hori K, Sen A, Kirchhausen T, Artavanis-Tsakonas S. Regulation of ligand-independent Notch signal through intracellular trafficking. Commun Integr Biol. 2012;5(4):374-376.
32. Kanwar R, Fortini ME. Notch signaling: a different sort makes the cut. Curr Biol. 2004; 14(24):R1043-1045.
33. Hori K, Fostier M, Ito M, et al. Drosophila deltex mediates suppressor of Hairless-independent and late-endosomal activation of Notch signaling. Development. 2004; 131(22):5527-5537.
34. Hori K, Sen A, Kirchhausen T, Artavanis-Tsakonas S. Synergy between the ESCRT-III complex and Deltex defines a ligand-independent Notch signal. J Cell Biol. 2011; 195(6):1005-1015.
35. Wilkin M, Tongngok P, Gensch N, et al. Drosophila HOPS and AP-3 complex genes are required for a Deltex-regulated activation of notch in the endosomal trafficking pathway. Dev Cell. 2008;15(5):762-772.
36. Griffith M, Spies NC, Krysiak K, et al. CIViC is a community knowledgebase for expert crowdsourcing the clinical interpretation of variants in cancer. Nat Genet. 2017;49(2): 170-174.

ARTICLE

Impact of cytogenetic abnormalities on outcomes of adult Philadelphia-negative acute lymphoblastic leukemia after allogeneic hematopoietic stem cell transplantation: a study by the Acute Leukemia Working Committee of the Center for International Blood and Marrow Transplant Research

Aleksandr Lazaryan,[1] Michelle Dolan,[2] Mei-Jie Zhang,[3,4] Hai-Lin Wang,[3] Mohamed A. Kharfan-Dabaja,[5] David I. Marks,[6] Nelli Bejanyan,[7] Edward Copelan,[8] Navneet S. Majhail,[9] Edmund K. Waller,[10] Nelson Chao,[11] Tim Prestidge,[12] Taiga Nishihori,[13] Partow Kebriaei,[14] Yoshihiro Inamoto,[15] Betty Hamilton,[16] Shahrukh K. Hashmi,[17,18] Rammurti T. Kamble,[19] Ulrike Bacher,[20] Gerhard C. Hildebrandt,[21] Patrick J. Stiff,[22] Joseph McGuirk,[23] Ibrahim Aldoss,[24] Amer M. Beitinjaneh,[25] Lori Muffly,[26] Ravi Vij,[27] Richard F. Olsson[28,29], Michael Byrne,[30] Kirk R. Schultz,[31] Mahmoud Aljurf,[18] Matthew Seftel,[32] Mary Lynn Savoie,[33] Bipin N. Savani,[34] Leo F. Verdonck,[35] Mitchell S. Cairo,[36] Nasheed Hossain,[37] Vijaya Raj Bhatt,[38] Haydar A. Frangoul,[39] Hisham Abdel-Azim,[40] Monzr Al Malki,[24] Reinhold Munker,[41] David Rizzieri,[42] Nandita Khera,[43] Ryotaro Nakamura,[44] Olle Ringdén,[45] Marjolein van der Poel,[46] Hemant S. Murthy,[47] Hongtao Liu,[48] Shahram Mori,[49] Satiro De Oliveira,[50] Javier Bolaños-Meade,[51] Mahmoud Elsawy,[52] Pere Barba,[53] Sunita Nathan,[54] Biju George,[55] Attaphol Pawarode,[56] Michael Grunwald,[57] Vaibhav Agrawal,[58] Youjin Wang,[59] Amer Assal,[60] Paul Castillo Caro,[61] Yachiyo Kuwatsuka,[62] Sachiko Seo, [63]Celalettin Ustun,[64] Ioannis Politikos,[65] Hillard M. Lazarus,[66] Wael Saber,[3] Brenda M. Sandmaier,[67] Marcos De Lima,[68] Mark Litzow,[69] Veronika Bachanova[70] and Daniel Weisdorf,[71] Acute Leukemia Committee of the CIBMTR[3]

[1]H. Lee Moffitt Cancer Center and Research Institute, Tampa, FL, USA; [2]University of Minnesota Medical Center, Minneapolis, MN, USA; [3]CIBMTR (Center for International Blood and Marrow Transplant Research), Department of Medicine, Medical College of Wisconsin, Milwaukee, WI, USA; [4]Division of Biostatistics, Institute for Health and Equity, Medical College of Wisconsin, Milwaukee, WI, USA; [5]Division of Hematology-Oncology, Blood and Marrow Transplantation Program, Mayo Clinic, Jacksonville, FL, USA; [6]Adult Bone Marrow Transplant, University Hospitals Bristol NHS Trust, Bristol, UK; [7]Department of Blood and Marrow Transplant and Cellular Immunotherapy, Moffitt Cancer Center, Tampa, FL, USA; [8]Levine Cancer Institute, Atrium Health, Carolinas HealthCare System, Charlotte, NC, USA; [9]Blood & Marrow Transplant Program, Cleveland Clinic Taussig Cancer Institute, Cleveland, OH, USA; [10]Department of Hematology and Medical Oncology, Winship Cancer Institute, Emory University, Atlanta, GA, USA; [11]Division of Cell Therapy and Hematology, Department of Medicine, Duke University Medical Center, Durham, NC, USA; [12]Blood and Cancer Centre, Starship Children's Hospital, Auckland, New Zealand; [13]Department of Blood and Marrow Transplantation, H. Lee Moffitt Cancer Center and Research Institute, Tampa, FL, USA; [14]Department of Stem Cell Transplantation, Division of Cancer Medicine, The University of Texas MD Anderson Cancer Center, TX, USA; [15]Division of Hematopoietic Stem Cell Transplantation, National Cancer Center Hospital, Tokyo, Japan; [16]Blood & Marrow Transplant Program, Cleveland Clinic Taussig Cancer Institute, Cleveland, OH, USA; [17]Department of Internal Medicine, Mayo Clinic, MN, USA; [18]Oncology Center, King Faisal Specialist Hospital and Research Center, Riyadh, Saudi Arabia; [19]Division of Hematology and Oncology, Center for Cell and Gene Therapy, Baylor College of Medicine, Houston, TX, USA; [20]Department of Hematology, Inselspital, Bern University Hospital, Switzerland; [21]Markey Cancer Center, University of Kentucky, Lexington, KY, USA; [22]Loyola University Medical Center, Maywood, IL, USA; [23]University of Kansas Medical Center, Westwood, KS, USA; [24]City of Hope Comprehensive Cancer Center, Duarte, CA, USA; [25]University of Miami, Miami, FL, USA; [26]Division of Blood and Marrow Transplantation, Stanford University, Stanford, CA, USA; [27]Division of Hematology and Oncology, Washington University School of Medicine, St. Louis, MO, USA; [28]Department of Laboratory Medicine, Karolinska Institutet, Stockholm, Sweden; [29]Centre for Clinical Research Sormland, Uppsala University, Uppsala, Sweden; [30]Vanderbilt University Medical Center, Nashville, TN, USA; [31]Department of Pediatric Hematology, Oncology and Bone Marrow Transplant, British Columbia's Children's Hospital, The University of British Columbia, Vancouver, British Columbia, Canada; [32]Department of Medical Oncology and Hematology, CancerCare Manitoba, Winnipeg, Manitoba, Canada; [33]Tom Baker Cancer Centre, Calgary, Alberta, Canada; [34]Division of Hematology/Oncology, Department of Medicine, Vanderbilt University Medical Center, Nashville, TN, USA; [35]Department of

Ferrata Storti Foundation

Haematologica 2020
Volume 105(5):1329-1338

Correspondence:

ALEKSANDR LAZARYAN
aleksandr.lazaryan@moffitt.org

Received: March 12, 2019.

Accepted: September 20, 2019.

Pre-published: September 26, 2019.

doi:10.3324/haematol.2019.220756

Check the online version for the most updated information on this article, online supplements, and information on authorship & disclosures: www.haematologica.org/content/105/5/1329

Hematology/Oncology, Isala Clinic, Zwolle, the Netherlands; [36]Division of Pediatric Hematology, Oncology and Stem Cell Transplantation, Department of Pediatrics, New York Medical College, Valhalla, NY, USA; [37]Loyola University Chicago Stritch School of Medicine, Maywood, IL, USA; [38]The Fred and Pamela Buffett Cancer Center, University of Nebraska Medical Center, Omaha, NE, USA; [39]The Children's Hospital at TriStar Centennial and Sarah Cannon Research Institute, Nashville, TN, USA; [40]Division of Hematology, Oncology and Blood & Marrow Transplantation, Children's Hospital Los Angeles, University of Southern California Keck School of Medicine, Los Angeles, CA, USA; [41]Section of Hematology/Oncology, Department of Internal Medicine, Louisiana State University Health Shreveport, Shreveport, LA, USA; [42]Division of Hematologic Malignancies and Cellular Therapy, Duke University, Durham, NC, USA; [43]Department of Hematology/Oncology, Mayo Clinic, Phoenix, AZ, USA; [44]Department of Hematology & Hematopoietic Cell Transplantation, City of Hope, Duarte, CA, USA; [45]Translational Cell Therapy Group, CLINTEC (Clinical Science, Intervention and Technology), Karolinska Institutet, Stockholm Sweden; [46]Academische Ziekenhuis Maastricht, Maastricht, the Netherlands; [47]Mayo Clinic Florida, Jacksonville, FL, USA; [48]University of Chicago Medicine, Chicago, IL, USA; [49]Blood & Marrow Transplant Center, Florida Hospital Medical Group, Orlando, FL, USA; [50]UCLA Medical Center, Los Angeles, CA, USA; [51]The Sidney Kimmel Comprehensive Cancer Center at Johns Hopkins, Baltimore, MD, USA; [52]QE II Health Sciences Centre, Dalhousie University, Halifax, Nova Scotia, Canada; [53]Hospital Vall d'Hebron, Barcelona, Spain; [54]Rush University Medical Center, Chicago, IL, USA; [55]Christian Medical College, Vellore, India; [56]Blood and Marrow Transplantation Program, Division of Hematology/Oncology, Department of Internal Medicine, The University of Michigan Medical School, Ann Arbor, MI, USA; [57]Department of Hematologic Oncology and Blood Disorders, Levine Cancer Institute, Atrium Health, Charlotte, NC, USA; [58]Division of Hematology-Oncology, Indiana University School of Medicine, Indianapolis, IN, USA; [59]National Cancer Institute (NCI), Rockville, MD, USA; [60]New York Presbyterian Hospital/Columbia University Medical Center, New York, NY, USA; [61]UF Health Shands Children's Hospital, Gainesville, FL, USA; [62]Department of Advanced Medicine, Nagoya University Hospital, Nagoya, Japan; [63]Department of Hematology and Oncology, Dokkyo Medical University, Tochigi, Japan; [64]Division of Hematology/Oncology/Cell Therapy, Rush University, Chicago, IL, USA; [65]Memorial Sloan Kettering Cancer Center, New York, NY, USA; [66]Case Western Reserve University, Cleveland, OH, USA; [67]Division of Medical Oncology, University of Washington and Clinical Research Division, Fred Hutchinson Cancer Research Center, Seattle, WA, USA; [68]Department of Medicine, Seidman Cancer Center, University Hospitals Case Medical Center, Cleveland, OH, USA; [69]Division of Hematology and Transplant Center, Mayo Clinic Rochester, Rochester, MN, USA; [70]Blood and Marrow Transplant Program, University of Minnesota Medical Center, Minneapolis, MN, USA and [71]Division of Hematology, Oncology and Transplantation, Department of Medicine, University of Minnesota Medical Center, Minneapolis, MN, USA.

ABSTRACT

Cytogenetic risk stratification at diagnosis has long been one of the most useful tools to assess prognosis in acute lymphoblastic leukemia (ALL). To examine the prognostic impact of cytogenetic abnormalities on outcomes after allogeneic hematopoietic cell transplantation, we studied 1731 adults with Philadelphia-negative ALL in complete remission who underwent myeloablative or reduced intensity/non-myeloablative conditioning transplant from unrelated or matched sibling donors reported to the Center for International Blood and Marrow Transplant Research. A total of 632 patients had abnormal conventional metaphase cytogenetics. The leukemia-free survival and overall survival rates at 5 years after transplantation in patients with abnormal cytogenetics were 40% and 42%, respectively, which were similar to those in patients with a normal karyotype. Of the previously established cytogenetic risk classifications, modified Medical Research Council-Eastern Cooperative Oncology Group score was the only independent prognosticator of leukemia-free survival (P=0.03). In the multivariable analysis, monosomy 7 predicted post-transplant relapse [hazard ratio (HR)=2.11; 95% confidence interval (95% CI): 1.04-4.27] and treatment failure (HR=1.97; 95% CI: 1.20-3.24). Complex karyotype was prognostic for relapse (HR=1.69; 95% CI: 1.06-2.69), whereas t(8;14) predicted treatment failure (HR=2.85; 95% CI: 1.35-6.02) and overall mortality (HR=3.03; 95% CI: 1.44-6.41). This large study suggested a novel transplant-specific cytogenetic scheme with adverse [monosomy 7, complex karyotype, del(7q), t(8;14), t(11;19), del(11q), tetraploidy/near triploidy], intermediate (normal karyotype and all other abnormalities), and favorable (high hyperdiploidy) risks to prognosticate leukemia-free survival (P=0.02). Although some previously established high-risk Philadelphia-negative cytogenetic abnormalities in ALL can be overcome by transplantation, monosomy 7, complex karyotype, and t(8;14) continue to pose significant risks and yield inferior outcomes.

Introduction

Allogeneic hematopoietic cell transplantation (HCT) is a potentially curative therapy for patients with acute lymphoblastic leukemia (ALL). Risk stratification of ALL varies across studies and generally includes a spectrum of demographic (e.g., age), clinical (e.g., white blood cell count, minimal residual disease, steroid sensitivity), phenotypic (B- *versus* T-cell origin), and cytogenetic characteristics. Several cytogenetic risk stratification schemes have been developed and are used as prognostic tools at diagnosis of ALL to guide treatment decisions. However, most prior studies focusing on the prognostic significance of cytogenetics in ALL were influenced by inclusion of patients with Philadelphia chromosome-positive (Ph^+) B-ALL and defined for patients who received conventional chemotherapies.

Pivotal Medical Research Council–Eastern Cooperative Oncology Group (MRC-ECOG) and Southwest Oncology Group (SWOG) clinical trials identified commonly recognized Ph-negative (Ph^-) cytogenetic risks, including *KMT2A* (*MLL*) translocations at 11q23 associated with

t(4;11)(q21;q23), complex karyotype, t(8;14)(q24;q32), low hypodiploidy, or near triploidy, among others.[1] However, only a subset of Ph⁻ patients underwent allogeneic HCT in those trials. Thus, the applicability of existing cytogenetic risk classifications for allogeneic transplant recipients with ALL remains uncertain due to the relatively low frequency of specific Ph⁻ cytogenetic abnormalities and the modest size of prior studies. In a single-center retrospective cohort study of 333 allograft recipients with ALL, cytogenetic risk did not predict survival after allogeneic HCT.[2] Notably, in that study Ph⁺ patients accounted for the majority of patients in the poor-risk cytogenetic group, and the cytogenetic risk scheme used was chosen arbitrarily. Another study on allogeneic HCT in Ph⁻ ALL (n=373), conducted in Japan, found no difference in overall survival between patients with high-risk [t(4;11), t(8;14), low hypodiploidy, and complex karyotype] and standard-risk cytogenetics.[3] A more recent analysis of Ph⁻ B-ALL patients from GRAALL clinical trials identified t(4;11)/*KMT2A-AFF1* and t(v;14q32)/*IGH* as markers of poor clinical outcome; however, only a third of the trial patients underwent allogeneic HCT in first complete remission.[4]

In view of the conflicting prior data, we analyzed Center for International Blood and Marrow Transplant Research (CIBMTR) registry data to determine the prognostic impact of individual conventional (G-banding) cytogenetic abnormalities and major previously established Ph⁻ cytogenetic risk classifications (Table 1) on outcomes of allogeneic HCT. We also developed an allogeneic HCT–specific cytogenetic classification of Ph⁻ ALL for prediction of post-transplant relapse and survival.

Methods

Data source

Study data were obtained from the CIBMTR registry which is a voluntary network of over 450 blood and marrow transplant centers in the USA and around the world. Participating centers contributed detailed transplant-related information longitudinally to the centralized data management and statistical centers at the Medical College of Wisconsin (Milwaukee, WI, USA) and the National Marrow Donor Program (NMDP) (Minneapolis, MN, USA). Like all observational research conducted by the CIBMTR, this study adhered to strict federal regulations for the protection of human research subjects. Protected health information used in this study was collected and maintained in CIBMTR's capacity as a Public Health Authority under the Health Insurance Portability Accountability (HIPAA) Privacy Rule.

Table 1. Major established cytogenetic risk classifications of Philadelphia chromosome-negative acute lymphoblastic leukemia.

Study	Design highlights	Risk group	Cytogenetic abnormalities
MRC-ECOG (Moorman *et al.* Blood 2007)	• Randomized phase III • 796 pts with abnormal cytogenetics • 310 alloHCT	Poor	t(4;11), t(8;14)*, complex* (≥5 abnormalities without translocations), low hypodiploidy (30-39 chr)/near triploidy (60-78 chr)*
		Other	All other karyotypes
		Good	High hyperdiploidy (>50), del(9p)
Modified MRC-ECOG (Pullarkat *et al.* Blood 2008)	• Randomized phase III • 140 pts with evaluable cytogenetics • Re-classified by MRC-ECOG • 19 alloHCT	Very high	t(4;11), t(8;14), complex (≥5 abnormalities without translocations), low hypodiploidy (30-39 chr)/near triploidy (60-78 chr)
		High	Other 11q23/*MLL*, monosomy 7[§], del(7p), +8[§], t(1;19) or t(17;19), t(5;14)
		Intermediate	Normal diploid, low hyperdiploidy (47-50 chr), abnormal 11q (not *MLL*), del(6q), del(17p), del(9p), del(12p), del(13q), t14q32, t(10;14), tetraploidy (>80 chr), or any karyotype abnormalities not identified with a different risk group
		Standard	High hyperdiploidy (>50 chr)
SWOG (Pullarkat *et al.* Blood 2008)	• Randomized phase III trial • 140 pts with evaluable cytogenetics • 19 alloHCT	Unfavorable	Monosomy 7, +8, and 11q23/*MLL* gene rearrangements
		Miscellaneous	Any other abnormal karyotype
		Normal	Normal karyotype
NILG-ALL (Bassan *et al.* Blood 2009)	• Phase II • 276 with evaluable cytogenetics	Adverse	t(4;11) and/or MLL-AF4, +8, near triploidy, low hypodiploidy, complex (≥3 abnormalities), del(6q), t(8;14)
		Non-adverse	t(1;19) and/or *E2A-PBX1*, hyperdiploid, other karyotype abnormalities not identified with a different risk group
		Normal	Normal karyotype
North UK (Moorman *et al.* Blood 2010)	• Observational • 292 pts with evaluable cytogenetics	Poor	t(4;11), t(8;14), t(14;18), complex (≥5 abnormalities without translocations), low hypodiploidy (30-39 chr)/near triploidy (60-78 chr)
		Standard	All other karyotypes
GIMEMA 0496 (Mancini *et al.* Blood 2005)	• Phase II • 282 pts with evaluable cytogenetics	High	t(4;11), t(1;19)
		Intermediate	del(6q) and other karyotypes
		Standard	normal karyotype, del(9p)

MRC-ECOG: Medical Research Council-Eastern Cooperative Oncology Group; SWOG: Southwest Oncology Group; NILG: Northern Italy Leukemia Group; GIMEMA: Gruppo Italiano Malattie EMatologiche dell'Adulto; alloHCT: allogeneic hematopoietic cell transplantation; pts: patients; chr: chromosomes; *MLL*: mixed lineage leukemia *Independent predictors. [§]Unfavorable by Cancer and Leukemia Group B classification.

Selection of patients

The initial study population included 3,275 adults (age ≥16 years) with Ph⁻ ALL in first or second complete remission (CR1 or CR2, corresponding to morphological remission with <5% bone marrow blasts) who underwent allogeneic HCT between 1995-2011 and whose data were reported to the CIBMTR. Further restriction of the study population to the recipients of HLA-matched sibling and unrelated donor peripheral blood or bone marrow allografts (with consent to submit at least 100 days of post-transplant research reports) resulted in 2,903 eligible study participants. The CIBMTR data center requested original cytogenetic reports for cases with reportedly abnormal or unknown cytogenetics at either the time of diagnosis or prior to allogeneic HCT. Cytogenetic reports were received from participating centers for 1,013 cases, all of which were reviewed and validated by the study's principal investigators (AL, MD). Data on cytogenetics from the existing CIBMTR records were used for 743 cases for which no original cytogenetic reports were received from the queried centers. For 342 cases (12%) with prior CIBMTR cytogenetics status reported as "unknown" or "not tested" the original cytogenetic reports were requested, but not received from the transplant centers. Normal conventional cytogenetic results were confirmed with over 95% accuracy upon review of all original reports received and the remaining 805 cases with normal cytogenetics were included in the final study sample of 1,099 patients with normal cytogenetics reported. Patients with abnormal conventional cytogenetics (n=632) were included in the study population after review of all available original cytogenetic reports. Thus, a total study population of 1,731 patients from 256 reporting centers and 38 countries was analyzed.

Cytogenetics

Blood and marrow samples at the time of ALL diagnosis and prior to transplantation were cultured and evaluated for cytogenetic abnormalities by G-banding according to the standard practices of the participating centers. Original cytogenetic data reported to the CIBMTR conformed to the International System of Cytogenetic Nomenclature (ISCN).[5] According to the ISCN, a clonal abnormality was defined as the presence of a gain of the same chromosome or the presence of the same structural abnormality in ≥2 cells or the loss of the same chromosome in ≥3 cells. A normal conventional cytogenetic result was defined as the absence of clonal abnormalities in at least 20 metaphase cells. Abnormal cytogenetics were classified according to previously established cytogenetic risk classifications for Ph⁻ ALL (Table 1). Standard definitions for hypodiploid, hyperdiploid, complex, and monosomal karyotypes were based on the following modal chromosome numbers: (i) low hypodiploidy (30-39 chromosomes), (ii) high hypodiploidy (40-43), (iii) low hyperdiploidy (47-50), (iv) high hyperdiploidy (>50), (v) near triploidy (60-78), (vi) tetraploidy (>80), (vii) complex with ≥5 abnormalities[6-8] (adopted here) in the absence of established translocations or ploidy abnormalities; or ≥3 abnormalities used exclusively by the Northern Italy Leukemia Group (NILG)[9] (Table 1), and (viii) monosomal (≥2 autosomal monosomies or a single autosomal monosomy combined with a single structural abnormality). Fluorescence *in situ* hybridization (FISH) findings and/or other molecular data were available for the minority of patients and were, therefore, only used to validate cytogenetic reports when available.

Statistical analysis

Individual Ph⁻ cytogenetic abnormalities were included in the analysis if they were detected in ≥20 patients or in <20 patients but with previously established prognostic significance in ALL. Cytogenetic abnormalities included high hyperdiploidy (n=29), tetraploidy (n=9), near triploidy (n=6), low hypodiploidy (n=11), complex karyotype (n=51), monosomal karyotype (n=84), monosomy 17 (n=21), i(17q) (n=5), del(17p) (n=6), t(1;19) (n=33), t(4;11) (n=95), t(8;14) (n=10), t(10;11) (n=8), t(11;19) (n=10), add(5q) (n=7), del(5q) (n=20), add(7p) (n=8), i(7q) (n=10), add(12p) (n=10), del(12p) (n=18), t(14;18) (n=6), del(6q) (n=48), del(7q) (n=7), monosomy 7 (n=33), add(9p) (n=11), del(9p) (n=52), i(9q) (n=17), add(12p) (n=10), del(12p) (n=18), del(11q) (n=18), del(13q) (n=12), and trisomy 8 (n=35). Each cytogenetic abnormality was tested individually for its association with post-HCT relapse while adjusted for potential confounders. Statistically significant (P<0.05) clinical factors other than cytogenetics [conditioning regimen, remission status, donor type, and graft-*versus*-host disease (GvHD) prophylaxis among other potential confounders] were retained in the multivariable Cox proportional hazards model. Abnormalities with a hazard ratio (HR) ≥1.4 for relapse were subsequently grouped as adverse risk; abnormalities with a HR ≤0.6 for relapse were grouped as favorable, whereas all other abnormalities, and normal cytogenetics, were grouped as intermediate risk. Relapse was used as the primary endpoint for evaluation of individual cytogenetic abnormalities and it was calculated as the cumulative incidence of ALL recurrence with treatment-related mortality as the competing risk. Leukemia-free survival was used as the primary endpoint for evaluation of previously established and study-derived cytogenetic risk classifications and was defined as the time to death or relapse with survivors in continuing complete remission censored at last follow-up. Adjusted probabilities of leukemia-free survival and relapse were calculated using multivariable models, stratified by cytogenetic risk scheme and weighted by the pooled sample proportion value for each prognostic factor.[10,11] Overall survival was a secondary study endpoint and was defined as the time to death from any cause with surviving patients censored at last follow-up. Treatment failure (1 – leukemia-free survival) and overall mortality (1 – overall survival) were used to model all Cox regression HR estimates. SAS version 9.4 (SAS Institute, Cary, NC, USA) and GraphPad Prism version 7.04 were used for all data analysis and graphics.

Results

Study population and transplant characteristics

A description of the entire study population and the distribution of the main study variables among patients with abnormal and normal cytogenetics are summarized in Table 2. The study cohort consisted predominantly of young (82% <45 years) male (63%) patients with B-precursor ALL (69%). Patients with hyperleukocytosis (white blood cell count >30×10⁹/L for B-ALL and >100×10⁹/L for T-ALL) at the time of initial diagnosis accounted for 22% of the entire cohort and 57% of patients underwent allogeneic HCT in CR1 with a median time to achieve CR1 of 6 weeks (range, 1-123).

Post-transplant outcomes classified by established cytogenetic schemes

Patients with abnormal cytogenetics had 5-year leukemia-free and overall survival rates of 40% and 42%, respectively, which were similar to those of patients with a normal karyotype (both P>0.6). The cytogenetic risk categories defined by the MRC-ECOG, SWOG, NILG-ALL, North UK, and GIMEMA 0496 (Table 1) had no prognostic significance for leukemia-free survival, relapse, or overall survival (all P-values >0.15). However, the cytogenetic risk

Table 2. Patient and transplant characteristics.

Variables	All	Cytogenetics Abnormal	Cytogenetics Normal
Number of patients	1731	632 (36.5)	1099 (63.5)
Number of centers	256	178	226
Recipient age, median (range), years	29 (16-68)	28 (16-65)	29 (16-68)
Gender, female, n (%)	636 (37)	234 (37)	402 (37)
Recipient race, n (%)			
Caucasian	1429 (83)	534 (84)	895 (81)
African-American	42 (2)	12 (2)	30 (3)
Asian	154 (9)	49 (8)	105 (10)
Other	106 (7)	37 (6)	69 (6)
Karnofsky score ≥ 90%, n (%)	1245 (72)	459 (73)	786 (72)
Disease status prior to alloHCT, n (%)			
CR1	990 (57)	395 (62.5)	595 (54)
CR2	741 (43)	237 (37.5)	504 (46)
Time to CR1, median (range), weeks	6 (1-123)	5 (2-123)	6 (1-113)
Time from CR1 to alloHCT[1], median (range), months	3 (<1-16)	3 (<1-13)	4 (<1-16)
Time from CR1 to relapse[2], median (range), months	20 (<1-111)	18 (<1-103)	21 (1-111)
ALL lineage, n (%)			
B-ALL	1197 (69)	474 (75)	723 (66)
T-ALL	393 (23)	121 (19)	272 (25)
Unknown	141 (8)	37 (6)	104 (9)
Hyperleukocytosis at diagnosis, n (%)			
B-ALL (>30x10^9 WBC/L)	299 (17)	150 (24)	149 (14)
T-ALL (>100x10^9 WBC/L)	81 (5)	31 (5)	50 (4)
Extramedullary ALL at diagnosis, n (%)			
CNS	105 (6)	35 (6)	70 (6)
Non-CNS	202 (12)	70 (11)	132 (12)
Conditioning intensity, n (%)			
MAC (+TBI)	1343 (78)	522 (83)	821 (75)
MAC (-TBI)	254 (15)	72 (11)	182 (17)
NMA/RIC	98 (6)	28 (5)	70 (7)
Unknown	36 (2)	10 (2)	26 (2)
GvHD prophylaxis, n (%)			
Tacrolimus-based	576 (33)	217 (34)	359 (33)
Cyclosporine A-based	1000 (58)	350 (55)	650 (59)
T-cell depletion (*ex-vivo*)	123 (7)	55 (9)	68 (6)
In-vivo T-cell depletion, n (%)			
Alemtuzumab	46 (3)	19 (3)	27 (2)
ATG	286 (17)	99 (16)	187 (17)
Graft source, n (%)			
Bone marrow	790 (46)	281 (44)	509 (46)
Peripheral blood	941 (54)	352 (46)	590 (54)
Donor type, n (%)			
HLA-identical sibling	819 (47)	270 (43)	549 (50)
Well-matched unrelated donor	469 (27)	188 (30)	281 (26)
Partially-matched/mismatched unrelated donor	357 (21)	141 (22)	216 (20)
Other related/unrelated donor	172 (10)	70 (11)	102 (9)
Donor/recipient CMV serostatus, n (%)			
Donor+/recipient+	574 (33)	170 (27)	404 (37)
Donor+/recipient-	193 (11)	78 (12)	115 (10)
Donor-/recipient+	385 (22)	143 (23)	242 (22)
Donor-/recipient-	494 (29)	210 (33)	284 (26)
Unknown	85 (5)	31 (5)	54 (5)
Donor/recipient gender match, n (%)			
Male-male	691 (40)	256 (41)	435 (40)
Male-female	340 (20)	127 (20)	213 (19)
Female-male	401 (23)	142 (22)	259 (24)
Female-female	295 (17)	107 (17)	188 (17)
Unknown	4 (<1)	0	4 (<1)
Year of alloHCT, n (%)			
1995-2000	557 (32)	194 (31)	363 (33)
2001-2005	604 (35)	217 (34)	387 (35)
2006-2011	570 (33)	221 (35)	349 (32)
Median follow up of survivors (range), months	75 (2-224)	87 (3-224)	73 (2-218)

continued in next column

continued from previous column

alloHCT: allogeneic hematopoietic cell transplantation; CR1: first complete remission; CR2: second complete remission; ALL: acute lymphoblastic leukemia; WBC: white blood cell; CNS: central nervous system; MAC: myeloablative conditioning; TBI: total body irradiation; NMA: non-myeloablative; RIC: reduced-intensity conditioning; HLA: human leukocyte antigen; GvHD: graft-*versus*-host disease; ATG: antithymocyte globulin; CMV: cytomegalovirus. [1]Referred to patients in CR1. [2]Referred to patients in CR2.

classification defined by the modified MRC-ECOG was significantly associated with both treatment failure (overall P=0.02) and overall survival (overall P=0.03) in multivariable analyses adjusted for recipient age, disease status, conditioning intensity, Karnofsky Performance Status, donor type, and GvHD prophylaxis (Figures 1A and 2). Significant associations between the modified MRC-ECOG classification and major clinical outcomes appeared to be largely driven by the favorable outcomes of patients with standard-risk cytogenetics (n=24), all with a high hyperdiploid karyotype. There was no difference between high or very high modified MRC-ECOG cytogenetic risk groups compared to the intermediate group. In contrast, good-risk cytogenetics according to the MRC-ECOG classification included del(9p), in addition to high hyperdiploidy, and was not significantly associated with any of the clinical outcomes of interest.

Individual cytogenetic abnormalities: relapse

Monosomy 7 [HR=2.11; 95% confidence interval (CI): 1.04-4.27, P=0.04] and complex karyotype (HR=1.69; 95% CI: 1.06-2.69, P=0.03) were both associated with increased risk of relapse in multivariable analysis adjusted for conditioning intensity, ALL remission status prior to transplantation, and monosomal karyotype (Figure 3, Table 3). Patients with high hyperdiploidy had an estimated 54% lower risk of relapse, whereas those with del(7q), t(8;14), t(11;19), del(11q), or a tetraploid/near triploid karyotype had a HR of at least 40% higher for relapse, which did not reach statistical significance (Figure 3). The magnitude and strength of associations with relapse for the remaining individual cytogenetic categories, such as trisomy 8, monosomal karyotype, monosomy 17, del(17p)/i(17p), low hypodiploidy, del(6q), t(1;19), t(4;11), and normal karyotype, did not demonstrate any meaningful clinical associations (all HR between 0.6 and 1.4), and none was statistically significant (all P-values >0.1).

A significant interaction was detected between t(4;11) and pre-transplant remission status (P<0.001) with the adverse impact of t(4;11) on relapse observed only in patients undergoing allogeneic HCT in CR2 (HR=2.82; 95% CI: 1.25-6.36, P=0.01), but not in CR1 (HR=0.86,95% CI: 0.53-1.41, P=0.55).

Individual cytogenetic abnormalities: treatment failure

Monosomy 7 (HR=1.97; 95% CI: 1.20-3.24, P=0.007) and t(8;14) (HR=2.85; 95% CI: 1.35-6.02, P=0.006) were

prognostic for treatment failure after adjustments for recipient age, pre-transplant remission status, conditioning intensity, donor type, and GvHD prophylaxis in multivariable analyses (Table 4). Trends toward increased risk of treatment failure were observed for patients with del(7q) (HR=2.16; 95% CI: 0.95-4.90, *P*=0.06) and del(17p)/i(17q) (HR=1.95; 95% CI: 0.80-4.75, *P*=0.1). In contrast, patients with high hyperdiploidy (HR=0.62; 95% CI: 0.37-1.04, *P*=0.07) and monosomal karyotype (HR=0.73; 95% CI: 0.54-1.01, *P*=0.05) trended toward less risk of treatment failure. Although t(4;11) was not associated with treatment failure (HR=1.12; 95% CI: 0.85-1.48, *P*=0.41) within the entire cohort or in CR1 patients (n=83) (HR=0.98; 95% CI: 0.72-1.33, *P*=0.89), it was associated with a significantly higher risk of treatment failure in CR2 patients (n=11) (HR=2.35; 95% CI: 1.25-4.43, *P*=0.008).

Individual cytogenetic abnormalities: overall mortality

After adjustment for recipient age (HR=1.55; 95% CI: 1.17-2.06, *P*<0.01 for age >55 years *versus* <40 years), Karnofsky Performance Status <90 (HR=1.29; 95% CI: 1.12-1.48, *P*<0.001), ALL in CR2 (HR=1.56; 95% CI: 1.36-1.77, *P*<0.001), myeloablative conditioning without total body irradiation (HR=1.35; 95% CI: 1.13-1.62, *P*<0.001), mismatched unrelated donor (HR=1.49; 95% CI: 1.27-1.76, *P*<0.001), and GvHD prophylaxis (HR=1.41; 95% CI: 1.11-1.79, *P*=0.005 for non-calcineurin inhibitor- *versus* tacrolimus-based) in multivariable analysis, only t(8;14) was associated with higher mortality after allogeneic HCT (HR=3.03; 95% CI: 1.44-6.41, *P*=0.004).

Novel allogeneic hematopoietic cell transplantation-specific cytogenetic classification

Based on the relapse model adjusted for significant clinical factors and individual cytogenetic abnormalities (Figure 3), the following cytogenetic markers with HR≥1.4 were categorized as adverse risk (n=125): monosomy 7, complex karyotype, del(7q), t(8;14), t(11;19), del(11q), and tetraploid/near triploid karyotype. Conversely, high hyperdiploidy (n=29) was identified as

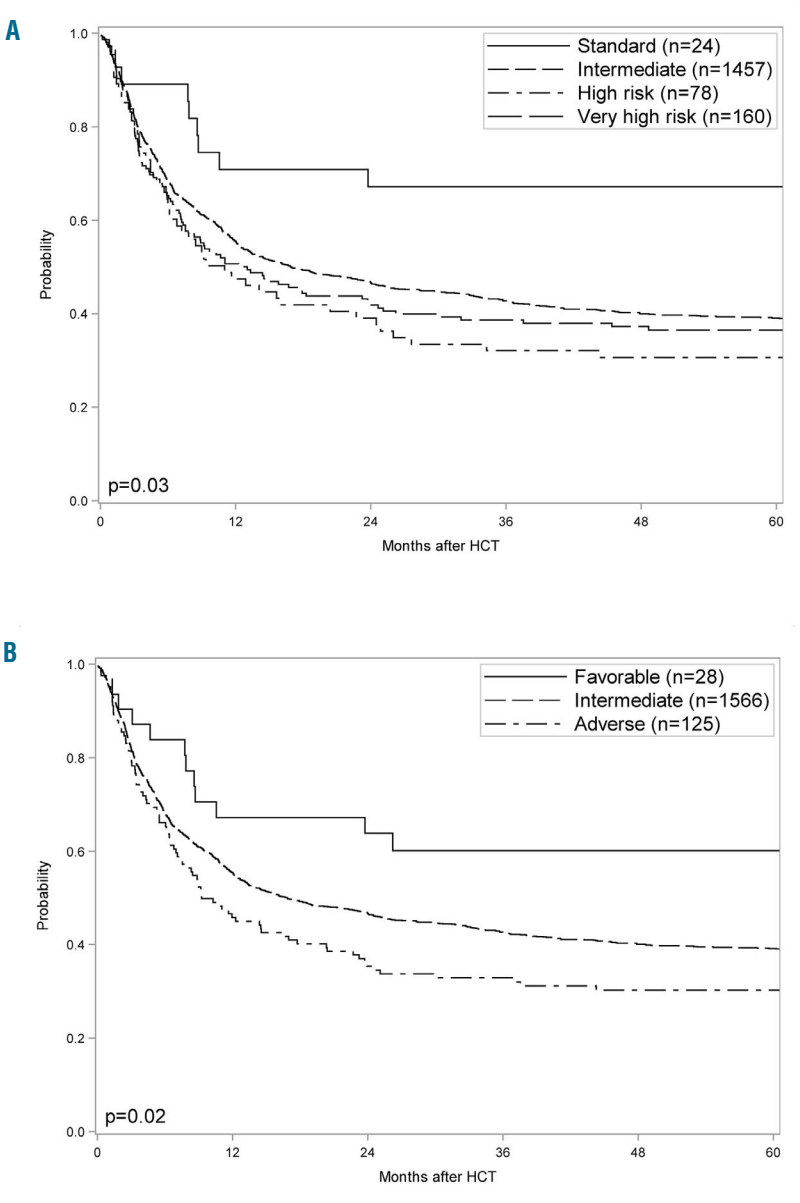

Figure 1. Adjusted leukemia-free survival by cytogenetic risk classifications. (A) Adjusted leukemia-free survival by modified Medical Research Council – Eastern Cooperative Oncology Group cytogenetic risk classification. (B) Adjusted leukemia-free survival by Center for International Blood and Marrow Transplant Research acute lymphoblastic leukemia risk classification. HCT: hematopoietic cell transplantation.

the sole cytogenetic abnormality with a HR≤0.6 for relapse, and was categorized as favorable risk. The remaining cytogenetic markers, including normal cytogenetics, were categorized as intermediate risk (n=1566). This novel allogeneic HCT-specific cytogenetic risk classification (hereafter called CIBMTR ALL risk) was found to be prognostic for both post-transplant relapse (*Online Supplementary Figure S1*) and leukemia-free survival (log-rank *P*=0.04) (Figure 1B). Furthermore, in the multivariable Cox proportional hazards model adjusted for recipient age, pre-transplant remission status, conditioning intensity, Karnofsky Performance Status, donor type, and GvHD prophylaxis, patients with CIBMTR adverse-risk cytogenetics had a higher risk of treatment failure (HR=1.26; 95% CI: 1.01-1.57, *P*=0.04), and those with favorable risk had a lower risk (HR=0.6; 95% CI: 0.35-1.02, *P*=0.06) compared to those with intermediate-risk cytogenetics (Table 5). There was a significantly greater risk of treatment failure in those with adverse *versus* favorable risk cytogenetic abnormalities (HR=2.10; 95% CI: 1.19-3.70, *P*=0.01). Similarly, there was a significantly greater risk of overall mortality in patients with adverse *versus* favorable risk cytogenetic abnormalities (HR=1.91; 95% CI: 1.08-3.38, *P*=0.03).

Discussion

This large CIBMTR analysis of allogeneic HCT recipients with Ph- ALL defined a cytogenetic classification specific to allogeneic transplantation. Of the established

Table 3. Multivariable model of prognostic factors for post-transplant relapse.

Factors	N	HR (95% CI)	*P*-value
Conditioning regimens			
MAC (+TBI)	1334	1.0	
MAC (-TBI)	253	1.54 (1.22-1.96)	<0.001
RIC/NMA	96	1.9 (1.38-2.61)	<0.001
Remission status pre-alloHCT			
CR1	986	1.0	
CR2	733	1.71 (1.44-2.04)	<0.001
Cytogenetics			
Complex karyotype*	51	1.69 (1.06-2.69)	0.03
Monosomy 7*	33	2.11 (1.04-4.27)	0.04

N: number; HR: hazard ratio; 95% CI: 95% confidence interval; MAC: myeloablative conditioning; TBI: total body irradiation; RIC: reduced-intensity conditioning; NMA: non-myeloablative; alloHCT: allogeneic hematopoietic cell transplantation; CR1: first complete remission; CR2: second complete remission. *Adjusted for monosomal karyotype.

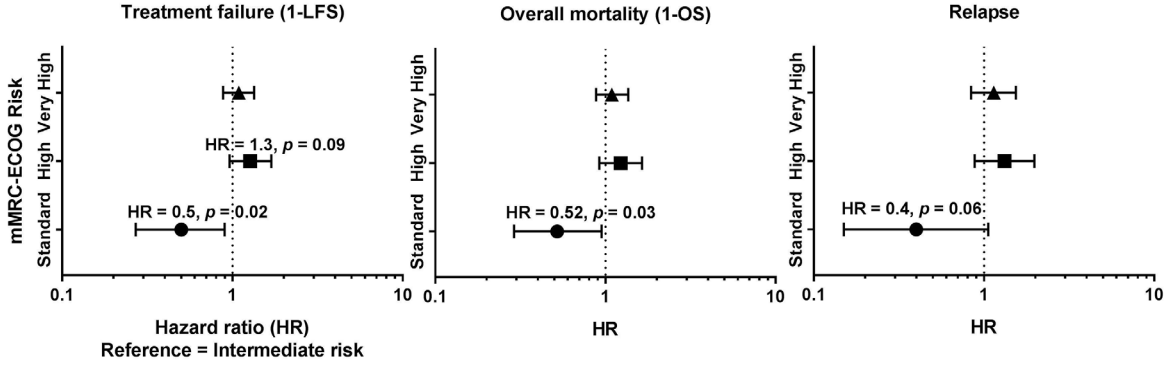

Figure 2. Cytogenetic risks by modified Medical Research Council – Eastern Cooperative Oncology Group cytogenetic risk classification and post-transplant outcomes. All multivariable models were adjusted for recipient age, disease status, conditioning intensy, Karnofsky Performance Status, donor type and graft-*versus*-host disease prophylaxis. mMRC-ECOG: modified Medical Research Council-Eastern Cooperative Oncology Group classification with its three cytogenetic risk groups on Y-axis, relative to the Intermediate risk (reference with HR=1) on X-axis; LFS: leukemia-free survival; OS: overall survival.

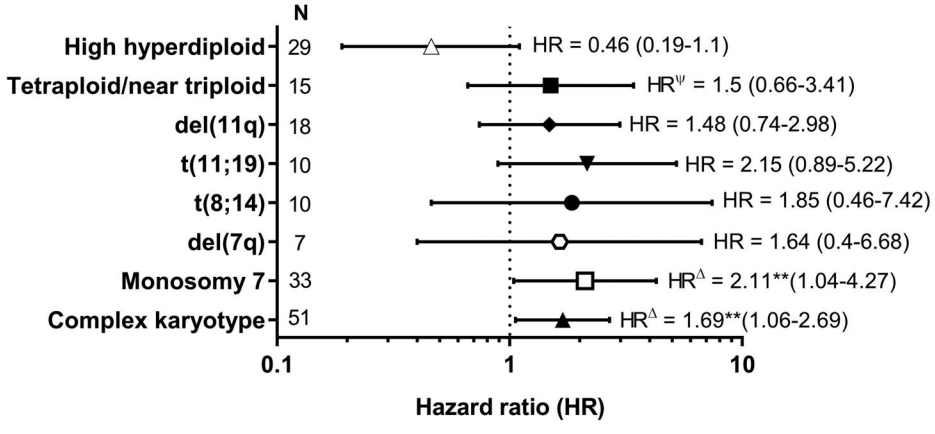

Figure 3. Forest plots of cytogenetic markers associated with post-transplant relapse. All hazard ratios (HR) and corresponding 95% confidence intervals (CI) are adjusted for conditiong intensity and remisssion status; CK: complex karyotype; N: sample size of carriers of each cytogenetic marker. * Defined as 40% risk increase or decrement; **Markers with *P*<0.05; ΨAdjusted also for complex karyotype. ΔAdjusted also for monosomal karyotype.

major ALL cytogenetic risk schemes, only the modified MRC-ECOG classification could be validated in our dataset for its association with post-transplant outcomes. The association of the modified MRC-ECOG classification was largely explained by favorable outcomes for patients with high hyperdiploidy, a factor known to be associated with better outcomes.[12,13] While a few individual high-risk cytogenetic abnormalities maintained their prognostic relevance for recipients of allogeneic HCT, many others had no significant prognostic influence on the transplant outcomes. Thus, the aggregate effects of previously established high or very high risk cytogenetic groups defined by MRC-ECOG, SWOG, NILG-ALL, North UK, and GIMEMA 0496 were overcome by allogeneic HCT and did not predict the outcomes of the transplant recipients. High-risk cytogenetic abnormalities including trisomy 8, low hypodiploidy, t(1;19), del(6q) could be overcome, in part, by the graft-*versus*-leukemia effect of allogeneic HCT, and thus, were not unfavorable in this analysis. In contrast to findings in acute myeloid leukemia[14,15] and recently reported cases of ALL,[4,16] in our dataset and elsewhere,[17] monosomal karyotype did not predict poor post-transplant outcomes for Ph$^-$ ALL. Similarly, our analysis did not confirm the adverse effect of t(4;11) on relapse or leukemia-free survival among all carriers of this well-known cytogenetic risk, but uncovered a differential effect of t(4;11) on transplant outcomes which was modified by pre-transplant disease status. Nevertheless, given the relatively small subset of patients with t(4;11) in CR2, the results of our post-hoc analysis should be interpreted with caution. Moreover, the infrequency of CR2 allografts in patients with t(4;11) may reflect intrinsic difficulty for those patients to effectively maintain maintain subsequent remissions. A recent comparison of allograft recipients with t(4;11) and normal karyotype in CR1 demonstrated relatively favorable survival of patients with t(4;11) and especially those with undetectable pretransplant minimal residual disease.[18] Allogeneic HCT in CR1 for adult ALL patients with t(4;11) remains valuable.[19]

High-risk cytogenetic abnormalities found in this study included t(8;14), complex karyotype, and monosomy 7, previously known poor-risk categories in major classification schemes, excluding GIMEMA 0496 (Table 1). Patients with these high-risk cytogenetic abnormalities were predominantly young adults, most of whom received myeloablative conditioning and still had poor outcomes, thus confirming the high-risk nature of cytogenetic abnormalities.

The t(8;14) is a rare recurrent abnormality among patients with ALL[20-23] and has been associated with a poor outcome.[7] It was observed in ten allogeneic HCT recipients (median age, 21) who had a nearly 3-fold significantly lower leukemia-free survival in our cohort. In addition to the *IGH-MYC* fusion resulting from the t(8;14), other *IGH* translocations involving *BCL2* (when present together

Table 4. Multivariable model of prognostic factors for post-transplant treatment failure.

Factors	N	HR (95% CI)	*P*-value
Age, years			
16-39	1270	1.0	
40-55	363	1.21 (1.04-1.41)	0.02
55+	86	1.42 (1.07-1.88)	0.01
Remission status pre-alloHCT			
CR1	986	1.0	
CR2	733	1.53 (1.34-1.74)	<0.001
Conditioning regimens			
MAC (+TBI)	1334	1.0	
MAC (-TBI)	253	1.4 (1.18-1.66)	<0.001
MAC (+TBI)	1334	1.0	
RIC/NMA	96	1.26 (0.97-1.64)	0.09
Performance status			
KPS≥90	1234	1.0	
KPS<90	423	1.32 (1.15-1.52)	<0.001
Donor type			
MSD	818	1.0	
Matched URD	464	1.06 (0.9-1.24)	0.49
Mismatched URD	351	1.43 (1.21-1.68)	<0.001
Other RD/URD	86	1.36 (1.02-1.81)	0.03
GvHD prophylaxis			
Tac-based	569	1.0	
CsA-based	996	1.11 (0.96-1.28)	0.15
Other	134	1.39 (1.1-1.75)	0.006
Cytogenetics			
t(8;14)	10	2.85 (1.35-6.02)	0.006
Monosomy 7*	33	1.97 (1.2-3.24)	0.007

N: number; HR: hazard ratio; 95% CI: 95% confidence interval; alloHCT: allogeneic hematopoietic cell transplantation; CR1: first complete remission; CR2: second complete remission; MAC: myeloablative conditioning; TBI: total body irradiation; RIC: reduced-intensity conditioning; NMA: non-myeloablative; KPS: Karnofsky Performance Status; MSD: matched sibling donor; RD: related donor; URD: unrelated donor; GvHD: graft-*versus*-host disease; CSA: cyclosporine. *Adjusted for monosomal karyotype.

Table 5. Novel Center for International Blood and Marrow Transplant Research risk scheme for post-transplant Philadelphia-negative acute lymphoblastic leukemia outcomes

Cytogenetic risk groups	N	HR (95% CI)*		
		Treatment failure(1-LFS)	Relapse	Overall mortality (1-OS)
Favorable (high hyperdiploidy)	28	0.6 (0.35-1.02)	0.39 (0.15-1.05)	0.64 (0.37-1.08)
Intermediate (normal karyotype and all other abnormalities[§])	1578	1.0 (Reference)	1.0 (Reference)	1.0 (Reference)
Adverse (monosomy 7, complex karyotype, del(7q), t(8;14), t(11;19), del(11q), tetraploidy/near triploidy)	125	1.26 (1.01-1.57)	1.48 (1.09-2.0)	1.22 (0.97-1.53)
Adverse vs. favorable	-	2.1 (1.19-3.7)	3.78 (1.36-1.76)	1.91 (1.08-3.38)

HR: hazard ratio; 95% CI: 95% confidence interval; LFS: leukemia-free survival; OS: overall survival. *Adjusted for conditioning intensity, disease status prior to transplantation, recipient age, Karnofsky Performance Status, donor type, graft-versus-host disease prophylaxis, as applicable based on the individual models. §Except for those included in the adverse and favorable groups

with *IGH-MYC*) and *CRLF2* have also been reported to yield poor outcomes.[24-26]

Our study confirmed the previously established unfavorable risk associated with a complex karyotype[6,27] after allogeneic HCT. Notably, we observed substantial overlap between complex karyotype, monosomal karyotype, and other common abnormalities, mandating careful data analysis and interpretation of complex cytogenetics in future studies.

Monosomy 7 was consistently associated with worse post-transplant outcomes in this and prior studies.[8] Multiple mechanisms have been proposed to explain the effects of monosomy 7 on leukemogenesis including, but not limited to, loss of tumor suppressor genes, haploinsufficiency, or monoallelic loss of *IKZF1*, an important adverse prognostic marker in B-cell ALL which is localized to chromosome 7p.[28,29] Haploinsufficient deletions of *IKZF1* are enriched among Ph- ALL cases and associated with inferior survival.[30]

Our observed higher risk of relapse among allogeneic HCT recipients with t(11;19) was also consistent with the previously reported poor survival of ALL patients with t(11;19)(q23;p13.3).[31]

We propose an allogeneic HCT-specific cytogenetic risk classification for Ph- ALL separating patients into three prognostic risk categories based on the presence of monosomy 7, del(7q), t(8;14), t(11;19), del(11q), complex, tetraploid/near triploid, and high hyperdiploid karyotypes (Table 5). This novel CIBMTR ALL risk classification of Ph- patients treated with allogeneic HCT is directly relevant to pre-HCT decision-making and might help in stratifying clinical trial candidates undergoing allogeneic HCT for Ph- ALL.

Unfortunately we could not account in our analysis for pre-transplant minimal residual disease (MRD), defined by flow cytometry or FISH/molecular testing. Pre-transplant MRD has been important in predicting ALL relapse and future research should combine cytogenetic classifications with pre-transplant MRD status. Pretreatment complex karyotype and low hypodiploidy/near-triploidy portended poor survival after adjustment for MRD in a recent single-institution study.[27] Our analysis validated other established patient- and transplant-related prognostic factors and thereby confirmed the additional importance of the cytogenetic groupings. As most patients in this cohort received allografts with myeloablative conditioning, future validation of the CIBMTR ALL risk scheme among recipients treated with reduced intensity conditioning will test this prognostic tool in older and/or less fit ALL patients.

Our study focused on the transplant period preceding Food and Drug Administration approvals and broader use of liposomal vincristine, blinatumomab, inotuzumab ozogamycin, or tisagenlecleucel, and it thereby focused on a more homogeneous patient population with no differential effect on treatment outcomes found according to quinquennial transplant periods from 1995 to 2011.

While many patients with previously established high-risk Ph- cytogenetic abnormalities can benefit from allogeneic HCT, those with monosomy 7, complex karyotype, and t(8;14) remain at high risk for treatment failure after transplantation. Selective targeting of these and other clinically-defined high-risk cohorts will be necessary to improve post-transplant survival of patients with Ph- ALL.

Acknowledgments

*The CIBMTR is supported primarily by a public health service grant/cooperative agreement U24CA076518 from the National Cancer Institute (NCI), the National Heart, Lung and Blood Institute (NHLBI) and the National Institute of Allergy and Infectious Diseases (NIAID); grant/cooperative agreement U24HL138660 from the NHLBI and NCI; grant U24CA233032 from the NCI; grants OT3HL147741, R21HL140314 and U01HL128568 from the NHLBI; a contract HHSH250201700006C with Health Resources and Services Administration (HRSA/DHHS); grants N00014-18-1-2888 and N00014-17-1-2850 from the Office of Naval Research; and grants from *Actinium Pharmaceuticals, Inc.; Adaptive Biotechnologies; *Amgen, Inc.; Anonymous donation to the Medical College of Wisconsin; *Anthem, Inc.; Astellas Pharma US; Atara Biotherapeutics, Inc.; Be the Match Foundation; *bluebird bio, Inc.; Boston Children's Hospital; *Bristol Myers Squibb Co.; *Celgene Corp.; Children's Hospital of Los Angeles; *Chimerix, Inc.; *CSL Behring; *CytoSen Therapeutics, Inc.; Dana Farber Cancer Institute; *Daiichi Sankyo Co., Ltd.; Fred Hutchinson Cancer Research Center; *Gamida-Cell, Ltd.; Gilead Sciences, Inc.; *GlaxoSmithKline (GSK); HistoGenetics, Inc.; Immucor; Incyte Corporation; Janssen Biotech, Inc.; *Janssen Pharmaceuticals, Inc.; Janssen Scientific Affairs, LLC; *Jazz Pharmaceuticals, Inc.; Karius, Inc.; Karyopharm Therapeutics, Inc.; *Kite, a Gilead Company; *Magenta Therapeutics; Medac GmbH; The Medical College of Wisconsin; Mediware; Merck & Company, Inc.; *Mesoblast; MesoScale Diagnostics, Inc.; Millennium, the Takeda Oncology Co.; *Miltenyi Biotec, Inc.; Mundipharma EDO; National Marrow Donor Program; Novartis Oncology; Novartis Pharmaceuticals Corporation; *Omeros Corporation; *Oncoimmune, Inc.; PCORI; *Pfizer, Inc.; *Phamacyclics, LLC; PIRCHE AG; *Regeneron Pharmaceuticals, Inc.; REGiMMUNE Corp.; *Sanofi Genzyme; *Seattle Genetics; *Shire; Sobi, Inc.; Spectrum Pharmaceuticals, Inc.; St. Baldrick's Foundation; Swedish Orphan Biovitrum, Inc.; *Takeda Oncology; University of Minnesota; University of Pittsburgh; University of Texas-MD Anderson; University of Wisconsin – Madison and Viracor Eurofins. The views expressed in this article do not reflect the official policy or position of the National Institute of Health, the Department of the Navy, the Department of Defense, Health Resources and Services Administration (HRSA) or any other agency of the U.S. Government. *Corporate Members.*

References

1. Goldstone AH, Richards SM, Lazarus HM, et al. In adults with standard-risk acute lymphoblastic leukemia, the greatest benefit is achieved from a matched sibling allogeneic transplantation in first complete remission, and an autologous transplantation is less effective than conventional consolidation/maintenance chemotherapy in all patients: final results of the International ALL Trial (MRC UKALL XII/ECOG E2993). Blood. 2008;111(4):1827-1833.
2. Aldoss I, Tsai NC, Slovak ML, et al. Cytogenetics does not impact outcomes in adult patients with acute lymphoblastic leukemia undergoing allogeneic hematopoietic cell transplantation. Biol Blood Marrow Transplant. 2016;22(7):1212-2017.
3. Shimizu H, Saitoh Y, Okamoto S, et al.

Prognostic impact of cytogenetic abnormalities in adult patients with Philadelphia-chromosome (Ph)-negative acute lymphoblastic leukemia (ALL) who underwent allogeneic stem cell transplant (allo-SCT). Blood. 2015;126(23):2024.
4. Lafage-Pochitaloff M, Baranger L, Hunault M, et al. Impact of cytogenetic abnormalities in adults with Ph-negative B-cell precursor acute lymphoblastic leukemia. Blood. 2017;130(16):1832-1844.
5. Shaffer L, McGowan J, Schmid M. ISCN 2013: An International System for Human Cytogenetic Nomenclature. Basel. S Krager AG, 2012.
6. Moorman AV, Harrison CJ, Buck GA, et al. Karyotype is an independent prognostic factor in adult acute lymphoblastic leukemia (ALL): analysis of cytogenetic data from patients treated on the Medical Research Council (MRC) UKALLXII/Eastern Cooperative Oncology Group (ECOG) 2993 trial. Blood. 2007;109(8):3189-3197.
7. Moorman AV, Chilton L, Wilkinson J, Ensor HM, Bown N, Proctor SJ. A population-based cytogenetic study of adults with acute lymphoblastic leukemia. Blood. 2010;115(2): 206-214.
8. Pullarkat V, Slovak ML, Kopecky KJ, Forman SJ, Appelbaum FR. Impact of cytogenetics on the outcome of adult acute lymphoblastic leukemia: results of Southwest Oncology Group 9400 study. Blood. 2008;111(5):2563-2572.
9. Bassan R, Spinelli O, Oldani E, et al. Improved risk classification for risk-specific therapy based on the molecular study of minimal residual disease (MRD) in adult acute lymphoblastic leukemia (ALL). Blood. 2009;113(18):4153-4162.
10. Zhang X, Zhang MJ. SAS macros for estimation of direct adjusted cumulative incidence curves under proportional subdistribution hazards models. Comput Methods Programs Biomed. 2011;101(1):87-93.
11. Zhang X, Loberiza FR, Klein JP, Zhang MJ. A SAS macro for estimation of direct adjusted survival curves based on a stratified Cox regression model. Comput Methods Programs Biomed. 2007;88(2):95-101.
12. Paulsson K, Johansson B. High hyperdiploid childhood acute lymphoblastic leukemia. Genes Chromosomes Cancer. 2009;48(8): 637-660.
13. Hakeem A, Shiekh AA, Bhat GM, Lone AR. Prognostification of ALL by cytogenetics. Indian J Hematol Blood Transfus. 2015;31 (3):322-331.
14. Breems DA, Lowenberg B. Acute myeloid leukemia with monosomal karyotype at the far end of the unfavorable prognostic spectrum. Haematologica. 2011;96(4):491-493.
15. Breems DA, Van Putten WL, De Greef GE, et al. Monosomal karyotype in acute myeloid leukemia: a better indicator of poor prognosis than a complex karyotype. J Clin Oncol. 2008;26(29):4791-4797.
16. Motllo C, Ribera JM, Morgades M, et al. Prognostic significance of complex karyotype and monosomal karyotype in adult patients with acute lymphoblastic leukemia treated with risk-adapted protocols. Cancer. 2014;120(24):3958-3964.
17. Kenderian SS, Al-Kali A, Gangat N, et al. Monosomal karyotype in Philadelphia chromosome-negative acute lymphoblastic leukemia. Blood Cancer J. 2013;3(7):e122.
18. Esteve J, Labopin M, Czerw T, et al. Allogeneic hematopoietic cell transplantation (alloHCT) for adult patients with t(4;11)(q21;q23) KMT2A/AFF1 (MLL/AF4) B-acute lymphoblastic leukemia in first complete remission (CR1): favorable outcome of patients with negative minimal residual disease (MRD) status at transplant. a report from the Acute Leukemia Working Party of the European Society for Blood and Bone Marrow Transplantation (ALWP-EBMT). Blood. 2017;130(Suppl 1):669.
19. Marks DI, Moorman AV, Chilton L, et al. The clinical characteristics, therapy and outcome of 85 adults with acute lymphoblastic leukemia and t(4;11)(q21;q23)/MLL-AFF1 prospectively treated in the UKALLXII/ECOG2993 trial. Haematologica. 2013;98(6):945-952.
20. Moore S, Suttle J, Bain S, Story C, Rice M. Acute lymphoblastic leukemia characterized by t(8;14)(q11.2;q32). Cancer Genet Cytogenet. 2003;141(1):1-4.
21. Messinger YH, Higgins RR, Devidas M, Hunger SP, Carroll AJ, Heerema NA. Pediatric acute lymphoblastic leukemia with a t(8;14)(q11.2;q32): B-cell disease with a high proportion of Down syndrome: a Children's Oncology Group study. Cancer Genet. 2012;205(9):453-458.
22. Kubo Y, Kakazu N, Tasaka T, et al. Acute lymphoblastic leukemia (ALL) with t(8;14)(q11.2;q32) in an elderly patient. Leuk Res. 2010;34(3):e82-84.
23. Dyer MJ, Akasaka T, Capasso M, et al. Immunoglobulin heavy chain locus chromosomal translocations in B-cell precursor acute lymphoblastic leukemia: rare clinical curios or potent genetic drivers? Blood. 2010;115(8): 1490-1499.
24. Liu W, Hu S, Konopleva M, et al. De novo MYC and BCL2 double-hit B-cell precursor acute lymphoblastic leukemia (BCP-ALL) in pediatric and young adult patients associated with poor prognosis. Pediatr Hematol Oncol. 2015;32(8):535-547.
25. Russell LJ, Enshaei A, Jones L, et al. IGH@ translocations are prevalent in teenagers and young adults with acute lymphoblastic leukemia and are associated with a poor outcome. J Clin Oncol. 2014;32(14):1453-1462.
26. Herold T, Schneider S, Metzeler KH, et al. Adults with Philadelphia chromosome-like acute lymphoblastic leukemia frequently have IGH-CRLF2 and JAK2 mutations, persistence of minimal residual disease and poor prognosis. Haematologica. 2017;102 (1):130-138.
27. Issa GC, Kantarjian HM, Yin CC, et al. Prognostic impact of pretreatment cytogenetics in adult Philadelphia chromosome-negative acute lymphoblastic leukemia in the era of minimal residual disease. Cancer. 2017;123(3):459-467.
28. Iacobucci I, Iraci N, Messina M, et al. IKAROS deletions dictate a unique gene expression signature in patients with adult B-cell acute lymphoblastic leukemia. PloS one. 2012;7(7):e40934.
29. Mullighan CG, Su X, Zhang J, et al. Deletion of IKZF1 and prognosis in acute lymphoblastic leukemia. N Engl J Med. 2009;360(5):470-480.
30. Dupuis A, Gaub MP, Legrain M, et al. Biclonal and biallelic deletions occur in 20% of B-ALL cases with IKZF1 mutations. Leukemia. 2013;27(2):503-507.
31. Moorman AV, Hagemeijer A, Charrin C, Rieder H, Secker-Walker LM. The translocations, t(11;19)(q23;p13.1) and t(11;19)(q23;p13.3): a cytogenetic and clinical profile of 53 patients. European 11q23 Workshop participants. Leukemia. 1998; 12(5):805-810.

ARTICLE

An intronic deletion in megakaryoblastic leukemia 1 is associated with hyperproliferation of B cells in triplets with Hodgkin lymphoma

Julien Record,[1*] Anton Sendel,[1*] Joanna S. Kritikou,[1] Nikolai V. Kuznetsov,[1] Hanna Brauner,[1] Minghui He,[1] Noemi Nagy,[1] Mariana M.S. Oliveira,[1] Elena Griseti,[1] Christoph B. Haase,[1] Jenny Dahlström,[2] Sanjaykumar Boddul,[2] Fredrik Wermeling,[2] Adrian J. Thrasher,[3] Chaohong Liu,[4] John Andersson,[1,5] Hans-Erik Claesson,[2] Ola Winqvist,[2] Siobhan O. Burns,[6,7] Magnus Björkholm[2] and Lisa S. Westerberg[1]

[1]Department of Microbiology, Tumor and Cell Biology, Biomedicum, Karolinska Institutet, Stockholm, Sweden; [2]Department of Medicine Solna, Karolinska University Hospital, Stockholm, Sweden; [3]Institute of Child Health, University College London, London, UK; [4]Department of Pathogen Biology, School of Basic Medicine, Huazhong University of Science and Technology, Wuhan, China; [5]Department of Medical Epidemiology and Biostatistics, Karolinska Institutet, Stockholm, Sweden; [6]Institute of Immunity and Transplantation, University College London, London, UK and [7]Department of Immunology, Royal Free London NHS Foundation Trust, London, UK

** JR and AS contributed equally to this work*

Ferrata Storti Foundation

Haematologica 2019
Volume 105(5):1339-1350

ABSTRACT

Megakaryoblastic leukemia 1 (MKL1) is a coactivator of serum response factor and together they regulate transcription of actin cytoskeleton genes. MKL1 is associated with hematologic malignancies and immunodeficiency, but its role in B cells is unexplored. Here we examined B cells from monozygotic triplets with an intronic deletion in *MKL1*, two of whom had been previously treated for Hodgkin lymphoma (HL). To investigate MKL1 and B-cell responses in the pathogenesis of HL, we generated Epstein-Barr virus-transformed lymphoblastoid cell lines from the triplets and two controls. While cells from the patients with treated HL had a phenotype close to that of the healthy controls, cells from the undiagnosed triplet had increased *MKL1* mRNA, increased MKL1 protein, and elevated expression of MKL1-dependent genes. This profile was associated with elevated actin content, increased cell spreading, decreased expression of CD11a integrin molecules, and delayed aggregation. Moreover, cells from the undiagnosed triplet proliferated faster, displayed a higher proportion of cells with hyperploidy, and formed large tumors *in vivo*. This phenotype was reversible by inhibiting MKL1 activity. Interestingly, cells from the triplet treated for HL in 1985 contained two subpopulations: one with high expression of CD11a that behaved like control cells and the other with low expression of CD11a that formed large tumors *in vivo* similar to cells from the undiagnosed triplet. This implies that pre-malignant cells had re-emerged a long time after treatment. Together, these data suggest that dysregulated MKL1 activity participates in B-cell transformation and the pathogenesis of HL.

Introduction

Hodgkin lymphoma (HL) is a B-cell malignancy of largely unknown etiology. Familial clustering and twin concordance are seen, as are links with viral infections such as Epstein-Barr virus (EBV).[1,2] The malignant HL Reed-Sternberg cells have frequently undergone class switch recombination and likely originate from germinal center B cells that fail to undergo apoptosis despite destructive somatic mutations.[1,3,4] Various studies have shown the ability of EBV to rescue crippled germinal center B cells from apoptosis, supporting the role of this virus in the pathogenesis of HL.[5,6]

Megakaryoblastic leukemia 1 (MKL1; also known as MRTF-A, MAL, or BSAC) is

Correspondence:

LISA WESTERBERG
lisa.westerberg@ki.se

Received: March 7, 2019.

Accepted: September 26, 2019.

Pre-published: October 3, 2019.

doi:10.3324/haematol.2019.216317

Check the online version for the most updated information on this article, online supplements, and information on authorship & disclosures: www.haematologica.org/content/105/5/1339

a transcriptional coactivator of serum response factor (SRF) and binds to globular (G-)actin via an RPEL motif.[7,8] As cytoplasmic G-actin is polymerized into filamentous (F)-actin, the G-actin pool diminishes. This leads to MKL1 translocation into the nucleus where it interacts with SRF to induce transcription of cytoskeleton-related genes, including actin, integrin molecules, and SRF itself.[7-10] Indeed, inducible expression of SRF in response to serum stimulation is dependent on SRF and MKL1 activity.[9,11] Actin polymerization and MKL1-SRF activity are additionally regulated by extracellular signaling through several integrin molecules which activate the small Rho GTPases, including RhoA.[12]

MKL1 was initially described as part of a fusion protein in megakaryoblastic leukemia of poor prognosis.[13,14] MKL1 expression is detected in malignant cells in breast and liver cancer and is associated with increased cell proliferation, anchorage-independent cell growth, and metastasis.[15,16] Small molecule inhibitors of the MKL1-SRF pathway have been identified, facilitating studies on the biological activity of MKL1, and are being tested as potential cancer therapeutic agents.[17] One of these compounds is CCG-1423, which was originally identified as a RhoA-MKL1-SRF pathway inhibitor and later discovered to target MKL1 directly.[17,18]

A loss-of-function mutation in *MKL1* was recently identified in a 4-year old girl with severe primary immunodeficiency.[19] MKL1 deficiency caused reduced G-actin and F-actin content in the patient's neutrophils, leading to reduced phagocytosis and migration.[19] In 2013, a familial case of two monozygotic triplets who developed HL at the age of 40 and 63 was described.[20] Both patients are in remission following HL treatment in 1985 and 2008, respectively, and the third triplet remains undiagnosed. Using microarray comparative genomic hybridization, a 15-31 kb deletion in intron 1 of *MKL1* was identified in the triplets.[20] The impact of this mutation on MKL1 expression and B-cell function remains unknown.

Here we took the approach of generating EBV-transformed lymphoblastoid cell lines (LCL) from the triplets with the deletion in *MKL1* intron 1 (HL0, HL1, and HL2) and from two healthy controls (C1 and C2). We found that the LCL from the undiagnosed triplet had increased MKL1 and SRF expression, and elevated G-actin content. This was associated with hyperproliferation, genomic instability, and tumor formation when the cells were injected into immunocompromised mice. When compared to control LCL with high CD11a expression and capacity to form large aggregates, HL0 LCL expressed low CD11a and had reduced capacity to form aggregates. The HL1 LCL showed a bimodal expression of CD11a and when sorted for CD11a low and CD11a high cells, CD11a high cells mimicked the response of control LCL whereas the H10 CD11a low cells mimicked the response of HL0 cells with increased proliferation and tumor formation. Finally, treatment of HL0 cells with the MKL1 inhibitor CCG-1423 reverted the phenotype and prevented tumor growth *in vivo*. These data show that unregulated MKL1 alters B-cell cytoskeletal responses leading to B-cell transformation.

Methods

Human blood samples and Epstein-Barr virus transformation

Whole blood samples were obtained from the triplets and age-matched controls after informed consent was given. This study was performed according to the principles expressed in the Helsinki Declaration and with approval from the local ethics committee (Dnr 2015/416-31). For analysis of primary cells, the first experiment included samples from HL0, HL1, and a control (not used for EBV-transformation) collected in February 2015 and the second experiment was conducted on samples from HL2 and C1, collected in May 2015. To establish the EBV-transformed LCL, peripheral blood mononuclear cells from HL0, HL1, and HL2, and two age- and sex-matched controls (C1 and C2), all collected in November 2015, were cultured with supernatant of the virus-producing B95-8 line.[21]

Mice

NOD/SCID-IL2rγ^{null} (NSG) mice were bred and maintained at the animal facility of the Department of Microbiology, Tumor and Cell Biology at Karolinska Institutet under specific pathogen-free conditions. Female mice were used and all animal experiments were performed after approval from the local ethics committee (the Stockholm District Court, permit N77/13 and N272/14). For inhibitor treatment, 10 μM CCG-1423 or dimethylsulfoxide was injected intratumorally for 6 consecutive days. The volume of the tumor was calculated at the endpoint using a caliper.

Flow cytometry and microscopy

Flow cytometry was performed on peripheral blood mononuclear cells, LCL, and cultured primary B cells using an LSRFortessa X-20 (BD Biosciences). The results were processed using FlowJo v10 software (TreeStar Inc., St. Ashland, OR, USA). To determine integrin expression at the cell surface, LCL were labeled with an anti-human CD11a antibody (TS2/4; Biolegend) for total CD11a expression, or an anti-human CD11a antibody (Hl111; Biolegend) for inactive/closed conformation-CD11a expression, or an anti-human CD54 antibody (Biolegend), followed by an anti-mouse-Alexa647 antibody (ThermoFisher Scientific). To determine F- and G-actin content in two LCL samples side by side, one sample was incubated with an anti-human CD54 antibody (Biolegend) for 30 min on ice and thereafter labeled with DNaseI-Alexa488 (ThermoFisher Scientific) and phalloidin-Alexa568 (ThermoFisher Scientific).

Results

The *MKL1* intron 1 deletion is associated with increased expression of MKL1 and MKL1-induced genes

To understand how the deletion in *MKL1* intron 1 affected actin cytoskeleton regulation in B cells, we examined freshly isolated cells and LCL from the triplets (HL0, HL1, and HL2) and two healthy controls (C1 and C2) (Figure 1A, B). We reasoned that cells from the undiagnosed HL0 triplet may be in a pre-HL stage, whereas HL1 and HL2 cells may be more similar to control cells because of successful treatment for HL in 1985 and 2008, respectively. MKL1 protein in primary blood lymphocytes was higher in the cells from all triplets than in control cells, as assessed by flow cytometry (Figure 1C and *Online Supplementary Figure S1A*). Using primer walking and sequencing, we confirmed that the triplets' cells contained a heterozygous deletion of *MKL1* intron 1 (*Online Supplementary Figure S2A*). The intron 1 is in the 5´ untranslated region of the *MKL1* gene. We examined exon boundaries of exons 1-4 in the 5' untranslated region and found normal expression of adjacent exons,

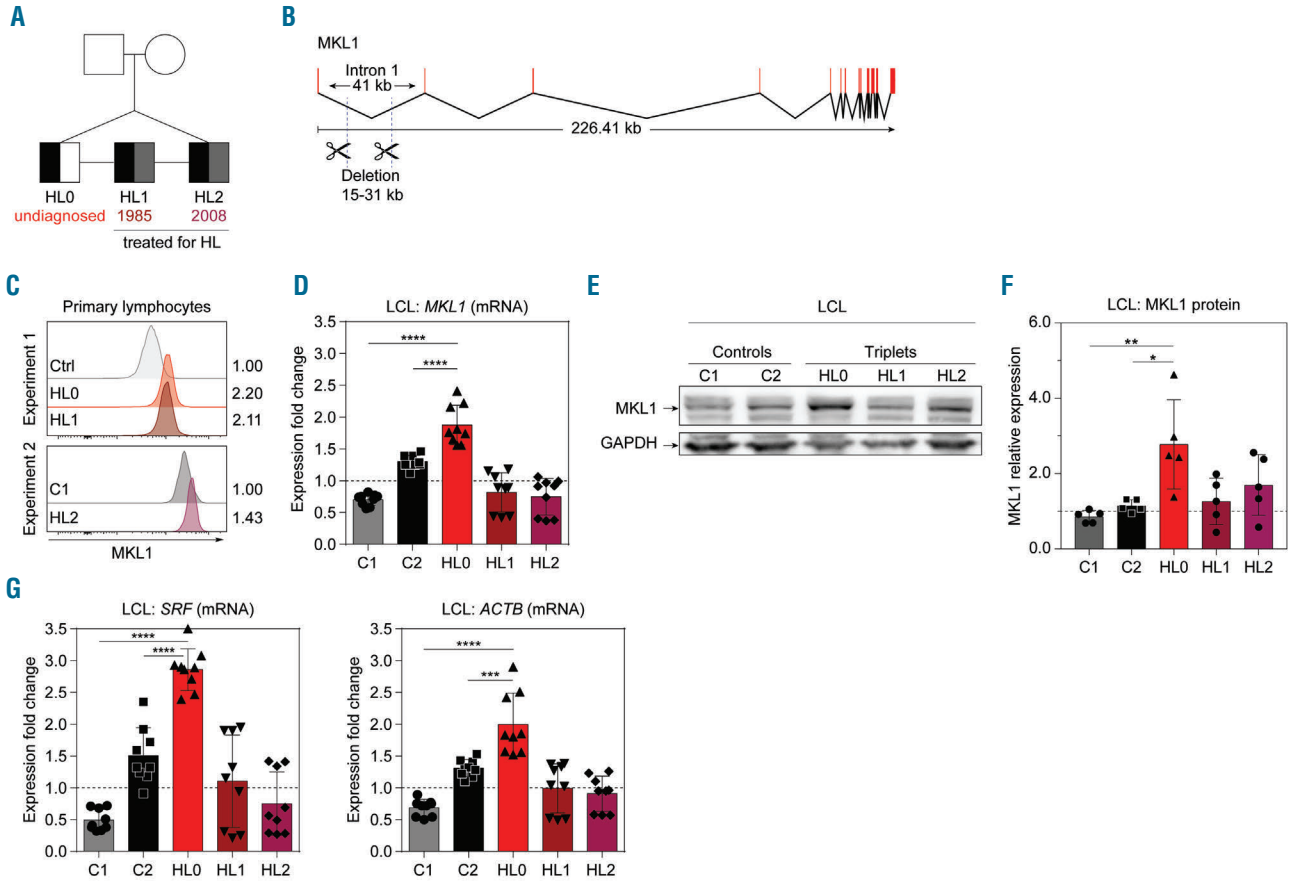

Figure 1. The *MKL1* intronic deletion is associated with increased expression of *MKL1* and MKL1-induced genes. (A) Pedigree of genetically identical triplets (HL0, HL1, HL2) of whom two have been diagnosed with Hodgkin lymphoma (HL). Presence of the *MKL1* intronic deletion is indicated in black, a diagnosis of HL in gray, and undiagnosed in white. Numbers indicate year of treatment. (B) Overview of *MKL1* indicating the deletion in intron 1. (C) MKL1 protein expression in primary lymphocytes, determined by flow cytometry, in two separate experiments. Experiment 1: control (Ctrl), HL0, and HL1. Experiment 2: C1 and HL2. Numbers indicate the fold-change in expression normalized to the ctrl and C1 values, respectively. (D) *MKL1* mRNA expression. (E) Representative image of MKL1 protein expression. (F) MKI1 expression normalized to GAPDH expression. (G) Expression of MKL1-induced genes by real-time quantitative polymerase chain reaction. (D, F, G) Combined data from three experiments; experiments with primary lymphocytes (C) were performed once. For bar graphs, the dotted line indicates normalization to the mean of C1 and C2. All panels display data from lymphoblastoid cell lines except (C), which displays data from primary lymphocytes. Error bars represent the standard deviation of the measurements. Symbols represent technical replicates from three independent experiments in (D) and (G), and single values from independent experiments in (F). All data were analyzed using analysis of variance with a post-hoc Tukey test. ***P<0.001, ****P<0.0001.

suggesting that the intron 1 deletion did not affect splicing of *MKL1* (*Online Supplementary Figure S3*). *MKL1* intron 1 contains many transcription binding sites (*Online Supplementary Figure S2B*) that may affect MKL1 transcription. We examined *MKL1* mRNA expression in LCL by real-time quantitative polymerase chain reaction (RT-qPCR). The LCL from HL0 (the undiagnosed triplet) had higher expression of *MKL1* when compared to that of the siblings (HL1 and HL2) and controls (C1 and C2) (Figure 1D). Protein studies indicated that the levels of MKL1 were higher in HL0 than in C1 and C2 (Figure 1E, F and *Online Supplementary Figure S1B*). To investigate whether increased MKL1 expression was associated with increased MKL1 activity, we examined mRNA expression of specific MKL1-dependent genes including *SRF* and *ACTB*.[19] HL0 LCL had the highest expression of both these MKL1-dependent genes (Figure 1G). This suggests that the intron 1 deletion in *MKL1* directly influences the expression of MKL1 and MKL1 target genes.

Increased actin content and actin-dependent spreading in HL0 and HL1 cells

To understand how the deletion in *MKL1* intron 1 affected actin content and responses, we examined F-actin content in primary lymphocytes by flow cytometry. No difference was seen when comparing HL0 and HL1 to control lymphocytes while HL2 had a higher F-actin content compared to that of C1 (Figure 2A). In primary monocytes gated based on forward and side scatter profiles by flow cytometry, the triplets' cells had higher MKL1 expression (*Online Supplementary Figure S1C*) and higher F-actin content (*Online Supplementary Figure S1D*). Monocyte-derived dendritic cells from whole blood of the controls and HL patients displayed a similar ability to form podosomes (*Online Supplementary Figure S4A, B*). To exclude a possible effect of cell size and different hematopoietic cell subsets of primary cells, we compared actin content in cells from the triplets' LCL with those of controls side by side by alternately labeling one cell pop-

ulation with anti-CD54 antibodies after fixation and before mixing the two populations. Thereafter, we detected G-actin using DNAse1, and F-actin using phalloidin (Figure 2B and *Online Supplementary Figure S1E, F*). HL0 cells had increased G-actin and a tendency for increased F-actin (Figure 2B-D). To examine whether increased actin content had any impact on cytoskeletal rearrangement, the triplets' and control LCL were examined microscopically on glass surfaces coated with fibronectin and anti-CD19 antibodies. HL0 and HL1 cells had increased capacity to spread, with formation of long dendritic protrusions (Figure 2E, F and *Online Supplementary Figure S5A*), and increased adhesive area measured by interference reflection microscopy (Figure 2G, H). This indicates that the deletion in *MKL1* intron 1 was associated with increased actin content and actin-dependent B-cell spreading.

HL0 cells display decreased aggregation and reduced CD11a integrin expression

LCL grow in clusters by homotypic aggregation dependent on leukocyte function antigen-1 (LFA-1, consisting of subunits CD11a/integrin αL and CD18/integrin β2) and intercellular adhesion molecule-1 (ICAM-1/CD54) (*Online Supplementary Figure S6*).[22-24] When culturing LCL, we observed decreased clustering of the triplets' cells, an effect that was especially pronounced for HL0 LCL (*Online Supplementary Figure S5B*). To quantify this, we measured aggregation from single cell suspensions by live cell imaging over 2 h. LCL from C1, C2, HL1, and HL2 formed aggregates instantly, whereas those from HL0 displayed impaired aggregation with delayed formation of small aggregates over 2 h (Figure 3A, B). We investigated whether decreased aggregation resulted from altered surface expression of adhesion receptors. C1, C2,

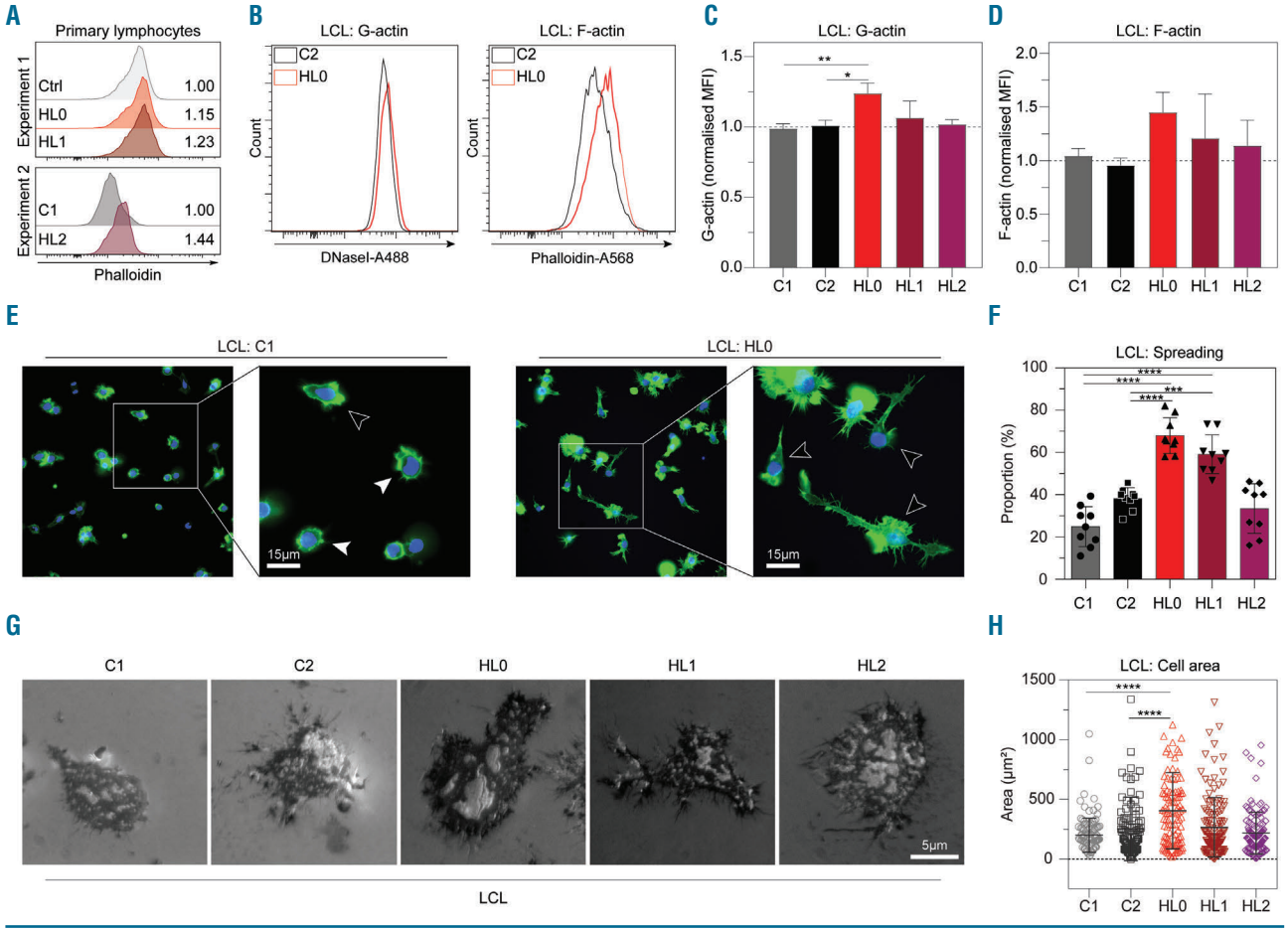

Figure 2. Increased actin content and actin-dependent spreading in HL0 and HL1 cells. (A) Phalloidin expression in primary lymphocytes determined by flow cytometry. Experiment 1: Control (Ctrl), HL0, and HL1. Experiment 2: C1 and HL2. Numbers indicate fold-change in expression normalized to ctrl and C1, respectively. (B) Representative flow cytometry plot of G-actin and F-actin content in C2 and HL0 and (C, D) quantification of G- and F-actin content in control and the triplets' lymphoblastoid cell lines (LCL). (E) Immunocytochemistry of LCL adhering to glass slides coated with fibronectin and anti-CD19 antibody. Spread cells are defined as those with lamellipodia-like structures and/or long protrusions. White arrowheads indicate examples of spread cells; black arrowheads indicate non-spread cells. Cells stained with phalloidin-Alexa488 (green color) and mounted in Vectashield Antifade Mounting Medium with 4',6-diamidino-2- phenylindole (DAPI, blue color). Original magnification x400. (F) Proportion of spread LCL. The experiment was repeated three times and cell spreading was determined each time in three separate fields of view. Total cells counted: C1: 800; C2: 1356; HL0: 1081; HL1: 1062; HL2: 983; and 200 cells or more were counted per sample per experiment. (G) Interference reflection microscopy of LCL adhering to cover slips coated with fibronectin and anti-CD19 antibody. Original magnification x630. (H) Area of LCL spread on coverslips. Total cells counted: C1: 119; C2: 109; HL0: 109; HL1: 131; HL2: 123. (C, D, F) Combined data from three experiments. (H) Combined data from two experiments. (A) The experiments with primary lymphocytes were performed once. (B) Representative histograms. (E, G) Representative images. For bar graphs, the dotted line indicates normalization to the mean of C1 and C2. All panels display data from LCL except (A), which displays data from primary lymphocytes. Error bars represent the standard deviation of the measurements. Symbols represent technical replicates from three independent experiments in (F), and pooled single values from three independent experiments in (H). All data were analyzed using analysis of variance with the post-hoc Tukey test. *P<0.05, **P<0.01, ***P<0.001, ****P<0.0001.

HL1, and HL2 cells displayed similar expression of total surface and intracellular CD11a, and inactive CD11a (Figure 3C-G and *Online Supplementary Figure S5C*). HL0 cells displayed lower expression of total surface and intracellular CD11a, and inactive CD11a as well as lower CD11a mRNA (*ITGAL*) (Figure 3C-G and *Online Supplementary Figure S5C*). Interestingly, cells lacking MKL1 expression[19] showed higher surface CD11a expression when compared to control cells (*Online Supplementary Figure S4C*). LCL from the triplet and controls had similar expression of CD54 (Figure 3H and *Online Supplementary Figure S5C*). This shows that HL0

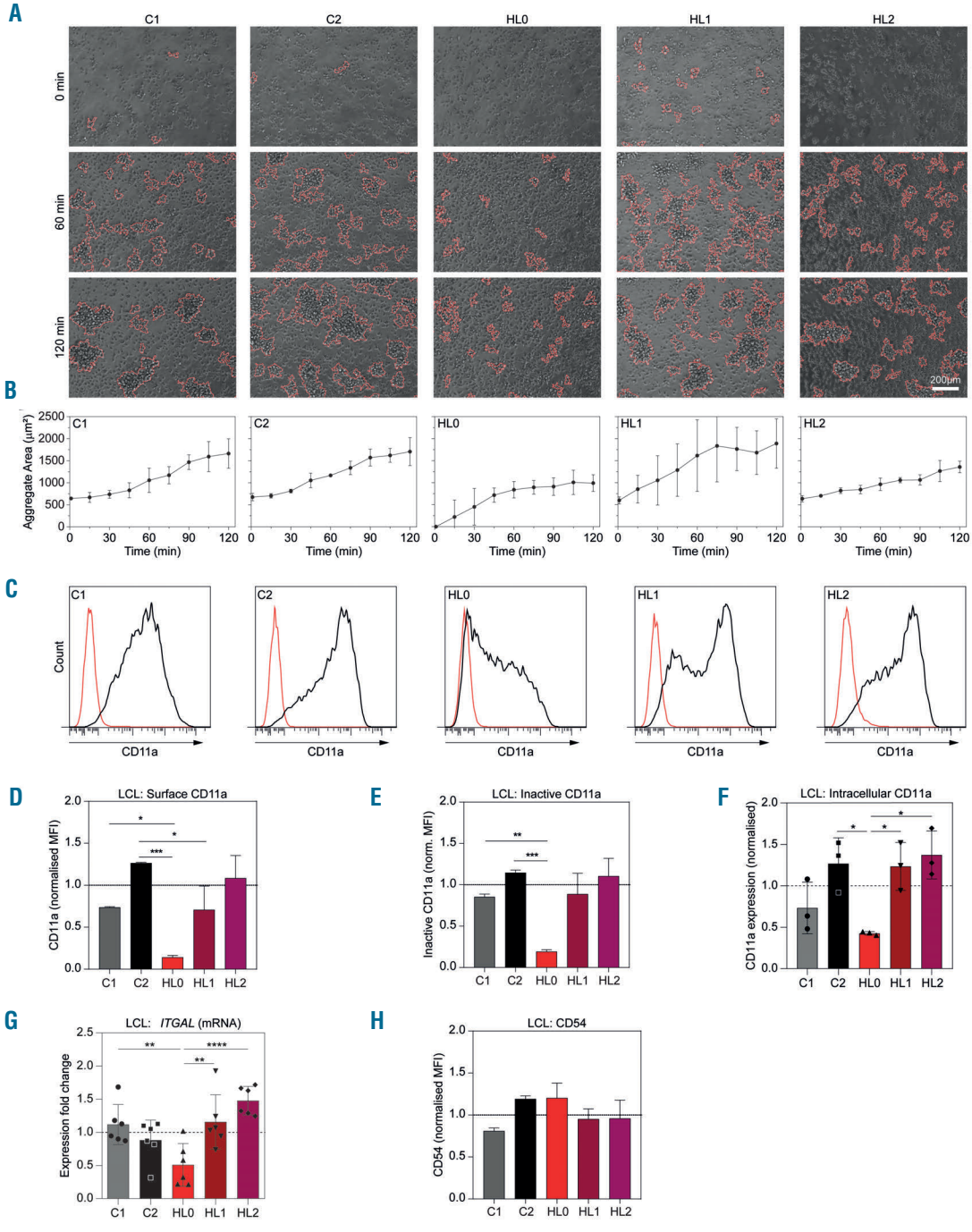

Figure 3. HL0 cells display decreased aggregation and reduced CD11a integrin expression. (A) Aggregation of lymphoblastoid cell lines (LCL), representative images. (B) Average area of aggregates observed in (A). (C) Representative flow cytometry plots of total CD11a surface expression in LCL. (D) Quantification of CD11a surface expression as seen in (C). (E, F) Quantification of inactive CD11a surface expression and intracellular CD11a expression as seen in *Online Supplementary Figure* S3. (G) Expression of *ITGAL* (CD11a) by real-time quantitative polymerase chain reaction. (H) Quantification of CD54 surface expressio. (B, D-F) Combined data from three experiments. (G-H) Combined data from two experiments. For bar graphs, the dotted line indicates normalization to the mean of C1 and C2. All panels display data from LCL. Error bars represent the standard deviation of the measurements. Symbols represent technical replicates from three independent experiments in (G), and single values from three independent experiments in (F). All data were analyzed using analysis of variance with the post-hoc Tukey test. **P*<0.05, ***P*<0.01, ****P*<0.001.

cells had reduced capacity to form aggregates and this was associated with low expression of CD11a.

HL0 cells display increased proliferation and genomic instability

HL has previously been associated with immunodeficiency and altered proliferation.[25,26] To examine for immunodeficiency, we used flow-cytometric assay of specific cell-mediated immune response in activated whole blood (FASCIA) analysis to detect B- and T-cell responses to various antigens.[27] We found that the triplets' B cells displayed a decreased response to pokeweed mitogen but had normal T-cell responses (*Online Supplementary Table S1*). To address how increased MKL1 expression correlated to proliferation, primary B cells were cultured with anti-CD40 antibodies and interleukin-4 for 72 h and labeled with the proliferation marker Ki-67 (Figure 4A and *Online Supplementary Figure S5D*). The triplets' samples had more Ki-67$^+$ proliferating B cells than those of the controls (Figure 4A). To exclude that any variation was due to sample collection time when using Ki-67, we measured proliferation in LCL by DNA synthesis over 20 h using ^{3}H-thymidine incorporation. Compared to controls, HL0 cells had greater DNA synthesis (Figure 4B). To examine whether proliferation rate was associated with cell cycle alterations, we used DNA-specific Hoechst labeling to evaluate cells in the G0/G1 (2n DNA content), S, and G2/M (4n DNA content) phases. The proportion of cells in S or G2/M phase was higher in HL0 LCL (Figure 4C). Three percent of HL0 cells had more than 4n DNA content, compared to 0–1% of control cells (Figure 4D). Since EBV has been shown to induce multiple nuclei in transformed cells,[28] we counted nuclei in the LCL from the triplets and controls to evaluate whether multinuclearity could explain the proportion of cells with more than 4n DNA content. No correlation

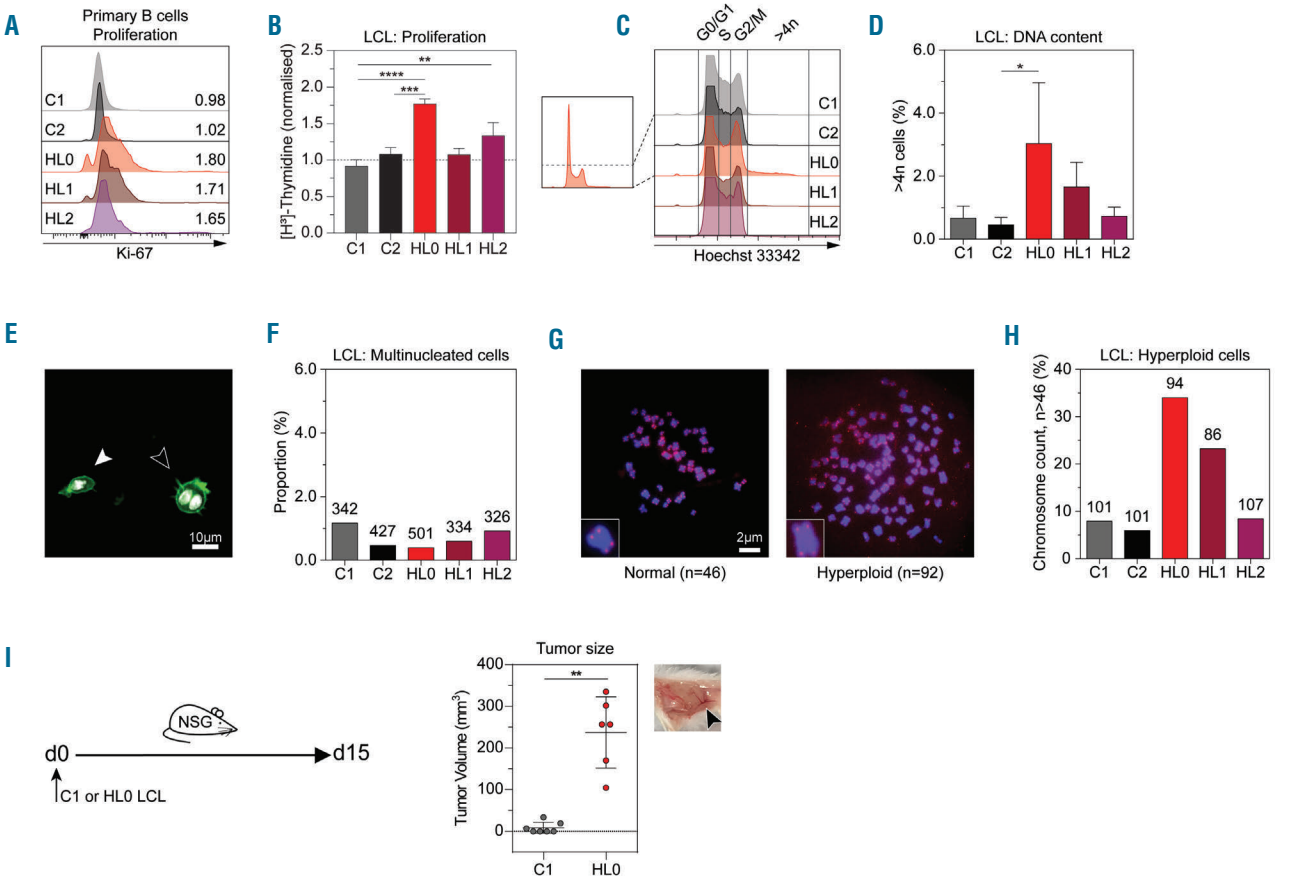

Figure 4. HL0 cells display increased proliferation and genomic instability. (A) Expression of the proliferation marker Ki-67 by flow cytometry on primary B cells cultured 48 h with interleukinIL-4 and anti-CD40 antibodies. Numbers indicate fold-change of expression normalized to the mean of C1 and C2. (B) DNA synthesis rate as measured by radiation from incorporated 3H-thymidine after 48 h. (C) Proportions of cell cycle phases (G0/G1, S and G2/M) determined by Hoechst 33342 staining, measured by flow cytometry (representative histograms). Left graph shows how the Y-axis was cut to allow for emphasized visualization of hyperploid cells with >4n of DNA content, quantified in (D). (E) Comparison of mononuclear (indicated by white arrowhead) and multinuclear (black arrowhead) cells of lymphoblastoid cell lines (LCL). White color: 4',6-diamidino-2- phenylindole (DAPI); green color: phalloidin-Alexa488. (F) Proportion of multinucleated LCL cells, as assessed by manual microscopical counting of nuclei stained with DAPI. Numbers indicate counted cells for each sample. (G) Telomere-fluorescence *in situ* hybridization on chromosomes in metaphase. Representative images of a normal cell with 46 chromosomes and a hyperploid cell with 92 chromosomes; insets show magnified representative chromosomes. Original magnification x1000. Chromosomes hybridized with TelG-Cy3 PNA probe (red color) and mounted in Vectashield Antifade Mounting Medium with DAPI (blue color). (H) Proportion of metaphases with a hyperploid amount of chromosomes (>46). Numbers indicate counted metaphases for each sample. (I) Subcutaneous injection of C1 and HL0 LCL in NSG mice and measurement of tumor mass at day 9. Each circle represents one mouse. Right subpanel: representative image of tumor mass assessed at the endpoint. Black arrowhead indicates angiogenesis. (A) Data from one experiment. (B, D, F, H) Combined data from three experiments. (I) Combined data from two experiments. For bar graphs, the dotted line indicates normalization to the mean of C1 and C2. All panels display data from LCL except (A), which displays data from primary B cells. Error bars represent the standard deviation of the measurements. All data were analyzed using analysis of variance with the post-hoc Tukey test, except (I) that was analyzed using a *t*-test. **P*<0.05, ***P*<0.01, ****P*<0.001, *****P*<0.0001.

was seen between multinuclearity and DNA content (Figure 4E, F), indicating that increased DNA content could have resulted from genomic instability. When arresting LCL from the triplets and controls in metaphase, HL0 and HL1 had higher proportions of cells (approximately 25–35%) with more than 46 chromosomes (Figure 4G, H). To investigate the growth of HL0 and C1 cells *in vivo*, the cells were injected subcutaneously into NSG mice that lack a functional immune response and cell growth was examined as tumor mass on day 9. C1 cells failed to form a tumor mass whereas HL0 cells formed tumors with distinct angiogenesis (Figure 4I). Together these observations suggest that increased MKL1 expression and activity is directly associated with hyperproliferation and genomic instability leading to formation of a tumor mass *in vivo*.

HL1 cells contain two distinct populations of which one shows an HL0 phenotype

We noticed that HL1 cells recurrently showed an intermediate phenotype when compared to HL0 and control cells. HL1 cells showed a bimodal expression of CD11a and we examined whether this represented two populations of cells with different phenotypes. We used fluorescence activated cell sorting (FACS) to sort out CD11a low and CD11a high cells from the HL1 cells (Figure 5A). PCR of genomic DNA showed that sorted HL1 CD11a low and HL1 CD11a high cells contained the heterozygous deletion of *MKL1* intron 1 (*Online Supplementary Figure S2A*). CD11a low cells had increased MKL1 protein and increased cell spreading when compared to CD11a high cells (Figure 5B, C). We quantified aggregation over 2 h and found that CD11a low cells had a reduced capacity to aggregate compared to that of CD11a high cells (Figure 5D, E). To examine proliferation, we sorted 250,000 CD11a low and CD11a high cells and counted them between days 3 and 8. The CD11a high cells showed only modest proliferation whereas the CD11a low cells expanded 3- to 4-fold in the period between day 3 and day 8 (Figure 5F). To examine proliferation of cells *in vivo*, we injected CD11a low and CD11a high cells into NSG mice and determined tumor growth on day 15. CD11a low cells formed a large tumor mass with visible angiogenesis, whereas CD11a high cells formed a smaller tumor mass (Figure 5G). To address whether the control C1 and C2 cells also contained a stable CD11a low population, we used FACS and cultured the C1 and C2 CD11a low and CD11a high cells for 17 days. The C1 and C2 CD11a low cells gained expression of CD11a during the culture, suggesting that the CD11a phenotype in control cells was unstable (*Online Supplementary Figures S7* and *S8*). We next examined whether alterations in CD11a expression were present in the L1236 HL cell line derived from a primary isolate of a patient with advanced HL.[29] The L1236 cells contained large Reed-Sternberg-like cells and smaller cells (Figure 5H). Using flow cytometry, small and large cells were identified based on forward and side scatter. Small cells had low expression of CD11a and the large cells were devoid of CD11a expression (Figure 5H). Together, these data suggest that low expression of CD11a may be a characteristic feature of pre-malignant B cells in HL.

Inhibition of MKL1 activity in HL0 cells induces a phenotype similar to that of control cells

We next investigated whether we could revert the phenotype of HL0 cells to that of control cells using the MKL1 small molecule inhibitor CCG-1423.[17,18] To define the dose range, HL0 cells were treated with different doses of CCG-1423 and cell death measured by flow cytometry. At doses of 2-10 μM CCG-1423, 90% of cells were viable (Figure 6A). HL0 cells treated with CCG-1423 displayed dose-dependent lowering of MKL1 protein and decreased SRF expression (Figure 6B-D). The spreading capacity of HL0 cells was reduced upon CCG-1423 treatment (Figure 6E). Lowering MKL1 protein and activity led to increased aggregate formation and reduced proliferation (Figure 6F-H). To examine whether the MKL1 inhibitor could suppress tumor growth *in vivo*, HL0 cells were injected into NSG mice by subcutaneous injections. From day 6 to day 12, a daily dose of 10 μM CCG-1423 was injected intratumorally. Compared to treatment with vehicle (dimethylsulfoxide), treatment with the MKL1 inhibitor led to reduced HL0 tumor mass in mice (Figure 6I).

Discussion

Dysregulation of MKL1 expression and the actin cytoskeleton has been implicated in hematologic malignancies, although the exact mechanism has not been determined (*Online Supplementary Figure S9*).[30,31] Mutated MKL1 was originally described in patients with acute megakaryoblastic leukemia in whom *MKL1* was fused with *RBM15* by a chromosomal translocation.[13,14] The role of MKL1 in megakaryocyte differentiation, migration, and in the formation of proplatelets was subsequently described in MKL1-deficient mice.[32,33] In humans, MKL1 deficiency has a profound affect on the hematopoietic cell actin cytoskeleton resulting in severely impaired cell migration and phagocytosis.[19] Genetically identical triplets with a large deletion in *MKL1* intron 1, of whom two affected by HL and one undiagnosed, provided a unique opportunity to investigate MKL1 and B-cell responses in the pathogenesis of HL. We found that increased activity of MKL1 in B cells led to the classical hallmarks of cancer cells: hyperproliferation, genomic instability, and formation of tumors with induction of angiogenesis.[34]

In this study we mainly used EBV-transformed B cells (LCL) from two controls and the triplets. To minimize possible variation due to EBV transformation, all samples were EBV-transformed under the same conditions with regards to day of transduction, virus batch and concentration. The EBV cells enabled an extensive investigation of the impact of the *MKL1* intron 1 deletion on B cells and importantly they allowed us to perform controlled experiments in which cells from the controls and the triplets could be compared side by side. A limitation with EBV transformation is that highly proliferative B cells are favored during EBV transformation.[35] Moreover, the donor distribution of naïve, non-switched memory, and switched memory B cells is reflected in the EBV-transformed B cells.[35,36] We cannot exclude that the EBV transformation induced expansion of a dominant subclone; however, CD11a staining revealed variable expression of CD11a in each sample although with different distributions. In fact, the variable CD11a expression allowed us to define different subpopulations in the HL0 and HL1 samples and argue against a dominant subclone upon EBV transformation.

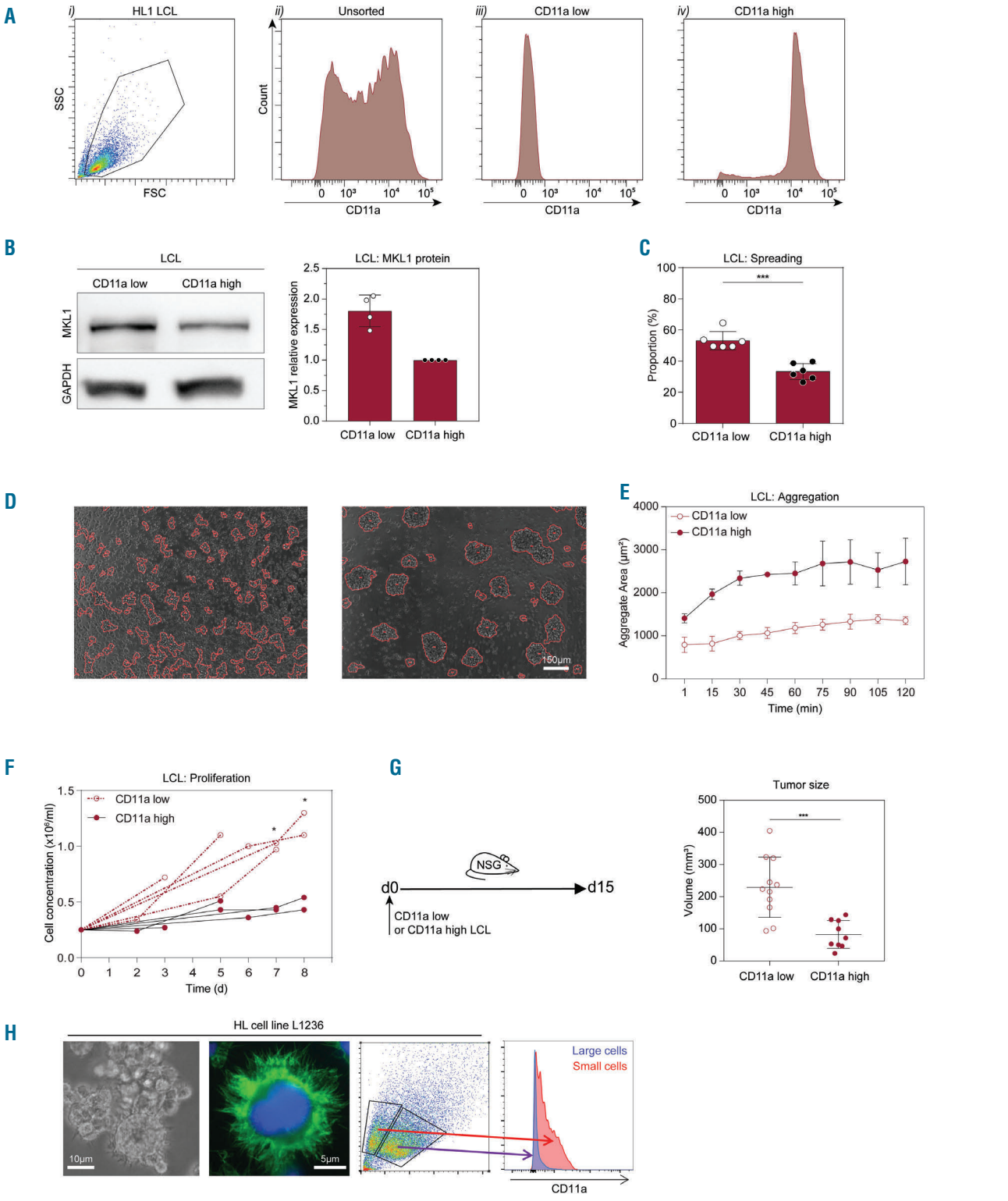

Figure 5. HL1 cells comprise two distinct populations of which one shows an HL0 phenotype. (A) (i) Representative flow cytometry plots from eight experiments showing gating on lymphoblastoid cell lines (LCL) using side scatter (SSC) *vs.* forward scatter (FSC). (ii) CD11a expression in HL1 cells. HL1 cells were sorted according to CD11a surface expression resulting in the two populations, CD11a low and CD11a high, cells shown in (iii) and (iv), respectively. (B) MKL1 expression in CD11a low and CD11a high LCL was evaluated by western blot. Left subpanel: representative western blot showing MKL1 expression in CD11a low and CD11a high cells. Right subpanel: quantification by densitometry of MKL1 expression relative to GAPDH expression in four independent experiments. (C) Proportion of spread LCL. CD11a low and high cells were allowed to spread on glass slides coated with fibronectin and anti-CD19 antibody. The experiment was repeated two times and cell spreading was determined each time in three separate fields of view. Total cells counted: CD11a low: 689; CD11a high: 579; and 200 cells or more were counted per sample per experiment. (D) Aggregation of CD11a low and high LCL, representative images. (E) Average area of aggregates. Results from three independent experiments. (F) Concentration of CD11a low and CD11a high LCL cells over 8 days. Results from five independent experiments. (G) Left subpanel: CD11a low or CD11a high LCL cells were injected subcutaneously into NSG mice and the tumor size was measured 15 days later. Right subpanel: quantification of the tumor size in NSG mice injected with either CD11a low or high LCL cells. Results from three independent experiments. (H) Microscopy of the L1236 HL cell line. Green: F-actin; blue: nuclear stain. CD11a expression determined by flow cytometry. Symbols represent single values from four independent experiments in (B) and (F), and technical replicates from two and three independent experiments in (C) and (G), respectively. Error bars represent the standard deviation of the measurements. All data were analyzed using *t*-tests. **P*<0.05, ****P*<0.001.

Since the deletion in *MKL1* is intronic, we did not anticipate any changes in the amino acid sequence and found that the MKL1 expressed was of normal size. The first intron is often essential for the regulation of gene expression,[37,38] which is why we investigated possible alterations of MKL1 expression in the triplets' cells and found that those from the undiagnosed triplet (HL0) displayed the highest expression of MKL1 while cells from HL1 and HL2, the triplets who were successfully treated for HL, showed an intermediate phenotype. This suggests a phenotypic difference between the triplets based on the onset and treatment of the disease. MKL1, via its interac-

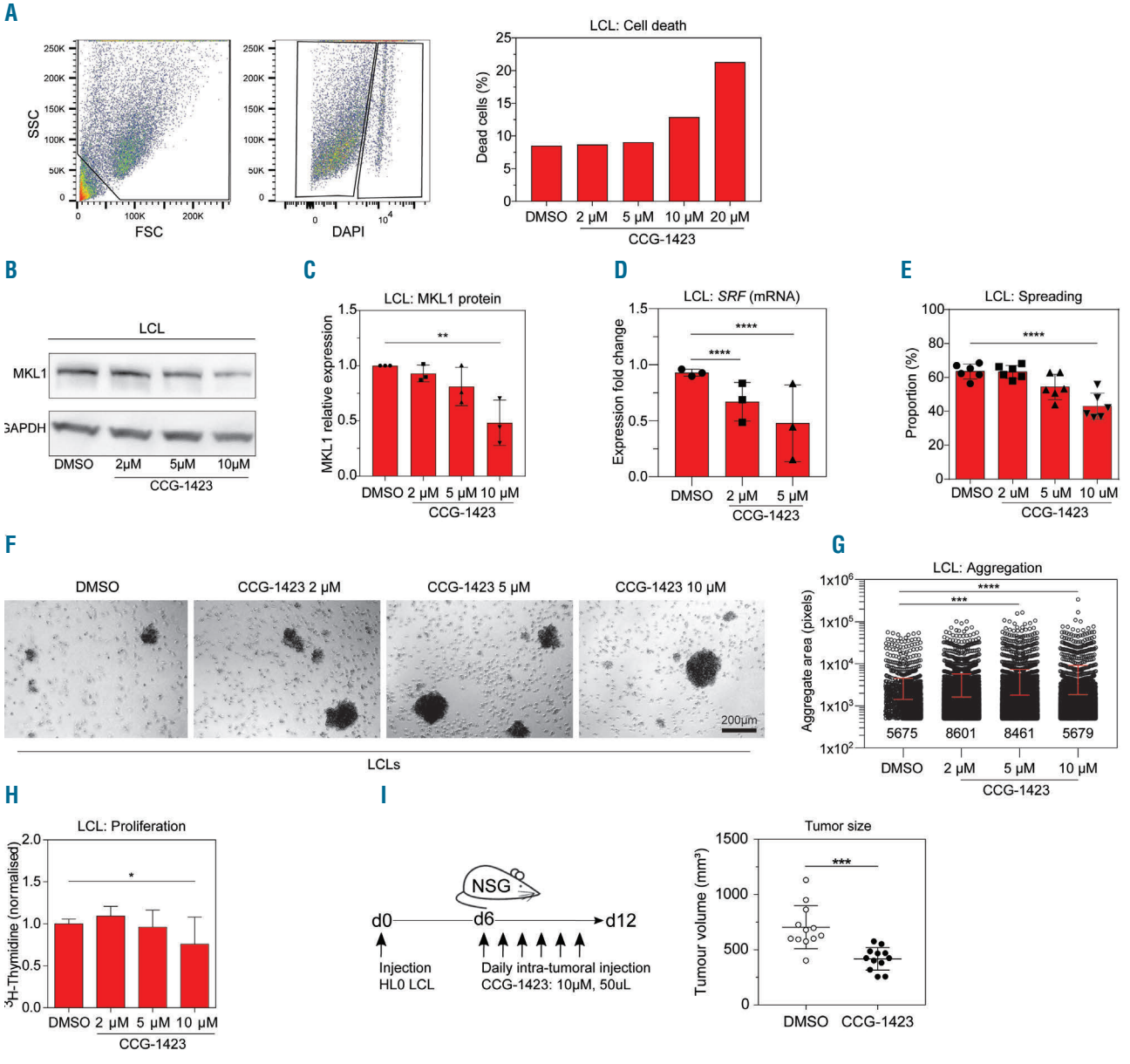

Figure 6. Inhibition of MKL1 activity in HL0 cells induces a phenotype similar to that of control cells. (A) Left and middle subpanels: representative flow cytometry plots showing gating for size, granularity, and 4',6-diamidino-2- phenylindole (DAPI) fluorescence intensity as a measure of the proportion of dead cells of HL0 lymphoblastoid cell lines (LCL) treated with 10 µM of CCG-1423 for 24 h. Right subpanel: quantification of death of HL0 cells treated with dimethylsulfoxide (DMSO), as the control, or CCG-1423 for 24 h. Representative graph of three independent experiments. (B) Representative image of MKL1 protein expression in HL0 LCL treated with DMSO or CCG-1423 for 24 h. (C) Quantification of MKL1 expression levels normalized to GAPDH in HL0 LCL treated with DMSO or CCG-1423 for 24 h. Results from three independent experiments. (D) Expression of *SRF* mRNA, determined by real-time quantification polymerase chain reaction, in HL0 LCL treated with DMSO or CCG-1423 for 24 h. Results from three independent experiments. (E) Proportion of spread HL0 LCL after treatment with DMSO or CCG-1423 for 48 h. The experiment was repeated twice and cell spreading was determined each time in three separate fields of view. Total cells counted: DMSO: 541; 2 µM: 517; 5 µM: 454; 10 µM: 271; and 100 cells or more were counted per sample per experiment. (F) Aggregation in culture of HL0 LCL treated with DMSO or CCG-1423 for 24 h. More than 15 fields were randomly chosen for quantification. Original magnification x40. (G) Quantification of aggregation observed in (F) using ImageJ. Data representative of two independent experiments. Numbers indicate counted aggregates for each sample. (H) DNA synthesis rate in HL0 LCL as measured by radiation from incorporated 3H-thymidine after 48 h of treatment with DMSO or CCG-1423. (I) HL0 LCL cells were injected into NSG mice. From day 6, 50 µL of DMSO or 10 µM of CCG-1423 were injected intratumorally daily for 6 days. Tumor size was measured on day 12. Error bars represent the standard deviation of the measurements. Symbols represent single values from three independent experiments in (C), mean values in (D), and technical replicates from two independent experiments in (C) and (G). All data were analyzed using analysis of variance with the post-hoc Tukey test. *P<0.05, **P<0.01, ***P<0.001, ****P<0.0001.

tion with SRF, regulates expression of hundreds of genes involved in cell migration, adhesion, and differentiation.[15,39] We show that the high mRNA and protein expression of MKL1 in HL0 cells correlated with high expression of the MKL1 target genes *SRF* and *ACTB*. MKL1 activity promotes migration and proliferation of cancer cells,[16,40,41] suggesting that HL0 LCL could be pre-malignant.

Because the absence of MKL1 results in a severely impaired actin cytoskeleton,[19] we reasoned that overexpression of MKL1 could result in a more active actin cytoskeleton. Actin cytoskeleton proteins are upregulated in invasive cancer,[42] suggesting that the increased activity of the actin cytoskeleton in the HL0 cells could enhance cell migration and cell division, promoting invasion of cells and growth of tumors. In support of this, HL0 cells with the highest MKL1 expression had higher G- and F-actin content and displayed increased spreading, a process that depends on actin cytoskeleton dynamics. The migration and hyperproliferation of cancer cells are also regulated by alteration of integrin expression at the cell surface and modification of the subsequent intracellular integrin signaling.[43] EBV-transformed B cells aggregate in cell culture via the interaction between the integrin CD11a (a subunit of LFA-1) and the adhesion molecule ICAM-1 (this study).[22-24] We examined LCL aggregation *in vitro* and observed that HL0 cells aggregated poorly, while HL1 cell aggregation varied and HL2 cell aggregation was similar to that of control cells. We found that the levels of surface and total protein as well as mRNA expression of CD11a were low in HL0 cells, but similar to control levels in HL2 cells. Interestingly, CD11a expression in HL1 cells showed a bimodal distribution with CD11a low and CD11a high cells, which might be the cause of the high variation of HL1 cell aggregation results. It is possible that the overactive actin cytoskeleton in HL0 cells prevented correct translocation of adhesion receptors to the cell surface or affected integrin inside-out and outside-in signaling.

Because of the possible pre-malignant stage of HL0 cells, we investigated cell proliferation *in vitro* and *in vivo* through formation of tumor mass. HL0 cells were hyperproliferative *in vitro* and also *in vivo* where they rapidly formed tumors in immunocompromised NSG mice. The HL0 population showed increased DNA content and a higher percentage of hyperploid cells. Because polyploidy is a result of incomplete cytokinesis,[44] the increased hyperploidy of HL0 cells could be due to an elevated rate of cytokinesis failure, possibly connected to overactivity of the actin cytoskeleton as shown previously when the actin regulator WASp is overactive.[45,46] Reed-Sternberg cells originate from failed cytokinesis and re-fusion of HL daughter cells.[47,48] This suggests that the failure of HL0 cells to complete cytokinesis could lead to the formation of giant multinucleated cells similar to Reed-Sternberg cells.

The variable phenotype of the HL1 and HL2 triplets treated for HL in 1985 and 2008, respectively, was at first puzzling. Since all triplets contained the heterozygous deletion of *MKL1* intron 1, we reasoned that whether a cell expresses the healthy *MKL1* allele or the intron 1-deleted allele of *MKL1* must be a stochastic event. Transcription of the *MKL1* gene is quite complex, with several sets of transcripts. The transcriptional start site is in exon 4, placing intron 1 in the 5' untranslated region of *MKL1*. To understand the MKL1-associated phenotype, we took advantage of the bimodal expression of CD11a in HL1 cells to sort out CD11a low and CD11a high cells. CD11a high cells behaved similarly to the control cells, displaying low expression of MKL1, low spreading and proliferation, together with a strong aggregation response. In contrast, CD11a low cells behaved similarly to HL0 cells with high expression of MKL1, decreased aggregation, as well as increased proliferation *in vitro* and tumor formation *in vivo*. We also sorted out the small population of CD11a low cells from control (C1 and C2) cells; however, control CD11a low cells were not stable in culture and started to express CD11a during 17 days of culture. This suggests that the stable CD11a low phenotype in HL0 cells and sorted HL1 cells is associated with increased MKL1 expression. Interestingly, HL Reed-Sternberg cells are characterized by low mRNA expression of CD11a.[49,50] Thus, since the HL0 triplet has not received HL treatment we reason that HL0 cells could represent a pre-HL stage. The presence of CD11a low cells in HL1, who was treated for HL with mustargen, oncovin, procarbazine, prednisone/adriamycin, bleomycin, vinblastine, and dacarbazine in 1985,[20] may indicate *de novo* HL with the CD11a low cells possibly outgrowing the healthy CD11a high cells. With this reasoning, the HL2 patient who received adriamycin, bleomycin, vinblastine and dacarbazine to treat HL in 2008[20] should have predominantly CD11a high cells, assuming that the highly proliferative CD11a low cells would have been mostly eradicated by the HL treatment.

Finally, we investigated whether the HL0 cell phenotype could be reverted by inhibition of MKL1 using the small molecule CCG-1423.[17,18] HL0 cells treated with this MKL1 inhibitor showed decreased expression of MKL1 protein and the MKL1 target gene *SRF*, as well as reduced cell spreading. Importantly, using the MKL1 inhibitor we could revert the hyperproliferation of HL0 cells *in vitro* and also, by intratumoral injections, *in vivo*.

We present here the first example of an intron mutation in *MKL1*, resulting in increased MKL1 expression, increased actin content, decreased aggregation, hyperproliferation, and genomic instability in B cells. Of the triplets' samples, those from HL0 showed the most pronounced difference in both MKL1 expression and activity, as well as in cellular responses when compared to controls. Cells from HL1 and HL2, successfully treated for HL, had a phenotype closer to that of healthy controls. This finding, together with the known role of MKL1 in metastasis[15] and with high mRNA expression of MKL1 in many types of lymphomas, suggests that increased MKL1 expression actively participates in B-cell transformation and the pathogenesis of HL.

Acknowledgments

We are grateful to the family and healthy controls for providing blood samples. We thank Dr Kaisa Lehti, Dr Peter Bergman, and Dr Andreas Lundqvist for valuable input. This work was supported by a postdoctoral fellowship from the Swedish Childhood Cancer Fund and the Swedish Society of Medical Research to JR, an MD-PhD (CSTP) fellowship and a clinical internship (research AT) from Karolinska Institutet to AS, a clinical postdoctoral fellowship from the Swedish Society of Medical Research to HB, a postdoctoral fellowship from Olle Engqvist Byggmästare to MH, a PhD fellowship from Fundação para a Ciência e a Tecnologia to MMSO, funds from the Swedish Medical Society to HB and LSW, Groschinsky Foundation and Åke Wiberg

Foundation to HB and LSW, the Swedish Cancer Society to MB and LSW, as well as the Swedish Research Council, the Swedish Childhood Cancer Fund, Karolinska Institutet, the European Commission 7th Framework Program, Åke Olsson Foundation, Jeansson Foundation, and Bergvall Foundation to LSW. LSW is a Ragnar Söderberg Fellow in Medicine.

References

1. Borchmann S, Engert A. The genetics of Hodgkin lymphoma: an overview and clinical implications. Curr Opin Oncol. 2017;29(5):307-314.
2. Goldin LR, Bjorkholm M, Kristinsson SY, et al. Highly increased familial risks for specific lymphoma subtypes. Br J Haematol. 2009;146(1):91-94.
3. Kanzler H, Kuppers R, Hansmann ML, et al. Hodgkin and Reed-Sternberg cells in Hodgkin's disease represent the outgrowth of a dominant tumor clone derived from (crippled) germinal center B cells. J Exp Med. 1996;184(4):1495-1505.
4. Martin-Subero JI, Klapper W, Sotnikova A, et al. Chromosomal breakpoints affecting immunoglobulin loci are recurrent in Hodgkin and Reed-Sternberg cells of classical Hodgkin lymphoma. Cancer Res. 2006;66(21):10332-10338.
5. Bechtel D, Kurth J, Unkel C, et al. Transformation of BCR-deficient germinal-center B cells by EBV supports a major role of the virus in the pathogenesis of Hodgkin and posttransplantation lymphomas. Blood. 2005;106(13):4345-4350.
6. Mancao C, Altmann M, Jungnickel B, et al. Rescue of "crippled" germinal center B cells from apoptosis by Epstein-Barr virus. Blood. 2005;106(13):4339-4344.
7. Wang DZ, Li S, Hockemeyer D, et al. Potentiation of serum response factor activity by a family of myocardin-related transcription factors. Proc Natl Acad Sci U S A. 2002;99(23):14855-14860.
8. Miralles F, Posern G, Zaromytidou AI, et al. Actin dynamics control SRF activity by regulation of its coactivator MAL. Cell. 2003;113(3):329-342.
9. Cen B, Selvaraj A, Burgess RC, et al. Megakaryoblastic leukemia 1, a potent transcriptional coactivator for serum response factor (SRF), is required for serum induction of SRF target genes. Mol Cell Biol. 2003;23(18):6597-6608.
10. Selvaraj A, Prywes R. Expression profiling of serum inducible genes identifies a subset of SRF target genes that are MKL dependent. BMC Mol Biol. 2004;5:13.
11. Spencer JA, Misra RP. Expression of the serum response factor gene is regulated by serum response factor binding sites. J Biol Chem. 1996;271(28):16535-16543.
12. Hermann MR, Jakobson M, Colo GP, et al. Integrins synergise to induce expression of the MRTF-A-SRF target gene ISG15 for promoting cancer cell invasion. J Cell Sci. 2016;129(7):1391-1403.
13. Ma Z, Morris SW, Valentine V, et al. Fusion of two novel genes, RBM15 and MKL1, in the t(1;22)(p13;q13) of acute megakaryoblastic leukemia. Nat Genet. 2001;28(3):220-221.
14. Mercher T, Coniat MB, Monni R, et al. Involvement of a human gene related to the Drosophila spen gene in the recurrent t(1;22) translocation of acute megakaryocytic leukemia. Proc Natl Acad Sci U S A. 2001;98(10):5776-5779.
15. Medjkane S, Perez-Sanchez C, Gaggioli C, et al. Myocardin-related transcription factors and SRF are required for cytoskeletal dynamics and experimental metastasis. Nat Cell Biol. 2009;11(3):257-268.
16. Muehlich S, Hampl V, Khalid S, et al. The transcriptional coactivators megakaryoblastic leukemia 1/2 mediate the effects of loss of the tumor suppressor deleted in liver cancer 1. Oncogene. 2012;31(35):3913-3923.
17. Evelyn CR, Wade SM, Wang Q, et al. CCG-1423: a small-molecule inhibitor of RhoA transcriptional signaling. Mol Cancer Ther. 2007;6(8):2249-2260.
18. Hayashi K, Watanabe B, Nakagawa Y, et al. RPEL proteins are the molecular targets for CCG-1423, an inhibitor of Rho signaling. PLoS One. 2014;9(2):e89016.
19. Record J, Malinova D, Zenner HL, et al. Immunodeficiency and severe susceptibility to bacterial infection associated with a loss-of-function homozygous mutation of MKL1. Blood. 2015;126(13):1527-1535.
20. Bjorkholm M, Sjoberg J, Nygell UA, et al. Development of Hodgkin lymphoma in homozygotic triplets with constitutional deletion in MKL1. Blood. 2013;121(23):4807.
21. Nagy N, Adori M, Rasul A, et al. Soluble factors produced by activated CD4+ T cells modulate EBV latency. Proc Natl Acad Sci U S A. 2012;109(5):1512-1517.
22. Patarroyo M, Beatty PG, Nilsson K, Gahmberg CG. Identification of a cell-surface glycoprotein mediating cell adhesion in EBV-immortalized normal B cells. Int J Cancer. 1986;38(4):539-547.
23. Gronberg A, Halapi E, Ferm M, Petersson M, Patarroyo M. Regulation of lymphocyte aggregation and proliferation through adhesion molecule CD54 (ICAM-1). Cell Immunol. 1993;147(1):12-24.
24. Rothlein R, Springer TA. The requirement for lymphocyte function-associated antigen 1 in homotypic leukocyte adhesion stimulated by phorbol ester. J Exp Med. 1986;163(5):1132-1149.
25. Merk K, Bjorkholm M, Tullgren O, Mellstedt H, Holm G. Immune deficiency in family members of patients with Hodgkin's disease. Cancer. 1990;66(9):1938-1943.
26. Bjorkholm M, Holm G, Mellstedt H. Persisting lymphocyte deficiences during remission in Hodgkin's disease. Clin Exp Immunol. 1977;28(3):389-393.
27. Marits P, Wikstrom AC, Popadic D, Winqvist O, Thunberg S. Evaluation of T and B lymphocyte function in clinical practice using a flow cytometry based proliferation assay. Clin Immunol. 2014;153(2):332-342.
28. Shumilov A, Tsai MH, Schlosser YT, et al. Epstein-Barr virus particles induce centrosome amplification and chromosomal instability. Nat Commun. 2017;8:14257.
29. Wolf J, Kapp U, Bohlen H, et al. Peripheral blood mononuclear cells of a patient with advanced Hodgkin's lymphoma give rise to permanently growing Hodgkin-Reed Sternberg cells. Blood. 1996;87(8):3418-3428.
30. Verrills NM, Liem NL, Liaw TY, Hood BD, Lock RB, Kavallaris M. Proteomic analysis reveals a novel role for the actin cytoskeleton in vincristine resistant childhood leukemia--an in vivo study. Proteomics. 2006;6(5):1681-1694.
31. Rath N, Olson MF. Rho-associated kinases in tumorigenesis: re-considering ROCK inhibition for cancer therapy. EMBO Rep. 2012;13(10):900-908.
32. Gilles L, Bluteau D, Boukour S, et al. MAL/SRF complex is involved in platelet formation and megakaryocyte migration by regulating MYL9 (MLC2) and MMP9. Blood. 2009;114(19):4221-4232.
33. Smith EC, Thon JN, Devine MT, et al. MKL1 and MKL2 play redundant and crucial roles in megakaryocyte maturation and platelet formation. Blood. 2012;120(11):2317-2329.
34. Hanahan D, Weinberg RA. Hallmarks of cancer: the next generation. Cell. 2011;144(5):646-674.
35. Dorner M, Zucol F, Berger C, et al. Distinct ex vivo susceptibility of B-cell subsets to epstein-barr virus infection according to differentiation status and tissue origin. J Virol. 2008;82(9):4400-4412.
36. Heath E, Begue-Pastor N, Chaganti S, et al. Epstein-Barr virus infection of naive B cells in vitro frequently selects clones with mutated immunoglobulin genotypes: implications for virus biology. PLoS Pathog. 2012;8(5):e1002697.
37. Huang GL, Li BK, Zhang MY, et al. Allele loss and down-regulation of heparanase gene are associated with the progression and poor prognosis of hepatocellular carcinoma. PLoS One. 2012;7(8):e44061.
38. Shaul O. How introns enhance gene expression. Int J Biochem Cell Biol. 2017;91(Pt B):145-155.
39. Baarlink C, Wang H, Grosse R. Nuclear actin network assembly by formins regulates the SRF coactivator MAL. Science. 2013;340(6134):864-867.
40. Cheng X, Yang Y, Fan Z, et al. MKL1 potentiates lung cancer cell migration and invasion by epigenetically activating MMP9 transcription. Oncogene. 2015;34(44):5570-5581.
41. Hu Q, Guo C, Li Y, Aronow BJ, Zhang J. LMO7 mediates cell-specific activation of the Rho-myocardin-related transcription factor-serum response factor pathway and plays an important role in breast cancer cell migration. Mol Cell Biol. 2011;31(16):3223-3240.
42. Yamaguchi H, Condeelis J. Regulation of the actin cytoskeleton in cancer cell migration and invasion. Biochim Biophys Acta. 2007;1773(5):642-652.
43. Hamidi H, Pietila M, Ivaska J. The complexity of integrins in cancer and new scopes for therapeutic targeting. Br J Cancer. 2016;115(9):1017-1023.
44. Nguyen HG, Ravid K. Polyploidy: mechanisms and cancer promotion in hematopoietic and other cells. Adv Exp Med Biol. 2010;676:105-122.
45. Moulding DA, Moeendarbary E, Valon L, Record J, Charras GT, Thrasher AJ. Excess F-actin mechanically impedes mitosis leading to cytokinesis failure in X-linked neutropenia by exceeding Aurora B kinase error cor-

rection capacity. Blood. 2012;120(18):3803-3811.
46. Westerberg LS, Meelu P, Baptista M, et al. Activating WASP mutations associated with X-linked neutropenia result in enhanced actin polymerization, altered cytoskeletal responses, and genomic instability in lymphocytes. J Exp Med. 2010;207(6):1145-1152.
47. Rengstl B, Newrzela S, Heinrich T, et al. Incomplete cytokinesis and re-fusion of small mononucleated Hodgkin cells lead to giant multinucleated Reed-Sternberg cells. Proc Natl Acad Sci U S A. 2013;110(51):20729-20734.
48. Cuceu C, Hempel WM, Sabatier L, Bosq J, Carde P, M'Kacher R. Chromosomal instability in Hodgkin lymphoma: an in-depth review and perspectives. Cancers. 2018;10(4).
49. Schwering I, Brauninger A, Klein U, et al. Loss of the B-lineage-specific gene expression program in Hodgkin and Reed-Sternberg cells of Hodgkin lymphoma. Blood. 2003;101(4):1505-1512.
50. Tiacci E, Doring C, Brune V, et al. Analyzing primary Hodgkin and Reed-Sternberg cells to capture the molecular and cellular pathogenesis of classical Hodgkin lymphoma. Blood. 2012;120(23):4609-4620.

ARTICLE

Identification of a *miR-146b*-Fas ligand axis in the development of neutropenia in T large granular lymphocyte leukemia

Barbara Mariotti,[1*] Giulia Calabretto,[2,3*] Marzia Rossato,[1§] Antonella Teramo,[2,3] Monica Castellucci,[1†] Gregorio Barilà,[2,3] Matteo Leoncin,[2,3] Cristina Vicenzetto,[2,3] Monica Facco,[2,3] Gianpietro Semenzato,[2,3] Flavia Bazzoni,[1,*] and Renato Zambello[2,3,*]

[1]Department of Medicine, Division of General Pathology, University of Verona, Verona; [2]Department of Medicine, Hematology and Clinical Immunology section, University of Padua, Padua and [3]Venetian Institute of Molecular Medicine (VIMM), Padua, Italy

[§]*Present affiliation for MR is: Department of Biotechnology, University of Verona, Verona, Italy;*

[†]*Present affiliation for MC is: Genomics and transcriptomics platform, CPT, University of Verona, Verona, Italy*

**BM, GC, FB and RZ contributed equally to this work.*

Ferrata Storti Foundation

Haematologica 2020
Volume 105(5):1351-1360

ABSTRACT

T large granular lymphocyte leukemia (T-LGLL) is characterized by the expansion of several large granular lymphocyte clones, among which a subset of large granular lymphocytes showing constitutively activated STAT3, a specific $CD8^+/CD4^-$ phenotype and the presence of neutropenia has been identified. Although STAT3 is an inducer of transcription of a large number of oncogenes, so far its relationship with miRNAs has not been evaluated in T-LGLL patients. Here, we investigated whether STAT3 could carry out its pathogenetic role in T-LGLL through an altered expression of miRNAs. The expression level of 756 mature miRNA was assessed on purified T large granular lymphocytes (T-LGLs) by using a TaqMan Human microRNA Array. Hierarchical Clustering Analysis of miRNA array data shows that the global miRNome clusters with CD8 T-LGLs. Remarkably, CD8 T-LGLs exhibit a selective and STAT3-dependent repression of miR-146b expression, that significantly correlated with the absolute neutrophil counts and inversely correlated with the expression of Fas ligand (FasL), that is regarded as the most relevant factor in the pathogenesis of neutropenia. Experimental evidence demonstrates that the STAT3-dependent reduction of miR-146b expression in CD8 T-LGLs occurs as a consequence of miR-146b promoter hypermethylation and results in the disruption of the HuR-mediated post-transcriptional machinery controlling FasL mRNA stabilization. Restoring miR-146b expression in CD8 T-LGLs lead to a reduction of HuR protein and, in turn, of FasL mRNA expression, thus providing mechanistic insights for the existence of a STAT3-miR146b-FasL axis and neutropenia in T-LGLL.

Introduction

T large granular lymphocytes leukemia (T-LGLL) is a rare disease characterized by the abnormal expansion of T large granular lymphocytes (T-LGLs) in the peripheral blood.[1,2] While the aetiology of the disease is still elusive, LGL proliferation is thought to be maintained through an impairment of the apoptotic machinery due to the activation of many survival signals.[3] Among these, JAK/STAT signalling represents one of the most important deregulated pathways in T-LGLL. In particular, leukemic LGLs are equipped with STAT3 constitutively over-expressed and in some cases over-activated.[4,5] Moreover, in 30-40% of patients, STAT3 has been demonstrated to carry hot-spot mutations, likely resulting in STAT3 activation.[6,7] This genetic lesion was also correlated by some authors with increased frequency of neutropenia[5,7,8] which represents the most frequent cause of symptomatic dis-

Correspondence:

FLAVIA BAZZONI
flavia.bazzoni@univr.it

Received: May 3, 2019.

Accepted: August 23, 2019.

Pre-published: August 29, 2019.

doi:10.3324/haematol.2019.225060

Check the online version for the most updated information on this article, online supplements, and information on authorship & disclosures: www.haematologica.org/content/105/5/1351

ease in LGLL patients, often requiring specific therapy. The pathogenesis of neutropenia, although not properly elucidated thus far, seems to be multifactorial. Multiple mechanisms have been postulated, including destruction of mature neutrophils and myeloid progenitors *via* Fas/Fas ligand (FasL). Mechanisms leading to neutropenia are not completely characterized, although we[5] and others[9-12] provided evidence that extremely high concentrations of FasL are detectable in T-LGLL patients suggesting that soluble FasL is involved in this process. We also demonstrated that STAT3 plays a central role in FasL transcription and we showed that high levels of STAT3 activation correlated with high levels of FasL expression in T-LGLL patients.[5] However, the molecular mechanism through which STAT3 regulates FasL production in these patients has not yet been clarified.

Although STAT3 is an inducer of transcription of a large number of oncogenes, its relationship with microRNAs (miRNAs) has not yet been evaluated in T-LGLL patients. As a matter of fact, several miRNAs contribute to normal hematopoietic processes and many miRNAs act both as tumor suppressors and oncogenes in the pathogenesis of hematological malignancies, including acute and chronic leukemias and lymphomas, where they contribute to lymphomagenesis acting in various cellular functions, such as the regulation of cell survival and proliferation.[13,14]

In this study a high throughput quantitative and qualitative analysis of the miRNA expression profile in leukemic LGLs was performed with the aim to investigate the role of miRNAs in clinical and biological features of T-LGLL, thus playing a role in the pathogenesis of neutropenia in T-LGLL patients.

Methods

Patients

Thirty T-LGLL patients and nine age and sex-matched healthy donors were enrolled in the study. Clinical and biological characteristics of patients are summarized in the *Online Supplementary Table S1*. At the time of the study, no patients had received treatment, with a follow-up ranging from 1 to 16 years. LGL proliferation ranged from 48% to 91% of the lymphocyte pool. T-LGLL clonality was demonstrated as previously reported.[15] The Padova Institutional Review Board approved this study and written informed consent in accordance with the Declaration of Helsinki was obtained by each subject.

Cell isolation and culture

T-LGLs were purified from peripheral blood mononuclear cells (PBMC) using the anti-CD57 microbeads (Milteny Biotec), as previously reported.[16] $CD8^+CD57^+$ cells used as control, were obtained from PBMCs of healthy donors by the FACSAria cell sorter (BD biosciences). Purity and viability of cell preparation were both >95%. The LGL phenotype was assessed by flow cytometry. In selected experiments PBMC from T-LGLL patients (2×10^6 cells/mL) were cultured in RPMI1640 (EuroClone) supplemented with 10% FCS (Sigma-Aldrich), 2mM Gln 25mM Hepes, 100 U/mL penicillin and 100 μg/mL streptomycin (EuroClone) in the presence of 2.5 μM 5-aza-2'-deoxycytidine (DAC, Sigma-Aldrich) for three days, 15 μM STATTIC (Shelleckchem) for 24 hours (h) or DMSO (Sigma-Aldrich) as control.

miRNA and Gene-Expression Analysis

RNA was purified from CD57+ cells using the miRCURY RNA Isolation Kit (Exiqon) according to the manufacturer's instructions. High throughput and single miRNA expression were analysed using the TaqMan® Human microRNA Array (Card Set v3.0, Applied Biosystems) and the TaqMan® microRNA Human Assays (Applied Biosystems), respectively, as previously described.[17] Expression of DNMT1, FasL, FasL-Primary Transcript (PT), HuR, GAPDH, pri-miR-146b and RPL32 mRNA was quantified by real-time quantitative PCR (RT-qPCR) as previously described,[18] using specific primer pairs listed in the *Online Supplementary Table S2*.

Methylated DNA Immunoprecipitation (meDIP) assay

Genomic DNA was purified from $CD57^+$ T-LGLs with the AllPrep DNA/RNA/miRNA Universal Kit (Qiagen), according to the manufacturer's instructions and methylated DNA Immunoprecipitation (meDIP) assay was performed as reported by Mohn *et al.*[19] with minor modifications. The methylation levels of miR-146b promoter was analysed by qPCR using specific primers (Invitrogen, Thermo Scientific) listed in the *Online Supplementary Table S2*.

Western blot

T-LGLs ($2.5x10^5$) and Jurkat cells were lysed in Sample Buffer (40mM tris (hydroxymethyl) aminomethane HCl pH6.8, 7.5% glycerol, 1% sodium dodecyl sulphate). Total cell lysates were resolved on SDS-PAGE and transferred onto nitrocellulose (Millipore). The blots were incubated with specific antibodies and detected using the ImageQuant LAS 500 or the Odyssey infrared imaging system (LI-COR Biosciences).

Cell transfection

Jurkat cells (10^6) or freshly purified $CD57^+$ T-LGL (10^7) were transfected with the indicated amount of specific oligonucleotide using the Amaxa Nucleofector (Lonza) and the Ingenio Electroporation Solution (Mirus Bio).

Enzyme-linked immunosorbent assay (ELISA)

Secreted FasL in plasma were determined by ELISA kit (RayBiotech, Georgia, USA), following the manufacturer's recommendations.

Statistics

Statistical evaluation was performed by using the Mann-Whitney U-test, the Wilcoxon signed-rank test or Student *t*-test, as appropriate, with α set to 0.05. Correlation coefficient was determined using the Spearman Rank Correlation.

For detailed information on the materials and methods used, see the *Online Supplementary Material and Methods*.

Results

Characterization of T-LGL miRNome

To identify miRNAs potentially involved in T-LGLL, the miRNA pattern of expression was investigated in CD57+ cells purified from six patients affected by T-LGLL and three healthy donors, using Taq-Man Human microRNA Array. Unsupervised Hierarchical Clustering Analysis (HCA) of normalized array data led to the identification of two clusters: cluster A including LGL1, LGL3, LGL5 and LGL9, and cluster B including LGL10, LGL17 together with the three healthy donors (HD1, HD2, HD4), (Figure 1A). Interestingly, according to the characterization of the T-LGLL patients enrolled in the study, LGL samples in cluster A share the $CD4^-CD8^+CD16^+CD56^-CD57^+$ (CD8 T-LGLs) immunophenotype, while LGLs in cluster B share

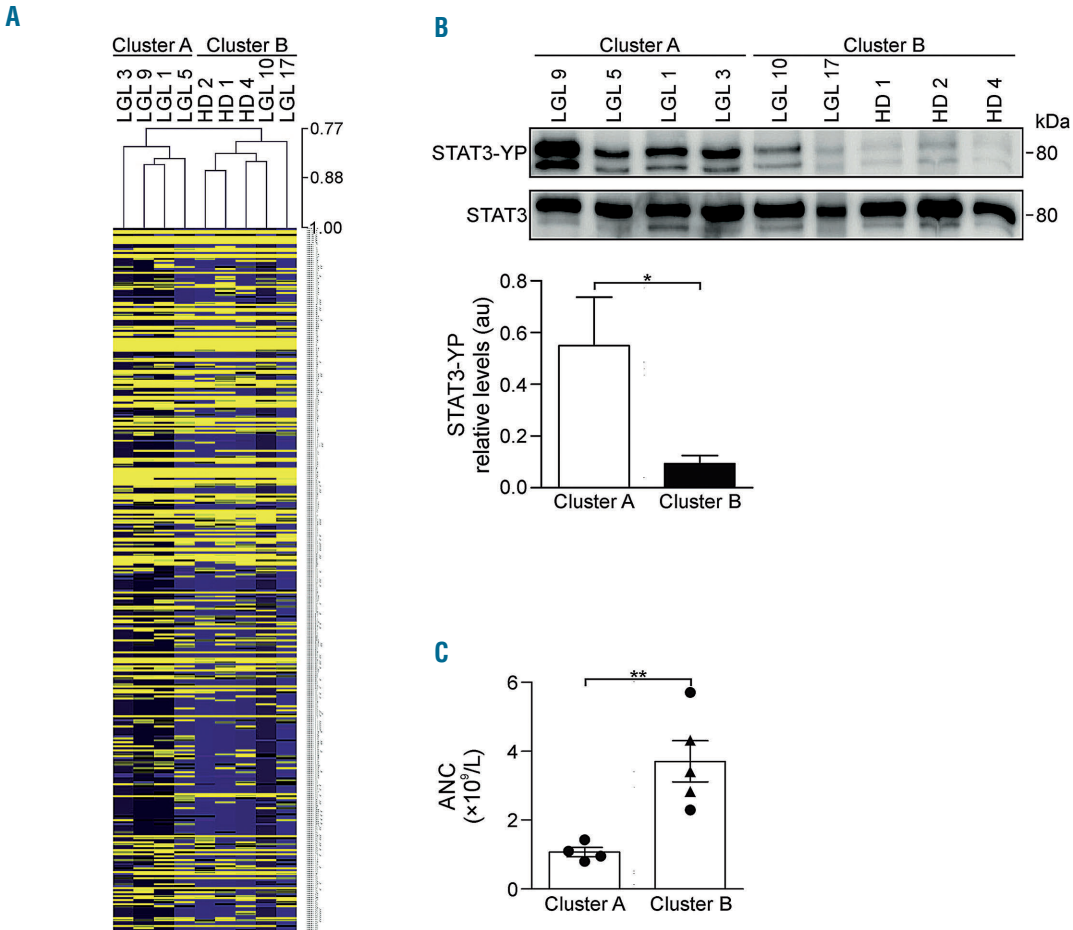

Figure 1. miRNome of T-LGLL patients correlates with STAT3 phosphorylation. Peripheral blood CD57⁺ T cells from T large granular lymphocyte leukemia (T-LGLL) patients (n=6) and healthy donors (HD, n=3) were collected. (A) Heatmap representation of the 756 miRNAs analyzed using the TaqMan microRNA array as described in the *Methods*. Results are expressed as arbitrary units (au) using U6 as reference control. (B) Whole-cell extracts (250x10³ cells) purified from the same cells as in (A) were loaded on gels and analyzed for STAT3-YP and total STAT3 expression level. Quantification of the relative normalized STAT3-YP protein levels are reported as arbitrary units (au) below the Western blot. Mean ± standard error of the mean (SEM) is shown, **P*<0.05 by unpaired *t*-test. (C) Absolute neutrophil counts in each CD8 and CD4 T-LGLL patient (circle) and HD (triangle). Mean ± SEM is shown. ***P*<0.01 by unpaired t-test. Patients analyzed in each panel are specified in the *Online Supplementary Table S5*.

the $CD4^+CD8^+CD16^-CD56^+CD57^+$ (CD4 T-LGLs) immunophenotype (*Online Supplementary Table S1*). We have recently shown that $CD8^+CD16^+CD56^-CD57\pm$ immunophenotype identifies a subset of patients characterized by the presence of STAT3 mutation and/or activation and neutropenia, whereas STAT3 mutations are lacking in CD4 T-LGLL patients, usually displaying normal neutrophil counts.[5] Confirming our previous observation, high levels of STAT3-YP, detected by Western blot analysis (Figure 1B), characterized the CD8 T-LGLL patients, three of whom carry STAT3 mutations (*Online Supplementary Table S1*). Conversely, no STAT3 mutations (*Online Supplementary Table S1*) nor constitutive activation (Figure 1B) were detected in CD4 T-LGLs. No variation in the total STAT3 levels between CD8 and CD4 samples was detected (Figure 1B). Moreover, and consistent with our previous observation, CD8 T-LGLL patients are characterized by a significantly (P=0.0066) different absolute neutrophil counts (ANC) as compared to CD4 T-LGLL patients, that shows normal neutrophil counts (Figure 1C). Taken together, our data show that the global miRNome clusters with STAT3-activated/CD8 phenotype, that is, in turn, characterized by neutropenia.

miR-146b is differentially expressed in CD8 *versus* CD4 T-LGLs and inversely correlates with neutropenia

On the basis of the above correlation between the global mature miRNA expression profile and the presence of activated STAT3 (Figure 1), and taking into account that a pathogenic link between CD8 phenotype and STAT3 activation has been demonstrated,[5] we hypothesized that a STAT3 activation-dependent, CD8-specific miRNAs expression pattern is in place. To get insights into this immunophenotype-specific miRNome, miRNAs expressed in CD8 and CD4 T-LGLs were subjected to differential expression analysis. miRNAs showing threshold cycle (Ct) value <32, and Fold Change (FC) value >2 or <0.5 were considered as differentially modulated. Accordingly, twenty-four miRNA emerged as up-regulated and only one miRNA, namely miR-146b, as down-regulated in a statistically significant manner (P<0.05) in CD8 as compared to CD4 T-LGLs (*Online Supplementary Figure S1* and *Online Supplementary Table S3*).

Based on our recent data indicating that high level of STAT3 activation correlates not only with CD8 T-LGLs phenotype, but also with the presence of symptomatic disease, mostly as a consequence of neutropenia,[5] all the miRNAs differentially expressed in CD8 and CD4 T-LGL (*Online Supplementary Table S3*) were analysed for correlation with the ANC. Correlation analysis highlighted only two miRNAs, namely miR-630 and miR-146b, whose expression correlated with ANC (P=-0.886, P=0.033 and P=0.866, P=0.030, respectively) and simultaneously with the levels of STAT3-YP (P=1.00, P=0.003 and P=-0.866, P=0.033, respectively) (*Online Supplementary Table S4*). None of the remaining differentially modulated miRNA correlated with the absolute neutrophil count in a statistically significant manner (*Online Supplementary Table S4*). RT-qPCR single assay on additional T-LGLL patients confirmed the downregulation of miR-146b expression in CD8 T-LGLs, compared to CD4 T-LGLs (P=0.018) or to T lymphocytes from healthy donors (P=0.024) (Figure 2A). Accordingly, miR-146b was found to inversely correlate simultaneously with the levels of activated STAT3 (P=-0.846, P=0.0005) and with ANC (P=0.707, P=0.0012) (Figure 2B). Consistently, in the additional T-LGLL patients a significant correlation between STAT3 activation and neutropenia was confirmed as well (P=-0.867, P=0.0003) (Figure 2B, right panel). On the contrary, miR-630 was confirmed as differentially expressed in CD4 T-LGLs as compared to CD8 T-LGLs, but the correlation with ANC was not validated (*not shown*).

To gain insights into the cause-effect relationship between the degree of STAT3 activation and the lack of miR-146b expression, CD8 T-LGLs were incubated with non-toxic doses of the STAT3 inhibitor STATTIC and the level of miR-146b expression was analyzed. Figure 2C shows that blocking STAT3 activity in CD8 T-LGLs unleashed miR-146b transcription, thus demonstrating that suppression of miR-146b expression in CD8 T-LGLs is secondary to constitutive STAT3 activation.

STAT3 is a well-known transcriptional activator for many genes,[20] and it has also been reported to inhibit gene expression by promoting methylation of the target genes promoter.[21-23] In normal tissues STAT3 is reported to activate miR-146b transcription.[24,25] However, in several systems miR-146b promoter methylation has been shown to prevent miR-146b expression, even in the presence of constitutively activated STAT3.[26,27] According to the publically available methylome data (*https://genome-euro.ucsc.edu/cgi-bin/hgTracks?db=hg19&lastVirtModeType=default&lastVirtModeExtraState=&virtModeType=default&virtMode=0&nonVirtPosition=&position=chr10%3A104196181104196428&hgsid=230688991_Xz5zjxAjb58tIT5oL9i5MkaweCLp*), four cytosine located upstream (-570bp, -63bp, -56bp, -26bp) and two located downstream (-71bp, and -273bp) the miR-146b TSS (*Online Supplementary Figure S2*) have been identified as differentially methylated in different cell lines. On these bases, we analyzed the level of miR-146b promoter methylation in CD8 and CD4 T-LGLs that are characterized by the presence or absence of activated STAT3, respectively. Our results showed a significantly higher level of 5meC in the regions -687bp/-496bp (+141.21%, P<0.01) and -149bp/+98bp (+58.46%, P<0.05) upstream miR-146b TSS in CD8 T-LGLs compared to CD4 T-LGLs (Figure 3A). As a control, methylation of the region downstream (+44bp/+315bp) miR-146b TSS in CD8 and CD4 T-LGL was comparable (Figure 3A). Inhibition of methyl-transferase activity with 5-aza-2-deoxycytidine (DAC) restored the expression of the miR-146b primary transcript (pri-miR-146b) in CD8 T-LGLs (Figure 3B), further proving that miR-146b promoter methylation prevents miR-146b expression in CD8 T-LGLs. Remarkably, STAT3 inhibition led to a statistically significant reduction of the level of DNMT1 expression, thus suggesting that constitutive STAT3 activation may lead to miR-146b promoter methylation (Figure 3B, left panel). Collectively, these data suggest a cause-effect link between the lack of miR-146b expression and constitutive STAT3-activation in CD8 T-LGLs.

FasL mRNA-stabilizing protein HuR is target of miR-146b

To gain insights into the molecular mechanisms underlying the correlation between miR-146b expression and ANC (Figure 2B, central panel), we focused our subsequent analysis on FasL. In fact, increased release of FasL has long been reported as one of the most relevant factor in the pathogenesis of neutropenia in LGLL patients.[9,12,28]

According to our published data,[5] RT-qPCR analysis showed that FasL mRNA expression correlates with the degree of STAT3 activation (P=0.762, P=0.0368) (Figure 4A) and simultaneously inversely correlates with ANC (P=-0.727, P=0.0096) (Figure 4B). Most importantly, an inverse correlation between miR-146b and FasL mRNA expression (Figure 4C) and the release of soluble FasL (sFasL) (Figure 4D) were detected. Consistently, FasL mRNA expression was higher in CD8 T-LGLL patients (MNE 0.0306±0.0067) compared to the non-neutropenic patients belonging to the CD4 T-LGLL subset (MNE 0.0119±0.0026, P=0.02) (Figure 4E). Interestingly, no difference in the level of FasL primary transcript (FasL-PT) expression between CD8 and CD4 T-LGLs was observed (Figure 4E), suggesting that a mechanism controlling FasL expression at a post-transcriptional level is defective in CD8 T-LGLL subset, that therefore display higher levels of FasL mRNA as compared to CD4 T-LGLL subset.s

In order to demonstrate that miR146b and FasL expression were causally linked, miR-146b was overexpressed in Jurkat and the level of FasL mRNA was analyzed 48 h post transfection. miR-146b-overexpressing cells have reduced levels of FasL mRNA (MNE $2\times10^{-5}\pm5.77\times10^{-6}$) compared to cells transfected with a scramble control miRNA (MNE $3.67\times10^{-5}\pm6.67\times10^{-6}$) (Figure 5A), suggesting a role of miR-146b in the regulation of FasL expression. Nevertheless, in silico miR-target prediction analysis performed by seven different target prediction software (microT4, miRanda, Pictar2, PITA, RNA22, miRWalk and TargetScan) did not identify FasL among the putative miR-146b target genes, thus suggesting that miR-146b eventually affects FasL expression indirectly, by targeting genes involved in FasL mRNA stability. Among the sixteen genes retrieved as putative miR-146b targets commonly predicted by all software only one, namely the ribonucleoprotein Human Antigen R (HuR, also known as ELAVL1), plays a well-

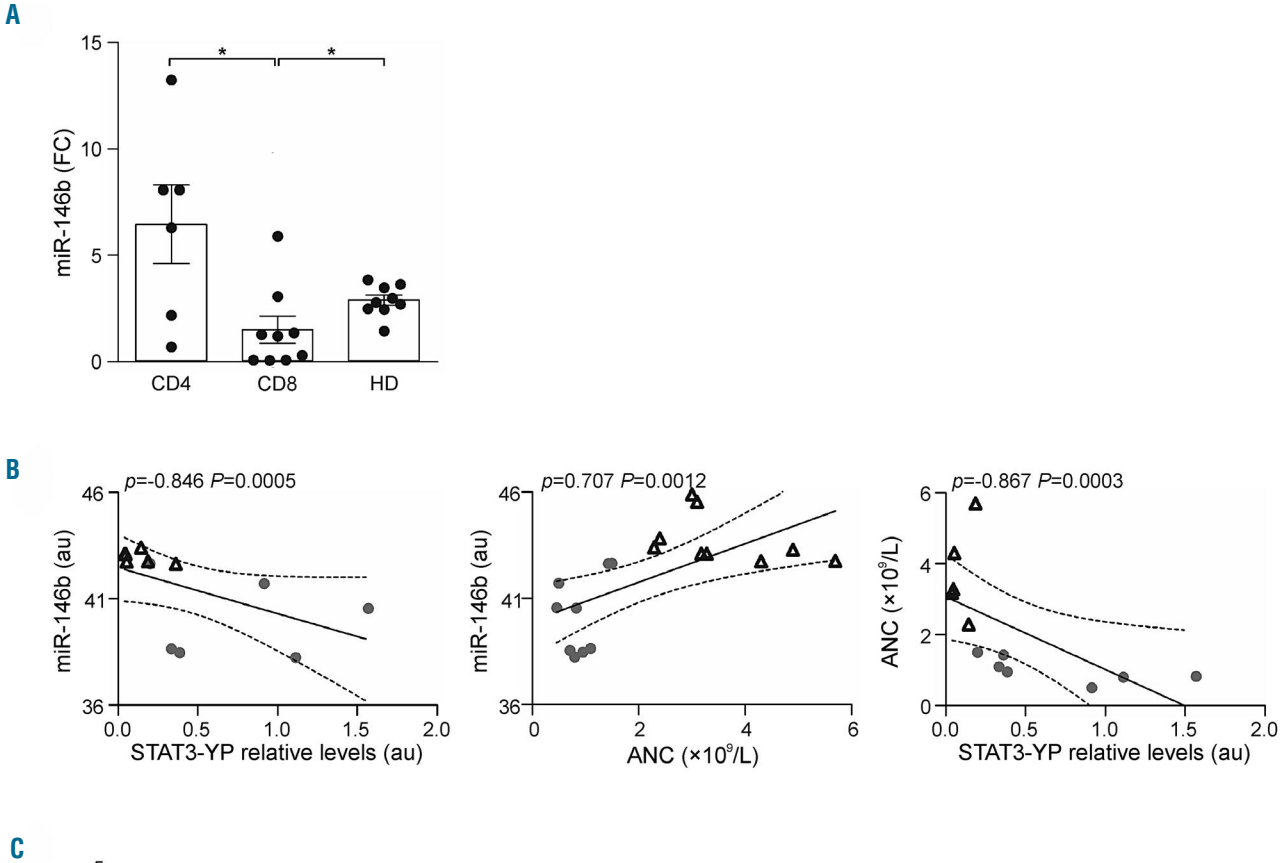

Figure 2. STAT3-dependent inhibition of *miR-146b* expression in CD8 T large granular lymphocytes. (A) miR-146b expression level in each CD8 (n=9) and CD4 (n=6) T large granular lymphocytes (T-LGLs) as well as in HD (n=9) together with mean±standard error of the mean (SEM) are shown. *P<0.05 by Kruskal-Wallis tests. (B) Correlation analysis between miR-146b expression and STAT3-YP (left, n=12), miR-146b expression and absolute neutrophil count (ANC) (central, n=18), and between ANC and STAT3-YP levels (right, n=12). Grey circles identify CD8 T-LGLs, empty triangles identify CD4 T-LGLs. miR-146b expression analyzed in real-time quatitative PCR (RT-qPCR) is reported as arbitrary units after U6 normalization. The relative STAT3-YP protein levels, normalized for total STAT3, are reported as arbitrary units (au). ANC is reported as cell×10^9/L. Spearman correlation coefficient (p) and P-values are reported. (C) CD8 T-LGLs were cultured for 24 hours (h) in presence of 15 μM STATTIC or DMSO as control (n=7). miR-146b primary transcript (pri-miR-146b) expression, analyzed by RT-qPCR, is reported as Fold Induction (FI) relative to DMSO treated cells, after RPL32 normalization. Mean ± SEM are shown. ***P<0.001 by Wilcoxon signed-rank. Patients analyzed in each panel are specified in the *Online Supplementary Table S5*.

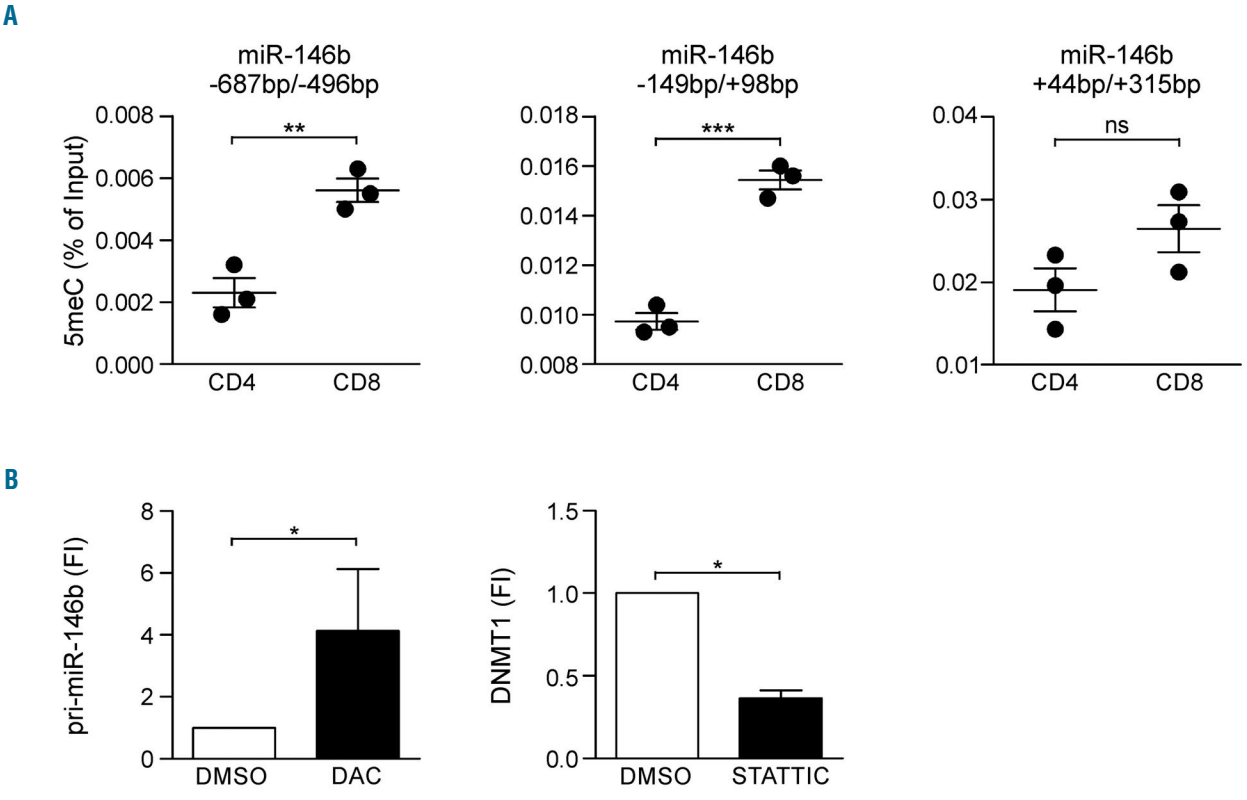

Figure 3. Promoter methylation prevents *miR-146b* expression in CD8 T large granular lymphocytes. (A) The methylation level of -687/-496, -149/+98 miR-146b promoter region and +44/+315 downstream region was analyzed by meDIP assay with anti-5meC antibody (Ab) in CD4 (n=3) and CD8 (n=3) T large granular lymphocyte leukemia (T-LGLs). Single value and mean±standard error of the mean (SEM) are reported as percentage over input. ***P*<0.01, ****P*<0.001, not significant (ns) *P*>0.05 by unpaired t-test. (B) PBMCs from CD8 T-LGLL patients were cultured in presence of 2.5 μM 5-aza-2'-deoxycytidine (DAC) for three days (left) or 15 μM STATTIC for 24 hours (h) (right). pri-miR-146b (left) and DNMT1 (right) expression was analyzed. Data are expressed as Fold Induction (FI) relative to the untreated condition (DMSO). Mean±SEM of six (left panel) and seven (right panel) independent experiments is shown. **P*<0.05, by Wilcoxon signed-rank test. Patients analyzed in each panel are specified in the *Online Supplementary Table S5.*

defined role in mRNA stabilization, and has been reported to be absolutely required for FasL expression in T lymphocytes.[29] Moreover, the potential miR-146b binding site in the 3' UTR of HuR (*Online Supplementary Figure S3*) has been demonstrated to be functional by 3'UTR reporter assay.[30,31] Consistently, overexpression of miR-146b in Jurkat cells led to a reduction of the intracellular HuR protein levels (-34.05±3.74%, n=2) (Figure 5B). Likewise, silencing HuR with a specific HuR siRNA caused a parallel reduction of FasL mRNA expression (Figure 5C), thus providing further evidence for the causal link between miR-146b-mediated reduction of the FasL mRNA-stabilizing protein HuR and the consequent decrease of FasL mRNA. Most importantly, restoring miR-146b expression in purified CD8 T cells from LGLL patients caused a reduction of HuR mRNA expression (Figure 6A), thus validating HuR as endogenous miR-146b target in primary CD8 T-LGLs as well. Concurrently, FasL mRNA, but not FasL primary transcript, expression was reduced (Figure 6A), thus demonstrating that miR-146b-mediated reduction of HuR protein post-transcriptionally controls FasL expression. To ascertain that HuR protein expression inversely correlates with the levels of endogenous miR-146b expression, the intracellular levels of HuR protein in CD8 and CD4T-LGLs were examined. Remarkably, endogenous HuR protein was detected in CD8 T-LGLs, that express low levels of miR-146b, at levels significantly higher (*P*=0.003) than those detected in miR-146b-expressing CD4 T-LGLs (Figure 6B). Collectively, these data show that in CD8 T-LGLs constitutively activated STAT3 leads to the loss of miR-146b, that in turn unleashes the translation of HuR protein. As a consequence, HuR stabilizes FasL mRNA and increases FasL production, causing, in turn, neutropenia.

Discussion

MicroRNAs are regarded as important gene expression regulators often involved in the pathogenesis of a variety of conditions such as cancer and autoimmunity. In this study, by exploring a relevant number of miRNAs, we report the first characterization of a restricted pattern of miRNAs differentially expressed in T-LGLL patients. Unsupervised hierarchical clustering analysis identified a correlation between the miRNA expression profile and individual T-LGL subset, characterized by a specific $CD8^+$ phenotype, by high levels of constitutive STAT3 phosphorylation and by the presence of specific clinical features. Noticeably, miRNA expression correlates mostly with STAT3 activation status, rather than with the presence of STAT3 mutations. Several authors suggested a pathogenic

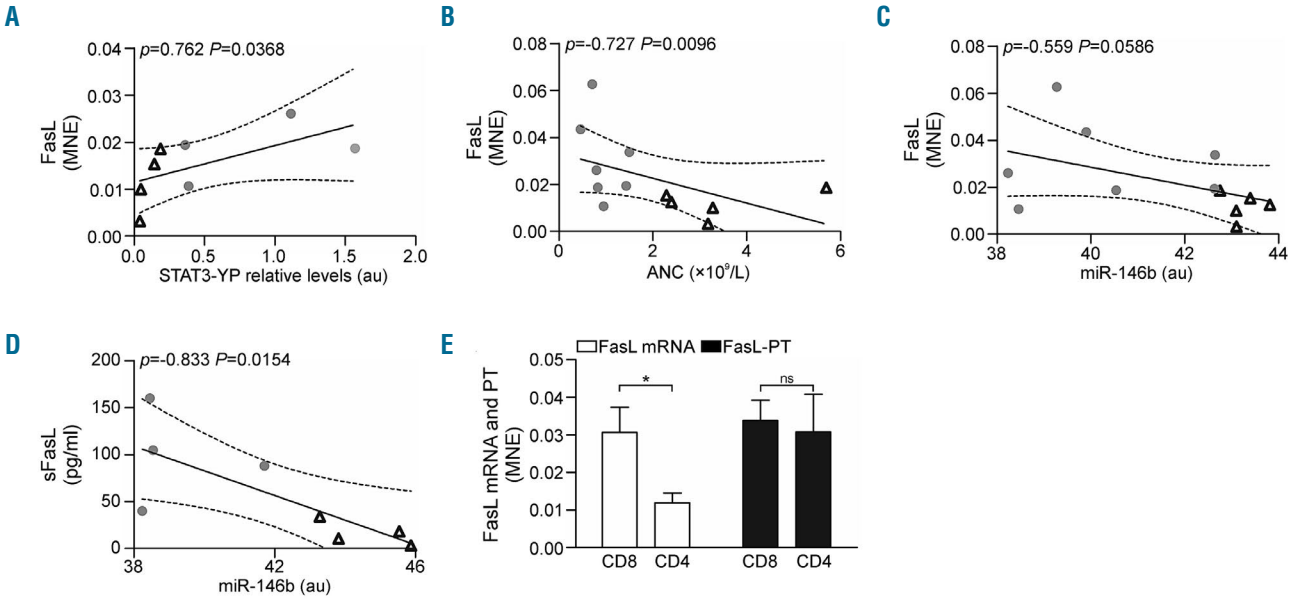

Figure 4. *miR-146b* controls Fas ligand mRNA expression targeting HuR. Correlation analysis between Fas ligand (FasL) mRNA expression and STAT3-YP levels (A; n=8), FasL mRNA expression and ANC (B; n=12), FasL mRNA expression and miR-146b expression levels (C; n=12) and soluble FasL (sFasL) and miR-146b expression levels (D; n=8). FasL mRNA is expressed as MNE relative to GAPDH, while miR-146b is expressed as au after U6 normalization. ANC is reported as cellx10^9/L and sFasL is expressed in pg/mL. Spearman correlation coefficient (*p*) and *P* are reported. (E) FasL mRNA and FasL primary transcript (PT) were analyzed in CD8 (n=7) and CD4 (n=5) T-LGLs by real-time quatitative PCR (RT-qPCR). Data are expressed as MNE relative to GAPDH. Data are reported as mean ± standard error of the mean (SEM). **P*<0.05, ns, not significant by Mann-Whitney *U*-test. Grey circles identify CD8 T-LGLs, empty triangles identify CD4 T-LGLs. Patients analyzed in each panel are specified in the *Online Supplementary Table S5*.

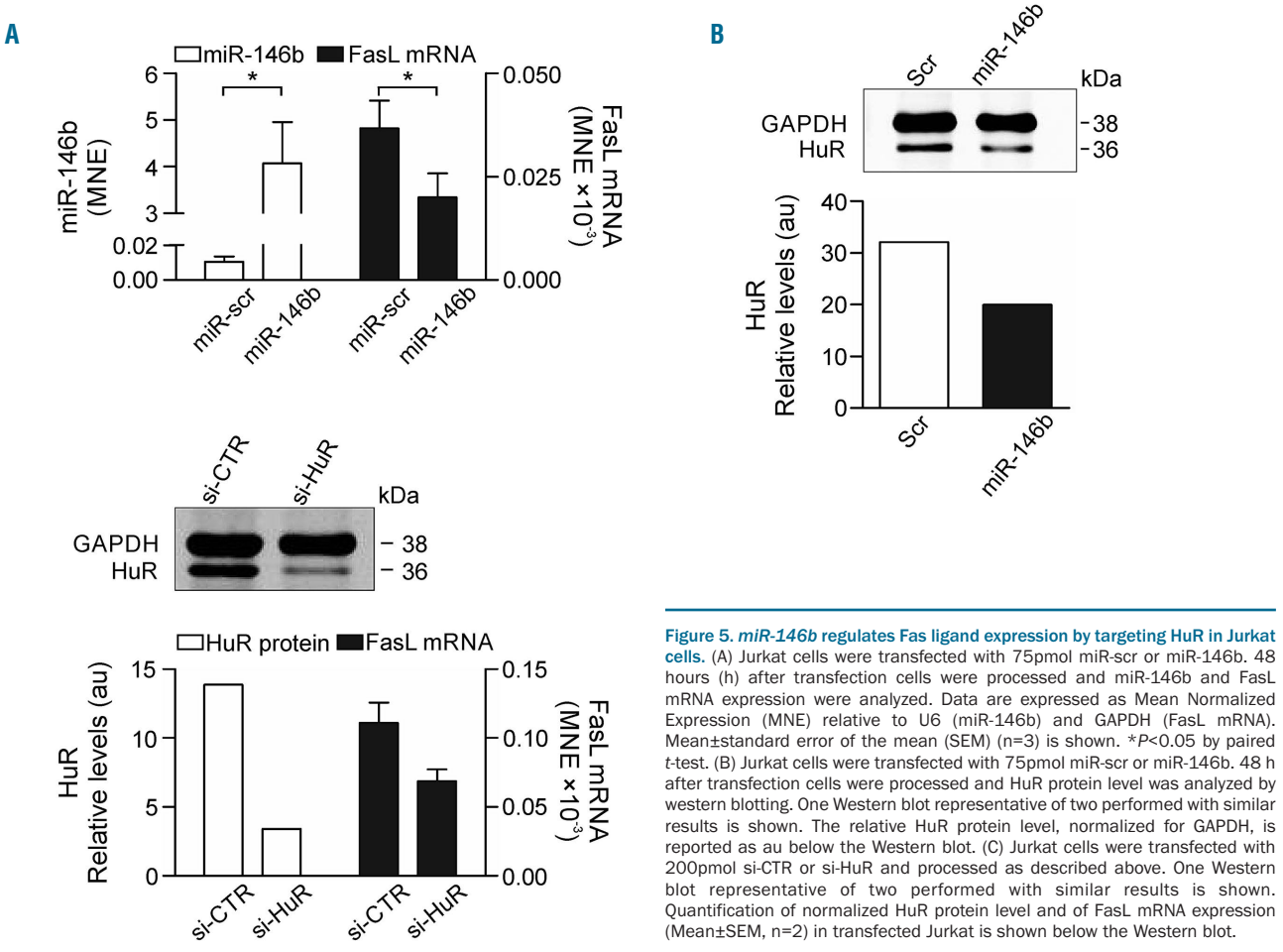

Figure 5. *miR-146b* regulates Fas ligand expression by targeting HuR in Jurkat cells. (A) Jurkat cells were transfected with 75pmol miR-scr or miR-146b. 48 hours (h) after transfection cells were processed and miR-146b and FasL mRNA expression were analyzed. Data are expressed as Mean Normalized Expression (MNE) relative to U6 (miR-146b) and GAPDH (FasL mRNA). Mean±standard error of the mean (SEM) (n=3) is shown. **P*<0.05 by paired *t*-test. (B) Jurkat cells were transfected with 75pmol miR-scr or miR-146b. 48 h after transfection cells were processed and HuR protein level was analyzed by western blotting. One Western blot representative of two performed with similar results is shown. The relative HuR protein level, normalized for GAPDH, is reported as au below the Western blot. (C) Jurkat cells were transfected with 200pmol si-CTR or si-HuR and processed as described above. One Western blot representative of two performed with similar results is shown. Quantification of normalized HuR protein level and of FasL mRNA expression (Mean±SEM, n=2) in transfected Jurkat is shown below the Western blot.

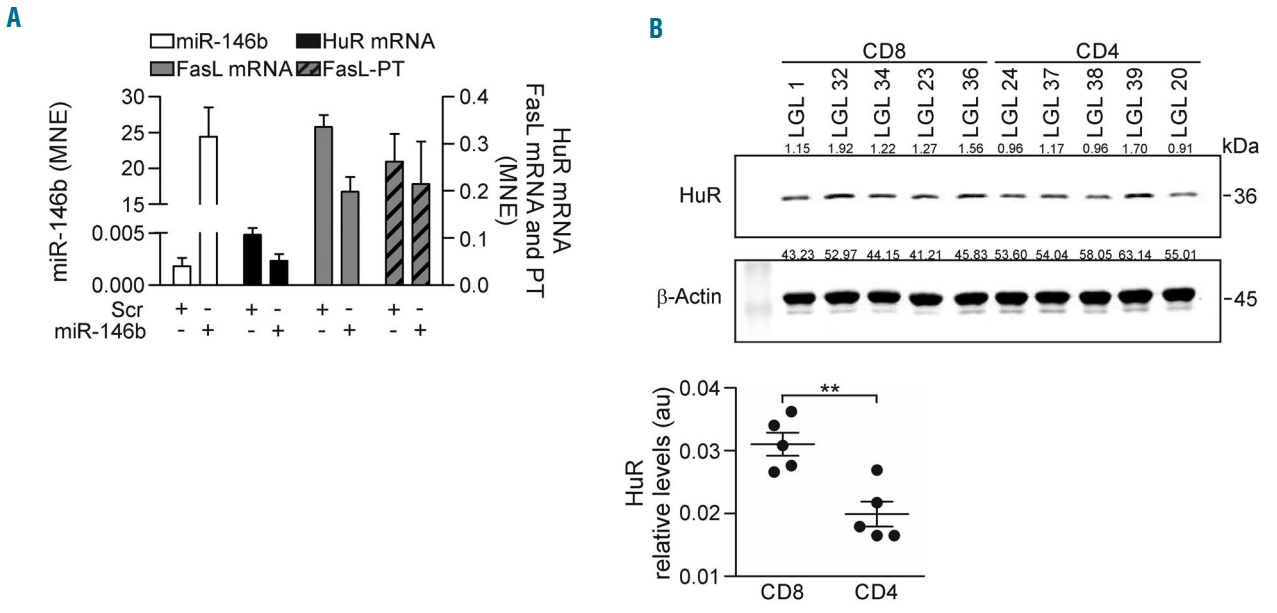

Figure 6. HuR is the endogenous *miR-146b* target gene in CD8 T large granular lymphocytes. (A) CD8 T large granular lymphocytes (T-LGL) were transfected with 200 pmol miR-scr or miR-146b. 24 hours (h) after transfection cells were processed and miR-146b, HuR mRNA, FasL mRNA and primary transcript (PT) expression were analyzed by real-time quatitative PCR (RT-qPCR). Data are expressed as MNE relative to U6 (miR-146b) and RPL32 (HuR, FasL mRNA and PT). Mean±standard error of the mean (SEM) of two independent experiments is shown. (B) HuR protein level was analyzed by Western blot as described in the Methods in CD8 (n=5) and CD4 (n=5) whole-cell extracts (15 μg). Normalized HuR protein levels are reported as arbitrary units (au) below the Western blot. **P*<0.01 by unpaired *t*-test. Patients analyzed in each panel are specified in the *Online Supplementary Table S5*.

role for STAT3 mutations in this disease.[6,7] However these mutations, mostly of the activating type, involve a variable percentage of pathological clones and in many cases are present in a very low percentage of LGL.[32] Our results point to the role of STAT3 activation as the dominant factor in the pathogenesis of the disease and in the induction of a specific miRNA profile. These findings are consistent with recent data from our lab indicating a correlation between STAT3 activation, phenotypic pattern of proliferating LGLs and the presence of symptomatic disease, mostly characterized by neutropenia.[5]

The mechanism sustaining neutropenia in LGLL patients still remains poorly clarified. Since infiltration of pathological LGLs usually play only a marginal role in the pathogenesis of neutropenia, soluble factors have been reported to be the more relevant players in this feature. Among them, FasL has been detected at very high concentrations in LGLL patients.[9,12,28] In particular, a significant increase in FasL mRNA and protein expression was reported in patients with $CD8^+CD16^+CD56^-$ phenotype.[5,9-12] Consistently, we also found that the CD8 T-LGL population under investigation is characterized by higher levels of FasL expression. Comparative analysis of the differentially expressed miRNAs within different T-LGL subsets allowed us to identify miR-146b as a unique miRNA. In fact, miR-146b expression is decreased in CD8 T-LGLL, that is distinguished from the CD4 T-LGLL phenotype by high levels of constitutive STAT3 activation. Moreover, miR-146b expression inversely correlates with the levels of STAT3 tyrosine phosphorylation, with neutropenia and concurrently with FasL expression, suggesting the existence of a STAT3-miR146b-FasL axis in T-LGL leukemia. Inhibition of constitutively activated STAT3 by STATTIC in CD8 T-LGLL patients increased miR-146b expression, thus providing experimental evidence for a mechanistic link between constitutively activated STAT3 and inhibition of miR-146b expression in CD8 T-LGLs. This finding is in line with data showing that induction of miR-146b expression by STAT3 occurs under normal physiological conditions only in non-transformed cells, but is lost in malignancy, mostly has a consequence miR-146b promoter methylation, that prevents miR-146b expression even in the presence of constitutively activated STAT3.[26,27] Here we provide the first evidence of miR-146b promoter methylation at the expected sites, thus pointing that a similar mechanism might also take place in CD8 T-LGLL. Inhibition of this process using DAC restored miR146b levels. Moreover, a direct role of activated STAT3 in inducing miR-146b promoter methylation, through regulating expression of DNA methyltransferase 1 (DNMT1) has been demonstrated in solid tumors[27] and in malignant T lymphocytes.[33] Similarly, we show that inhibition of constitutively active STAT3-YP reduces the expression of DNMT1, thereby providing a functional and mechanistic link between activation of STAT3 signaling pathway and its epigenetic control. Interestingly, a role for epigenetic mechanisms taking place in chronic LGL proliferations has been already reported by Caligiuri *et al.* in T-LGLL[34] and by our group in CLPD-NK,[35] and our data contribute to unravel the machineries differently activated in each subsets of patients (i.e. $CD8^+$ *vs.* $CD4^+$ LGLL) with relevant clinical impact.

Restoration of miR-146b expression in Jurkat cells and, most importantly, in patients CD8 T-LGLL, resulted in a significant reduction of the FasL mRNA expression level, which occurs in the absence of modification of the FasL primary transcript expression. Collectively, these data indicate that miR-146b affects FasL expression at a post-

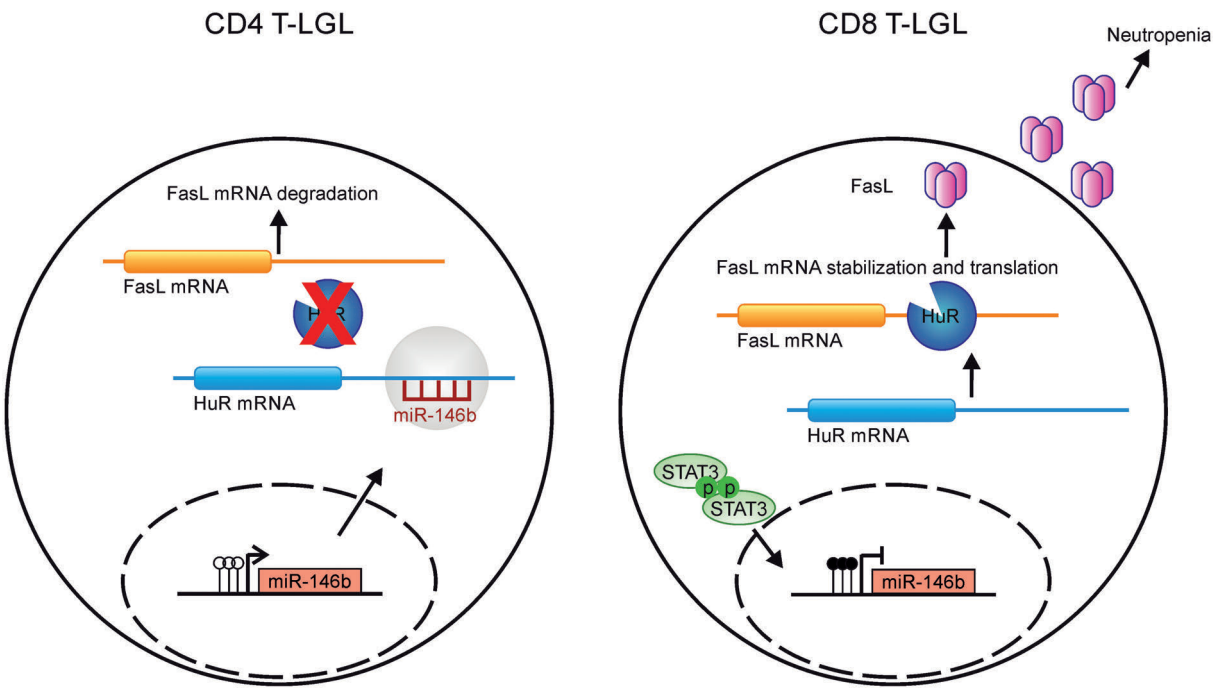

Figure 7. Schematic representation of the pathogenic link between constitutively active STAT3, defective *miR-146b* expression and Fas ligand-mediated neutropenia, that specifically characterizes the CD8 subset of large granular lymphocyte leukemia. Methylation status of miR-146b promoter is represented as circles: empty circles mean not methylated cytosine, while black circles represent methylated cytosine.

transcriptional level. Nevertheless, in silico miR-target prediction analysis did not identify FasL among the putative miR-146b target genes, thus suggesting that miR-146b eventually affects FasL expression indirectly, by targeting genes involved in FasL mRNA stability. In fact, we demonstrated that the intracellular mRNA level of HuR (one of the sixteen genes retrieved as putative miR-146b targets independently predicted by seven miRNA-target prediction software) is affected by miR-146b over-expression. HuR, a ubiquitously expressed member of the HuR family of RNA-binding proteins, has a known role in mRNA stabilization and has been reported to be associated to the ARE-containing 3'UTR of FasL mRNA, which is mandatory for its expression.[29,36] Remarkably, HuR has been experimentally validated as miR-146b target genes in glioma stem cells[31] and endothelial cells,[30] and the predicted miR-146b seed region located in the 3'UTR of HuR mRNA has been demonstrated to be functional.[30,31] According to these published data, restoration of miR-146b in CD8 T-LGLs decreases the levels of HuR mRNA and, consistently, of FasL. Noticeably, a statistically significant difference in the levels of endogenous HuR protein between CD8 and CD4 T-LGLs is detectable. The suggested pathogenetic link between constitutively active STAT3, defective miR-146b expression and neutropenia, that specifically characterizes the CD8 subset of LGLL, is schematically shown in Figure 7. In conclusion, even though the lack of miR-146b expression may have additional effects on the development and progression of CD8 T-LGL leukemia, in this study we convincingly demonstrated that a STAT3-dependent abrogation of miR-146b expression plays a direct role in the development of neutropenia reported in a subset of LGLL patients, representing a potential target for individualized therapeutic approach.

Funding

The authors have been supported by AIRC (Milan), by Università degli Studi di Padova, Progetti di Ateneo, by Fondo Unico per la Ricerca (BAZZONI-FUR) and by Fondazione CARIPLO (2015-0584).

References

1. Lamy T, Moignet A, Loughran TP, Jr. LGL leukemia: from pathogenesis to treatment. Blood. 2017;129(9):1082-1094.
2. Semenzato G, Zambello R, Starkebaum G, Oshimi K, Loughran TP, Jr. The lymphoproliferative disease of granular lymphocytes: updated criteria for diagnosis. Blood. 1997;89(1):256-260.
3. Leblanc F, Zhang D, Liu X, Loughran TP. Large granular lymphocyte leukemia: from dysregulated pathways to therapeutic targets. Future Oncol. 2012;8(7):787-801.
4. Epling-Burnette PK, Zhong B, Bai F, et al. Cooperative regulation of Mcl-1 by Janus kinase/stat and phosphatidylinositol 3-kinase contribute to granulocyte-macrophage colony-stimulating factor-delayed apoptosis in human neutrophils. J Immunol. 2001;166(12):7486-7495.
5. Teramo A, Barila G, Calabretto G, et al. STAT3 mutation impacts biological and clinical features of T-LGL leukemia. Oncotarget. 2017;8(37):61876-61889.
6. Jerez A, Clemente MJ, Makishima H, et al. STAT3 mutations unify the pathogenesis of chronic lymphoproliferative disorders of NK cells and T-cell large granular lymphocyte leukemia. Blood. 2012;120(15):3048-3057.
7. Koskela HL, Eldfors S, Ellonen P, et al. Somatic STAT3 mutations in large granular

lymphocytic leukemia. N Engl J Med. 2012; 366(20):1905-1913.
8. Qiu ZY, Fan L, Wang L, et al. STAT3 mutations are frequent in T-cell large granular lymphocytic leukemia with pure red cell aplasia. J Hematol Oncol. 2013;6:82.
9. Lamy T, Liu JH, Landowski TH, Dalton WS, Loughran TP, Jr. Dysregulation of CD95/CD95 ligand-apoptotic pathway in CD3(+) large granular lymphocyte leukemia. Blood. 1998;92(12):4771-4777.
10. Liu JH, Wei S, Lamy T, et al. Chronic neutropenia mediated by fas ligand. Blood. 2000;95(10):3219-3222.
11. Perzova R, Loughran TP, Jr. Constitutive expression of Fas ligand in large granular lymphocyte leukaemia. Br J Haematol. 1997; 97(1):123-126.
12. Tanaka M, Suda T, Haze K, et al. Fas ligand in human serum. Nat Med. 1996;2(3):317-322.
13. Ikeda S, Tagawa H. Dysregulation of microRNAs and their association in the pathogenesis of T-cell lymphoma/leukemias. Int J Hematol. 2014; 99(5):542-552.
14. Lawrie CH. MicroRNAs in hematological malignancies. Blood Rev. 2013;27(3):143-154.
15. Gattazzo C, Teramo A, Passeri F, et al. Detection of monoclonal T populations in patients with KIR-restricted chronic lymphoproliferative disorder of NK cells. Haematologica. 2014;99(12):1826-1833.
16. Teramo A, Gattazzo C, Passeri F, et al. Intrinsic and extrinsic mechanisms contribute to maintain the JAK/STAT pathway aberrantly activated in T-type large granular lymphocyte leukemia. Blood. 2013;121(19): 3843-3854, S1.
17. Bazzoni F, Rossato M, Fabbri M, et al. Induction and regulatory function of miR-9 in human monocytes and neutrophils exposed to proinflammatory signals. Proc Natl Acad Sci U S A. 2009;106(13):5282-5287.
18. Rossato M, Cencig S, Gasperini S, Cassatella MA, Bazzoni F. IL-10 modulates cytokine gene transcription by protein synthesis-independent and dependent mechanisms in lipopolysaccharide-treated neutrophils. Eur J Immunol. 2007;37(11):3176-3189.
19. Mohn F, Weber M, Schubeler D, Roloff TC. Methylated DNA immunoprecipitation (MeDIP). Methods Mol Biol. 2009;507:55-64.
20. Yu H, Pardoll D, Jove R. STATs in cancer inflammation and immunity: a leading role for STAT3. Nat Rev Cancer. 2009;9(11):798-809.
21. Lee H, Deng J, Xin H, Liu Y, Pardoll D, Yu H. A requirement of STAT3 DNA binding precludes Th-1 immunostimulatory gene expression by NF-kappaB in tumors. Cancer Res. 2011;71(11):3772-3780.
22. Niu G, Wright KL, Ma Y, et al. Role of Stat3 in regulating p53 expression and function. Mol Cell Biol. 2005;25(17):7432-7440.
23. Zhang Q, Wang HY, Marzec M, Raghunath PN, Nagasawa T, Wasik MA. STAT3- and DNA methyltransferase 1-mediated epigenetic silencing of SHP-1 tyrosine phosphatase tumor suppressor gene in malignant T lymphocytes. Proc Natl Acad Sci U S A. 2005;102(19):6948-6953.
24. Curtale G, Mirolo M, Renzi TA, Rossato M, Bazzoni F, Locati M. Negative regulation of Toll-like receptor 4 signaling by IL-10-dependent microRNA-146b. Proc Natl Acad Sci U S A. 2013;110(28):11499-11504.
25. Renzi TA, Rubino M, Gornati L, Garlanda C, Locati M, Curtale G. MiR-146b Mediates Endotoxin Tolerance in Human Phagocytes. Mediators Inflamm. 2015;2015:145305.
26. Villela D, Ramalho RF, Silva AR, et al. Differential DNA Methylation of MicroRNA Genes in Temporal Cortex from Alzheimer's Disease Individuals. Neural Plast. 2016;2016:2584940.
27. Xiang M, Birkbak NJ, Vafaizadeh V, et al. STAT3 induction of miR-146b forms a feedback loop to inhibit the NF-kappaB to IL-6 signaling axis and STAT3-driven cancer phenotypes. Sci Signal. 2014;7(310):ra11.
28. Saitoh T, Karasawa M, Sakuraya M, et al. Improvement of extrathymic T cell type of large granular lymphocyte (LGL) leukemia by cyclosporin A: the serum level of Fas ligand is a marker of LGL leukemia activity. Eur J Haematol. 2000;65(4):272-275.
29. Drury GL, Di Marco S, Dormoy-Raclet V, Desbarats J, Gallouzi IE. FasL expression in activated T lymphocytes involves HuR-mediated stabilization. J Biol Chem. 2010; 285(41):31130-31138.
30. Cheng HS, Sivachandran N, Lau A, et al. MicroRNA-146 represses endothelial activation by inhibiting pro-inflammatory pathways. EMBO Mol Med. 2013;5(7):1017-1034.
31. Yang W, Yu H, Shen Y, Liu Y, Yang Z, Sun T. MiR-146b-5p overexpression attenuates stemness and radioresistance of glioma stem cells by targeting HuR/lincRNA-p21/beta-catenin pathway. Oncotarget. 2016;7(27): 41505-41526.
32. Clemente MJ, Przychodzen B, Jerez A, et al. Deep sequencing of the T-cell receptor repertoire in CD8+ T-large granular lymphocyte leukemia identifies signature landscapes. Blood. 2013;122(25):4077-4085.
33. Zhang Q, Wang HY, Woetmann A, Raghunath PN, Odum N, Wasik MA. STAT3 induces transcription of the DNA methyltransferase 1 gene (DNMT1) in malignant T lymphocytes. Blood. 2006;108(3):1058-1064.
34. Mishra A, Liu S, Sams GH, et al. Aberrant overexpression of IL-15 initiates large granular lymphocyte leukemia through chromosomal instability and DNA hypermethylation. Cancer Cell. 2012;22(5):645-655.
35. Gattazzo C, Teramo A, Miorin M, et al. Lack of expression of inhibitory KIR3DL1 receptor in patients with natural killer cell-type lymphoproliferative disease of granular lymphocytes. Haematologica. 2010;95(10):1722-1729.
36. Zhu H, Berkova Z, Mathur R, et al. HuR Suppresses Fas Expression and correlates with patient outcome in liver cancer. Mol Cancer Res. 2015;13(5):809-818.

ARTICLE

CXCR4 upregulation is an indicator of sensitivity to B-cell receptor/PI3K blockade and a potential resistance mechanism in B-cell receptor-dependent diffuse large B-cell lymphomas

Linfeng Chen,[1,2] Jing Ouyang,[1*] Kirsty Wienand,[1*] Kamil Bojarczuk,[1,3*] Yansheng Hao,[1,4] Bjoern Chapuy,[1,5] Donna Neuberg,[6] Przemyslaw Juszczynski,[1,3] Lee N. Lawton,[1] Scott J. Rodig,[7] Stefano Monti[8] and Margaret A. Shipp[1]

[1]Department of Medical Oncology, Dana-Farber Cancer Institute, Boston, MA, USA; [2]Current address: H3 Biomedicine, Cambridge, MA, USA; [3]Current address: Department of Experimental Hematology, Institute of Hematology and Transfusion Medicine, Warsaw, Poland; [4]Current Address: Department of Pathology, Mount Sinai Hospital, New York, NY, USA; [5]Current Address: Department of Hematology and Oncology, University Medical Center Göttingen, Göttingen, Germany; [6]Department of Biostatistics and Computational Biology, Dana-Farber Cancer Institute, Boston, USA; [7]Department of Pathology, Brigham and Women's Hospital, Boston, MA, USA and [8]Section of Computational Biomedicine, Boston University School of Medicine, Boston, MA, USA

**JO, KW and KB contributed equally to this work.*

Ferrata Storti Foundation

Haematologica 2020
Volume 105(5):1361-1368

ABSTRACT

B-cell receptor (BCR) signaling pathway components represent promising treatment targets in multiple B-cell malignancies including diffuse large B-cell lymphoma (DLBCL). In *in vitro* and *in vivo* model systems, a subset of DLBCLs depend upon BCR survival signals and respond to proximal BCR/phosphoinositide 3 kinase (PI3K) blockade. However, single-agent BCR pathway inhibitors have had more limited activity in patients with DLBCL, underscoring the need for indicators of sensitivity to BCR blockade and insights into potential resistance mechanisms. Here, we report highly significant transcriptional upregulation of C-X-C chemokine receptor 4 (CXCR4) in BCR-dependent DLBCL cell lines and primary tumors following chemical spleen tyrosine kinase (SYK) inhibition, molecular SYK depletion or chemical PI3K blockade. SYK or PI3K inhibition also selectively upregulated cell surface CXCR4 protein expression in BCR-dependent DLBCLs. CXCR4 expression was directly modulated by forkhead box O1 via the PI3K/protein kinase B/forkhead box O1 signaling axis. Following chemical SYK inhibition, all BCR-dependent DLBCLs exhibited significantly increased stromal cell-derived factor-1α (SDF-1α) induced chemotaxis, consistent with the role of CXCR4 signaling in B-cell migration. Select PI3K isoform inhibitors also augmented SDF-1α induced chemotaxis. These data define CXCR4 upregulation as an indicator of sensitivity to BCR/PI3K blockade and identify CXCR4 signaling as a potential resistance mechanism in BCR-dependent DLBCLs.

Introduction

Diffuse large-B-cell lymphomas (DLBCLs) are clinically and genetically heterogeneous diseases.[1] Our previous studies demonstrated that a subset of DLBCLs rely upon B-cell receptor (BCR)-dependent survival signals.[2,3] BCR signaling activates proximal pathway components including the spleen tyrosine kinase (SYK) and downstream effectors such as phosphatidylinositol-3-kinase (PI3K)/AKT and the Bruton's tyrosine kinase (BTK)/ nuclear factor-κB (NF-κB).[3,4] In prior studies, we, and others, characterized distinct BCR/PI3K-dependent viability pathways in DLBCL cell lines and primary tumors with low- or high-baseline NF-κB activity

Correspondence:

MARGARET A. SHIPP
margaret_shipp@dfci.harvard.edu

Received: January 7, 2019.

Accepted: September 26, 2019.

Pre-published: October 3, 2019.

doi:10.3324/haematol.2019.216218

Check the online version for the most updated information on this article, online supplements, and information on authorship & disclosures: www.haematologica.org/content/105/1361

(germinal center B- (GCB-) and activated B-cell like (ABC)-type tumors, respectively).[3,5-7]

In both types of BCR-dependent DLBCLs, inhibition of SYK or PI3K decrease the phosphorylation of AKT and Forkhead Box O1 (FOXO1) and increase the nuclear retention and associated activity of unphosphorylated FOXO.[13,8] BCR-dependent DLBCLs with low baseline NF-κB (GCB tumors) frequently exhibit inactivating mutations or copy loss of Phosphatase and tensin homolog (*PTEN)* and decreased abundance of the PTEN protein.[1,3,6] In these DLBCLs, proximal inhibition of BCR signaling primarily modulates the PI3K/AKT pathway.[3,5-7,9] In contrast, SYK/PI3K blockade additionally limits BTK/NF-κB signaling in BCR-dependent DLBCLs with high baseline NF-κB activity and frequent *MYD88*^{L265P} and/or *CD79B* mutations (ABC tumors).[1,3,7,9]

We sought to identify an indicator of BCR dependence in DLBCLs with low or high baseline NF-κB and noted that C-X-C chemokine receptor 4 (CXCR4) transcripts were significantly more abundant in both DLBCL subtypes following the inhibition of proximal BCR signaling.[3] In experimental model systems, BCR engagement promotes the internalization of CXCR4 and limits stromal cell-derived factor-1α) (SDF-1α)-induced chemotaxis.[10] For these reasons, we hypothesized that BCR blockade might increase CXCR4 expression and associated tumor cell migration.

Physiologically, the CXCR4 chemokine receptor binds to SDF-1αand plays a critical role in the chemotaxis of normal germinal center (GC) B cells.[11-13] CXCR4 is a known FOXO1 target gene that is induced in normal FOXO1-rich dark zone GC B-cells.[13] In the GC, CXCR4$^+$ B-cells migrate in response to a SDF-1α chemokine gradient.[11]

CXCR4 transduces SDF-1α signals via G-protein coupled activation of PI3K isoforms.[14-18] As a consequence, CXCR4 is also considered to be a possible therapeutic target in multiple B-cell malignancies, including DLBCL.[19-24] Herein, we assess CXCR4 modulation and signaling as both an indicator of sensitivity to BCR blockade and a potential resistance mechanism in DLBCL.

Methods

Cell lines and culture conditions

The DLBCL cell lines, SU-DHL4 (DHL4), SU-DHL6 (DHL6), OCI-LY7 (LY7), HBL1, TMD8, U-2932, Karpas 422 (K422), Toledo and OCI-LY4 (LY4), were cultured as previously described.[25] The identities of the DLBCL cell lines used in this study were confirmed via STR profiling with PowerPlex ®1.2 system (Promega, Madison, WI, USA). DHL4, DHL6, LY7, HBL1 and U-2932 were previously characterized as BCR-dependent and K422, Toledo and LY4 were BCR-independent.[3,9]

Primary tumor specimens

Cryopreserved viable primary DLBCL samples were obtained according to the Institutional Review Board (IRB) – approved protocols from the Brigham and Women's Hospital Department of Pathology. These anonymous primary tumor specimens were considered discarded tissues which did not require informed consent. The six primary DLBCLs were previously characterized for surface immunoglobulin (Ig) expression, BCR signaling and baseline NF-κB activity.[3]

Chemical inhibition of SYK, PI3K or BTK

The chemical SYK inhibitor, R406, was a gift from Rigel Pharmaceuticals (San Francisco, CA, USA). R406 was dissolved in DMSO at a concentration of 10 mM and stored at -80°C. For immediate inhibition, cells were incubated with 1 μM R406 or vehicle alone (in PBS) in a 37°C water bath for 2 hours (h). For long-term inhibition, R406 was added to cell culture medium at a final concentration of 1 μM and cells were maintained in an incubator at 37°C for 24 h. The chemical pan-PI3K inhibitor, LY294002, was purchased from Sigma-Aldrich (Saint Louis, MO, USA), The chemical SYK inhibitor, GS-9973 (entospletinib), the PI3K isoform-predominant inhibitors, GDC-0941 (pictilisib, PI3K α/δ>β/γ), CAL101 (idelalisib, δ) and IPI145 (duvelisib, δ/γ) and the BTK inhibitor, PCI-32765 (ibrutinib) were purchased from Selleckchem (Houston, TX, USA). DLBCL cell lines were treated with GS-9973 (2 μM), LY294002 (10 μM), GDC-0941 (0.5 μM), CAL101 (2 μM), IPI145 (1 μM), PC1-32765 (0.1 μM) or vehicle (DMSO) for 24 h as previously described.[9] The doses of SYK, PI3K and BTK inhibitors used in these studies were determined based on prior analyses of the respective agent EC50s of these agents;[9] the LY294002 dose was chosen based on previously reported studies.[3,16] Following treatment with chemical SYK, PI3K or BTK inhibitors, cells were harvested for additional analyses (*below*).

Quantitative RT-PCR (qRT-PCR)

QRT-PCR was performed as previously described[9] (*Online Supplementary Materials and Methods*).

Flow cytometry

A PE-conjugated mouse anti-human CD184 (CXCR4) antibody (BD Bioscience, CA, USA) was used for flow cytometry analysis on a FACS Canto II flow cytometer (BD Biosciences) and the data were analyzed with FlowJo 10 software (Flowjo Data analysis software LLC, Ashland, OR, USA).

Lentiviral-mediated shRNA transduction

The shRNA knockdown of target genes was performed as previously described[3] (*Online Supplementary Materials and Methods*).

Transduction with myristoylated AKT

DLBCL cell lines were retrovirally transduced with constructs encoding constitutively active (myristoylated) AKT (pMIG-mAKT1-IRES-GFP) or pMIG-IRES-GFP as previously described.[3] After 72 h, GFP$^+$ cells were sorted, treated with R406 or vehicle, and analyzed for CXCR4 expression by flow cytometry.

Chemotaxis assay

DLBCL cell lines were treated with vehicle, R406 (1 μM), GDC-0941 (0.5 μM), Ibrutinib (0.1 μM), AMD3100 (10 μM) or R406 + AMD3100 for 24 h. Before the chemotaxis assay, Permeable Polycarbonate Membrane Inserts in the Corning™ Transwell™ 24-well plate (Fisher Scientific, pore size 8 μm) were pretreated by adding 600 μL of RPMI-1640 media containing 0.5% bovine serum albumin (Sigma) with or without SDF-1α (25-100 ng/mL, R&D Systems) into the bottom chamber at 37°C for 1 h. Each lot of SDF-1α was individually titrated for activity in the chemotaxis assay prior to use. Treated cells were harvested and resuspended in RPMI-1640 media for a final density of 2×10^6/mL. 100 μL of cell suspension was transferred to each top chamber and incubated at 37 °C for 2-4 h. Cells in the lower chambers were harvested and cell numbers were determined by manual counting. Each condition was set up in triplicate.

Results

SYK inhibition selectively induces CXCR4 expression in BCR-dependent DLBCL cell lines and primary tumors

To identify potential compensatory signaling pathways in DLBCL treated with chemical BCR inhibitors, we reviewed the transcriptional profiles of five BCR-dependent DLBCL cell lines treated with the chemical SYK inhibitor, R406, or vehicle (DMSO).[3] Differential analysis of treated *versus* untreated samples revealed that CXCR4 transcripts were significantly upregulated in all five BCR-dependent DLBCL cell lines (DHL4, DHL6, LY7, HBL1, U-2932) following 6-24 h of R406 treatment (*P*-value=0.00052 at 24 h; *Online Supplementary Figure S1*).

To expand on these findings, we treated an extended panel of BCR-dependent and BCR-independent DLBCL cell lines with R406 (or vehicle) and evaluated CXCR4 transcript abundance by qRT-PCR. The extended DLBCL cell line panel included five BCR-dependent DLBCL cell lines (DHL4, DHL6, LY7 [low NF-κB, GCB]; and HBL1 and U-2932 [high NF-κB, ABC])[3] and an additional ABC DLBCL cell line, TMD8, that is sIgM$^+$, BCR-dependent,

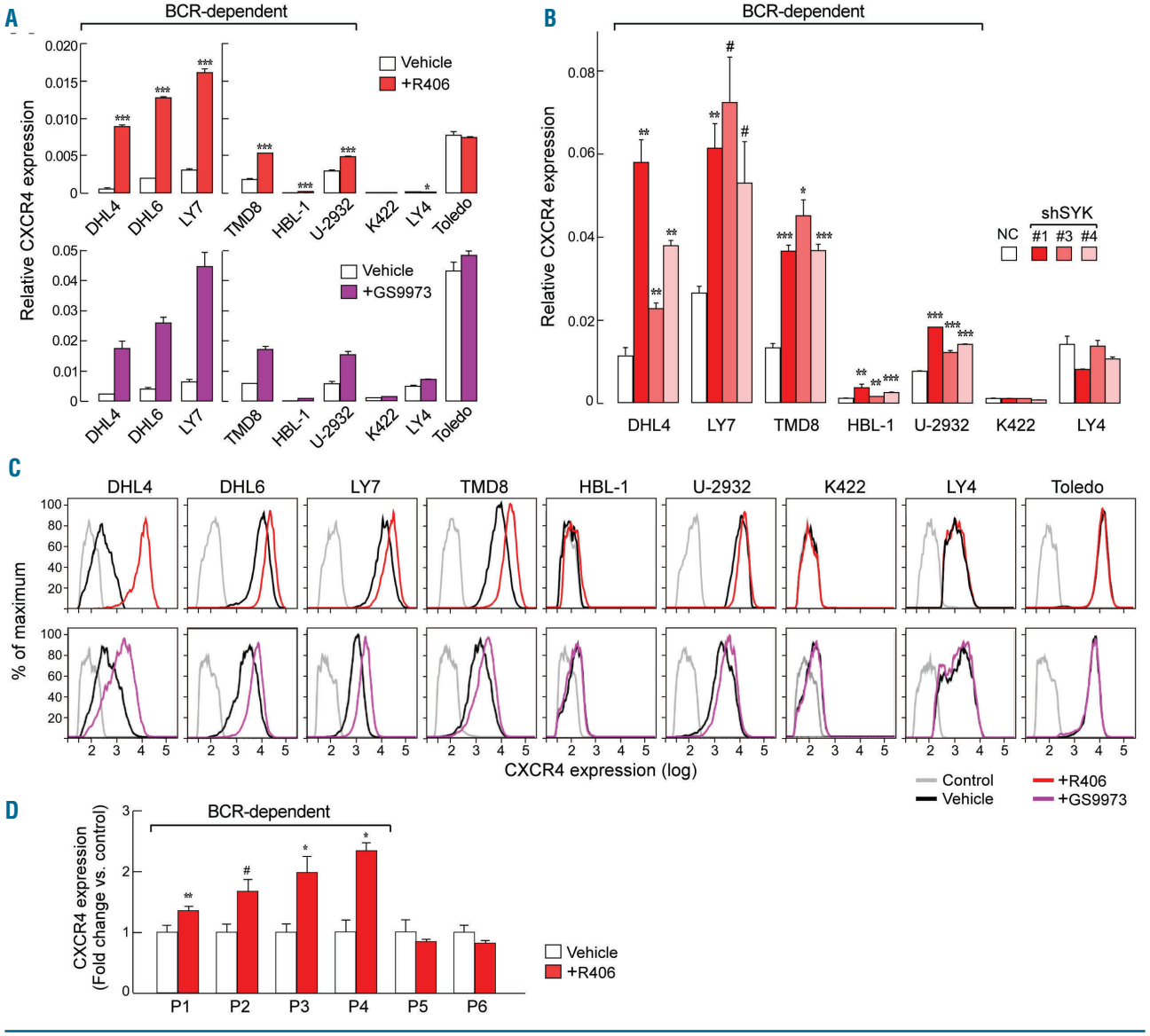

Figure 1. CXCR4 is upregulated in BCR-dependent DLBCL cell lines following SYK inhibition. (A) CXCR4 transcript abundance in diffuse large B-cell lymphoma (DLBCL) cell lines treated with 1 μM R406 (upper panel) or 2 μM GS-9973 (lower panel) for 24 hours (h) was determined by quantitative RT-PCR (qRT-PCR) relative to PPIA. The P-values for vehicle versus R406 treated or GS-9973 treated were determined with a one-sided Welch *t*-test. ***P<0.0001; *P<0.01. Error bars represent the SD of three independent assays in a representative experiment. (B) CXCR4 transcript abundance in SYK-depleted DLBCL cell lines (72 h following completion of puromycin selection) was determined by qRT-PCR relative to PPIA. NC (negative control) shRNA. The *P*-values for NC *versus* shSYK constructs were determined with a one-sided Welch *t*-test. ***P<0.0001; **P<0.001; *P<0.01; #P<0.05. Error bars represent the SD of three independent assays in a representative experiment. (C) Cell surface expression of CXCR4 in DLBCL cell lines treated for 24 h with vehicle or 1 μM R406 (upper panel), or vehicle or 2 μM GS-9973 (lower panel) was measured by flow cytometry. Isotype-matched control in gray. (D) CXCR4 expression in primary DLBCL patient samples following SYK inhibition. Cryopreserved viable DLBCL tumor cell suspensions from newly diagnosed patients were thawed and treated with vehicle or 1 μM R406 for 24 h. RNA samples were prepared and CXCR4 expression was determined by qRT-PCR relative to PPIA. The *P*-values for vehicle *versus* R406 treatment were determined with a one-sided Welch t-test. **P<0.001; *P<0.01; #P<0.05. Error bars represent the SD of three independent assays in a representative experiment.

and sensitive to chemical SYK inhibition (R406) and molecular depletion of SYK (*Online Supplementary Figure S2*). Consistent with its designation as an ABC-type DLBCL cell line, TMD8 exhibited high baseline expression of the NF-κB target, BCL2A1, that was markedly reduced following SYK depletion (*Online Supplementary Figure S2*). The extended cell line panel also included three BCR-independent DLBCL cell lines, K422, Toledo and LY4.[3]

In the DLBCL cell line panel, chemical SYK inhibition with R406 selectively increased CXCR4 transcript levels in all six BCR-dependent DLBCL cell lines; however, the baseline CXCR4 levels in HBL1 were low. Chemical SYK inhibition did not modulate CXCR4 transcript abundance in the three BCR-independent DLBCL cell lines (Figure 1A, top panel). Similar results were obtained with a more selective chemical SYK inhibitor, GS-9973, that is currently under evaluation in lymphoma clinical trials (Figure 1A, lower panel).[26-28]

SYK depletion with three independent shRNAs significantly increased CXCR4 transcripts in BCR-dependent, but not BCR-independent DLBCL cell lines, phenocopying the CXCR4 induction following chemical SYK inhibition (Figure 1B). Consistent with these findings, chemical inhibition of SYK with either R406 or GS-9973 selectively increased cell surface CXCR4 protein expression in the BCR-dependent DLBCLs (with the least effect in HBL1), but not in the BCR-independent DLBCLs (Figure 1C, R406, top panel; GS-9973, bottom panel).

After identifying selective CXCR4 induction in BCR-dependent DLBCLs cell lines, we assessed the same parameters in primary DLBCLs. For these studies, we utilized aliquots of six cryopreserved viable tumor suspensions of primary DLBCL that were previously characterized as BCR-dependent with low baseline NF-κB activity (P1 and P2), BCR-dependent with high baseline NF-κB activity (P3 and P4); or BCR-independent (P5 and P6).[3] As in the DLBCL cell lines, chemical SYK inhibition selectively induced CXCR4 in all four BCR-dependent primary DLBCLs (P1-P4) but not in the two BCR-independent primary DLBCLs (P5 and P6) (Figure 1D).

Prolonged chemical SYK inhibition increases SDF-1α associated migration of BCR-dependent DLBCLs

We next assessed the functional significance of CXCR4 induction following prolonged SYK inhibition by performing a transwell chemotaxis assay using SDF-1α as the chemoattractant. Prolonged SYK blockade selectively enhanced the migration of all examined BCR-dependent DLBCL cell lines to SDF-1α; the migration of the BCR-independent DLBCL cell lines was unchanged (Figure 2A). The R406-augmented, SDF-1α associated cellular migration was abrogated when the chemotaxis assay was performed in the presence of the specific CXCR4 inhibitor, AMD3100, confirming the specificity of the observed effect (Figure 2B).

PI3K/AKT signaling regulates CXCR4 expression in BCR-dependent DLBCL cell lines

We previously described the central role of PI3K/AKT in SYK-mediated BCR-signaling in DLBCLs.[3,9] These data prompted us to evaluate the function of PI3K/AKT in the regulation of CXCR4 upon proximal BCR/PI3K inhibition. For these studies, representative BCR-dependent DLBCL

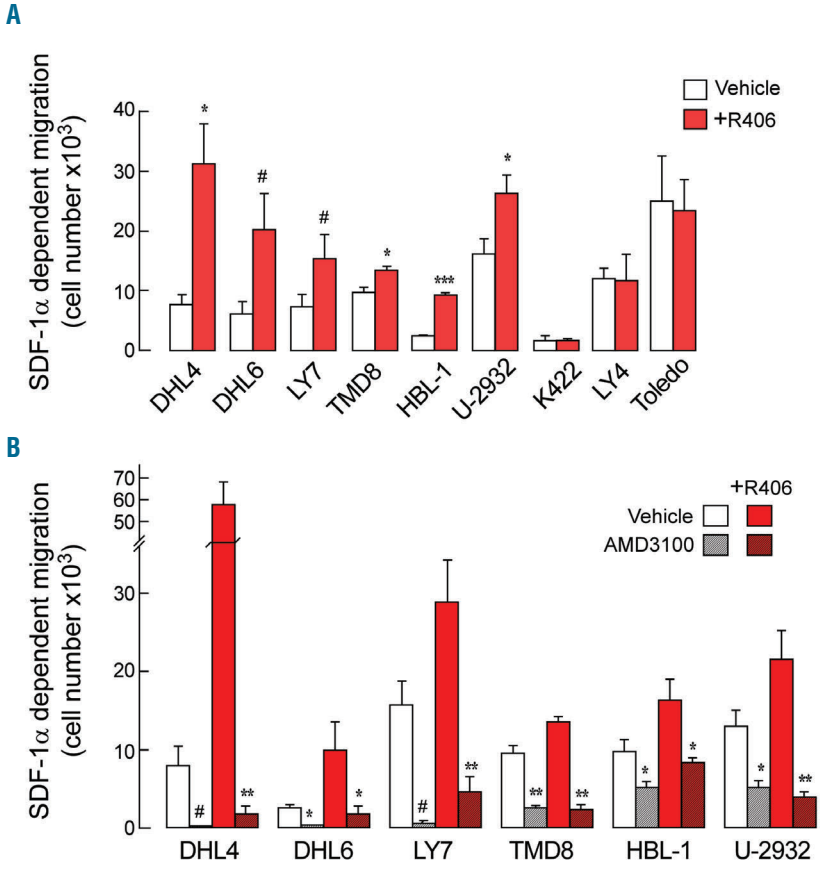

Figure 2. SDF-1α induced cell migration in DLBCL cell lines following SYK inhibition. (A) DLBCL cells were treated with vehicle or R406 for 24 hours (h), then assayed for migration in response to 100 ng/mL SDF-1α for 4 h ($2x10^5$ cells per condition). (B) BCR-dependent DLBCL cell lines were treated with vehicle, 10 μM AMD3100, 1 μM R406 or combination of AMD3100 and R406 for 24 h, then assayed for migration in response to SDF-1α. The *P*-values for vehicle- *versus* R406-treated (A) and vehicle- *versus* AMD3100-treated or R406 alone *versus* AMD3100+R406 (B) were determined with a one-sided Welch *t*-test. ***$P<0.0001$; **$P<0.001$; *$P<0.01$; #$P<0.05$. Error bars represent the SD of three independent assays in a representative experiment.

cell lines (DHL4, DHL6, LY7 [low NF-κB]; and TMD8 [high NF-κB]), were transduced with a vector encoding constitutively active (myristoylated) AKT1 (mAKT) or an empty vector control.[29] Thereafter, GFP+-selected cells were treated with vehicle control or R406 and analyzed for CXCR4 expression. Following R406 treatment, all four BCR-dependent DLBCL cell lines infected with the control vector expressed increased CXCR4 (Figure 3A, top panel). In contrast, chemical SYK inhibition did not modulate CXCR4 expression in mAKT-expressing DLBCL cell lines with constitutive activation of AKT1 (Figure 3A, lower panel). These data confirmed the role of PI3K/AKT in SYK-dependent modulation of CXCR4 expression.

Given these findings, we assessed the consequences of chemical pan-PI3K inhibition on CXCR4 expression in BCR-dependent DLBCL cell lines (Figure 3B) using the tool compound, LY294002. Like chemical SYK inhibition, pan-PI3K blockade with LY294002 increased CXCR4 transcript abundance (Figure 3B) and cell surface expression (Figure 3C).

We next examined the mechanism by which prolonged SYK/PI3K inhibition induces CXCR4 expression in BCR-dependent DLBCLs. BCR signaling is known to promote CXCR4 internalization and inhibit SDF-1α induced

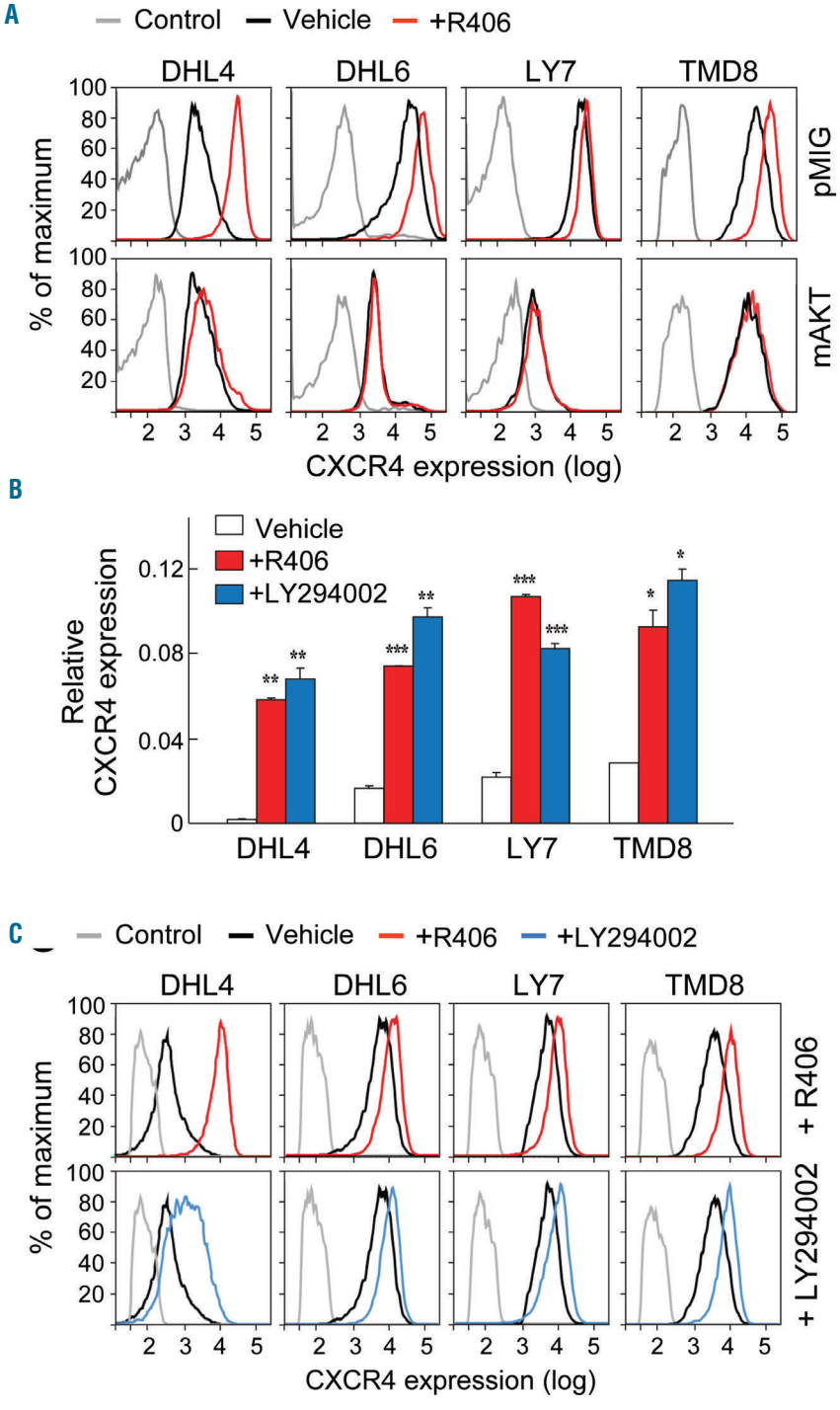

Figure 3. PI3K/AKT signaling regulates CXCR4 expression in BCR-dependent DLBCL cell lines. (A) BCR-dependent DLBCL cell lines, DHL4, DHL6, LY7 and TMD8, were retrovirally transduced with pMIG-mAKT1-IRES-GFP or pMIG-IRES-GFP vector, FACS-sorted for GFP expression, treated with 1 μM R406 or vehicle for 24 h (h), and analyzed for CXCR4 expression by flow cytometry. (B) BCR-dependent DLBCL cell lines were treated with 1 μM R406 (red), 10 μM LY294002 (blue) or vehicle for 24 h. Thereafter, CXCR4 expression was analyzed by qRT-PCR relative to PPIA. The *P*-values for vehicle *versus* R406 treated or vehicle *versus* LY294002 treated were determined with a one-sided Welch *t*-test. ***$P<0.0001$; **$P<0.001$; *$P<0.01$. Error bars represent the SD of three independent assays in a representative experiment. (C) Cell surface expression of CXCR4 was measured by flow cytometry in DLBCL cell lines treated with vehicle (black), R406 (red) or LY294002 (blue) for 24 h.

chemotaxis.[10] Therefore, molecular depletion or chemical inhibition of SYK or pan-PI3K blockade may limit CXCR4 internalization and increase residual cell surface CXCR4 expression. However, SYK/PI3K inhibition also increases nuclear localization of FOXO1 and associated FOXO1-mediated transactivation of CXCR4[3,8,13,30] For these reasons, we depleted FOXO1 in a BCR-dependent DLBCL cell line (DHL4), treated the cells with vehicle or R406 and subsequently measured CXCR4 expression by flow cytometry (*Online Supplementary Figure S3*). SYK inhibition induced less CXCR4 in FOXO1-depleted cells (*Online Supplementary Figure S3)*, highlighting the role of FOXO1 in CXCR4 expression.

After demonstrating CXCR4 upregulation following SYK or pan-PI3K inhibition (Figure 1 and Figure 3), we assessed the consequences of more selective PI3K isoform or BTK blockade using the PI3Kα/δ>β/γ, PI3Kδ and PI3Kδ/γ predominant inhibitors, GDC-0941, CAL101 and IPI145, respectively, and the BTK inhibitor, PCI-32765 (ibrutinib)[9] (Figure 4A). In each of the evaluated BCR-dependent DLBCL cell lines (DHL4, DHL6 and TMD8), more selective PI3K isoform inhibition with GDC-0941, CAL101 or IPI145 increased CXCR4 transcript abundance (Figure 4A) and CXCR4 cell surface protein expression (Figure 4B). In contrast, BTK blockade had more modest effects on CXCR4 transcript and protein expression in the

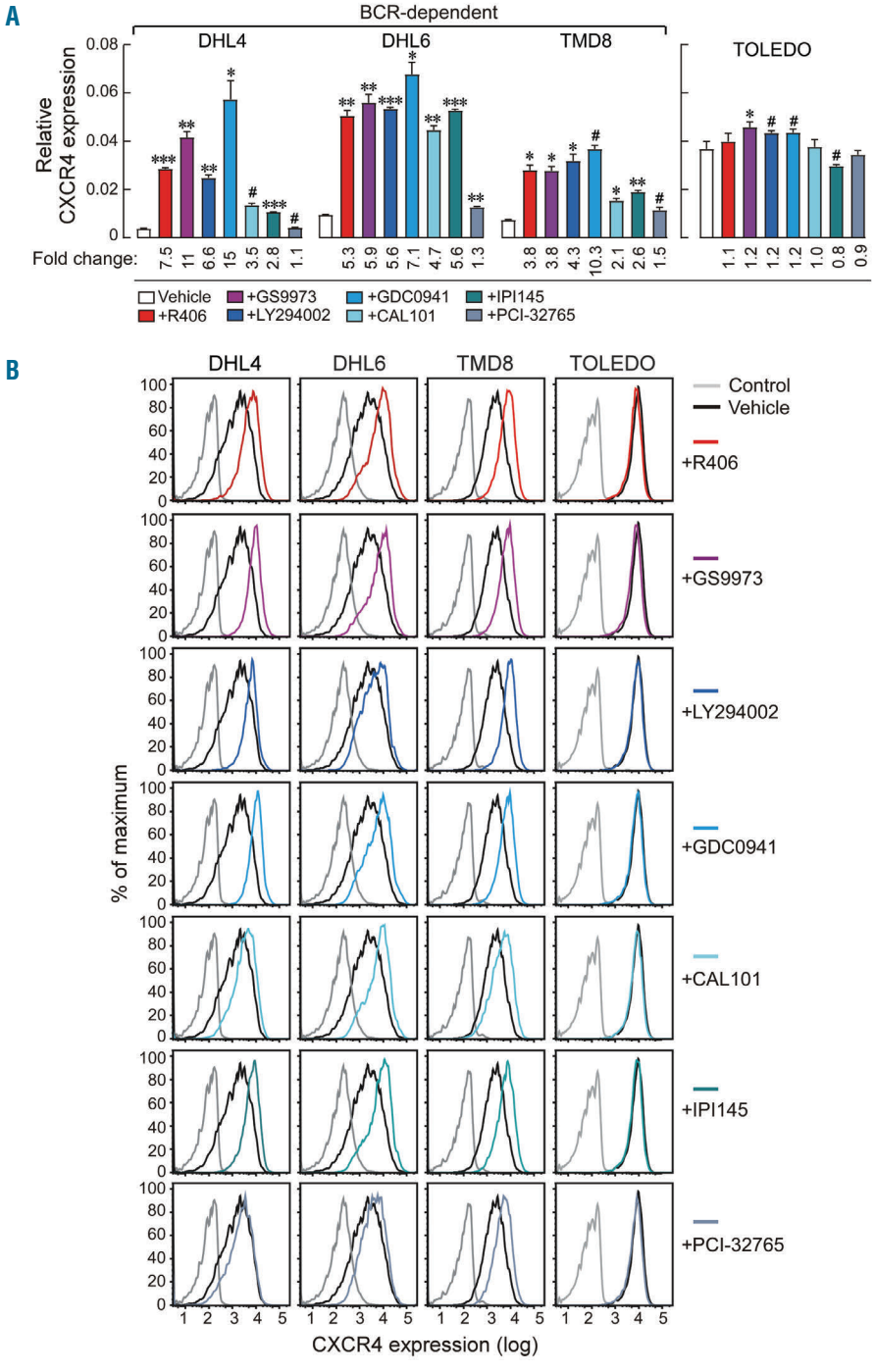

Figure 4. CXCR4 expression in BCR-dependent and BCR-independent DLBCL cell lines following SYK, PI3K or BTK inhibition. BCR-dependent diffuse large B-cell lymphoma (DLBCL) cell lines (DHL4, DHL6 and TMD8) and a BCR-independent DLBCL cell line (Toledo) were treated with DMSO, R406 (1 μM), GS-9973 (2 μM), LY294002 (10 μM), GDC-0941 (0.5 μM), CAL101 (2 μM), IPI145 (1 μM), PCI-32765 (0.1 μM) for 24 hours (h). Thereafter, CXCR4 expression was analyzed by qRT-PCR relative to PPIA (A) or flow cytometry (B) as in Figure 1A and Figure 1C. (A) CXCR4 transcript abundance. Fold changes in CXCR4 transcript abundance relative to DMSO are shown below each inhibitor for the four cell lines. The *P*-values for vehicle *versus* R406, GS-9973, LY294002, GDC-0941, CAL101, IPI145 and PCI-32765 treated were determined with a one-sided Welch *t*-test. ***$P<0.0001$; **$P<0.001$; *$P<0.01$; #$P<0.05$. Error bars represent the SD of three independent assays in a representative experiment. (B) CXCR4 cell surface expression in DLBCL cell lines treated with vehicle (black) or the above-mentioned inhibitors (see key) for 24 h. Isotype-matched control in gray.

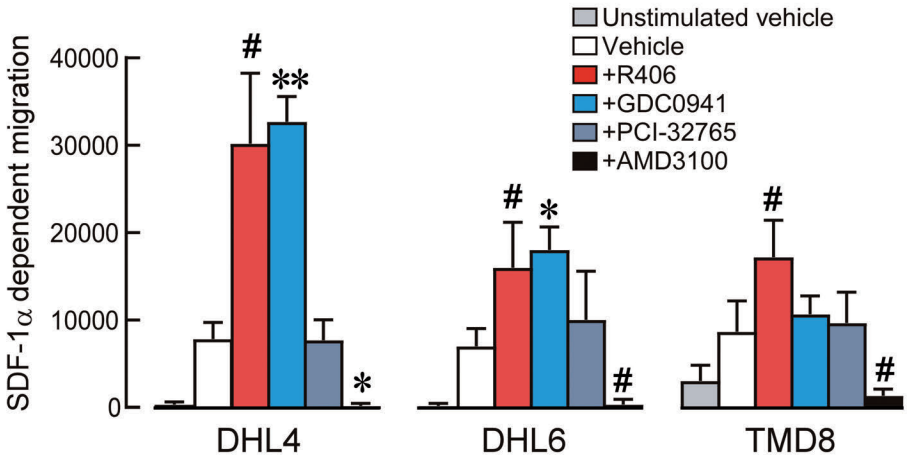

Figure 5. SDF-1α induced cell migration in BCR-dependent DLBCL cell lines following SYK, PI3K or BTK inhibition. Three representative BCR-dependent DLBCL lines (DHL4, DHL6 and TMD8) were treated with vehicle, 1 μM R406, 0.5 μM GDC-0941, 0.1 μM PCI-32765 or 10 μM AMD3100 for 24 (h), assayed for migration in response to 25 ng/mL of SDF-1α for 2 h ($2x10^5$ cells per condition). Vehicle-treated cells without SDF-1α stimulation were used as controls. The *P*-values for vehicle *versus* inhibitor-treated samples were determined using one-tailed Welch's *t*-test. $^{**}P<0.001$; $^{*}P<0.01$; $^{\#/*}P<0.05$. Error bars represented the SD of three independent assays in a representative experiment.

BCR-dependent lines. As expected, none of the compounds modulated CXCR4 expression in a BCR-independent DLBCL cell line (Toledo) (Figure 4A-B).

Consistent with these observations, chemical inhibition of SYK/PI3K was more effective than BTK blockade in augmenting SDF-1α– induced chemotaxis (Figure 5).

Discussion

In this study, we identify CXCR4 upregulation as an indicator of sensitivity to targeted inhibition of BCR/PI3K signaling in DLBCL cell lines and primary tumor cell suspensions. Chemical SYK inhibition, genetic *SYK* depletion and PI3K inhibition all increased CXCR4 expression in BCR-dependent DLBCLs. In DLBCLs with low or high baseline NF-κB, CXCR4 expression was modulated in a PI3K/AKT/FOXO1-dependent manner at the level of transcription (Figure 6). In addition to enhanced CXCR4 expression, proximal BCR(SYK)/PI3K inhibition induced chemotaxis of DLBCL cell lines to the CXCR4 ligand, SDF-1α.

In the current studies, we find induction of CXCR4 at the transcript level within 6 h of proximal BCR signaling blockade. Thereafter, increased CXCR4 cell surface expression is readily detectable by flow cytometry within 24 h of SYK or PI3K inhibition in almost all BCR-dependent DLBCLs. In recent studies, PI3K/mammalian target of rapamycin chemical inhibition also increased CXCR4 transcript abundance in BCR-dependent DLBCL cell lines.[31] Taken together, these data suggest that CXCR4 upregulation is an indicator of sensitivity to inhibition of proximal BCR/PI3K signaling in DLBCLs.

CXCR4 is a FOXO1 target gene which, under physiological conditions, contributes to the polarization of light zone and dark zone GC-B cells.[13] Upon inhibition of the BCR/SYK/PI3K/AKT axis, FOXO1 is dephosphorylated and retained in the nucleus, initiating transcription of its target genes.[8] FOXO1 is considered to be a homeostatic regulator with targets that include pro-apoptotic mediators of cell death such as *BIM, HRK* or *p27*, as well as BCR/PI3K signaling pathway components including *SYK, PIK3CA* and CXCR4.[1,3,13] Therefore, FOXO1-dependent upregulation of CXCR4 can be regarded as a potential compensatory signaling pathway in DLBCLs following proximal BCR/PI3K inhibition.

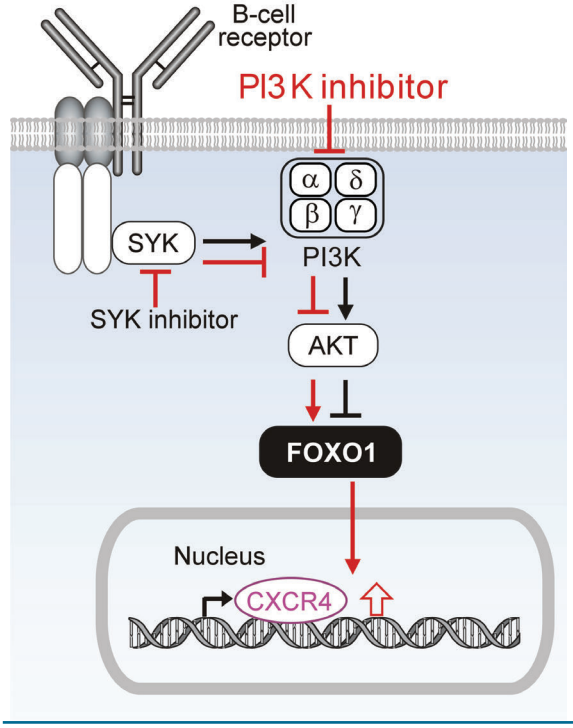

Figure 6. Model for B-cell receptor/SYK/PI3K regulation of CXCR4 signals. Red arrows indicate consequences of spleen tyrosine kinase (SYK) and/or phosphatidylinositol-3-kinase (PI3K) inhibition including increased nuclear localization of FOXO1 and C-X-C chemokine receptor 4 (CXCR4) upregulation.

In Waldenström's Macroglobulinemia (WM), nearly 30% of patients exhibit an activating somatic mutation of *CXCR4*[32] that increases AKT and extracellular signal-regulated kinases signaling and mediates increased migration, adhesion, survival and resistance to ibrutinib.[24] In our *in vitro* analyses of BCR-dependent DLBCLs, inhibition of SYK or PI3K signaling was more effective than BTK blockade in upregulating CXCR4 expression. In our recent genomic characterization of 304 primary DLBCLs, we did not observe recurrent *CXCR4* mutations.[1] However, immunohistochemical assessment of clinically annotated cohorts of *de novo* DLBCLs identified heterogeneity of CXCR4 expres-

sion and adverse prognostic significance of CXCR4 staining.[33,34]

These observations are noteworthy because CXCR4 may also be a relevant treatment target. There are ongoing clinical trials incorporating either the CXCR4 inhibitor (AMD3100, plerixafor) or a monoclonal antibody against CXCR4 (ulocuplumab) into existing therapies of WM.[35] Additionally, multiple CXCR4 antagonists are reported to enhance the cytotoxic effect of rituximab or additional agents in diverse *in vitro* lymphoma models, including those of DLBCLs.[19-23,36]

Taken together, these data identify CXCR4 upregulation as an indicator of sensitivity to proximal BCR/PI3K blockade. These findings will potentially aid in the development of representative model systems and analyses of BCR/PI3K pathway-specific inhibitors. CXCR4 upregulation may also be an important and potentially targetable resistance mechanism in BCR-dependent DLBCLs.

Funding

This work was supported by a 'Mobility Plus' fellowship from the Polish Ministry of Science and Higher Education (1261/MOB/IV/2015/0) (KB) and a Leukemia and Lymphoma Society SCOR award (MA. and SJR).

References

1. Chapuy B, Stewart C, Dunford AJ, et al. Molecular subtypes of diffuse large B cell lymphoma are associated with distinct pathogenic mechanisms and outcomes. Nat Med. 2018;24(5):679-690.
2. Chen L, Monti S, Juszczynski P, et al. SYK-dependent tonic B-cell receptor signaling is a rational treatment target in diffuse large B-cell lymphoma. Blood. 2008;111(4):2230-2237.
3. Chen L, Monti S, Juszczynski P, et al. SYK inhibition modulates distinct PI3K/AKT-dependent survival pathways and cholesterol biosynthesis in diffuse large B cell lymphomas. Cancer Cell. 2013;23(6):826-838.
4. Bojarczuk K, Bobrowicz M, Dwojak M, et al. B-cell receptor signaling in the pathogenesis of lymphoid malignancies. Blood Cells Mol Dis. 2015;55(3):255-265.
5. Havranek O, Xu J, Kohrer S, et al. Tonic B-cell receptor signaling in diffuse large B-cell lymphoma. Blood. 2017;130(8):995-1006.
6. Pfeifer M, Grau M, Lenze D, et al. PTEN loss defines a PI3K/AKT pathway-dependent germinal center subtype of diffuse large B-cell lymphoma. Proc Natl Acad Sci U S A. 2013;110(30):12420-12425.
7. Erdmann T, Klener P, Lynch JT, et al. Sensitivity to PI3K and AKT inhibitors is mediated by divergent molecular mechanisms in subtypes of DLBCL. Blood. 2017; 130(3):310-322.
8. Szydlowski M, Kiliszek P, Sewastianik T, et al. FOXO1 activation is an effector of SYK and AKT inhibition in tonic BCR signal-dependent diffuse large B-cell lymphomas. Blood. 2016;127(6):739-748.
9. Bojarczuk K, Wienand K, Ryan JA, et al. Targeted inhibition of PI3Kalpha/delta is synergistic with BCL-2 blockade in genetically defined subtypes of DLBCL. Blood. 2019;133(1):70-80.
10. Guinamard R, Signoret N, Ishiai M, Marsh M, Kurosaki T, Ravetch JV. B cell antigen receptor engagement inhibits stromal cell-derived factor (SDF)-1alpha chemotaxis and promotes protein kinase C (PKC)-induced internalization of CXCR4. J Exp Med. 1999;189(9):1461-1466.
11. Allen CD, Ansel KM, Low C, et al. Germinal center dark and light zone organization is mediated by CXCR4 and CXCR5. Nat Immunol. 2004;5:943-952.
12. Victora GD, Dominguez-Sola D, Holmes AB, Deroubaix S, Dalla-Favera R, Nussenzweig MC. Identification of human germinal center light and dark zone cells and their relationship to human B-cell lymphomas. Blood. 2012;120(11):2240-2248.
13. Dominguez-Sola D, Kung J, Holmes AB, et al. The FOXO1 Transcription factor instructs the germinal center dark zone Program. Immunity. 2015;43(6):1064-1074.
14. Thorpe LM, Yuzugullu H, Zhao JJ. PI3K in cancer: divergent roles of isoforms, modes of activation and therapeutic targeting. Nat Rev Cancer. 2015;15(1):7-24.
15. Janas ML, Varano G, Gudmundsson K, Noda M, Nagasawa T, Turner M. Thymic development beyond beta-selection requires phosphatidylinositol 3-kinase activation by CXCR4. J Exp Med. 2010;207 (1):247-261.
16. Li M, Sun X, Ma L, et al. SDF-1/CXCR4 axis induces human dental pulp stem cell migration through FAK/PI3K/Akt and GSK3beta/beta-catenin pathways. Sci Rep. 2017;7:40161.
17. Reiske HR, Kao SC, Cary LA, Guan JL, Lai JF, Chen HC. Requirement of phosphatidylinositol 3-kinase in focal adhesion kinase-promoted cell migration. J Biol Chem. 1999;274(18):12361-12366.
18. Wang JF, Park IW, Groopman JE. Stromal cell-derived factor-1alpha stimulates tyrosine phosphorylation of multiple focal adhesion proteins and induces migration of hematopoietic progenitor cells: roles of phosphoinositide-3 kinase and protein kinase C. Blood. 2000;95(8):2505-2513.
19. Reinholdt L, Laursen MB, Schmitz A, et al. The CXCR4 antagonist plerixafor enhances the effect of rituximab in diffuse large B-cell lymphoma cell lines. Biomark Res. 2016; 4:12.
20. Beider K, Ribakovsky E, Abraham M, et al. Targeting the CD20 and CXCR4 pathways in non-hodgkin lymphoma with rituximab and high-affinity CXCR4 antagonist BKT140. Clin Cancer Res. 2013;19(13): 3495-3507
21. O'Callaghan K, Lee L, Nguyen N, et al. Targeting CXCR4 with cell-penetrating peptducins in lymphoma and lymphocytic leukemia. Blood. 2012;119(7):1717-1725.
22. Buchner M, Brantner P, Stickel N, et al. The microenvironment differentially impairs passive and active immunotherapy in chronic lymphocytic leukaemia - CXCR4 antagonists as potential adjuvants for monoclonal antibodies. Br J Haematol. 2010;151(2):167-178.
23. Recasens-Zorzo C, Cardesa-Salzmann T, Petazzi P, et al. Pharmacological modulation of CXCR4 cooperates with BET bromodomain inhibition in diffuse large B-cell lymphoma. Haematologica. 2019;104(4):778-788.
24. Cao Y, Hunter ZR, Liu X, et al. The WHIM-like CXCR4(S338X) somatic mutation activates AKT and ERK, and promotes resistance to ibrutinib and other agents used in the treatment of Waldenstrom's Macroglobulinemia. Leukemia. 2015;29 (1):169-176.
25. Chapuy B, McKeown MR, Lin CY, et al. Discovery and characterization of super-enhancer-associated dependencies in diffuse large B cell lymphoma. Cancer Cell. 2013;24(6):777-790.
26. Currie KS, Kropf JE, Lee T, et al. Discovery of GS-9973, a selective and orally efficacious inhibitor of spleen tyrosine kinase. J Med Chem. 2014;57(9):3856-3873.
27. Sharman J, Hawkins M, Kolibaba K, et al. An open-label phase 2 trial of entospletinib (GS-9973), a selective spleen tyrosine kinase inhibitor, in chronic lymphocytic leukemia. Blood. 2015;125(15):2336-2343.
28. Andorsky DJ, Kolibaba KS, Assouline S, et al. An open-label phase 2 trial of entospletinib in indolent non-Hodgkin lymphoma and mantle cell lymphoma. Br J Haematol. 2019;184(2):215-222.
29. Kharas MG, Okabe R, Ganis JJ, et al. Constitutively active AKT depletes hematopoietic stem cells and induces leukemia in mice. Blood. 2010;115(7):1406-1415.
30. Ochiai K, Maienschein-Cline M, Mandal M, et al. A self-reinforcing regulatory network triggered by limiting IL-7 activates pre-BCR signaling and differentiation. Nat Immunol. 2012;13(3):300-307.
31. Tarantelli C, Gaudio E, Arribas AJ, et al. PQR309 is a novel dual PI3K/mTOR inhibitor with preclinical antitumor activity in lymphomas as a single agent and in combination therapy. Clin Cancer Res. 2018; 24(1):120-129.
32. Hunter ZR, Xu L, Yang G, et al. The genomic landscape of Waldenstrom macroglobulinemia is characterized by highly recurring MYD88 and WHIM-like CXCR4 mutations, and small somatic deletions associated with B-cell lymphomagenesis. Blood. 2014;123 (11):1637-1646.
33. Chen J, Xu-Monette ZY, Deng L, et al. Dysregulated CXCR4 expression promotes lymphoma cell survival and independently predicts disease progression in germinal center B-cell-like diffuse large B-cell lymphoma. Oncotarget. 2015;6(8):5597-5614.
34. Moreno MJ, Bosch R, Dieguez-Gonzalez R, et al. CXCR4 expression enhances diffuse large B cell lymphoma dissemination and decreases patient survival. J Pathol. 2015; 235(3):445-455.
35. Treon SP. How I treat Waldenstrom macroglobulinemia. Blood. 2015;126(6): 721-732.
36. Xu ZZ, Shen JK, Zhao SQ, Li JM. Clinical significance of chemokine receptor CXCR4 and mammalian target of rapamycin (mTOR) expression in patients with diffuse large B-cell lymphoma. Leuk Lymphoma. 2018;59(6): 1451-1460.

ARTICLE

An increase in *MYC* copy number has a progressive negative prognostic impact in patients with diffuse large B-cell and high-grade lymphoma, who may benefit from intensified treatment regimens

Francesca Schieppati,[1*] Piera Balzarini,[2*] Simona Fisogni,[2] Alessandro Re,[1] Chiara Pagani,[1] Nicola Bianchetti,[1] Lorenzo Micheli,[2] Angela Passi,[1] Samantha Ferrari,[1] Adriana Maifredi, [1]Chiara Bottelli,[1] Rossella Leopaldo,[1] Vilma Pellegrini,[2] Fabio Facchetti,[2] Giuseppe Rossi[1] and Alessandra Tucci[1]

[1]Department of Hematology, ASST Spedali Civili di Brescia and [2]Department of Molecular and Translational Medicine, Section of Pathology, University of Brescia, Brescia, Italy

**FS and PB contributed equally to this work.*

Ferrata Storti Foundation

Haematologica 2020
Volume 105(1):1369-1378

ABSTRACT

MYC translocations, a hallmark of Burkitt lymphoma, occur in 5-15% of diffuse large B-cell lymphoma, and have a negative prognostic impact. Numerical aberrations of *MYC* have also been detected in these patients, but their incidence and prognostic role are still controversial. We analyzed the clinical impact of *MYC* increased copy number on 385 patients with diffuse large B-cell lymphoma screened at diagnosis for *MYC*, *BCL2*, and *BCL6* rearrangements. We enumerated the number of *MYC* copies, defining as amplified those cases with an uncountable number of extra-copies. The prevalence of *MYC* translocation, increased copy number and amplification was 8.8%, 15%, and 1%, respectively. Patients with 3 or 4 gene copies, accounting for more than 60% of patients with *MYC* copy number changes, had a more favorable outcome compared to patients with >4 copies or translocation of MYC, and were not influenced by the type of treatment received as first-line. Stratification according to the number of *MYC* extra-copies showed a negative correlation between an increasing number of copies and survival. Patients with >7 copies or the amplification of *MYC* had the poorest prognosis. Patients with >4 copies of MYC showed a similar, trending towards worse prognosis compared to patients with *MYC* translocation. The survival of patients with >4 copies, translocation or amplification of *MYC* seemed to be superior if intensive treatments were used. Our study underlines the importance of fluorescence *in situ* hybridization testing at diagnosis of diffuse large B-cell lymphoma to detect the rather frequent and clinically significant numerical aberrations of *MYC*.

Introduction

Diffuse large B-cell lymphoma (DLBCL) is a clinically and biologically heterogeneous group of diseases.[1] The survival of patients with DLBCL has significantly improved since rituximab (R) was added to cyclophosphamide, doxorubicin, vincristine and prednisone (CHOP) therapy, and R-CHOP has now become the standard of care. The International Prognostic Index (IPI)[2] and the Revised-International Prognostic Index (R-IPI)[3] are useful tools to stratify patients in different risk classes. However, despite this, 30-40% of these patients are not cured by R-CHOP or R-CHOP-like regimens.[4] In the last two decades, much effort has been made to identify patients at high risk of treatment failure, using morphological subtyping,[5,6] identification of cell of origin by gene expression profiling,[7] BCL2 and MYC protein expression by immunohistochemistry,[8] and molecular insights by genetic studies.[9,10] In particular, different authors have demonstrated a negative prognostic impact of chromosomal aberration affecting the *MYC* gene locus in patients with

Correspondence:

FRANCESCA SCHIEPPATI
fschieppati@gmail.com

Received: April 6, 2019.

Accepted: August 8, 2019.

Pre-published: August 8, 2019.

doi:10.3324/haematol.2019.223891

Check the online version for the most updated information on this article, online supplements, and information on authorship & disclosures: www.haematologica.org/content/105/5/1369

DLBCL studied by interphase fluorescence *in situ* hybridization (FISH), both before[11] and after[12,13] the introduction of rituximab. Overall, *MYC* genetic rearrangements have been described in 5-10% DLBCL at diagnosis.[10,11] The presence of dual translocations involving both *MYC* and *BCL2* ("double-hit"), associated or not to the translocation of BCL6 ("triple-hit"), have shown a dismal clinical course.[14] The importance of the molecular study of *MYC*, *BCL2* and BCL6 status is highlighted by the updated World Health Organization (WHO) classification of 2016, which identifies a specific diagnostic category called "High Grade Lymphoma with *MYC* and *BCL2* with or without *BCL6* translocation", irrespective of the morphological subtype of DLBCL. In addition, preliminary studies suggest that the partner gene in the *MYC* translocation may also influence tumor behavior.[15] In particular, *MYC* rearrangements with immunoglobulin genes, but not with other partner genes, seem to have a negative prognostic impact on patients with DLBCL treated with immunochemotherapy.[16,17]

Recent studies have revealed that also numerical alterations of *MYC* gene detected by FISH can occur in DLBCL.[18] In the same way as chromosome translocations juxtapose oncogenes to the promoter of genes that are constitutively expressed, a gain of gene copy-number or the amplification of *MYC* may cause its over-transcription and protein over-expression leading to uncontrolled proliferation.[19] Different studies have shown that numerical alterations of *MYC* may influence the outcome of patients with DLBCL, but their incidence and prognostic relevance is still controversial.[19,20] Moreover, the definition of *MYC* copy number changes is not homogeneous across studies, where the terms "gain" and "amplification" are used to define different conditions. In the present study, we analyzed the frequency and the clinical outcome of patients with *MYC* numerical aberrations in the setting of DLBCL with particular emphasis on the number of *MYC* extra-copies, on their frequency, and on their correlation with the clinical outcome in a consecutive series of DLBCL patients.

Methods

Study design and participants

In this retrospective, observational study, participants were enrolled between January 2011 and June 2016. Eligible patients were consecutive adults receiving a diagnosis of DLBCL during the study period. FISH study at diagnosis was performed on patients considered fit for treatment with curative intent. Tumors were classified according to the 2008 WHO Classification. No immunodeficiency-associated lymphomas were included. Disease burden was assessed by Ann-Arbor staging and IPI classification.[2] All patients signed informed consent to provide material for biological studies. The study was conducted in accordance with good clinical practice guidelines and approved by the institutional ethical committee. All patients with DLBCL were treated with rituximab-containing immuno-chemotherapy programs. The following were considered standard dose regimens: CHOP, and COMP (cyclophosphamide, vincristine, liposomal doxorubicin, and prednisone), whereas the following were considered intensified regimens: GMALL B-ALL/NHL 2002 protocol,[21] and DA-EPOCH (dose adjusted etoposide, doxorubicin, cyclophosphamide vincristine, and prednisone). Autologous stem cell transplantation (ASCT) was used in approximately 25% of cases as intensification of first-line treatment, using BEAM/FEAM as conditioning regimens [carmustine (BCNU) or fotemustine, etoposide, cytarabine, melphalan followed by autologous stem cell infusion]. ASCT as intensification of a first-line treatment with R-CHOP was considered an intensified regimen.

Interphase fluorescence *in situ* hybridization analysis

Fluorescence *in situ* hybridization analysis was performed on 4-µm sections of formalin-fixed paraffin-embedded (FFPE) tissue using break-apart DNA probes (Dako, Glostrup, Denmark) for c-MYC (8q24), BCL2 (18q21) and BCL6 (3q27). FISH was carried out according to the manufacturer's guideline. FISH images were captured at x100 magnification and elaborated using the Genikon software (Nikon Instruments S.p.A., Italy). The presence of three or more red/green signals of *MYC, BCL-2* or *BCL-6* was considered to indicate an increased copy number of these genes (namely MYC-ICN, BCL2-ICN, and BCL6-ICN).[20] A "cloud-like" FISH pattern due to countless copies of *MYC* was defined as "amplification" (MYC-AMP) (Figure 1). We did not regularly use a chromosome 8 centromeric probe in this study. However, in 11 cases with MYC-ICN, single centromeric chromosome 8 probe (CEP8 SpectrumGreen, Abbott Molecular Inc., USA) was also used in order to exclude polysomy as cause of MYC-ICN.

Immunohistochemistry

Four-micron thick tissue sections were used for immunohistochemical staining for c-MYC (clone Y69, -Abcam; dilution 1:75), which was performed on a Bond III automated immunostainer (Leica Microsystem, Bannockburn, IL, USA) using controls in parallel. Diaminobenzidine was used to reveal the *in situ* hybridization (ISH) reaction and sections were counterstained with hematoxylin. A cut-off of >40% was used for positive MYC expression by immunohistochemistry (IHC).

Response criteria and statistical analysis

Standard definitions of complete response (CR), progression-free survival (PFS), and overall survival (OS) were used.[22] Categorical data were compared using Fisher's exact test, whereas the Mann-Whitney test was used for continuous parameters. OS was measured from date of diagnosis to death from any cause, and PFS from the date of treatment start to the date of disease progression, relapse or death. The actuarial survival analysis was carried out according to the method described by Kaplan and Meier and the curves compared by the log-rank test with 95% confidence intervals (CI).[23] Differences between the results of comparative tests were considered significant at two-sided $P<0.05$.

Results

General clinical characteristics and outcome of the study population

Of 504 patients diagnosed with DLBCL at our Institution, FISH was performed on 385 consecutive patients considered fit for treatment with curative intent. Tumors were classified according to the WHO 2008 Classification of Tumours of Haematopoietic and Lymphoid Tissues, as follows: 365 DLBCL not otherwise specified (NOS) (95%), and 20 B-cell lymphoma, unclassifiable (BCLU), with features intermediate between diffuse large B-cell lymphoma and Burkitt lymphoma (5%). Thirty-four (8.3%) cases were transformed from a low-grade lymphoma.

Ninety-five patients of the whole cohort of DLBCL had a structural or numerical aberration of *MYC* at FISH (25%),

and these constituted our study cohort. Figure 2 shows the flow diagram of the entire study population. The patients' main clinical characteristics at diagnosis are presented in Table 1, both for the whole cohort with FISH abnormalities and for the subgroups with either structural or numerical *MYC* aberrations. In addition, MYC protein expression by immunostaining was available for 52 patients, and was positive in 88%: among them, all patients with a translocation of *MYC* (MYC-T) over-expressed the MYC protein, whereas seven patients with numerical aberrations of *MYC* (11%) showed <40% expression of MYC protein by IHC. Five patients initially considered fit for curative therapy received palliative/symptomatic treatment and were therefore excluded from the survival analyses. The remaining 90 patients received immuno-chemotherapy: standard dose in 46 patients or intensified regimens in 44 patients. Twenty-three patients received ASCT as intensification of first-line treatment. Median follow up was 38 months (range 0-79). A complete response (CR) was achieved in 55 patients (61%). Overall, there was no difference in achievement of CR between patients receiving intensified and those receiving standard treatment (57% *vs.* 65%,

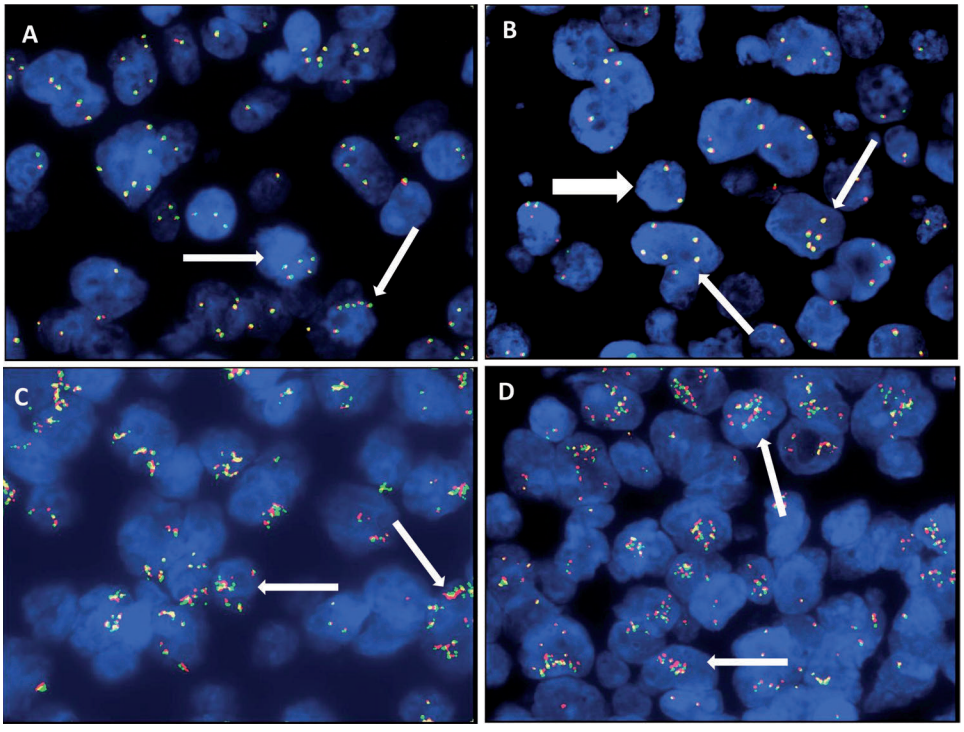

Figure 1. Numerical aberrations of *MYC* by fluorescence *in situ* hybridization (FISH). (A and B) Thin white arrows show *MYC* increased copy number (MYC-ICN); white thick arrow shows MYC wild type. (C and D) Thin white arrows show *MYC* amplification (MYC-AMP).

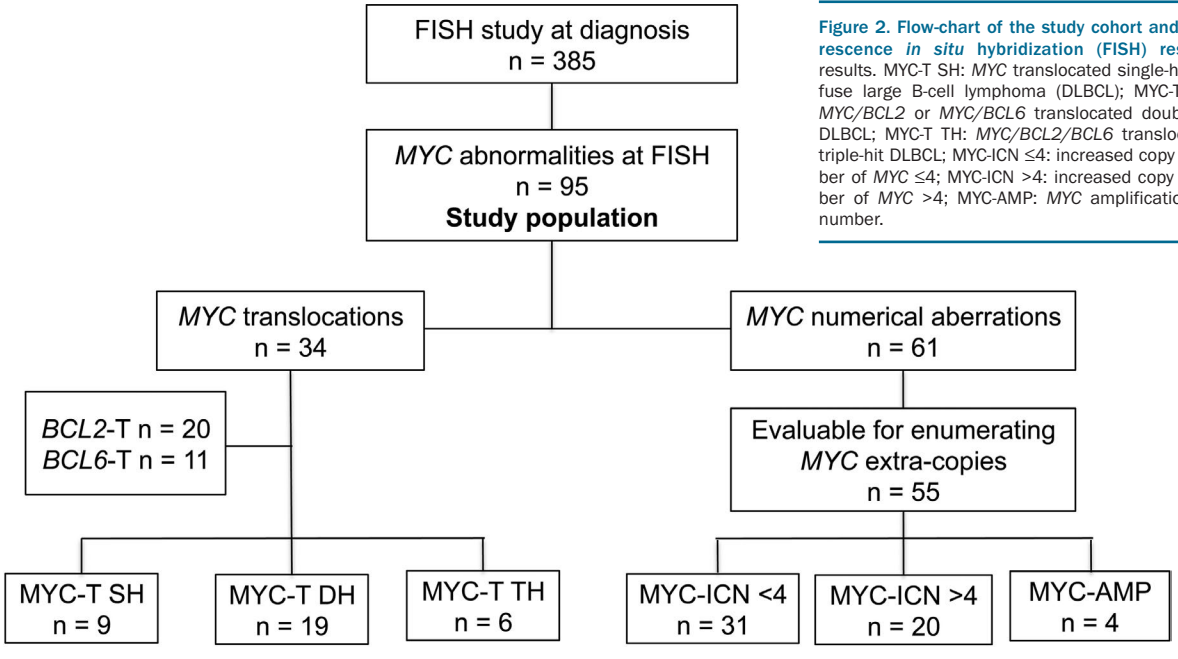

Figure 2. Flow-chart of the study cohort and fluorescence *in situ* hybridization (FISH) results. results. MYC-T SH: *MYC* translocated single-hit diffuse large B-cell lymphoma (DLBCL); MYC-T DH: *MYC/BCL2* or *MYC/BCL6* translocated double-hit DLBCL; MYC-T TH: *MYC/BCL2/BCL6* translocated triple-hit DLBCL; MYC-ICN ≤4: increased copy number of *MYC* ≤4; MYC-ICN >4: increased copy number of *MYC* >4; MYC-AMP: *MYC* amplification. n: number.

P=0.41). Median OS and PFS at three years were 58.8% and 54.8%, respectively, with no significant differences between the groups treated with intensified or standard regimens (*P*=0.93 and *P*=0.69, respectively). Outcome was similar in the two groups receiving standard or intensified regimens, despite the different treatment schemes. Twenty patients received R-COMP due to age over 70 years or cardiac dysfunction; none received consolidation with ASCT. The other 26 patients in the standard regimen arm received R-CHOP, and no differences in the outcome were seen between patients treated with the R-COMP and those treated with R-CHOP (OS 73% *vs.* 53%, *P*=0.2). In the intensified group, one patient with a transformed lymphoma received R-ESHAP and ASCT due to the risk of cardiotoxicity related to prior anthracycline therapy. There was no significant difference in OS among patients receiving R-CHOP-like + ASCT, GMALL-like ± ASCT, or R-DA-EPOCH ± ASCT (OS 69% vs. 51% vs. 69%, respectively, *P*=0.8).

Table 1. Clinical characteristics of the patients with structural and numerical aberrations of *MYC* at fluorescence *in situ* hybridization.

	All patients (n =95) n (%)	MYC-T (n=34) n (%)	MYC-ICN/ MYC AMP (n=61) n (%)
Age, median (range)	67 (21-88)	66.5 (27-88)	67 (21-84)
Male sex	63 (66)	24 (71)	39 (64)
Ann Arbor stage III-IV	76 (80)	30 (88)	46 (75)
IPI High intermediate/ High risk	66 (69)	24 (71)	42 (69)
IHC MYC positivity	**n=52** 46 (88)	**n=24** 24 (100)	**n=28** 21 (75)
Histopathology			
DLBCL, NOS	87 (92)	27 (79)	60 (98)
BCLU	8 (8)	7 (21)	1 (2)
BCL2 and BCL6 status			
BCL2-T	34 (36)	20 (59)	14 (23)
BCL6-T	29 (31)	2 (6)	27 (44)
BCL2-ICN	23 (24)	11 (32)	12 (20)
BCL6-ICN	21 (22)	5 (15)	16 (27)
Treatment regimen			
Standard			
R-CHOP/R-CHOP-like	46 (48)	9 (26)	37 (61)
- R-CHOP	26 (27)	6 (17)	20 (33)
- R-COMP	20 (21)	3 (9)	17 (28)
Intensified	44 (46)	22 (65)	22 (36)
GMALL-like ± ASCT	15 (23)	10 (29)	5 (8)
R-DA-EPOCH ± ASCT	13 (14)	10 (29)	3 (5)
R-CHOP/R-CHOP-like + ASCT	16 (17)	2 (6)	14 (23)
- R-CHOP + ASCT	15 (16)	1 (3)	14 (23)
- R-ESHAP + ASCT	1 (1)	1 (3)	0
Palliative	5 (5)	3 (9)	2 (3)
Total ASCT consolidation	23 (24)	8 (23)	15 (25)
Response	**n=90**	**n=31**	**n=59**
CR	55 (61)	18 (58)	37 (63)
PR	12 (13)	4 (13)	8 (14)
NR/disease progression	23 (26)	9 (29)	14 (24)

DLBCL: diffuse large B-cell lymphoma; NOS: not otherwise specified; BCLU: B-cell lymphoma, unclassifiable; IPI: International Prognostic Index; IHC: immunohistochemistry; ASCT: autologous stem cell transplantation; CR: complete response; PR: partial response; NR: no response; n: number.

MYC, BCL2 and *BCL6* translocations

A *MYC* translocation (MYC-T) by FISH study was observed in 34 patients (8.8%). With respect to *BCL2* and *BCL6, MYC* translocation occurred as a single-hit (SH) aberration in 9 of 34 patients (26%), whereas 19 (56%) and 6 (18%) patients had a "double-hit" (DH) and "triple-hit" (TH) DLBCL, respectively. The clinical characteristics in terms of age, gender, histopathology, MYC protein expression by IHC, Ann Arbor and IPI stage were not significantly different among patients with SH, DH or TH DLBCL (Table 2). Three patients who received palliative/symptomatic treatment were excluded from the survival analyses. Overall, nine patients were treated with a standard regimen and 22 with an intensified regimen, with similar distribution among the SH, DH and TH DLBCL groups. After a median follow up of 33 months, the 2.5-year OS was similar among SH, DH, and TH DLBCL patients.

Numerical aberrations *MYC* by fluorescence *in situ* hybridization

We observed an increased number of *MYC* gene copies (16%) in tumor samples from 61 patients negative for *MYC* translocations. Fifty-seven cases (15%) were referred to as to "increased copy number of *MYC*" (MYC-ICN) DLBCL, while four cases (1%) showed amplification of *MYC* (MYC-AMP) (Figure 1). The exact number of

Table 2. Clinical characteristics of the patients with single-hit (SH), double-hit (DH) or triple-hit (TH) diffuse large B-cell lymphoma at fluorescence *in situ* hybridization.

	MYC-T SH (n=9) n (%)	MYC-T DH (n=19) n (%)	MYC-T TH (n=6) n (%)	*P*
Age, median (range)	71 (29-74)	63 (29-88)	62 (58-83)	0.71
Male gender	4 (44)	15 (79)	5 (83)	0.13
Ann Arbor stage III-IV	7 (78)	18 (95)	5 (83)	0.39
IPI High intermediate/ High risk	8 (89)	12 (63)	4 (67)	0.36
IHC MYC positivity	**n=5** 5 (100)	**n=15** 15 (100)	**n=4** 4 (100)	–
Histopathology				
DLBCL, NOS	7 (78)	15 (79)	5 (83)	0.96
BCLU	2 (22)	4 (21)	1 (17)	
Treatment regimen				
Standard				
R-CHOP/R-CHOP-like	2 (22)	4 (21)	3 (50)	0.35
Intensified				
GMALL-like ± ASCT	4 (45)	5 (27)	1 (17)	0.46
R-DA-EPOCH ± ASCT	0	8 (42)	2 (33)	0.07
R-CHOP/R-CHOP-like + ASCT	1 (11)	1 (5)	0	0.65
Palliative	2 (22)	1 (5)	0	0.23
Total ASCT consolidation	1 (11)	6 (36)	1 (17)	0.44
Response	**n=7**	**n=18**	**n=6**	
CR	5 (71)	9 (50)	4 (67)	0.69
PR	0	4 (22)	0	0.16
NR/disease progression	2 (29)	5 (28)	2 (33)	0.89
2.5-year OS	47%	58%	62%	0.96

DLBCL: diffuse large B-cell lymphoma; NOS: not otherwise specified; BCLU: B-cell lymphoma, unclassifiable; IPI: International Prognostic Index; IHC: immunohistochemistry; ASCT: autologous stem cell transplantation; CR: complete response; PR: partial response; NR: no response; OS: overall survival; n: number.

extra-copies (EC) of *MYC* was not assessable in six cases. In the remaining 51, 3-10 gene copies per cell were found in at least 50% of the analyzed nuclei. In detail, the distribution of *MYC* gene copies in the MYC-ICN cases was: 3 copies in 12 cases (24%), 4 copies in 19 (37%), 5 copies in 8 (15%), 6 copies in 4 (8%), 7 copies in 5 (10%), and 8-10 copies in 3 (6%). Of note, more than 60% of cases presented 3-4 copies of *MYC*. Since ICN aberration was identified during routine *MYC* analysis for which the break-apart probe is regularly used in our laboratory, information on the copies of chromosome 8 was available in only 11 cases showing MYC-ICN, where a single centromeric chromosome 8 probe was also used. No abnormal copies of chromosome 8 were detected in any of these cases, whereas identical MYC-ICN was found, thus excluding polysomy as cause of MYC-ICN.

An excess of copies of *BCL2* (BCL2-ICN) and *BCL6* (BCL6-ICN) was also found in these cases (in 44% and 27%, respectively), whereas *BCL2* and *BCL6* translocations (BCL2-T and BCL6-T) were observed in 23% and 20% of cases with numerical aberrations of *MYC*, respectively (Table 1).

Clinical impact of numerical and structural aberrations of *MYC*

The overall prognosis of patients with *MYC* numerical aberrations showed a negative correlation between increasing number of *MYC* copies and survival (Figure 3). Patients with MYC-ICN ≤4 had a more favorable outcome, with 2.5-year OS of 73% (95%CI: 50-84) compared to 30% (95%CI: 15-43) of the patients with MYC-ICN >4 (P=0.007) (Figure 3A). Having MYC-ICN>7 or MYC-AMP was associated with the worst prognosis, with a median OS of 8 and 8.5 months, respectively (P=0.0008) (Figure 3B). When comparing the outcome of patients with MYC-ICN ≤4 and MYC-ICN >4 with the outcome of patients with MYC-T or MYC-AMP, the presence of MYC-ICN ≤4 was associated with a better outcome (P=0.01) (Figure 3C), while patients with MYC-ICN >4 had no significant difference in OS compared to MYC-T (P=0.1), and both these groups of patients had a better survival compared to MYC-AMP (P=0.05 and P=0.01, respectively).

The demographic and clinical characteristics of the patients with MYC-ICN ≤4, MYC-ICN >4, MYC-T, and MYC-AMP in terms of age, gender, histopathology, MYC

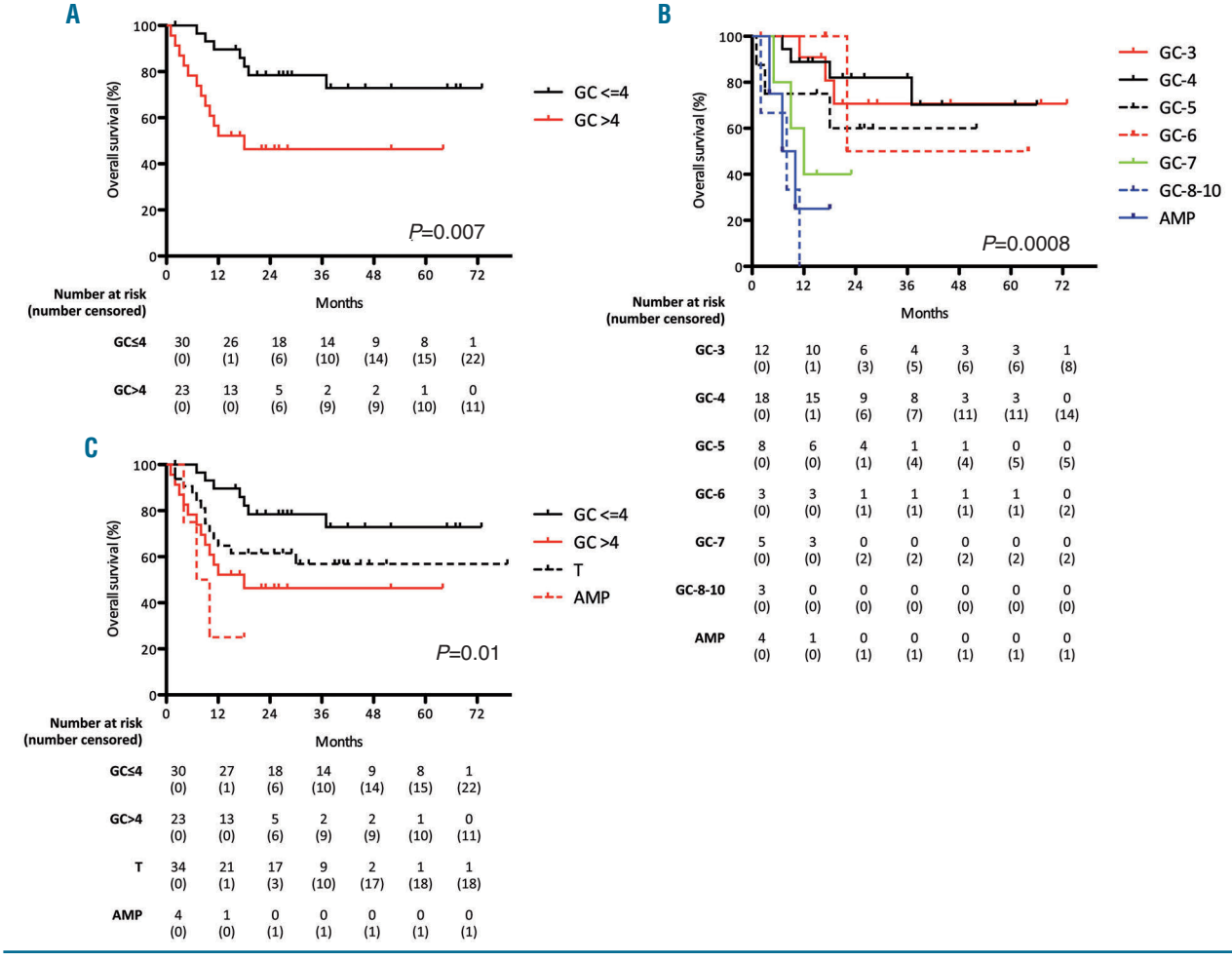

Figure 3. Negative correlation between increasing number of MYC copies and survival. (A) Kaplan-Meier curve comparing 2.5 year overall survival (OS) of patients with *MYC*-ICN ≤4 and patients with *MYC*-ICN >4. (B) Negative correlation between increasing number of *MYC* copies and survival: patients with *MYC* gene copies (MYC-GC) >7 and MYC-AMP showed the worse prognosis. (C) Comparison of the outcome of patients with MYC-ICN ≤4 and MYC-ICN >4 with patients with *MYC* translocation (MYC-T) or MYC-AMP: while MYC-ICN ≤4 conferred the best outcome, patients with MYC-ICN >4 had no significant difference in OS compared to MYC-T, and both these groups of patients had a better survival compared to MYC-AMP; GC: gene copies.

protein expression by IHC, Ann Arbor and IPI stage, were not significantly different, except that patients with a histological diagnosis of BCLU clustered in the MYC-T and MYC-AMP groups (P=0.03) (Table 3). Notably, all patients with MYC-AMP showed aggressive clinical features, although one did not show MYC protein overexpression by IHC.

The treatment type and the response to treatment in each FISH category are reported in Table 3. Patients with MYC-ICN preferentially received standard treatment (61% MYC-ICN ≤4 and 65% MYC-ICN >4, respectively, P=0.008), unlike patients with MYC-T and MYC-AMP who received an intensified regimen in 65% and 75% of cases, respectively (P=0.02).

Patients with MYC-ICN ≤4 had a higher overall response rate (ORR) and complete response rate (CRR) compared to the other FISH groups (ORR 93% *vs.* 59%, P=0.0009; CRR 73% *vs.* 57%, P=0.16), and also a significantly lower progression rate (7% *vs.* 41%, P=0.0009). In the MYC-ICN ≤4 subgroup, there was neither a difference in terms of ORR and CRR achievement, nor a significant advantage in terms of OS and PFS between patients treated with standard or intensified regimens. At a median follow up of 3.5 years, OS was 73% and 70%, respectively. In the MYC-T group, ORR was similar in patients treated with standard or intensive induction therapy, and CRR was slightly higher in the intensified-regimen group (64% *vs.* 55%) (Table 3).

Patients with MYC-ICN >4 and MYC-T receiving a first-line intensified regimen showed a non-significant trend toward a better outcome (2.5-year OS of 40% for standard treatment vs. 60% for intensified treatment in MYC-ICN >4; OS of 53% for standard treatment vs. 65% for intensified treatment in MYC-T). The same trend was seen combining MYC-AMP group with MYC-ICN >4 and MYC-T groups (2.5-year OS of 32% for standard *vs.* 57% for intensified treatment).

Table 3. Clinical characteristics of the patients with MYC-ICN ≤4, MYC-ICN >4, MYC-T, and MYC-AMP.

All patients	MYC-ICN ≤4 (n=31) n (%)	MYC-ICN >4 (n=20) n (%)	MYC-T (n=34) n (%)	MYC-AMP (n=4) n (%)	*P*
Age, median (range)	65 (21-84)	73 (30-81)	66.5 (27-88)	66 (57-73)	0.81
Male gender, n. (%)	20 (65)	9 (45)	24 (72)	4 (100)	0.15
Ann Arbor stage III-IV	22 (71)	15 (75)	30 (91)	4 (100)	0.77
IPI High intermediate/ High risk	19 (61)	16 (80)	24 (72)	4 (100)	0.31
IHC MYC positivity	**n=13** 9 (69)	**n=11** 9 (81)	**n=24** 24 (100)	**n=3** 2 (66)	0.21
Histopathology					
DLBCL, NOS	31 (100)	20 (100)	27 (82)	3 (75)	0.06
BCLU	0	0	6 (18)	1 (25)	**0.03**
Treatment regimen					
Standard					
R-CHOP/R-CHOP-like	19 (61)	13 (65)	9 (26)	1 (25)	**0.008**
Intensified	11 (35)	6 (30)	22 (65)	3 (75)	**0.02**
GMALL-like ± ASCT	1 (3)	2 (10)	10 (29)	1 (25)	**0.02**
R-DA-EPOCH ± ASCT	0	2 (10)	10 (29)	1 (25)	**0.008**
R-CHOP/R-CHOP-like + ASCT	10 (33)	2 (10)	2 (6)	1 (25)	**0.03**
Palliative	1 (3)	1 (5)	3 (9)	0	0.74
Total ASCT consolidation	10 (33)	2 (11)	8 (23)	1 (25)	0.38
Response	**n=30**	**n=19**	**n=31**	**n=4**	
ORR	28 (93)	11 (63)	20 (64)	1 (25)	**0.0009***
Standard	17/19 (89)	8/13 (61)	6/9 (67)	0	
Intensified	11/11 (100)	3/6 (50)	14/22 (64)	1/3 (33)	
CR	22 (73)	11 (58)	19 (61)	1 (25)	0.16*
Standard	14/19 (74)	8/13 (61)	5/9 (55)	0/1 (0)	
Intensified	8/11 (73)	3/6 (50)	14/22 (64)	1/3 (33)	
PR	6 (20)	0	1 (3)	0	**0.03***
Standard	3/19 (16)	0/13	1/9 (11)	0/1	
Intensified	3/11 (27)	0/6	0/22	0/3	
NR/disease progression	2 (7)	8 (42)	11 (36)	3 (75)	**0.0009***
Standard	2/19 (10)	5/13 (38)	3/9 (33)	1/1 (100)	
Intensified	0/11 (0)	3/6 (50)	8/22 (36)	2/3 (67)	

DLBCL: diffuse large B-cell lymphoma; NOS: not otherwise specified; BCLU: B-cell lymphoma, unclassifiable; IPI: International Prognostic Index; IHC: immunohistochemistry; ASCT: autologous stem cell transplantation; ORR: overall response rate; CR: complete response; PR: partial response; NR: no response; n: number. *Overall response (OR), CR, PR and NR/disease progression rates of MYC-ICN<4 compared to the combination of other fluorescence *in situ* hybridization (FISH) groups.

Among intensified regimens, in MYC-T and MYC-AMP subgroups, patients treated with R-DA-EPOCH showed an advantage in ORR compared to patients treated with GMALL B-ALL/NHL 2002 protocol or R-CHOP followed by ASCT (ORR 82% *vs.* 36%, *P*=0.04), and a trend toward a better survival was also seen (2.5-year OS of 81% *vs.* 46%, *P*=0.08) (Figure 4). Five patients initially considered fit for curative treatment and tested by FISH, were eventually treated with palliative care due to rapidly worsening clinical conditions. Palliative regimens were single-agent cyclophosphamide for three patients, and single-agent vincristine for two patients; among these five patients, three had MYC-T (1 double-hit MYC-T/BCL2-T, 2 single-hit lymphomas), one MYC-ICN≤4, and one MYC-ICN>4. They experienced a dismal outcome irrespective of MYC status (median survival of 2 months for the MYC-T group and 1 month for each of the other 2 patients, *P*=0.7) (data not shown).

Finally, we analyzed the impact of *BCL2* and *BCL6* numerical and structural aberrations on the outcome of patients with numerical aberrations of *MYC* (MYC-ICN/MYC-AMP). BCL2-ICN did not influence patient survival, which was very similar to patients with wild-type (WT) BCL2 (2.5-year OS 70% *vs.* 69%, respectively). However, BCL2-T negatively influenced patient outcome compared to BCL2-WT and BCL2-ICN patients (2.5-year

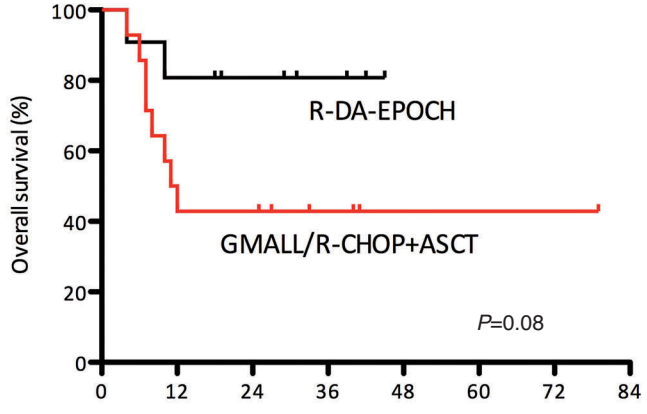

Number at risk (number censored)							
R-DA-EPOCH	11 (0)	8 (1)	6 (3)	5 (4)	0 (9)	0 (9)	0 (9)
GMALL/ R-CHOP+ASCT	15 (0)	7 (0)	6 (0)	3 (3)	1 (5)	1 (5)	1 (5)

Figure 4. Analysis of response to treatment with R-DA-EPOCH. In the MYC-T and MYC-AMP subgroups, patients treated with R-DA-EPOCH showed an advantage in ORR and trend toward a better survival compared to patients treated with GMALL B-ALL/NHL 2002 protocol or R-CHOP followed by autologous stem cell transplantation (ASCT).

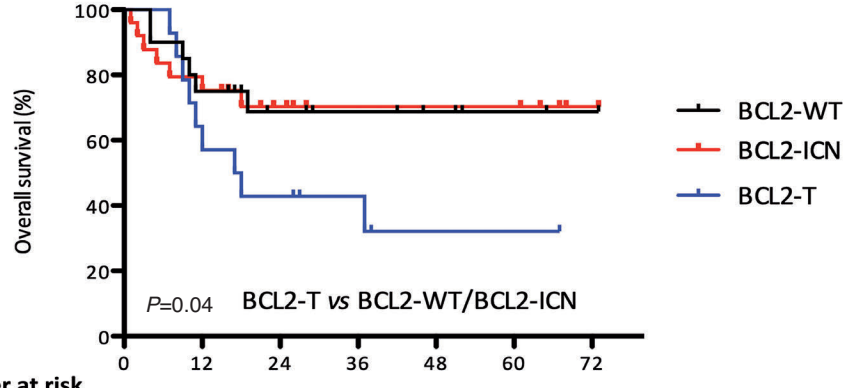

Number at risk (number censored)							
BCL2-WT	20 (0)	15 (0)	10 (4)	8 (6)	5 (9)	2 (12)	1 (13)
BCL2-ICN	25 (0)	19 (1)	10 (8)	7 (11)	7 (11)	7 (11)	1 (17)
BCL2-T	14 (0)	9 (0)	6 (0)	4 (2)	2 (3)	2 (3)	0 (5)

Figure 5. Negative impact of *BCL2* translocation on the outcome of patients with MYC-ICN. BCL2-ICN did not influence survival of patients with MYC-ICN, whereas BCL2-T negatively influenced the outcome of these patients compared to BCL2-WT and BCL2-ICN patients. Notably, among patients with MYC-ICN and BCL2-T, the group with >4 copies had a significantly worse prognosis than patients with ≤4 copies [median overall survival (OS) of 11 months compared to a 2.5-year OS of 75%, *P*=0.004] (*data not shown*).

OS 32% *vs.* 70%, *P*=0.04) (Figure 5), whereas BCL6-ICN and BCL6-T did not significantly impact on patient outcome compared to WT *BCL6* (*data not shown*). Of note, among patients with MYC-ICN and BCL2-T, the group with ≥4 *MYC* copies had a significantly worse prognosis than patients with <4 copies (median OS of 11 months compared to a 2.5-year OS of 75%, P=0.004) (data not shown). Only one patient with MYC-AMP was positive for *BCL2* translocation; survival was seven months.

Discussion

MYC rearrangement is considered to confer a poor prognosis to DLBCL patients and to represent an adverse prognostic factor in patients treated with R-CHOP. In our study, the prevalence of MYC translocations was 8.8%, in accordance with data from the literature.[10] A single-hit MYC aberration was present in 26% of patients, while 74% had classical DH/TH aberrations. Although a worse prognosis of patients with DH/TH compared to SH DLBCL has been described,[24,25] we could not confirm a significant difference in the outcome of SH *versus* DH/TH patients, as reported also by Copie-Bergman.[16] Among patients with MYC-T eligible for curative chemotherapy, 65% were treated with an intensified regimen, obtaining a slight advantage in terms of response rate but no significant advantage in survival compared to standard dose chemo-immunotherapy, confirming data reported by Petrich *et al.*[26]

In addition to *MYC* gene rearrangements, an increase in *MYC* copy number was observed in 16% of patients, a nearly 2-fold more than that of *MYC* translocations. The presence of MYC-ICN has been analyzed in several studies; frequency ranged from 7% to 21%,[18,20,27-29] but its prognostic significance is still controversial. Yoon reported ICN in 7% of 156 DLBCL patients,[18] with an adverse prognostic significance, while Testoni *et al*. found an ICN of no more than 4 gene copies in 10% of 166 patients, and the negative prognostic impact was limited to patients with a concomitant del (8p) chromosomal aberration.[28] Valera *et al*. found 3-4 MYC ICN in 19% and >4 MYC-ICN in 2% of 176 patients, with a negative impact on outcome in the few patients with >4 MYC-ICN.[20] In the group of 22 patients with >4 MYC ICN analyzed by Landsburg *et al*., neither the 2-year PFS (48%) or OS (71%) were significantly lower than those of patients with normal MYC.[29] More recently, in a large study reported by Quesada on 663 DLBCL patients, 76 (12%) had MYC-ICN, and 16% of them had >4 extra-copies. The CR and OS of patients with MYC-ICN were significantly worse compared to patients with normal *MYC* gene, irrespective of the number of *MYC* extra-copies.[27]

A number of *MYC* copies >4 has been defined in some studies as *MYC* amplification.[20,30] In the present study, we have analyzed the 61 patients with MYC-ICN by exactly enumerating the number of *MYC* extra-copies, defining as amplified those cases with an uncountable number of *MYC*-copies. The same criteria and terminology have been adopted in a recent study by Pophali *et al*.[31] We, like other authors,[20,31] did not systematically use a chromosome 8 centromeric probe for this study. Nevertheless, we analyzed chromosome 8 in 11 cases with MYC-ICN, and no abnormal copies of chromosome 8 were detected, thus excluding polysomy as cause of MYC-ICN.

Our patients with 3 or 4 gene copies, accounting for more than 60% of MYC-ICN, had a more favorable outcome than patients with MYC-ICN >4, and their ORR and CRR were higher compared to the other FISH groups, and were not influenced by the type of treatment received as first-line. There was no difference in OS between patients with 3 or 4 *MYC* gene copies. On the other hand, by stratifying them according to the exact number of *MYC* extra-copies, a negative correlation between an increasing number of *MYC* copies and survival was observed. Patients with MYC-ICN >7 had the worst prognosis, and patients with an amplification of MYC at FISH had a particularly aggressive disease and a dismal prognosis. Of note, the single MYC-AMP patient who did not show MYC protein positivity by immunohistochemistry was also the only patient who responded to treatment. Notably, a correlation between an excess of *MYC* copies, MYC protein overexpression and poor outcome has been previously described.[32] In our study, patients with MYC-ICN >4 seemed to have a more favourable outcome compared to MYC-T patients, whereas Quesada and colleagues observed the opposite result, although this outcome was not statistically significant in both studies.[27]

Taken together, our results show a prognostic role of the number of MYC extra-copies. In accordance with other studies, results underline that, among MYC-ICN, the presence of >4 *MYC* gene copies, and particularly of countless numbers of *MYC* as in MYC-AMP, is associated with a worse prognosis and does identify a category of patients with a prognosis similar to double-hit lymphoma. Of note, the 24 patients with >4 MYC copies represented 6.6% of our entire series, further supporting the potential usefulness of a routine use of FISH at diagnosis in DLBCL.[12,13,33] We did not identify specific clinical characteristic of patients associated with the presence of different FISH patterns, except that a significant higher percentage of patients with BCLU histology clustered in the MYC-T group. Notably, 7 of 8 patients with BCLU carried MYC-T and one patient MYC-AMP. Since 5 patients with BCLU and MYC-T had a double- or triple-hit lymphoma, they would now be defined as high grade B-cell lymphoma (HGBCL) with *MYC* and *BCL2* and/or *BCL6* translocations according to the updated 2016 WHO classification of lymphoid neoplasms.[1]

Although there have been no published prospective trials in double-hit lymphoma, retrospective studies seem to suggest that aggressive induction regimens may confer a superior outcome.[34] In a large retrospective series, patients receiving a Burkitt-like regimen (cyclophosphamide, vincristine, doxorubicin, methotrexate, ifosfamide, etoposide, cytarabine, CODOX-M/IVAC) and consolidation with ASCT appeared to have favorable outcomes over historical controls; however, the 2-year PFS was only 44%, with early progressions precluding ASCT in 41% of patients.[35] In another non-randomized retrospective study comparing R-CHOP with R-DA-EPOCH and other intensified regimens, response rates were higher for dose-adjusted R-EPOCH.[26,36]

In addition to its retrospective nature, a major limitation of our study in evaluating the impact of different treatment strategies on lymphoma outcome was the heterogeneity of the regimens used, including ASCT, and the small number of patients in each subgroup with different *MYC* abnormalities. Moreover, the exclusion of patients not treated with curative intent does not allow the frequency of *MYC* abnormalities in these patients or their

impact on the efficacy of less intensive treatments to be evaluated. In any case, the treatment choice was based on the individual clinician's decision.

Overall, no differences emerged between standard chemo-immunotherapy and more aggressive regimens both in CR achievement and in survival, particularly in the subgroup of patients with a limited number of *MYC* abnormalities (≤4). On the other hand, the survival of patients with MYC-T, MYC-ICN >4 and MYC-AMP seemed to be superior if intensive treatments were used, and DA-EPOCH among intensive treatments seemed to be the most effective for patients with MYC-T and MYC-AMP. Nevertheless, these retrospective data should be interpreted with caution, particularly in the absence of statistical significance; further studies are need in larger groups of patients and these results confirmed in prospective studies.

The present study further confirms that the occurrence of a *BCL-2* translocation has a negative prognostic influence. In contrast to the presence of *MYC* extra-copies, the presence of extra-copies of *BCL-2* and *BCL-6* genes did not carry any adverse prognostic significance. Likewise, *BCL-2* and *BCL-6* extra-copies did not worsen the outcome of patients with MYC-ICN in the study by Quesada *et al.*[27]

In conclusion, our study shows that, in DLBCL patients, *MYC* extra-copies are more frequently detected by FISH studies than *MYC* translocations, highlighting the importance of FISH testing at diagnosis of DLBCL. While having 3-4 copies of *MYC* correlated with a high rate of treatment response and a good prognosis also with standard immuno-chemotherapy, lymphoma showing >4 copies of *MYC* had a more aggressive disease, comparable to *MYC*-translocated DLBCL, and may be more responsive to intensified treatment approaches. Further investigation is warranted to clarify the biological implications of numerical aberrations of *MYC* and the possible benefit of specific or intensified therapeutic strategies.

Acknowledgments

The authors would like to thank all doctors and nurses who provided patients' care at the Department of Hematology, ASST Spedali Civili di Brescia.

References

1. Swerdlow SH, Campo E, Pileri SA, et al. The 2016 revision of the World Health Organization classification of lymphoid neoplasms. Blood. 2016;127(20):2375-2391.
2. International Non-Hodgkin's Lymphoma Prognostic Factors Project. A predictive model for aggressive Non-Hodgkin's Lymphoma. N Engl J Med. 1993; 329(14):987-994.
3. Sehn LH, Berry B, Chhanabhai M, et al. The revised International Prognostic Index (R-IPI) is a better predictor of outcome than the standard IPI for patients with diffuse large B-cell lymphoma treated with R-CHOP. Blood. 2015;109(5):1857-1862.
4. Green TM, Young KH, Visco C, et al. Immunohistochemical double-hit score is a strong predictor of outcome in patients with diffuse large B-cell lymphoma treated with rituximab plus cyclophosphamide, doxorubicin, vincristine, and prednisone. J Clin Oncol. 2012;30(28):3460-3467.
5. Jaffe E, Harris N, Stein H, Vardiman J. Pathology and Genetics of Tumours of Haematopoietic and Lymphoid Tissues. WHO Classification of Tumours, Third Edition. 3. 2001;3.
6. Swerdlow SH, Campo E, Harris NL, et al. WHO Classification of Tumours, Fourth Edition. IARC WHO Classif Tumours. 2008; 2.
7. Rosenwald A, Wright G, Chan WC, et al. The Use of Molecular Profiling to Predict Survival after Chemotherapy for Diffuse Large-B-Cell Lymphoma. N Engl J Med. 2002;346(25):1937-1947.
8. Hu S, Xu-Monette ZY, Tzankov A, et al. MYC/BCL2 protein coexpression contributes to the inferior survival of activated B-cell subtype of diffuse large B-cell lymphoma and demonstrates high-risk gene expression signatures: A report from the International DLBCL Rituximab-CHOP Consortium Program. Blood. 2013; 121(20): 4021-4031.
9. Kramer MH, Hermans J, Wijburg E, et al. Clinical relevance of BCL2, BCL6, and MYC rearrangements in diffuse large B-cell lymphoma. Blood. 1998;92(9):3152-3162.
10. Horn H, Ziepert M, Becher C, et al. MYC status in concert with BCL2 and BCL6 expression predicts outcome in diffuse large B-cell lymphoma. Blood. 2013;121(12):2253-2263.
11. Klapper W, Stoecklein H, Zeynalova S, et al. Structural aberrations affecting the MYC locus indicate a poor prognosis independent of clinical risk factors in diffuse large B-cell lymphomas treated within randomized trials of the German High-Grade Non-Hodgkin's Lymphoma Study Group (DSHNHL). Leukemia. 2008;22(12):2226-2229.
12. Savage KJ, Johnson N a, Ben-neriah S, et al. MYC gene rearrangements are associated with a poor prognosis in diffuse large B-cell lymphoma patients treated with R-CHOP chemotherapy. Blood. 2009;114(17):3533-3537.
13. Barrans S, Crouch S, Smith A, et al. Rearrangement of MYC is associated with poor prognosis in patients with diffuse large B-cell lymphoma treated in the era of rituximab. J Clin Oncol. 2010;28(20):3360-3365.
14. Snuderl M, Kolman O, Chen Y-B, et al. B-cell Lymphomas with Concurrent IGH-BCL2 and MYC Rearrangements Are Aggressive Neoplasms with Clinical and Pathologic Features Distinct from Burkitt Lymphoma and Diffuse Large B-cell Lymphoma. Am J Surg Pathol. 2010;34(3):327-340.
15. Campo E. MYC in DLBCL: Partners matter. Blood. 2015;126(22):2439-2440.
16. Copie-Bergman C, Cuillière-Dartigues P, Baia M, et al. MYC-IG rearrangements are negative predictors of survival in DLBCL patients treated with immunochemotherapy: A GELA/LYSA study. Blood. 2015; 126(22):2466-2474.
17. Pedersen MO, Gang AO, Poulsen TS, et al. MYC translocation partner gene determines survival of patients with large B cell lymphoma with MYC or double hit MYC/BCL2 translocations. Eur J Haematol. 2014;92(1):42-48.
18. Yoon S, Jeon Y, Paik J, et al. MYC translocation and an increased copy number predict poor prognosis in adult diffuse large B-cell lymphoma (DLBCL), especially in germinal centre-like B cell (GCB) type. Histopathology. 2008;53(2):205-217.
19. Stasik CJ, Nitta H, Zhang W, et al. Increased MYC gene copy number correlates with increased mRNA levels in diffuse large B-cell lymphoma. Haematologica. 2010;95(4):597-603.
20. Valera A, López-Guillermo A, Cardesa-Salzmann T, et al. MYC protein expression and genetic alterations have prognostic impact in patients with diffuse large B-cell lymphoma treated with immunochemotherapy. Haematologica. 2013;98(10):1554-1562.
21. Hoelzer D, Walewski J, Hartmut D, et al. Improved outcome of adult Burkitt lymphoma/leukemia with rituximab and chemotherapy : report of a large prospective multicenter trial. Blood. 2014;124(26):3870-3880.
22. Cheson BD, Pfistner B, Juweid ME, et al. Revised response criteria for malignant lymphoma. J Clin Oncol. 2007;25(5):579-586.
23. Kaplan EL, Meier P. Nonparametric Estimation from Incomplete Observations. J Am Stat Assoc. 1958;53(282):457-481.
24. Cohen JB, Geyer SM, Lozanski G, et al. Complete Response to Induction Therapy in Patients With Myc-Positive and Double-Hit Non-Hodgkin Lymphoma Is Associated With Prolonged Progression-Free Survival. Cancer. 2014;120(11):1611-1613.
25. Landsburg DJ, Nasta SD, Svoboda J, Morrissette JJD, Schuster SJ. ' Double-Hit ' cytogenetic status may not be predicted by baseline clinicopathological characteristics

and is highly associated with overall survival in B cell lymphoma patients. Br J Haematol. 2014;166(3):369–374.
26. Petrich AM, Gandhi M, Jovanvoic B, et al. Impact of induction regimen and stem cell transplantation on outcomes in patients with double-hit lymphoma : a large multicenter retrospective analysis. Blood. 2014;124(15):1-9.
27. Quesada A, Medeiros L, Desai P, et al. Increased MYC copy number is an independent prognostic factor in patients with diffuse large B-cell lymphoma. Mod Pathol. 2017;30(12):1688-1697.
28. Testoni M, Kwee I, Greiner TC, et al. Gains of MYC locus and outcome in patients with diffuse large B-cell lymphoma treated with R-CHOP. Br J Haematol. 2011;155(2):274-277.
29. Landsburg DJ, Falkiewicz MK, Petrich AM, et al. Sole rearrangement but not amplification of MYC is associated with a poor prognosis in patients with diffuse large B cell lymphoma and B cell lymphoma unclassifiable. Br J Haematol. 2016;175(4):631-640.
30. Testoni M, Zucca E, Young KH, Bertoni F. Genetic lesions in diffuse large B-cell lymphomas. Ann Oncol. 2015;26(6):1069-1080.
31. Pophali P, Marinelli LM, Ketterling RP, et al. High Level MYC Amplification in Aggressive B-Cell Lymphomas: Is It a Marker of Aggressive Disease? Blood. 2018;132(Suppl 1):1693.
32. Valentino C, Kendrick S, Johnson N, et al. Colorimetric In Situ Hybridization Identifies MYC Gene Signal Clusters Correlating With Increased Copy Number, mRNA, and Protein in Diffuse Large B-cell Lymphoma Carlo. Am J Clin Pathol. 2013;139(2):242-254.
33. Swerdlow SH. Diagnosis of 'double hit' diffuse large B-cell lymphoma and B-cell lymphoma, unclassifiable, with features intermediate between DLBCL and Burkitt lymphoma: when and how, FISH versus IHC. Hematol Am Soc Hematol Educ Program. 2014;2014(1):90-99.
34. Friedberg JW. How I Treat How I treat double-hit lymphoma. Blood. 2017;130(5):590-597.
35. Sun H, Savage K, Karsan A, et al. Outcome of Patients With Non-Hodgkin Lymphomas With Concurrent MYC and BCL2 Rearrangements Treated With CODOX-M/IVAC With Rituximab Followed by Hematopoietic Stem Cell Transplantation. Clin Lymphoma Myeloma Leuk. 2015;15(6):341-348.
36. Oki Y, Noorani M, Lin P, et al. Double hit lymphoma : the MD Anderson Cancer Center clinical experience. Br J Haematol. 2014;166:891-901.

ARTICLE

Genomic alterations in high-risk chronic lymphocytic leukemia frequently affect cell cycle key regulators and NOTCH1-regulated transcription

Jennifer Edelmann,[1,2] Karlheinz Holzmann,[3] Eugen Tausch,[1] Emily A. Saunderson,[2] Billy M. C. Jebaraj,[1] Daniela Steinbrecher,[1] Anna Dolnik,[1] Tamara J. Blätte,[1] Dan A. Landau,[4,5] Jenny Saub,[1] Sven Estenfelder,[1] Stefan Ibach,[6] Florence Cymbalista,[7] Veronique Leblond,[8] Alain Delmer,[9] Jasmin Bahlo,[10] Sandra Robrecht,[10] Kirsten Fischer,[10] Valentin Goede,[10] Lars Bullinger,[1,11] Catherine J. Wu,[4] Daniel Mertens,[1], Gabriella Ficz,[2] John G. Gribben,[2] Michael Hallek,[10] Hartmut Döhner[1] and Stephan Stilgenbauer[1]

[1]Department of Internal Medicine III, Ulm University, Ulm, Germany; [2]Centre for Haemato-Oncology, Barts Cancer Institute, Queen Mary University of London, London, UK; [3]Genomics Core Facility, Ulm University, Ulm, Germany; [4]Department of Medical Oncology, Dana Farber Cancer Institute, Boston, MA, USA; [5]New York Genome Center, New York, NY, USA; [6]Wissenschaftlicher Service Pharma GmbH (WiSP), Langenfeld, Germany; [7]Service d'Hématologie Biologique, Hôpital Avicenne, Bobigny, France; [8]Service d'Hématologie, Hôpital Pitié-Salpêtrière, Paris, France; [9]Service d'Hématologie Clinique, CHU de Reims, Reims, France; [10]Department of Internal Medicine I, University of Cologne, Cologne, Germany and [11]Department of Hematology, Oncology and Tumor Immunology, Charité University Medicine Berlin, Campus Virchow Klinikum, Berlin, Germany

Ferrata Storti Foundation

Haematologica 2020
Volume 105(5):1379-1390

ABSTRACT

To identify genomic alterations contributing to the pathogenesis of high-risk chronic lymphocytic leukemia (CLL) beyond the well-established role of *TP53* aberrations, we comprehensively analyzed 75 relapsed/refractory and 71 treatment-naïve high-risk cases from prospective clinical trials by single nucleotide polymorphism arrays and targeted next-generation sequencing. Increased genomic complexity was a hallmark of relapsed/refractory and treatment-naïve high-risk CLL. In relapsed/refractory cases previously exposed to the selective pressure of chemo(immuno)therapy, gain(8)(q24.21) and del(9)(p21.3) were particularly enriched. Both alterations affect key regulators of cell-cycle progression, namely *MYC* and *CDKN2A/B*. While homozygous *CDKN2A/B* loss has been directly associated with Richter transformation, we did not find this association for heterozygous loss of *CDKN2A/B*. Gains in 8q24.21 were either focal gains in a *MYC* enhancer region or large gains affecting the *MYC* locus, but only the latter type was highly enriched in relapsed/refractory CLL (17%). In addition to a high frequency of *NOTCH1* mutations (23%), we found recurrent genetic alterations in *SPEN* (4% mutated), *RBPJ* (8% deleted) and *SNW1* (8% deleted), all affecting a protein complex that represses transcription of NOTCH1 target genes. We investigated the functional impact of these alterations on *HES1*, *DTX1* and *MYC* gene transcription and found derepression of these NOTCH1 target genes particularly with *SPEN* mutations. In summary, we provide new insights into the genomic architecture of high-risk CLL, define novel recurrent DNA copy number alterations and refine knowledge on del(9p), gain(8q) and alterations affecting NOTCH1 signaling. This study was registered at ClinicalTrials.gov with number NCT01392079.

Correspondence:

JENNIFER EDELMANN
jennifer.edelmann@uniklinik-ulm.de

Received: February 5, 2019.

Accepted: August 23, 2019.

Pre-published: August 29, 2019.

doi:10.3324/haematol.2019.217307

Check the online version for the most updated information on this article, online supplements, and information on authorship & disclosures: www.haematologica.org/content/105/5/1379

Introduction

Advanced understanding of the pathophysiology of chronic lymphocytic leukemia (CLL) has led to targeted therapy approaches such as inhibition of B-cell receptor signaling by BTK inhibitors or PI3K inhibitors and antagonism of BCL-2.[1,2] These treatment strategies clearly improved the clinical outcome of high-risk CLL,[1,2] although inadequate responses have been observed in as yet insufficiently characterized subgroups of patients.[3-5] In the era of chemo(immuno)therapy, high-risk CLL was defined by *TP53* deletion/mutation or refractoriness to purine analog-based treatment (no response or progression-free survival <6 months).[6] For chemotherapy-free regimens, the prognostic value of *TP53* alterations is less clear, but the presence of a complex karyotype, which often occurs together with *TP53* deletion/mutation,[7] has been identified as an independent risk factor for early progression during venetoclax or ibrutinib treatment.[8,9] However, a more recent study has shown that CLL with a complex karyotype is a heterogeneous group with variable clinical behaviors.[10]

To better understand treatment failure in CLL, a comprehensive characterization of the genomic architecture in high-risk CLL is vital. With 5-10% high-risk cases included in large-scale studies on DNA copy number changes and gene mutations, these cases were underrepresented for systematic analyses restricted to this subgroup.[11-14]

Available results from single nucleotide polymorphism (SNP)-array profiling of high risk CLL support the notion of increased genomic complexity in the majority of these cases.[11-13] However, it should be noted that TP53 dysfunction and defects in other DNA damage response systems such as ATM cause chromosomal instability with random secondary events not necessarily associated with adverse prognosis.[15] This constitutes a challenge, to identify those alterations contributing to a high-risk form of disease.

In order to get a more thorough understanding of the pivotal genomic alterations contributing to high-risk CLL biology, we performed high-resolution SNP-array profiling and targeted sequencing on 75 relapsed/refractory CLL cases including 18 cases without *TP53* alterations. We extended our cohort by including 71 treatment-naïve, *TP53*-deficient, primary high-risk cases. All patients' samples were derived from prospective clinical trials of the French/German CLL study groups (FCLLSG/GCLLSG).

To identify DNA copy number alterations (CNA) occurring more often than would be expected by chance, we applied the Genomic Identification of Significant Targets in Cancer algorithm 2.0 (GISTIC2.0).[16] In relapsed/refractory CLL, in which tumor cell clones underwent selective pressure imposed by therapy, CNA with significance assigned by GISTIC2.0 harbored genes with key roles in cell-cycle control. Furthermore, we identified NOTCH1 as a central pathway frequently affected by genomic alterations enhancing its signaling strength.

Methods

Patients and samples

The study included peripheral blood mononuclear cells (PBMC) from 146 high-risk cases (*TP53* aberration or refractoriness to purine analogs) enrolled on prospective trials of the GCLLSG/FCLLSG (CLL2O trial, clinicaltrials.gov identifier: NCT01392079; CLL8 trial, NCT00281918; CLL11 trial, NCT01010061). Written informed consent from all patients and ethics committee approval were obtained in accordance with the Declaration of Helsinki.

Selection of cases was guided by sample availability and included 110 of 135 cases from the CLL2O trial,[17] 27 of 51 cases with 17p deletion from the CLL8 trial[18] and nine of 52 cases with 17p deletion from the CLL11 trial.[19] All samples were taken at trial enrollment and tumor cells were enriched via CD19 immunomagnetic beads (MACS, Miltenyi Biotec®, Bergisch Gladbach, Germany). CD19 negative PBMC fractions with a tumor cell load <5% were available for paired analysis in 91 cases. Cases lacking matched normal material were analyzed against a pool of ten gender-matched reference samples.

IGHV mutational analysis, fluorescence *in situ* hybridization (FISH) studies for 11q22.3, 13q14, 12p11.1-q11, 17p13.1, t(11;14)(q13;q23) and *TP53* mutational analysis were performed at trial enrollment. Cases positive for t(11;14)(q13;q23) were excluded from the study. Telomere length was determined as described previously.[20]

Single nucleotide polymorphism array and gene enrichment analysis

Analysis for CNA, including copy neutral losses of heterozygosity, was done using 6.0 SNP arrays (Affymetrix®, Santa Clara, CA, USA). CNA positions and gene locations were determined with the UCSC Genome Browser, assembly March 2006, NCBI36/hg18. CNA frequencies were compared to those observed in treatment-naïve, standard-risk cases (n=304, no *TP53* deletion/mutation).[13] Microarray raw data were made publicly available at Gene Expression Omnibus (GEO accession number: GSE131114).

GISTIC2.0 was applied on manually curated DNA copy number data.[16] According to default settings, CNA with a *q* value <0.25 were defined as significant. CNA that reached high confidence levels for being significantly enriched (*q* value <0.01) were manually curated for minimally affected regions. Genes located within these minimally affected regions were assigned to WikiPathways[21,22] and analyzed for pathway enrichments using PathVisio, version 3.2.3.[23,24]

Next-generation sequencing

Amplicon-based, targeted next-generation sequencing (tNGS) was performed on *TP53* exons 2-11, *NOTCH1* exon 34, and *SF3B1* exons 13-16. In 17 cases *TP53*, *NOTCH1* and *SF3B1* mutational status was determined as previously described.[25] All coding regions of *MGA*, *SPEN*, *RBPJ*, and *SNW1* (in 108 cases each), and *CDKN2A* and *MYC* (in 93 cases each) were screened by tNGS.

Quantitative gene expression analysis

Gene expression of *CCAT1*, *MGA*, *RBPJ*, *SNW1*, *HES1*, *DTX1*, *MYC*, *CDKN2A*, *p14ARF*, and *p15INK4b* was analyzed by quantitative reverse transcription (qRT) polymerase chain reaction (PCR) (TaqMan® Gene Expression Assays; Applied Biosystems®, Foster City, CA, USA). Sample selection was based on highly clonal presence of respective CNA/gene mutations ($\log_2$ ratio <-0.8 for deletions and >0.75 for gains; variant allele frequency >0.3 for mutations). Promoter DNA methylation of *CDKN2A/B* transcripts was assessed by bisulfite PCR followed by Sanger sequencing.

Statistical analysis

Associations between genomic alterations were tested by Fisher exact tests; differences between datasets by Mann

Whitney tests. All statistical tests were two-sided and conducted in GraphPad Prism® version 7.0.

Further details are available in the *Online Supplementary Methods*.

Results

Cohort characteristics

High-resolution genome-wide copy number analysis was performed on CD19-enriched PBMC from 146 CLL patients with high-risk disease. Cases belonged to the following subgroups. (i) Patients refractory to purine analogs from the CLL2O trial (n=49), who had received a median of three previous lines of therapy (range, 1 to 7 lines of therapy). This cohort encompassed patients with *TP53* loss and/or mutation (n=31; refractory^{TP53-}) and patients without *TP53* aberration (n=18; refractory$^{TP53\ intact}$). (ii) Relapsed patients with *TP53* loss from the CLL2O trial (n=26; relapsed^{TP53-}), who had received a median of two previous lines of therapy (range, 1 to 4 lines of therapy). (iii) Primary high-risk treatment-naïve patients with *TP53* loss (n=71; treatment-naïve^{TP53-}) from the CLL2O (n=35), CLL8 (n=27) and CLL11 trials (n=9). Standard-risk cases used as the reference cohort were derived from the CLL8 trial and included all available cases without a *TP53* alteration (n=304; treatment naïve$^{TP53\ intact}$) (Figure 1; characteristics of the patients and samples are provided in *Online Supplementary Table S1*).

Landscape of genomic copy number alterations in high-risk chronic lymphocytic leukemia

First, we assessed genomic complexity in cases grouped by clinical and genetic characteristics. For this, we used paired cases only to focus on somatically acquired CNA. No difference in median CNA numbers was observed between 39 treatment-naïve^{TP53-} primary high-risk and 38 relapsed^{TP53-}/refractory^{TP53-} high-risk tumors (5.6 *versus* 5.8 CNA per case mean) so that genomic complexity with TP53 deficiency was independent of previous therapy. In the absence of *TP53* abnormalities, tumors with *ATM* loss (n=7) had 5.4 CNA per case mean. Refractory high-risk cases lacking *TP53* and *ATM* abnormalities had two or fewer CNA in the majority of cases (5 of 7 cases) (Figure 2).

More than half of the high-risk cases showed complex CNA with two or more switches between two copy number states on at least one chromosome (87/146 cases, 60%). Thirteen CNA in 12/146 cases (8%) fulfilled the formal criteria of chromothripsis, which is defined by ten or more switches between two or more copy number states on an individual chromosome.[26] Reducing the required number of copy number switches to eight and six increased numbers to 23 CNA in 16 cases (11%) and 50 CNA in 32 cases (22%), respectively.

Overall, the cohort of high-risk CLL cases comprised more than 1,500 individual copy number changes (*Online Supplementary Table S2*). To identify CNA that were significantly enriched, we conducted GISTIC2.0 analysis. While therapy-naïve$^{TP53\ intact}$ patients only had 11 significantly enriched CNA, GISTIC2.0 assigned significance to 28 CNA within the treatment-naïve^{TP53-} cohort and to 20 CNA within the relapsed^{TP53-}/refractory cohort when using the default *q* value of 0.25 as the cut-off for significance (Figure 3).

To further reduce complexity, we focused our analysis on CNA that reached high confidence levels for being significantly enriched. High confidence was defined by a GISTIC *q* value <0.01 in at least one of three GISTIC2.0 analyses: (i) the entire high-risk cohort, (ii) the treatment naïve^{TP53-} cohort, and (iii) the relapsed^{TP53-}/refractory cohort (for minimally affected regions and confidence levels see Table 1). We compared frequencies observed in high-risk

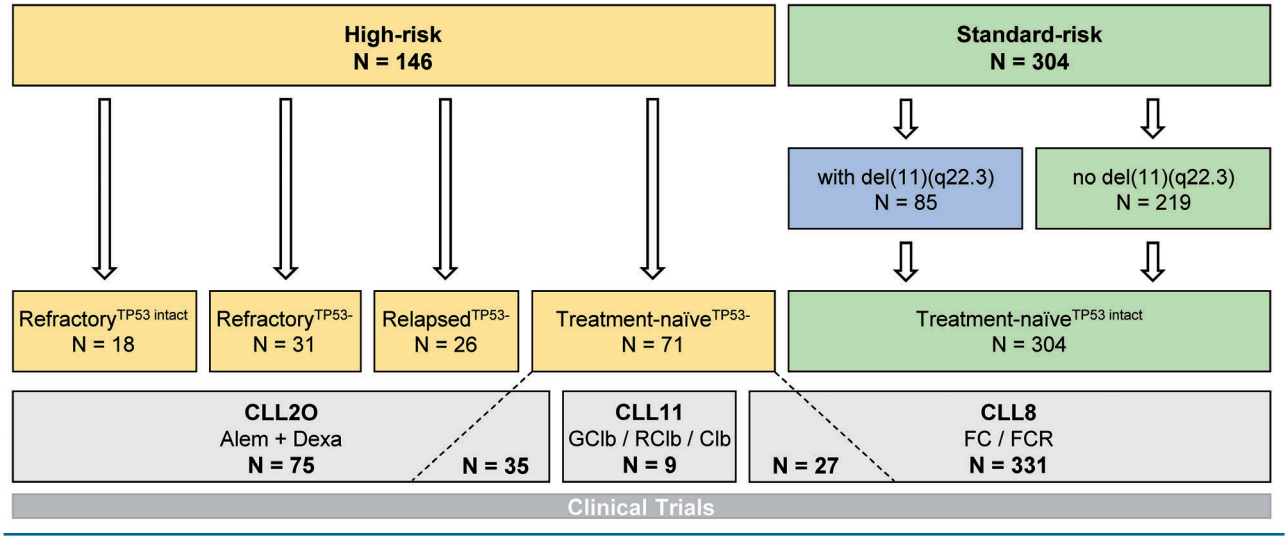

Figure 1. Description of the sample cohort. High-risk cases of chronic lymphocytic leukemia (CLL) comprised refractory cases (no response or progression-free survival <6 months) with or without *TP53* alterations (refractory^{TP53-}, refractory$^{TP53\ intact}$, respectively), relapsed cases (response >6 months) with *TP53* alterations (relapsed^{TP53-}), and treatment-naïve cases with *TP53* alterations (treatment-naïve^{TP53-}). Standard-risk cases were treatment-naïve cases without *TP53* alterations (treatment-naïve$^{TP53\ intact}$), comprising cases carrying del(11)(q22.3) and cases not carrying del(11)(q22.3). Patients' samples were derived from the CLL2O trial, in which patients were treated with alemtuzumab plus dexamethasone, the CLL11 trial, in which treatment with obinutuzumab plus chlorambucil was compared with rituximab plus chlorambucil or chlorambucil monotherapy, and the CLL8 trial, in which treatment with fludarabine/cyclophosphamide (FC) was compared with FC plus rituximab. Alem: alemtuzumab; dexa: dexamethasone; G: obinutuzumab; Clb: chlorambucil; R: rituximab; F: fludarabine; C: cyclophosphamide

cases with those observed in treatment-naïve standard-risk cases. Apart from +(2)(p16.1 p15) and del(6)(q21), all CNA listed in Table 1 occurred at least two times more often in the cohort of high-risk cases: +(8)(q24.21) in 16.4% *versus* 3.6%, del(8)(p23.1) in 15.8% *versus* 0.3%, del(18)(p11.31) in 13.7% *versus* 2.0%, del(10)(q24.32) in 11.0% *versus* 1.3%, del(15)(q15.1) in 10.3% *versus* 3.6%, del(3)(p21.31) in 10.3% *versus* 0.3%, and del(14q) in 7.5% *versus* 0.7%. Losses in 14q were heterogeneous and a continuous minimally deleted region could not be identified. The two minimally deleted regions in 14q24.3 and 14q31.3 were defined by one case with a discontinuous deletion.

GISTIC2.0 also assigned *q* values <0.01 to novel CNA: +(17)(p11.2) found in 8.2%, +(17)(q23.2) in 7.5%, del(3)(p25.3) in 9.6%, del(3)(p24.1) in 8.9%, del(4)(p15.2) in 8.2%, and del(9)(p21.3) in 8.9% of high-risk cases. Boundaries of minimally affected chromosomal regions in 3p25.3, 3p24.1, and 17q23.2 derived from complex discontinuous CNA.

GISTIC2.0 results for the treatment naïve^{TP53-} and relapsed^{TP53-}/refractory cohort shared similarities, but the latter group had fewer significant CNA. This suggested a selection of clones with CNA contributing to CLL high-risk biology and failure of previous chemo(immuno)therapy. In the relapsed^{TP53-}/refractory cohort, only gain(8)(q24.21) and del(9)(p21.3) retained GISTIC *q* values <0.01 beyond CNA routinely assessed by FISH (Table 1). Of note, the minimally affected regions in 8q24.21 and 9p21.3 both contained key regulators of cell cycle progression, namely *MYC* and *CDKN2A/B*.

In contrast, del(18p), del(15)(q15.1), del(4)(p15), del(14q) and gain(2p) failed to reach significant GISTIC *q* values in the relapsed^{TP53-}/refractory cohort, so that these CNA less likely conferred refractoriness.

We next analyzed the 146 high-risk cases for associations between genomic lesions. The distribution of genomic lesions across samples is depicted in Figure 4 for relapsed^{TP53-}/refractory cases and in *Online Supplementary Figure S1* for treatment naïve^{TP53-} cases. Comparing cases with and without *TP53* alteration, only del(11)(q22.3) significantly associated with refractory$^{TP53\ intact}$ cases (P<0.01). Testing for dependence of a genomic lesion on the presence of a *TP53* alteration was hampered by the low number of refractory$^{TP53\ intact}$ cases included in the study. Loss of *CDKN2A/B* was associated with gain of the *MYC* gene locus, with *MGA* mutation, and with loss of *MGA* by del(15)(q15.1) (P=0.028, P=0.044, and P=0.03, respectively). Interestingly, cases with co-occurring *CDKN2A/B* loss and *MYC* gain were among those with the shortest telomeres as a potential sign of higher proliferation rates in these tumors. Co-occurrence of coding *NOTCH1* and *SF3B1* mutations was lower than would have been expected to occur by chance (3/145 cases, P=0.034), although both mutations were frequent. *NOTCH1* mutations occurred in 24% relapsed^{TP53-}/refractory and 21% treatment-naïve^{TP53-} cases and *SF3B1* mutations in 24% relapsed^{TP53-}/refractory and 23% treatment naïve^{TP53-} cases.

Lastly, to identify distinct molecular pathways affected by CNA with significant GISTIC *q* values, we analyzed genes located in minimally involved regions as shown in Table 1 by PathVisio. PathVisio assigned significance to 29 pathways. Due to *TP53*, *ATM*, and *CDKN2A/B* loss and *MYC* gain, 12 of 29 pathways were related to DNA damage response, apoptosis or cell cycle control. Of note, "NOTCH1 signaling" was identified as one significant pathway based on loss of two genes associated with NOTCH1 target gene repression (*RPBJ* and *SNW1*) and gain of the NOTCH1 target gene *MYC*. Toll like receptor signaling was the pathway with the most significant *P*

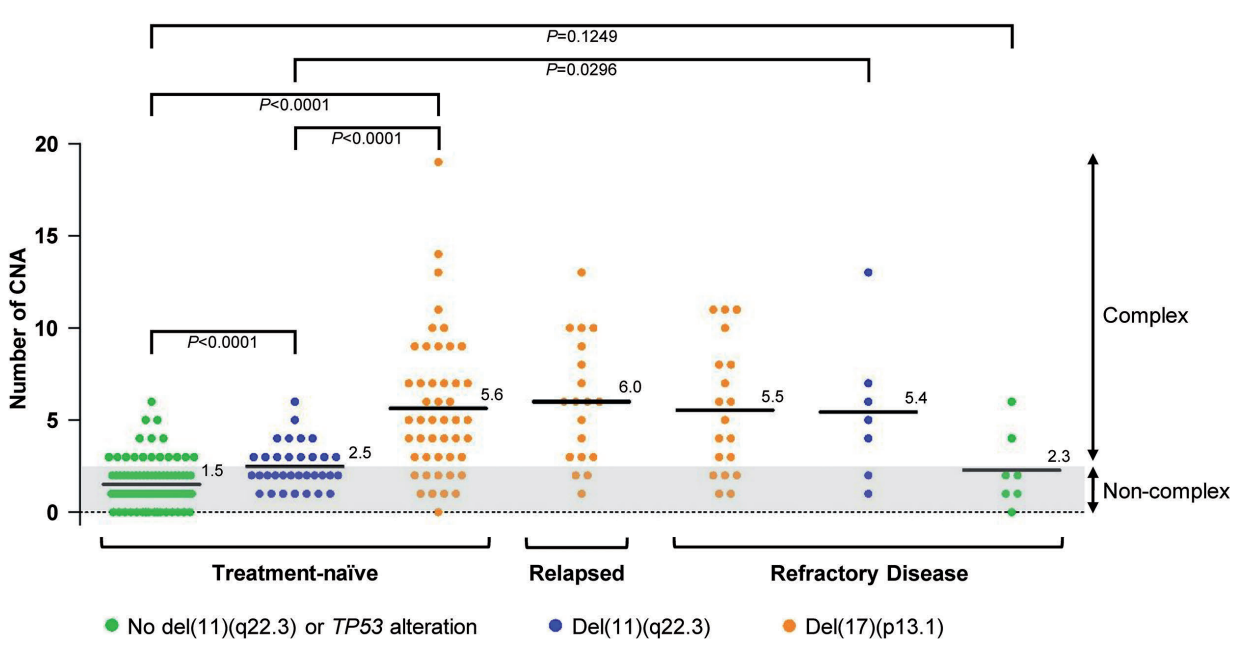

Figure 2. Mean number of copy number alterations in clinically and genetically determined subgroups of patients with chronic lymphocytic leukemia. Numbers of copy number alterations (CNA) for all patients who were analyzed against their intra-individual reference DNA (paired). The mean value of CNA numbers is highlighted within each subgroup of patients defined by genetic alterations and disease stage. *P* values are based on Mann-Whitney tests.

value, but this was due to loss of an interferon cluster located in 9p21.3 (Figure 5).

Since our results drew attention to CDKN2A/B, MYC and NOTCH1 signaling, we next shed more light on genetic lesions relating to them.

Characterization of del(9)(p21.3) as a novel recurrent copy number alteration in high-risk chronic lymphocytic leukemia

Deletions in 9p21.3 were found in 13 patients (7% treatment-naïve^{TP53-}; 11% relapsed^{TP53-}/refractory cases). This

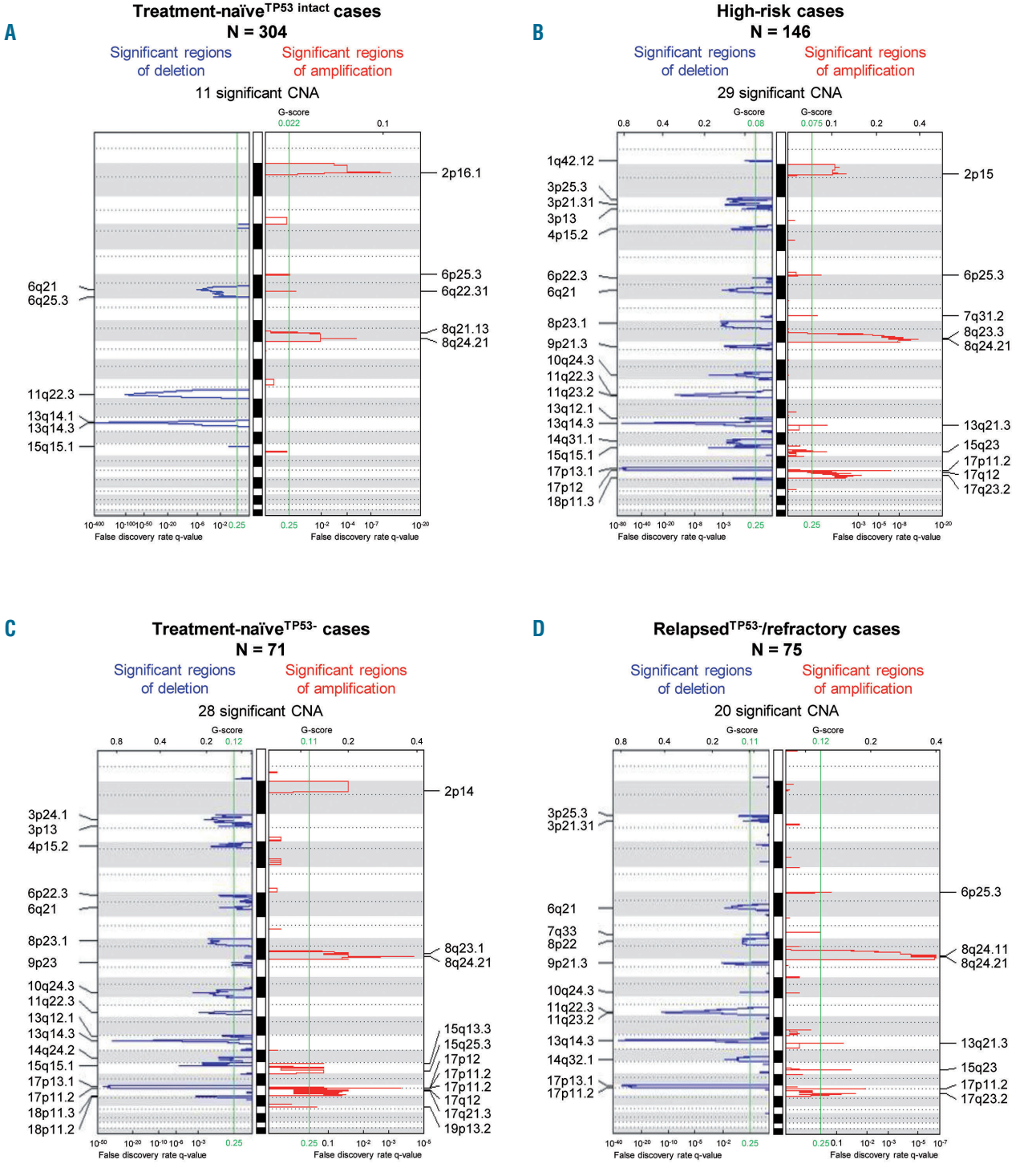

Figure 3. Identification of significant copy number gains and losses by GISTIC2.0. (A-D) GISTIC2.0 results of four separate analyses conducted on the following cohorts: (A) treatment-naïve$^{TP53\ intact}$ standard-risk cases (n=304); (B) all high-risk cases (n=146); (C) treatment-naïve^{TP53-} primary high-risk cases (n=71); and (D) relapsed^{TP53-}/refractory high-risk cases (n=75). False discovery rate *q* values are plotted along the x axis. Chromosomal positions are plotted along the y axis. Altered regions with significance levels exceeding 0.25 (marked by vertical green lines) were deemed to be significant.

Table 1. DNA copy number alterations with high confidence levels for being significantly enriched in high-risk chronic lymphocytic leukemia.

	Cytoband	Start	Stop	All high-risk cases [N=146] GISTIC q-value	Treatment-naïve high-risk cases [N=71]	Relapsed / refractory cases [N=75]
Amplification	2p16.1-p15	59,872,879	61,781,897	0.0070	0.0308	not significant
	8q24.21	128,276,750	128,338,750	< 0.0001	< 0.0001	< 0.0001
	17p11.2	no common MAR [1]		< 0.0001	0.1248	0.0118
	17q23.2	no continuous MAR [2]		0.0006	0.0308	0.0260
Deletion	3p26.1-p25.3	8,459,754	9,005,743	0.0025	not significant	0.0867
	3p24.1	29,680,087	29,722,568	not significant	0.0039	not significant
	3p21.31	46,872,865	47,222,966	0.0016	not significant	0.1355
	4p15.2-p15.1	25,031,670	30,250,789	0.0070	0.0140	not significant
	6q21	no common MDR [3]		0.0008	0.0497	0.0119
	8p21.3	22,075,838	23,155,110	0.0005	0.0083	0.1181
	9p21.3	21,151,950	22,445,892	0.0012	not significant	0.0076
	10q24.32	103,862,811	104,452,562	< 0.0001	0.0003	0.0960
	11q22.3	107,595,005	107,673,512	< 0.0001	0.0013	< 0.0001
	13q14.3	49,541,515	49,786,376	< 0.0001	< 0.0001	< 0.0001
	14q24.3-q32.1	no continuous MDR [4]		0.0023	0.0418	not significant
	15q15.1	39,834,465	39,925,748	< 0.0001	< 0.0001	not significant
	17p13.1	7,223,868	7,604,837	< 0.0001	< 0.0001	< 0.0001
	18p11.32-p11.31	1,339,610	6,397,482	0.0094	0.0006	not significant

[1]Chr 17: 19,330,676 – 20,077,185 is the most frequent MAR [10/12 cases]; [2]Chr 17: 56,343,164 – 57,575,244 and 58,167,359 – 58,198,114; [3]Chr 6: 106,415,362 –106,820,208 is the most frequent MDR [12/14 cases]; [4]Chr 14: 77,238,552 – 77,275,608 and 77,898,877 – 93,494,856. Listed are all copy number alterations (CNA) with their minimally amplified region (MAR) / minimally deleted region (MDR) that reached high confidence levels for being significantly enriched in high-risk CLL (GISTIC *q* value <0.01) in at least one of three GISTIC2.0 analyses: (i) all high-risk cases, (ii) treatment-naïve^{TP53-} cases, (iii) relapsed^{TP53-}/refractory cases. According to the default settings of GISTIC2.0, CNA with a *q* value <0.25 were deemed significant.

high frequency was surprising, since del(9)(p21.3) has not been observed in standard-risk cases at treatment initiation.[13] The minimally deleted region encompassed *CDKN2A, CDKN2B, MTAP, DMRTA1* and an interferon gene cluster (Figure 6A). Two cases had focal homozygous deletions within larger monoallelic deletions, but the *CDKN2A/B* loci were covered by the homozygous deletion in only one case. The minimally deleted homozygous region contained only *DMRTA1* coding for a transcription factor with unknown target genes (Figure 6B). Somatic *CDKN2A* mutations were not found in the high-risk cases screened by tNGS.

Consistent with a role of CDKN2A/B in proliferation control, loss of their gene loci has been directly associated with Richter transformation (RT), since del(9)(p21) had so far been only observed in lymph node biopsies with histologically confirmed RT and not in corresponding peripheral blood samples acquired during the CLL phase.[27,28] We, therefore, next investigated associations between del(9)(p21.3) and the development of RT, the presence of which had been an exclusion criterion at enrollment on each clinical trial. During the observation period, only one patient with del(9)(p21.3) developed histologically confirmed RT. This patient was under alemtuzumab maintenance therapy and was diagnosed with RT 557 days after trial enrollment. The observation periods for the other 11 patients ranged from 15 to 1387 days. Short periods of less than 4 months, observed in five of the 11 patients, were related to progressive disease (n=2; 38 and 75 days after trial enrollment), fatal infections (n=3), or early patient dropout (n=1). The first patient with progressive disease had marked lymphadenopathy (abdominal lymph nodes >10 cm) but a normal lactate dehydrogenase level of 227 U/L. The second patient had a homozygous *CDKN2A* deletion with a concurrent *MYC* gain, rapidly progressive lymphadenopathy, and a vastly increased lactate dehydrogenase level of 1026 U/L. Lymph node biopsies were not taken in either case.

We also searched for patients who developed RT during their observation period and identified 14 patients with histologically confirmed RT all of whom belonged to the relapsed^{TP53-}/refractory cohort. The diagnosis of RT was made at a median of 407 days after trial enrollment (range, 21-568 days). In general, genomic profiles obtained from tumor cell-enriched PBMC taken at trial enrollment did not differ between patients who developed RT during follow up and the other relapsed^{TP53-}/refractory cases (*Online Supplementary Figure S2*). Three tumors transformed during the first 6 weeks after trial enrollment (#2O_CLLL033 at day 21; #2O_CLL056 at day 36; and #2O_CLL037 at day 41). Interestingly, these three tumors had alterations affecting NOTCH1 as well as MYC signaling alongside TP53 dysfunction (*Online Supplementary Tables S1* and *S2*).

Overall, del(9)(p21.3) was less frequently associated with RT than previous publications had suggested. Our next aim was, therefore, to understand whether *CDKN2A/B* expression was compensated by the second allele in cases with heterozygous loss. In 9p disome cases, gene expression levels of *CDKN2A* and *CDKN2B* were variable. Although the median expression levels of *CDKN2A* transcripts were significantly lower in cases with del(9)(p21.3), the respective values in cases with heterozygous loss did not fall below the range of values observed in 9p disome cases (Figure 6C, details in *Online Supplementary Table S3*). Promoter methylation, serving as an explanation of abnormally reduced *CDKN2A/B* expres-

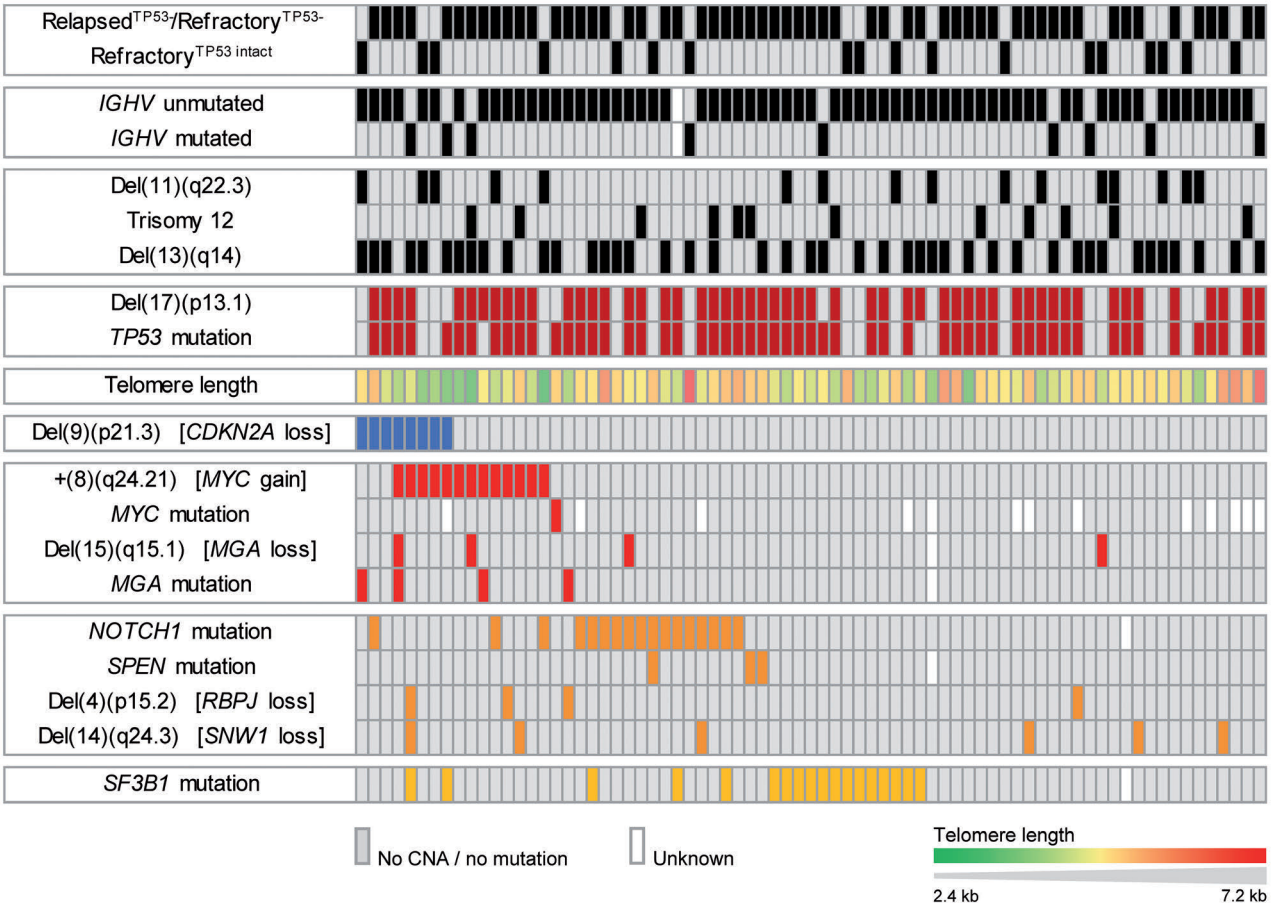

Figure 4. Distribution of genetic characteristics across relapsed^{TP53-}/refractory cases. CNA: copy number alteration.

sion in 9p-disome cases, was not found for *p14^{ARF}*, *p16INK4A* and *p15INK4B* transcripts (based on 8 selected 9p disome cases including 2 cases with noticeably low expression levels of *CDKN2A* transcripts and *p14^{ARF}*; *data not shown*).

Characterization of genomic lesions relating to *MYC*

Gains on 8q were found in 16% of high-risk cases, with a comparable distribution between treatment-naïve^{TP53-} and relapsed^{TP53-}/refractory cases (15% and 17%, respectively). Two types of gains were identified: (i) broad gains covering the *MYC* locus; (ii) focal gains with a size <500 kb in 8q24.21 affecting a super enhancer region proximal of the *MYC* locus. The broad type of gains was far more frequent in high-risk cases than in standard-risk ones (14.4% *versus* 2.2%). The frequency of focal gains was comparable in both risk groups (1.4% and 1.3%) and no relapsed^{TP53-}/refractory case was affected. Only one COSMIC-listed *MYC* mutation was found in 93 high-risk cases screened.

Despite their low frequency, the focal gains in 8q24.21 raised our interest, since they were the only recurrent gains in non-coding DNA regions found throughout the entire CLL genome. Their minimally gained region encompassed three long non-coding RNA, namely *CASC19*, *CCAT1*, and *CASC21* (*Online Supplementary Figure S3*). Of these, *Colon Cancer Associated 1* (*CCAT1*) has been associated with adverse risk in several solid cancers,[29,30] since its transcript has been described to stabilize a chromosome loop between *MYC* and the enhancer region.[31] However, *CCAT1* expression in CLL cases with 8q gain did not exceed normal expression levels (*Online Supplementary Figure S4*).

Besides chromosomal gains on 8q, we and others have previously identified *MGA* deletion/mutation as a potential alternative mechanism for increased MYC activity in CLL.[13,32] MGA is a protein that forms a heterodimer with MAX and this heterodimer antagonizes MYC induced transcriptional changes.[33] Against the background of frequent *MYC* gain in relapsed^{TP53-}/refractory cases, loss of a significant GISTIC *q* value for del(15)(q15.1) in the relapsed/refractory cohort was surprising, since its minimally deleted region encompasses the *MGA* gene locus. We performed qRT PCR to determine *MGA* gene expression in cases with heterozygous 15q deletion relative to 15q disome cases and found that *MGA* transcription in cases with heterozygous *MGA* loss was fully compensated by the remaining allele (*Online Supplementary Figure S5*). Nonetheless, we found an increased frequency of truncating *MGA* mutations with five mutations in 4/108 high-risk cases (3.7%). As all *MGA* mutated cases belonged to the relapsed^{TP53-}/refractory cohort, they were clearly enriched in this cohort (4/74 cases; 5.4%).

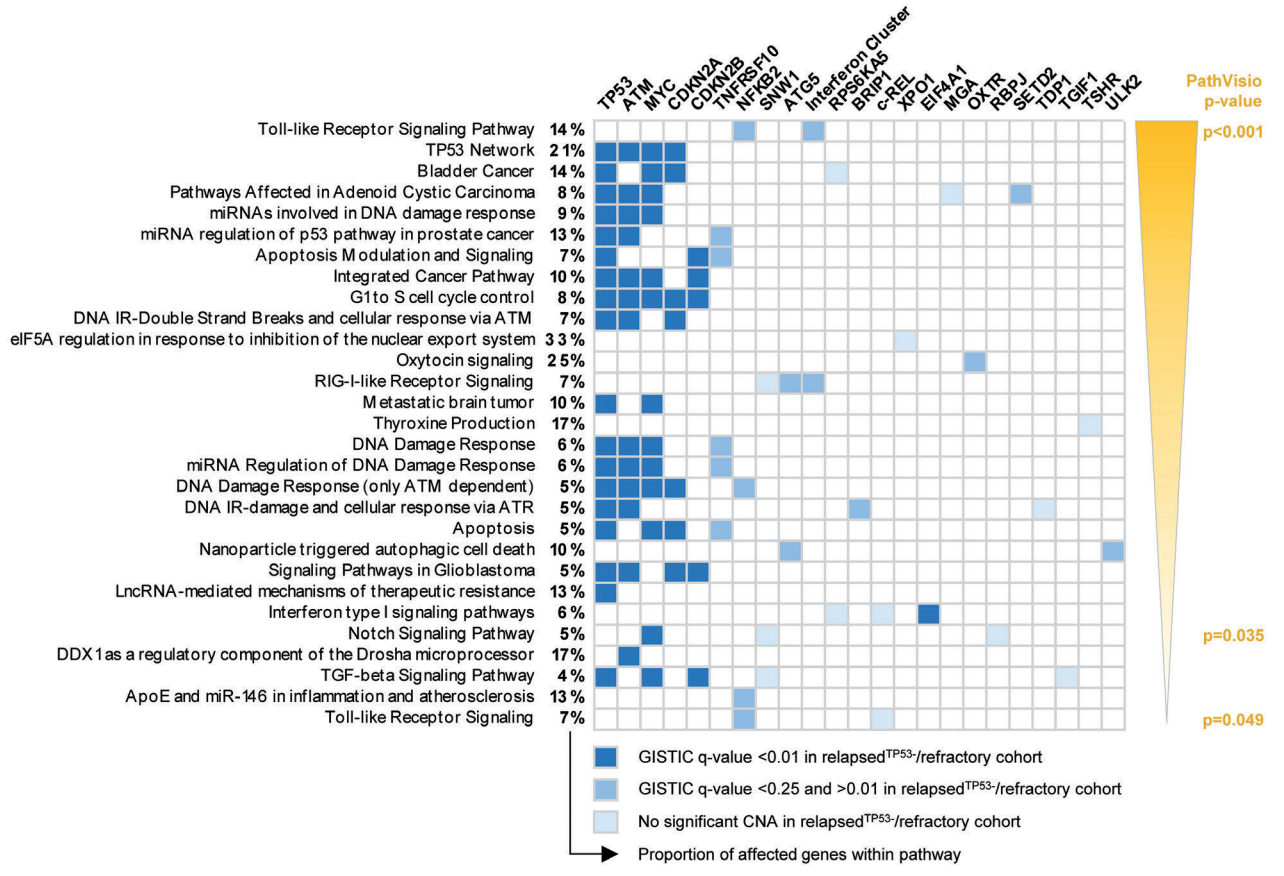

Figure 5. Biological pathways significantly affected by copy number alterations. Significant biological pathways as identified by PathVisio. All genes located within the minimally affected regions of copy number alterations (CNA) that are listed in Table 1 were included in the analysis and genes were assigned to WikiPathways. Pathways are listed by *P* values as determined via PathVisio. The percentages provided refer to the proportion of affected genes within the respective pathway. The color coding for affected genes refers to the GISTIC *q* value, which was assigned to the respective CNA.

Characterization of genomic lesions related to NOTCH1 signaling

Based on our PathVisio results, we also investigated genomic alterations associated with NOTCH1 signaling. As a novel finding, three components of a protein complex repressing NOTCH1 target genes were recurrently affected: *RBPJ* in 4p15.2 was deleted in 8.2%; *SPEN* was mutated in 3.7% (4/108 cases); and *SNW1* in 14q24.3 coding for an unconfirmed component of the repressor complex was deleted in 7.5% of cases (Figure 7A, C, E).

RBPJ is essential for DNA binding of the NOTCH1 intracellular domain (NICD1), which is released as a transcription factor upon activation of the NOTCH1 cell surface receptor. In the absence of NICD1 in the nucleus, RBPJ forms a protein complex with SHARP encoded by *SPEN* and other proteins that recruit histone deacetylases to condense the chromatin around NOTCH1 target genes.[34-36] Disruption of this repressor complex has been associated with tumorigenesis.[37] SKIP encoded by *SNW1* is an unconfirmed complex component that has been associated with recruitment of histone deacetylases to NOTCH1-regulated genes.[34]

Median gene expression levels of *RBPJ* and *SNW1* were lower in cases with deletion, supporting a potential functional relevance of RBPJ and SNW1 loss (Figure 7B, D). This led us to hypothesize that disruption of the NOTCH1 repressor complex might lead to de-repression of NOTCH1 target genes. We therefore measured expression levels of *HES1*, *DTX1* and *MYC* as genes known to be NOTCH1-regulated in primary CLL samples.[38,39] Non-CD19-enriched PBMC samples were used for this analysis of NOTCH1 target gene expression, since EDTA-containing sorting buffer used for cell enrichment can activate NOTCH1 signaling *ex vivo* (*Online Supplementary Figure S6*).[40] Sample suitability was determined by the following selection criteria: (i) tumor cell count ≥70%; (ii) variant allele frequency >0.3 for *SPEN* and *RBPJ* mutations; and (iii) $\log_2$ ratio <-0.8 for del(4)(p15.2) or del(14)(q24.3)

Six of nine available *SPEN* mutant samples and one available *RBPJ* mutant sample fulfilled these requirements. Target gene expression did not correlate with the number of non-B cells per sample (*Online Supplementary Figure S7*). In line with our hypothesis, *SPEN* mutant tumors had significantly higher median expression levels of *HES1* and *DTX1* and four *SPEN* mutant cases had remarkably high expression levels of *MYC*.

Of 14 *RBPJ*-deleted samples with available RNA, seven fulfilled our requirements. In this highly selected group of cases, *RBPJ* deletion occurred together with an activating *NOTCH1* mutation in three out of the seven cases. *HES1*

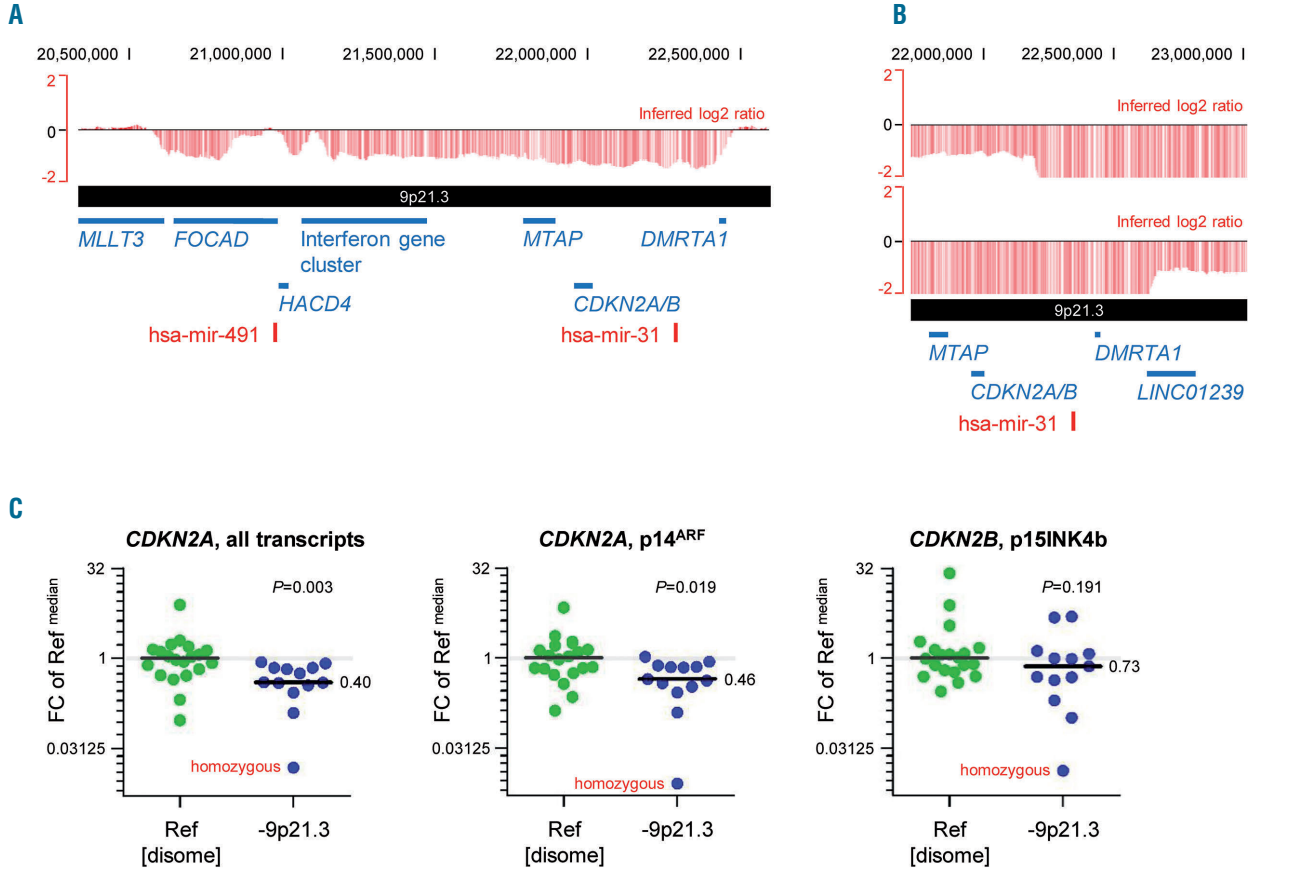

Figure 6. Del(9)(p21.3) leads to loss of *CDKN2A/B*. (A) Minimal consensus region of monoallelic del(9)(p21.3). Raw $\log_2$ ratio, chromosome 9, case #2O_CLL047 displayed with the UCSC genome browser (hg18). Red bars represent determined $\log_2$ ratios of single probe sets sorted by their physical position along the chromosome. The minimal consensus region of monoallelic del(9)(p21.3) harboring the *CDKN2A/B* gene loci is shown. (B) Minimal consensus region of biallelic del(9)(p21.3). Raw $\log_2$ ratio, chromosome 9, cases #2O_CLL011 and #2O_CLL050 displayed with the UCSC genome browser (hg18). The minimal consensus region of biallelic del(9)(p21.3) harboring the *DMRTA1* gene locus only is shwon. (C) Expression levels of *CDKN2A/B* transcripts in cases with del(9)(p21.3). Gene expression levels of *CDKN2A* transcripts (left: all transcripts, middle: $p14^{ARF}$ transcript alone) as well as the *CDKN2B* transcript p15INK4B (right) were calculated relative to *ACTB* expression levels. Fold changes (FC) were calculated towards the median ΔCt value of all reference samples (Ref). Median expression levels within each group of samples are highlighted and differences between groups were analyzed by the Mann-Whitney test. All available 9p-deleted cases were included in the analysis.

expression was very variable, but in cases with combined *RBPJ* and *NOTCH1* disruption it was highly increased. *DTX1* expression was more independent of the *NOTCH1* mutation status and its median was significantly higher in cases with *RBPJ* loss. However, expression of *MYC* was not altered in 4p deleted cases.

Of 12 *SNW1*-deleted cases with available RNA, only two cases fulfilled our requirements (Figure 7F; details in *Online Supplementary Table S4*).

Discussion

Genome-wide screening for CNA in high-risk CLL revealed complex genomic aberrations in the majority of cases, which was in contrast to the high genomic stability observed in treatment-naïve, standard-risk CLL without *TP53* or *ATM* alterations.[13] Our cohort consisted mainly of *TP53*-deficient cases and we found genomic instability to the same degree in patients who had or had not been previously treated.

Our focus was to identify CNA within complex genomic rearrangements relevant to the development of high-risk CLL. Using GISTIC2.0 as a systematic approach to distinguish meaningful chromosomal aberrations from random background alterations,[16] we identified *CDKN2A/B* loss, *MYC* gain and abnormally strong NOTCH1 signaling as significantly enriched alterations. The genomic profiles observed in peripheral blood CLL cells taken from high-risk patients shared extensive similarities with the profiles found in RT, in which *CDKN2A/B* loss, *MYC* gain and activating *NOTCH1* mutations have also been identified as hallmark genomic lesions alongside *TP53* alterations.[27,28] However, none of the respective alterations could be directly associated with transformation so that extrinsic stimuli from the microenvironment and/or additional intrinsic stimuli are required to induce transformation.

Loss of *CDKN2A/B* is a sparsely described CNA in CLL,[41] although homozygous deletion has recently been associated with resistance to venetoclax treatment.[5] The role in CLL progression of the signaling network around

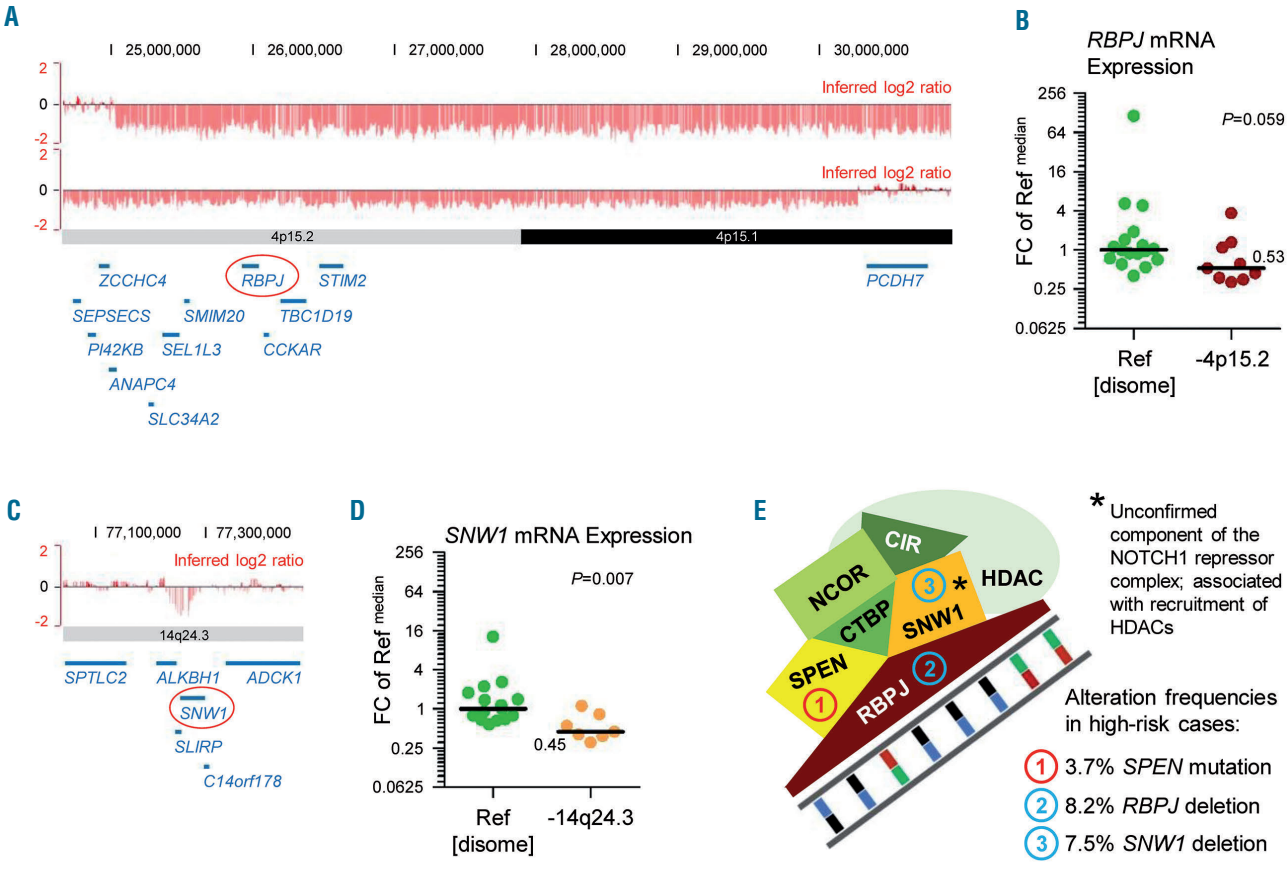
A
25,000,000
26,000,000
27,000,000
28,000,000
29,000,000
30,000,000
Inferred log2 ratio
Inferred log2 ratio
4p15.2
4p15.1
ZCCHC4
RBPJ
STIM2
PCDH7
SEPSECS
SMIM20
TBC1D19
PI42KB
SEL1L3
CCKAR
ANAPC4
SLC34A2
B
RBPJ mRNA Expression
FC of Ref median
P=0.059
0.53
Ref
-4p15.2
[disome]
C
77,100,000
77,300,000
Inferred log2 ratio
14q24.3
SPTLC2
ALKBH1
ADCK1
SNW1
SLIRP
C14orf178
D
SNW1 mRNA Expression
FC of Ref median
P=0.007
0.45
Ref
-14q24.3
[disome]
E
CIR
NCOR
CTBP
SNW1
HDAC
SPEN
RBPJ
* Unconfirmed component of the NOTCH1 repressor complex; associated with recruitment of HDACs
Alteration frequencies in high-risk cases:
1 3.7% SPEN mutation
2 8.2% RBPJ deletion
3 7.5% SNW1 deletion
F
HES1 mRNA Expression
FC of Ref median
P=0.002
P=0.197
2.7
13.9
Ref
NOTCH1mut
RBPJDel SNW1Del Repressor Complex Deletion
SPENMut RBPJMut Repressor Complex Mutation
DTX1 mRNA Expression
FC of Ref median
P=0.006
P=0.01
4.1
14.7
Ref
NOTCH1mut
RBPJDel SNW1Del Repressor Complex Deletion
SPENMut RBPJMut Repressor Complex Mutation
with trisomy 12
no trisomy 12
c-MYC mRNA Expression
FC of Ref median
P=0.282
5.6
Ref
RBPJDel SNW1Del Repressor Complex Deletion
SPENMut RBPJMut Repressor Complex Mutation
Reference sample from CLL8 trial (13q single in FISH)
Reference sample from CLL2O trial
Sample with SPEN alteration
Sample with RBPJ alteration
Sample with SNW1 alteration
Sample with additional NOTCH1 mutation in the respective group

Figure 7. Disruption of the NOTCH1 transcription repressor complex adds to the overall frequency of altered NOTCH1 signaling in high-risk chronic lymphocytic leukemia. (A) Minimal consensus region of del(4)(p15) covering the *RBPJ* gene locus. Raw $\log_2$ ratio, chromosome 4, cases #2O_CLL036 and #2O_CLL068 displayed with the UCSC genome browser (hg18). Red bars represent determined $\log_2$ ratios of single probe sets sorted by their physical position along the chromosome. The minimal consensus region of del(4)(p15) harboring the *RBPJ* gene locus is shown. (B) *RBPJ* expression levels in cases with del(4)(p15). *RBPJ* gene expression levels were calculated relative to *ACTB* expression levels and fold changes (FC) were calculated towards the median ΔCt value of all reference samples (Ref). Median expression levels within each group of samples are highlighted and the difference between the two groups was analyzed by the Mann-Whitney test. Only 4p-deleted cases with a $\log_2$ ratio lower than 0.89 were included. (C) Minimal consensus region of del(14)(q24.3) covering the *SNW1* gene locus. Raw $\log_2$ ratio, chromosome 14, case #2O_CLL027. The minimal consensus region of del(14)(q24.3) harboring the *SNW1* gene locus is shown. (D) *SNW1* expression levels in cases with del(14)(q24.3). *SNW1* gene expression levels were calculated relative to *ACTB* expression levels and FC were calculated towards the median ΔCt value of all reference samples (Ref). Median expression levels within each group of samples are highlighted and the difference between the two groups was analyzed by the Mann-Whitney test. Only 14q-deleted cases with a $\log_2$ ratio lower than 0.87 were included. (E) Composition of the NOTCH1 transcription repressor complex. Simplified illustration of the NOTCH1 transcription repressor complex. The mutation frequency of *SPEN* is based on targeted next-generation sequencing results on 108 cases from the high-risk cohort. The deletion frequencies of *RBPJ* and *SNW1* are based on the entire high-risk cohort (n=146). SNW1/SKIP is an unconfirmed component of the NOTCH1 repressor complex, which has been associated with the recruitment of histone deacetylases. (F) *HES1*, *DTX1* and *MYC* expression levels in cases with genomic alterations affecting the NOTCH1 transcription repressor complex. *HES1*, *DTX1* and *MYC* gene expression levels were calculated relative to *18S* expression levels and FC were calculated towards the median ΔCt value of all reference samples (Ref). Median expression levels within each group of samples are highlighted and differences between groups were analyzed by the Mann-Whitney tests. Non-purified peripheral blood mononuclear cells with a tumor cell load >70% were used for the experiment. Reference samples without evidence of a genetic alteration affecting NOTCH1 signaling were taken from the CLL8 trial (favorable risk cases with 13q deletion as sole abnormality in routine fluorescence *in situ* hybridization analysis; light green) and from the CLL2O trial (high risk cases; dark green). Additionally, three cases with a highly clonal *NOTCH1* mutation were included (blue). Cases with *RBPJ* alteration are shown in dark red, samples with *SNW1* alteration in orange, and samples with *SPEN* alteration in pale red. Samples with additional *NOTCH1* mutation are indicated in blue within their respective sample group. The *DTX1* gene locus is located on chromosome 12. In the figure illustrating *DTX1* expression levels, cases without trisomy 12 are indicated by a round symbol and cases with trisomy 12 are indicated by a square symbol. Trisomy 12 appeared to be enriched in samples with mutations affecting the repressor complex. A gene dosage effect on *DTX1* gene expression was not apparent.

MYC, which comprises transcriptional inhibitors such as MGA,[42] is poorly understood. The *CDKN2A/B* gene loci encode cell-cycle regulators decelerating cell proliferation at multiple levels.[43] The *CDKN2A* gene product $p14^{ARF}$ tightly controls pro-proliferative activities of MYC so that reduced *CDKN2A* expression in combination with increased *MYC* expression can result in accelerated proliferation.[44] Enrichment of *CDKN2A/B* loss and *MYC* gain in the relapsed^{TP53-}/refractory cohort and frequent co-occurrence of both aberrations therefore hints at a key role for deficient cell-cycle control in the development of high-risk CLL.

The small focal gains within the 8q24.21 super-enhancer region are relevant with regard to them harboring binding sites for the NICD1 transcription factor.[38] *MYC* is a well established target gene of NOTCH1,[39] and tight bonds between aberrantly strong NOTCH1 signaling and increased MYC activity have been observed in T-cell acute lymphoblastic leukemia and were also shown to exist in CLL.[38,39] Hence, genomic aberrations with an activating effect on NOTCH1 signaling strength can indirectly increase the number of cases with enhanced MYC activity. Besides coding activating NOTCH1 mutations, which prolong NICD1 transcription factor activity,[45] various other genomic alterations were identified to interfere with NOTCH1 signaling. These alterations include non-coding *NOTCH1* mutations in the 3' untranslated region,[46] *FBXW7* mutations,[47] *MED12* mutations,[48] as well as *SPEN* mutations and probably also *RBPJ* alterations.

The fact that *NOTCH1* and *SF3B1* mutations are often mutually exclusive raises the question as to what extent *SF3B1* mutation can disturb the physiological balance between NOTCH1 signaling and *MYC* transcription. This question is based on the observation that the strength of NOTCH1 signaling depends on *DVL2*, which inhibits transcriptional activation by NOTCH1.[49] Mutations in *SF3B1* lead to alternative splicing of *DVL2* and the resulting splice variant has been shown to lack its ability to modulate NOTCH1 signaling.[50] *SF3B1* mutations may, therefore, constitute another frequent mechanism to strengthen the NOTCH1-MYC signaling axis.

Taken together, our results raise the hypothesis that multiple genetic lesions in high risk CLL converge in upregulated MYC activity. Testing this hypothesis requires an integrative analysis of the genome, transcriptome and proteome in samples strictly processed at 4°C and in the absence of calcium chelators. For translation of our results into clinical practice, a systematic record of genomic alterations identified as meaningful in our study needs to be obtained in more recent, prospective clinical trials including treatment arms based on BTK or Pi3K inhibition and/or antagonism of BCL-2. Novel potential markers must be tested for relevance in each treatment arm and markers proving to be relevant must be utilized for the assembly of a genomic clinical database. In the long-term, such an approach will allow an estimation of the likelihood of benefit or disadvantage from a given treatment regimen, hence paving the way towards more personalized treatment choices in the future management of CLL patients.

Acknowledgments

The authors would like to thank the patients who participated in the CLL2O, CLL8, and CLL11 trials; the investigators who treated patients and submitted samples; and Christina Galler, Sabrina Rau, and Jacqueline Fiegel for excellent assistance and support.

Funding

This study was supported by the German Research Foundation (DFG: ED 256/1 1; SFB 1074/B2 and Z1), by grants from the German Federal Ministry of Education and Research (BMBF, PRECiSe) and by the Barts Charity Fund. Central genetic diagnostics were partly funded by F. Hoffmann-La Roche.

References

1. Hallek M, Shanafelt TD, Eichhorst B. Chronic lymphocytic leukaemia. Lancet. 2018;391(10129):1524-1537.
2. Parikh SA. Chronic lymphocytic leukemia treatment algorithm 2018. Blood Cancer J. 2018;8(10):93.
3. Woyach JA, Johnson AJ. Targeted therapies in CLL: mechanisms of resistance and strategies for management. Blood. 2015;126(4):471-477.
4. Burger JA, Landau DA, Taylor-Weiner A, et al. Clonal evolution in patients with chronic lymphocytic leukaemia developing resistance to BTK inhibition. Nat Commun. 2016;7:11589.
5. Herling CD, Abedpour N, Weiss J, et al. Clonal dynamics towards the development of venetoclax resistance in chronic lymphocytic leukemia. Nat Commun. 2018;9 (1):727.
6. Stilgenbauer S, Zenz T. Understanding and managing ultra high-risk chronic lymphocytic leukemia. Hematology Am Soc Hematol Educ Program. 2010;2010:481-488.
7. Haferlach C, Dicker F, Schnittger S, Kern W, Haferlach T. Comprehensive genetic characterization of CLL: a study on 506 cases analysed with chromosome banding analysis, interphase FISH, IgV(H) status and immunophenotyping. Leukemia. 2007;21 (12):2442-2451.
8. Anderson MA, Tam C, Lew TE, et al. Clinicopathological features and outcomes of progression of CLL on the BCL2 inhibitor venetoclax. Blood. 2017;129(25): 3362-3370.
9. Thompson PA, O'Brien SM, Wierda WG, et al. Complex karyotype is a stronger predictor than del(17p) for an inferior outcome in relapsed or refractory chronic lymphocytic leukemia patients treated with ibrutinib-based regimens. Cancer. 2015;121(20):3612-3621.
10. Baliakas P, Jeromin S, Iskas M, et al. Cytogenetic complexity in chronic lymphocytic leukemia: definitions, associations, and clinical impact. Blood. 2019;133(11):1205-1216.
11. Gunnarsson R, Isaksson A, Mansouri M, et al. Large but not small copy-number alterations correlate to high-risk genomic aberrations and survival in chronic lymphocytic leukemia: a high-resolution genomic screening of newly diagnosed patients. Leukemia. 2010;24(1):211-215.
12. Ouillette P, Collins R, Shakhan S, et al. Acquired genomic copy number aberrations and survival in chronic lymphocytic leukemia. Blood. 2011;118(11):3051-3061.
13. Edelmann J, Holzmann K, Miller F, et al. High-resolution genomic profiling of chronic lymphocytic leukemia reveals new recurrent genomic alterations. Blood. 2012;120(24): 4783-4794.
14. Landau DA, Tausch E, Taylor-Weiner AN, et al. Mutations driving CLL and their evolution in progression and relapse. Nature. 2015;526(7574):525-530.
15. Negrini S, Gorgoulis VG, Halazonetis TD. Genomic instability--an evolving hallmark of cancer. Nat Rev Mol Cell Biol. 2010;11(3):220-228.
16. Mermel CH, Schumacher SE, Hill B, Meyerson ML, Beroukhim R, Getz G. GISTIC2.0 facilitates sensitive and confident localization of the targets of focal somatic copy-number alteration in human cancers. Genome Biol. 2011;12(4):R41.
17. Stilgenbauer S CF, Leblond V, Delmer A, et al. Alemtuzumab combined with dexamethasone, followed by alemtuzumab maintenance or allo-SCT in "ultra high-risk" CLL: final results from the CLL2O phase II study. Blood. 2014;124 (21):1991.
18. Hallek M, Fischer K, Fingerle-Rowson G, et al. Addition of rituximab to fludarabine and cyclophosphamide in patients with chronic lymphocytic leukaemia: a randomised, open-label, phase 3 trial. Lancet. 2010;376 (9747):1164-1174.
19. Goede V, Fischer K, Busch R, et al. Obinutuzumab plus chlorambucil in patients with CLL and coexisting conditions. N Engl J Med. 2014;370(12):1101-1110.
20. Steinbrecher D, Jebaraj BMC, Schneider C, et al. Telomere length in poor-risk chronic lymphocytic leukemia: associations with disease characteristics and outcome. Leuk Lymphoma. 2018;59(7):1614-1623.
21. Kelder T, van Iersel MP, Hanspers K, et al. WikiPathways: building research communities on biological pathways. Nucleic Acids Res. 2012;40(Database issue):D1301-1307.
22. Kutmon M, Riutta A, Nunes N, et al. WikiPathways: capturing the full diversity of pathway knowledge. Nucleic Acids Res. 2016;44(D1):D488-494.
23. van Iersel MP, Kelder T, Pico AR, et al. Presenting and exploring biological pathways with PathVisio. BMC Bioinformatics. 2008;9:399.
24. Kutmon M, van Iersel MP, Bohler A, et al. PathVisio 3: an extendable pathway analysis toolbox. PLoS Comput Biol. 2015;11(2): e1004085.
25. Stilgenbauer S, Schnaiter A, Paschka P, et al. Gene mutations and treatment outcome in chronic lymphocytic leukemia: results from the CLL8 trial. Blood. 2014;123(21):3247-3254.
26. Rausch T, Jones DT, Zapatka M, et al. Genome sequencing of pediatric medulloblastoma links catastrophic DNA rearrangements with TP53 mutations. Cell. 2012;148(1-2):59-71.
27. Chigrinova E, Rinaldi A, Kwee I, et al. Two main genetic pathways lead to the transformation of chronic lymphocytic leukemia to Richter syndrome. Blood. 2013;122(15): 2673-2682.
28. Fabbri G, Khiabanian H, Holmes AB, et al. Genetic lesions associated with chronic lymphocytic leukemia transformation to Richter syndrome. J Exp Med. 2013;210(11):2273-2288.
29. Xin Y, Li Z, Shen J, Chan MT, Wu WK. CCAT1: a pivotal oncogenic long non-coding RNA in human cancers. Cell Prolif. 2016;49(3):255-260.
30. Chen Y, Xie H, Gao Q, Zhan H, Xiao H, Zou Y, et al. Colon cancer associated transcripts in human cancers. Biomed Pharmacother. 2017;94:531-540.
31. Kim T, Cui R, Jeon YJ, et al. Long-range interaction and correlation between MYC enhancer and oncogenic long noncoding RNA CARLo-5. Proc Natl Acad Sci U S A. 2014;111(11):4173-4178.
32. De Paoli L, Cerri M, Monti S, et al. MGA, a suppressor of MYC, is recurrently inactivated in high risk chronic lymphocytic leukemia. Leuk Lymphoma. 2013;54(5): 1087-1090.
33. Hurlin PJ, Steingrimsson E, Copeland NG, Jenkins NA, Eisenman RN. Mga, a dual-specificity transcription factor that interacts with Max and contains a T-domain DNA-binding motif. EMBO J. 1999;18(24):7019-7028.
34. Kao HY, Ordentlich P, Koyano-Nakagawa N, et al. A histone deacetylase corepressor complex regulates the Notch signal transduction pathway. Genes Dev. 1998;12 (15):2269-2277.
35. Oswald F, Kostezka U, Astrahantseff K, et al. SHARP is a novel component of the Notch/RBP-Jkappa signalling pathway. EMBO J. 2002;21(20):5417-5426.
36. Borggrefe T, Oswald F. The Notch signaling pathway: transcriptional regulation at Notch target genes. Cell Mol Life Sci. 2009;66(10):1631-1646.
37. Kulic I, Robertson G, Chang L, et al. Loss of the Notch effector RBPJ promotes tumorigenesis. J Exp Med. 2015;212(1):37-52.
38. Fabbri G, Holmes AB, Viganotti M, et al. Common nonmutational NOTCH1 activation in chronic lymphocytic leukemia. Proc Natl Acad Sci U S A. 2017;114(14):E2911-E2919.
39. Palomero T, Lim WK, Odom DT, et al. NOTCH1 directly regulates c-MYC and activates a feed-forward-loop transcriptional network promoting leukemic cell growth. Proc Natl Acad Sci U S A. 2006;103(48): 18261-18266.
40. Rand MD, Grimm LM, Artavanis-Tsakonas S, et al. Calcium depletion dissociates and activates heterodimeric notch receptors. Mol Cell Biol. 2000;20(5):1825-1835.
41. Martel V, Guerci A, Humbert JC, et al. De novo methylation of tumour suppressor genes CDKN2A and CDKN2B is a rare finding in B-cell chronic lymphocytic leukaemia. Br J Haematol. 1997;99(2):320-324.
42. Grandori C, Cowley SM, James LP, Eisenman RN. The Myc/Max/Mad network and the transcriptional control of cell behavior. Ann Rev Cell Dev Biol. 2000;16:653-699.
43. Hannon GJ, Beach D. p15INK4B is a potential effector of TGF-beta-induced cell cycle arrest. Nature. 1994;371(6494):257-261.
44. Cleveland JL, Sherr CJ. Antagonism of Myc functions by Arf. Cancer Cell. 2004;6(4):309-311.
45. Weng AP, Ferrando AA, Lee W, et al. Activating mutations of NOTCH1 in human T cell acute lymphoblastic leukemia. Science. 2004;306(5694):269-271.
46. Puente XS, Bea S, Valdes-Mas R, et al. Non-coding recurrent mutations in chronic lymphocytic leukaemia. Nature. 2015;526 (7574):519-524.
47. Close V, Close W, Kugler SJ, et al. FBXW7 mutations reduce binding of NOTCH1, leading to cleaved NOTCH1 accumulation and target gene activation in CLL. Blood. 2019;133(8):830-839.
48. Wu B, Slabicki M, Sellner L, et al. MED12 mutations and NOTCH signalling in chronic lymphocytic leukaemia. Br J Haematol. 2017;179(3):421-429.
49. Collu GM, Hidalgo-Sastre A, Acar A, et al. Dishevelled limits Notch signalling through inhibition of CSL. Development. 2012;139(23):4405-4415.
50. Wang L, Brooks AN, Fan J, et al. Transcriptomic characterization of SF3B1 mutation reveals its pleiotropic effects in chronic lymphocytic leukemia. Cancer Cell. 2016;30(5):750-763.

ARTICLE

IL6R-STAT3-ADAR1 (P150) interplay promotes oncogenicity in multiple myeloma with 1q21 amplification

Phaik Ju Teoh,[1,2] Tae-Hoon Chung,[1] Pamela Y.Z. Chng,[1] Sabrina H. M. Toh[1] and Wee Joo Chng[1,2,3]

[1]Cancer Science Institute of Singapore, National University of Singapore; [2]Department of Medicine, Yong Loo Lin School of Medicine, National University of Singapore and [3]Department of Haematology-Oncology, National University Cancer Institute of Singapore, National University Health System, Singapore

Ferrata Storti Foundation

Haematologica 2020
Volume 105(5):1391-1404

ABSTRACT

1q21 amplification is an important prognostic marker in multiple myeloma. In this study we identified that *IL6R* (the interleukin-6 membrane receptor) and *ADAR1* (an RNA editing enzyme) are critical genes located within the minimally amplified 1q21 region. Loss of individual genes caused suppression to the oncogenic phenotypes, the magnitude of which was enhanced when both genes were concomitantly lost. Mechanistically, *IL6R* and *ADAR1* collaborated to induce a hyper-activation of the oncogenic STAT3 pathway. High IL6R confers hypersensitivity to interleukin-6 binding, whereas, ADAR1 forms a constitutive feed-forward loop with STAT3 in a P150-isoform-predominant manner. In this respect, ADAR1-P150 acts as a direct transcriptional target for STAT3 and this STAT3-induced-P150 in turn directly interacts with and stabilizes the former protein, leading to a larger pool of proteins acting as oncogenic transcription factors for pro-survival genes. The importance of both IL6R and ADAR1-P150 in STAT3 signaling was further validated when concomitant knockdown of both genes impeded IL6-induced-STAT3 pathway activation. Clinical evaluation of various datasets of myeloma patients showed that low expression of either one or both genes was closely associated with a compromised STAT3 signature, confirming the involvement of IL6R and ADAR1 in the STAT3 pathway and underscoring their essential role in disease pathogenesis. In summary, our findings highlight the complexity of the STAT3 pathway in myeloma, in association with 1q21 amplification. This study therefore reveals a novel perspective on 1q21 abnormalities in myeloma and a potential therapeutic target for this cohort of high-risk patients.

Introduction

Multiple myeloma (MM) is a latent type of hematologic malignancy characterized by abnormal accumulation of plasma cells in the bone marrow. It is well established that MM cells are highly dependent on the bone marrow microenvironment enriched with growth factors for support and propagation.[1-3] Among these factors, interleukin-6 (IL6), which is secreted in an autocrine and paracrine fashion, is pivotal for the survival and proliferation of MM cells: high expression of IL6 prevents drug-induced-apoptosis.[1,4-6] Blood serum from MM patients contains elevated levels of IL6 and this is significantly associated with worse disease outcome.[6,7]

Mechanistically, IL6 confers oncogenicity through the activation of the Janus kinases (JAK)/signal transducers and activators of transcription 3 (STAT3) pathway, initiated with its binding to the transmembrane receptor IL6R.[4,8,9] STAT3 is activated when its tyrosine-705 (Y705) is phosphorylated by JAK upon IL6 stimulation, leading to transcription of various pro-survival and anti-apoptotic genes such as *MCL1* and *BCL2*.[10,11] In line with this mechanism of action, primary MM tumors possess constitutive activation of the STAT3 pathway (incidence rate of 40-60%) with close correlation with poor prognosis and chemoresistance,[9,12-14] suggesting that IL6/STAT3 signaling is essential for MM therapeutic targeting.

Correspondence:

WEE JOO CHNG
csicwj@nus.edu.sg

Received: March 6, 2019.

Accepted: August 12, 2019.

Pre-published: August 14, 2019.

doi:10.3324/haematol.2019.221176

Check the online version for the most updated information on this article, online supplements, and information on authorship & disclosures: www.haematologica.org/content/105/5/1391

Cytogenetic abnormalities remain one of the main hallmarks of MM. 1q21 amplification [1q21(amp)], the most commonly identified chromosomal aberration, present in 36-48% of newly diagnosed cases of MM, is an important prognostic marker.[15-18] Previous studies revealed that *CKS1B* and *PMSD4* are genes that putatively drive disease aggressiveness in 1q21(amp) cases;[18-20] nevertheless, biological and functional reports on these genes conferring oncogenic phenotypes are lacking. In reality, the critical genes within the minimally amplified region have yet to be fully characterized.

IL6R, the gene encoding the transmembrane receptor protein for IL6 is located on chromosome 1q21. Although it has been shown that *IL6R* has a role in predicting patients' outcome,[5,21,22] it remains unknown whether *IL6R* expression is associated with 1q21(amp) or could cause the hyperactivation of STAT3 signaling that could potentially contribute to adverse disease manifestations.

Importantly, our group and Lazzari *et al*. have recently reported that overexpression of *ADAR1*, an RNA editing enzyme, residing in the 1q21 region near the aforementioned *IL6R*, also has significant prognostic value in MM.[23,24] The protein exists in two distinct isoforms, namely the short P110 and the long P150 isoforms. While P110 is constitutively expressed in the nucleus, P150 expression is interferon-inducible and can shuttle between the nucleus and cytoplasm due to the presence of a nuclear export signal on its extended amino terminal domain.[25-27] Although interferon and IL6 are both members of the cytokine family and can be upregulated upon infection and inflammation, a possible cross-talk between IL6/STAT3 signaling and ADAR1 expression has not been thoroughly investigated. Aberrant adenosine-to-inosine editing events arising from deregulated ADAR1 been widely reported in cancers,[27-31] however, the general knowledge on its upstream regulators and the mechanisms mediating its overexpression have remained elusive, not to mention in MM.

In view of both *IL6R* and *ADAR1* being located in close proximity on 1q21 and having been independently reported to be prognostically important for MM, we sought to delineate their potential collaboration in the pathogenesis of MM and to determine how they are associated with STAT3 signaling. Here, we report that 1q21(amp) leads to elevated expression of IL6R and ADAR1. ADAR1-P150 and STAT3 form a regulatory feedback loop mediating the growth and proliferation of MM cells; the convergence of regulatory signals from both IL6R and ADAR1-P150 confers hyperactivation of STAT3 signaling, potentially driving the malicious evolution of MM. Critically, MM patients with concurrent overexpression of both proteins had a poorer prognosis than those who had no abnormality or a single one.

Methods

Patients' samples and human multiple myeloma cell lines

Primary samples from the healthy volunteers and MM patients were collected after obtaining informed consent, according to conditions stated by the Institutional Review Board, National University Hospital. All human MM cell lines used have been previously characterized.[32] Isolation of patients' samples and culture conditions for them and human MM cell lines are described in the *Online Supplementary Information*. The purity of CD138$^+$ cells of the patients' samples was checked with anti-κ and anti-λ immunofluorescence staining (*Online Supplementary Figure S5*).

Gene expression profiling, genomic hybridization and biostatistics

Details of the multiple gene expression profiling and array comparative genomic hybridization datasets analyzed are provided in *Online Supplementary Table S1*. Analyses of *IL6R/ADAR1* copy number and expression and STAT3 signature/index are described in the *Online Supplementary Information*. Statistical analyses between two groups in the patients' datasets were performed with the Wilcoxon test. *P*-values between two groups from *in vitro* studies were computed with an independent *t*-test, assuming a normal distribution of the means. All experiments were repeated at least twice (biological replicates) and the error bars in the graphs represent the means ± standard deviations.

ADAR1-P150, IL6R and STAT3 knockdown and overexpression

We knocked down ADAR1-P150 and IL6R in human MM cell lines with specific shRNA through lentivirus infection. shRNA sequences are available in the *Online Supplementary Information* (*Online Supplementary Table S3*). pCDNA-Flag-tagged vector encoding for P150 protein was transfected into MM cells using an electroporation method (Neon, Invitrogen). siRNA against STAT3 and pIRES-STAT3 plasmids were also introduced into MM cells via Neon transfection. Based on the basal level of the proteins (Figure 1B), we picked H929 and U266 cell lines for P150 and IL6R knockdown and the OCIMY5 and KMS12BM lines for P150 overexpression.

Assays

Details of the chromatin immunoprecipitation (ChIP), luciferase, co-immunoprecipitation, immunofixation and functional assays (cell growth, colony formation and cell cycle) are available in the *Online Supplementary Information*. Blots and images presented are representative of multiple repeats (at least two) of the experiments.

RNA-sequencing and analysis of global RNA editing events

Total RNA from IL6-treated MM cells was isolated using the RNeasy kit (Qiagen) according to the manufacturer's protocol. Whole transcriptome sequencing was done on an Illumina Hi-Seq-4000 platform (Supplier). Detailed information about variant calling and RNA editing analysis are provided in the *Online Supplementary Information*.

Results

ADAR1-P150 and IL6R are associated with 1q21 copy number and IL6 stimulation

Since *IL6R* and *ADAR1* genes are located in close proximity (*Online Supplementary Figure S1A*), we postulated that 1q21(amp) could lead to concomitant increases in the expression of both. *In silico* analyses revealed that 1q21 status was indeed closely associated with *IL6R* and *ADAR1* levels in diverse patients' datasets and human MM cell lines (Figure 1A and *Online Supplementary Figure S1B*). Quantitative polymerase chain reaction (qPCR) and western blotting confirmed the upregulation of ADAR1 and IL6R at the mRNA and protein levels, respectively, in cell lines with 1q21(amp) compared to the levels in the wild-type (WT) line (Figure 1B).

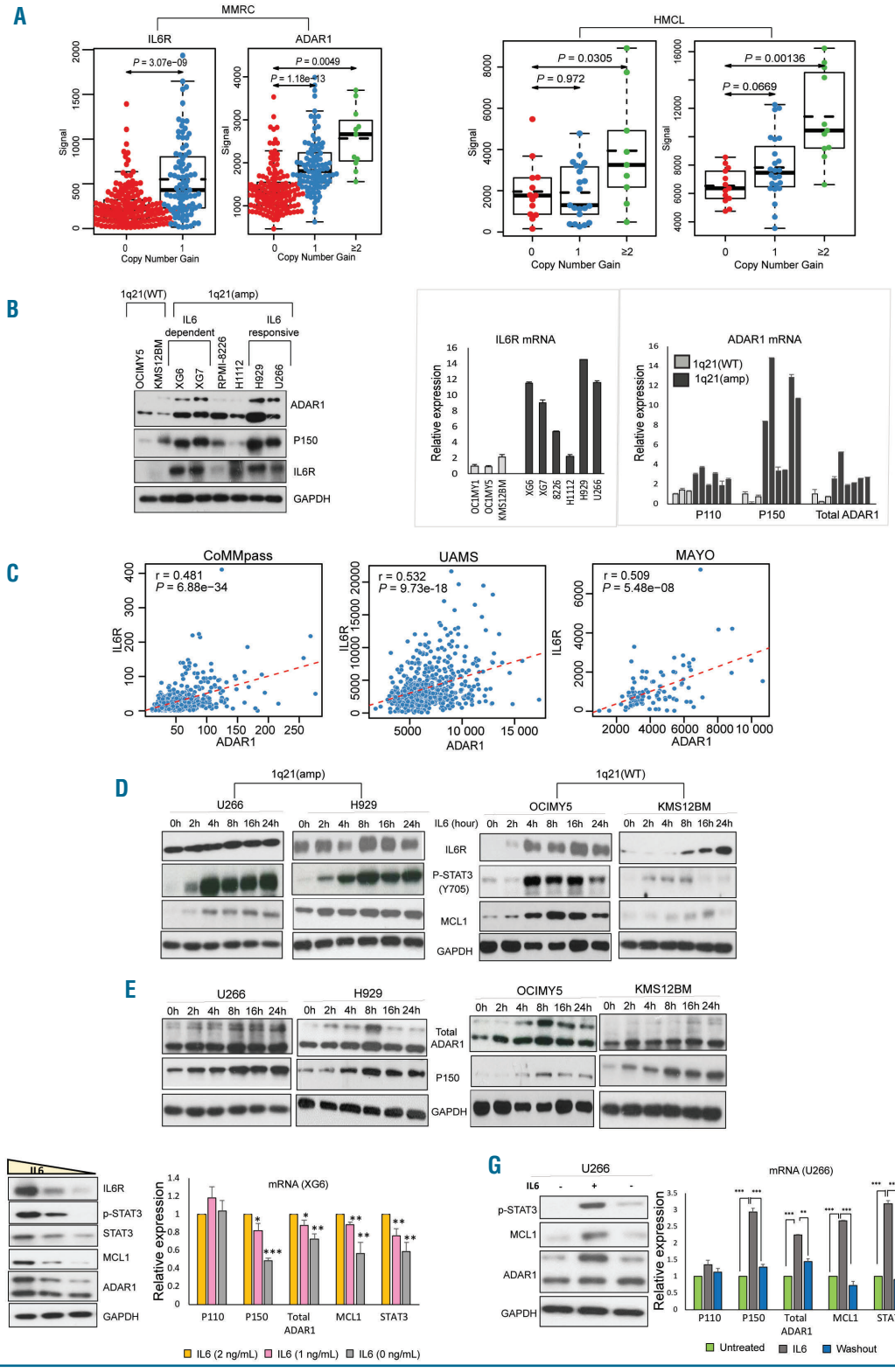

Figure 1. IL6R and ADAR1-P150 are closely associated with 1q21 copy number and IL6 stimulation. (A) Gene expression levels of *IL6R* and *ADAR1* in the Multiple Myeloma Research Consortium (MMRC) patients' dataset (left) and human multiple myeloma cell lines (HMCL) (right) according to 1q21 status. 0- no copy number gain (wildtype, WT), 1- one copy gain, ≥2- two or more copy gains. *IL6R* and *ADAR1* copy number and expression values were determined as described in the *Online Supplementary Information*. (B) Basal protein (left) and mRNA (right) expression of IL6R and ADAR1 in HMCL as detected by western blot and real time quantitative polymerase chain reaction (RT-qPCR). (C) Correlation of ADAR1 with IL6R in different patients' datasets computed using the Pearson correlation test. 'r' is the correlation coefficient and P-values indicate whether the correlation coefficient is different from 0. (D, E) Western blot analysis of IL6/STAT3 pathway components (D) and ADAR1 expression (E) in cells with 1q21(amp) (U266 and H929) and 1q21(WT) (OCIMY5 and KMS12BM) upon IL6 stimulation (10 ng/mL) at different time points. The top band in total ADAR1 refers to the P150 isoform, while the bottom band is the P110 isoform. The single P150 band in the second blot was probed with a specific antibody that can only detect P150 but not P110 (Ab126745). (F) Western blot and RT-qPCR analysis of protein (left) and mRNA (right) expression of ADAR1 and STAT3 pathway markers in the XG6 cell line which was cultured in conditions with gradual IL6 deprivation (3 ng/mL, 2 ng/mL, 1 ng/mL) for 24 h. (G) U266 was stimulated with IL6 (10 ng/mL) for 8 h before the IL6-containing medium was washed off, and the cells were resuspended in IL6-free medium again for 24 h. ADAR1 and STAT3 pathway components were checked for expression via western blot (left) and qRT-PCR (right). *P<0.05, **P<0.01, ***P<0.0001. MMRC: Multiple Myeloma Research Consortium; HMCL: human multiple myeloma cell lines; WT: wildtype; IL6: interleukin-6.

With regards to ADAR1, interestingly, we observed that among the 1q21(amp) cells, P150 isoform expression was prominently higher in IL6-responsive and -dependent cells, while the expression of P110 isoform did not vary much (Figure 1B). Importantly, we also observed a consistent positive correlation between ADAR1 and IL6R in patients from several clinical datasets (Figure 1C) suggesting that the ADAR1-P150 isoform, just like IL6R, could be involved in IL6 signaling.

To test this hypothesis, we treated human MM cell lines with IL6 for different periods and investigated the expression profile of various markers involved in IL6-signaling. We observed that IL6 caused an induction of STAT3 signaling in MM cells regardless of the cells' 1q21 status, albeit at different levels. While there was a gradual and time-dependent accumulation of IL6R in the 1q21(WT) cells, the 1q21(amp) cells showed only a minimal increase, largely due to its already heightened endogenous level, even in the unstimulated state (Figure 1D). As expected, IL6 led to robust upregulation of phospho-STAT3 in both cell types; however, close scrutiny of the time kinetics revealed that 1q21(amp) cells had more rapid and sustainable phospho-STAT3 induction than the 1q21(WT), concomitantly with its downstream target MCL1. This indicated that the STAT3 signaling in 1q21(amp) cells was hypersensitized, potentially in relation to the constitutively expressed IL6R.

With regards to ADAR1 expression, the P150 isoform was evidently upregulated upon IL6 stimulation, whereas, P110 seemed to show minimal changes, at both the protein (Figure 1E) and mRNA levels (*Online Supplementary Figure S1C*), irrespective of 1q21 status. An antibody specific for the P150 isoform was also used to confirm our observations. We further validated our observations by starving the IL6-dependent-cells lines XG6 and XG7 of IL6, which demonstrated depleted P150, and an attenuation of IL6R, concomitantly with MCL1; P110 was again mildly affected (Figure 1F and *Online Supplementary Figure S1D*). The specific correlation of IL6 induction with P150 was also recapitulated when the rescue of IL6 stimulation in a IL6-sensitive cell line, U266, returned P150 expression to its basal level (Figure 1G). In corroboration, *in vitro* IL6 starvation of $CD138^{+}$ cells harvested from patients' samples (n=2) compromised the STAT3 pathway, concomitantly with P150 downregulation (*Online Supplementary Figure S1E*). Collectively, these data suggest that besides potently activating the STAT3 pathway, IL6 has a role in mediating ADAR1-P150 expression in MM cells.

STAT3 transcriptionally regulates ADAR1-P150 expression

Considering that IL6 robustly activated STAT3 signaling, we next proceeded to investigate the direct role of STAT3 transcription factor on ADAR1-P150. Utilizing mouse liver cells with STAT3-$WT^{+/+}$ and $null^{-/-}$ genotypes, we observed that the absence of STAT3 ($STAT3^{-/-}$) grossly compromised the upregulation of IL6-induced-P150 (Figure 2A). Pharmacological inhibition of STAT3 in H929 cells with two specific inhibitors (STA-21 and LLL12) caused a gradual reduction of P150 expression in a time- and dosage-dependent manner (Figure 2B), concomitantly with phospho-STAT3 and MCL1. At the mRNA level, knocking down STAT3 and overexpressing the constitutively-activated-STAT3 (CA-Y705), but not the dominant negative mutant derivative, caused a reduction and an increase of P150 mRNA, respectively (Figure 2C, D). These data strongly suggest that STAT3 plays a role in regulating the transcription and expression of P150.

Indeed, our hypothesis was validated when the ChIP-qPCR assay showed an enrichment of STAT3 protein on the promoter regions of P150 and its known target MCL1 (Figure 2E). There was no change in the binding enrichment of STAT3 on the IL6R promoter (*Online Supplementary Figure S2B*). A luciferase reporter assay provided further evidence of STAT3's transcriptional regulation of P150 where IL6 stimulation (Figure 2F) and the overexpression of STAT3-CA (but not the dominant negative mutant) (Figure 2G) resulted in enhancement of the luciferase signal as compared to their respective controls.

P150 is important for the growth and proliferation of multiple myeloma cells

The above results demonstrated that P150 overexpression in MM can arise from the combined effects of 1q21(amp) (Figure 1) and constitutive activation of STAT3 (Figure 2). This double-pronged regulation of P150 suggests that aberrant expression of the isoform may have important biological and functional effects. To elucidate the oncogenic role of IL6/STAT3-induced-P150 in MM, we cloned P150-specific sequences into a pCDNA-overexpressing plasmid and transfected them into OCIMY5 cells, after which we performed various functional assays. Effective overexpression of P150 but not P110 (Figure 3A) allowed us to study the P150-specific oncogenic properties. P150 enrichment in the cells conferred a growth advantage (Figure 3B), increased colony-forming ability (Figure 3C) and a more proliferative cell cycle profile (cellular enrichment in S/G2 phase) (Figure 3D). Conversely, knocking down P150 in U266 cells (Figure 3A) was detrimental to the cells' survival, with the P150-depleted cells demonstrating a slower growth rate, loss of colony-forming ability and a higher fraction of cells undergoing apoptosis (sub-G1 population enrichment in the cell cycle and increased annexin-V positivity) (Figure 3B-E). These phenotypes were replicated in P150-overexpressing KMS12BM cells (*Online Supplementary Figure S3*) and shP150-H929 cells (*Online Supplementary Figure S4*).

To further ensure that our observations thus far were P150-specific, we performed a rescue experiment by introducing the P150 isoform back into the shP150 cells (Figure 3F). The re-introduction of P150 clearly led to a rescue of growth (Figure 3G) and colony-forming ability (Figure 3H), suggesting that the growth disadvantage observed in the shP150 cells in Figure 3B-E was, in part, mediated by the lack of P150.

ADAR1-P150 in turn mediates IL6-induced STAT3 signaling

Interestingly, we also observed evidence of STAT3 activity being mediated by ADAR1. In the ADAR1 knockdown cells, IL6 delayed the activation of STAT3 signaling, as shown by slower induction of phospho-STAT3 and its direct target, MCL1. Up to 8 h were needed for the mechanism to start in U266-shADAR1, whereas, U266-shCtr already demonstrated STAT3 activation at 4 h after IL6 stimulation. This was completely reversed in the OCIMY5 cells which overexpressed ADAR1 (Figure 4A). Importantly, this protein expression profile was commensurate with the cellular phenotypes, in which the more

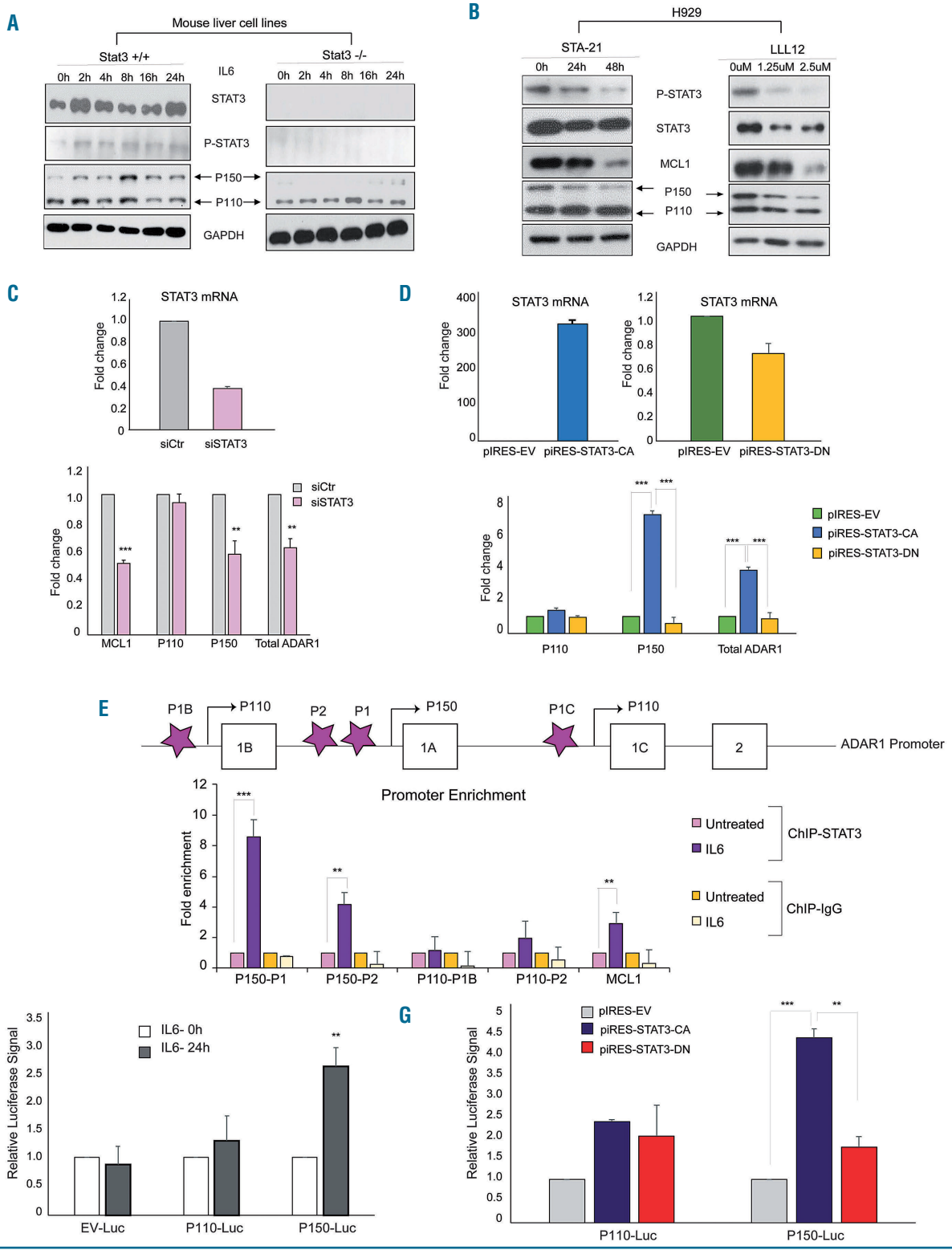

Figure 2. STAT3 transcriptionally regulates ADAR1-P150 expression. (A) Wildtype (STAT3$^{+/+}$) and STAT3 knockout (STAT3$^{-/-}$) mouse liver cell lines were treated with IL6 (10 ng/mL) for different periods and the protein expression profile was checked with western blotting. (B) Western blot analysis of H929 cells treated with STAT3 inhibitors, STA-21 (10 μM for 24 h and 48 h) and LLL12 (for 24 h at 1.25 μM and 2.5 μM). (C) Top panel: real-time quantitative polymerase chain reaction (RT-qPCR) analysis of *STAT3* mRNA expression after siRNA-mediated-*STAT3* knockdown in H929 cells (24 h). Bottom panel: MCL1 and *ADAR1* mRNA expression 24 h after STAT3 knockdown. (D) H929 transfected with pCDNA plasmid transcribing for constitutively-activated STAT3 (STAT3-CA) and its dominant negative mutant (STAT3-DN) (24 h). STAT3-CA is artificially phosphorylated at Y705, while the STAT3-DN is transcriptionally defective and has a gain-of-function of inhibiting endogenous STAT3 expression. Top panel: the transfection efficiency was checked with qRT-PCR. Bottom panel: ADAR1 mRNA expression after STAT3 overexpression. CA: constitutively activated, DN: dominant negative. (E) Top panel: depiction of primers (purple stars) designed to encompass different regions of *ADAR1* promoters. Promoters 1B and 1C transcribe for the P110 isoform and promoter 1A transcribes for the P150 isoform. Bottom panel: H929 cells were stimulated with IL6 (10 ng/mL for 6 h) and STAT3 enrichment on the different regions of *ADAR1* promoter was investigated with chromatin immunoprecipitation and qPCR with primers depicted in the top panel. (F, G) H929 cells were transfected with a luciferase-reporter vector encoding for either P110 or P150 promoter regions. At 24 h after transfection, the cells were treated with (F) either phosphate-buffered saline (PBS) or IL6 (10 ng/mL) for 8 h or (G) further transfected with either STAT3-CA or STAT3-DN and the cells were left to grow for another 24 h. The luciferase activity was analyzed with a Tecan plate reader. EV: empty vector.

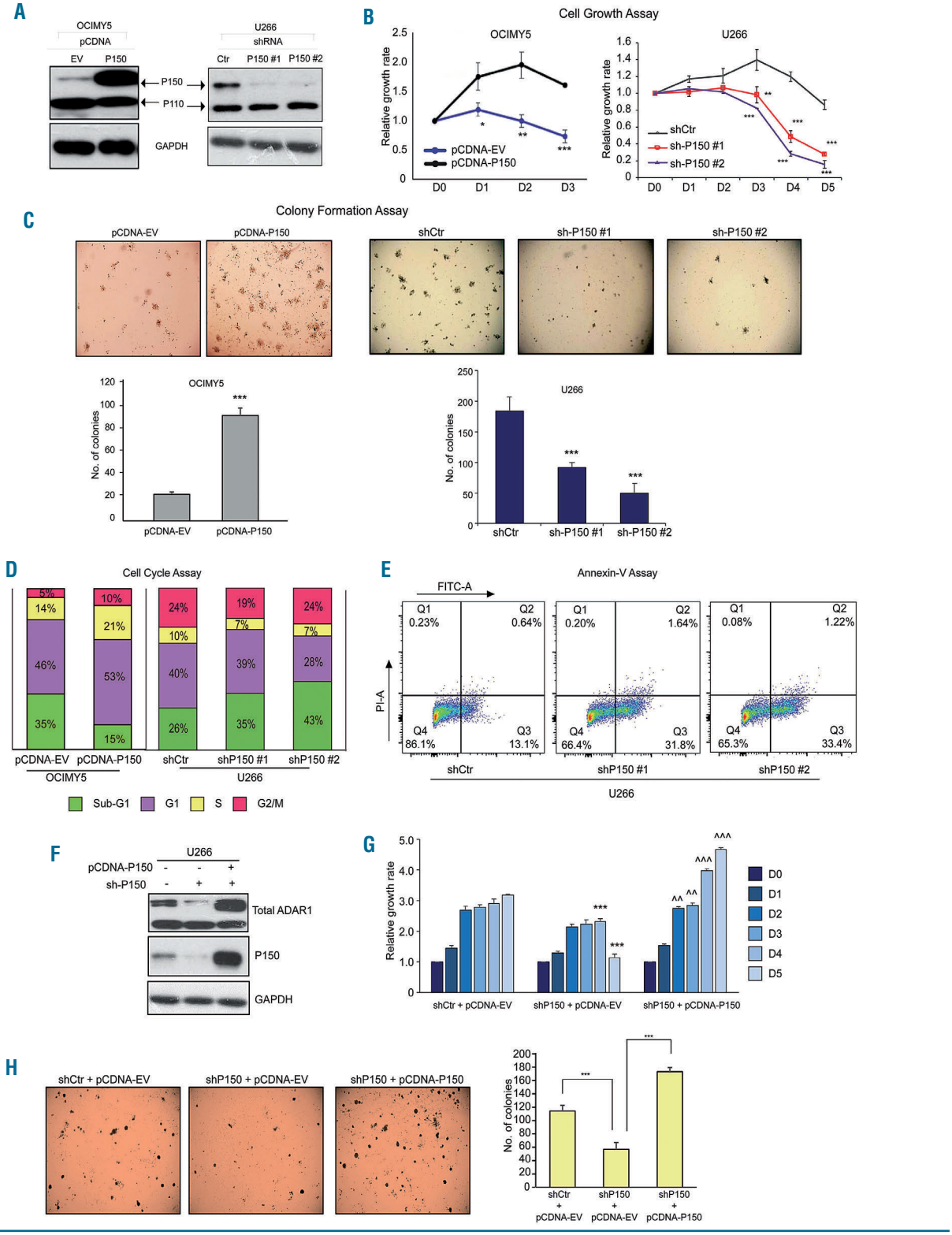

Figure 3. ADAR1-P150 is important for the growth and proliferation of multiple myeloma cells. (A) Western blot analysis to check for the efficiency of P150 overexpression in OCIMY5 cells and lentivirus-mediated-shRNA knockdown of P150 in U266 cells. Cells were harvested at 48 h after manipulation for protein isolation. The shRNA sequences are available in the *Online Supplementary Information*. (B) Daily cell growth assay (CTG assay) depicting the growth profile of multiple myeloma cells with manipulated levels of P150. The reading for day 0 (D0) was taken 48 h after manipulation. (C) Colony-formation assay assessing the ability of the cells to form colonies upon P150 overexpression and knockdown. Top panel: representative images of the soft agar incubated over 7-14 days. Bottom panel: quantification of the colonies formed in triplicate wells of soft agar. (D) Cell cycle analysis (propidium iodide staining) of P150-overexpressed OCIMY5 cells and P150-depleted U266 cells. Cells were harvested 48 h after manipulation for analysis. The percentage on each bar represents the number of the cell population within the cell cycle phase out of the total number of cells captured and analyzed. *P<0.05 **P<0.001 ***P<0.0001 (E) Annexin-V-FITC apoptosis assay of U266 cells 48 h after P150 knockdown. (F) Western blot analysis for the expression of total ADAR1 and P150 24 h after transfection with shP150 or upon co-transfection with shP150 and pCDNA-P150 in U266 cells. (G) Daily cell growth assay of U266 cells with different levels of P150. The reading for day 0 (D0) was taken 48 h after manipulation. **P<0.05 against shCtr+pCDNA-EV, ***P<0.001 against shCtr+pCDNA-EV, ^^P<0.05 against shP150+pCDNA-EV, ^^^P<0.001 against shP150+pCDNA-EV. (H) Left panel: representative photographs of colonies formed in triplicate wells of soft agar over 14 days. Right panel: quantification of the number of colonies in U266 cells with different levels of P150. ***P<0.0001.

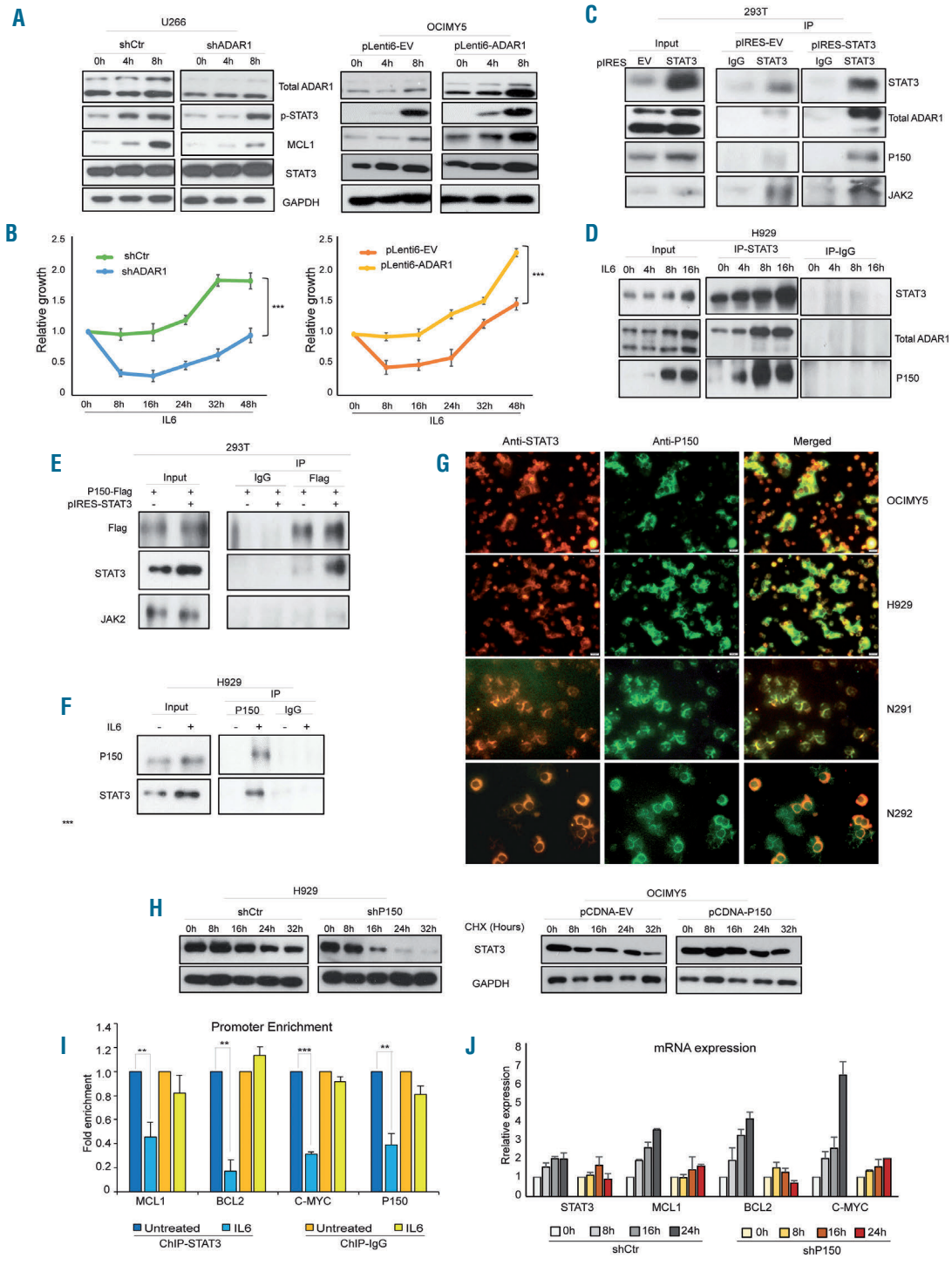

Figure 4. STAT3-induced-ADAR1-P150 in turn mediates STAT3 signaling. (A) Stable isogenic cell lines (U266 and OCIMY5) with different levels of ADAR1 expression that have been previously established[24] were treated with IL6 (10 ng/mL) at different time points before western blotting was done to analyze the protein expression profile. (B) Daily cell growth of IL6-stimulated-U266 and OCIMY5 with differential ADAR1 expression. The reading for day 0 (D0) was taken 48 h after manipulation. ***P<0.0001. (C) 293T cells were transfected with either an empty vector (pIRES-EV) or a STAT3-overexpressing vector (pIRES-STAT3) for 24 h and cells were collected for protein extraction and subsequent co-immunoprecipitation experiments. The total cell lysate was incubated with either IgG control antibody or a specific STAT3 antibody. Its potential interaction with endogenous ADAR1 was checked with western blot analysis. JAK2 served as the positive control. (D) Phospho-STAT3 was induced with IL6 (10 ng/mL) in H929 cells which were harvested to determine their total protein level. Protein was pulled down with either STAT3 or IgG antibodies and western blot was used to check for the potential interaction. (E) 293T cells were transfected with either P150-Flag only or with both P150-Flag and STAT3 and reciprocal immunoprecipitation was done with IgG and Flag-antibody. The interaction between P150-Flag and STAT3 was checked with western blot analysis. (F) H929 cells were stimulated with IL6 (10 ng/mL) for 16 h and endogenous P150 was pulled down with its specific antibody or negative control IgG, for reciprocal immunoprecipitation. Its interaction with STAT3 was assessed with western blot. (G) Cytospin slides consisting of cells from multiple myeloma cell lines (OCIMY5 and H929) and patients' samples (N291 and N292) were immunostained with STAT3- and P150-specific antibodies. Immunofluoresence signals for both proteins were analyzed under a fluorescence microscope. Total magnification used was 400x. Red (Alexa-Fluor-555): STAT3; green (Alexa-Flour-488): P150; yellow: co-localization. (H) A cycloheximide (CHX) chase assay was performed to identify the stability of the STAT3 protein. P150-knockdown U266 cells and P150-overexpressing OCIMY5 cells with their respective control cells were treated with the protein synthesis inhibitor CHX at 50 µg/mL to elucidate the time kinetics for STAT3 protein degradation. The intracellular content of STAT3 protein was analyzed by western blotting. (I) Fold enrichment of STAT3 occupancy on its target gene promoters before and after P150 knockdown in U266 cells, as analyzed with chromatin immunoprecipitation quantitative polymerase chain reaction analysis (qPCR). **P<0.05, ***P<0.001 (J) Reat-time qPCR analysis for the mRNA induction of STAT3 target genes in response to IL6 (10 ng/mL) treatment at different time points in control (shCtr) and P150-knockdown (shP150) U266 cells.

rapid STAT3 activation (in U266-shCtr and OCIMY5-pLenti6-ADAR1) was associated with significantly accelerated IL6-induced growth (Figure 4B).

To elucidate the potential mechanism, we first checked for a possible ADAR1-STAT3 interaction. Pulling down STAT3 from STAT3-overexpressing 293T cells showed enrichment of endogenous P150 and its known interacting partner, JAK2, in the immunoprecipitated fraction but not in the IgG control fraction. On the other hand, P110 seemed to form only a loose interaction with STAT3 (Figure 4C). Consistently, in IL6-responsive H929 cells, accumulation of IL6-induced phospho-STAT3 led to a gradual increase of interaction with endogenous ADAR1, particularly P150 (Figure 4D), indicating that it was the main interacting isoform. To confirm this observation, we performed reciprocal immunoprecipitation. Co-transfection of P150-Flag and STAT3 plasmids into 293T cells and pulling down only the P150 isoform also revealed efficient co-precipitation with STAT3 protein (Figure 4E). There was no interaction of P150 with JAK2. Similarly, P150 could be seen co-precipitating with endogenous STAT3 in the IL6-induced fraction of H929 cells (Figure 4F).

Subsequently, we checked for the localization of ADAR1 and STAT3 in human MM cell lines (OCIMY5 and H929) and patients' samples (N291 and N292), and found that STAT3 was localized in both the nucleus and cytoplasm, whereas, P150 was predominant in the cytoplasm. Merged images of individual proteins clearly showed co-localization of STAT3 and P150 in the cytoplasm (Figure 4G). It is therefore plausible that this cytoplasmic co-localization could have rendered the environment conducive for their physical interaction.

Next, we investigated how this interaction could enhance STAT3 activity. A cycloheximide chase assay revealed that P150 could promote the stability of STAT3 protein. Knocking down P150 enhanced STAT3 degradation (Figure 4H). At 8 h, STAT3 already showed signs of degradation and was almost completely degraded at 24 h after cycloheximide treatment in the shADAR1 cells, in contrast to the shCtr cells which required up to 16 h for a mild cycloheximide effect to be visible. Similarly, the P150-overexpressed cells also took longer (up to 24 h) to show signs of STAT3 protein degradation.

These data suggest that P150 could mediate the activity of STAT3 signaling via a direct physical interaction, which leads to stabilization of the latter, thus, more is shuttled into the nucleus to transcribe various pro-oncogenic genes. This hypothesis was validated when the loss of P150 led to compromised STAT3 binding to its target gene promoters (Figure 4I) and sub-optimal induction of its target genes (Figure 4J).

Combined IL6R and P150 suppression leads to reduced IL6-induced oncogenicity

The more rapid and sustainable STAT3 signaling in the 1q21(amp) cells (which express IL6R constitutively) (Figure 1D), coupled with the STAT3- P150 feedback regulatory loop (Figure 4) led us to hypothesize that the concomitant gain of IL6R and ADAR1 may lead to hyperactivation of STAT3 signaling, conferring a more malignant state to 1q21(amp) cells. Indeed, the observation of 1q21(amp) patients having significantly higher STAT3 indices (STAT3 pathway activation) further supports the basis of our hypothesis (Figure 5A).

We further investigated this by first comparing the growth profile of 1q21(WT) and 1q21(amp) upon IL6 stimulation. Not surprisingly, exogenous IL6 conferred more active growth to all tested cell lines compared to untreated ones (Figure 5B). Importantly, however, 1q21(amp) cells demonstrated more pronounced growth than the WT cells. The growth rate of the IL6-stimulated 1q21(amp) cells already surpassed that of the unstimulated ones as soon as 4 h after IL6 induction. In contrast, the 1q21(WT) cells required up to 24 h after IL6 stimulation to display a differential growth phenotype. This implies that the 1q21(amp) cells had a sensitized IL6/STAT3 pathway and that there was a possibility that the pathway-related genes within 1q21 could be driving this phenotype.

To elucidate the potential importance of IL6R and P150, we performed single and co-depletion of IL6R and P150 and assessed the functional consequences for STAT3 activity and MM cell growth. Suppression of IL6R or P150 alone obliterated the IL6-induced STAT3 pathway, manifested by the weaker induction of phospho-STAT3 and its downstream factors (Figure 5C). Inhibition of this pathway was detrimental to MM cells, which experienced growth retardation (Figure 5D), impeded colony formation (Figure 5E) and halted IL6-induced-cell cycle progression (as compared to IL6-treated shCtr cells which progressed through the S/G2 phase) (Figure 5F), suggesting that both factors are individually important for IL6-induced STAT3 activation. Notably, the combined loss of IL6R and P150 resulted in more deleterious cellular phenotypes as compared to the loss of just one respective protein, consistent with the more prominent attenuation of IL6-induced STAT3 signaling (Figure 5C). A similar trend was also observed in H929 cells (*Online Supplementary Figure S6*).

IL6R, ADAR1 and STAT3 demonstrate good clinical correlation

Having shown the biological association of both IL6R and ADAR1-P150 with STAT3, we then investigated the clinical correlations by analyzing publicly available patients' datasets. Positive correlations were consistently observed between the STAT3 signatures and the expression of STAT3, IL6R and ADAR1 in various patients' datasets (Figure 6A).

To demonstrate the importance of the combined gain of both genes within 1q21, we computed the correlation between STAT3 signature enrichment and overall survival in patients with differential expression of these genes. Six out of seven datasets revealed a significantly enriched STAT3 signature in the high-ADAR1+high-IL6R as compared to the low-ADAR1+low-IL6R groups of patients (Figure 6B). We also found that lack of expression of either gene resulted in a lower STAT3 signature expression and, more importantly, loss of both genes caused an even more significant suppression of the signature (Figure 6C), signifying that both factors are influential players in the STAT3 pathway. Importantly, this differential STAT3 activity in different groups was also closely associated with the patients' prognosis. Patients with high expression of both genes had a worse overall survival than those with low expression of both genes (Figure 6B and *Online Supplementary Figure S7*) further supporting our hypothesis that the concomitant gain of IL6R and ADAR1 is critical in driving poor disease outcome in the 1q21(amp) cases.

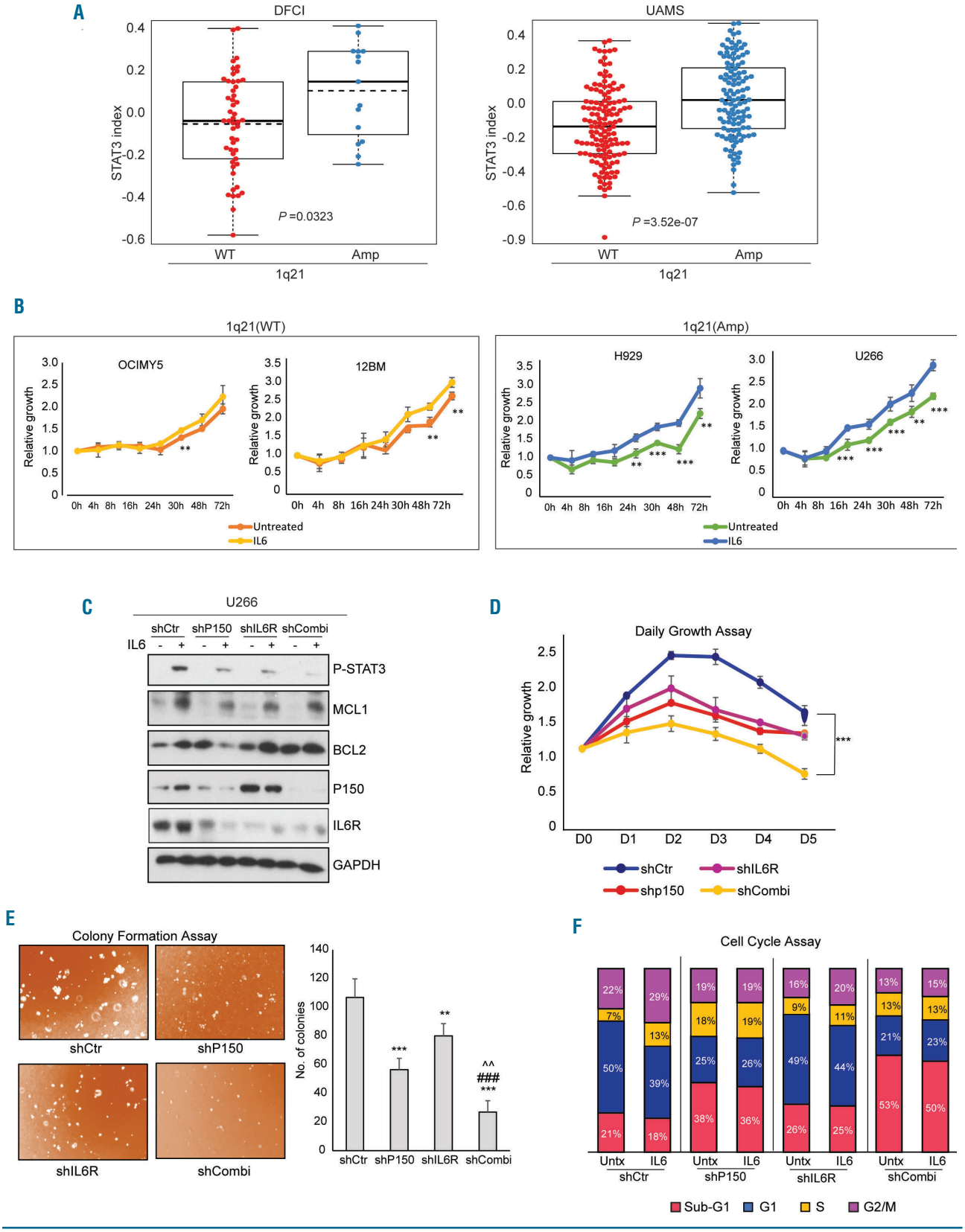

Figure 5. Combined IL6R and P150 suppression led to reduced IL6-induced oncogenicity. (A) The association between 1q21 status and STAT3 signature in Dana Farber Cancer Institute (DFCI) and University for Arkansas Medical School (UAMS) patient's datasets. WT- wildtype, Amp- two or more copies. (B) CTG assay assessing the growth rate of multiple myeloma cell lines with different 1q21 status over a 72 h time course. $^{**}P<0.05$, $^{***}P<0.001$ (C) At 48 h after lentivirus infection, U266 cells with shRNA-mediated P150 and/or IL6R knockdown were treated with IL6 (10 ng/mL) for 8 h and then the STAT3 pathway protein expression profile was analyzed by western blotting. (D-F) Daily growth assays (D), colony formation assays (E) and cell cycle assays (F) were done 48 h after lentivirus infection of shRNA to elucidate the phenotypes associated with loss of either one or both P150 and IL6R. For the cell cycle assays, the cells were stimulated with IL6 (10 ng/mL) for 24 h (to induce STAT3 signaling) before being fixed for fluorescence activated cell sorting analysis. This was to study the direct effects of loss of expression of these genes on the STAT3-mediated cell cycle profile. $^{**}P<0.05$ against shCtr, $^{***}P<0.001$ against shCtr, $^{\#\#\#}P<0.001$ against shP150, $^{\wedge\wedge}P<0.05$ against shIL6R.

A

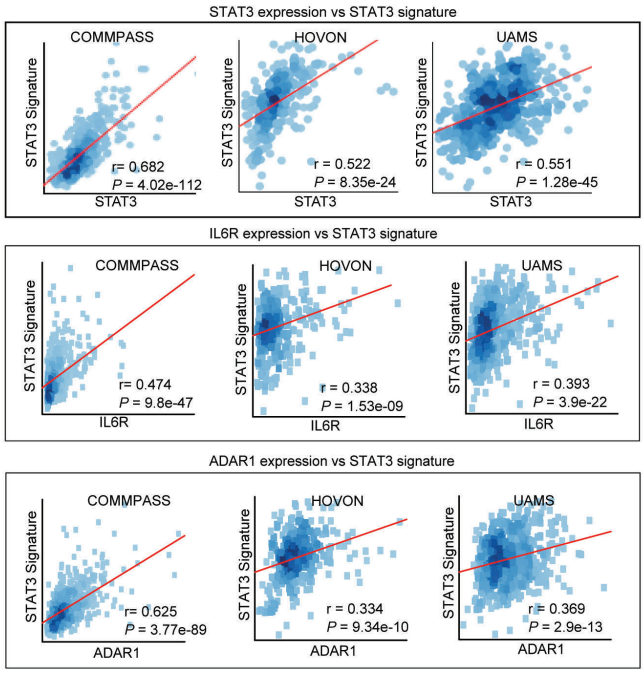

B

(High-ADAR1, High-IL6R) vs (Low-ADAR1, Low-ADAR1)	MAYO	ITALY	APEX	UAMS	HOVON	MMRC	CoMMpass
STAT3 signature (*P*-value)	0.266	5.5E-07	0.0239	1.11E-16	8.18E-07	2.52E-09	1.07E-13
Overall survival (HR)	N.A.	N.A.	1.67	2.12	1.58	N.A.	2.33
Overall survival (p-value)	N.A.	N.A.	0.012	0.0047	0.0865	N.A.	0.0008

C

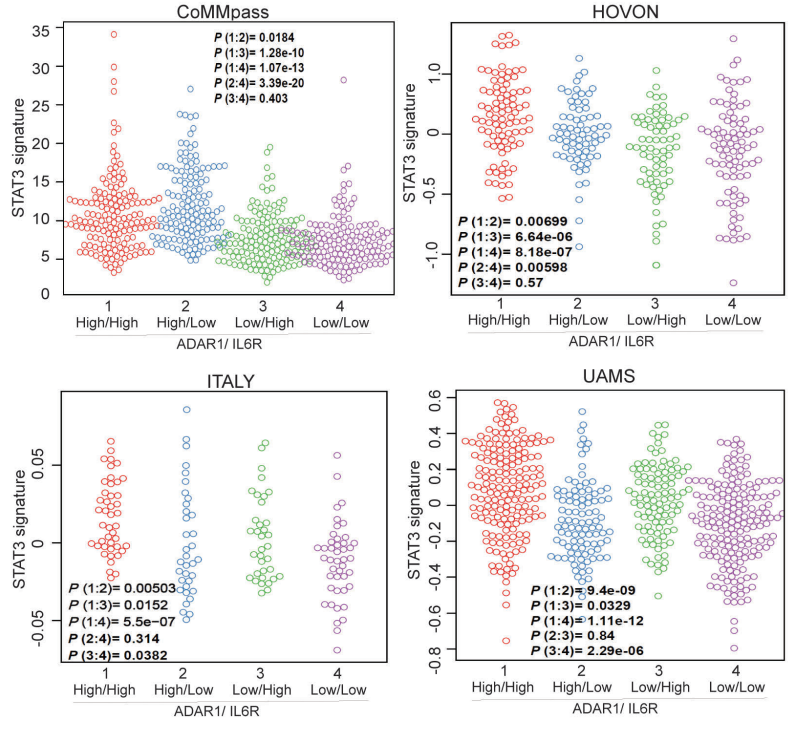

Figure 6. IL6R, ADAR1 and STAT3 demonstrated good clinical correlation. (A) Pearson correlation between the STAT3 signature and STAT3 (top panel), IL6R (central panel) and ADAR1 (bottom panel) expression in different patients' datasets. r is the correlation coefficient and P-values indicate whether the correlation coefficient is different from 0. (B) Comparison of the STAT3 signature and overall survival between patients with high expression of both ADAR1 and IL6R and patients with low expression of both genes. *P*-values highlighted in red indicate statistical significance ($P<0.05$). (High-ADAR1, High-IL6R indicates high expression of both genes; Low-ADAR1 and Low-IL6R indicates low expression of both genes. HR: hazard ratio. N.A.: information not available in that particular dataset, therefore analysis cannot be done. (C) Comparison of the STAT3 signature in patients with different levels of ADAR1 and IL6R expression. High/high: the expression of both genes is high. High/low: ADAR1 expression is high, IL6R expression is low. Low/high: ADAR1 expression is low, IL6R expression is high, Low/low: the expression of both genes is low. *P*(1:2) represents the *P*-value between group 1 (high/high) and group 2 (high/low). Similarly, the rest of the comparisons are done according to the group numbers. The STAT3 signature reflects the activity of the signaling pathway.

Potential therapeutic implications of the IL6R-P150-STAT3 interaction

The STAT3 inhibitor, LLL12, was reported to be effective in MM cells *in vitro*,[33] but the study did not highlight its association with a differential degree of STAT3 activity. We postulated that the prolonged and amplified STAT3 signals from P150-induced STAT3 stabilization could have an impact on cellular responsiveness to LLL12. Here, we demonstrated that cells with ectopically expressed P150 were indeed more sensitive to LLL12 treatment and that the cellular inhibition effect was further enhanced under IL6 stimulation (Figure 7A). This suggests that the lengthened STAT3 signaling event from IL6 induction and stabilization of the protein by the downstream P150 provides an ample target for the drug, rendering the cells hypersensitive to LLL12. To determine whether this principle holds true in 1q21(amp) cells, which have another hit of STAT3 activation through IL6R overexpression, we knocked down P150, IL6R or both and compared the cells' responsiveness to LLL12. Depletion of either gene did indeed compromise the sensitivity of the cells (under persistent IL6 stimulation) to the drug and loss of both genes caused the cells of both lines tested to be even more resistant (Figure 7B).

Discussion

The growth privilege of MM cells is widely attributed to their concerted interactions with the bone marrow microenvironment and the growth factors enriched within the bone marrow are, therefore, deemed indispensable for MM survival.[3,5] Studies over the years have provided solid evidence that among these growth factors, IL6 is one of the key cytokines driving the growth and proliferation of MM cells, and its oversecretion could lead to drug resistance.[1,4,13] IL6 induces STAT3 activation and this signaling pathway has been a long-standing oncogenic player.[1,33] Various therapies targeting this pathway have been developed and although *in vitro* and *in vivo* laboratory testing in MM had shown some potential,[34-36] the outcome of clinical trials on anti-IL6 antibodies was less meaningful.[37,38] The stumbling block was probably the lack of complete biological understanding of the IL6/STAT3 pathway itself. Our current work focuses on further dissecting this pathway and here we report novel IL6-induced oncogenicity in myeloma. Our data unveil a close interplay between IL6R, ADAR1 and STAT3 proteins, which could contribute to the hyperactivation of STAT3 signaling, consequently causing a more proliferative cellular profile in MM.

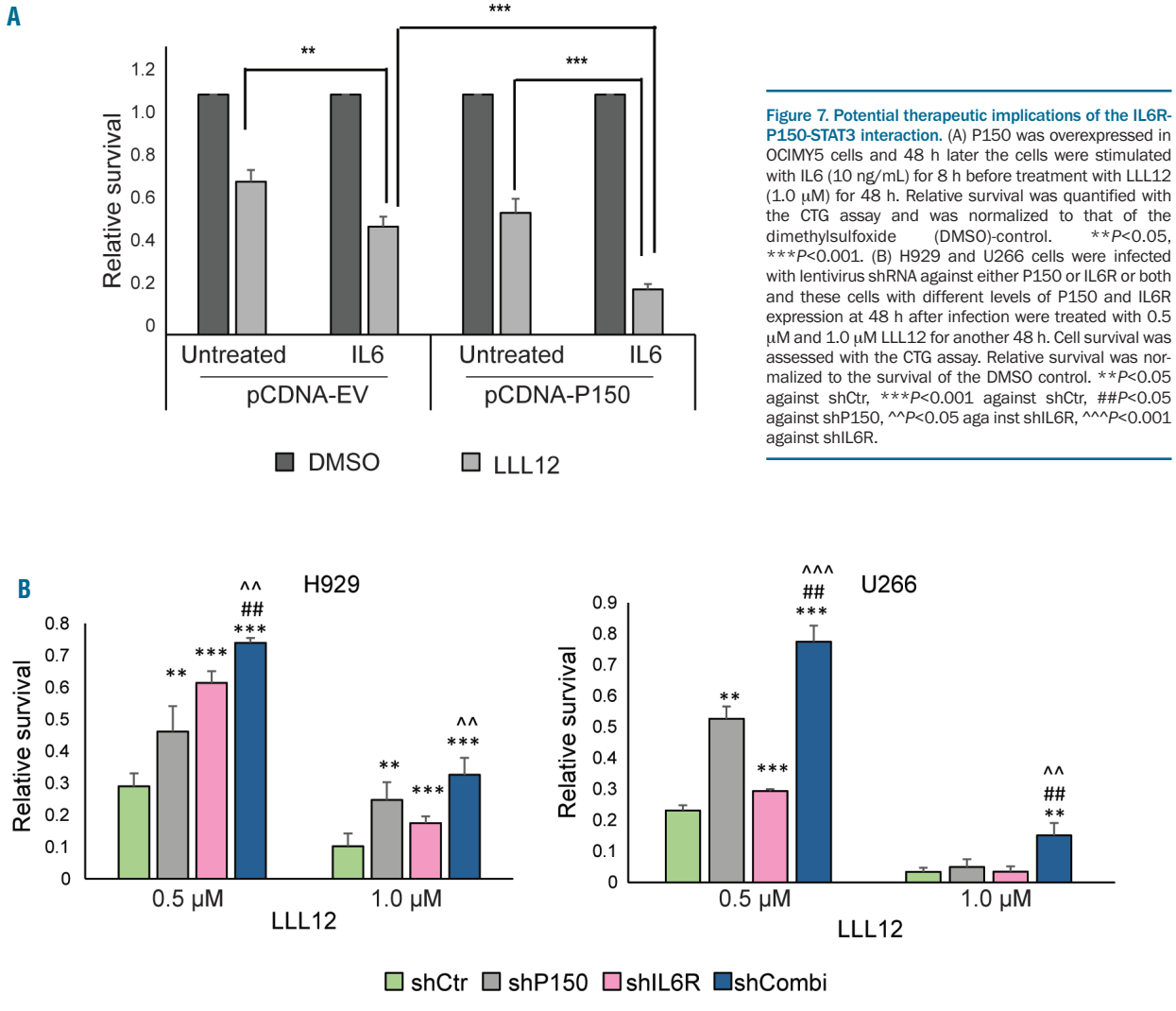

Figure 7. Potential therapeutic implications of the IL6R-P150-STAT3 interaction. (A) P150 was overexpressed in OCIMY5 cells and 48 h later the cells were stimulated with IL6 (10 ng/mL) for 8 h before treatment with LLL12 (1.0 μM) for 48 h. Relative survival was quantified with the CTG assay and was normalized to that of the dimethylsulfoxide (DMSO)-control. $^{**}P<0.05$, $^{***}P<0.001$. (B) H929 and U266 cells were infected with lentivirus shRNA against either P150 or IL6R or both and these cells with different levels of P150 and IL6R expression at 48 h after infection were treated with 0.5 μM and 1.0 μM LLL12 for another 48 h. Cell survival was assessed with the CTG assay. Relative survival was normalized to the survival of the DMSO control. $^{**}P<0.05$ against shCtr, $^{***}P<0.001$ against shCtr, $^{\#\#}P<0.05$ against shP150, $^{\wedge\wedge}P<0.05$ aga inst shIL6R, $^{\wedge\wedge\wedge}P<0.001$ against shIL6R.

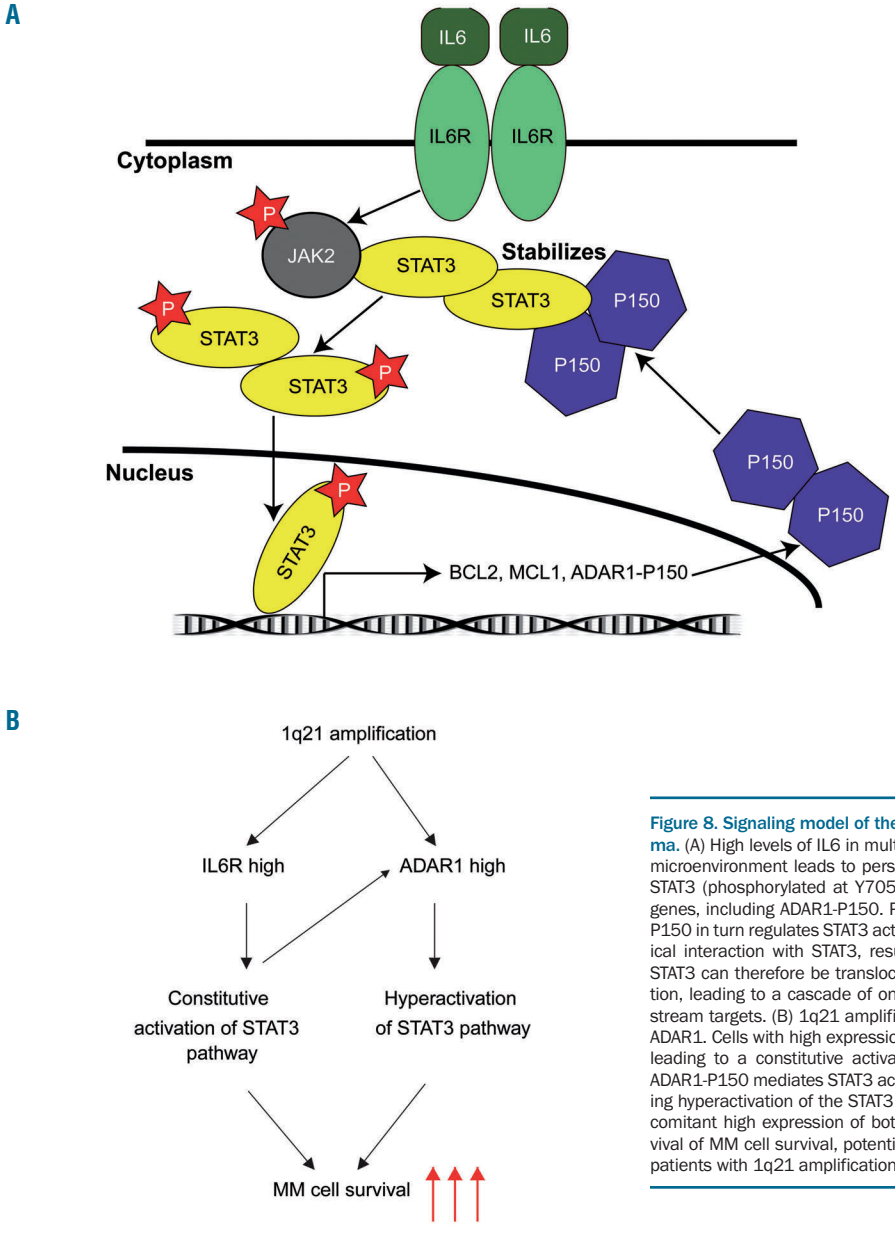

Figure 8. Signaling model of the IL6R-ADAR1-STAT3 interplay in multiple myeloma. (A) High levels of IL6 in multiple myeloma (MM) cells within the bone marrow microenvironment leads to persistent activation of the STAT3 pathway. Activated STAT3 (phosphorylated at Y705 by JAK) will drive the transcription of its target genes, including ADAR1-P150. P150 shuttles in and out of nucleus. Cytoplasmic P150 in turn regulates STAT3 activity in a positive feedback loop by forming a physical interaction with STAT3, resulting in protein stabilization of the latter. More STAT3 can therefore be translocated into the nucleus for its transcriptional function, leading to a cascade of oncogenicity deriving from the actions of its downstream targets. (B) 1q21 amplification leads to high expression of both IL6R and ADAR1. Cells with high expression of IL6R are highly sensitized to IL6 stimulation, leading to a constitutive activation of the STAT3 pathway. High expression of ADAR1-P150 mediates STAT3 activity in a feedback loop, as described in (A), causing hyperactivation of the STAT3 pathway. Convergence of mechanisms from concomitant high expression of both IL6R and ADAR1 culminates in enhanced survival of MM cell survival, potentially contributing to the poor disease prognosis in patients with 1q21 amplification.

To date, 1q21(amp) has remained a high-risk prognostic factor in MM. This poses a serious hurdle in myeloma management since a high percentage of newly diagnosed patients present with this abnormality and they are reported to be resistant to standard and novel therapies.[16,17,39,40] Although the clinical significance of *CKS1B*, the most commonly reported candidate driver gene,[18,39] has already been established, we believe that other genes within the amplified region may also be of pathogenic importance. Here, we impart novel information about the pathogenesis of 1q21(amp) and provide compelling evidence that *IL6R* and *ADAR1* on chromosome 1q21 are critical genes for myeloma pathogenesis. Concomitant gain of their genomic loci conferred growth and proliferation privilege to MM cells, working through hyperactivation of the STAT3 pathway. With regards to ADAR1, we saw an isoform-predominant phenomenon in which the P150 isoform was found to be intertwined in the STAT3 pathway by being its downstream transcriptional target and its upstream mediator. This feed-forward regulatory loop causes an augmented oncogenic effect, with both STAT3-induced P150 expression and P150-induced STAT3 protein stabilization acting in concert to promote manifestation of an aggressive disease. Coupled with the overexpression of IL6R that drives the hypersensitivity of the STAT3 pathway, it is plausible that these multi-oncogenic hits could contribute to the poor prognosis in the 1q21(amp) patients.

Although IL6R has been documented to be a predictor of poor outcome in myeloma patients,[5,21,22,41] there have not been proper biological studies associating it to myelomagenicity. Our notion of high IL6R acting as an ever-ready receptor for the IL6 ligand was proven when 1q21(amp) cells which constitutively express endogenous IL6R showed hastened and sustainable STAT3 pathway activation and enhanced IL6-induced-growth. This suggests that

high levels of IL6R hypersensitize the cells to IL6 binding. Consequently, activated STAT3 leads to the transcription of not only its classical target gene, thereby mediating growth and proliferation, but also ADAR1-P150, which also has oncogenic roles, thereby augmenting proliferative phenotypes.

Since ADAR1 is a well-known RNA editing enzyme, we also investigated whether our observations were related to the canonical function of this enzyme. IL6 treatment of MM cells for up to 24 h did not lead to much change in the total number of global editing events at the whole transcriptome level (*Online Supplementary Figure S8A*). A more complex picture emerged at the gene-specific level, whereby, genes of hyper-editing, hypo-editing and no-change of editing frequency appeared without distinct functional segregation among them (*Online Supplementary Figure S8B*). Analysis on the CoMMpass dataset revealed that the STAT3 signature, an indicator of collective STAT3 activity, was poorly correlated with the number of global editing events (r=0.115) (*Online Supplementary Figure S8C*). While we could not definitively conclude that the RNA editing's role of the IL6-induced P150 was not involved in conferring growth benefits to the cells, the fact that the localization of P150 was predominantly cytoplasmic even after IL6 stimulation (*Online Supplementary Figure S8D*) suggests that RNA editing is not likely to be the prevailing mechanism, as this process takes place in the nucleus where double-stranded mRNA are abundant.

Instead, we opine that the oncogenic effects are likely driven by P150-induced hyperactivation of the STAT3 pathway. The close association between ADAR1 and STAT3 signature strongly indicates that high ADAR1 expression contributes to STAT3 pathway activation, culminating in a conducive growth-promoting environment within the bone marrow. ADAR1 has been reported before to have an editing-independent role,[42-45] albeit not an extensive one, thus, our finding adds to the important pool of knowledge on the novel non-canonical function of ADAR1, specifically of its P150 isoform.

The fact that we also found a close correlation between IL6R and ADAR1, and the STAT3 signature, as well as between these and patients' survival, gives the strong impression that there is a close interplay between these factors which drives disease prognosis. We summarize our findings in a schematic diagram illustrating how 1q21(amp) can result in the overexpression of IL6R and ADAR1, eventually leading to more intensified oncogenic effects from the aberrantly amplified STAT3 activity (Figure 8A, B).

In conclusion, our current work highlights the complexity of the STAT3 pathway in MM and for the very first time we report its important association with the 1q21(amp) phenotype. It should, however, be noted that our data do not demonstrate a direct causal effect of 1q21 abnormalities, but rather a close relationship, which we showed through our detailed mechanistic study on human cell lines, supported by robust clinical data. Our data suggesting that 1q21(amp) cells are more responsive to the STAT3 inhibitor (LLL12) indicates that these cells have a close association and dependency on STAT3 pathway activity. This study further highlights the potential complex biological impact imparted by 1q21(amp), of which oncogenic phenotypes are conferred by potentially more than just *CSK1B*. It is plausible that a cascade of survival signals, produced by the gain of other critical oncogenes within this region, and in our case, IL6R and ADAR1-P150, led to the alteration of cytokine-mediated signaling and the intrinsic cellular phenotypes. Our results could explain why targeting IL6 may not be enough BUT targeting STAT3 activity may ACTUALLY be more beneficial. This study provides a new perspective on the STAT3 pathway in MM and the potential therapeutic means for high-risk 1q21(amp) patients.

Acknowledgment

WJC is supported by NMRC Singapore Translational Research (STaR) Investigatorship. This research is partly supported by the National Research Foundation Singapore and the Singapore Ministry of Education under the Research Centers of Excellence initiative as well as the RNA Biology Center at the Cancer Science Institute of Singapore, NUS, as part of funding under the Singapore Ministry of Education's Tier 3 grants, grant number MOE2014-T3-1-006. The computational work for this article was partially performed with resources of the National Supercomputing Center, Singapore (https://www.nscc.sg). We thank Dr Chen Leilei for providing experimental advice and vital reagents. We would also like to thank Dr Zhou Jianbiao for kindly contributing the STAT3 plasmids for our experiments.

References

1. Matthes T, Manfroi B, Huard B. Revisiting IL-6 antagonism in multiple myeloma. Crit Rev Oncol hematol. 2016;105:1-4.
2. Lee C, Oh J-I, Park J, et al. TNFα mediated IL-6 secretion is regulated by JAK/STAT pathway but not by MEK phosphorylation and AKT phosphorylation in U266 multiple myeloma cells. Biomed Res Int. 2013; 2013:580135.
3. Mondello P, Cuzzocrea S, Navarra M, Mian M. Bone marrow micro-environment is a crucial player for myelomagenesis and disease progression. Oncotarget. 2017;8(12): 20394-20409.
4. Gado K, Domjan G, Hegyesi H, Falus A. Role of interleukin-6 in the pathogenesis of multiple myeloma. Cell Biol Int. 2000;24(4):195-209.
5. Barille S, Bataille R, Amiot M. The role of interleukin-6 and interleukin-6/interleukin-6 receptor-alpha complex in the pathogenesis of multiple myeloma. Eur Cytokine Netw. 2000;11(4):546-551.
6. Bataille R, Jourdan M, Zhang XG, Klein B. Serum levels of interleukin 6, a potent myeloma cell growth factor, as a reflect of disease severity in plasma cell dyscrasias. J Clin Invest. 1989;84(6):2008-2011.
7. Pelliniemi TT, Irjala K, Mattila K, et al. Immunoreactive interleukin-6 and acute phase proteins as prognostic factors in multiple myeloma. Finnish Leukemia Group. Blood. 1995;85(3):765-771.
8. Song Z, Ren D, Xu X, Wang Y. Molecular cross-talk of IL-6 in tumors and new progress in combined therapy. Thorac Cancer. 2018;9(6):669-675.
9. Sikka S, Shanmugam MK, Kannaiyan R, et al. Suppression of essential pro-inflammatory signaling pathways by natural agents for the therapy of multiple myeloma. Phytochem Rev. 2014;13(1):79-106.
10. Xiong A, Yang Z, Shen Y, Zhou J, Shen Q. Transcription factor STAT3 as a novel molecular target for cancer prevention. Cancers (Basel). 2014;6(2):926-957.
11. Yu H, Lee H, Herrmann A, Buettner R, Jove R. Revisiting STAT3 signalling in cancer: new and unexpected biological functions. Nat Rev Cancer. 2014;14(11):736-746.
12. Jung YY, Lee JH, Nam D, et al. Anti-myeloma effects of Icariin are mediated through the tttenuation of JAK/STAT3-dependent signaling cascade. Front Pharmacol. 2018; 9:531.
13. Catlett-Falcone R, Landowski TH, Oshiro MM, et al. Constitutive activation of Stat3 signaling confers resistance to apoptosis in human U266 myeloma cells. Immunity. 1999;10(1):105-115.
14. Quintanilla-Martinez L, Kremer M, Specht

K, et al. Analysis of signal transducer and activator of transcription 3 (Stat 3) pathway in multiple myeloma: Stat 3 activation and cyclin D1 dysregulation are mutually exclusive events. Am J Pathol. 2003;162(5):1449-1461.
15. An G, Acharya C, Deng S, et al. Cytogenetic and clinical marks for defining high-risk myeloma in the context of bortezomib treatment. Exp Hematol. 2015;43(3):168-176.
16. An G, Xu Y, Shi L, et al. Chromosome 1q21 gains confer inferior outcomes in multiple myeloma treated with bortezomib but copy number variation and percentage of plasma cells involved have no additional prognostic value. Haematologica. 2014;99(2):353-359.
17. Yu W, Guo R, Qu X, et al. The amplification of 1q21 is an adverse prognostic factor in patients with multiple myeloma in a Chinese population. Onco Targets Ther. 2016;9:295-302.
18. Fonseca R, Van Wier SA, Chng WJ, et al. Prognostic value of chromosome 1q21 gain by fluorescent in situ hybridization and increase CKS1B expression in myeloma. Leukemia. 2006;20(11):2034-2040.
19. Chang H, Qi X, Jiang A, Xu W, Young T, Reece D. 1p21 deletions are strongly associated with 1q21 gains and are an independent adverse prognostic factor for the outcome of high-dose chemotherapy in patients with multiple myeloma. Bone Marrow Transplant. 2010;45(1):117-121.
20. Shaughnessy JD, Jr., Qu P, Usmani S, et al. Pharmacogenomics of bortezomib test-dosing identifies hyperexpression of proteasome genes, especially PSMD4, as novel high-risk feature in myeloma treated with Total Therapy 3. Blood. 2011;118(13):3512-3524.
21. Pulkki K, Pelliniemi TT, Rajamaki A, Tienhaara A, Laakso M, Lahtinen R. Soluble interleukin-6 receptor as a prognostic factor in multiple myeloma. Finnish Leukaemia Group. Br J Haematol. 1996;92(2):370-374.
22. Ohtani K, Ninomiya H, Hasegawa Y, et al. Clinical significance of elevated soluble interleukin-6 receptor levels in the sera of patients with plasma cell dyscrasias. Br J Haematol. 1995;91(1):116-120.
23. Lazzari E, Mondala PK, Santos ND, et al. Alu-dependent RNA editing of GLI1 promotes malignant regeneration in multiple myeloma. Nat Commun. 2017;8(1):1922.
24. Teoh PJ, An O, Chung TH, et al. Aberrant hyperediting of myeloma transcriptome by ADAR1 confers oncogenicity and is a marker of poor prognosis. Blood. 2018;132(12):1304-1317.
25. Nishikura K. Functions and regulation of RNA editing by ADAR deaminases. Ann Rev Biochem. 2010;79(1):321-349.
26. Song C, Sakurai M, Shiromoto Y, Nishikura K. Functions of the RNA editing enzyme ADAR1 and their relevance to human diseases. Genes (Basel). 2016;7(12).
27. Jiang Q, Crews LA, Barrett CL, et al. ADAR1 promotes malignant progenitor reprogramming in chronic myeloid leukemia. Proc Natl Acad Sci U S A. 2013;110(3):1041-1046.
28. Chen L, Li Y, Lin CH, et al. Recoding RNA editing of AZIN1 predisposes to hepatocellular carcinoma. Nat Med. 2013;19(2):209-216.
29. Chan TH, Qamra A, Tan KT, et al. ADAR-Mediated RNA editing predicts progression and prognosis of gastric cancer. Gastroenterology. 2016;151(4):637-650.
30. Paz N, Levanon EY, Amariglio N, et al. Altered adenosine-to-inosine RNA editing in human cancer. Genome Res. 2007;17(11):1586-1595.
31. Fumagalli D, Gacquer D, Rothé F, et al. Principles governing A-to-I RNA editing in the breast cancer transcriptome. Cell Rep. 2015;13(2):277-289.
32. Teoh PJ, Chung TH, Sebastian S, et al. p53 haploinsufficiency and functional abnormalities in multiple myeloma. Leukemia. 2014;14(10):102.
33. Johnson DE, O'Keefe RA, Grandis JR. Targeting the IL-6/JAK/STAT3 signalling axis in cancer. Nat Rev Clin Oncol. 2018;15(4):234-248.
34. Lin L, Benson DM, DeAngelis S, et al. A small molecule, LLL12 inhibits constitutive STAT3 and IL-6-induced STAT3 signaling and exhibits potent growth suppressive activity in human multiple myeloma cells. Int J Cancer. 2012;130(6):1459-1469.
35. Scuto A, Krejci P, Popplewell L, et al. The novel JAK inhibitor AZD1480 blocks STAT3 and FGFR3 signaling, resulting in suppression of human myeloma cell growth and survival. Leukemia. 2011;25(3):538-550.
36. Bataille R, Barlogie B, Lu ZY, et al. Biologic effects of anti-interleukin-6 murine monoclonal antibody in advanced multiple myeloma. Blood. 1995;86(2):685-691.
37. Voorhees PM, Manges RF, Sonneveld P, et al. A phase 2 multicentre study of siltuximab, an anti-interleukin-6 monoclonal antibody, in patients with relapsed or refractory multiple myeloma. Br J Haematol. 2013;161(3):357-366.
38. San-Miguel J, Bladé J, Shpilberg O, et al. Phase 2 randomized study of bortezomib-melphalan-prednisone with or without siltuximab (anti–IL-6) in multiple myeloma. Blood. 2014;123(26):4136.
39. Nemec P, Zemanova Z, Greslikova H, et al. Gain of 1q21 is an unfavorable genetic prognostic factor for multiple myeloma patients treated with high-dose chemotherapy. Biology Blood Marrow Transplant. 2010;16(4):548-554.
40. Smetana J, Berankova K, Zaoralova R, et al. Gain(1)(q21) is an unfavorable genetic prognostic factor for patients with relapsed multiple myeloma treated with thalidomide but not for those treated with bortezomib. Clin Lymphoma Myeloma Leuk. 2013;13(2):123-130.
41. Kim SY, Min HJ, Park HK, et al. Increased copy number of the interleukin-6 receptor gene is associated with adverse survival in multiple myeloma patients treated with autologous stem cell transplantation. Biol Blood Marrow Transplant. 2011;17(6):810-820.
42. Nemlich Y, Baruch EN, Besser MJ, et al. ADAR1-mediated regulation of melanoma invasion. Nat Commun. 2018;9(1):2154.
43. Qi L, Song Y, Chan Tim Hon M, et al. An RNA editing/dsRNA binding-independent gene regulatory mechanism of ADARs and its clinical implication in cancer. Nucleic Acids Res. 2017;45(18):10436-10451.
44. Nie Y, Ding L, Kao PN, Braun R, Yang J-H. ADAR1 interacts with NF90 through double-stranded RNA and regulates NF90-mediated gene expression independently of RNA editing. Mol Cell Biol. 2005;25(16):6956-6963.
45. Wang IX, So E, Devlin JL, Zhao Y, Wu M, Cheung VG. ADAR regulates RNA editing, transcript stability, and gene expression. Cell Rep. 2013;5(3):849-860.

ARTICLE

Cardiac biomarkers are prognostic in systemic light chain amyloidosis with no cardiac involvement by standard criteria

Faye A. Sharpley, Marianna Fontana, Ana Martinez-Naharro, Richa Manwani, Shameem Mahmood, Sajitha Sachchithanantham, Helen J. Lachmann, Julian D. Gillmore, Carol J. Whelan, Philip N. Hawkins and Ashutosh D. Wechalekar

National Amyloidosis Centre, University College London, London, UK

Ferrata Storti Foundation

Haematologica 2020
Volume 105(5):1405-1413

ABSTRACT

Patients with systemic immunoglobulin light chain amyloidosis (AL) with no evidence of cardiac involvement by consensus criteria have excellent survival, but 20% will die within 5 years of diagnosis and prognostic factors remain poorly characterised. We report the outcomes of 378 prospectively followed Mayo stage I patients (N-terminal pro b-type natriuretic peptide <332 ng/L, high sensitivity cardiac troponin <55 ng/L). The median presenting N-terminal pro b-type natriuretic peptide was 161 ng/L, high sensitivity cardiac troponin 10 ng/L, creatinine 76 μmol/L and mean left ventricular septal wall thickness, 10 mm. Median follow up was 42 (1-117 months), with 71 deaths; median overall survival was not reached (78% survival at 5 years). Although no patients had cardiac involvement by echocardiogram, a proportion (n=25/90, 28%) had cardiac involvement by cardiac magnetic resonance imaging. Age, autonomic nervous system involvement, N-terminal pro b-type natriuretic peptide >152 ng/L, high sensitivity cardiac troponin >10 ng/L and cardiac involvement by magnetic resonance imaging were predictive for survival; on multivariate analysis only N-terminal pro b-type natriuretic peptide >152 ng/L (P<0.008, hazard ratio [HR] 3.180, confidence interval [CI]: 1.349-7.495) and cardiac involvement on magnetic resonance imaging (P=0.026, HR=5.360, CI: 1.219-23.574) were prognostic. At 5 years, 70% of patients with N-terminal pro b-type natriuretic peptide >152 ng/L were alive. In conclusion, N-terminal pro b-type natriuretic peptide is prognostic for survival in patients with no cardiac involvement by consensus criteria and cardiac involvement is detected by magnetic resonance imaging in such cases. This suggests that N-terminal pro b-type natriuretic peptide thresholds for cardiac involvement in AL may need to be redefined.

Introduction

Systemic immunoglobulin light chain amyloidosis (AL) is characterised by the extracellular deposition of misfolded immunoglobulin light chains resulting in progressive organ dysfunction. Patient outcomes are largely dependent upon the severity and pattern of organ involvement.[1] Accurate stratification of patients is needed to assess prognosis and to facilitate treatment decisions. Cardiac involvement is the critical determinant of survival. NT-proBNP (N-terminal pro b-type natriuretic peptide) is a remarkably sensitive marker of cardiac involvement and is one of the cornerstones of the international amyloidosis consensus group diagnostic criteria for cardiac involvement.[2] Change in NT-proBNP is crucial in monitoring the effect of therapy in patients with cardiac amyloidosis.[3] These findings have followed from the seminal work by the Mayo clinic group discovering NT-proBNP and troponin T (TNT) as sensitive biomarkers for prognosis in AL[4] and the development of the 2004 Mayo prognostic scoring system, which has been further refined in 2012.[5] The widely used 2004 staging system uses thresholds of NT-proBNP <332 ng/L and a TNT <0.035 μg/L to classify patients into stage I, II or

Correspondence:

FAYE A. SHARPLEY
f.sharpley@gmail.com

Received: February 7, 2019.

Accepted: August 7, 2019.

Pre-published: August 8, 2019.

doi:10.3324/haematol.2019.217695

Check the online version for the most updated information on this article, online supplements, and information on authorship & disclosures: www.haematologica.org/content/105/5/1405

III if both biomarkers are normal, one biomarker elevated or both biomarkers elevated respectively.[4] This is with progressively poorer prognosis (median survival of 27.2, 11.1 and 4.1 months respectively). Lately, with the move to high sensitivity TNT (hsTNT), the threshold for troponin is <55 ng/L.

Recent studies of patients with normal NT-proBNP and hsTNT without cardiac involvement, (so called Mayo stage I disease) show excellent outcomes with median overall survival (OS) not reached at 5 years. There are still deaths in this group of patients and few have explored factors predictive of poor survival. There are a number of novel prognostic variables in AL including: the number of organs involved, a high percentage of bone marrow plasma cells,[6] raised von Willebrand factor[7] and high growth differentiation factor-15 levels.[8] None of the studies have focused specifically on the stage I patients. Liver involvement is widely believed to contribute to the poor prognosis of such cases but in the vast majority of cases this is associated with other organ involvement.[9]

We designed this study to assess prognostic variables in patients with systemic AL who had no evidence of cardiac involvement by echocardiographic criteria and who had normal cardiac biomarkers (Mayo 2004 stage I).

Methods

This study included all prospectively followed up patients with AL from an ongoing prospective observational study (Alchemy) from 2009-2017, with Mayo stage I disease (defined by normal cardiac biomarkers (NT-proBNP <332 ng/L, hsTnT <55 ng/L)). A threshold of hsTNT of 55 ng/L was used (equivalent to 0.035 g/L cTNT) and this has been used by our laboratory since we moved from standard TNT measurements to using hsTNT measurements at our centre.

A diagnosis of amyloidosis was confirmed by Congo-red staining of a tissue biopsy, with the demonstration of characteristic birefringence under cross polarized light, and AL typing was confirmed by immunohistochemistry, with specific antibodies or by mass spectrometry. Hereditary amyloidosis was excluded by appropriate gene sequencing, if there was a doubt about the diagnosis of AL. As part of the study protocol, all patients had a detailed baseline assessment of organ function, including biomarker measurements and imaging with echocardiogram and ^{123}I-labelled serum amyloid P (SAP) scintigraphy. Organ involvement was defined according to the international amyloidosis consensus (ISS) criteria.[2] Specifically, the echocardiogram was considered to show cardiac involvement if the patients had mean left ventricular (LV) wall thickness >12 mm, in the absence of any other cause of left ventricular hypertrophy. NT-proBNP was <335 ng/L and hsTNT <55 ng/L in all cases. Cardiac magnetic resonance imaging (CMR) was added to routine baseline assessments from late 2015 onwards and the result of the baseline CMR was recorded, where available. A typical pattern of late gadolinium enhancement and an extracellular volume (ECV) >0.30 on an magnetic resonance imaging (MRI) scan were used as criteria suggestive of cardiac involvement by CMR.[10]

OS was calculated from the date of diagnosis to death or last follow-up. Factors were analysed for their impact on survival and this included: age, sex, type and number of organ involvement, difference in serum free light chains (dFLC) and markers of cardiac, renal and liver function and treatment given. Since asymptomatic liver involvement is often detected by ^{123}I -SAP scintigraphy[11] we assessed the prognostic significance of amyloid load by this imaging method. Survival outcomes were analysed using the Kaplan-Meier method with comparisons done using the log rank test. All *P*-values were two sided with a significance level of <0.05 and median values were used to dichotomise continuous variables. Any factors found to be significant on univariate analysis were further assessed in multivariate modelling by Cox's regression analysis. Statistical analysis was performed using SPSS (IBM Corp. Released 2012. IBM SPSS Statistics for Windows, Version 21.0. Armonk, NY, USA) and Stata (StataCorp LLC. 2017. Stata Statistical Software: Release 15. College Station, TX, USA). Approval for analysis and publication was obtained from the National Health Service institutional review board and written consent was obtained from all patients in accordance with the Declaration of Helsinki.

Results

A total of 378 patients were included in this study. The patient baseline characteristics are outlined in Table 1. The median patient age was 69 years (range 35-92 years); 212 (56.1%) were men. The median number of organs involved was two (range: 1-7). None of the patients had cardiac involvement by standard criteria.[12] The majority of patients had renal involvement (n=277, 73.3%). Thirty-nine patients (10.3%) had liver involvement by ISS criteria, whilst liver was abnormal by ^{123}I-SAP scintigraphy in 111 (29.4%). By ^{123}I-SAP scintigraphy, amyloid deposition was seen in 255 patients with the distribution: no amyloid in 122 patients (32.4%); 181 patients (48.0%) had a small or moderate amyloid load and 74 (19.6%) had a large amyloid load. The mean LV wall thickness was 10 mm (range: 6-13 mm). Six patients had a mean LV thickness of 13 mm, but none with echocardiogram appearances suggestive of cardiac amyloidosis based on their preserved global strain pattern. In all six patients the NT-proBNP was <335 ng/L, and co-existing hypertension was present in 5 of 6. The median NT-proBNP was 161 ng/L (range: 8-330 ng/L) and hsTNT was 10 ng/mL (range: 3-51 ng/L). Peripheral and autonomic neuropathy were seen in 43 (11.4%) and 30 (7.9%) cases respectively.

The median follow up was 42 months (1-117 months). There were 71 deaths. Median OS was not reached (Figure 1A). The OS at 1, 3, and 5 years was 96%, 87% and 78% respectively. Liver involvement by ISS (ALP >1.5 times upper limit of normal [ULN]) was not prognostic for survival (*P*=0.204, HR: 1.518, CI: 0.797-2.891), neither was any abnormality in the ALP (defined by an ALP outside the ULN of 129U/L) (*P*=0.753, hazard ratio [HR]: 0.923, confidence interval [CI]: 0.561-1.519) (Figure 1B). Although liver involvement was detected more frequently on SAP scintigraphy, neither liver involvement by SAP (*P*=0.284, HR: 0.750, CI: 0.443-1.269), nor the amyloid load on SAP scans (*P*=0.894, HR: 0.956, CI=0.489-1.869) were prognostic for survival. Renal involvement was not predictive of outcome using the standard consensus criteria definition,[12] (*P*=0.396, HR: 0.804, CI=0.486-1.330), or an estimated glomerular filtration rate (GFR) of <30 mL/min (*P*=0.483, HR: 2.11, CI: 0.262-17.047), but only 14 patients had an eGFR <30 mL/min and only five patients had an eGFR <20 mL/min. Patients with autonomic nervous system involvement had significantly poorer outcomes on univariate analysis (*P*=0.018, HR: 2.177, CI: 1.144-4.142), but patient numbers were small. Age was predictive of survival on univariate analysis (*P*=0.005,

Table 1. Baseline patient characteristics (total patients, n=378) including univariate analysis.

Factor assessed for significance	Median (range), n(%)	HR (CI)	Cox regression *P*
Age (years), >70 years	69 (35-92), 93 (25)	1.034(1.010-1.059)	0.005
Male sex	212 (56.1)	0.850(0.667-1.082)	0.186
Number of organs involved	2 (1-7)		
Renal	277 (73.3)	0.804 (0.486-1.330)	0.396
PNS	43 (11.4)	1.612 (0.866-3.000)	0.132
ANS	30 (7.9)	2.177 (1.144-4.142)	0.018
Soft Tissue	44 (11.7)	1.792 (0.982-3.273)	0.057
GI	36 (9.5)	1.428 (0.731-2.789)	0.297
Spleen	160 (42.3)	1.279 (0.759-2.154)	0.354
Renal parameters			
Creatinine (μmol/L)	76 (27-487)	1.004 (1. 000-1.008)	0.036
eGFR (mL/min)	69 (18- >90)	0.990 (0.972-1.008)	0.274
EGFR < 30 mL/min	14 (3.73)	2.11 (0.262-17.047)	0.483
Proteinuria (g/24h)	4.28 (0.03- 58.46)	0.99 (0.997-1.001)	0.198
Liver parameters			
Albumin (g/L)	32 (15-50)	0.994(0.968-1.020)	0.633
Bilirubin (mmol/L)	5 (1-57)	1.00(0.998-1.001)	0.630
ALP (U/L	77 (31-2,113)	0.923 (0.561-1.519)	0.753
Abnormal ALP (<129U/L)	47 (22.9)	0.872(0.352-2.155)	0.766
Liver involvement (ALP 1.5x upper limit)	39 (10.3)	1.518 (0.797-2.891)	0.204
SAP liver involvement	111 (29.4)	0.750 (0.443-1.269)	0.284
SAP load			0.894
None/equivocal	122 (32.4)		
Small/moderate	181 (48.0)	0.956(0.489-1.869)	
Large	74 (19.6)		
Cardiac parameters			
NT-pro-BNP (ng/L)	161 (8-330)	1.006 (1.003-1.009)	<0.001
NT-pro-BNP >152 (ng/L)	208 (55)	2.413 (1.448-4.021)	0.001
hsTNT (ng/L)	10 (3-51)	1.032 (1.011-1.054)	0.003
hsTNT >10 (ng/L)	76 (37.1)	1.249(0.554-2.813)	0.592
Echocardiogram (mean LVW)	10 (6-13)	0.998(0.820-1.215)	0.984
Hematological parameters			
Presenting κ (mg/L)	22.55 (1.5 -935)	1.101 (0.847-1.203)	0.916
Presenting λ (mg/L)	26.6(1.9- 6,180)	0.991 (0.831-1.181)	0.917
dFLC (mg/L)	1.40 (0.1- 6,064)	0.991 (0.831-1.181)	0.919
dFLC > 50 mg/L	104 (28.2)	1.431 (0.859-2.384)	0.202
dFLC >180 mg/L	51 (13.5)	1.590(0.848-2.979)	0.143
Treatments			
PI based	248 (67.4)	0.732 (0.417-1.287)	0.279
Alkylator	43 (11.7)	1.560 (0.937-2.599)	0.088
ASCT	55 (14.9)	1.084 (0.529-2.224)	0.825
No treatment/ trial treatment*	24 (6.5)	0.476 (0.143-1.591)	0.137
Missing data	10 (2.6)		
Treatment interval			
2008-2012	29 (8.4)		
2012-2016	88 (25.5)		
2014-2016	80 (23.2)		
2016-2018	77 (22.3)		
No treatment/ missing data	33 (9.6)		

*Trial treatment MLN9708. PNS: peripheral nervous system ; ANS: autonomic nervous system ; GI: gastrointestinal; NT-pro BNP: N-terminal pro b-type natriuretic peptide; hsTNT: high-sensitive cardiac troponin T; dFLC: difference between involved and uninvolved serum free light chains; ALP: alkaline phosphatase; SAP: 123I labelled serum amyloid P component (SAP) scintigraphy; LVW: left ventricle wall; eGFR: estimated glomerular filtration rate; Imid: immunomodulatory therapy: PI: proteasome inhibitor; HR: hazard ratio; CI: confidence interval.

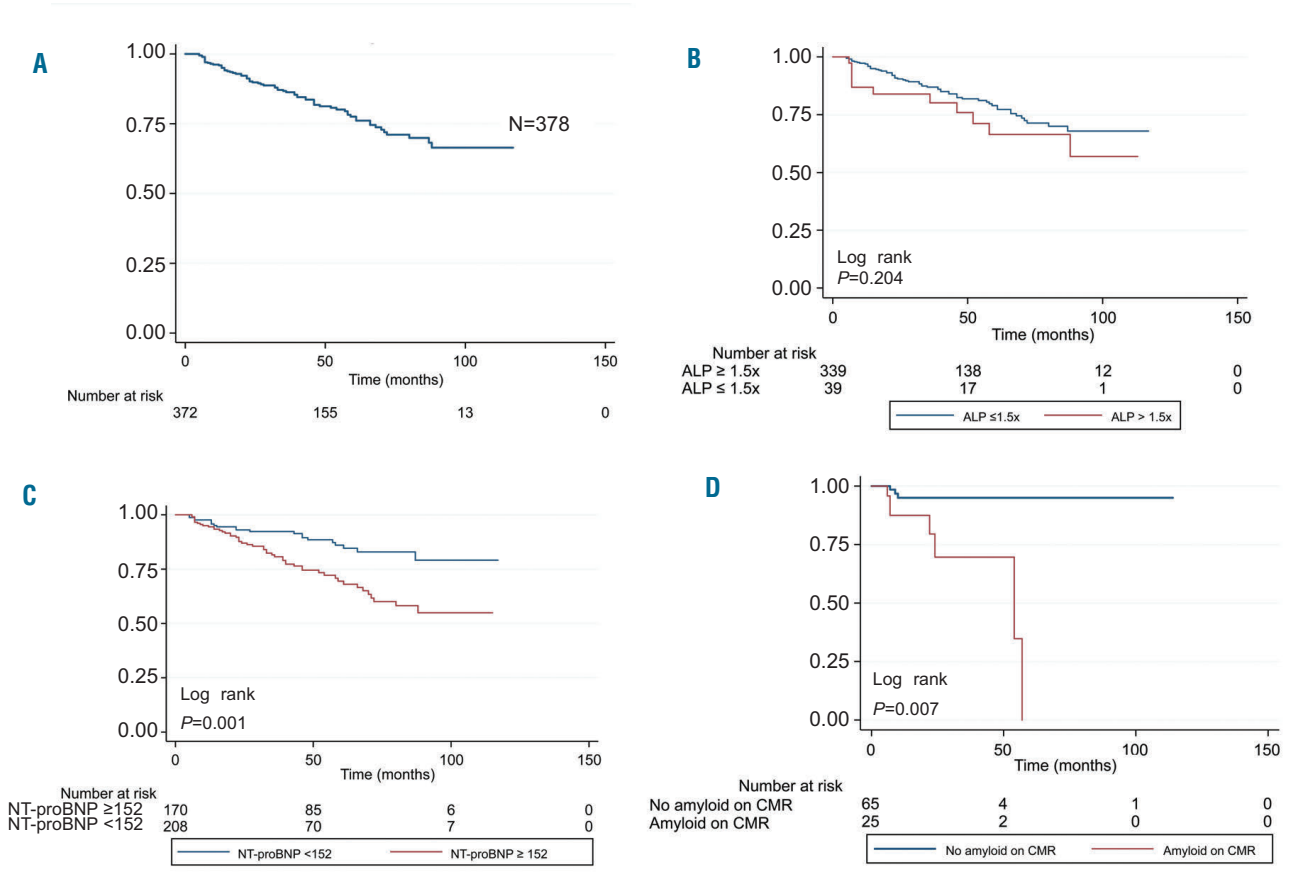

Figure 1. Survival curves for Mayo stage I patients demonstrating. (A) Overall survival was not reached; overall survival at 1, 3, and 5 years was 95%, 87% and 76% respectively. (B) The impact of haematological response to treatment at six months and survival outcomes, patients achieving a complete response to treatment *versus* not a complete response (log rank *P*<0.001). (C) N-terminal pro b-type natriuretic peptide (NT-pro-BNP) above and below 152 ng/L showing poorer outcome for patients with NT-proBNP >152 ng/L, (log rank *P*=0.001). (D) Cardiac magnetic resonance imaging findings demonstrating a significantly poorer outcome for patients with cardiac amyloid deposition, (log *P*=0.007)

HR: 1.034, CI: 1.010-1.059) but using receiver operating characteristic (ROC) analysis there was no clearly identifiable threshold for poorer outcomes. The presenting free light chains (FLC) were not prognostic for survival in this cohort as a continuous variable or a dichotomous variable above or below a difference between involved and uninvolved FLC (dFLC) of 50 mg/L or 180 mg/L (Table 1). At four years 83% *versus* 77% of patients with a dFLC above or below a value of 50 mg/L were alive (log rank *P*=0.202).

Although all the patients included in this study had no evidence of cardiac involvement, and cardiac biomarkers below the threshold for defining cardiac involvement, hsTNT and NT-proBNP were still prognostic for survival both on univariable analysis and only NT-proBNP on multivariate analysis. We undertook ROC analysis to define thresholds for NT-proBNP and hsTNT, (identified as 152 ng/L and 10 ng/L respectively), as prognostic cut offs for poorer survival. The OS was significantly better for patients with NT-proBNP <152 ng/L *versus* those with a greater value (although median OS not reach for either group) (log rank *P*≤0.001; Figure 1C). At 1, 3, and 5 years, for patients with NT-proBNP below and above 152 ng/L, the OS was 96% *versus* 94%; 91% *versus* 82%; and 83% *versus* 70% respectively. The OS at 1, 3, and 5 years for patients with hsTNT below and above 10 ng/L was 98%% *versus* 93%%, 91% *versus* 84% and 87% *versus* 70% respectively. The median OS was not reached for either group. There was no significant difference in the median creatinine or eGFR for patients with a NT-proBNP value </≥152 ng/L (*P*=0.091 and 0.206 respectively) ruling out impairment of renal function as a cause of abnormal NT-proBNP in this cohort.

CMR was undertaken since 2015 and results were available on 90/378 (24%) patients. Twenty-eight percent (n=25/90) of patients had cardiac involvement by CMR. In the patients who had a CMR with NT-proBNP below (32 patients) and above (58 patients) 152 ng/L, the CMR was positive for amyloid deposition in 22% *versus* 31% of cases, respectively (*P*=0.353) (see Table 2). There was a trend towards higher NT-proBNP in patients with a positive CMR median NT-proBNP 220 ng/L *versus* 169 ng/L (*P*=0.089) (Figure 2). The median LV wall thickness by echocardiogram (11 mm *vs.* 10 mm [*P*=0.1902]) and hsTNT values (17 ng/L *vs.* 14 ng/L [*P*=0.373]) were not significantly different in those patients with CMR positivity for amyloid deposition compared to those patients with negative CMR findings respectively. After gadolinium contrast, the extracellular volume fraction (which directly reflects myocardial interstitial expansion by amyloid deposition) was calculated with a median ECV of 0.33 (0.24-0.71). The mean ECV of patients with cardiac involvement was 0.44 *versus* 0.31 (*P*<0.0001) for those without cardiac involvement. Cardiac involvement on CMR was prognostic for OS with the 1- and 2-year survival for patients with CMR positive *versus* negative being 86% *versus* 98% and 69% *versus* 98% respectively (*P*=0.007,

Table 2. A comparison of patients with N-terminal pro b-type natriuretic peptide >152 ng/L *versus* <152 ng/L.

	NT- proBNP ≤152 g/L (n=170)	NT-pro BNP >152 ng/L (n=208)	*P**
Other biomarkers			
High-sensitive cardiac troponin T	7	11	<0.001
dFLC	10.90	18.70	0.204
ALP (U/L)	170	207	0.994
Cardiac magnetic resonance imaging (CMR) findings:			
CMR positive for amyloidosis (n=90)	7(22%)	18(31%)	0.364
Extracellular volume	0.327	0.355	0.470
Echocardiogram parameters			
Echo global strain (%)	-21.96	-20.34	0.40
Echo IVS (mm)	10	10	0.914

*Mann-Whitney U-test for non-parametric variables; Chi-squared for categorical variables. NT-pro BNP: N-terminal pro b-type natriuretic peptide; ALP: alkaline phosphatase; CMR: cardiac magnetic resonance imaging; IVS: interventricular septal thickness; dFLC: difference between involved and uninvolved serum free light chains.

Table 3. Factors included in a multivariate analysis and their significance (separate multivariate models were developed with and without cardiac magnetic resonance imaging [CMR] due to smaller patient numbers with CMR data).

	Analysis excluding CMR findings	Analysis including CMR findings
Factor in multivariate analysis	*P*/ HR (CI)	
Age	0.269/1.021(0.984-1.058)	0.363/0.967(0.900-1.039)
ANS	0.624/0.696(0.164-2.962)	0.322/6.749(0.154-295.885)
NT-proBNP> 152 ng/L	**0.008**/3.180(1.349-7.495)	0.918/1.074(0.999-1.154)
HsTNT >10 ng/L	0.771/0.880(0.370-2.091)	0.073/1.059(0.995-1.128)
CMR positivity	–	**0.026/5.360(1.219-23.574)**

HR: hazard ratio; CI: confidence interval; ANS: autonomic nervous system; NT-proBNP: N-terminal pro b-type natriuretic peptide; hsTNT: high-sensitive cardiac troponin T; ImiD: immunomodulatory drug; CMR: cardiac magnetic resonance imaging.

HR: 6.563, CI: 1.689-25.492) (Figure 1D). Too few patients have sufficient follow up for meaningful longer-term survival analysis at present.

Treatment details were available in 97% of cases (n=368/378) and are outlined in Table 1. A total of 91% (n=346/378) patients were treated with chemotherapy. The most common treatment given was bortezomib (mostly cyclophosphamide-bortezomib-dexamethasone) (n= 246/368, 67%) followed by thalidomide (mainly cyclophosphamide-thalidomide-dexamethasone) (n=110/369, 30%). Fifteen percent (n=55/368) of patients has an upfront autologous stem cell transplant (ASCT). Treatment type was not prognostic for survival on univariate analysis (Table 1).

In the 346 patients who received chemotherapy 89% (n=337/378) were evaluable at six months. Haematological response was as follows: complete response (CR) 51% (n=173/378, very good partial response (VGPR) 13% (n=46/346), partial response (PR) 3% (n=12/346), no response (NR) 4% (n=14/346) and progressive disease (PD) 17% (n=58/346). The OS of patients who achieved a CR to treatment was significantly longer than those who did not achieve a CR (median OS 109 *vs.* 75 months, *P*<0.001). The six-month landmark analysis was as follows: CR- median survival not reached, non-CR median survival 88 months, *P*<0.001. Survival at 1 and 3 years by NT-proBNP <152 ng/L was: CR: 100%, 96% *versus* non-CR: 90%, 69% respectively, and for patients with NT-proBNP >152 ng/L: CR: 96%, 80% and non-CR: 91%, 53% respectively, *P*<0.001. A total of 95 patients had NT-proBNP >152 ng/L and achieved a CR at six months. Of these patients, 15% (n=14/95) achieved a reduction in the invloved FLC (iFLC) to <10 mg/L at six months. There was no significant survival difference between those patients who achieved an iFLC <10 mg/L at six months *versus* those who did not (*P*=0.396). Of the 95 patients with NT-proBNP >152 ng/L who achieved a CR at six months, 8% (n=8/95) achieved a CR at one month, and 39% (n=37/95) after three months. There was no significant difference in OS between those patients who achieved a CR *versus* non-CR at one month (*P*=0.281), or three months (*P*=0.402).

Of the 346 patients treated, 80% (n=277/346) had NT-proBNP readings at 12 months. Based on a 30% change in NT-proBNP to define response: 32% (n=88/277) patients had reduction in their NT-proBNP levels, 50% (n=138/277) patients' values increased and 18% (n=51/277) patients did not reach either criteria. When analysing the entire cohort there was no significant difference in survival between patients who had an NT-proBNP response *versus* no response/ progression, (*P*=0.193); the 3- year survival of patients was 76% *versus* 70% for patients with an NT-proBNP response compared with unchanged/progression, respectively. However, when the analysis was restricted to patients with NT-proBNP >152 ng/L, outcomes were significantly poorer in the patients with a baseline NT-proBNP level of >152 ng/L who progressed (*P*=0.001).

Multivariate models were developed using variables significant on univariate analysis, defined as a *P*-value <0.05, (Table 3). A model including CMR was done separately due to the limited number of patients with CMR data. On

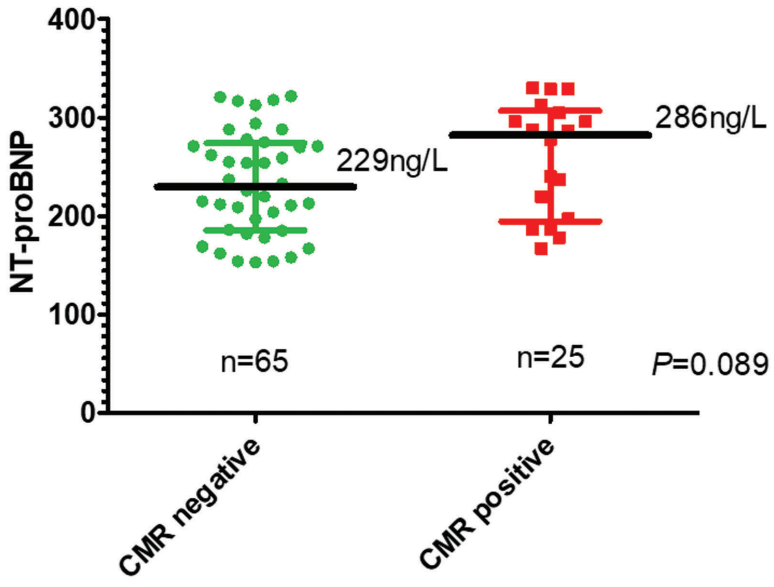

Figure 2. The difference in N-terminal pro b-type natriuretic peptide (NT-pro-BNP) between patients with, and without, evidence of cardiac involvement on cardiac magnetic resonance imaging (CMR).

multivariate model including age, autonomic nervous system involvement, NT-proBNP >152 ng/L, hsTNT >10ng/L, only NT-proBNP (*P*=0.008, HR: 3.180, CI: 1.349-7.495) was an independent predictor of survival (Table 1). When cardiac involvement by MRI was added to the model, only cardiac amyloid on CMR (*P*=0.026, HR: 5.360, CI: 1.219-23.574) remained an independent predictor of outcome.

The cause of death was available for 20 of 71 patients (28.2 %). The most common cause of death was progressive amyloidosis (five patients), end stage renal failure (four patients), and pneumonia (three patients). Two patients died of splenic haemorrhage and two due to complications of treatment. One patient each died of a fall, heart failure, sepsis and a fatal arrthymia respectively. Of the 71 patients who died, 82% (n=58/71) had a repeat echocardiogram. In 12% (n=7/58) cases the echocardiogram was clearly suggestive of cardiac amyloid progression based on an interventricular septum (IVS) >12 mm and a reduced global strain pattern. In 57% (n=4/7) of these patients their baseline NT-proBNP was above our threshold of 152 ng/L suggesting that in at least a proportion of patients the cause of death was progressive cardiac amyloidosis.

Discussion

Patients with AL amyloidosis without cardiac involvement by the consensus criteria have excellent outcomes. These patients have normal cardiac biomarkers and therefore, by definition, have Mayo (2004) stage I disease. Whilst this study confirms the excellent long-term outcomes of patients with this early disease, 22% of patients died within 5 years of diagnosis. We report here that cardiac biomarkers remain prognostic even in this group of patients at a lower threshold (NT-proBNP <152 ng/L) than previously outlined. We also show that patients with AL have CMR scans showing cardiac involvement, with adverse prognostic implications, even in patients with low biomarker levels and with echocardiogram features not suggestive of amyloidosis.

Cardiac involvement in A is currently defined by both echocardiogram criteria (>12 mm mean wall thickness in diastole by echocardiogram in absence of other causes of left ventricular hypertrophy) and by elevation of the cardiac biomarker (NT-proBNP >332 ng/L), in the absence of renal failure or atrial fibrillation. NT-proBNP is unquestionably one of most sensitive markers of cardiac stress in AL reflecting the direct pathological activity of amyloidogenic light chains/toxic oligomers, mediated by activation of the p38-MAP kinase pathway. The importance of NT-proBNP for defining cardiac involvement is reflected in the initial Mayo staging scoring system where a threshold for NT-pro-BNP was defined using a multivariate model with a value of 332 ng/L (the upper reference limit of normal for women older than 50 years) providing the best fit and the highest HR (Table 4).[4] The prognostic importance of this value has since been confirmed in a number of studies although the threshold value itself has never been systematically re-examined. In 2011 we reported a small cohort of patients with NT-proBNP <127 ng/L had much better outcomes and those with NT-proBNP >127 ng/L had a higher risk of developing cardiac amyloidosis on longer term follow up.[13] In the 2011 cohort, we had not access to MRI scanning understand the relevance of these findings. Dittick *et al*. have also highlighted the difficulty of using current Mayo staging scores in the setting of renal impairment and atrial fibrillation.[14] The Mayo Clinic data, and data from the international collaborative series, were also generated in the era where highly effective novel agent-based therapies were not routinely available. The survival of patients with stage I disease in these earlier series may now be considered relatively poor compared with contemporary survival outcomes – allowing for a potential opportunity to revisit the NT-proBNP threshold for defining cardiac involvement.

This current data suggests that the extreme sensitivity of NT-proBNP in AL extends to a much a lower value of 152 ng/L and patients with a subtle increase in NT-proBNP (>152 ng/L) had poorer outcomes (HR: 3.180 [CI: 1.329-7.495]). The "normal" range for NT-proBNP is between 100-125 ng/L for those aged less than 70 years which is lower than the prognostic threshold identified in this

Table 4. A review of the literature to outline previous studies and the previous prognostic thresholds of N-terminal pro b-type natriuretic peptide.

Study details	NT-proBNP threshold	Survival
Palladini G. *et al.*[19]	152 pmol/L=1,288 ng/L	7.6 per 100 person-years (95% CI: 3.6-15.7) and 72.2 per 100 person-years (95% CI: 54.2-86.1)
Dispenzieri A. *et al.*[4]	332 ng/L	<332 pg/mL survival 20 months >332 pg/mL 5.8 months
Kumar SK *et al.*[20]	332 ng/L	Median OS from diagnosis for patients NT proBNP <332 ng/L was 4.0 years *versus* 2.4 years if either NT-proBNP was >332 ng/L or cTnT >0.035 g/L.
Wechalekar AD *et al.*[13]	NT-proBNP <15 pMol/L=127 ng/L	5-year survival 98% *versus* 88% for those above and below respectively
Kumar S *et al.*[25]	1,800 pg/mL=1,800 ng/L	NT-ProBNP ≥ 1,800 pg/mL was 10.5 months, compared with median not reached for those with NT-ProBNP <1,800 pg/mL

NT-proBNP: N-terminal pro b-type natriuretic peptide; CI: confidence interval; OS: overall survival.

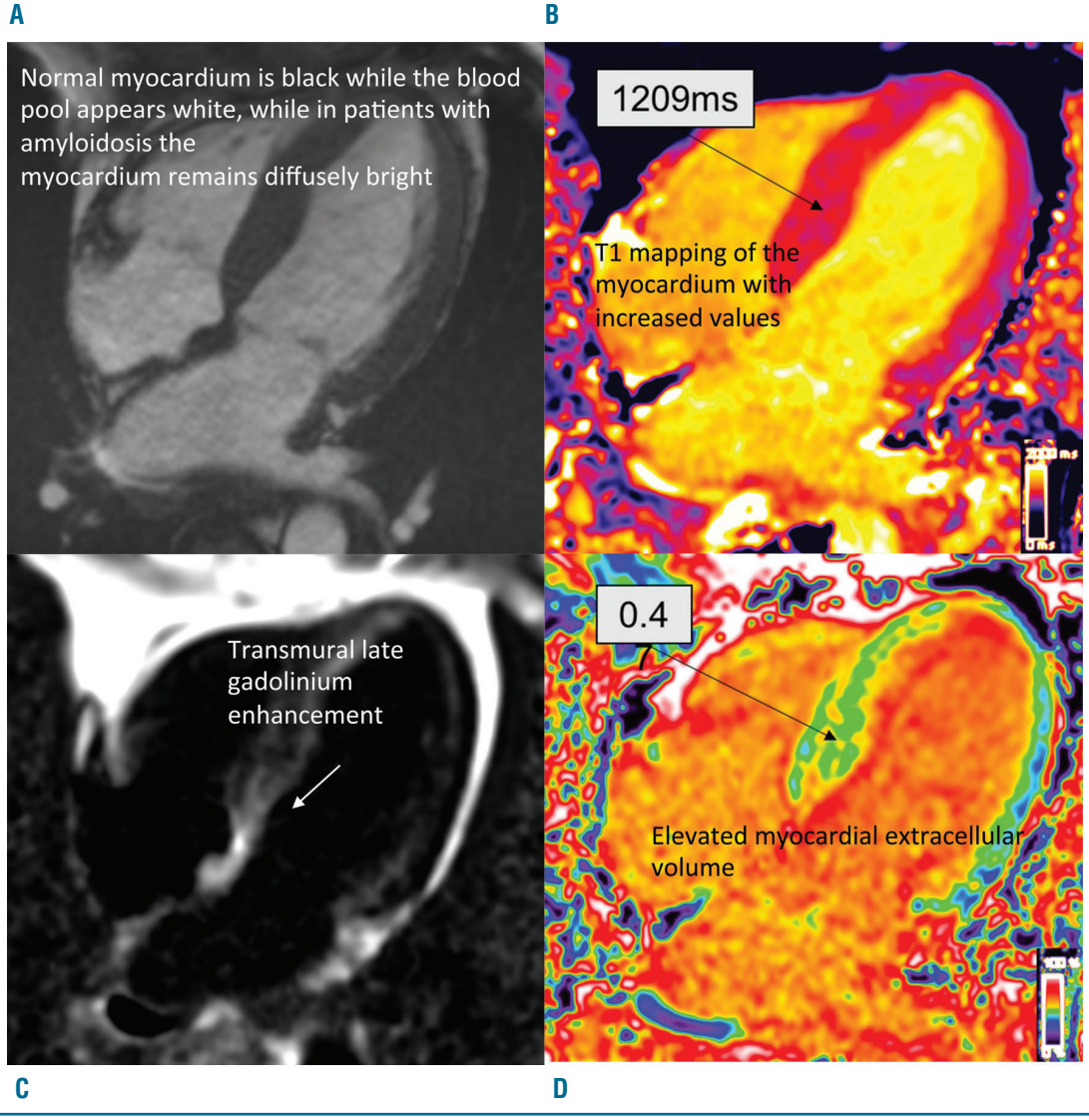

Figure 3. Cardiac magnetic resonance image of a patient with no evidence of cardiac amyloidosis by echocardiogram and NT-BNP <332 ng/L showing characteristic features of cardiac involvement. (A) Four-chamber steady state free precession (SSFP) cine (top right panel). (B) Corresponding native T1 map (top left panel) with an elevated value of 1209 m. (C) Corresponding phase sensitive inversion recovery late gadolinium enhancement (PSIR LGE) image showing subendocardial LGE (bottom right panel).(D) Corresponding extracellular volume (ECV) map with an elevated value of 0.47 (bottom left panel).

cohort. Other factors can influence NT-proBNP levels such as age. There was a correlation of NT-proBNP with age (P=0.002) but there was no significant difference in the numbers of patients over or below 75 years with NT-proBNP < or > 152 ng/L. Additionally, age was not significant in the multivariable analysis.

The exquisite prognostic sensitivity of NT-proBNP in AL may suggest either early cardiac involvement or light chain proteotoxicity. The structurally established echocardiographic criteria for AL cardiac involvement is an LV wall of >12 mm (in the absence of other causes). It is conceivably possible for a patient with baseline 8-10 mm LV wall could have substantial amyloid deposition before the threshold of 12 mm is reached. The opportunity to track changes in NT-proBNP during development of cardiac AL is rare. The kinetics of NT-proBNP increase as well as its correlation with LV wall thickness at early stage of the disease process remain largely unknown.

CMR is an alternative method of monitoring patients with cardiac amyloidosis. In this current cohort, a third of all patients who had a CMR showed features of cardiac amyloidosis. Moreover, the presence of amyloid deposition on CMR was an independent prognostic marker. CMR, with late gadolinium enhancement (LGE) and T1 mapping, is emerging as a highly sensitive and specific tool for diagnosis and characterisation of cardiac amyloidosis in AL (Figure 3).[15] Transmural LGE with phase-sensitive inversion recovery (PSIR) is associated with the burden of cardiac amyloid and predicts death independent of NT-pro-BNP and other known prognostic factors.[10] In this cohort, it clearly identified cardiac involvement in patients where the echocardiogram was not suggestive of cardiac amyloidosis but not all patients with NT-proBNP >152 ng/L had abnormal CMR (31% had abnormal CMR) and not all patients with NT-proBNP <152 ng/L had normal CMR (22% had abnormal CMR). This suggests that CMR provided complementary information on patients' cardiac damage. NT-proBNP may be detecting cardiac damage by light chain proteotoxicity before structural amyloid deposition is apparent on CMR, conversely, some patients may have non-proteotoxic light chains (analogous to cardiac amyloid deposition in transthyretin amyloidosis [ATTR]) where the structural changes are apparent on CMR before biomarkers become abnormal. In this early stage of the disease, NT-proBNP and CMR findings should be used together for defining cardiac involvement.

In this study, liver involvement, a previously reported poor prognostic marker,[9,16] did not significantly impact survival. Relatively few patients had significant liver involvement - only 10% by consensus criteria (although a third had asymptomatic liver involvement on ^{123}I-SAP scintigraphy). The strict exclusion of cardiac involvement by consensus criteria may have excluded patients with advanced liver involvement since the latter patients often have multi-organ amyloidosis. Likewise, although the majority of patients had renal involvement, 277 (73.3%) the median presenting creatinine was low (76 μmol/L), with only a small proportion (n=14/375, 3.7%) with an eGFR <30 mL/min, which may explain why neither the presence of renal involvement nor proteinuria was a predictor of survival. Autonomic involvement (ANS) was significant on univariate but not multivariate analysis, but the number of patients was small.

This study has limitations and needs to be interpreted in this context. This is single centre data but we are planning validation in an international collaborative data set. One major limitation is that the exact cause of death was only available in a small proportion of patients and when the cause was recorded as "amyloidosis" this does not elucidate whether cardiac amyloidosis was the real cause of death. Progressive cardiac amyloidosis does appear to be the cause of death in at least a proportion of patients in this study, based on serial echocardiogram imaging. The use of a very sensitive marker of cardiac disease like NT-proBNP at a low level is also challenging as other unrelated factors can impact upon NT-proBNP (such as age, renal function, sex, body mass index as evidenced by the Framingham study from 2011, and a more recent study by Dittrick *et al.*[14,17] Finally, only a proportion of patients had CMR scans. Larger studies are needed to address these limitations.

In conclusion, this study demonstrates that in patients with AL with no cardiac involvement by consensus criteria even small elevations of NT-proBNP as well as cardiac involvement by CMR are factors highly prognostic for survival. This novel finding offers some insight into the heterogeneity in survival of Mayo stage I patients. There findings have implications for clinical practice. We suggest that a baseline cardiac MRI scan should be considered at diagnosis for stage I AL patients, if possible. Better outcomes for patients in a CR and those with decrease in NT-proBNP, suggest that in "high risk" stage I patients (those with NT-proBNP >152 ng/L) the goal of therapy should be similar to those with cardiac AL *i.e.* a complete haematological response. The follow up of such patients should include routine NT-proBNP measurement including assessment of response (as patients with presenting NT-proBNP >152 ng/L and NT-proBNP progression [>30% increase] had poorer outcomes); those with NT-proBNP progression should be considered for further treatment. The "high risk relapse criteria" defined by the Italian amyloidosis group, should be applied for treatment at relapse for patients with NT-proBNP >152 ng/L (high risk stage I).[18] Serial CMR data is needed to assess cardiac structure and functional changes to delineate the natural history of 'high risk' patients and to help identify interventions to prevent progressive cardiac involvement.

References

1. Kyle RA, Greipp PR, O'Fallon WM. Primary systemic amyloidosis: multivariate analysis for prognostic factors in 168 cases. Blood. 1986;68(1):220-224.
2. Gertz MA, Comenzo R, Falk RH, et al. Definition of organ involvement and treatment response in immunoglobulin light chain amyloidosis (AL): a consensus opinion from the 10th International Symposium on Amyloid and Amyloidosis, Tours, France, 18-22 April 2004. Am J Haematol. 2005;79(4):319-328.
3. Palladini G, Dispenzieri A, Gertz MA, et al. New criteria for response to treatment in immunoglobulin light chain amyloidosis based on free light chain measurement and cardiac biomarkers: impact on survival outcomes. J Clin Oncol. 2012;30(36):4541- 4549.
4. Dispenzieri A, Gertz MA, Kyle RA, et al. Serum cardiac troponins and N-terminal pro-brain natriuretic peptide: a staging system for primary systemic amyloidosis. J Clin Oncol. 2004;22(18):3751-3757.
5. Kumar S, Dispenzieri A, Lacy MQ, et al. Revised prognostic staging system for light chain amyloidosis incorporating cardiac biomarkers and serum free light chain measurements. J Clin Oncol. 2012; 30(9):989-995.
6. Moreau P, Leblond V, Bourquelot P, et al. Prognostic factors for survival and response

after high-dose therapy and autologous stem cell transplantation in systemic AL amyloidosis: a report on 21 patients. Br J Haematol. 1998;101(4):766-769.
7. Kastritis E, Papassotiriou I, Terpos E, et al. Clinical and prognostic significance of serum levels of von Willebrand factor and ADAMTS-13 antigens in AL amyloidosis. Blood. 2016;128(3):405-409.
8. Kastritis E, Papassotiriou I, Merlini G. Growth differentiation factor-15 is a new biomarker for survival and renal outcomes in light chain amyloidosis. Blood. 2018;131(14):1568-1575.
9. Russo P, Palladini G, Foli A, et al. Liver involvement as the hallmark of aggressive disease in light chain amyloidosis: distinctive clinical features and role of light chain type in 225 patients. Amyloid. 2011;18 Suppl 1:92-93.
10. Fontana M, Pica S, Reant P, et al. Prognostic value of late gadolinium enhancement cardiovascular magnetic resonance in cardiac amyloidosis. Circulation. 2015;132(16): 1570-1579.
11. Lovat LB, Persey MR, Madhoo S, Pepys MB, Hawkins PN. The liver in systemic amyloidosis: insights from 123I serum amyloid P component scintigraphy in 484 patients. Gut. 1998;42(5):727-734.
12. Gertz MA, Comenzo R, Falk RH, et al. Definition of organ involvement and treatment response in immunoglobulin light chain amyloidosis (AL): a consensus opinion from the 10th International Symposium on Amyloid and Amyloidosis, Tours, France, 18-22 April 2004. Am J Hematol. 2005;79(4):319-328.
13. Wechalekar AD, Gillmore JD, Wassef N, Lachmann HJ, Whelan C, Hawkins PN. Abnormal N-terminal fragment of brain natriuretic peptide in patients with light chain amyloidosis without cardiac involvement at presentation is a risk factor for development of cardiac amyloidosis. Haematologica. 2011;96(7):1079-1080.
14. Dittrich T, Benner A, Kimmich C, et al. Performance analysis of AL amyloidosis cardiac biomarker staging systems with special focus on renal failure and atrial arrhythmia. Haematologica. 2019;
15. Wan K, Sun J, Han Y, et al. Increased prognostic value of query amyloid late enhancement score in light-chain cardiac amyloidosis. Circ J. 2018;82(3):739-746.
16. Gertz MA, Kyle RA. Hepatic amyloidosis: clinical appraisal in 77 patients. Hepatology. 1997;25(1):118-121.
17. Fradley MG, Larson MG, Cheng S, et al. Reference limits for N-terminal-pro-B-type natriuretic peptide in healthy individuals (from the Framingham Heart Study). Am J Cardiol. 2011;108(9):1341-1345.
18. Palladini G, Milani P, Foli A, et al. Presentation and outcome with second-line treatment in AL amyloidosis previously sensitive to nontransplant therapies. Blood. 2018;131(5):525-532.
19. Palladini G, Campana C, Klersy C, et al. Serum N-terminal pro-brain natriuretic peptide is a sensitive marker of myocardial dysfunction in AL amyloidosis. Circulation. 2003;107(19):2440-2445.
20. Kumar SK, Gertz MA, Lacy MQ, et al. Recent improvements in survival in primary systemic amyloidosis and the importance of an early mortality risk score. Mayo Clin Proc. 2011;86(1):12-18.

Ferrata Storti Foundation

Dynamin 2 is required for GPVI signaling and platelet hemostatic function in mice

Nathan Eaton,[1,2] Caleb Drew,[1] Jon Wieser,[1] Adam D. Munday,[3,4] and Hervé Falet[1,2]

[1]Blood Research Institute, Versiti, Milwaukee, WI; [2]Department of Cell Biology, Neurobiology, and Anatomy, Medical College of Wisconsin, Milwaukee, WI; [3]Bloodworks Northwest Research Institute, Seattle, WA and [4]Division of Hematology, Department of Medicine, University of Washington, Seattle, WA, USA

Haematologica 2020
Volume 105(5):1414-1423

ABSTRACT

Receptor-mediated endocytosis, which contributes to a wide range of cellular functions, including receptor signaling, cell adhesion, and migration, requires endocytic vesicle release by the large GTPase dynamin 2. Here, the role of dynamin 2 was investigated in platelet hemostatic function using both pharmacological and genetic approaches. *Dnm2*$^{fl/fl}$ Pf4-Cre (*Dnm2*$^{Plt-/-}$) mice specifically lacking dynamin 2 within the platelet lineage developed severe thrombocytopenia and bleeding diathesis and *Dnm2*$^{Plt-/-}$ platelets adhered poorly to collagen under arterial shear rates. Signaling *via* the collagen receptor GPVI was impaired in platelets treated with the dynamin GTPase inhibitor dynasore, as evidenced by poor protein tyrosine phosphorylation, including that of the proximal tyrosine kinase Lyn on its activating tyrosine 396 residue. Platelet stimulation *via* GPVI resulted in a slight decrease in GPVI, which was maintained by dynasore treatment. Dynasore-treated platelets had attenuated function when stimulated *via* GPVI, as evidenced by reduced GPIbα downregulation, α-granule release, integrin αIIbβ3 activation, and spreading onto immobilized fibrinogen. By contrast, responses to the G-protein coupled receptor agonist thrombin were minimally affected by dynasore treatment. GPVI expression was severely reduced in *Dnm2*$^{Plt-/-}$ platelets, which were dysfunctional in response to stimulation *via* GPVI, and to a lesser extent to thrombin. *Dnm2*$^{Plt-/-}$ platelets lacked fibrinogen in their α-granules, but retained von Willebrand factor. Taken together, the data show that dynamin 2 plays a proximal role in signaling *via* the collagen receptor GPVI and is required for fibrinogen uptake and normal platelet hemostatic function.

Correspondence:

HERVÉ FALET
hfalet@versiti.org

Received: February 19, 2019.

Accepted: July 9, 2019.

Pre-published: July 11, 2019.

doi:10.3324/haematol.2019.218644

Check the online version for the most updated information on this article, online supplements, and information on authorship & disclosures: www.haematologica.org/content/105/5/1414

Introduction

Receptor-mediated endocytosis (RME), the process by which cells internalize and sort specific extracellular material, plasma membrane proteins, and lipids, contributes to a wide range of cellular functions, including receptor signaling, cell adhesion, and migration.[1] RME requires membrane fission by the large and ubiquitous GTPase dynamin 2 (DNM2), which polymerizes at the neck of budding endocytic vesicles to mediate the GTP-dependent membrane fission required for their release into the cytosol prior to their incorporation into the endosomal compartment.[2] Consistent with its indispensable role in cellular homeostasis, *DNM2* mutations have been associated with Charcot-Marie-Tooth disease, centronuclear myopathy, and early T-cell precursor acute lymphoblastic leukemia (ETP-ALL),[3-5] and *Dnm2* deletion results in early embryonic lethality in mice.[6] While other classical dynamins (DNM1 and DNM3) are critical for activity-dependent vesicle recycling in presynaptic neurons,[7,8] their functions in other cells remain less clear.

The most well-characterized physiological roles of RME are to regulate uptake of nutrients such as cholesterol and iron and to down-modulate cytokine receptor signaling.[1] Lack of DNM2-dependent RME enhances responses to thrombopoietin in platelets and megakaryocytes (MK),[9] and to epidermal growth factor and inter-

leukins 5 and 7 in other cells,[10-12] the proposed mechanism associating *DNM2* loss-of-function mutations and ETP-ALL development.[5] Further, previous studies using pharmacological approaches have suggested that dynamin GTPase activity contributes to receptor desensitization in human platelets, as in the case of the purinergic receptors P2Y1 and P2Y12.[13]

Human platelets express all three classical dynamins,[14,15] including an inactive DNM3 spliced variant, for which a single nucleotide polymorphism has been associated with platelet size.[16] In comparison, mouse platelets express predominantly the ubiquitous DNM2,[14,17] thus providing a valuable model to study DNM2-dependent RME in platelet and MK biology, independent of neuronal DNM1 and DNM3. We have previously shown that $Dnm2^{fl/fl}$ Pf4-Cre ($Dnm2^{Plt-/-}$) mice specifically lacking DNM2 in the platelet lineage develop severe macrothrombocytopenia due to membrane fission arrest and accumulation of clathrin-coated vesicles obstructing the MK demarcation membrane system, the highly organized membrane reservoir for future platelets.[9] Here we investigated the role of DNM2 in platelet hemostatic function using both pharmacological and genetic approaches. Our data show that DNM2 regulates proximal signaling *via* the platelet collagen receptor GPVI and that DNM2-dependent RME is required for the accumulation of plasma fibrinogen into α-granules to facilitate normal platelet hemostatic function.

Table 1. Primary antibodies used.

Target	Host	Type	Company
pTyr (4G10 Platinum)	Mouse	Monoclonal	EMD Millipore
pLyn (Y396)	Rabbit	Monoclonal	Boster Biological
Lyn	Mouse	Monoclonal	Santa Cruz
DNM2	Mouse	Monoclonal	Santa Cruz
β-actin	Rabbit	Polyclonal	Abcam
β-tubulin	Mouse	Monoclonal	Sigma-Aldrich
GPVI (JAQ1)	Rat	Monoclonal	Emfret Analytics
GPIbα (CD42b)	Rat	Monoclonal	Emfret Analytics
P-selectin (CD62P)	Rat	Monoclonal	BD Biosciences
αIIb (CD41)	Rat	Monoclonal	R&D Systems
Fibrinogen	Rabbit	Polyclonal	DAKO
vWF	Rabbit	Polyclonal	DAKO
Clathrin Heavy Chain	Mouse	Monoclonal	EMD Millipore
Cavin 2 (SDPR)	Rabbit	Polyclonal	Proteintech
Caveolin 1	Rabbit	Monoclonal	Cell Signaling
Rab5	Rabbit	Monoclonal	Cell Signaling
Rab7	Rabbit	Monoclonal	Cell Signaling
Rab11	Rabbit	Monoclonal	Cell Signaling
Flotillin 1	Mouse	Monoclonal	BD Biosciences

pTyr: phosphotyrosine; pLyn: phosphorylated Lyn; vWF: von Willebrand factor.

Methods

Mice

$Dnm2^{Plt-/-}$ mice were described previously.[9] Mice were treated according to the National Institutes of Health and Medical College of Wisconsin Institutional Animal Care and Use Committee guidelines.

Platelet count

Platelet count was measured on a Sysmex XT-2000i automatic hematology analyzer using blood collected by mouse retro-orbital plexus bleeding and immediately diluted in Cellpack (Sysmex) supplemented with EDTA and PGE1.[18]

Tail bleeding time

Bleeding time was determined by snipping 2 mm of distal mouse tail and immediately immersing the tail in 37°C isotonic saline.[19] A complete cessation of bleeding was defined as the bleeding time.

Ex vivo perfusion assay

Platelet interaction with immobilized type I collagen was performed using the VenaFlux Platform and Vena8Fluor+ biochips (Cellix).[20] Additional information can be found in the *Online Supplementary Methods*.

Platelet preparation and flow cytometry

Blood was collected by mouse retro-orbital plexus bleeding and was anticoagulated in acid-citrate-dextrose.[19] Platelets were isolated by sequential centrifugation, resuspended at $5x10^8$ platelets/mL, and incubated for 30 minutes (min) at 37°C with 100 μM of the non-competitive inhibitor of dynamin GTPase activity, dynasore (EMD Millipore),[13,21-23] or vehicle (0.1% DMSO).

Platelets were activated or not with collagen-related peptide (CRP; Protein Chemistry Core Laboratory, Blood Research Institute, Versiti, USA) or human thrombin (Roche) for 2-3 min at 37°C and stained with FITC-labeled rat anti-mouse GPIbα or FITC-labeled rat anti-mouse P-selectin antibodies (Table 1) or Oregon Green 488-labeled fibrinogen (Thermo Fisher Scientific).[19] Fluorescence was quantified using an Accuri C6 flow cytometer (BD Biosciences) and FlowJo software. A total of 10,000 events were analyzed for each sample.

Immunoblot analysis

Platelets were lysed as described.[19] Platelet proteins were separated by SDS-PAGE, transferred onto an Immobilon-P membrane (EMD Millipore), and probed with antibodies directed against proteins of interest (Table 1). Platelet fibrinogen content was quantitated using purified mouse fibrinogen (Enzyme Research) as standard.

Lipid rafts were isolated from human platelets as described.[24] Blood was collected from volunteers by venipuncture and was anticoagulated in acid-citrate-dextrose. Approval was obtained from the Western Institutional Review Board and informed consent was approved according to the Declaration of Helsinki.

Immunofluorescence microscopy

Samples were imaged on Nikon Structured Illumination Microscopy (N-SIM, NIS-Elements AR v4.40.00 software) and Olympus Confocal FV1000-MPE (FluoView software) platforms under 100x oil objectives.[9,25] Additional information can be found in the *Online Supplementary Methods.*

Statistical analysis

All experiments were performed at least in triplicate. Results were compared with the unpaired Student *t*-test (simple), two-way ANOVA followed by Bonferroni correction (multiple), or the Kaplan-Meier analysis (time-to-event) using Prism software (GraphPad). $P<0.05$ was considered significant.

Results

Hemostatic defects in *Dnm2*$^{Plt-/-}$ mice

Dnm2$^{Plt-/-}$ mice developed severe thrombocytopenia, with 152±15x10^3 platelets/μL [mean±standard error of mean SEM); n=15], compared to 1,299±54x10^3 platelets/μL in control *Dnm2*$^{fl/fl}$ mice (n=18) (P<0.0001), an 88% reduction (Figure 1A), as described previously.[9] The role of DNM2 in platelet hemostatic function was evaluated using the tail bleeding time assay (Figure 1B). Control mice had a median tail bleeding time of 1.16 min. By contrast, *Dnm2*$^{Plt-/-}$ mice had a profound bleeding diathesis with all mice studied bleeding for 10 min, our experimental end-point measurement (n=12 in each group) (Log-rank P<0.0001).

Following blood vessel injury and disruption of the vascular endothelium, platelets are exposed to basement membrane proteins and soluble agonists, which initiate platelet adhesion and activation, leading to thrombus formation and preventing excessive bleeding. At arterial shear rates, initial platelet adhesion is mediated by collagen-bound von Willebrand factor (vWF) binding to the GPIb-IX complex, followed by platelet activation *via* the collagen receptor GPVI.[26] The functionality of *Dnm2*$^{Plt-/-}$ platelets in whole blood was tested in flow chamber experiments using the VenaFlux platform,[20] where binding to a collagen-coated surface was measured under arterial shear rate (1500 s^{-1}) to mediate the interaction of plasma vWF with surface-bound collagen (Figure 1C-F). After 4 min, control platelets covered 18.0±5.1% (mean±SEM; n=7) of the collagen-coated surface (Figure 1E). Adhesion was markedly decreased in *Dnm2*$^{Plt-/-}$ platelets, with only 0.6±0.1% (n=4) (P=0.0333) of surface coverage, a 97% reduction.

The dwell time of individual control and *Dnm2*$^{Plt-/-}$ platelets was analyzed under the same experimental conditions (Figure 1F). After initial tethering, control platelets dwelled for a median time of 61 seconds (s) (n=60). *Dnm2*$^{Plt-/-}$ platelets dwelled for a significantly lower median time of 33 s (n=61) (Log-rank P=0.0331), indicating that a decreased stability of the GPIbα-vWF interaction contributes to the poor adhesion of *Dnm2*$^{Plt-/-}$ platelets to collagen under arterial shear rates and the profound bleeding diathesis of *Dnm2*$^{Plt-/-}$ mice.

Impaired GPVI signaling in dynasore-treated and *Dnm2*$^{Plt-/-}$ platelets

Collagen binding to its platelet receptor GPVI initiates a signaling pathway that sequentially involves activation of the Src family tyrosine kinases Fyn and Lyn, phosphorylation of the GPVI-associated FcR γ-chain, and recruitment, tyrosine phosphorylation, and activation of the tyrosine kinase Syk, leading to activation of phospholipase C-γ2 (PLC-γ2).[27] The ability of DNM2 to regulate GPVI signaling was investigated (Figure 2). Control platelets, platelets treated with 100 μM dynasore to inhibit DNM2 GTPase activity pharmacologically, and *Dnm2*$^{Plt-/-}$ platelets were activated with the GPVI agonist CRP. In control platelets,

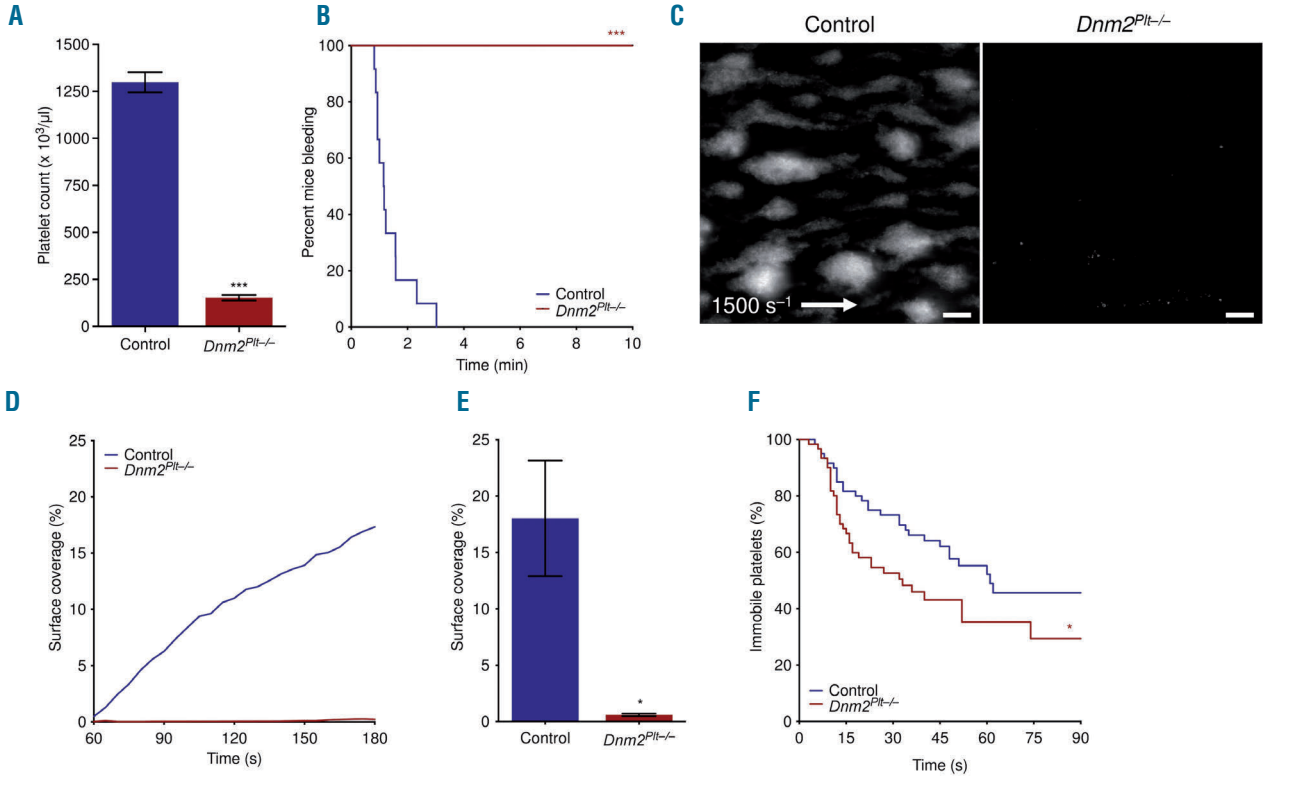

Figure 1. Hemostatic defects in *Dnm2*$^{Plt-/-}$ mice. (A) Blood platelet count of control *Dnm2*$^{fl/fl}$ (n = 18) and *Dnm2*$^{Plt-/-}$ mice (n=15; ***P<0.0001). (B) Tail bleeding time of control *Dnm2*$^{fl/fl}$ and *Dnm2*$^{Plt-/-}$ mice (n=12 in each group; Log-rank ***P<0.0001). (C-F) PPACK-anticoagulated whole blood from control and *Dnm2*$^{fl/fl}$ mice was labeled and perfused on type I collagen-immobilized surface at an arterial shear rate of 1500 s^{-1}. (C) Representative still image at 4 min. Scale bars, 100 μm. (D) Representative time-course surface coverage, as labeled platelets accumulate in the field of view. (E) Surface coverage at 4 min (mean ± SEM; 7 control and 4 *Dnm2*$^{Plt-/-}$; *P=0.0333). (F) Dwell time of individual control and *Dnm2*$^{Plt-/-}$ platelets (n=60 in each group; Log-rank *P=0.0331).

CRP stimulation induced tyrosine phosphorylation of several proteins, including proteins at 125, 72, 68, 56, 52, and 38 kDa (Figure 2A). Dynasore-treated platelets had a moderate reduction of tyrosine phosphorylation of these proteins in response to CRP stimulation, and *Dnm2*$^{Plt-/-}$ platelets failed to increase protein tyrosine phosphorylation, even at high doses of CRP.

Because of its proximal role in the GPVI signaling pathway,[28] Lyn activation was probed using an antibody specifically directed against its phosphorylated activating tyrosine 396 (Tyr396) residue (Figure 2B). Stimulation of control platelets with CRP induced a 62±19% increase in Lyn Tyr396 phosphorylation that peaked at 2.5 μg/mL CRP (mean±SEM; n=3 in each group) (P=0.0408). Lyn Tyr396 phosphorylation was attenuated in dynasore-treated platelets and markedly reduced in *Dnm2*$^{Plt-/-}$ platelets.

GPVI expression in control, dynasore-treated, and *Dnm2*$^{Plt-/-}$ platelets was further evaluated by immunoblot analysis using the monoclonal antibody JAQ1 (Figure 2C). Following stimulation of control platelets with 25 μg/mL CRP, JAQ1 signal decreased by 15%, compared to resting levels. Dynasore treatment resulted in a 10% increase in JAQ1 signal, which was maintained following CRP stimulation. Taken together, the data show that DNM2 contributes to GPVI homeostasis at rest and GPVI downregulation and Lyn activation following GPVI ligation. As reported previously, GPVI expression was markedly decreased in *Dnm2*$^{Plt-/-}$ platelets,[9] and was unaffected by CRP.

Impaired GPIbα downregulation in CRP-stimulated dynasore-treated and *Dnm2*$^{Plt-/-}$ platelets

GPIbα is internalized during platelet activation,[29] a phenomenon that is expected to negatively affect initial platelet adhesion to collagen-bound vWF and for which a role of dynamin has been reported, based on pharmacological inhibition.[22] The role of DNM2 in this process was investigated in response to the GPVI agonist CRP or the soluble G-protein-coupled receptor agonist thrombin (Figure 3). Expression of surface GPIbα decreased to about 30% of resting levels following stimulation of control platelets with CRP (Figure 3A) or thrombin (Figure 3B).

In response to stimulation with CRP, expression of surface GPIbα decreased to 60% of resting levels in dynasore-treated platelets, a 50% reduction compared to controls, and *Dnm2*$^{Plt-/-}$ platelets failed to down-regulate GPIbα (Figure 3A). By contrast, dynasore treatment or *Dnm2* deletion did not affect GPIbα downregulation when platelets were stimulated with thrombin (Figure 3B).

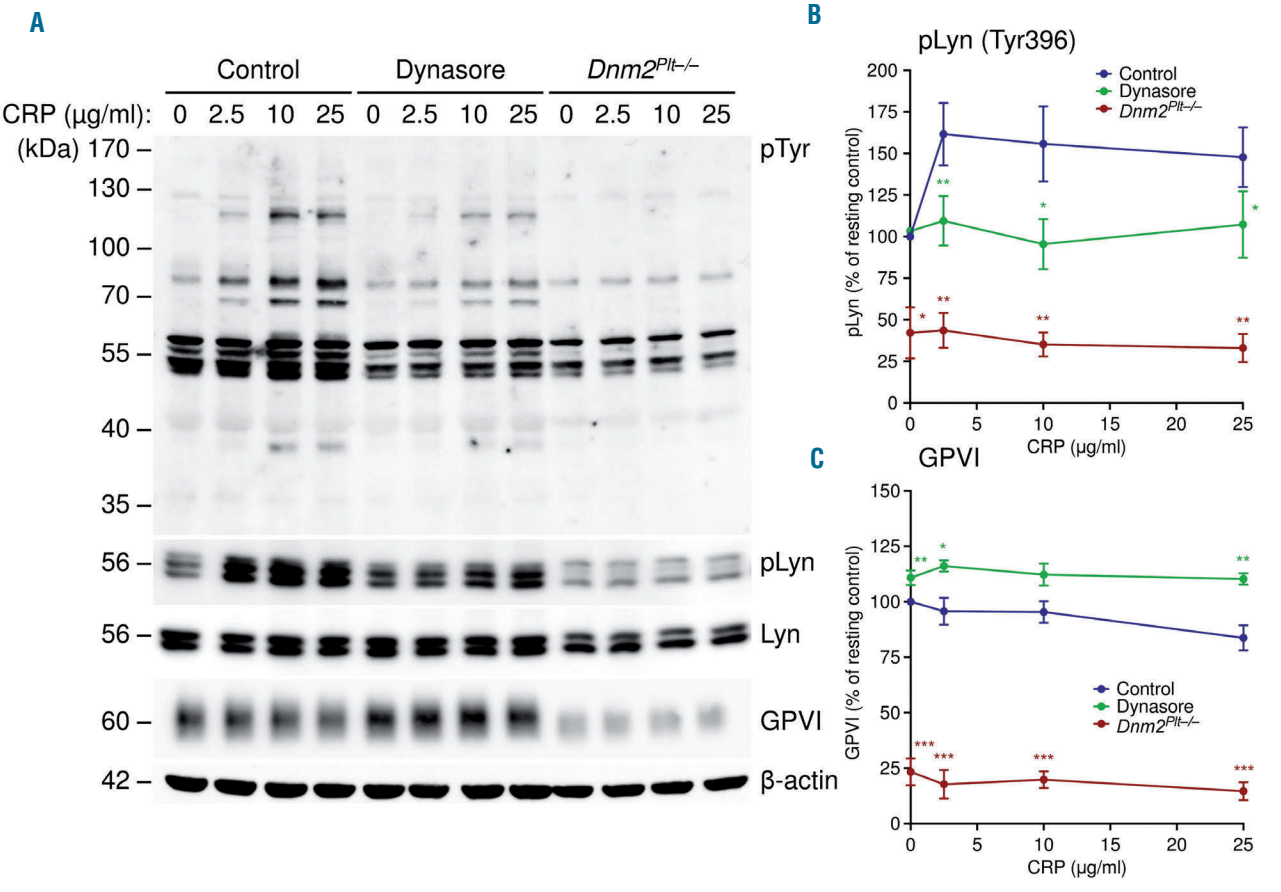

Figure 2. GPVI signaling defects in dynasore-treated and *Dnm2*$^{Plt-/-}$ platelets. Control platelets, platelets treated with 100 μM dynasore, and *Dnm2*$^{Plt-/-}$ platelets were activated or not with CRP for 2 minutes at 37 °C as indicated. (A) Platelet lysates corresponding to 2 μg of protein were subjected to SDS-PAGE and probed for phosphotyrosine (pTyr), phosphorylated Lyn Tyr396 (pLyn), Lyn, GPVI, and β-actin as a loading control. Results are representative of five independent experiments. Assessment of Lyn Tyr396 phosphorylation (B) and GPVI expression (C) in CRP-stimulated control, dynasore-treated, and *Dnm2*$^{Plt-/-}$ platelets. Results represent mean±standard error of mean (SEM) of 3-4 independent experiments, and are compared statistically to control (*P<0.05; **P<0.01; ***P<0.001).

The decreased GPIbα surface expression was due to internalization, and not to shedding, as total GPIbα expression was maintained during the course of the experiment, as shown by immunoblot analysis (Figure 3C). Taken together, the data show that DNM2 specifically regulates GPVI signaling, rather than GPIbα downregulation.

Impaired α-granule secretion and integrin αIIbβ3 activation in CRP-stimulated dynasore-treated and *Dnm2*$^{Plt-/-}$ platelets

Following activation by collagen or soluble agonists, platelets secrete their granule contents and activate their surface integrin αIIbβ3 in order to recruit circulating platelets and mediate platelet aggregation, respectively. The significance of DNM2 in these platelet hemostatic processes was assessed by flow cytometry (Figure 4). Control platelets, dynasore-treated platelets, and *Dnm2*$^{Plt-/-}$ platelets were activated with CRP (Figure 4A and C) or thrombin (Figure 4B and D), and analyzed for P-selectin (CD62P) expression, a marker for α-granule secretion (Figure 4A and B), and binding of fluorescently-labeled fibrinogen, a marker for integrin αIIbβ3 activation (Figure 4C and D).[19] Both CRP and thrombin induced a concentration-dependent increase of α-granule secretion and integrin αIIbβ3 activation in control platelets, reaching about 80% of platelets expressing CD62P or binding fibrinogen with 25 μg/mL CRP or 0.25 U/mL thrombin, respectively. Dynasore treatment resulted in a significant decrease in platelet responses to CRP, as only 30-40% platelets expressed CD62P and bound fibrinogen with 50 μg/mL CRP. By contrast, platelet responses to thrombin were not significantly affected by dynasore treatment. CRP-dependent CD62P expression and fibrinogen binding were completely abolished in *Dnm2*$^{Plt-/-}$ platelets and only about 20% expressed CD62P and bound fibrinogen in response to 0.5 U/mL thrombin.

Altered spreading of dynasore-treated and *Dnm2*$^{Plt-/-}$ platelets

Following activation, platelets rapidly change shape from resting disc-like entities to morphologically distinct forms, first by rounding, then by extending finger-like filopodia and spreading thin sheet-like lamellipodia.[30] The significance of DNM2 in platelet spreading was examined (Figure 5). Control platelets, dynasore-treated, and *Dnm2*$^{Plt-/-}$ platelets were activated with either 1 μg/mL CRP or 0.01 U/mL thrombin and allowed to adhere onto immobilized fibrinogen. In control platelets, stimulation with CRP or thrombin resulted in filopodia extension and lamellipodia spreading, as evidenced by phalloidin staining, a marker for polymerized actin, with the greatest difference being more angular or rounded appearance, respectively (Figure 5A). Treatment with dynasore mitigated lamellipodia formation in CRP-stimulated platelets (Figure 5B), and to a lesser, non-statistically significant degree in thrombin-stimulated platelets (Figure 5C), although it did not prevent filopodia growth.

Dnm2$^{Plt-/-}$ platelets displayed great heterogeneity in shape change with either agonist (Figure 5A), wherein spread platelet surface area varied between below control levels or up to a 5-fold increase in size following stimulation, reflecting the increased size of these platelets.[9] *Dnm2*$^{Plt-/-}$ platelets revealed extreme irregularity in their cytoskeletal and overall morphological arrangement, consistent with altered spreading capacity.

Absence of fibrinogen in *Dnm2*$^{Plt-/-}$ platelets

The fibrinogen content of platelet α-granules derives from the integrin αIIbβ3-dependent uptake of plasma-

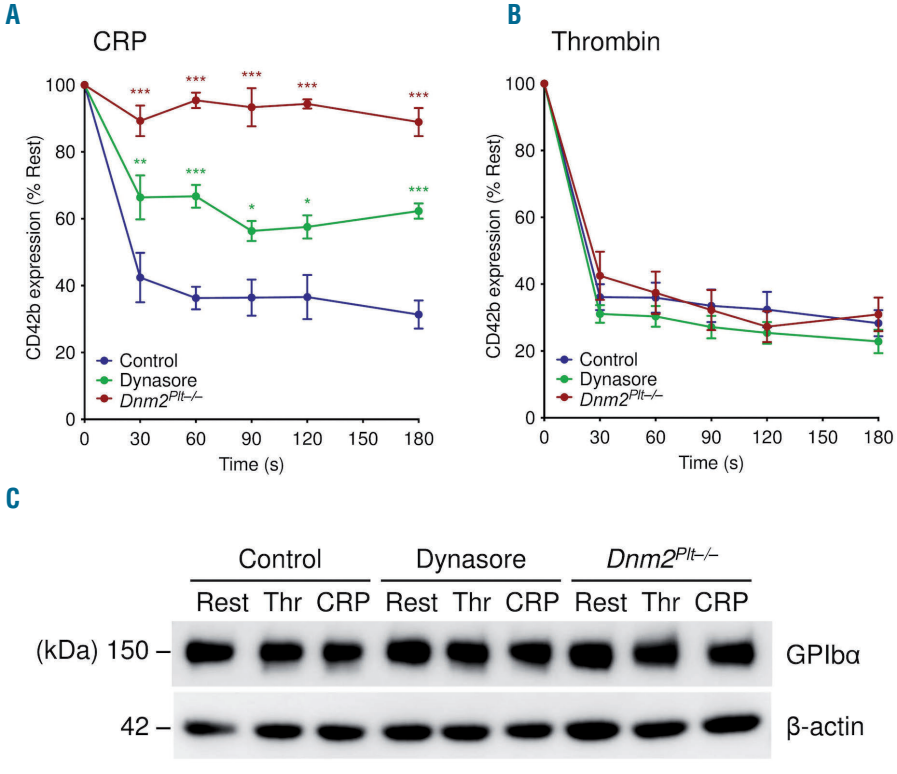

Figure 3. Impaired GPIbα downregulation in CRP-stimulated dynasore-treated and *Dnm2*$^{Plt-/-}$ platelets. Control platelets, platelets treated with 100 μM dynasore, and *Dnm2*$^{Plt-/-}$ platelets were activated for 3 minutes (min) at 37°C with 25 μg/mL CRP (A) or 0.1 U/ml thrombin (B), incubated with FITC-labeled anti-mouse CD42b antibody, and analyzed by flow cytometry. Results are expressed as percentage of CD42b expression at rest, represent mean±standard error of mean (SEM) of three independent experiments, and are compared statistically to control (*P<0.05; **P<0.01; ***P<0.001). (C) Control, dynasore-treated, and *Dnm2*$^{Plt-/-}$ platelets were activated or not with 0.1 U/mL thrombin or 25 μg/mL CRP for 3 min at 37°C as indicated. Platelet lysates were subjected to SDS-PAGE and probed for GPIbα and β-actin as loading control, as indicated. Results are representative of three independent experiments.

derived fibrinogen.[31,32] To evaluate the contribution of DNM2-dependent RME in the process, the fibrinogen content of *Dnm2*$^{Plt-/-}$ platelets was compared to that of vWF, which is synthesized by MK and is also stored in platelet α-granules (Figure 6A).[33] Immunoblot analysis showed severe fibrinogen reduction in *Dnm2*$^{Plt-/-}$ platelet lysates, but normal expression of vWF. Quantification of the immunoblots using purified mouse fibrinogen as standard revealed that 10^6 *Dnm2*$^{Plt-/-}$ platelets contained 71±6 ng fibrinogen, compared to 333±27 ng in 10^6 control platelets (n=3 in each group) (P=0.0007), a 79% decrease (Figure 6B).

The fibrinogen content of control and *Dnm2*$^{Plt-/-}$platelets was further evaluated by structured illumination microscopy and compared to that of the αIIb subunit (CD41) of its receptor, the integrin αIIbβ3 (Figure 6C, top panels). In control platelets fibrinogen was observed in large puncta, consistent with its presence in α-granules.[33] By contrast, *Dnm2*$^{Plt-/-}$ platelets had severely reduced fibrinogen content, with about 90% of *Dnm2*$^{Plt-/-}$ platelets presenting barely detectable fibrinogen positive α-granules. CD41 resided on the platelet surface and in small vesicles or granules within platelets, independent of DNM2 expression, consistent with the association of the integrin αIIbβ3 with multiple intracellular platelet compartments that include α-granules and the open canalicular system.[34] By contrast, vWF was normally packaged in *Dnm2*$^{Plt-/-}$ platelets (Figure 6C, bottom panels). Taken together, the data show that integrin αIIbβ3-dependent uptake of plasma-derived fibrinogen requires DNM2-dependent RME.

Platelet endocytic and endosomal components

Thin-section electron microscopy studies have subdivided RME into clathrin- and caveolae-mediated endocytosis (CME and CavME, respectively).[1] CME is found in virtually all cells and requires cargo receptor binding to clathrin-associated adaptor protein 2 complexes to form clathrin-coated vesicles.[35] Caveolae are invaginated lipid rafts rich in cholesterol, sphingolipids, and scaffolding proteins called caveolins and cavins that are found in many mammalian cell types.[36] Platelet endocytic and endosomal components were investigated in the presence or absence of DNM2 (Figure 6A). Platelets contained clathrin heavy chain required for CME and its expression was increased in *Dnm2*$^{Plt-/-}$ platelets. Cavin 2 (also known as SDPR, PS-p68) was detected in platelets, but not caveolin 1, which is required for CavME. Ruling out poor antibody reactivity, a strong caveolin 1 signal was observed at the expected molecular weight of 21 kDa with mouse lung tissue lysates (*data not shown*).[37]

As an additional control and because cavin 2 associates

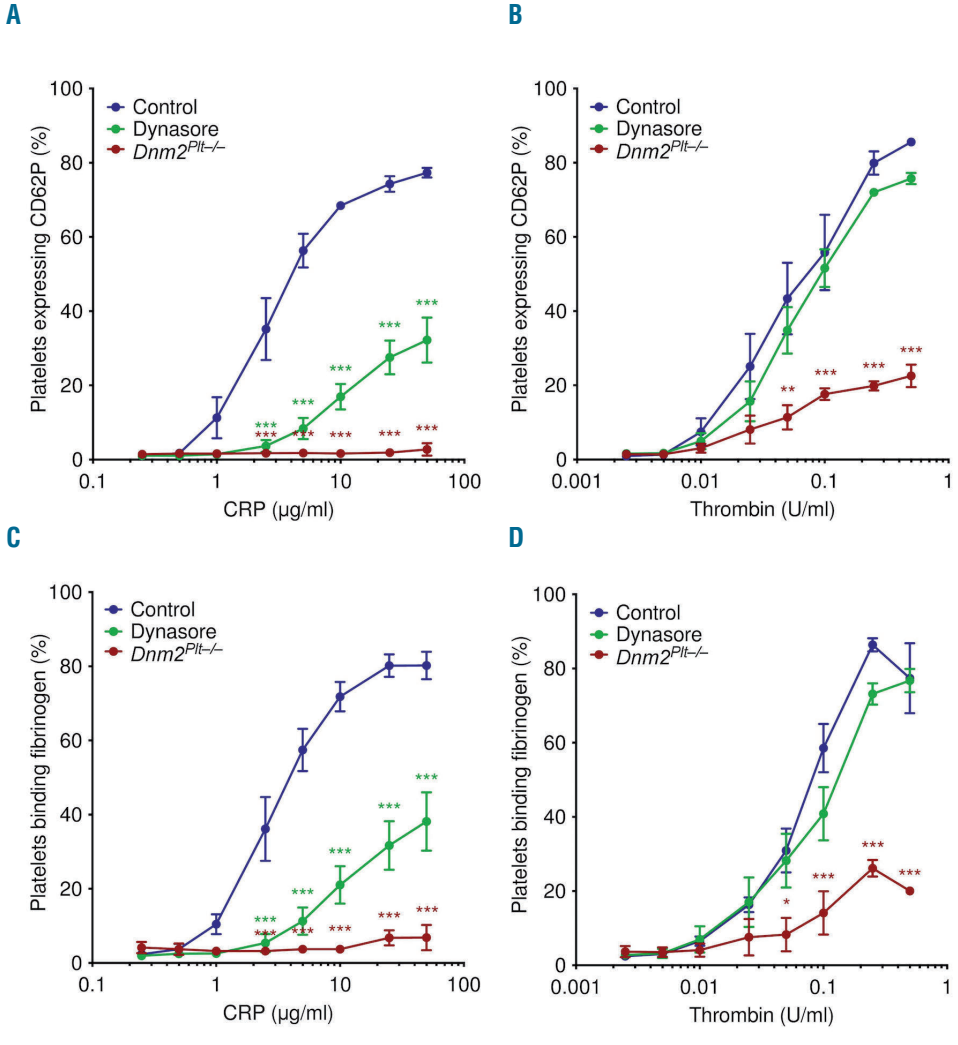

Figure 4. Hemostatic defects of CRP-stimulated dynasore-treated and *Dnm2*$^{Plt-/-}$ platelets. Control platelets, platelets treated with 100 μM dynasore, and *Dnm2*$^{Plt-/-}$ platelets were activated for 2 min at 37°C with CRP (A and C) or thrombin (B and D) as indicated. Platelets were then incubated with FITC-labeled anti-mouse CD62P antibody (A and B) or Oregon green 488-labeled fibrinogen (C and D) and analyzed by flow cytometry. Results are expressed as percentage of positive platelets, represent mean±standard error of mean (SEM) of 3-6 independent experiments, and are compared statistically to control (*P<0.05; **P<0.01; ***P<0.001).

with insoluble lipid rafts in cells expressing caveolin 1,[38] the association of cavin 2 with detergent-resistant platelet lipid rafts was investigated using a sucrose gradient in human platelet lysates (Figure 6D), which also lack caveolin 1 (*data now shown*). Cavin 2 did not associate with the insoluble sucrose gradient fractions rich in GM1 ganglioside and flotillin 1. Taken together, the data show that platelets contained the endocytic machinery required for CME, but not for CavME.

Early, late, and recycling endosomal compartments are distinguished by their association with specific members of the Rab family of small GTPases. Platelets contained Rab5 (early), Rab7 (late), and Rab11 (recycling), as described previously,[33,39] and their expression levels were not affected by the lack of DNM2 (Figure 6A).

Discussion

The cellular mechanisms and proteins regulating platelet and MK RME are poorly understood.[39] Here, using both pharmacological and genetic approaches, we described the role of the endocytic GTPase DNM2 in intracellular signaling *via* the collagen receptor GPVI and platelet hemostatic function.

In control platelets, ligation of the collagen receptor GPVI by its soluble agonist CRP induced an increase in protein tyrosine phosphorylation, including that of the proximal protein tyrosine kinase Lyn on its activating residue Tyr396, and a decrease in GPVI expression. Following dynasore treatment, phosphorylation of Lyn Tyr396 was attenuated and GPVI expression was maintained. Recent studies have shown that common dynamin inhibitors, such as dynasore and Dyngo-4a, not only inhibit dynamin GTPase activity, but also disrupt the organization of cholesterol-rich membrane rafts in a dynamin-independent manner.[40,41] Dynasore-treated platelets elicited defects in GPIbα downregulation, α-granule secretion, integrin αIIbβ3 activation, and spreading onto fibrinogen when stimulated *via* GPVI, but not by thrombin. By contrast, the cholesterol-lowering reagent, methyl-β-cyclodextrin, inhibits GPVI signaling, as well as platelet responses to the G-protein-coupled receptor agonists, thrombin and ADP.[42,43] Hence, the data argue

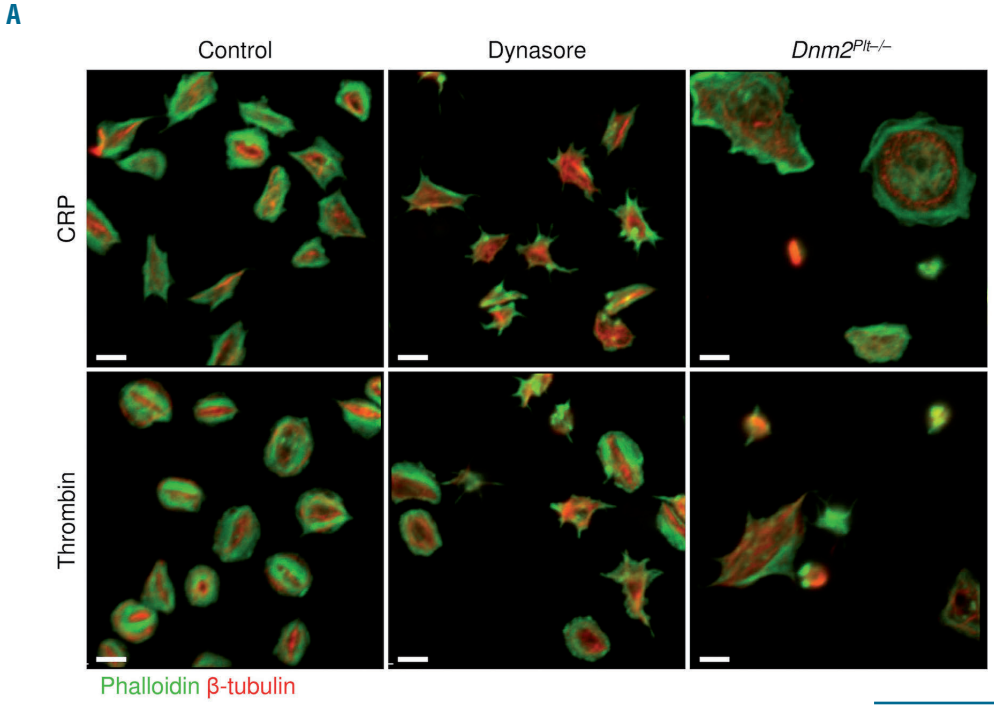

Figure 5. Altered spreading of CRP-stimulated dynasore-treated and *Dnm2*$^{Plt-/-}$ platelets. (A) Control platelets, platelets treated with 100 μM dynasore, and *Dnm2*$^{Plt-/-}$ platelets were activated with 1 μg/mL CRP or 0.01 U/mL thrombin and spread onto fibrinogen-coated coverslips for 30 minutes (min) as indicated. Fixed platelets were stained for polymerized actin (phalloidin; green) and β-tubulin (red) and analyzed by confocal microscopy. Images are representative of at least three independent experiments. Scale bars, 3 μm. (B) Assessment of platelet spreading in response to 1 μg/mL CRP. Total platelets scored were 374 control, 275 dynasore-treated, and 187 *Dnm2*$^{Plt-/-}$. (C) Assessment of platelet spreading in response to 0.01 U/mL thrombin. Total platelets scored were 298 control, 226 dynasore-treated, and 192 *Dnm2*$^{Plt-/-}$ (*P<0.05; **P<0.01; ***P<0.001).

against membrane raft disruption and indicate that DNM2 plays a proximal role in GPVI signaling.

The positive role of DNM2 in GPVI signaling contrasts with its commonly reported function in attenuating receptor signaling. Lack of DNM2-dependent RME enhances responses to thrombopoietin in platelets and MK and to epidermal growth factor and interleukins 5 and 7 in other cells.[9-12] Dynasore treatment also inhibits the desensitization of the purinergic receptors P2Y1 and P2Y12 in human platelets.[13] Thus, DNM2 differentially regulates signaling depending on the receptor it is linked to. The GPVI-associated FcR γ-chain contains two putative endocytic YxxL motifs that are present within its immunoreceptor tyrosine-based activation motif. Whether these motifs recruit the endocytic machinery necessary to down-regulate GPVI is unclear, as their mutation in mouse platelets abol-

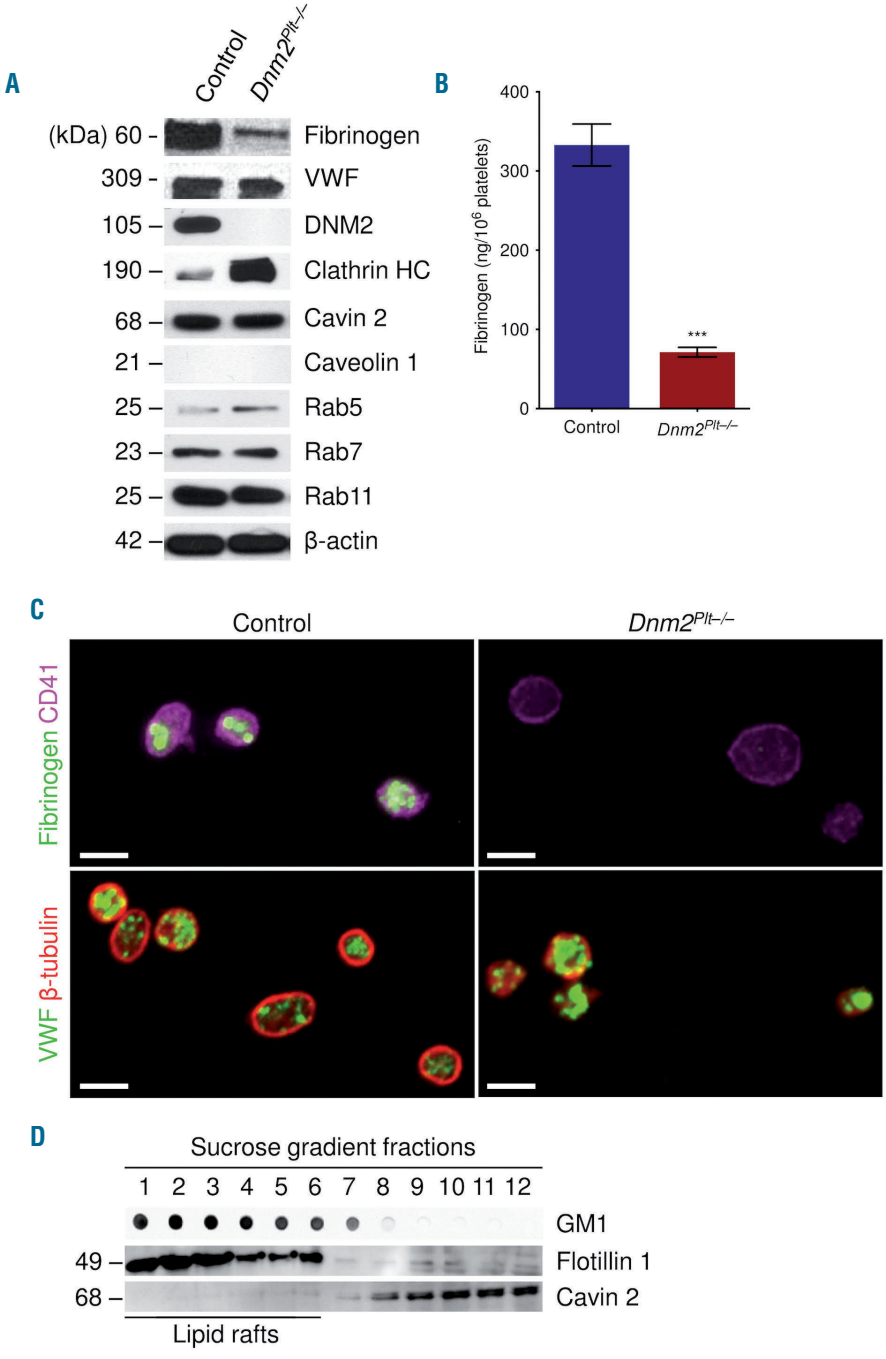

Figure 6. Cargo, endocytic, and endosomal proteins in *Dnm2*$^{Plt-/-}$ platelets. (A) Control and *Dnm2*$^{Plt-/-}$ platelet lysates corresponding to 2 μg of protein were subjected to SDS-PAGE and probed for cargo, endocytic, and endosomal proteins, and β-actin as loading control, as indicated. Results are representative of three independent experiments. HC: heavy chain. (B) The fibrinogen content of control and *Dnm2*$^{Plt-/-}$ platelets was evaluated by immunoblot analysis using purified mouse fibrinogen as standard. Results are expressed as ng/10^6 platelets and represent mean±standard error of mean (SEM) of three independent experiments (***P=0.0007). (C) Structured illumination microscopy analysis of fibrinogen (green) and CD41 (magenta; top panels) and confocal microscopy analysis of vWF (green) and β-tubulin (red; bottom panels) in control and *Dnm2*$^{Plt-/-}$ platelets. Scale bars, 3 μm. (D) Sucrose density fractions of human platelet lysates were dot-blotted and probed with HRP-conjugated cholera toxin B subunit to detect GM1 ganglioside or immunoblotted for flotillin 1 and cavin 2.

ishes both GPVI signaling and internalization.[44] Besides its role in membrane fission during RME, DNM2 can also serve as a scaffolding protein for signaling intermediates.[2] In T cells, DNM2 directly interacts with the guanine nucleotide exchange factor Vav1 to regulate activation of PLC-γ1 and the accumulation of cortical actin at sites of T-cell receptor activation, thereby regulating T-cell receptor signaling.[45] Vav1 and Vav3 play critical but redundant roles in the activation of PLC-γ2 downstream of GPVI,[46] and clustering of GPVI dimers, the mechanism of which depends on a dynamic actin cytoskeleton, contributes to GPVI signaling.[47] It is, therefore, tempting to speculate that platelet DNM2 serves as a scaffolding protein for signaling intermediates and/or actin-regulatory proteins downstream of GPVI.

Dnm2$^{Plt-/-}$ mice had a severe bleeding diathesis, which was intrinsic to platelets as *Dnm2* deletion under control of the *Pf4* promoter is specific to the platelet lineage.[9] Consistently, *Dnm2*$^{Plt-/-}$ platelets adhered poorly to collagen under arterial shear rates and were depleted of fibrinogen. Further, α-granule secretion, integrin αIIbβ3 activation, and spreading onto fibrinogen were markedly reduced in *Dnm2*$^{Plt-/-}$ platelets stimulated through GPVI or with thrombin. The lack of GPVI signaling is likely explained by the profound deficit in GPVI expression.[9] Whether this deficit is due to decreased GPVI synthesis in *Dnm2*$^{Plt-/-}$ MK, increased internalization and degradation, or ADAM10-mediated extracellular domain shedding is unclear. The differences between the pharmacological and genetic approaches indicate that either dynasore treatment does not completely inhibit platelet DNM2 GTPase activity or *Dnm2*$^{Plt-/-}$ platelets acquire defects during production affecting their functional responses. Because RME is a critical component of cellular cholesterol homeostasis,[1] it is possible that *Dnm2* genetic deletion impacts cell membrane composition and lipid raft organization, thereby affecting signaling in cholesterol-rich membrane domains. While the tail bleeding time in mice is largely unaffected by severe reduction of platelet count or lack of GPVI,[48,49] it cannot be excluded that the macrothrombocytopenia of *Dnm2*$^{Plt-/-}$ mice combined with the profound deficit in GPVI expression contributes to the bleeding diathesis.

The severe reduction in fibrinogen content of *Dnm2*$^{Plt-/-}$ platelets is consistent with impaired RME and a role for DNM2 downstream of integrin αIIbβ3 function as plasma fibrinogen is taken up by platelets and MK in an integrin αIIbβ3-mediated manner.[31,32] Beside fibrinogen, platelets and MK take up and store in their α-granules a long list of plasma proteins such as coagulation factor V and regulators of angiogenesis.[50,51] While the hypothesis was not tested here, endocytosed proteins are expected to be absent in *Dnm2*$^{Plt-/-}$ platelets due to defective RME, affecting other biological processes aside from hemostasis.

Platelets contained major endocytic and endosomal proteins such as clathrin and Rab GTPases.[33,39] The increased expression of clathrin heavy chain in *Dnm2*$^{Plt-/-}$ platelets likely reflects the accumulation of clathrin-coated vesicles observed in the demarcation membrane system of *Dnm2*$^{Plt-/-}$ MK.[9] Caveolin 1 was not detected in platelets, consistent with mRNA and protein profiling,[14,15,17] and cavin 2, a detergent-insoluble caveolae marker in cells expressing caveolin 1,[38] remained soluble following sucrose gradient of human platelet lysates. While cavin 2 is abundantly expressed in platelets,[14,15,17] where it was originally characterized,[52] its role in the absence of caveolin 1 is unclear. Taken together, the observations show that CME is the primary mechanism for RME in platelets. Consistently, fibrinogen uptake involves the recruitment of clathrin-associated adaptor protein 2 complexes to the β3 subunit of the integrin αIIbβ3 *via* clathrin adaptor proteins such as Dab2 and Numb.[53,54] After its uptake by CME and transport *via* the early (Rab5) and late (Rab7) endosome, fibrinogen is retained within α-granules by mechanisms dependent on NBEAL2, mutated in gray platelet syndrome.[33] The remaining fibrinogen content of *Dnm2*$^{Plt-/-}$ platelets is likely associated with the plasma membrane or trapped in the open canalicular system.

In conclusion, our work provides pharmacological and genetic evidence for a role of DNM2 in GPVI signaling and platelet hemostatic function. DNM2 regulates signaling events downstream of the collagen receptor GPVI, including the activation of the proximal tyrosine kinase Lyn, and is required for the integrin αIIbβ3-mediated accumulation of plasma fibrinogen into α-granules. Our data also show that DNM2 does not contribute to GPIbα downregulation, as dynasore-treated platelets and *Dnm2*$^{Plt-/-}$ platelets down-regulated GPIbα normally in response to thrombin. Whether DNM2 is a reasonable target for antithrombotic therapies remains to be determined.

Acknowledgments

The authors would like to thank Emily Legan and Scott Wood for technical assistance and Drs. Harry Heijnen, Karin Hoffmeister, and Walter Kahr for helpful discussions. This work was supported by the American Society of Hematology Foundation and National Institutes of Health R01 grant HL126743 (HF).

References

1. Doherty GJ, McMahon HT. Mechanisms of endocytosis. Annu Rev Biochem. 2009;78:857-902.
2. Ferguson SM, De Camilli P. Dynamin, a membrane-remodelling GTPase. Nat Rev Mol Cell Biol. 2012;13(2):75-88.
3. Züchner S, Noureddine M, Kennerson M, et al. Mutations in the pleckstrin homology domain of dynamin 2 cause dominant intermediate Charcot-Marie-Tooth disease. Nat Genet. 2005;37(3):289-294.
4. Bitoun M, Maugenre S, Jeannet PY, et al. Mutations in dynamin 2 cause dominant centronuclear myopathy. Nat Genet. 2005;37(11):1207-1209.
5. Zhang J, Ding L, Holmfeldt L, et al. The genetic basis of early T-cell precursor acute lymphoblastic leukaemia. Nature. 2012;481(7380):157-163.
6. Ferguson SM, Raimondi A, Paradise S, et al. Coordinated actions of actin and BAR proteins upstream of dynamin at endocytic clathrin-coated pits. Dev Cell. 2009;17(6):811-822.
7. Ferguson SM, Brasnjo G, Hayashi M, et al. A selective activity-dependent requirement for dynamin 1 in synaptic vesicle endocytosis. Science. 2007;316(5824):570-574.
8. Raimondi A, Ferguson SM, Lou X, et al. Overlapping role of dynamin isoforms in synaptic vesicle endocytosis. Neuron. 2011;70(6):1100-1114.
9. Bender M, Giannini S, Grozovsky R, et al. Dynamin 2-dependent endocytosis is required for normal megakaryocyte development in mice. Blood. 2015;125(6):1014-1024.
10. Gorska MM, Cen O, Liang Q, Stafford SJ, Alam R. Differential regulation of inter-

leukin 5-stimulated signaling pathways by dynamin. J Biol Chem. 2006;281(20):14429-14439.
11. Sousa LP, Lax I, Shen H, Ferguson SM, De Camilli P, Schlessinger J. Suppression of EGFR endocytosis by dynamin depletion reveals that EGFR signaling occurs primarily at the plasma membrane. Proc Natl Acad Sci U S A. 2012;109(12):4419-4424.
12. Tremblay CS, Brown FC, Collett M, et al. Loss-of-function mutations of Dynamin 2 promote T-ALL by enhancing IL-7 signalling. Leukemia. 2016;30(10):1993-2001.
13. Mundell SJ, Barton JP, Mayo-Martin MB, Hardy AR, Poole AW. Rapid resensitization of purinergic receptor function in human platelets. J Thromb Haemost. 2008;6(8):1393-1404.
14. Rowley JW, Oler AJ, Tolley ND, et al. Genome-wide RNA-seq analysis of human and mouse platelet transcriptomes. Blood. 2011;118(14):e101-111.
15. Burkhart JM, Vaudel M, Gambaryan S, et al. The first comprehensive and quantitative analysis of human platelet protein composition allows the comparative analysis of structural and functional pathways. Blood. 2012;120(15):e73-82.
16. Nürnberg ST, Rendon A, Smethurst PA, et al. A GWAS sequence variant for platelet volume marks an alternative DNM3 promoter in megakaryocytes near a MEIS1 binding site. Blood. 2012;120(24):4859-4868.
17. Zeiler M, Moser M, Mann M. Copy number analysis of the murine platelet proteome spanning the complete abundance range. Mol Cell Proteomics. 2014;13(12):3435-3445.
18. Lorenz V, Ramsey H, Liu ZJ, et al. Developmental Stage-Specific Manifestations of Absent TPO/c-MPL Signalling in Newborn Mice. Thromb Haemost. 2017;117(12):2322-2333.
19. Falet H, Pollitt AY, Begonja AJ, et al. A novel interaction between FlnA and Syk regulates platelet ITAM-mediated receptor signaling and function. J Exp Med. 2010;207(9):1967-1979.
20. Kanaji T, Kanaji S, Montgomery RR, Patel SB, Newman PJ. Platelet hyperreactivity explains the bleeding abnormality and macrothrombocytopenia in a murine model of Sitosterolemia. Blood. 2013;122(15):2732-2742.
21. Koseoglu S, Dilks JR, Peters CG, et al. Dynamin-related protein-1 controls fusion pore dynamics during platelet granule exocytosis. Arterioscler Thromb Vasc Biol. 2013;33(3):481-488.
22. Jones CI, Sage T, Moraes LA, et al. Platelet endothelial cell adhesion molecule-1 inhibits platelet response to thrombin and von Willebrand factor by regulating the internalization of glycoprotein Ib via AKT/glycogen synthase kinase-3/dynamin and integrin alphaIIbbeta3. Arterioscler Thromb Vasc Biol. 2014;34(9):1968-1976.
23. Gao W, Shi P, Chen X, et al. Clathrin-mediated integrin alphaIIbbeta3 trafficking controls platelet spreading. Platelets. 2018;29(6):617-621.
24. Munday AD, Gaus K, Lopez JA. The platelet glycoprotein Ib-IX-V complex anchors lipid rafts to the membrane skeleton: implications for activation-dependent cytoskeletal translocation of signaling molecules. J Thromb Haemost. 2010;8(1):163-172.
25. Begonja AJ, Pluthero FG, Suphamungmee W, et al. FlnA binding to PACSIN2 F-BAR domain regulates membrane tubulation in megakaryocytes and platelets. Blood. 2015;126(1):80-88.
26. Nieswandt B, Watson SP. Platelet-collagen interaction: is GPVI the central receptor? Blood. 2003;102(2):449-461.
27. Watson SP, Auger JM, McCarty OJ, Pearce AC. GPVI and integrin alphaIIb beta3 signaling in platelets. J Thromb Haemost. 2005;3(8):1752-1762.
28. Ezumi Y, Shindoh K, Tsuji M, Takayama H. Physical and functional association of the Src family kinases Fyn and Lyn with the collagen receptor glycoprotein VI-Fc receptor gamma chain complex on human platelets. J Exp Med. 1998;188(2):267-276.
29. Michelson AD, Barnard MR. Thrombin-induced changes in platelet membrane glycoproteins Ib, IX, and IIb-IIIa complex. Blood. 1987;70(5):1673-1678.
30. Falet H. Anatomy of the Platelet Cytoskeleton. In: Gresele P, Kleiman NS, López JA, Page CP, eds. Platelets in Thrombotic and Non-Thrombotic Disorders: Pathophysiology, Pharmacology and Therapeutics: an Update: Springer; 2017:139-156.
31. Harrison P, Wilbourn B, Debili N, et al. Uptake of plasma fibrinogen into the alpha granules of human megakaryocytes and platelets. J Clin Invest. 1989;84(4):1320-1324.
32. Handagama P, Scarborough RM, Shuman MA, Bainton DF. Endocytosis of fibrinogen into megakaryocyte and platelet alpha-granules is mediated by alpha IIb beta 3 (glycoprotein IIb-IIIa). Blood. 1993;82(1):135-138.
33. Lo RW, Li L, Leung R, Pluthero FG, Kahr WHA. NBEAL2 (Neurobeachin-Like 2) Is Required for Retention of Cargo Proteins by alpha-Granules During Their Production by Megakaryocytes. Arterioscler Thromb Vasc Biol. 2018;38(10):2435-2447.
34. Cramer EM, Savidge GF, Vainchenker W, et al. Alpha-granule pool of glycoprotein IIb-IIIa in normal and pathologic platelets and megakaryocytes. Blood. 1990;75(6):1220-1227.
35. Kaksonen M, Roux A. Mechanisms of clathrin-mediated endocytosis. Nat Rev Mol Cell Biol. 2018;19(5):313-326.
36. Parton RG, del Pozo MA. Caveolae as plasma membrane sensors, protectors and organizers. Nat Rev Mol Cell Biol. 2013;14(2):98-112.
37. Guo YH, Hernandez I, Isermann B, et al. Caveolin-1-dependent apoptosis induced by fibrin degradation products. Blood. 2009;113(18):4431-4439.
38. Hansen CG, Bright NA, Howard G, Nichols BJ. SDPR induces membrane curvature and functions in the formation of caveolae. Nat Cell Biol. 2009;11(7):807-814.
39. Banerjee M, Whiteheart SW. The ins and outs of endocytic trafficking in platelet functions. Curr Opin Hematol. 2017;24(5):467-474.
40. Park R, Shen H, Liu L, Liu X, Ferguson SM, De Camilli P. Dynamin triple knockout cells reveal off target effects of commonly used dynamin inhibitors. J Cell Sci. 2013;126(22):5305-5312.
41. Preta G, Cronin JG, Sheldon IM. Dynasore - not just a dynamin inhibitor. Cell Commun Signal. 2015;13:24.
42. Ezumi Y, Kodama K, Uchiyama T, Takayama H. Constitutive and functional association of the platelet collagen receptor glycoprotein VI-Fc receptor gamma-chain complex with membrane rafts. Blood. 2002;99(9):3250-3255.
43. Quinton TM, Kim S, Jin J, Kunapuli SP. Lipid rafts are required in Galpha(i) signaling downstream of the P2Y12 receptor during ADP-mediated platelet activation. J Thromb Haemost. 2005;3(5):1036-1041.
44. Rabie T, Varga-Szabo D, Bender M, et al. Diverging signaling events control the pathway of GPVI down-regulation in vivo. Blood. 2007;110(2):529-535.
45. Gomez TS, Hamann MJ, McCarney S, et al. Dynamin 2 regulates T cell activation by controlling actin polymerization at the immunological synapse. Nat Immunol. 2005;6(3):261-270.
46. Pearce AC, Senis YA, Billadeau DD, Turner M, Watson SP, Vigorito E. Vav1 and vav3 have critical but redundant roles in mediating platelet activation by collagen. J Biol Chem. 2004;279(52):53955-53962.
47. Poulter NS, Pollitt AY, Owen DM, et al. Clustering of glycoprotein VI (GPVI) dimers upon adhesion to collagen as a mechanism to regulate GPVI signaling in platelets. J Thromb Haemost. 2017;15(3):549-564.
48. Kato K, Kanaji T, Russell S, et al. The contribution of glycoprotein VI to stable platelet adhesion and thrombus formation illustrated by targeted gene deletion. Blood. 2003;102(5):1701-1707.
49. Morowski M, Vogtle T, Kraft P, Kleinschnitz C, Stoll G, Nieswandt B. Only severe thrombocytopenia results in bleeding and defective thrombus formation in mice. Blood. 2013;121(24):4938-4947.
50. Gould WR, Simioni P, Silveira JR, Tormene D, Kalafatis M, Tracy PB. Megakaryocytes endocytose and subsequently modify human factor V in vivo to form the entire pool of a unique platelet-derived cofactor. J Thromb Haemost. 2005;3(3):450-456.
51. Klement GL, Yip TT, Cassiola F, et al. Platelets actively sequester angiogenesis regulators. Blood. 2009;113(12):2835-2842.
52. Burgener R, Wolf M, Ganz T, Baggiolini M. Purification and characterization of a major phosphatidylserine-binding phosphoprotein from human platelets. Biochem J. 1990;269(3):729-734.
53. Tsai HJ, Huang CL, Chang YW, et al. Disabled-2 is required for efficient hemostasis and platelet activation by thrombin in mice. Arterioscler Thromb Vasc Biol. 2014;34(11):2404-2412.
54. Yu CH, Rafiq NB, Cao F, et al. Integrin-beta3 clusters recruit clathrin-mediated endocytic machinery in the absence of traction force. Nat Commun. 2015;6:8672.

Ferrata Storti Foundation

Haematologica 2020
Volume 105(5):1424-1435

The contact system proteases play disparate roles in streptococcal sepsis

Juliane Köhler,[1] Claudia Maletzki,[2] Dirk Koczan,[3] Marcus Frank,[4] Carolin Trepesch,[1*] Alexey S. Revenko,[5] Jeffrey R. Crosby,[5] A. Robert Macleod,[5] Stefan Mikkat[6] and Sonja Oehmcke-Hecht[1]

[1]Institute of Medical Microbiology, Virology and Hygiene, Rostock University Medical Center, Rostock, Germany; [2]Department of Internal Medicine, Medical Clinic III - Hematology, Oncology, Palliative Care, Rostock University Medical Center, Rostock, Germany; [3]Center for Medical Research – Core Facility Micro-Array-Technologie, Rostock University Medical Center, Rostock, Germany; [4]Medical Biology and Electron Microscopy Centre, Rostock University Medical Center, Rostock, Germany; [5]Department of Antisense Drug Discovery, Ionis Pharmaceuticals Inc., Carlsbad, CA, USA and [6]Core Facility Proteome Analysis, Rostock University Medical Center, Rostock, Germany

**Current address: Department of Anesthesiology and Operative Intensive Care Medicine, Campus Virchow-Klinikum, Charité - Universitätsmedizin Berlin; Freie Universität Berlin, Humboldt-Universität zu Berlin, and Berlin Institute of Health, Berlin, Germany*

ABSTRACT

Sepsis causes an activation of the human contact system, an inflammatory response mechanism against foreign surfaces, proteins and pathogens. The serine proteases of the contact system, factor XII and plasma kallikrein, are decreased in plasma of septic patients, which was previously associated with an unfavorable outcome. However, the precise mechanisms and roles of contact system factors in bacterial sepsis are poorly understood. We, therefore, studied the physiological relevance of factor XII and plasma kallikrein in a mouse model of experimental sepsis. We show that decreased plasma kallikrein concentration in septic mice is a result of reduced mRNA expression plasma prekallikrein gene, indicating that plasma kallikrein belong to negative acute phase proteins. Investigations regarding the pathophysiological function of contact system proteases during sepsis revealed different roles for factor XII and plasma kallikrein. *In vitro*, factor XII decelerated bacteria induced fibrinolysis, whereas plasma kallikrein supported it. Remarkably, depletion of plasma kallikrein (but not factor XII) by treatment with antisense-oligonucleotides, dampens bacterial dissemination and growth in multiple organs in the mouse sepsis model. These findings identify plasma kallikrein as a novel host pathogenicity factor in *Streptococcus pyogenes* sepsis.

Correspondence:

SONJA OEHMCKE-HECHT
sonja.oehmcke-hecht@med.uni-rostock.de

Received: April 3, 2019.

Accepted: July 12, 2019.

Pre-published: July 18, 2019.

doi:10.3324/haematol.2019.223545

Check the online version for the most updated information on this article, online supplements, and information on authorship & disclosures: www.haematologica.org/content/105/5/1424

Introduction

Sepsis and severe sepsis are life-threatening complications caused by a dysregulated host response to bacterial infection and activation of coagulation. The liver plays a key role in these events due to the acute phase protein response, an increased or decreased synthesis of host defense and coagulation proteins. Increased production of acute phase proteins contribute to a procoagulant state in sepsis, especially by enhancing production of procoagulants such as fibrinogen, and by decreasing liver synthesis of antithrombin.[1] A procoagulant state is thought to be protective against bacterial dissemination, as local activation of coagulation traps bacteria in a fibrin mesh and activates inflammatory reactions.[2,3] Inhibition of fibrinolysis may support this process further, since highly invasive pathogens exploit the host fibrinolytic system to degrade fibrin clots and overcome tissue barriers.[2] *Streptococcus pyogenes* is a Gram-positive major human pathogen causing mainly local infections of the skin and mucous membranes such as erysipelas or tonsillitis. Local infections occasionally develop into serious systemic complications, of which streptococcal toxic shock syndrome and necrotizing fasciitis are associated with high morbidity and mortality.[3]

Virulence factors of *S. pyogenes* have been studied intensively, and conversion of human plasminogen to plasmin by bacterial streptokinase is a mechanism which supports bacterial dissemination.[4] Streptokinase-activated plasmin also activates the human contact system, an inflammatory response mechanism against artificial material and pathogens.[5] The human contact system consists of two proteases, factor XII (FXII) and plasma prekallikrein (PPK), as well as the co-factor high molecular weight kininogen (HK). The proteins are produced in the liver and circulate as zymogens in the blood stream or are assembled on endothelial cells, neutrophils, and platelets. When blood is exposed to foreign artificial or biological surfaces, contact factors bind to it, and FXII becomes auto-activated and converts PPK to plasma kallikrein (PK). PK, which circulates in a non-covalent complex with HK,[6] cleaves HK and the proinflammatory peptide bradykinin is released.[7] In severe sepsis, activation of the contact system is archetypal[8] and multiple animal studies with different pharmacological interventions that inhibit FXII, bradykinin receptors or the interaction of contact factors with the bacterial surface[9] were carried out to evaluate potential therapeutic options.[10] However, surprisingly little is known about the precise role of contact factors during microbial sepsis. Here, therefore, we studied the physiological role of FXII- and PK in a mouse model of experimental sepsis. We found that hepatic expression of *F12* and *Klkb1* genes after infection with *S. pyogenes* is quickly reduced upon streptococcal infection. Moreover, a knockdown of *Klkb1* gene expression by antisense-oligonucleotide (ASO) technology prior to infection diminishes bacterial spreading, but knockdown of F12 did not influence bacterial dissemination. Our data indicate different *in vivo* roles for FXII and PK in streptococcal sepsis.

Methods

A detailed description of materials and methods with additional information is provided in the *Online Supplementary Appendix*.

Antisense-oligonucleotides

Antisense-oligonucleotides (ASO) for *Klkb1* or *F12* mRNA knockdown *in vivo* were provided by Ionis Pharmaceuticals and have been described previously.[11]

Infection of HepG2 cells

Details are provided in the *Online Supplementary Appendix*.

mRNA analysis

Total RNA was isolated from HepG2 cells or homogenized mouse liver with RNeasy Plus Mini Kit (Qiagen). RNA quality was checked with Agilent RNA 6000 Nano Kit (Agilent Technologies) and RNA concentration determined with Qubit™ RNA HS Assay Kit (Invitrogen). All analyses were performed according to the manufacturer's instructions. 800 ng total RNA was converted to cDNA using the High-Capacity cDNA Reverse Transcription Kit (Applied Biosystems) and the complementary DNA obtained used for real-time quantitative polymerase chain reaction (PCR). Reaction mixture (20 ML) containing gene specific nuclease assay (Taqman Universal PCR Master Mix; Applied Biosystems) and cDNA was amplified as follows: denaturation at 95°C for 10 minutes (min) and 45 cycles at 95°C for 15 seconds (sec) and 60°C for 1 min. GAPDH (human or rodent) was used as housekeeping gene. Relative expression was calculated using the 2– ct method.

Clotting assays

Details are provided in the *Online Supplementary Appendix*.

Clot lysis time

A clot was generated in human normal, FXII- or PK-deficient plasma by addition of PT-Reagent. In some experiments, CTI (75 μg/mL), PKSI (10 M), FXIIa (50 μg/mL) or PK (50 μg/mL) was added before clot formation was induced. The clot was incubated for 5 min at 37°C before Streptokinase (100 Units), uPA (10 μg/mL g) or tPa (10 μg) was added. Time until clot lysis was determined in a coagulometer.

Measurement of FXII and plasma kallikrein in plasma

Details are provided in the *Online Supplementary Appendix*.

Proteolytic potential for plasma kallikrein/factor XIIa activity in mouse plasma

Pooled plasma from four mice/group was incubated with Dapptin and FXIIa/PK activity was determined in a microplate reader by chromogenic substrate S-2302 (Chromogenix). (*See Online Supplementary Appendix*).

Plasma clot escape experiments

See *Online Supplementary Appendix*.

Light and scanning electron microscopy

See *Online Supplementary Appendix* and Oehmcke *et al.*[12] and Isenring *et al.*[13]

Fibrinogen degradation

Fibrinogen was mixed with either plasmin, plasminogen and streptokinase, FXII, PPK, or PBS as negative control. (See *Online Supplementary Appendix*). The mix was incubated at 37°C and at indicated time points samples were analyzed by SDS-Page and western blot using fibrinogen antibody (Santa Cruz). Relative fibrinogen levels were determined by densitometry analysis (ImageStudioLite 5.2.5).

Animal experiments

Eight-week-old female BALB/c mice (weight 16-18g) (Charles River Laboratories) were treated with ASO through intraperitoneal injections, with a dose of 800 μg/mouse, twice per week for three weeks (total 7 injections, each with 800 μg ASO/mouse).

The subcutaneous infection model with *S. pyogenes* AP1 strain and determination of bacterial dissemination were performed as described previously.[12] (See also *Online Supplementary Appendix*). This study was performed in strict accordance with the recommendations in the Guide for the Care and Use of Laboratory Animals of the National Institutes of Health. The protocol was approved by the Committee on the Ethics of Animal Experiments the Landesveterinär- und Lebensmitteluntersuchungsamt Rostock (Permit n. 7221.3-1-002/16).

Plasma proteome

The methods are provided in the *Online Supplementary Appendix*.

Patient samples

Patients with sepsis, severe sepsis, or septic shock were enrolled from the Intensive Care Medicine Unit at University Medical Center of Rostock, as described previously.[14] The protocol had been approved by our Institutional Ethics committee (A 201151), and informed consent was obtained from the patients or their caring relatives.

Results

Plasma proteome from septic mice

In order to gain more information about contact factors in sepsis, we performed a quantitative proteome analysis of plasma from healthy or *S. pyogenes*-infected mice. The subcutaneous infection model has been shown to become septic and activate the contact system,[9] which is similar to the situation encountered in human streptococcal toxic shock syndrome.[15] Plasma was collected 24 hours (h) after infection and a total number of 137 proteins including PK, kininogen-1 and FXII could be quantified based on the abundance of at least two peptides (*Online Supplementary Table S1*). There was a rise in the concentration of 38 proteins due to infection (*Online Supplementary Table S2*). Within this set of elevated proteins, typical positive acute phase proteins such as serum amyloid, C-reactive protein or fibrinogen were detected. In addition, we also identified 47 proteins with significantly decreased concentration due to infection (Table 1). Here, again, we found classical negative acute phase proteins such as retinol binding protein or antithrombin III. PK concentrations were significantly reduced in infected animals (Table 1). Kininogen-1 and FXII levels were also reduced; however, this was not statistically significant (*Online Supplementary Table S1*).

F12 and Klkb1 mRNA levels decline *in vitro* and *in vivo* after infection with *S. pyogenes*

We next investigated *in vitro* how mRNA expression of contact factors is affected in liver cells in response to infection. HepG2 cells were treated with IL6 or living bacteria and mRNA was analyzed by quantitative real-time PCR. In accordance with Citarella *et al.*,[16] F12 mRNA levels were significantly decreased in cells treated with IL6 for 6 and 24 h (Figure 1A). The same was observed in cells infected with *S. pyogenes* (Figure 1A). *Klkb1* mRNA levels also significantly declined upon treatment with either IL6 or *S. pyogenes* (Figure 1B).

To investigate the hepatic expression of Klkb1 and F12 mRNA *in vivo*, we used the streptococcal murine sepsis model. Mice were infected subcutaneously with 1.5-2x10^7 colony forming units (CFU) of *S. pyogenes* and samples collected 6 and 24 h after infection. Six h after infection, *Klkb1* mRNA levels were reduced by approximately 50% compared to non-infected controls (Figure 1C). Twenty-four h after infection, *Klkb1* mRNA levels dropped down to undetectable levels (Figure 1C), indicating that *Klkb1* mRNA production was discontinued upon bacterial spreading. Relative expression of F12 was also significantly reduced at 6 and 24 h after infection (Figure 1D); however, this effect was not as pronounced as for the *Klkb1* gene. We also measured fibrinogen alpha (FGA) mRNA levels and found significantly increased FGA expression at 6 and 24 h after infection (Figure 1E), which is consistent with the data from proteome analysis. Ninety-percent of mice were bacteremic at 6 h after infection, containing bacteria in their liver and/or spleen (Figure 1F).

Plasma kallikrein concentration decline significantly *in vivo* after infection with *S. pyogenes*

In accordance with the quantitative proteome analysis and *Klkb1* mRNA data, we detected a significant decrease in PK levels in mice 24 h after infection, and an even greater decrease 48 h after infection (Figure 2A). This was accompanied by a decreased proteolytic potential of PK/FXIIa in plasma after activation with Dapptin reagent (Figure 2B), and a significantly prolonged activated partial thromboplastin time (aPTT) (Figure 2C) but not PT (Figure 2D). In accordance with mass spectrometry data, FXII plasma levels did not change significantly in infected mice (*data not shown*).

Knockdown of plasma prekallikrein diminishes streptococcal dissemination, dampens kidney damage, cyto- and chemokines, but raises RANTES

Such quick downregulation of protein expression during sepsis implicates that the protein is not required, or is even harmful, under these conditions. To investigate the functional contribution of PK and FXII during sepsis, we inhibited *Klkb1* or *F12* gene expression by antisense oligonucleotides (ASO), using established protocols,[11,17] prior to infection with *S. pyogenes*. As expected, pre-treatment of female BALB/c mice with PPK ASO (*Online Supplementary Figure S1A*) or FXII ASO (*Online Supplementary Figure S1B*) reduces relative expression levels more than 90%, which is in accordance with previous studies in male BALB/c mice. As shown before,[11,17] plasma protein level of PPK on FXII depletion, or FXII on PPK depletion, were increased (*Online Supplementary Figure S1C-F*). This indicates stabilization of FXII or PPK as response to decreased basal activation. As a consequence of PPK or FXII knockdown, decreased proteolytic potential of PK/FXIIa (*Online Supplementary Figure S1G*) and prolongation of activated partial thromboplastin time (aPTT) (*Online Supplementary Figure S1H*) in plasma was demonstrated, compared to mice treated with control ASO. Moreover, as expected, PT was not affected by the treatment with either ASO (*data not shown*).

The PPK and FXII-depleted mice were challenged with *S. pyogenes* as described above. Bacterial dissemination and histopathology of the kidneys was determined 24 h after infection. PPK-depleted mice had significantly fewer bacteria in the spleen and blood compared to control-ASO mice (Figure 3A and B). Intriguingly, there was no difference in bacterial loads in spleen, blood or kidneys between FXII-depleted mice and controls (*data not shown*).

Formation of microvascular fibrin deposition in kidneys was described in lethal human sepsis.[18] In our animal model, fibrin was detected 24 h after subcutaneous (sc.) infection in kidneys from septic animals (Figure 3C). A quantification of fibrin areas (> 5 μm) on a scale from 0 to 3 (0: absent; 1: ≤ 20 fibrin areas; 2: 20-50 fibrin areas; 3: >50 fibrin areas) revealed that the mean score in PPK-ASO treated animals was lower (1.7) than that of the control-ASO treated group (2.0) or the FXII-ASO treated group (2.5). This was reflected by increased creatinine values in plasma from control-ASO (8±2.9 μmol/L) and FXII-ASO (8.25±1.9 μmol/L) mice, compared to values in PPK-ASO mice (6±1 μmol/L).

In addition, a panel of 20 cytokines, chemokines and growth factors was measured in healthy, infected control-ASO and PPK-ASO treated mice. Infection boosted the pro-inflammatory response yielding a robust increase of 17 cytokines/chemokines. In agreement with lower bacterial loads, infected PPK-ASO treated mice had significantly lower levels of Gm-CsF (Figure 4A) MIP-1 beta (Figure 4B), and MIP-2 (Figure 4C) compared to infected control mice. Interestingly, CCL5 was significantly increased in infected PPK-ASO mice compared to infected controls (Figure 4D).

Table 1. Plasma proteins from infected mice detected by mass spectrometry analysis that were significantly down-regulated, compared to healthy mice.

Accession	Protein	Fold change infected/control	Anova (*P*)
Q00724	Retinol-binding protein 4	0.08	2.17E-09
P49182	Heparin cofactor 2	0.19	1.50E-05
O70362	Phosphatidylinositol-glycan-specific phospholipase D	0.21	7.41E-06
P41317	Mannose-binding protein C	0.32	2.66E-04
P01675	Ig kappa chain V-VI region XRPC 44	0.32	5.87E-04
P03987	Ig gamma-3 chain C region	0.32	4.16E-06
Q61268	Apolipoprotein C-IV	0.33	5.79E-04
P26262	Plasma kallikrein	0.37	2.42E-04
P42703	Leukemia inhibitory factor receptor	0.38	1.30E-04
Q9DBB9	Carboxypeptidase N subunit 2	0.40	8.67E-07
P01898	H-2 class I histocompatibility antigen_ Q10 alpha chain	0.42	2.00E-04
Q9JJN5	Carboxypeptidase N catalytic chain	0.42	2.95E-04
Q07968	Coagulation factor XIII B chain	0.44	3.61E-07
Q9Z1R3	Apolipoprotein M	0.44	8.43E-04
Q61730	Interleukin-1 receptor accessory protein	0.45	6.01E-05
Q8BH61	Coagulation factor XIII A chain	0.45	1.18E-02
Q9R098	Hepatocyte growth factor activator	0.46	3.31E-04
Q06770	Corticosteroid-binding globulin	0.47	2.25E-04
Q8VCS0	N-acetylmuramoyl-L-alanine amidase	0.48	1.55E-03
O89020	Afamin	0.49	1.28E-06
P33622	Apolipoprotein C-III	0.49	3.90E-04
Q60994	Adiponectin	0.50	1.33E-02
P01887	Beta-2-microglobulin	0.50	1.98E-03
P01642	Ig kappa chain V-V region L7 (Fragment)	0.50	1.26E-03
P01863	Ig gamma-2A chain C region_ A allele	0.50	2.38E-02
P51885	Lumican	0.51	1.81E-03
P07309	Transthyretin	0.51	5.89E-04
P03953	Complement factor D	0.53	2.81E-02
P13020	Gelsolin	0.53	1.87E-04
Q9QWK4	CD5 antigen-like	0.54	1.19E-03
Q06890	Clusterin	0.54	6.55E-05
P01787	Ig heavy chain V regions TEPC 15/S107/HPCM1/HPCM2/HPCM3	0.55	1,75E-02
P29699	Alpha-2-HS-glycoprotein	0.55	2.09E-04
P01806	Ig heavy chain V region 441	0.56	2.29E-02
Q64726	Zinc-alpha-2-glycoprotein	0.60	3.34E-05
P28665	Murinoglobulin-1	0.63	1.80E-04
P28666	Murinoglobulin-2	0.64	2.88E-04
P14106	Complement C1q subcomponent subunit B	0.64	1.23E-02
P01631	Ig kappa chain V-II region 26-10	0.65	1.55E-02
Q9ESB3	Histidine-rich glycoprotein	0.65	1.06E-02
P01867	Ig gamma-2B chain C region	0.66	3.93E-02
P23953	Carboxylesterase 1C	0.66	5.23E-03
Q61129	Complement factor I	0.66	3.33E-04
P32261	Antithrombin-III	0.66	1.07E-03
P01872	Immunoglobulin heavy constant mu	0.66	6.51E-03
P01843	Ig lambda-1 chain C region	0.67	2.40E-02
P01868	Ig gamma-1 chain C region secreted form	0.67	4.62E-03

Role of contact factors in bacterial-triggered fibrinolysis

S. pyogenes activates plasminogen to escape from the local site of infection;[4] however, knockdown of PPK decelerated bacterial spreading in mice, implicating a role of PK in bacteria-induced fibrinolysis. To further explore the human relevance to our findings, we employed *in vitro* plasma clot-lysis assays in normal human plasma and congenital FXII- or PPK-deficient plasma, followed by incubation with streptokinase or the host plasminogen activators uPA and tPA. Clot lysis in PPK-deficient plasma was significantly longer, regardless of the fibrinolysis activator used (Figure 5A). In contrast, clot lysis in FXII-deficient plasma was significantly shorter compared to normal plasma. When corn trypsin inhibitor (CTI), a FXII inhibitor, was added to normal plasma, the clot lysis, induced by streptokinase, was again significantly shorter compared to normal plasma (Figure 5B). Similarly, the addition of the PK

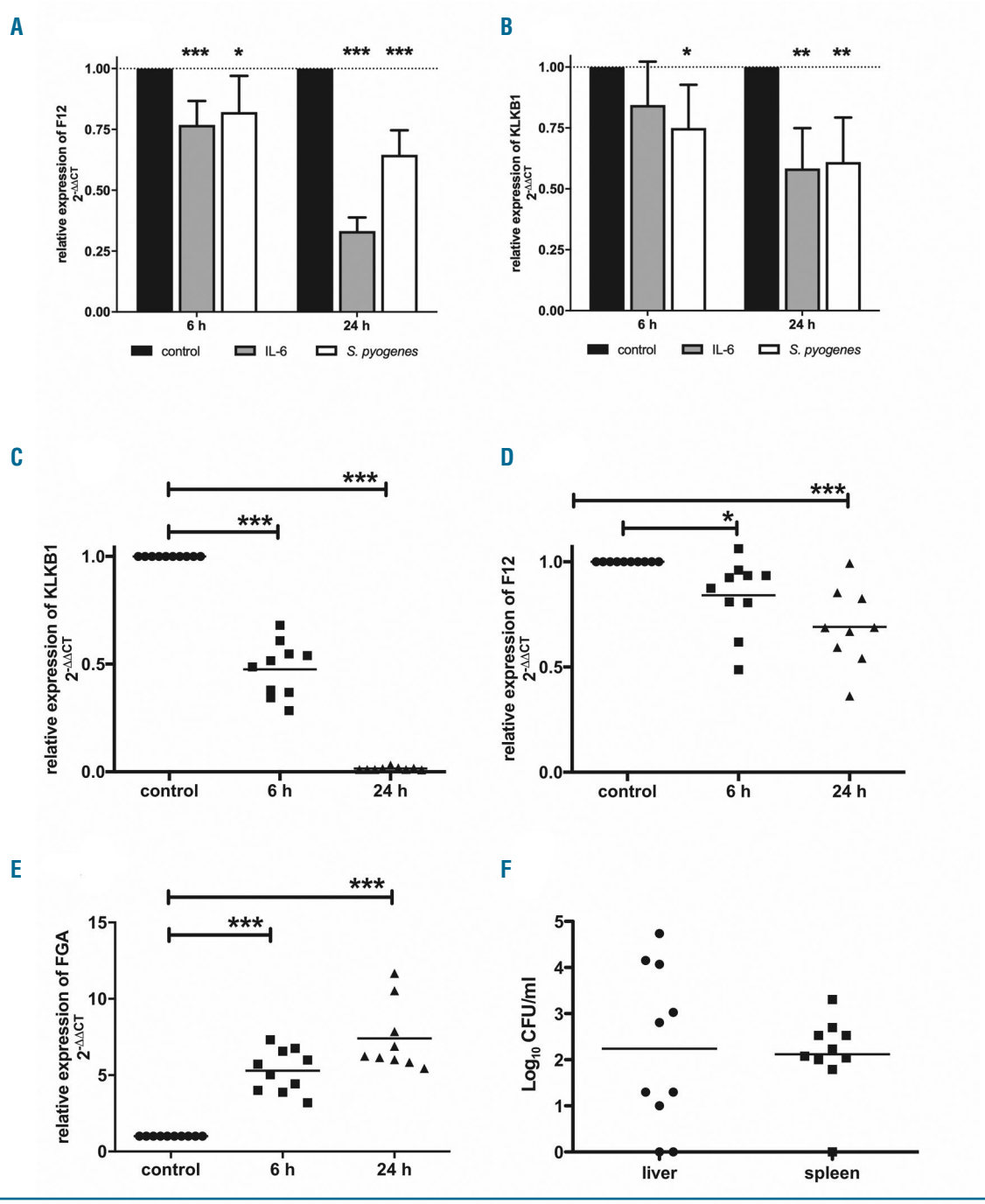

Figure 1. Decreased mRNA levels of *F12* and *Klkb1 in vitro* and *in vivo* after infection with *S. pyogenes*. (A and B) HepG2 cells (2x10^5 cells/mL) were incubated with IL6 (50 ng/mL) or *S. pyogenes* [2x10^6 colony forming units (CFU)/mL] for 6 hours (h). After incubation, cells were washed and the medium was replaced with fresh medium containing 1% PenStrep. After 6 and 24 h, cells were harvested, total RNA was isolated, and real-time polymerase chain reaction (PCR) TaqMan® gene expression assays were performed. N≥9. (*P≤0.05; **P≤0.01; ***P≤0.001). (C-F) Groups of mice (n=8-10) were subcutaneously (sc.) infected with 2x10^7 CFU/mouse of *S. pyogenes* AP1. Animals were killed 6 and 24 h after infection, and liver tissue was collected for total RNA isolation (C-E) and real-time PCR TaqMan® gene expression assays were performed. (F) Spleen and liver were homogenized and the number of CFU was quantified 6 h after infection. *P≤0.05; ***P≤0.001.

inhibitor PKSI19 to normal plasma prolonged clot lysis induced by streptokinase (Figure 5B). Complementation of human congenital FXII- or PPK-deficient plasma with activated enzymes (FXIIa or PK) could reverse shortening or prolongation of clot lysis by streptokinase (Figure 5B). Plasminogen content was slightly reduced in FXII-deficient plasma (97±5 μg/mL) comparing to pooled normal plasma (141μ8 μg/mL) or PPK deficient plasma (123μ28 μg/mL). However, plasmin activity after activation with streptokinase was similar in all plasma types (*Online Supplementary Figure S2A*), providing proof that the streptokinase/plasmin activity is not inhibited due to different donors.

Activation of fibrinolysis results in the release of D-dimer from cross-linked fibrin; thus, we measured the content of D-dimer in the supernatant from human plasma clots, which contained *S. pyogenes* bacteria. Twenty minutes after incubation, D-dimer were detected in samples from clots in FXII-deficient plasma, but not in samples from clots in normal or PPK-deficient plasma (Figure 5C). Thirty minutes after incubation, D-dimer could be detected from clots in normal plasma and FXII-deficient plasma complemented with FXIIa, but still not from clots in PPK-deficient plasma. Forty-five minutes after incubation, D-dimer were detected in the supernatant of PPK-deficient plasma, and this time-lag could be reversed by complementation with PK (Figure 5C). As expected, in plasminogen-depleted plasma, no D-dimer were detected within 180 min, but after complementation with plasminogen D-dimer, release occurred after 30 min. Complete clot lysis by the bacteria could be observed when D-dimer concentration was at the highest level, i.e. after 20 min in FXII-deficient plasma, after 30 min in normal plasma, and after 45-50 min in PPK-deficient plasma.

As clot lysis time and D-dimer production were decelerated in PPK-def. plasma, we investigated whether PK might accelerate plasmin degradation of fibrinogen. Western blot analysis shows that pure fibrinogen is degraded by the streptokinase/plasminogen complex within 5- 10 min, and addition of PPK supports fibrinogen degradation further (Figure 5D and F). Of note, PPK was activated by Ska/plasminogen in the presence of fibrinogen (*Online Supplementary Figure S2C and D*). If PPK and FXII were added to fibrinogen it was degraded within 30 min, comparable to plasmin (Figure 5E and G). PPK or FXII alone had marginal effects on fibrinogen degradation, and blocking the proteases by PKSI or CTI inhibited degradation (*Online Supplementary Figure S2B*). Intriguingly, the degradation pattern of PK cleaved alpha chain of fibrinogen was different, compared to the FXII or the plasmin cleavage pattern (*Online Supplementary Figure S2E*). We conclude that PPK, activated either by streptokinase/plasminogen or by FXIIa supports plasmin mediated degradation of fibrinogen.

We also investigated the structure of plasma clots by scanning electron microscopy. Clots derived from PPK-deficient plasma had thinner fibrin strands than clots from normal or FXII-deficient plasma (Figure 5H).

Plasma kallikrein promotes bacterial escape from mouse plasma clots

Streptokinase was shown to specifically activate human plasminogen,[20] but *S. pyogenes* is able to escape from

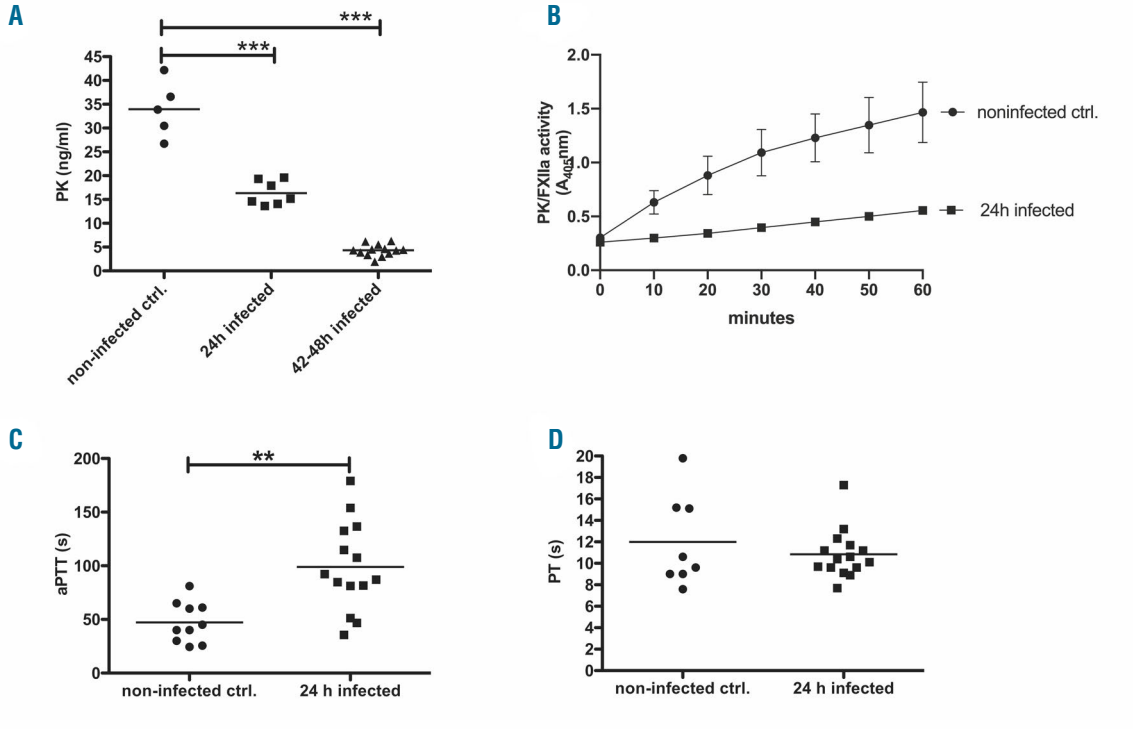

Figure 2. Analysis of plasma samples from mice after infection with *S. pyogenes*. Groups of mice (n=4-10) were subcutaneously (sc.) infected with $2x10^7$ colony forming units (CFU)/mouse of *S. pyogenes*. (A) Plasma prekallikrein (PPK) concentration in plasma was measured after 24 and 42-48 hours (h) of infection by a specific sandwich enzyme-linked immunosorbent assay. (B) Plasma samples from four mice per group were pooled and proteolytic potential of plasma kallikrein (PK)/factor XIIa (FXIIa) activity was measured using chromogenic substrate S-2302 for PK and FXIIa. (C) Activated partial thromboplastin time (aPTT) and (D) prothrombin time (PT) in plasma of infected and non-infected animals were measured using a coagulometer. *P≤0.05; **P≤0.001; ***P≤0.0001. ctrl: control.

mouse (C57BL/6)-derived plasma clots.[21] To test whether *S. pyogenes* can survive in, and escape from, plasma clots of BALB/c mice, plasma samples from control- or PPK-ASO treated animals were clotted with thrombin in the presence of *S. pyogenes*. Clots were covered with 1% plasma and incubated for up to 4 h at 37°C. Viable *S. pyogenes* count assays from the supernatants and the clots were performed. Two hours after incubation, no bacteria could be detected in the supernatant. Four hours after incubation, the supernatants of PPK-depleted clots contained significantly fewer viable bacteria compared to supernatants from control-ASO clots (Figure 6A). Thus, *S. pyogenes* is able to escape from BALB/c mouse plasma clots and PK plays an important role in this process. The relative importance of PK was confirmed in PPK-depleted plasma reconstituted with human PK, where significantly more viable bacteria (compared to PPK-depleted plasma clots) could be detected in the supernatants (Figure 6A). No difference in CFU could be determined inside the clots (Figure 6B).

It has previously been shown that PK activates plasminogen,[22] which would enhance plasmin concentration in control mice. To address this experimentally, circulating plasmin 2-antiplasmin (PAP) complexes were quantified in infected control- and PPK-ASO treated mice (Figure 6C). However, no difference between the two groups was observed, supporting the assumption that PK assist in fibrinogen degradation and might be relevant for the observed bacterial dissemination. Importantly, there was no difference in the plasminogen concentration between healthy control and PPK-ASO treated mice (Figure 6D).

Finally, plasma clots from control ASO or PPK-depleted animals incubated with *S. pyogenes* were imaged with scanning electron microscopy. Clots derived from control mice and incubated with bacteria lost their structural integrity (Figure 6E), fibrin fibers were degraded, and bacteria could not be detected within the clot (Figure 6E, left). If PPK was absent, intact fibrin fibers were visible, with bacteria trapped inside of them (Figure 6E, right).

Taken together, the data show that PK supports degradation and streptococcal escape from mouse plasma clots leading to increased bacteremia and infection of tissues.

Plasma kallikrein and FXII concentrations are significantly decreased in plasma of septic patients

We further investigated PK and FXII concentrations in plasma of 23 patients with sepsis, severe sepsis or septic shock, collected 1, 2 and 3 days after admission to the Intensive Care Unit (ICU). In most of the patients, multiple infectious sources and bacterial isolates were identified and, importantly, non-survivors had significantly prolonged aPTT compared to survivors.[14] Plasma samples from 12 healthy persons were used as controls. Both PK and FXII levels are significantly reduced in all patients compared to healthy controls (Figure 7A and B). There is no significant difference between survivors and non-survivors, or between the days of admission. The data support earlier studies, and clearly show that reduction of PK and FXII in plasma is not restricted to *S. pyogenes* sepsis.

Discussion

Local activation of contact factors on the bacterial surface may be protective against infections, due to the

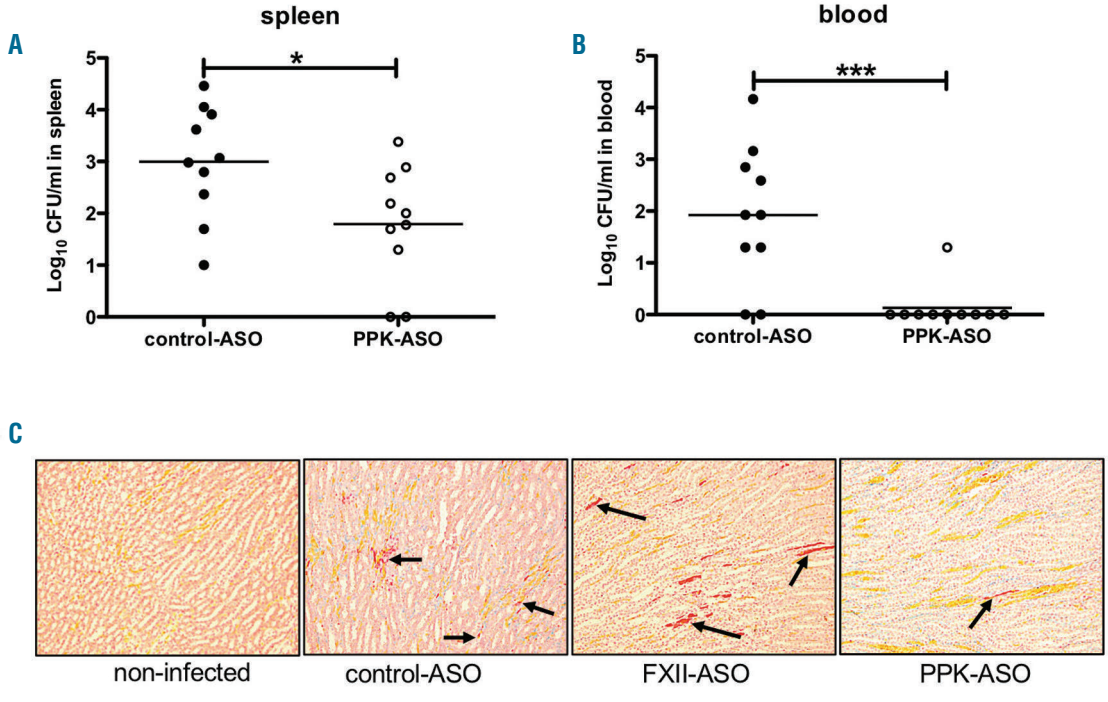

Figure 3. Bacterial spreading and histopathology of kidneys from plasma prekallikrein (PPK)- or factor XII (FXII)-depleted mice infected with *S. pyogenes*. Groups of mice were infected subcutaneously (sc.) with 1.6-2 x10^7 colony forming units (CFU)/mouse *S. pyogenes* AP1. Twenty-four hours after infection, samples were collected and (A) spleen or (B) blood of infected control-antisense-oligonucleotide (ASO) or PPK-ASO treated mice were homogenized and the number of CFU was quantified. Data are presented as means of ten mice per group and were obtained from two independent experiments. *$P \leq 0.05$; ***$P \leq 0.0001$. (C) Representative kidney tissue sections showing the medullary rays, from non-infected, control-, PPK, or FXII-ASO animals. Sections were stained (MSB-Lendrum) and fibrin depositions (marked by arrows) were detected and scored as described in the Methods section (10 x magnification).

release of antimicrobial peptides and bradykinin from HK, which trigger inflammatory reactions. On the other hand, activation of the system by the pathogen may provoke invasive spreading *via* bradykinin-induced vascular leakage.[5] We previously reported that *S. pyogenes* triggers activation of the contact system by streptokinase with the liberation of bradykinin. In addition, we showed that *S. pyogenes* isolates from invasive infections trigger an activation of the contact system more potently than strains isolated from non-invasive infections. Intriguingly, no significant difference was observed when plasmin activation was analyzed,[23] supporting the idea that the ability of certain strains to activate contact factors is associated with improved bacterial dissemination. The current study showed that PK, a serine protease of the contact system, is involved in fibrinolysis triggered by *S. pyogenes*, and supports streptococcal dissemination in mice. *In vitro*, degradation of fibrinogen and lysis of plasma clots (induced by streptokinase) was impaired in the absence of PK. We therefore, suggest that PK assist in degradation of fibrin by plasmin. This hypothesis is supported by *ex vivo* and *in vivo* experiments showing that PK is involved in *S. pyogenes* escape from mouse plasma clots and dissemination. On the other hand, our data do not exclude a direct plasminogen activation by PK that was shown before *in vitro*.[22] Of note, a knock-out of the *Klkb1* gene in mice results in an antithrombotic phenotype.[11,24] However, reduced thrombosis in *Klkb1* KO mice was not due to defective contact activation but was a result of reduced aortic tissue factor in this mouse;[24] thus, this mouse would be not suitable for our investigations. In the present study, we demonstrated that the selective reduction of PPK by ASO-technology decelerated bacterial spreading, dampens inflammatory cytokine and chemokines, and raises CCL5 (RANTES). RANTES acts as a chemoattractant for monocytes, memory Th cells, and eosinophils. As in our animal model, in humans, the level of RANTES was inversely associated with bacteremia[25] and the APACHE II score, thus low levels were predictive with poor outcome.[26,27]

FXII is the main physiological activator of PPK but, surprisingly, a knockdown of *F12* gene had no influence on bacterial dissemination in our sepsis model. Beside its function as an activator for PPK, FXII directly increases the fiber density within a clot and makes it more resistant to fibrinolysis.[28,29] Consequently, deficiency of FXII in mice or human impairs thrombus stability.[30,31] The present study supports these findings, as fibrinolysis, initiated *in vitro* by bacteria or pure streptokinase, was faster in the absence of FXII. A recent study by Stroo *et al.* showed that FXII deficiency in mice improved survival and reduced bacterial outgrowth in an airway infection model with the Gram-negative *Klebsiella pneumoniae*. However, and similar to our data, FXII deficiency did not protect mice when the Gram-positive *Streptococcus pneumoniae* was used in the airway infection model.[32]

A depletion of contact factors is often seen in sepsis patients,[15,33,34] and this was confirmed in the present study. Depletion of contact factors has been assigned to consumption resulting from massive activation of the contact system. However, although a prolonged aPTT indicated a consumption of FXII and PK in these patients, we could not observe a massive HK cleavage.[14] As contact factors are mainly synthesized in the liver, an alternative explana-

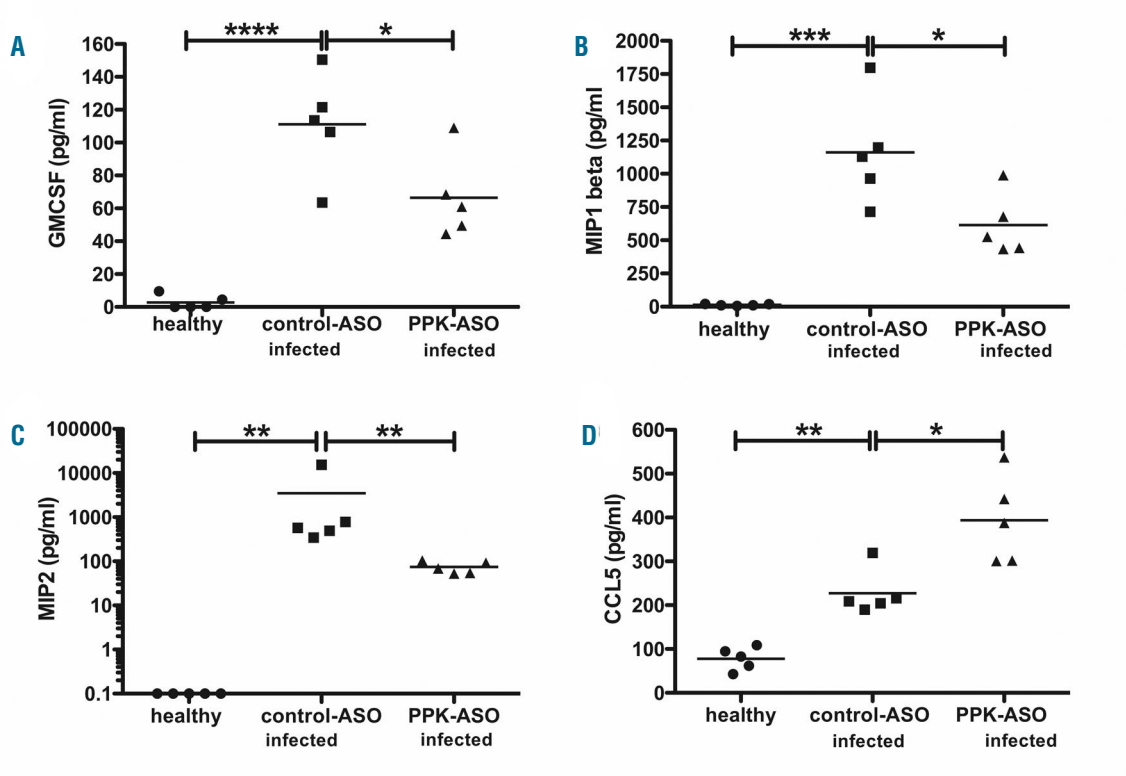

Figure 4. Proinflammatory response in plasma prekallikrein (PPK)-depleted mice infected with *S. pyogenes*. Groups of mice (n=5 per group) were infected subcutaneously (sc.) with $2x10^7$ colony forming units (CFU)/mouse *S. pyogenes* AP1. Twenty-four hours after infection animals were collected and EDTA plasma were analyzed for GmCSF (A), MIP-1 beta (B), MIP-2 (C), CCL5 (RANTES) (D), using a Multi-Plex immunoassay. *$P \leq 0.05$; **$P \leq 0.01$; ***$P \leq 0.0002$; ***$P \leq 0.0001$.

tion for low contact factor levels is downregulation of gene expression in the liver, as shown in the present study for *F12* and *Klkb1* genes in the mouse sepsis model. The knowledge about the pathophysiological role of contact factor gene expression is important for the understanding of their general functions in infection. Expression of *Klkb1* was quickly decreased due to invasive infection in mice and accompanied by a fast decrease in the protein in plasma. In addition, an earlier study has shown that the clearance rate of PK by the liver is significantly increased during the acute phase reaction.[35] Both mechanisms could contribute to low PK levels in plasma of septic patients, and this suggests that the fast reduction of PK is part of the physiological acute phase response, which supports the antifibrinolytic state. The role of the acute phase response is to enhance host defense to prevent injury of the host

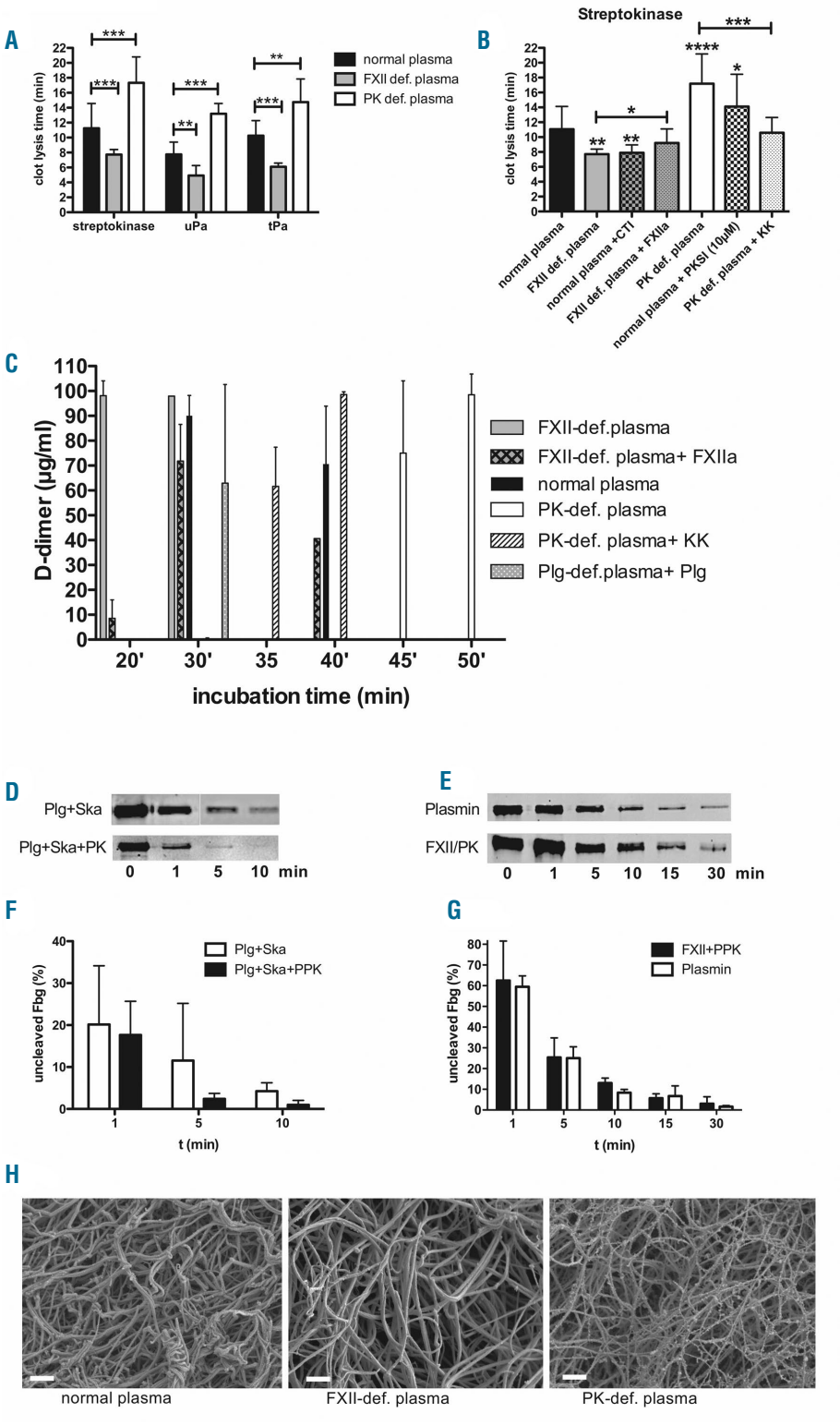

Figure 5. Effect of human congenital factor XII (FXII) or plasma prekallikrein (PPK) deficiency on fibrinolysis induced by streptokinase or *S. pyogenes* bacteria. (A) A clot was derived in normal, FXII- or PPK-deficient plasma by thromboplastin (PT)-reagent and time until clot lysis was measured after addition of streptokinase, uPA or tPA. (B) A clot was derived in normal, FXII- or PPK-deficient (def) plasma that was, if indicated, pre-incubated with CTI (75 µg/mL), PKSI (10 µM), FXIIa (50 µg/mL) or PK (50 µg/mL). Time until clot lysis was measured after addition of streptokinase. (C) Growing *S. pyogenes* ($2x10^8$ CFU/mL) were mixed with plasma, and thrombin was used to form a stable clot. The plasma clot was overlaid with PBS and D-dimer concentration in the supernatant was measured after different time points, using an ELISA. (D and E) Representative western blot analysis of fibrinogen incubated for up to 30 minutes with plasminogen+streptokinase (Plg/Ska), plasminogen+streptokinase+PPK (Plg/Ska/PPK), Plasmin, or FXII+PPK (FXII/PPK) (F and G) relative levels of uncleaved fibrinogen (Fbg), quantified by densitometry from three independent experiments. (H) Plasma clots were induced by thrombin, fixed and analyzed by Scanning electron microscopy. Bars represent 2 µm. *$P \leq 0.05$; **$P \leq 0.01$; ***$P \leq 0.001$; ****$P \leq 0.0001$. min: minutes.

within the process of killing bacteria.[1] A procoagulant state with inhibition of fibrinolysis may help to contain the bacteria at the primary site of infection. The impairment of fibrinolysis is mediated by different mechanisms, i.e. by decreasing liver synthesis of anticoagulants such as antithrombin III,[36] or increasing production of fibrinolysis inhibitors, such as thrombin-activatable fibrinolytic inhibitor (TAFI)[37] or plasminogen-activator-inhibitor 1 (PAI1).[38,39] Our investigations suggest that down-regulated *Klkb1* expression during infection likewise contributes to inhibited fibrinolysis.

The intrinsic coagulation pathway does not contribute

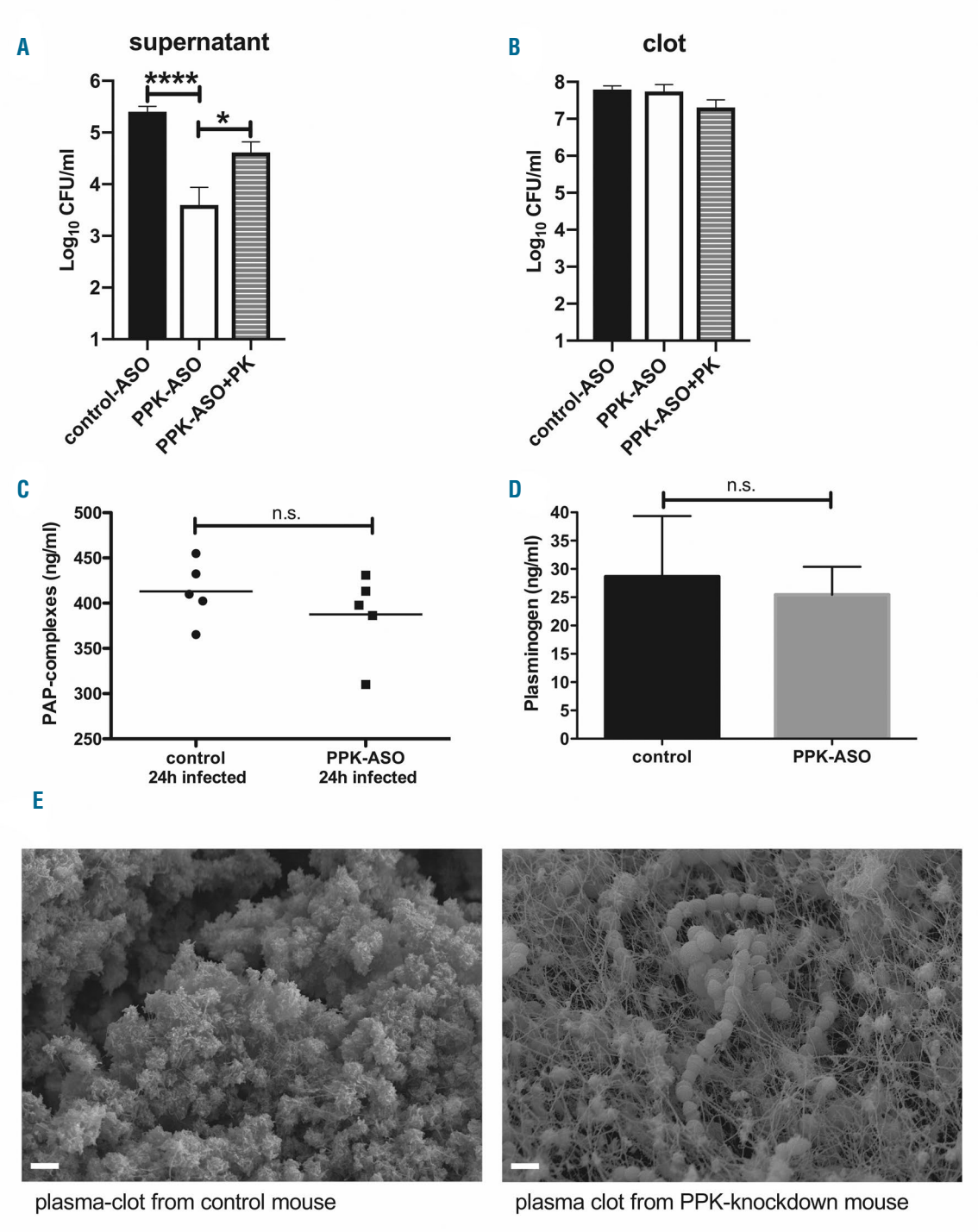

Figure 6. Antisense-oligonucleotide (ASO)-mediated plasma prekallikrein (PPK) depletion reduced bacterial escape and inhibited bacteria-triggered fibrinolysis in mouse plasma clots. (A and B) Plasma from four mice per group was pooled and mixed with $1x10^7$ colony forming units (CFU)/mL *S. pyogenes*, a stable clot was induced by addition of thrombin and $CaCl_2$, and overlaid with PBS, containing 1% plasma. After 4 hours (h), the bacterial loads in the supernatant (A) and homogenized clots (B) were determined by plating. N=4. *P=0.0323; ****P<0.0001. (C) PAP complexes or plasminogen content (D) were determined in EDTA plasma from infected control- or PPK-ASO treated mouse, n=5 per group. (E) Plasma was mixed with $1x10^9$ CFU/mL *S. pyogenes* and clot formation was induced by addition of thrombin and $CaCl_2$. After 4 h of incubation at 37 °C, clots were fixed and analyzed by Scanning electron microscopy. Bars represent 2 μm. PK: plasma kallikrein; n.s. not significant.

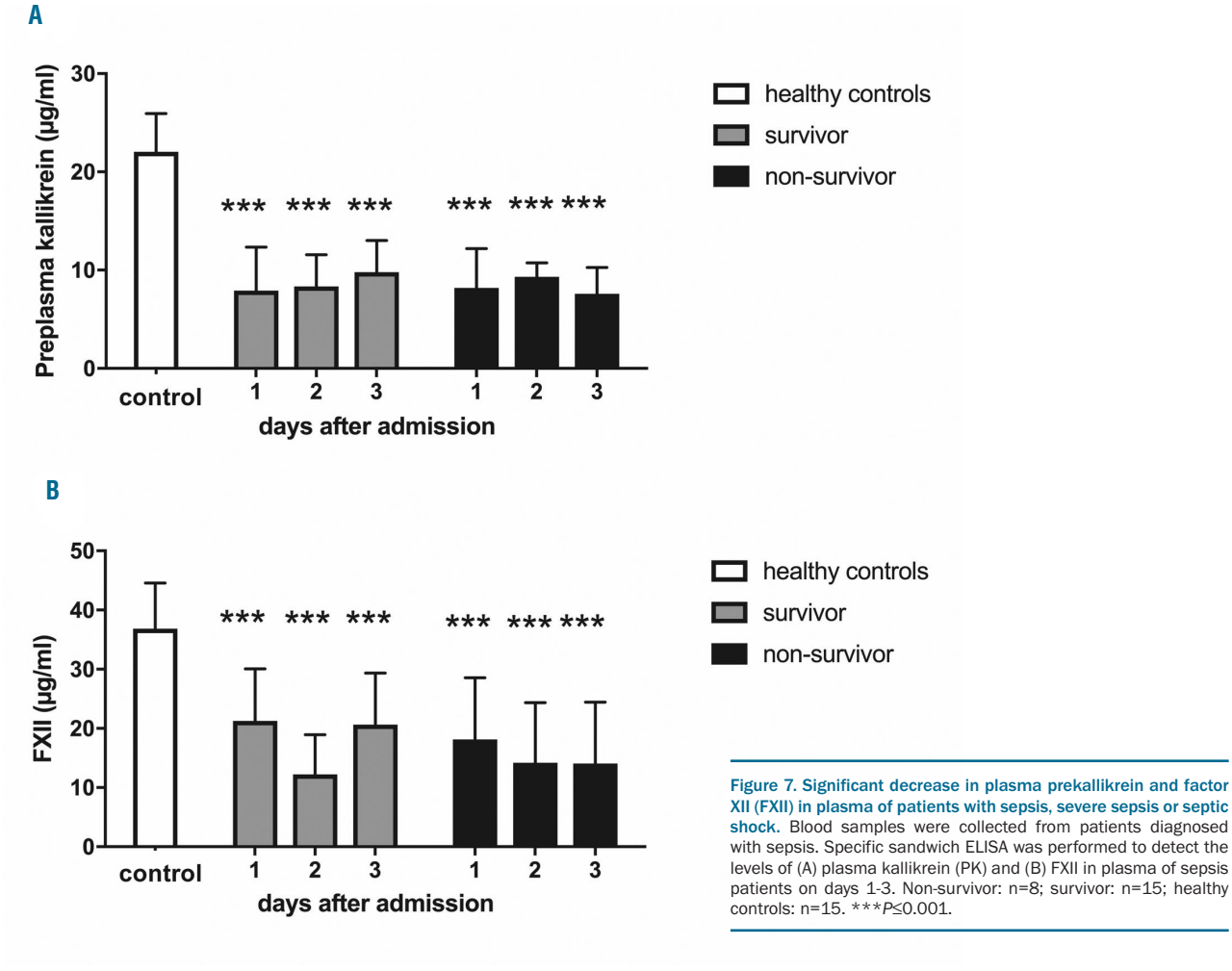

Figure 7. Significant decrease in plasma prekallikrein and factor XII (FXII) in plasma of patients with sepsis, severe sepsis or septic shock. Blood samples were collected from patients diagnosed with sepsis. Specific sandwich ELISA was performed to detect the levels of (A) plasma kallikrein (PK) and (B) FXII in plasma of sepsis patients on days 1-3. Non-survivor: n=8; survivor: n=15; healthy controls: n=15. ***$P \leq 0.001$.

to physiological hemostasis, and activation occurs *in vivo* always under pathological conditions, such as thrombosis, sepsis, or ARDS.[40-42] This is the first study that investigated the functional contribution of PK in host defense to bacterial sepsis in rodent and human systems. The study shows that FXII and PK play distinct roles within the infection process. PK supports streptococcal spreading by its profibrinolytic function, whereas, in our model, FXII did not influence bacterial dissemination.

Acknowledgments

We thank Jana Bull (IMIKRO) and Dr. Armin Springer (EMZ) for excellent technical assistance and Dr. Ulf Broschewitz for assessment of histology. We are also grateful to Ionis Pharmaceutical for providing us with ASO.

Funding

This study was supported by a grant from the Deutsche Forschungsgemeinschaft (project OE 547/ 4-1). SOH was supported by the Federal Excellence Initiative of Mecklenburg Western Pomerania and European Social Fund (ESF) Grant KoInfekt (ESF_14-BM-A55-00xx_16) and by a grant from the Medical Faculty of the University of Rostock in the framework of the FORUN program 2018.

References

1. Dhainaut JF, Marin N, Mignon A, Vinsonneau C. Hepatic response to sepsis: Interaction between coagulation and inflammatory processes. Crit Care Med. 2001;29(7):S42–S47.
2. Lähteenmäki K, Edelman S, Korhonen TK. Bacterial metastasis: the host plasminogen system in bacterial invasion. Trends Microbiol. 2005;13(2):79–85.
3. Walker MJ, Barnett TC, McArthur JD, et al. Disease manifestations and pathogenic mechanisms of group a Streptococcus. Clin Microbiol Rev. 2014;27(2):264–301.
4. Sun H, Ringdahl U, Homeister JW, et al. Plasminogen is a critical host pathogenicity factor for group A streptococcal infection. Science. 2004;305(5688):1283–1286.
5. Oehmcke-Hecht S, Köhler J. Interaction of the human contact system with pathogens-An update. Front Immunol. 2018;9:312.
6. Mandle RJ, Colman RW, Kaplan AP. Identification of Prekallikrein and High-Molecular-Weight Kininogen as a Complex in Human-Plasma. Proc Natl Acad Sci USA. 1976;73(11):4179–4183.
7. Colman RW, Schmaier AH. Contact system: a vascular biology modulator with anticoagulant, profibrinolytic, antiadhesive, and proinflammatory attributes. Blood. 1997;90(10):3819–3843.
8. Schmaier AH. Physiologic activities of the contact activation system. Thromb Res. 2014;133 Suppl 1:S41–44.
9. Oehmcke S, Shannon O, Köckritz-Blickwede von M, et al. Treatment of invasive streptococcal infection with a peptide derived from human high-molecular weight kininogen. Blood. 2009;114(2):444–451.

10. Nicola H. The role of contact system in septic shock: the next target? An overview of the current evidence. J Intensive Care. 2017;5(1):31.
11. Revenko AS, Gao D, Crosby JR, et al. Selective depletion of plasma prekallikrein or coagulation factor XII inhibits thrombosis in mice without increased risk of bleeding. Blood. 2011;118(19):5302–5311.
12. Oehmcke S, Westman J, Malmström J, et al. A novel role for pro-coagulant microvesicles in the early host defense against streptococcus pyogenes. PLoS Pathog. 2013;9(8):e1003529.
13. Isenring J, Köhler J, Nakata M, et al. Streptococcus gallolyticus subsp. gallolyticus endocarditis isolate interferes with coagulation and activates the contact system. Virulence. 2017;9(1):1–31.
14. Trepesch C, Nitzsche R, Glass A, et al. High intravascular tissue factor-but not extracellular microvesicles-in septic patients is associated with a high SAPS II score. J Intensive Care. 2016;4:34.
15. Sriskandan S, Cohen J. Kallikrein-kinin system activation in streptococcal toxic shock syndrome. Clin Infect Dis. 2000;30(6):961–962.
16. Citarella F, Felici A, Brouwer M, et al. Interleukin-6 downregulates factor XII production by human hepatoma cell line (HepG2). Blood. 1997;90(4):1501–1507.
17. Bhattacharjee G, Revenko AS, Crosby JR, et al. Inhibition of vascular permeability by antisense-mediated inhibition of plasma kallikrein and coagulation factor 12. Nucleic Acid Ther. 2013;23(3):175–187.
18. Aslan A, van den Heuvel MC, Stegeman CA, et al. Kidney histopathology in lethal human sepsis. Crit Care. 2018;22(1):359.
19. Wanaka K, Okamoto S, Bohgaki M, et al. Effect of a highly selective plasma-kallikrein synthetic inhibitor on contact activation relating to kinin generation, coagulation and fibrinolysis. Thromb Res. 1990;57(6):889–895.
20. Wulf RJ, Mertz ET. Studies on Plasminogen .8. Species Specificity of Streptokinase. Can J Biochem. 1969;47(10):927–931.
21. Shannon O, Rydengård V, Schmidtchen A, et al. Histidine-rich glycoprotein promotes bacterial entrapment in clots and decreases mortality in a mouse model of sepsis. Blood. 2010;116(13):2365–2372.
22. Colman RW. Activation of plasminogen by human plasma kallikrein. Biochem Biophys Res Commun. 1969;35(2):273–279.
23. Nitzsche R, Rosenheinrich M, Kreikemeyer B, Oehmcke-Hecht S. Streptococcus pyogenes triggers activation of the human contact system by streptokinase. Infect Immun. 2015;83(8):3035–3042.
24. Stavrou EX, Fang C, Merkulova A, et al. Reduced thrombosis in Klkb1-/- mice is mediated by increased Mas receptor, prostacyclin, Sirt1, and KLF4 and decreased tissue factor. Blood. 2015;125(4):710–719.
25. Mosevoll KA, Skrede S, Markussen DL, et al. Inflammatory Mediator Profiles Differ in Sepsis Patients With and Without Bacteremia. Front Immunol. 2018;9:691.
26. Cavaillon JM, Adib-Conquy M, Fitting C, Adrie C, Payen D. Cytokine cascade in sepsis. Scand J Infect Dis. 2003;35(9):535–544.
27. Ng PC, Li K, Leung TF, et al. Early prediction of sepsis-induced disseminated intravascular coagulation with interleukin-10, interleukin-6, and RANTES in preterm infants. Clin Chem. 2006;52(6):1181–1189.
28. Konings J, Govers-Riemslag JWP, Philippou H, et al. Factor XIIa regulates the structure of the fibrin clot independently of thrombin generation through direct interaction with fibrin. Blood. 2011;118(14):3942–3951.
29. Konings J, Hoving LR, Ariëns RS, et al. The role of activated coagulation factor XII in overall clot stability and fibrinolysis. Thromb Res. 2015;136(2):474–480.
30. Renné T, Pozgajová M, Grüner S, et al. Defective thrombus formation in mice lacking coagulation factor XII. J Exp Med. 2005;202(2):271–281.
31. Pluthero FG, Ryan C, Williams S, Brandão LR, Kahr WHA. Decreased in vitro thrombin generation and clot stability in human FXII-null blood and plasma. Br J Haematol. 2011;152(1):111–112.
32. Stroo I, Zeerleder S, Ding C, et al. Coagulation factor XI improves host defence during murine pneumonia-derived sepsis independent of factor XII activation. Thromb Haemost. 2017;117(8):1601–1614.
33. Mason JW, Kleeberg U, Dolan P, Colman RW. Plasma kallikrein and Hageman factor in Gram-negative bacteremia. Ann Intern Med. 1970;73(4):545–551.
34. Aasen AO, Smith-Erichsen N, Amundsen E. Plasma kallikrein-kinin system in septicemia. Arch Surg. 1983;118(3):343–346.
35. Martins B, Kouyoumdjian M, Limaos EA, Borges DR. The Clearance Rate of Plasma Kallikrein by the Liver Increases During the Acute-Phase Response to Inflammation. Agents Actions. 1992;37(1-2):111–113.
36. Niessen RW, Lamping RJ, Jansen PM, et al. Antithrombin acts as a negative acute phase protein as established with studies on HepG2 cells and in baboons. Thromb Haemost. 1997;78(3):1088–1092.
37. Sato T, Miwa T, Akatsu H, et al. Pro-carboxypeptidase R is an acute phase protein in the mouse, whereas carboxypeptidase N is not. J Immunol. 2000;165(2):1053–1058.
38. Renckens R, Roelofs JJTH, Bonta PI, et al. Plasminogen activator inhibitor type 1 is protective during severe Gram-negative pneumonia. Blood. 2007;109(4):1593–1601.
39. Kager LM, Wiersinga WJ, Roelofs JJTH, et al. Plasminogen activator inhibitor type I contributes to protective immunity during experimental Gram-negative sepsis (melioidosis). J Thromb Haemost. 2011;9(10):2020–2028.
40. Renné T, Schmaier AH, Nickel KF, Blomback M, Maas C. In vivo roles of factor XII. Blood. 2012;120(22):4296–4303.
41. Oehmcke S, Herwald H. Contact system activation in severe infectious diseases. J Mol Med. 2010;88(2):121–126.
42. Hess R, Wujak L, Hesse C, et al. Coagulation factor XII regulates inflammatory responses in human lungs. Thromb Haemost. 2017;117(10):1896–1907.

Ferrata Storti Foundation

Haematologica 2020
Volume 105(5):1436-1442

Accuracy of the Ottawa score in risk stratification of recurrent venous thromboembolism in patients with cancer-associated venous thromboembolism: a systematic review and meta-analysis

Aurélien Delluc,[1] Sébastien Miranda,[2] Paul den Exter,[3] Martha Louzada,[4] Adriano Alatri,[5] Shin Ahn,[6] Manuel Monreal,[7] Alok Khorana,[8] Menno V. Huisman,[3] Philip S. Wells[1] and Marc Carrier[1]

[1]Department of Medicine, Ottawa Hospital Research Institute at the University of Ottawa, Ottowa, Ontario, Canada; [2]Normandie University, UNIROUEN, INSERM U1096 and Rouen University Hospital, Department of Internal Medicine, Vascular and Thrombosis Unit, F 76000 Rouen, France; [3]Department of Thrombosis and Hemostasis, Leiden University Medical Center, Leiden, the Netherlands; [4]Department of Medicine, Division of Hematology, University of Western Ontario, London, Ontario, Canada; [5]Division of Angiology, Lausanne University Hospital, Lausanne, Switzerland; [6]Department of Emergency Medicine, Asan Medical Center, University of Ulsan College of Medicine, Seoul, South Korea; [7]Department of Internal Medicine. Hospital Universitari Germans Trias i Pujol, Badalona, Spain and [8]Cleveland Clinic-Taussig Cancer Center, Cleveland, OH, USA

ABSTRACT

In patients with cancer-associated venous thromboembolism, knowledge of the estimated rate of recurrent events is important for clinical decision-making regarding anticoagulant therapy. The Ottawa score is a clinical prediction rule designed for this purpose, stratifying patients according to their risk of recurrent venous thromboembolism during the first six months of anticoagulation. We conducted a systematic review and meta-analysis of studies validating either the Ottawa score in its original or modified versions. Two investigators independently reviewed the relevant articles published from 1st June 2012 to 15th December 2018 and indexed in MEDLINE and EMBASE. Nine eligible studies were identified; these included a total of 14,963 patients. The original score classified 49.3% of the patients as high-risk, with a sensitivity of 0.7 [95% confidence interval (CI): 0.6-0.8], a 6-month pooled rate of recurrent venous thromboembolism of 18.6% (95%CI: 13.9-23.9). In the low-risk group, the recurrence rate was 7.4% (95%CI: 3.4-12.5). The modified score classified 19.8% of the patients as low-risk, with a sensitivity of 0.9 (95%CI: 0.4-1.0) and a 6-month pooled rate of recurrent venous thromboembolism of 2.2% (95%CI: 1.6-2.9). In the high-risk group, recurrence rate was 10.2% (95%CI: 6.4-14.6). Limitations of our analysis included type and dosing of anticoagulant therapy. We conclude that new therapeutic strategies are needed in patients at high risk for recurrent cancer-associated venous thromboembolism. Low-risk patients, as per the modified score, could be good candidates for oral anticoagulation. (This systematic review was registered with the International Prospective Registry of Systematic Reviews as: PROSPERO CRD42018099506).

Correspondence:

AURÉLIEN DELLUC
adelluc@toh.ca

Received: March 27, 2019.

Accepted: June 28, 2019.

Pre-published: July 4, 2019.

doi:10.3324/haematol.2019.222828

Check the online version for the most updated information on this article, online supplements, and information on authorship & disclosures: www.haematologica.org/content/105/5/1436

Introduction

Cancer is one of the most frequent risk factors for venous thromboembolism (VTE) and for VTE recurrence while on anticoagulation.[1,2] In patients with VTE and cancer, the rate of recurrent VTE despite anticoagulation can reach up to 20% after six months of therapy, but this rate highly depends on several patient and cancer characteristics.[3] For example, age, residual thrombosis, previous history of VTE, surgical procedures within three months prior to VTE, cancer stage, and the site and

histology of the malignancy all impact the 6-month rate of recurrent VTE.[4-8] The anticoagulant therapy used [e.g. vitamin K antagonist, direct oral anticoagulants or low molecular weight heparin (LMWH)] may also influence the rate of recurrent VTE. Reliable identification of which patients are at high or low risk of recurrent VTE recurrence must be performed to aid clinical decision-making regarding the type of anticoagulant therapy.

For this, the Ottawa score was designed to stratify the risk of recurrent VTE during the first six months of anticoagulant therapy in patients with cancer-associated VTE.[9] Two scores were derived. The original score (female sex, lung cancer, and prior history of VTE each give 1 point; breast cancer gives a negative point; cancer stage I gives 2 negative points) dichotomizes patients into low (score ≤ 0) or high (score ≥ 1) risk for VTE recurrence. The modified score (female sex, lung cancer, and prior history of VTE each give 1 point; breast cancer and cancer stage I + II each give a negative point) classifies patients into low (score ≤–1), intermediate (score = 0), and high (score ≥ 1) risk for VTE recurrence. However, the accuracy of these two clinical models remains to determine.

To determine if the Ottawa risk score (i.e. original and modified) can reliably identify the risk of recurrent VTE during the first six months of anticoagulation in cancer patients with VTE, we conducted a systematic review and meta-analysis of the literature.

Methods

The guidelines of the Preferred Reporting Items for Systematic reviews and Meta-Analyses (PRISMA) Statement were followed. The systematic review was registered with the International Prospective Registry of Systematic Reviews (PROSPERO CRD42018099506).

Search strategy and study selection

We systematically searched Medline and Embase, using the following key words: recurrent venous thromboembolism AND cancer AND (decision tree OR clinical prediction rule OR clinical prediction score OR clinical decision rule OR management stud-

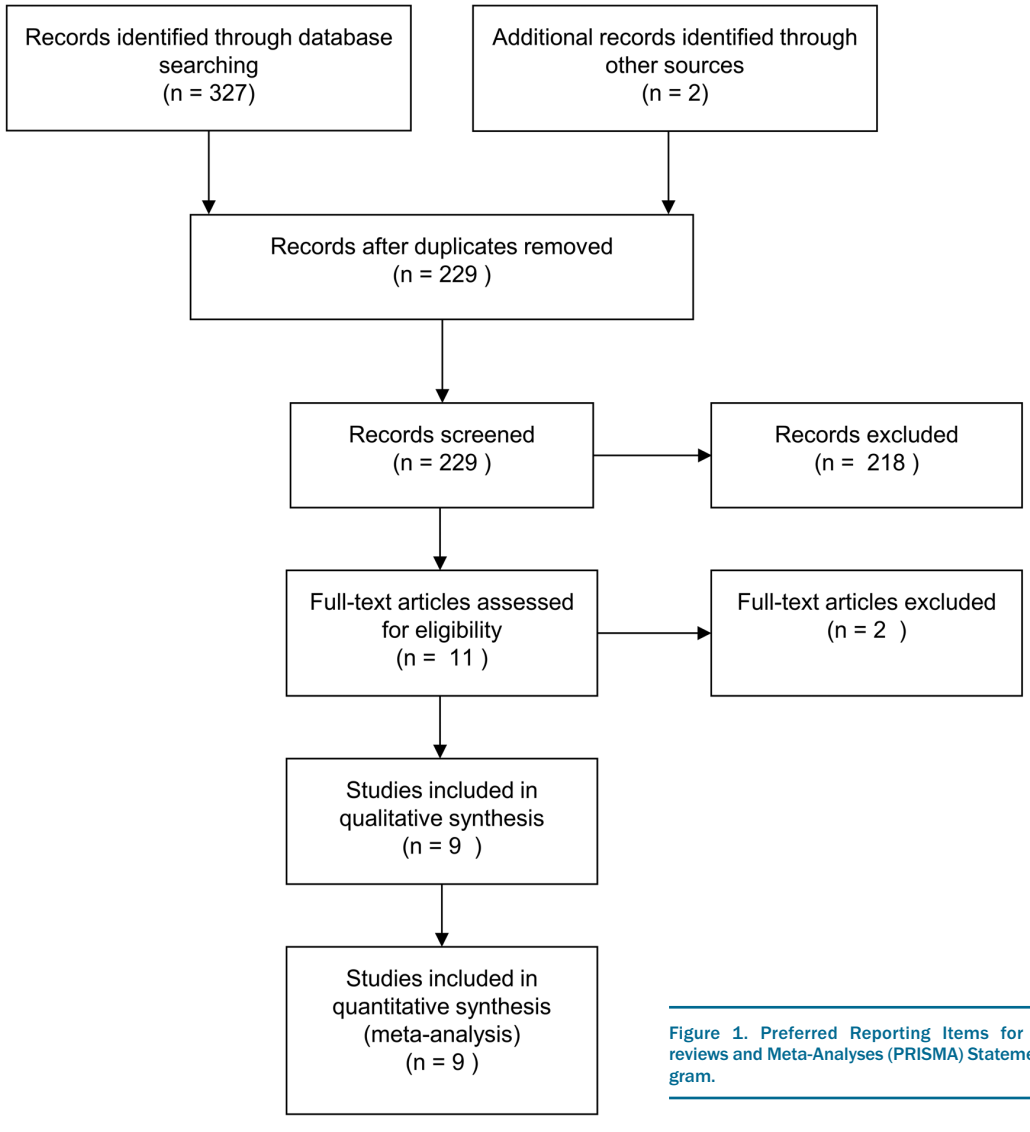

Figure 1. Preferred Reporting Items for Systematic reviews and Meta-Analyses (PRISMA) Statement flow diagram.

ies OR outcome studies OR decision support techniques), (venous thromboembolism recurrence) AND cancer AND (decision tree OR clinical prediction rule OR clinical prediction score OR clinical decision rule OR management studies OR outcome studies OR decision support techniques). The search was limited to English and French language studies. Literature search was restricted to 1st June 2012 to 15th December 2018, since the Ottawa score was published online in June 2012. To ensure a comprehensive literature search, we examined reference lists from retrieved articles and reference literature (guidelines and systematic reviews), and contacted experts in the management of cancer-associated VTE for possible missing studies. Eligible studies were those validating either the original or the modified Ottawa scores. If key data were missing, study authors were contacted to request the relevant data. Two investigators independently evaluated studies for possible inclusion (AD and SM). They independently assessed study quality and extracted the data on study design and patient characteristics. Disagreements about extracted data were resolved by consensus or by discussion with a third reviewer (MC).

Quality assessment and data extraction

Methodological quality of included studies was assessed independently by two observers (AD and SM) using the Hayden quality assessment tool specifically developed for systematic reviews of prognosis studies.[10] This tool assesses six potential biases. 1) Is the population of interest represented in the study sample? 2) Are there cases of Loss to Follow Up that are not associated with key characteristics? 3) Is there adequate measurement of the prognostic factors? 4) Is there adequate measurement of the outcome of interest? 5) Are important confounders accounted for? 6) Has the appropriate statistical analysis been conducted? Regarding the study population criterion, we considered as representative cohorts those that included consecutive patients with documented cancer-associated VTE with at least six months of follow up.

We collected the following data for each study: year of publication, score evaluated (original or modified), data collection methods (retrospective or prospective), setting (outpatient, inpatient or both), geographic location, demographics (mean age, percentage of women), follow-up duration, overall prevalence of recurrent VTE, distribution of patients in each pre-test probability group, and prevalence of VTE in each pre-test probability group.

The primary outcome of the study was the pooled prevalence of recurrent VTE in each risk group after six months of anticoagulation.

Data analysis

Publication bias was explored by funnel plots and Egger's test. We determined the 95% confidence intervals (CI) of the prevalence of recurrent VTE in the various clinical probability categories using the exact method. The prevalence of VTE in each level of clinical probability was separately assessed using the method of the inverse variance on the arcsine-transformed proportions. Heterogeneity was tested with the Cochran Q statistic and also quantified by the indicator I^2 (ranging from 0% for perfect homogeneity to 100% for extreme heterogeneity). In case of heterogeneity (Cochran Q test with a P-value < 0.10 or I2 > 50%), a random effects model was used.[11]

All analyses were performed using STATA14 (StataCorp, College Station, TX, USA) using the metaprop command.[12]

Table 1. Characteristics of the studies.

Studies	Score	Characteristics*	Setting	Inclusion period	N	Age (mean)	Female sex	Lung cancer	Breast cancer	Metastases	History of VTE	VTE recurrence rate
Louzada derivation (2012)[9]	Original Modified	R, D	Single-center	2002-2004 2007-2008	543**	63	303 (55.8%)	96 (17.7%)	85 (15.6%)	321 (66.2%)	46 (8.5%)	55 (10.1%)
Louzada validation (2012)[9]	Modified	P, V	Multicenter	1995-1999 1999-2001	819	–	427 (52.1%)	106 (12.9%)	139 (17.0%)	526 (71.8%)	96 (11.7)	86 (10.5%)
Louzada validation (2012)[14]	Original	R, V	Multicenter	2006-2010 2009-2011	353	64	204 (57.7%)	62 (17.5%)	39 (11.0%)	230 (75.7%)***	77 (21.8%)	44 (12.5%)
Den Exter (2013)[17]	Modified	P, V	Multicenter	2001-2010	419	60	197 (47.0%)	64 (15.3%)	33 (7.9%)	252 (71.2%)	39 (9.3%)	35 (8.4%)
Ahn (2013)[19]	Original	R, V	Single-center	2007-2010	546	58	294 (53.8%)	94 (17.2%)	36 (6.6%)	406 (74.4%)	26 (4.8%)	99 (18.1%)
Astruc (2016)[13]	Modified	P, V	Single-center	2000-2010	156	69	70 (44.8%)	23 (14.7%)	17 (10.9%)	62 (39.8%)	36 (23.1%)	14 (11.9%)
Alatri (2017)[16]	Modified	P, V	Multicenter	2001-2016	11123	67	5145 (46.2%)	1691 (15.2%)	1407 (12.6%)	6127 (55.1%)	1347 (12.1%)	477 (4.3%)
Khorana (2017)[18]	Modified	P, V	Multicenter	2010-2013	900	59	537 (59.6%)	104 (11.5%)	84 (9.3%)	492 (54.7%)	57 (6.3%)	76 (8.4%)
van Es (2018)[15]	Original	P, V	Multicenter	2012-2014	117	63	59 (50.4%)	26 (22.2%)	10 (8.5%)	89 ((76.0%)	0	11 (9.4%)

*P: prospective; R: retrospective; V: validation; D: derivation; **Missing data for 13 patients; *** TNM>1; N: number; VTE: venous thromboembolism; ***Tumor node metastasis>1.

Results

Study selection

The literature search identified 329 article records of which 229 were assessed for eligibility (Figure 1). Nine studies reporting data on 14,963 patients were eligible and were included in the analyses.[9,13-19]

Study characteristics

Study characteristics are depicted in Table 1. Of the reported studies, six were prospective, six were multicenter, and four used the original score. In total, seven studies were validation studies of the Ottawa score. Mean age of the patients was 58-69 years; female gender accounted for 45-59% of the patients.

Risk of bias within studies

Risk of bias is summarized in *Online Supplementary Appendix 1*. For six studies, at least four out of six potential bias areas were judged satisfied.[9,14-16,18] Confounding measurement was not accounted for in all studies, and attrition was accounted for in only one study.[18] A significant publication bias between the studies was observed (P=0.001) (*Online Supplementary Appendix 2A*). This bias was only observed in studies reporting on the modified score (*Online Supplementary Appendix 2B and C*).

Synthesis of results

All nine identified studies were included in the meta-analysis. Data were extracted from original publications for six studies[9,13-15,19] or, after that, additional data were provided by corresponding authors.[16-18] The overall 6-month rate of recurrent VTE varied from 4.3% to 18.1% in the different studies; the overall 6-month pooled rate was 9.8% (95%CI: 6.4-13.8; I^2=96%).

The original Ottawa score was derived in one and validated in three studies.[9,14,15,19] The total number of patients included in these studies was 1,558 with an overall pooled 6-month rate of recurrent VTE of 12.7% (95%CI: 8.9-17.2, I^2=81%). Overall, 763 (49.3%) patients were classified in

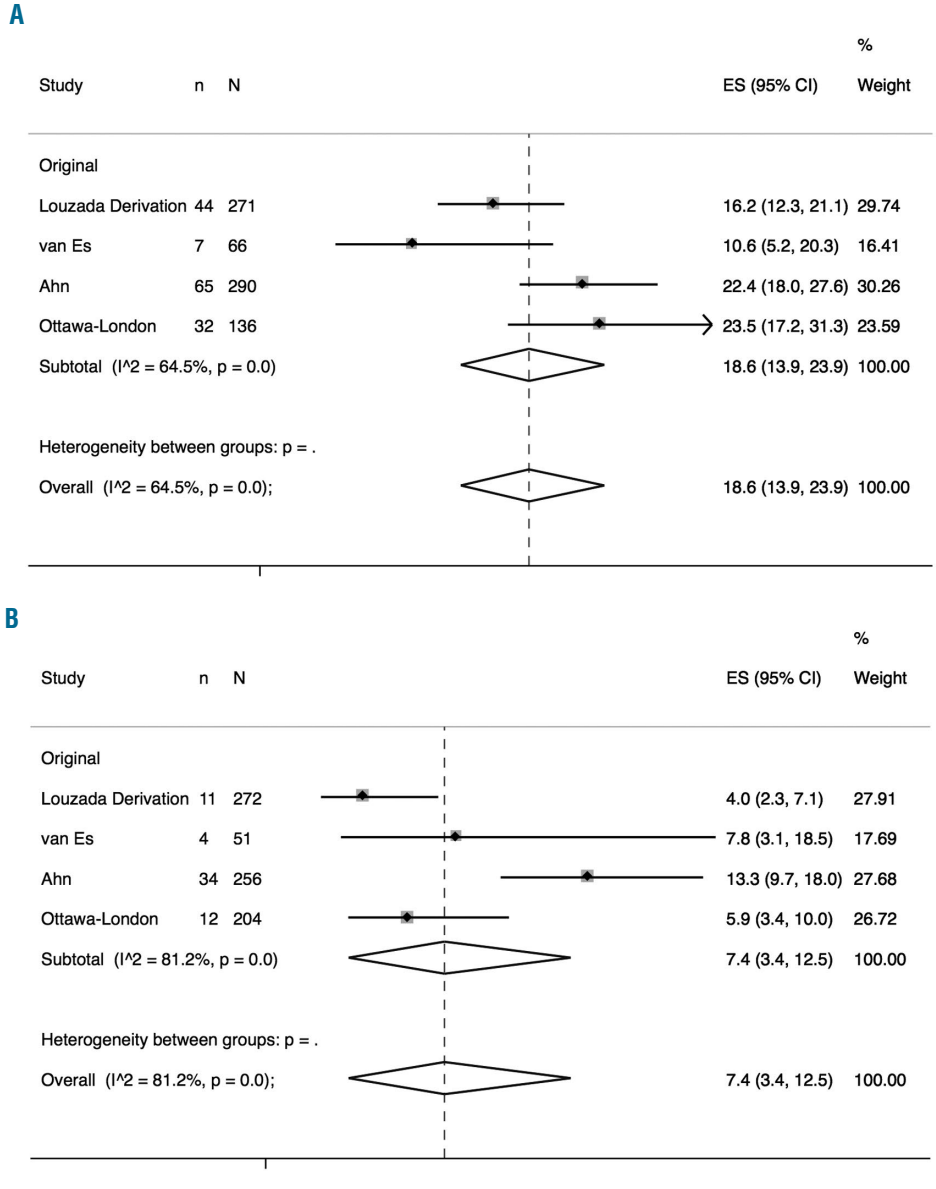

Figure 2. Pooled recurrence rates of venous thromboembolism for the original Ottawa score. (A) Pooled recurrence rates of venous thromboembolism for the original Ottawa score in high-risk patients. (B) Pooled recurrence rates of venous thromboembolism for the original Ottawa score in low-risk patients

the high-risk category with a pooled 6-month recurrence rate of VTE of 18.6% (95%CI: 13.9-23.9) (I^2=64%, P=0.04) (Figure 2A). Of the remaining 795 patients (classified in the low-risk category), the pooled 6-month rate of recurrent VTE was 7.4% (95%CI: 3.4-12.5) (I^2=81%, P<0.01) (Figure 2B). The estimated pooled sensitivity, specificity, and Area Under the Receiver Operating Characteristic curve (AUROC) of the original score to identify high-risk patients were 0.7 (95%CI: 0.6-0.8), 0.5 (95%CI: 0.5-0.6), and 0.7 (0.6-0.8), respectively.

The modified score was derived in one and validated in four studies.[9,13,16-18] The pooled 6-month rate of recurrent VTE in the 13,419 studied patients was 7.85% (95%CI: 4.79-11.57) (I^2=95%, P<0.01). The modified score classified 5,307 (39.5%) patients in the high-risk category, in which the pooled 6-month rate of recurrent VTE was 10.2% (95%CI: 6.4-14.6) (I^2=89%, P<0.01) (Figure 3A). A total of 2,653 patients (19.8%) were classified in the low-risk category with a pooled 6-month rate of recurrent VTE of 2.2% (95%CI: 1.6-2.9) (I^2=0%, P=0.51) (Figure 3B). For the remaining 5,459 patients in the intermediate-risk category, the pooled 6-month rate of recurrent VTE was 7.1% (3.8-11.3) (I^2=90%, P<0.01) (Figure 3C).

The estimated pooled sensitivity, specificity, and AUROC of the modified score to identify high-risk patients were 0.5 (95%CI: 0.5-0.6), 0.6 (95%CI: 0.5-0.7), and 0.5 (95%CI: 0.5-0.6), respectively. For the identification of low-risk patients these characteristics were 0.9 (95%CI: 0.8-1.0), 0.2 (95%CI: 0.1-0.2), and 0.5 (95%CI: 0.5-0.7), respectively.

Pooled incidences of recurrent VTE for each point category using the original and the modified Ottawa scores are reported in *Online Supplementary Appendix 3*. The rates of recurrent VTE ranged from 0 to 37.1% (95%CI: 12.7-64.7) with a dose-effect association in studies applying the original score and ranged from 0 to 9.1% (95%CI: 0.2-24.7) in studies applying the modified score with a stepwise association.

Discussion

This systematic review and meta-analysis of nine studies involving a total of 14,963 patients with cancer-associated VTE, confirms that the Ottawa score is an accurate tool to stratify the risk for recurrent VTE within the first six months of anticoagulation. The original Ottawa score can reliably identify patients with cancer-associated VTE at high risk of recurrent events, whereas the modified score is best suitable for identifying cancer patients with low risk of VTE recurrence. The original score classified 49.3% of the patients into the high-risk group with a sensitivity of 71% and the modified score classified 19.8% of the patients into the low-risk group with a sensitivity of 92%.

The Ottawa scores (original and modified) are the only tools available to stratify the risk for recurrence of cancer-associated VTE. The scores can help identify patients with a rate of recurrent VTE >10%. This has been suggested as clinically relevant and considered as a "high-risk" category.[20] The Ottawa scores have better accuracy than the reported sensitivity, specificity or AUROC values, which were calculated based on crude rates of recurrent

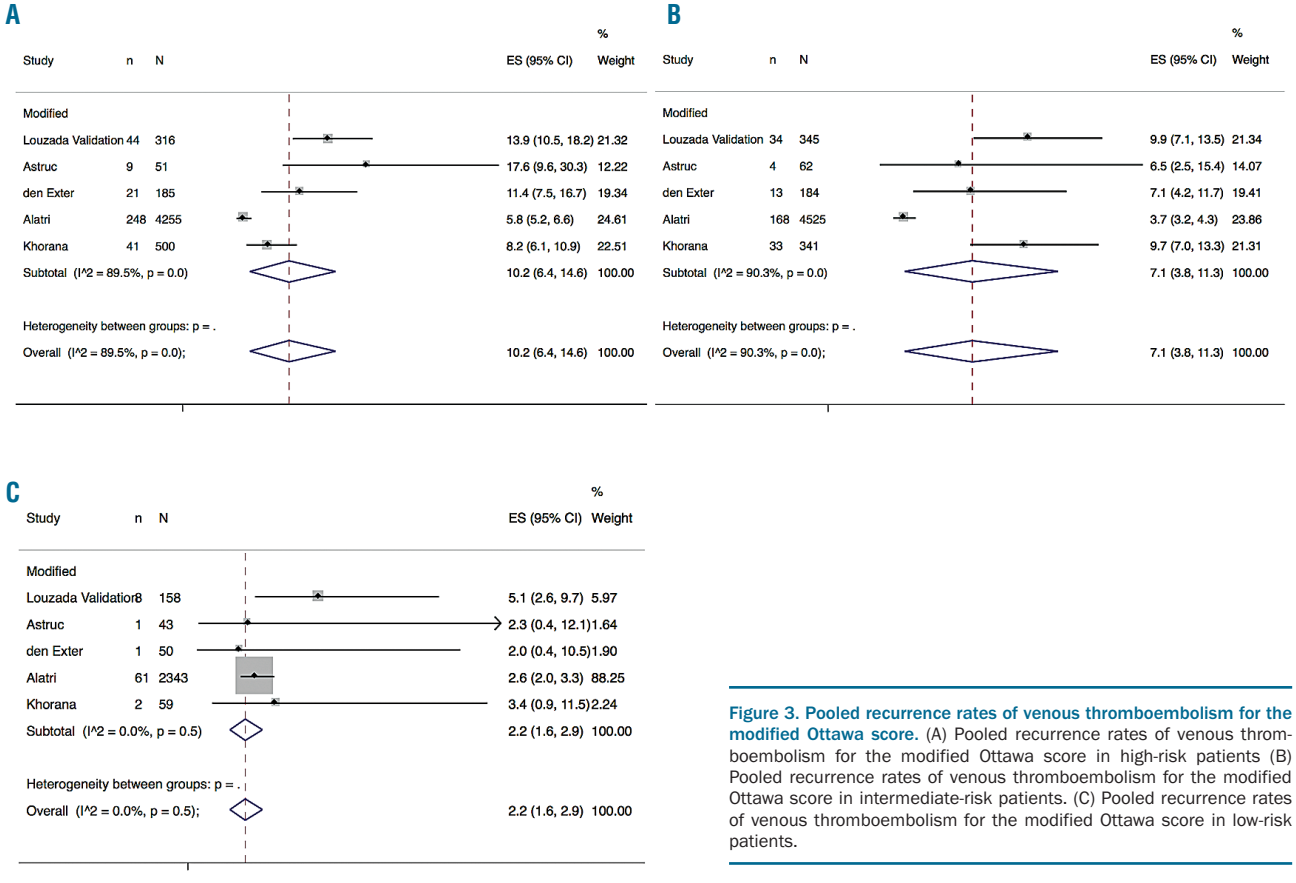

Figure 3. Pooled recurrence rates of venous thromboembolism for the modified Ottawa score. (A) Pooled recurrence rates of venous thromboembolism for the modified Ottawa score in high-risk patients (B) Pooled recurrence rates of venous thromboembolism for the modified Ottawa score in intermediate-risk patients. (C) Pooled recurrence rates of venous thromboembolism for the modified Ottawa score in low-risk patients.

VTE as opposed to correct classification. If patients were classified *a priori* by risk categories (i.e. "high-risk", "low-risk") similar to how a diagnostic test would be reported as "disease", or "no disease", it is very likely that estimates of intrinsic properties of the Ottawa score would improve. Furthermore, when considering our meta-analysis across each sum of points, we could demonstrate a dose-effect relationship, either continuous (original score) or stepwise (modified score), which confirmed the accuracy of the risk classification of the Ottawa scores.

The accuracy of the modified Ottawa score to identify patients at low risk for VTE recurrence has a potential major therapeutic impact that should be considered for implementation into daily practice. The low 2.2% risk of recurrent VTE in this patient population closely mirrors the recurrent risk of the general VTE population[21,22] (refer to DOAC trials). In this setting, the potential advantages of LMWH over oral anticoagulation are clearly counterbalanced by their cost, their negative impact on quality of life, and the expected low absolute risk reduction of recurrent VTE (<2% based on a 50% relative risk reduction).[23,24] The use of oral anticoagulants in low-risk patients is, therefore, clinically relevant and could be systematically considered as first line in this specific risk group. In contrast, 49.3% of the patients were classified in the high-risk group by the original Ottawa score. The unacceptable 18.6% estimated rate of recurrent VTE, despite anticoagulant treatment, in this group warrants the urgent development of new therapeutic strategies.

Strengths of our study include its comprehensiveness and the large number of patients included; however, we acknowledge several limitations. First, there was a significant heterogeneity between studies and some publication bias, particularly in validation studies of the modified score. Nevertheless, most of the studies were of good quality. A major source of heterogeneity was the large difference in incidence rates of recurrent VTE across the studies. Most datasets were old and included patients receiving out-dated cancer therapies. These therapies may have exposed patients to higher risk of recurrent VTE, leading to an overestimation of the current risk. However, the most recent study using the original or modified scores reported an overall recurrence rate of VTE of 9.4 and 8.4%, respectively, which remains high and clinically relevant.[15,18] Specific center-related factors that could also potentially affect recurrence-rate of VTE include academic centers, age of included patients and their socio-economic level, number of comorbidities, higher stage disease, history of VTE, and ethnicity. The second limitation of our study was we were unable to account for the type of anticoagulation used. None of the studied patients were treated with a direct oral anticoagulant. Data on exposure to LMWH or vitamin K antagonist was not available in any of the identified studies. In the derivation and in some of the validation studies, the type of anticoagulation was not a significant predictor for VTE recurrence. However, among all randomized trials, only one showed the superiority of LMWH over vitamin K antagonists to treat cancer-associated VTE.[25] Third, we could not assess the importance of other risk factors for VTE recurrence (e.g. interruption of anticoagulants for an invasive procedure, age, etc.) during follow up. However, the Ottawa scores were derived without accounting for these confounders and appeared to accurately classify patients. Fourth, patients classified by the original score in the low-risk category had an estimated rate of VTE recurrence of 7.4%, which cannot be considered as low. However, when the score was initially derived, the objective was to identify patients with an *a priori* risk for VTE recurrence during anticoagulation of <7%. In that instance, our data confirm the accuracy of the original score.

In conclusion, the Ottawa score, either in its original or modified form, is a useful tool to stratify the 6-month risk for VTE recurrence during anticoagulation in patients with cancer-associated VTE. Specifically, the original and modified Ottawa score can accurately identify patients with cancer-associated VTE at high and low risk of recurrent events, respectively. There is an urgent need for the development of new therapeutic strategies to prevent recurrent VTE in high-risk patients. The original score is an accurate tool to define inclusion criteria of future studies.

Funding

Dr. Khorana acknowledges additional research support from the Sondra and Stephen Hardis Chair in Oncology Research and the National Heart, Lung and Blood Institute (Consortium Linking Oncology with Thrombosis - U01HL143402; R34 HL127156).

References

1. Delluc A, Tromeur C, Le Ven F, et al. Current incidence of venous thromboembolism and comparison with 1998: a community-based study in Western France. Thromb Haemost. 2016;116(5):967-974.
2. Prandoni P, Lensing AWA, Piccioli A, et al. Recurrent venous thromboembolism and bleeding complications during anticoagulant treatment in patients with cancer and venous thrombosis. Blood. 2002; 100(10): 3484-3488.
3. Chew HK, Wun T, Harvey D, Zhou H, White RH. Incidence of venous thromboembolism and its effect on survival among patients with common cancers. Arch Intern Med. 2006;166(4):458-464.
4. Trujillo-Santos J, Nieto JA, Tiberio G, et al. Predicting recurrences or major bleeding in cancer patients with venous thromboembolism. Findings from the RIETE Registry. Thromb Haemost. 2008;100(3):435-439.
5. Napolitano M, Saccullo G, Malato A, et al. Optimal duration of low molecular weight heparin for the treatment of cancer-related deep vein thrombosis: the Cancer-DACUS Study. J Clin Oncol. 2014;32(32):3607-3612.
6. Descourt R, Le Gal G, Couturaud F, et al. Recurrent venous thromboembolism under anticoagulant therapy: a high risk in adenocarcinoma? Thromb Haemost. 2006; 95(5):912-913.
7. Louzada ML, Majeed H, Dao V, Wells PS. Risk of recurrent venous thromboembolism according to malignancy characteristics in patients with cancer-associated thrombosis: a systematic review of observational and intervention studies. Blood Coagul Fibrinolysis. 2011;22(2):86-91.
8. Noel-Savina E, Sanchez O, Descourt R, et al. Tinzaparin and VKA use in patients with cancer associated venous thromboembolism: a retrospective cohort study. Thromb Res. 2015;135(1):78-83.
9. Louzada ML, Carrier M, Lazo-Langner A, et al. Development of a clinical prediction rule for risk stratification of recurrent venous thromboembolism in patients with cancer-associated venous thromboembolism. Circulation. 2012;126(4):448-454.
10. Hayden JA, Cote P, Bombardier C. Evaluation of the quality of prognosis studies in systematic reviews. Ann Intern Med. 2006;144(6):427-437.
11. Ceriani E, Combescure C, Le Gal G, et al. Clinical prediction rules for pulmonary embolism: a systematic review and meta-analysis. J Thromb Haemost. 2010; 8(5):957-970.

12. Nyaga VN, Arbyn M, Aerts M. Metaprop: a Stata command to perform meta-analysis of binomial data. Archives of public health = Archives belges de sante publique. 2014; 72(1):39.
13. Astruc N, Ianotto JC, Metges JP, Lacut K, Delluc A. External validation of the modified Ottawa score for risk stratification of recurrent cancer-associated thrombosis. Eur J Intern Med. 2016;36:e11-e12.
14. Louzada ML, Bose G, Cheung A, Chin-Yee BH, Wells S, Wells PS. Predicting Venous Thromboembolism Recurrence Risk in Patients with Cancer: A Validation Study. Blood. 2012;120(21):394-394.
15. van Es N, Louzada M, Carrier M, et al. Predicting the risk of recurrent venous thromboembolism in patients with cancer: A prospective cohort study. Thromb Res. 2018;163:41-46.
16. Alatri A, Mazzolai L, Font C, et al. Low discriminating power of the modified Ottawa VTE risk score in a cohort of patients with cancer from the RIETE registry. Thromb Haemost. 2017;117(8):1630-1636.
17. den Exter PL, Kooiman J, Huisman MV. Validation of the Ottawa prognostic score for the prediction of recurrent venous thromboembolism in patients with cancer-associated thrombosis. J Thromb Haemost. 2013;11(5):998-1000.
18. Khorana AA, Kamphuisen PW, Meyer G, et al. Tissue Factor As a Predictor of Recurrent Venous Thromboembolism in Malignancy: Biomarker Analyses of the CATCH Trial. J Clin Oncol. 2017;35(10):1078-1085.
19. Ahn S, Lim KS, Lee YS, Lee JL. Validation of the clinical prediction rule for recurrent venous thromboembolism in cancer patients: the Ottawa score. Supportive care in cancer: official journal of the Multinational Association of Supportive Care in Cancer. 2013;21(8):2309-2313.
20. Prandoni P, Lensing AW, Cogo A, et al. The long-term clinical course of acute deep venous thrombosis. Ann Intern Med. 1996;125(1):1-7.
21. Agnelli G, Buller HR, Cohen A, et al. Oral apixaban for the treatment of acute venous thromboembolism. N Engl J Med. 2013; 369(9):799-808.
22. Büller HR, Prins MH, Lensin AWA, et al. Oral rivaroxaban for the treatment of symptomatic pulmonary embolism. N Engl J Med. 2012;366(14):1287-1297.
23. Lloyd AJ, Dewilde S, Noble S, Reimer E, Lee AYY. What Impact Does Venous Thromboembolism and Bleeding Have on Cancer Patients' Quality of Life? Value in health : the journal of the International Society for Pharmacoeconomics and Outcomes Research. 2018;21(4):449-455.
24. Carrier M, Cameron C, Delluc A, Castellucci L, Khorana AA, Lee AY. Efficacy and safety of anticoagulant therapy for the treatment of acute cancer-associated thrombosis: a systematic review and meta-analysis. Thromb Res. 2014;134(6):1214-1219.
25. Lee AY, Levine MN, Baker RI, et al. Low-molecular-weight heparin versus a coumarin for the prevention of recurrent venous thromboembolism in patients with cancer. N Engl J Med. 2003;349(2): 146-153.

ARTICLE

Relationship between factor VIII activity, bleeds and individual characteristics in severe hemophilia A patients

João A. Abrantes,[1] Alexander Solms,[2] Dirk Garmann,[3] Elisabet I. Nielsen,[1] Siv Jönsson[1] and Mats O. Karlsson[1]

[1]Department of Pharmaceutical Biosciences, Uppsala University, Uppsala, Sweden; [2]Bayer, Berlin, Germany and [3]Bayer, Wuppertal, Germany

Ferrata Storti Foundation

Haematologica 2020
Volume 105(5):1443-1453

ABSTRACT

Pharmacokinetic-based prophylaxis of replacement factor VIII (FVIII) products has been encouraged in recent years, but the relationship between exposure (factor VIII activity) and response (bleeding frequency) remains unclear. The aim of this study was to characterize the relationship between FVIII dose, plasma FVIII activity, and bleeding patterns and individual characteristics in severe hemophilia A patients. Pooled pharmacokinetic and bleeding data during prophylactic treatment with BAY 81-8973 (octocog alfa) were obtained from the three LEOPOLD trials. The population pharmacokinetics of FVIII activity and longitudinal bleeding frequency, as well as bleeding severity, were described using non-linear mixed effects modeling in NONMEM. In total, 183 patients [median age 22 years (range, 1-61); weight 60 kg (11-124)] contributed with 1,535 plasma FVIII activity observations, 633 bleeds and 11 patient/study characteristics [median observation period 12 months (3.1-13.1)]. A parametric repeated time-to-categorical bleed model, guided by plasma FVIII activity from a 2-compartment population pharmacokinetic model, described the time to the occurrence of bleeds and their severity. Bleeding probability decreased with time of study, and a bleed was not found to affect the time of the next bleed. Several covariate effects were identified, including the bleeding history in the 12-month pre-study period increasing the bleeding hazard. However, unexplained inter-patient variability in the phenotypic bleeding pattern remained large (111%CV). Further studies to translate the model into a tool for dose individualization that considers the individual bleeding risk are required. Research was based on a *post-hoc* analysis of the LEOPOLD studies registered at *clinicaltrials.gov identifiers: 01029340, 01233258 and 01311648.*

Introduction

Hemophilia A is an X-linked hereditary bleeding disorder caused by the deficiency of coagulation factor VIII (FVIII). The severity of the disease is inversely correlated with the amount of factor that an individual is able to produce, and nearly half of the cases correspond to the severe laboratory phenotype (endogenous plasma FVIII activity levels <1 IU/dL).[1,2] Prophylaxis with FVIII concentrates is currently considered the treatment of choice to decrease the frequency of bleeding and preserve musculoskeletal function.[3-5] The population pharmacokinetics (PK) of FVIII products has been extensively studied, and it has been seen that the elimination half-life varies substantially between patients.[6,7] Thus, the individual disposition of FVIII cannot be adequately predicted by average PK parameters and demographic characteristics, and PK-based dosing has been encouraged to optimize dosing regimens in the prophylactic setting.[8-10] In brief, PK-based dosing relies on Bayesian estimation to estimate the individual PK parameters by combining patient information (dose, FVIII activity measurements and demographic characteristics, e.g. age, body weight) with information previously collected from a patient population by means of a population PK model.[11,12] Based on the estimated

Correspondence:

MATS O. KARLSSON
mats.karlsson@farmbio.uu.se

Received: February 1, 2019.

Accepted: July 23, 2019.

Pre-published: August 1, 2019.

doi:10.3324/haematol.2019.217133

Check the online version for the most updated information on this article, online supplements, and information on authorship & disclosures: www.haematologica.org/content/105/5/1443

individual PK parameters, a patient-specific dosing regimen can be suggested.[13] Recently, the shift from standard prophylaxis to PK-based prophylaxis was facilitated by the development of dosing tools, which are hemophilia-specific for one (e.g. my PKFit, Shire Pharmaceutical Holdings Ireland Limited, Dublin, Ireland; *www.mypkfit.com*) or multiple (WAPPS-Hemo, McMaster University, Hamilton, Ontario, Canada, *www.wapps-hemo.org*) FVIII products, or generic tools (e.g. DoseMe LLC, Taringa Qld, Australia; *www.doseme-rx.com*; InsightRX Inc., San Francisco, CA, USA, *www.insight-rx.com*), which also support drugs from other clinical areas.[14]

The choice of individual dosing regimens in PK-based prophylaxis is based on information about the individual PK, but is also based on other components such as the patient's bleeding pattern, joint status or physical activity. From a PK perspective, the dose and dosing interval that generates an individual trough plasma FVIII activity above a certain target level, traditionally 1 IU/dL, is selected.[1,15] However, even though this level was not supposed to be an end in itself,[16] but rather an orientation, until recently it was the main target used to build prophylaxis regimens. Several studies showed that some patients still bleed with higher trough values, while others do not bleed despite having trough values below 1 IU/dL, suggesting that a "one-target-fits-all" strategy is not appropriate.[16-22] Other measures of target FVIII exposure have been associated with bleeding,[23] and different target levels for different patients that take into consideration individual lifestyle were recently suggested.[24]

One of the most important clinical endpoints to assess efficacy in hemophilia is bleeding frequency. This is often reported as the absolute number of bleeds during the study duration or annualized bleeding rate with the respective dispersion (e.g. range or standard deviation).[25] Whereas these bleeding outcome measures may be useful to report efficacy, they are not adequate to study predictors of bleeding as they do not account for complex aspects, such as individual differences in FVIII disposition or bleeding phenotype, or time-varying factors, such as changes in dosing regimens or bleeding patterns. However, using an integrated model-based analysis overcomes these limitations. Repeated time-to-event modeling, an extension of parametric time-to-event survival analysis using non-linear mixed effects modeling, accounts for the occurrence of multiple events (e.g. bleeds) within an individual.[26,27] This methodology enables the characterization of time-varying patterns in the occurrence of events (e.g. bleeding patterns changing over time) or predictors of events (e.g. FVIII activity) and has successfully been applied to several clinical areas, e.g. to describe the analgesic consumption in postoperative pain,[28] or the time to the occurrence of epileptic seizures.[29] This technique can be further extended to capture how consecutive events may be related to each other (Markovian dependence), or to include the severity of the events [repeated time-to-categorical event (RTTCE) modeling].[30]

To better understand the link between prophylactic FVIII replacement therapy and bleeding patterns in patients with severe hemophilia A, the aim of this study was to characterize the relationship between FVIII doses, FVIII activity in plasma, and the occurrence of bleeds, as well as bleeding severity (mild, moderate or severe).

Methods

For a detailed description of the methods used, see the *Online Supplementary Appendix.*

Patients and data

This *post-hoc* analysis was based on dosing, PK, bleeding and patient characteristics data obtained from the three LEOPOLD trials (LEOPOLD I *clinicaltrials.gov identifier: 01029340*, LEOPOLD II *clinicaltrials.gov identifier: 01233258* and LEOPOLD kids *clinicaltrials.gov identifier: 01311648*),[31-33] evaluating efficacy, safety and PK of a full-length recombinant human FVIII product, BAY 81-8973 (octocog alfa, Kovaltry®),[34] in severe hemophilia A (endogenous FVIII activity <1 IU/dL) patients. Previously treated patients with no history of FVIII inhibitors, receiving on-demand or prophylactic treatment at screening, aged 12-64 years (LEOPOLD I and II) and ≤12 years (LEOPOLD kids) were included. Single doses of 50 IU/kg or 20-50 IU/kg 2-3 times/week (LEOPOLD I), 20-40 IU/kg 2-3 times/week (LEOPOLD II), and 25-50 IU/kg at least 2 times/week (LEOPOLD kids) were administered. The study protocols were reviewed and approved by each site's independent ethics committee or institutional review board.

Factor VIII activity was measured by the chromogenic assay. Bleeding episodes observed during prophylactic treatment were included in the analysis, which included spontaneous, trauma-related and untreated bleeds (i.e. bleeds not requiring FVIII infusions in addition to scheduled treatment), and unspecified events requiring FVIII treatment. Date and time of injection, and bleeding data (date, time, severity and location) were self-reported by the patient or caregiver using an electronic patient diary. A maximum of one bleed per calendar day was recorded, and spontaneous joint or muscle bleeds were not registered if occurring within 72 hours (h) of another bleed at the same site or respective infusion.

Model development and assessment

Model estimation was performed using non-linear mixed effects modeling in NONMEM® 7.4.3.[35] The PK and RTTCE models were estimated simultaneously and covariates integrated afterwards. Model assessment was based on scientific plausibility, changes in the objective function value (OFV, -2·log-likelihood), goodness-of-fit plots and precision of parameter estimates. For nested models, the likelihood ratio test was used [difference in OFV (ΔOFV) >6.64 considered significant at =0.01, 1 *d.f.*].

Population pharmacokinetic model

The population PK analysis started from the model by Garmann *et al*. using the corresponding set of data.[36] The included association between lean body weight (LBW) and clearance (CL) and central volume of distribution (V1) was retained given the wide age range of patients. The previous model assumptions were comprehensively assessed.

Repeated time-to-categorical bleed model

The probability density of each bleed, as well as the probability associated with each severity was estimated from the observed time of bleeding and severity score (mild, moderate, severe) using a combination of parametric survival analysis and proportional odds model for ordered categorical data,[26,27,37,38] i.e. the RTTCE model.[30] The distribution of time of bleeds was explored using exponential, Weibull and Gompertz hazard functions. Inter-individual variability was considered on the overall bleeding hazard and on the logit transform of the severity probability. The censoring time for bleeds was set at the end of the individual bleeding observation period (right-censored observation).

The influence of individual plasma FVIII activity predicted from

the estimated individual PK parameters and recorded dose information was explored on the baseline hazard using either a linear, exponential or maximum inhibition (Imax) model. Furthermore, a time-dependency between consecutive bleeds was assessed with a Markov hazard rate through a function depending on the time since the previous bleed.

The final RTTCE model, developed based on data of all bleeds, was re-estimated including only data concerning joint spontaneous bleeds from the studies LEOPOLD I and II to characterize the joint bleeding patterns in patients aged 12 years or older.

Covariate analysis

The correlation between covariates (patient and study characteristics), PK, bleeding hazard (all bleeds), and bleeding severity were evaluated using full random effects modeling.[39,40] This methodology allows the characterization of all model parameter-covariate relationships in a single step and does not require imputation of pre-defined values when covariate data are missing. The covariates explored were: age, body weight, body mass index, lean body weight, race, von Willebrand factor (vWF), number of bleeds in the 12-month pre-study period, previous therapy history, on-demand or prophylaxis treatment, number of target joints for bleeds at study start obtained from the case report forms, ratio of the number of bleeds in the 12-month pre-study period to the number of target joints for bleeds at study start and during the study. In the original PK model development,[36] vWF was not available; this covariate was, therefore, tested for the first time in this analysis. Relevant parameter-covariate relationships were identified by the correlation coefficient (r), uncertainty of the effect size, and scientific plausibility.

Results

Patients and data

The final analysis included 1,535 FVIII activity observations from 183 patients, 633 bleeds from 172 patients, and 11 covariates. The median bleeding observation period was approximately 12 months for LEOPOLD I and II, and six months for LEOPOLD kids. Eleven patients had PK observations available but did not contribute with bleeding information because either they only received on-demand treatment (n=5) or only participated in the PK part of the trial (n=6). The median patient was a 22-year old 60-kg white male, with a vWF level of 104%, one target joint at study start, and receiving prophylactic treatment before the study. In total, 116 patients (67% of total) had at least one bleed during the observation period (median 2, range 0-33), and the median time to first bleed was 48.2 days (range 14.5 hours-352 days). Descriptive statistics of study, patient characteristics and information on bleeding episodes are available in Table 1. (This information by age cohort is available in the *Online Supplementary Appendix).*

Population pharmacokinetic model

The PK component of the final model provided a good description of the PK data, similarly to the previously reported model.[36] In addition to inter-individual variability on CL and V1, adding inter-individual variability on the residual error improved both model fit (ΔOFV=-199) and parameter precision. The median estimated individual CL was 1.80 dL/h (range 0.579-4.73 dL/h) and V1 was 29.5 dL (range 5.68-51.1 dL). The distribution of model-predicted plasma FVIII activity at the time of bleeding was strongly positively skewed with a median of 5.81 IU/dL (mean 11.6 IU/dL, range <1.50-140 IU/dL). The parameter estimates of the final model are available in Table 2.

Repeated time-to-categorical bleed model

A Gompertz hazard function with decreasing bleeding hazard over time provided an adequate description of the time-to-bleed data and was superior to the Weibull and exponential models. The effect of FVIII activity on the bleeding hazard was characterized by an Imax model (P<0.001; ΔOFV=-146), with full inhibition for high FVIII activity values. An exponential effect performed almost as well (ΔOFV=-133), while a linear relationship performed substantially worse (ΔOFV=-23). The final hazard equation was given by:

$$h(t) = \lambda \cdot e^{\gamma \cdot (t-1)} \cdot \left(1 - \frac{FVIII(t)}{FVIII(t) + IF50}\right) \cdot e^{\eta}$$

where h(t) is the time-varying bleeding hazard, λ and γ are the scale and shape factors of the Gompertz distribution, FVIII(t) is the individual PK model-predicted FVIII activity at time t, IF50 is the FVIII activity resulting in half-maximum inhibition of the hazard, and η is a log-normally distributed random effect describing the unexplained inter-individual variability of the bleeding hazard in the population. Instead of representing the bleeding hazard when FVIII activity in plasma is zero, λ and IF50 were re-parametrized to represent the bleeding hazard when plasma FVIII activity was 0.5 IU/dL and 20 IU/dL ($\lambda_{0.5IU/dL}$ and $\lambda_{20IU/dL}$, respectively) one year after study start. The assessment of a time dependency between consecutive bleeds, given by a transient effect where the occurrence of a bleed changed the bleeding hazard of a new bleed, could not be identified (P>0.05 for Markov component). The estimated probability of a bleed during the study to be mild, moderate or severe was 39.6, 55.7 and 4.72%, respectively.

The observed Kaplan-Meier curves for the first three bleeding episodes and the 95% confidence interval (CI) of the model predictions, showing how well the model described the data, are presented in Figure 1, and the parameter estimates of the final model are available in Table 2. An additional model diagnostic plot is available in the *Online Supplementary Appendix* (*Online Supplementary Figure S1*).

The re-estimated model accounting for the spontaneous joint bleeding information only was found to describe the data well (*Online Supplementary Figure S2*), and the final parameter estimates are available in Table 3. As expected, when including only spontaneous joint bleeds, the bleeding hazard as well as the IF50 parameter decreased, reflecting less frequent events and higher potency for the replacement therapy, respectively.

Covariate analysis

The estimated correlations between the model parameters (CL, V1, PK residual error, bleeding hazard and bleeding severity including all bleeds) and the co-variates are illustrated in Figure 2. The strongest relationships found were: vWF on CL (r=-0.54; decreased unexplained inter-individual variability by 4.7%) and number of bleeds in the 12-month pre-study period on the bleeding hazard (r=0.45; decreased unexplained inter-individual variability by 15%). The effect of LBW on CL and V1 was included *a*

Table 1. Patients' characteristics, treatment and bleeding data by study for patients with plasma factor VIII (FVIII) observations enrolled in the bleeding observation period.

Study	LEOPOLD I	LEOPOLD II	LEOPOLD kids	Total
Patients with PK and bleeding data, n (% of total)	62 (36)	59 (34)	51 (30)	172 (100)
Duration of bleeding observation period, months				
Mean±SD	11.8 ± 1.53	12.2 ± 0.165	6.12 ± 0.544	10.3 ± 2.86
Median [range]	12.0 [3.08-13.1]	12.2 [11.7-12.5]	6.09 [3.78-7.22]	12.0 [3.08-13.1]
Individual FVIII dose during treatment period (IU/kg)				
Mean±SD	38.4 ± 9.24	38.9 ± 9.37	36.2 ± 10.5	38.2 ± 9.60
Median [range]	37.9 [4.25-80.9]	38.7 [5.85-199]	34.1 [19.2-106]	37.9 [4.30-199]
Patients' characteristics				
Age, years				
Mean±SD	31.5 ± 12.7	29.0 ± 11.1	6.59 ± 2.94	23.2 ± 14.9
Median [range]	30.0 [12.0-61.0]	27.0 [14.0-59.0]	6.00 [1.00-11.0]	22.0 [1.00-61.0]
Weight, kg				
Mean±SD	76.7 ± 17.3	64.9 ± 13.2	25.9 ± 10.8	57.6 ± 25.5
Median [range]	76.0 [39.0-124]	64.0 [46.0-98.0]	22.6 [11.0-59.0]	60.0 [11.0-124]
Lean body weight,[a] kg				
Mean±SD	58.4 ± 8.88	52.8 ± 7.18	23.3 ± 8.66	46.0 ± 17.1
Median [range]	58.5 [35.5-79.2]	52.2 [40.9-68.4]	20.8 [9.25-48.9]	50.9 [9.25-79.2]
Body mass index,[a] $kg \cdot m^{-2}$				
Mean±SD	25.2 ± 4.63	21.4 ± 3.94	16.4 ± 2.55	21.3 ± 5.25
Median [range]	25.2 [16.2-38.3]	20.8 [15.0-30.9]	15.7 [13.0-24.6]	20.3 [13.0-38.3]
von Willebrand factor level,[b] %				
Mean±SD	107 ± 34.3	110 ± 38.9	NA	109 ± 36.5
Median [range]	103 [53.0-200]	104 [43.0-242]	NA	104 [43.0-242]
Race, n (%)				
White	55 (89)	30 (51)	47 (92)	132 (77)
Black	4 (6.5)	1 (1.7)	3 (5.9)	8 (4.7)
Asian	0 (0.0)	23 (39)	0 (0.0)	23 (13)
Hispanic	2 (3.2)	5 (8.5)	1 (2.0)	8 (4.7)
Unknown	1 (1.6)	0 (0.0)	0 (0.0)	1 (0.60)
Treatment history, n (%)				
On-demand	11 (18)	59 (100)	11 (22)	81 (47)
Prophylaxis	51 (82)	0 (0.0)	40 (78)	91 (53)
N. of target joints at study start[c]				
Median [range]	1 [1-4]	2 [1-5]	1 [1-2]	1 [1-5]
Summary of bleeding episodes				
Total number of bleeds, n (% of total)	240 (38)	292 (46)	101 (16)	633 (100)
Patients with at least one bleed, n (% of total)	45 (39)	43 (37)	28 (24)	116 (100)
Individual n. of bleeds				
Median [range]	2 [0-26]	2 [0-33]	1 [0-9]	2 [0-33]
Time to first bleed,[d] days				
Mean±SD	91.8 ± 96.7	63.9 ± 66.0	58.0 ± 46.6	73.3 ± 76.8
Median [range]	49.1 [1.00-351.9]	43.0 [0.606-265]	5.00 [1.17-182]	48.2 [0.606-352]
Bleed type, n (%)				
Spontaneous	155 (65)	209 (72)	24 (24)	388 (61)
Non-spontaneous	85 (35)	83 (28)	77 (76)	245 (39)
Spontaneous bleed location, n (%)				
Joint	131 (55)	189 (65)	8 (7.9)	328 (52)
No joint	109 (45)	103 (35)	93 (92)	305 (48)
Bleed severity, n (%)				
Mild	123 (51)	120 (41)	52 (52)	295 (47)
Moderate	91 (38)	139 (48)	46 (46)	276 (44)
Severe	26 (11)	33 (11)	3 (3.0)	62 (9.8)
N. of bleeds in the 12 months prior to study start[e]				
Median [range]	5.5 [0-55]	36 [3-106]	4 [0-55]	11 [0-106]

N/n: number; PK: pharmacokinetics; NA: not available; SD: standard deviation. [a]Lean body weight and body mass index missing for one patient. [b]von Willebrand factor levels missing for 55 patients. [c]Number of target joints missing for 61 patients. [d]Time to first bleed based on data from patients experiencing at least one bleed. [e]Number of bleeds in the last 12 months missing for 3 patients.

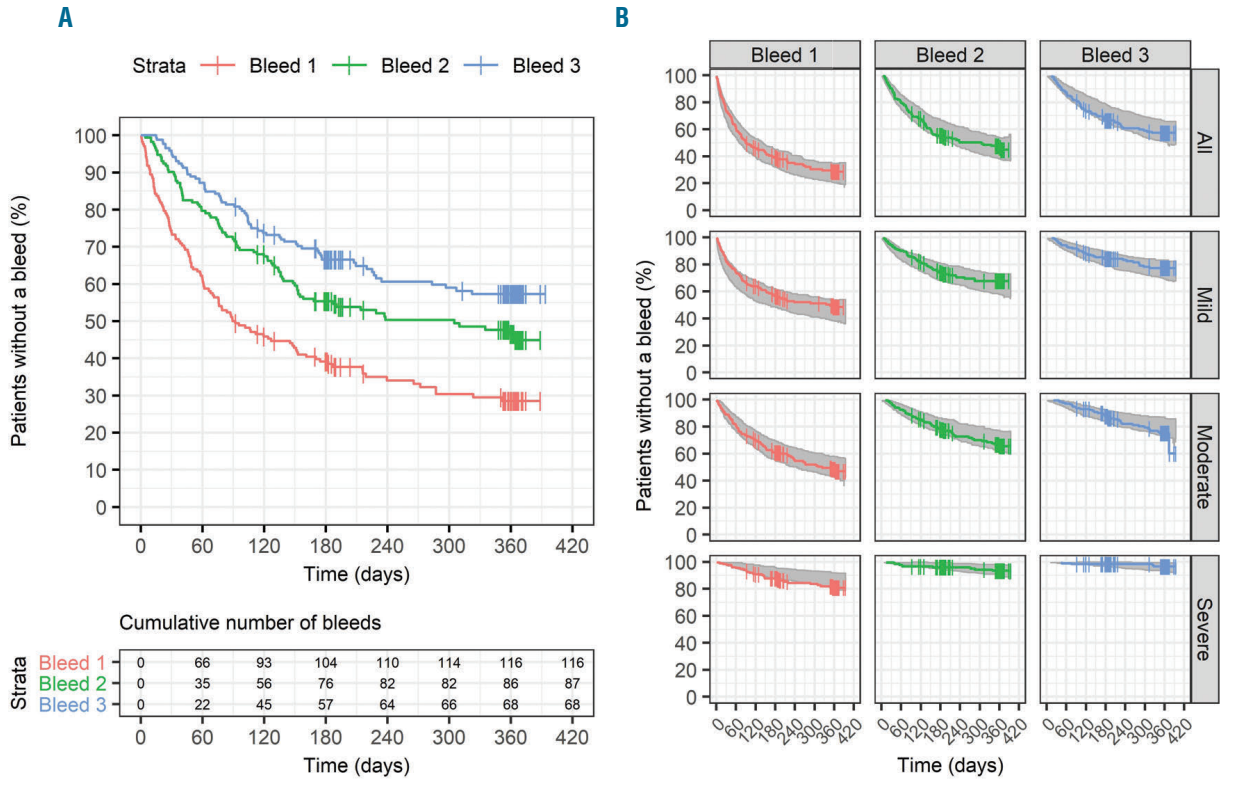

Figure 1. Observed and model-predicted Kaplan-Meier curves depicting the percentage of bleed-free patients *versus* time after start of the LEOPOLD studies, for the first, second and third individual bleed. (A) Observed Kaplan-Meier curves (plot) and cumulative number of bleeds throughout time (table). (B) Observed Kaplan-Meier curves by number of bleeds (first, second or third in the study) and bleeding severity (mild, moderate or severe) overlaid with the 95% confidence interval of the model-predicted Kaplan-Meier curves (shaded area), based on 200 simulations. Vertical lines indicate that a patient was censored.

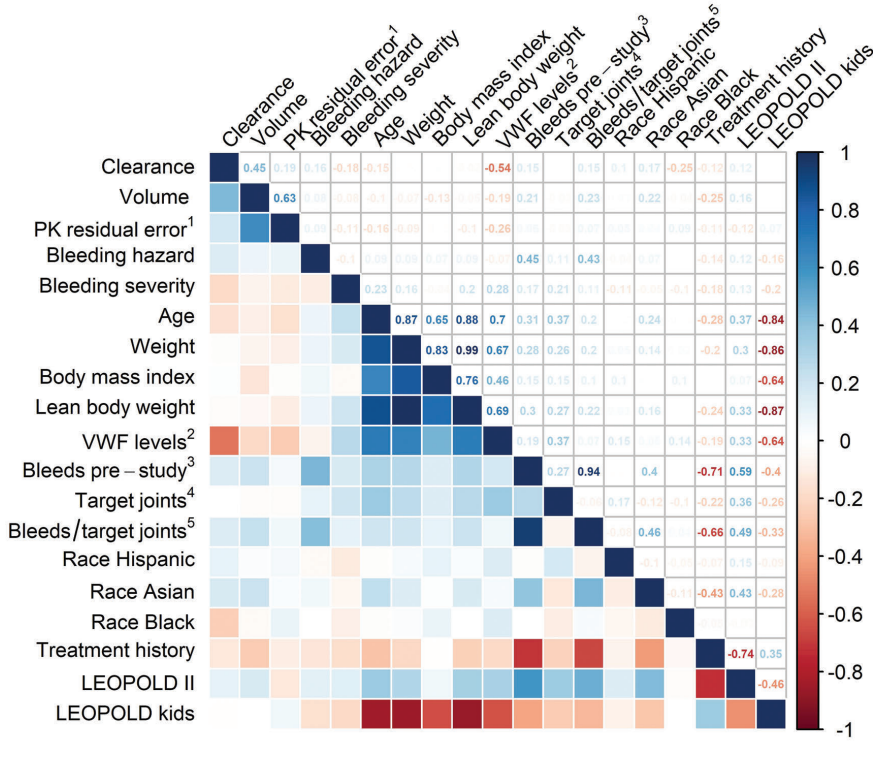

Figure 2. Correlation matrix illustrating the correlations between model parameters and observed study or patient characteristics (covariates). Each square illustrates the correlation between two variables (model parameters or covariates). The same variables are represented in the rows and columns, and the diagonal line shows that each variable correlates perfectly with itself. The first five rows/columns depict the relationship between the model parameters associated with inter-individual variability [clearance, central volume of distribution, pharmacokinetic (PK) residual error, bleeding hazard and bleeding severity] and the covariates, and the remaining rows/columns represent the correlations between the observed covariate values (on the log-scale). The matrix is symmetrical, and the correlations below the main diagonal line are represented with colors. The darker the color, the stronger the interdependence of the two variables, with strong negative correlations represented in dark red (r=-1), i.e. one variable increases as the other decreases, and strong positive correlations represented in dark blue (r=+1), i.e. one variable increases as the other increases. Correlations above the main diagonal line are represented with numbers detailing the correlation coefficient values (r). [1]Unexplained inter-individual variability on the residual error. [2]VWF: von Willebrand factor. [3]Number of bleeds in the 12-month pre-study period. [4]Number of target joints for bleedings at study start. [5]Ratio of the number of bleeds in the 12 months pre-study period to the number of target joints for bleedings at study start.

priori in the PK structural model and the absence of a correlation between LBW on CL or V1 in the covariate analysis indicates that the relationship was well captured by the model. Other characteristics showed lower correlation coefficients, namely, Black race and Asian race decreasing and increasing CL (r=-0.25 and 0.17), respectively, and age and vWF being positively correlated to the severity of bleeding (r=0.23 and 0.28). In addition, correlations were identified between model parameters (e.g. CL and V1, r=0.45) and between covariates (e.g. treatment history and number of bleeds pre-study period, r=-0.71).

The effect sizes of the most relevant parameter-covariate interactions are shown in Figure 3. The number of bleeds in the 12-month pre-study period correlating with the bleeding hazard was the most relevant interaction found. Compared to a mean patient with 8.2 bleeds in the pre-study period, a patient who had one bleed (5th percentile of the observed data) or 84 bleeds (95th percentile) pre-study was found to have a 54% lower (95%CI: 40-65) or 147% higher (95%CI: 79-226) hazard, respectively. These values translate into a bleeding hazard ($\lambda_{0.5\ IU/dL}$) of 1.30 year^{-1} (95%CI: 0.99-1.68) (1 pre-study bleed), and 6.97 year^{-1} (95%CI: 5.05-9.18) (84 pre-study bleeds). von Willebrand factor levels and race were found to correlate with CL. A patient with a vWF level of 64% (5th percentile) or 179% (95th percentile) had an estimated CL of 2.30 dL/h (95%CI: 2.17-2.45; terminal half-life 11.6 h) and 1.59 dL/h (95%CI: 1.47-1.69; terminal half-life 16.5 h), respectively. Patients of Black race had an estimated CL of 1.41 dL/h (95%CI: 1.16-1.71), Asian 2.21 dL/h (95%CI: 1.97-2.48), and Caucasian 1.93 dL/h (95%CI:1.80-2.07). A modest correlation was identified between vWF and bleeding severity, with a patient with a vWF level of 64% having a probability of having a moderate or severe bleed of 57% (95%CI: 55-59), while the corresponding probability for a patient with a vWF level of 179% was 68% (95%CI: 62-75); a similar trend was found for age.

Simultaneous model predictions

An illustration of the observed plasma FVIII activity and time-to-bleed data for three patients, and the respective model-based predictions are available in Figure 4.

Variability in the bleeding hazard

The inclusion of all available covariates in the model resulted in a decrease of 25% in the inter-individual variability on the bleeding hazard, with a final unexplained inter-individual variability value of 111%. Figure 5 shows how this variability translates into bleeding frequency by using the model to simulate the occurrence of bleeds during one year in a group of virtual patients with median characteristics, following doses leading to a given plasma FVIII activity trough value: 1, 3, 5 and 15 IU/dL. Plasma FVIII activity-time profiles with higher trough values were linked to lower bleeding hazards, leading to an expected lower simulated bleeding frequency. The median cumulative number of simulated bleeds for the given dosing scenarios ranged between 0.745 (FVIII activity trough 15 IU/dL) and 2.73 (FVIII activity trough 1 IU/dL) bleeds, and the 90th percentile, representing the inter-patient variability on the bleeding hazard (underlying bleeding tendency), ranged between 3.00 and 11.2 bleeds.

Discussion

We developed a comprehensive mathematical model describing the relation between the dose of a recombinant FVIII product, plasma FVIII activity, the bleeding outcome as well as severity and the correlation with covariates, fol-

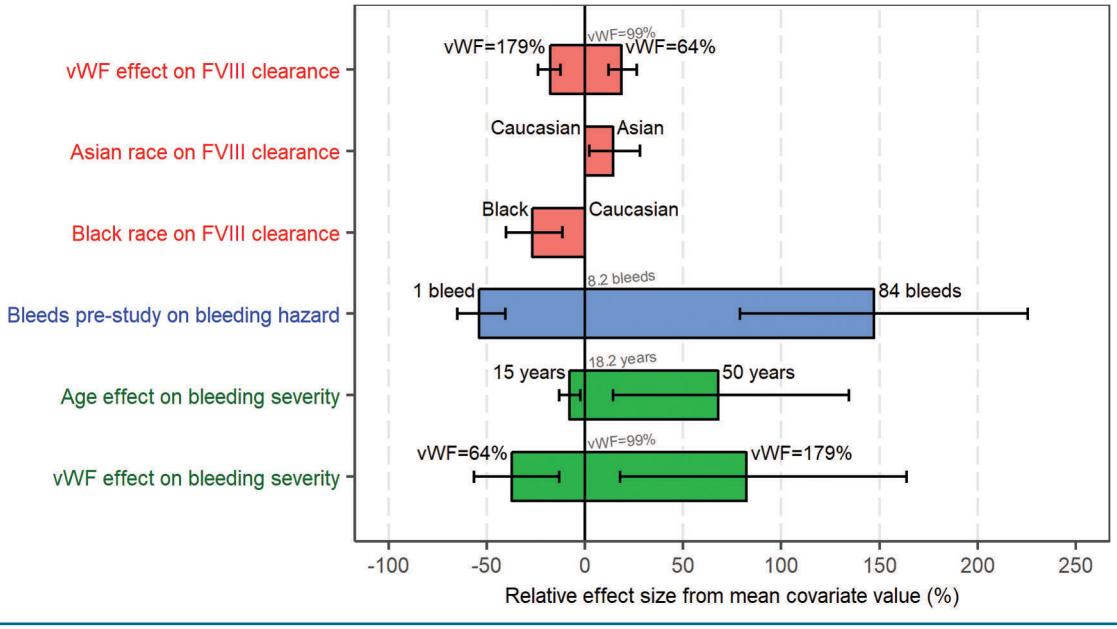

Figure 3. Effect sizes of the most relevant covariates on the estimated model parameters when compared to the mean covariate value, with uncertainty. For continuous covariates (vWF: von Willebrand factor, bleeds pre-study period, and age) the effects at the 5th and 95th percentiles of the covariates are shown, and the geometric mean value is represented in gray. For the categorical covariate race, the effect of the presented category is compared to the most frequent category. The black error bars represent the 95% confidence interval given by the uncertainty of the estimated model parameters. FVIII: factor VIII.

lowing prophylactic treatment in patients with severe hemophilia A. To our knowledge, this is the first reported model characterization including longitudinal bleeding events for a replacement FVIII product. The model was based on observed data of plasma FVIII activity (PK component), bleeding time and severity (RTTCE component) and covariates, collected during the LEOPOLD studies. The final model satisfactorily described plasma FVIII activity and time- and PK-related probability of bleeding. Besides LBW (included *a priori* influencing CL and V1), vWF and race correlated with CL, number of bleeds in the 12-month pre-study period correlated with the bleeding hazard, and age and vWF affected the severity of bleeding. However, even after identifying these covariate effects, the unexplained inter-individual variability on the bleeding hazard was high.

The covariate analysis allowed the exhaustive assessment of the clinical relevance of the correlation between

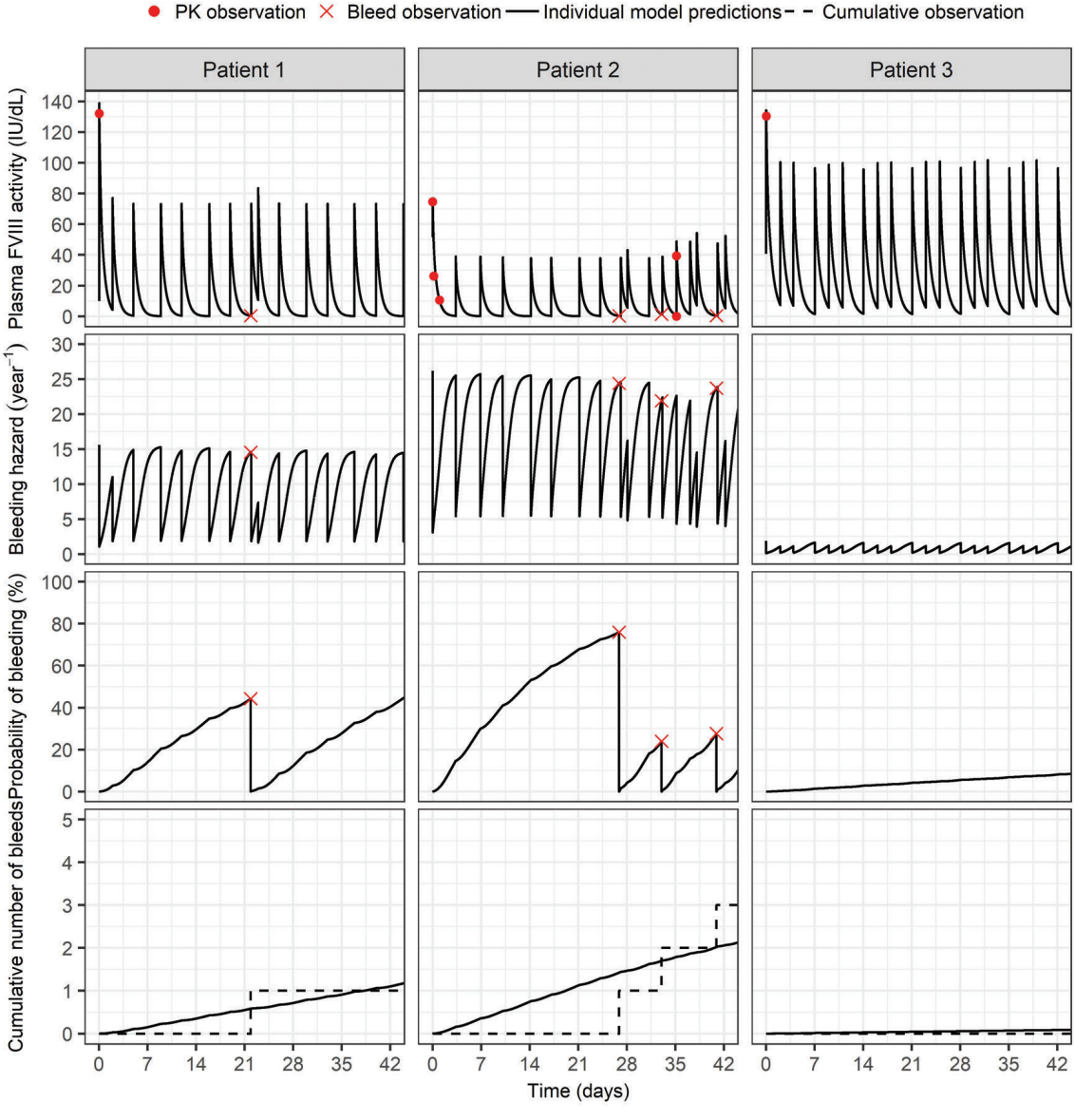

Figure 4. Illustration of the observed pharmacokinetics (PK), observed time-to-bleed data and model predictions (including co-variates) for three illustrative patients during the first six weeks in the study. Patient 1 participated in the LEOPOLD I trial and was 44 years old, weighed 107 kg, received prophylactic treatment before the study started and had six bleeds in the 12 months pre-study period; a PK sample was collected 25 min post-dose on day 1; a bleed occurred on day 22. Patient 2 participated in the LEOPOLD kids trial and was 11 years old, weighed 40 kg, received prophylactic treatment before the study started and had 15 bleeds in the 12 months pre-study period; PK samples were collected at 0.6, 4.25 and 24.2 h post-dose on day 1, and pre-dose and 0.5 h post-dose on day 35. Bleeds occurred on days 27, 33 and 41. Patient 3 participated in the LEOPOLD II trial and was 19 years old, weighed 68 kg, received on-demand treatment before the study started and had 36 bleeds in the 12 months pre-study period; a PK sample was collected at 25 min post-dose on day 1; no bleeds were observed. The first row shows the PK observations (circles), respective model predictions (solid lines) and the time of bleeds (crosses). At the time of the bleeds, the model-predicted factor VIII (FVIII) activity values were 0.38 IU/dL (patient 1) and 0.30, 1.39 and 0.367 IU/dL (patient 2), all values below the lower limit of quantification. The second row depicts the predicted individual bleeding hazard, which is inversely correlated with plasma factor VIII activity, and decreases throughout the time of the study. The third row depicts the individual probability of bleeding, which was calculated based on the individual bleeding hazard (the higher the hazard, the faster the increase in the probability of bleeding) and was reset to zero every time a bleed occurred. The fourth row shows the observed and predicted cumulative number of bleeds over time. Further details on the mathematical derivation of the curves related to bleeding can be found in the *Online Supplementary Appendix*.

Table 2. Parameter estimates for the simultaneous estimation of the pharmacokinetic and repeated time-to-categorical event (RTTCE) sub-components of the final model.

Parameters	Estimate	RSE (%)
PK model		
Structural model		
CL, dL/h	1.93	3.54
V1, dL	30.3	1.72
Q, dL/h	1.69	23.0
V2, dL	6.29	8.79
Covariate parameters		
Effect of LBW on CL[a]	0.646	10.0
Effect of LBW on V1[a]	0.958	3.13
Inter-individual variability		
CL, %CV	30.2[b]	7.31[c]
V1, %CV	15.1[b]	8.75[c]
Residual error, %CV	63.1[b]	7.23[c]
Residual variability		
Additive, IU/dL	1.52	11.0
Proportional, %CV	20.3	5.52
RTTCE model (all bleeds)		
Structural model		
$\lambda_{0.5\ IU/dL}$, year^{-1}	2.82	17.6
$\lambda_{20\ IU/dL}$, year^{-1}	1.00	17.3
$\lambda_{(0\ IU/dL,\ 1\ year)}$ (derived)[d], year^{-1}	2.96	–
IF50 (derived)[d], IU/dL	10.2	–
γ, year^{-1}	-0.566	26.1
b_1	0.424	68.2
b_2	-3.43	6.42
$P_{mild\ bleed}$ (derived),[d,e] %	39.6	–
$P_{moderate\ bleed}$ (derived),[d,e] %	55.7	–
$P_{severe\ bleed}$ (derived),[d,e] %	4.72	–
Inter-individual variability		
λ, %CV	136b	7.95[c]
b_1 and b_2, SD	1.67[b]	10.8[c]

b_1 and b_2: baseline logits of the cumulative bleeding severity probabilities; PK: pharmacokinetics; CL: clearance; CV: coefficient of variation; IF50: factor VIII activity resulting in half-maximum inhibition; LBW: lean body weight; P: probability; Q: inter-compartmental clearance; RSE: relative standard error; RTTCE: repeated time-to-categorical event; SD: standard deviation; V1: central volume of distribution; V2: peripheral volume of distribution; λ: bleeding hazard; γ: shape factor of the Gompertz distribution. [a]typical $CL = CL \cdot \left(\frac{LBW}{51.1}\right)^{effect}$, typical $V1 = V1 \cdot \left(\frac{LBW}{51.1}\right)^{effect}$ [b]η-shrinkage was 10.4, 16.1, 11.2, 15.1, and 26.7% on CL, V1, PK residual error, λ and b, respectively. [c]Relative standard error for inter-individual variability parameters reported on the approximate standard deviation scale (standard error/variance estimate)/2. [d]Derivations and further details available in *Online Supplementary Appendix*. [e]Probability of observing a mild, moderate or severe bleed.

Table 3. Parameter estimates for the repeated time-to-categorical event (RTTCE) sub-component of the final model, including only joint spontaneous bleeds.

Parameters	Estimate	RSE (%)
RTTCE model (only joint spontaneous bleeds)		
Structural model		
$\lambda_{0.5\ IU/dL}$, year^{-1}	1.65	23.8
$\lambda_{20\ IU/dL}$, year^{-1}	0.386	22.9
$\lambda_{(0\ IU/dL,\ 1\ year)}$ (derived)[d], year^{-1}	1.80	–
IF50 (derived)[a], IU/dL	5.45	–
γ, year^{-1}	-0.706	27.6
b_1	0.831	57.6
b_2	-3.95	9.40
$P_{mild\ bleed}$ (derived),[a,b] %	30.3	–
$P_{moderate\ bleed}$ (derived),[a,b] %	65.4	–
$P_{severe\ bleed}$ (derived),[a,b] %	4.23	–
Inter-individual variability		
λ, %CV	157[c]	11.4[d]
b_1 and b_2, SD	2.13[c]	17.0[d]

b_1 and b_2: baseline logits of the cumulative bleeding severity probabilities; CV: coefficient of variation; IF50: FVIII activity resulting in half-maximum inhibition; P: probability; RSE: relative standard error; RTTCE: repeated time-to-categorical event; SD: standard deviation; λ: bleeding hazard; γ : shape factor of the Gompertz distribution. The pharmacokinetics model was the same as presented in Table 2. [a]Derivations and further details available in the *Online Supplementary Appendix*. [b]Probability of observing a mild, moderate or severe bleed. [c]η-shrinkage was 21.8, and 35.1% on λ and b, respectively. [d]Relative standard error for inter-individual variability parameters reported on the approximate standard deviation scale (standard error/variance estimate)/2.

the covariates available and the model parameters. For PK, higher vWF levels were associated with a decreased FVIII CL; an expected finding since the complex FVIII-vWF is known to protect FVIII from proteolytic degradation.[41] The impact was, however, modest, with the typical value of CL being 2.30 and 1.59 dL/h at vWF levels of 64% and 179% (5th and 95th percentiles). The magnitude of the vWF effect on CL is in agreement with results of other population PK studies.[42,43] Interestingly, Black race was associated with a 27% (95%CI: 12-40) lower CL compared to Caucasians. A similar trend was previously identified for a B-domain deleted recombinant FVIII product,[6] and might be in part due to higher vWF levels in Black race patients or other unknown factors.[44] Moreover, Asian race had a 14.2% (95%CI: 2.0-28) higher CL compared to Caucasians. Such a trend had been identified during the previous development of the population PK model, but the relation was not retained due to lack to statistical significance.[36] Due to the modest effect sizes, and the high uncertainty associated with the low number of patients of these races (Asian 31, Black 10), these correlations should be interpreted with caution.

The RTTCE component of the model describes the bleeding probability throughout the study period and the likelihood of that bleed to be mild, moderate or severe. The hazard function describes the distribution of bleeds in time, and represents the instantaneous risk of having a bleed per unit of time. Thus, the cumulative hazard gives the likely number of events in a given time interval. In this analysis, the hazard described a declining bleeding probability with time. The estimated lambda parameter (λ) represents the bleeding hazard at the end of the LEOPOLD I and II studies (1 year), and the shape parameter (γ) describes whether the hazard decreases, remains stable or increases with time. The bleeding hazard estimates for a typical patient at the end of the study were 2.7, 2.0 and 1.2 year-1 for the thresholds of 1, 5 and 15 IU/mL, reflecting the model-predicted annual bleeding rates of patients constantly at a trough value. For instance, a typical patient with a permanent level of 1 IU/dL would be expected to have approximately three bleeds per year, if he remained

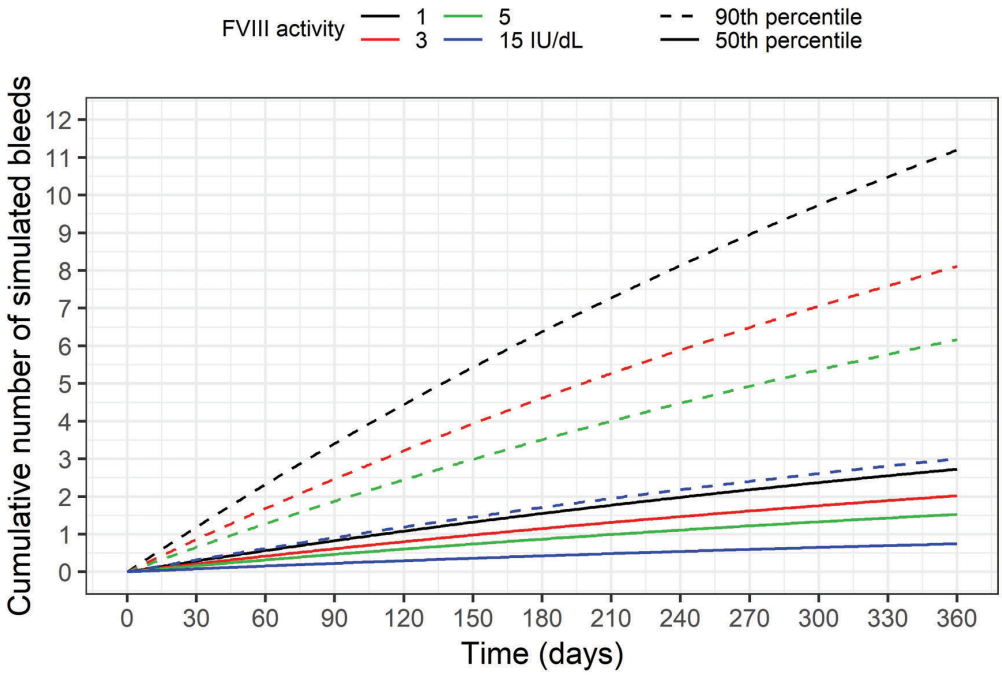

Figure 5. The 50th and 90th percentiles of the cumulative number of simulated bleeds during 1 year after starting treatment assuming only inter-individual variability on the bleeding hazard unexplained by any covariates. The doses considered were 420 IU, 1260 IU, 2100 IU and 6240 IU administered every two days, which correspond to trough factor VIII (FVIII) activity values at steady-state of 1, 3, 5 and 15 IU/dL. Results based on 2000 simulations for a median patient weighing 60 kg.

at the same hazard that was estimated at the end of the study. This numerical summary ignores protective effects against bleeds provided by higher levels and overall exposure, and therefore less bleeds would be expected in a real-world scenario. No additional correlations between PK and the bleeding hazard were found, besides the time-varying FVIII activity.

A time trend was identified in the hazard with a typical patient having 5.0 bleeds/year at the start of the study and 2.8 bleeds/year at the end (assuming a constant plasma FVIII activity of 0.5 IU/dL). The lower bleeding rate at the end of the study most likely captures a treatment effect, not explained by plasma FVIII activity, and can be a consequence of a normalization of the clotting system due to prophylactic treatment or a better adherence to treatment in a clinical trial setting. The number of bleeds in the 12-month pre-study period was found to be a strong predictor of the bleeding frequency. This finding can be explained by the individual-specific bleeding risk given, for example, by pre-existing joint disease and extent of joint damage, comorbidities or level of physical exercise.

The estimated unexplained inter-individual variability on the bleeding hazard was high (111%), representing the variability in the bleeding tendency not being explained by the time-varying plasma FVIII activity or other covariates. Figure 5 shows that even when virtual patients with identical characteristics had a plasma FVIII activity trough of 5 IU/dL, i.e. moderately above the common target of 1 IU/dL, the cumulative number of simulated bleeds was still highly variable at one year, with a median 1.53 bleeds, and 40% of the patients having 1.53 - 6.17 bleeds, and 10% having more than 6.17 bleeds. Such high variability agrees with the clinical observation that patients may respond differently to identical plasma FVIII activity values, thus requiring also individual FVIII trough target levels. Part of this variability may be explained by factors that are known to influence the bleeding tendency in severe hemophilia A patients but that were not available to our study, such as *FVIII* gene mutation type, or physical activity patterns.[45,46] However, even though the magnitude of inter-patient variability potentially explained by missing co-variates is unknown, variability in a real-world scenario is still expected to be high due, for example, to lack of adherence to treatment, or unidentified hemostatic factors playing a role in the occurrence of bleeds.

This study has limitations. First, the LEOPOLD trials were not designed for the aims of this post-hoc analysis or to characterize the individual bleeding pattern. Information, for example, on pre-existing joint disease, comorbidities or level of physical exercise before and during the trials could have been useful to better characterize the bleeding patterns. Second, bleeds (occurrence and severity) and doses were self-reported, which may result in uncertainty of timing and occurrence of bleeds (although the data were reviewed and validated by study staff in an effort to reduce uncertainty). Third, patients without any bleeds (33% of those enrolled in the bleeding observation period) contributed with PK and co-variate information, but with little information to the characterization of the FVIII activity-bleeding hazard relationship. Finally, in the absence of data from on-demand treatment or placebo, we are not able to estimate a bleeding hazard corresponding to untreated patients. Thus, our results cannot be applied to treatment strategies other than prophylaxis.

The individual bleeding hazard estimated by the presented mathematical model is a numerical translation of the individual bleeding phenotype and may be used to further optimize the individualization of dosing regimens of replacement FVIII products. Using this model for dose

individualization, a pre-defined FVIII activity target would not be required, in contrast to the current implementation of PK-based dosing. Instead, the full model would be employed using a Bayesian approach, with the estimation of the individual bleeding hazard in addition to the individual PK parameters. Thus, the individualized dose and dosing interval would be selected not only based on the individual pharmacokinetics, but also the individual bleeding risk. This implementation warrants further study; namely, to understand which information is required to allow a precise estimation of the individual bleeding risk and which target to aim for in the dose calculation.[47]

In conclusion, we have developed an integrated population PK and repeated time-to-categorical bleed model based on data from patients with severe hemophilia A following prophylactic treatment. This combined model characterizes the relationship between the dose of a recombinant FVIII product, plasma FVIII activity, the bleeding outcome, as well as severity and the correlation with covariates. In the future, this model may be used for dose-tailoring using covariate, PK and/or bleeding information. Such an application requires a detailed theoretical assessment as well as robust data on bleeding and other factors, such as lifestyle or comorbidities, with the final goal of suggesting a more effective individualized FVIII dose.

Acknowledgments

The authors would like to thank Gunnar Yngman for skillful assistance during the implementation of the full random effects modeling approach.

References

1. Ahlberg A. Haemophilia in Sweden. VII. Incidence, treatment and prophylaxis of arthropathy and other musculo-skeletal manifestations of haemophilia A and B. Acta Orthop Scand Suppl. 1965:Suppl 77:73-132.
2. Geraghty S, Dunkley T, Harrington C, Lindvall K, Maahs J, Sek J. Practice patterns in haemophilia A therapy -- global progress towards optimal care. Haemophilia. 2006; 12(1):75-81.
3. Manco-Johnson MJ, Abshire TC, Shapiro AD, et al. Prophylaxis versus episodic treatment to prevent joint disease in boys with severe hemophilia. N Engl J Med. 2007; 357(6):535-544.
4. Fischer K, Ljung R. Primary prophylaxis in haemophilia care: Guideline update 2016. Blood Cells Mol Dis. 2017;67:81-85.
5. Iorio A, Marchesini E, Marcucci M, Stobart K, Chan AK. Clotting factor concentrates given to prevent bleeding and bleeding-related complications in people with hemophilia A or B. Cochrane Database Syst Rev 2011;9:CD003429.
6. Abrantes JA, Nielsen EI, Korth-Bradley J, Harnisch L, Jonsson S. Elucidation of Factor VIII Activity Pharmacokinetics: A Pooled Population Analysis in Patients With Hemophilia A Treated With Moroctocog Alfa. Clin Pharmacol Ther. 2017; 102(6):977-988.
7. Collins PW, Fischer K, Morfini M, Blanchette VS, Bjorkman S, International Prophylaxis Study Group Pharmacokinetics Expert Working G. Implications of coagulation factor VIII and IX pharmacokinetics in the prophylactic treatment of haemophilia. Haemophilia. 2011;17(1):2-10.
8. Iorio A, Blanchette V, Blatny J, Collins P, Fischer K, Neufeld E. Estimating and interpreting the pharmacokinetic profiles of individual patients with hemophilia A or B using a population pharmacokinetic approach: communication from the SSC of the ISTH. J Thromb Haemost. 2017; 15(12):2461-2465.
9. Berntorp E. If you know you will also see: population pharmacokinetics is the way to personalize and optimize prophylaxis in hemophilia. J Thromb Haemost. 2017;15(6):1103-1105.
10. Stemberger M, Kallenbach F, Schmit E, et al. Impact of Adopting Population Pharmacokinetics for Tailoring Prophylaxis in Haemophilia A Patients: A Historically Controlled Observational Study. Thromb Haemost. 2018;119(3):368-376.
11. Sheiner LB, Beal S, Rosenberg B, Marathe VV. Forecasting individual pharmacokinetics. Clin Pharmacol Ther. 1979;26(3):294-305.
12. Bjorkman S, Collins P. Measurement of factor VIII pharmacokinetics in routine clinical practice. J Thromb Haemost. 2013; 11(1):180-182.
13. Iorio A. Using pharmacokinetics to individualize hemophilia therapy. Hematology Am Soc Hematol Educ Program. 2017; 2017(1):595-604.
14. Iorio A, Edginton AN, Blanchette V, et al. Performing and interpreting individual pharmacokinetic profiles in patients with Hemophilia A or B: Rationale and general considerations. Res Pract Thromb Haemost. 2018;2(3):535-548.
15. Collins PW, Blanchette VS, Fischer K, et al. Break-through bleeding in relation to predicted factor VIII levels in patients receiving prophylactic treatment for severe hemophilia A. J Thromb Haemost. 2009;7(3): 413-420.
16. Bjorkman S. Prophylactic dosing of factor VIII and factor IX from a clinical pharmacokinetic perspective. Haemophilia. 2003;9Suppl1:101-108; discussion109-110.
17. Valentino LA, Mamonov V, Hellmann A, et al. A randomized comparison of two prophylaxis regimens and a paired comparison of on-demand and prophylaxis treatments in hemophilia A management. J Thromb Haemost. 2012;10(3):359-367.
18. Ahnstrom J, Berntorp E, Lindvall K, Bjorkman S. A 6-year follow-up of dosing, coagulation factor levels and bleedings in relation to joint status in the prophylactic treatment of haemophilia. Haemophilia. 2004;10(6):689-697.
19. Aledort LM, Haschmeyer RH, Pettersson H. A longitudinal study of orthopaedic outcomes for severe factor-VIII-deficient haemophiliacs. The Orthopaedic Outcome Study Group. J Intern Med. 1994;236(4): 391-399.
20. Petrini P. What factors should influence the dosage and interval of prophylactic treatment in patients with severe haemophilia A and B? Haemophilia. 2001;7(1):99-102.
21. Fischer K, Berntorp E. Targeting factor replacement therapy in severe hemophilia: which level is important? Semin Thromb Hemost. 2015;41(8):860-863.
22. Petrini P, Valentino LA, Gringeri A, Re WM, Ewenstein B. Individualizing prophylaxis in hemophilia: a review. Expert Rev Hematol. 2015;8(2):237-246.
23. Valentino LA, Pipe SW, Collins PW, et al. Association of peak factor VIII levels and area under the curve with bleeding in patients with haemophilia A on every third day pharmacokinetic-guided prophylaxis. Haemophilia. 2016;22(4):514-520.
24. Iorio A, Iserman E, Blanchette V, et al. Target plasma factor levels for personalized treatment in haemophilia: a Delphi consensus statement. Haemophilia. 2017;23(3): e170-e179.
25. Chai-Adisaksopha C, Hillis C, Thabane L, Iorio A. A systematic review of definitions and reporting of bleeding outcome measures in haemophilia. Haemophilia. 2015;21(6):731-735.
26. Karlsson KE, Plan EL, Karlsson MO. Performance of three estimation methods in repeated time-to-event modeling. AAPS J. 2011;13(1):83-91.
27. Cox EH, Veyrat-Follet C, Beal SL, Fuseau E, Kenkare S, Sheiner LB. A population pharmacokinetic-pharmacodynamic analysis of repeated measures time-to-event pharmacodynamic responses: the antiemetic effect of ondansetron. J Pharmacokinet Biopharm. 1999;27(6):625-644.
28. Juul RV, Rasmussen S, Kreilgaard M, Christrup LL, Simonsson US, Lund TM. Repeated Time-to-event Analysis of Consecutive Analgesic Events in Postoperative Pain. Anesthesiology. 2015;123(6):1411-1419.
29. Lindauer A, Laveille C, Stockis A. Time-to-Seizure Modeling of Lacosamide Used in Monotherapy in Patients with Newly Diagnosed Epilepsy. Clin Pharmacokinet. 2017;56(11):1403-1413.
30. Plan EL, Karlsson KE, Karlsson MO. Approaches to simultaneous analysis of frequency and severity of symptoms. Clin Pharmacol Ther. 2010;88(2):255-259.
31. Saxena K, Lalezari S, Oldenburg J, et al. Efficacy and safety of BAY 81-8973, a full-length recombinant factor VIII: results from the LEOPOLD I trial. Haemophilia. 2016;22(5):706-712.

32. Kavakli K, Yang R, Rusen L, et al. Prophylaxis vs. on-demand treatment with BAY 81-8973, a full-length plasma protein-free recombinant factor VIII product: results from a randomized trial (LEOPOLD II). J Thromb Haemost. 2015;13(3):360-369.
33. Ljung R, Kenet G, Mancuso ME, et al. BAY 81-8973 safety and efficacy for prophylaxis and treatment of bleeds in previously treated children with severe haemophilia A: results of the LEOPOLD Kids Trial. Haemophilia. 2016;22(3):354-360.
34. Shah A, Solms A, Garmann D, et al. Improved Pharmacokinetics with BAY 81-8973 Versus Antihemophilic Factor (Recombinant) Plasma/Albumin-Free Method: A Randomized Pharmacokinetic Study in Patients with Severe Hemophilia A. Clin Pharmacokinet. 2016;56(9):1045-1055.
35. Beal SL, Sheiner LB, Boeckmann AJ, Bauer RJ (eds). NONMEM 7.4 Users Guides. ICON plc, Gaithersburg, MD. (1989–2018). [https://nonmem.iconplc.com/nonmem743]
36. Garmann D, McLeay S, Shah A, Vis P, Maas Enriquez M, Ploeger BA. Population pharmacokinetic characterization of BAY 81-8973, a full-length recombinant factor VIII: lessons learned - importance of including samples with factor VIII levels below the quantitation limit. Haemophilia. 2017;23(4):528-537.
37. Agresti A. Modelling ordered categorical data: recent advances and future challenges. Stat Med. 1999;18(17-18):2191-2207.
38. Sheiner LB. A new approach to the analysis of analgesic drug trials, illustrated with bromfenac data. Clin Pharmacol Ther. 1994;56(3):309-322.
39. Yngman G, Nyberg J, Jonsson N, Karlsson MO. Practical considerations for using the full random effects modeling (FREM) approach to covariate modeling. 2017. PAGE 26. Abstr 7365 [www.page-meeting.org/?abstract=7365].
40. Karlsson MO. A full model approach based on the covariance matrix of parameters and covariates. 2012. PAGE 21. Abstr 2455 [www.page-meeting.org/?abstract=2455].
41. Weiss HJ, Sussman, II, Hoyer LW. Stabilization of factor VIII in plasma by the von Willebrand factor. Studies on post-transfusion and dissociated factor VIII and in patients with von Willebrand's disease. J Clin Invest. 1977;60(2):390-404.
42. Nestorov I, Neelakantan S, Ludden TM, Li S, Jiang H, Rogge M. Population pharmacokinetics of recombinant factor VIII Fc fusion protein. Clin Pharmacol Drug Dev. 2015;4(3):163-174.
43. Zhang Y, Roberts J, Tortorici M, et al. Population pharmacokinetics of recombinant coagulation factor VIII-SingleChain in patients with severe hemophilia A. J Thromb Haemost. 2017;15(6):1106-1114.
44. Conlan MG, Folsom AR, Finch A, et al. Associations of factor VIII and von Willebrand factor with age, race, sex, and risk factors for atherosclerosis. The Atherosclerosis Risk in Communities (ARIC) Study. Thromb Haemost. 1993;70(3):380-385.
45. Carcao MD, van den Berg HM, Ljung R, Mancuso ME. Correlation between phenotype and genotype in a large unselected cohort of children with severe hemophilia A. Blood. 2013;121(19):3946-3952.
46. Broderick CR, Herbert RD, Latimer J, et al. Association between physical activity and risk of bleeding in children with hemophilia. JAMA. 2012;308(14):1452-1459.
47. Abrantes JA, Solms A, Garmann D, Nielsen EI, Jönsson S, Karlsson MO. Bayesian forecasting utilizing bleeding information to support dose individualization of factor VIII. CPT Pharmacometrics Syst Pharmacol. 2019;8(12):894-903.

Ferrata Storti Foundation

Pre-transplant testosterone and outcome of men after allogeneic stem cell transplantation

Aleksandar Radujkovic,[1] Lambros Kordelas,[2] Julia Krzykalla,[3] Axel Benner,[3] David Schult,[1] Joshua Majer-Lauterbach,[1] Dietrich W. Beelen,[2] Carsten Müller-Tidow,[1] Christian Kasperk,[4] Peter Dreger[1] and Thomas Luft[1]

[1]Department of Internal Medicine V, University of Heidelberg, Heidelberg; [2]Department of Bone Marrow Transplantation, University Hospital, Essen; [3]Division of Biostatistics, German Cancer Research Center, Heidelberg and [4]Department of Internal Medicine I, University of Heidelberg, Heidelberg, Germany

Haematologica 2020
Volume 105(5):1454-1464

ABSTRACT

Testosterone is an important determinant of endothelial function and vascular health in men. As both factors play a role in mortality after allogeneic stem cell transplantation (alloSCT), we retrospectively evaluated the impact of pre-transplant testosterone levels on outcome in male patients undergoing alloSCT. In the discovery cohort (n=346), an impact on outcome was observed only in the subgroup of patients allografted for acute myeloid leukemia (AML) (n=176, hereafter termed 'training cohort'). In the training cohort, lower pre-transplant testosterone levels were significantly associated with shorter overall survival (OS) [hazard ratio (HR) for a decrease of 100 ng/dL: 1.11, *P*=0.045]. This was based on a higher hazard of non-relapse mortality (NRM) (cause-specific HR: 1.25, *P*=0.013), but not relapse (cause-specific HR: 1.06, *P*=0.277) in the multivariable models. These findings were replicated in a confirmation cohort of 168 male patients allografted for AML in a different center (OS, HR: 1.15, *P*=0.012 and NRM, cause-specific HR: 1.23; *P*=0.008). Next, an optimized cut-off point for pre-transplant testosterone was derived from the training set and evaluated in the confirmation cohort. In multivariable models, low pre-transplant testosterone status (<250 ng/dL) was associated with worse OS (hazard ratio 1.95, *P*=0.021) and increased NRM (cause-specific HR 2.68, *P*=0.011) but not with relapse (cause-specific HR: 1.28, *P*=0.551). Our findings may provide a rationale for prospective studies on testosterone/androgen assessment and supplementation in male patients undergoing alloSCT for AML.

Correspondence:

THOMAS LUFT
thomas.luft@med.uni-heidelberg.de

Received: February 23, 2019.

Accepted: July 10, 2019.

Pre-published: July 11, 2019.

doi:10.3324/haematol.2019.220293

Check the online version for the most updated information on this article, online supplements, and information on authorship & disclosures: www.haematologica.org/content/105/5/1454

Introduction

Allogeneic stem cell transplantation (alloSCT) is an effective therapy for many hematologic malignancies, but is still hampered by substantial procedure-related mortality and morbidity. Today, there is growing recognition that endothelial dysfunction is implicated in the pathogenesis of a variety of potentially fatal early and late complications of alloSCT, such as transplant-associated thrombotic microangiopathy, cardiovascular disorders, and graft-*versus*-host disease (GvHD).[1,2]

In particular, therapy refractory GvHD is a substantial determinant of non-relapse mortality (NRM) after alloSCT, and "endothelial vulnerability" was proposed as a hypothesis to explain why some patients with acute GvHD fail to respond to escalating immunosuppressive therapy and ultimately succumb to GvHD and/or treatment related complications.[3-6]

In male individuals, low serum testosterone has been linked to endothelial dysfunction and all-cause and cardiovascular disease-related mortality in various non-transplant settings.[7-9] This is of particular importance as alloSCT is increasingly used in elderly populations characterized by declining sex hormone activity. Notably, with regard to hematologic malignancies, testosterone and androgens have also been used as adjunct in the treatment of acute myeloid leukemia (AML).[10-12]

Based on these considerations, we sought to evaluate the impact of pre-transplant testosterone levels on outcome in male patients undergoing alloSCT.

Methods

Patients

Patients were eligible for this study if they were allografted for a hematologic malignancy between 2002 and 2017 at the University Hospital Heidelberg, Germany, and had serum samples available for measurement of pre-transplant testosterone levels. Pre-transplant testosterone levels were assessed in all male patients meeting these criteria (discovery cohort, n=346). The independent confirmation cohort consisted of male patients diagnosed with AML who had undergone allografting at the University Hospital Essen between 2009 and 2013 and had serum samples available for measurement of testosterone levels (n=168). In addition, pre-transplant testosterone levels were also measured in a small pilot cohort of female patients allografted for AML in Heidelberg (n=32).

Written informed consent for sample and data collection according to the Declaration of Helsinki was obtained for all patients, and the local ethics committees approved the study. Patient data were obtained from medical records and chart review. Disease status prior to alloSCT was assessed applying published criteria.[13] Further details regarding transplant procedure are provided in the *Online Supplementary Appendix.*

Assessment of pre-transplant testosterone serum levels

Serum samples were collected between 0 and 2 weeks before alloSCT and cryopreserved at –80°C. Serum levels of total testosterone were assessed retrospectively in the last serum sample before start of the conditioning treatment. The measurements were carried out using accredited laboratory methods. A detailed description of the methodology is provided in the *Online Supplementary Appendix*. Serum concentrations of total testosterone were expressed in ng/dL (for conversion of ng/dL into nM divide by a factor of 28.8). None of the patients had received sex hormone therapy previous to, or at the time of, sample collection.

Statistical analysis

Overall survival (OS), progression-free survival (PFS) (time to relapse or death from any cause), time to relapse, and non-relapse mortality (NRM) (time to death in absence of prior relapse) were calculated from the date of alloSCT to the appropriate end point. NRM and recurrence of the underlying malignancy were considered as competing events. Since acute GvHD and its treatment are major contributors to post-transplant mortality, OS, PFS, incidence of NRM and relapse were also assessed after acute GvHD (i.e. in patients who developed acute GvHD, from the date of its onset).

Since the normal physiological range of serum testosterone has not been well defined, pre-transplant testosterone was first analyzed as a continuous variable in the uni- and multivariable models. Cox proportional hazards regression analysis was applied for OS, PFS, and OS and PFS after acute GvHD. Relapse and NRM were analyzed by cause-specific Cox models. Prognostic impact of pre-transplant testosterone on OS, PFS, OS and PFS after acute GvHD was assessed by hazard ratios (HR) and, in case of time to relapse and NRM, by cause-specific hazard ratios (CHR) from corresponding (cause-specific) Cox models. Multivariable (cause-specific) Cox regression models were used to adjust for additional co-variates. All statistical tests were two-sided. For further details on the statistical methods used for analysis see the *Online Supplementary Appendix.*

Results

Discovery cohort

Patients', disease and transplant characteristics of the male patients of the discovery cohort (n=346) are summarized in *Online Supplementary Table S1*. Median follow up of survivors was 65 months (95%CI: 57-73). Median pre-transplant total testosterone serum level was 400 ng/dL [interquartile range (IQR) 269-584].

In univariable analysis, lower pre-transplant testosterone as continuous variable was significantly associated with shorter OS and PFS (HR for a decrease of 100 ng/dL, 1.11, 95%CI: 1.03-1.20, *P*=0.005 and HR 1.12, 95%CI: 1.05-1.20, *P*=0.001, respectively). This was due to a significantly higher risk of both NRM and relapse (CHR 1.15, 95%CI: 1.02-1.28, *P*=0.018 and CHR 1.11, 95%CI: 1.01-1.20, *P*=0.023, respectively). However, in both the "slim" and "full" multivariable models, significant associations of pre-transplant testosterone with any end point could not be confirmed. This was based on a statistically significant interaction between pre-transplant testosterone and the diagnosis AML for the end point NRM (*Online Supplementary Table S2*).

Accordingly, lower levels of pre-transplant testosterone were significantly associated with shorter OS and PFS, and higher hazard of NRM and relapse only in the subgroup of patients allografted for AML (n=176) but not for other diagnoses (n=170) as revealed by the univariable models (*Online Supplementary Table S3*). Patients' and transplant characteristics of AML *versus* non-AML patients are also provided in *Online Supplementary Table S1.* Consequently, further analyses were restricted to male patients with AML, henceforth referred to as the 'training cohort' (n=176).

Pre-transplant testosterone and post-transplant outcome in the training cohort

Patients', disease and transplant characteristics of the training cohort are summarized in Table 1. Median pre-transplant total testosterone serum level was 423 ng/dL (IQR 256-611; for distribution, see histogram in *Online Supplementary Figure S1A*) and the estimated median follow up of survivors was 36 months (95%CI: 32-47). The cumulative incidence of acute GvHD grade 3-4 on day +100 post-transplant was 5.1% (95%CI: 1.7-8.4). Pre-transplant testosterone had no impact on the hazard of acute GvHD grade 3-4 (HR 0.92 95%CI: 0.74-1.15, *P*=0.448).

Since testosterone might also reflect the individual's health and nutritional status prior to alloSCT, pre-transplant testosterone levels were correlated to additional patients' characteristics: body-mass index (BMI), levels of C-reactive protein (CRP), performance status and comorbidities prior to alloSCT. These data were only available for the training cohort and are summarized in *Online Supplementary Table S4*. Pre-transplant testosterone levels were weakly negatively correlated to pre-transplant CRP levels (Spearman's rho: -0.17, P=0.025) and were not correlated to the BMI (Spearman's rho: -0.12, *P*=0.107). However, pre-transplant testosterone levels were lower in obese patients of the training cohort (BMI ≥30 kg/m^2, *P*=0.028) (*Online Supplementary Figure S2A*). The median pre-transplant testosterone levels were similar between patients with elevated (>5 mg/L) and non-elevated (≤5

Table 1. Patients' disease and transplant characteristics of male acute myeloid leukemia (AML) patients of the training and confirmation cohorts.

	Training cohort n=176	Confirmation cohort n=168	P
Parameter			
Age [years] at alloSCT (median, IQR)	59 (50-64)	56 (45-63)	0.818
Disease stage before alloSCT[a], n (%)			0.022
Early	74 (42)	78 (47)	
Intermediate	32 (18)	45 (27)	
Late	69 (39)	44 (26)	
NA	1	1	
Conditioning[b], n (%)			0.003
RIC	114 (65)	132 (80)	
MAC	62 (35)	34 (20)	
NA	0	2	
Stem cell source, n (%)			0.632
Peripheral blood	168 (96)	158 (94)	
Bone marrow	8 (4)	10 (6)	
Donor, n (%)			0.182
Related	41 (23)	29 (17)	
Unrelated	135 (77)	139 (83)	
Recipient – donor sex match, n (%)			0.078
Matched	127 (72)	135 (80)	
Male – female	49 (28)	33 (20)	
Pre-transplant testosterone, ng/dL (median, IQR)	423 (256-611)	469 (309-580)	0.043

alloSCT: allogeneic stem cell transplantation; AML: acute myeloid leukemia; CI: confidence interval; IQR: interquartile range; MAC: myeloablative conditioning; NA: not available or not assessable; RIC: reduced intensity conditioning. [a]According to Gratwohl *et al.*[13] [b]According to Bacigalupo *et al.*[37] and Bornhäuser *et al.*[38]

mg/L) CRP levels prior to alloSCT (P=0.127) (*Online Supplementary Figure S2B*). There was a trend towards lower pre-transplant testosterone levels in patients with lower Karnofsky performance status (KPS ≤80%), whereas testosterone levels were similar between the low hematopoietic cell transplantation-specific comorbidity index[14] group (HCT-CI 0), intermediate (HCT-CI 1 to 2), and high risk (HCT-CI 3 or more) HCT-CI groups (*Online Supplementary Figure S2C and D*; for further details see the *Online Supplementary Appendix*).

In univariable analysis, lower pre-transplant testosterone was correlated with shorter post-transplant OS and PFS, due to higher hazards of both relapse and NRM. Low pre-transplant testosterone was also associated with non-relapse and overall mortality after onset of acute GvHD. The results of the univariable analyses of the training cohort are given in Table 2.

In the multivariable models, lower levels of pre-transplant testosterone were significantly associated with worse OS (HR for a decrease of 100 ng/dL, 1.11, P=0.045) and PFS (HR 1.11, P=0.022) ("full" models). Other factors with a statistically significant impact on OS and PFS were patient age and advanced disease stage (Table 3). Notably, lower pre-transplant testosterone was associated with a higher hazard of NRM (CHR 1.25, P=0.013) rather than relapse (CHR 1.06, P=0.277) in patients allografted for AML as revealed by the "slim" models (Table 3).

In contrast to the univariable models (Table 2), no significant association of testosterone with survival after onset of acute GvHD could be observed in multivariable analysis (Table 3). Consequently, and due to the relatively low number of events, no multivariable models were fitted for NRM/relapse following acute GvHD. When pre-transplant testosterone as continuous variable was analyzed in multivariable models including age, CRP, BMI, KPS and comorbidities as co-variates, the associations of lower testosterone with worse OS and shorter PFS remained significant (*Online Supplementary Table S5*).

Finally, pre-transplant testosterone was assessed and evaluated in a small pilot cohort of female patients allografted for AML in the Heidelberg center (n=32) (*Online Supplementary Table S6*). As expected, median pre-transplant total testosterone serum levels were substantially (20-fold) lower than in males. Importantly, no association of testosterone (per decrease of 10 ng/dL) with any end point was observed in the univariable models (*Online Supplementary Table S7*).

Pre-transplant testosterone and post-transplant outcome in the confirmation cohort

Patients', disease and transplant characteristics of the confirmation cohort are summarized in Table 1. As compared to the training cohort, significantly fewer patients were transplanted for late-stage disease and were allografted after myeloablative conditioning (Table 1). In the confirmation cohort, median pre-transplant total testosterone serum level was 469 ng/dL (IQR 309-580) (*Online Supplementary Figure S1B*). The estimated median follow up of survivors was 47 months (95%CI: 39-53). The cumulative incidence of acute GvHD grade 3-4 on day

Table 2. Univariable analysis of pre-transplant testosterone in the training (n=176) and in the confirmation (n=168) cohorts.

	Training cohort (n=176) Testosterone per 100 ng/dL decrease		Confirmation cohort (n=168) Testosterone per 100 ng/dL decrease	
	HR 95%CI	P	HR 95%CI	P
End point				
OS	1.16 (1.05-1.28)	0.002	1.12 (1.03-1.25)	0.027
PFS	1.18 (1.08-1.28)	0.0005	1.09 (0.99-1.20)	0.088
OS after acute GvHD	1.19 (1.01-1.41)	0.040	1.15 (1.03-1.30)	0.012
PFS after acute GvHD	1.22 (1.04-1.43)	0.015	1.12 (1.01-1.23)	0.037
	CHR 95%CI	P	CHR 95%CI	P
NRM	1.28 (1.09-1.52)	0.003	1.19 (1.03-1.30)	0.019
Relapse	1.12 (1.01-1.25)	0.033	1.01 (0.88-1.15)	0.916
NRM after acute GvHD	1.45 (1.11-1.89)	0.005	1.19 (1.03-1.39)	0.022
Relapse after acute GvHD	1.06 (0.86-1.32)	0.552	1.05 (0.91-1.22)	0.490
	HR 95%CI	P	HR 95%CI	P
Acute GvHD grade 3-4	0.92 (0.74-1.15)	0.448	1.23 (0.99-1.54)	0.055

AML: acute myeloid leukemia; CHR: cause-specific hazard ratio; CI: confidence interval; GvHD: graft-*versus*-host disease; HR: hazard ratio; OS: overall survival; PFS: progression-free survival; NRM: non-relapse mortality.

+100 post-transplant was 11.9% (95%CI: 7.0-16.8) and pre-transplant testosterone had no significant impact on risk of acute GvHD grade 3-4 (HR 1.23 95%CI: 0.99-1.54, *P*=0.055).

In univariable analysis, similar to the training cohort, lower pre-transplant testosterone (as continuous variable) showed significant associations with shorter OS, and worse OS and PFS after onset of acute GvHD. In this cohort of AML patients, this was due in both instances to a higher hazard of NRM rather than relapse (Table 2). These findings were further substantiated in the corresponding multivariable models of the confirmation cohort (Table 4).

Optimized pre-transplant testosterone cut-off value and illustration of outcome correlations

Continuous effects, in general, are less instructive and often hard to interpret, particularly with regard to interventions in a possible future clinical trial setting. Therefore, in order to facilitate further evaluation of pre-transplant testosterone status, an optimal cut-off determination with regard to post-transplant OS was conducted in the training cohort. The analysis revealed multiple cut-off points (*Online Supplementary Figure S3*). The value of 250 ng/dL (corresponding to 8.7 nM, significance level of *P*=0.018) was used as optimal cut-off point, since it agrees with the reports in the literature on testosterone and mortality[15,16] and exactly reflects the lower level of our center's reference range (250-1000 ng/dL).

When the optimized cut-off of 250 ng/dL was analyzed in multivariable models including age, CRP, BMI, KPS and comorbidities as confounding variables, the associations of lower testosterone status (<250 ng/dL) with worse OS and shorter PFS remained significant (HR 2.0 for both OS and PFS) in the training cohort (*Online Supplementary Table S8*).

The optimized cut-off of 250 ng/dL was next evaluated in the multivariable models of the confirmation cohort, showing that low pre-transplant testosterone status (<250 ng/dL) was correlated with worse survival both post transplant (HR approx. 2) and after onset of acute GvHD (HR approx. 2.3) (Table 5). Again, the association of low pre-transplant status with OS after alloSCT was mainly driven by a nearly 2.7-fold increased hazard of NRM (Table 5).

For illustration purpose, patients of both cohorts were stratified according to high (≥250 ng/dL) and low (<250 ng/dL) pre-transplant testosterone status; the corresponding plots for the end points post-transplant and after onset of acute GvHD are given in Figure 1 and Figure 2, respectively.

Non-relapse causes of death

To further explore the association of pre-transplant testosterone with NRM, we made a detailed analysis of non-relapse causes of death in both cohorts. In the training cohort, a total of 35 non-relapse deaths occurred. These were caused by severe infections (including sepsis) in 20 (57%), acute GvHD (i.e. lethal complications of acute GvHD and/or its treatment) in 13 (37%), and cardiovascular events in two (6%) patients. In the confirmation cohort, a total of 47 non-relapse deaths occurred. Again, the most common non-relapse cause of death was infection/sepsis in 32 (68%) followed by lethal acute GvHD in nine (19%), and cardiovascular events in six (13%) patients, respectively. Notably, as compared to patients not succumbing to NRM, in both cohorts, serum levels of pre-transplant testosterone tended to be lower in patients who died of lethal complications of acute GvHD (Figure 3).

Correlation of pre-transplant testosterone with pre-transplant serum levels of suppressor of tumorigenicity-2

When both cohorts were combined, pre-transplant serum levels of soluble suppressor of tumorigenicity-2 (ST2) were available for a total of 218 patients. Pre-transplant testosterone levels were weakly negatively correlated to pre-transplant soluble ST2 levels (Spearman's rho: -0.13, *P*=0.048). However, when regarding the pre-transplant testosterone cut-off value of 250 ng/dL, median pre-transplant ST2 was significantly higher in patients with low pre-transplant testosterone status (<250 ng/dL) as compared to patients of the high (≥250 ng/dL) pre-transplant testosterone group (573 pg/mL, IQR 255-2082 *vs.* 350 pg/mL, IQR 212-587, *P*=0.005, respectively) (*Online Supplementary Figure S4*).

Discussion

The present study is, to the best of our knowledge, the first to evaluate testosterone status in the context of outcome and mortality after alloSCT. So far, studies in the alloSCT setting have focused on the impact of chronic GvHD and its treatment on the androgen status,[17] or have investigated the relationship between sex hormone levels and overall gonadal function, mainly in the context of late complications after alloSCT.[18,19] Evaluation of testosterone status in the context of outcome and mortality after alloSCT, therefore, appears to meet an unmet need, given that sex hormones are involved in the regulation of a wide range of physiological processes that affect metabolism, tissue and cardiovascular homeostasis, inflammatory and immune responses,[20] and thus may interfere with alloSCT outcome.

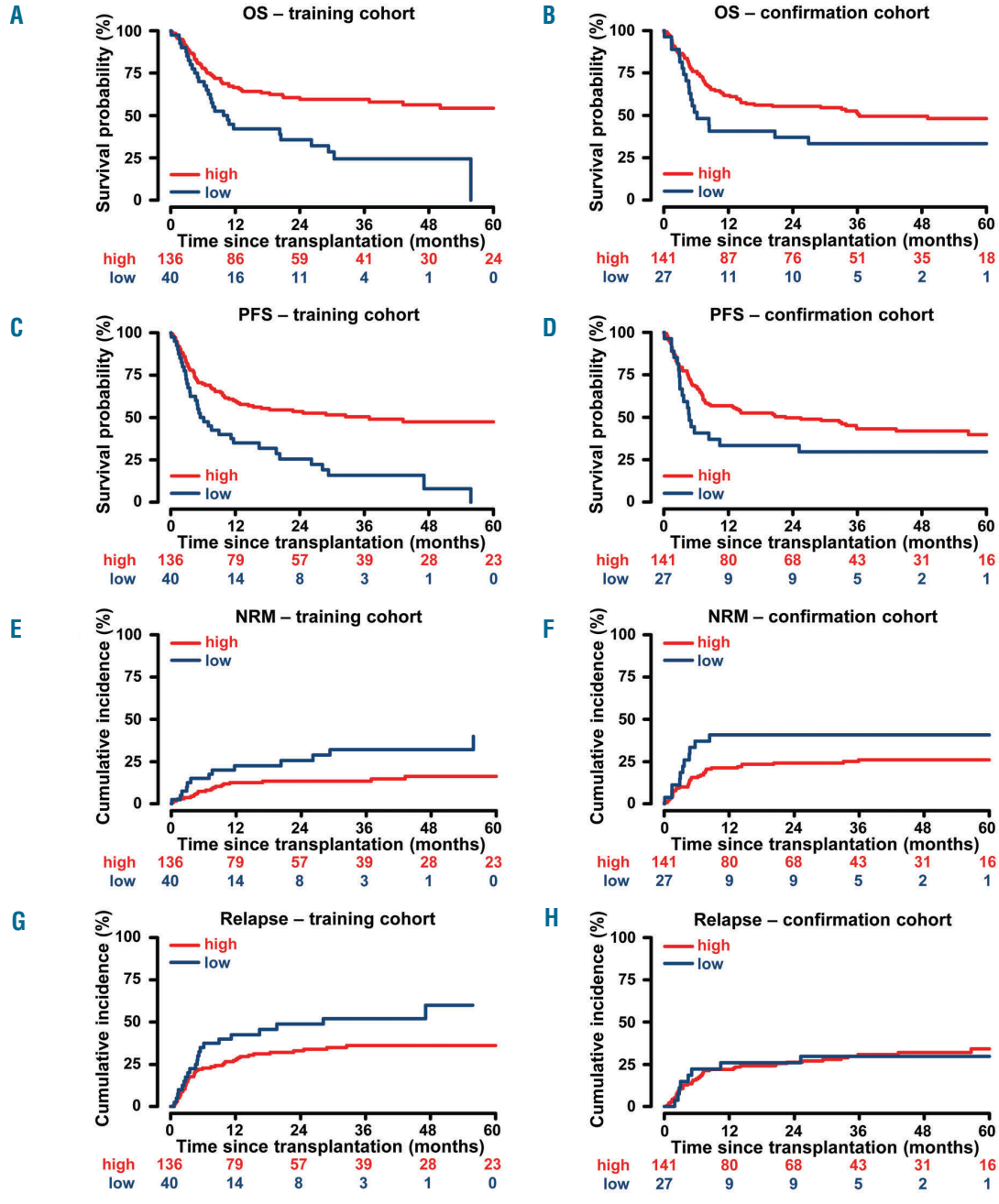

Figure 1. Impact of pre-transplant testosterone status on outcome measures after allogeneic stem cell transplantation (alloSCT) in the training and in the confirmation cohorts. The cut-off point of 250 ng/dL was derived from the Heidelberg training cohort of men allografted for acute myeloid leukemia (AML) (n=176). It was used to stratify patients in low (<250 ng/dL) and high (≥250 ng/dL) pre-transplant testosterone groups, and then applied to an independent cohort of male AML patients who underwent alloSCT in the Essen center (confirmation cohort, n=168) (see *Online Supplementary Figure S1*). (A and C) Distribution of overall survival (OS) and progression-free survival (PFS) since transplant in the training cohort. (B and D) Distribution of OS and PFS since transplant in the confirmation cohort. (E and G) Incidence curves of non-relapse mortality (NRM) and relapse after alloSCT in the training cohort. (F and H) Incidence curves of NRM and relapse after alloSCT in the confirmation cohort. Curves of patients with low (<250 ng/dL) and high (≥250 ng/dL) pre-transplant testosterone status are shown in blue and in red, respectively.

In our study, impact of pre-transplant testosterone on outcome was observed only in the subgroup of male patients allografted for AML. Lower levels of pre-transplant testosterone were associated with worse OS and PFS post-transplant, largely due to a significantly increased risk of NRM. The reason for this disease-specific association is unclear.

In general, testicular damage and dysfunction, which result in low testosterone status, appear to be rather long-term sequelae of cytotoxic chemotherapy, and the clinically most significant toxicities are observed after regimens employing higher doses of alkylating agents.[21] In contrast, adult AML patients considered eligible for alloSCT are usually treated by combination therapy employing anthracyclines and antimetabolites in both first-line and salvage treatment approaches. As patients in advanced disease stage are likely to have received more aggressive therapy prior to transplant and to account for the more deleterious effect of treatment intensity, we have considered disease stage prior to alloSCT as confounding variable in all multivariable models. In both cohorts, the associations of pre-transplant testosterone with worse outcome were not confounded by disease stage prior to transplant.

One possible explanation for the observed disease-specific association may be related to the immunoregulatory cytokine network in human AML, including leukemia cell-derived angiopoietins and the interleukin-33/ST2 axis, and the likely cross-talk between leukemic and endothelial cells.[22-26] Notably, soluble ST2 and angiopoietin-2 were known to be associated with endothelial dysfunction and cardiovascular risk,[27,28] and in the context of alloSCT, both were highly correlated with therapy-refractoriness of acute GvHD and high overall mortality.[3,29] Given the inverse correlation of pre-transplant serum levels of testosterone with soluble ST2 observed in our patients, some speculation about endothelial involvement in the present study may appear justified.

Analysis of non-relapse causes of death revealed that pre-transplant testosterone levels tended to be lower in patients that later succumbed to acute GvHD and/or its treatment, and lower pre-transplant testosterone levels were also associated with shorter survival after onset of GvHD. In this regard, our findings fit into the concept of "endothelial vulnerability".[3,4] In the setting of alloSCT, this concept describes a condition/predisposition that manifests itself particularly after a severe challenge, such as conditioning therapy or GvHD. Since this "vulnerability" is, at least in part, a characteristic of the recipient's endothelial cell system, a corresponding increased risk of mortality may already be identified prior to transplantation by assessing endothelial biomarkers. Accordingly, low(er) pre-transplant testosterone, which represents a known determinant of endothelial dysfunction in men,[7] may therefore promote and/or enhance this "vulnerability", resulting in the observed increase in treatment-related mortality.

However, it should be noted that our study design is not able to definitely support (or refute) the hypothesis of endothelial involvement. Although the associations of lower pre-transplant testosterone levels with worse outcome in the training cohort continued to hold true when additional confounding variables that reflect comorbidities and the patients' nutritional and overall status were included in the multivariable models, the possibility that lower pre-transplant testosterone is primarily an expres-

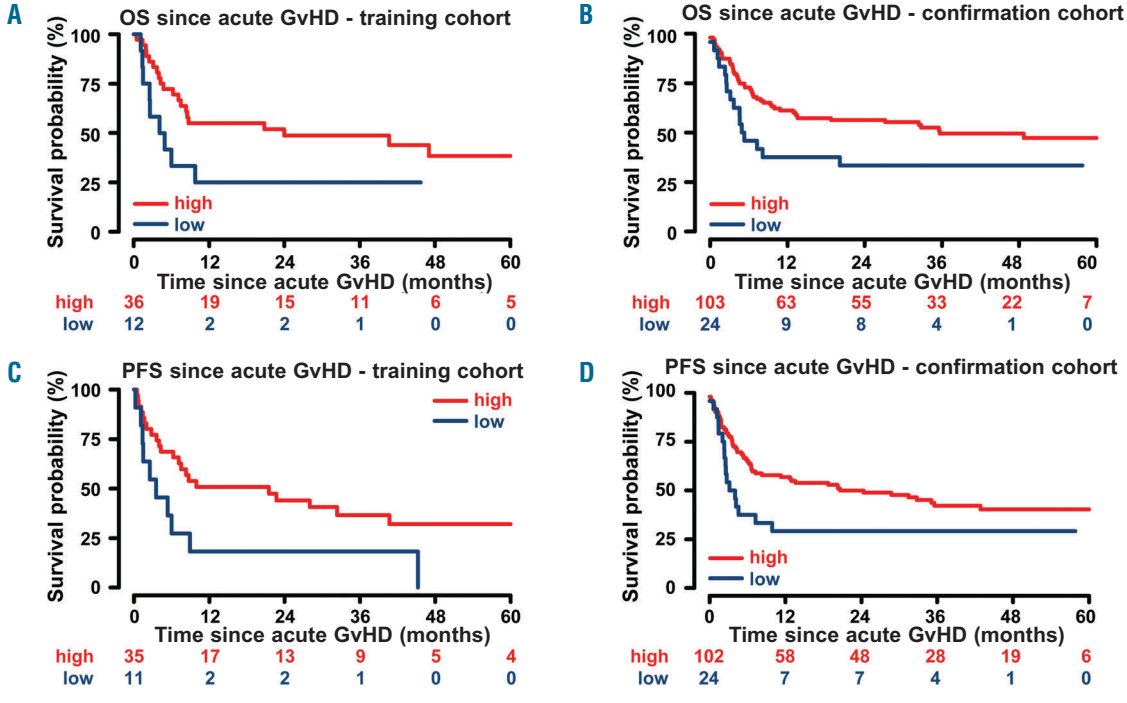

Figure 2. Impact of pre-transplant testosterone status on outcome measures after onset of acute graft-*versus*-host disease (GvHD) in the training and in the confirmation cohorts. (A and C) Distribution of overall survival (OS) and progression-free survival (PFS) since onset of acute GvHD in the training cohort. (B and D) Distribution of OS and PFS since onset of acute GvHD in the confirmation cohort. Curves of patients with low (<250 ng/dL) and high (≥250 ng/dL) pre-transplant testosterone status are shown in blue and in red, respectively.

sion of patients' general health status prior to alloSCT cannot be ruled out.

Currently, there is an ongoing "testosterone debate" in the field of cardiovascular medicine. Although the association between testosterone levels and cardiovascular mortality seems to be conclusive, prospective data on testosterone treatment are scarce, and so far no prospective controlled study has been able to show that treatment with testosterone or normalization of testosterone levels can reduce cardiovascular events.[30] On the contrary, results of a recently published prospective controlled study, which is one of seven co-ordinated National Institutes of Health (NIH)-supported trials of testosterone treatment in elderly men ("T Trials"),[31] indicate that testosterone may even increase cardiovascular risk, as reflected by increasing coronary artery plaque volume following testosterone treatment.[32] Thus, although of potential clinical value, any long-term health benefits of testosterone supplementation remain to be established.

As regards myeloid malignancies, testosterone among other sex steroids has been shown to exert cytostatic and cytotoxic effects on several myeloid leukemia cell lines *in vitro*.[33] However, although an early pilot study on AML patients using androgens as an adjunct in different first-line and maintenance treatment approaches showed an unexpectedly high rate of long-term survivors in a group of patients who achieved complete remission,[10] larger randomized studies failed to show beneficial effects on overall and disease-free survival.[11] Only recently, a prospective controlled trial in elderly patients with AML suggested that maintenance therapy with low-dose oral norethandrolone, a synthetic androgen with similar anabolic activity to testosterone, significantly improves overall, disease- and event-free survival,[12] and this has renewed interest in this treatment approach. However, in this study, the beneficial effects of androgen maintenance therapy were observed only in patients with low disease burden at diagnosis and only in the absence of relapse during the first year of treatment.[12] This might imply that androgen treatment has had some impact on disease-independent mortality. Interestingly, in the aforementioned trial, female patients were also treated, and the multivariable

Table 3. Multivariable analysis of the training cohort with the end points overall survival (OS), progression-free survival (PFS), non-relapse mortality (NRM), and relapse following allogeneic stem cell transplantation and OS and PFS after onset of acute graft-*versus*-host disease (GvHD) (complete case analysis).

	OS (n=175)		PFS (n=175)		NRM* (n=175)		Relapse* (n=175)		OS after acute GvHD* (n=48)		PFS after acute GvHD* (n=45)	
	HR 95% CI	*P*	HR 95% CI	*P*	CHR 95% CI	*P*	CHR 95% CI	*P*	HR 95% CI	*P*	HR 95% CI	*P*
Covariate												
Testosterone	1.11		1.11		1.25		1.06		1.14		1.12	
(per 100 ng/dL decrease)	(1.00-1.22)	0.045	(1.02-1.22)	0.022	(1.05-1.47)	0.013	(0.95-1.19)	0.277	(0.95-1.35)	0.152	(0.95-1.33)	0.171
Disease stage†												
Early	Ref		Ref		Ref		Ref		Ref		Ref	
Intermediate	0.92		0.94		0.62		1.14		3.65		3.35	
	(0.46-1.86)	0.822	(0.50-1.78)	0.857	(0.19-1.95)	0.411	(0.55-2.36)	0.720	(1.26-10.61)	0.017	(1.13-9.88)	0.029
Late	1.87		1.74		2.11		2.17		2.98		4.59	
	(1.03-3.36)	0.038	(1.04-3.08)	0.036	(1.00-4.45)	0.050	(1.25-3.76)	0.006	(1.16-7.64)	0.023	(1.80-11.68)	0.001
Age (per 10-year increase)	1.26		1.28		1.13		1.28		1.11		1.13	
	(1.02-1.54)	0.029	(1.06-1.55)	0.010	(0.84-1.52)	0.415	(1.01-1.61)	0.040	(0.78-1.59)	0.564	(0.80-1.59)	0.498
Conditioning												
MAC	Ref		Ref		–	–	–	–	–	–	–	–
RIC	0.70 (0.41-1.21)	0.203	0.69 (0.41-1.15)	0.152								
Donor												
Related donor	Ref		Ref		–	–	–	–	–	–	–	–
Unrelated Donor	1.36		1.35									
	(0.82-2.26)	0.233	(0.84-2.15)	0.214								
Recipient - donor sex match												
Matched	Ref		Ref		–	–	–	–	–	–	–	–
Male recipient /	0.77		0.89									
female donor	(0.46-1.31)	0.341	(0.55-1.43)	0.630								
Donor source												
PB	Ref		Ref		–	–	–	–	–	–	–	–
BM	1.60		1.24									
	(0.62-4.13)	0.333	(0.49-3.15)	0.652								

Number of events: OS, n=87; PFS, n=102; NRM, n=35; relapse, n=67; OS after acute GvHD, n=30; PFS after acute GvHD, n=32. *Slim model. †According to Gratwohl *et al.*[13] BM: bone marrow; CHR: cause-specific hazard ratio; CI: confidence interval; HR: hazard ratio; MAC: myeloablative conditioning; PB: peripheral blood; RIC: reduced intensity conditioning.

models revealed no impact of gender on survival. In our cohorts of male patients allografted for AML, pre-transplant testosterone did not correlate with post-transplant relapse risk, suggesting an only limited, if any, impact on disease control. Conversely, and similar to the androgen maintenance trial,[12] in our patients, the associations of testosterone with post-transplant survival were largely driven by increased NRM.

Besides its retrospective nature, several potential limitations of our study need to be addressed. First, and as already stated above, we cannot definitely exclude the possibility that testosterone solely reflects the individual's health and nutritional status prior to alloSCT, and thus unknown confounders cannot be ruled out. Second, due to its observational character, our study does not provide evidence for causality between testosterone and post-transplant outcome, and therefore our results here need to be interpreted with caution. Further, measurements of

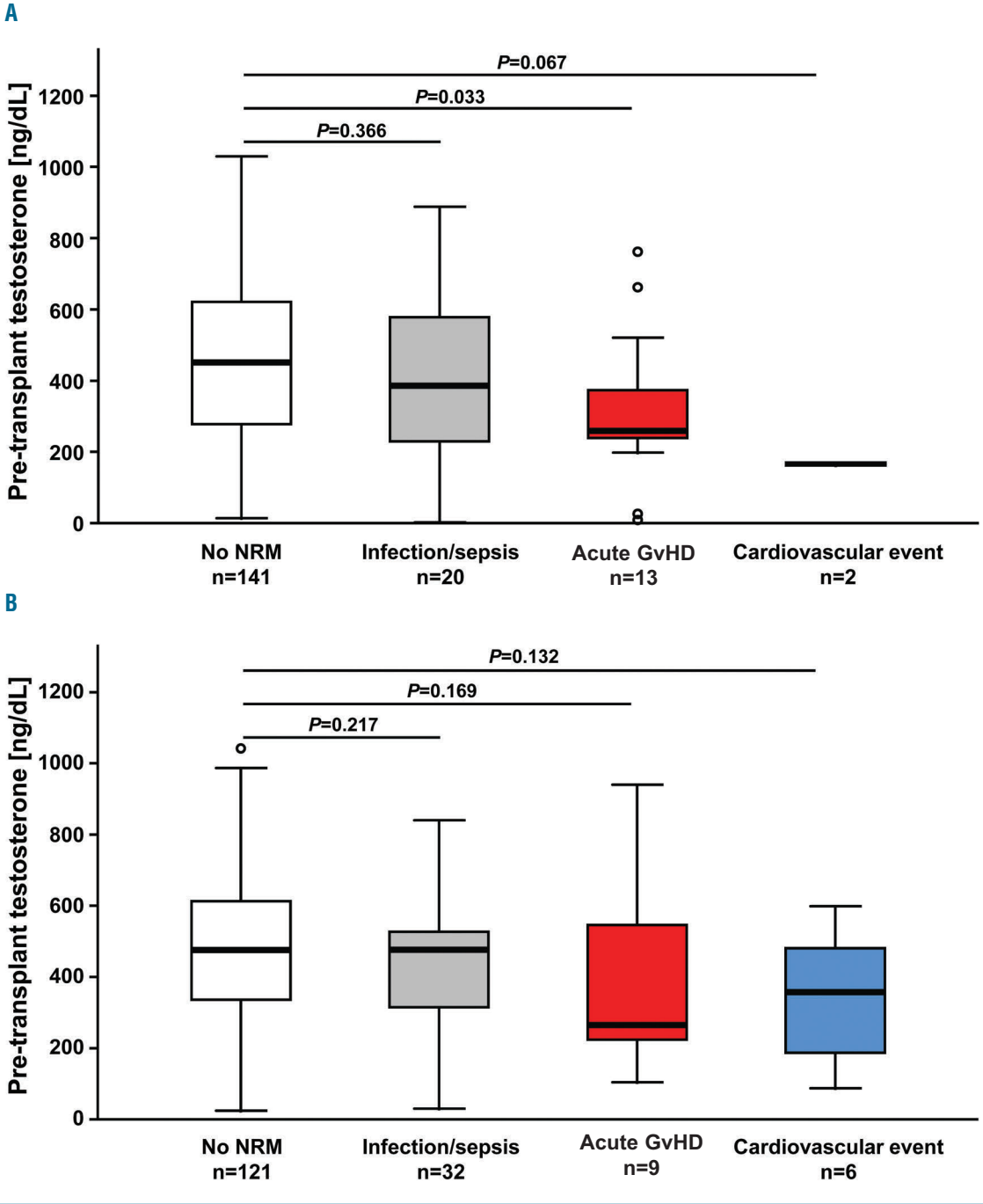

Figure 3. Comparison of pre-transplant testosterone serum levels according to different non-relapse causes of death in the training and in the confirmation cohorts. Non-relapse causes of death were grouped into three categories: severe infection/sepsis, death due to acute graft-*versus*-host disease (GvHD) (i.e. lethal complications of acute GvHD and/or its treatment), and cardiovascular events. In both the training (A) and the confirmation (B) cohorts, as compared to patients not succumbing to non-relapse mortality (NRM), serum levels of pre-transplant testosterone tended to be lower in patients who died of lethal complications of acute GvHD. Box plots are depicted. Number of patients/events for each group is indicated. *P*-values by Mann-Whitney U test.

Table 4. Multivariable analysis of the confirmation cohort with the end points overall survival (OS), progression-free survival (PFS), non-relapse mortality (NRM), and relapse following allogeneic stem cell transplantation and OS and PFS after onset of acute graft-*versus*-host disease (GvHD) (complete case analysis).

	OS (n=165)		PFS (n=165)		NRM* (n=165)		Relapse* (n=165)		OS after acute GvHD* (n=127)		PFS after acute GvHD* (n=126)	
	HR 95% CI	P	HR 95% CI	P	CHR 95% CI	P	CHR 95% CI	P	HR 95% CI	P	HR 95% CI	P
Co-variate												
Testosterone	1.15		1.10		1.23		1.02		1.19		1.15	
(per 100 ng/dL decrease)	(1.03-1.28)	0.012	(0.99-1.22)	0.062	(1.05-1.43)	0.008	(0.88-1.16)	0.818	(1.05-1.33)	0.004	(1.03-1.28)	0.011
Disease stage†												
Early	Ref		Ref		Ref		Ref		Ref		Ref	
Intermediate	1.62		1.55		1.88		1.22		2.01		1.75	
	(0.93-2.83)	0.088	(0.92-2.62)	0.101	(0.87-4.09)	0.109	(0.61-2.45)	0.579	(1.09-3.74)	0.026	(0.98-3.10	0.057
Late	2.48		2.43		3.30		1.98		3.21		2.95	
	(1.48-4.15)	<0.001	(1.48-3.97)	<0.001	(1.65-6.62)	<0.001	(1.03-3.78)	0.039	(1.78-5.80)	<0.001	(1.70-5.12	<0.001
Age (per 10-year increase)	1.12		1.09		1.32		1.02		1.22		1.16	
	(0.90-1.37)	0.307	(0.89-1.33)	0.424	(1.03-1.71)	0.031	(0.82-1.26)	0.893	(0.99-1.50)	0.068	(0.96-1.40)	0.127
Conditioning												
MAC	Ref		Ref		–	–	–	–	–	–	–	–
RIC	1.81		1.65									
	(0.88-3.71)	0.10	(0.85-3.21)	0.137								
Donor												
Related donor	Ref		Ref		–	–	–	–	–	–	–	–
Unrelated Donor	1.22		0.93									
	(0.65-2.29)	0.528	(0.52-1.65)	0.806								
Recipient - donor sex match												
Matched	Ref		Ref		–	–	–	–	–	–	–	–
Male recipient /	1.63		1.15									
female donor	(0.95-2.81)	0.075	(0.68-1.97)	0.604								
Donor source												
PB	Ref		Ref		–	–	–	–	–	–	–	–
BM	1.29		1.75									
	(0.49-3.39)	0.605	(0.77-3.97)	0.182								

Number of events: OS, n=87; PFS, n=97; NRM, n=46; relapse, n=51; OS after acute GvHD, n=67; PFS after acute GvHD, n=75. *Slim model. †According to Gratwohl *et al.*[13] BM: bone marrow; CHR: cause-specific hazard ratio; CI: confidence interval; HR: hazard ratio; MAC: myeloablative conditioning; PB: peripheral blood; RIC: reduced intensity conditioning.

total testosterone levels were based on a single serum sample. However, it should be noted that single-point measurements of total testosterone and androgens were demonstrated to be a reliable indication of the long-term hormonal status of men.[34] Certainly, further prospective, and preferably interventional, studies are needed to confirm our findings.

As regards intervention, the "optimal" cut-off value for definition of "low testosterone" needs to be discussed. Most studies on cardiovascular health and cardiovascular risk assessment applied values between 100-350 ng/dL (corresponding to 3.5-12.1 nM), as indicated by a recent systematic review.[35] In the prospective "T trials", testosterone levels <275 ng/dL (approx. 9.5 nM) were used as indications for intervention.[31] However, men undergoing alloSCT represent a distinct patient cohort. And although the available evidence indicates that testosterone replacement therapy is largely considered to be safe in most men, some controversies remain, and the inherent risk of adverse effects, particularly in selected high-risk populations, should not be ignored.[36] In our study, median pre-transplant testosterone levels in all male cohorts were above the aforementioned range. It should further be noted that, since data on clinical signs of hypogonadism cannot be ascertained retrospectively, patients of the low pre-transplant testosterone group (<250 ng/dL) in our study may not necessary be androgen deficient. In the present study, an optimized cut-off point of 250 ng/dL was derived and was shown to be associated with a 2-fold risk of death post transplant and after onset of acute GvHD in men allografted for AML. This cut-off value of 250 ng/dL is consistent with one definition of "low testosterone"[35] and was shown to be associated with mortality also in non-transplant settings,[15,16] and may thus be applied in a pilot clinical trial. Certainly, any future prospective study should also assess clinical signs of androgen deficiency, including additional biochemical testing.

In summary, our study suggests that pre-transplant testosterone has an impact on NRM and thus may be a determinant of outcome in male patients allografted for

Table 5. Multivariable analysis of the confirmation cohort with optimized pre-transplant testosterone cut-off value (complete case analysis).

	OS (n=165)		PFS (n=165)		NRM (n=165)		Relapse (n=165)		OS after acute GvHD* (n=127)		PFS after acute GvHD* (n=126)	
	HR 95% CI	P	HR 95% CI	P	CHR 95% CI	P	CHR 95% CI	P	HR 95% CI	P	HR 95% CI	P
Co-variate												
Testosterone												
≥250 ng/dL	Ref		Ref		Ref		Ref		Ref		Ref	
<250 ng/dL	1.95		1.81		2.68		1.28		2.29		2.29	
	(1.11-3.43)	0.021	(1.05-3.12)	0.033	(1.25-5.74)	0.011	(0.57-2.84)	0.551	(1.27-4.12)	0.006	(1.29-4.10)	0.005
Disease stage†												
Early	Ref		Ref		Ref		Ref		Ref		Ref	
Intermediate	1.67		1.62		2.04		1.35		2.12		1.90	
	(0.96-2.93)	0.072	(0.95-2.75)	0.076	(0.92-4.51)	0.079	(0.66-2.77)	0.417	(1.13-3.96)	0.019	(1.05-3.42)	0.033
Late	2.53		2.46		3.09		2.04		3.27		3.09	
	(1.51-4.23)	<0.001	(1.51-4.00)	<0.001	(1.51-6.33)	0.002	(1.03-4.05)	0.042	(1.80-5.93)	<0.001	(1.76-5.40)	<0.001
Age (per 10-year	1.12		1.10		1.28		0.98		1.23		1.17	
increase)	(0.91-1.39)	0.280	(0.90-1.35)	0.353	(0.93-1.64)	0.121	(0.68-1.28)	0.873	(0.99-1.53)	0.065	(0.96-1.43)	0.117
Conditioning												
MAC	Ref		Ref		Ref		Ref		–		–	
RIC	1.79		1.63		1.62		1.69					
	(0.88-3.67)	0.110	(0.84-3.15)	0.146	(0.56-4.64)	0.370	(0.71-4.01)	0.233				
Donor												
Related donor	Ref		Ref		Ref		Ref		–		–	
Unrelated Donor	1.19		0.91		1.25		0.72					
	(0.64-2.22)	0.579	(0.52-1.61)	0.753	(0.50-3.13)	0.634	(0.35-1.49)	0.375				
Recipient - donor sex match												
Matched	Ref		Ref		Ref		Ref		–		–	
Male recipient /	1.57		1.13		1.45		0.93					
female donor	(0.93-2.65)	0.094	(0.67-1.91)	0.643	(0.70-3.00)	0.316	(0.44-1.98)	0.854				
Donor source												
PB	Ref		Ref		Ref		Ref		–		–	
BM	1.42		1.92		1.59		2.01					
	(0.53-3.78)	0.485	(0.83-4.42)	0.125	(0.35-7.30)	0.551	(0.74-5.49)	0.173				

Number of events: OS, n=87; PFS, n=97; NRM, n=46, relapse, n=51; OS after acute GvHD, n=67; PFS after acute GvHD, n=75. *Slim model. †According to Gratwohl *et al.*[13] Number of events: OS, n=87; PFS, n=97; NRM, n=46; relapse, n=51; OS after acute GvHD, n=67; PFS after acute GvHD, n=75. *Slim model. †According to Gratwohl *et al.*[13] PFS: progression-free survival; BM: bone marrow; CHR: cause-specific hazard ratio; CI: confidence interval; GvHD: graft-*versus*-host disease; HR: hazard ratio; MAC: myeloablative conditioning; PB: peripheral blood; RIC: reduced intensity conditioning; OS: overall survival; NRM: non-relapse mortality.

AML. Considering recent successful post-remission androgen maintenance treatment approaches in AML,[12] and the fact that an individual's testosterone status is modifiable, our results may provide a rationale for the design of interventional clinical studies evaluating testosterone/androgen status and supplementation in patients undergoing alloSCT.

Acknowledgments

The authors wish to acknowledge the great work of the physicians and the nursing staff of both transplant units and the patients for making the study possible. The authors thank Michael Hess and Alexandra Hof for their expert technical assistance, and the construction and maintenance of the serum biobank. We would also like to acknowledge the help of Markus Zorn at the Department of Clinical Chemistry of the Heidelberg University Hospital and the help of Ina Rehberger at the Steroid Lab of the Institute of Pharmacology, University Heidelberg.

Funding

This work was supported by B.L.U.T. e.V. (Weingarten, Germany).

References

1. Tichelli A, Bucher C, Rovó A, et al. Premature cardiovascular disease after allogeneic hematopoietic stem-cell transplantation. Blood. 2007;110(9):3463-3671.
2. Cooke KR, Jannin A, Ho V. The contribution of endothelial activation and injury to end-organ toxicity following allogeneic hematopoietic stem cell transplantation. Biol Blood Marrow Transplant. 2008;14(1 Suppl 1):23-32.
3. Luft T, Dietrich S, Falk C, et al. Steroid-refractory GvHD: T-cell attack within a vulnerable endothelial system. Blood. 2011;118(6):1685-1692.
4. Radujkovic A, Dai H, Kordelas L, et al.

Asymmetric dimethylarginine serum levels are associated with early mortality after allogeneic stem cell transplantation. Haematologica. 2019;104(4):827-834.
5. Lindås R, Tvedt TH, Hatfield KJ, Reikvam H, Bruserud O. Preconditioning serum levels of endothelial cell-derived molecules and the risk of posttransplant complications in patients treated with allogeneic stem cell transplantation. J Transplant. 2014;2014:404096.
6. Tatekawa S, Kohno A, Ozeki K, et al. A Novel Diagnostic and Prognostic Biomarker Panel for Endothelial Cell Damage-Related Complications in Allogeneic Transplantation. Biol Blood Marrow Transplant. 2016;22(9):1573-1581.
7. Akishita M, Hashimoto M, Ohike Y, et al. Low testosterone level is an independent determinant of endothelial dysfunction in men. Hypertens Res. 2007;30(11):1029-1034.
8. Empen K, Lorbeer R, Dörr M, et al. Association of testosterone levels with endothelial function in men: results from a population-based study. Arterioscler Thromb Vasc Biol. 2012;32(2):481-486.
9. Araujo AB, Dixon JM, Suarez EA, Murad MH, Guey LT, Wittert GA. Clinical review: Endogenous testosterone and mortality in men: a systematic review and meta-analysis. J Clin Endocrinol Metab. 2011;96(10):3007-3019.
10. Hollard D, Sotto JJ, Berthier R, Leger J, Michallet M. High rate of long-term survivals in AML treated by chemotherapy and androgenotherapy: a pilot study. Cancer. 1980;45(7):1540-1548.
11. Hayat M, Jehn U, Willemze R, et al. A randomized comparison of maintenance treatment with androgens, immunotherapy, and chemotherapy in adult acute myelogenous leukemia. A Leukemia-Lymphoma Group Trial of the EORTC. Cancer. 1986;58(3):617-623.
12. Pigneux A, Béné MC, Guardiola P, et al. Addition of Androgens Improves Survival in Elderly Patients With Acute Myeloid Leukemia: A GOELAMS Study. J Clin Oncol. 2017;35(4):387-393.
13. Gratwohl A, Stern M, Brand R, et al. Risk score for outcome after allogeneic hematopoietic stem cell transplantation: a retrospective analysis. Cancer. 2009; 115(20):4715-4726.
14. Sorror ML, Maris MB, Storb R, et al. Hematopoietic cell transplantation (HCT)-specific comorbidity index: a new tool for risk assessment before allogeneic HCT. Blood. 2005;106(8):2912-2919.
15. Shores MM, Matsumoto AM, Sloan KL, Kivlahan DR. Low serum testosterone and mortality in male veterans. Arch Intern Med. 2006;166(15):1660-1605.
16. Haring R, Völzke H, Steveling A, et al. Low serum testosterone levels are associated with increased risk of mortality in a population-based cohort of men aged 20-79. Eur Heart J. 2010;31(12):1494-1501.
17. Björk Y, Smith Knutsson E, Ankarberg-Lindgren C, et al. Androgens in women after allogeneic hematopoietic cell transplantation: impact of chronic GvHD and glucocorticoid therapy. Bone Marrow Transplant. 2017;52(3):431-437.
18. Grigg AP, McLachlan R, Zaja J, Szer J. Reproductive status in long-term bone marrow transplant survivors receiving busulfan-cyclophosphamide (120 mg/kg). Bone Marrow Transplant. 2000;26(10):1089-1095.
19. Tauchmanovà L, Selleri C, De Rosa G, et al. Gonadal status in reproductive age women after haematopoietic stem cell transplantation for haematological malignancies. Hum Reprod. 2003;18(7):1410-1416.
20. dos Santos RL, da Silva FB, Ribeiro RF Jr, Stefanon I. Sex hormones in the cardiovascular system. Horm Mol Biol Clin Investig. 2014;18(2):89-103.
21. Howell SJ, Shalet SM. Testicular function following chemotherapy. Hum Reprod Update. 2001;7(4):363-369.
22. Zhang J, Ye J, Ma D, et al. Cross-talk between leukemic and endothelial cells promotes angiogenesis by VEGF activation of the Notch/Dll4 pathway. Carcinogenesis. 2013;34(3):667-677.
23. Cogle CR, Goldman DC, Madlambayan GJ, et al. Functional integration of acute myeloid leukemia into the vascular niche. Leukemia. 2014;28(10):1978-1987.
24. Hatfield K, Øyan AM, Ersvaer E, et al. Primary human acute myeloid leukaemia cells increase the proliferation of microvascular endothelial cells through the release of soluble mediators. Br J Haematol. 2009; 144(1):53-68.
25. Reikvam H, Hatfield KJ, Fredly H, Nepstad I, Mosevoll KA, Bruserud Ø. The angioregulatory cytokine network in human acute myeloid leukemia - from leukemogenesis via remission induction to stem cell transplantation. Eur Cytokine Netw. 2012; 23(4):140-153.
26. Afferni C, Buccione C, Andreone S, et al. The Pleiotropic Immunomodulatory Functions of IL-33 and Its Implications in Tumor Immunity. Front Immunol. 2018; 9:2601.
27. Andersson C, Enserro D, Sullivan L, et al. Relations of circulating GDF-15, soluble ST2, and troponin-I concentrations with vascular function in the community: The Framingham Heart Study. Atherosclerosis. 2016;248:245-251.
28. Patel JV, Lim HS, Varughese GI, Hughes EA, Lip GY. Angiopoietin-2 levels as a biomarker of cardiovascular risk in patients with hypertension. Ann Med. 2008;40(3):215-222.
29. Vander Lugt MT, Braun TM, Hanash S, et al. ST2 as a marker for risk of therapy-resistant graft-versus-host disease and death. N Engl J Med. 2013;369(6):529-539.
30. Gencer B, Mach F. Testosterone: a hormone preventing cardiovascular disease or a therapy increasing cardiovascular events? Eur Heart J. 2016;37(48):3569-3575.
31. Snyder PJ, Ellenberg SS, Cunningham GR, et al. The Testosterone Trials: Seven coordinated trials of testosterone treatment in elderly men. Clin Trials. 2014;11(3):362-375.
32. Budoff MJ, Ellenberg SS, Lewis CE, et al. Testosterone Treatment and Coronary Artery Plaque Volume in Older Men With Low Testosterone. JAMA. 2017;317(7):708-716.
33. Blagosklonny MV, Neckers LM. Cytostatic and cytotoxic activity of sex steroids against human leukemia cell lines. Cancer Lett. 1994;76(2-3):81-86.
34. Vermeulen A, Verdonck G. Representativeness of a single point plasma testosterone level for the long term hormonal milieu in men. J Clin Endocrinol Metab. 1992;74(4):939-942.
35. Huo S, Scialli AR, McGarvey S, et al. Treatment of Men for "Low Testosterone": A Systematic Review. PLoS One. 2016;11(9):e0162480.
36. Grech A, Breck J, Heidelbaugh J. Adverse effects of testosterone replacement therapy: an update on the evidence and controversy. Ther Adv Drug Saf. 2014;5(5):190-200.
37. Bacigalupo A, Ballen K, Rizzo D, et al. Defining the intensity of conditioning regimens: working definitions. Biol Blood Marrow Transplant. 2009;15(12):1628-1633.
38. Bornhäuser M, Kienast J, Trenschel R, et al. Reduced-intensity conditioning versus standard conditioning before allogeneic haemopoietic cell transplantation in patients with acute myeloid leukaemia in first complete remission: a prospective, open-label randomised phase 3 trial. Lancet Oncol. 2012;13(10):1035-1044.

ERRATA CORRIGE

Association of early disease progression and very poor survival in the GALLIUM study in follicular lymphoma: benefit of obinutuzumab in reducing the rate of early progression

John F. Seymour,[1] Robert Marcus,[2] Andrew Davies,[3] Eve Gallop-Evans,[4] Andrew Grigg,[5] Andrew Haynes,[6] Michael Herold,[7] Thomas Illmer,[8] Herman Nilsson-Ehle,[9] Martin Sökler,[10] Ulrich Dünzinger,[11] Tina Nielsen,[12] Aino Launonen[12] and Wolfgang Hiddemann[13]

[1]Peter MacCallum Cancer Centre, Royal Melbourne Hospital and University of Melbourne, Victoria, NSW, Australia; [2]Kings College Hospital, London, UK; [3]Cancer Research UK Centre, University of Southampton, Southampton, UK; [4]Velindre Cancer Centre, Cardiff, UK; [5]Austin Hospital, Melbourne, Victoria, NSW, Australia; [6]Nottingham University Hospitals NHS Trust, Nottingham, UK; [7]HELIOS-Klinikum Erfurt, Germany; [8]BAG Freiberg-Richter, Jacobasch, Illmer and Wolf, Dresden, Germany; [9]Section of Hematology and Coagulation, Department of Medicine, Sahlgrenska University Hospital, Gothenburg, Sweden; [10]Eberhard-Karls-University Tübingen, Tübingen, Germany; [11]Roche Pharma AG, Grenzach-Wyhlen, Germany; [12]F. Hoffmann-La Roche Ltd., Basel, Switzerland and [13]Department of Medicine III, Ludwig-Maximilians-University, München, Germany

doi:10.3324/haematol.2020.246991

In the article by Seymour JF, Marcus R, Davies A, Gallop-Evans E, Grigg A, Haynes A, Herold M, Illmer T, Nilsson-Ehle H, Sökler M, Dünzinger U, Nielsen T, Launonen A, Hiddemann W entitled 'Association of early disease progression and very poor survival in the GALLIUM study in follicular lymphoma: benefit of obinutuzumab in reducing the rate of early progression', published in Haematologica supplement 2019 Jun;104(6):1202-1208, there is a small data error in the *Online Supplementary Table S6*, the number of low-risk FLIPI patients with POD24 in the G-chemo group percentage has been miscalculated, it should read (9.4) not (44.4).

Online Supplementary Table S6. POD24 and post-progression mortality rates, stratified by FLPI score category.

FLIPI score category	Number of POD24 patients (n/N, %)		24-month CIF rate, % (95% CI)		POD24 risk reduction, % (95% CI)	2-year PPS		Crude PPS death rates	
	G-chemo	R-chemo	G-chemo	R-chemo		G-chemo	R-chemo	G-chemo	R-chemo
High	30/249 (12.0)	54/253 (21.3)	12.7 (8.8-17.3)	22.2 (17.2-27.6)	46.4 (16.2-65.7)	0.60	0.56	26.07 (15.3-44)	27.65 (18.8-40.6)
Intermediate	15/225 (6.7)	31/223 (13.9)	7.2 (4.2-11.2)	14.8 (10.4-20.0)	54.6 (15.8-75.5)	0.86	0.73	6.62 (1.7-26.5)	13.99 (7-28)
Low	12/127 (9.4)	13/125 (10.4)	10.0 (5.5-16.2)	11.6 (6.5-18.3)	15.0 (-83.3-61.2)	0.73	0.77	11.86 (3.8-36.8)	10.67 (3.4-33.1)

CI: confidence interval; FLIPI: Follicular Lymphoma International Prognostic Index; G-chemo: obinutuzumab plus chemotherapy; POD: progressive disease or death; PPS: post-progression survival; R-chemo: rituximab plus chemotherapy.

RESEARCH, READ & CONNECT

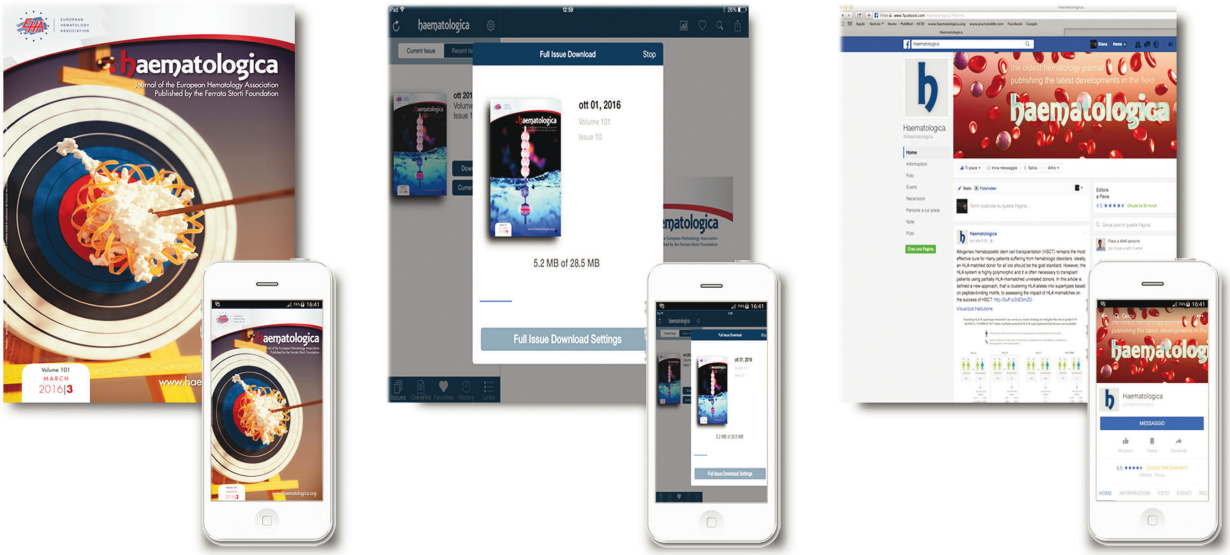

We reach more than
6 hundred thousand readers each year

The first Hematology Journal in Europe

Impressions YTD

9,621,645

Digital Readers

4,431

Total Audience

554,484

Worldwide rank	Impact factor	Total citations
7 th	7.570	16,255

haematologica

Journal of the Ferrata Storti Foundation

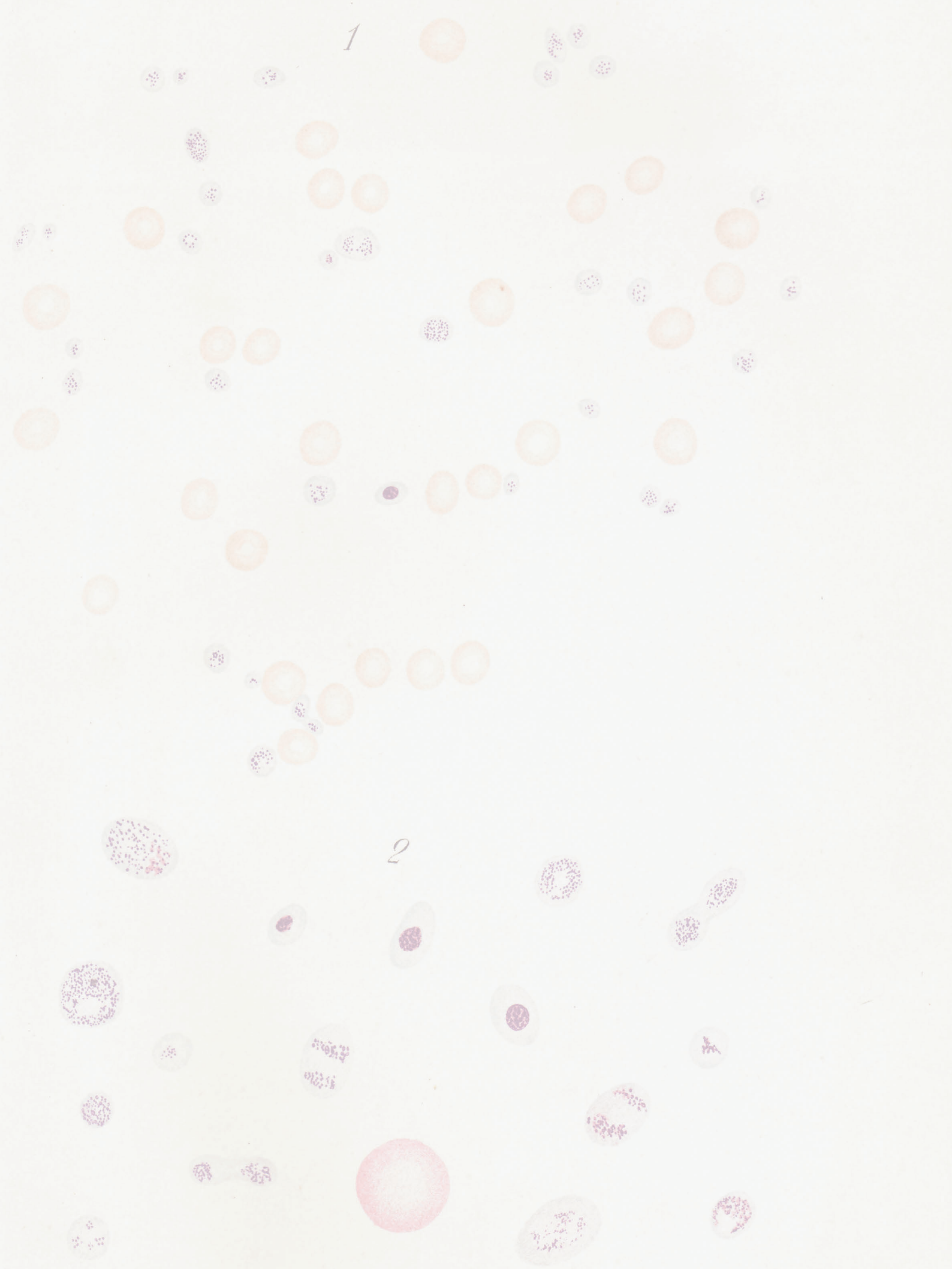
1
2

haematologica — Vol. 105 n. 5 — May 2020 — 1169-1466